

49A 124400

2

**MINUTES
OF THE TWENTIETH
EXPLOSIVES SAFETY SEMINAR
VOLUME I**

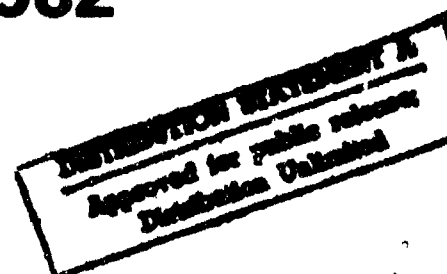


**OMNI INTERNATIONAL HOTEL
NORFOLK, VIRGINIA**

24 - 25 - 26 AUGUST 1982

DTIC FILE COPY

**SPONSORED BY
DEPARTMENT OF DEFENSE EXPLOSIVES SAFETY BOARD
ALEXANDRIA, VA**



88 01 31 .012

REPORT DOCUMENTATION PAGE		READ INSTRUCTIONS BEFORE COMPLETING FORM
1. REPORT NUMBER	2. GOVT ACCESSION NO. AD-A124400	3. RECIPIENT'S CATALOG NUMBER
4. TITLE (and Subtitle) MINUTES OF THE TWENTIETH EXPLOSIVES SAFETY SEMINAR _ Volume I		5. TYPE OF REPORT & PERIOD COVERED
7. AUTHOR(s)		6. PERFORMING ORG. REPORT NUMBER
9. PERFORMING ORGANIZATION NAME AND ADDRESS		8. CONTRACT OR GRANT NUMBER(s)
11. CONTROLLING OFFICE NAME AND ADDRESS Chairman, DDESB 2461 Eisenhower Avenue Alexandria, Virginia 22331		10. PROGRAM ELEMENT, PROJECT, TASK AREA & WORK UNIT NUMBERS
12. REPORT DATE August 24-26, 1982		13. NUMBER OF PAGES 948
14. MONITORING AGENCY NAME & ADDRESS (if different from Controlling Office)		15. SECURITY CLASS. (of this report) Unclassified
		15a. DECLASSIFICATION/DOWNGRADING SCHEDULE
16. DISTRIBUTION STATEMENT (of this Report) Approved for Public Release - Distribution Unlimited		
17. DISTRIBUTION STATEMENT (of the abstract entered in Block 20, if different from Report)		
18. SUPPLEMENTARY NOTES		
19. KEY WORDS (Continue on reverse side if necessary and identify by block number) Ammunition Explosives Safety		
20. ABSTRACT (Continue on reverse side if necessary and identify by block number)		

DTIC
JAN 31 1983
H

(1)

DTIC
FEB 7 1983

COMPONENT PART NOTICE

THIS PAPER IS A COMPONENT PART OF THE FOLLOWING COMPILATION REPORT: **A**

(TITLE): Minutes of the Explosives Safety Seminar (20th) Held at OMNI International
Hotel, Norfolk, Virginia on 24-26 August 1982. Volume I.

(SOURCE): Department of Defense Explosives Safety Board, Alexandria, Va.

TO ORDER THE COMPLETE COMPILATION REPORT USE AD-A124 400.

THE COMPONENT PART IS PROVIDED HERE TO ALLOW USERS ACCESS TO INDIVIDUALLY AUTHORED SECTIONS OF PROCEEDINGS, ANNALS, SYMPOSIA, ETC. HOWEVER, THE COMPONENT SHOULD BE CONSIDERED WITHIN THE CONTEXT OF THE OVERALL COMPILATION REPORT AND NOT AS A STAND-ALONE TECHNICAL REPORT.

THE FOLLOWING COMPONENT PART NUMBERS COMPRISE THE COMPILATION REPORT:

AD#: P000	TITLE:
427	Detonability of Agent BZ - Pyromix.
AD-P000 428	Hazard Classification Testing of Ammonium Perchlorate.
AD-P000 429	Classification and In-Process Classification Testing - Where Do We Go From Here?
AD-P000 430	Blast Parameters from Cylindrical Charges Detonated on the Surface of the Ground.
AD-P000 431	Blast Predictions for Coyote Canyon Explosions.
AD-P000 432	The Contaminated Waste Processor for Incineration of Explosives Contaminated Waste.
AD-P000 433	Industrial Robots Present State of Development.
AD-P000 434	Barricade/Shield Testing New Thinking on Heat Flux Requirements.
AD-P000 435	Developments in Shearing of Ammunition for DEMIL.
AD-P000 436	Naval Explosives Safety Improvement Program - Plans and Programs.
AD-P000 437	Yield and Blast Analyses with a Unified Theory of Explosions.
AD-P000 438	Design Criteria for Frangible Covers in Ordnance Facilities.
AD-P000 439	Internal Blast Measurements in a Model of the Panter Damaged Weapons Facility.
AD-P000 440	Quasi-Static Pressure, Duration, and Impulse for Explosions in Structures.
AD-P000 441	Viper Round Containment Vessel Development.
AD-P000 442	Behavior of Gun Propellant to Ignitions of Different Intensities.
AD-P000 443	The Response of RDX/TNT Filled Shell to Thermal Stimuli.
AD-P000 444	Sparrow (AIM/RIM-7M) with EX-114 Mod 1 Warhead Quantity-Distance Study for Handling Operations.
AD-P000 445	Basic Tow Missile (BGM-71A-1) Quantity-Distance Hazard Study for Handling Operations.
AD-P000 446	Half-Scale Submarine Tender Workshop Explosion Hazards.
AD-P000 447	Explosion Containment: Progress, Scaling Laws, and Material Properties.

COMPONENT PART NOTICE (CON'T)

AD#: P000 448	TITLE: Design of a Detonation Chamber for Demilitarizing Munitions.
AD-P000 449	Design of the Advanced High Kinetic Energy Launch System.
AD-P000 450	Design and Evaluation of Damaged Weapon Facility.
AD-P000 451	DoD Ammunition and Explosives Safety Standards. Chapter 13. Personnel Protection.
AD-P000 452	Fire Hazards of Combustible Ammunition in Storage or Transport.
AD-P000 453	Measurement and Prediction of Heat Flux in Gun Propellant Fires.
AD-P000 454	Quantity-Distances for Hazard Division 1.3 Mass Fire Risk Explosives.
AD-P000 455	Improved Thermal Protection for Pyrotechnic Workers.
AD-P000 456	General Risk Analysis Methodological Implications to Explosives Risk Management Systems.
AD-P000 457	Risk Analysis for Explosives Operations.
AD-P000 458	Building Damages Due to Airblast from an Accidental Explosion.
AD-P000 459	Modeling Debris Effects Produced by a High Yield Explosion.
AD-P000 460	Response of the Flash X-Ray Building at Site 300 to Explosions on Its Firing Table.
AD-P000 461	Structural Damage to Building Frames from Accidental or Terrorist Explosions.
AD-P000 462	Lightning Warning Systems for Explosive Operations/Facilities.
AD-P000 463	Dielectric Radio Frequency Heating of Propellants Incident Investigation and Applications.
AD-P000 464	Safety of High Explosives Commutation Processes.
AD-P000 465	Static Electricity Phenomena in the Manufacture and Handling of Solid Propellants.
AD-P000 466	Risk Analysis - Grasping the Nettle.
AD-P000 467	The Low Probability of Accidental Explosions: Isn't it Worth a Cent in Explosives Safety?

Accession For	
NTIS GRA&I	<input checked="" type="checkbox"/>
DTIC TAB	<input type="checkbox"/>
Unannounced	<input type="checkbox"/>
Justification	
By	
Distribution/	
Availability Codes	
Dist	Avail and/or Special
A	

This document has been approved for public release and sale; its distribution is unlimited.

MINUTES OF THE
TWENTIETH EXPLOSIVES SAFETY SEMINAR

Volume I

Omni International Hotel
Norfolk, Virginia

24-25-26 August 1982

Sponsored by

Department of Defense Explosives Safety Board
Alexandria, Virginia 22331

Approved for public release; distribution unlimited

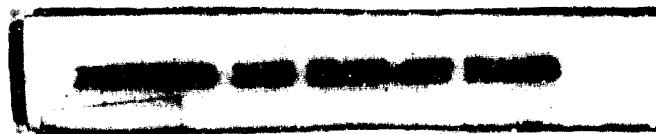
PREFACE

This Seminar is held as a medium by which there may be a free exchange of information regarding explosives safety. With this idea in mind, these minutes are being provided for your information. The presentations made at this Seminar do not imply indorsement of the ideas, accuracy of facts presented, or any product, by either the Department of Defense Explosives Safety Board or the Department of Defense.

D. G. HOECH
Captain, USN
Chairman



Accession For	
NTIS GPO&I	<input checked="" type="checkbox"/>
DTIC T-8	<input type="checkbox"/>
Unannounced	<input type="checkbox"/>
Justification	
By _____	
Distribution/	
Availability Codes	
Dist	Avail and/or Special
A	



These proceedings are published for information as an
accommodation to the participants at the Seminar.

The Department of Defense Explosives Safety Board cannot
accept responsibility for the correctness of those papers
which have been directly reproduced from copy furnished
by the authors.

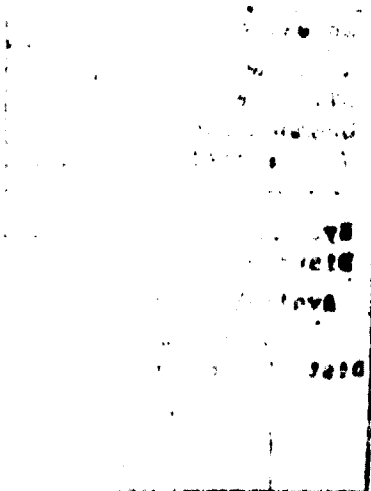


TABLE OF CONTENTS

VOLUME I

<i>PREFACE</i>	111
<i>WELCOME</i>	1
COLONEL Alton W. Powell, USAF, Chairman, Department of Defense Explosives Safety Board	
<i>KEYNOTE ADDRESS</i>	3
Dr. Sharon Lord, Deputy Assistant Secretary for Equal Opportunity and Safety Policy	
<i>THE EFFECTS OF THE HEALTH AND SAFETY AT WORK ACT, 1974, ON MILITARY EXPLOSIVES SAFETY MANAGEMENT IN THE UNITED KINGDOM</i>	7
Air Commodore Frank Robinson, Vice President, UK Ordnance Board	
 SESSION - HAZARD CLASSIFICATION TESTING	
Moderator - Mr. Eric T. Olson	
<i>DETONABILITY OF AGENT BZ - PYROMIX</i>	19
Dr. B. D. Trott and Mr. James Stuart	
<i>HAZARD CLASSIFICATION TESTING OF AMMONIUM PERCHLORATE</i>	55
Messrs. Joseph P. Caltagirone, Darl E. Westover and Fred L. McIntyre	
<i>CLASSIFICATION AND IN-PROCESS CLASSIFICATION TESTING - WHERE DO WE GO FROM HERE?</i>	73
Mr. F. L. McIntyre	
 SESSION - HIGH EXPLOSIVE AIRBLAST PARAMETERS	
Moderator - Mr. C. N. Kingery	
<i>BLAST PARAMETERS FROM CYLINDRICAL CHARGES DETONATED ON THE SURFACE OF THE GROUND</i>	87
Messrs. G. Guerke and G. Scheklinski-Glueck	
<i>EFFECTS OF LOW LOADING DENSITY ON BLAST PROPAGATION FROM EARTH COVERED MAGAZINES</i>	115
Messrs. George Coulter and Charles Kingery	
<i>BLAST PREDICTIONS FOR COYOTE CANYON EXPLOSIONS</i>	169
Mr. Jack W. Reed	
 SESSION - AMMUNITION PECULIAR EQUIPMENT	
Moderator - Mr. Mark Zaugg	
<i>THE CONTAMINATED WASTE PROCESSOR FOR INCINERATION OF EXPLOSIVES CONTAMINATED WASTE</i>	203
Dr. Solim S. W. Kwak	

INDUSTRIAL ROBOTS PRESENT STATE OF DEVELOPMENT..... 223
Directorate for Ammunition Equipment

BARRICADE/SHIELD TESTING NEW THINKING ON HEAT FLUX REQUIREMENTS..... 237
Mr. Jerry Miller

DEVELOPMENTS IN SHEARING OF AMMUNITION FOR DEMIL..... 261
Mr. Kenneth O. Rhea, Jr.

SESSION - NAVAL EXPLOSIVES SAFETY IMPROVEMENT PROGRAM I

Moderator - Mr. Edward A. Daugherty

NAVAL EXPLOSIVES SAFETY IMPROVEMENT PROGRAM - PLANS AND PROGRAMS..... 285
Mr. Michael M. Swisdak, Jr.

YIELD AND BLAST ANALYSES WITH A UNIFIED THEORY OF EXPLOSIONS..... 303
Mr. Francis B. Porzel

SESSION - BLAST LOADS INSIDE STRUCTURES

Moderator - Mr. William A. Keenan

DESIGN CRITERIA FOR FRANGIBLE COVERS IN ORDNANCE FACILITIES..... 333
Messrs. William A. Keenan and James E. Tancreto

*INTERNAL BLAST MEASUREMENTS IN A MODEL OF THE PANTEX
DAMAGED WEAPONS FACILITY..... 363*
Messrs. J. C. Hokanson, E. D. Esparza, W. E. Baker and N. R. Sandoval

*QUASI-STATIC PRESSURE, DURATION, AND IMPULSE FOR EXPLOSIONS
IN STRUCTURES..... 389*
Messrs. W. E. Baker, Charles E. Anderson, Jr., Bruce L. Morris and
Ms. Donna K. Wauters

VIPER ROUND CONTAINMENT VESSEL DEVELOPMENT..... 415
Mr. C. James Dahn

SESSION - RESPONSE OF AMMUNITION TO THERMAL STIMULI

Moderator - Mr. Eugene G. Clark

BEHAVIOR OF GUN PROPELLANT TO IGNITIONS OF DIFFERENT INTENSITIES..... 441
Mr. Roland Wild

THE RESPONSE OF RDX/TNT FILLED SHELL TO THERMAL STIMULI..... 449
Messrs. A. S. Dyer, C. D. Hutchinson, P. J. Hubbard and J. Connor

SESSION - NAVAL EXPLOSIVES SAFETY IMPROVEMENT PROGRAM II

Moderator - Mr. Edward A. Daugherty

SPARROW (AIM/RIM-7M) WITH EX-114 MOD 1 WARHEAD QUANTITY-DISTANCE STUDY FOR HANDLING OPERATIONS.....	459
Dr. Jerry M. Ward and Richard A. Lorenz	
BASIC TOW MISSILE (BGM-71A-1) QUANTITY-DISTANCE HAZARD STUDY FOR HANDLING OPERATIONS.....	487
Mr. Richard A. Lorenz and Dr. Jerry M. Ward	
HALF-SCALE SUBMARINE TENDER WORKSHOP EXPLOSION HAZARDS.....	507
Mr. Joseph G. Connor, Jr.	

SESSION - BLAST CONTAINMENT STRUCTURES

Moderator - Dr. W. E. Baker

EXPLOSION CONTAINMENT: PROGRESS, SCALING LAWS, AND MATERIAL PROPERTIES.	519
Messrs. John J. White, III and B. Dale Trott	
DESIGN OF A DETONATION CHAMBER FOR DEMILITARIZING MUNITIONS.....	549
Messrs. M. G. Whitney, W. E. Baker, J. R. Riegel III and L. R. Garza	
DESIGN OF THE ADVANCED HIGH KINETIC ENERGY LAUNCH SYSTEM.....	571
Mr. W. V. Hill	
DESIGN AND EVALUATION OF DAMAGED WEAPON FACILITY.....	589
Messrs. Norval Dobbs and Samuel Weissman	

SESSION - THERMAL HAZARDS AND PROTECTION

Moderator - Mr. Eugene G. Clark

DoD 5154.4S, "DoD AMMUNITION AND EXPLOSIVES SAFETY STANDARDS," CHAPTER 13, PERSONNEL PROTECTION.....	607
Dr. R. A. Scott	
FIRE HAZARDS OF COMBUSTIBLE AMMUNITION IN STORAGE OR TRANSPORT.....	611
Messrs. R. Pape, T. E. Waterman and Ms. H. Napadensky	
MEASUREMENT AND PREDICTION OF HEAT FLUX IN GUN PROPELLANT FIRES.....	629
Mr. J. P. Lucotte	
QUANTITY-DISTANCES FOR HAZARD DIVISION 1.3 MASS FIRE RISK EXPLOSIVES....	643
Mr. W. S. N. Tinkler	
IMPROVED THERMAL PROTECTION FOR PYROTECHNIC WORKERS.....	661
Messrs. Jim I. Martin, Don W. Moore and Tracy K. Bramlett	

SESSION - RISK ANALYSIS I
Moderator - Mr. Peter Rutledge

<i>GENERAL RISK ANALYSIS METHODOLOGICAL IMPLICATIONS TO EXPLOSIVES RISK MANAGEMENT SYSTEMS.....</i>	<i>703</i>
<i>Mr. Lloyd L. Philipson</i>	
<i>RISK ANALYSIS FOR EXPLOSIVES OPERATIONS.....</i>	<i>725</i>
<i>LTC Alan C. Graham, Jr.</i>	

SESSION - STRUCTURAL RESPONSE TO AIRBLAST
Moderator - Mr. Norval Dobbs

<i>BUILDING DAMAGES DUE TO AIRBLAST FROM AN ACCIDENTAL EXPLOSION.....</i>	<i>737</i>
<i>Mr. Hansjorg Rytz</i>	
<i>MODELING DEBRIS EFFECTS PRODUCED BY A HIGH YIELD EXPLOSION.....</i>	<i>759</i>
<i>Messrs. A. Longinow, T. E. Waterman and Ms. H. S. Napadensky</i>	
<i>RESPONSE OF THE FLASH X-RAY BUILDING AT SITE 300 TO EXPLOSIONS ON ITS FIRING TABLE.....</i>	<i>781</i>
<i>Messrs. C. F. Baker, C. Y. King, J. W. Lyle, R. K. Mullins, D. S. Ravenscroft and W. M. Shay</i>	
<i>STRUCTURAL DAMAGE TO BUILDING FRAMES FROM ACCIDENTAL OR TERRORIST EXPLOSIONS.....</i>	<i>801</i>
<i>Mr. Bruce L. Morris</i>	

SESSION - EXPLOSIVES AND PROPELLANT MANUFACTURING
Moderator - Mr. Glen Leach

<i>LIGHTNING WARNING SYSTEMS FOR EXPLOSIVE OPERATIONS/FACILITIES.....</i>	<i>831</i>
<i>Mr. Mitchell A. Guthrie</i>	
<i>DIELECTRIC RADIO FREQUENCY HEATING OF PROPELLANTS INCIDENT INVESTIGATION AND APPLICATIONS.....</i>	<i>853</i>
<i>Mr. Melvin C. Hudson</i>	
<i>SAFETY OF HIGH EXPLOSIVES COMMINUTION PROCESSES.....</i>	<i>865</i>
<i>Mr. R. Applin</i>	
<i>STATIC ELECTRICITY PHENOMENA IN THE MANUFACTURE AND HANDLING OF SOLID PROPELLANTS.....</i>	<i>883</i>
<i>Mr. Ralph Kent</i>	

SESSION - RISK ANALYSIS II
Moderator - Mr. Peter Rutledge

RISK ANALYSIS - GRASPING THE NETTLE..... 901
Mr. R. R. Watson

*THE LOW PROBABILITY OF ACCIDENTAL EXPLOSIONS: ISN'T IT WORTH
A CENT IN EXPLOSIVES SAFETY?*..... 925
Mr. Hans A. Merz

Volume II contains pages 941 thru 1923

WELCOME

Colonel Alton W. Powell, USAF
Chairman
Department of Defense Explosives Safety Board

Good morning, ladies and gentlemen. I am Colonel Alton Powell, Chairman, Department of Defense Explosives Safety Board.

It is with considerable pleasure that I welcome you to our Twentieth Explosives Safety Seminar. It is good to see so many friends and familiar faces. Since it is the mission of the DDESB to keep informed of conditions affecting safety wherever U.S. titled ammunition and explosives are found, I have traveled extensively during my three years as Chairman. Thus I have met many of you on your home turf and become aware, first hand, of the problems and concerns you must deal with day-by-day. With the onslaught of the electronic/computer age, we are able to solve many problems of yesteryear, but new problems have arisen; how far are we to permit the computer to control production/manufacturing processes, test and operate weapon systems, etc.? Concessions have been made with respect to quantity-distance requirements for insensitive high explosive substances and articles. How much more relaxation should be permitted? Should the tools of the systems engineers, such as risk analysis be used more in the explosives safety decision making process? Some people think so. There are many more problems/questions that face us today which are demanding answers. That is one of the important reasons for holding this seminar: to provide you (hopefully) answers to some of your questions: but, more than that, this seminar is being held to stimulate you professionally by providing you avenues to knowledge with which to aid you in seeking solutions not provided here. Solving your problem will make our nation's defense posture not only safer but stronger. With world events as they are today, that should be foremost. I, therefore, challenge you to use this seminar as a vehicle for solving your problems and answering your questions. We encourage you to fully participate. I believe our program will make you want to do just that!

Let me now introduce the current members of the Explosives Safety Board. Colonel Bobby Robinson is the Department of the Army Board Member. Colonel Robinson is Chief of the Chemical Division, Deputy Chief of Staff, Operations and Plans. Unfortunately Colonel Robinson could not be with us today. In his stead we have Department of the Army Alternate Board Member, Mr. James Coakley. Jim is on the staff of the Army Safety Program Director. From the Department of the Navy, Captain Virgil E. Strickland Jr. Virgil is Head of the Ordnance Materiel Management Branch in the Office of Chief of Naval Operations. Regrettably also, Captain Strickland could not be with us today. In his stead we have Department of the Navy Alternate Board Member, Mr. Carlo Ferraro, Jr. Carlo is Head of the Explosives and Nuclear Weapons Safety Section in CNO. From the Department of the Air Force, Colonel Jim McQueen. Jim is the Chief of Weapons Safety, Deputy Inspector General, Headquarters Air Force.

I would also like to particularly welcome several of our professional friends in the audience from other countries: from France, General Toche and General Roure; from the United Kingdom, Air Commodore Robinson.

At this time, it is my pleasure to introduce our keynote speaker, Dr. Sharon B. Lord, Deputy Assistant Secretary for Equal Opportunity and Safety Policy.

MANAGEMENT OF
EXPLOSIVES SAFETY WITHIN
THE DEPARTMENT OF DEFENSE

By

Dr. Sharon Lord
Deputy Assistant Secretary
for Equal Opportunity and Safety Policy

At

Twentieth Department of Defense Explosives Safety Seminar
Norfolk, Virginia
August 24, 1982

I am delighted to be with you here in Norfolk today. This is a wonderful opportunity to meet the people who are in the forefront of the continuing effort to control the awesome but indiscriminate destructive power of the explosive materials and devices upon which we rely for the defense of our nation. That this is a matter of international concern is attested by the large number of persons here representing other nations. We welcome all of you and hope this will be a mutually beneficial experience. Our common cause of protecting life and property from the harmful effects of accidents involving ammunition and explosives is certainly one that all nations can support.

Apart from sincere humanitarian concern for the safety of our personnel, DoD has a most vital concern for the prevention of all avoidable mishaps in terms of readiness to perform our national defense mission. Every man or woman, military or civilian, who is incapacitated and every piece of equipment or system accidentally damaged or destroyed diminishes that readiness. Accordingly, an essential element of overall DoD policy is:

- . To protect all DoD personnel from on-the-job injuries and occupational illnesses
- . To protect DoD material resources from accidental damage or destruction
- . To protect the public from possible hazards associated with DoD operations, and
- . To comply with applicable safety and occupational health regulations which Federal or State regulatory agencies promulgate.

Because of the inherent hazard potential of ammunition and explosives, in no other element of the overall DoD safety program is it more important that these policies be effectively implemented. For that reason, as well as the fact that this is an explosives safety seminar, I will focus on that aspect of the DoD Safety Program.

In consonance with the Administration's and Secretary Weinberger's policies, we in office, Secretary of Defense are working to ease excessive regulatory burdens wherever possible; to move progressively from micro-management toward more general oversight and evaluation of bottom-line results, and to use our influence to support safety management initiatives of the DoD components. We are acutely aware that being a responsibility of management, safety policy is subject to the same threats to good management as any other function, and safety is perhaps more critical. If other management techniques are grossly inefficient, time and money are lost and perhaps an enterprise fails. If our management of safety is bad, lives are lost. Knowing this, there is a natural tendency to overmanage--to write standing operating procedures rather than policies, and specification-type rather than performance-type safety standards. There is that fear that if we at the top do not think of every possibility and provide for it, an accident may happen and a life may be lost. Noble as the intent may be, we can't

think of them all and, by attempting to do so, we stifle initiatives at lower levels that are likely to be more effective. Many of these initiatives are the direct result of knowledge gained and ideas spawned by these biennial explosives safety seminars.

We fully realize that our safety program has to be a balance between one that provides for total protection of life and property and one that permits operators to conduct activities in a "laissez-faire" manner without considerations for preservation of life and property. A proper approach to safety is a reasonable application of safety principles that enhance, not inhibit, operations. The guarded interests of both safety and operations can be served by establishing an awareness of safety principles in operators that results in preservation of assets and creates a safe working environment that increases worker efficiency. To accomplish this in the area of explosives safety, DoD has published ammunition and explosives safety standards that, when applied with general safety principles, will provide for containment of the accident and reasonable protection for life and property.

The objective of our explosives safety program is to provide maximum protection against injury to personnel and damage to property consistent with operational requirements. Toward this end our goals are;

- ✓ To eliminate unnecessary risks to life and property from the harmful effects of accidents;
- ✓ To make safety an essential consideration in all facilities and operations planning;
- ✓ To insure that safety is a total life-cycle consideration for ammunition and explosives; and
- ✓ To eliminate deviations from ammunition and explosives safety standards that are not essential or are not justified on the basis that the increased risks are insignificant in comparison with the cost of achieving compliance.

We are making progress. Improvements in explosives safety have occurred through reductions of exposure of personnel and property both inside and outside installation boundaries. The greatest emphasis has been in reducing or eliminating exposure outside installations where we have no control over development and encroachment is likely to occur. Encroachment on DoD explosives facilities has been a problem and many installations cannot make maximum use of existing explosives storage structures because to do so would endanger life and improved property located on non-Federal land. A serious explosives accident with effects off-base may result in not only loss of life and property, but also credibility for DoD. Without elaborating on this, I am sure you can see the many damaging ramifications of such an accident.

Other recent achievements of note are:

- . Gains have been made in reducing exposure inside installation boundaries through new construction projects and restriction of storage and operations.
- . DoD ammunition and explosives safety standards have been extended to cover chemical agents and ammunition, and worker protection.
- . Knowledge about model testing has been gained through comparison of model scale tests with results of full scale tests of like structures in the distant runner series of tests at White Sands last fall.
- . Criteria have been developed for testing and hazard classifying insensitive high explosives substances and articles containing insensitive high explosives.
- . Increased efforts by the services to insure that all construction projects involving ammunition and explosives receive complete safety review and that new facilities are sited to provide long term protection against encroachment.

Despite these improvements in explosives safety, there is still much to be accomplished. The DoD explosives safety program must be a dynamic flexible program that can adapt to changes in explosives technology, weapons technology, and explosives weapon storage and employment requirements. To this end, the DoD will be undertaking a critical review of explosives safety standards to ensure they are "state-of-the-art" standards. Expansion of these standards may be in order to ensure all significant hazards have been properly addressed. Consequently, we will review the standards for completeness. Our explosives safety surveys will continue to seek out problems and identify practical solutions. We look to the DoD components to accept the challenge of our goals and will seek evidence of positive action in our safety program oversight reviews and evaluations of bottom-line results. With your help we can succeed. We ask no more--we can accept no less.

I've looked at your program and I find it quite impressive, both in terms of subjects covered and the expertise of those participating. I am certain that no matter what your specific explosives safety interests are, the next three days will afford you the opportunity to explore them profitably--I wish you every possible success.

Thank you.

ADDRESS

by

AIR COMMODORE FRANK ROBINSON

Ministry of Defence

Chairman Defence Explosives Safety Authority
Chairman Explosives Storage and Transport Committee
Vice-President Ordnance Board
London, England

at

Twentieth Department of Defense Explosives Safety Seminar
Norfolk, Virginia

August 24, 1982

THE EFFECTS OF THE HEALTH AND SAFETY AT WORK ACT, 1974, ON
MILITARY EXPLOSIVES SAFETY MANAGEMENT IN THE UNITED KINGDOM

GOOD MORNING, LADIES AND GENTLEMEN.

I AM INDEED HONOURED TO ADDRESS THIS DISTINGUISHED GATHERING OF EXPLOSIVES SAFETY EXPERTS HERE TODAY. MY THANKS THEREFORE TO THE DEPARTMENT OF DEFENSE EXPLOSIVES SAFETY BOARD AND TO COLONEL ALTON POWELL FOR INVITING ME TO SPEAK.

MY SUBJECT TODAY IS THE EFFECT OF THE HEALTH AND SAFETY AT WORK ACT, 1974 ON MILITARY EXPLOSIVES SAFETY MANAGEMENT IN THE UNITED KINGDOM, AND, IN PARTICULAR THE FORMATION OF THE DEFENCE EXPLOSIVES SAFETY AUTHORITY (DESA). THE HSW ACT FOR THE VERY FIRST TIME, GRANTED THE OVERALL RESPONSIBILITY FOR MONITORING EXPLOSIVES SAFETY IN THE UK - INCLUDING SPONSORSHIP OF THE NECESSARY LEGISLATION - TO AN INDEPENDENT BODY CALLED THE HEALTH AND SAFETY EXECUTIVE (HSE). SO THE MINISTRY OF DEFENCE, BY THIS ONE ACT, LOST ITS SOLE CONTROL OVER MILITARY EXPLOSIVES.

HOW DID THE 1974 ACT COME ABOUT? WELL IN 1972, THE GOVERNMENT OF THE DAY FORMED THE 'ROBEN'S COMMITTEE' TO SEE HOW THEY COULD BRING TOGETHER THE MASSIVE REGULATIONS AND ACTS THEN EXISTING - SUCH AS THE EXPLOSIVES ACT, THE FACTORIES ACT, MINES AND QUARRIES ACT, OFFICES, SHOPS AND RAILWAY PREMISES ACT, BUILDING REGULATIONS, AND SO ON - WHICH ALL IMPOSE HEALTH AND SAFETY DUTIES ON PEOPLE AT WORK, AND SWEEP THEM UP UNDER THE UMBRELLA OF ONE ALL EMBRACING ACT. THE OUTCOME OF THIS STUDY WAS THE INTRODUCTION OF THE 1974 HSW ACT.

THE OBJECTIVES OF THE ACT ARE TO:

- a. SECURE THE HEALTH, SAFETY AND WELFARE OF PEOPLE AT WORK.
- b. PROTECT THE GENERAL PUBLIC AGAINST RISKS TO THEIR HEALTH AND SAFETY ARISING OUT OF WORK ACTIVITIES.
- c. CONTROL THE KEEPING AND USE OF EXPLOSIVES OR HIGHLY FLAMMABLE OR OTHERWISE DANGEROUS SUBSTANCES AND GENERALLY PREVENT PEOPLE FROM UNLAWFULLY HAVING AND USING SUCH SUBSTANCES.

d. CONTROL THE RELEASE INTO THE ATMOSPHERE OF NOXIOUS OR OFFENSIVE SUBSTANCES.

THE ACT ESTABLISHED TWO NEW BODIES UNDER THE SECRETARY OF STATE FOR EMPLOYMENT; THE HEALTH AND SAFETY COMMISSION (HSC) AND THE HEALTH AND SAFETY EXECUTIVE (HSE), IN ORDER TO PROMOTE THE OBJECTIVES OF THE ACT AND TO ENSURE ITS PROVISIONS WERE IMPLEMENTED.

THE HEALTH AND SAFETY COMMISSION CONSISTS OF A FULL-TIME CHAIRMAN AND BETWEEN SIX AND NINE PART-TIME MEMBERS, ALL OF WHOM ARE APPOINTED BY THE SECRETARY OF STATE FOR EMPLOYMENT (S OF S). THE S OF S IS REQUIRED TO CONSULT EMPLOYERS' ORGANISATIONS ABOUT THREE MEMBERS, EMPLOYEES' ORGANISATIONS I.E. THE TRADE UNIONS, ABOUT THREE OTHER MEMBERS AND LOCAL AUTHORITIES AND OTHER APPROPRIATE ORGANISATIONS, INCLUDING PROFESSIONAL BODIES, ABOUT THE REST.

THE COMMISSION'S DUTIES INCLUDE PROMOTING THE OBJECTIVES OF THE ACT, CARRYING OUT AND ENCOURAGING RESEARCH AND TRAINING INTO SAFETY, PROVIDING AN INFORMATION AND ADVISORY SERVICE AND ADVISING THE GOVERNMENT OF ANY REGULATIONS UNDER THE ACT.

THE HEALTH AND SAFETY EXECUTIVE CONSISTS OF THREE FULL-TIME MEMBERS, WHO ARE APPOINTED BY THE HSC PLUS A SUPPORTING STAFF.

THE EXECUTIVE'S DUTIES INCLUDE MAKING ARRANGEMENTS FOR ENFORCEMENT OF THE LEGISLATION, INITIATING NEW LEGISLATION AND CARRYING OUT OTHER TASKS GIVEN TO IT BY THE COMMISSION. IN PRACTICE, HSE CARRIES OUT THE DAY-TO-DAY WORK NECESSARY TO ENABLE THE COMMISSION TO PERFORM ITS FUNCTIONS. TO DO THIS, IT HAS SIX INSPECTORATES COVERING AGRICULTURE, ALKALINE AND CLEAN AIR, EXPLOSIVES, FACTORIES, MINES AND QUARRIES AND NUCLEAR INSTALLATIONS. THERE ARE ALSO POLICY BRANCHES, A RESEARCH DIVISION PLUS OTHER STAFF TO ENABLE IT TO CARRY OUT THE COMMISSION'S FUNCTIONS.

TODAY WE SHALL CONCERN OURSELVES WITH THE INSPECTORATE OF EXPLOSIVES, AND THE CHANGES WHICH HAVE OCCURRED IN THE MOD DEFENCE STRUCTURE IN ORDER TO CATER FOR THE IMPLICATIONS OF THE 1974 HSW ACT.

AT THE RISK OF BORING SOME OF YOU BUT FOR THE BENEFIT OF THOSE NOT CONVERSANT WITH THE UK MILITARY EXPLOSIVES SAFETY MANAGEMENT SYSTEM, PLEASE ALLOW ME TO DWELL A MOMENT ON THE HISTORY OF THE ORGANISATION.

WE START WAY BACK IN OCTOBER 1874, WHEN A TRAIN OF SIX LIGHT BARGES WAS PASSING ALONG THE REGENTS PARK CANAL IN LONDON. LET ME NOW QUOTE FROM THE ILLUSTRATED LONDON NEWS DATED 10 OCTOBER 1874.

"AMONG THESE BARGES WAS THE UNFORTUNATE TILBURY WHOSE CARGO CONTAINED SUGAR, NUTS, STRAWBOARDS, COFFEE, TWO OR THREE BARRELS OF PETROLEUM AND ABOUT FIVE TONS OF GUNPOWDER.

THE POWDER WAS EN ROUTE TO NOTTINGHAM FROM THE WALTHAM ABBEY MILLS, ESSEX. THE TILBURY WAS DIRECTLY UNDER THE MACCLESFIELD ROAD BRIDGE WHEN, BY SOME MEANS UNEXPLAINED, THE POWDER CAUGHT FIRE AND THE WHOLE WAS BLOWN UP. THE BRIDGE WAS ENTIRELY DESTROYED: SEVERAL OF THE NEIGHBOURING HOUSES WERE HALF-RUINED, THEIR ROOFS AND WALLS BEING GREATLY INJURED, AND IN HUNDREDS OF OTHER HOUSES, A MILE EAST OR WEST OF THE PLACE, THE WINDOWS WERE BROKEN, AND MANY FRAGILE ARTICLES OF FURNITURE.'

LET ME ADD FOR THOSE INTERESTED IN TAKING TERRAIN INTO ACCOUNT WHEN CALCULATING SAFETY DISTANCES THAT AS THE ILLUSTRATED LONDON NEWS GOES ON TO SAY:

"IT MUST, HOWEVER, BE CONFESSED THAT THE EFFECT OF SUCH AN EXPLOSION MIGHT HAVE BEEN MUCH WORSE, IF IT HAD TAKEN PLACE IN A TUNNEL AMIDST THE CROWDED BUILDINGS OF FINSBURY OR PENTONVILLE, OR AT ANY POINT WHERE, AS IN KENTISH TOWN, THE SURFACE OF THE WATER IS NEAR THE LEVEL OF THE ADJOINING STREETS. THE FRAGMENTS OF THE BARGE AND CARGO WOULD, IN THE LATTER CASE, HAVE BEEN HURLED RIGHT AND LEFT, A HUNDRED YARDS OR MORE WITH TERRIBLE FORCE AND EFFECT; INSTEAD OF WHICH THEY WERE MOSTLY CONFINED TO THE DEEP CUTTING OF THE CANAL."

THE RESULTANT PUBLIC OUTCRY LED TO THE PARLIAMENT OF THE DAY PASSING THE EXPLOSIVES ACT, 1875. HOWEVER IT WAS SAID AT THE TIME BY THE EDITOR OF THE ILLUSTRATED LONDON NEWS, THAT:

"SUCH CASUALTIES AS THAT OF FRIDAY MORNING NEVER HAPPEN IN CONNECTION WITH EITHER THE ARMY OR THE NAVY, BECAUSE THE STORAGE AND CONVEYANCE OF GUNPOWDER FOR AND BY EITHER ARE ALWAYS CONDUCTED UNDER THE STRICTEST REGULATIONS."

THIS DOUBTLESS LED TO SECTION 97 OF THE ACT, WHEREBY THE CROWN WAS EXEMPTED, AND THE SECRETARY OF STATE FOR DEFENCE WAS EMPOWERED TO MAKE REGULATIONS FOR THE SAFE CONDUCT OF MILITARY EXPLOSIVES AFFAIRS. THIS HAS REMAINED SO, RIGHT UP TO THE PASSING OF THE 1974 HSW ACT, WHEN, DESPITE PLEAS FOR THE CONTINUANCE OF THE CROWN EXEMPTION, NO SUCH EXEMPTION WAS GRANTED, AND, AS I SAID EARLIER, MOD LOST ITS ABSOLUTE CONTROL OVER ITS OWN EXPLOSIVES AFFAIRS.

AFTER WORLD WAR I, THE CONTINUING EXPANSION OF EXPLOSIVES ACTIVITIES IN THE UK, RESULTING FROM THE FORMATION OF THE RAF, THE CONTINUANCE OF A LARGE NAVY AND ARMY PLUS AN INCREASING RESEARCH, DEVELOPMENT AND MANUFACTURING CAPABILITY, LED TO THE DECISION THAT SOME CENTRALISED BODY WAS NEEDED TO INFLUENCE MANAGEMENT OF THE

MILITARY EXPLOSIVES SAFETY FIELD. SO, IN 1925, THE EXPLOSIVES STORAGE AND TRANSPORT COMMITTEE (ESTC) WAS FORMED. EVER SINCE, THE ESTC HAS BEEN THE MEANS THROUGH WHICH THE S OF S FOR DEFENCE HAS DISCHARGED THE RESPONSIBILITIES DELEGATED TO HIM BY THE 1875 EXPLOSIVES ACT.

TO FULFIL ITS ROLE, THE BASIC TASKS OF THE ESTC, WHICH ARE INTER-RELATED AND FOLLOW IN A LOGICAL PATTERN, ARE AS FOLLOWS. FIRSTLY, HAZARD CLASSIFICATION OF EVERY MUNITION BY TEST, OR ANALOGY TO PREVIOUS LIKE MUNITIONS - THE PRIME TASK, FOR, FROM THIS ALL OUR OTHER WORK FOLLOWS - AND, LIKE OTHER NATIONS, WE NOW FOLLOW THE UN CLASSIFICATIONS AS PUBLISHED IN 1970. SECONDLY, THE COMMITTEE FORMULATES AND ISSUES THE PRESCRIPTIONS FOR EXPLOSIVES QUANTITY DISTANCES. THIRDLY, THERE IS THE FORMULATION AND ISSUING OF PRESCRIPTIONS COVERING THE CONSTRUCTION OF EXPLOSIVES STORAGE BUILDINGS, TRAVERSES OR BARRICADES. FOURTHLY, IS THE RAISING OF STATUTORY INSTRUMENTS (SIs) REGULATING THE MOVEMENT OF MUNITIONS; THERE ARE, AT PRESENT, THREE SUCH SIs, COVERING PORTS AND HARBOURS, ROADS AND RAIL.

TO COVER THESE TASKS THE ESTC HAS A NUMBER OF SUB-COMMITTEES, EACH COMPRISING EXPERTS IN A PARTICULAR AREA. THESE COMMITTEES ARE ADDED TO OR DISBANDED TO SUIT PREVAILING CIRCUMSTANCES.

THE PLACE OF THE ESTC IN THE UK ORGANISATION FOR EXPLOSIVES SAFETY IS SHOWN ON THIS SLIDE. FOR MILITARY EXPLOSIVES THE CLOSE ASSOCIATION BETWEEN THE ESTC AND THE ORDNANCE BOARD (OB) IS DEPICTED (IN FACT THE CHAIRMAN OF THE ESTC IS ALSO A VICE-PRESIDENT OF THE OB).

THE IMPORTANT FACT TO BEAR IN MIND IS THAT THE ESTC, IS AN INDEPENDENT BODY. IT OWES ITS ALLEGIANCE TO THE MINISTRY OF DEFENCE (MOD) BUT NOT TO THE INDIVIDUAL SERVICES. IT ALSO GATHERS ITS INFORMATION AND ADVICE FROM PERSONS BOTH WITHIN AND OUTSIDE THE MOD AND INCLUDES MEMBERS OF THE HSE ON ITS MAIN AND SOME OF ITS SUB-COMMITTEES.

THE NUB OF THE RELATIONSHIP WITH MOD STAFFS IS THAT WHILE THE ESTC PREPARES ADVICE AND THE MOD STAFFS INVARIABLY TAKE NOTE OF IT, THERE IS NO LEGAL OBLIGATION FOR STAFFS TO OBSERVE OR ENFORCE ESTC PRESCRIPTIONS. THE INDIVIDUAL SERVICE AND PE ELEMENTS OF MOD WRITE THEIR OWN EXPLOSIVES REGULATIONS BASED ON ESTC PRESCRIPTIONS AND ARE SEPARATELY RESPONSIBLE FOR ENFORCEMENT.

HAVING LOOKED AT THE PAST, NOW LET US SEE WHAT CHANGES ARE NECESSARY IN ORDER TO MEET THE REQUIREMENTS OF THE 1974 HSW ACT. HERE IT IS IMPORTANT TO BEAR IN MIND THAT THE HSE HAVE THE POWER, AND THE INTENTION, TO EMBARK ON A COMPLETE MODERNISATION OF EXPLOSIVES LAW, INCLUDING THE REPLACEMENT OF THE EXPLOSIVES ACT 1875. FURTHER, IT IS THEY WHO ARE NOW EMPOWERED WITH ISSUING THE SIS COVERING THE STORAGE AND TRANSPORTATION OF EXPLOSIVES - BOTH FOR CIVIL AND MILITARY USES. FINALLY, THEY ARE REQUIRED TO OVERSEE THE ENFORCEMENT OF MOD'S EXPLOSIVES REGULATIONS THROUGHOUT THE SERVICE DEPOTS, STORAGE AREAS, RESEARCH ESTABLISHMENTS AND THE ROYAL ORDNANCE FACTORIES (WHICH STILL MAINTAIN THE MAJOR MILITARY EXPLOSIVES MANUFACTURING AND FILLING FACILITIES IN THE UK.) SO, UNLIKE THE ESTC, WHICH IS AN INDEPENDENT ADVISORY BODY WITHOUT ANY EXECUTIVE AUTHORITY, THE HSE IS AN ENFORCING AUTHORITY.

EVER SINCE THE PASSING OF THE 1974 HSW ACT, DISCUSSIONS AND NEGOTIATIONS HAVE FOLLOWED CONCERNING THE BEST WAY THAT HSE SHOULD TAKE ON ITS NEW ROLE IN THE MOD EXPLOSIVES AREAS. THE OUTCOME OF THESE NEGOTIATIONS WAS THE FORMATION ON 1 JANUARY, 1982, OF THE DEFENCE EXPLOSIVES SAFETY AUTHORITY (DESA). ITS AIM IS THE PROVISION OF MACHINERY TO ASSIST WITH THE MONITORING OF MOD EXPLOSIVES AREAS TO ENSURE COMPLIANCE WITH THE HSW ACT. IT IS A FORUM IN WHICH CONFLICTS BETWEEN DEFENCE IMPERATIVES AND THE OBLIGATIONS OF THE HSW ACT AND OTHER

LEGISLATION WILL BE RECONCILED. IT MUST OVERSEE THE PROVISIONS FOR HEALTH AND SAFETY IN MOD EXPLOSIVES AREAS, ARRANGE FOR AUDITING OF THESE PROVISIONS AND GIVE GUIDANCE ON ENFORCEMENT POLICY WHERE THIS IS NECESSARY.

DESA IS MADE UP OF FOUR DISTINCT PARTS EACH HAVING A DEFINITIVE ROLE TO PLAY:

- a. A MANAGEMENT COMMITTEE COMPRISING THE DIRECTOR GENERAL DG/HSE AND THE PERMANENT UNDER SECRETARY (2nd PUS)/MOD.
- b. A CENTRAL COMMITTEE WHICH REPORTS TO THE MANAGEMENT COMMITTEE MADE UP OF EXPERTS IN EXPLOSIVES POLICY AND TECHNOLOGY FROM MOD AND HSE.
- c. THE INTERNAL INSPECTORATE ORGANISATION WHICH ALREADY EXISTS WITHIN MOD UNDER THE COMMAND OF DEPARTMENTAL CHIEF INSPECTORS AND WHICH RESPONDS TO THE CENTRAL COMMITTEE THROUGH THEM.
- d. AN AUDIT TEAM WHICH IS UNDER THE COMMAND OF HM CHIEF INSPECTOR OF EXPLOSIVES HSE AND WHICH RESPONDS TO THE CENTRAL COMMITTEE THROUGH HIM.

THE MANAGEMENT COMMITTEE WILL PROVIDE A GENERAL OVERSIGHT OF THE WORK OF DESA. IN ADDITION, IT WILL TRY TO RESOLVE ANY MAJOR DISAGREEMENTS WHICH MIGHT ARISE BETWEEN MOD AND HSE IN THE CONDUCT OF HSW AFFAIRS.

THE CENTRAL COMMITTEE IS CHAIRED BY THE VICE-PRESIDENT OF THE ORDNANCE BOARD WHO IS ALSO CHAIRMAN OF THE ESTC. THE VICE-CHAIRMAN IS THE HEAD OF EXPLOSIVES POLICY AT THE HSE. THESE TWO POSTS ROTATE ANNUALLY. MEMBERSHIP IS DRAWN FROM THE CHIEF INSPECTORS OF EXPLOSIVES OF THE 3 SERVICES AND THE PROCUREMENT EXECUTIVE, PLUS HM CHIEF INSPECTOR OF EXPLOSIVES HSE (WHO IS THE DESA CHIEF AUDIT INSPECTOR),

TOGETHER WITH REPRESENTATIVES FROM INTERESTED MOD DEPARTMENTS AND THE HSE.

ITS RESPONSIBILITIES COVER:

- a. INTRODUCING PROCEDURES THROUGH THE MEDIUM OF PRESCRIPTIONS ALLOWING DESA TO PERFORM ITS FUNCTIONS UNDER THE AGREEMENT.
- b. AGREEING STANDARDS FOR COMPLIANCE WITH THE HSW ACT REQUIREMENTS IN MOD EXPLOSIVES AREAS.
- c. REVIEWING THE PROCEDURES FOR CONCESSIONS AGAINST THE AGREED SAFETY STANDARDS.
- d. AGREEING DESA MONITORING PROGRAMMES AND RECEIVING REPORTS FROM THE DEPARTMENTAL CHIEF INSPECTORS AND THE CHIEF INSPECTOR OF AUDIT.
- e. RECEIVING ACCIDENT AND DANGEROUS OCCURRENCE REPORTS AND THE RESULTS OF ENQUIRIES INTO EXPLOSIVE INCIDENTS.
- f. RESOLVING DIFFICULTIES ARISING OUT OF CROWN NOTICE ACTION.
- g. REVIEWING NEW HSE LEGISLATION CONCERNING MOD CONVENTIONAL EXPLOSIVES AND THE IMPLICATIONS OF SUCH LEGISLATION ON DESA STANDARDS AND DEFENCE IMPERATIVES.
- h. LIAISON WITH THE ESTC.
- j. PRODUCING AN ANNUAL REPORT FOR THE MANAGEMENT COMMITTEE.

THE SERVICE AND PE EXPLOSIVES INSPECTORATES ARE RESPONSIBLE FOR THE DAY-TO-DAY COMPLIANCE OF THE HSW ACT IN ACCORDANCE WITH THE STANDARDS AGREED BY THE CENTRAL COMMITTEE.

THE AUDIT TEAM IS RESPONSIBLE FOR MONITORING COMPLIANCE WITH THE REQUIREMENT OF THE HSW ACT IN MOD EXPLOSIVES AREAS. TO DO THIS IT NEEDS TO:

- a. MONITOR ALL INTERNAL INSPECTION REPORTS AND ATTEND SELECTED MOD INTERNAL INSPECTIONS BY AGREEMENT.

b. CONDUCT SAFETY AUDITS IN MOD CONVENTIONAL EXPLOSIVES AREAS, USING AGREED STANDARDS, WITH A REPRESENTATIVE OF THE INTERNAL INSPECTORATE IN ATTENDANCE.

c. EXAMINE EXPLOSIVES LICENSING ARRANGEMENTS.

d. CONDUCT OR PARTICIPATE IN ACCIDENT/INCIDENT INVESTIGATIONS, AS CONSIDERED APPROPRIATE BY THE CHIEF INSPECTOR OF AUDIT.

e. INVESTIGATE COMPLAINTS ABOUT DEFICIENCIES IN HEALTH AND SAFETY.

f. WHEN NO OTHER ACTION IS POSSIBLE, TAKE ENFORCING ACTION, BY SERVING CROWN PROHIBITION, OR IMPROVEMENT NOTICES, AGAINST MOD ESTABLISHMENTS AND CONDUCTING PROSECUTION ACTION, IF NECESSARY. AS YOU CAN WELL IMAGINE, THIS LATTER POINT HAS BEEN AN AREA OF GREAT CONCERN TO THE MOD FOR IT HAS VERY WIDE CONNOTATIONS AND IMPLICATIONS ON THE WAY WE IN THE SERVICES DO OUR JOB. NEVERTHELESS, IT HAS BEEN AGREED THAT THE HSW ACT WILL NOT TAKE PRECEDENCE OVER THE SERVICE DISCIPLINE ACTS AND IT HAS TO BE RECOGNISED THAT THE SAFETY OF THE REALM IS TO BE CONSIDERED THE PARAMOUNT FACTOR. FURTHERMORE, IT HAS BEEN AGREED THAT THE HSE HAS NO INTENTION OF PROSECUTING AN INDIVIDUAL CIVIL SERVANT IN SUBSTITUTION FOR HIS DEPARTMENT. THE HSE WOULD ONLY PROSECUTE AN INDIVIDUAL CIVIL SERVANT WHERE THERE IS WILFUL OR RECKLESS DISREGARD OF HEALTH OR SAFETY REQUIREMENTS. WITH SERVICEMEN THE SERVICES WOULD USE THEIR OWN POWERS TO DEAL WITH DISCIPLINARY CHARGES AND ONLY IN VERY EXCEPTIONAL CIRCUMSTANCES AND WITH THE APPROVAL OF THE MANAGEMENT COMMITTEE WOULD CIVIL COURTS BE INVOLVED.

FINALLY, THE AREA THAT WILL BE COVERED BY DESA WITH RESPECT TO BOTH STANDARDS AND ENFORCEMENT, WILL BE IN THOSE NON CONVENTIONAL EXPLOSIVES AREAS COVERING MANUFACTURE, PRODUCTION, STORAGE, CONVEYANCE, RESEARCH, DEVELOPMENT, PROOF AND TRIALS. IT WILL NOT BE RESPONSIBLE FOR:

- a. EXPLOSIVES HELD READY FOR OPERATIONAL USE, IN HM SHIPS AND RFAs, IN ARMY OPERATIONAL UNITS OR IN RAF AIRCRAFT OR STOCKS DISPERSED TO SQUADRON OPERATING AREAS IN A READY-FOR-USE STATE.
- b. AMMUNITION AND EXPLOSIVES BEING USED FOR OPERATIONAL TRAINING PURPOSES BY OPERATIONAL UNITS OR TRAINING ESTABLISHMENTS.
- c. STATIC ESTABLISHMENTS DURING PERIODS WHEN THEY ARE SUPPORTING OPERATIONS OR DURING MOBILISATION EXERCISES.

NOTE: HSE's RESPONSIBILITIES CONCERNING VISITING FORCES ARE AT PRESENT UNDER INVESTIGATION BUT IT IS ENVISAGED THAT DESA WILL TREAT THEM IN THE SAME WAY AS THEY DO THE UK SERVICES.

SO IN SUMMING UP, WHAT HAS BEEN THE EFFECT OF THE HSW ACT 1974, ON THE UNITED KINGDOM MILITARY EXPLOSIVES SAFETY MANAGEMENT AREA:

- a. THE MOST IMPORTANT, ALTHOUGH IT WILL BE A LONG TIME BEFORE IT TAKES EFFECT, IS THAT AN OUTSIDE BODY, THE HSE, IS NOW RESPONSIBLE FOR RAISING THE LEGISLATION, THAT IS THE SIAs, CONCERNING THE MANUFACTURE, STORAGE AND TRANSPORTATION BY ROAD, SEA AND AIR OF MILITARY EXPLOSIVES WITHIN THE UK. HOWEVER, IT IS STILL ENVISAGED THAT THE ESTC WILL PLAY A MAJOR PART IN THE INTRODUCTION OF SUCH LEGISLATION.
- b. THE INDIVIDUAL SERVICE AND PE EXPLOSIVES INSPECTORATES WILL NO LONGER BE SELF ACCOUNTING. THE DESA AUDIT INSPECTORS WILL IN FUTURE MONITOR THEIR WORK.

WHAT HAS NOT CHANGED, AND WILL NOT CHANGE, IS THAT THE OPERATIONAL SIDE OF THE SERVICES WILL REMAIN SOLELY UNDER THE CONTROL OF THE INDIVIDUAL SERVICES AND WILL, IN NO WAY BE INFLUENCED BY THE HSC OR THE HSE. FURTHERMORE, DURING PERIODS OF TENSION, PROVISION HAS BEEN MADE FOR THE SERVICES TO HAVE COMPLETE FREEDOM OF ACTION.

BEFORE CONCLUDING, YOU MAY WELL ASK WHAT IS THE FUTURE OF THE ESTC. WELL, I FORECAST THAT ONCE DESA HAS RESPONSIBILITIES FOR BOTH NUCLEAR AND CONVENTIONAL WEAPONS, THE ESTC MIGHT WELL BE SUBSUMED INTO BEING PART OF THE DESA FRAMEWORK. FOR, WITH THE HSE BEING RESPONSIBLE FOR ALL UK EXPLOSIVES' LEGISLATION, PLUS ITS AUDITING FUNCTION, IT IS ONLY LOGICAL THAT GIVEN TIME, THE DEMAND WILL COME FOR THE STANDARDISATION OF THE MOD EXPLOSIVES REGULATIONS WHICH CURRENTLY ARE IN 4 VERSIONS (ALL DIFFERENT) FOR THE RN, ARMY, RAF AND PE. ONCE THIS STANDARDISATION IS ACHIEVED THE NEXT STEP WILL BE THE LEGISLATION OF ESTC PRESCRIPTIONS - WHICH ARE CURRENTLY ADVISORY ONLY. THE WAY TO DO THIS WILL BE UNDER THE MANTLE OF DESA. HOWEVER, THIS IS LOOKING A LONG WAY AHEAD.

IN CONCLUSION, MAY I SAY THAT IT IS EARLY DAYS YET, FOR DESA WAS ONLY FORMED IN JANUARY OF THIS YEAR, BUT I REMAIN CONFIDENT THAT SAFETY IN THE UK MILITARY EXPLOSIVES AREA CAN ONLY BE ENHANCED BY THESE NEW MEASURES, WHILE, AT THE SAME TIME, THE OPERATIONAL ROLE OF THE SERVICES TOGETHER WITH DEFENCE IMPERATIVES, WILL IN NO WAY BE JEOPARDISED. INDEED, IT IS MY RESPONSIBILITY, AS THE CHAIRMAN, TO ENSURE THAT THIS REMAINS SO.

THANK YOU.

"BRITISH CROWN COPYRIGHT. Not to be reproduced without permission from the Controller, Her Britannic Majesty's Stationery Office."

AD P000427

DETONABILITY OF AGENT

BZ - PYROMIX

by

B. D. Trott
Battelle Columbus Laboratories

and

James Stuart
Pine Bluff Arsenal

INTRODUCTION AND SUMMARY

The U.S. Army Toxic and Hazardous Materials Agency is preparing to demilitarize the U.S. inventory of munitions containing the incapacitating agent BZ. As employed in the munitions, BZ is blended with an energetic pyrotechnic mixture. The mixture is 50% BZ, 23% KClO_3 , 9% S, and 18% NaHCO_3 . In normal functioning, this mixture is ignited along central core holes in the munitions and reacts over a few tens of seconds to produce an aerosol cloud of BZ. However, upper limit theoretical calculations suggested that this mixture could potentially be detonable, but it was not known if actual detonation could occur. To facilitate selection from among five candidate demilitarization concepts⁽¹⁾ it was desirable that the detonability of the munitions be established. To this end, a series of experimental tests as described in this paper was conducted. These tests gave conclusive evidence of non-detonability.

The potentially most detonable item in the BZ inventory was selected for detonability tests. This is the bomblet with the largest continuous diameter, 72 mm of BZ-pyrotechnic mix, the M138. This bomblet also has the thickest steel walls, 3 mm, for radial confinement. The M138 is comprised of 4 individual M7 cannisters loaded inside a steel tube casing. An individual M138 bomblet is one of 57 packed in each M43 cluster munition. As such, adjacent M138s in the close-packed array could provide a full-length additional 3-mm steel radial confinement along 6 line contacts with the M138. Therefore, the M138, fitted inside an additional close-fitting steel tube with 2.3 mm wall thickness (nearest to 3 mm thickness available), was selected as the configuration for detonability tests. Proof of non-detonability of this item would constitute proof of non-detonability of the entire BZ-containing munition inventory.

The test configuration included a full munition diameter donor explosive charge of composition C-4 in firm contact with one end of the munition. The primary indication of detonability was from dynamic instrumentation, epoxy potted into the entire length of the core hole, which showed the steady decay of the input shock velocity to sonic values as the shock progressed down the munition. Examination of the munition remains provided a secondary indication.

The tests were conducted in a sealed blast containment chamber inside an igloo at Pine Bluff Arsenal. A pilot plant incinerator, previously qualified for destruction of BZ, was used to dispose of the BZ released during the tests.

Of 17 tests attempted, 14 tests provided detonability data. In two tests the munitions self-ignited during heating to the original target preheat temperature of 105 C. This self-ignition resulted in lowering the preheat temperature to 80 C on remaining tests. Data from the third test were lost due to an equipment malfunction. To provide the broadest possible sampling base, the tested munitions were drawn from all of the eight manufacturing lots from which M138s had been downloaded from the original M43 cluster configuration. These lots were judged to be reasonably representative of the total inventory on the basis of available lot characterization data. Seven tests were conducted at ambient temperature and seven were conducted after preheating the munitions to 80 C. Four of the ambient temperature tests were conducted on munitions "inerted" by immersion in a water-plus 0.01% Avirol-113 wetting agent. The BZ-pyrotechnic mixture was ignited by the shock wave in most tests, although one or more of the 0.1-m M7 canisters remained intact in half of the tests.

There was no significant difference in the observed shock decay between inerted, ambient live, and preheated live munitions. The average shock wave travel, above the apparent sonic velocity of 2.0 mm/microsec, was 115.1% 8.5 mm through the munitions for all tests. A shock travel of 130 mm above 2.0 mm/microsec was observed in a similiar detonability test on a mockup which contained no reactive ingredients. These results, together with the recovery of intact portions of the munitions in many tests, are conclusive evidence for non-detonability of the munitions.

The body of this paper is organized into four major sections following this introduction and summary. Section 2 describes the technical approach, the background for selection of the detonability test configuration, the basis for selection of test conditions, and the basis for interpretation of the results obtained. Section 3 describes the specialized experimental apparatus used for these tests. Section 4 presents the experimental procedures used and the results obtained. Section 5 lists conclusions from this work.

2. TECHNICAL APPROACH

2.1 Background

The process of detonation can be described as a supersonic compressive shock wave driven through a reactive material by the energy released in the Chapman-Jouguet (C-J) reaction zone immediately behind the shock wave. The adiabatic heating associated with the shock compression of the material triggers the chemical reaction(s) responsible for the energy release. Immediately behind the shock wave, the particle or mass velocity is in the same direction as the shock wave velocity. The mass velocity, pressure, and internal energy decay behind the shock wave front. The energy released behind the shock wave front can contribute to driving the shock front only in the zone in which the energy transfer speed (the sum of the local sonic velocity plus the mass velocity) is equal to or greater than the shock velocity. As the mass velocity, pressure, and temperature decay behind the shock front, a limiting boundary is reached where the energy transfer speed drops below the shock velocity. The shock wave and this boundary define the C-J reaction zone. Chemical reaction may continue behind this boundary and can contribute to the total energy released during explosion but cannot influence the detonation (or shock wave) velocity. In a uniform charge of constant cross sectional area and confinement along its length, a steady detonation velocity is normally achieved in which the energy released in the reaction zone is equal to the energy required to drive the shock wave (the energy required to shock compress the unreacted material).

However, at the lateral surfaces of the charge, a portion of energy released in the reaction zone is also expended in the production of lateral mass velocity components and resultant lateral expansion of the charge. This energy is lost for the purpose of driving the detonation front, but must be included in the energy balance which determines the detonation velocity. Because the ratio of lateral surface area to reaction zone volume increases as the charge diameter decreases, the fraction of energy lost laterally increases with decreasing charge diameter. This effect can lead to a decreasing detonation velocity with charge diameter because the energy required to drive the shock front decreases with shock velocity. With decreasing shock velocity, the shock pressure and induced temperature rise also decrease. These decreases lead, in turn, to a generally

exponential rate of decrease in chemical reaction rate. The detonation velocity does not decrease below a certain level which depends on the detailed characteristics of the reactive material. Instead, a minimum diameter (the critical diameter) is reached below which a sustained detonation is not possible.

Because the critical diameter arises due to lateral energy losses from the reaction zone, the critical diameter of a given reactive material also depends on the lateral confinement of the charge. Thus the critical diameter for a charge inside a confinement tube is less, perhaps much less, than for an unconfined charge.

In sufficiently large charge diameters, many energetic materials such as gun and rocket propellants can be detonated. These materials are not commonly referred to as detonable materials because their critical diameters for a sustained detonation are simply larger than are normally prepared and/or no sufficiently large initiating shocks (in magnitude and cross-sectional area) are available to start the detonation process.

2.2 Selection of Test Configuration

The determination of the detonability of the material of interest here, i.e. BZ-pyromix, from a practical viewpoint need not be an absolute determination, but rather a determination of detonability under the combined conditions of maximum existing charge diameter and lateral confinement. Within the BZ munition inventory, these conditions are fulfilled by the M138 bomblet packed into the M43 cluster munition, see Figures 1 and 2.

The array of 19 M138 bomblets through a cross-section of an M43 cluster might be considered to form an equivalent diameter larger than a single M138 from the standpoint of critical diameter for detonation. However, a deflagration-to-detonation transition (DDT) must occur over a diameter at least equal to the critical diameter to develop a self-sustaining detonation. Thus, if the critical diameter is greater than the diameter of a single M138, but smaller than an M43, a DDT must occur simultaneously in three or more contiguous M138s. A DDT in a single M138, being below the critical diameter, could not occur and an induced detonation wave in a single M138 would be quenched. The likelihood of a DDT occurring simultaneously across the junctures of the M138s so that the resultant detonation wave was contiguous across the junctures of the M138s appears negligibly small under any conceivable real circumstances during demilitarization. Hence, we believe that proof of the critical diameter for detonation of BZ-pyromix being greater than that of a single M138, as confined inside an M43, is sufficient to support an assessment of non-detonability for all of the BZ munitions.

An M138 inside an M43 is confined around its perimeter by line contacts with six adjacent M138s along its length. The combined wall thickness of the M138 case and contained M7 canister cases approximates 3 mm of steel. Hence, a test of an M138 contained inside a steel tube with a 3-mm wall thickness would provide an over-test of the confinement provided by the adjacent M138's in an M43 cluster. Thus the munition selected for detonability tests was a single M138 housed inside a close-fitting steel tube with a 2.3-mm wall thickness, (the nearest standard size to 3 mm).

From the standpoint of theoretical predictions of detonability, the maximum possible energy release from the reaction of the BZ-pyromix can be equated to the

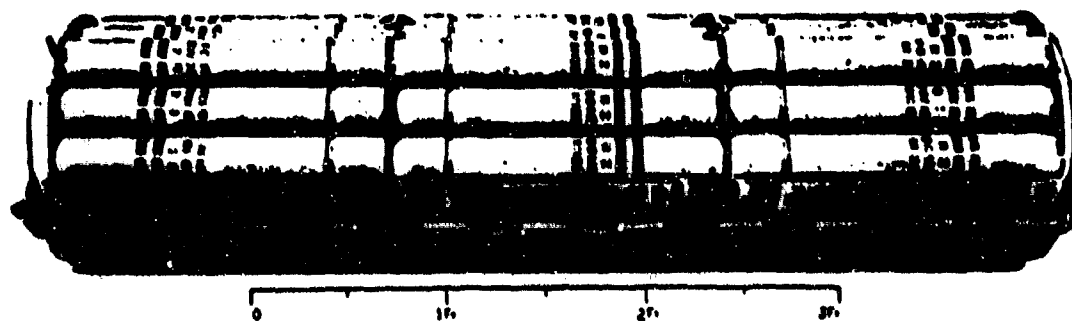


FIGURE 1. M43 BOMB CLUSTER SHOWING INTERIOR

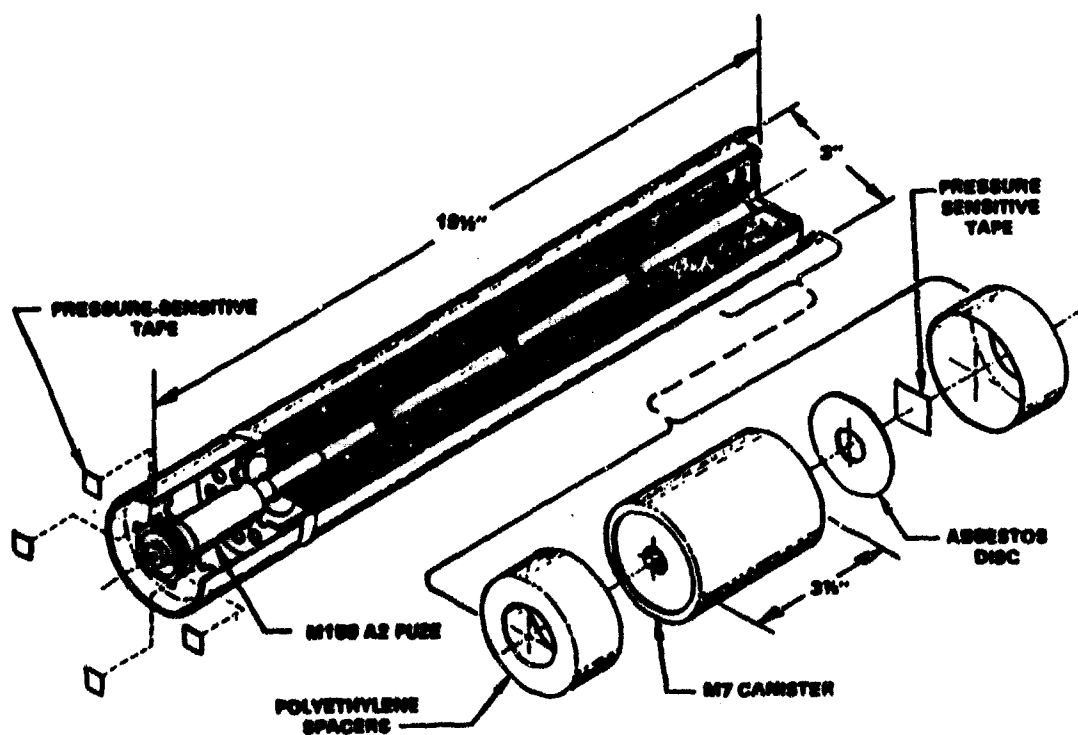


FIGURE 2. M138 BZ BOMB ASSEMBLY

energy required to drive a shock wave through the unreacted material. By ignoring lateral energy losses, the problem is simplified and becomes equivalent to mocking up very large or well confined charges. A calculational scheme based on the above premises has been built into a computer program called TIGER.

It should be noted that this calculation cannot predict whether detonation will or can occur because it cannot be predicted at present whether the hypothesized reactions can occur rapidly enough to take place within the C-J reaction zone. Thus, this calculation is a prediction of the theoretical upper limit for the detonation velocity and pressure within the uncertainty of knowledge of the required inputs to the code calculation. The TIGER code was run for the BZ-pyromix composition by Robert Gentner of ARRADCOM(2), Dover Site. The theoretically predicted detonation velocity was 3.3 mm/microsec at a pressure of about 2.5 GPa (25 kbar).

Thus for detonability testing, a donor charge which provides a shock velocity (and pressure) input to a confined M138 over its entire cross sectional area in excess of the predicted upper limit sustained detonation velocity (and pressure) is all that is required. In the absence of a detonation, the input shock would be expected to decay along the length of the M138. The shock pressure would decay from the initial high input pressure from the donor charge to very low levels. Accompanying the pressure decay, the shock velocity would decay from high initial values of 5 mm/microsec down to the sonic velocity in BZ-pyromix. There does not appear to be any sonic velocity data available for BZ-pyromix. However, based on comparisons with other materials it seems unlikely that the sonic velocity will exceed 2.3 mm/microsec, and may be appreciably lower.

2.3 Basis for Interpretation of Results

Historically, and commonly, the occurrence of a detonation is signalled by the perforation of a steel witness plate in close proximity to the charge⁽³⁾. However, in the case of BZ-pyromix, the predicted upper limit detonation parameters are sufficiently low that such perforation might not occur even in the presence of a detonation. Instead, a dual basis for the test interpretation was developed. One relies on instrumentation in the core hole to measure the shock front position with time (and hence shock velocity by differentiation) along the length of the M138. The other relies on visual observation of the remaining metal parts after the test. In the event of failure of the real time instrumentation or as confirmation, a post-test examination which shows major parts of the M138 remaining intact, or broken into fairly large pieces, constitutes evidence for non-detonation. A measured sustained shock velocity in the M138 near 3 mm/microsec coupled with fragmentation of the metal parts would constitute evidence for detonation. On the other hand, a decaying shock velocity to 2.3 mm/microsec which remains below this value together with some metal parts remaining intact, or only fractured in relatively large pieces, would constitute a non-detonation. In this context, "relatively large" pieces means fragments approximate to the length of an M7 canister and wide enough to span about one-half the M138 circumference.

2.4 Test Conditions and Lot Selection

Processes being evaluated for application to the demilitarization of the BZ munition inventory involve handling of the munitions in both inventory condition and after

inerting by submersion in an inerting liquid. Destruction is expected to occur by burning off the BZ-pyromix in a heating chamber or rotary kiln, with subsequent incineration of the evolved BZ vapor or aerosol. Thus it is desirable to obtain data on the detonability of munitions at ambient temperatures in (1) the inventory condition, (2) after short (5-minute) inerting liquid submersion and (3) after normal (2-hour) inerting liquid submersion for a plant design to withstand detonation effects, if shown to be necessary. Since heating of munitions is also contemplated, it is desirable to obtain detonability data on preheated munitions as an aid in assessing the requirements for the heating-functioning furnace or kiln.

Bomblets which had been downloaded from M43s were available for testing from several different lots of production. Production testing showed the burning (normal functioning) rates to vary appreciably from lot to lot. Although there is no known correlation between detonability and burning rate in the normal functioning mode, the burning rate data seemed likely to be the most significant data available. Thus M138 munitions were selected for test from all available lots, but with replications of the fastest burning and near the slowest burning time munitions available. The numerical values of this parameter are reported in Section 4.1 on test conditions and lot selection.

3. EXPERIMENTAL APPARATUS

To conduct the planned series of detonability tests, two major items of equipment were required:

- An explosive and gas containment vessel capable of containing the detonation of at least 1.5 kg TNT-equivalent high explosive and retaining the gases and aerosol without significant leakage
- A vapor incinerator, afterburner, and water quench system capable of reducing the BZ content and temperature of gases resulting from the detonability tests to a level allowable for discharge into the igloo environment.

The vapor incinerator, afterburner, and water quench system was constructed to obtain preliminary plant design information as well as to destroy the BZ vapor/aerosol generated during these tests. The incinerator system was extensively tested and qualified for the destruction of BZ prior to the conduct of these tests. It has been described in detail elsewhere.⁽⁴⁾

3.1 Blast Containment Sphere

The blast containment vessel was modified from a previously constructed, 1.07-m- diameter spherical chamber with an average wall thickness of 22.9 mm.⁽⁵⁾ For this application, the original port reinforcing ring and door were replaced by an O-ring-sealed door externally mounted and secured by a double row of bolts. This port design was patterned after similar closures which had been qualified for blast containment at Los

Alamos National Laboratory. Additional penetrations were a high-pressure, 28-pin electrical lead-through manufactured by D. G. O'Brien, incorporated for heater and instrumentation connections, and two Swagelok® high voltage lead-throughs for the exploding bridgewire detonators. Piping connections for the pressure transducer and for gas purging were made through the door. After modification, the sphere was requalified by the test firing of a 1.82 Kg spherical composition C-4 test charge, as well as static gas pressure tests at 2.27 MPa. These tests have been previously described in detail.⁽⁶⁾

3.2 Fragment Restraint Assembly

Figure 3 shows a schematic of a hot detonability test assembly arranged inside the containment sphere. To provide protection for the sphere interior from fragment damage, a 0.46-m-length of 0.41-m O.D. pipe with near 25.4-mm wall thickness was hung, as shown, on the sphere horizontal centerline. This pipe was specially constructed of high toughness steel alloy. It was fitted with a replaceable, mild steel liner rolled from 9.61-mm-thickness plate. The pipe provided the structural strength to absorb the fragment momentum while the liner absorbed the fragment craters. About midway through the test series, the liner was replaced as planned, to prevent penetration of the accumulated fragment craters through the liner.

3.3 Detonability Assemblies

Inside the fragment restraint pipe, the detonability assembly was supported on the sphere centerline by a thin steel cradle. The assembly shown schematically in Figure 3 is for a preheated detonability test. At the heart of the assembly is a specially instrumented M138 bomblet which is described in the following section (Section 3.4). The bomblet is secured inside a 13-gage steel tube over its full length to provide the desired additional confinement. This tube in turn was fitted with two separate fiberglass-insulated electrical heating tapes, a main heater and an end compensating heater. Each heater was controlled with the aid of a thermocouple, hard-soldered to the confinement tube. The two control thermocouples were connected to strip chart recorder-controllers. The heaters were powered through variable autotransformers which were adjusted during heating to maintain the center and end thermocouple at near the same temperature and to maintain good temperature control once the heating jacket reached the desired temperature.

The 1.3-lb composition C-4 donor charge was designed to provide a charge length at full diameter equal to the charge diameter plus a conical lead-in to insure near-planar, axial symmetry of the detonation shock entering the munition. For the pre-heated tests, it was supported inside a fiberglass-reinforced silicone plastic tube, separated from the M138 by a 51-mm air space during heating to minimize preheating of the C-4. After the desired preheat, a specially-designed electric gearmotor actuator moved the charge into firm contact with the M138 just before detonation. The C-4 charge was contained inside a 0.20- to 0.46-mm thick vacu-formed PVC container. This container was supported by a strong, wooden mold during packing of the C-4 plastic explosive to allow the production of a fully densified charge of the correct dimensions. After packing, the thin plastic container provided sufficient support to allow easy handling of the explosive charge.

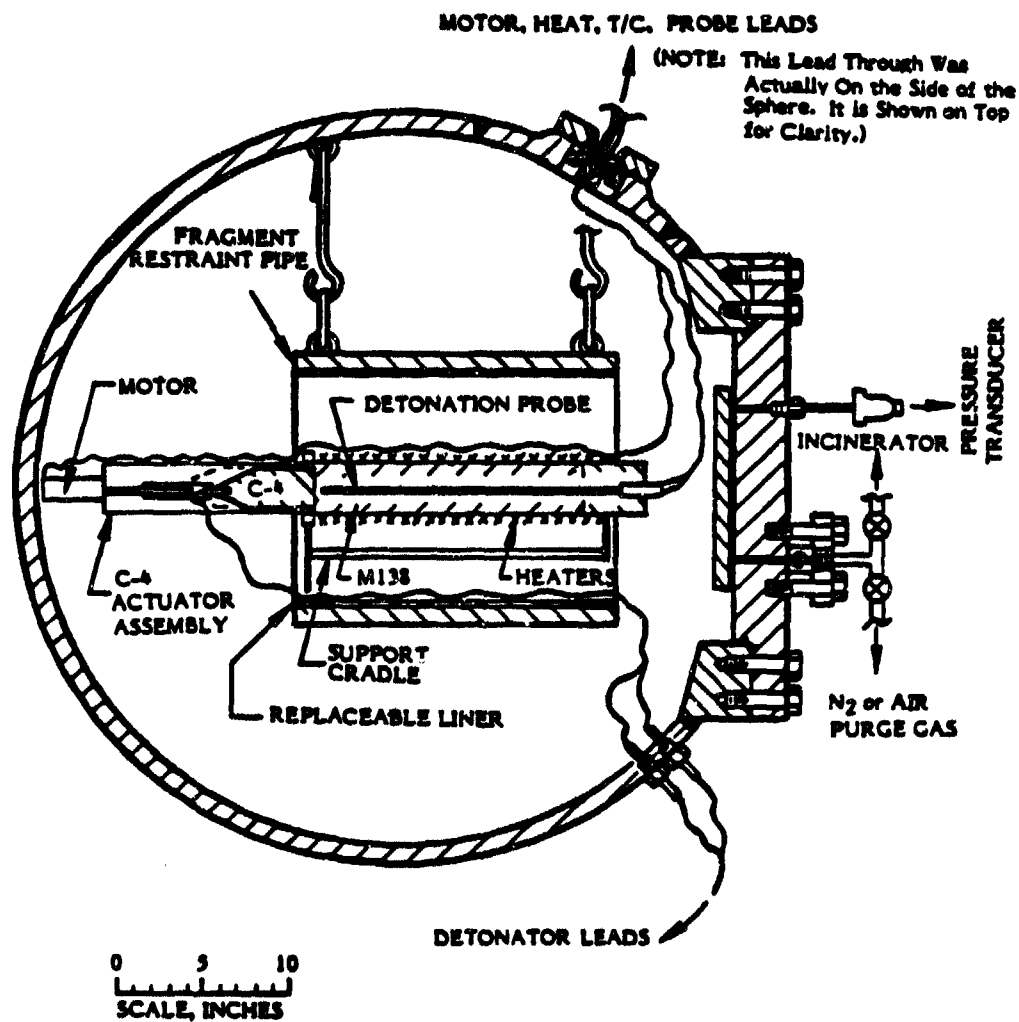


FIGURE 3. SPHERE ASSEMBLY

The C-4 charge was detonated by an RP-83 exploding bridgewire detonator. This detonator was selected to provide safety from stray electrical currents during loading operations. The exploding bridgewires were fired by a Model FS-10 firing unit manufactured by Reynolds Products, Inc.

The confinement tube for the unheated M138 munitions was identical to that for the heated munitions. For these tests, the composition C-4 charges were secured in firm contact with the munitions by the force of several strong rubber bands between the M138 and a specially shaped, wooden block across the base of the C-4 charge.

3.4 Instrumented M138 Assembly

The M138 itself was fitted with a special detonation probe assembly inserted into the core hole of the munition. Figure 4 shows the detonation probe assembly. As shown, the assembly was comprised of two 28 ga type K (Chromel-Alumel) thermocouples and two detonation probes potted inside a low-density polyethylene tube. The header assembly served to protect the otherwise extremely fragile connection between the detonation probes and the coaxial cables used to connect the probes to the exterior instrumentation.

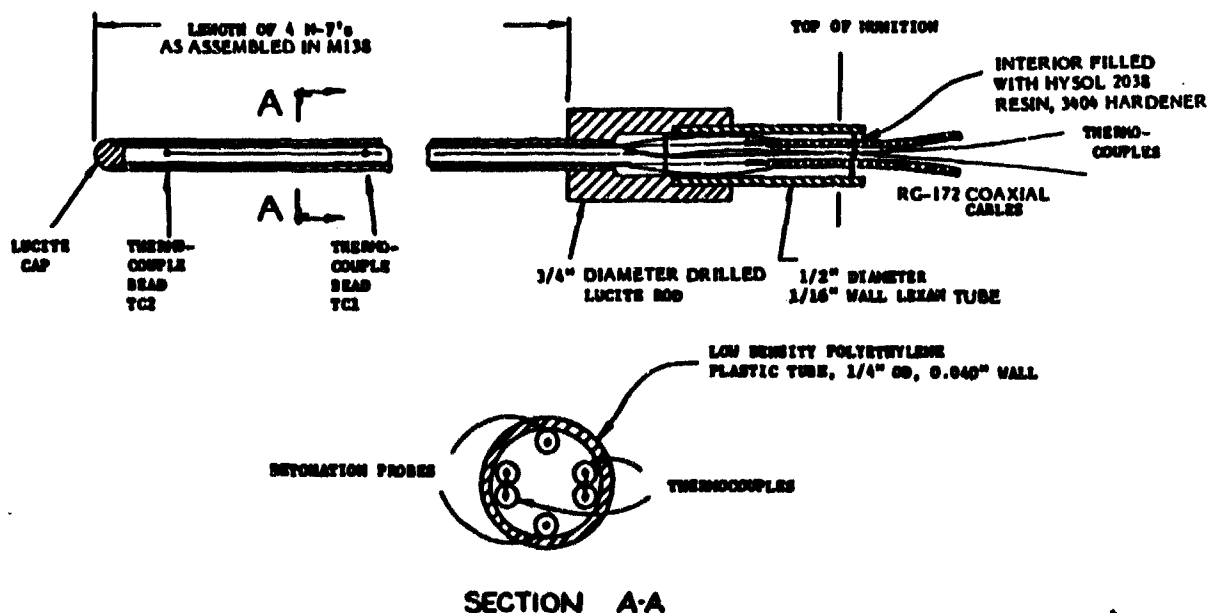


FIGURE 4. DETONATION PROBE ASSEMBLY

Two detonation probes were used in each assembly to provide redundant information on the position of the shock front (Figure 4). Each probe was comprised of a 0.51-mm-diameter aluminum tube (0.038-mm wall thickness) containing an 0.025-mm-diameter Moleculloy® resistance wire (0.33 ohms/mm resistance). The resistance wire was insulated by skip-wound nylon. The resistance wire was soldered to the aluminum tube at one end and connected to the center wire of the coaxial signal cable at the other. The aluminum tube was connected to the coaxial cable shield.

In operation, a high pressure shock wave travelling up the M138 and probe from the originally shorted end progressively shorted out more of the resistance wire by crushing the aluminum tubing against the wire. Of course, if the pressure in the shock wave dropped below that required to crush the tube, the probe would cease to provide position data; at pressure levels near the threshold, the crushing of the tube could be expected to be somewhat erratic. The circuitry associated with each probe consisted of a battery-powered, constant current source and a high-impedance measurement of the variation in voltage across the probe with time. With appropriate calibrations, the measured voltage could be related to the position of the shock front (as described in detail in Appendix A). The constant current supply was adjusted to provide ~74 mA through the probe resistance of ~121 ohms, giving an initial voltage of ~9V. This represents a power dissipation of ~2/3 Watt so that negligible heating was produced by the probe excitation current.

The detonation probe assemblies for the ambient temperature tests were identical to those shown in Figure 4 except the thermocouples were not installed.

To insure that no interference would be encountered during assembly of the 6.4-mm probes into the M138 munition, each core hole was optically gaged with the aid of a small (2 mW) He-Ne laser fitted with a beam expander which provided a 12-mm diameter parallel light beam. If the light beam was unobstructed over at least a 6.4-mm diameter after passing through the core hole of the munition, the probe could be safely inserted. This optical gaging technique showed that all munitions were safe to insert the 6.34-mm probe.

One detonation probe assembly was potted inside the core-hole of each M138 bomblet tested. The core hole surrounding the detonation probe was filled with a low viscosity epoxy resin (Hysol® resin R8-2038 with HD-3404 hardner). The active end of the actual detonation probes were approximately 1/4-inch, or 6.3 mm, from the end of the bottom M7 canister. The fuze cavity at the lead end of the M138 was filled with another epoxy potting compound (Hysol® C8-4143 resin with HD-3404 hardener). This resin contains 50% silica filler to reduce shrinkage during curing. Both epoxy resins were pre-checked for temperature rise during curing in the configurations used and found to be satisfactory. The resultant instrumented M138 was mechanically quite strong to allow handling and installation into the blast containment sphere for testing. All electrical leads were pre-connected and potted into a large, 28-pin plug which mated with the lead-through mounted in the blast container wall. Thus it was possible for operating personnel in Level B protective clothing (gas masks, rubber aprons, boots and gloves) to assemble and install these highly instrumented assemblies into the blast containment sphere without recourse to soldering operations.

It should be noted that both ends of the coaxial cables used for the detonation probe leads were entirely sealed by immersion in epoxy potting. In addition,

the plug O-ring sealed into the containment lead-through socket. Thus the entire probe circuits were protected from the short-circuiting effects of the high pressure, ionized air-shock wave generated by detonation of the C-4 charge, assuring against premature loss of the detonation probe signal from this source.

Another result of installation of the detonation probe assembly was to provide additional lateral confinement of the M138 by preventing the free expansion of the reaction products into the core hole, which would normally occur with inventory munitions. This provided an additional degree of overtest which was necessitated by the requirement to provide a continuous shock path through solid material from the BZ-pyromix fill to the detonation probes.

3.5 Electronic Data Acquisition Apparatus

A block diagram of the apparatus used for gathering the sphere pressure and detonation probe data is shown in Figure 5, together with the detonator firing circuit.

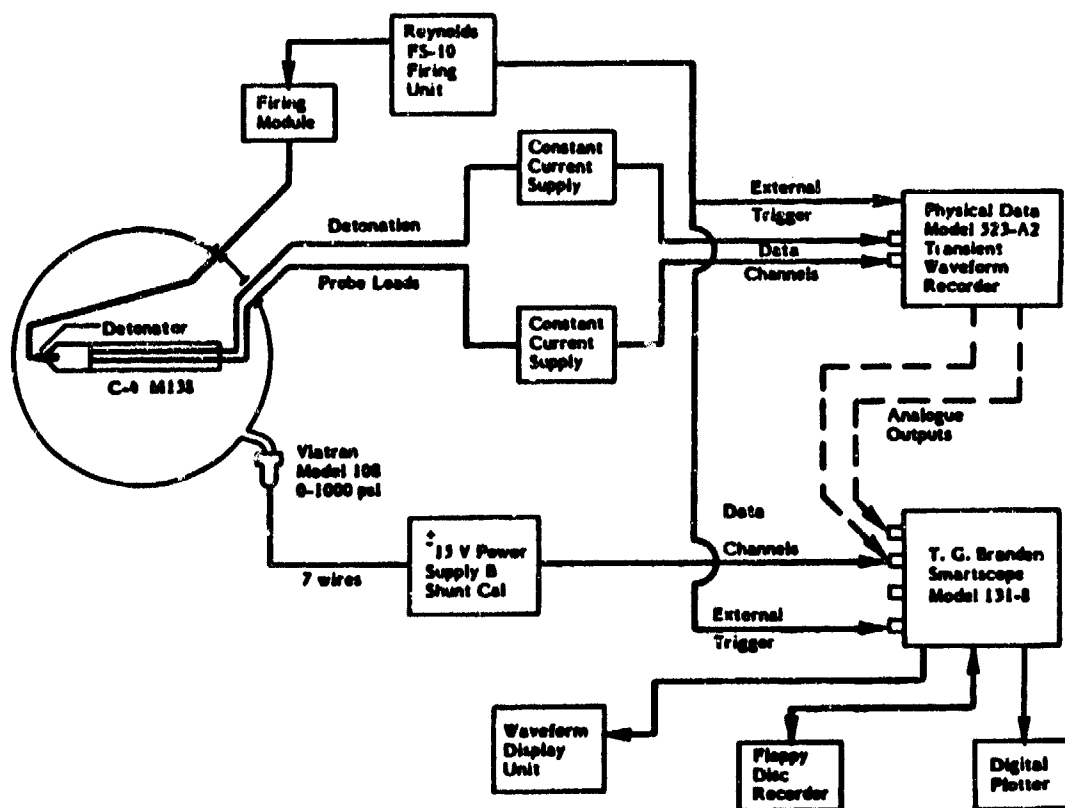


FIGURE 5. DATA ACQUISITION SYSTEM FOR THE DETONATION PROBES AND SPHERE INTERNAL PRESSURE

In operation, the shot was fired by a push button on the FS-10 firing unit. This unit, through the firing module, produced pulse needed to fire the exploding bridgewire detonator, Reynold's RP-83. At the same time the firing pulse was initiated, a 30-V pulse was generated which served as a trigger signal for the fast data acquisition system.

The fast data acquisition system was comprised of two major parts, the detonation probe and pressure-signal processing subsystems. The detonation probe subsystem consisted of two adjustable constant current power supplies and a Physical Data Inc. Model 523-A2 two-channel transient waveform recorder. This unit provided 4096 digital samples for each channel at 0.1 microsec per sample. After temporary digital storage in the unit, it was subsequently transferred at a reduced rate, in analog form to the Smartscope® where it was re-digitized and processed. The plots shown in this paper were generated directly on the Smartscope plotter.

The internal pressure in the sphere was monitored by a Viatran Model 108 pressure transducer and recorded on the Smartscope where it was sampled over a 10-sec period with 1-msec resolution. The appropriate calibrations were input to the Smartscope so that its digital plotter produced the pressure time records directly.

4. EXPERIMENTAL PROCEDURES AND RESULTS

The detonability tests were conducted in a storage igloo at Pine Bluff Arsenal, Pine Bluff, Arkansas. This igloo was equipped with a personnel change house, filtered ventilation system, and the necessary gas and power supplies. It also housed the pilot scale incinerator used to dispose of resultant BZ aerosol. After initial training, all munition preparations and test operations inside the igloo were conducted by technicians from Pine Bluff Arsenal. Explosive charge preparation, and all handling operations involving explosive and detonators, were performed by members of the 52nd E.O.D. Detachment at Pine Bluff Arsenal.

4.1 Test Conditions and Lot Selection

As described in the technical approach, munitions were selected from all available downloaded lots to provide as broad a sampling base as possible. In addition, where duplicate tests were possible, they were grouped at the extremes of low and high burning times. Table 1 shows the test sequence. As shown, the tests were in four groups. The first two tests were conducted on "inerted" M138 munitions. Inerting was done by immersion for 2 hours in a vertical position in water with 0.01% Avirol-113 (a wetting agent), after removal of the sealing tapes from the ends of the core holes. After inerting, the munitions were allowed to drain overnight in a vertical position, before potting the instrumentation into the core hole.

The short inerting on the second two munitions was done the same as for the inerted munitions except the immersion time was 5 minutes.

The third group of three munitions were tested in the inventory condition. All three of these groups were tested at ambient temperature (~27 C).

Table 1. Test Variables for M138 Detonability Tests

Test No.	Munition Lot No. 1021-	Burning ^(a) Time Secs.	Test Conditions	
			Preparation	Temperature C
D1	35-153	31.2	inerted	ambient
D2	44-1123	17.0	inerted	ambient
D3	35-153	31.2	short inerted	ambient
D4	44-1123	17.0	short inerted	ambient
D5	35-153	31.2	live inventory	ambient
D6	41-187	26.5	live inventory	ambient
D7	44-1123	17.0	live inventory	ambient
D8	35-153	31.2	live inventory	intended 105 ^(b)
D9	41-1113	30.7	live inventory	intended 105 ^(b)
D10	35-153	31.2	live inventory	74
D11	41-187	26.5	live inventory	81
D12	41-1103	23.3	live inventory	81
D13	36-160	22.5	live inventory	82
D14	44-1123	17.0	live inventory	84
D15	36-181	28.0	live inventory	81
D16	36-157	21.0	live inventory	81
D17	41-1113	30.7	live inventory	80

(a) Of all M43s produced, the shortest burn time measured was 15.3 sec. Only 5 lots had burn times less than 17.0 sec. Some production lots burned considerably slower than the slowest lot available for these tests; five lots had burn times greater than 40 sec.

(b) Munition functioned during heating.

The fourth group of ten munitions were tested in a preheated condition. As shown in Table 1, it was intended to preheat the munitions to a temperature of 105 C. This temperature was chosen to provide a 5 C margin of safety over tests with an inert simulant which caused extrusion of the fill(7). The preheating protocol was to heat the outer shell to the desired test temperature then maintain this shell temperature until the core temperature reached the approximate shell temperature. During heating of test D8, the BZ-pyromix ignited after the heater shell had been at 106-107 C for 58 minutes and the core thermocouples were indicating 75-77 C. No previous ignition of starter mix or BZ-pyromix at this low temperature had been observed. Hence a second attempt to preheat to 105 C was made in test D9. Again, ignition occurred before the test temperature was reached. This time ignition occurred 74 minutes after the outer shell reached 105-106 C and at an indicated core temperature of 88 C. Ignition of the pyromix caused the Composition C-4 to burn as well, so that no safety problem occurred. No detonability data were obtained from these two tests and it was decided to reduce the test temperature to 80 C.

When the outer shell temperature was restricted to 80 C, the heating time was too long to allow the core to reach 80 C. Thus test D10 was fired at a core temperature of 74 C, 2.4 hours after the shell reached 80 C. In subsequent tests, the shell temperature was raised to 90-93 C to provide an increased thermal gradient to drive the core temperature up to 80 C. Slightly before the test, the shell temperature was allowed to cool to near 80 C, so that near isothermal conditions were established.

In test D11, the actuator motor to move the Composition C-4 donor charge into contact with the M138 was found to be jammed in an attempt to operate the motor after preheating. Due to possible safety problems in handling a previously preheated device, the donor charge was fired, aborting test D11.

All remaining tests provided detonability data for the M138 configuration tested. However, much of the data obtained was quite noisy, which required the use of special techniques to extract meaningful data from the records. These data reduction techniques were carried out on the data as stored within the Smartscope so that the data plots presented herein were entirely machine-produced.

4.2 Typical Results Obtained

The results obtained from detonation test D7 are fairly representative of the data obtained from each test. In some cases data from only one probe were obtained and the data ranged from somewhat less to somewhat more noisy. In this section all of the intermediate steps in the data reduction of test D7 are shown in graphical form.

The graphs presented are:

- Original data as recorded and transferred to the Smartscope
- Conversion of the probe voltage data to shock position data after application of the basic data reduction constants
- Velocity determined after application of the data smoothing operations to reduce the noise content

- Comparison of the smoothed position-time data from the two probes
- Stepwise slope (finite-difference differential shock velocity) of the position-time data
- Cross-plots of the shock velocity versus shock position data.

Figure 6 shows the original voltage versus time data recorded from the two probes of test D7. The initial large amplitude ringing noise shown on this record appeared only after a replacement Physical Data recorder was put in service. It was not possible to find and eliminate this noise source during the time frame of these experiments.

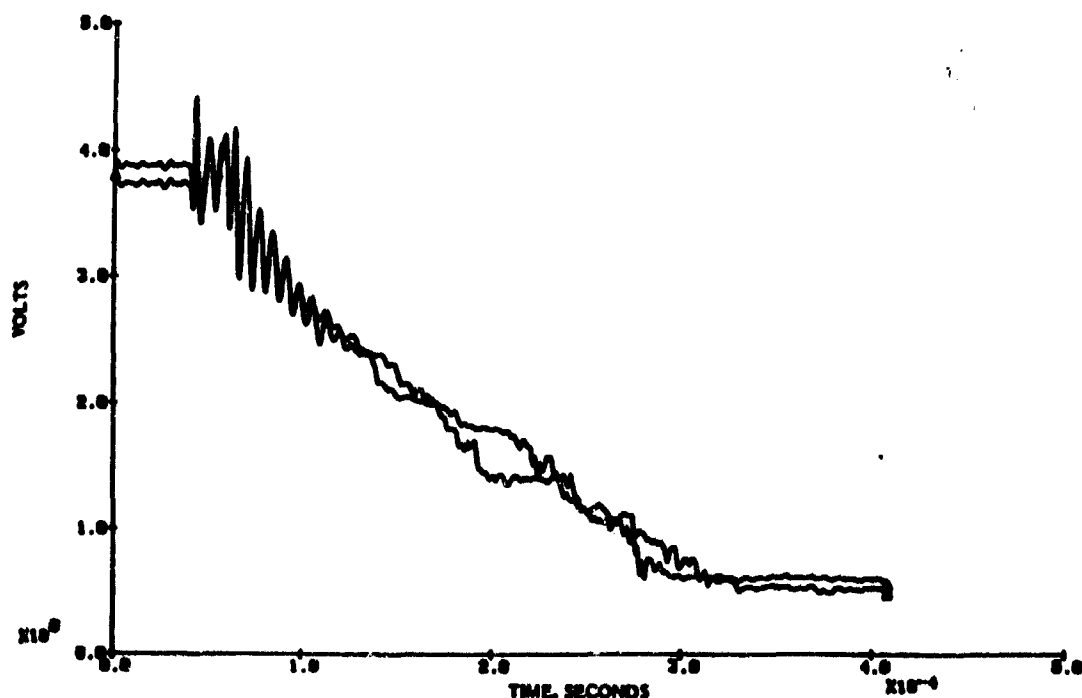


FIGURE 6. EXAMPLE ORIGINAL DETONATION PROBE VOLTAGE—TIME DATA AFTER A MINOR SMOOTHING OPERATION. (TEST D7)

Figure 7 shows the probe voltage curves after conversion to position-time data. This step is described in detail in Appendix A. Briefly, the constant current value is obtained from an auxiliary measurement of the voltage through a known resistance. With the current known, changes in voltage can be related to changes in probe resistance.

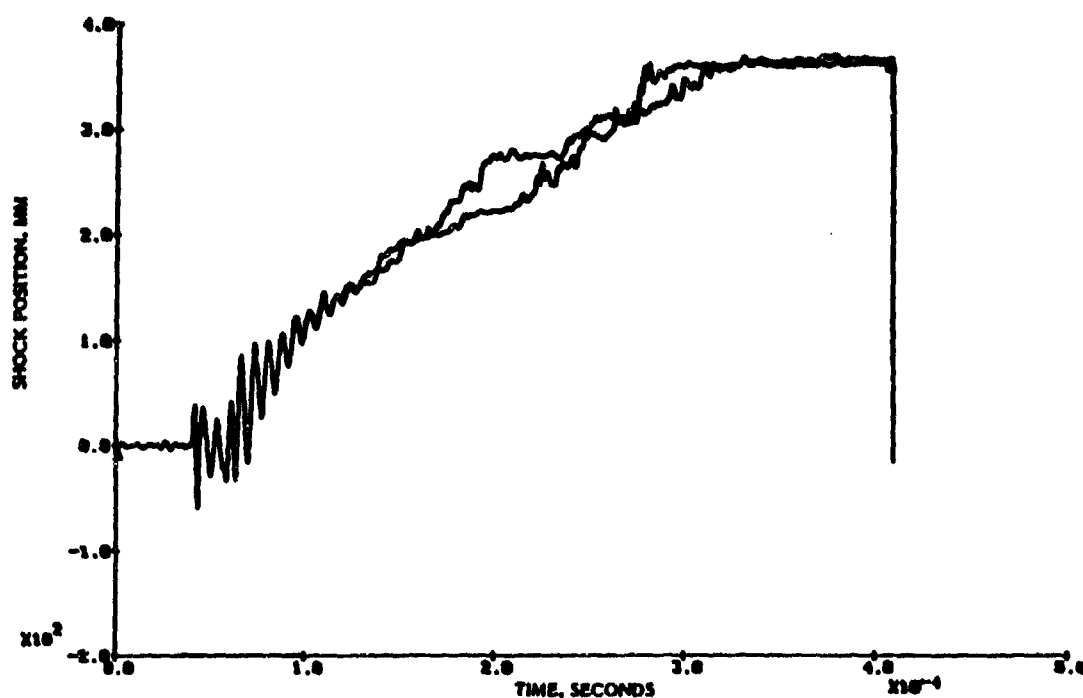


FIGURE 7. EXAMPLE ORIGINAL VOLTAGE DATA CONVERTED TO POSITION DATA BY APPLICATION OF CALIBRATION CONSTANTS AND RESISTANCE/UNIT LENGTH OF THE PROBE RESISTANCE WIRE. (TEST D7)

Likewise, with the resistance change known, and the probe resistance per unit length known, the shock position can be derived as shown. The deviation between the two curves at long (200 mm) shock travel distances arises because the low pressure which exists in this region is unable to produce precision crushing and shorting of the detonation probes, as it does in regions of higher pressure (smaller travel distances).

An example of reduction of noisy data by smoothed line construction is shown in Figure 8. The basis for drawing the smooth line is as follows. In the initial time region where the data curve is dominated by a ringing-type noise, the smoothed line is made up of a number of short straight line segments drawn through the average value of the initial ringing signal period by period. Later, the data was smoothed on the basis of engineering judgment as to the probable average position of the shock pressure front, with the guideline that the actual shock front progress has momentum associated with it and would be expected to follow a smooth line of progress. Of course, the munition itself is not homogeneous along its length, but is made up of four M7 canisters stacked end to end. Each M7 has 1.5-mm steel end closures, separated by a 1.0-mm thick plastic spacer. These discontinuities occur at three places along the munition length, as shown in Table 2, which also gives the total BZ-pyromix length. The detonation probe records frequently stop changing with time before the full length of the munition is reached. This means that the shock pressure had dropped too low to continue crushing the detonation probe tube.

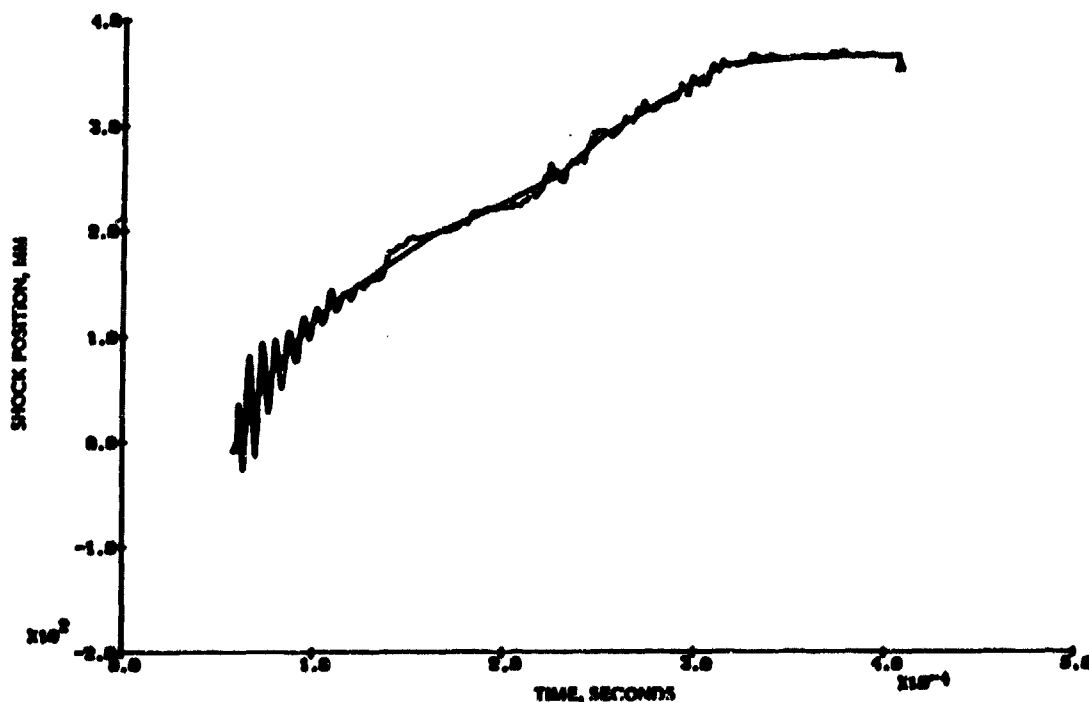


FIGURE 8. EXAMPLE SHOWING SMOOTHED LINE THROUGH THE ORIGINAL POSITION—TIME DATA. (TEST D7, PROBE 1)

Table 2. Locations of Discontinuities for Shock Travel Along M138 Length

Discontinuity	Location, mm	
	From Shock Entrance	As Plotted
Inside Rear of 1st Canister	95.5	89.2
Inside Front of 2nd Canister	101.0	94.7
Inside Rear of 2nd Canister	195.1	188.8
Inside Front of 3rd Canister	200.6	194.3
Inside Rear of 3rd Canister	294.6	288.3
Inside Front of 4th Canister	300.1	293.8
Inside Rear of 4th Canister	396.2	389.9
Outside Rear of 4th Canister (End of BZ-Pyromix Containers)	397.2	390.9

Note: The words "rear" and "front" mean the ends encountered last and first respectively by the shock wave.

Figure 9 shows a comparison of the two smoothed location - time curves from test D7. The curves track very well together until near the 200 mm location. This is after the shock velocity has decayed to the apparent sonic velocity in the material indicating that the pressures are no longer high.

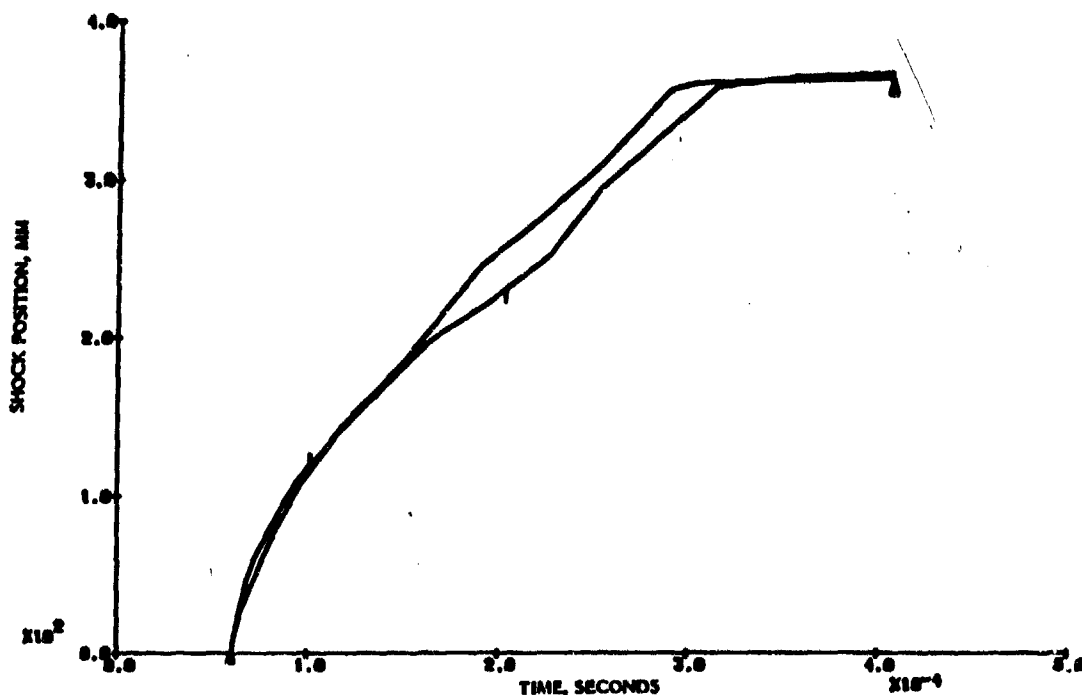


FIGURE 9. EXAMPLE COMPARISON OF THE TWO SMOOTHED POSITION-TIME CURVES OBTAINED FROM THE SAME TEST (TEST D7)

Figure 10 shows a velocity versus time record obtained by simply taking the slope of the position time curve at 10-microsec intervals along its length, and plotting this velocity as a constant over that time period. Figure 11 shows a final plot of shock velocity versus shock position. This plot is cross plot of the position data from the upper curve of Figure 10 and velocity data from the lower curve using time as a parameter. From plots of this type, the determination of shock travel at velocities greater than 2.0 mm/microsec was made. The discontinuities near 200 and 300 mm travel are apparent on these plots, coinciding with the ends of the M7 canisters.

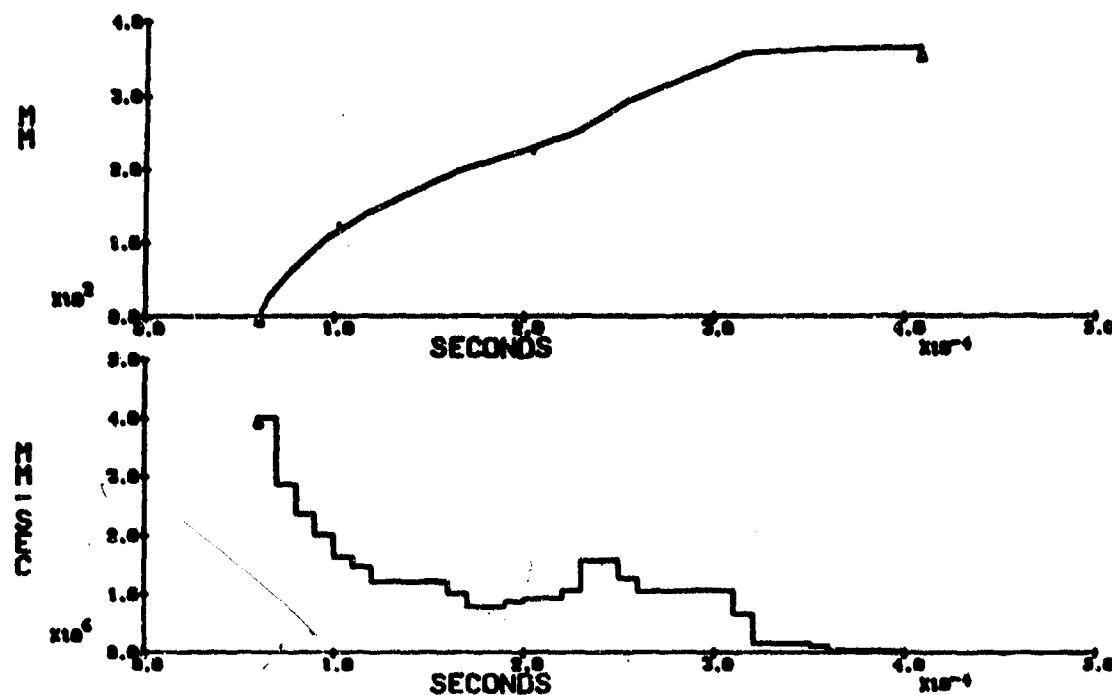


FIGURE 10. UPPER CURVE SMOOTHED POSITION—TIME DATA.
LOWER CURVE STEPWISE VELOCITY DATA FROM
UPPER CURVE (TEST D7 PROBE 1)

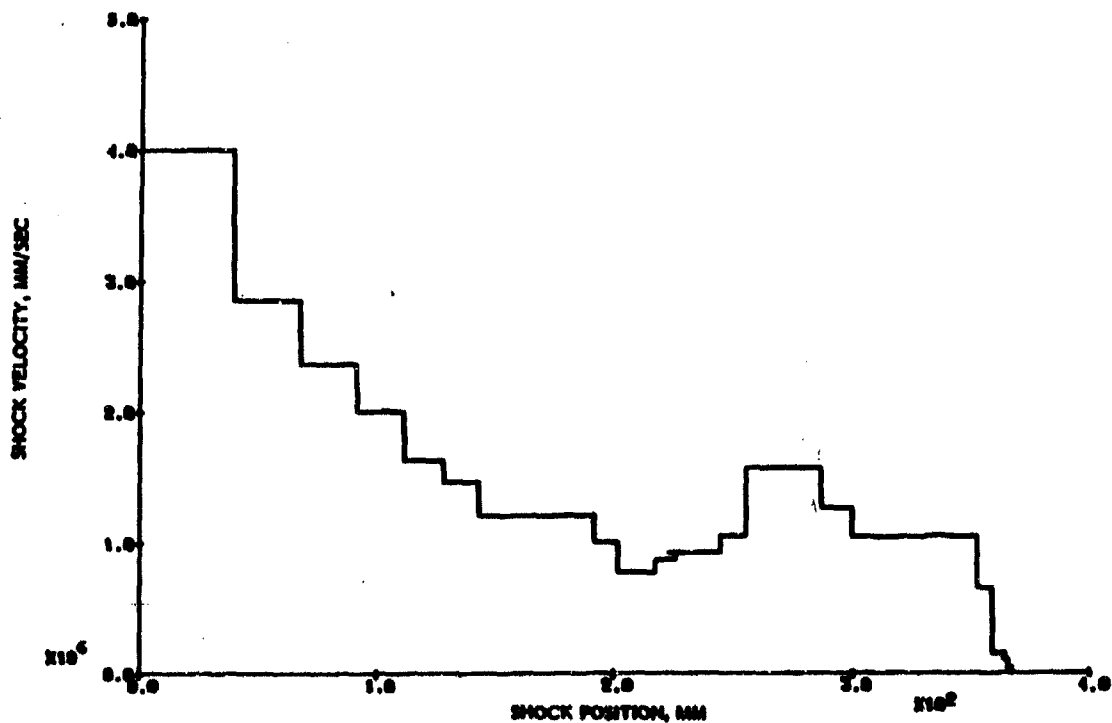


FIGURE 11. CROSS PLOT SHOWING VELOCITY DECAY WITH DISTANCE
ALONG THE M138. (TEST D7 PROBE 1)

4.3 Results

From each final plot, the shock travel at a velocity greater than 2.0 mm/microsec was measured and is tabulated in Table 3. Here, the limiting value of 2.0 mm/microsec was chosen over the initially selected 2.3 mm/microsec value after examination of the data which showed that the observed velocities generally fell below this level. (Results using 2.0 mm/microsec versus 2.3 mm/microsec are conservative.) Occasionally, near the end of a record, velocities slightly over 2.0 mm/microsec were observed; this was attributed to the irregular performance of the probes at low pressure levels. This conclusion is supported by the recovery in several tests of intact portions of munitions which came from the same regions where these late velocity excursions were observed. It should be noted that the shock travel at velocities greater than 2.0 mm/microsec for an simulated non detonable test item⁽⁷⁾ was 130 mm, with a very similar velocity decay curve. Improved data reduction techniques from those used in Reference 7 were used on the current data set* so that the difference between the current data and the simulated non-detonable item may be less than suggested by the numbers. In any event, the results obtained from the current tests on live BZ-pyromix were quite similar to those obtained on the simulated non-detonable mockup item.

With respect to the munition remains after the test, about two-thirds of the original munition remained intact, with no burning of the remaining BZ-pyromix-filled canisters in the inerted and short-time inerted munitions tests. For the non-inerted munitions, a vigorous reaction of most or all the BZ-pyromix occurred. Although the entire munition was broken up, many large fragments with areas almost one-half that of a single canister case remained, indicating that the pressures developed prior to canister burst were not appreciably above the minimum pressure required to burst them, far below the predicted detonation pressure. In the unheated non-inerted tests and preheated tests D11 and D12, all canisters were destroyed. In the other preheated tests, one distorted but intact M7 canister remained, except in test D17 where two M7s remained intact. In test D17 there also was evidence of unburned BZ-pyromix. The bursting of the M7 canister's M138 sleeve and the added confinement tube in these tests due to the reaction of BZ-pyromix was to be expected because the core hole (which normally vents the generated gases and BZ aerosol) was securely plugged with epoxy resin cast in place.

Both the active instrumentation and the post-shot appearance of the munition remains confirm that no sustained detonation occurred, nor does there appear to be any evidence for a fading detonation as would occur with a material which would support a sustained detonation in a slightly larger charge diameter.

* The difference arises principally in the use of an additional calibration which eliminates the effect of long term drift in the constant current. It was found after the tests of Reference 7 that the current provided by the constant current supply slowly drifted up with time between pre-calibration measurements and conduct of the test. This drift went undetected in the initial non-agent tests.

Table 3. Shock Travel at Velocity Greater Than 2.0 mm/microsec

Test No.	Probe 1 mm	Probe 2 mm	Average Within Groups mm	Standard Deviation of Group mm
D1	100	-	103.5	± 4.9
D2	107	-		
D3	116	-	104	± 17.0
D4	92	92		
D5	98	116	109	± 10.1
D6	115	125		
D7	100	100		
D9	-	-		
D10	120	130	111.6	± 6.6
D11	58 ^(a)	59 ^(a)		
D12	108	-		
D13	108	112		
D14	102	110		
D15	115	-		
D16	109	106		
D17	106	113		
Overall Average			108.8	± 8.5

(a) Not included in averages because of no contact between donor charge and M138 munition.

Notes: The total shock travel distance is 6.3 mm greater than the values shown because the end of the active probe was 6.3 mm from the lower end of the munition.

Additional evidence regarding the reaction of the BZ-pyromix was obtained from the measurement of pressure inside the sphere following the detonability tests. An example pressure measurement record is shown in Figure 12 for test D7. As demonstrated in this example, all records showed an initial spike pressure which rapidly decayed to a more slowly changing pressure, called the initial steady pressure. Ten of the 15 records obtained showed a small increase to a maximum pressure in a small fraction of a second, followed by a steady pressure decay to the last accurately measured pressure at 10 seconds after the test.

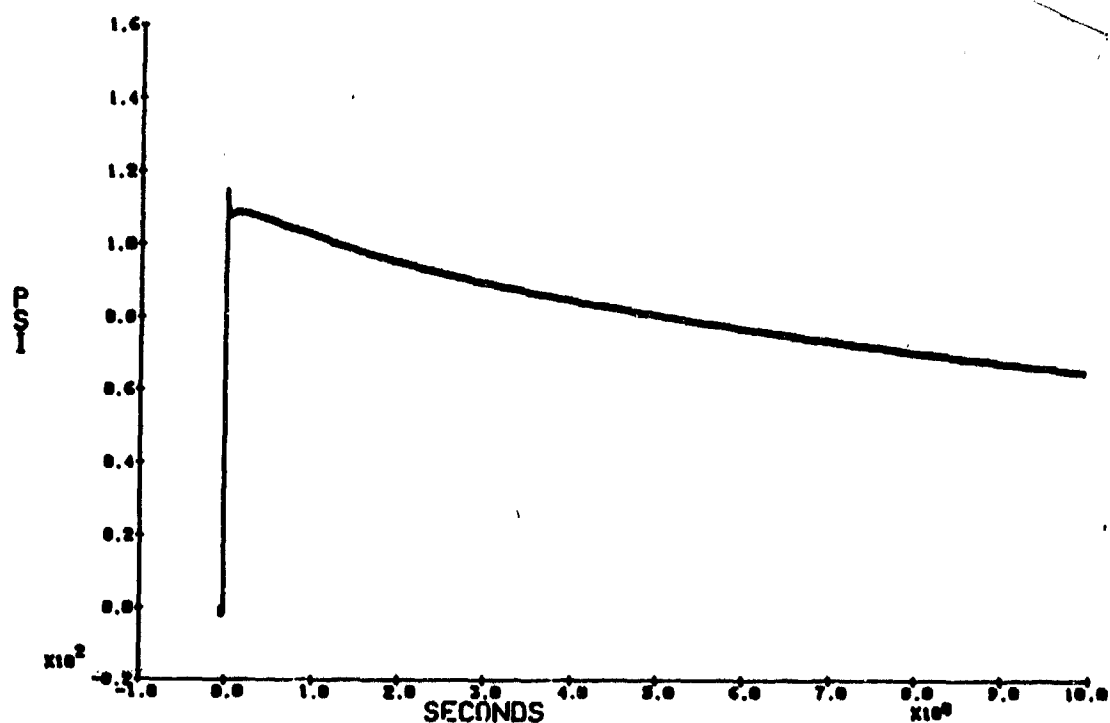


FIGURE 12. EXAMPLE PRESSURE MEASUREMENT RECORD. (TEST D7)

Table 4 shows a tabulation of the measured pressures from the records as identified in the example above. Examination of this data shows that the initial spike and maximum pressures fall into three groups corresponding to the inerted, short-time inerted, and live munitions. The live munition group includes both the ambient and preheated munitions mixed together. This grouping is shown graphically in Figure 13. The separation of these initial and maximum pressures may be taken as an indication of the fraction of the BZ-pyromix which reacted in the first few tenths of a second. Thus there appears to be no significant difference in the amount of BZ-pyromix reacted during shock wave passage (or detonation if it occurred) between the ambient temperature live munitions and the preheated live munitions.

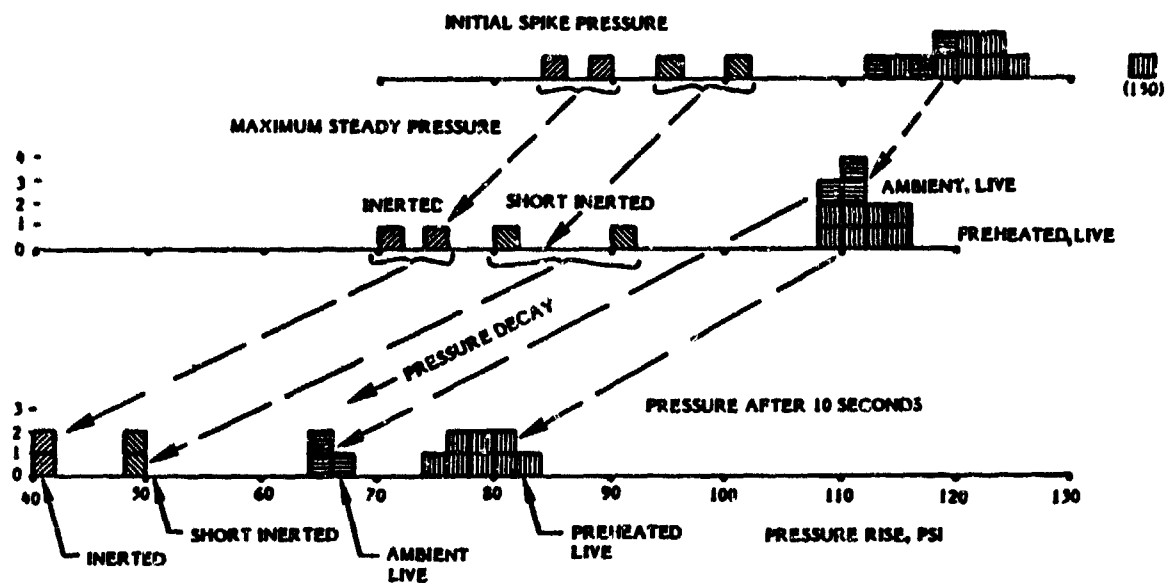


FIGURE 13. PRESSURE DISTRIBUTION HISTOGRAMS,
CLASS INTERVAL 2 PSI

During the decay of pressure in the first ten seconds, however, the ambient temperature and preheated tests divide into two groups as shown in Figure 13. Significantly less pressure decay occurs in the preheated group than in the ambient temperature group. This shows that the reaction of the BZ-pyromix which remained after initial shock wave passage in the preheated group was taking place faster during the first ten seconds than in the unheated group, but by a gradual and progressive process, not a detonation.

Table 4. Sphere Pressure Rise

Test No.	Initial Spike Pressure psi	Initial Steady Pressure psi	Maximum		After 10 Sec Pressure psi
			Pressure psi	Time sec	
D1	88.2	69.2	70.9	.16	40.1
D2	84.3	75.0	75.0	-	40.7
D3	94.5	80.0	80.0	-	48.8
D4	101.5	90.9	90.9	-	48.5
D5	118.0	108.5	108.5	-	64.2
D6	113.8	107.8	111.6	-	67.4
D7	116.1	108.8	110.0	.11	65.8
D10	119.5	110.4	113.4	.41	83.2
D11	121.4	113.5	114.7	.13	79.4
D12	122.8	112.2	114.5	.18	80.8
D13	123.3	110.8	111.6	.13	77.8
D14	125.4	108.4	109.1	.18	77.6
D15	150.0	109.8	109.8	-	80.1
D16	120.8	112.5	113.8	.07	78.0
D17	115.6	109.8	111.0	.07	74.8

4.4 Analysis of Results

The effects of pre-treatment inerting, short-time inerting, ambient or preheated condition on the shock travel distance at velocities greater than 2.0 mm/microsec was analyzed by comparing the average run distances and standard deviations between groups with different pre-treatments as shown in the two right hand columns of Table 3. The standard deviations of groups generally overlap the means of other groups. It appears that there is no significant difference in shock travel distance between different pre-treatments.

The effect of lot burn time on the shock travel distance at velocities greater than 2.0 mm/microsec observed was analyzed. Again no significant correlation was found.

The effect of pre-treatment on the pressures developed within the sphere and the subsequent pressure decay has been presented in Figure 13. Analysis for additional correlation of the pressure parameters shown in Table 4 with the measured burn times for each lot showed no correlation between burn time and any of the individual pressure parameters.

5. CONCLUSIONS

Based on the results obtained during these tests and their analysis, the following conclusions are drawn:

1. The BZ-pyromix contained in the M138 bomblet configuration is non-detonable.
2. The observed shock wave decay in the munitions from the C-4 donor charge was not affected by pre-treatment inerting by immersion in a water/wetting agent solution, nor by preheating to 80 C.
3. The observed shock wave decay agreed, within experimental error, with the observed shock wave decay in a previous test of an inert mockup munition.
4. No significant correlation exists between a tendency to react during passage of a high pressure shock wave and munition burn time.

ACKNOWLEDGEMENTS

This program was conducted under the able direction of the USATHAMA project manager for BZ demilitarization, Mr. Richard Roux, with assistance from Mr. Edward Meseke. Their support and insistence on the achievement of high technical standards are gratefully acknowledged. A large number of people contributed to the successful conduct of the detonability tests. The specialized apparatus used in these tests was designed, constructed and proof-tested at Battelle Columbus Laboratories prior to shipment to Pine Bluff Arsenal where the tests were conducted. The contributions of the following members of the Battelle staff are acknowledged in the areas noted.

Overall Program Management BZ Incinerator, Afterburner	Wayne E. Ballantyne Albert E. Weller David R. Hopper
Proof Tests of Blast Containment Sphere	William F. Schola
Installation at Pine Bluff Arsenal	David R. Hopper
Qualification of Potting Resins	Eugene J. Mezey
Construction of Detonation Probes	Harvey N. Ebersole
Operation of the Detonation Tests Data Acquisition System	Harvey N. Ebersole David W. Carpenter
Reduction of the Detonability Data	Harvey N. Ebersole

The test director at Pine Bluff Arsenal was Mr. James C. Stuart who had overall responsibility for the tests at Pine Bluff Arsenal. He was responsible for the igloo modifications including the ventilation and cooling systems, power and utilities supplies, the line for input of materials, and change-house for personnel. He arranged all logistic support and staffing for the tests, wrote the Standing Operating Procedures and secured local approvals for them, and personally supervised all the operations of the testing proper, including assurance of testing the correct munition lot numbers and other innumerable details. He was assisted by several members of the Pine Bluff Arsenal staff. The contributions of Mr. Huey Desoto in the area of electrical controls and instrumentation, and of Mr. Floyd Hickerson and Alvin Wooten in leading and directing the technicians who conducted the munition preparations and performed the testing inside the igloo are particularly acknowledged.

REFERENCES

1. Ballantyne, W. E., Zeidman, G. G., "Final System Concept Report for Demilitarizing the BZ Item/Munition Inventory", Contract DAAK11-78-C-0096 to the U.S. Army Toxic and Hazardous Materials Agency by Battelle Columbus Laboratories, April 24, 1980.
2. Gentner, Robert of ARRADCOM, Dover Site, reported of a meeting at USATHAMA HQ., Aberdeen Proving Ground, Maryland, February 28, 1979.
3. "Explosives Hazard Classification Procedures" Department of the Army Technical Bulletin DSAR 8220.1, May 19, 1967.
4. Weller, A. E., "Test Report on Incineration Detonation Studies", Contract DAAK-11-78-C-0096 to U.S. Army Toxic and Hazardous Materials Agency by Battelle Columbus Laboratories, June 30, 1981.
5. Trott, B. D. and White, J. J., III, "Design and Evaluation of An Experimental Multipurpose Blast Containment Chamber", NAVEODFAC Technical Report TR-196. Naval Explosive Ordnance Disposal Facility, Indian Head, Md., October, 1978 (AD B033 126b).
6. Trott, B.D. "Test Report for Containment Sphere Leak and Proof Tests", Contract DAAK11-78-C-0096 to U.S. Army Toxic and Hazardous Materials Agency by Battelle Columbus Laboratories, October 15, 1980.
7. Weller, A. E., et al, "Test Report on Non-Agent Tests of Incineration/Detonation Test Equipment", Contract DAAK-11-78-C-0096 to U.S. Army Toxic and Hazardous Materials Agency by Battelle Columbus Laboratories, January 22, 1981.

APPENDIX A

RESISTANCE PROBE DATA REDUCTION

APPENDIX A

Resistance Probe Data Reduction

The resistance probe circuit is shown in Figure B-1. It consists of the detonation probe supply circuit connected to the detonation probe and to the recording device. The constant current supply makes the output voltage to the recording device proportional to the resistance to ground. In operation, the switch is turned first to "operate" and the output current is adjusted to make the output voltage near the upper limit of the recording scale being used on the recording device to provide optimum resolution of recording. Once the current is adjusted, it is not further changed intentionally. However, in practice the current from the supply remained constant over short time periods, but drifted slowly upwards over longer time periods, such as the time between calibration measurements and shot time. To compensate for this drift, calibration measurements made before the test were adjusted at the time of the experiments with the aid of the pre-detonation baseline voltage measured from the actual detonation probe dynamic voltage record.

Three initial calibration voltage measurements were made at the recording device:

V_{ol} obtained with the switch in the "operate" position,

V_{cal} obtained with the switch in the "120 ohm cal" position,

and

V_{gl} obtained with the switch in the "short" position.

These three measurements were made over a short time period to insure against current drift in the constant current supply. The measurement of V_{ol} was repeated after measurement of V_{gl} . No change in V_{ol} assured that the initial measuring current I , had indeed remained constant. From Ohms' Law we wrote

$$V_{ol} = I_1 R_p \quad (1)$$

$$V_{cal} = I_1 (R_{sw} + R_{cal}) \quad (2)$$

$$V_{gl} = I_1 R_{sw} \quad (3)$$

where

R_p = is the total resistance in the probe circuit

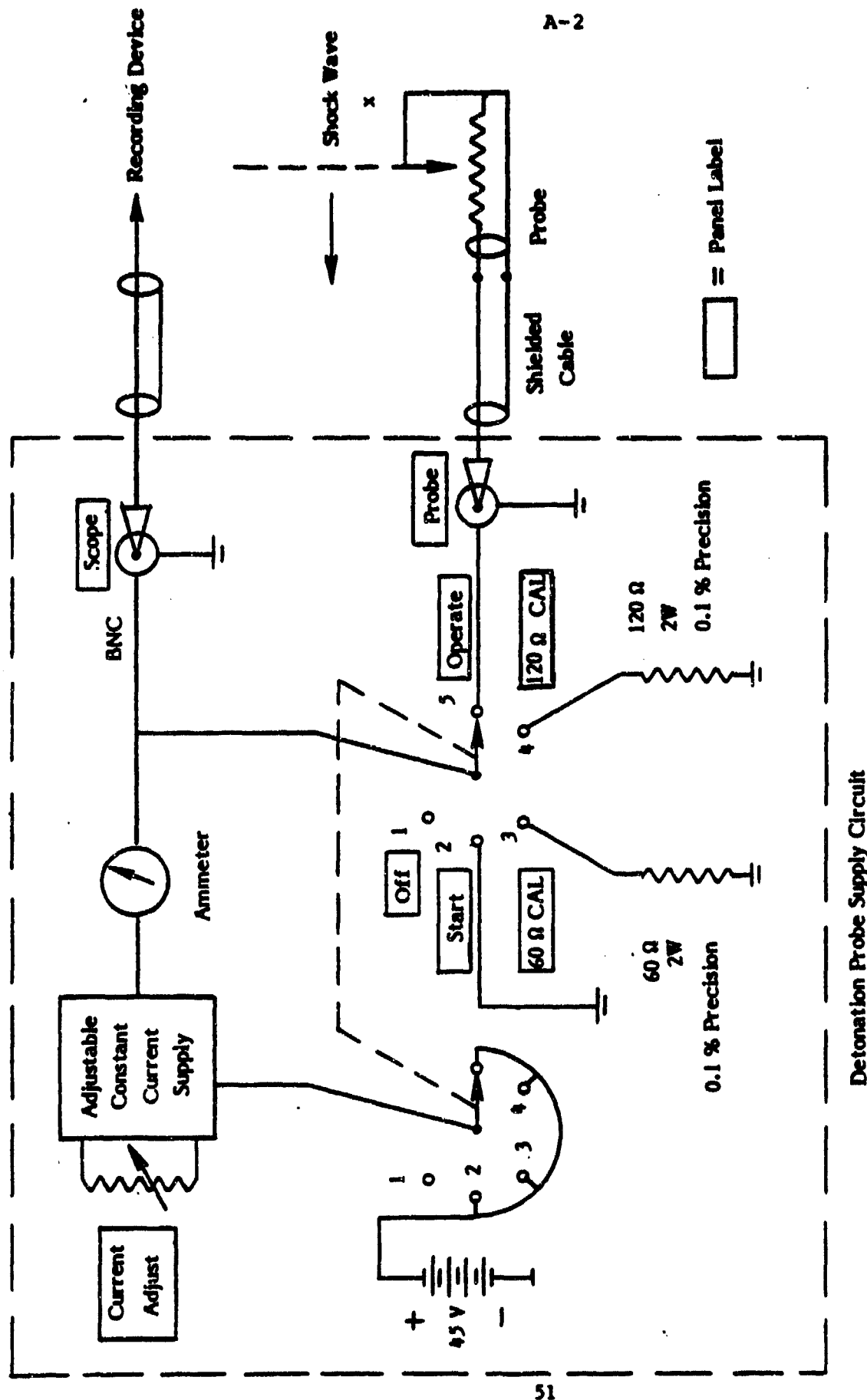


FIGURE A-1. DETONATION PROBE CIRCUIT

R_{sw} = resistance of the switch contacts and directly associated circuitry

R_{cal} = resistance of precision resistance = 120 Ω

By subtracting (3) from (2) the unknown switch contact resistance was eliminated, or at least errors from this source reduced, and an expression for the initial measuring current was obtained:

$$I_1 = (V_{cal} - V_{g1})/R_{cal} \quad (4)$$

After the shot was fired (switch in operate position), a measurement of the initial, predetonation baseline voltage, say V_{o2} yielded:

$$R_p = V_{o2}/I_2 \quad (5)$$

where I_2 = the measuring current at shot time

This expression for R_p was equated to the value of R_p from equation (1) yielding:

$$\frac{I_1}{I_2} = \frac{V_{o1}}{V_{o2}} \quad (6)$$

Finally the value of the total probe resistance is given by

$$R_p = R_{ld} + r_p (L - x) \quad (7)$$

where

R_{ld} is the resistance of the connecting lead wires to the probe

r_p is the specific resistance of the probe wire (in the present case

$r_p = 0.2892 \Omega/\text{mm}$ or $88.15 \Omega/\text{ft}$).

L is the total length of the probe resistance wire

and

x is the length of probe resistance shorted out by crushing of the surrounding tube by the shock wave pressure. This is taken as the shock wave position which is the value to be determined.

At shot time, V_{o2} from (5) and (7) is given by:

$$V_{o2} = I_2 (R_{ld} + r_p L) \quad (8)$$

and V_s the dynamic value of the signal voltage during the shot is given by

$$V_s = I_2 (R_{ld} + r_p (L-x)) \quad (9)$$

By subtracting V_s (9) from V_{o2} (8) the unknown probe lead resistance R_{id} and the probe total length were eliminated. The resultant expression solved for x :

$$x = (V_{o2} - V_s) / I_2 r_p. \quad (10)$$

The value for I_2 was found from equations (6) and (4) and substituted into (10) to yield the final expression for x in terms of known constants or measured quantities:

$$x = \frac{R_{cal} V_{o1} (V_{o2} - V_s)}{r_p V_{o2} (V_{cal 1} - V_{g1})}. \quad (11)$$

In practice, evaluation of (11) merely meant subtracting the time varying signal V_s from the constant V_{o2} and multiplying the difference by the experimentally derived constant for each experiment of $R_{cal} V_{o1} / r_p V_{o2} (V_{cal 1} - V_{g1})$. (12)

The indicated operations were carried out by the signal processing capability of the Smartscope.



AD P000428

HAZARDS CLASSIFICATION TESTING

OF

AMMONIUM PERCHLORATE

by

Joseph P. Caltagirone, ARRADCOM

Darl E. Westover, ARRADCOM

Fred L. McIntyre, Computer Science Corp.

ABSTRACT

Based upon laboratory test results, the West German representative to the UN Committee on the Transportation of Dangerous Goods has recommended that Ammonium Perchlorate(AP) of all particle sizes be classified as a Class 1.1 explosive. If this recommendation is adopted it will have a drastic effect on the transportation of ammonium perchlorate with commercial concerns and military agencies. Under current regulations, only AP with a particle size less than 45 microns is considered Class 1.1 (the latest DARCOM regulation specifies 15 microns or less). Above 45 microns, AP is classified as a 5.1 oxidizer. In order to resolve this difference, a plan for conducting UN Test Series 6 for packaged AP, 200 micron size in 30 gallon, 250 lb steel drums was developed in cooperation with the JANNAF Interagency Propulsion Committee and DARCOM Safety Office. This paper discusses the test plan, testing, results and recommendations.

FORWARDED PAGE BLANK-NOT FILMED

INTRODUCTION

Ammonium perchlorate (AP) is an oxidizer ingredient used in the manufacture of composite solid propellants. Under current UN regulation ammonium perchlorate with a particle size less than 45 microns is considered a Class 1.1 explosive (latest DARCOM reg specifies 15 microns or less). Above 45 microns, it is classified as a 5.1 oxidizer. The hazards classification of ammonium perchlorate UN No. 1442 (AP oxidizer) has recently been questioned by the UN Committee of Experts on the Transport of Dangerous Goods. If classified as a 1.1 explosive, it will have a drastic effect on shipping with commercial concerns and military agencies. To resolve this conflict, a series of tests was conducted in March 1982 in accordance with INTEREG, Transportation of Dangerous Goods, 1981 edition. These tests were managed by the Energetic Systems Process Division, Large Caliber Weapon Systems Lab, ARRADCOM and conducted at NASA National Space Technology Laboratories under the direction of the ARRADCOM Resident Operations Office (AROO). This paper summarizes the test plan, tests, results and recommendations. A more detailed account may be obtained from ARRADCOM Report No. ARLCD-CR-82026, "Hazards Testing of Ammonium Perchlorate," May 1982.

TEST MATERIAL

Ammonium perchlorate, nominal 200 micron size, manufactured by Kerr-McGee Chemical Corporation, was provided for testing. The package is a 113.6 l (30 gal) DOT 37A-350 20-gage steel drum with a bolted ring closure. The dimensions of the drum are 0.74m high by 0.49m diameter with 0.8mm thick walls. (Note: This is a heavier gage (20 vs 24) drum than required for U.S. shipment of this material. The material was packed inside the drum in two conductive polyethylene bags with approximately 4.5 kg (10 lb) of dessicant placed atop the ammonium perchlorate inside the inner bag. Gross weight of the drum and contents averaged 119.5 kg (264 lb).

The test plan called for sample analysis to verify particle size distribution and moisture content of each drum. Particle size distribution was determined in accordance with MIL-STD-286B and ASTM 300. Two samples from each drum were removed from the center by a standard core sampler. The 50 g sample was weighed and placed on a U.S. standard number 50 sieve. Number 80, 100, 120, 140, 200, 325 sieves and a catch pan were placed beneath. All sieves were inserted into a Tyler Model RX-21 portable sieve shaker for five minutes. The amount of material remaining on each sieve was weighed. After particle size analysis, the individual samples were recombined, weighed, then placed in a vacuum oven at 75°C (167°F) temperature for two hours at 29 inches vacuum. Each sample was reweighed and the weight loss recorded as the moisture content, which was specified as 0.007 percent.

TESTS

The tests required by INTEREG, Transportation of Dangerous Goods, 1981, for determining the hazards classification (Class 1.1, 1.2, 1.3, 1.4) are:

1. Test Series 6a: Three single package tests
2. Test Series 6b: Three stack tests (5 packages minimum)
3. Test Series 6c: One external fire test (5 packages minimum)

Single Package Test

The purpose of this test is to determine whether initiation or ignition in the package causes burning or explosion and whether burning or explosion propagates within the package; also, how the surroundings are affected.

Two series of single package tests were conducted three times each. For both, a drum of ammonium perchlorate was placed on a steel witness plate 0.81m X 0.81m X 12.7mm thick (2.67 ft X 2.67 ft X 0.5 in) at ground level. A Chromed/Alumel thermocouple was positioned inside the drum 25.4mm (1 in) above the ignition/initiation source. An additional thermocouple was fixed to the outside of the drum near the center. The drum was confined by 1m (3.28 ft) of sandbags in all directions to provide confinement as specified in the INTEREG. For the first series of 6a single package tests, an S94 squib with 56.7g (2 oz) of FFF black powder was placed in the center of the material as the ignition source. A typical test setup is shown in figure 1. The second series of 6a single package tests were conducted using a No. 8 blasting cap as an initiation source in place of the S94 squib and black powder ignition source.

An additional test, not specified in the INTEREG procedures, was conducted on an unconfined drum ignited by an S94 squib and 56.7g (2 oz) of black powder.

Stack Test

The purpose of this test is to determine whether and in what way burning or explosion in the stack propagates from one package to another and how the surroundings are endangered in this event.

It was planned to conduct the stack tests (6b) as shown in figure 2. Five drums would be placed on ground level with a witness plate under the donor drum which would be ignited by an S94 squib and 56.7g (2 oz) of black powder. Sandbags were to be placed around the entire stack 1m (3.28 ft) thick. Thermocouples would be placed in the donor drum as in the single package tests.

However, since there was no explosive reaction in the 6a single package tests, the series 6b stack tests were deleted per paragraph 4.5.5 of the INTEREG.

External Fire Test

The objective of this test series is to determine how the packages in the stack behave when involved in an external fire and whether and in what way the surroundings are endangered by blast waves, heat radiation, and/or fragment projection.

One test was conducted as required. Five drums, each containing 113.4 kg (250 lb) of ammonium perchlorate, were placed on a steel crib 1m (3.28 ft) above the ground surface as shown in figure 3. They were banded together with two steel bands to maintain drum contact during the test. Air dried lumber, 50.8mm by 101.6mm X 1.5m (2 in by 4 in by 59 in) was placed beneath the crib in a lattice with a lateral separation of 101.6mm (4 in). The entire crib was surrounded by the same size lumber to a minimum thickness of 508mm (20 in). The entire mass was drenched with 53 l (14 gal) of diesel fuel/gasoline mixture (9/1 ratio) and ignited remotely by two electric matches each with 56.7g (2 oz) of FFF black powder 180° apart at the base.

INSTRUMENTATION

The test setup and instrumentation are shown in figure 4. Instrumentation consisted of: pressure transducers, thermocouples, heat flux gages, motion picture cameras, fiducial markers, and fragment assessor panels for the external fire test only.

Pressure transducers in a 90° array were used to measure potential incident overpressure resulting from an explosion or partial explosion. Twelve were used for the single package tests from 1.19 to 17.85 m/kg^{1/3} (3 to 45 ft/lb^{1/3}) and eight for the external fire test from 1.98 to 17.85 m/kg^{1/3} (5 to 45 ft/lb^{1/3}).

Temperature measurements in the test material using 22 gage Chromel/Alumel thermocouples were obtained for the single package tests only. One thermocouple was attached to the outside center of the drum and the other was in the center 25.4mm (1 in) above the ignitor/initiator.

Thermal radiation data establish the intensity, duration, and spatial characteristics as functions of material, size of combustion zone and burning rate to determine the distance at which a value of 0.3 calories per square centimeter per second from the material is obtained.

Motion picture coverage consisted of three cameras operating at 500 frames per second (fps) and one at 24 fps. Locations of the camera are shown in figure 4. A video recorder was also used to tape the events. Color still photographs were taken before and after each test showing typical setup and post-test results. Standard meteorological data were recorded for each test.

Fragment assessor panels (fiberboard) banded to make a pack 3.66mm X 1.22m X 2.44m high (12 ft X 4 ft X 8 ft high) as shown in figure 3 were placed as shown in figure 5. The purpose of these is to make an assessment of the number of projections emanating from the material in the event of an explosion. This was done only for the external fire test as required by the INTEREG.

RESULTS

Data Analysis

Data analysis for end-item stores is based upon the 'Go/No-Go' results of the prescribed tests as outlined in the INTEREG, Chapter 4 and TB700-2, Department of Defense Explosives Hazard Classification Procedure.

The flowchart for interpretation of test series 6 is shown in figure 6.

Discussion

Particle size analyses were in general agreement with the specified data. Any differences may be attributable to transportation or material handling where additional shearing or grinding occurred. The sampling technique may also account for the minor differences. Moisture analyses were somewhat different from the specified data. The differences are attributable to sampling techniques as well as the humidity difference between the test site (high relative humidity) and the processing location.

A total of six type 6a, single package tests were conducted with a minimum of 1m (3.28 ft) of sandbag confinement. In the first three tests an ignition source (S94 squib and black powder) was used, while in the second three tests an initiation source (No. 8 blasting cap) was used. Figures 7 and 8 show the typical test setup. Figure 7 shows the drum before totally confined with sandbags. Figure 8 shows total confinement before ignition/initiation. The results of all six tests were similar. Upon ignition/initiation, white smoke was visible within five seconds; a red/orange smoke was visible near the lid of the drum after one minute. Within 18 to 20 minutes there was an increase of red/orange smoke lasting 30 to 45 seconds. The average total thermal decomposition time for each drum was 27 minutes.

There were no overpressures detected in any of the single package tests. There was no fragmentation from the drums. Heat flux values were several orders of magnitude less than the $0.3 \text{ cal}/(\text{cm}^2\text{s})$ at or beyond 30.48m (100 ft) radius that is being considered for Division 1.4 material by the UN Committee of Experts on the Transportation of Dangerous Goods. Figures 9 and 10 show typical post-test results for the confined single package tests. The drum was discolored from the heat but was not ruptured, split, fragmented or even significantly deformed. There was no deformation of the witness plate.

Results of the single package test without confinement (figure 11) were different from the previous tests. The lid of the drum relieved. None of the ammonium perchlorate ignited. Some material was spilled on the ground as the result of ignition.

A summary of all single package tests is contained in Table 1.

The external fire test configuration with all lumber in place is shown in figure 12. Following ignition of the lumber and visual observation of a sustained fire, the lids of individual drums began to relieve starting at 42 seconds for the first drum following ignition to 84 seconds for the fifth. The ammonium perchlorate burned for 5 minutes when the majority of the material had been consumed. The reaction was more intense for a 30 second period during the 5 minutes. The wood fire burned substantially longer than the 30 minutes required by the test procedures. There was no explosion, no rupture, splitting, or fragmenting of the drums, and the fire effects were minimal. The post-test result is shown in figure 13. Table 2 summarizes the external fire test.

CONCLUSIONS

Based upon test results of the single package and external fire tests and interpretation of results as outlined in figure 6 (figure 4.3 of the INTEREG) and paragraph 6.5 of the Dod Explosives Hazard Classification Procedure, TB700-2, there are no indications that ammonium perchlorate with nominal particle size of 200 microns exhibited explosive behavior. Specifically:

1. There was no explosion, no overpressure detected, no rupture, splitting, or fragmenting of the drums, and no radiant heat hazard, during the 6a, single package tests.
2. There was no mass detonation, no fragmentation, no mass fire effect, and little or no damage to the shipping drums as a result of the 6c, external fire test.
3. Ammonium perchlorate did not react when primed by a S94 squib and 56.7g (2 oz) of FFF black powder without confinement.
4. There was no explosive hazard exhibited during any of the tests performed as required by the INTEREG.

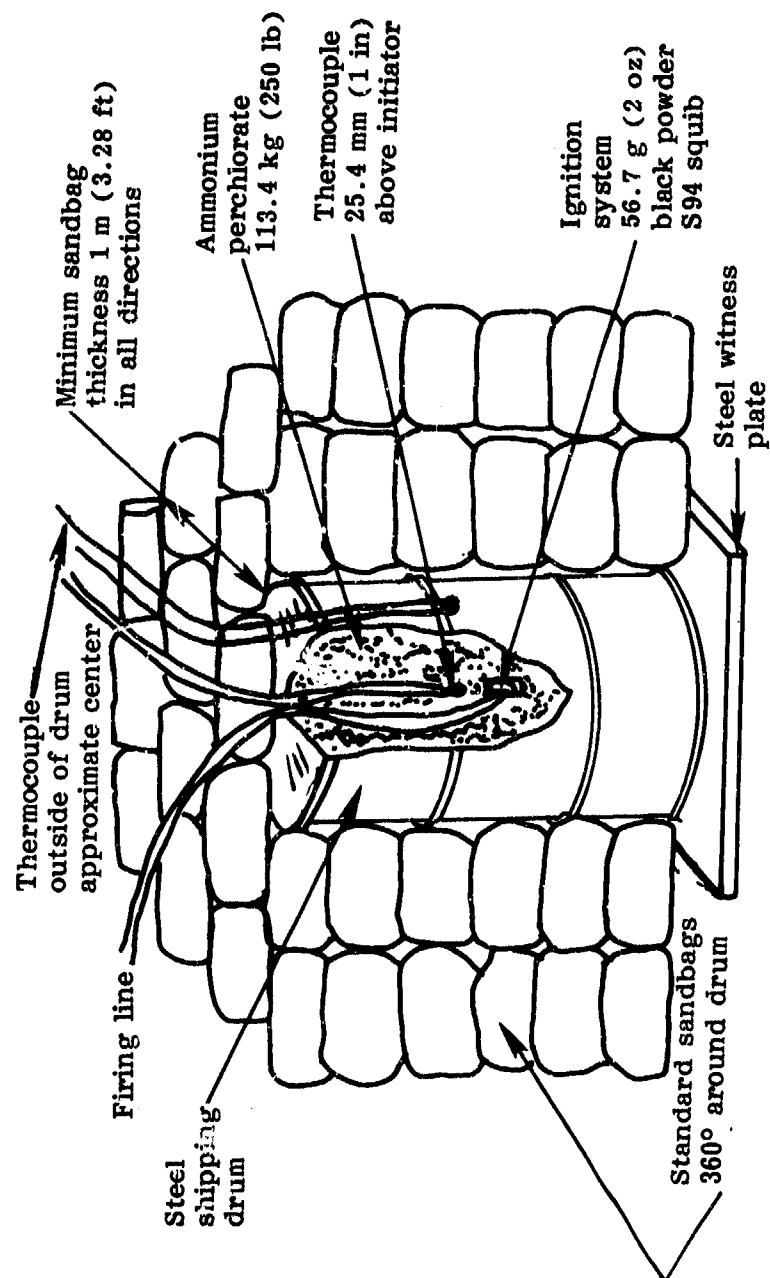


Figure 1. Single Package Test Configuration
(S94 squib with BP)

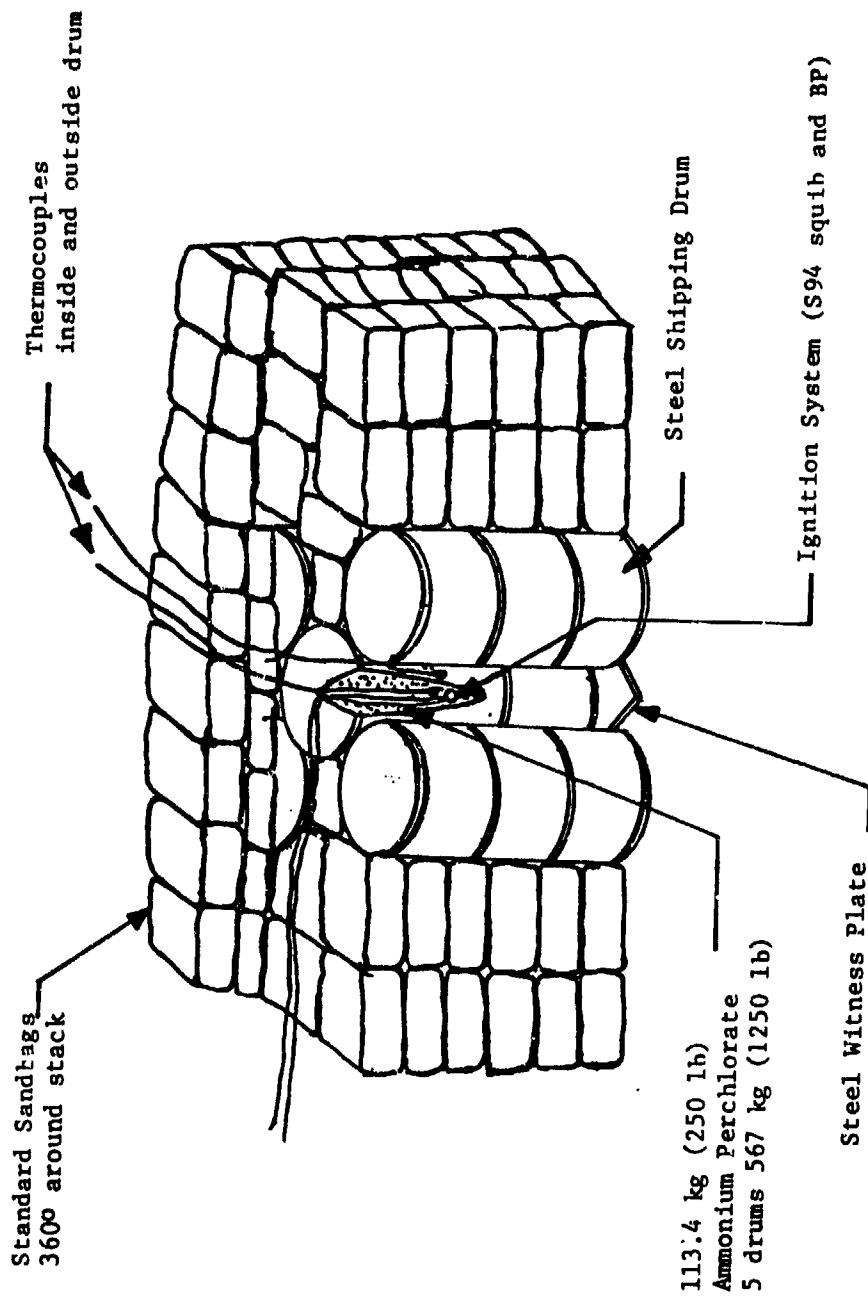


Figure 2. Stack Test Configuration

Fragment Assessor Panels
(3 locations, see fig. 5)

113.4 kg (250 lb)
Ammonium perchlorate
5 drums 567 kg (1250 lb)

Steel bands

METER

Air dried wood
50.8 by 101.6 mm
(2 by 4 in)
with lateral
distance between
laths 101.6 mm (4 in)

Drum support
frames (steel)

Wood shall be
piled beneath and
360° around the
stack to a minimum
of 508 mm (20 in)

Figure 3. External Fire Test Setup

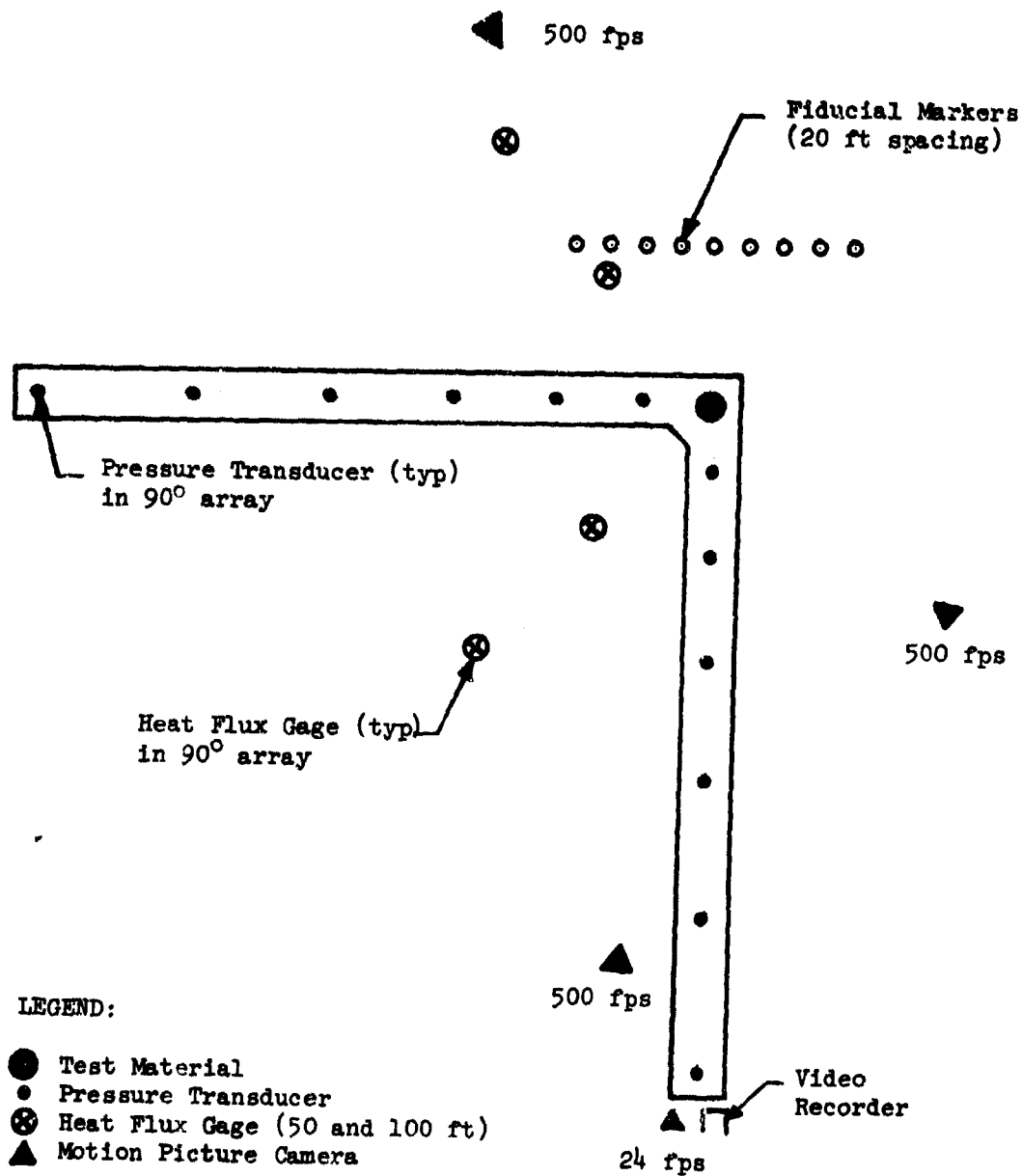


Figure 4. Typical Instrumentation Setup

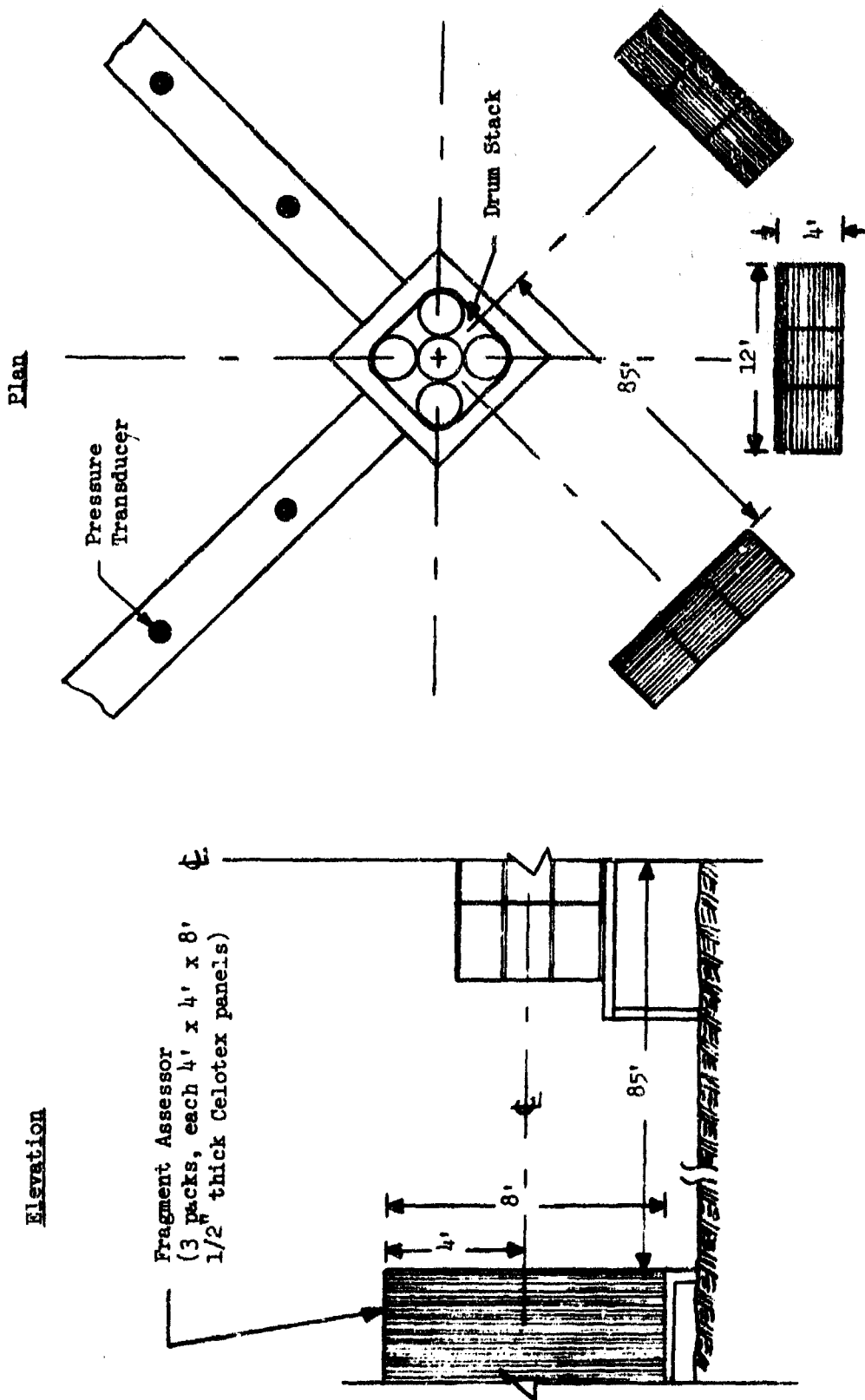


Figure 5. Location of Fragment Assessor Panels

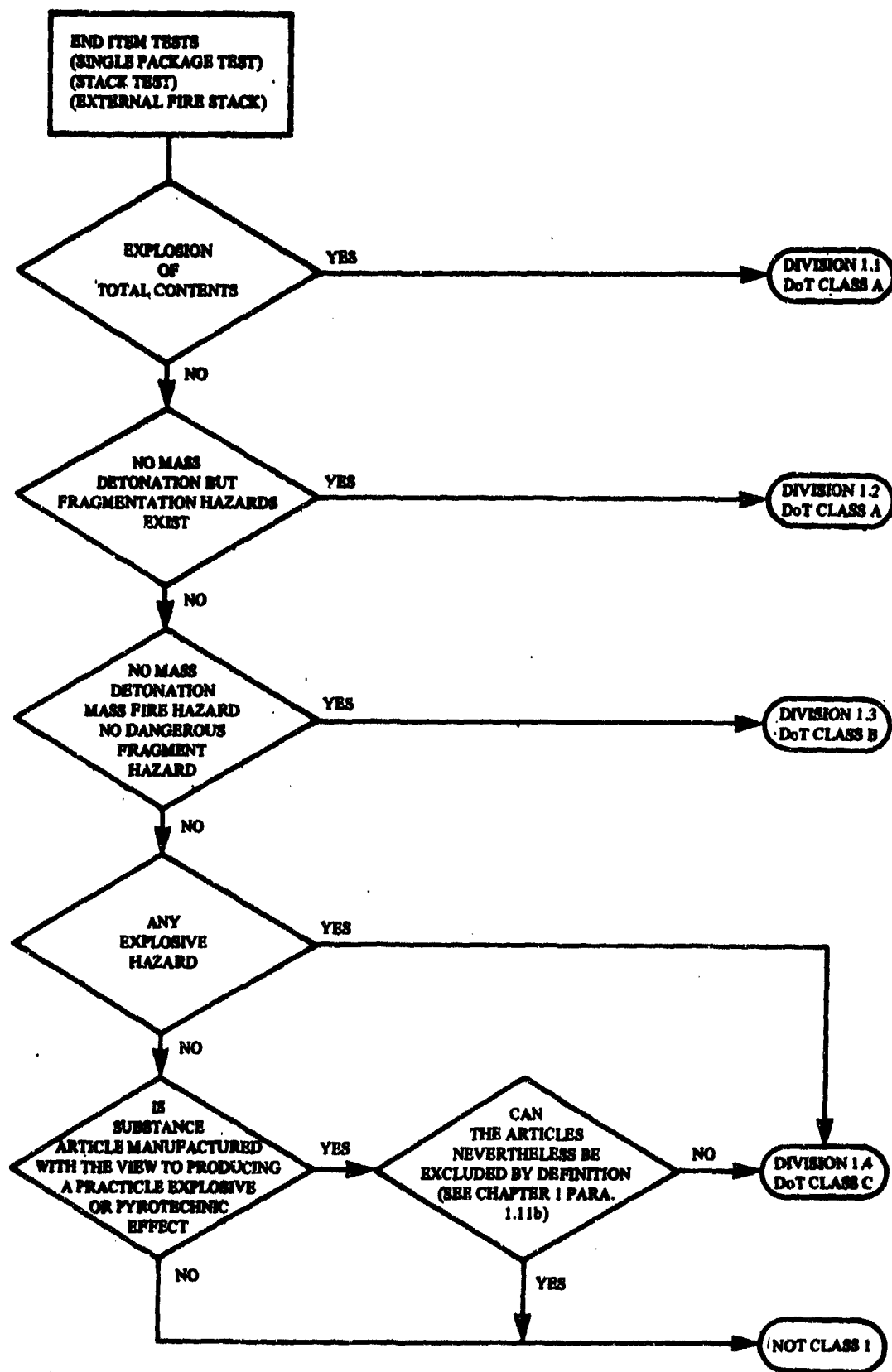


Figure 6. Interpretation of Test Results

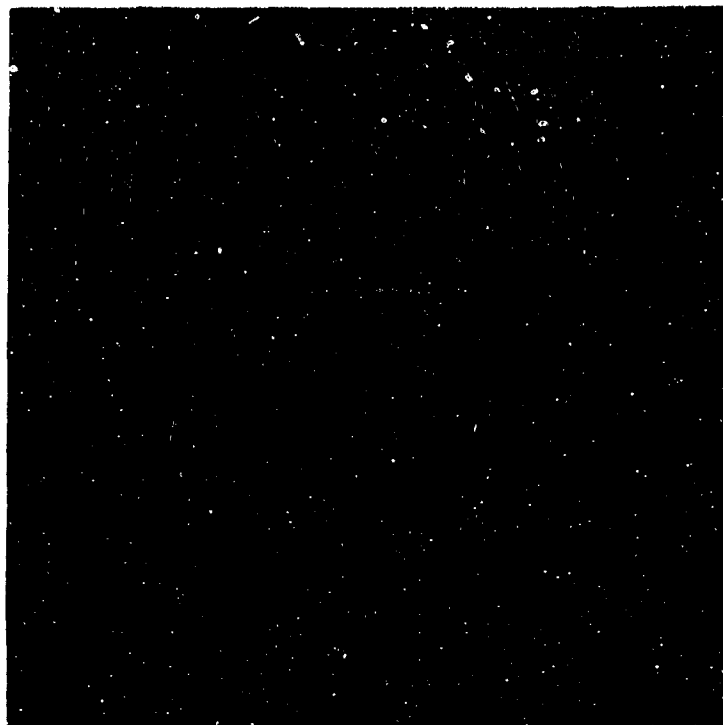


Figure 7. Single Package Setup Before Confinement



Figure 8. Single Package Setup with Total Confinement



Figure 9. Typical Single Package Results Showing Burned Sandbags



Figure 10. Typical Single Package Results Showing Drum



Figure 11. Results of Unconfined Single Package Test

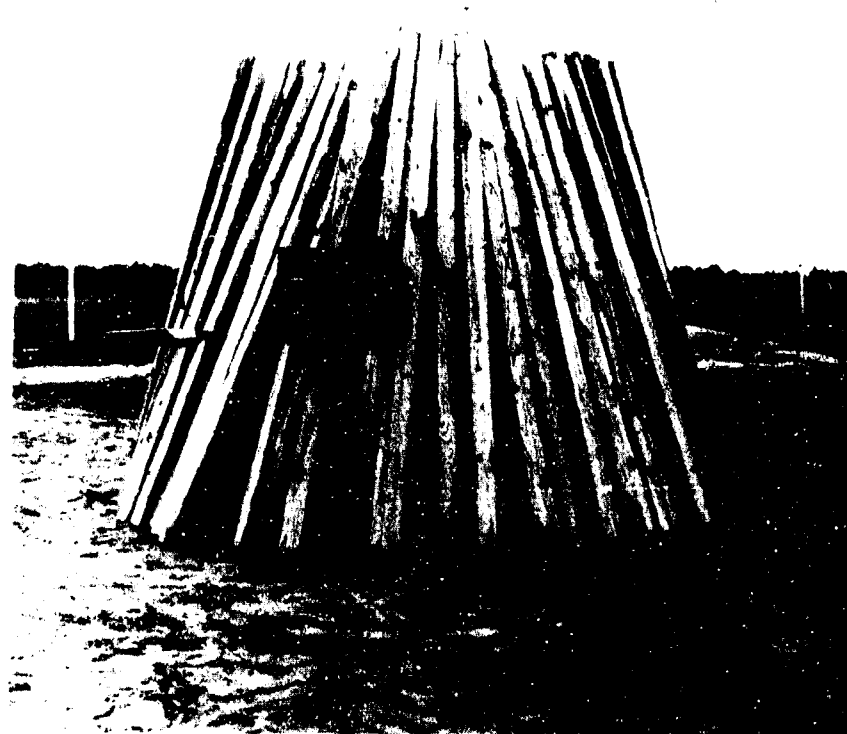


Figure 12. External Fire Test Setup



Figure 13. External Fire Test Results

Material	Ignition/initiation method	Confinement	Results
113.4 kg Ammonium perchlorate in steel drums	S94 squib and 56.7 g black powder	1 m (3.28 ft) Sand bags	No explosion, drum body intact, no explosive hazard
113.4 kg Ammonium perchlorate in steel drums	S94 squib and 56.7 g black powder	1 m (3.28 ft) Sand bags	No explosion, drum body intact, no explosive hazard
113.4 kg Ammonium perchlorate in steel drums	S94 squib and 56.7 g black powder	1 m (3.28 ft) Sand bags	No explosion, drum body intact, no explosive hazard
113.4 kg Ammonium perchlorate in steel drums	Number 8 blasting cap	1 m (3.28 ft) Sand bags	No explosion, drum body intact, no explosive hazard
113.4 kg Ammonium perchlorate in steel drums	Number 8 blasting cap	1 m (3.28 ft) Sand bags	No explosion, drum body intact, no explosive hazard
113.4 kg Ammonium perchlorate in steel drums	Number 8 blasting cap	1 m (3.28 ft) Sand bags	No explosion, drum body intact, no explosive hazard
113.4 kg Ammonium perchlorate in steel drums	S94 squib and 56.7 g black powder	None	No ignition of material, lid relieved, no fragmentation, no explosive hazard

Table 1. Single Package Test Results

Material	Ignition method	Confinement	Results
5 each 113.4 kg ammonium perchlorate in steel drums 567 kg (1250 lb) total weight	2 each electric matches with 56.7 g black powder 180° apart at base of steel crib	Steel banded	No explosion, drum body intact, no explosive hazard

Table 2. External Fire Test Results

AD P000429

CLASSIFICATION AND IN-PROCESS CLASSIFICATION TESTING -
WHERE DO WE GO FROM HERE?

by

F. L. McINTYRE
COMPUTER SCIENCES CORPORATION
NASA NATIONAL SPACE TECHNOLOGY LABORATORIES
NSTL STATION, MS 39529

ABSTRACT

In 1974, an agreement was reached between DoD and NATO to standardize Hazards Classification Procedures and adopt the UN Classification System. Implementation by DoD was scheduled for 1976. Actual adoption occurred in 1978; however, TB 700-2 was not released until March 1982.

Basically this procedure does not change the existing Bulk Interim Qualification Tests which still include: Card Gap; Detonation; Ignition and Unconfined Burning; Impact and Thermal Stability Tests. End-item classification testing changed significantly and includes: Single Package, Stack Test and External Fire Stack Test. Additional constraints on End-item Munition Testing Require Heat Flux and Firebrand Data for 1.3 and 1.4 materials and TNT Equivalency and Fragmentation Assessment for 1.1 and 1.2 class munitions.

This new procedure was instantly open to criticism. Card Gap and Impact Sensitivity tests are too severe for most materials, particularly small arms propellants and pyrotechnics. The Ignition and Unconfined Burning Test is not applicable to pyrotechnics. End-item tests are more costly in terms of the amount of munitions required as well as instrumentation requirements (Heat Flux and TNT Equivalency). Finally in-process classification was excluded.

I hope to briefly discuss the new Hazards Classification Procedures, the need for In-process Classification, and Pyrotechnic Test Procedures proposed by the Pyrotechnic Committee at the Second International Conference on Standardization of Safety and Performance Tests for Energetic Materials. It is impossible to cover all in great detail - rather, my intention is to provoke thought and, possibly, some action.

INTRODUCTION

An end-item has been produced for several years and although a different type of liner was substituted for the existing one, there was no change in the formulation. In another instance the granulation size of the oxidizer was changed; the binder of another formulation was changed; the fuel/oxidizer ratio of a given mixture was changed by two percent, and finally, there was an improvement in packaging technique for a particular end-item.

All of the above scenarios have one thing in common. These seemingly subtle changes constitute a new or improved end-item that requires reclassification for transportation and storage. The classification testing would be performed in accordance with the DoD Explosives Hazard Classification Procedure TB 700-2, March 1981⁽¹⁾.

However, none of the above scenarios or gross changes of any kind would affect classification during the manufacturing process. Manufacturing processes are exempt from classification unless the materials are transported by public conveyance. Generally, during manufacturing, all bulk mixtures are considered as 1.1 explosives until the mixture is consolidated into an end-item. At such time, the classification for that particular end-item would prevail.

BACKGROUND

Classification of hazardous materials is the systematic arrangement of such materials into groups or categories according to established safety criteria. This is accomplished by subjecting the specimen to standardized initiating influences (Figure 1). The output reactions being observed as either mass detonation or a fire hazard are then used to determine into which classification the specimen will be categorized in order that it may be transported and/or stored within acceptable safety limits.

Since 1967, the prescribed authority for determining hazards classification of explosives (pyrotechnics are defined as explosives), propellants, and end-items was the U.S. Army Technical Bulletin 700-2, NAVORDINST 8020.3 TO 11A-1-47⁽²⁾. The prescribed initiating influences for bulk materials were

limited to the selected tests such as Card Gap, Detonation, Ignition and Unconfined Burning, Impact Sensitivity, and Thermal Stability Tests. The initiating influences for end-items were limited to Detonation Test "A", Detonation Test "B", and External Heat Test "C".

In 1974, an agreement was reached between DoD Components and NATO. A new document was to be written and published as early as 1976 that would incorporate the United Nations Classification System and incorporate similar tests as outlined in the Transport of Dangerous Goods NATO INTEREG ST/SG/AC.10/1/⁽³⁾. The final version of this document, The DoD Explosives Hazard Classification Procedures, was published March 1982⁽¹⁾.

During this period, a significant amount of research and testing was devoted to developing In-process Hazards Classification Procedures. A NATO Committee was established to standardize test procedures. ARRADCOM, under the auspices of Single Service Management for the Manufacture of Munitions, proposed in-process classification to reduce the number of incident/accidents associated with manufacturing. In 1980, a safety committee also established the need for In-process Hazards Classification and Identification. These concepts and studies have met considerable resistance and basically have remained ignored since their inception.

DISCUSSION

Changes in the new DoD Explosives Hazard Classification Procedures deal with terminology, adaptation of the UN Classification System and new End-item Classification requirements. There is a distinction between bulk and end-item classification; bulk material testing is referred to as interim qualification and end-item testing as classification. Figure 2 shows the interpretation for interim qualification. Other significant changes deal primarily with end item testing.

End-item testing has changed significantly. Three types of tests are conducted: Single Package Test; Stack Test; and External Fire Stack Test. The number of tests per configuration have been reduced from five to three

for the Single Package and Stack Test versus five each tests for the Detonation Tests "A" and "B" configurations. However, the Stack Test now requires five items versus two for the Detonation "B" test. Five items are also required for the External Fire Stack Test versus two to six for the External Heat Test "C". Another major change for pyrotechnic end-items now requires confinement ranging from a minimum of 0.5 m (1.64 ft) to a maximum of 1 m (3.28 ft) dependent upon the size of the external packages.

Other changes require that radiant flux, firebrand, and fragment density be reported for division 1.3 and 1.4 materials. TNT equivalency and fragmentation assessments are required for divisions 1.1 and 1.2 materials. Interpretation of the end-item results is shown in Figure 3.

Criticisms came from several areas. End-item tests were costly, as instrumentation for heat flux and TNT equivalency is expensive. Fragmentation assessment was costly and time-consuming. Confinement (up to 1 m (3.28 ft)) was too severe. Bulk Interim Qualification tests remained unchanged. These tests were either too severe for small arms propellants and pyrotechnics, or they did not apply. Other participants were concerned that their proposed tests had not been included. As a result In-process Classification was still excluded.

Such criticisms are unwarranted, as the critics fail to grasp the intent of the classification procedures. TB700-2 is used to determine the effects of accidental initiation and to set parameters to protect property and personnel. This is accomplished by conducting a limited number of tests representing "worst case" situations; then reporting the results, at the same time providing for an acceptable safety margin. It is not intended that these tests replace parametric, stability, sensitivity and performance (output) tests which are obtained separately, or in conjunction with, and included in component data safety statements. The component data safety statements and hazards classification results can ultimately be combined to represent the hazards associated with handling, transporting, storage and use of a particular item. The existing classification procedure meets this objective. Based upon a survey of incident/accidents⁽⁴⁾, there is no known incident/accident attributed to

the item's being categorized in the wrong division. The opposite is true when classification is assigned by analogy without testing to support the assigned hazards division.

The same incident/accident analysis also indicated that the majority of all incidents were associated with manufacturing. This is understandable because the manufacturing process is in a constant state of change and the amount of data available concerning in-process hazards are not readily available. The next logical step in the classification process would then be to screen or classify the materials during various stages of manufacturing. Potential problems would be identified and prevented. An initial attempt at in-process classification was developed by Pape and Napadensky⁽⁵⁾ whose efforts concentrated on propellants and explosives. The study was based upon several factors including: Historical Accident Survey; Engineering Analysis; Survey of Existing Test Methods; Definition of the Classification Procedure Structure; Selection of Candidate Tests; and Validation and Finalization of the Proposed Tests Procedures. Their scheme is illustrated in Figure 4. The potential of the study represents a quantum step forward in reducing potential mishaps during the manufacturing process.

In 1977 and 1979, the International Conference on the Standardization of Safety and Performance Tests for Energetic Materials^(6,7), through several international agreements, strove to develop a document on the principles and methodology for the acceptability of energetic materials for military use. This manual makes possible the international and interservice acceptance of qualification data obtained by individual services and industrial laboratories. The Pyrotechnics Subcommittee established at the second conference⁽⁷⁾ recommended a series of tests applicable to pyrotechnic (Table 1) including mandatory and prescribed tests. The submissions were accepted without prejudice with the only stipulation being that sufficient information to understand and duplicate the test results be submitted. It was also noted that additional changes could be submitted when better procedures were developed. The mandatory test methods submitted included: Hygroscopicity, Heat of Combustion, TNT Equivalency, Dust Explosion, Linear Burn Rate and Pressure Time, all of which have standard procedures. Additional mandatory tests

which do not have a standard developed procedure include: Ignitibility Burning Rate (Flares), Candle Power, Efficiency, IR Calibration, Chromaticity, High Pressure, Heat Flux and Chemiluminescence. In the case of an illuminant output measurement it was felt that no standard test could be developed until the instrumentation could be standardized. None of these proposed tests were considered for incorporation to the TB700-2 or ST/SG/AC.10/1/Rev 1 NATO Transport of Dangerous Goods ⁽³⁾.

The cursory synopsis of changes in test methods during the past decade will have a significant impact on the pyrotechnic community. Generally pyrotechnics are grouped under the broad term of "explosives." Classification tests are now more rigorous due to confinement and the slightest change in the formulation of a given mixture would require reclassification. The accomplishments of Pape and Napadinsky's study on in-process classification and the efforts of the pyrotechnic subcommittee at the Second International Conference of the Standardization of Safety and Performance Tests for Energetic Materials are basically unknown. Probably the most serious result of this is the fact that the formation of the International Pyrotechnic Society is still a well kept secret.

It is imperative that we in pyrotechnics adopt some positive action to bring our plight to the forefront. Such steps are beginning to surface. McDonald, Robinson and Johnson ⁽⁸⁾ have proposed in-process classification for pyrotechnics. They have also proposed an in-process hazards identification scheme. The identification scheme has considerable merit. Logically, it follows that we should consider in-process classification as a means of reducing incidents during manufacturing. This can only be accomplished when a united group clamor for changes. In discussing in-process classification with various DoD safety components, all indicate a need for it, but each is waiting for someone else to take the initiative. In-process classification would be welcomed when and if such techniques were validated. The initiative is ours.

If we are to have any input into the Allied Ordinance Publication ⁽⁹⁾ concerning pyrotechnic performance testing, we should take advantage of the test methods proposed by the subcommittee at the Second Standardization Conference ⁽⁷⁾ or substitute updated more germane test methods. A possible

update could indicate friction testing using the Rotary Friction Device Standardized by Naval Weapons Support Center. Another area would be to validate the 20 liter and 1 m³ dust chambers and substitute these procedures for the Hartmann Test. Possibilities are limitless.

CONCLUSIONS

1. We have a new updated DoD Explosives Hazard Classification Procedure that we must take the time to understand and use as it was intended. It will stand the test of time.
2. In-process classification is feasible and some form of in-process classification should be validated.
3. In-process classification techniques demonstrate the potential to reduce manufacturing incidents.
4. Through international agreements it is possible to use, validate, or submit standardized test methods applicable to the pyrotechnic community that allow for international and interservice acceptance.
5. Cognizant DoD safety representatives understand the need for in-process classification but they are waiting for others to take the initiative.
6. The initiative is ours.

REFERENCES

1. Department of Defense Explosive Hazard Classification Procedures, Army Technical Bulletin TB700-2, NAVSEAINST 8020.3, TO 11A-1-47, DLAR 8220.1 March 1981
2. Department of the Army Technical Bulletin TB700-2, NAVORDINST 8020.3, TO 11-A-47 DSAR 8220.1, 19 May 1967
3. Transport of Dangerous Goods NATO INTEREG ST/SG/AC.10/1/, December 1980 Addendum 3 Annex 4
4. McIntyre, F. L. Edgewood Arsenal Contractor Report EM-CR-76001-EA-5711 Incident/Accident Survey (1950-1974), December 1975
5. Napadensky, Hyla; Pape, Ronald; Recommended Hazard Classification Procedures for In-process Propellant and Explosive Material. U.S. Army ARRADCOM Large Caliber Weapons System Laboratory, Dover, New Jersey September 1980
6. L. Avrami, H. J. Matsuguma, R. F. Walker (Editors), "Proceedings of the Conference on the Standardization of the Safety and Performance Tests for Energetic Materials - Volume 1" ARRADCOM Special Publication ARLCD-SP-77004, U.S. Army, Army Armament Research and Development Command, Dover, NJ, September 1977 (AD-E400-004)
7. R. F. Walker, H. S. Matsuguma, L. Avrami (Editors), Minutes of the Second International Conference on the Standardization of Safety and Performance Tests for Energetic Materials, January 1980, Held at ARRADCOM, Dover, New Jersey, 15-19 October 1979
8. McDonald, J. P.; Johnson, D. M.; and Robinson, C. O., A System For In-process Hazards Classification and Identification for Pyrotechnic Materials, Presented at ADPA Pyrotechnics and Explosives Meeting at Livermore National Laboratories, CA. November 4-5, 1981.
9. Allied Ordnance Publication Number 7.

Table 1. Proposed Pyrotechnic Standardized Test Methods

Test Requirement	Status	Typical Test Method
Hygroscopicity	Mandatory All Mixtures	U.K. MOAD Method 303 US EA4D01 Final Report
Heat of Combustion	Mandatory All Mixtures	MIL-STD-268-B UK/Performance/Pyrotechnics-2
TNT Equivalency	Mandatory All Mixtures	TB 700-2 UK To Be Written Up
Ignitability	Mandatory All Mixtures	Radiation Pulse Test UK Bickford Fuze Test
Dust Explosion	Mandatory Mixtures and Constituents	Harmann, 1 m ³ Dr Passman, Holland 20 liter Dr Passman, Holland
Linear Burn Rate	Mandatory, Delays Only	UK/Pyrotechnic Performance/1 ARRADCOM Procedure, NSWC US Navy Procedure
Burning Rate	Mandatory, Lined Candle & Bare Grain	No Standard Test Method Submitted
Candle Power (CANDELA)	Mandatory, Photoflash and Illuminants	UK Performance/Pyrotechnic/4
Efficiency (Candle/Sec-kg)	Mandatory, Photoflash and Illuminants	UK Performance/Pyrotechnic/4
Chromaticity	Mandatory, Colored Flares	No Standard Test Method Submitted
Chemiluminescence	Mandatory Illuminants	No Standard Test Method Submitted
IR Calibration	Mandatory IR Items	UK Performance/Pyrotechnics/5
KTA-8	Mandatory for Smoke	
Pressure/Time	Mandatory for Explosion Charges	D. Dillehay 5th IPS
Spin	Mandatory (TRACER)	Valcartier, Canada Test Method Frankford Arsenal Spin Test USA
High Pressure Vessel	Mandatory (TRACER)	Gun Breech Simulator UK Valcartier, Canada Test Method
Heat Flux	Desirable for Incendiaries	TB 700-2
Bullet Impact	Desirable	Method 107 US EA4D01 Final Report

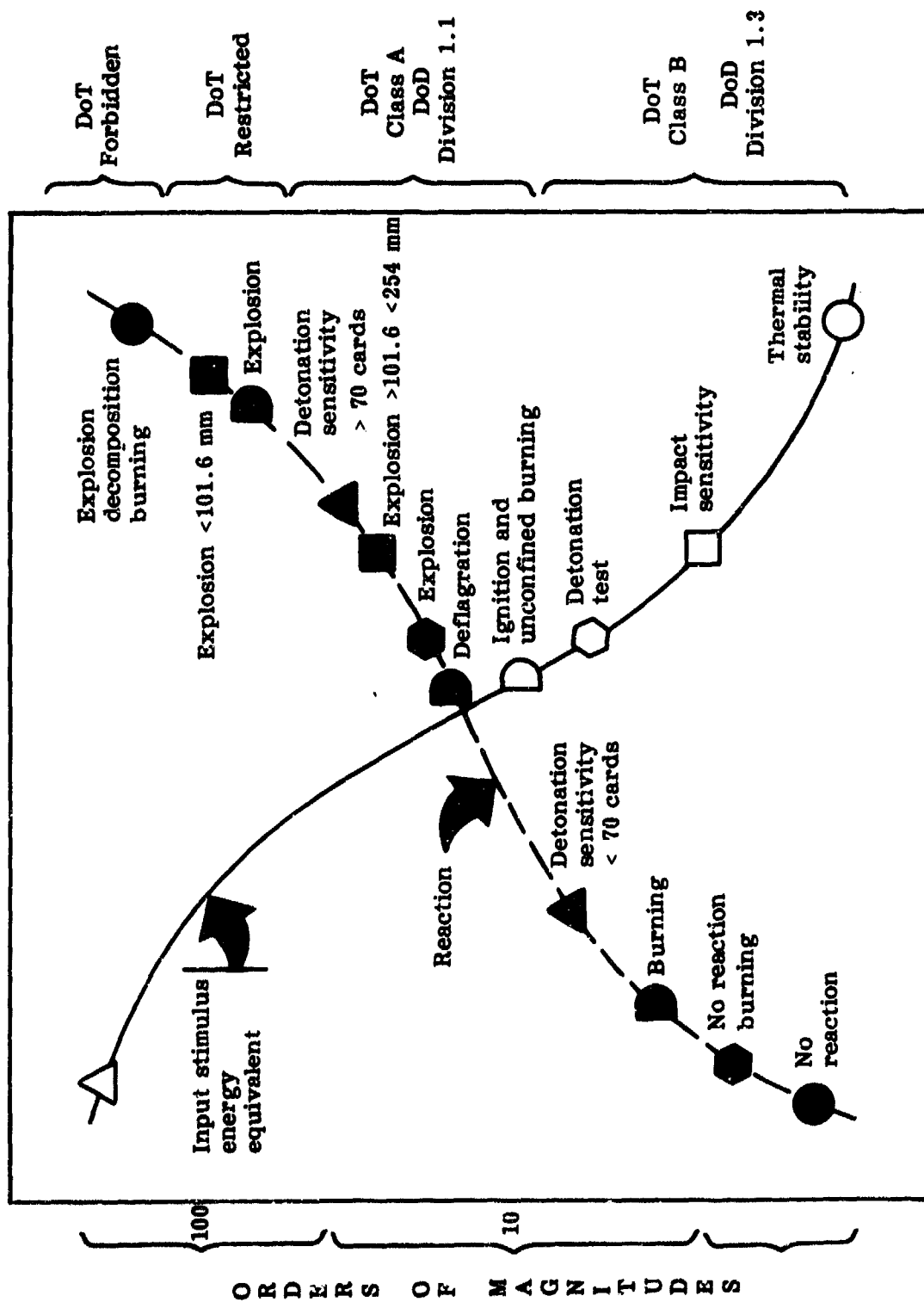


Figure 1. Interim qualification for bulk materials per DoD explosives classification procedures initiation susceptibility versus output reaction

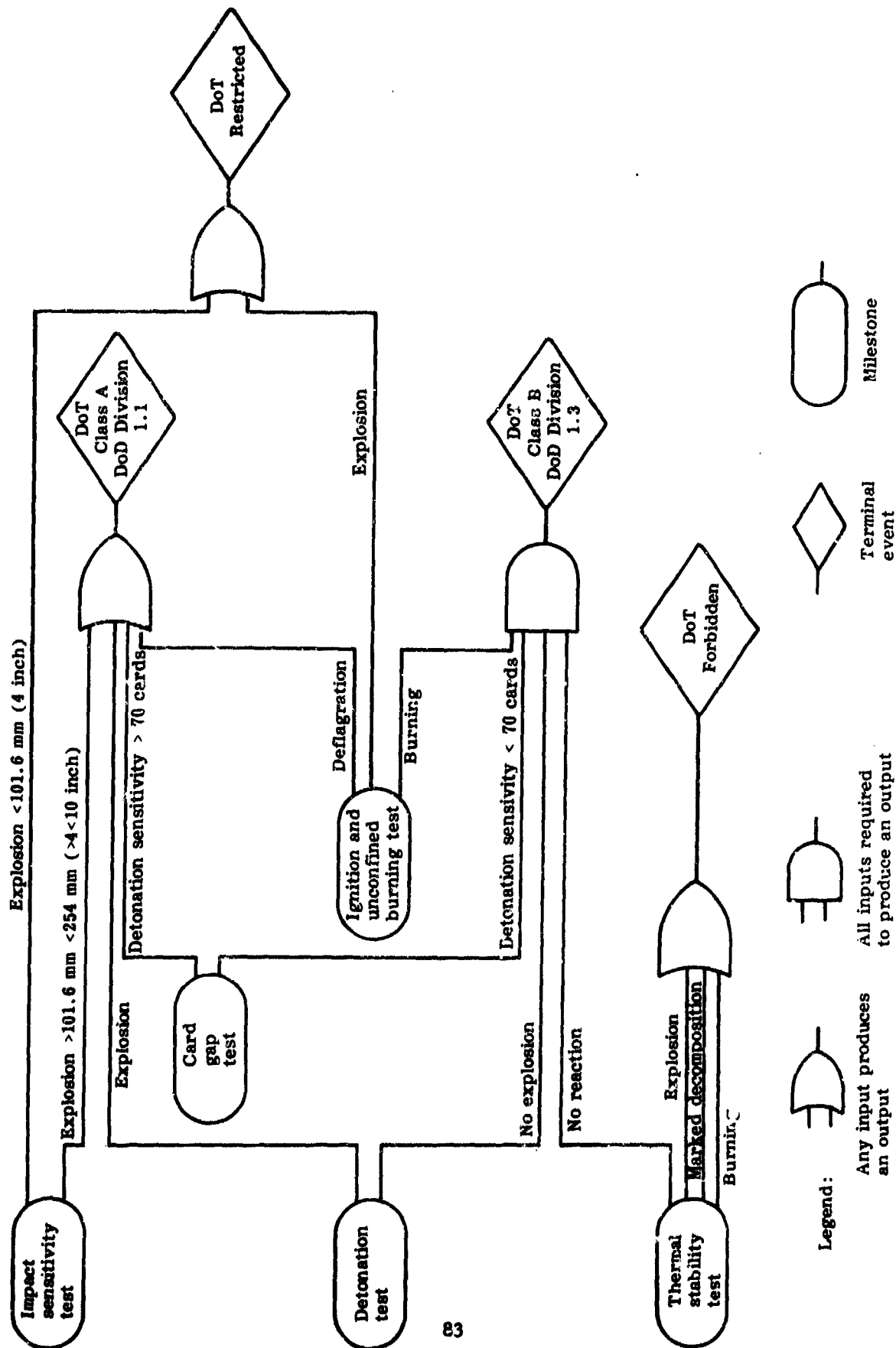


Figure 2. Interpretation of interim qualification tests paragraph 5.4 DoD explosives hazards classification procedures TB 700-2

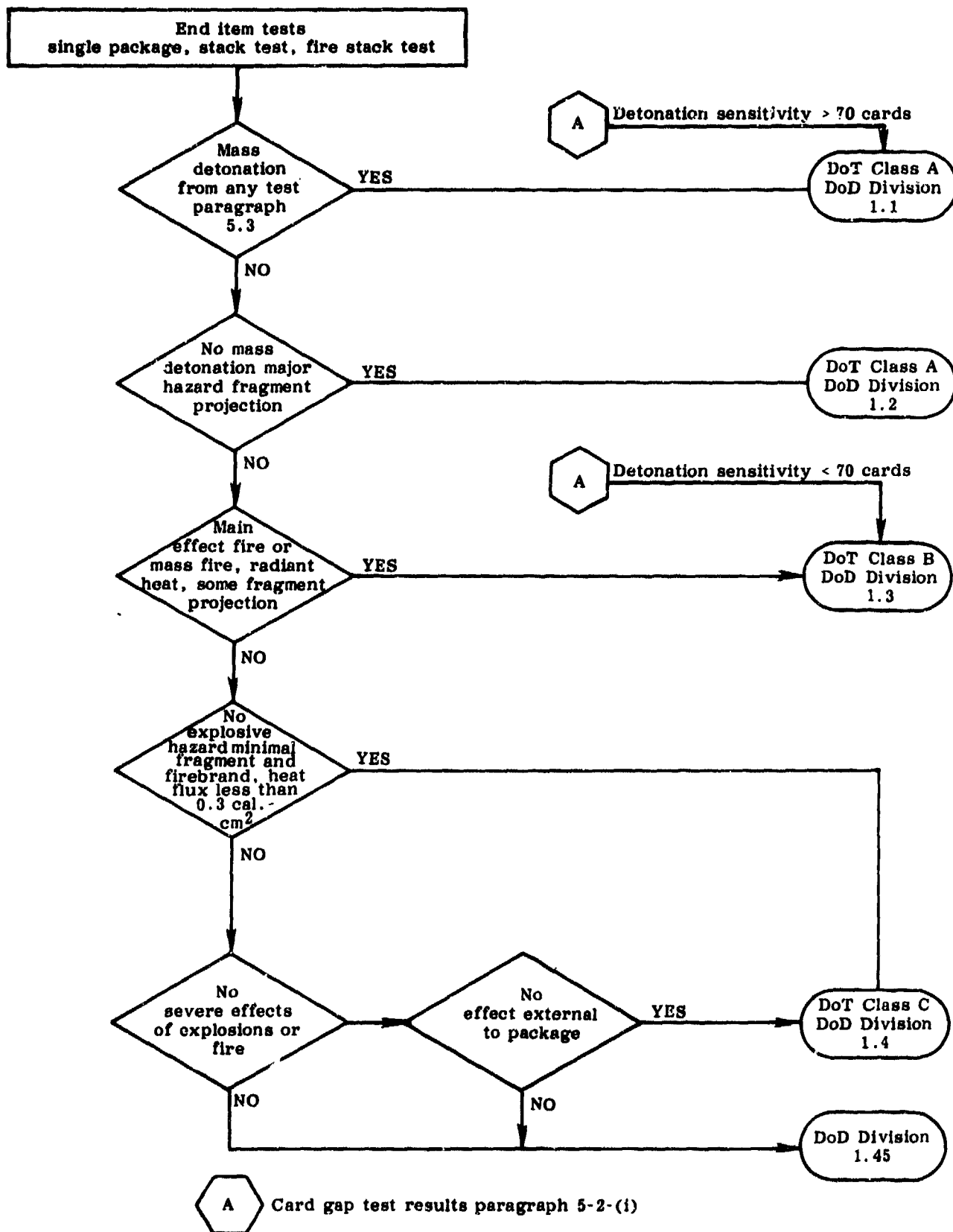


Figure 3. Interpretation of results for end item classification tests

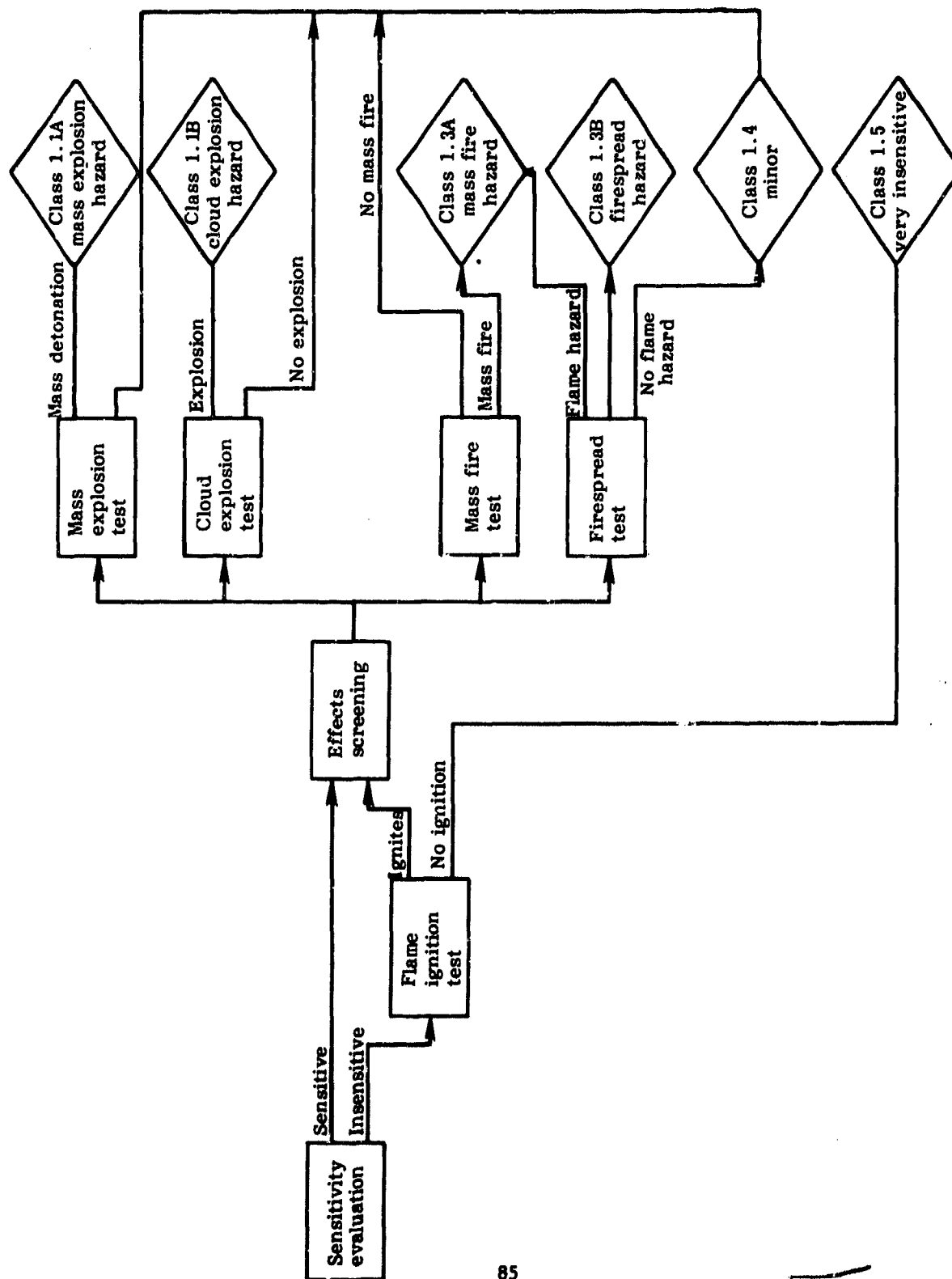


Figure 4. Proposed in-process hazards classification procedure

↓
Blast Parameters from Cylindrical Charges Detonated
on the Surface of the Ground

G. Guerke, G. Scheklinski-Glueck
Ernst-Mach-Institut, Freiburg
Germany

degruet

Abstract

↓
Tables and diagrams of scaled side-on blast parameters are available for time of shock front arrival, primary shock front overpressure, overpressure impulse and positive duration for cylindrical RDX explosives having length to diameter ratios of 1 and 5. Charges were placed in a vertical, a horizontal and a 60° inclined position to the surface of the ground. Initiation point was at one end. Blast parameters were measured along 9 blast lines at scaled standoffs from 0.5 to 32 mkg^{-1/3}.

to the same 1/3 power

1. Introduction
2. Experimental Program
3. Scaling Law
4. Shock Front Contour
5. Blast Parameters as a Function of Azimuth Angle
6. Blast Parameters versus Scaled Distance
7. References

FORWARDED PAGE BLANK-NOT FILLED

1. Introduction

The objective of this report is to present a compilation of blast data from a series of small scale HE tests with cylindrical charges detonated at the surface of the ground. In a literature search we found just one investigation concerning blast data of cylindrical charges fired on the ground surface (Ref. 1, 1975). In agreement with a recent manual for the prediction of blast loadings on structures (Ref. 3, 1980) we decided, that the existing data for explosions of elongated charges on the ground surface are not extensive enough to develop prediction curves and equations, and are not adequate to check scaling laws. Hence an experimental program was designed to gather more data on the blast from cylindrical charges fired on the surface of the ground oriented with the axis parallel, oblique and normal to the surface.

2. Experimental Program

The experimental program is delineated in Table 1. Cylindrical charges having length to diameter ratios of 1 and 5 were selected. Rounds were fired for each geometry with the charge in vertical position and with the initiation from the top (No. 4 in Table 1). In the next group, charges were placed in a horizontal position on the ground and detonated from one end (No. 1 in Table 1). Figure 2.1 shows a top plan of the cylindrical charge with the initiation point at the end in line with the 0 degree line. Keeping the charge fixed and moving clockwise we have the instrument line at 9 different azimuth angles H at 0, 22.5, 45, 67.5, 90, 112.5, 135, 157.5, 180 degrees to the ground zero point.

Table 1 Test Plan

A three-number code is used to characterize the test arrangement. Initiation point is at $H = 0$. The code:
L/D ratio - Azimuth Angle H - Angle of Inclination V

1. Horizontal Cylinders (Angle of Inclination $V = 0$)

5 - 0 - 0	1 - 0 - 0
5 - 22,5 - 0	1 - 45 - 0
5 - 45 - 0	1 - 90 - 0
5 - 67,5 - 0	1 - 112,5 - 0
5 - 90 - 0	1 - 135 - 0
5 - 112,5 - 0	
5 - 135 - 0	
5 - 157,5 - 0	
5 - 180 - 0	

2. 45 Degrees Inclined Cylinders

5 - 0 - 45	1 - 0 - 45
5 - 90 - 45	1 - 90 - 45
5 - 180 - 45	1 - 180 - 45

3. 60 Degrees Inclined Cylinders

5 - 0 - 60	1 - 0 - 60
5 - 45 - 60	1 - 90 - 60
5 - 90 - 60	1 - 180 - 60
5 - 135 - 60	
5 - 180 - 60	

4. Vertical Cylinders (Symmetric in azimuth angle)

5 - S - 90	1 - S - 90
------------	------------

5. Hemispherical Charges

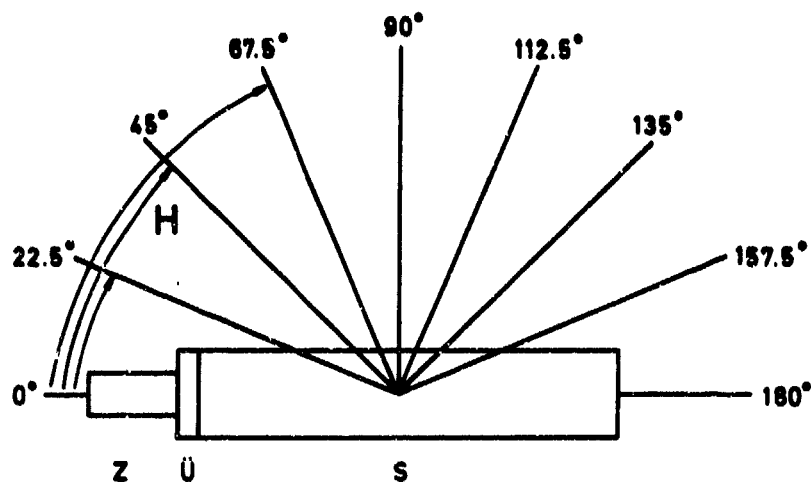


Fig. 2.1

**Top Plan of Blast Lines at Azimuth Angles H.
Initiation Point at $H = 0$.**

Z = Igniter Ü = Propagation Charge

S = RDX cylinder

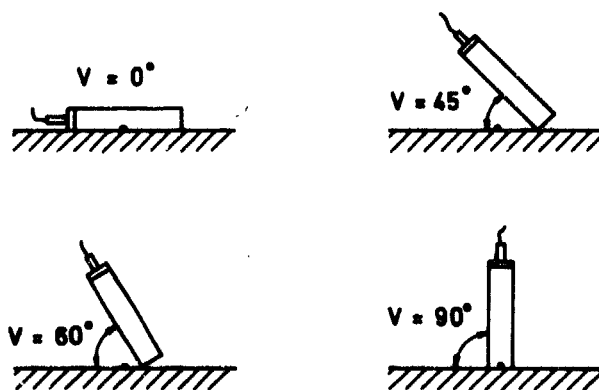


Fig. 2.2

**Side View of Cylindrical Charges Inclined
to the Surface of the Ground**

As Figure 2.2 shows each of the two L/D geometries was fired in a position at vertical elevation $V = 60^\circ$ degrees inclined to the ground surface with end initiation away from the ground (No. 3 in Table 1). To complete the program some rounds were fired in a position $V = 45^\circ$ degrees to the ground surface (No. 2 in Table 1). Semispherical charges of identical masses and identical type of HE were initiated at their center of mass in order to get reference values for the semi-spherical blast propagation (No. 5 in Table 1).

All charges, as shown in Table 2, were bare RDX with nominal weight of 0.016 kg, 0.128 kg and 1.024 kg.

Table 2 Explosives Specifications

Cylindrical Charges S 94.5 % RDX
 4.5 % Wax
 1.0 % Graphite

Charge Density 1680 kg m^{-3}

Precision Microsecond Igniter PL 464 Dynamit Nobel

L = Charge Length D = Charge Diameter \bar{U} = Propagation Charge

Mass in kg	L/D = 1		L/D = 5		\bar{U} in g	S in g
	D in cm	L in cm	D in cm	L in cm		
0.016	2,3	2,3	1,35	6,7	2	14
0.128	4,6	4,6	2,7	13,4	5	123
1.024	9,2	9,2	5,4	26,8	8	1016

Firings were made on heavy steel plates that were nearly perfect reflectors of blast waves. Restoration of the plates and of the compacted sand under them was carried out after each event. Shown in Figure 2.3 is the field layout.

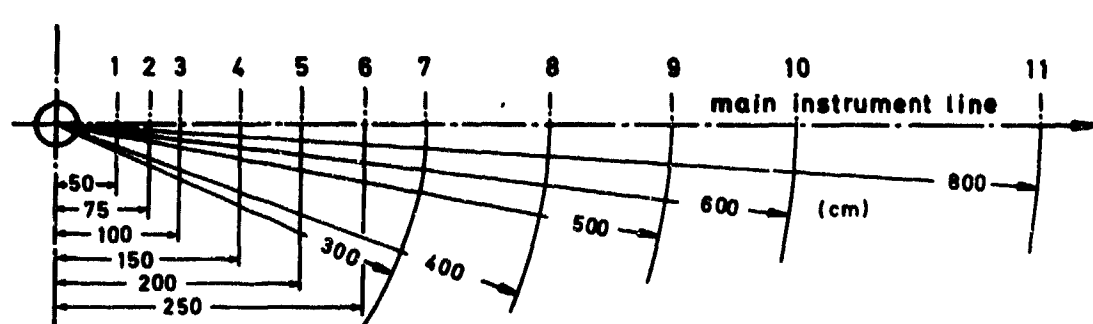


Fig. 2.3

Top Plan of the Field Layout

Blast Gages No 1 to 11 along the Main Instrument Line. All distances in centimeters

The geometric center or a projection thereof was used as the ground zero point. Eleven blast gages were installed along the main instrument line extending from 0.5 meter to 8 meter, corresponding to scaled distances from $Z = 0.5$ to $Z = 32 \text{ m kg}^{-1/3}$. Two additional control gages were located at an off angle at 90° equal to station 2 at 0.75 meter and to station 4 at 1.5 meter. The pressure transducers were Kistler Instruments model 603 B piezoelectric sensing elements having a natural

Table 3

BLASTPARAMETER , ZYLINDRISCHE LADUNGEN , ANORDNUNG 5 - 90 - 0

NR.	Z	TA	PS	IS+	T+
1	0.50	1.17E-01	I	2.00E+00	1.99E-01
2	0.60	1.45E-01	I	2.88E+00	2.49E-01
3	0.70	1.74E-01	I	2.88E+00	3.02E-01
4	0.80	2.06E-01	I	2.88E+00	3.56E-01
5	1.00	2.74E-01	8.10E+01	2.88E+00	4.69E-01
6	1.25	3.70E-01	5.79E+01	2.68E+00	6.19E-01
7	1.50	4.78E-01	4.11E+01	2.08E+00	7.75E-01
8	1.75	5.97E-01	2.95E+01	2.88E+00	9.30E-01
9	2.00	7.20E-01	2.15E+01	2.58E+00	1.11E+00
10	2.25	8.71E-01	1.58E+01	2.88E+00	1.28E+00
11	2.50	1.02E+00	1.10E+01	2.85E+00	1.46E+00
12	2.75	1.27E+00	7.60E+00	2.29E+00	1.64E+00
13	3.00	1.56E+00	5.40E+00	1.87E+00	1.83E+00
14	3.50	2.24E+00	2.95E+00	1.31E+00	2.21E+00
15	4.00	3.07E+00	1.75E+00	9.09E-01	2.62E+00
16	4.50	4.05E+00	1.10E+00	7.91E-01	2.82E+00
17	5.00	5.27E+00	7.68E-01	6.99E-01	3.00E+00
18	5.50	6.32E+00	6.01E-01	6.25E-01	3.18E+00
19	6.00	7.43E+00	4.84E-01	5.64E-01	3.36E+00
20	7.00	9.79E+00	3.36E-01	4.70E-01	3.69E+00
21	8.00	1.23E+01	2.50E-01	4.02E-01	4.01E+00
22	9.00	1.50E+01	1.95E-01	3.50E-01	4.31E+00
23	10.00	1.77E+01	1.58E-01	3.09E-01	4.60E+00
24	11.00	2.05E+01	1.32E-01	2.76E-01	4.87E+00
25	12.00	2.34E+01	1.13E-01	2.49E-01	5.14E+00
26	14.00	2.92E+01	8.67E-02	2.08E-01	5.65E+00
27	16.00	3.51E+01	7.05E-02	1.77E-01	6.09E+00
28	18.00	4.09E+01	5.95E-02	1.54E-01	6.15E+00
29	20.00	4.66E+01	5.18E-02	1.36E-01	6.20E+00
30	22.00	5.22E+01	4.61E-02	1.22E-01	6.25E+00
31	24.00	5.77E+01	4.17E-02	1.10E-01	6.29E+00
32	28.00	6.82E+01	3.56E-02	9.18E-02	6.37E+00
33	32.00	7.80E+01	3.17E-02	7.84E-02	6.43E+00

KOEFFIZIENTEN DER AUSGLEICHSFUNKTION , ANORDNUNG 5 - 90 - 0

VON Z	BIS Z	GRAD	R SQU	B0	B1	B2
TA :						
0.50	2.50	2	0.998	-0.5623	1.3159	0.3125
2.50	5.00	1	1.000	-0.9309	2.3556	
5.00	32.00	2	1.000	-0.9111	2.7476	-0.5881
PS :						
0.87	2.50	2	1.000	1.9129	-1.3696	-1.8590
2.50	5.00	1	0.995	2.6033	-3.9207	
5.00	32.00	2	0.995	2.2610	-4.1797	1.1172
IS+ :						
0.50	2.50	1	0.000	0.4594	0	
2.50	4.00	1	0.999	1.3691	-2.2979	
4.00	32.00	1	0.998	0.6682	-1.1785	
T+ :						
0.50	4.00	1	1.000	-0.3286	1.2386	
4.00	16.00	1	0.999	0.0488	0.6136	
16.00	32.00	1	0.924	0.6389	0.0794	

frequency of 500 kc. Signals were recorded on Transient Recorders having a frequency bandpass 0 - 150 kc. The data was reduced with the aid of a HP 9830 A desk computer. Scaled arrival time $TA \cdot Q^{-1/3}$, shock front overpressure PS, scaled overpressure impuls $IS \cdot Q^{-1/3}$ and scaled positive duration $T \cdot Q^{-1/3}$ were obtained from more than 1200 records.

A final report covers the reduced data of the entire program (Ref. 4). Interested people will find 35 Tables and 35 Diagrams in the report belonging to different charge orientations and directions of blast propagation (see Table 1). One example is to be seen in Tab. 3, in order to show the arrangement of data. At 33 values of the scaled distance parameter Z the scaled blast parameters have been listed at distances that allow linear interpolation. Also coefficients of least-squares regression power functions of blast data as a function of scaled distance have been listed. Blast data can be taken from the tables directly for 1 kilogram charges but must be multiplied by the cube root of the charge mass for all charges heavier or lighter than 1 kilogram. A procedure that is well known to people who handle TNT standard curves or tables. Remember that the scaling of blast data works correctly as long as the basic assumptions of Hopkinson-Cranz scaling rules are fulfilled.

3. Scaling Laws

Tests were conducted at three different charge masses of RDX at identical charge geometries and identical test arrangements. Table 4 may show as an example that Cranz-Hopkinson scaling proofed well throughout our test series. Time of arrival data have been listed for the test-arrangement 1-90-0 ($L/D = 1$, charge axis parallel to the ground, direction of blast measurement 90°). Direct comparison of test results can be made at scaled distances between $Z = 2$ and $Z = 8$. Time-of-arrival measurements in milliseconds differ by a factor of about 4 between 16 gram and 1 kilogram charges, but scaled time-of-arrival data correspond within 3 per cent.

Table 4 Check of Scaling Laws
Time of Shock Front Arrival for 3 Different
Charge Masses. Test Arrangement 1-90-0

<div><div>Q</div><div>Z</div></div>	0.016 kg			0.128 kg			1.024 kg		
R/Q ^{1/3}	R in m	t _A in ms	t _A /Q ^{1/3}	R in m	t _A in ms	t _A /Q ^{1/3}	R in m	t _A in ms	t _A /Q ^{1/3}
2	0.5	0.21	0.83	1	0.42	0.83	2	0.82	0.81
4	1	1.03	4.09	2	2.0	3.97	4	4.10	4.08
8	2	3.55	14.1	4	7.22	14.3	8	14.4	14.3

Fig. 3.1 shows just one example of measured pressure-time histories at tests with different charge masses at identical scaled distances. Time and impulse scales are scaled to 1 kilogram. It is easily to be seen, that measurements are nearly identical.

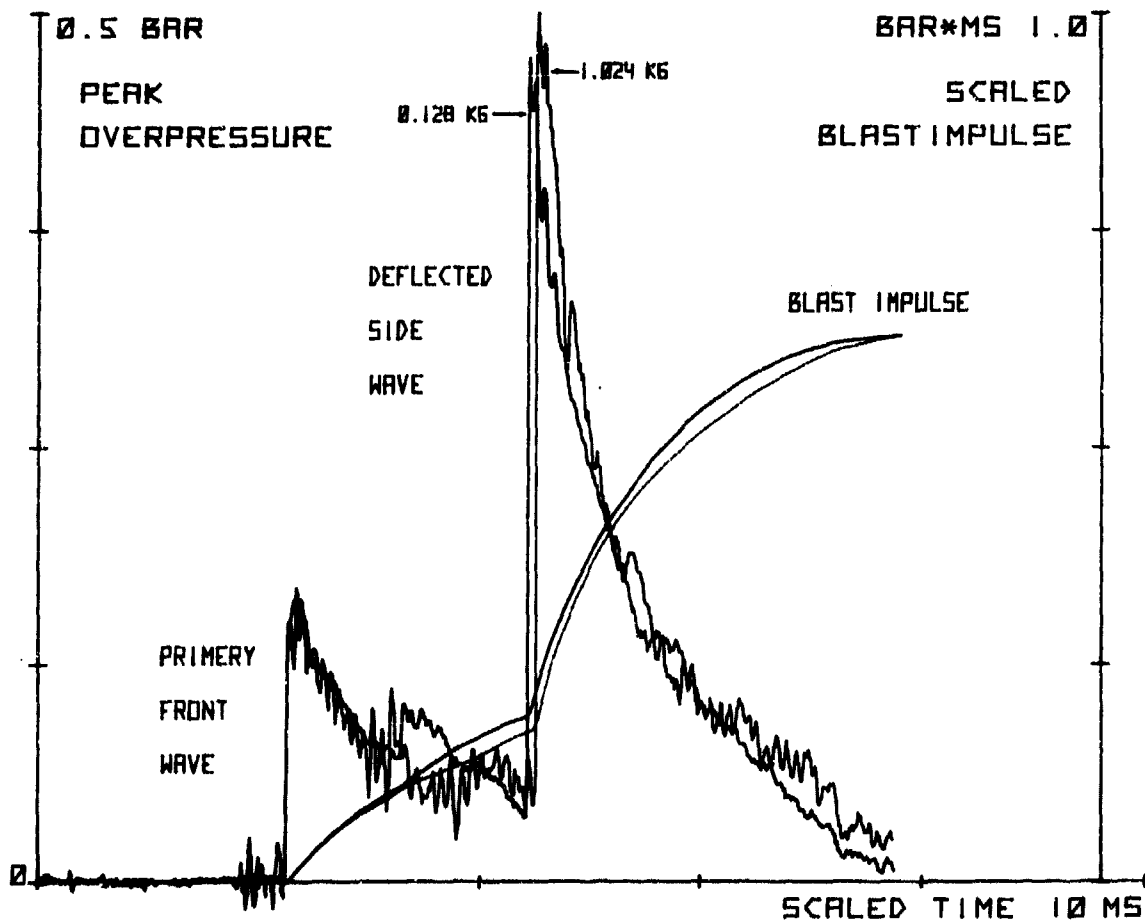


FIG.3.1

PRESSURE-TIME RECORDS SCALED TO 1 KG-EQUIVALENT.

TEST ARRANGEMENT S - 180 - 0

4. Shock Front Contour

For a charge of cylindrical geometry as standoff increases the shock front becomes more spherical. This is shown in Figures 4.1 to 4.3. Iso time of arrival lines that mark the shock front contours are shown for 3 scaled arrival times TA 0.874; 5.6; 46.6 after ignition time. Semicircles mark the shock front from semispherical charges at identical arrival time. Peak overpressure is identical along the semicircles 7 bar (100 psi); 0.7 bar (10 psi); 0.07 bar (1 psi). At the same instant after charge ignition the shock front contour of the cylindrical charge is asymmetric with largest distance from the explosion center at 90° , $112,5^\circ$ and 180° (Fig. 4.1). The peak overpressure at the shock front is far from uniform for cylindrical charges. It is given in small figures along the contour. High peak overpressure in 90° direction in Fig. 4.1 is due to the side-wave and in 180° it is due to the front wave. Highest peak overpressure in $112,5^\circ$ direction is produced by the asymmetric ignition at 0° . In that case the detonation gas has a forward velocity component that may cause the strongest shock not in 90° but in a forward direction. The falling back shock front and low pressure at 0° to 45° is produced by asymmetric ignition.

The Figures 4.2 and 4.3 show that the shock front contour becomes more spherical. But even in the far field, where semispherical charges produce a peak overpressure of 0.07 bar (1 psi), the cylindrical charge produces peak overpressures from 0.05 to 0.1 bar at the shock front.

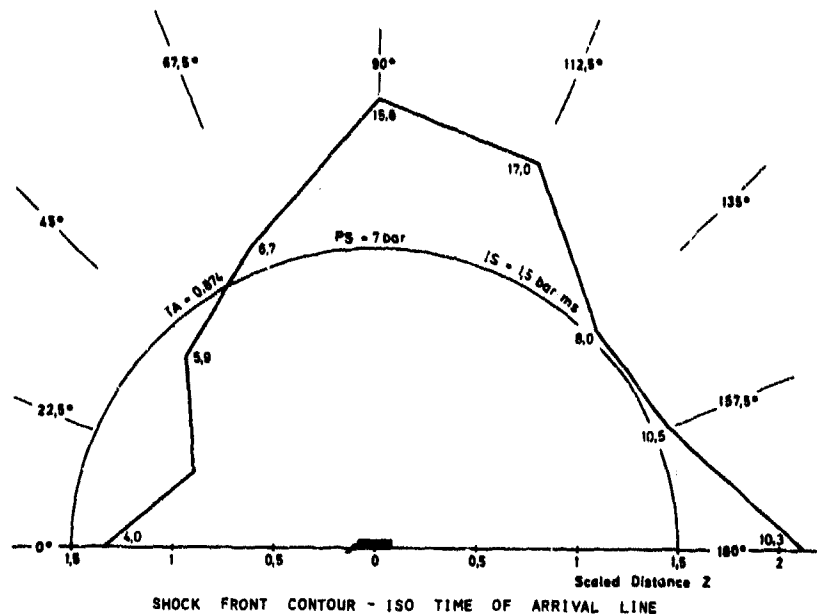


FIG. 4.1

CYLINDRICAL RDX CHARGE $L/D = 5$; $V = 0$; IGNITION AT 0° VARIABLE SHOCK FRONT OVERPRESSURE ALONG THE ISO LINE, SEMICIRCLE: SHOCK FRONT CONTOUR FOR SEMISPHERICAL CHARGE OF IDENTICAL MASS, SCALED DISTANCE $Z = 1.5$, SHOCK FRONT OVERPRESSURE $PS = 7 \text{ BAR}$.

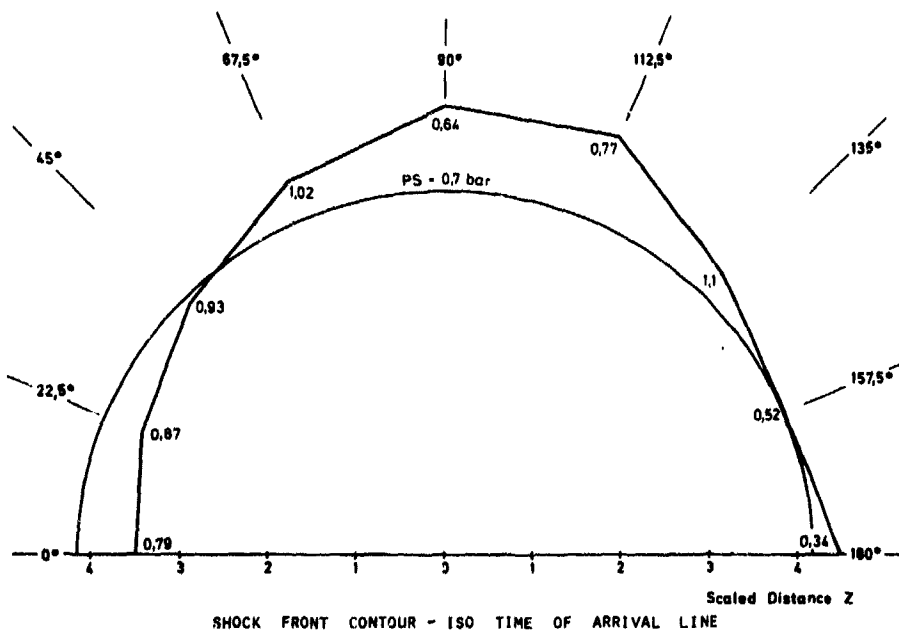
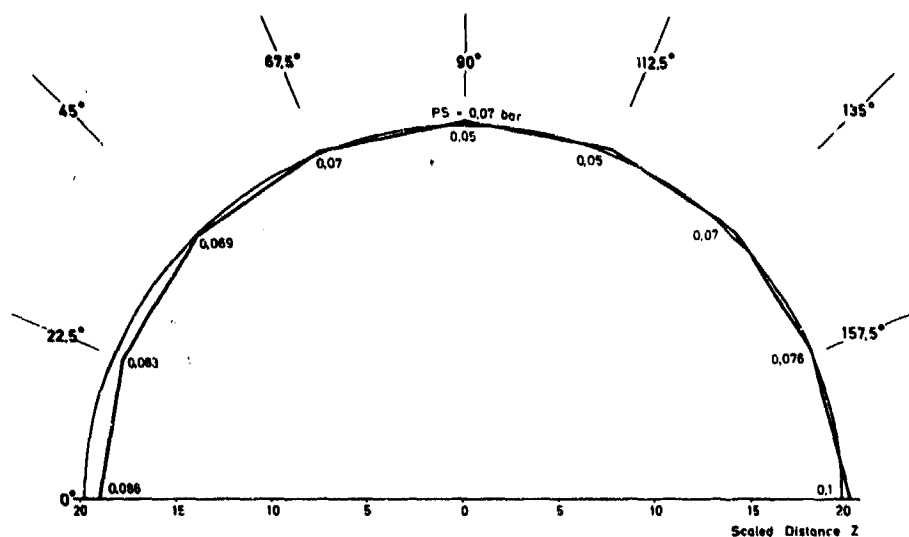


FIG. 4.2

CYLINDRICAL RDX CHARGE $L/D = 5$; $V = 0$; IGNITION AT 0° VARIABLE SHOCK FRONT OVERPRESSURE ALONG THE ISO LINE, SEMICIRCLE: SHOCK FRONT CONTOUR FOR SEMISPHERICAL CHARGE OF IDENTICAL MASS, SCALED DISTANCE $Z = 4.2$, SHOCK FRONT OVERPRESSURE $PS = 0.7 \text{ BAR}$.



SHOCK FRONT CONTOUR - ISO TIME OF ARRIVAL LINE

$$TA \ Q^{-1/3} = 46.6 \text{ MS } \text{KG}^{-1/3}$$

FIG. 4.3

CYLINDRICAL RDX CHARGE $L/D = 5$; $V = 0$; IGNITION AT 0° VARIABLE SHOCK FRONT OVERPRESSURE ALONG THE ISO LINE, SEMICIRCLE: SHOCK FRONT CONTOUR FOR SEMISPHERICAL CHARGE OF IDENTICAL MASS. SCALED DISTANCE $Z = 20$ SHOCK FRONT OVERPRESSURE $PS = 0.07 \text{ BAR}$.

5. Blast Parameters as a Function of Azimuth Angle

If a hemispherical charge resting on a flat surface is initiated at its center of mass a shock wave will travel through the surrounding air, its strength a function of radial standoff from the center of the explosion. For a cylindrical charge that is initiated at one end the shock wave will not enter the surrounding air as a spherical wave, nor at the same time over the entire charge surface. The shape and strength of the shock wave will depend upon the length to diameter ratio, and upon the location at which initiation occurred. The blast parameters will be functions not only of radial standoff, but also of azimuth.

Figures 5.1 through 5.4 are plots comparing blast data of cylindrical charges to hemispherical charges. Primary shock front peak overpressure and positive pressure impulse are plotted as a function of azimuth angle H and scaled distance Z , for cylindrical charges having length to diameter ratios of 1 and 5. Our final report covers data from the entire program (Lit. 4).

Results of semispherical charges are plotted as horizontal lines. Azimuthal symmetry is valid at that case. Unsymmetrical blast propagation around cylindrical charges is identified very clearly at this type of diagram that has been used in Ref. 3.

Figure 5.2a summarizes primary shock front overpressure data in the near field at scaled distances from $Z = 1$ to $Z = 2.5$ for $L/D = 5$. Maximum peak overpressure of about 150 bar at $Z = 1$ was measured in $H = 112.5^\circ$ direction. Former investigators who had measuring lines at 90° and 135° could not detect this effect of the asymmetric expansion of the detonation gases as a consequence of ignition at C° .

Minimum peak overpressure at $Z = 1$ occurred at $H = 22.5^\circ$ direction of about 5.5 bar as a consequence of asymmetric ignition and the bridge wave phenomenon. Very high peak overpressure was observed at $Z = 1$ at $H = 180^\circ$ direction as an effect of the front wave. Errors of about a factor of 10 in peak overpressure may be induced in the near field by neglecting the charge shape.

Most people think that blast parameters from non-spherical charges smoothen continuously to spherical parameters in the far field. In fact the peak overpressure from cylinders with $L/D = 5$ seems to smoothen at scaled distance $Z = 7$ in figure 5.2b. Former investigator only measured up to this distance. But far out can we recognize the effect that at distances from $Z = 10$ to $Z = 20$ peak overpressure is very small at $H = 90^\circ$ and $H = 112.5^\circ$ directions and high in $H = 0^\circ$ and $H = 180^\circ$. This type of overreaction corresponds to reflection and diffraction phenomena of primary side waves and end waves from the cylindrical explosives. Pressure-distance relationships are determined not only by one shock front, but by side-waves, end-waves and bridge-waves that result in multiple pressure peaks. Some wave fronts tend to heal by overtaking and merging with the primary front while others tend to recede. As a result even in the far field, at $Z = 20$, errors of about a factor of 2 (100 percent) in peak overpressure are induced by neglecting the charge shape.

Figures 5.1a and 5.1b summarize peak overpressure data from cylinders with $L/D = 1$. There are some remarkable differences between length to diameter ratios 5 and 1. All of them can be qualitatively explained by the different charge geometry and the observation that high peak overpressure in a certain direction tends to fall down to very low pressure at increasing distances. The rate of change in peak overpressure

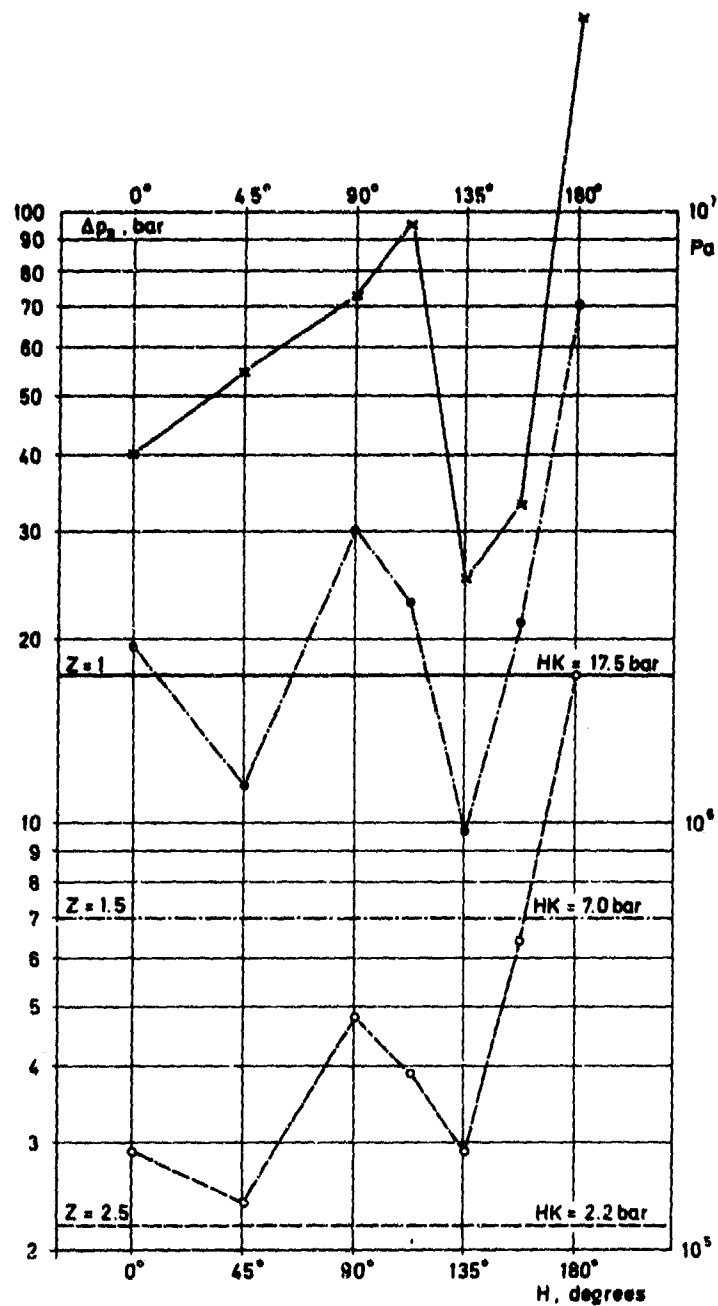


Fig 5.1a Primary Shock Front Side-on Overpressure as a Function of Azimuth Angle H and Scaled Distance $Z = R \cdot Q^{-1/3}$ in $\text{mkg}^{-1/3}$ for Cylindrical Charges with L/D Ratio of 1. Horizontal Lines Indicate Shock Front Overpressure of Semispherical Charges of Identical Mass at the Same Scaled Distance.

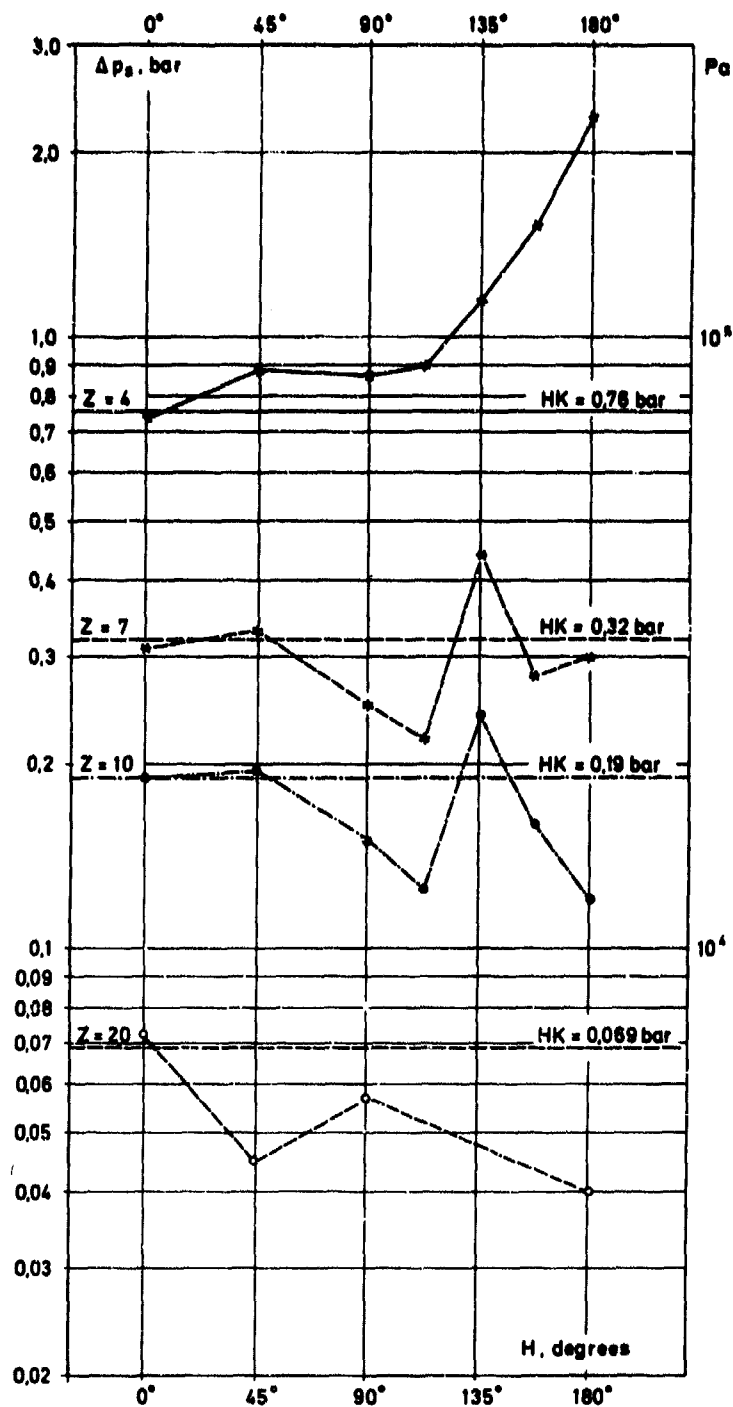


Fig. 5.1b Primary Shock Front Side-on Overpressure as a Function of Azimuth Angle H and Scaled Distance $Z = R \cdot Q^{-1/3}$ in $\text{mkg}^{-1/3}$ for Cylindrical Charges with L/D Ratio of 1. Horizontal Lines Indicate Shock Front Overpressure of Semispherical Charges of Identical Mass at the Same Scaled Distance.

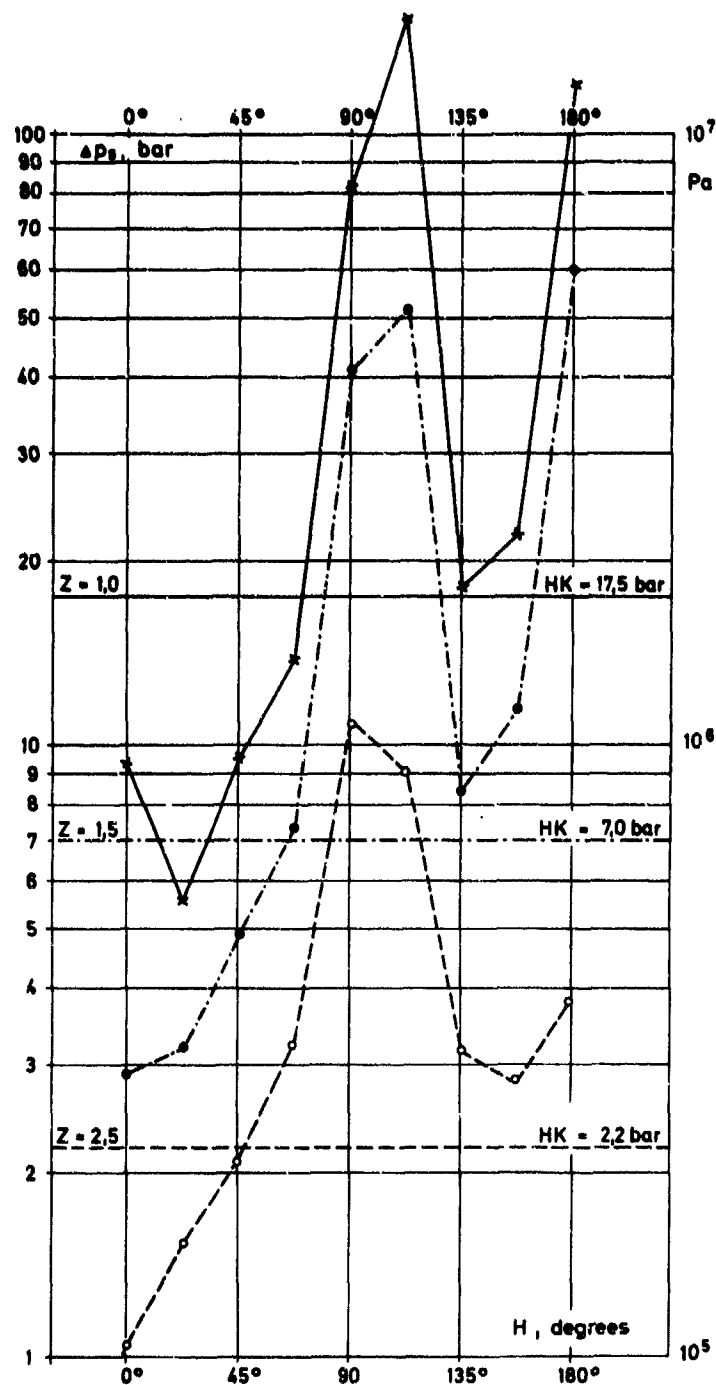


Fig. 5.2a Primary Shock Front Side-on Overpressure as a Function of Azimuth Angle H and Scaled Distance $Z = R \cdot Q^{-1/3}$ in $\text{mkg}^{-1/3}$ for Cylindrical Charges with L/D Ratio of 5. Horizontal Lines Indicate Shock Front Overpressure of Semispherical Charges of Identical Mass at the Same Scaled Distance.

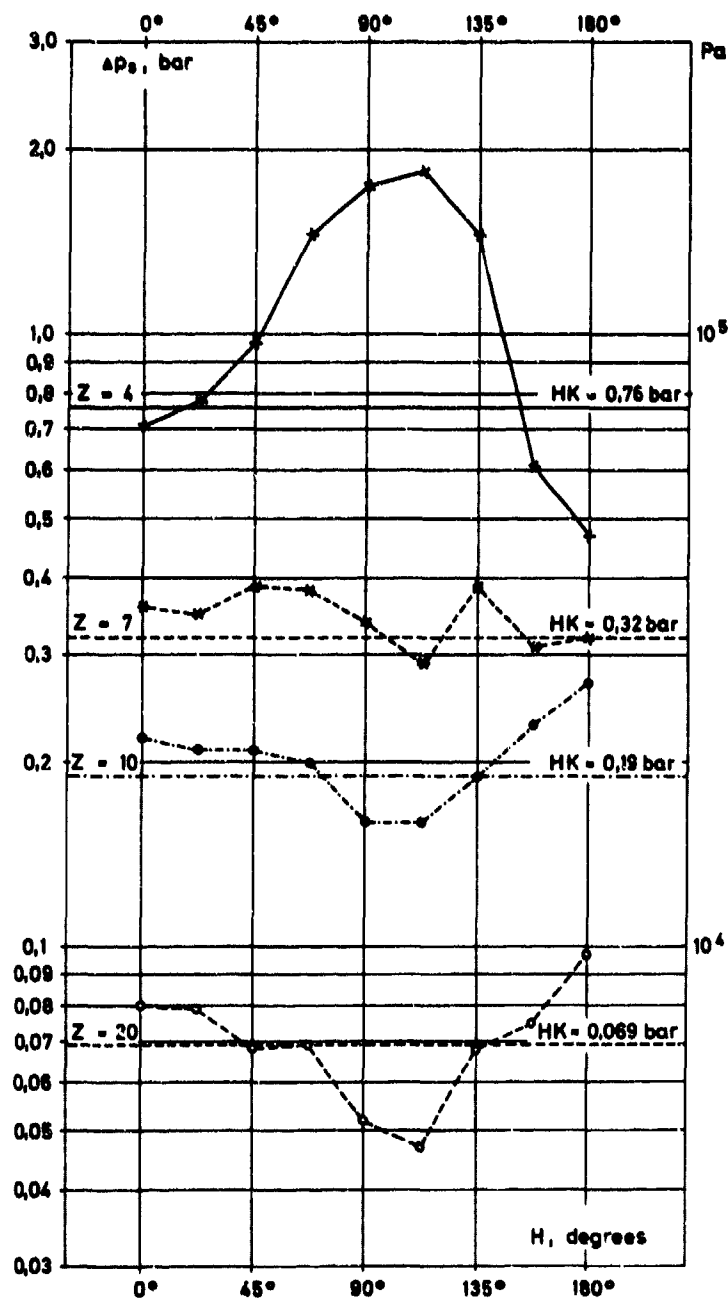


Fig. 5.2b Primary Shock Front Side-on Overpressure as a Function of Azimuth Angle H and Scaled Distance $Z = R \cdot Q^{-1/3}$ in $\text{mkg}^{-1/3}$ for Cylindrical Charges with L/D Ratio of 5. Horizontal Lines Indicate Shock Front Overpressure of Semispherical Charges of Identical Mass at the Same Scaled Distance.

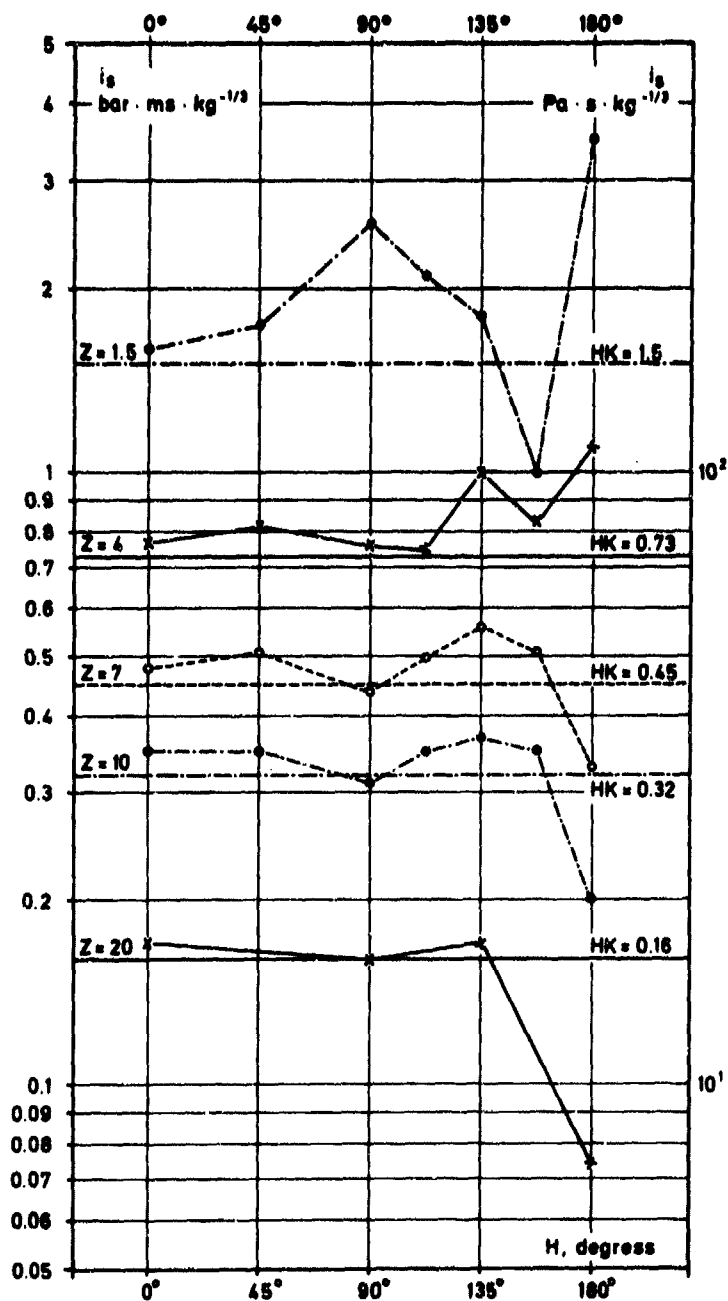


Fig. 5.3 Side-on Overpressure - Impulse as a Function of Azimuth Angle H and Scaled Distance Z in $\text{mkg}^{-1/2}$ for Cylindrical Charges with L/D Ratio of 1. Horizontal Lines Indicate Impulses of Semispherical Charges of Identical Mass at the Same Scaled Distance.

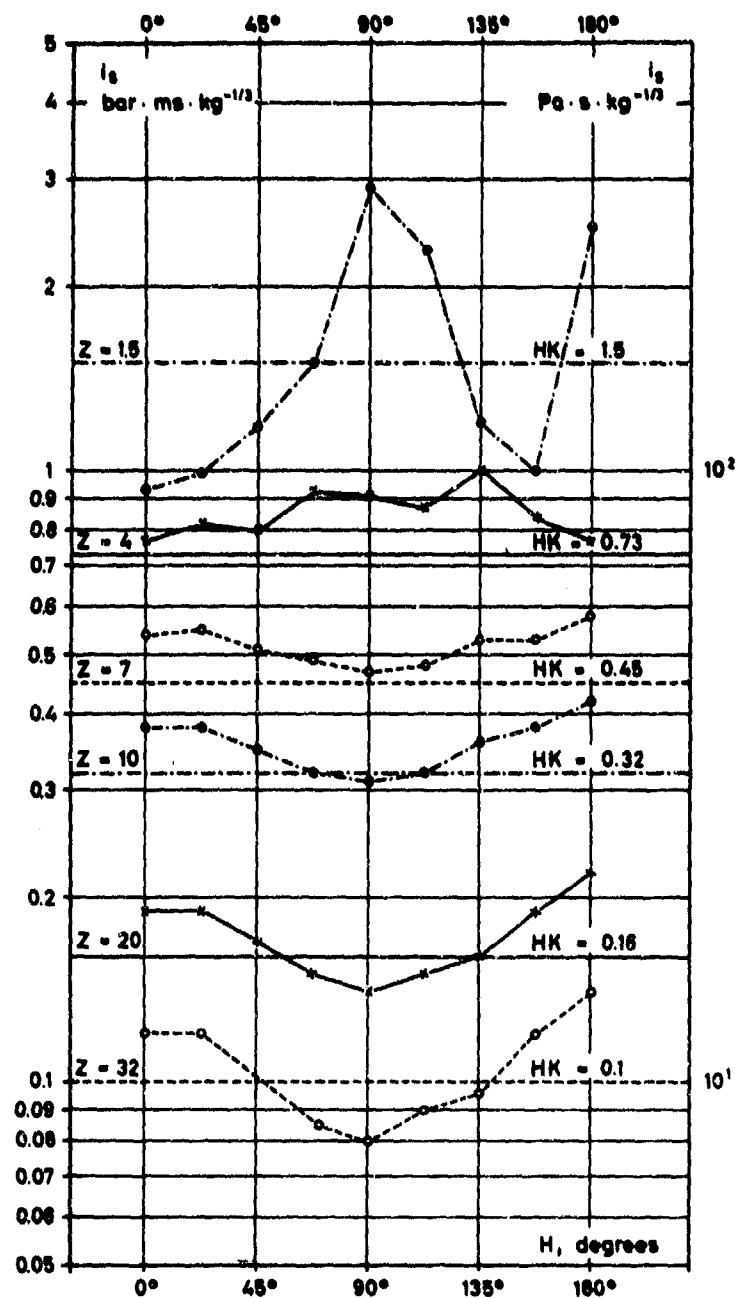


Fig. 5.4 Side-on Overpressure - Impulse as a Function of Azimuth Angle H and Scaled Distance Z in $\text{m} \cdot \text{kg}^{-1/3}$ for Cylindrical Charges with L/D Ratio of 5. Horizontal Lines Indicate Impulses of Semispherical Charges of Identical Mass at the Same Scaled Distance.

depends upon the impulse that is included in the first pressure peak (not to be confused with the total overpressure impulse).

Figures 5.3 and 5.4 summarize total side-on overpressure impulse for $L/D = 1$ and 5. Multiple shocks are included. It is remarkable that at some distances blast impulses at the surface of the ground show higher values at any direction around a cylindrical charge than around a hemispherical charge. Again this phenomenon may be explained by geometrical effects, that the cylinder presents greater surface area in the direction of the ground surface than the hemisphere. Also blast impulses that show very high values in a certain direction in the near field (e.g. 180° in Fig. 5.4) tend to fall down to rather low values at greater distances.

6. Blast Parameters versus Scaled Distance

The diagrams'- figures 6.1 to 6.4-contain a presentation of primary shock front peak overpressure versus scaled distance values and positive pressure impulse versus scaled distance values derived from our small scale measurements. The values of blast parameters in Ref. 4 were all scaled to a kilogram equivalent at standard sea level conditions. To use the curves for predicting blast data for other yields at other than standard sea level conditions standard scaling procedures should be used. This type of diagram has been used in Ref. 1 and may give the most complete presentation of our results.

As reference values results from semispherical charge detonations were fit into the diagrams that may make clear the big differences in peak overpressure in different directions around elongated charges. Kingery (Ref. 1) has fitted experimental peak overpressure data from hemispherical charges. The curve fit is of the functional form

$$P_s = f(Z)$$

P_s = peak side-on overpressure

Z = scaled distance.

Plooster (Ref. 5) has curve-fit the experimental peak side-on overpressure data obtained from a test program conducted at Denver Research Institute for cylindrical charges in free air. Much more data are needed in order to make a curve fit of the functional form

$$P_s = f(Z; L/D; H)$$

P_s = peak side-on overpressure

Z = scaled distance

L/D = cylinder length to diameter ratio

H = azimuth angle

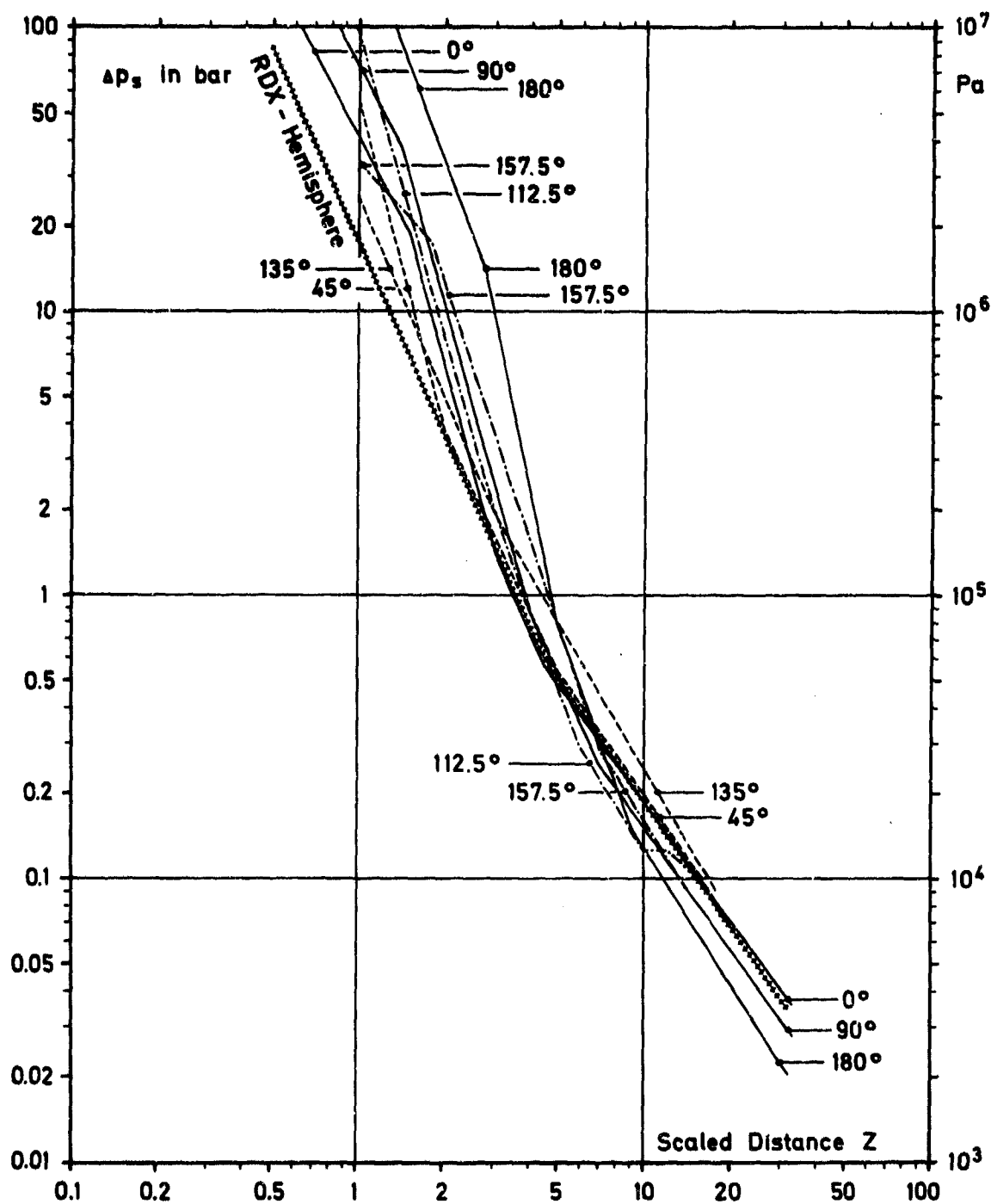


Fig. 6.1

**Primary Shock Front Overpressure vs. Scaled Distance
for Cylindrical RDX Surface Bursts $L/D = 1$**

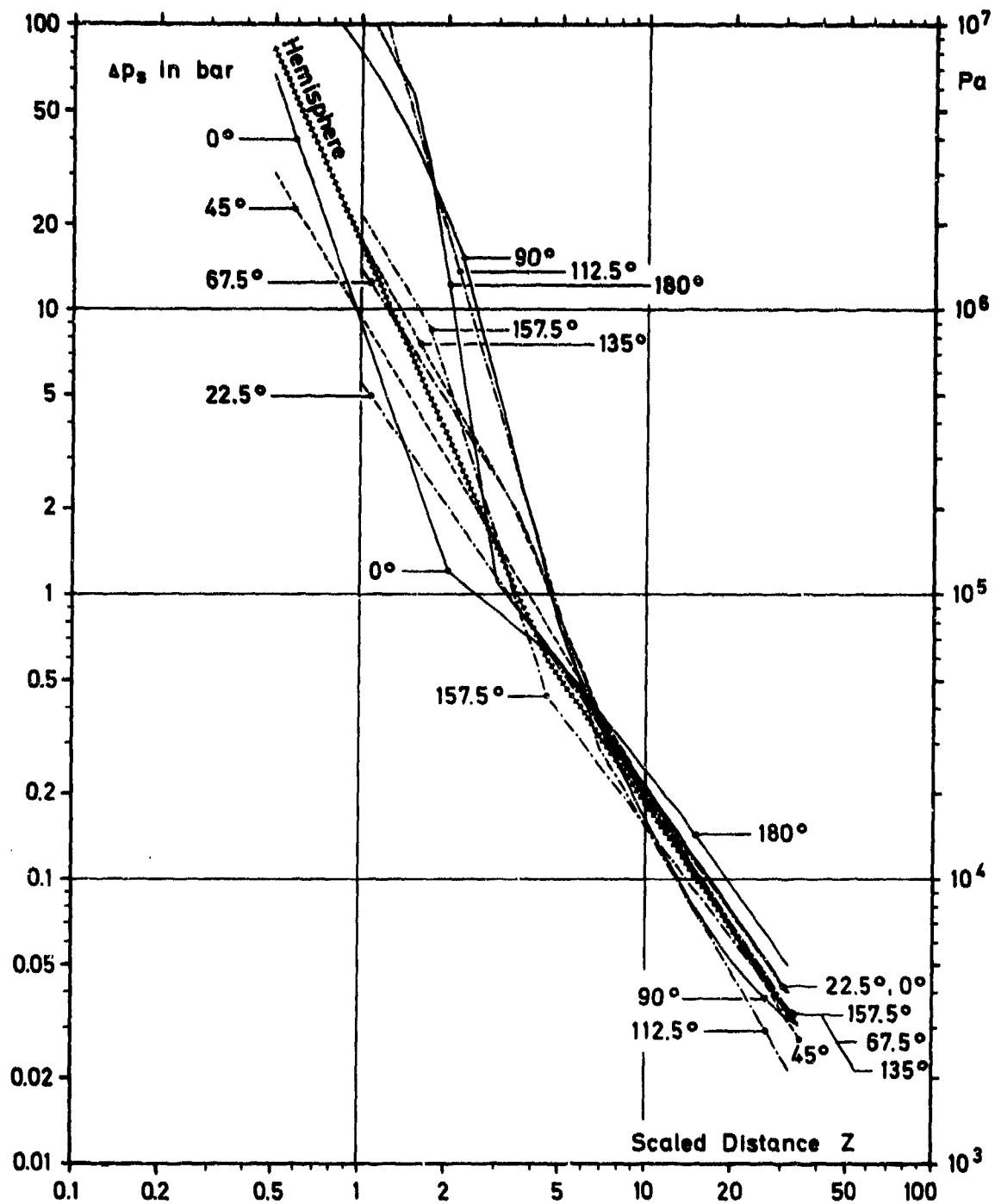


Fig. 6.2
Primary Shock Front Overpressure vs. Scaled Distance
for Cylindrical RDX Surface Bursts $L/D = 5$

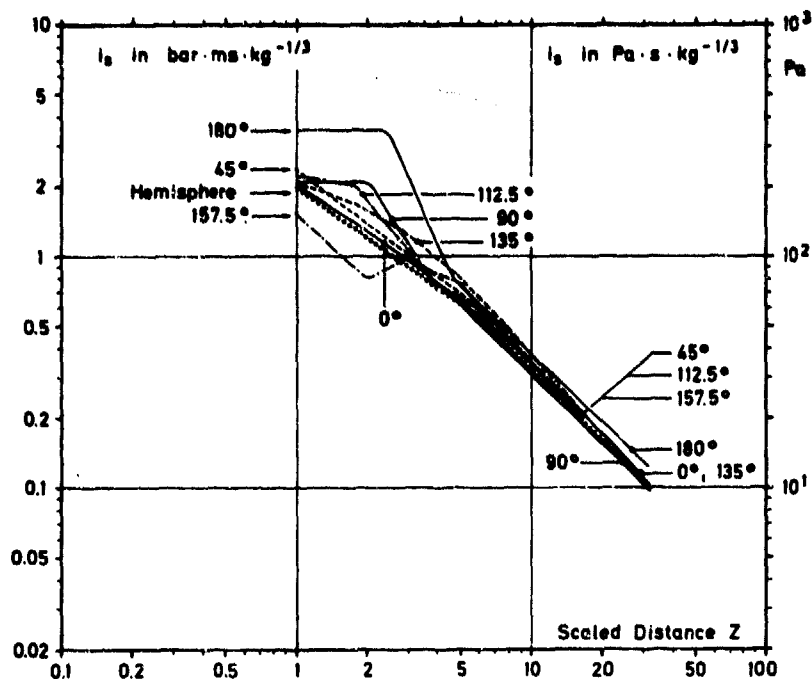


Fig. 6.3 Overpressure - Impulse vs. Scaled Distance
for Cylindrical RDX Surface Bursts $L/D = 1$

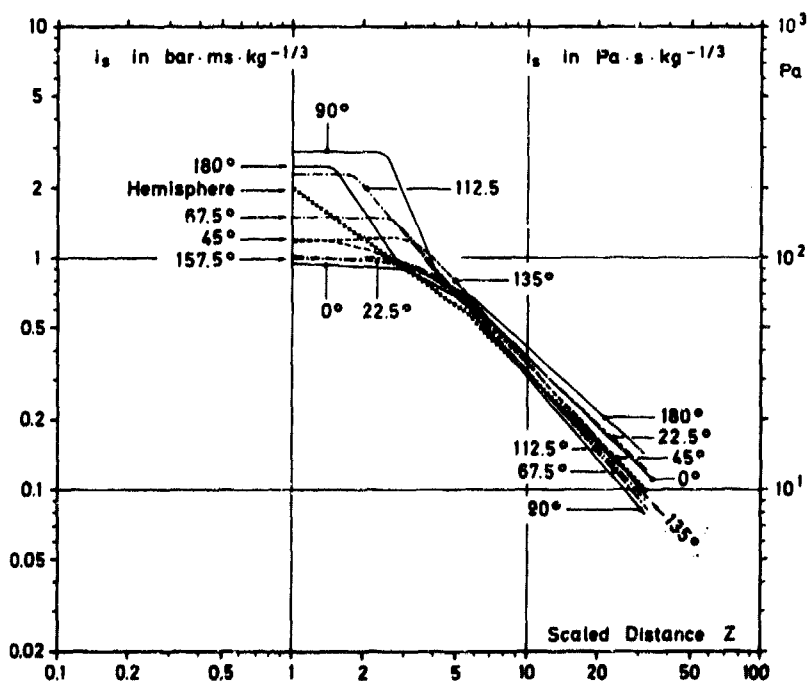


Fig. 6.4 Overpressure - Impulse vs. Scaled Distance
for Cylindrical RDX Surface Bursts $L/D = 5$

Curve fitting of the data presented in this report has not yet been completed. It is more complicated than in Ref. 5 as a wider range of distances, peak overpressures and blast impulses was investigated.

7. References

1. Kingery C.N., Pannill B.F.
"Peak Overpressure vs Scaled Distance for TNT Surface Bursts (Hemispherical Charges)", Ballistic Research Laboratories, Memorandum Report No. 1518, Apr. 1964
2. Reisler R.E., Giglio-tos L., Teel G.D
"Air Blast Parameters from Pentolite Cylinders Detonated on the Ground", Ballistic Research Laboratories, Memorandum Report No. 2471, Apr. 1975
3. "A Manual for the Prediction of Blast and Fragment Loadings on Structures". U.S. Department of Energy (prepared by Southwest Research Institute, San Antonio, Texas), DOE/TIC-11268, Nov. 1980
4. Gürke G., Scheklinski-Glück G., Detterer M., Mehlin H.P.
"Blastparameter bei der Oberflächendetonation von Explosivstoffzylindern". Bericht des Ernst-Mach-Instituts, No. E 6/82, März 1982
5. Plooster M.N.
"Blast Front Pressure from Cylindrical Charges of High Explosives", Naval Weapons Center, Technical Memorandum No. 3631, Sept. 1978.

**EFFECTS OF LOW LOADING DENSITY ON BLAST PROPAGATION
FROM EARTH COVERED MAGAZINES**

By

George Coulter
Charles Kingery

U.S. ARMY ARMAMENT RESEARCH & DEVELOPMENT COMMAND
BALLISTIC RESEARCH LABORATORY
ABERDEEN PROVING GROUND, MARYLAND 21005

ABSTRACT

This report contains the results from a series of high explosive tests designed to determine the airblast parameters propagating to the front, side, and rear of an earth covered munition storage magazine with a low loading density. The tests were conducted with 1/30th-scale donor models and hemi-cylindrical pentolite charges of 0.227, 0.363, 1.066, 1.814, and 5.040 kg masses. These charge masses simulate full size munition storage magazines filled with 6130, 9800, 28780, 48980 and 136080 kg of explosive. The 48980 kg full size load was used as the baseline for comparing blast attenuation or enhancement from a full size load of 6130 kg. There was attenuation of both peak overpressure and impulse to the side and rear of the structure at the lower loading density. The impulse propagating to the front of the structure was enhanced while the peak overpressure showed no significant effect of the low loading density.

RESEARCH AND DEVELOPMENT

I. INTRODUCTION

A. Background

This study is an extension of earlier work sponsored by the Department of Defense Explosives Safety Board (DDESB) to determine the airblast parameters propagating to the front, side, and rear of a munition storage magazine in event of an accidental explosion. In Reference 1 the model (1/50th-scale) study was based on 226800 kg, 136100 kg, and 45400 kg of explosive stored in a standard (18.3 metre length), steel single arch magazine.

Comparisons of the results from the model tests with full scale test results were excellent and added to the validity of using scaled models to simulate blast effects from full scale accidental explosions.

There are requirements for storing, in standard magazines, net explosive quantities, smaller than those tested in Reference 1. The earth cover suppresses the blast to the side and rear of the magazine in the near field but there is no suppression effect at the explosive work shop distance* and beyond for a Q of 45400 kilograms. It is surmised that there will be some suppressive effect at the greater distances, ($> 7.14 Q^{1/3} \text{ m}$) for smaller quantities stored in this magazine. If true it would permit siting of operating buildings and other controlled facilities closer to the above ground storage magazines.

B. Objectives

The objective of this series of tests is to obtain from scale-model experiments data on the suppression of blast propagation from stored quantities of munition in the range from 45400 kg (100090 lbm) down to approximately 4540 kg (10009 lbm).

This should provide a basis for establishing the quantity-distances to certain exposures from igloos containing small quantities of explosives. The distances of interest range from the safe separation distance $0.5Q^{1/3} \text{ m}$ ($1.25 w^{1/3} \text{ ft}$) out to $16Q^{1/3} \text{ m}$ ($40 w^{1/3} \text{ ft}$) where Q is in kilograms and distance is metres, and w is in pounds mass and distance is in feet.

A second objective was added to the program after the first series of tests were completed. Because the overlap of data from the 1/50th-scale model results simulating 45400 kg full scale and the 1/30th-scale model simulating 45400 kg full scale were not within an acceptable error band it was proposed to fire a 5.04 kg charge in the 1/30th-scale donor model to check the full scale magazine loaded with 136080 kg (300,000 lbm) as reported in Reference 1.

¹ C. Kingery, G. Coulter, and T. Watson, "Blast Parameters from Explosions in Model Earth Covered Magazines," BRL-MR-2680, Sept 1976.

* The explosive work shop distance is defined as $d_e = 7.14 \text{ m/kg}^{1/3}$, scaled to the cube root of the mass Q(kg) of explosive: $D_e = d_e \times Q^{1/3}$.

TEST PROCEDURE

The test procedures followed to meet the objective were to (1) design the scale model, (2) design the explosive source, and (3) establish the instrumentation and blast lines.

A. Design of Magazine Model

The standard munitions storage magazine being modeled for this series of tests is shown in Figure 1. The overall width including the earth cover is 27.43 metres (90 feet) and the length is 28.96 metres (95 feet). The total volume of earth cover is 1665 m^3 ($58,812 \text{ ft}^3$). The volume of the interior of the magazine is 496 m^3 ($17,500 \text{ ft}^3$).

The model scale in Reference 1 was 1/50th and was sufficient for the simulation of large quantities of explosives. In order to simulate smaller quantities of explosives and work with similar size scaled charges a decision was made to use 1/30th-scale donor models. All linear dimensions were scaled down by a factor of 30. The scaled down model, with dimensions, is presented in Figure 2. The total volume of modeling sand is 0.0617 m^3 (2.178 ft^3) and the interior volume of the model is 0.018 m^3 (0.648 ft^3). A photograph of the interior portion of the model without the sand cover is shown in Figure 3. The model arch is aluminum rather than steel as used in the full-size magazines. Scaled steel doors were attached to the masonite headwall to more nearly simulate the suppression of blast associated with the closed doors.

The donor magazine model with the steel doors and modeling sand cover is shown in Figure 4.

B. Test Charges

The test charges used as the explosive source were cast Pentolite (50 PETN/50 TNT). The mass of the charges are usually based on the quantity to be stored in the full size magazine. For this series of tests the three molds for the hemi-cylindrical charges used in the tests reported in Reference 1 were still available and therefore a 1/30th-scale was selected to meet the range of explosive quantities of interest. Two additional molds were designed and manufactured, one to cover the low end of the desired range, and one for the additional high range shot.

The range of scaled charge weights tested were 0.227 kg, 0.363 kg, 1.066 kg, 1.814 kg and 4.99 kg (0.5, 0.8, 2.4, 4.0 and 11.0 lbm). When these masses are scaled up by 30^3 (27,000) then the full scale simulation is 6130 kg, 9800 kg, 28780 kg, 48980 kg, and 134730 kg (13,510, 21,605, 64,750, 107,980, and 297,000 lbm). These charges cover a range from 134730 kg down to 6130 kg which is very close to the original request for a range of 136080 kg down to 4536 kg.

The test charge was always placed with the flat side down and with the center of flat side at the geometric center of the magazine floor. The point of initiation was on the end toward the doors or along the zero degree blast line. The ratio of the mass of the model charge to the interior volume of the model was the same as the mass of the explosive in the storage magazine to the interior volume of the storage magazine.

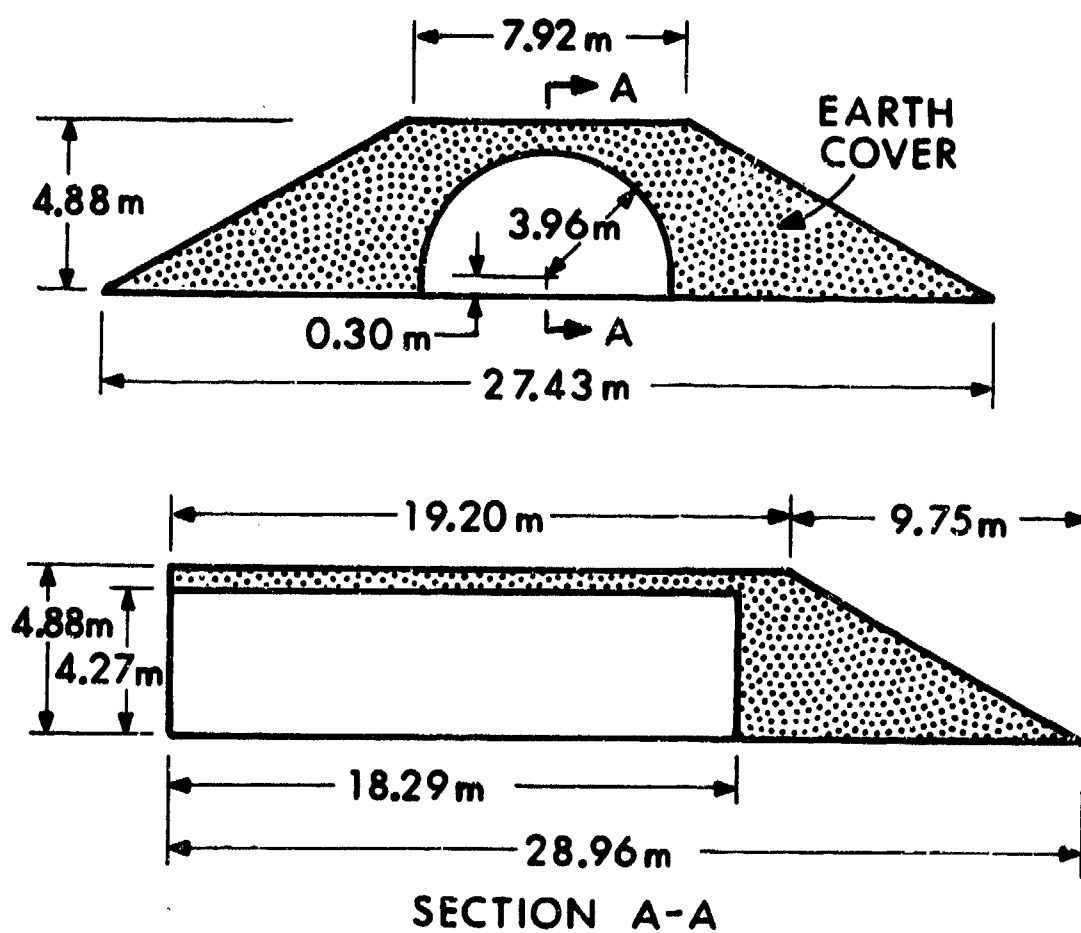
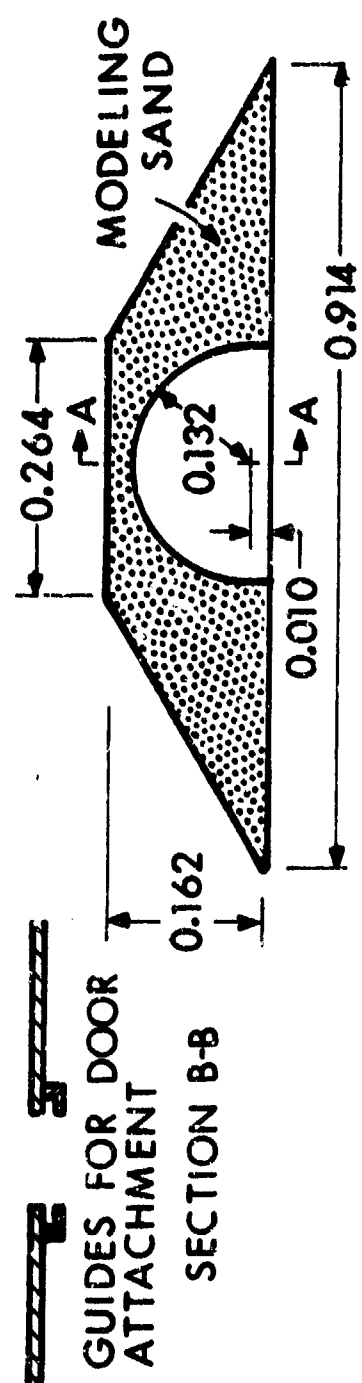
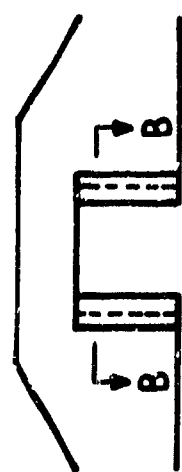
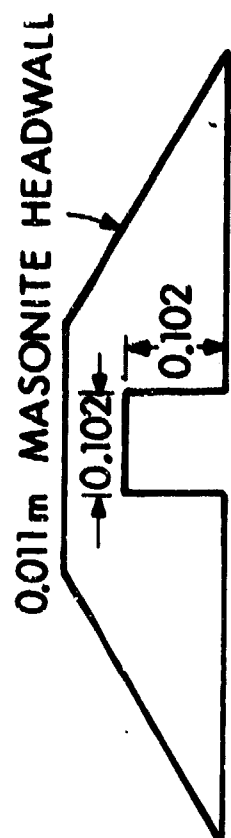


Figure 1. Standard munition storage magazine.



DIMENSIONS IN METRES

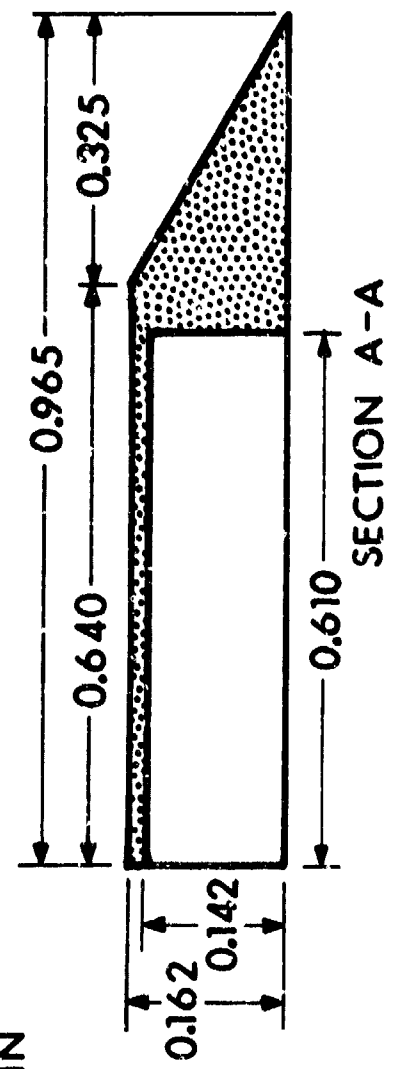
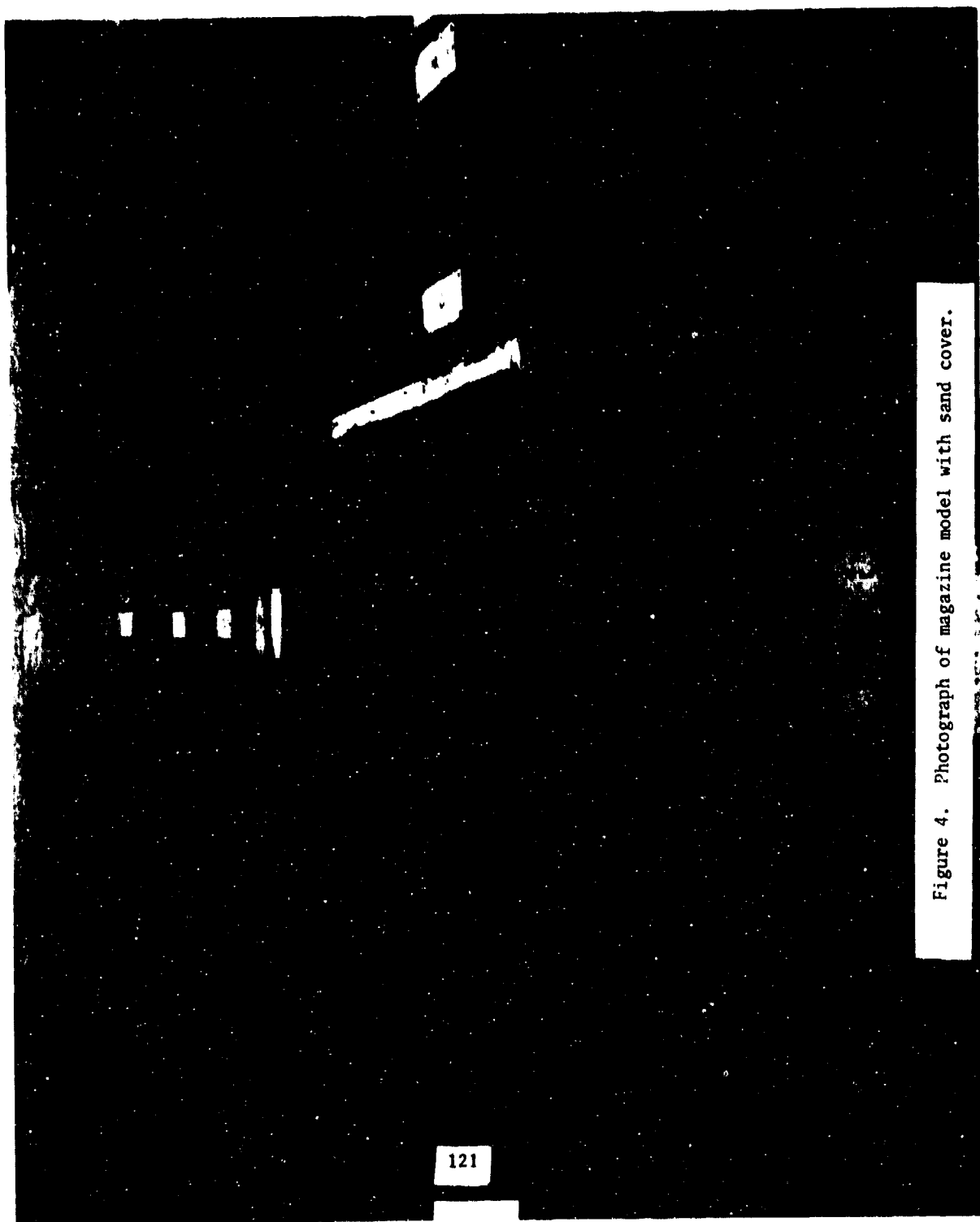


Figure 2. 1/30th-scale munition storage magazine model.



Figure 3. Photograph of internal portion of the magazine model.



C. Test Instrumentation

The instrumentation for this test series consisted of pressure transducers, magnetic tape recorder/playback, and a data reduction system. A block diagram is shown in Figure 5.

1. Pressure Transducers. Piezo-electric pressure transducers were used for this series of tests. The PCB Electronics Inc., models 113A22, 113A24, and 113A28, with quartz sensing elements and built-in source followers were used extensively.

2. Tape Recorder System. The tape recorder consisted of three basic units, the power supply and voltage calibrator, the amplifiers, and the FM recorder. The FM tape recorder was a Honeywell 7600 having a frequency response of 80 kHz. Once the signal was recorded on the magnetic tape it was played back and recorded on a Honeywell Visicorder. This oscillograph has 5 kHz frequency response and the overpressure versus time recorded at the individual stations can be read directly from the playback records for preliminary data analysis.

3. Data Reduction System. For the final data output, the tape signals were processed through an analog-to digital converter, to a digital recorder-reproducer, and then to a computer. The computer (TEKTRONX 4051) was programmed to apply the calibration values and present the data in the proper units for analysis. From the computer, the data is put on a digital tape from which the final form can be plotted or tabulated. The digital tape can be also stored for future analysis.

D. Test Layout

The objective of this program was to document the blast propagation from a scaled munition magazine model assuming an accidental explosion of a specific amount of explosive. This required three lines instrumented with pressure transducers. One to the front of the magazine, designated the 0-degree blast line. One to the side of the magazine, designated the 90-degree blast line, and one to the rear of the magazine designated the 180-degree blast line. The field test layout is shown in Figure 6.

1. Donor Charges in Magazine. When the tests are conducted with the donor charge in the magazine model there are specific distances that should be documented along the blast line. The first of those is the "safe separation" distance. This is defined as the required separation of munition storage magazines. It is a function of the quantity of explosive to be stored and relative locations of the magazines. The safe separation distance to the front and rear of the donor magazine, the 0-degree and 180-degree blast line, is defined as

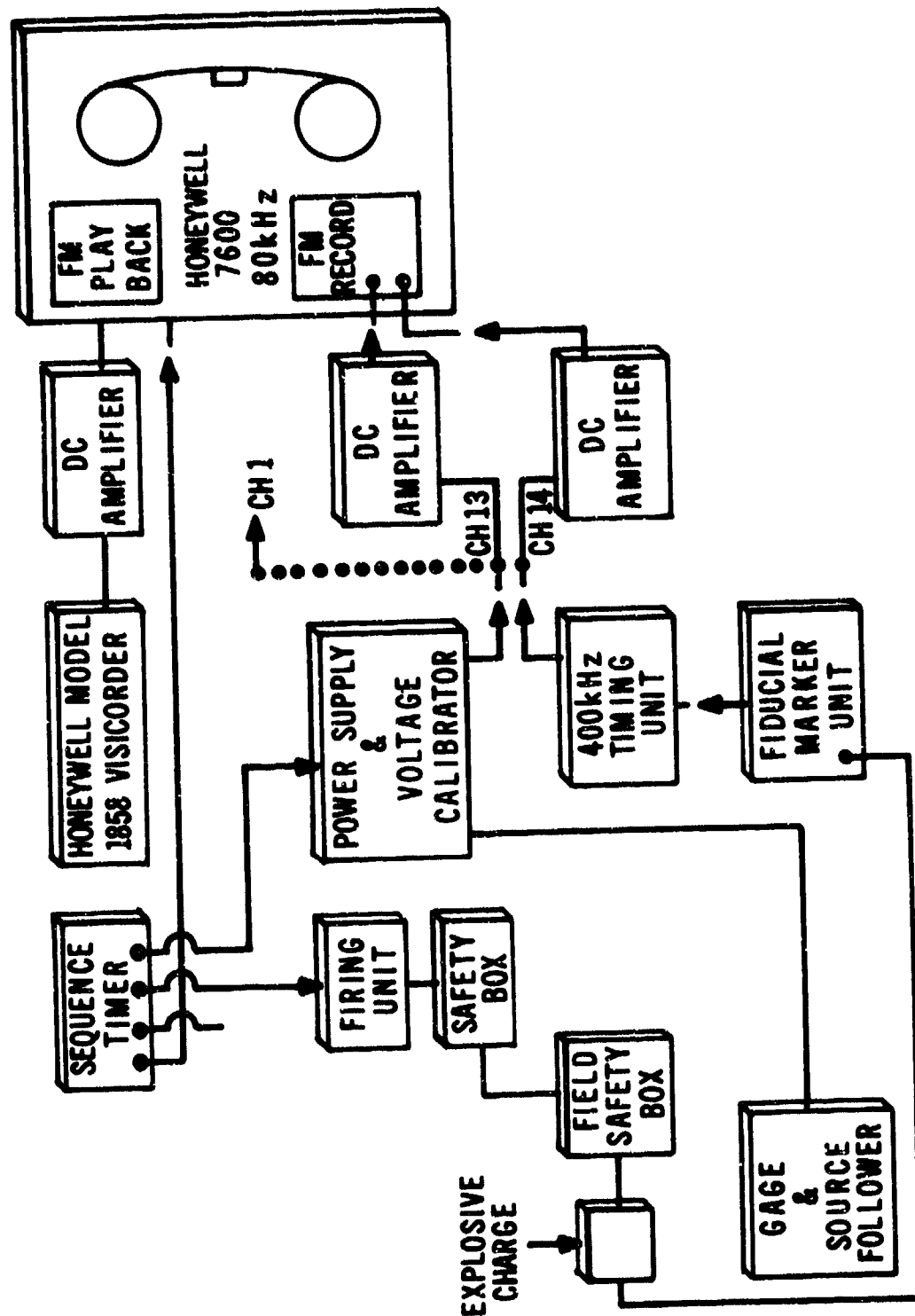


Figure 5. Instrumentation block diagram.

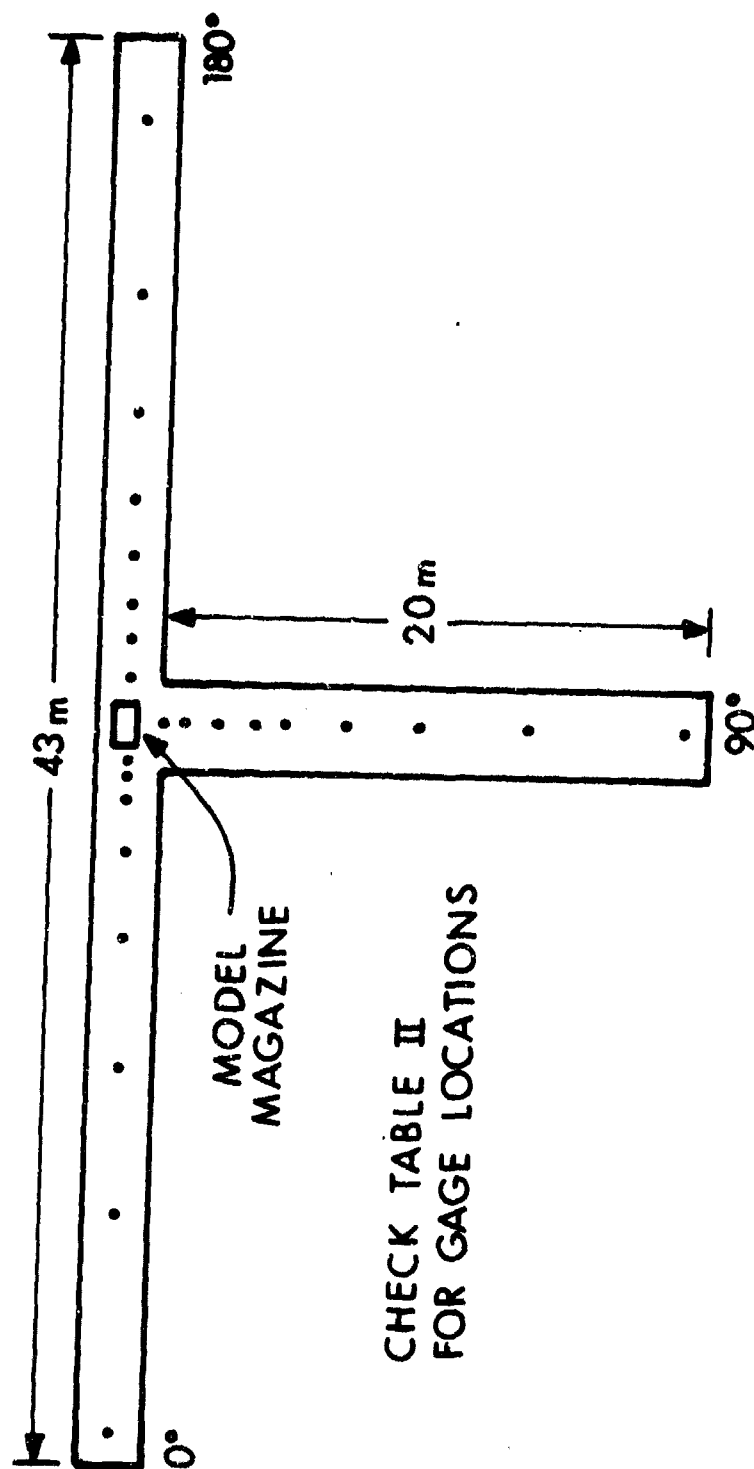


Figure 6. Test field layout.

$$D_{SF} 0-180 = 0.8 \times Q^{1/3} \text{ m.} \quad (1)$$

To the side of the magazine (the 90-degree blast line) the separation distance is defined as

$$D_{SF} 90 = 0.5 \times Q^{1/3} \text{ m.} \quad (2)$$

The safe separation distance is measured from the interior walls of the magazine. The pressure transducer station distances are measured from the geometric center of the floor of the magazine. An adjusted distance of 0.305 m was added to the 0-degree and 180-degree line safe separation distance for the first station and 0.132 m was added to the 90-degree line safe separation distance for the location of the first station. That is

$$D_{SF} 0/180 + 0.305 = 0.8Q^{1/3} + 0.305 \quad (3)$$

$$D_{SF} 90 + 0.137 = 0.5Q^{1/3} + 0.137 \quad (4)$$

Table 1 shows the location of the first station on each blast line for the five charge weights.

TABLE 1. LOCATION OF FIRST STATIONS

Q	$Q^{1/3}$	$.8Q^{1/3}$ m	0 and 180 $.8Q^{1/3} + .305$ m	$.5Q^{1/3}$ m	90 $.5Q^{1/3} + .132$ m
.227	.610	.488	.793	0.305	0.437
.363	.713	.570	.875	0.357	0.487
1.089	1.029	.823	1.128	0.514	0.646
1.814	1.220	.976	1.281	0.610	0.742
4.990	1.709	1.367	1.672	0.855	0.987

The station locations for the five charge weights and the three blast lines are listed in Table 2. The distances range from 0.57 m to 21.3 m with many station distances repeated for the different charge masses in order to keep movement of gage stations to a minimum and thereby keep the turn around time per test as short as possible. Station 90-1 was placed no closer than 0.57 m because the sand cover, the masonite base, and the gage mount would not allow the measurement to be made closer.

2. Donor Charge Unconfined. To meet the objectives of the test and determine the suppressive effect of the earth cover one must establish a base for comparison. Therefore the blast parameters along the 0, 90, and 180-degree blast lines were determined for four charge masses without the magazine in place, ie, charge unconfined. The 5.0 kg charge was not tested unconfined.

E. Test Matrix

The series was designed to conduct the minimum number of tests to meet the objective. Tests were conducted both with the charges covered, ie, in the

TABLE 2. GAGE STATION LOCATIONS

Charge Mass (kg)	4.99	1.814	1.066	0.363	0.227
Station	Distance m	Distance m	Distance m	Distance m	Distance m
0-1	1.68	1.27	1.12	0.87	0.79
0-2	2.29	1.68	1.27	1.27	1.27
0-3	3.20	2.29	1.68	1.68	1.68
0-4	4.27	3.20	2.29	2.29	2.29
0-5	6.00	4.27	3.20	3.20	3.20
0-6	8.40	9.14	6.10	6.10	4.27
0-7	14.00	12.80	10.67	10.67	6.10
0-8	21.00	21.34	18.29	18.29	10.67
90-1	0.99	0.74	0.64	0.61 ^a	0.57 ^a
90-2	1.50	1.12	1.12	1.12	1.14
90-3	2.00	1.27	1.27	1.27	1.68
90-4	3.20	1.68	1.68	1.68	2.30
90-5	4.50	2.29	2.29	2.29	3.35
90-6	6.00	3.20	5.03	5.03	5.03
90-7	8.00	6.71	6.10	6.80	6.80
90-8	12.50	12.80	12.80	12.80	9.14
90-9	21.00	21.34	18.29	18.29	12.80
180-1	1.68	1.27	1.12	0.87	0.79
180-2	2.29	1.68	1.27	1.27	1.27
180-3	3.20	2.29	1.68	1.67	1.68
180-4	4.27	3.20	2.29	2.29	2.29
180-5	6.00	4.27	3.20	3.20	3.20
180-6	8.40	6.10	6.10	6.10	4.27
180-7	14.00	12.80	10.67	10.67	6.10
180-8	21.00	21.34	18.29	18.29	10.67

^aStation was as close as the sand covered slope would allow.

magazine, and uncovered to establish any suppressive effect at the lower stored quantities of munitions. The number of tests and conditions planned are listed in Table 3.

TABLE 3. PLANNED TEST MATRIX

Charge Mass kg	Charge In-Magazine Tests	Charge Unconfined Tests
.227	2	1
.363	2	1
1.089	2	1
1.814	2	1
5.040	2	0

If large variations were found in the results from the two "in-magazine tests" then a third test would be conducted. Likewise if the uncovered shots do not follow the trend established in Reference 1, then a repeat test would be conducted.

III. RESULTS

The results will be presented in the form of tables and graphs. Each blast line will be treated separately for the various charge masses in order to show any suppressive effect the earth cover might have at the lower loading densities.

The program was modified during the field test phase because the overlap expected at the 45360 kg charge mass between the 1/50th-scale (Reference 1) and the 1/30th-scale results did not occur at the safe separation distance. A test series to include the simulation of a full-scale 136,080 kg in a standard magazine was added to further check the 1/50 and 1/30 scaled model results.

There is also some concern in the comparison of the suppressive effect of the earth cover when using a hemicylindrical charge as the donor because of the second shock pulse that develops at the greater distances when detonated in an uncovered environment. Test Number 7 was added in which a hemispherical charge of 1.128 kg was tested in the 1/30th-scaled magazine model of a standard munition storage magazine. The results of this test will be compared with the in-magazine hemicylindrical charge tests. They may also be compared with the standard hemispherical surface burst data.² The tests as conducted are listed in Table 4.

² C.N. Kingery, "Air Blast Parameters versus Distance for Hemispherical TNT Surface Burst," BRL R 1344, September 1960.

TABLE 4. TEST MATRIX AS CONDUCTED

Test No.	Charge Mass, kg	Charge Environment
1	1.814	in magazine
2	1.814	in magazine
3	1.814	free-field
4	1.070	in magazine
5	1.066	in magazine
6	1.066	in magazine
7 ^a	1.128	in magazine
8	1.066	free-field
9	0.363	in magazine
10	0.363	in magazine
11	0.363	free-field
12	0.227	in magazine
13	0.227	in magazine
14	0.227	in magazine
15	0.227	free-field
16	4.99	in magazine
17	4.99	in magazine

^a hemisphere

A. Blast Parameters Along the 0-Degree Blast Line.

The 0-degree blast line extends to the front of the magazine. The results from Reference 1 indicate an enhancement of the blast parameters because of the focusing effect of the three earth barriers and the weakness of the headwall and door. As listed in Table 4 either two or three tests were conducted for the covered conditions therefore an average value is listed in the data tables. Only one test was conducted for the unconfined charges. The 5.0 kg charge was not fired unconfined. The blast parameters for all blast lines and charge masses are listed in Table 5 through 14.

1. Peak Overpressure versus Scaled Distance, 0-Degree Blast Line. The average peak overpressures versus scaled distances recorded at Stations 0-1 through 0-8 for the unconfined tests are listed in Tables 6, 8, 10, and 12. The values are plotted in Figure 7. Where double peaks were recorded along the blast line only the maximum values are plotted. There is excellent agreement between the various charge masses when scaled to 1 kg mass. The results follow the same trend as established in Reference 1.

The peak overpressure versus scaled distance along the 0-degree blast line for the five charge masses, tested in magazine, are plotted in Figure 8. The results indicate a smooth pressure decay with distance over the full range of measurements. It was unexpected that the 5.0 kg tests would produce pressure values lower than average at scaled distances greater than $3 \text{ m/kg}^{1/3}$.

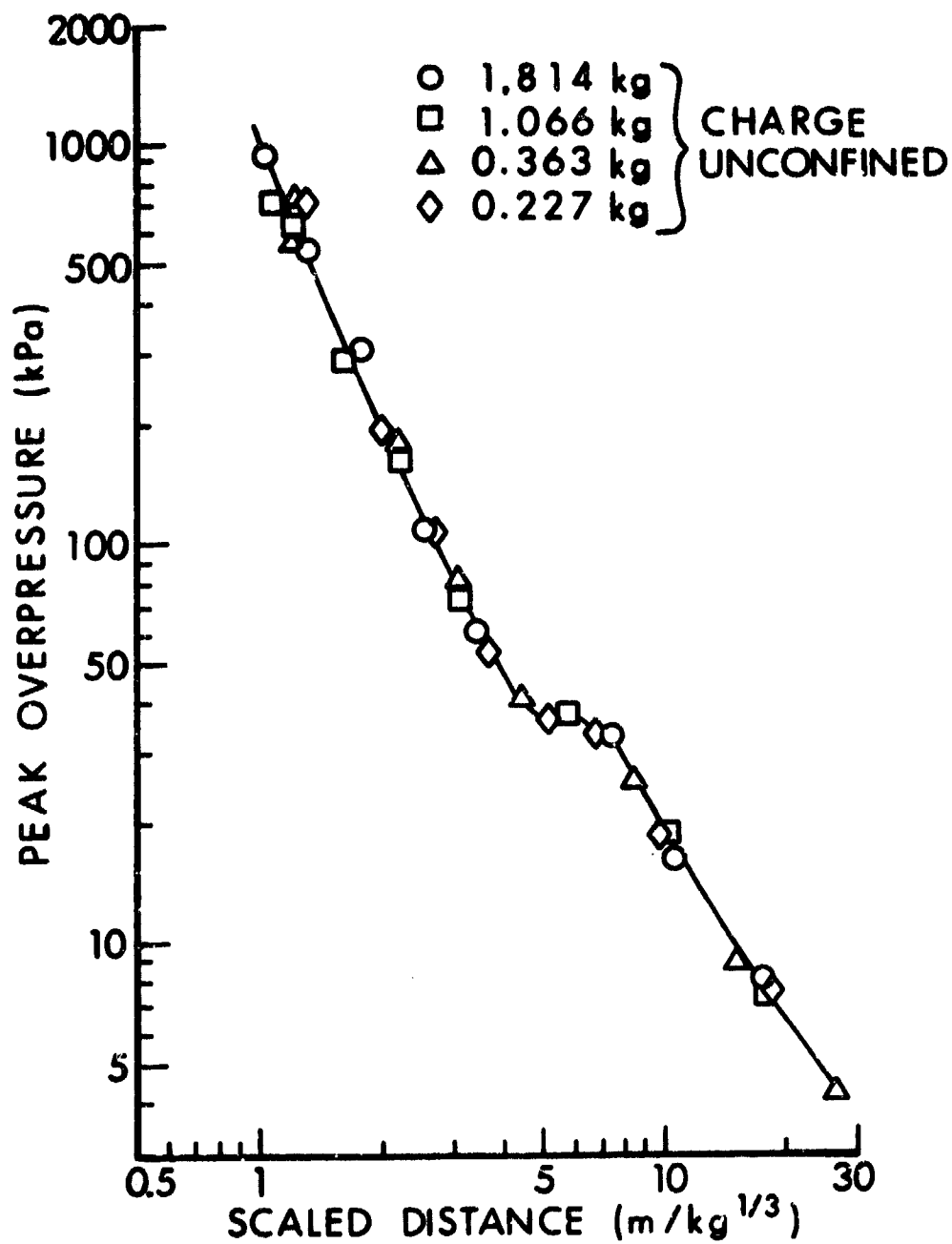


Figure 7. Peak overpressure versus scaled distance along the 0-degree blast line, charge unconfined.

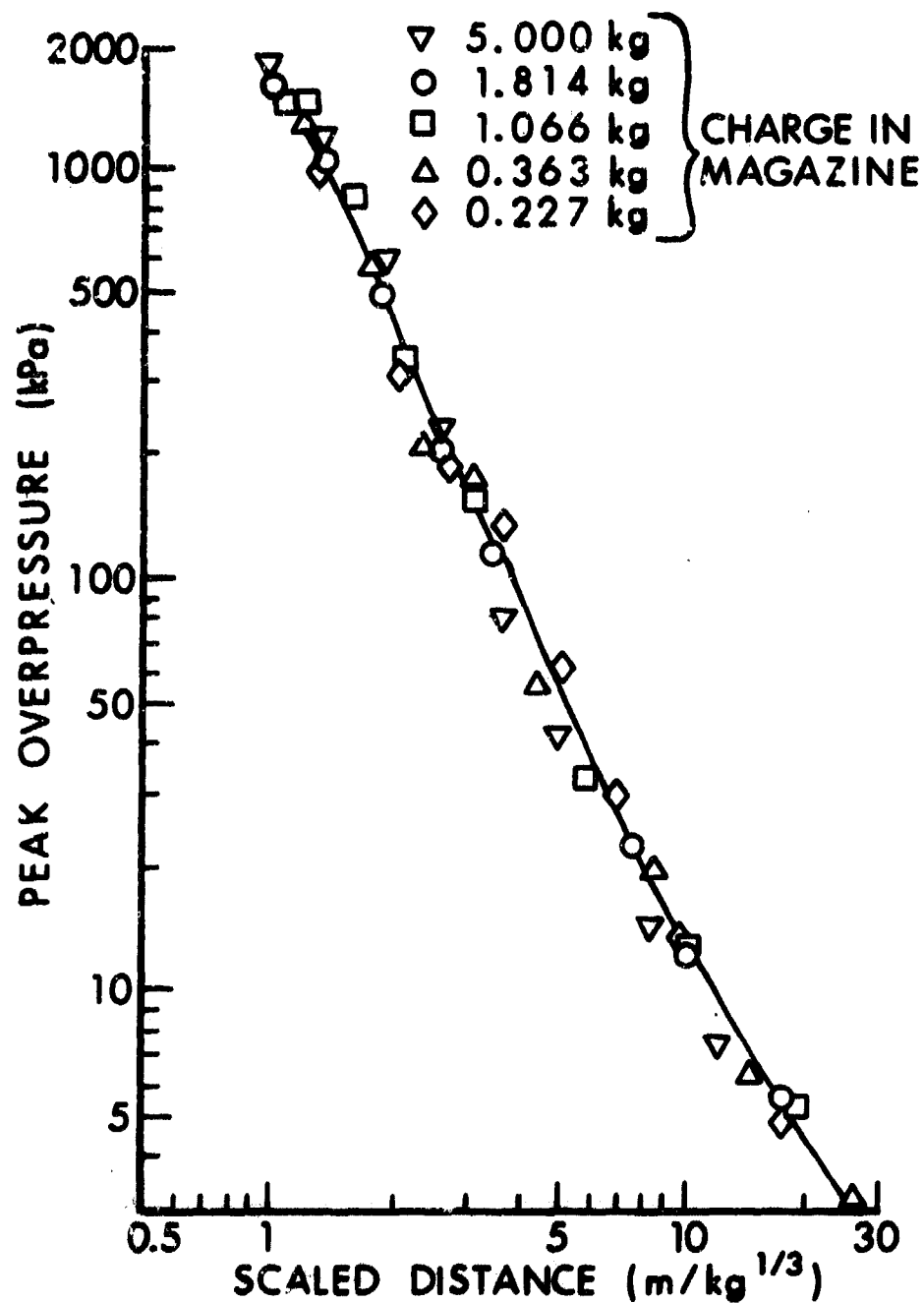


Figure 8. Peak overpressure versus scaled distance along the 0-degree blast line, charges in magazine.

TABLE 5. AIR BLAST PARAMETERS FROM 1.814 kg IN MAGAZINE

Station	Distance from Ground Zero		Peak Overpressure		Overpressure Impulse		Arrival Time		Positive Duration		Scaled Distance		Scaled Impulse	
	metres	feet	kPa	psi	kPa-ms	psi-ms	ms	ms	ms	ms	m/kg ^{1/3}	m/kg ^{1/3}	kPa-ms/kg ^{1/3}	kPa-ms/kg ^{1/3}
0-1	1.27	4.17	1504	218	292	42.3	0.528	0.95			1.04		239	
0-2	1.68	5.50	1001	145	257	37.3	0.861	1.31			1.38		211	
0-3	2.29	7.50	572	83	212	30.8	1.536	2.51			1.88		174	
0-4	3.20	10.50	225	33	137	19.8	2.870	2.60			2.62		112	
0-5	4.27	14.00	113	16.1	99.6	14.4	5.185	2.75			3.50		81.7	
0-6	9.14	30.00	22.4	3.25	34.9	5.06	18.00	4.15			7.49		28.6	
0-7	12.80	42.00	12.4	1.79	25.6	3.71	28.51	4.50			10.50		21.0	
0-8	21.34	70.00	5.49	0.80	14.4	2.09	53.21	5.60			17.50		11.8	
90-1	0.74	2.42	273/390	39.6/56.6	135	19.6	1.075	1.24			0.61		111	
90-2	1.12	3.68	304	44.0	126	18.2	1.630	1.44			0.92		103	
90-3	1.27	4.17	333	48.3	123	17.8	1.885	1.39			1.04		101	
90-4	1.68	5.50	228	33.1	115	16.8	2.560	1.87			1.38		94.3	
90-5	2.29	7.50	157	22.8	113	16.4	3.765	2.56			1.88		92.7	
90-6	3.20	10.50	94.9	13.8	90.1	13.1	5.935	2.77			2.62		73.9	
90-7	6.71	22.01	36.3	5.26	52.7	7.65	14.93	4.37			5.50		43.2	
90-8	12.80	42.00	12.0	1.75	29.8	4.33	32.11	5.33			10.50		24.4	
90-9	21.34	70.00	5.99	0.87	18.8	2.77	56.84	6.55			17.50		15.4	
180-1	1.27	4.17	288	41.8	95.5	13.8	1.760	1.93			1.04		78.3	
180-2	1.68	5.51	209	30.3	88.0	12.8	2.420	1.66			1.38		72.2	
180-3	2.29	7.51	113	16.5	76.9	11.2	3.745	2.52			1.88		63.1	
180-4	3.20	10.50	66.9	9.70	57.8	8.38	5.875	2.99			2.62		47.4	
180-5	4.27	14.00	44.0	6.38	49.1	7.12	8.663	3.65			3.50		40.3	
180-6	6.10	20.01	27.5	4.00	39.9	5.78	13.56	4.55			5.00		32.7	
180-7	12.80	42.00	8.24	1.20	20.5	2.98	32.67	5.41			10.50		16.8	
180-8	21.34	70.00	4.50	0.65	12.5	1.81	57.62	6.04			17.50		10.2	

TABLE 6. AIR BLAST PARAMETERS FROM 1.814 kg UNCONFINED

Station	Distance from Ground Zero		Peak Overpressure		Overpressure Impulse		Arrival Time ms	Positive Duration ms	Scaled Distance m/kg ^{1/3}	Scaled Impulse kPa-ms/kg ^{1/3}
	metres	feet	kPa	psi	kPa-ms	psi-ms				
0-1	1.27	4.17	911	132	269	39.0	0.462	1.27	1.04	220
0-2	1.68	5.50	543	787	182	26.4	0.907	1.82	1.38	149
0-3	2.29	7.50	304	44.1	124	18.0	1.790	1.93	1.88	102
0-4	3.20	10.50	106	15.4	104	15.1	3.510	3.50	2.62	85.3
0-5	4.27	14.00	61.0/48.8	8.8/7.1	94.3	12.6	6.060	3.75	3.50	77.3
0-6	9.14	30.00	33.8	4.90	53.9	7.81	19.32	4.90	7.49	44.2
0-7	12.80	42.00	16.1	2.34	36.6	5.30	29.44	5.10	10.50	30.0
0-8	21.34	70.00	8.09	1.17	22.4	3.25	53.92	6.10	17.50	18.4
90-1	0.74	2.42	4153	602	215	31.2	0.125	0.28	0.61	176
90-2	1.12	3.68	2462	357	251	36.4	0.290	0.49	0.92	206
90-3	1.27	4.17	—	—	—	—	—	—	1.04	—
90-4	1.68	5.50	1508	219	303	44.0	0.665	1.12	1.38	248
90-5	2.29	7.50	550	79.8	155	22.5	1.350	1.24	1.88	127
90-6	3.20	10.50	216	31.4	110	16.0	2.990	3.98	2.62	90.2
90-7	6.71	22.01	40.5	5.87	60.4	8.77	11.52	4.91	5.50	49.6
90-8	12.80	42.00	11.6	1.69	34.2	4.96	28.78	6.42	10.50	28.0
90-9	21.34	70.00	5.48	0.80	21.2	3.07	53.84	7.25	17.50	17.4
180-1	1.27	4.17	—	—	—	—	—	—	1.04	—
180-2	1.68	5.51	—	—	—	—	—	—	1.38	—
180-3	2.29	7.51	—	—	—	—	—	—	1.88	—
180-4	3.20	10.50	332	48.1	109	15.8	1.690	1.61	2.62	89.2
180-5	4.27	14.00	68.9	10.0	66.7	9.67	3.855	3.68	3.50	54.7
180-6	6.10	20.01	24.6/39.6	3.57/5.74	76.4	11.1	8.637	7.68	5.00	62.7
180-7	12.80	42.00	4.43/18.8	.643/2.73	37.4	5.43	28.01	7.12	10.50	30.7
180-8	21.34	70.00	2.25/8.28	.327/1.20	22.0	3.20	53.27	7.13	17.50	18.1

TABLE 7. AIR BLAST PARAMETERS FROM 1.066 kg IN MAGAZINE

Station	Distance from Ground Zero		Peak Overpressure		Overpressure Impulse		Arrival Time		Positive Duration		Scaled Distance		Scaled Impulse	
	metres	feet	kPa	psi	kPa-ms	psi-ms	ms	ms	ms	ms	m/kg ^{1/3}	m/kg ^{1/3}	kPa-ms/kg ^{1/3}	kPa-ms/kg ^{1/3}
0-1	1.12	3.68	1400	203	203	29.5	0.491	0.75	1.10	198				
0-2	1.27	4.17	1430	207	257	37.3	0.596	1.10	1.24	251				
0-3	1.68	5.50	827	120	241	35.0	0.980	2.20	1.64	236				
0-4	2.29	7.50	356	51.6	146	21.2	1.772	2.34	2.24	143				
0-5	3.20	10.50	166	24.1	96	13.4	3.462	2.77	3.13	94				
0-6	6.10	20.00	33.1	4.80	40.4	5.87	10.76	3.00	5.97	39.5				
0-7	10.67	35.00	12.7	1.85	25.6	3.71	23.82	3.97	10.44	25.0				
0-8	18.29	60.00	5.28	0.77	12.1	1.75	45.76	4.41	17.90	11.9				
90-1	0.64	2.10	282/317	40.9/46.0	109	15.8	1.060	1.22	0.63	107				
90-2	1.12	3.68	194/226	28.1/32.8	100	14.5	1.782	1.49	1.10	97.9				
90-3	1.27	4.17	200	29.0	97.4	14.1	2.067	1.68	1.24	95.4				
90-4	1.68	5.50	163	23.6	91.8	13.3	2.850	1.98	1.64	89.9				
90-5	2.29	7.50	116	16.8	84.0	12.1	4.178	2.24	2.24	82.2				
90-6	5.03	16.50	44.0	6.39	52.8	7.65	11.21	3.26	4.92	51.6				
90-7	6.10	20.00	29.5	4.28	39.0	5.66	14.06	3.77	5.97	38.2				
90-8	12.80	42.00	8.72	1.27	19.4	2.82	33.28	4.70	12.53	19.0				
90-9	18.29	60.00	5.15	0.75	14.0	2.02	49.38	5.65	17.90	13.7				
180-1	1.12	3.68	249	36.1	77.2	11.2	1.554	1.14	1.10	75.6				
180-2	1.27	4.17	223	32.3	75.0	10.9	1.801	1.32	1.24	73.4				
180-3	1.68	5.50	156	22.6	68.7	10.0	2.632	1.78	1.64	67.3				
180-4	2.29	7.50	90.2	13.1	55.2	8.00	3.977	2.29	2.24	54.0				
180-5	3.20	10.50	48.4	7.02	41.3	6.00	6.275	2.83	3.13	40.5				
180-6	6.10	20.00	18.4	2.66	26.3	3.82	14.21	4.56	5.97	25.8				
180-7	10.67	35.00	7.36	1.07	16.1	2.34	27.42	4.85	10.44	15.8				
180-8	18.29	60.00	3.71	0.54	8.96	1.30	49.90	5.34	17.90	8.78				

TABLE 8. AIR BLAST PARAMETERS FROM 1.066 kg UNCONFINED

Station	Distance from Ground Zero		Peak Overpressure		Overpressure Impulse		Arrival Time		Positive Duration		Scaled Distance		Scaled Impulse	
	metres	feet	kPa	psi	kPa-ms	psi-ms	ms	ms	ms	ms	m/kg ^{1/3}	m/kg ^{1/3}	kPa-ms/kg ^{1/3}	kPa-ms/kg ^{1/3}
0-1	1.12	3.68	708	03	185	27.0	0.422	1.21	1.10	182				
0-2	1.27	4.17	625	91.0	184	26.7	0.575	1.70	1.24	180				
0-3	1.68	5.50	290	39.5	108	15.7	1.170	1.50	1.64	106				
0-4	2.29	7.50	166	24.1	82.0	11.9	2.240	1.98	2.24	80.2				
0-5	3.20	10.50	67.5/73.2	9.79/10.5	84.6	12.3	4.290	3.00	3.13	82.8				
0-6	6.10	20.00	23.6/37.9	3.42/5.50	57.2	8.29	12.04	4.00	5.97	56.0				
0-7	10.67	35.00	18.2	2.63	35.8	5.19	24.70	4.50	10.44	35.0				
0-8	18.29	60.00	7.42	1.08	18.1	2.62	46.78	5.20	17.90	17.7				
90-1	0.64	2.10	2634	382	176	25.5	0.085	0.30	0.63	172				
90-2	1.12	3.68	2345	340	259	37.6	0.315	1.10	1.10	254				
90-3	1.27	4.17	1352	196	183	26.5	0.420	0.58	1.24	179				
90-4	1.68	5.50	849	123	180	26.1	0.775	0.88	1.64	176				
90-5	2.29	7.50	318	46.1	121	17.6	1.665	2.07	2.24	118				
90-6	5.03	16.50	56.1	8.14	64.1	9.29	8.165	4.00	4.92	62.7				
90-7	6.10	20.00	33.3	4.83	47.1	6.83	11.04	4.56	5.97	46.1				
90-8	12.80	42.00	8.80	1.28	23.5	3.41	30.39	5.55	12.53	23.0				
90-9	18.29	60.00	5.21	0.76	17.0	2.46	46.66	6.23	17.90	16.5				
180-1	1.12	3.68	4375	634	505	73.2	0.265	1.85	1.10	494				
180-2	1.27	4.17	—	—	—	—	—	—	1.24	—				
180-3	1.68	5.50	2193	318	205	29.7	0.535	0.65	1.64	200				
180-4	2.29	7.50	557	80.8	148	21.4	1.060	1.37	2.24	144				
180-5	3.20	10.50	94.8	13.7	72.9	10.6	2.815	4.49	3.13	71.3				
180-6	6.10	20.00	17.3/47.9	2.51/6.95	55.7	8.08	10.64	5.43	5.97	54.6				
180-7	10.67	35.00	4.70/19.4	0.68/2.81	33.2	4.81	24.10	5.35	10.44	32.4				
180-8	18.29	60.00	1.40/8.94	0.20/1.30	18.0	2.62	46.97	5.30	17.90	17.7				

TABLE 9. AIR BLAST PARAMETERS FROM 0.363 kg IN MAGAZINE

Station	Distance from Ground Zero		Peak Overpressure		Overpressure Impulse		Arrival Time		Positive Duration		Scaled Distance		Scaled Impulse	
	metres	feet	kPa	psi	kPa-ms	psi-ms	ms	ms	ms	ms	m/kg ^{1/3}	m/kg ^{1/3}	kPa-ms/kg ^{1/3}	kPa-ms/kg ^{1/3}
0-1	0.87	2.86	1215	176	173	25.1	0.541	0.54	0.54	0.54	1.22	1.22	243	243
0-2	1.27	4.17	572	83.0	148	21.4	0.969	1.44	1.44	1.44	1.78	1.78	207	207
0-3	1.68	5.50	201	29.2	102	14.8	1.620	1.56	1.56	1.56	2.35	2.35	143	143
0-4	2.29	7.50	176	25.5	74.7	10.8	2.900	2.03	2.03	2.03	3.20	3.20	105	105
0-5	3.20	10.50	55.7	8.08	46.7	6.77	4.940	2.98	2.98	2.98	4.49	4.49	65.5	65.5
0-6	6.10	20.00	19.6	2.85	22.5	3.27	12.88	3.40	3.40	3.40	8.55	8.55	31.6	31.6
0-7	10.67	35.00	6.28	0.91	11.4	1.65	26.30	3.96	3.96	3.96	14.96	14.96	16.0	16.0
0-8	18.29	60.00	3.10	0.45	6.00	0.87	48.95	4.46	4.46	4.46	25.64	25.64	8.41	8.41
90-1	0.61	2.00	85/.105	12.3/15.2	67.5	9.79	1.215	1.55	1.55	1.55	0.86	0.86	94.6	94.6
90-2	1.12	3.68	64.5/83.9	9.35/12.2	57.4	8.33	2.098	1.85	1.85	1.85	1.57	1.57	80.5	80.5
90-3	1.27	4.17	59.0/89.4	8.6/13.1	57.1	8.28	2.413	2.10	2.10	2.10	1.78	1.78	80.0	80.0
90-4	1.68	5.50	46.5/70.6	6.74/10.2	52.5	7.62	3.343	2.30	2.30	2.30	2.35	2.35	73.6	73.6
90-5	2.29	7.50	36.2/52.8	5.25/7.66	46.9	6.80	4.985	2.58	2.58	2.58	3.20	3.20	65.8	65.8
90-6	5.03	16.50	22.0	3.19	22.8	3.31	12.61	3.92	3.92	3.92	7.05	7.05	32.0	32.0
90-7	6.80	22.30	11.8	1.71	16.2	2.35	17.57	2.95	2.95	2.95	9.53	9.53	22.7	22.7
90-8	12.80	42.00	4.68	0.68	8.58	1.24	35.26	3.44	3.44	3.44	17.95	17.95	12.0	12.0
90-9	18.29	60.00	2.90	0.42	5.78	0.84	51.54	3.92	3.92	3.92	25.64	25.64	8.11	8.11
180-1	0.87	2.86	120	17.4	42.1	6.11	1.455	1.50	1.50	1.50	1.22	1.22	59.0	59.0
180-2	1.27	4.17	82.4	11.9	36.6	5.31	2.330	1.80	1.80	1.80	1.76	1.76	51.3	51.3
180-3	1.67	5.50	51.2	7.43	30.8	4.47	3.328	2.32	2.32	2.32	2.35	2.35	43.2	43.2
180-4	2.29	7.50	32.3	4.68	26.7	3.87	5.108	2.67	2.67	2.67	3.20	3.20	37.4	37.4
180-5	3.20	10.50	21.4	3.10	21.7	3.15	7.650	2.70	2.70	2.70	4.49	4.49	30.4	30.4
180-6	6.10	20.00	9.92	1.44	12.3	1.79	15.92	3.10	3.10	3.10	8.55	8.55	17.3	17.3
180-7	10.67	35.00	4.64	0.67	7.60	1.10	29.23	3.25	3.25	3.25	14.96	14.96	10.6	10.6
180-8	18.29	60.00	2.17	0.31	4.22	0.61	51.69	3.40	3.40	3.40	25.64	25.64	5.92	5.92

TABLE 10. AIR BLAST PARAMETERS FROM 0.363 kg UNCONFINED

Station	Distance from Ground Zero		Peak Overpressure		Overpressure Impulse		Arrival Time		Positive Duration		Scaled Distance		Scaled Impulse	
	metres	feet	kPa	psi	kPa-ms	psi-ms	ms	ms	ms	ms	m/kg ^{1/3}	m/kg ^{1/3}	kPa-ms/kg ^{1/3}	kPa-ms/kg ^{1/3}
0-1	0.87	2.86	568	82.4	104	15.1	0.490	0.95	—	—	1.22	—	146	—
0-2	1.27	4.17	—	—	—	—	—	—	—	—	1.78	—	—	—
0-3	1.68	5.50	173	25.1	71.4	10.4	1.825	1.77	—	—	2.35	—	—	—
0-4	2.29	7.50	80.5	11.7	62.4	9.04	3.165	2.10	—	—	3.20	—	100	—
0-5	3.20	10.50	40.8	5.91	46.7	6.78	5.530	2.40	—	—	4.49	—	87.4	—
0-6	6.10	20.00	25.2	3.66	27.7	4.02	13.44	3.19	—	—	8.55	—	65.5	—
0-7	10.67	35.00	8.96	1.29	16.1	2.34	26.57	3.66	—	—	14.96	—	38.8	—
0-8	18.29	60.00	4.17	0.61	8.70	1.26	49.04	4.13	—	—	25.64	—	22.6	—
90-1	0.61	2.00	2145	311	158	22.9	0.143	0.30	—	—	0.86	—	222	—
90-2	1.12	3.68	772	112	109	15.8	0.528	0.80	—	—	1.57	—	153	—
90-3	1.27	4.17	457	66.3	91.4	13.3	0.710	0.84	—	—	1.78	—	128	—
90-4	1.68	5.50	295	42.8	85.2	12.4	1.368	1.30	—	—	2.35	—	119	—
90-5	2.29	7.50	135	19.6	63.4	9.20	2.600	2.25	—	—	3.20	—	98.9	—
90-6	5.03	16.50	26.2	3.80	33.9	4.91	9.838	3.20	—	—	7.05	—	47.5	—
90-7	6.80	22.30	12.3	1.78	22.4	3.24	14.91	3.50	—	—	9.53	—	31.3	—
90-8	12.80	42.00	4.64	0.67	10.5	1.53	22.70	4.20	—	—	17.95	—	14.8	—
90-9	18.29	60.00	3.24	0.47	8.21	1.19	49.14	4.93	—	—	25.64	—	11.5	—
180-1	0.87	2.86	1713	248	174	25.2	0.168	0.60	—	—	1.22	—	244	—
180-2	1.27	4.17	836	121	128	18.6	0.465	1.58	—	—	1.78	—	179	—
180-3	1.67	5.50	239	34.7	65.6	9.51	1.022	1.70	—	—	2.35	—	92.0	—
180-4	2.29	7.50	89.4	13.0	55.2	8.01	2.230	3.50	—	—	3.20	—	77.4	—
180-5	3.20	10.50	33.2/34.8	4.82/5.05	52.5	7.61	4.560	3.90	—	—	4.49	—	73.6	—
180-6	6.10	20.00	10.5/27.7	1.52/4.02	30.6	4.44	12.74	4.05	—	—	8.55	—	42.9	—
180-7	10.67	35.00	4.00/14.0	0.58/2.03	17.9	2.60	26.08	4.10	—	—	14.9	—	25.1	—
180-8	18.29	60.00	4.46	0.65	9.49	1.38	48.40	4.10	—	—	25.64	—	13.3	—

TABLE 11. AIR BLAST PARAMETERS FROM 0.227 kg IN MAGAZINE

Station	Distance from Ground Zero		Peak Overpressure		Overpressure Impulse		Arrival Time		Positive Duration		Scaled Distance		Scaled Impulse	
	metres	feet	kPa	psi	kPa-ms	psi-ms	ms	ms	ms	ms	m/kg ^{1/3}	m/kg ^{1/3}	kPa-ms/kg ^{1/3}	kPa-ms/kg ^{1/3}
0-1	0.79	2.60	974	141	146	21.1	0.388	0.60	0.60	0.60	1.30	1.30	239	239
0-2	1.27	4.17	310	44.9	134	19.4	1.038	2.02	2.02	2.02	2.08	2.08	219	219
0-3	1.68	5.50	193/185	28.0/26.8	92.0	13.3	1.808	1.86	1.86	1.86	2.75	2.75	151	151
0-4	2.29	7.50	116/135	16.8/19.6	60.4	8.77	3.132	2.75	2.75	2.75	3.75	3.75	99.1	99.1
0-5	3.20	10.50	61.8	8.96	32.2	4.66	5.158	3.06	3.06	3.06	5.25	5.25	52.7	52.7
0-6	4.27	14.00	30.0	4.20	23.3	3.38	8.228	3.04	3.04	3.04	7.00	7.00	38.2	38.2
0-7	6.10	20.00	9.67/13.4	1.40/1.94	15.5	2.25	13.23	3.50	3.50	3.50	9.99	9.99	25.4	25.4
0-8	10.67	35.00	1.81/4.54	0.26/0.66	8.9	1.29	25.61	4.13	4.13	4.13	17.49	17.49	14.6	14.6
90-1	0.57	1.87	72.0/77.0	10.4/11.2	55.4	8.04	1.230	1.50	1.50	1.50	0.93	0.93	90.8	90.8
90-2	1.14	3.73	48.0/64.7	7.0/9.4	49.3	7.15	2.270	1.80	1.80	1.80	1.87	1.87	80.2	80.2
90-3	1.68	5.50	32.7/53.0	4.74/7.69	42.4	6.15	3.640	2.00	2.00	2.00	2.75	2.75	69.5	69.5
90-4	2.30	7.54	25.00/40.6	3.74/5.89	34.0	4.93	5.200	2.24	2.24	2.24	3.76	3.76	55.8	55.8
90-5	3.35	11.00	15.3/25.1	2.22/3.64	24.6	3.57	8.170	2.40	2.40	2.40	5.50	5.50	40.3	40.3
90-6	5.03	16.50	15.5	2.25	17.2	2.50	12.78	2.51	2.51	2.51	8.24	8.24	28.3	28.3
90-7	6.80	22.30	8.80	1.28	12.2	1.77	17.85	2.90	2.90	2.90	11.14	11.14	20.1	20.1
90-8	9.14	30.00	6.03	0.88	8.80	1.28	24.70	3.01	3.01	3.01	14.99	14.99	14.4	14.4
90-9	12.80	42.00	3.81	0.55	6.29	0.91	35.49	3.20	3.20	3.20	21.00	21.00	10.3	10.3
180-1	0.79	2.60	108	15.7	38.4	5.57	1.375	1.60	1.60	1.60	1.30	1.30	63.0	63.0
180-2	1.27	4.17	72.0	10.4	32.2	4.67	1.715	1.71	1.71	1.71	2.08	2.08	52.8	52.8
180-3	1.68	5.50	39.7	5.76	24.4	3.54	3.542	1.80	1.80	1.80	2.75	2.75	40.0	40.0
180-4	2.29	7.50	26.7	3.87	20.5	2.97	5.443	2.23	2.23	2.23	3.75	3.75	33.6	33.6
180-5	3.20	10.50	19.5	2.83	16.5	2.39	7.810	2.75	2.75	2.75	5.25	5.25	27.1	27.1
180-6	4.27	14.00	11.4	1.65	11.7	1.70	11.12	2.90	2.90	2.90	7.00	7.00	19.2	19.2
180-7	6.10	20.00	7.39	1.07	8.85	1.28	18.00	3.00	3.00	3.00	9.99	9.99	14.5	14.5
180-8	10.67	35.00	3.41	0.50	5.07	0.74	29.57	3.40	3.40	3.40	17.49	17.49	8.32	8.32

TABLE 12. AIR BLAST PARAMETERS FROM 0.227 kg UNCONFINED

Station	Distance from Ground Zero		Peak Overpressure		Overpressure Impulse		Arrival Time		Positive Duration		Scaled Distance		Scaled Impulse	
	metres	feet	kPa	psi	kPa-ms	psi-ms	ms	ms	ms	ms	m/kg ^{1/3}	m/kg ^{1/3}	kg-m/s/kg ^{1/3}	kg-m/s/kg ^{1/3}
0-1	0.79	2.60	760	110	102	14.8	0.322	0.80	0.80	0.80	1.30	1.30	167	167
0-2	1.27	4.17	186	27.0	57.3	8.31	1.045	0.94	0.94	0.94	2.08	2.08	93.9	93.9
0-3	1.68	5.50	101	14.7	51.4	7.45	1.902	1.76	1.76	1.76	2.75	2.75	84.3	84.3
0-4	2.29	7.50	53.3	7.73	45.8	6.65	3.330	1.98	1.98	1.98	3.75	3.75	75.1	75.1
0-5	3.20	10.50	35.1	5.09	33.9	4.92	5.715	2.23	2.23	2.23	5.25	5.25	55.6	55.6
0-6	4.27	14.00	32.8	4.76	29.8	4.32	8.500	2.60	2.60	2.60	7.00	7.00	48.8	48.8
0-7	6.10	20.00	18.7	2.71	20.6	2.99	13.46	3.09	3.09	3.09	9.99	9.99	33.8	33.8
0-8	10.67	35.00	7.04	1.02	11.8	1.71	26.26	3.38	3.38	3.38	17.49	17.49	19.3	19.3
90-1	0.57	1.87	1690	245	120	17.4	0.133	0.22	0.22	0.22	0.93	0.93	197	197
90-2	1.14	3.73	543	78.8	92.9	13.5	0.610	0.75	0.75	0.75	1.87	1.87	152	152
90-3	1.68	5.50	195	28.3	56.5	8.19	1.490	2.00	2.00	2.00	2.75	2.75	92.6	92.6
90-4	2.30	7.54	90.0	13.1	49.6	7.20	2.795	2.30	2.30	2.30	3.76	3.76	81.3	81.3
90-5	3.35	11.00	41.9	6.08	34.0	4.93	5.455	2.56	2.56	2.56	5.50	5.50	55.7	55.7
90-6	5.03	16.50	22.4	3.25	23.6	3.42	9.875	2.63	2.63	2.63	8.24	8.24	38.7	38.7
90-7	6.80	22.30	10.8	1.57	15.8	2.29	14.76	3.50	3.50	3.50	11.14	11.14	25.9	25.9
90-8	9.14	30.00	7.01	1.02	11.7	1.70	21.39	3.51	3.51	3.51	14.99	14.99	19.2	19.2
90-9	12.80	42.00	4.40	0.64	8.13	1.18	31.81	3.52	3.52	3.52	21.00	21.00	13.3	13.3
180-1	0.79	2.60	1858	269	130	18.9	0.362	1.00	1.00	1.00	1.30	1.30	213	213
180-2	1.27	4.17	474	68.8	91.0	13.2	0.490	1.50	1.50	1.50	2.08	2.08	149	149
180-3	1.68	5.50	142	20.6	55.8	8.09	1.097	2.30	2.30	2.30	2.75	2.75	91.5	91.5
180-4	2.29	7.50	49.0/20.0	7.11/2.90	44.3	6.43	2.450	3.80	3.80	3.80	3.75	3.75	72.6	72.6
180-5	3.20	10.50	20.00/38.4	2.90/5.57	36.8	5.34	4.870	3.60	3.60	3.60	5.25	5.25	60.3	60.3
180-6	4.27	14.00	10.53/34.4	1.52/5.00	28.7	4.16	7.845	3.80	3.80	3.80	7.00	7.00	47.1	47.1
180-7	6.10	20.00	6.44/23.4	0.93/3.39	22.9	3.32	13.04	3.95	3.95	3.95	9.99	9.99	37.5	37.5
180-8	10.67	35.00	2.08/9.05	0.30/1.31	12.3	1.78	26.20	3.50	3.50	3.50	17.49	17.49	20.2	20.2

TABLE 13. AIR BLAST PARAMETERS FROM 1.128 kg (HEMISPHERE) IN MAGAZINE

Station	Distance from Ground Zero		Peak Overpressure		Overpressure Impulse		Arrival Time		Positive Duration		Scaled Distance		Scaled Impulse	
	metres	feet	kPa	psi	kPa-ms	psi-ms	ms	ms	ms	ms	m/kg ^{1/3}	m/kg ^{1/3}	kPa-ms/kg ^{1/3}	kPa-ms/kg ^{1/3}
0-1	1.12	3.68	1288	187	195	28.3	0.415	0.40	0.40	0.40	1.08	1.08	187	187
0-2	1.27	4.17	1333	193	257	37.3	0.515	0.67	0.67	0.67	1.22	1.22	247	247
0-3	1.68	5.50	718	104	267	38.7	0.912	1.53	1.53	1.53	1.61	1.61	256	256
0-4	2.29	7.50	370	53.7	181	26.2	1.620	1.80	1.80	1.80	2.20	2.20	174	174
0-5	3.20	10.50	169	24.5	132	19.1	3.345	2.40	2.40	2.40	3.07	3.07	127	127
0-6	6.10	20.00	47.5	6.89	64.5	9.36	10.42	3.50	3.50	3.50	5.86	5.86	62.0	62.0
0-7	10.67	35.00	14.3	2.07	27.4	3.97	23.15	4.00	4.00	4.00	10.25	10.25	26.3	26.3
0-8	18.29	60.00	5.73	0.83	15.1	2.19	45.48	5.00	5.00	5.00	17.57	17.57	14.5	14.5
90-1	0.64	2.10	130/539	18.8/78.2	129	18.7	1.010	1.35	1.35	1.35	0.62	0.62	124	124
90-2	1.12	3.68	141/272	20.4/39.4	118	17.1	1.685	1.57	1.57	1.57	1.08	1.08	113	113
90-3	1.27	4.17	118/264	17.1/38.3	112	16.2	1.950	1.74	1.74	1.74	1.22	1.22	108	108
90-4	1.68	5.50	91.0/193	13.2/28.0	105	15.2	2.755	1.64	1.64	1.64	1.61	1.61	101	101
90-5	2.29	7.50	138	20.0	97.3	14.1	4.105	2.45	2.45	2.45	2.20	2.20	93.5	93.5
90-6	5.03	16.50	46.3	6.72	57.3	8.31	11.07	3.34	3.34	3.34	4.83	4.83	55.0	55.0
90-7	6.10	20.00	33.7	4.89	43.9	6.37	13.94	3.85	3.85	3.85	5.86	5.86	42.2	42.2
90-8	12.80	42.00	9.15	1.33	20.9	3.03	33.35	4.80	4.80	4.80	12.30	12.30	20.1	20.1
90-9	18.29	60.00	5.44	0.79	15.0	2.18	49.64	5.73	5.73	5.73	17.57	17.57	14.4	14.4
180-1	1.12	3.68	308	44.7	84.0	12.2	1.378	0.75	0.75	0.75	1.08	1.08	80.7	80.7
180-2	1.27	4.17	273	39.6	80.0	11.6	1.607	1.25	1.25	1.25	1.22	1.22	76.9	76.9
180-3	1.68	5.50	181	26.2	93.1	13.5	2.487	2.30	2.30	2.30	1.61	1.61	89.4	89.4
180-4	2.29	7.50	105	15.2	75.8	11.0	3.980	2.32	2.32	2.32	2.20	2.20	72.8	72.8
180-5	3.20	10.50	58.2	8.44	50.5	7.32	5.970	3.00	3.00	3.00	3.07	3.07	48.5	48.5
180-6	6.10	20.00	24.3	3.52	29.6	4.29	13.78	4.72	4.72	4.72	5.86	5.86	28.4	28.4
180-7	10.67	35.00	8.24	1.20	17.2	2.49	26.90	5.05	5.05	5.05	10.25	10.25	16.5	16.5
180-8	18.29	60.00	3.83	0.56	9.71	1.41	49.32	5.48	5.48	5.48	17.57	17.57	9.33	9.33

TABLE 14. AIR BLAST PARAMETERS FROM 4.99 kg IN MAGAZINE

Station	Distance from Ground Zero		Peak Overpressure		Overpressure Impulse		Arrival Time ms	Positive Duration ms	Scaled Distance $m/kg^{1/3}$	Scaled Impulse $kPa-ms/kg^{1/3}$
	metres	feet	kPa	psi	kPa-ms	psi-ms				
0-1	1.68	5.51	1837	266	328	47.6	.709	1.02	.983	192
0-2	2.29	7.51	1113	161	460	66.8	1.168	2.76	1.34	270
0-3	3.20	10.50	61.4	89.0	258	37.4	2.156	2.58	1.87	151
0-4	4.27	14.01	228	33.1	167	24.2	3.571	2.96	2.50	97.5
0-5	6.00	19.69	74.5	10.8	112	16.2	7.033	4.89	3.51	65.5
0-6	8.40	27.56	43.7	6.34	76.3	11.1	12.916	6.23	4.92	44.7
0-7	14.00	45.93	14.7	2.13	37.7	5.47	28.061	7.34	8.19	22.1
0-8	21.00	68.90	7.50	1.09	27.4	3.97	47.48	11.07	12.29	16.0
90-1	0.99	3.25	49.8	72.2	198	28.7	1.198	1.67	.579	116
90-2	1.50	4.92	338	49.0	186	27.0	1.87	1.93	.878	139
90-3	2.00	6.56	276	40.0	179	26.0	2.67	2.44	1.17	105
90-4	3.20	10.50	166	24.1	165	24.0	4.84	3.53	1.87	96.8
90-5	4.50	14.76	91.3	13.2	121	17.6	7.58	4.23	2.63	70.9
90-6	6.00	19.69	65.7	9.53	99.3	14.4	11.05	4.57	3.51	58.1
90-7	8.00	26.25	47.8	6.93	95.9	13.9	15.96	5.92	4.68	56.1
90-8	12.50	41.01	24.7	3.58	64.8	9.39	27.61	7.25	7.32	37.9
90-9	21.00	68.90	11.1	1.61	38.5	5.56	50.86	8.46	12.29	22.5
180-1	1.68	5.51	266	38.6	115	16.7	1.90	1.99	.983	67.2
180-2	2.29	7.51	196	28.4	116	16.8	2.94	2.72	1.34	67.9
180-3	3.20	10.50	102	14.8	101	14.7	4.75	3.35	1.87	59.2
180-4	4.27	14.01	70.4	10.2	88.3	12.8	7.09	3.96	2.50	51.7
180-5	6.00	19.69	45.0	6.53	78.0	11.3	11.29	6.78	3.51	45.7
180-6	8.40	27.56	29.2	4.24	62.0	9.00	17.43	6.87	4.92	36.3
180-7	14.0	45.93	17.5	2.54	40.5	5.88	32.46	7.91	8.19	23.7
180-8	21.0	68.90	8.63	1.25	27.8	4.04	51.76	8.75	12.29	16.3

As noted in Reference 1 the peak overpressures measured from the in-magazine charges are higher than recorded for the uncovered charges but only out to a scaled distance of $6.5 \text{ m/kg}^{1/3}$. In this region there is a cross-over and the uncovered charges produce higher values at the greater distances. This cross-over of peak overpressure is caused by a second peak wave which develops from a "bridge wave" as described in Reference 3. There is no suppressive effect noted along the 0-degree blast line for the in-magazine lower loading density. The in-magazine peak overpressure values are approximately 25 percent lower than the uncovered values at scaled distances greater than $8 \text{ m/kg}^{1/3}$.

2. Scaled Overpressure Impulse versus Scaled Distance, 0-Degree Blast Line. The scaled overpressure impulse versus scaled distance recorded at Stations 0-1 through 0-8 for the four unconfined charge masses are plotted in Figure 9. There is excellent correlation and with all values scaled to 1 kg there is no apparent mass effect. The scaled values for the five charge masses tested in-magazine are plotted in Figure 10. A phenomenon similar to that noted on the peak overpressure curves are noted on the scaled impulse curves. That is, the overpressure impulse recorded for the in-magazine tests are higher than those recorded on the unconfined tests out to a distance of approximately $5 \text{ m/kg}^{1/3}$ where there is a cross-over. Beyond this range the free-field values of impulse are larger than the in-magazine values. At distances greater than $7 \text{ m/kg}^{1/3}$ the in-magazine values of scaled impulse are approximately 25 percent lower than the unconfined values. The scaled impulse recorded from the larger charges tested in-magazine show greater attenuation at distances greater than $1.5 \text{ m/kg}^{1/3}$ than do the smaller charges. This is the reverse of what might be expected from lower density loading. It is surmised that for the larger charge masses the earth barriers have less effect on the focusing along the 0-degree blast line. As can be seen in Figure 10 the scaled values from the 0.227 kg charge are in general higher than the scaled values from the 5.0 kg charges.

B. Blast Parameters along the 90-Degree Blast Line

The 90-degree blast line extends to the side of the magazine. The gage station locations run from 90-1 to 90-9. The distances are listed in Table 2. The results are listed in Tables 5 through 14 for the five charge masses in-magazine and the four charge masses unconfined. The values of peak overpressure from the tables are plotted versus scaled distance in Figures 11 and 12. The values of scaled overpressure impulse versus scaled distance are plotted in Figures 13 and 14.

1. Peak Overpressure versus Scaled Distance, 90-Degree Blast Line. The values of peak overpressure versus scaled distance along the 90-degree blast line for the unconfined tests are plotted in Figure 11 and show excellent correlation of data when scaled to 1 kg. There is some scatter of data points at scaled distances less than $1 \text{ m/kg}^{1/3}$. The results follow the same trend as established in Reference 1.

³ R.E. Reisler, L. Giglio-Tos, and G.D. Teel, "Air Blast Parameters from Pentolite Cylinders Detonated on the Ground," BRL MR 2472, April 1975.

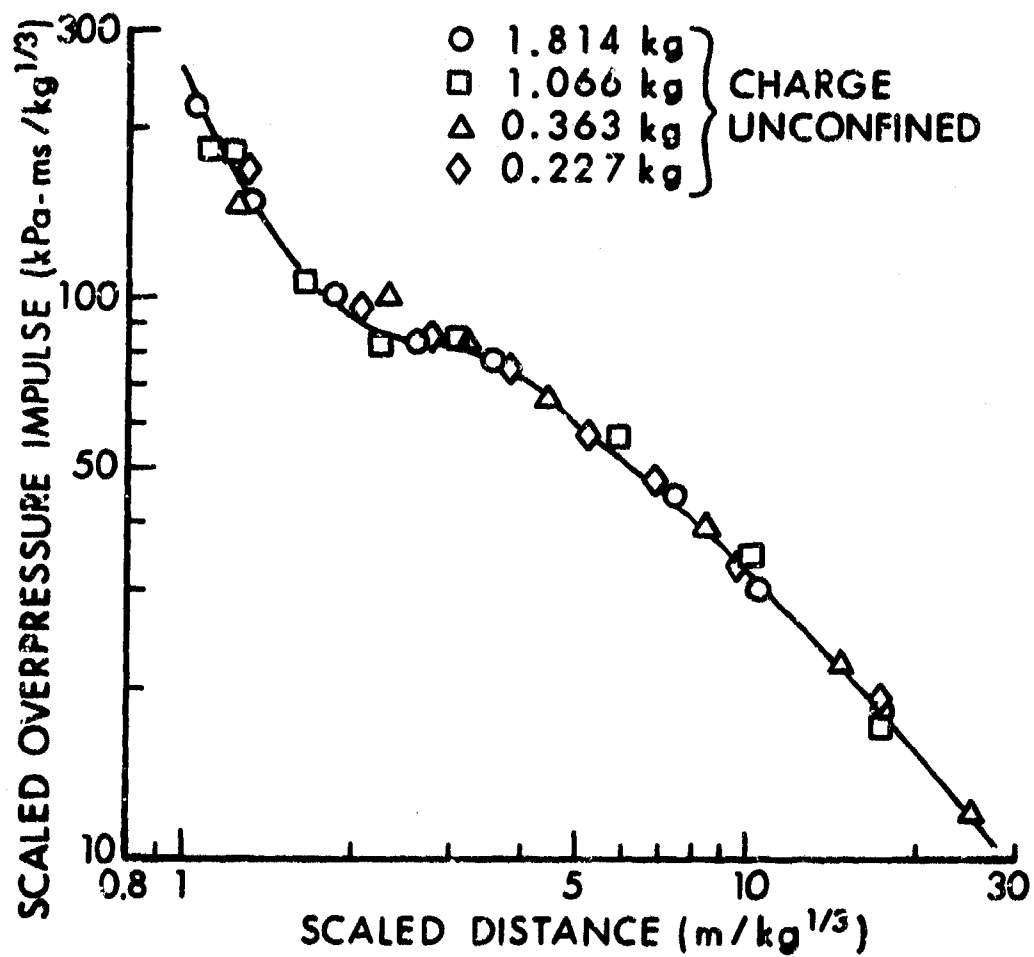


Figure 9. Scaled overpressure impulse versus scaled distance along the 0-degree blast line, charges unconfined.

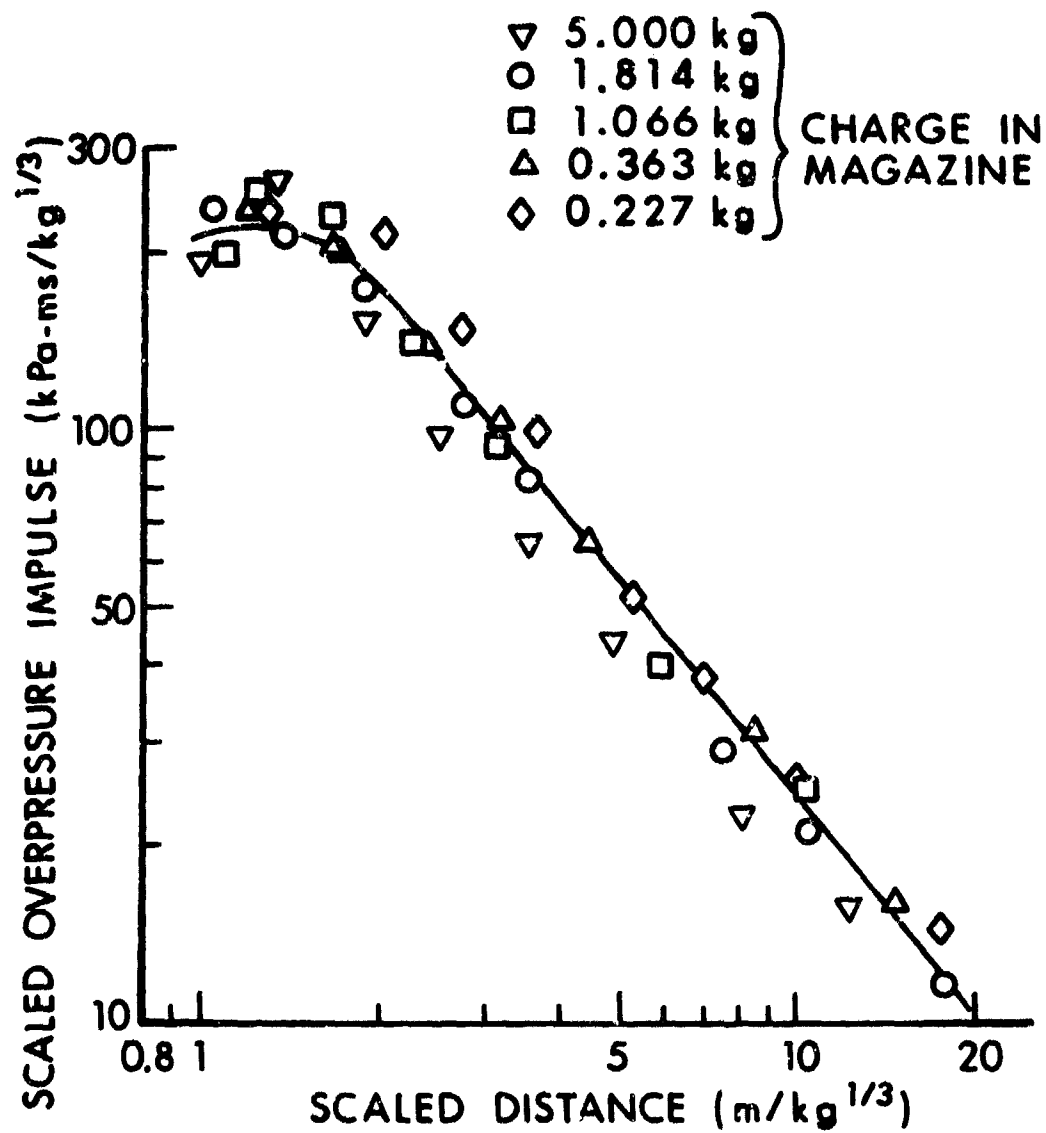


Figure 10. Scaled overpressure impulse versus scaled distance along the 0-degree blast line, charge in magazine.

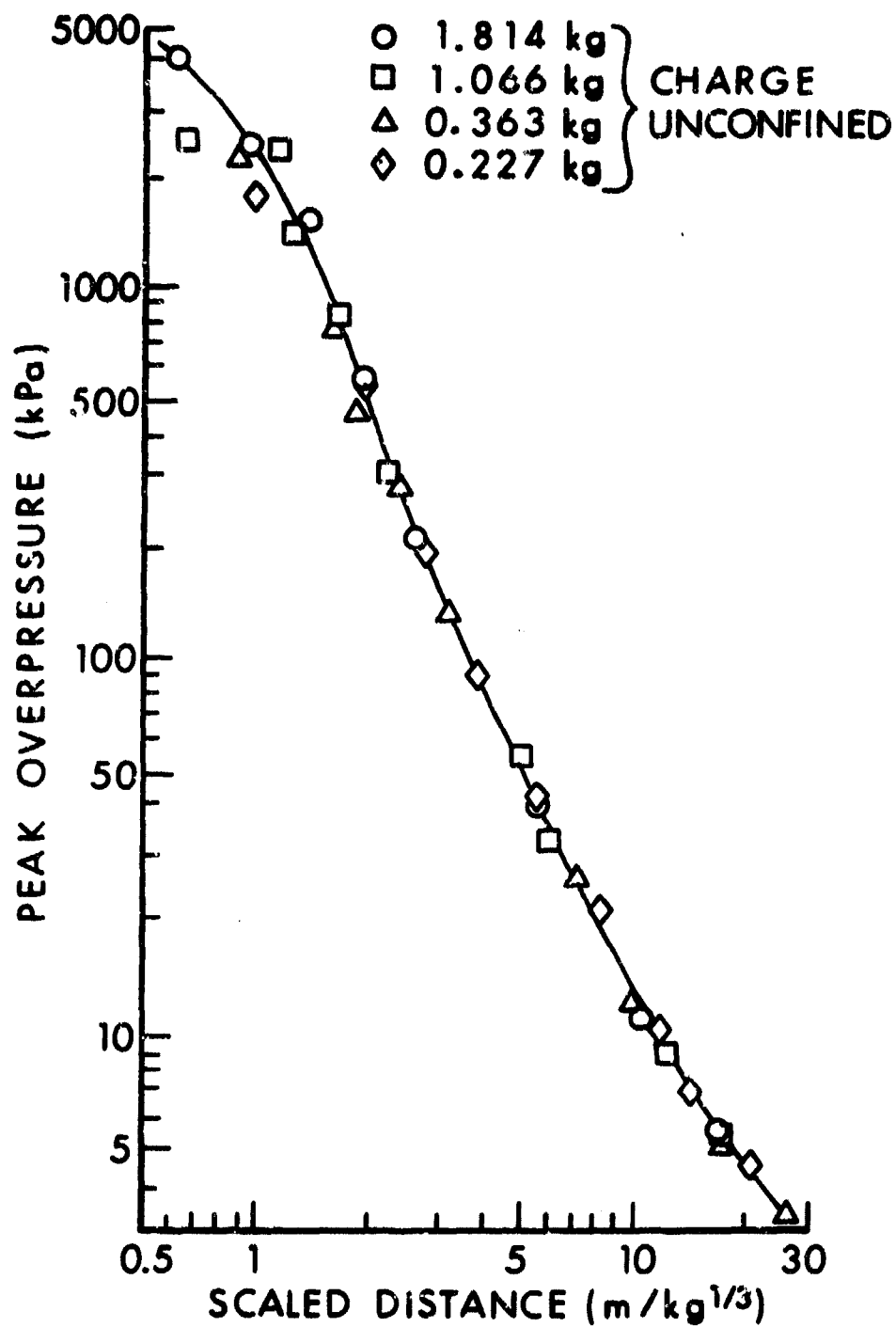


Figure 11. Peak overpressure versus scaled distance along the 90-degree blast line, charges unconfined.

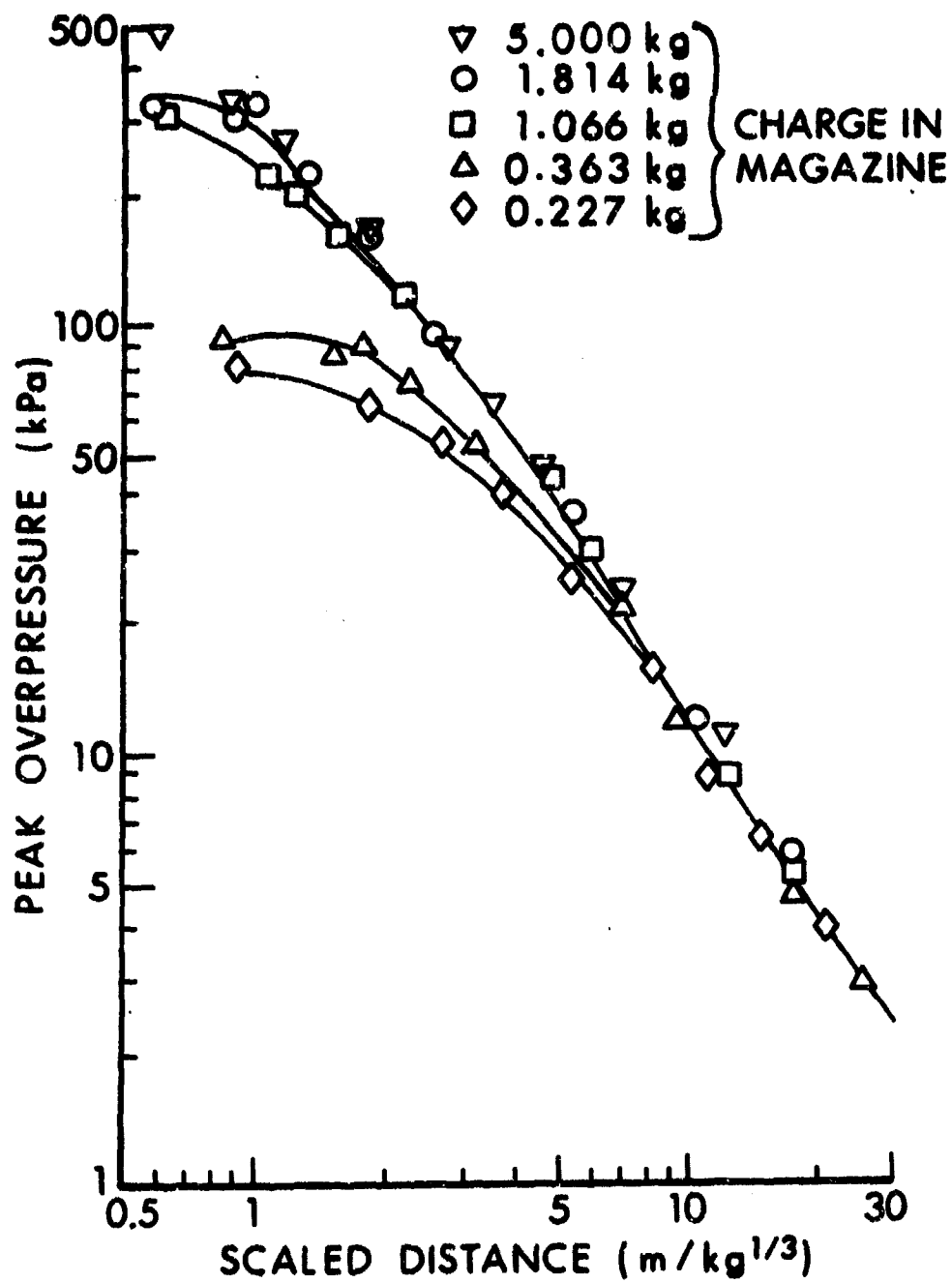


Figure 12. Peak overpressure versus scaled distance along the 90-degree blast line, charges in magazine.

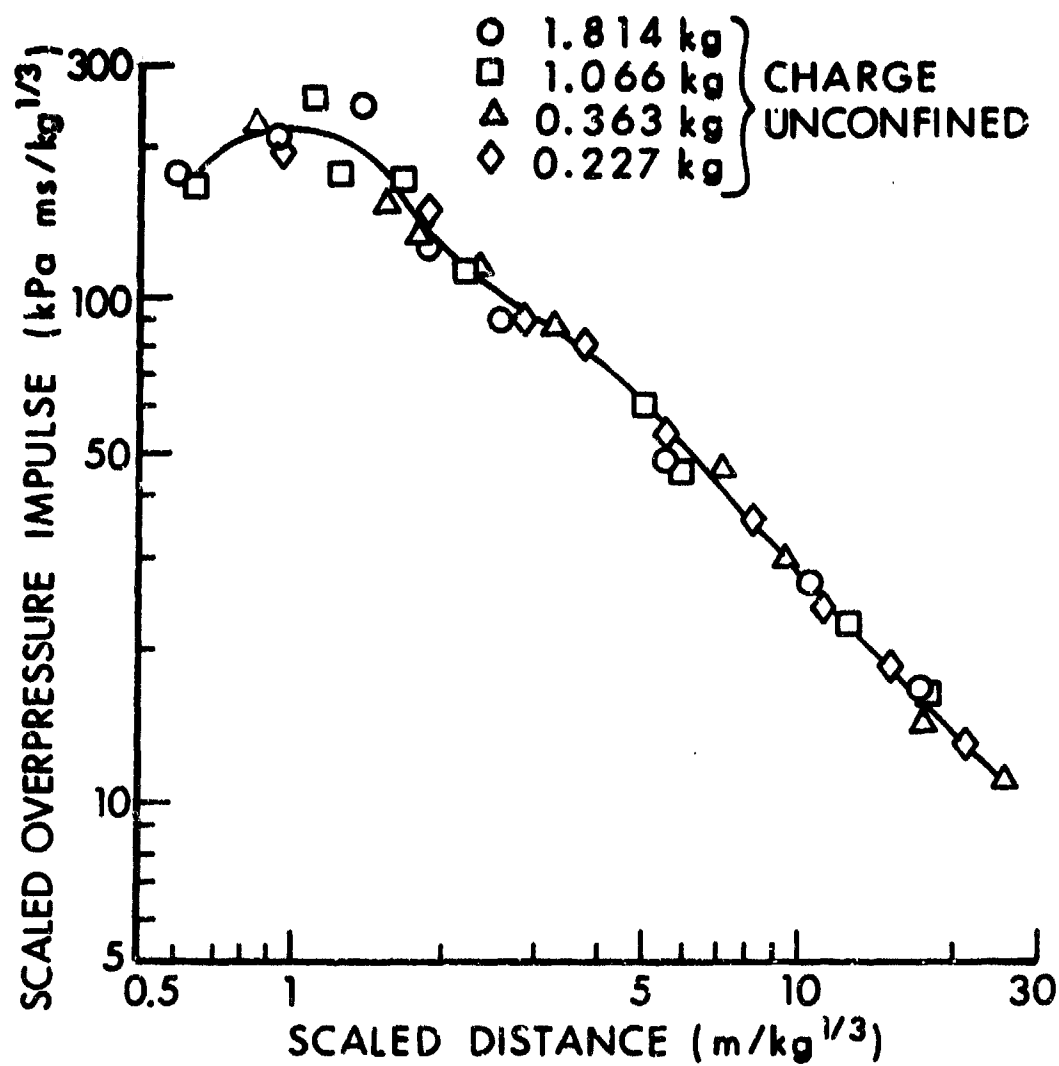


Figure 13. Scaled overpressure impulse versus scaled distance along the 90-degree blast line, charges unconfined.

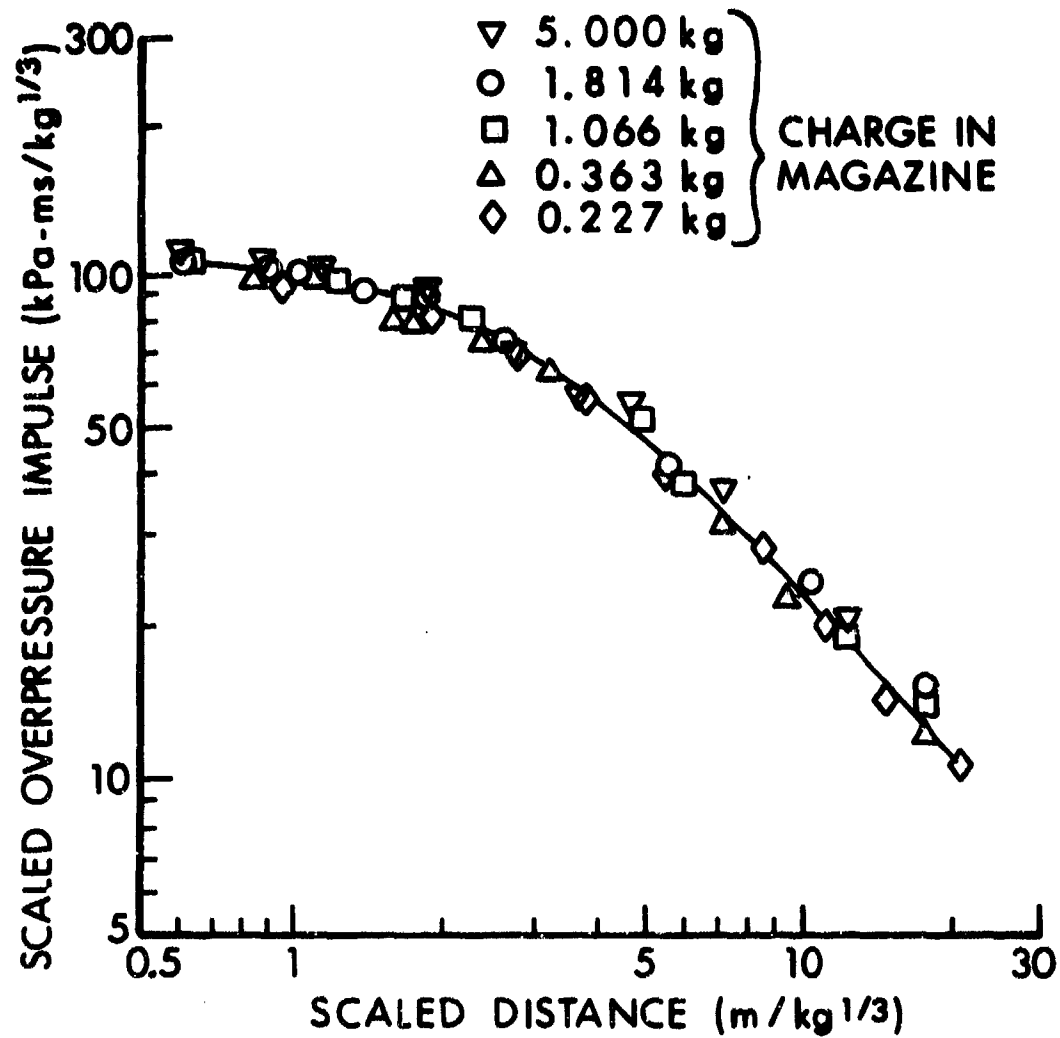


Figure 14. Scaled overpressure impulse versus scaled distance along the 90-degree blast line, charges in magazine.

The values of peak overpressure versus scaled distance along the 90-degree blast line for the five charge masses tested in the magazine are plotted in Figure 12. There is a very large loading density effect on the peak overpressure from a scaled distance of $0.6 \text{ m/kg}^{1/3}$ out to $6.0 \text{ m/kg}^{1/3}$. Beyond $6.0 \text{ m/kg}^{1/3}$ the suppression effect of the various loading densities becomes less evident. A discussion of the effect of low loading on the peak overpressure versus distance will be given later in this report.

2. Scaled Overpressure Impulse versus Scaled Distance, 90-Degree Blast Line. The values of scaled impulse versus scaled distance recorded along the 90-degree blast line for the four charge masses, unconfined, are plotted in Figure 13. The values establish a good trend and follow that reported in Reference 1. The charge masses range over a factor of 8, but using cube root scaling the scaled values show very little scatter.

The values of scaled impulse along the 90-degree blast line for the in-magazine tests are plotted in Figure 14. Although the peak overpressure values plotted in Figure 12 show a greater suppression at the lower loading densities (0.363 and 0.227 kg charges) this is not evident in the scaled overpressure impulse versus scaled distance presented in Figure 14. The peak overpressures were lower but because there were double peaks this apparently added to the impulse making only small differences in the scaled impulse. The second peak is an interior reflection from the magazine's arch.

When comparing the values of scaled impulse recorded from the in-magazine and uncovered charges there is suppression evident over the complete range of distances. From a scaled distance of $2 \text{ m/kg}^{1/3}$ out to $20 \text{ m/kg}^{1/3}$ the average attenuation of the in-magazine values is 25 percent of the unconfined values. The scaled impulse values do not merge into one curve at the greater distances as the peak overpressure values did along the 90-degree blast line.

In Figure 14 it can be seen that the suppression of the positive impulse along the 90-degree blast line is a function of loading density. The magnitude of this effect will be discussed later in this report.

C. Blast Parameters along the 180-Degree Blast Line

The 180-degree blast line extends to the rear of the magazine. This is away from the door and the point of initiation of the charge. The gage locations for stations 180-1 through 180-8 are listed in Table 2 while the peak overpressure and impulse values are listed in Tables 5 through 14.

1. Peak Overpressure versus Scaled Distance, 180-Degree Blast Line. The values of peak overpressure versus scaled distance along the 180-degree blast line for the unconfined tests are plotted in Figure 15. Here the effect of the configuration of the charge and point of detonation can clearly be seen. The station from 1.0 to $3.0 \text{ m/kg}^{1/3}$ record higher peak overpressure along the 180-degree blast line than along the 0-degree blast line. This is because detonation point is at 0-degree blast line end of the charge. A major curve inflection is noted at a scaled distance of $4.5 \text{ m/kg}^{1/3}$ where a second shock develops and becomes increasingly greater in

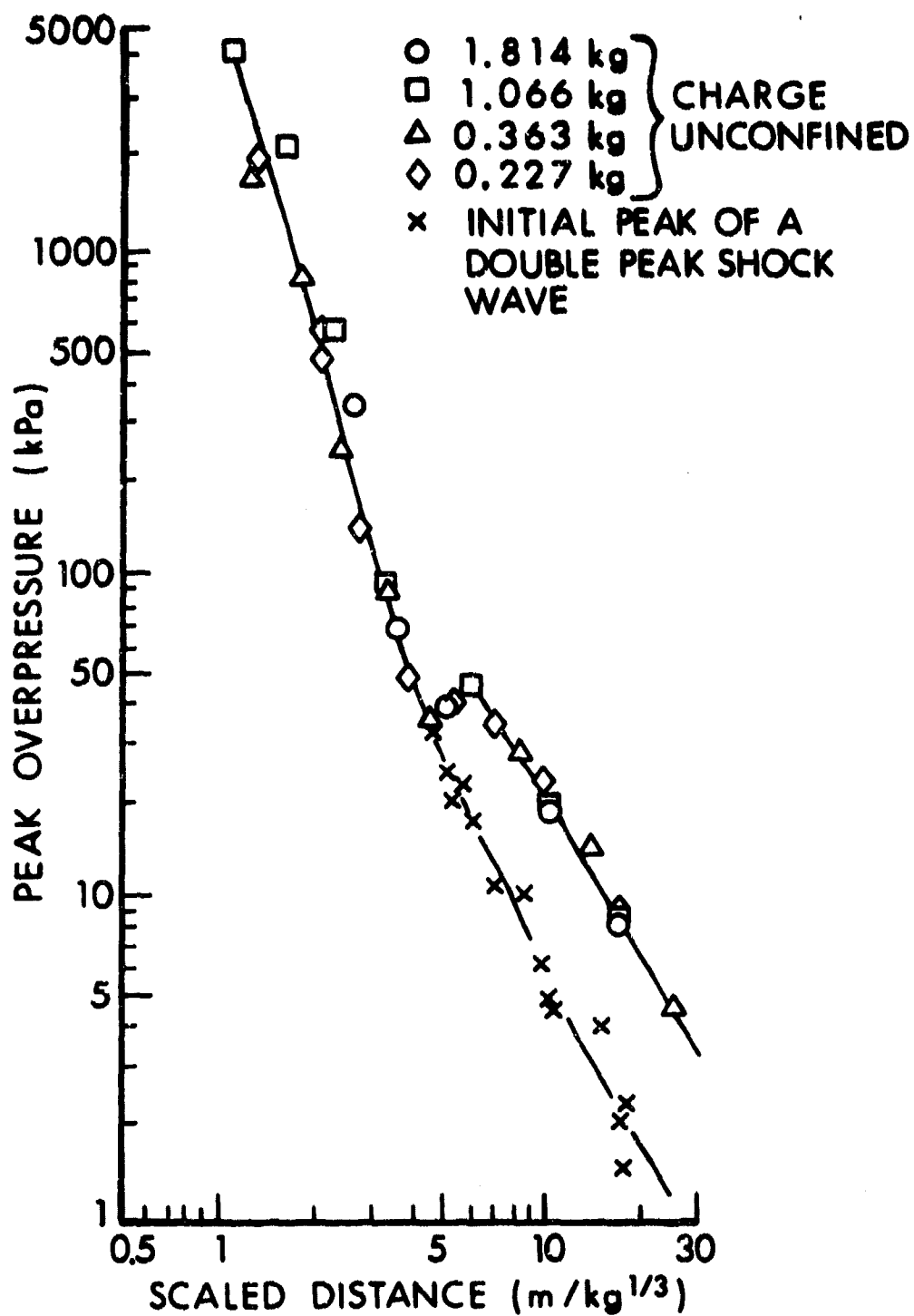


Figure 15. Peak overpressure versus scaled distance along the 180-degree blast line, charges unconfined.

magnitude than the initial shock as the distance increases. A second shock does not develop when the charge is tested in the storage magazine.

The values of peak overpressure recorded from the in-magazine tests are plotted versus scaled distance in Figure 16. Here we see a trend similar to that noted on the 90-degree blast line. The two small charge masses show some blast attenuation over the total range because of a loading density effect. The magnitude of the loading density effect will be discussed later.

When comparing the in-magazine tests (Figure 16) with the unconfined test (Figure 15) it is quite evident that there is blast attenuation over the complete range of measurements.

2. Scaled Impulse versus Scaled Distance, 180-Degree Blast Line. The scaled impulse values recorded for the unconfined charges are listed in Tables 6, 8, 10, and 12 and plotted in Figure 17. The change in the slope of the curve at scaled distance of $3\text{m/kg}^{1/3}$ is caused by the increase in impulse which in turn is caused by the second shock noted in Figure 15. The scaled impulse values for all four charge masses follow the same trend.

The values of a scaled overpressure impulse along the 180-degree blast line for the in-magazine tests are listed in Table 5, 7, 9, 11, and 14. These values are plotted in Figure 18. There appears to be some suppressive effect on scaled impulse along the 180-degree which is a function of loading density. The 1.814 kg values are ~ 10 percent less than the 5.04 kg values while the 1.066 kg values are ~ 10 percent less than the 1.814 kg values. The 0.363 and 0.227 kg values are ~ 10 percent less than the 1.066 kg values of scaled impulse. These suppressions of impulse are not great but they do appear consistent and valid.

The attenuation of scaled impulse because of confinement is 50 percent or greater along the 180-degree blast line. The attenuation of scaled impulse because of loading density is quite evident in Figure 18 and will be discussed in the following section.

D. Blast Attenuation as a Function of Loading Density

The preceding sections have pointed out the enhancement or attenuation of the blast waves as a function of a confined charge (in-magazine) relative to an unconfined charge. The following discussion will include the attenuation of the blast wave as a function of explosive loading density within the storage magazine model. The 1.814 kg charge which simulates a 48980 kg (107760 lbm) will be used as the baseline for comparison. The 0.227 kg charge will be used to determine the attenuation at selected distances. The four distances of primary interest are (1) the safe separation distance $0.8 Q^{1/3}$ m for 0 and 180-degree blast line and $0.5 Q^{1/3}$ m for the 90-degree blast line), (2) the unbarricaded intraline distance $7.2 Q^{1/3}$ m, (3) the public traffic routes $9.6 Q^{1/3}$ m, and (4) inhabited building distance $16 Q^{1/3}$ m. The attenuation or enhancement of peak overpressure will be treated in two ways. First the difference in peak overpressure at the selected distances and second the difference in

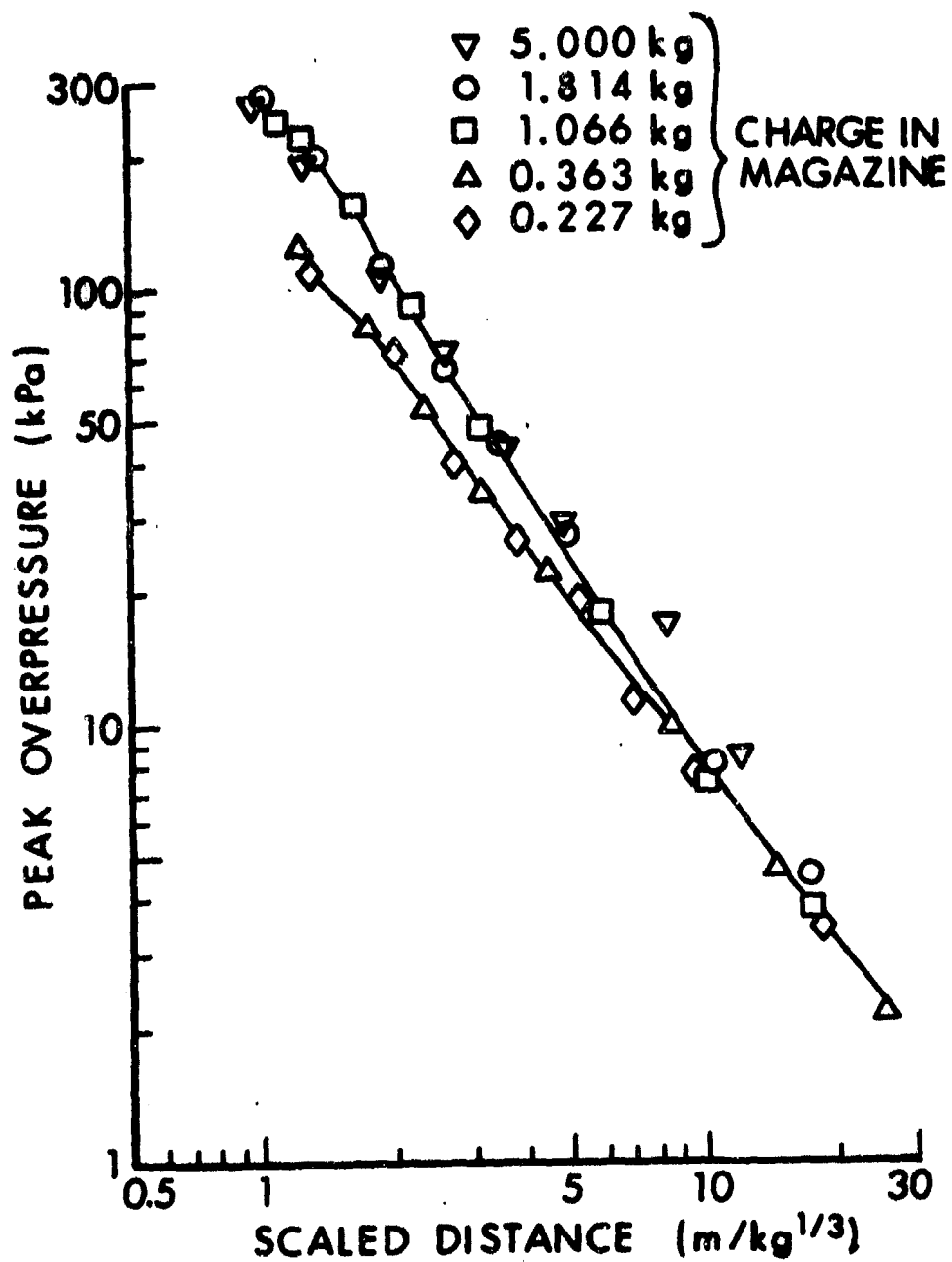


Figure 16. Peak overpressure versus scaled distance along the 180-degree blast line, charges in magazine.

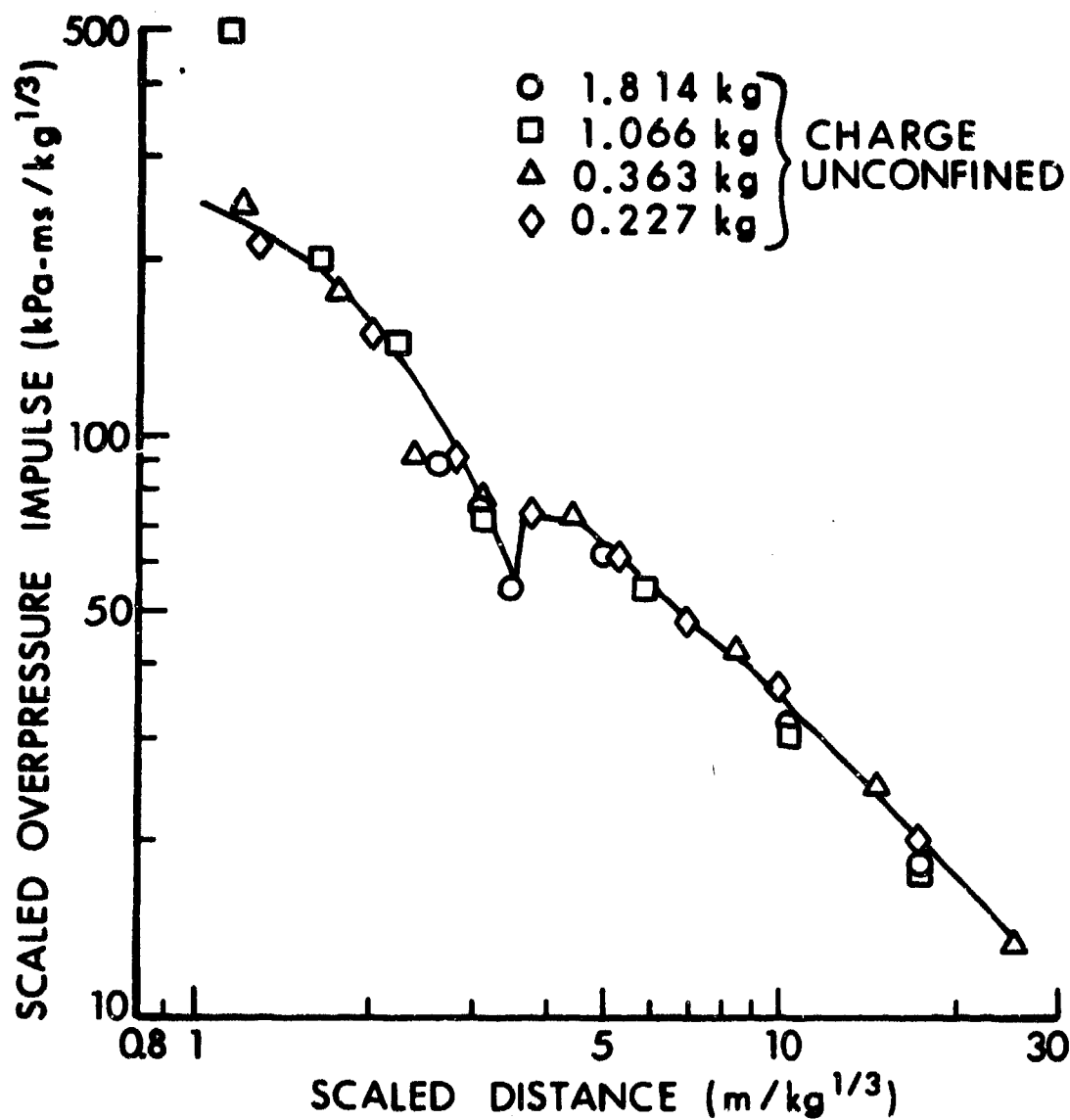


Figure 17. Scaled impulse versus scaled distance along the 180-degree blast line, charges unconfined.

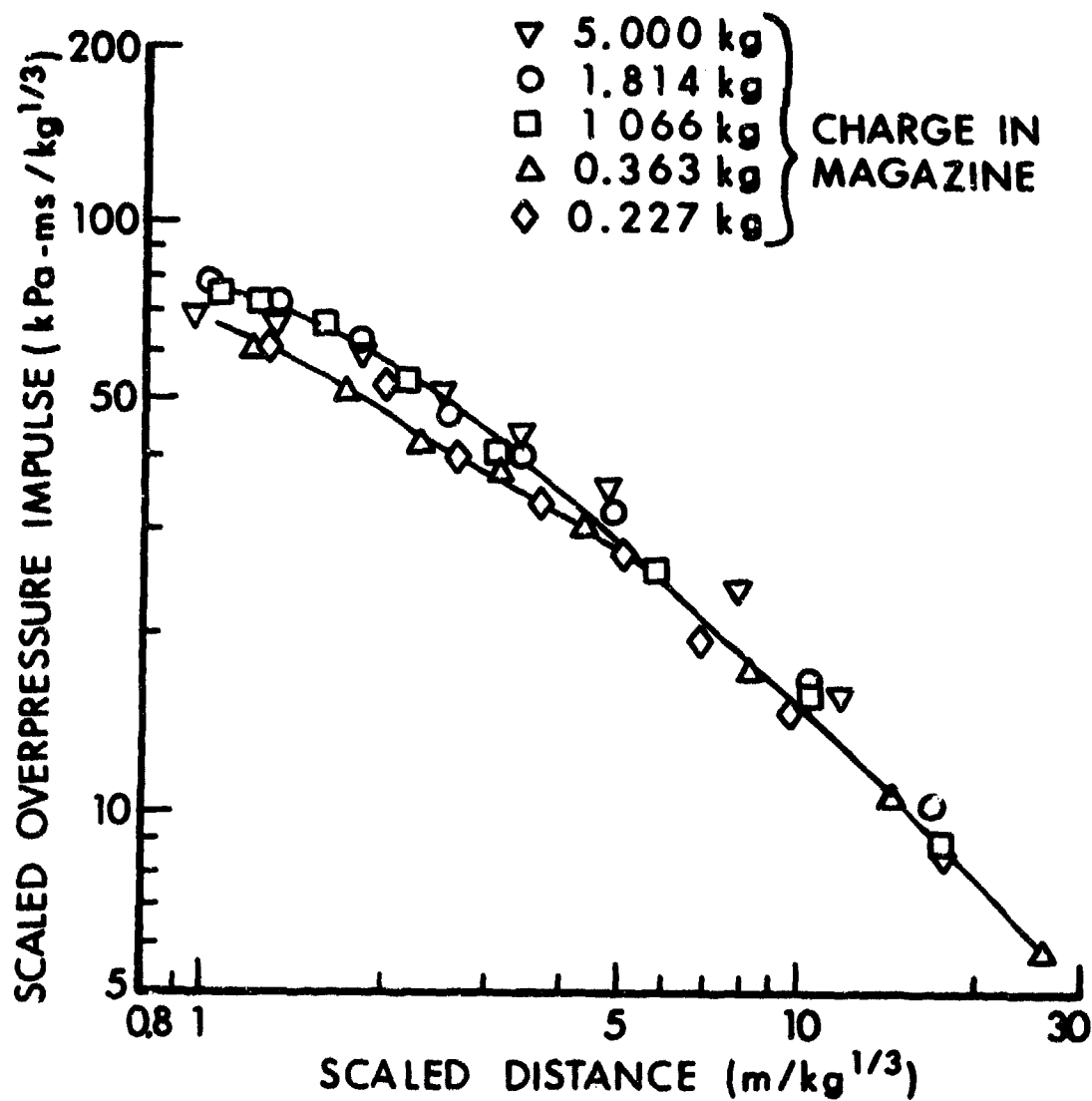


Figure 18. Scaled impulse versus scaled distance along the 180-degree blast line, charges in magazine.

scaled distance for the peak overpressure associated with the baseline curve. From the second method the equivalent mass factor will be determined.

The effect of loading density on the overpressure impulse will also be determined. This method will also be based on the equivalent mass factor. A ratio of the scale impulse/scaled distance for the baseline plot (1.814 kg scaled to 1 kg) will be computed and the scaled impulse versus scaled distance curve for 0.227 kg will be searched to determine an equal ratio. From this ratio the scaled distance will be determined and used to calculate the equivalent mass factor.

1. Loading Density Effects on Peak Overpressure. The effects of loading density on peak overpressure is presented in Table 15 for four selected distances along three blast lines. The percentage difference listed in column six is the difference in the low loading density (0.227 kg) relative to the medium loading density (1.814 kg).

There is little or no loading density effect on peak overpressure along the 0-degree blast line. An average of the percentage differences noted in column six would fall within a relative difference band of +6 percent.

Along the 90-degree blast line the major attenuation is at the safe-separation distance where it is 79.4 percent. The other three selected distances indicate an average of 14.6 percent attenuation of peak overpressure.

The attenuation of peak overpressure along the 180-degree blast line is also greatest at the safe separation distance (44 percent) while the average attenuation at the other three distances is 19 percent.

2. Effect of Pressure, Attenuation on Equivalent Yield. The attenuation of peak overpressure along the blast lines can also be expressed in equivalent yield or an equivalent mass factor (EMF). That is, the explosive yield of the attenuated pressure-distance curve relative to the baseline curve. The equivalent mass factors (EMF) are listed in column six of Table 16 for the three blast lines.

The EMF determined along the 0-degree blast line follows the same trend as the peak overpressure differences. Some are less than 1.0 and some greater than 1.0. The average is 0.98 indicating there is no significant effect of loading density on the EMF along the 0-degree line.

The EMF values based on pressure attenuation along the 90-degree blastline are listed in column six of Table 16. A value could not be calculated for the first distance but the last three distances give an average EMF of 0.69 + 7 percent.

The EMF determined for the 180-degree line for the last three selected distances is to .62, +5, -8 percent. This follows the same trend established in Table 15 where the 180-degree line recorded greater peak overpressure attenuation than the 90-degree line.

TABLE 15. LOADING DENSITY EFFECTS ON PEAK OVERPRESSURE

BLAST LINE	SCALED DISTANCE	PEAK OVERPRESSURE		DIFFERENCE	
		1.814 kg	0.227 kg	Δ	%
DEGREE	$m/kg^{1/3}$	kPa	kPa	kPa	
0	1.1	1400.0	1250.0	-150.0	-10.7
	7.2	24.5	28.0	+3.5	+14.0
	9.6	14.3	14.9	+0.6	+4.0
	16.0	6.2	5.4	-0.8	-15.0
90	0.63	378.0	78.0	-300.0	-79.4
	7.2	21.5	13.0	+3.5	-16.5
	9.6	13.6	11.9	+1.7	-11.8
	16.0	6.5	5.5	+1.0	-15.4
180	1.1	270.0	119.0	+151.0	-44.0
	7.2	13.8	11.1	+2.7	-20.0
	9.6	9.3	7.8	+1.5	-16.0
	16.0	4.9	3.8	+1.1	-22.0

TABLE 16. LOADING DENSITY EFFECTS ON EQUIVALENT YIELDS

BLAST LINE	PEAK OVERPRESSURE	SCALED DISTANCE		EMF $(R_2/R_1)^3$
		1.814 kg R_1	0.227 kg R_2	
DEGREES	kPa	m/kg ^{1/3}	m/kg ^{1/3}	
0	1400.0	1.10	1.02	0.80
	24.5	7.20	7.70	1.22
	14.3	9.60	9.80	1.06
	6.2	16.00	15.00	0.82
90	-	-	-	-
	21.5	7.20	6.25	0.65
	13.6	9.60	8.70	0.74
	6.5	16.00	14.10	0.68
180	-	-	-	-
	13.8	7.20	6.2	0.64
	9.3	9.60	8.3	0.65
	4.8	16.00	13.3	0.57

3. Loading Density Effects on Impulse. The effect of loading density on the overpressure impulse along the three blast lines is listed in Table 17. The percentage difference between the baseline curve and the low loading density curve is listed in column six for the four selected distances along each blast line.

Although the 0-degree blast line recorded very little difference in the peak overpressure because of loading density the impulse is enhanced. This enhancement is +7 percent at the first distance and an average of +21 percent for the last three stations.

Along the 90-degree blast line there is an attenuation of impulse as well as peak overpressure. The percentage difference appears to increase with distance, going from -7.8 percent at the first station to -20.5 percent at the last station.

The impulse recorded along the 180-degree blast line is also attenuated. The percentage attenuation of impulse at the last three stations is almost the same as recorded for peak overpressure at the last three stations shown in Table 15, ie, -18.8 vs -19.3 percent.

4. Effect of Impulse Variations on Equivalent Yield. The equivalent mass factors will be determined based on the variation of impulse along the blast lines as a function of loading density. The method described under Section D will be used to determine EMF. Values are listed in Table 18.

The values of the EMF determined along the 0-degree blast line based on impulse again show an enhancement. The average EMF is 1.31 showing that the low loading density will give higher scaled impulse values along the 0-degree blast line. The focusing effect of the three earth barricades is more effective for low density loads than the higher density loads. This is borne out in Figure 10 where the high loading density (5.0 kg) recorded much lower scaled impulse values than the low loading density (0.227 kg).

The average EMF along the 90-degree blast line was $0.81 + 7$ percent while the average EMF along the 180-degree blast line was $0.74 + 1.3$ percent.

E. Hemicylindrical versus Hemispherical Charges in Magazine

There was some difficulty in determining the effect of earth cover on the suppression of blast when comparing the confined (in-magazine) and unconfined hemicylindrical charge because of the double peaked shock waves recorded along both the 0-degree and 180-degree blast lines when unconfined. These double peaks did not materialize when the charges were confined.

1. Comparison of Peak Overpressure versus Scaled Distance. One test was conducted with a 1.128 kg hemispherical charge placed in a 1/30th-scale munition storage magazine model. The results from this test are listed in Table 13. The values listed in Table 13 were scaled to a 1 kg equivalent and are compared with a 1.066 kg hemicylindrical charge tested in the magazine model. The hemicylindrical charge values are listed in Table 7.

TABLE 17. LOADING DENSITY EFFECTS ON IMPULSE

BLAST LINE	SCALED DISTANCE	IMPULSE		DIFFERENCE	
		1.814 kg	0.227 kg	Δ	%
DEGREE	m/kg ^{1/3}	kPa-ms/kg ^{1/3}	kPa-ms/kg ^{1/3}	kPa-ms/kg ^{1/3}	
0	1.1	235.0	250.0	+15.0	+7.0
	7.2	30.0	37.0	+7.0	+23.0
	9.6	22.5	27.0	+4.5	+20.0
	16.0	12.8	15.5	+2.7	+21.0
90	.63	103.0	95.0	-8.0	-7.8
	7.2	34.5	32.0	-2.5	-7.2
	9.6	27.0	23.5	-3.5	-13.0
	16.0	17.0	13.5	-3.5	-20.5
180	1.1	78.0	68.0	-10.0	-12.5
	7.2	23.5	19.0	-4.5	-19.2
	9.6	18.0	14.8	-3.2	-17.7
	16.0	11.2	9.0	-2.2	-19.6

TABLE 18. EQUIVALENT YIELD FROM IMPULSE VARIATIONS

BLAST LINE DEGREE	1.814 kg		I_1/R_1	0.227 kg		EMF $(R_2/R_1)^3$
	SCALED DISTANCE	SCALED IMPULSE		SCALED DISTANCE	SCALED IMPULSE	
	R_1 $m/kg^{1/3}$	I_1 $kPa-ms/kg^{1/3}$		R_2 $m/kg^{1/3}$	I_2 $kPa-ms/kg^{1/3}$	
0	1.1	235.0	213.6	1.15	246.0	1.14
	7.2	30.0	4.2	8.0	33.0	1.37
	9.6	22.5	2.3	10.5	24.6	1.31
	16.0	12.8	0.8	18.0	14.0	1.42
90	0.63	103.0	163.0	0.59	96.0	0.81
	7.20	34.5	4.8	6.90	33.0	0.88
	9.60	27.0	2.8	9.00	25.5	0.82
	16.00	17.0	1.1	14.50	15.4	0.74
180	1.1	78.0	70.9	1.0	71.0	0.75
	7.2	23.5	3.3	6.5	21.2	0.74
	9.6	18.0	1.9	8.6	16.2	0.73
	16.0	11.2	0.7	14.5	10.1	0.74

The comparison of peak overpressure along the three blast lines are presented in Figures 19, 20, and 21. The peak overpressure versus scaled distance along the 0-degree blast line for the two charge configurations is shown in Figure 19.

The peak overpressures versus scaled distances along the 90-degree blast line for the two charge configurations are plotted in Figure 20. Here the peak overpressures recorded from the hemicylindrical charge are lower than the hemispherical charge out to a scaled distance of 4 $\text{m/kg}^{1/3}$. From 4 $\text{m/kg}^{1/3}$ out to the inhabited building distance (16 $\text{m/kg}^{1/3}$) there is no significant difference in the plotted data.

The peak overpressures versus scaled distance recorded along the 180-degree blast line are plotted in Figure 21. Here again the values from the hemicylindrical charge are lower than the values from the hemispherical charge out to a scaled distance of 2.2 $\text{m/kg}^{1/3}$. From 2.2 $\text{m/kg}^{1/3}$ out to 17.5 $\text{m/kg}^{1/3}$ there is no significant difference in the two sets of data.

2. Comparison of Scaled Impulse versus Scaled Distance. The values of scaled impulse versus scaled distances plotted in Figures 22, 23, and 24 were taken from Tables 7 and 13. In Figure 22, the 0-degree blast line, the values from the two charge configurations compare quite well at scaled distances from 1 $\text{m/kg}^{1/3}$ out to 2 $\text{m/kg}^{1/3}$ and from 10 $\text{m/kg}^{1/3}$ out to 20 $\text{m/kg}^{1/3}$. From 2 $\text{m/kg}^{1/3}$ to 10 $\text{m/kg}^{1/3}$ the scaled values of impulse from the hemicylindrical charge are lower.

Along the 90-degree blast line the values from the hemicylindrical charge as shown in Figure 23 are lower out to 4 $\text{m/kg}^{1/3}$ but beyond that there is no significant difference.

In Figure 24 the scaled impulse versus scaled distance values from the 180-degree blast line are plotted for the two charge configurations. The trend is similar to the 0-degree blast line where the beginning and end of the curves compare well. There is no significant difference in values beyond 6 $\text{m/kg}^{1/3}$.

For future tests where the suppression of blast parameters from earth cover is an objective it may be advisable to use hemispherical charges in the magazine model rather than hemicylindrical charges.

F. 1/30th-Scale versus 1/50th-Scale Testing

When simulating the effects of an accidental explosion in a munition storage magazine with an explosive source of 45360 kg (100,000 lbm) using munition storage magazine models a 0.363 kg charge was used in the 1/50th-scale tests and a 1.814 kg charge was used in the 1/30th-scale tests.

For the simulation of 136000 kg (300,000 lbm) a 1.080 kg charge was used for the 1/50th-scale tests while a 5.04 kg charge was used for the 1/30th-scale tests.

All data were scaled to a 1 kg equivalent for analysis and correlation of results.

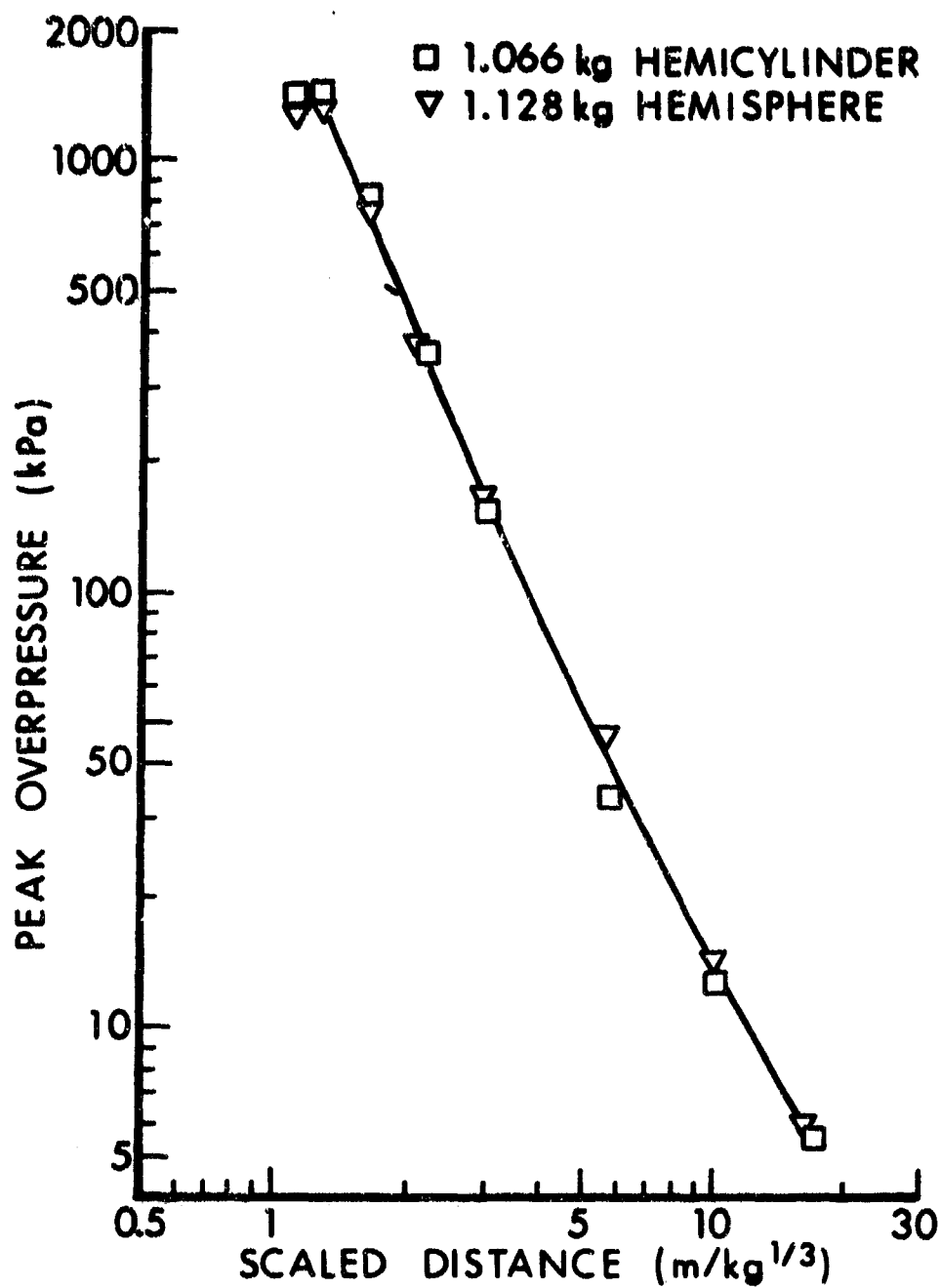


Figure 19. Peak overpressure versus scaled distance along the 0-degree blast line, hemicylinder and hemisphere in magazine.

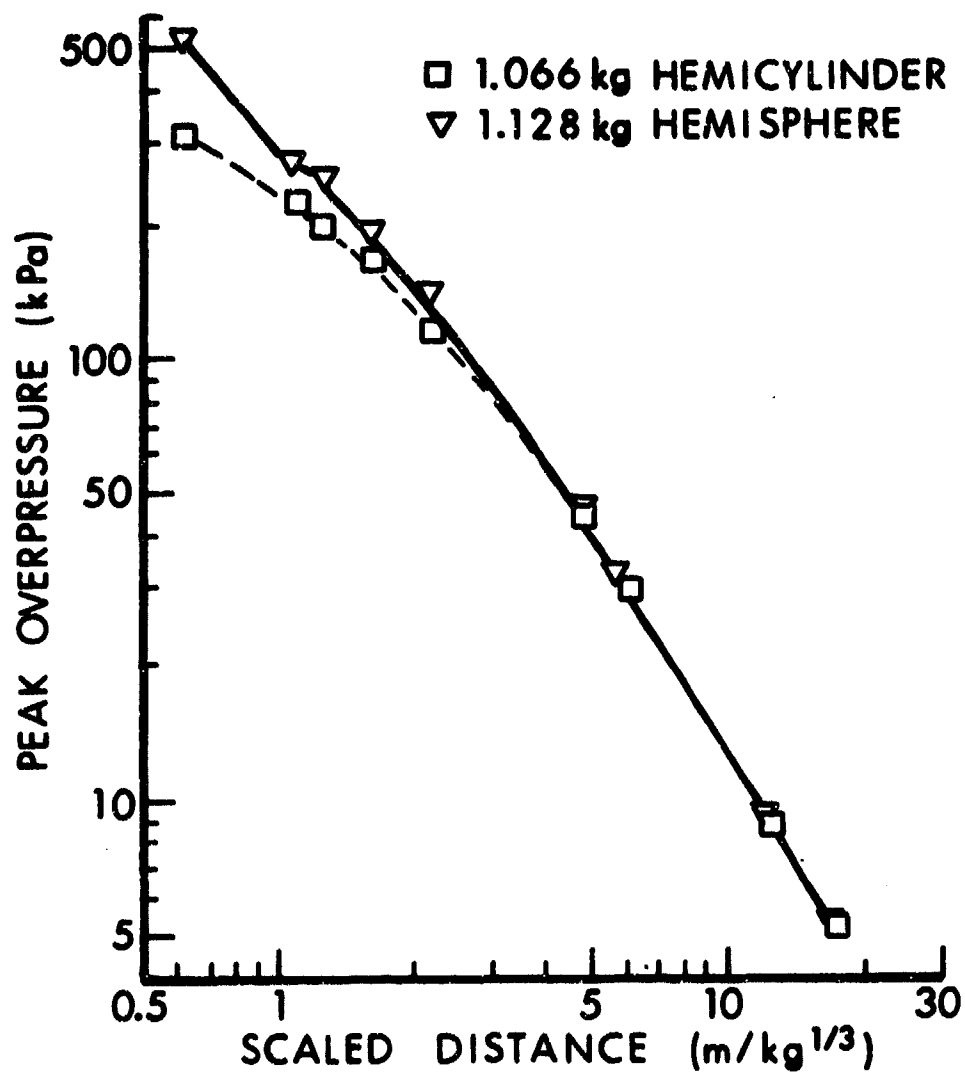


Figure 20. Peak overpressure versus scaled distance along the 90-degree blast line, hemicylinder and hemisphere in magazine.

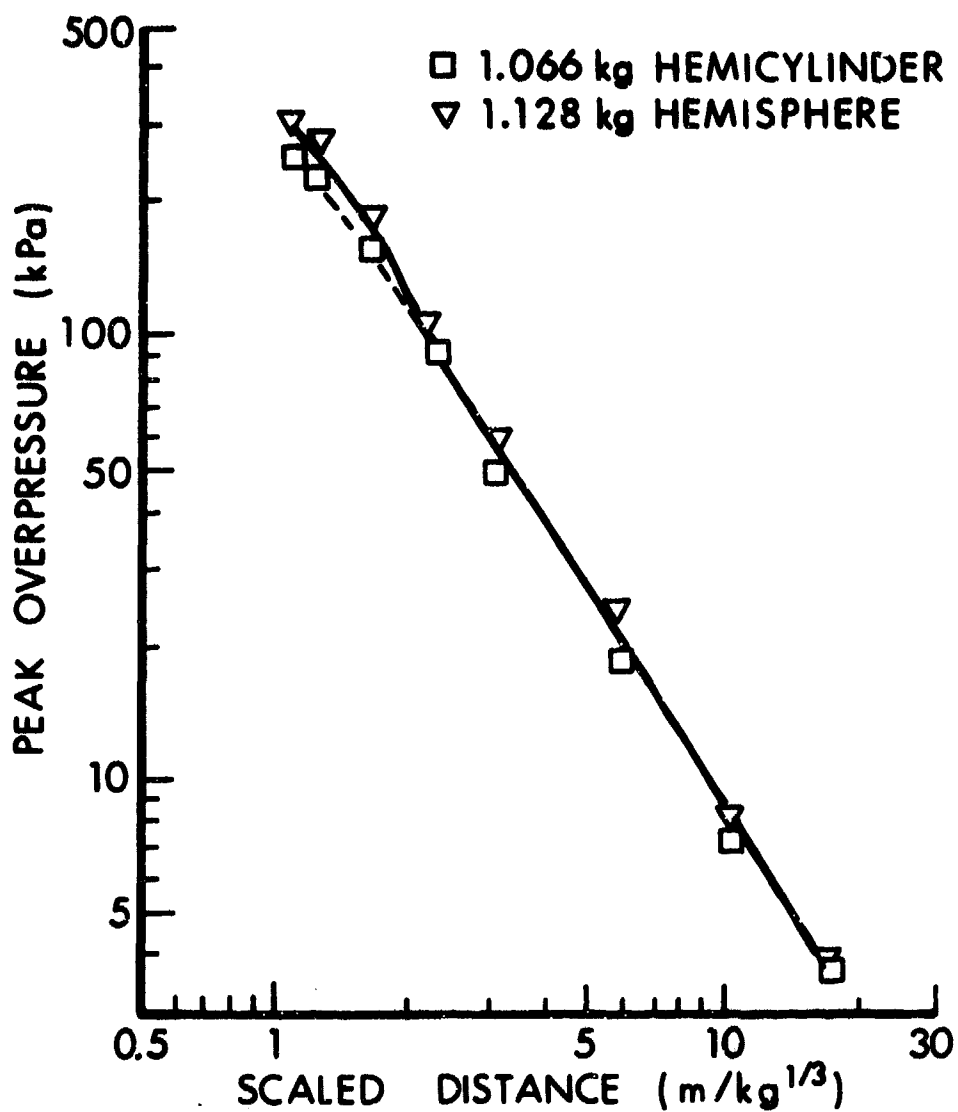


Figure 21. Peak overpressure versus scaled distance along the 180-degree blast line, hemicylinder and hemisphere in magazine.

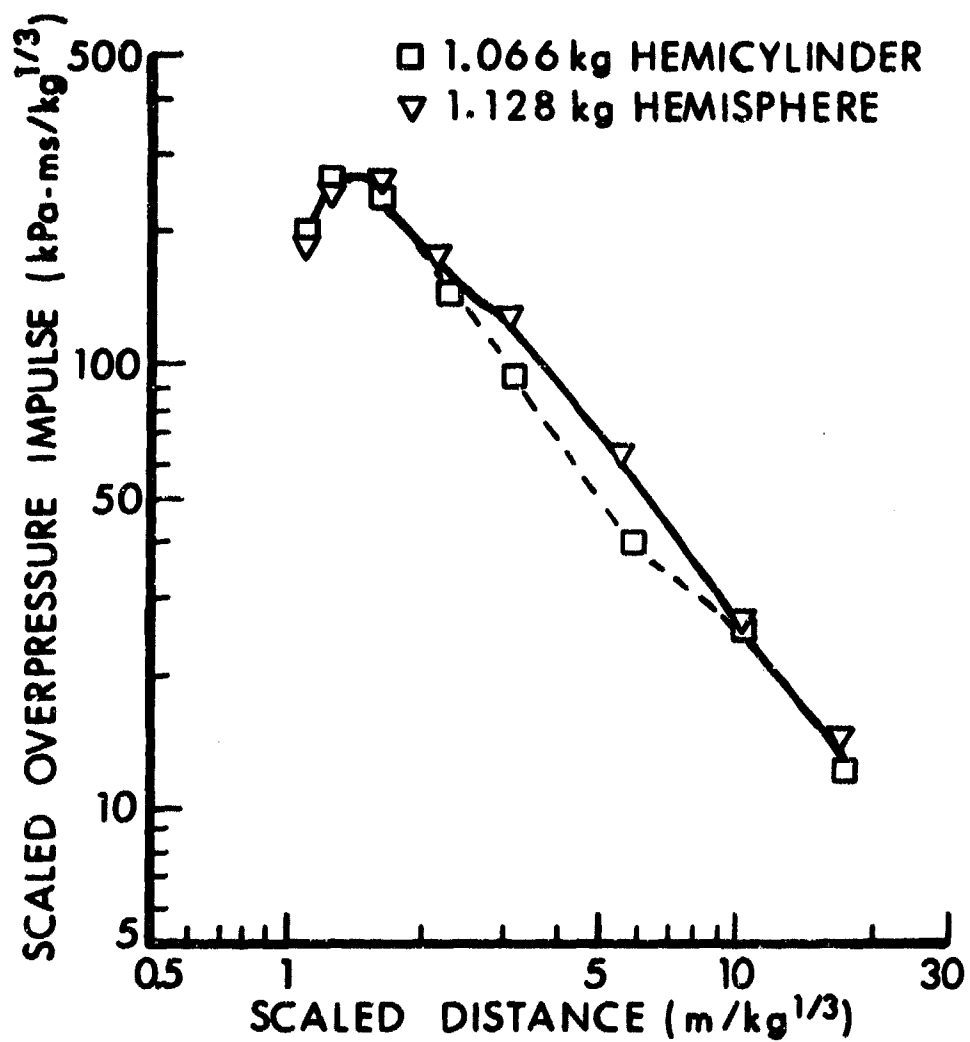


Figure 22. Scaled impulse versus scaled distance along the 0-degree blast line, hemicylinder and hemisphere in magazine.

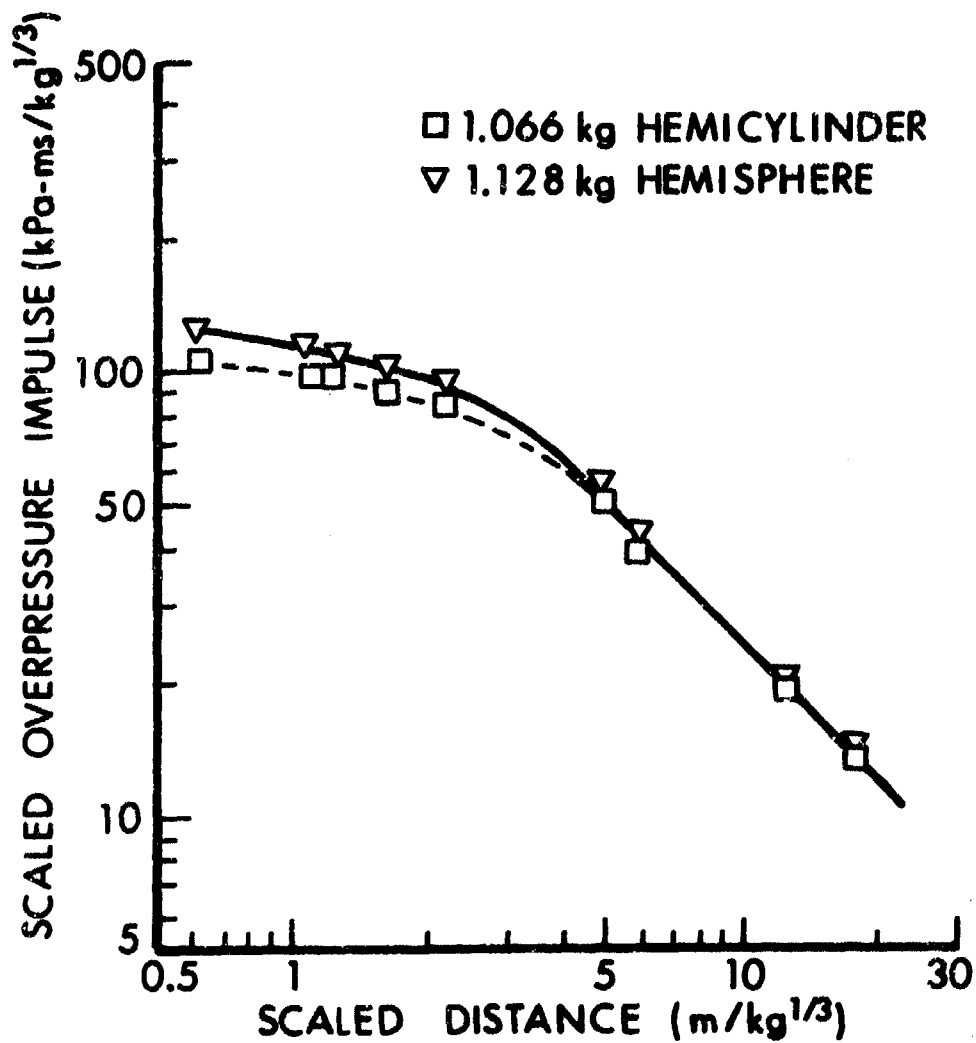


Figure 23. Scaled impulse versus scaled distance along the 90-degree blast line, hemicylinder and hemisphere in magazine.

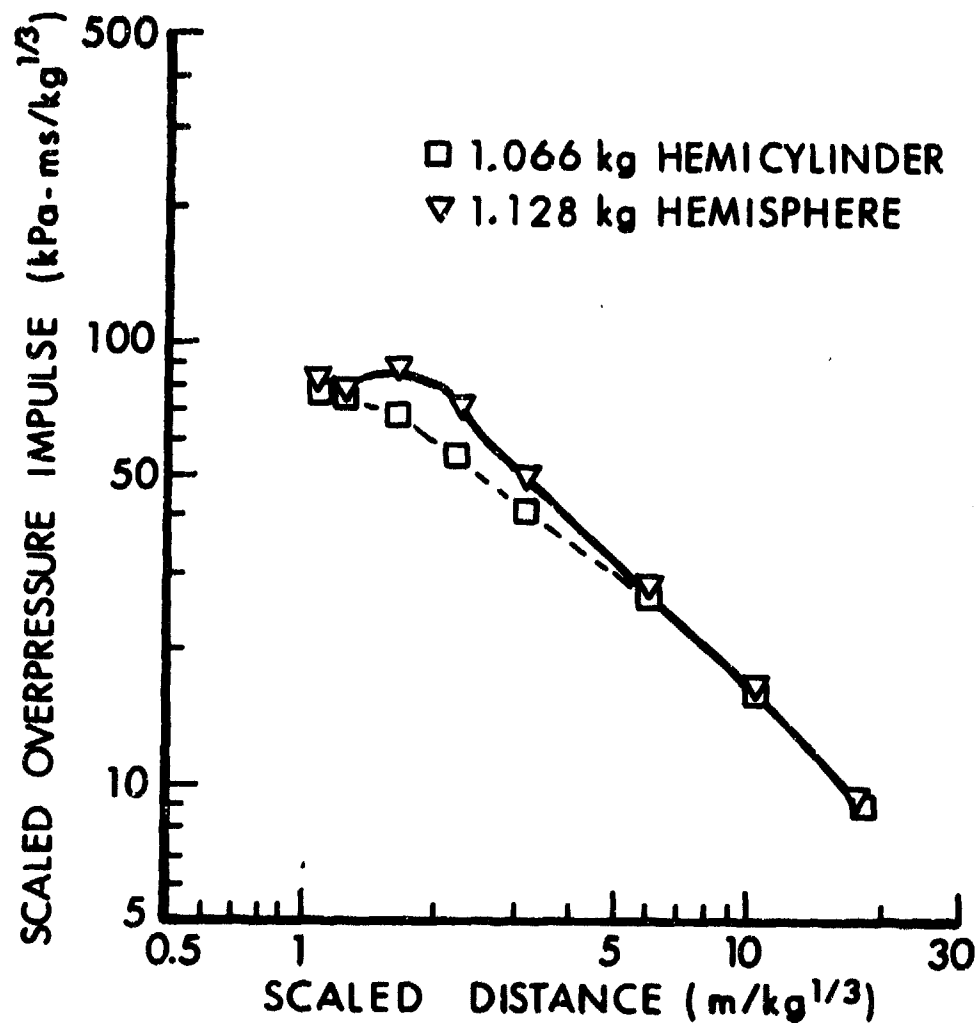


Figure 24. Scaled impulse versus scaled distance along the 180-degree blast line, hemicylinder and hemisphere in magazine.

The results published in Reference 1 (1/50th-scale) were compared with the present test results (1/30th-scale). The values of peak overpressure along the 0-degree blast line, recorded on the 1/50th-scale tests are approximately 25 percent lower than the 1/30th-scale test results at a scaled distance of $1 \text{ m/kg}^{1/3}$ but the results merge together at $2.5 \text{ m/kg}^{1/3}$ for both the 45360 kg and the 136000 kg full-size simulations. There is no significant differences in the impulse values along the 0-degree blast line when comparing the results from the 1/50th-scale and 1/30th-scale tests.

The peak overpressure along the 90-degree blast line were lower on the 1/50th-scale tests than the 1/30th-scale tests out to $2.5 \text{ m/kg}^{1/3}$ on the 45360 kg simulation. The comparison of peak overpressure is quite good between the two scaled tests on the 136000 kg simulation. The impulses recorded along the 90-degree blast line for the 1/50th-scale tests were 11 percent lower than those recorded on the 1/30th-scale tests for the 45360 kg simulation. The correlation of impulse recorded, on the 1/50th and 1/30th-scale tests along the 90-degree blast line for the 136000 kg simulation was good. Only one data point fell outside an acceptable scatter.

The largest difference noted in peak overpressure is along the 180-degree blast line when simulation 45360 kg full scale, the 1/50th-scale test results were 50 percent lower than the 1/30th-scale values at $1 \text{ m/kg}^{1/3}$. The data from the two scale tests merge and beyond the scaled distance of $2.5 \text{ m/kg}^{1/3}$ the values are the same. The peak overpressure along the 180-degree blast line for the 136000 kg simulation were an average of 13 percent lower on the 1/50th-scale results compared to the 1/30th-scale tests.

The impulse along the 180-degree blast line for the 45360 kg simulation from the 1/50th-scale tests were an average of 20 percent lower than the 1/30th-scale test results. Comparison of impulse for the 136000 kg simulation gave an average difference of less than ± 1 percent for the two scaled test results along 180-degree blast line.

A detailed analysis to determine the cause of the differences recorded between the 1/50th-scale test results and the 1/30th-scale test results has not been made. The larger differences are generally at scaled distances less than $2.5 \text{ m/kg}^{1/3}$.

IV. CONCLUSIONS

The conclusions reached after analysis and discussion of results are listed below.

1. There is a loading density effect on the blast propagation along the three blast lines.
2. Along the 0-degree blast line the lowest loading density tests (12.6 kg/m^3) gave the highest peak overpressures from a scaled distance of $3 \text{ m/kg}^{1/3}$ to $10 \text{ m/kg}^{1/3}$.

3. Along the 0-degree blast line the lowest loading density tests (12.6 kg/m^3) gave the highest scaled impulse values beyond a scaled distance of $1.5 \text{ m/kg}^{1/3}$.

4. Along the 90-degree blast line the lowest loading density tests (12.6 kg/m^3) gave lower peak overpressures and lower scaled impulses over the entire blast line.

5. Along the 180-degree blast line the two lower loading density tests (12.6 kg/m^3 and 20.2 kg/m^3) gave lower peak overpressure and lower scaled impulses over the entire blast line.

6. Quantity-distance criterion can be reduced for low loading densities along the 90-degree and 180-degree blast lines but should be increased along the 0-degree blast line.

7. The 1/30th-scale test results are recommended for 6130 kg (13,500 lbm) through 136000 kg (300,00 lbm) full size simulations. The 1/50th-scale tests are satisfactory for 226800 kg (500,000 lbm) full size simulations.

AD P000431

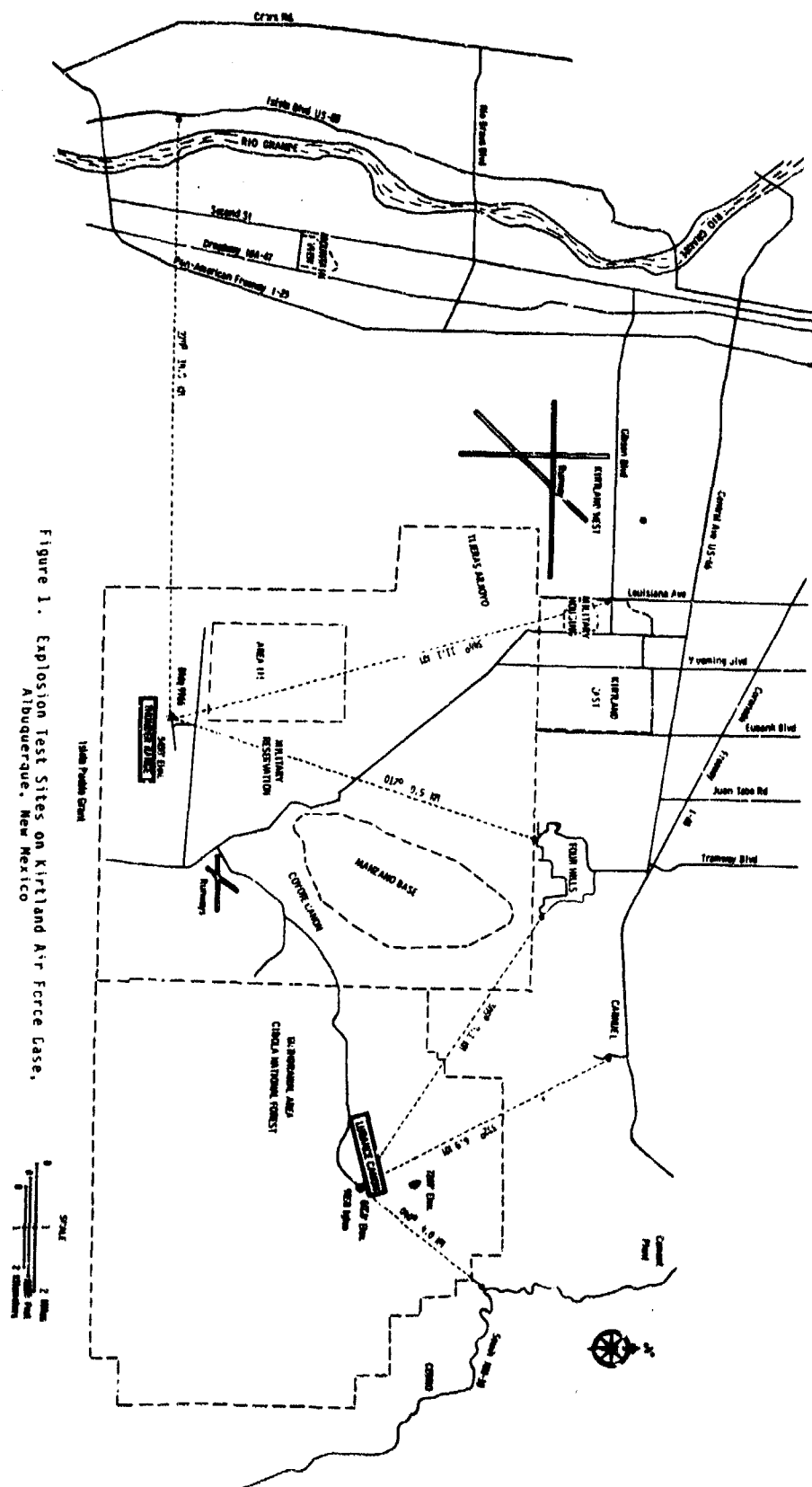
BLAST PREDICTIONS FOR COYOTE CANYON EXPLOSIONS

Jack W. Reed
Ground Motion & Seismic Division 7111
Sandia National Laboratories
Albuquerque, NM 87185

INTRODUCTION

Tests of small explosions of up to 7.5 tons (6.8 Mg) of TNT have frequently been conducted on Kirtland Air Force Base with only occasional nuisance damage to, or complaints from, the neighboring community of Albuquerque. Provisions were made for weather checks, including observations, forecasts, and acoustic propagation calculations, to determine whether or not a planned event could be tested as well as estimates of the delays needed to await suitable propagation weather.

We have developed a set of yield limits that may be fired without seriously disturbing our neighbors (located as shown in Figure 1) and without any check on weather conditions (assuming unlikely strong propagations). Operations are conducted at two primary firing sites, located in Coyote Canyon, the 200 km² test field that extends 10 km south from Kirtland AFB - East, (formerly named Sandia Base). In addition, limits have been produced for keeping below the threshold of damage, as well as the threshold for general audibility. All such thresholds have been based on extensive experience, including recent results of USAF- and NASA-supported airblast propagation tests at Cape Canaveral, Florida, where detailed meteorological data acquisition systems were available [1]. Finally, an up-to-date blast



prediction procedure, based on locally available weather observations and forecasts, has been developed for use by local USAF meteorologists.

BACKGROUND

Atmospheric Acoustic Refraction

Atmospheric acoustic refraction causes sound (or airblast) rays to bend upward, away from ground, when sound velocity decreases with height, as shown in Figure 2a, because higher portions of the wave travel in a slower velocity medium than lower wave portions. Conversely, when sound velocity increases with height (Figure 2c) emitted rays are bent toward ground, forming a sound duct and enhancing propagation. In the homogeneous atmosphere case (Figure 2b), with everywhere constant sound velocity, the hemispherical surface burst or spherical free air burst (FAB) explosion wave expands radially without distortion, and with characteristics that have been adequately defined by one-dimensional hydrodynamic models for explosions [2, 3].

Standard Explosion Definition

The standard 1-kt* nuclear explosion (NE), free-air burst (FAB), as computed by the USAF Weapons Laboratory (AFWL) [3], gives an airblast overpressure versus distance curve shown in Figure 3, using the distance scale at the top of the figure.

*The commonly used kiloton, abbreviated kt, was used rather than its SI equivalent, 4.2 TJ.

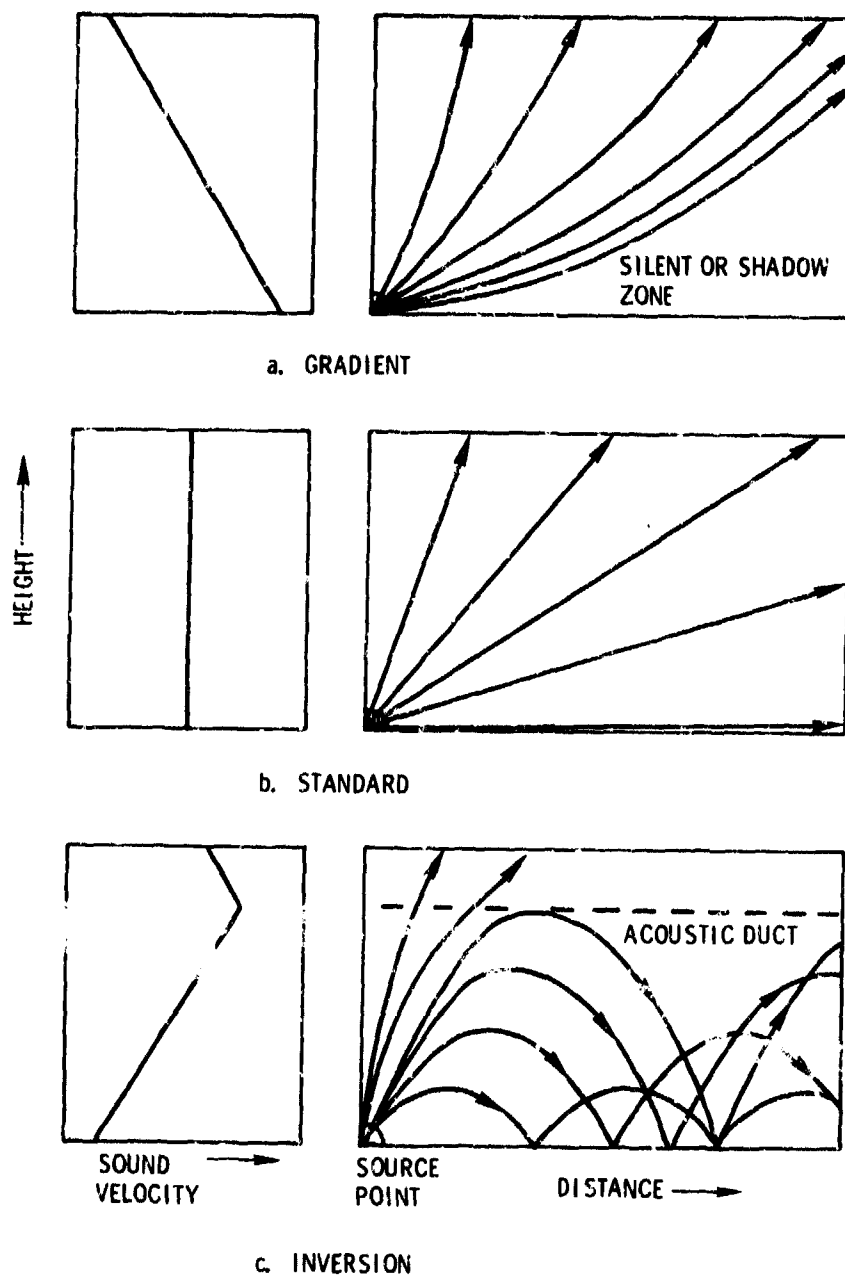
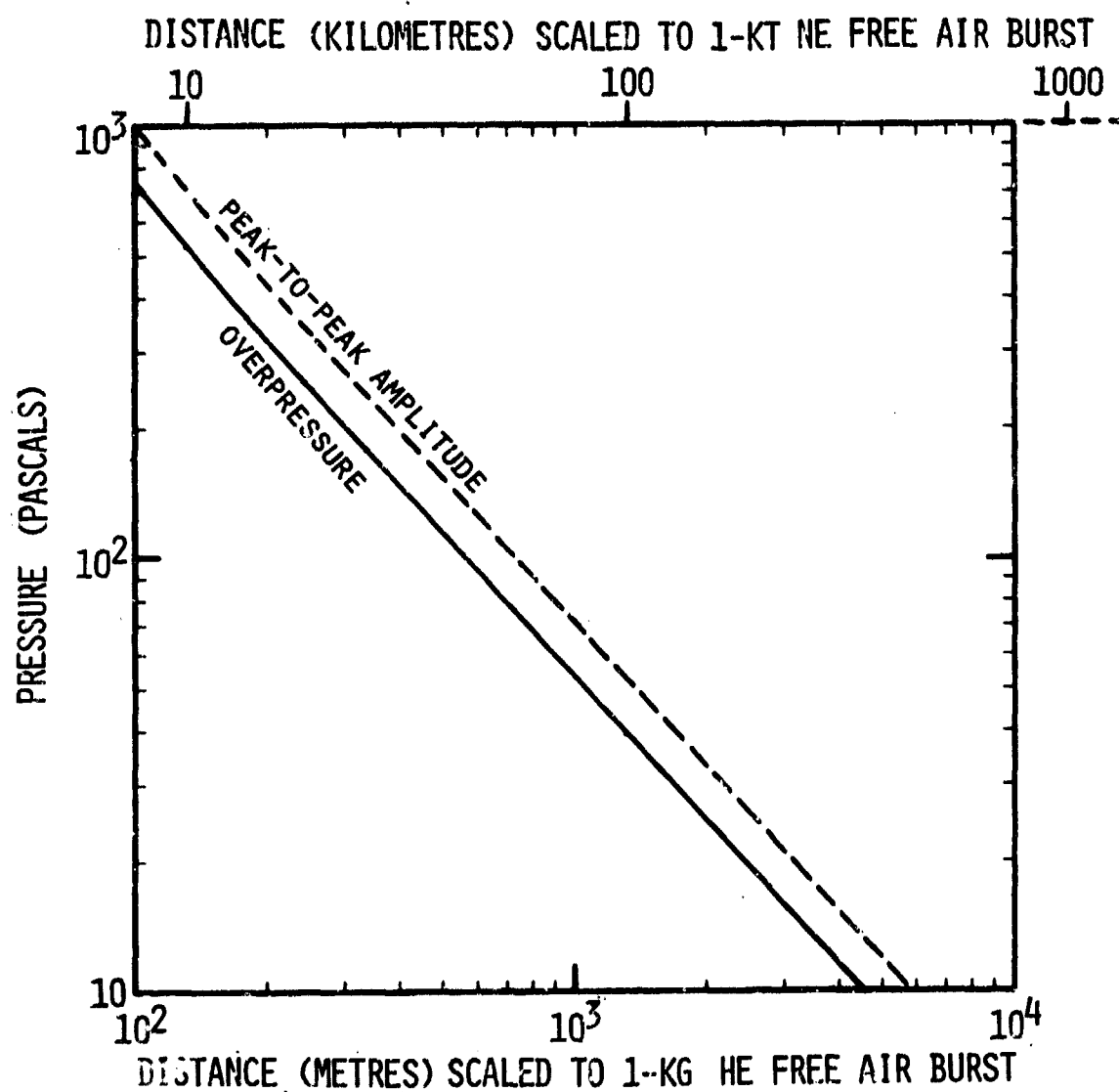


Figure 2. Atmospheric Refraction of Acoustic or Airblast Rays



STANDARD EXPLOSION AIRBLAST PRESSURE-DISTANCE CURVES
FOR MEAN SEA LEVEL PRESSURE-ALTITUDE.

Figure 3

The bottom scale has been adjusted to a 1 kg HE (TNT chemical high explosives) yield, following

$$R_1/R_2 = (W_1/W_2)^{1/3} \quad (1)$$

where R is radial distance and W is explosion yield. Also included in the Figure 3 scale shift is the generally accepted factor of two converting NE to HE yield [4].

Height-of-Burst (HOB)

Height-of-Burst is an important factor in determining explosion airblast source strength [4]. The reflection-formed hemispherical Mach wave appears to come from an enhanced yield, as shown in Figure 4, up to a yield-scaled height referred to as the "optimum" HOB. This gives the "most bang for the buck," or maximum radial extent of specific over-pressure or damage (up to a level of a few tens of kilo-pascals).

Atmospheric Effects on Propagation

Refractive distortion of a blast wave by the atmosphere may enhance or attenuate propagation. In addition, a wave may actually be focused along a circumferential arc (caustic) around an explosion under more complex atmospheric conditions [5]. Specifically, when directed sound velocity decreases, then increases with height to a velocity aloft that is greater than the surface velocity, as shown in Figure 5, an annular portion of an explosion hemisphere wave is essentially reflected aloft and returned to the ground in an ensonified ring, beyond a so-called "zone of silence."

Observations of atmospheric nuclear tests recorded an extreme of 5X magnification above standard unrefracted incident amplitude propagation [6], caused by jet stream winds near 10 km MSL (mean sea level) altitude. Up to 3X recordings near 220 km range were caused by the relatively warm atmospheric ozonosphere layer near 50 km altitude with seasonally directed winds and propagations at that level. Sandia experiments in Nevada with 1134 kg HE explosions showed up to 8.3X amplitude magnification from jet stream winds that were calculated by caustic ray path programs to cause a caustic at about 60 km distance [7].

Current interest in hot-fueled motors (Class VII explosive fuels) for such vehicles as the Trident [8], MX and Shuttle, led to an extensive experimental study of boundary layer (to 1.5 km MSL altitude) propagation at Cape Canaveral, Florida. Several hundred explosions, with yields ranging from 2.3 kg to 1145 kg TNT, were fired in 1979, under a variety of weather conditions [1]. Airblast amplitude records were obtained that allow quantitative relation of propagation (amplitude versus distance functions) to weather (sound velocity change; positive for inversions, negative in gradient conditions).

Figure 6 shows an empirical family of amplitude-distance curves (scaled to 1 kg HE FAB) that was obtained over flat Florida palmetto, sand, and swamp. Sound velocity differences are shown for each curve, representing the maximum deviation from surface level sound velocity that was observed in the boundary layer by a nearby 150 m meteorological tower. Figure

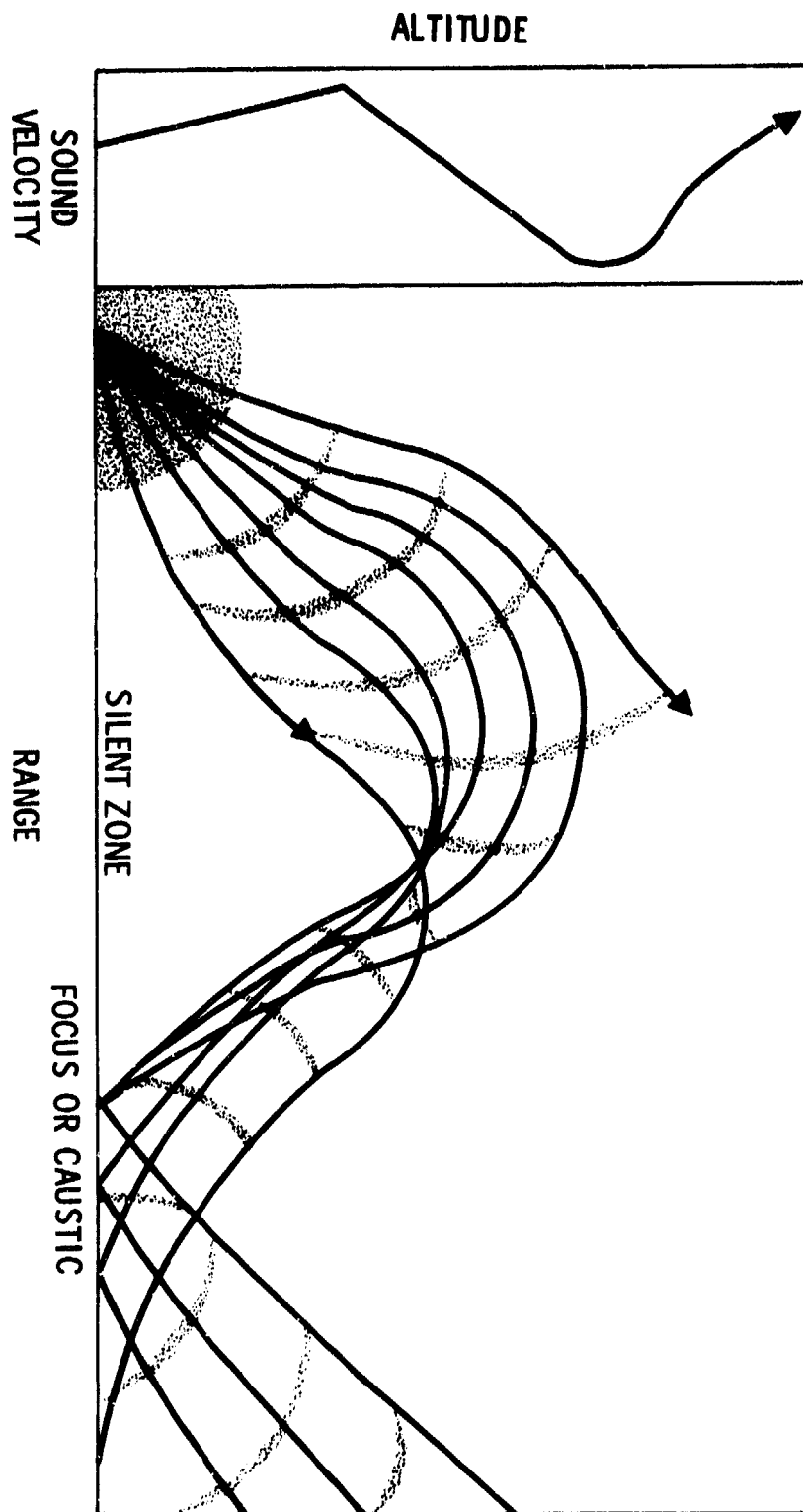
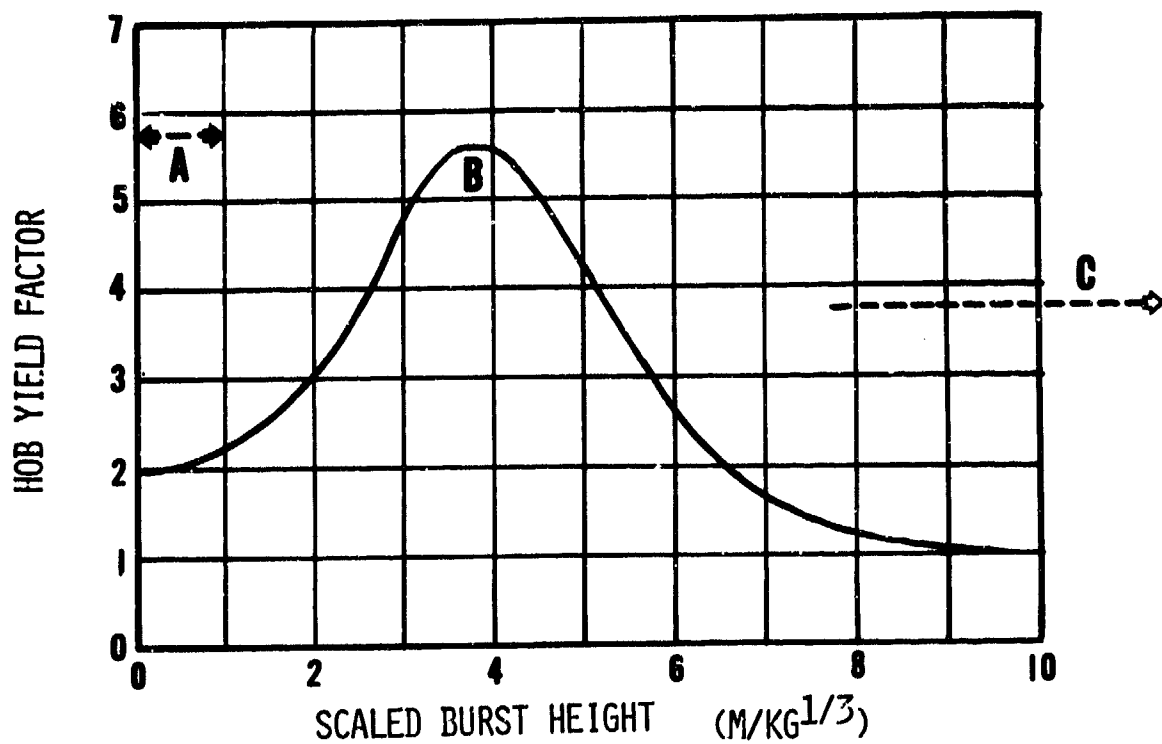


FIGURE 5. TYPICAL EXPLOSION RAY PATHS.

LEGEND

- A** SURFACE BURST REGIME
- B** OPTIMUM HOB
- C** FREE AIR BURST REGIME



AIRBLAST HEIGHT-OF-BURST EFFECT ON APPARENT YIELD,
 BASED ON HIGH EXPLOSIVES MACH-STEM PRESSURES NEAR
 $8 M/KG^{1/3}$ RADIUS.

Figure 4

scales have been shifted to Albuquerque pressure-altitude (83 kPa).

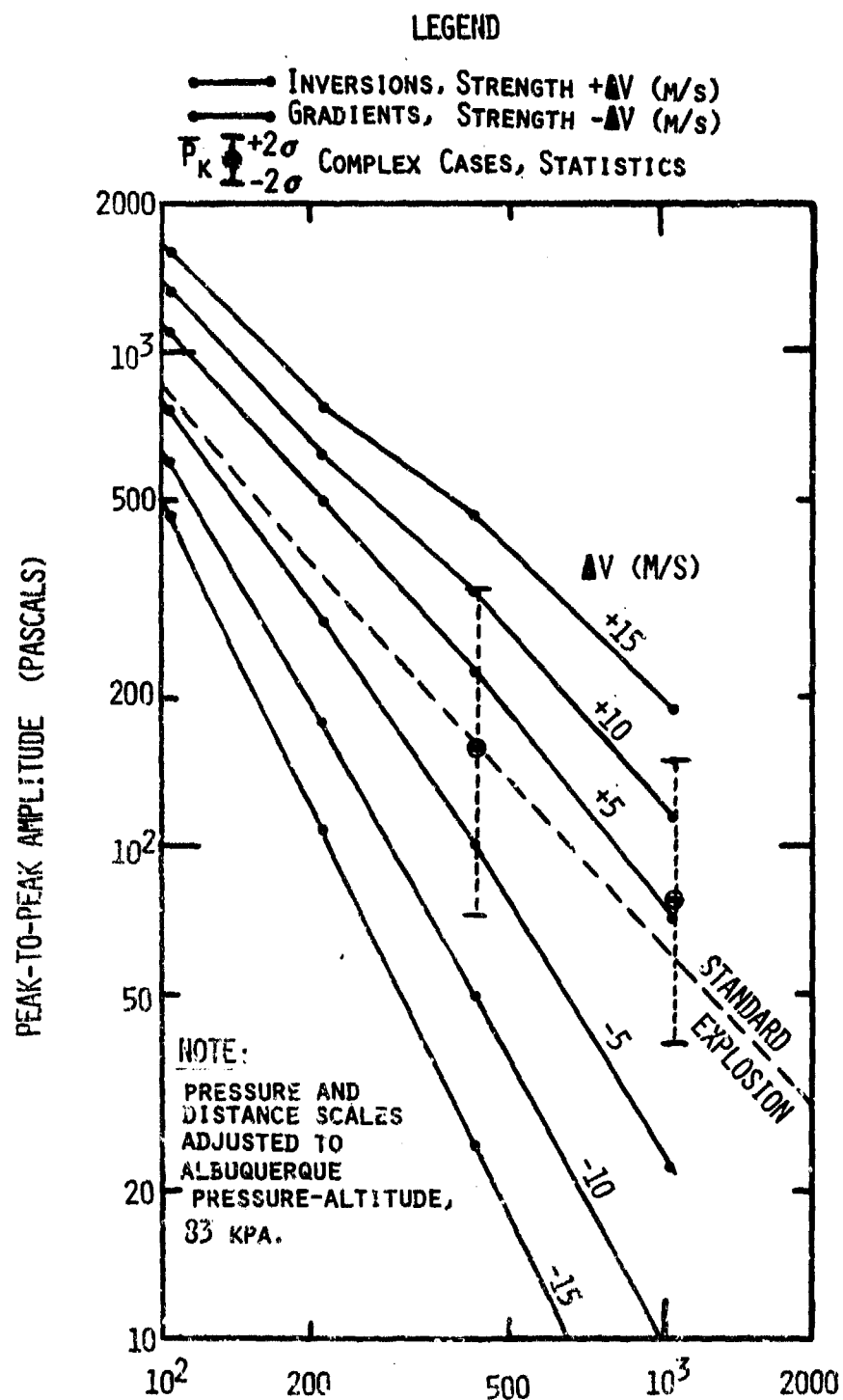
Some statistics of propagation measurements under complex conditions are also shown in Figure 6. Complex cases include both clear dog-leg $V(z)$ structures as well as what appear to be very nearly standard conditions ($V(z) = \text{constant}$). In near-standard cases there were occasional strong propagations caused by undetected sound velocity complexities.

Blast Noise Nuisance and Damage

Audible sounds generally range in frequencies from about 15 Hz to 20 kHz [5]. Low frequency explosion noises usually must reach about 20 Pa amplitude or 10 Pa overpressure (114 dB*) to be barely heard; 50 Pa overpressure (128 dB) usually arouses considerable attention from a typical community.

At long ranges, assumed for "distant" communities and low expected overpressures, the dominant frequency should be near 0.4 Hz from 1 kt NE and 30 Hz from 1 kg HE, except for added low frequency components caused by multi-path atmospheric propagations. On the other hand, it usually appears that much of what the public hears from distant explosions is the rattle of their houses in response to this low frequency pressure oscillation. Unfortunately, house-rattling often triggers a search for damage, and the years' accumulation of cracked

*Acoustic level $L = 20 \log_{10} (p/2 \times 10^{-5})$ decibels (dB), for pressure oscillation amplitude, p , in pascals.



DISTANCE (METRES) SCALED TO 1-KG HE FREE AIR BURST
AIRBLAST AMPLITUDE VERSUS DISTANCE, PROJECT PROPAGATOR.

Figure 6

plaster and windows is often claimed as the immediate consequence of an explosion.

Assessing true community damage from such weak explosion waves is quite complex. Experience with atmospheric nuclear tests has shown that a threshold for window damage appears to be about 400 Pa amplitude [9].

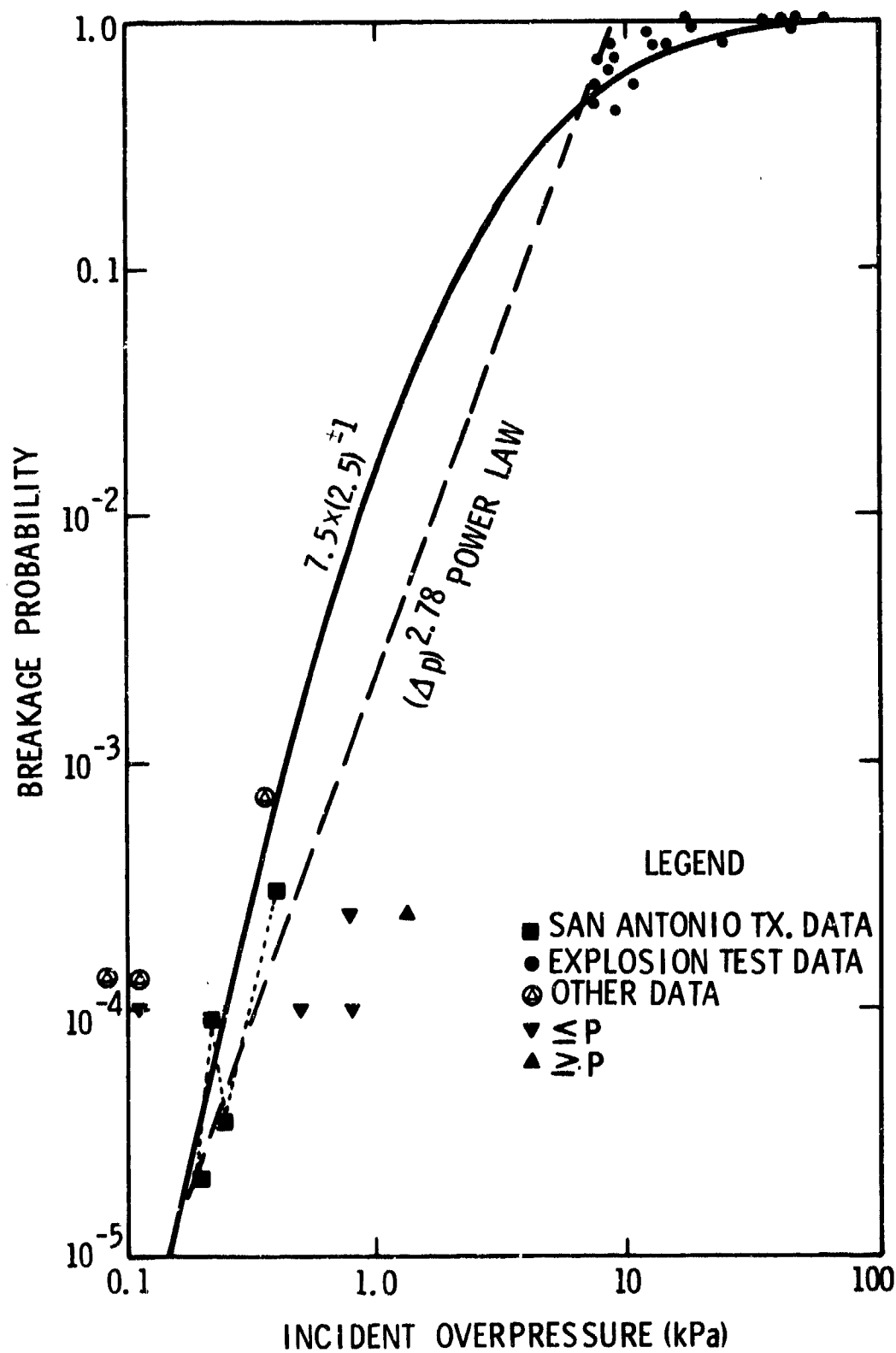
Window glass would seem to offer a relatively simple and sensitive structural component for airblast-damage correlations. Unfortunately, nothing is ever so simple as it seems, and to date, there is no satisfying and conclusive theoretical model for window damage response to airblast amplitude input. It appears that a simple empirical estimator, based on explosion test and accident results, gives the only satisfactory prediction [10]. As shown in Figure 7, the function relating breakage probability (on a community-wide basis of an assumed distribution of installations) to applied airblast overpressure, is the lognormal statistic

$$\Delta P_R = 7.5 \times (2.5)^{\pm} \text{ kPa}$$

YIELD LIMITATIONS, NO WEATHER CHECK

Acceptability Criteria

Cost effectiveness analysis would usually show that expenses of delaying an explosion test operation far exceed airblast damage costs, even under the worst weather conditions. Exceptions occur, of course, when someone is injured by falling or flying glass, or when community annoyance reaches such proportions



WINDOW BREAKAGE FROM AIRBLAST, THEORY & DATA

Figure 7

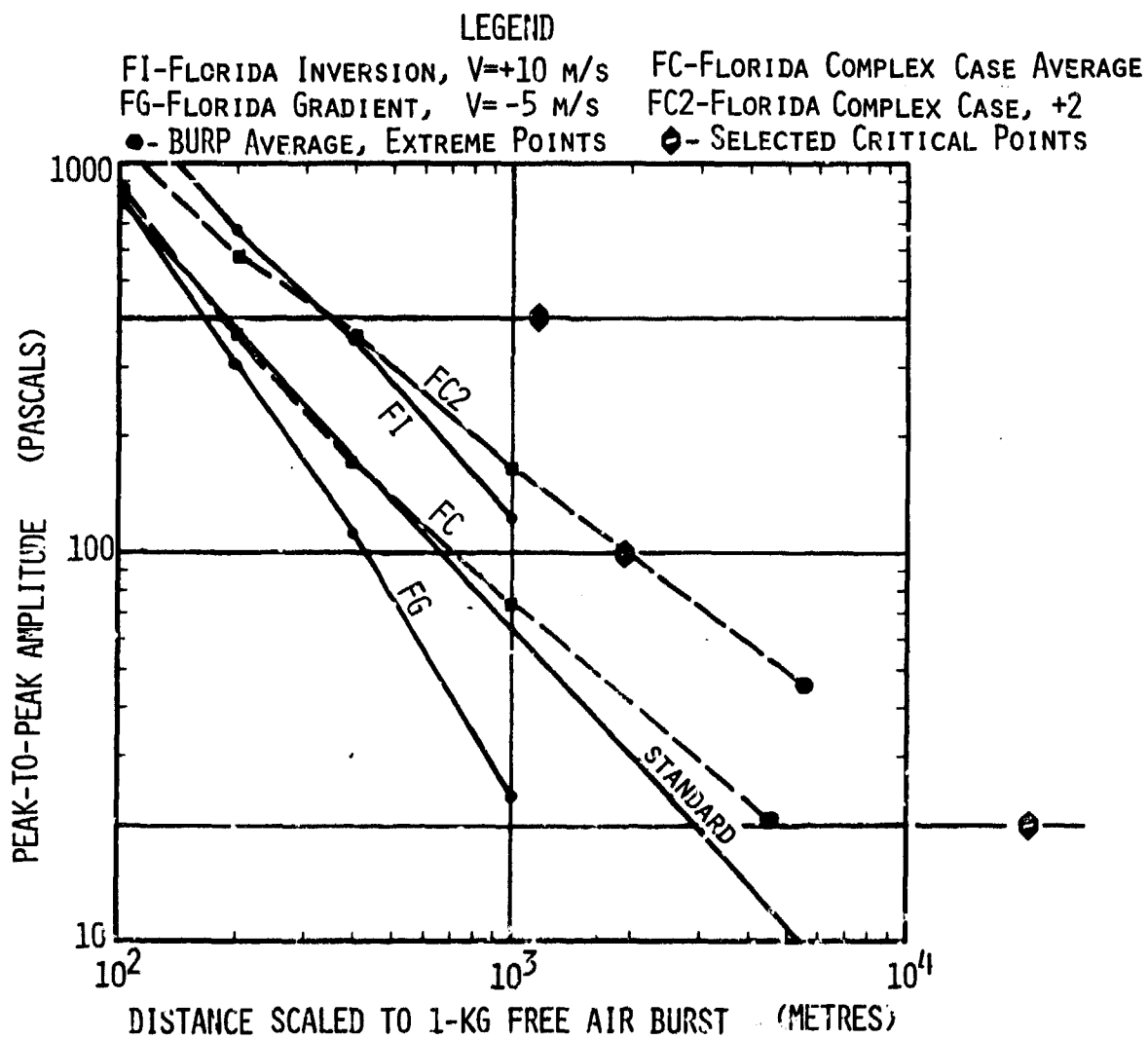
that political action is taken to suspend or radically change an operating program.

To avoid such consequences, limitations are commonly imposed and accepted by test managers to hold airblast noise levels down to mild rumbles, comparable to thunder. A recorded pressure amplitude of about 100 Pa corresponds to this noise level, at about one quarter the window damage threshold. Amplitudes of 20 Pa should pass unnoticed except by a forewarned and perceptive observer in a quiet ambience.

Relevant pressure-distance curves and data for establishing criteria are shown in Figure 8. Extreme propagation for 400 Pa damage has been adopted at a scaled distance of $1164 \text{ m/kg}^{1/3}$. Application of the 8.7X focus factor to long range gives the extreme range for minimal audibility (20 Pa) at $20 \text{ km/kg}^{1/3}$.

Operational decisions of whether or not a weather check is necessary may be made on the basis of generally accepting 100 Pa rumbings, while allowing that on rare occasions the rumble may be quite loud but not damaging.

Thus 100 Pa amplitude at $1950 \text{ m/kg}^{1/3}$ has been adopted, based on a $+2\sigma$ deviation from the average of complex condition propagations in Florida. With strong, simple inversions, $\Delta V = +10 \text{ m/s}$, 100 Pa would carry just beyond $1 \text{ km/kg}^{1/3}$ on the average and $+1\sigma$ in the distribution would fall near $1.5 \text{ km/kg}^{1/3}$. Florida test inversions never exceeded $\Delta V = +10 \text{ m/s}$. Stronger propagations will occur when there are complex conditions and focusing, but only 250 Pa would then be expected in the extreme cases of 8X



CRITICAL POINTS FOR COYOTE CANYON AIRBLAST PROPAGATION LIMITS.

Figure 8

magnification. No damage claims should arise from these rare incidents.

Calculated Limits for Various HOBs

Based on this criterion, that 100 Pa should extend to less than $1950 \text{ m/kg}^{1/3}$, explosion yield limits in Table I were calculated for critical target distances from two primary Coyote Canyon explosion test sites. Yield limits for not exceeding the 400 Pa damage threshold and the 20 Pa audibility threshold are also tabulated.

Table I shows that Lurance Canyon tests with surface bursts should be limited to 36 kg HE to hold propagation into Four Hills to less than 100 Pa amplitude under most weather conditions. Minor elevations of the charge can be accepted, up to 4 m, before HOB enhancement effects become significant. At optimum HOB, however, the limit is only 13 kg HE at 9 m above ground. Free air bursts, well above optimum HOB, could be 72 kg HE at 38 m or more, where FAB spherical wave formation is assured.

Thunder Range tests, at 9.5 km from the south boundary of Four Hills, should be restricted to 58 kg HE surface bursts. There have, in the past, been instances when minor airblast damage was caused by as little as 45 kg HE, as well as by rocket sled tests. Over thirty years of operation, such incidents have been so rare that they have been accepted by the community.

In general, it should take about four times the criteria yield limit, as well as extremely strong, focused propagations,

TABLE I.
Weather-Independent Explosion Yield Limits,
Coyote Canyon Tests

Blast Location:	Lurance Canyon Igloo 9830	Thunder Range Bldg 9966
Critical Target:	Four Hills 8.1 km	Four Hills 9.5 km
Surface Bursts	36 kg	58 kg
Maximum Height	4 m	5 m
Elevated Bursts	13 kg	21 kg
Optimum Height	9 m	11 m

to cause damage at critical target communities. On the other hand, barely audible sound might be observed from yields of only a few grams of HE. Only if a great number of such small explosions were planned, as on a small-weapon firing range, would there be any chance for significant public annoyance from such small shots.

YIELD LIMITS WITH GOOD WEATHER CONDITIONS

Gradient Conditions

Table II shows explosion yields that could reasonably be contemplated for Coyote Canyon testing, assuming that a weather watch is available and test delays are acceptable while awaiting suitably attenuated propagations. These optimistic estimates were based on good gradient propagation conditions of $\Delta V = -5$ m/s. Stronger gradients were occasionally observed during Florida tests, down to -10 m/s, but they included a wind component that would not usually prevail over the necessary range of azimuths. Under clear skies and generally light wind conditions, with firing restricted to early afternoon during the greatest temperature lapse rate, there should be a number of days in any season when $\Delta V \leq -5$ m/s would be directed toward all heavily inhabited directions. Fortunately, prevailing daytime winds in Albuquerque are from the south through northwest so that most of the city is frequently upwind of both firing sites.

Maximum Yield Estimates

It appears that 4-ton (3.6-mg) HE surface bursts in Lurance Canyon and 5.8 Mg (6.4-ton) HE at Thunder Range could be fired

TABLE II. Explosion Yields for Very Good Conditions ($\Delta v \leq -5\text{m/s}$)

CRITERIA	LURANCE CANYON			THUNDER RANGE		
	Four Hills	Carnuel	So. NM-10	Four Hills	La Blvd	Isleta Blvd
	8.1 km	6.9 km	4.0 km	7.5 km	11.1 km	14.8 km
<u>MODERATE NOISE</u> ($\leq 100\text{ Pa}$, $420\text{ m/kg}^{1/3}$)						
<u>Free Air Burst</u>						
Max W (kg)	7173	4434	864	11572	18460	43756
Min Ht (m)	179	152	88	209	245	326
<u>Surface Burst</u>						
Max W (kg)	3587	2217	432	5786	9230	21878
Max Ht (m)	18	16	9	21	25	33
<u>Optimum HOB</u>						
Max W (kg)	1281	792	154	2066	3296	7814
Opt Ht (m)	43	37	21	51	59	79
<u>Damage Threshold</u> (400 Pa , $165\text{ m/kg}^{1/3}$)						
FAB W (Mg)	118	73	14	190	304	722
Sfc W (Mg)	59	37	7	95	152	361
Opt HOB W (Mg)	21	13	3	34	54	129
<u>Audibility Threshold</u> (20 Pa , $1.1\text{ km/kg}^{1/3}$)						
FAB W (kg)	399	247	48	644	1028	2436
Sfc W (kg)	200	123	24	322	514	1218
Opt HOB W (kg)	71	44	9	115	183	435

under select weather conditions. This conclusion is in accord with historical experience, except for those few occasions when peculiar and unsuspected local weather influences caused trouble. Conceivably, even 59 Mg HE could be fired in Lurance Canyon without actual damage in Four Hills. Until mountain shadow effects are better understood, however, this yield would appear to hazard the whole Tijeras Canyon and NM-10 South region. Such large and expensive tests would be better conducted at a larger test range.

WEATHER WATCH & PREDICTION PROCEDURES

Outline

When an explosion test is planned to exceed yield limits shown in Table I, a weather watch and airblast prediction is required to assure that propagations will not unduly disturb the community. The recommended evaluation procedure follows the chronological order of occurrences:

- Source definition
- Propagation conditions
- Target effects assessment

Calculation forms have been provided for test operator use, along with various useful conversion tables and nomographs.

Source Definition

Equivalent yield was probably already determined in reaching a decision that detailed weather-dependent predictions were needed. Nevertheless, this source strength should be system-

atically determined by following the steps of Table III. Air-blast equivalent yield factors for common chemical explosives are available from several sources. An HOB yield enhancement factor should be estimated from the curve shown earlier in Figure 4. Results, in Lines 11-13, provide three points for plotting a standard pressure-distance curve for the indicated explosion.

Rather than attempting to reconstruct a yield-scaled family of propagation curves for various weather conditions, a background amplitude-distance pattern for 1 kg HE is shown in Figure 9 for use with a clear plastic overlay copy of Figure 10. The index arrow (at 1000 m or 1 km) is aligned under the overlaid distance scale at the kilometre distance given on Line 14 of Table III. This procedure, involving yield-scaling of distances, allows rapid evaluation for critical targets and weather threats, from a given explosion.

When the overlay has been aligned, the result shows the various weather-dependent propagation curves, with yield-scaled distances along the abscissa marked by ranges to specific local targets. Intersections of target distance lines (verticals) and propagation curves are used to establish limits on weather conditions to avoid exceeding pre-determined damage, noise, or audibility.

A number of notable incidents or test results have been shown by points on the Figure 9 background. Several incidents appear to show extreme propagations that exceeded results

TABLE III

EXPLOSION SOURCE STRENGTH CALCULATION

1. Type of chemical explosive		
2. Total explosive weight, W	lb	kg
3. Explosive yield equivalence factor (1.0 for TNT), k_e (see Table IV)		
4. TNT equivalent weight, $W_e = k_e \times W$	lb	kg
5. Yield scaling factor, $W_e^{1/3}$	lb ^{1/3}	kg ^{1/3}
6. Charge center height above ground, Z	ft	m
7. Yield-scaled height of burst, $HOB = Z / W_e^{1/3}$	ft/lb ^{1/3}	m/kg ^{1/3}
8. HOB yield enhancement factor, k_h (see Fig. 4)		
9. Apparent airblast yield, $W_a = k_h \times W_e$	lb	kg
10. Apparent yield scaling factor, $W_a^{1/3}$	lb ^{1/3}	kg ^{1/3}
11. Standard explosion 400 Pa distance, $R_A = 189.34 \times W_a^{1/3}$		m
12. Standard explosion 100 Pa distance, $R_g = 667.69 \times W_a^{1/3}$		m
13. Standard explosion 20 Pa distance, $R_C = 2884.04 \times W_a^{1/3}$		m
14. Index (Fig. 10) distance on overlay (Figure 11), Repeat Line 10 number entry.		km

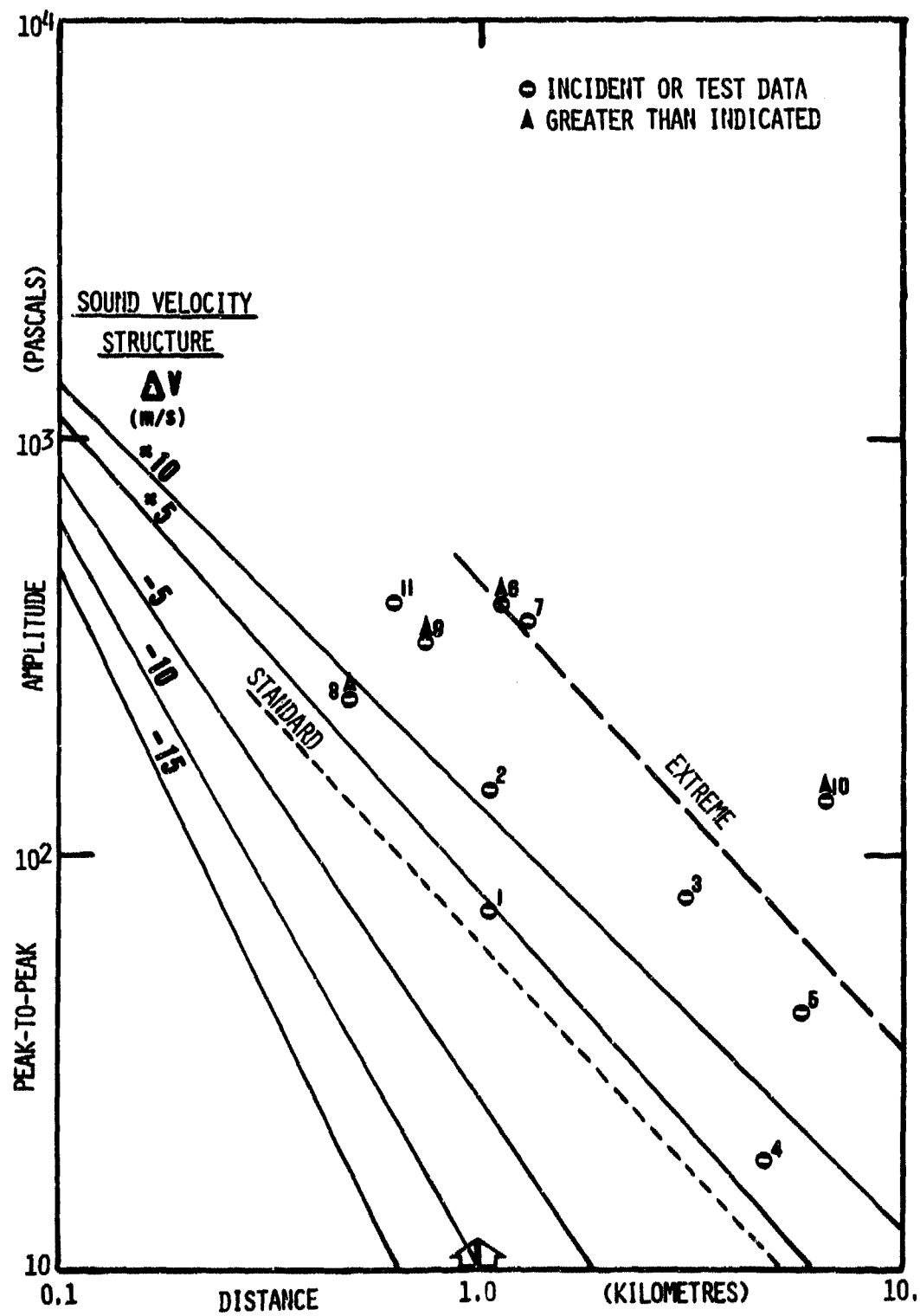


Figure 9. Explosion Pressure Amplitude Versus Distance Curves, Yield-Scaled to 1 kg HE

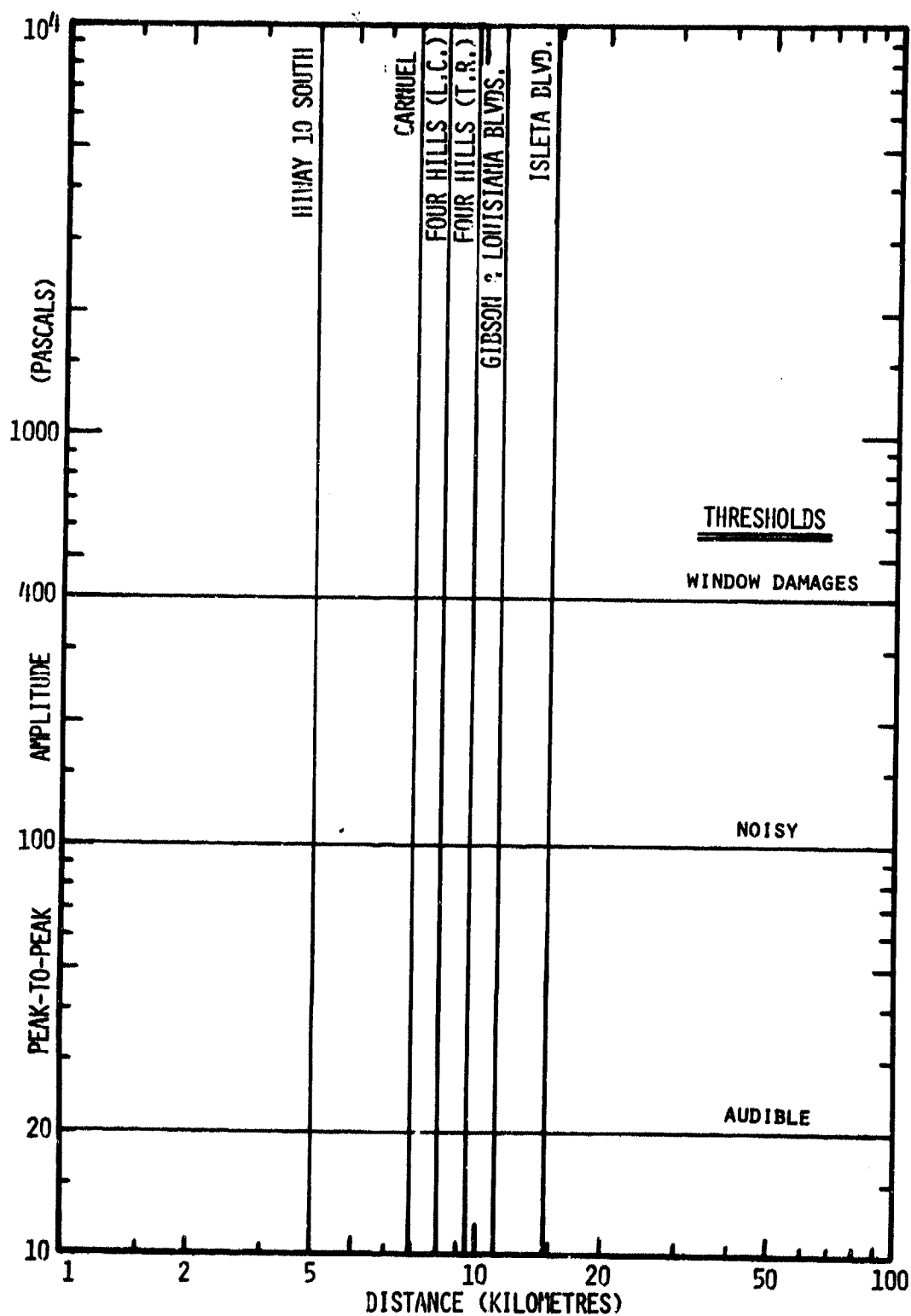


Figure 10. Target Distance Overlay for Amplitude-Distance Curves

obtained in experiments. As such, they indicate what could happen but not what might be expected to happen in a given situation. Except for the case shown by Point #10, extreme propagations appear to be bounded by the dashed line shown near 7X focus factor. In complex propagating conditions, either with a dog-leg sound velocity structure or near $\Delta V = 0$, and a yield that could conceivably cause damage to the community, a test delay should be recommended to await better weather. On the other hand, it may be necessary to proceed and fire some complicated or costly test explosions, with the remote chance of adverse response, even when the "Extreme" line is slightly exceeded. But if the amplitude of the exceedance is by about 50 percent or so, then there arises a real probability of injury caused by breaking or falling glass in any substantial population.

Well above the damage threshold level, and around 3 kPa overpressure (not amplitude), flying glass would have such density and velocity as to seriously threaten the safety of every resident [11]. This point is stressed here because there is a lingering remnant of misguided opinion that nearly 0.5-psi (3.5 kPa) is needed "to cause minor damage to the flimsiest structures." This conclusion, apparently originated by World War II bomb damage assessors and relevant only to the maintenance of building structural functions in war production, is still occasionally repeated with respect to sonic booms and mining activities [13].

Along similar lines, some obsolete analyses indicated 100X amplitude focusing potentials for atmospheric propagation [14]. All attempts to pin down the source data for this contention have been futile, but some clues have been obtained. Early (pre-1950) laboratory experiments made overpressure-distance measurements with small HE charges that showed $\Delta p \sim R^{-1.4}$, rather than $\Delta p \sim R^{-1.1}$ as now estimated for "standard" long range propagation. Similar rapid pressure-distance decays were later obtained from 0.4 g HE experiments [15]. Measurements at very long range from much larger explosions were apparently used to infer large magnification (referenced to the more rapid distance decay rate) in caustic zones. References to the new standard, however, should bring these amplifications down to or below the "Extreme" level shown in Figure 9.

Weather Observations and Calculations

Having established the explosion source strength and its potential for propagating unacceptable airblast amplitudes into some part of the surrounding community, the next step is to determine actual (or forecast) weather conditions and their capacity for causing airblast enhancements of unacceptable magnitude in critical directions. Surface and upper air observations of temperature and winds, as needed for this assessment, are entered in Table IV.

It is assumed that no humidity correction is needed for

TABLE IV. METEOROLOGICAL OBSERVATIONS & CALCULATIONS

Date: / / Mo Day Yr
 Time: M T
 GMT

L	E	Alti- tude	Temp- erature (°C)	Wind Direc- tion (deg)	Wind Speed (knots)	Sound Speed (m/s)	Directed Wind Components (m/s)				Directed Sound Velocities (m/s)				Sound Velocity Differences (m/s)			
							θ_1	θ_2	θ_3	θ_4	θ_1	θ_2	θ_3	θ_4	θ_1	θ_2	θ_3	θ_4
0																		
1																		
2																		
3																		
4																		
5																		
6																		
7																		
8																		
9																		
10																		

Date: / / Mo Day Yr
 Time: M T
 GMT

L	E	Alti- tude	Temp- erature (°C)	Wind Direc- tion (deg)	Wind Speed (knots)	Sound Speed (m/s)	Directed Wind Components (m/s)				Directed Sound Velocities (m/s)				Sound Velocity Differences (m/s)			
							θ_1	θ_2	θ_3	θ_4	θ_1	θ_2	θ_3	θ_4	θ_1	θ_2	θ_3	θ_4
0																		
1																		
2																		
3																		
4																		
5																		
6																		
7																		
8																		
9																		
10																		

sound speed calculation in dry Albuquerque air. Altitude, temperature, and wind reports are entered directly from provided surface weather observation (zero level) and upper air balloon rawinsonde reports. Airblast propagation is usually dominated by the atmospheric layer of depth less than about one-fifth, possibly one-fourth, of the horizontal distance of concern. Most concerns with Albuquerque and Coyote Canyon tests thus involve only about 3 km of atmosphere up to 4.5 km MSL, and typically the first seven levels of a winds-aloft report. Space is provided in the table for ten balloon data levels, should further information be desired.

Sound speed in air, C , may be calculated from absolute temperature, T in kelvins, by

$$C = 20.0555 T^{1/2} \text{ m/s,}$$

or read from prepared tables.

Selection of azimuthal directions for evaluation depends on target locations and directions as well as wind direction. One calculation should be made down-wind from the strongest wind in the lower two or three rawinsonde levels. Experience is useful in determining the fewest directional calculations that are necessary to establish the existence of a propagation problem.

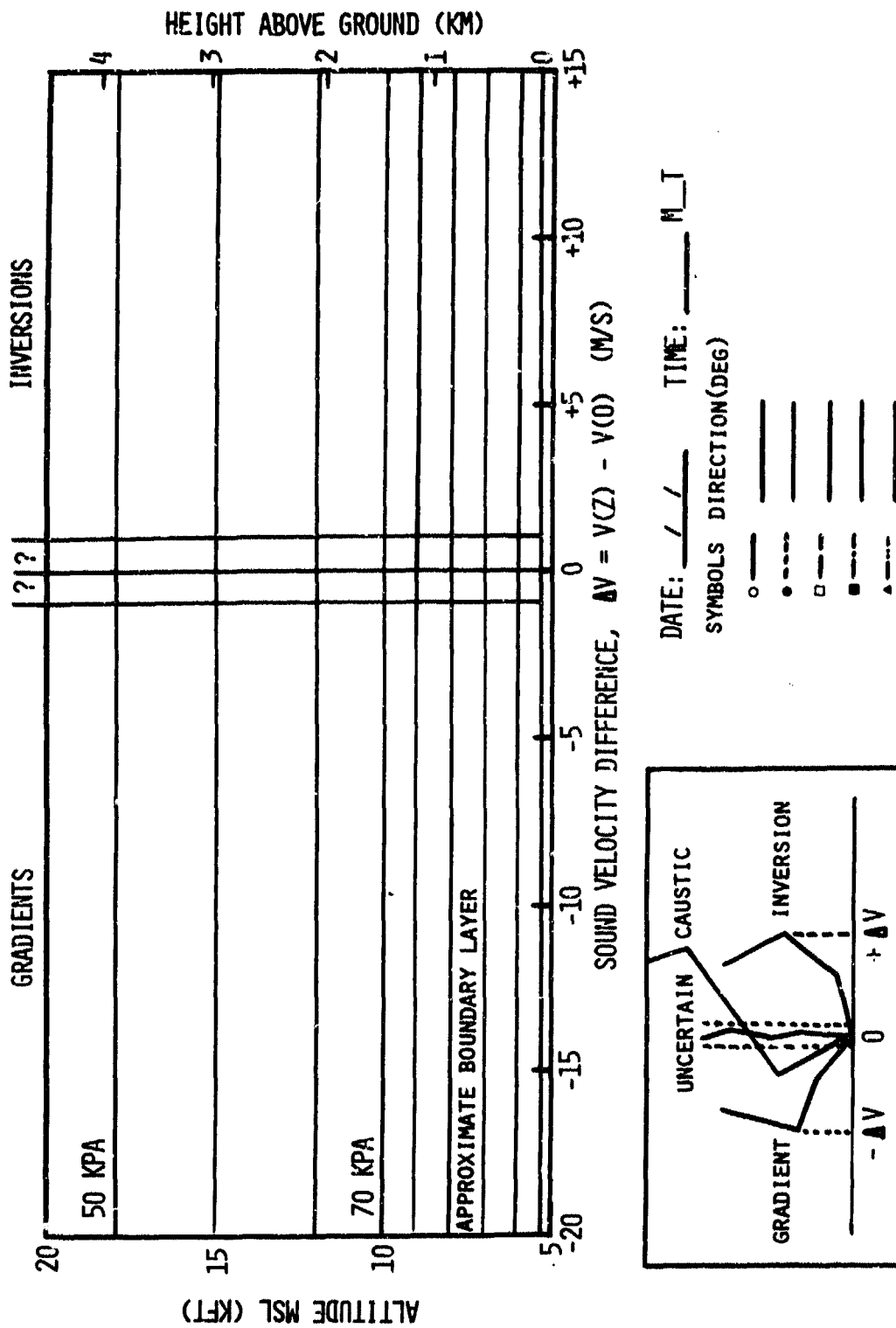
The directed wind component, U , along azimuth, θ , is resolved from the reported wind speed, W , and direction, D . Note that meteorological observing practice is to report winds according to the direction from which the wind blows. This convention, a

reversal from usual vector description, is defended to allow allusion to "cold north" and "warm south" winds, rather than vice versa.

Space is provided for analysis along four azimuthal bearings. Directed sound velocity at each level is obtained by simple addition of the directed wind component and sound speed. Sound velocity difference is obtained by subtracting the zero-level (surface) directed velocity from the upper level directed velocity. Difference curves are next plotted versus height on Figure 11. The apparent curve structure and, where applicable, the magnitude of the maximum boundary layer sound velocity difference provide the input to a propagation prediction from the yield-adjusted Figure 9/10 overlay.

Community Impact

Evaluation for community impact from the specified explosion and weather condition may be systematized by use of Table V. Values for the airblast assessment are read from the yield-adjusted Figure 9/10 overlay. The weather check, for complex structures as well as inversion or gradient intensities, is made from the directional curves drawn on Figure 11. YES-NO conclusions on acceptability are entered as appropriate, along with any remarks.



SOUND VELOCITY VERSUS HEIGHT PLOTS.

Figure 11

TABLE V. COMMUNITY IMPACT EVALUATION

Target	Azimuth (deg)	Distance (metres)	AIRBLAST ASSESSMENT					WEATHER CHECK			
			Scaled Dis- tance ($m/kg^{1/3}$)	Accep- table $\Delta V(100)$ (m/s)	Damage $\Delta V(400)$ (m/s)	Audible $\Delta V(20)$ (m/s)	Complex F(400) (σ)	Complex V-Struc- ture ? (yes/no)	OK? (yes/no)	ΔV (m/s)	OK? (yes/no)
LURANCE CANYON TESTS											
Cedro	070	5400									
NW-10 South	040	4000									
Cement Plant	010	7400									
Carnue	330	6900									
Four Hills Gibson & Louisiana	300 290	8100 15800									
Mountain View	260	22700									
THUNDER RANGE TESTS											
Four Hills Gibson & Louisiana Old Airport Terminal	020 340 320	9500 11100 12500									
Mountain View	290	11600									
Isleta Blvd	270	14800									

REFERENCES

1. J. W. Reed, "Project PROPA-GATOR - Intermediate Range Explosion Airblast Propagation Measurements," 19th DOD Explosive Safety Seminar, Los Angeles, CA, Sept. 9, 1980.
2. C. D. Broyles, "IBM Problem M Curves," Report SC-TM-268-56(51), Sandia Laboratories, Albuquerque, NM, Dec. 1956.
3. C. E. Needham, M. L. Havens, and C. S. Knauth, "Nuclear Blast Standard (1 kt)," Report AFWL-TR-73-55 (Rev.), Air Force Weapons Laboratory, Kirtland Air Force Base, NM, Apr. 1975.
4. S. Glasstone, S. (Editor). The Effects of Nuclear Weapons, Washington, DC: Government Printing Office, 1977.
5. E. F. Cox, Sound Propagation in Air, Chap. 22, Handbuch der Physik. Berlin: Springer-Verlag, 1958, Vol 48.
6. J. W. Reed, "Climatology of Airblast Propagations from Nevada Test Site Nuclear Airbursts," Report SC-RR-69-572, Sandia Laboratories, Albuquerque, NM, Dec. 1969.
7. J. W. Reed, "Explosion Wave Amplitude Statistics for a Caustic at Ranges of 30 to 45 Miles," Report SC-RR-67 860, Sandia Laboratories, Albuquerque, NM, Feb. 1968.
8. J. W. Reed, "Predictions of Nuisance Damage and Hazard from Accidental Explosions during Trident Missile Test Flights," SAND 79-0626, Sandia National Laboratories, Albuquerque, NM, March 1980.
9. E. F. Cox, Air Shocks at Large Distances from Atomic Explosions, Operation Tumbler-Snapper Report WT-504 Sandia Laboratories, Albuquerque, NM, January 1953.
10. J. W. Reed, Distant Blast Predictions for Explosions, Minutes 15th ESB Seminar, DOD-ESB, Washington, DC, 18 September 1973.
11. E. R. Fletcher, D. R. Richmond, and R. K. Jones, Velocities, Masses and Spatial Distributions of Glass Fragments from Windows Broken by Airblast, Defense Nuclear Agency Report (Albuquerque, NM, Lovelace Foundation), in preparation.
12. J. W. Reed, B. J. Pape, J. E. Minor, and R. C. Dehart, "Evaluation of Window Pane Damage Intensity in San Antonio Resulting from Medina Facility explosion on November 13, 1963," Annals of the New York Academy of Sciences, 152:Art 1, October 1968.

13. K. Shukla, "Blasting Concern for Neighbors and Operators," in Proc. 4th Conf on Explosives & Blasting Technique, Soc. of Explosives Engineers, New Orleans, LA, Feb. 1978.
14. B. Perkins, Jr., and W. F. Jackson, "Handbook for Prediction of Air Blast Focusing," BRL-1240, U.S. Army Ballistic Research Laboratories, Aberdeen, MD, Feb. 1964.
15. Sadwin, L. D., and E. A. Christian, "Characteristics of the Shock Wave Generated in Air by a Blasting Cap," NOLTR-71-105, U.S. Naval Ordnance Laboratory, Silver Spring, MD, June 1971.

AD P000432

THE CONTAMINATED WASTE PROCESSOR
FOR INCINERATION OF EXPLOSIVES CONTAMINATED
WASTE

BY

SOLIM S. W. KWAK, Ph.D.
AMMUNITION EQUIPMENT DIRECTORATE, TOOELE ARMY DEPOT, UTAH

INTRODUCTION

The purpose of this paper is to provide an update on the development, installation, and performance of the Contaminated Waste Processor (CWP), which was introduced during the developmental phase in a paper presented at the nineteenth Explosives Safety seminar in 1980 at Los Angeles, California.¹

Four systems are nearing completion, at Badger Army Ammunition Plant (AAP), Iowa AAP, Sunflower AAP, and Kansas AAP. Incineration tests for compliance with air emission standards have been successfully completed at Iowa AAP. Final equipment test and shakedown is ongoing at the four locations prior to turning the systems over to the installations.

BACKGROUND

During normal operations of Army ammunition plants and depots, considerable waste is generated that is contaminated, or is suspected of being contaminated with propellants or explosives. In addition, metals which are contaminated with explosives cannot be disposed of unless they are first flashed. Previously, the burning of such wastes and flashing of metals was accomplished on open burning grounds.

↙
The Clean Air Act and Resource Conservation and Recovery Act have resulted in restrictions in the open burning of such materials.

In response to the Army's search for an environmentally acceptable method of disposal of these materials, AED proposed that a modification to the Army's Standard APE 2048 Flashing Furnace would provide a system that could meet present and future air quality requirements. Under tasking by DARCOM, AED conducted a feasibility study which showed that a modified APE 2048 had excellent combustion characteristics which could meet all future requirements. The system concept was developed and named the Contaminated Waste Processor (CWP).
A

The Corps of Engineers, Huntsville Division, named AED at Tooele Army Depot to be the "Center of Technology" for design, development and installation of the CWP equipment.

SYSTEM DESCRIPTION

The CWP consists of three main subsystems with associated controls:

- (1) The carbottom furnace
- (2) The air pollution control system
- (3) The feed system(s)

NOTE: There are two sizes of CWP. The CWP Large Unit (CWPLU) has two feed systems, batch and continuous feed. The CWP Small Unit (CWPSU) has only one feed system, a batch feed.

The facility layout for the CWPLU and CWPSU is depicted in the artist's concepts in Figures 1, 2 and 3.

For the CWPLU, the waste material is dumped into the loading area where it can be loaded into baskets for batch feeding or it can be fed onto the conveyor for continuous feeding (See Figure 4). In the continuous feed system, materials are shredded in a low speed, high energy shredder to reduce size of materials. Shredded material is conveyed from the shredder to the furnace on an S-Conveyor and dumped

into the furnace through a double sliding valve (See Figures 5 and 6). During operations, should an explosion occur in the furnace or the shredder, personnel in the control and loading room are protected from primary fragments by reinforced concrete walls located by the furnace and shredder, and from secondary fragments by a steel barricade wall which separates the control and loading room from the rest of the building. The barricades are sized to protect against an explosion of up to 1 lb. of explosive. The feed system for the CWPSU consists of a batch loading system only.

The furnace for both the CWPLU and CWPSU is a carbottom furnace lined with ceramic fiber insulation. The only difference is in the size of the furnace. Both furnaces have a large and small burner, and automatically controlled air injection ports to control and optimize combustion of the waste materials.

Baskets loaded with waste materials are transported by an overhead automated trolley system and are fed into the furnace by placing the basket on the furnace car bottom and running it into the furnace (See Figure 7). Shredded material fed continuously into the furnace through the double sliding valves into the top of the furnace falls into a basket on the car bottom inside the furnace which facilitates subsequent removal of ashes (See Figure 8).

The CWP is designed to incinerate 600 lbs/hour of combustible waste when batch loaded, and is expected to incinerate 800-1000 lbs/hour of waste when operated with continuous feed. Approximately 10,000 lbs/hour of metal can also be flashed in the furnace. In actual operation, flashing of metal could be accomplished most efficiently by mixing it with combustible waste materials.

The CWP air pollution control system consists of a gas cooler, cyclone, baghouse, exhaust fan and exhaust stack. Exhaust gases from the furnace exit at temperatures up to 1600°F. They are cooled to approximately 900°F with dilution air before entering the gas cooler, where they are further cooled to approximately 250°F. Exhaust gases

next pass through the cyclone to remove particulate down to approximately the 30 micron size and then pass through the baghouse where particulate removal down to the 0.5 micron size is achieved. Cleaned exhaust gases then pass through the exhaust fan and out the exhaust stack.

CWP PROJECT STATUS

The CWP at Iowa AAP was the first system to come on line. Air compliance tests have been successfully completed on the furnace at Iowa AAP with the support of US Army Environmental Hygiene Agency. Iowa State air quality compliance officials were present at the test and were satisfied that the furnace operates within their standards. Preliminary data resulting from the air sampling are summarized in Figure 9.

Since the CWP at Iowa AAP is the first system to be constructed, it is essentially the pilot system. Some mechanical and electrical adjustments and corrections are in process and will be completed before the system can be totally turned over to the installation. System checkout and training will continue at Badger AAP, Sunflower AAP and Kansas AAP for the next few months prior to turning the systems over to the installations.

Four additional systems are presently in various stages of construction at Lexington-Blue Grass Depot Activity, Tooele Army Depot, Savanna Depot Activity, and Mississippi AAP. Equipment installation is scheduled to begin in the spring of 1983.

CONCLUSION

The CWP is proving to be an effective system for disposal of explosive contaminated wastes in compliance with state and federal air emission standards.

Minutes of the Nineteenth Explosives Safety Seminar, Volume II, Page 983, article entitled, "Contaminated Waste Processor," by Darrell W. Walker, PhD.

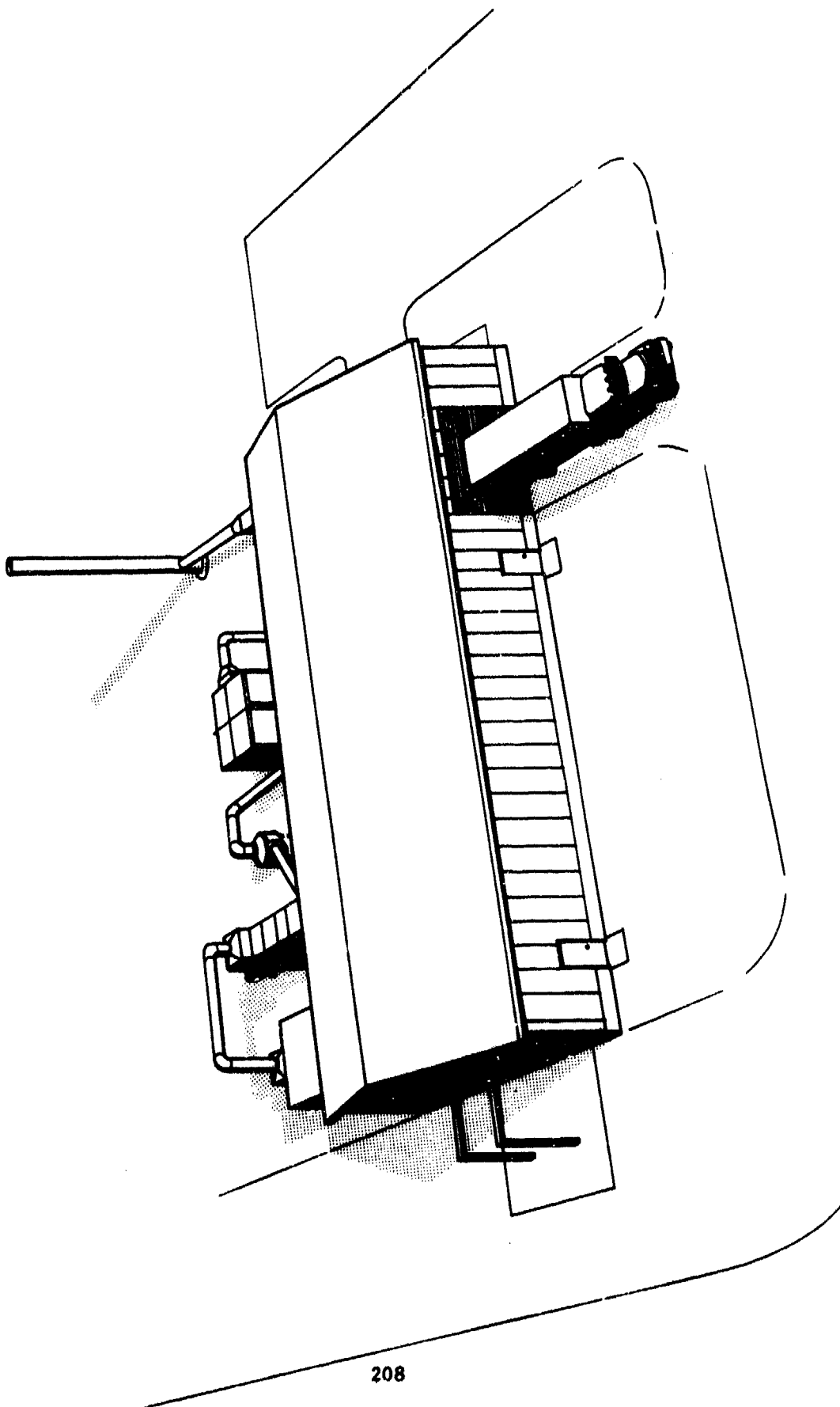
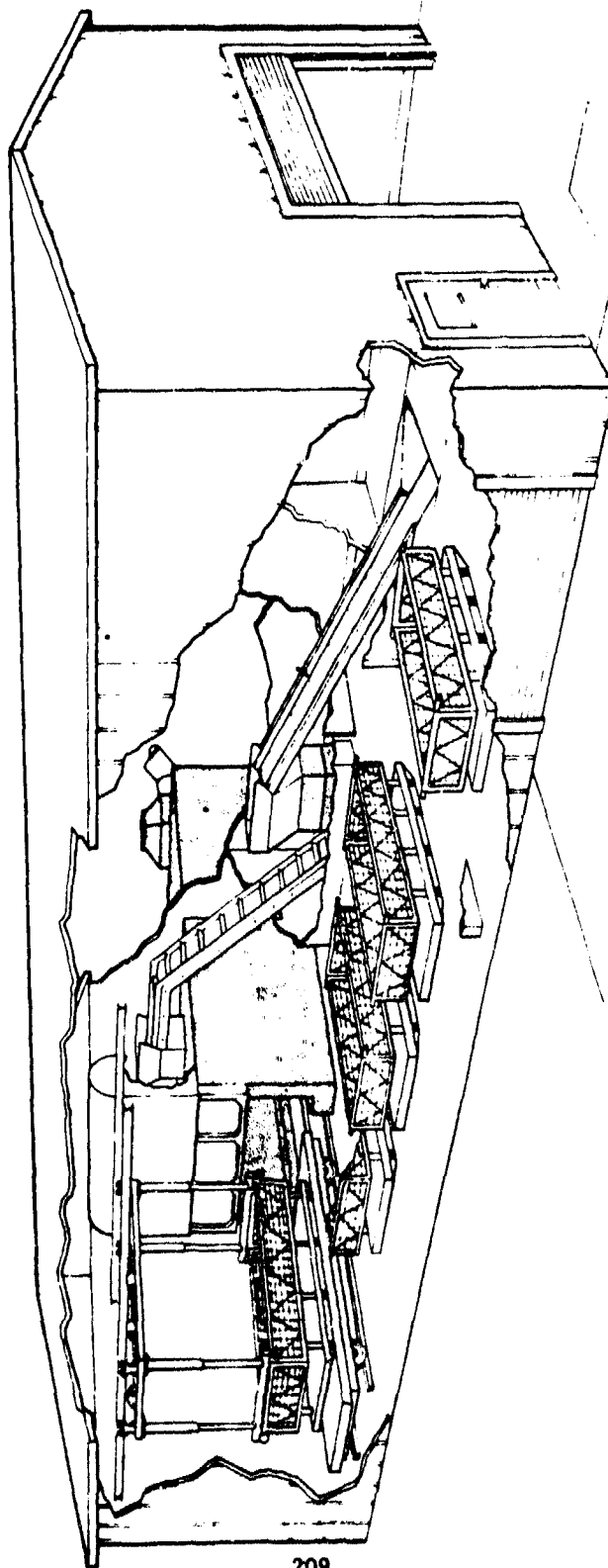


FIGURE 1
CONTAMINATED WASTE PROCESSOR LAYOUT



209

FIGURE 2
CONTAMINATED WASTE PROCESSOR
LARGE UNIT
(CWPLU)

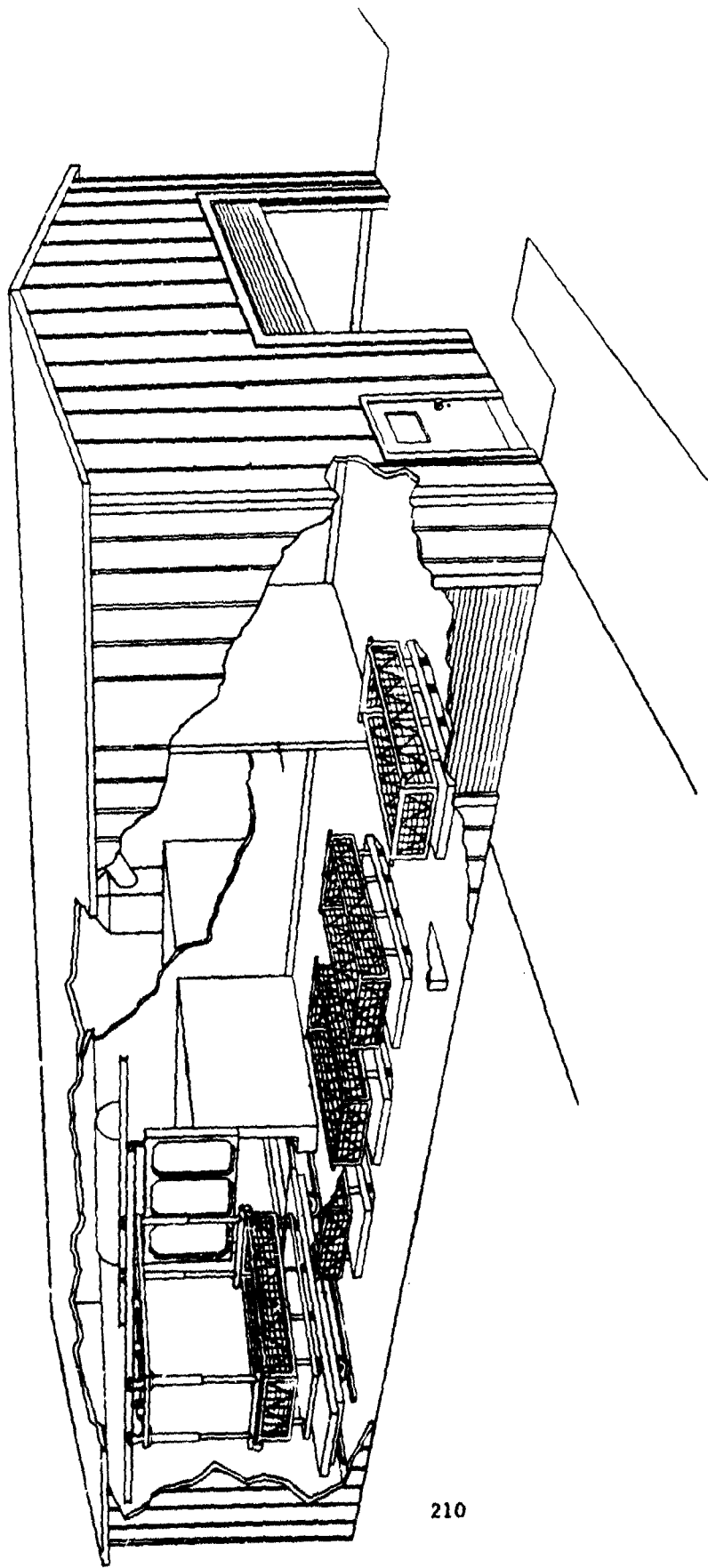


FIGURE 3
CONTAMINATED WASTE PROCESSOR
SMALL UNIT
(CWPSU)

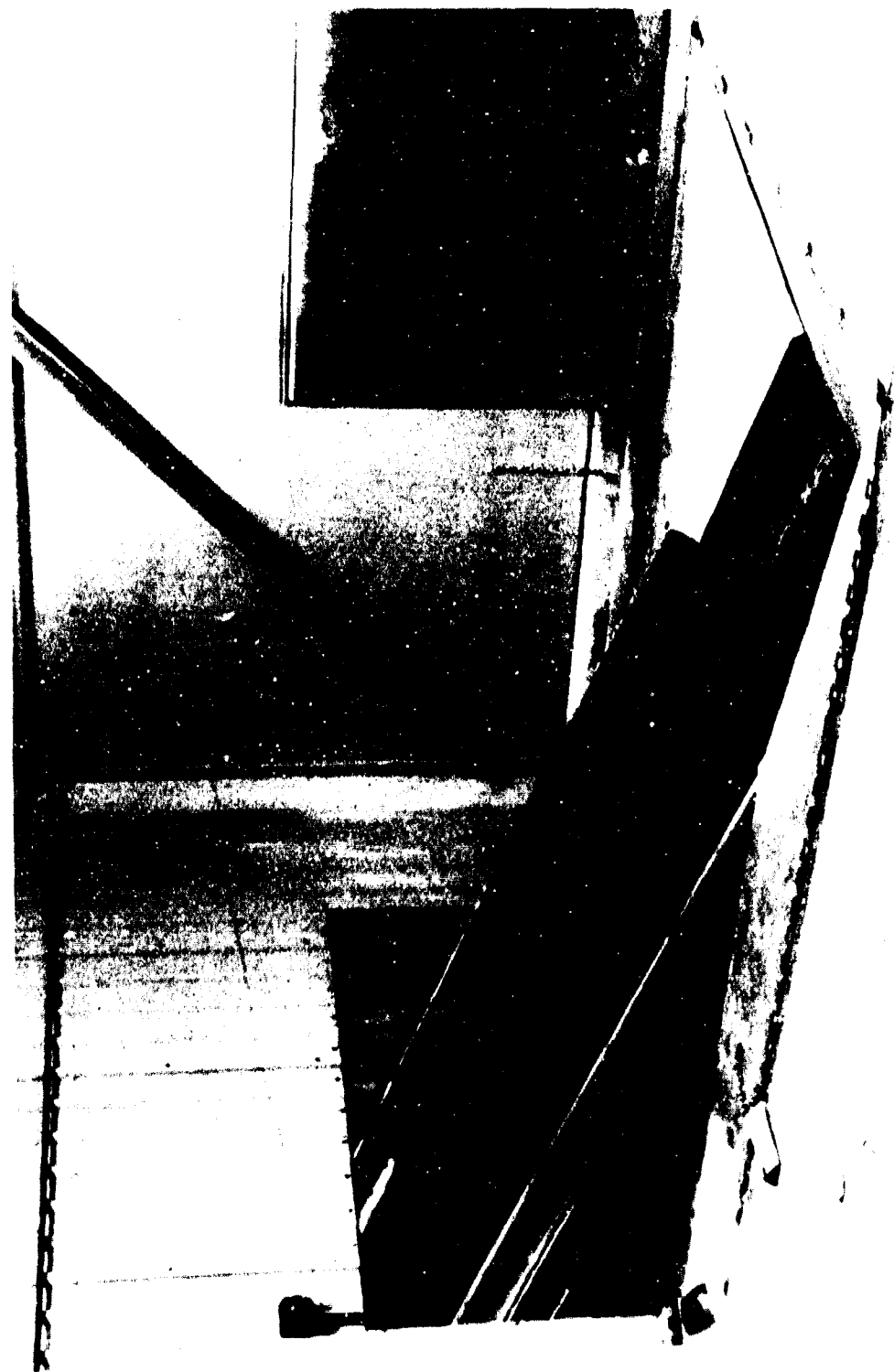


FIGURE 4 - FEED CONVEYOR IN FEED ROOM FOR
CONTINUOUS FEED

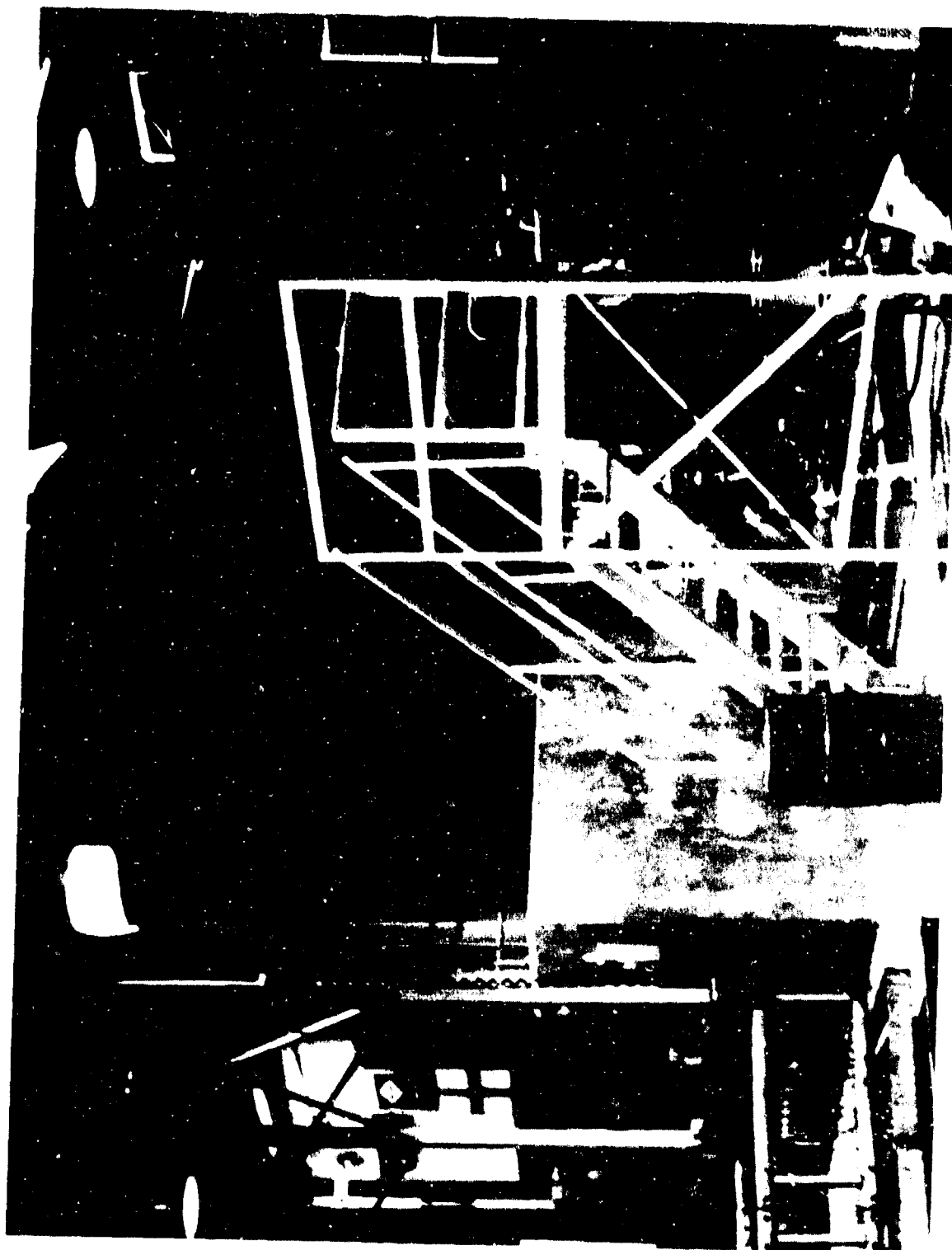


FIGURE 5 - LOW SPEED, HIGH ENERGY SHREDDER FOR
SHREDDING WASTE MATERIALS & S CONVEYOR

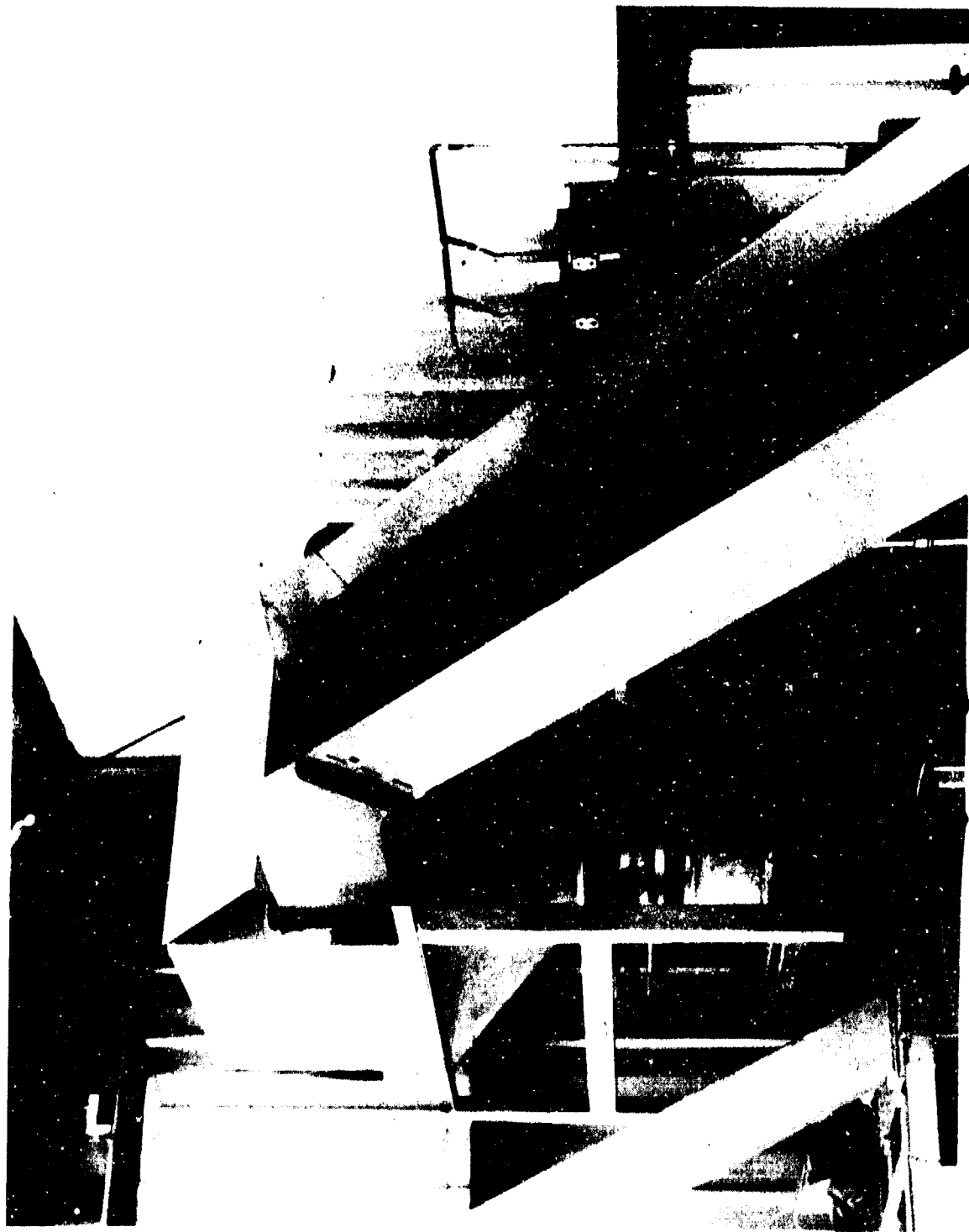


FIGURE 6 - S-CONVEYOR AND HOPPER WITH DOUBLE
SLIDING VALVE FOR CONTINUOUS FEED OF SHREDDED
WASTE MATERIALS INTO THE FURNACE

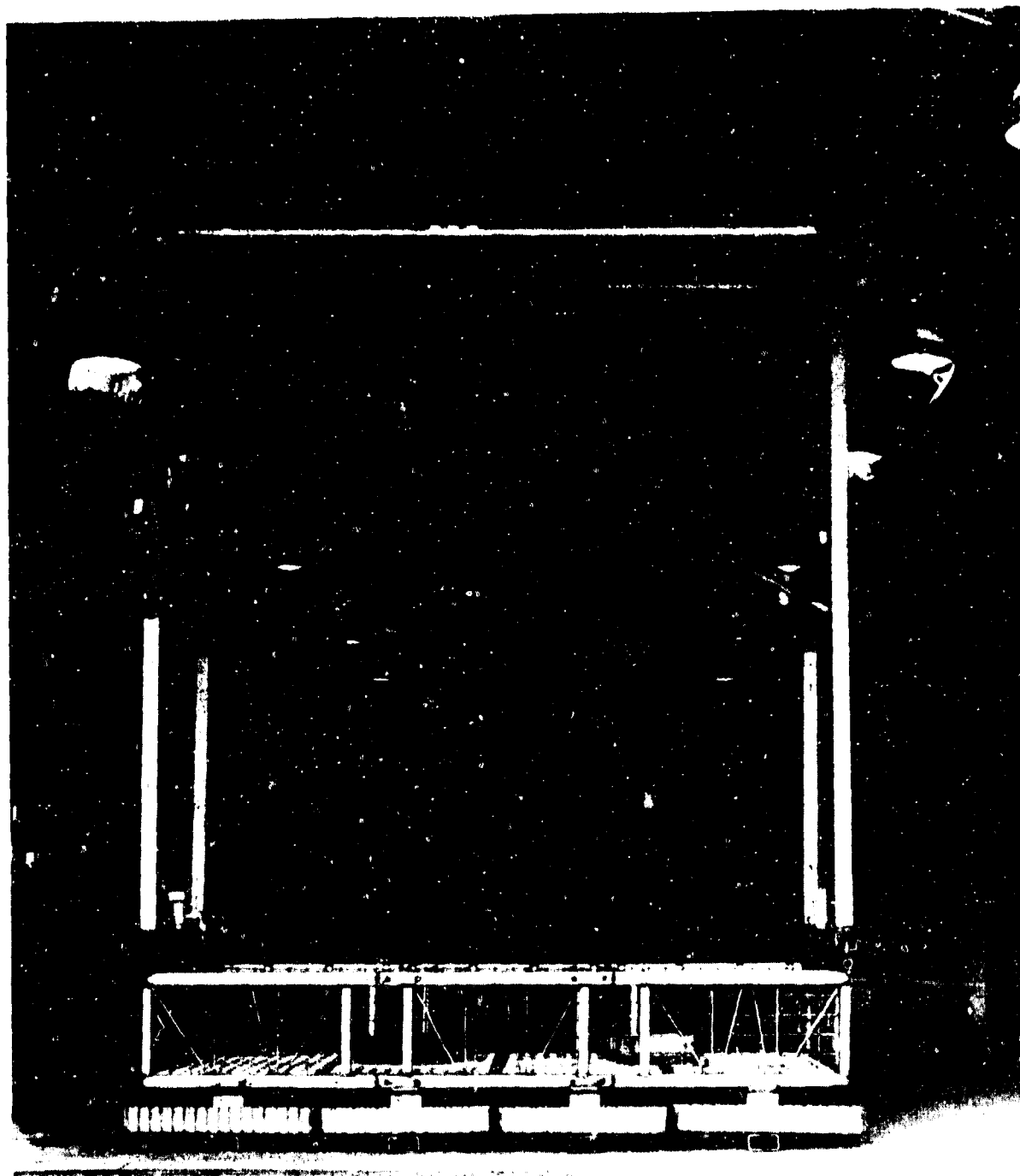


FIGURE 7 - OVERHEAD TROLLEY WITH WASTE
BASKET



FIGURE 8 - SHREDDED WASTE MATERIALS ON FURNACE
CAR BOTTOM DURING TEST OF SHREDDER SYSTEM.
SHREDDED WASTE WILL FALL INTO BASKET ON CAR
BOTTOM IN ACTUAL OPERATION

IOWA STATE AIR QUALITY STANDARD 0.35 GRAINS/SCF

TEST DATA*

RUN NO. 1	-	0.161 Grains/SCF
RUN NO. 2	-	0.116 Grains/SCF
RUN NO. 3	-	0.060 Grains/SCF

*All data corrected to 12% CO₂

FIGURE 9
PRELIMINARY AIR QUALITY TEST DATA
IOWA AAP - CWP

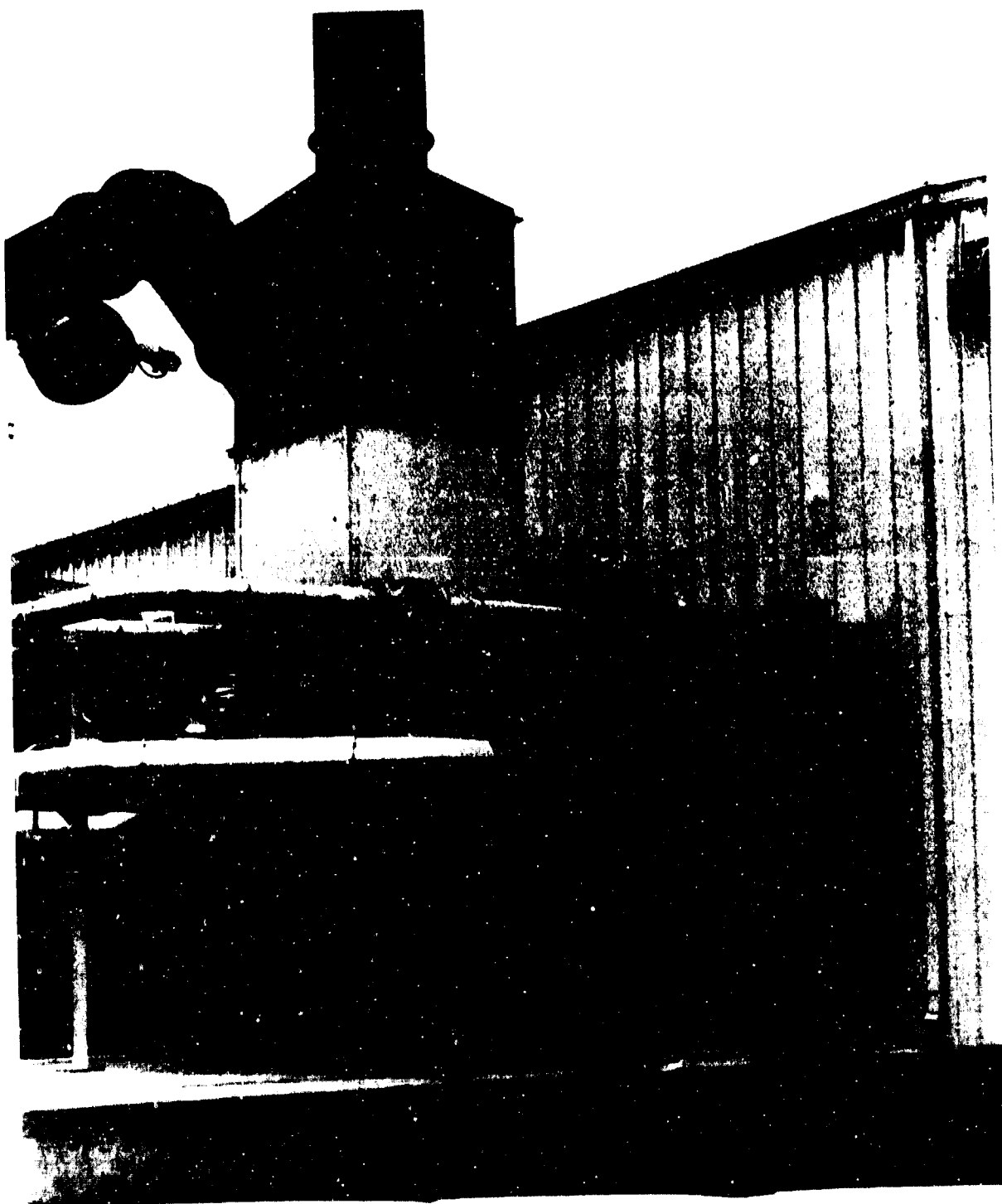


FIGURE 10 - BURNER END OF CAR BOTTOM FURNACE
WITH EXHAUST STACK FOR FURNACE START UP, AND
DILUTION AIR DAMPER

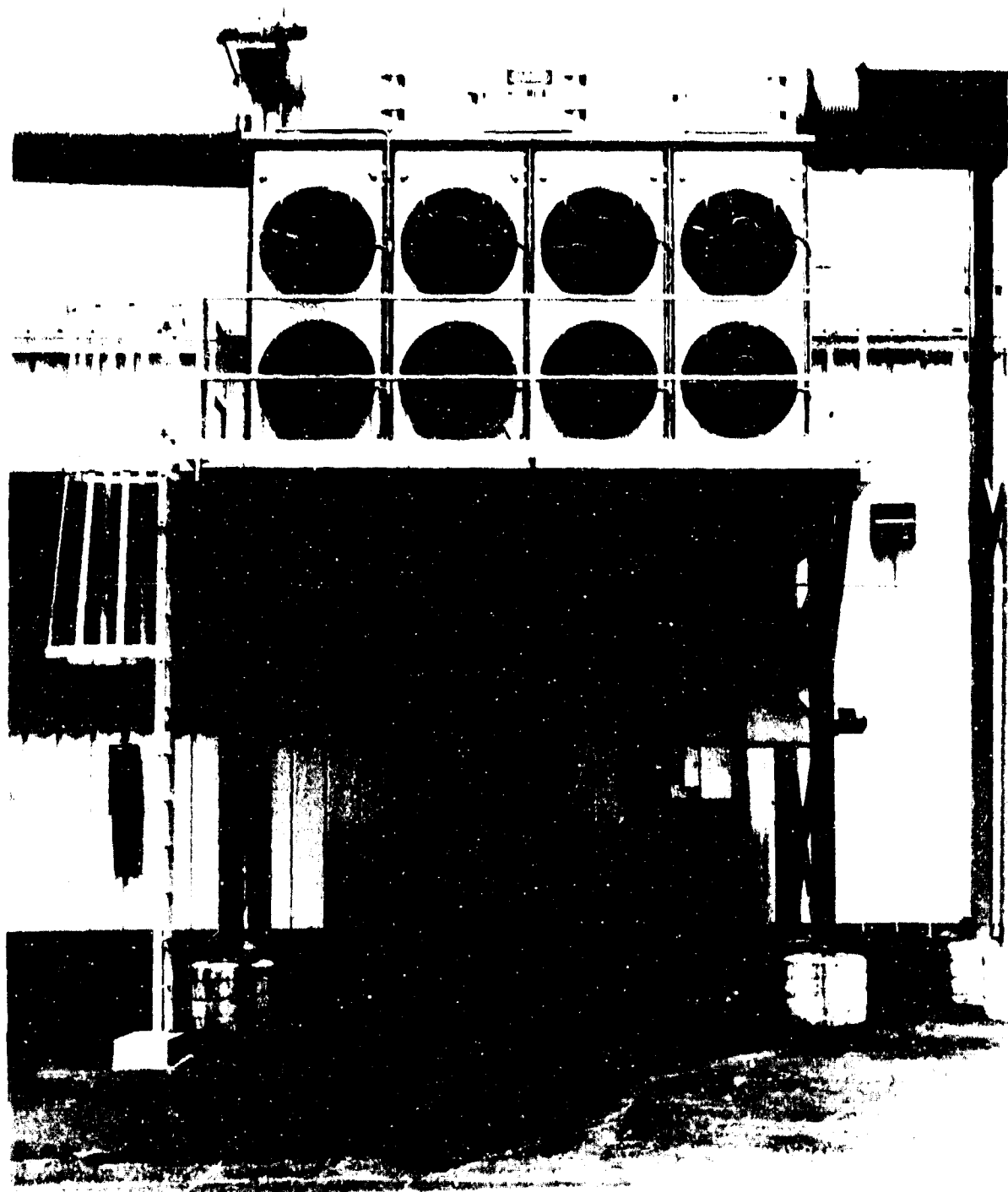


FIGURE 11 - CWP GAS COOLER 218



FIGURE 12 - CWP CYCLONE

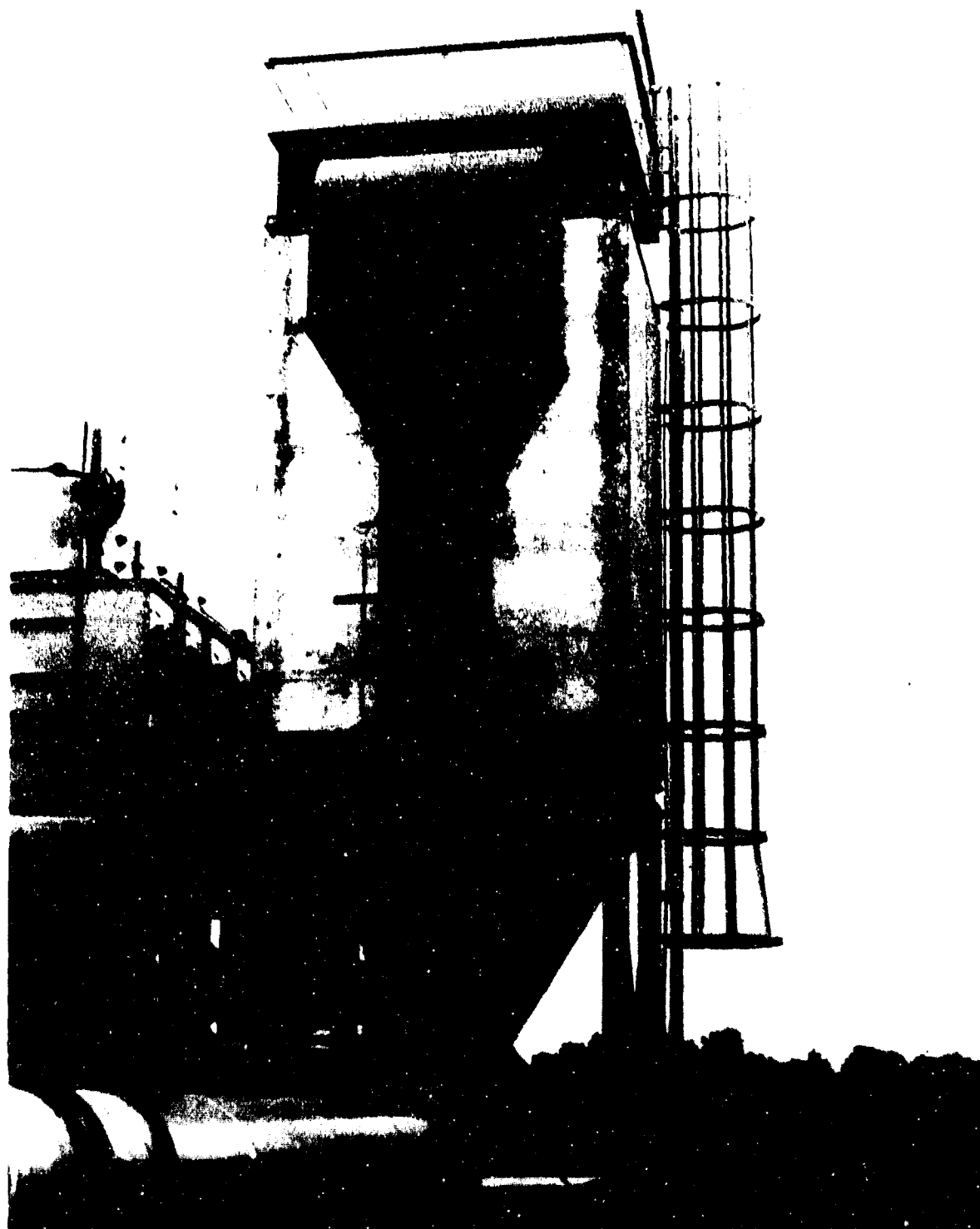


FIGURE 13 - CWP BAGHOUSE 220



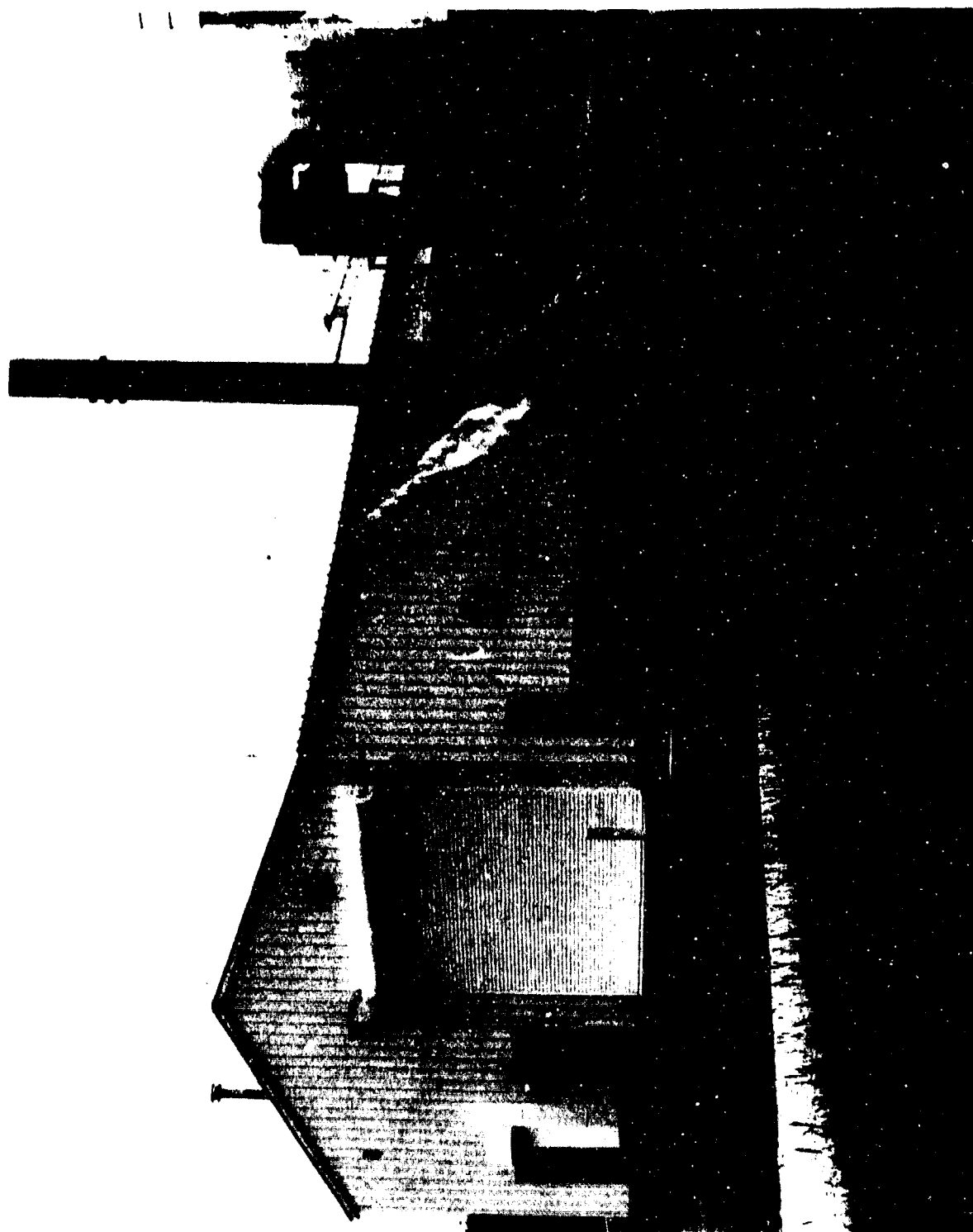


FIGURE 15 - CWPLU AT IOWA AAP

14
395031

AD P000433



INDUSTRIAL ROBOTS
PRESENT STATE OF DEVELOPMENT

DIRECTORATE FOR AMMUNITION EQUIPMENT
TOOELE ARMY DEPOT
TOOELE, UTAH 84074

SUMMARY

The Directorate for Ammunition Equipment (D/AE) was tasked in FY 81 to research the latest developments in robotics for potential applications of the Army's ammunition demilitarization and renovation lines.

This report discusses the present state of the art in robotics and covers in detail three major manufacturers of robots that this office has used in actual applications or has extensively evaluated for use in other applications.

INTRODUCTION

✓ In the past ten years the Directorate for Ammunition Equipment (D/AE) has been instrumental in the use of robots on ammunition related projects where this type of automation has been beneficial in either increasing the productivity or safety of a particular process. D/AE's first experience with automation began in the late 1960's when an industrial robot was used to download an M34 cluster bomb on the chemical agent filled bomb demilitarization program at Rocky Mountain Arsenal. Other experience has included use of an industrial robot to load and unload three detracer machines on a 40mm ammunition renovation line at Tooele Army Depot; and assignment as consultant to HQ ARRCOM for the installation of three large ton capacity robots at the Western Area Demil Facility (WADF) in Hawthorne, Nevada. These uses were not unconventional and placed robots in the common role of handling and transferring of material items. The items to be handled were mechanically delivered to an exact position where the robot then checked input signals supplied by interfaced equipment. It would then load and unload the machine it serviced and keep checks on the important parameters. ↗

Ⓛ The basic robots were purchased from commercial companies but the engineering to design the tooling used to handle the item, the controls to interface with the external machinery, the delivery system to supply the items to the delivery point, and in some cases the modification of the internal robot control, to allow it control features that it did not contain, were all done by D/AE.

The resultant hands-on design of system application gives D/AE a unique status among government agencies of having experience in a field where others have had little exposure.

Industrial Robot

A definition here is required to help accurately define what constitutes an industrial robot. These robots have often been classified as a type of an industrial manipulator. The term industrial manipulator helps to dissolve media-induced visions of a metal machine with human like abilities.

A common industrial standard unit will usually consist of a mechanical arm, hydraulically, electric servo, or pneumatically powered with three main axes of travel; horizontal, swing and vertical. On the end of this mechanical arm is a wrist to which the user designs the tooling or hand to manipulate the item. This wrist may also contain several axes of movement to assist the tooling to obtain the correct position. Each additional axis results in an additional degree of freedom. Some units may contain upwards of six degrees of freedom in a three dimension plane. The movement of the mechanical arm is programmed on a point to point basis or a continuous basis as in some welding applications. Feed back is generated by sensors mounted on the arm, wrist and tooling which determines where the mechanical arm moves. These signals are then fed to an internal controller which directs the arm to the next position.

Initially the user must supply the program to control the path of the robot. Many methods to program are used. Some have the operator take the mechanical arm and physically pull it through the path it must travel. The taught direction is retained on the memory system of the robot and repeated with great accuracy. This is done on many welding robots.

Another type of program system uses command potentiometers which set the location of the robot according to a voltage level defining a point in space. A potentiometer is, of course, required for each point of each degree of freedom. This older analogy system can in complex programs require the use of hundreds of voltage settings and can become impractical. The most

commonly used method today is accomplished by means of a teach control unit. It is used as follows:

The programmer switches the controls to a teach mode and directs the mechanical arm under very low speed to the desired position by pushing the various controls of the teach control unit which move the arm one axis at a time up and down, in or out, etc. Once the position is reached, the programmer then pushes the record button and that position is placed in the memory of the controls. Once all the positions of the operations have been recorded in memory, the robot will continue to follow these programmed instructions when directed through the sequence by its controller.

Factors to Consider Before Selecting a Robot

The robot is usually provided with a limited number of inputs which are used to monitor external functions of other equipment. Outputs are also available for the robot to energize as required. These outputs may, for example, be used on the conveyor system to deliver the item to the pickup area or to signal machinery that an operation has been completed. As discussed previously the amount of these input or output functions is both limited and basic in nature. Careful engineering is a must before any judgement feasibility of an application can be made. Below is a list of some facts to consider.

1. Draw or sketch the part to be handled to determine tooling required. Basic grippers can be purchased from the manufacturer but most applications will require some design by the user.
2. Determine machinery interferences, access openings, cylinder strokes, tooling clearances etc.
3. A floor plan layout of the area to scale or with dimensions is a must to detail relationship of the machines, conveyors, electrical panels, aisles, etc., to the robot.

4. Sketch concept of delivery and take-away conveyors.
5. Review increased production rates by determining how existing process will be improved with the robot. Interface robot cycle time with that of existing equipment. Try several approaches.
6. Consider the following facts about the part to be handled.
 - a. What is the material and weight of the part being handled.
 - b. If the part being handled is easily damaged what precautions should be taken?
 - c. Does the part require orientation at all stations?
 - d. If the part is delivered on an existing system, what is its height from the floor and distance from where the robot is to be installed? Consider this point and all other pickup and set down positions.
 - e. What programmed motions are required to load or unload the machine or conveyor, etc?
 - f. How does the part get to the robot from the preceding operation and can that system be automated to combine with the robot?
7. What type of environment will the robot have to operate in?
 - a. What is the ambient temperature?
 - b. Is the atmosphere corrosive, dry or humid, dirty, etc.?
 - c. Do hazards exist which will require special construction for meeting such things as explosion proof ratings?

8. Does the robot controller possess the ability to palletize? Can the robot handle a different pickup or set down location in a before hand preprogrammed order?

The above comments are somewhat general because they do not cover an exact application; however, these are the types of facts which the user must cover and study before the selection of the right industrial robot is made.

Status of Present State of Development

As noted in the last section's description, robots do not possess what is known as artificial intelligence. They can not see nor can they feel and evaluate conditions to make decisions in the normal sense. To make matters more complex, they must also be setup to fit within a structured environment with external items physically referenced to the robot's narrow internal coordinate system. These limitations have not stopped robots, however, from vastly increased production and accompanying reductions in operational costs. Robots have found a position doing the repetitive, around the clock tasks, that automation can produce without the boredom and fatigue associated with the human worker.

Although the United States has been the technology leader of robot development, the Japanese have surpassed us by using three times the number of robots working on actual assembly lines. The Robot Institute of America, a technical society dedicated to the advancement of robotics technology, lists some 39 U.S. robot companies along with 2 European and 4 Japanese companies. There is also an annual conference and exposition sponsored by the Society of Manufacturing Engineers each spring in Detroit, Michigan to provide the opportunity to see the latest developments, both domestic and foreign.

Three major U.S. manufacturers of industrial robots were selected to supply information for this report. They are as follows:

- a. Unimation Inc
Shelter Rock Lane
Danbury, Connecticut
- b. Cincinnati Milacron Inc
Mason Road and Route 48
Lebanon, Ohio
- c. Prab Conveyors, Inc/Robot Division
594412 Kilgove Road
Kalamazoo, Michigan

All have been the major suppliers of automated robot systems used in U.S. automobile assembly lines and other heavy industrial application. Somewhat disappointing is the fact that robot technology has not progressed as fast as one would have expected. It has been only recently that the use of computer systems have been incorporated for controls to expand the decision capabilities of commercial industrial robots. The same mechanical servo systems have been state of the art for years. The manufacturing industry is very conservative and future research, done mostly by university and private institutes of technology, awaits incorporation by the commercial concerns. This means that the U.S. lead, unless past performance improves, will continue to diminish.

DESCRIPTION OF SELECTED ROBOTS

Unimate Robots

Unimation Inc. has by far the largest share of today's robot market. They manufacture several different models, from small mini types to larger units that can lift upward of 450 pounds.

The small robot series 250, 500, 600, are constructed with a main boom that is jointed. This feature supplies a greater degree of dexterity. Drive

is accomplished by use of DC servos which are configured in five or six axes depending on model purchased. Lift capabilities are two to five pounds, but the small robots are designed to achieve accuracies of .004 inch and are used for small intricate work. Control on these models is advertised as one of the most advanced systems and uses the capabilities of a LSI 11 computer with Unimate's Val language. This gives the user the great control flexibility that many robots lack. The operator uses a detachable teach control to guide the robot through its task pattern. Control for each individual axis is provided to allow the operator to move the manipulator into the exact position.

Unimation's large robot series includes several models, but can be broken down to the 2000 and 4000 series. Both robots are similar but the 4000 can lift about 150 pounds more and has a heavier duty wrist. Both use a sequence step controller. Memory is on magnetic core and can store up to 2049 position points. The units are hydraulically powered and can achieve accuracies within .050 of an inch. A teach control is used to lead the arm through each successive position and that position is then recorded in memory for all five or six axes of movement as a program step. There are also a limited number of input/output functions on the robot which will allow it to receive signals from other machinery and control conveyors, or other machinery.

The advantages of the Unimate 2000 or 4000 are as follows:

a. Reliability- They have an established reputation among users for continual operation with little or no downtime. Manufacturer claims better than 98% uptime.

b. Programming - With the use of the hand held teach control programming is very easy. The user has only to lead the unit through the operation and record each point.

c. Unitized - The unit is self contained with everything including hydraulics and controls within the main frame housing. This allows quick installation and easy reinstallation when the robot is moved to be setup on another process.

The disadvantages are:

a. **Dexterity** - The series 1000, 2000, and 4000 use a turret or radial movement on the main arm. This results in less working area since the main arm can not retreat fully to the base and also sometimes results in difficulty in maneuvering the tooling into tight areas. Unimate has added a sixth axis model to help alleviate the problem but this then adds more size to the wrist and reduces the load limits. About anytime that the radial arm moves into a tight area not on the same horizontal level as the turret, this problem will occur.

b. **Robot Controller** - These larger robots use a simple sequence control which often causes the user to fight programming limitations. Jump or branch type instructions are difficult to perform. If an operational function is to be carried out repeatedly at many different locations within the total cycle it must be programmed each time. The unit can not connect with other computer interfaces or digital equipment at the level of intelligence possible with computer controlled robots.

c. **Servo Axis Control** - There is no coordinated control of all axes during the teach or automatic operational mode. Each of the five or six axes move randomly when directed to a programmed point. This means that the arm may move differently with changes in speed, etc, or that during teaching or programming positions, each axes must be moved one at a time. Again, the addition of a more powerful computer control has eliminated this problem in other models.

Cincinnati Milacron Robots

One of the more modern units available today is built by Cincinnati Milacron. This company is one of the leaders in the manufacture of numerical controlled machining equipment. The manufacturing of robots started as a side line, and although they only market one unit with two payload versions, they sell almost as many units as Unimate.

capacity. Control is accomplished by use of either a drum controller or a new solid state sequence control. Most operating components are standard industrial parts available from local suppliers. The value of the unit is its economical price, high reliability and ease of repair. The draw backs are that it is not suitable for most hazardous environments and does not have much flexibility when control amounts to more than pick and place operations.

Versatran Robots

Prab acquired the Versatran robot line from ANF and now markets it along with their basic model. The Versatran Model E was the first industrial application of robotics by our D/AE office. At Rocky Mountain Arsenal the Model E with the older basic analog controller was used to download and transfer to process equipment a large stockpile of GB filled cluster bombs for demil.

The physical construction of the Versatran robot is different both from the jointed main arm Cincinnati Milacron or the radial turret armed Unimate and Prab.

A main frame consisting of a square base and a vertical column form the robot. The boom or arm is mounted crosswise or horizontal to this column. When in operation the arm can travel up and down the main column, swing around 270°, or extend in and out. Tooling is mounted on the end of the arm which can supply up to three servo controlled degrees of freedom. This then makes up a total of six axes of movement. Versatran also uses a seventh servo on a traverse base to allow the robot the ability to move between work stations.

Experience from use of the Versatran line has revealed the following. The mechanical configuration of the design supplies good dexterity in moving in and out of tight areas with the tooling. It does not have the drawbacks of the turret radial design. Rear clearance behind the robot must be allowed for because the arm will project out the back when moved in toward

The T3 and heavier version HT3 use a jointed mechanical arm which is articulated to move in all six axes. The physical configuration of this jointed arm enlarges the working volume while increasing the dexterity. Payload capability is 175 pounds for the T3 and 250 pounds for the heavy duty HT3.

What makes this unit popular is the great flexibility it derives from a computer control. This company was one of the first to develop a strong computer software base to aid in robot control and in turn reduced much of the limitation of the more basic models.

A hand held teaching control is still used to guide the robot to the various positions. Positions are then recorded and stored in computer memory and can easily be modified or edited. The control console which houses the computer is equipped with a CRT to provide visual program readout. Each programmed point is displayed as X, Y and Z coordinates in space. Velocity, acceleration, input, output designation and other control status are displayed on the tube on a real time basis. Such tasks as programming randomly sequenced operations and interfacing between larger computer controlled processes and external equipment are all made easier because of the versatility of a computer aided robot.

A disadvantage of the T3 and HT3 robots are that they were not designed for quick reinstallation and are not unitized. The control console is separate as are the power distribution panel and hydraulic pump. If the robot were to be used in an explosive hazardous location much of this equipment would have to be installed remotely in a control room or utility area. This prevented the use of these units on our applications because we were installing equipment in existing older buildings.

Prab Conveyors Inc/Robot Division Robots

Prab's robot is much like the Unimate models 1000,2000 and 4000 in physical construction. The arm rotates on a radial turret. Four models are built around this design and vary only in reach and weight handling

the base. However, control of the robots have been modernized with the introduction of the series 600 computer control. Although Versatran has used the same LSI/11/02 computer as has the Milacron robot they do not offer as many options. This is a result of the executive program in the computer. The user is free to write his own program if they do not fit the application or he can have Versatran engineers work with him.

Versatran robots are not unitized.

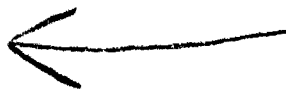
CONCLUSION

This report has been compiled for our own use or other parties which may be considering the use of robotics. Presently the design, building and marketing of robots is increasing rapidly. Because of this increase it is not possible to become knowledgeable with all robotic systems manufactured today. Major companies such as General Electric, Texas Instrument and IBM have invested large amounts of capital and have announced plans to market their own robot lines. The Japanese are making the majority of their own robots and these are now appearing in increasing numbers on the U.S. market. Older U.S. manufacturers which have controlled what was available on the market will soon be faced with fierce competition. However this will then result in better, more powerful robots as new technology is applied to gain advantage in sales.

Robots which were evaluated in this report were units on which we had formed opinions, either from actual industrial application or through study of the units for consideration in applications. A working hands-on knowledge was therefore gained both of the advantages and disadvantages of these models.

Future models of these robots will be caught up in rapid technological advances, making the conclusion of this report valid only for a short period of time. For example, Unimate will soon have a computer control system for their larger units and many of the criticisms of axis coordination and programming will be negated.

For the government to increase the productivity of its labor intensive manufacturing, renovation, and demil plants, a serious effort and investment of capital will need to be made toward the use of more robotic systems. Past experience has demonstrated, that where an application has been properly engineered, the investment has been paid back in a very short period.



13 P000434

BARRICADE/SHIELD TESTING
NEW THINKING ON HEAT FLUX REQUIREMENTS

BY JERRY MILLER, P.E.
AMMUNITION EQUIPMENT DIRECTORATE
TOOELE ARMY DEPOT

In 1976 MIL-STD 398 was published to help standardize on the criteria which must be met to properly protect an operator. As it states in the "Foreword" of this publication dated 5 Nov 1976;

"This standard defines the minimum criteria necessary to design an operational shield which will protect personnel and assets from thermal, pressure and fragmentation hazards resulting from an accidental or intentional detonation of ammunition or explosives, and identifies methods for testing prototype operational shields to assess the degree to which they meet the protection criteria specified; and

Criteria identified in this standard are recognized as providing an environment that affords adequate protection for personnel and assets."

Besides the area of overpressure, which is well documented and has transducers which can follow fast response pressure waves, the less defined and established area of heat flux was addressed.

It states in Section 4.1.3 that:

(a) "Shields shall be designed to limit exposure of personnel to a critical heat flux value based on the total time of exposure. This value of heat flux is determined by the following equation:

$$\dot{Q} = 0.62 t^{-.7423}$$

where

\dot{Q} = heat flux in cal/cm²-sec

t = total time in seconds that a person is exposed to the radiant

heat."

The equation was developed by plotting published heat flux data on log paper and establishing a best fit curve to this data. Further research

seems to indicate that the exponent in the equation ought to be 0.75 instead of 0.7423. Also, the safe heat flux level is based upon a pulse in the form of a square wave.

(b) "All operating personnel shall be located at a distance from the shield that assures their exposure is less than the flux determined by the above equation.

(c) The upper torso of an operator's body shall not be subjected to any visible fire or flame. Flame impingement upon the lower portion of the body may be permitted provided that the heat flux specified above is not exceeded."

A point of interest is that a former Ammunition Equipment Directorate (AED) engineer, Mr. K.T. Smith, was involved in the preparation of the heat flux section of the standard. In conjunction with his research, tests were performed at AED on various types of heat flux sensors under varying conditions.

As can be seen from the following film, there is concern for an operator's protection from the heat produced during a detonation/incident within a protective barricade. The first film shows what happens when M30 propellant is ignited inside an Ammunition Peculiar Equipment (APE) 1001 barricade. Since that date in 1979, much work has been done to reduce this heat problem to a minimum and there is now a fast response deluge system which suppresses the fire very quickly (in the order of 20-50 milliseconds).

The next sequence of film shows the test results on an APE 1202 operational shield. This shield evolved from an open back style to a total containment version while trying to meet the other safety criteria defined in MIL-STD-398. With a semicircular rear door added to the shield, the main areas where flame and heat can escape are around the rear door enclosure attachment mechanisms and around and over the turntable. Within the shield an internal barricade was designed to mostly enclose the turntable. Baffling was added to the turntable, and the gapping between the turntable and shield was reduced to a minimum. After these modifications the film shows that a detonation spray can still be seen coming out into the operator area at approximately chest height.

Some of the first work done in barricade testing centered around the testing of several types of heat flux sensors to determine the best for this application. These were the Gardon gage, Schmidt-Boelter and the platinum film gage. The platinum film gage was eliminated early in the testing because of problems with damage susceptibility, in calibrating, and filtering. The Gardon gage was supposed to have a faster response than the Schmidt-Boelter, but it was easily damaged during a detonation from the generated overpressure. Therefore, the Schmidt-Boelter gage appeared to best suit our requirements in measuring heat flux; but we knew it was limited due to its slow response.

Another concern, with any type transducer (gage, meter, etc.) is that because of the electrical noisy environment in which data is obtained, the transducer output must be in millivolts or larger. In no way could microvolts be measured with any certainty.

In 1980 Dr. Richard Ulrich, from the Brigham Young University was contracted to help look at concerns with the heat flux gages and the heat flux criteria as identified in MIL-STD-398. He is presently in the process of finalizing a report on certain aspects of his study to date.

Lets now look at the characteristics of the two gage types which seem to most adequately fit our requirements, the Gardon and Schmidt-Boelter. It must be realized that other names might be used to describe these types gages such as unidirectional, asymptotic, pyrohelometers, radiometers, etc. A discussion of the characteristics will eliminate possible misunderstanding of these designs.

In both types of sensors, heat flux is absorbed at the sensor surface and is transferred to an internal heat sink which remains at a temperature below that of the sensor surface. The difference in temperature between two points along the path of the heat flow from the temperature to the sink is proportional to the heat being transferred and therefore proportional to the heat flux being absorbed. At two such points, these transducers have thermocouple junctions which form a differential thermoelectric circuit providing a self-generated emf between the two output leads directly proportional to the heat transfer rate. No reference junction is needed.

Gardon gages, Figure 1, absorb heat in a thin metallic circular foil

and transfer the heat radially (parallel to the absorbing surface) to the heat sink attached to the periphery of the foil; the difference in temperature is taken between the center and edge of the foil.

Schmidt-Boelter gages, Figure 2, absorb the heat at one surface and transfer the heat in a direction normal to the absorbing surface; the difference in temperature is taken between the surface and a plane beneath the surface.

Both types are designed for operation in steady state and only then is there a direct proportional relationship between the measured temperature (or emf) and absorbed heat flux. Both types can be built having a "time constant" of as low as a few tens of milliseconds, say 40-80 milliseconds. However, the concept "time constant" has well-defined meaning only for first order systems and represents the time for a first order system to respond 63 percent to a step input. The path of the response curve is a well-defined exponential decay (or rise) from an initial to a steady state value and; if the time given (in number of time constants) is known, the response state is well known. However, neither type of heat flux gage can be well represented by a time constant since they can not be physically modeled accurately by a first order model. Of course the time for 63 percent response to a step input can be measured, but the response curve is not well represented by a single exponential equation. Because manufacturers often describe the response time by giving "time constants," that term will be used in this report.

The curve in Figure 3 shows a typical heat flux gage response from a particular barricade test. This response was produced by a Schmidt-Boelter type gage (a Medtherm 64 Series) having a "time constant" of about 55 milliseconds. First, assume that the heat flux versus time curve can be taken at its face value; that is, assume that the results are accurate. Does this particular curve satisfy the MIL-STD-398 equation?

$$q \leq 0.62t^{-.7423}$$

The obvious question is "what time should be used?" The film for this test show some visible effect for four to six milliseconds so the actual

time is probably some place between 5 and 700 milliseconds, a very wide range indeed.

The equation was developed from an extrapolation of rectangular wave shapes of heat flux versus time. The times were all longer than one second. Maybe, for these relatively short times, the integral of heat flux - time would make more sense as a limiting criteria.

Another problem arises due to the transient nature of the heat flux pulse when the gage is designed and calibrated for steady state use. Following is a discussion of the steps taken to understand and explain the data observed in Figure 3.

Schmidt-Boelter type heat flux gages are basically a many junction thermopile wrapped in series around a mandrel. This unit is mounted between plastic protectors and the entire system is mounted in a copper heat sink. The manufacturer is never sure of (exact) dimensions of the particular plastic layers so they need to calibrate each heat flux gage. The heat flux is indicated by the sum of voltage from the thermopile as the heat flows from the surface to the heat sink, since $Q = \frac{k\Delta T}{\Delta X}$, for steady state

operation. However, for unsteady state some energy is stored in various parts of the heat flux gage. This system was then modeled as shown in Figure 4, a node for the surface plastic, a node for the wire on top, a node for the mandrel, a node for wire on the bottom, a node for the plastic on the bottom and, a node for the heat sink. These nodes (or capacitors in the electrical analogy) are connected by resistors or conduction elements. For this system, a computer program was developed using estimated values for thicknesses and thermal properties, which would be modified to allow for matching computer output with field results.

This program is really two programs, or two phases in solving the specific problem. The first part solves the problem "given an unsteady input heat flux, what is the output, or indicated heat flux?" This program was developed and "calibrated". "Calibration" means that the parameters were chosen so the computer output matched the heat flux gage output for some known inputs. This demonstrated that the computer model fit of the physical model was adequate.

Having a good computer model then allowed for an inverse approach

program to be developed. That is "given the output from a heat flux gage during an unsteady operation, what was the input heat flux?" This was again used on some cases where the input and output were known and presented a good, if complex, result.

This program was then used on some real data from a barricade test and the result was that the calculated heat flux was about 50 percent greater than that indicated by the gage. The results are shown in Figure 5. No general rules of thumb were developed for estimating actual heat flux from indicated heat flux.

Another modeling and analysis technique was done to develop a method for interpreting data from unsteady usage from steady state calibrations of heat flux gages. It was done (in ME 542 Advanced Heat Transfer Design) under the direction of Dr. Ulrich by Max Howell and Brent Woodland. The heat flux step inputs were of small duration in comparison to the time constant of the gage.

The computer model again used resistors and capacitors to try to duplicate the response characteristics of a particular heat flux gage. A second computer program was written that would "back out" the step input given a typical response curve.

The computer programs, were then used to predict the actual input from a particular response curve. It was observed that the heat fluxes obtained from an APE 1202 barricade test probably passed the gage in two waves, a radiation pulse and a convection pulse. It was also seen that the maximum heat flux from the explosion was between four and seven times the indicated heat flux.

The heat flux gage was modeled as a 3 lump capacitance system as shown in Figure 6. The solutions to the three simultaneous differential equations indicated the Node Temperatures as a function of time. The three equations are:

$$dT_2 = \frac{dT}{C_1} \left(\frac{T_1 - T_2}{R_1} - \frac{T_2 - T_3}{R_2} \right)$$

$$dT_3 = \frac{dT}{C_2} \left(\frac{T_2 - T_3}{R_2} - \frac{T_3 - T_4}{R_3} \right)$$

$$dT_4 = \frac{dT}{C_3} \left(\frac{T_3 - T_4}{R_3} - \frac{T_4 - T_5}{R_4} \right)$$

Using this as an iterative model, time response curves were generated. By non-dimensionalizing the model output, the model could be geometrically adjusted to match the time response curve of the real gage. Figure 7 shows how closely the computer model matches the real gage response to a step input.

Assuming that the model is correct, it could be used to simulate various response characteristics that would be expected from the real gage. As long as both the model and the real gage data are in non-dimensionalized form, the response of the gage will always be the same. This being the case, the slope at a point on any reasonably smooth curve will correspond to a fraction of the steady state value. Figure 8 shows an example. This implies that for a general curve the instantaneous steady state value can be approximated since the ratio of the temperature difference to the steady state temperature difference is an instantaneous constant (h), where

$$h = \frac{\theta}{\theta_{ss}}$$

Using a non-dimensional model, a computer program was written which matched the slope of a particular output with the corresponding slope on the model. That slope identified what fraction of the steady state input the gage had attained. This process was repeated for numerous points along the output curve.

To test the accuracy of this technique, the model's response to several types of known inputs was generated. The slope-height technique was then applied to these response curves to see if it could accurately predict the input. Figure 9a is the model response to intermittent step waves of equal magnitude. It can be seen that the past history of the response does affect the current gage response. Figure 9b also shows that some error exists in the technique. This error could be compensated for, if necessary; however, for a single pulse this compensation is not needed. Figure 10 shows how the

computer program handled step inputs of varying magnitude.

Figure 11 shows how accurately the program was able to predict a single pulse square wave. The error in this prediction was very small.

The actual heat flux for a hand-grenade explosion in an APE 1202 barricade was predicted from test data. Figure 12a shows the data with time in milliseconds and the heat flux indicated (after smoothing) as a fraction of the calibrated flux on the gage (0.44 cal/cm sec). Figure 12b shows what the actual heat flux was predicted to be. It can be seen that the maximum heat flux is about seven times the flux indicated by the gage. This figure also shows two distinct impulses to which the gage may have been exposed.

The two pulses shown in Figure 12b may be interpreted as radiation and convection fluxes, respectively. This may be real since the pressure wave takes longer to reach the gage than the initial radiant burst of energy. By knowing the actual distance the gage was from the explosion, the beginning time of this impulse could be calculated to verify the prediction.

Figure 13 shows interesting contrasts, if the input data is not taken as a smooth pulse. This figure indicates that the maximum flux was only 4 times the gage value. This result seems to put the extremely high magnitude of 7 times the gage value in question. Good judgment would seem to suggest that the actual value is somewhere between the two. In other respects, this predicted heat flux is quite similar to that shown in Figure 12.

This slope-height technique is one way to determine the actual heat flux given the temperature-time response of a heat flux gage. This method does have inherent errors that seem to multiply for multiple-step inputs. However, for one or two pulses, it seems to do a very good job. For general interpretation of data the technique appears to be satisfactory, since more rigorous mathematical approaches are very laborious and time-consuming.

Another solution, to the problem of "given an indicated heat flux, what was the source heat flux?" was developed. This slope method is based on the idea that the response of the gage to a step input can be represented by a single exponential rise curve and that the time constant for the instrument is known. That is, assume τ_c is good indicator of 1 lump, i.e., $\tau_{c1} \ll \tau_{c2}$ for pulses where pulse width $< 1/4 \tau_{c1}$.

Then

$$q_1 = q_{ss} (1 - e^{-\tau/\tau_{c1}})$$

and near time = 0

$$\frac{dq_1}{d\tau} = \frac{q_{ss}}{\tau_{c1}} e^{-\tau/\tau_{c1}} = \frac{q_{ss}}{\tau_{c1}} = q_1' \Big|_0$$

Therefore, if we know τ_{c1} (measured or from the manufacturer) and measure

$$q_1' \Big|_0, \text{ then } q_{ss} = q_1' \Big|_0 \tau_{c1}$$

Thus, Figure 14, shows the step by step method of proceeding through this technique.

This method shows some promise and is still being developed. It is similar to the Howell-Woodland method, but much simpler to reduce data. All three methods need refining but they all show promise.

Several tests were done at Tooele Army Depot, Tooele, Utah, where a constant heat flux was impinged on the back of a large camera aperture. The opening was fixed in size and the time setting was varied from 1/4 to 1/125 of a second. The heat flux gage was shaded by the shutter and exposed for 1 sec (to get the steady state reading) then in sequence 1/4, 1/8, 1/15, 1/30, 1/60 and 1/125 of a second. The areas of the response curves were measured with a planimeter. These values were plotted versus time and the result was a straight line going through the origin, as shown in Figure 15, indicating that the total energy was registered by the heat flux gage, even if the instant rate was not registered. This was also proven using the analytical model.

The next phases of our heat flux studies will include the following:

1. Test several different manufacturer's heat flux gage types and models.
2. See if developed modeling techniques can be used on these sensors.
3. Perform statistical testing for more accurate evaluations of the modeling techniques.
4. Establish rules of thumb if possible.
5. Study the temperature of the surface of skin for various generated heat flux square waves to get T_s vs Q_{total} ($= \int q d\tau$).
6. Do skin modeling and look at temperature rise of skin due to generated square waves of heat flux.
7. Generate envelop of q vs T from energy, pressure, temperature, volume, etc.

When we feel that we can adequately model the heat flux measurements, we will present our findings to the U.S. Army Armament Command for review and possible revision of the heat flux section of MIL-STD-398.

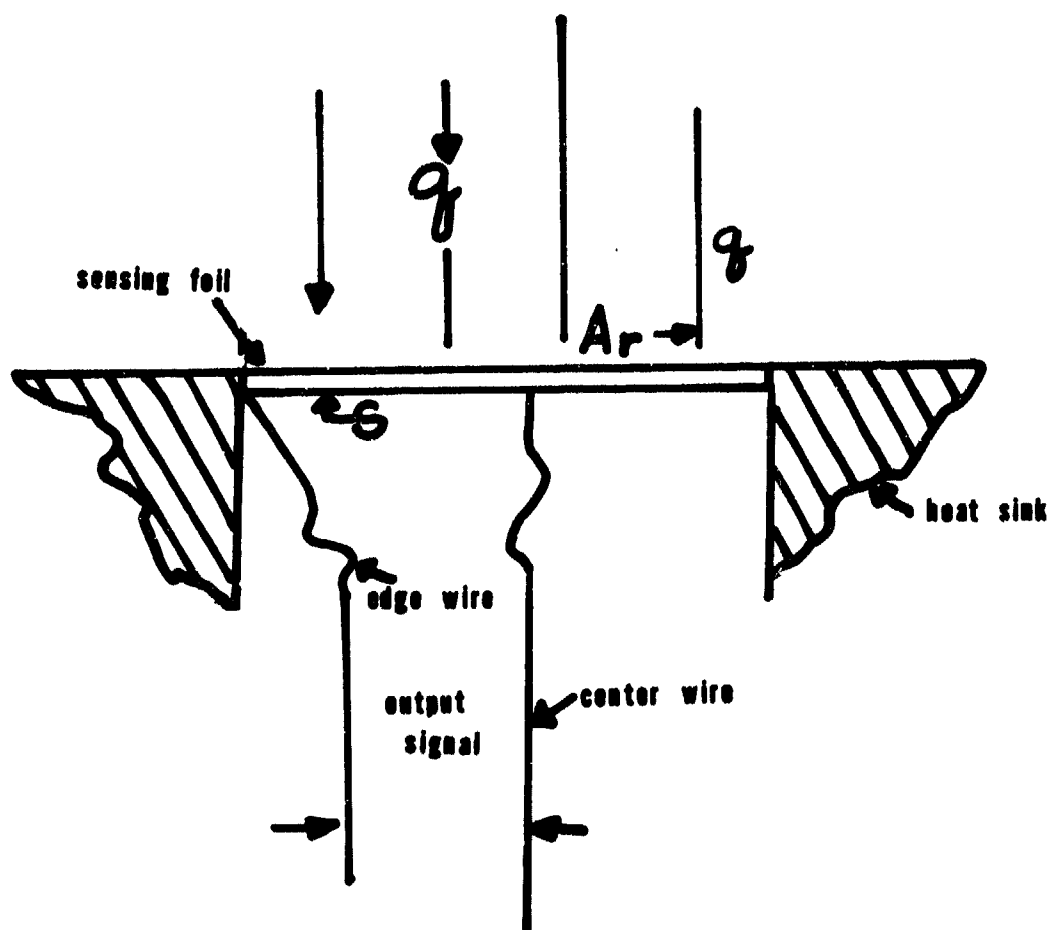


FIGURE 1 SIMPLIFIED GARDON GAGE

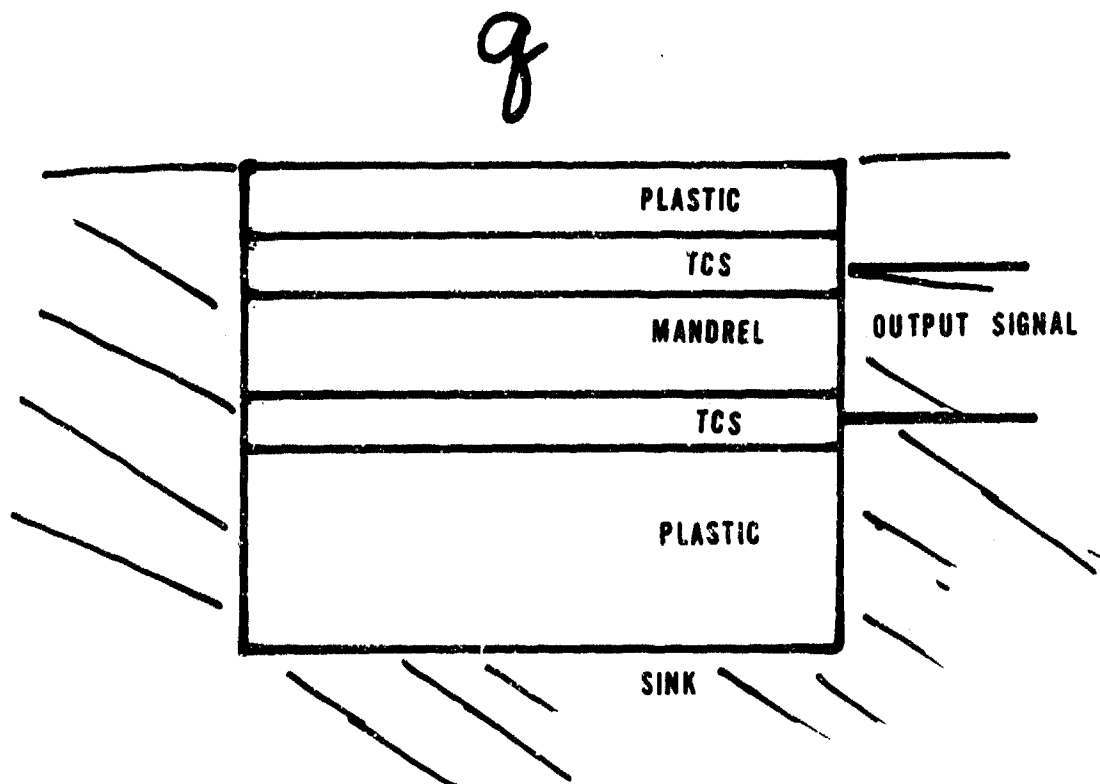
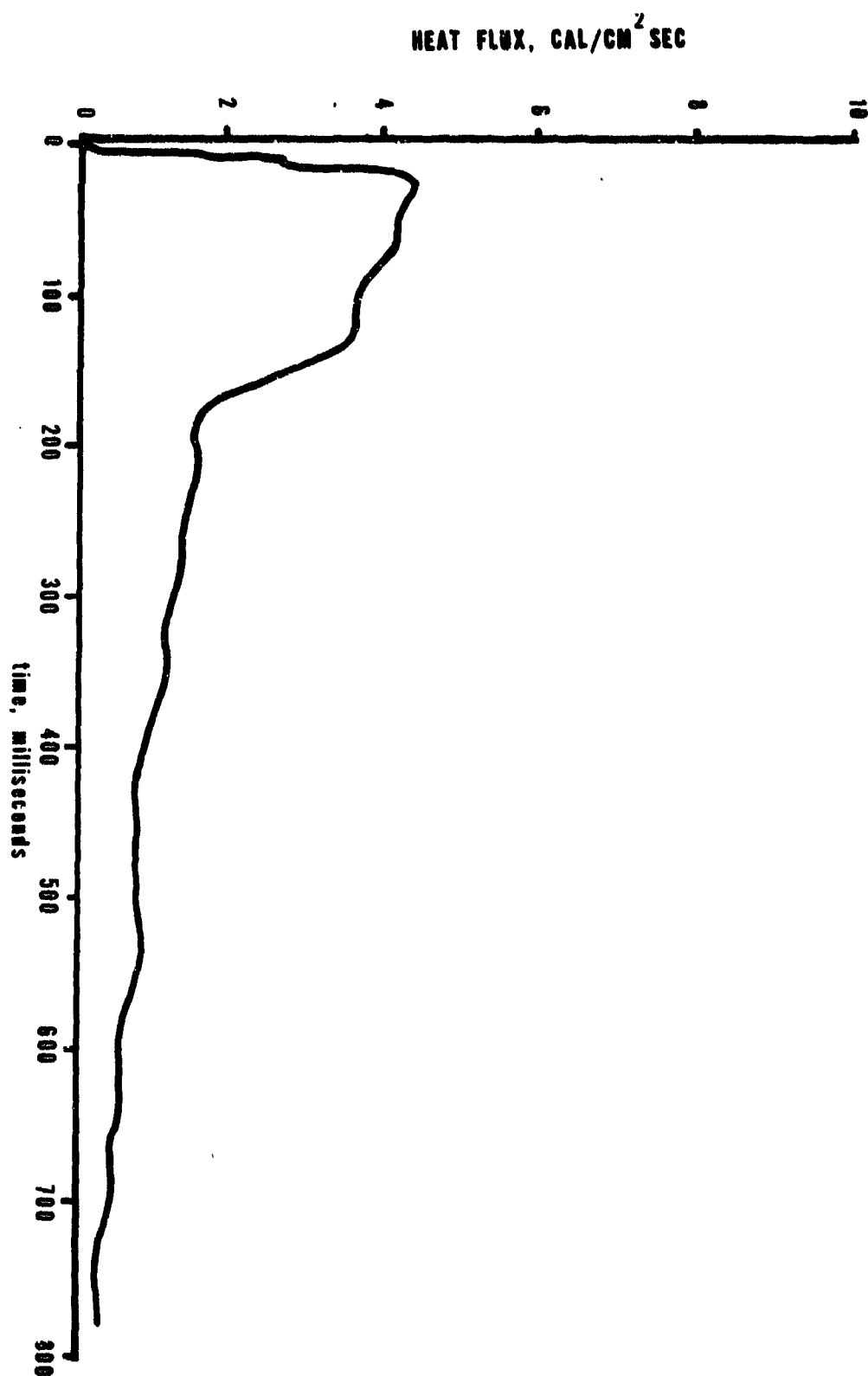


FIGURE 2 SIMPLIFIED SCHMIDT-BOELTER GAGE

FIGURE 3 TYPICAL HEAT FLUX RESPONSE
SCHMIDT BOELTER TYPE GAGE



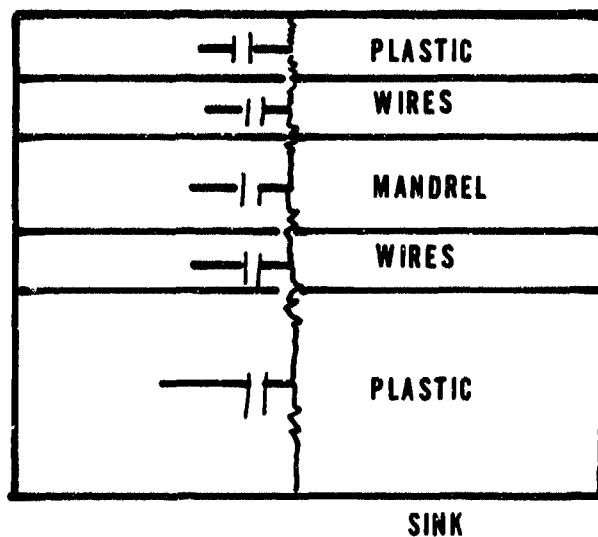


FIGURE 4 COMPUTER MODEL OF
SCHMIDT-BOELTER TYPE HEAT GAGE

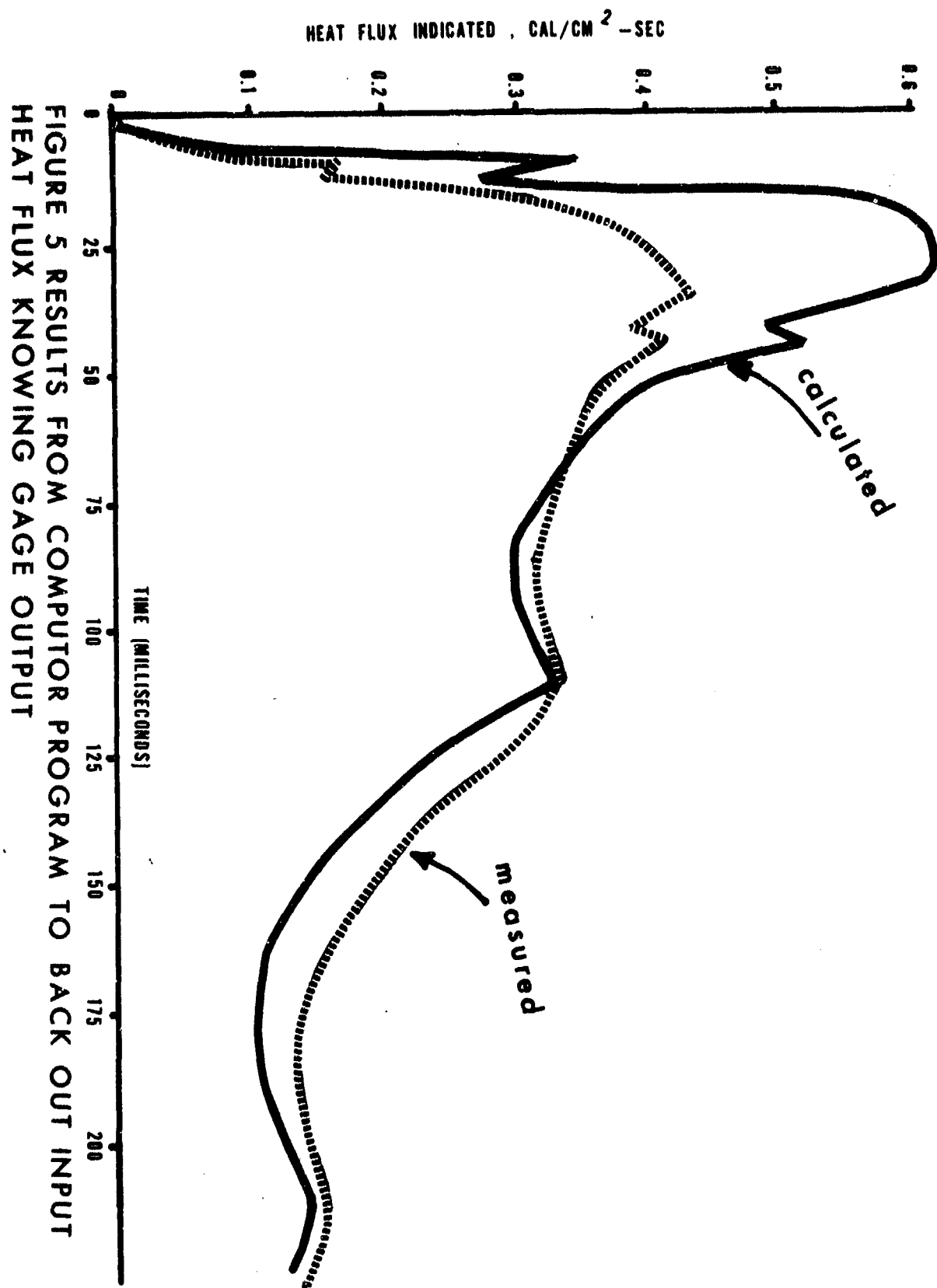


FIGURE 5 RESULTS FROM COMPUTER PROGRAM TO BACK OUT INPUT
HEAT FLUX KNOWING GAGE OUTPUT

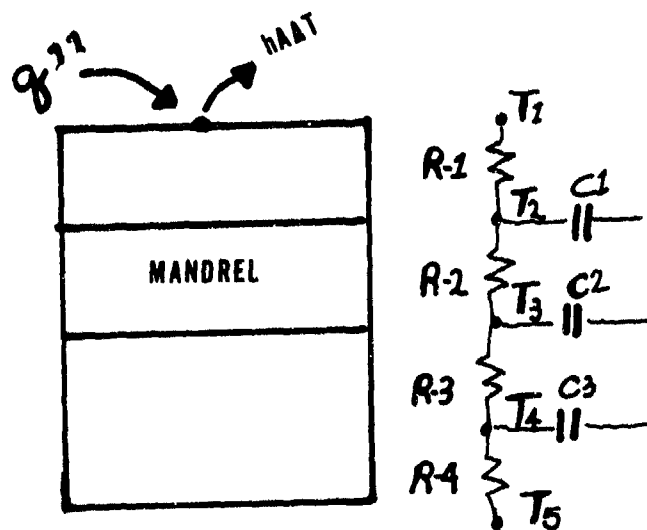


FIGURE 6 M. HOWELL/B. WOODLAND
COMPUTOR MODEL

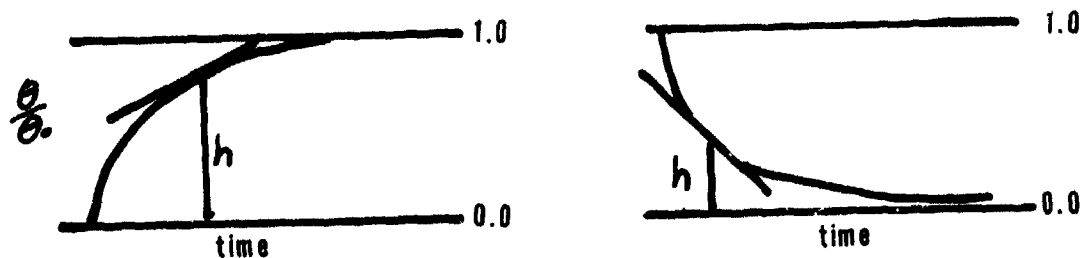


FIGURE 8 TECHNIQUE USED FOR
M. HOWELL/B. WOODLAND MODEL

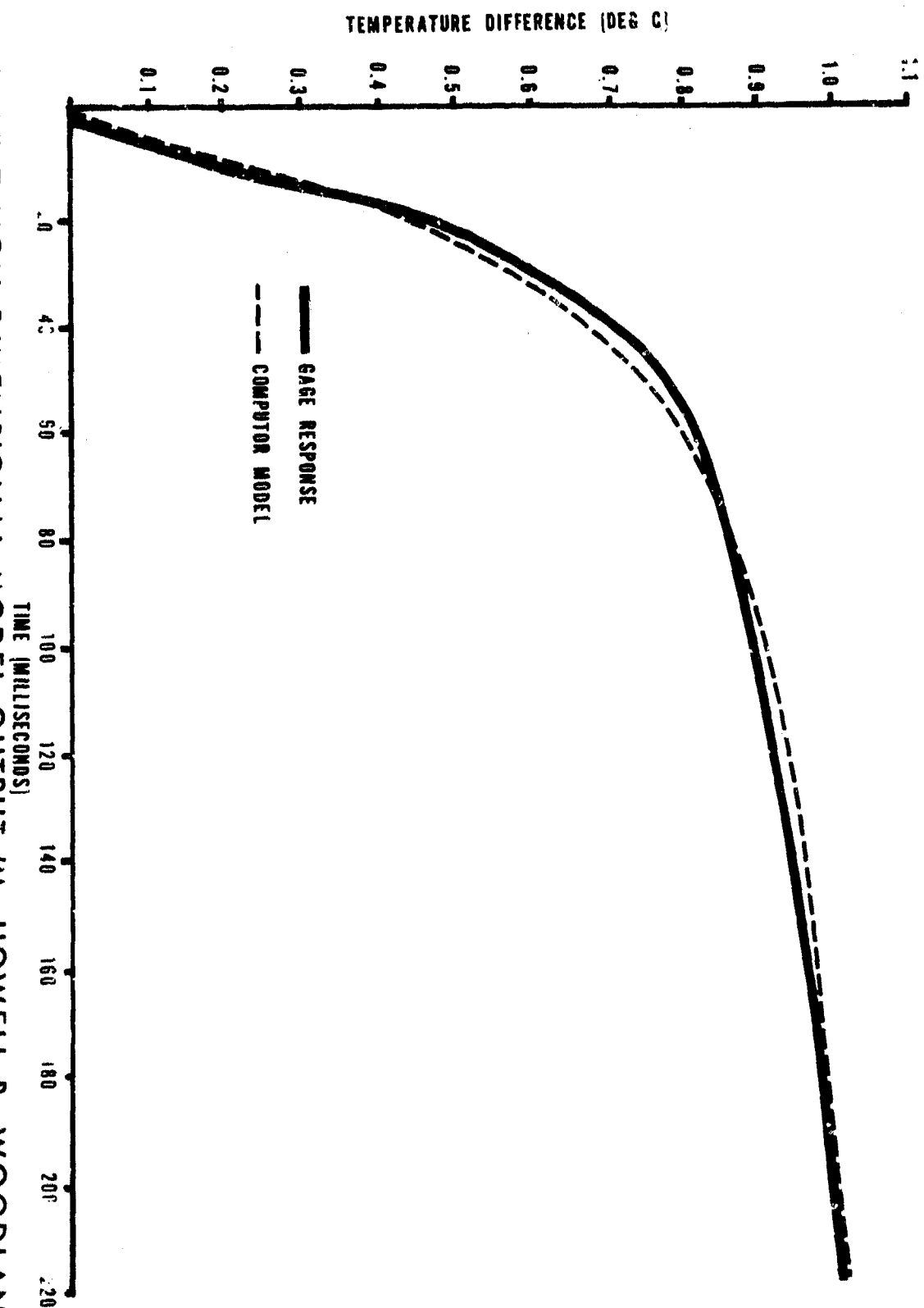


FIGURE 7 NON DIMENSIONAL MODEL OUTPUT (M. HOWELL B. WOODLAND)

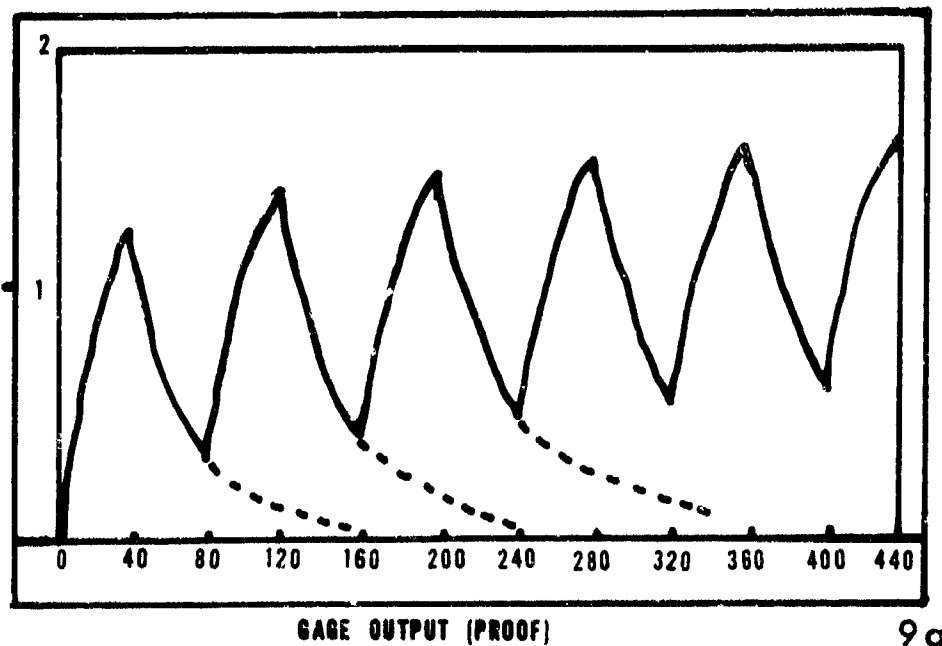
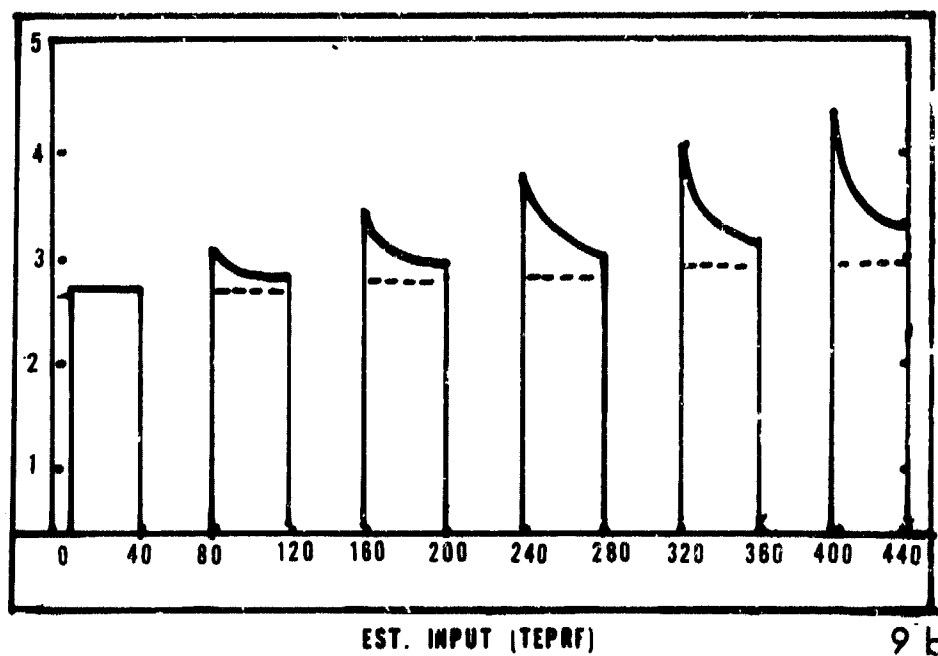


FIGURE 9 INTERMITTENT HEAT FLUX PULSE PREDICTIONS



10 a

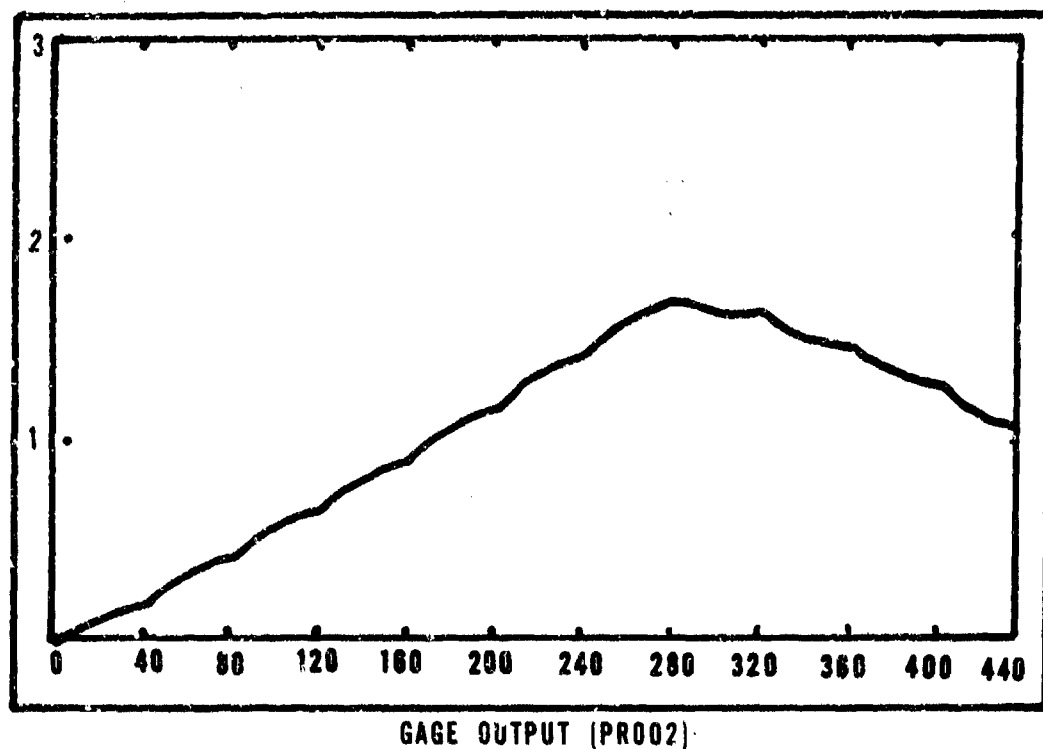
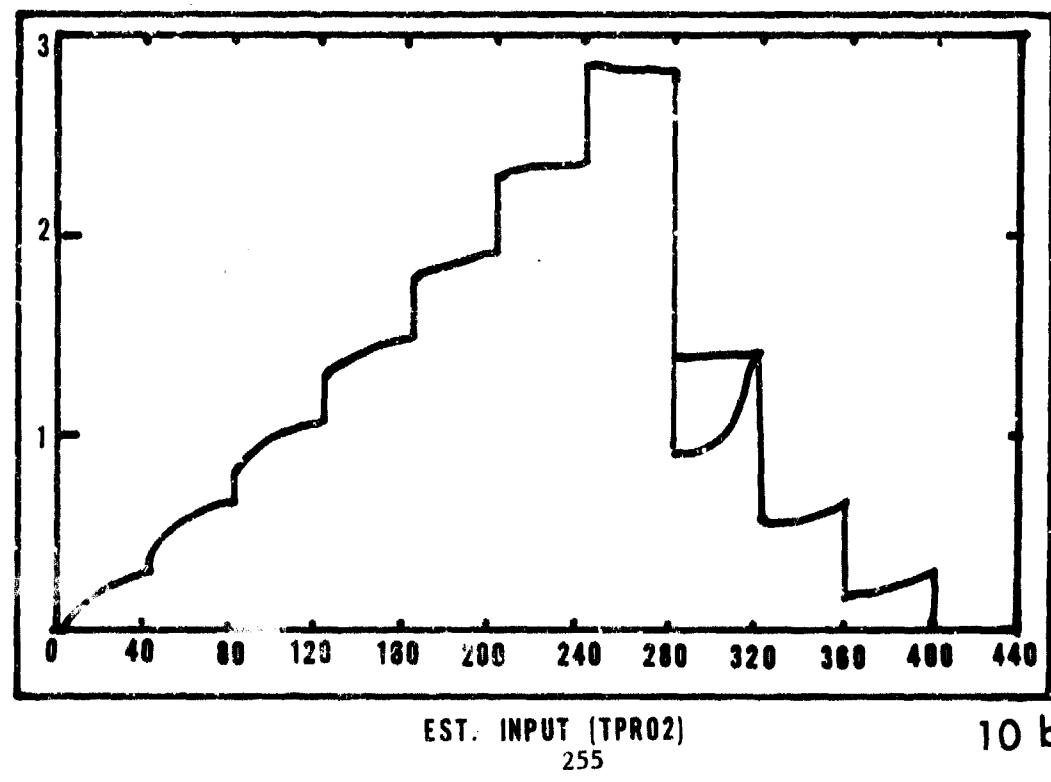
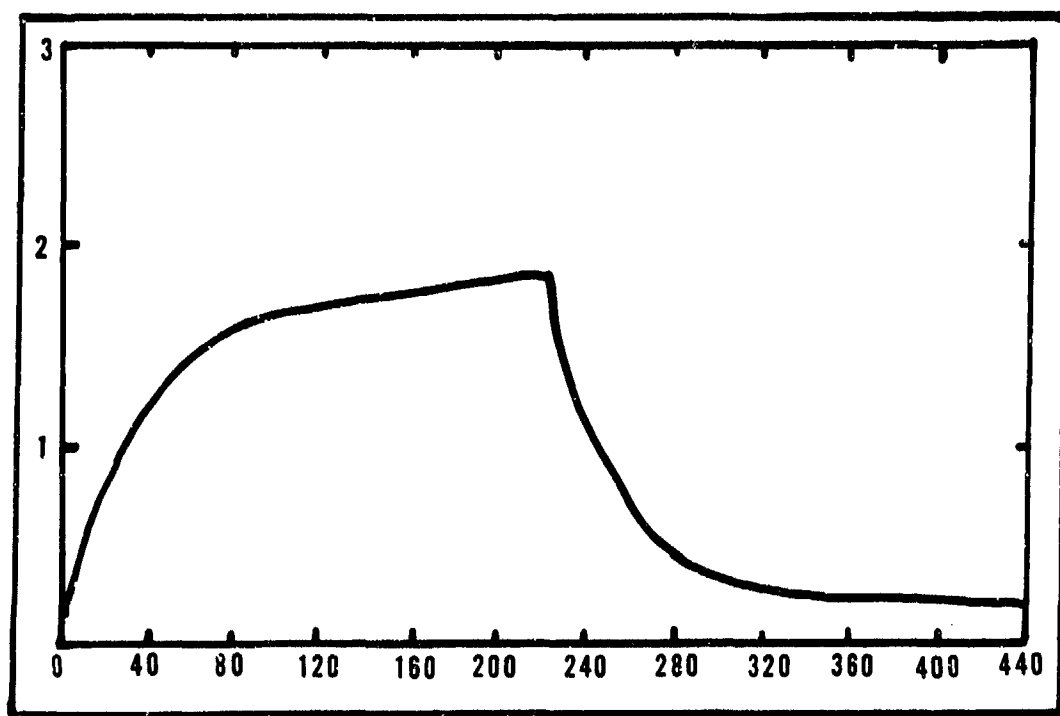


FIGURE 10 VARYING MAGNITUDE HEAT FLUX PULSE PREDICTIONS



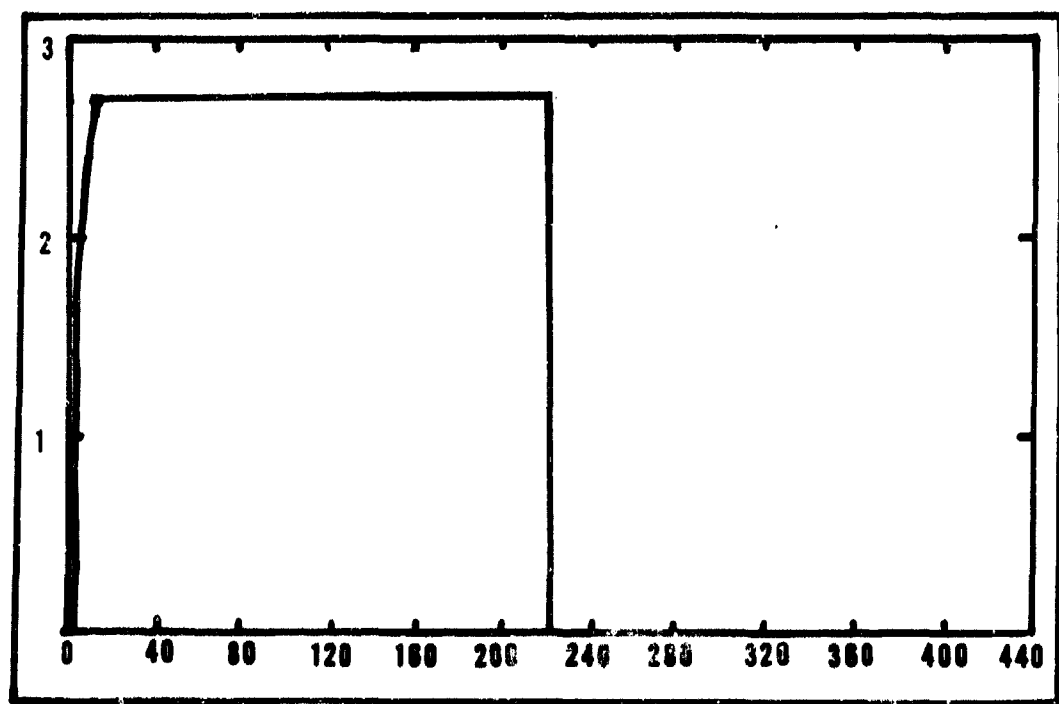
10 b



GAGE OUTPUT (SBMOD)

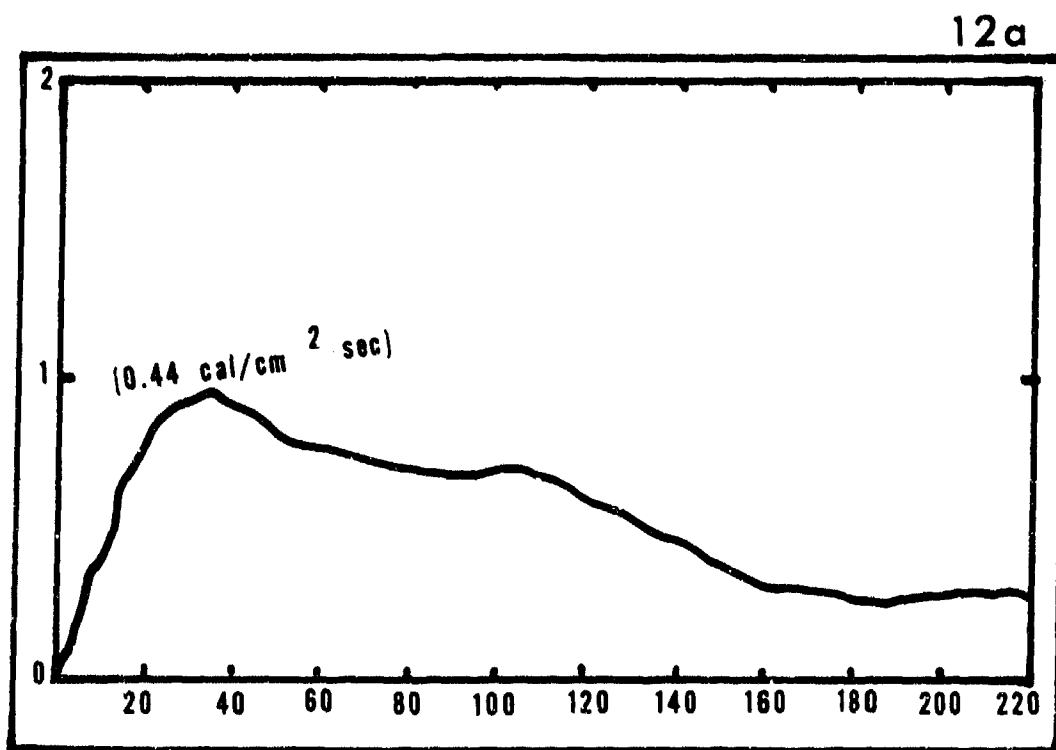
11a

FIGURE 11 SINGLE HEAT FLUX PULSE PREDICTION



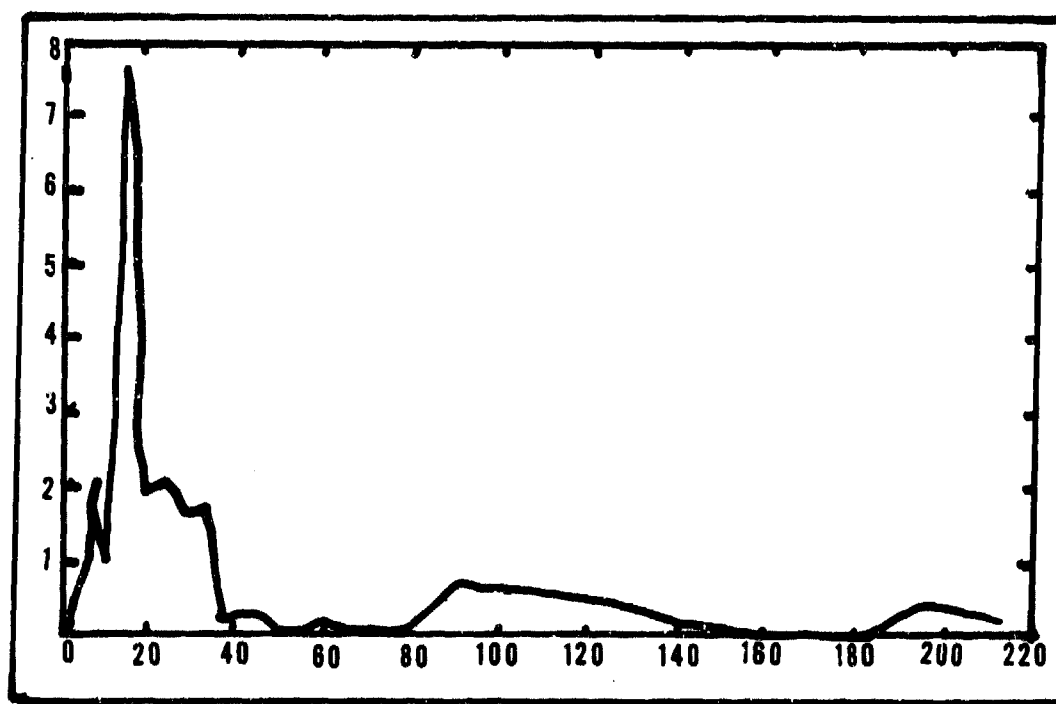
EST. INPUT (TEMOD)

11b



GAGE OUTPUT (ULRICH 1)

FIGURE 12 PREDICTED HEAT FLUX WAVE
FROM SMOOTHED GAGE OUTPUT



EST. INPUT (TESTU1)

12b

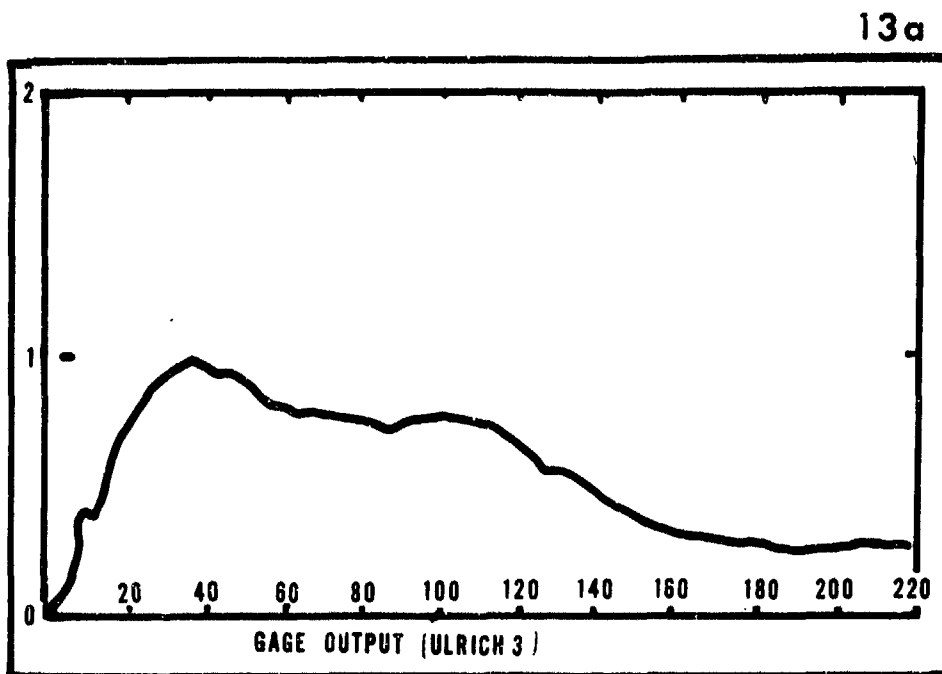
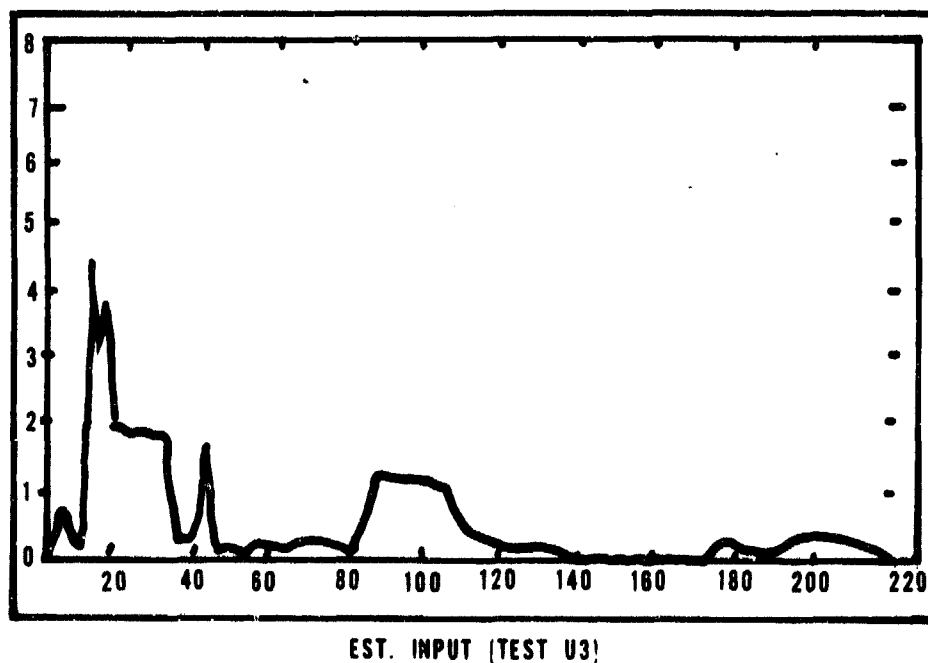


FIGURE 13 PREDICTED HEAT FLUX WAVE FROM
NON-SMOOTHED GAGE OUTPUT



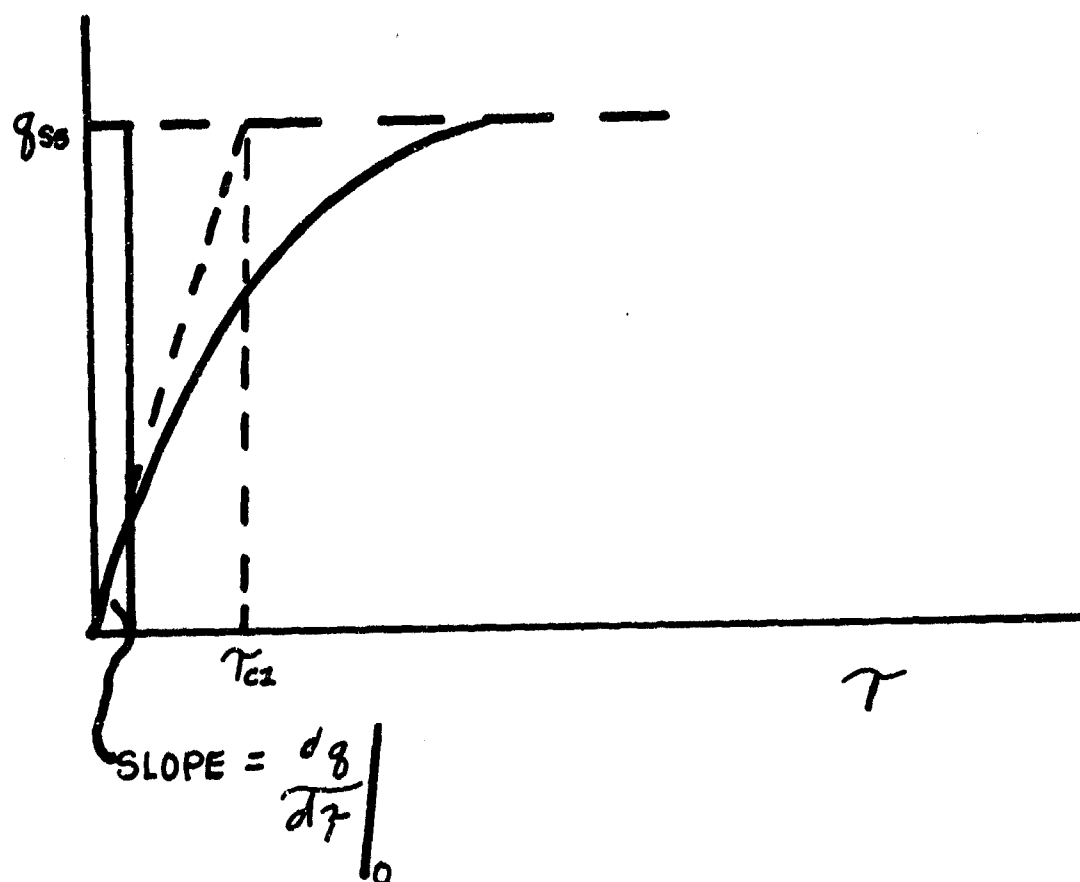


FIGURE 14 TECHNIQUE USING SINGLE EXPONENTIAL RISE CURVE

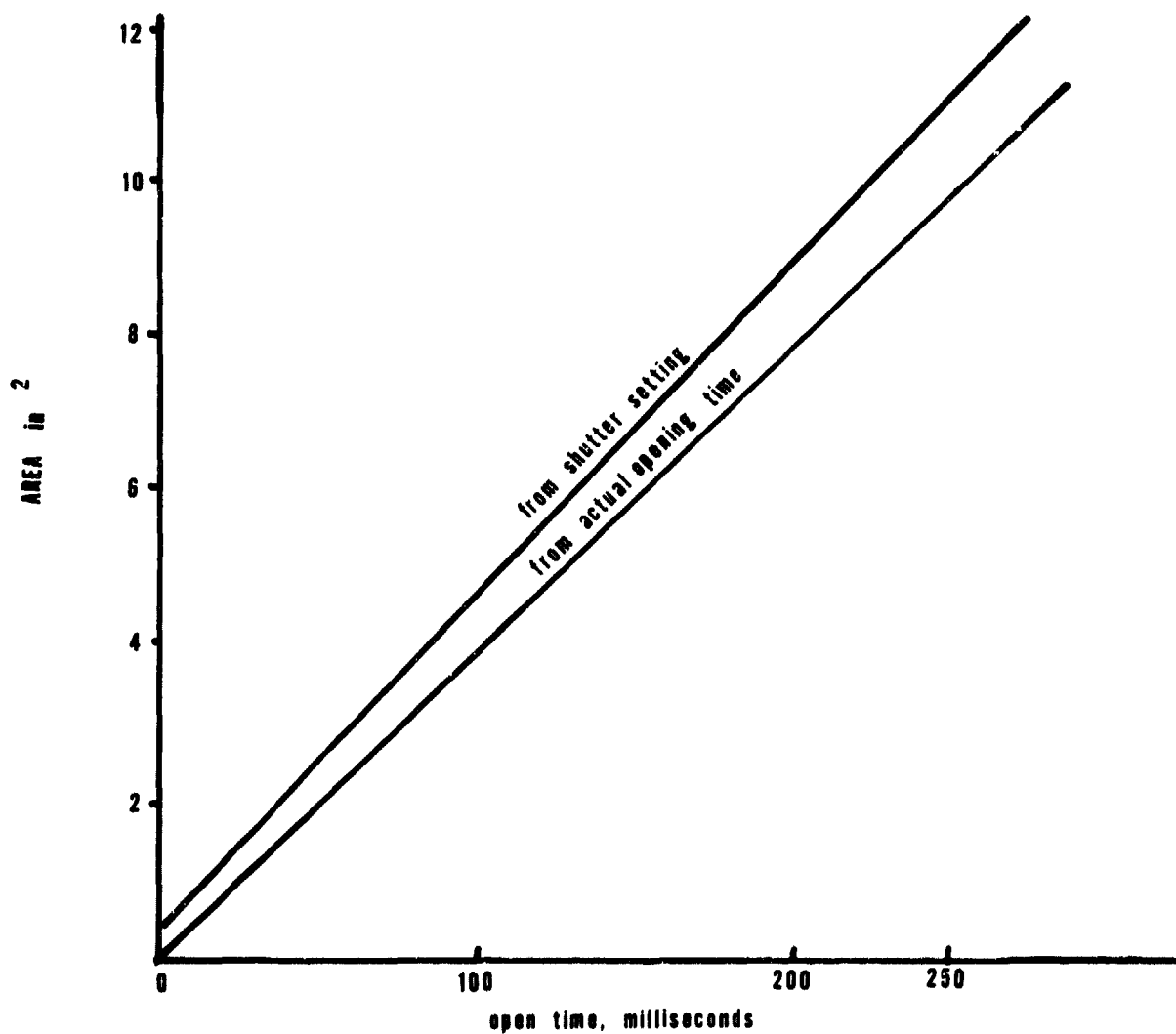


FIGURE 15 CAMERA APERTURE OPEN TIMES VS
AREA UNDER HEAT FLUX GAGE OUTPUT WAVES

AD P000435

DEVELOPMENTS IN SHEARING
OF
AMMUNITION FOR DEMIL

KENNETH O. RHEA, JR.
DIRECTORATE FOR AMMUNITION EQUIPMENT
TOOELE ARMY DEPOT, TOOELE, UTAH

INTRODUCTION

Ammunition Shearing originated in 1969 to aid in the demil of M125 bomblets. The success of that operation laid the ground work for more testing and the development of new equipment. Shearing munitions has been proven effective in reducing or eliminating high order detonations while demilling sheared or punched ammunition items in a deactivation furnace. Shearing has also been used to reduce the size of M55 and M61 chemical rockets by sectioning into seven sections. The sections can then be demilled in a deactivation furnace. Ammunition shearing is a fast and efficient method of expanding the capabilities of the APE 1236 Deactivation Furnace.

HISTORY OF SHEARING

Early work with the operation of shearing munitions centered around the demil of M125 chemical bomblets. The bomblet burster contained .55 pounds of tetryl, and was housed in the empty bomblet during the furnace demil. Burning 82 bomblets without shearing the burster resulted in 60% high order detonations. A series of tests of different punching and shearing techniques finally resulted in eliminating all high order detonations by completely severing the burster by shearing.

Based on the results of the testing, it was felt that this technique could possibly be used on other items to reduce or eliminate damaging high order detonations in the deactivation furnace.

The next series of tests were conducted in 1971 on M384 and M406 40MM grenades. In these tests it was determined that complete severance of the items was not required. Best results were obtained by merely stabbing the projectile 5/8" deep to expose the filler. Burning tests indicated a 91%

reduction in high order detonations. See Figures 1 and 2 for typical results. Tests were then run using M26 Hand Grenades, M21A4 boosters and M502 Artillery F booster with similar results. See Figures 3 through 7.

In 1975, design was begun on a pilot model production machine. The machine employed a nylon block with a machined cavity, Figure 8, to insure support and accurate placement of the shear tool. The machine, requiring a 7 step operation, would be controlled by a programmable controller, Figure 9. A single station machine was built and tested. A second station was then added to increase the production rate to 8 rounds per minute. The two station machine was then housed in an operational shield that had been tested and proven acceptable under the requirements of Mil Std 398 for up to 8 ounces of TNT.

Latest developments in shearing involve the sectioning of M55 and M61 chemical rockets into seven sections then destroying the sections in a furnace. This equipment will be installed in the Chemical Agent Munitions Demil System (CAMDS) at Tooele Army Depot.

The design has been completed on a three station, six cavity shearing, and burning facility for Mississippi Army Ammunition Plant, Figure 10. This equipment will be used to destroy manufacturing line rejected M42/46 grenades at a rate of 24 per minute.

PURPOSE OF SHEARING

There are three reasons for shearing munitions before demilling them in the deactivation furnace. They are:

- 1-To reduce the number of high order detonations in the furnace.
- 2-To reduce the size of an item entering the furnace.
- 3-To allow lower operating temperatures in the deactivation furnace.

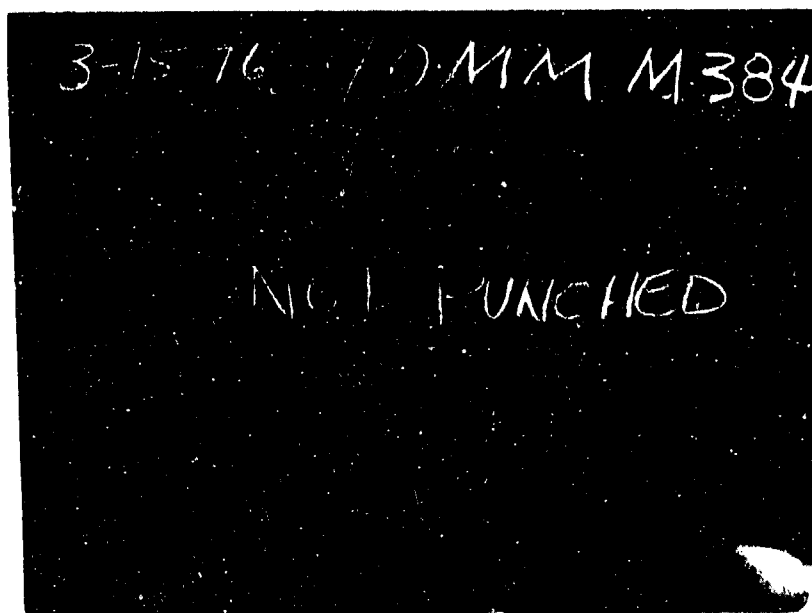


FIGURE 1 - 40MM GRENADES BURNED NOT PUNCHED

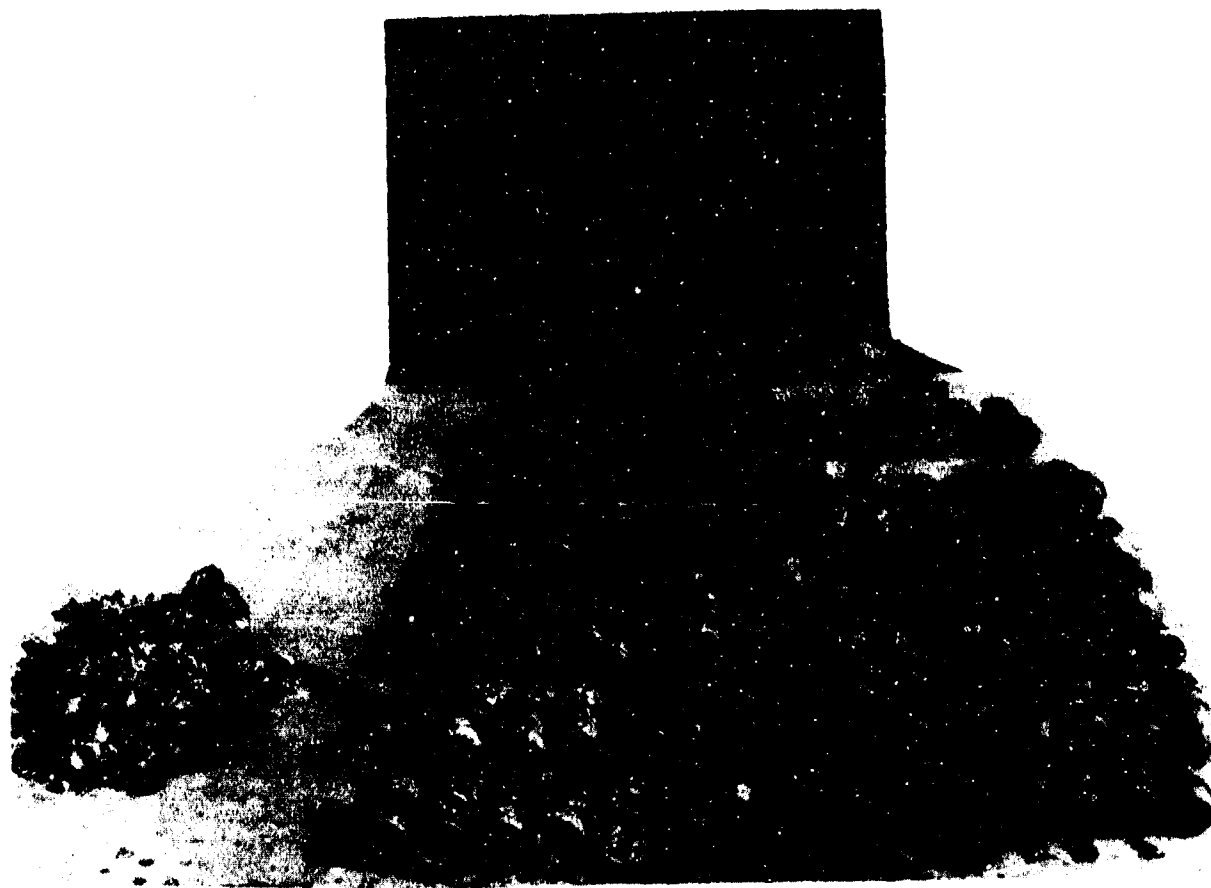


FIGURE 2 - 40MM GRENADES PUNCHED AND BURNED



FIGURE 3 - 40MM GRENADE, M406 PUNCHED AND BURNED

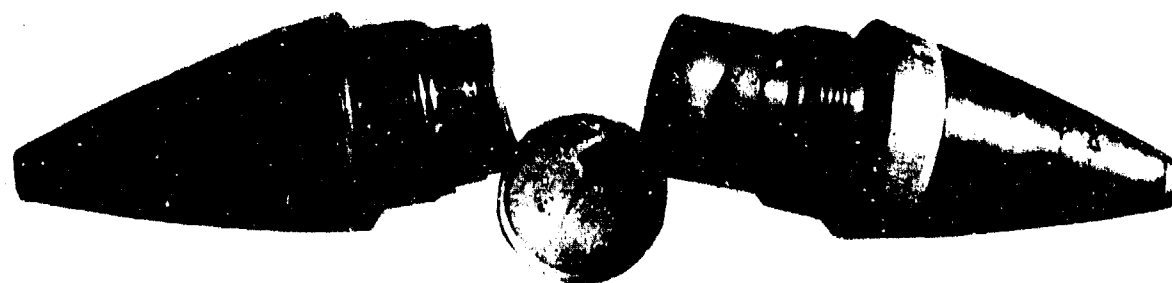


FIGURE 4 - M502 FUZE W/BOOSTER, SHEARED



FIGURE 5 - 40MM GRENADE, M384 SHEARED

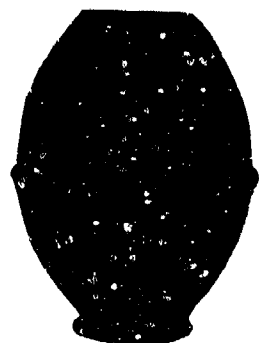


FIGURE 6 - M26 HAND GRENADE, PUNCHED

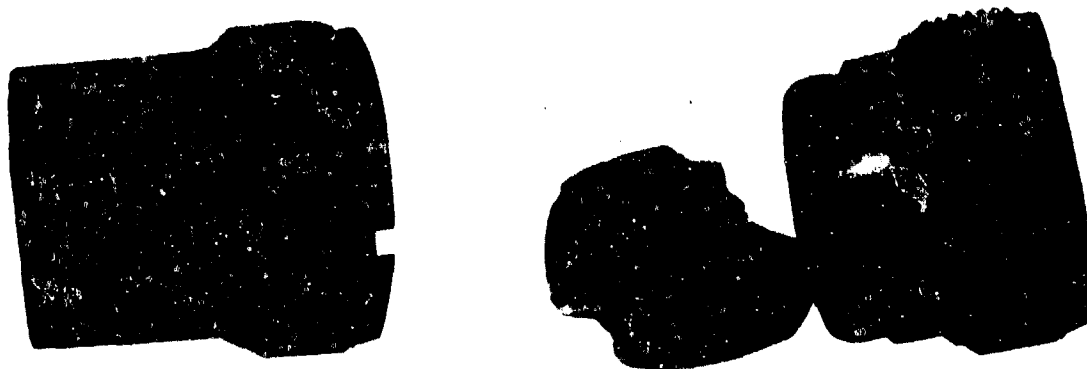


FIGURE 7 - M21A4 BOOSTER, SHEARED AND BURNED

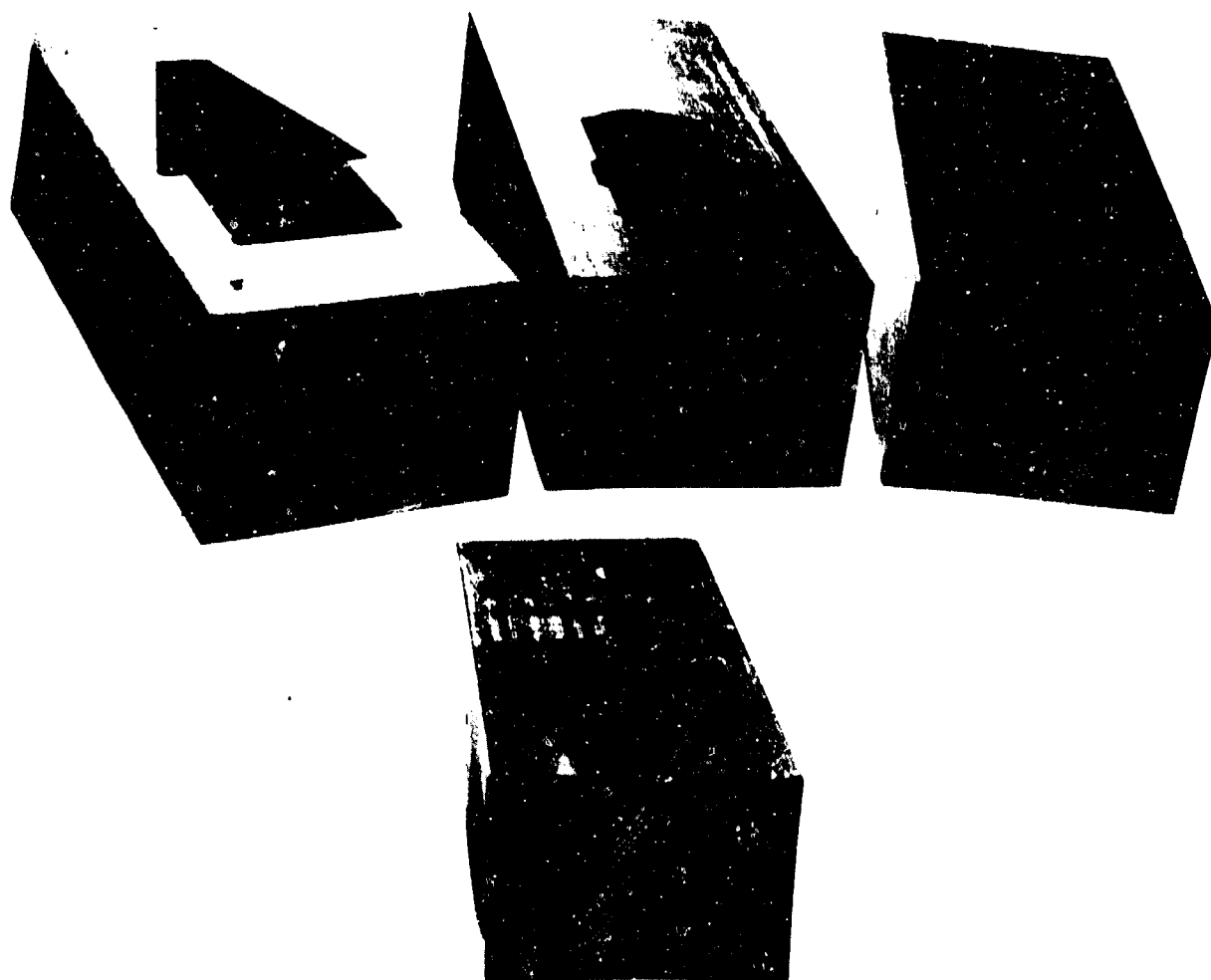


FIGURE 8 - MUNITION HOLDING BLOCKS

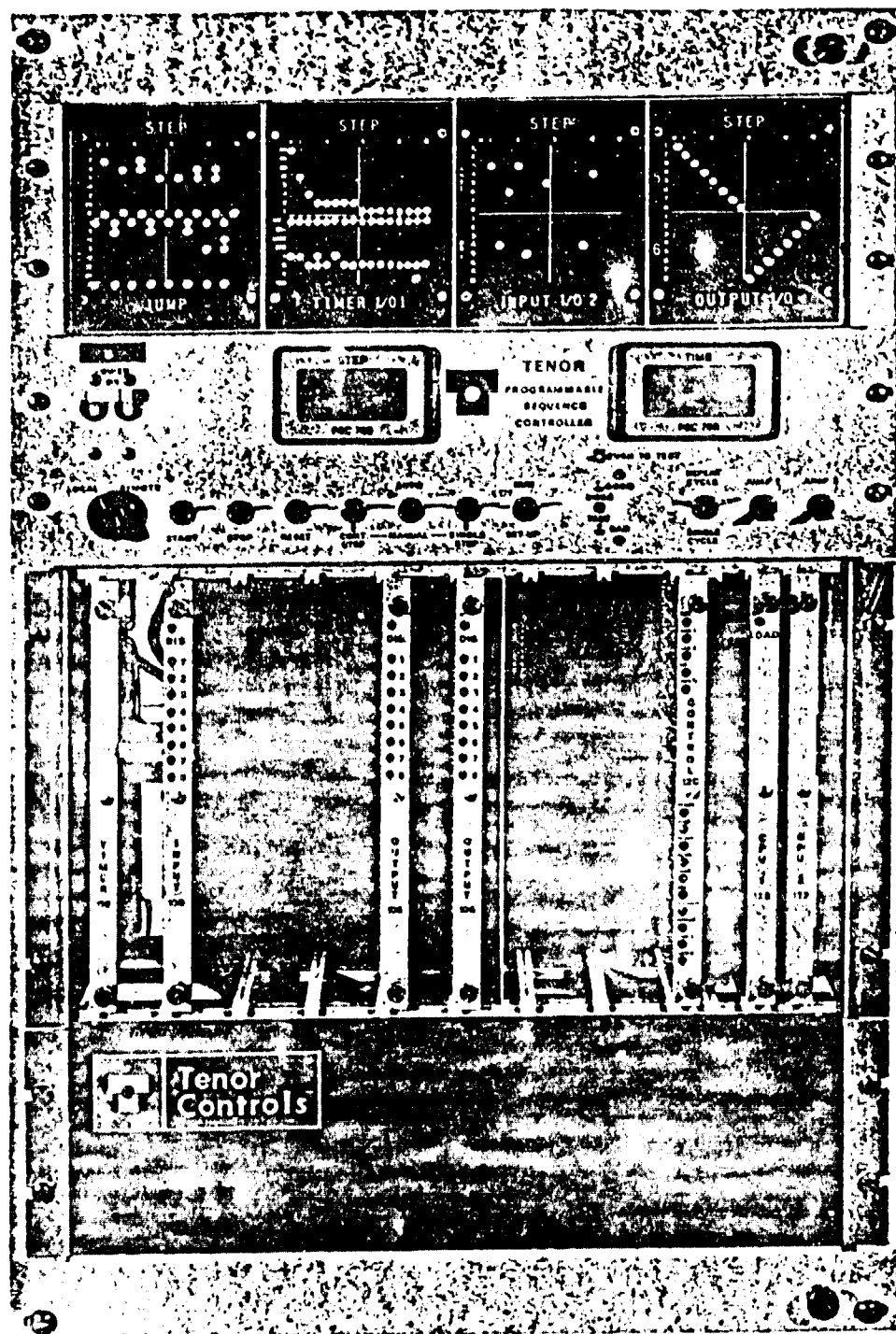
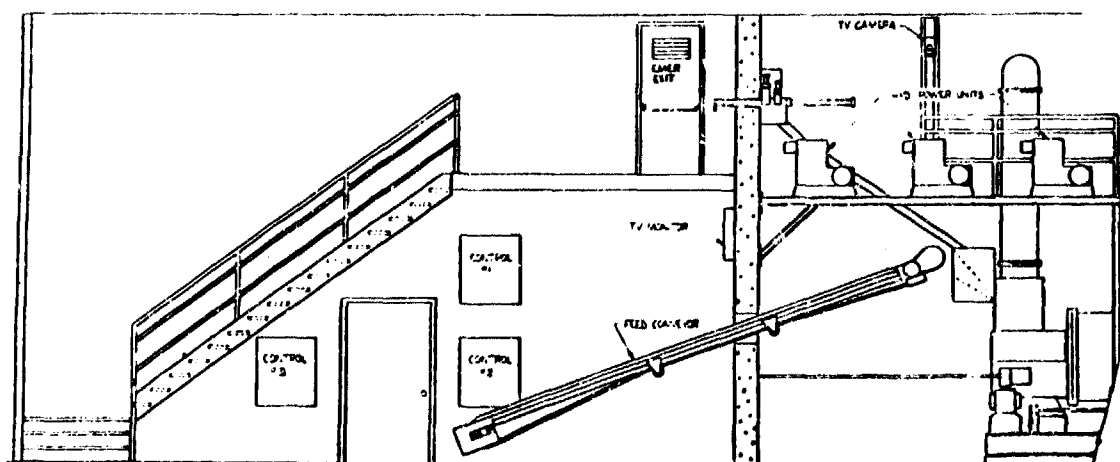
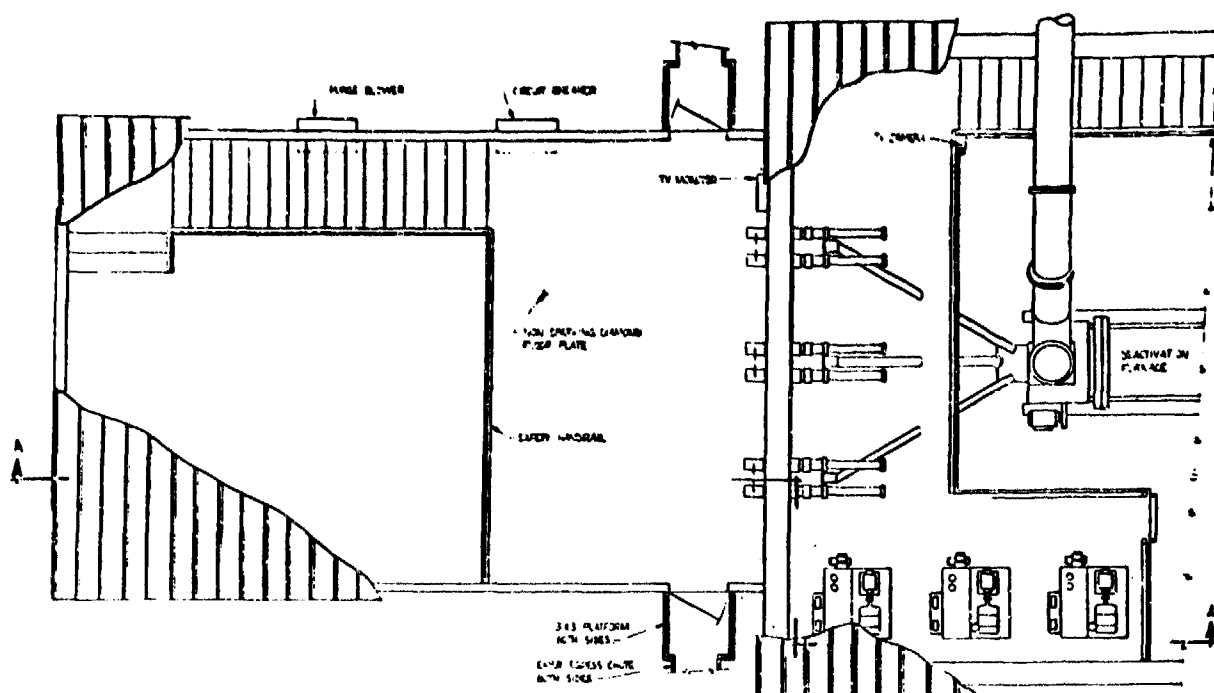


FIGURE 9 - PROGRAMMABLE CONTROLLER



SECTION A-A

FIGURE 10 - 3 STATION, 6 CAVITY SHEAR FACILITY

High order detonations in the furnace can be very damaging, particularly if they occur on a continuing basis. Not only is there risk involved in blowing out the flame and allowing items to exit the furnace that may not be completely demilled, but the equipment is subjected to unnecessary strain. Though the retort can withstand a 2 to 3 pound detonation, this occurrence can cause bulges and/or cracking.

The overpressures created by detonations weaken and/or distort the dampers in the air pollution control system. The production rate on items known to detonate high order must be reduced to protect the equipment. Shearing or punching ammunition items will greatly reduce or eliminate detonations by allowing the exposed explosive to ignite and burn before pressures and temperatures reach the detonation stage. The production rate can therefore be increased by punching or shearing the munition item.

To insure demil of a detonating item in the center (heavy duty) retorts, often the operating temperature must be increased. Since the bag house in the Air Pollution Control System is limited in the temperature it can withstand, the lower the temperature a furnace can operate at, the better. High furnace temperatures also create problems by melting metal such as aluminum and magnesium that are much more easily handled while in a solid state. Exposing the explosive filler by shearing creates a condition for igniting at lower temperatures; and the explosive burning is a much more easily controlled method of demil.

Using a shear operation to reduce the size of an item increases the usability of the deactivation furnace. In the case of the M55 and M61 rockets, the fuze, burster, rocket motor and igniter are all separated and reduced to a size the furnace can handle, Figures 11 through 13. The

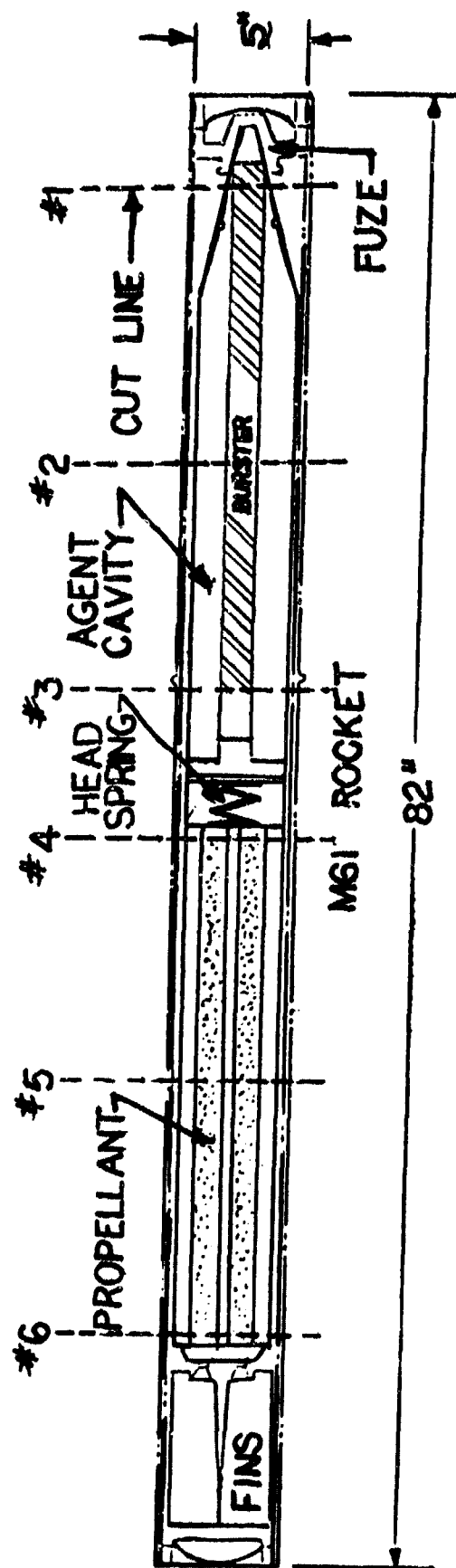


FIGURE 11 - M61 ROCKET, SHEARING LOCATIONS

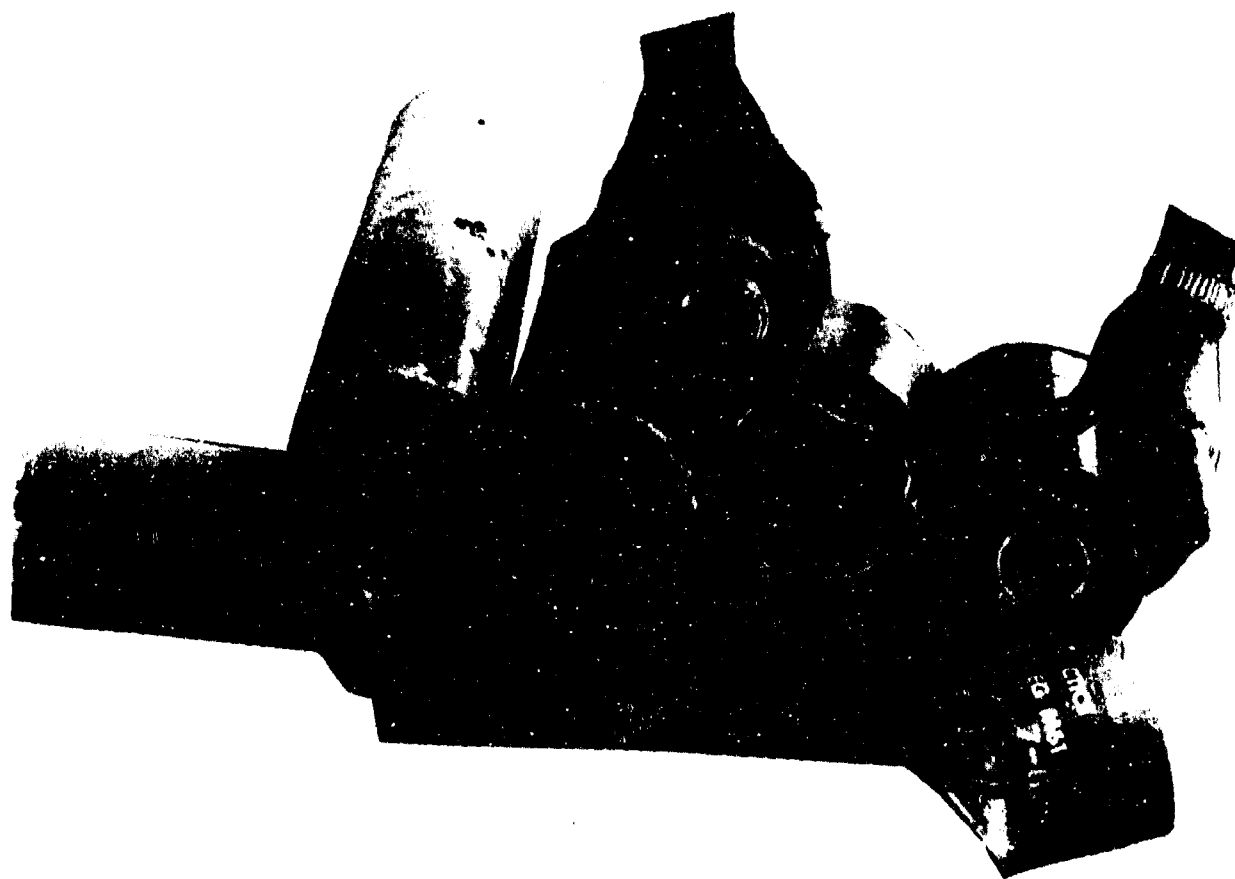


FIGURE 12 - M61 ROCKET SECTIONS

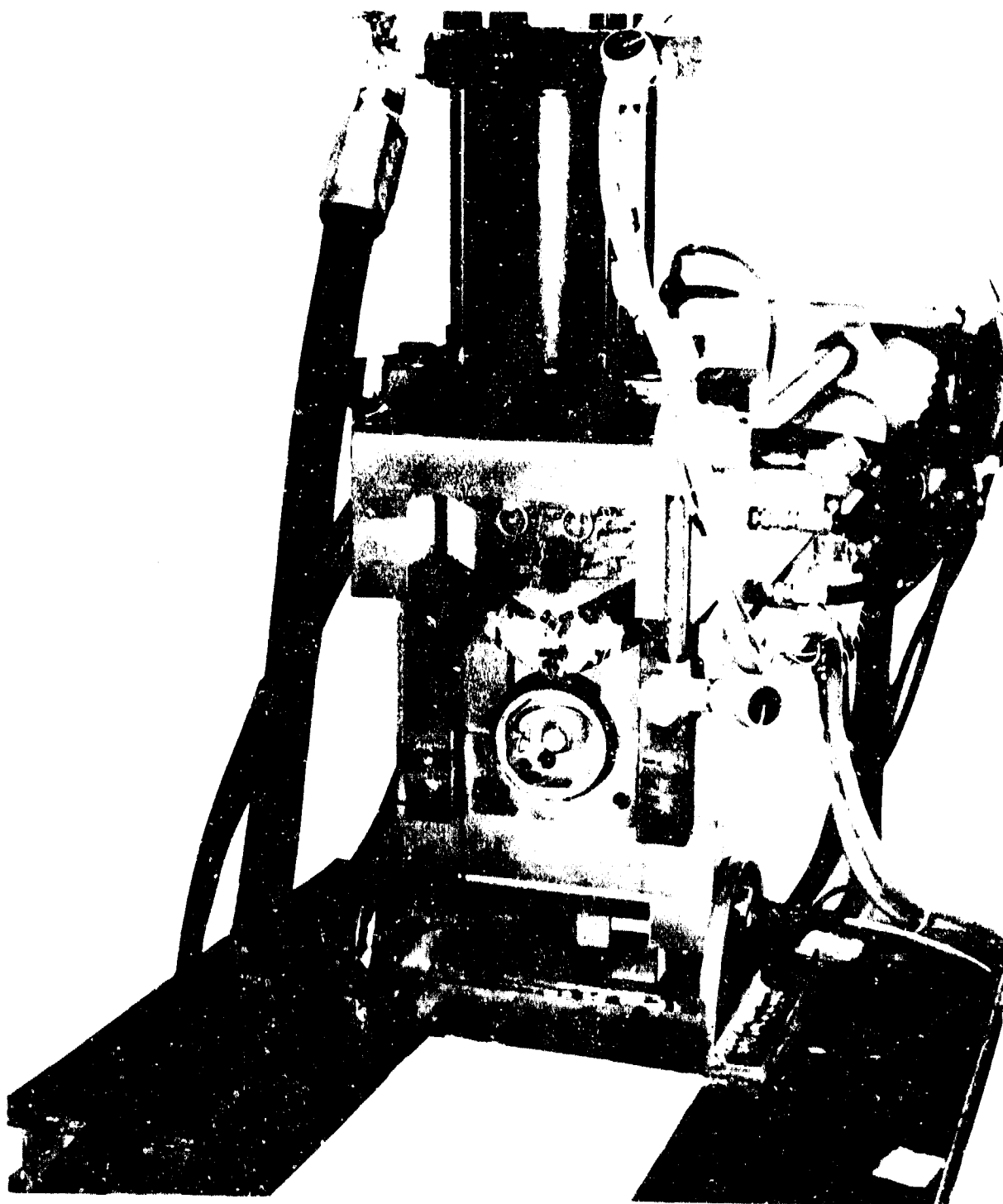


FIGURE 13 - SHEAR FIXTURE, M61 ROCKET

rocket shipping container is 82" long and 5" diameter. The proposed shearing operation sections the rocket housed in the container into seven sections that are easily handled by the furnace.

SHEARING ADVANTAGES

Exposing explosive filler or reducing the size of an item can be accomplished in several ways including sawing, drilling, flycutting or disassembly. Shearing has strong advantages over these other methods. Shearing is a relatively fast operation as opposed to sawing, drilling or disassembly.

The shear operation can be accomplished utilizing a relatively simple machine. The operation produces little or no metal chips and does not require any form of coolant.

However, like other methods of exposing the explosive, shearing or punching creates loose or powdered explosive that must be cleaned up almost continually; and special problems are created in handling an item containing exposed explosive.

DEVELOPMENT OF THE SHEAR PROCESS

Development of the shear process centers around maintaining less energy input to the item than is required to detonate the explosive filler. Several factors have bearing on this. They are:

- 1-Thickness of material to be penetrated.
- 2-Type of material to be penetrated.
- 3-Required size of the penetration.
- 4-Type of explosive being penetrated.
- 5-Type of penetration, i.e. round hole, triangular hole, complete sectioning.

Because of the many factors involved, each candidate must be considered on a case by case basis.

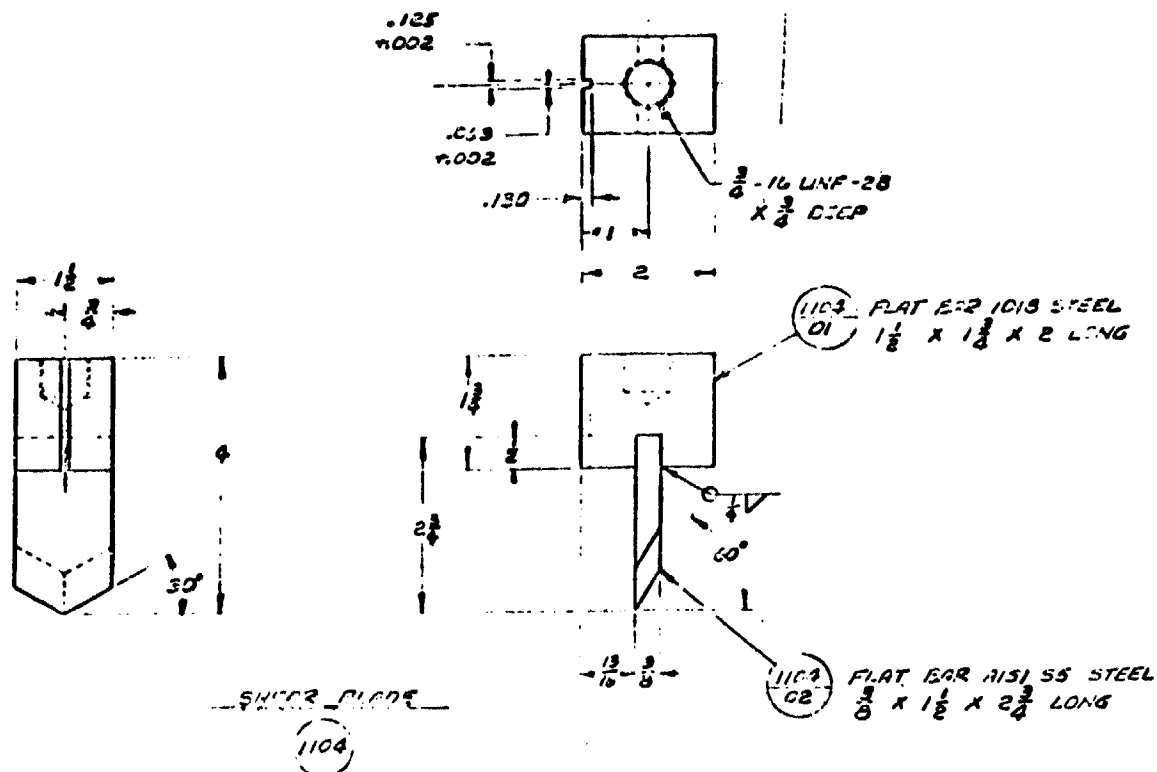
Considerable effort has been made to determine the best possible shear blade design. Though other designs may be better on items not yet tested, generally the tool that has proven the most successful is a single sided wedge shaped tool with the cutting edges sweeping back 30° from the point, Figure 14. Several designs have been tested including a double sided tool, single, straight cutting edge tool, and single sided rounded cutting edge tool. For punching the M42/46 grenades, a standard round punch is used. The standard punch is ground to a slightly rounded tip 3/8" in diameter. This tool is strong and most effective for punching the grenade body and continuing on to deform the shaped charge and expose the explosive.

Development of the shear process has not been without incident. While searching for the optimum punching location on M42 grenades, 16 high order detonations resulted.

Tests of shearing the M61 rockets using a straight edged blade resulted in ignition of the rocket motor. A single sided wedge shaped tool with swept back cutting edges has proven the best in this case also.

CURRENT CAPABILITIES

Currently, the APE 2196 Munition Shear Machine, Figures 15 through 18, design can handle small munition items up to 3 inches by 3 inches by 8 inches in size. The operational shield has been proven affective in protecting the operator against an 8 ounce TNT detonation of an offensive grenade or a 5.89 ounce Comp B detonation of a fragmenting grenade.



PART NO. 11-2-03 TO BE MACHINED AND HARDENED P₂ SS BEFORE WELDING.

FIGURE 14 - SHEAR BLADE

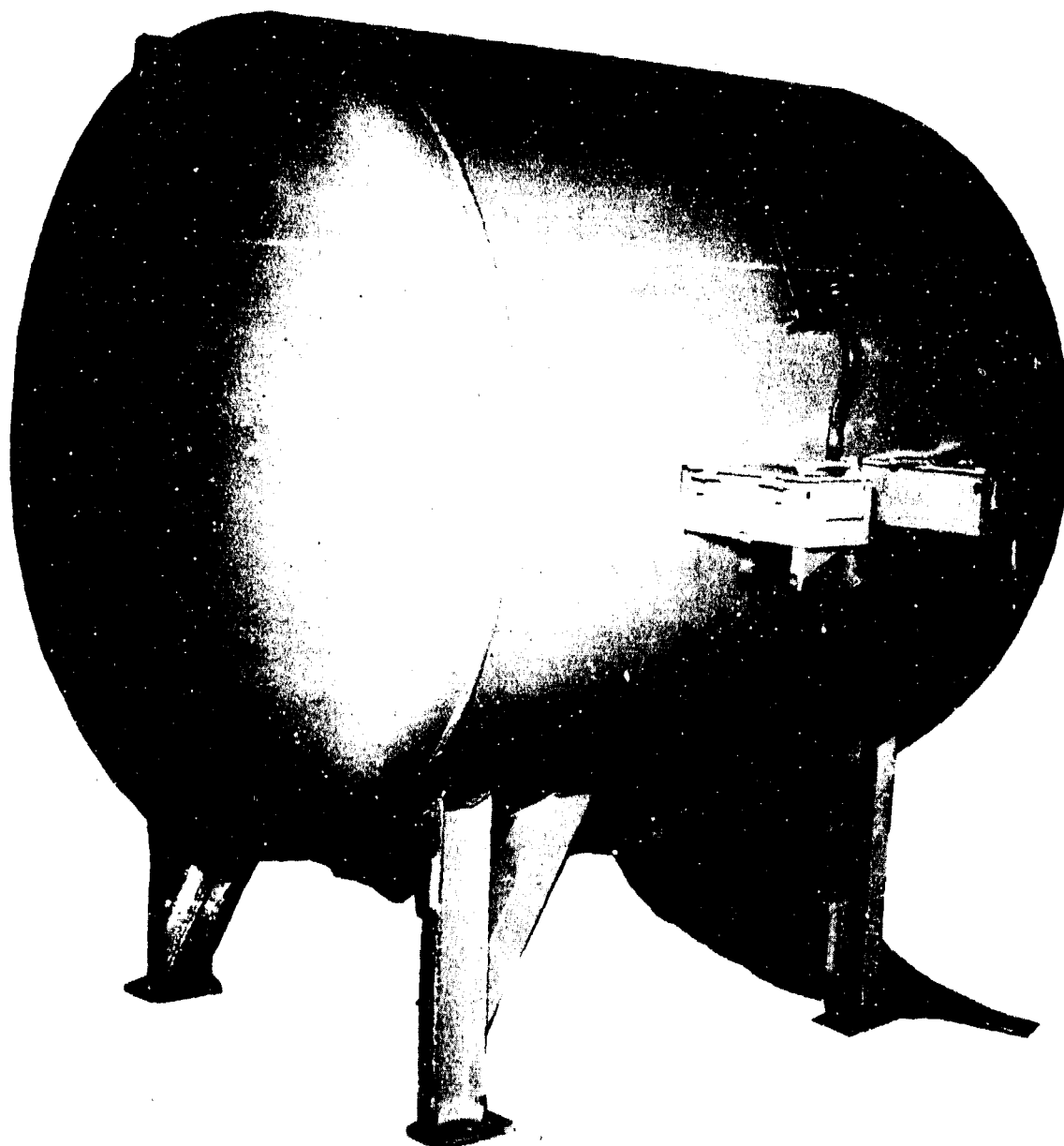


FIGURE 15 - APE 2196 MUNITIONS SHEAR MACHINE

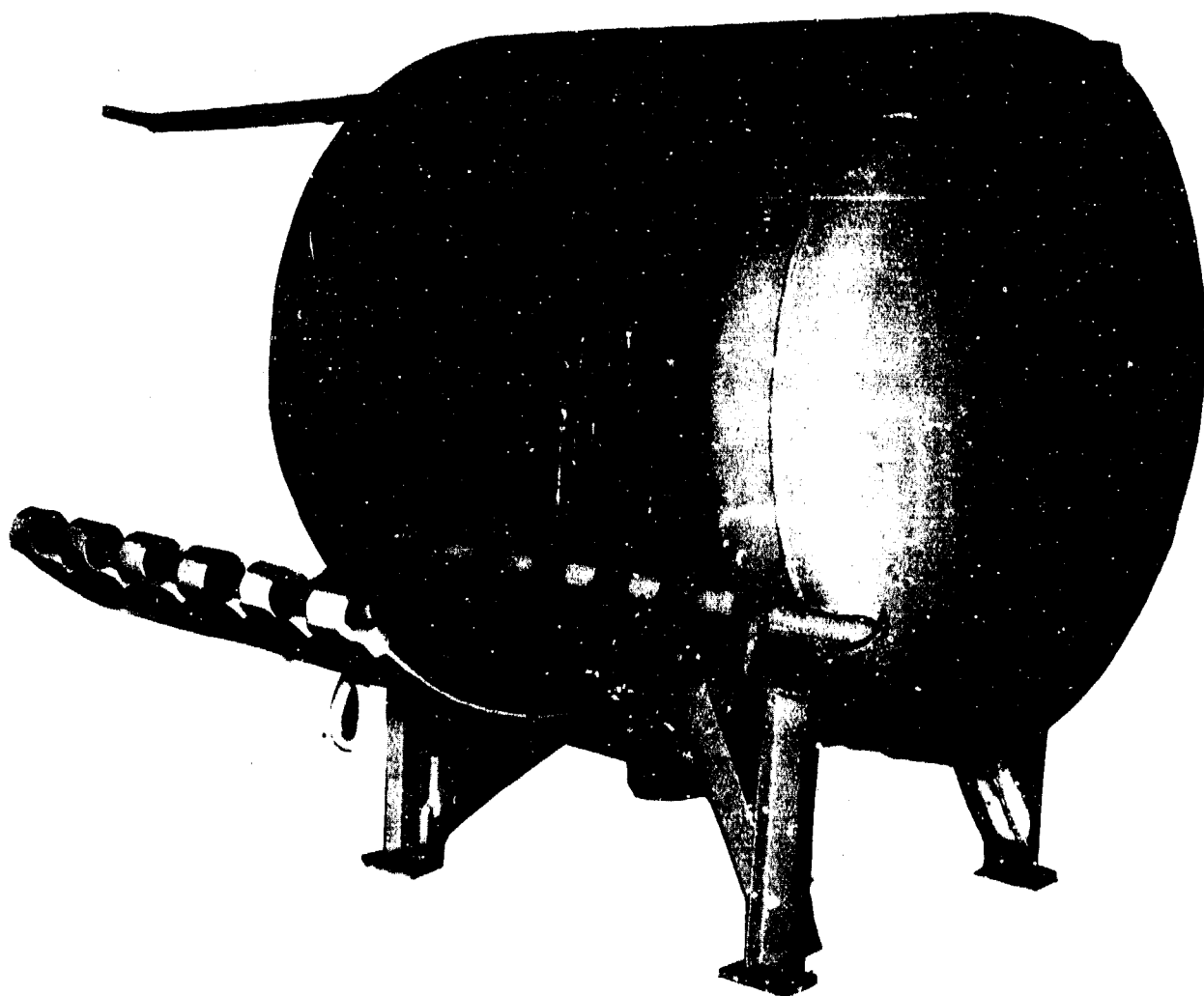


FIGURE 16 - SHEAR MACHINE ACCESS DOOR

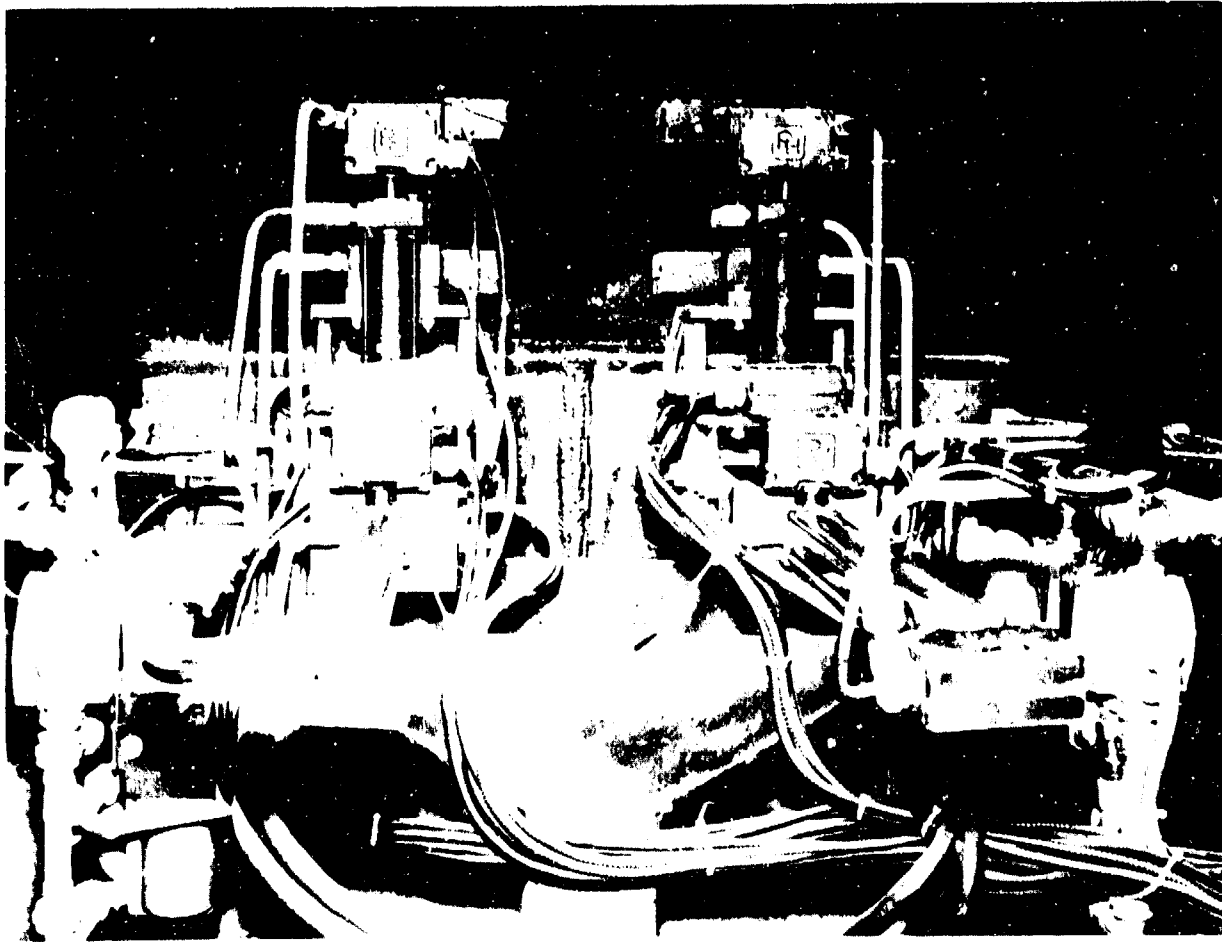


FIGURE 17 - SHEAR MACHINE INTERIOR

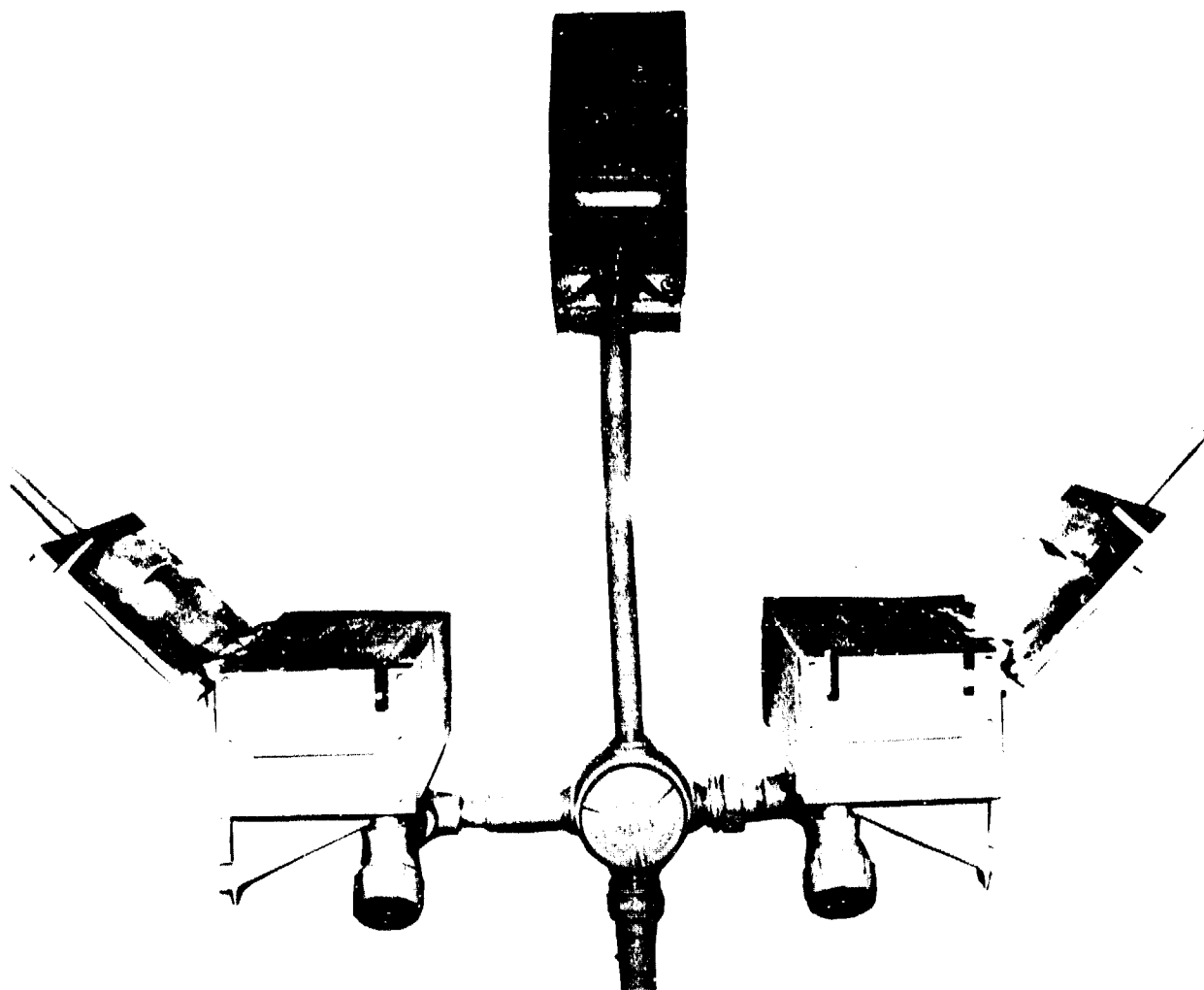


FIGURE 18 - SHEAR MACHINE INPUTS

Accessory kits are available for shearing M26 grenades (without fuze), M21A4 boosters, M502 artillery fuzes with M21A4 boosters, M384 and M406 40MM grenades, and M12/46 shaped charge grenades.

As shearing can be used to reduce the size of an item, any item that can be reduced to a six inch diameter and 22 inch length for feeding into the furnace is a possible candidate for a shearing and burning demil operation. The furnace is also limited in explosive amount to 5 pounds per flight, which must be considered when shearing large items for demil.

CONCLUSION

Shearing munitions for burning is a proven method of expanding the deactivation furnace capability. Particularly where open air detonation is limited, a shearing and burning operation could be utilized for destruction of small and medium sized explosive filled items.

**NAVAL EXPLOSIVE SAFETY
IMPROVEMENT PROGRAM**

(MILESTONE II-I)

PLANS AND PROGRAMS



MICHAEL M. SWISDAK, JR.

NAVAL SURFACE WEAPONS CENTER

NAVAL EXPLOSIVE SAFETY IMPROVEMENT PROGRAM
(MILESTONE II-1)
PLANS AND PROGRAMS

Michael M. Swisdak, Jr.
Naval Surface Weapons Center
White Oak, Silver Spring, Maryland 20910

The Naval Explosives Safety Improvement Program (NESIP), Milestone II-1, has as its objective the examination of Naval munitions in the quantities and scenarios experienced on Naval waterfronts, to determine fragment and blast hazard ranges. This paper will review the organization of the program, discuss several of its major on-going testing programs, review some of its many past accomplishments, and discuss its relationship with the Navy's Weapon System Explosive Safety Review Board. Specifically, the paper will review findings and testing concerning hazard ranges and sympathetic detonation of bombs and torpedoes in the open and torpedoes in certain classes of ships. It will discuss analytic studies of several Navy Weapon Systems including the Penguin Missile System and the Destructor MK 14 MOD 0. In addition it will present previously unpublished fragment velocity data taken from the NESIP data base.

The Chief of Naval Operations initiated the Naval Explosives Safety Improvement Program (NESIP). In 1974, the program was established for the purpose of assessing the Navy's compliance with DDESB standards on explosive handling waivers and explosive safety problems in general. A collateral objective was to develop military construction programs to eliminate such problem areas where possible.

The scope of the entire current NESIP effort is shown in a breakdown of tasks by Milestone number in Table 1. This paper will deal solely with Milestone II-1, "Prosecute Naval Explosive Safety Test (NEST) Program."

This Milestone (II-1) has as its objective the examination of Naval munitions, in the small quantities handled on Naval waterfronts, and in the several explosive handling scenarios which are experienced, to determine fragment and blast hazard ranges. The ultimate goal is the reduction of explosive-safety quantity-distance (ESQD) arcs which must be applied to small quantity handling evolutions. These define the basic scope of the program. The program deals with handling scenarios: transportation, loading, topping off, etc. It is also generally limited to small quantities of munitions. Small in the context of transportation and handling scenarios generally means no more than 1500 pounds Net Explosive Weight (NEW). (Note: The handling of small quantities of munitions excludes major facilities such as the Naval Weapon Station, Yorktown; it does include facilities such as those located at Charleston and San Diego).

In the past, the Navy has operated under Explosive Safety Quantity-Distance (ESQD) waivers at most of its tidewater port complexes during explosive handling operations which are necessary to maintain fleet operational readiness requirements. Much of the problem that brought about the imposition of these waivers in the first place resulted from the application of Department of Defense Explosive Safety Board (DDESB) general standards to specific Navy operations at these ports -- operations that are less severe and more limited in scope than those to which the DDESB standards are generally applied. These DDESB standards, as interpreted by the Navy are an ESQD arc of "... 670 feet for 100 pounds NEW (New Explosive Weight) or less. For 101 to 30,000 pounds NEW, the minimum distance will be 1250 feet unless it can be shown that fragments and debris from structural elements of the facility or process equipment will not present a hazard beyond the distance specified..."¹

The Navy recognizes the necessity of maintaining adequate safety standards. Moreover, it accepts the DDESB criteria for acceptable hazards. These criteria are:

1. Less than 1 psi blast overpressure, and
2. A hazardous fragment flux evaluated for the ground surface area of less than one hazardous fragment per 600 ft². A fragment is considered hazardous if it has an impact energy of 58 lb-ft or greater.

It is recognized that the DDESB's policy is to make changes in the ESQD tables if it is demonstrated that the new arcs for each specific scenario are realistic and do not compromise safety.

¹ Ammunition and Explosives Ashore: Safety Regulations for Handling, Storing, Production, Renovation, and Shipping, NAVSEA OP5, Vol. 1, Rev 10, 1 Nov 1981.

In essence then, each Naval munition or weapon system must be examined to answer the following questions:

1. Given the detonation of one round, what are its effects on any surrounding rounds? Will the surrounding ordnance sympathetically detonate? What is the Maximum Credible Event (MCE)?
2. For the MCE, and applying the DDESB standards given above, what is an appropriate ESQD arc?

The approach has been two-fold -- analytical and experimental. Predictions are made using the analytical techniques developed for this program. These predictions are then verified experimentally. When the theory is inadequate, it is developed/refined and experimental tests are conducted to determine relationships from the data. The analytical techniques form the NESIP Technology Base, which was described by Porzel² at the 1980 DDESB seminar. Currently, approximately 60% of the effort is analytical and 40% experimental. At the onset of the program, all analyses/predictions were verified experimentally (100% testing). As the results of these analyses and predictions were compared with the experimental data, it became obvious that less testing would be required. In every case in which differences occur between the Technology Base predictions and the experimental results, the Technology Base has been more conservative (i.e., required a larger ESQD arc). Because of the development of the Technology Base, answers to ESQD problems can now be obtained much more easily and reliably. The technology is now well-developed and operable. It is used for analysis and test guidance. Together -- analysis and tests -- they are giving the answers to the questions asked: "What are the ESQD values for specific Navy Scenarios?"

Because of the development of the Technology Base and its successful application, the CNO introduced^{3,4} in 1979 a mandatory requirement that all programs for the development and introduction of new weaponry into the fleet include analyses developed by the NESIP and/or verifying tests (as recommended by NESIP) to insure the timely availability of hazard information for review by the Weapon Systems Explosives Safety Review Board (WSESRB). The CNO specifically tasked Milestone II-1 of the NESIP to assess the sympathetic detonation characteristics and the explosion hazard effects of weapon systems that are presented to the WSESRB. These efforts are to be funded by the weapon systems project managers. If the weaponry is found to be unacceptably hazardous, then the NESIP Milestone II-1 is to fund an effort to reduce the hazard to an acceptable level.

²Porzel, F. B., "Technology Base of the Navy Explosives Safety Improvement Program," Minutes of the Nineteenth Explosives Safety Seminar, Los Angeles, CA, 11 September 1980.

³CNO ltr Ser 411F/316499 of 5 Feb 1979.

⁴NAVSEA ltr 04H3/EAD Ser 363 of 22 May 1979.

In 1978, Petes⁵ presented an outline of this milestone and certain of its accomplishments. Table 2 presents a summary of the weapons/scenarios which have been examined (analyzed and/or tested) since the program inception. Many of these findings have been reported previously in some detail^{12,6-15} in the open literature.

⁵Petes, J., "The Navy's Explosive Safety Improvement Program for Pier Side Munitions Operations," Minutes of the Eighteenth Explosives Safety Seminar, San Antonio, TX, 12-14 September 1978.

⁶Porzel, F. B., "Design of Lightweight Shields Against Blast and Fragments," Minutes of the 17th Explosives Safety Seminar, DOD Explosives Safety Board, Denver, CO, 1976.

⁷Porzel, F. B., "A Model and Methods for Control of Sympathetic Detonation," Minutes of the Eighteenth Explosives Safety Seminar, DOD Explosives Safety Board, San Antonio, TX, Sep 1978.

⁸Martin, G. H., "The Explosives Hazard Presented by the Torpedo Magazine of a Guided Missile Frigate (FFG Series) During Pier-side Topping-Off Operations," 19th DDESB Seminar, Los Angeles, CA, Sep 1980.

⁹Connor, J. G., "Hazards from Accidental Explosions in Submarine Tender Workshops," Minutes of the Nineteenth Explosives Safety Seminar, DOD Explosives Safety Board, Sep 1980.

¹⁰Ward, J. M., "Simulated Tomahawk Missile Handling Arc Test Results," Minutes of the Eighteenth Explosives Safety Seminar, DOD Explosives Safety Board, San Antonio, TX, Sep 1978.

¹¹Ward, J. M., "Blast/Fragment Hazards Associated with Accidental Explosion of a MK 82 Bomb Pallet," Minutes of the Nineteenth Explosives Safety Seminar, DOD Explosives Safety Board, Sep 1980.

¹²Porzel, F. B. and Ward, J. M., "Safety Analyses of the Machrihanish Magazine," NSWC TR 79-359, Naval Surface Weapons Center, White Oak Laboratory, 1979.

¹³Porzel, F. B., "Propagation of Explosions in the Machrihanish Magazine: Vulnerability of Thin-Cased Munitions to Massive Debris," Vol. 5, Seventh Quadripartite Ammunition Conference, London, England, Oct 1979.

¹⁴Swisdak, M., Jr., "Determination of the Safe Handling Arcs Around Nuclear Attack Submarine," Minutes of the Nineteenth Explosives Safety Seminar, DOD Explosives Safety Board, Los Angeles, CA, Sep 1980.

¹⁵Connor, J. G., "Shields for Decelerating Munitions Fragments," Minutes of the Eighteenth Explosives Safety Seminar, DOD Explosives Safety Board, San Antonio, TX, Sep 1978.

The remainder of this paper will review some of these findings. In addition, some of the previously unreported results will be presented. Other papers at this seminar will discuss still other facets of the work. Finally, several on-going experimental programs will be briefly discussed.

A major emphasis in the program has been the ESQD arcs required for torpedoes. The work was begun with obsolete MK 16's and is currently continuing with the newest MK 48's. It was discovered that the torpedo warhead fragments are not the culprits, since the warheads are relatively thin-skinned. The fragmentation hazard range is driven, rather, by parts of the truck or other vehicles used to transport the warheads. The ESQD arc for two torpedoes in the open is within 500 feet. When the torpedoes are placed on a truck, however, the ESQD arc extends well beyond 500 feet. This is because the truck becomes a major source of large secondary fragments. Through the use of a simple shield the warhead detonation was decoupled from the truck, reducing the hazard ranges to an acceptable level. This simple shield design is shown in Figure 1.6

Another part of the torpedo effort has been work done to reduce the MCE. At the spacings generally encountered in torpedo magazines aboard ship, if one torpedo detonates, the remainder should sympathetically detonate. The simple expedient of nose-to-tail stowage (as opposed to nose-to-nose stowage), as shown in Figure 2, reduces the likelihood of sympathetic detonation. If, in addition to nose-to-tail stowage, inhibitor plates are placed between rounds, the MCE can be limited to one warhead. (Note: sympathetic detonation is inhibited; lower order reactions such as burning are not automatically excluded). This has been demonstrated previously for MK 16 and MK 46 torpedo warheads. A recently completed experimental program has demonstrated the feasibility of this concept for MK 48 torpedo warheads.

It should be noted that the NESIP simply recommends methods of reducing sympathetic detonation and the ESQD arcs. The actual design and retro fit of these concepts are engineering problems that are being handled by the various ship engineering offices.

As part of these same studies, it was found that the OTTO Fuel does not detonate for the projected threat scenarios and thus does not contribute to the MCE.

Another effort¹¹ has involved the ESQD arcs produced by the detonation of pallet loads of MK 80 series bombs. The program has shown that if one H-6 filled bomb in a standard pallet configuration detonates, the remainder of the bombs within the pallet will also detonate within 300 microseconds. Furthermore, if pallets are stacked one on top of another or side-by-side as closely as possible, and if detonation begins in one pallet, it will spread to the surrounding pallets. Thus the MCE is the number of pallets in close proximity multiplied by the number of bombs in each pallet.

If the MCE is limited to a single pallet (approximately 900 to 1900 pounds NEW for bombs in the MK 80 series) resting on a flat surface in the open, the ESQD arc can be defined for this scenario. Test results indicate that for both MK 82 and MK 83 bombs (and by generalization all bombs in the MK 80 series), the ESQD arc is controlled by airblast and not by fragmentation. Figure 3 is a plot of NESIP generated pressure-distance data for MK 80 bombs (scaled to one

pound at sea level). One psi occurs at a scaled range of 56 ft/lb^{1/3} (approximately 600 feet for pallets of MK 82's and MK 83's and 700 feet for MK 84's). As part of the NESIP procedures, this data was compared with multi-source archival MK 80 data as shown in the next figure (Figure 4). The solid line in this figure is the NESIP Technology Base prediction for H-6 (Equivalent Weight of 1.3) in a steel case (case weight to explosive weight of 1.5). All of the data as well as the prediction are in excellent agreement.

As determined by NESIP tests, the ESQD arc based on fragmentation for single pallets of MK 80 series bombs is within 500 feet (i.e., less than one hazardous fragment per 600 square feet ground surface area). It should be noted that hazardous fragments do travel beyond 500 feet from ground zero. However, there is no physical reason why the ground surface areal density should be anything but a decreasing function with range beyond 500 feet for these naturally fragmenting bombs. This has been investigated in a series of tests conducted at White Sands Missile Range, New Mexico by the Terminal Effects Branch of the Naval Surface Weapons Center. In these tests, pallet loads of bombs were detonated and fragments recovered out to at least a range of 2000 feet. Analyses of these data are continuing.

A study was recently completed of the PENGUIN missile system. This is a Norwegian developed missile utilizing a BULLPUP A warhead as shown in Figure 5. The U. S. Navy plans to configure four missiles on a MK 3 patrol boat, as shown in Figure 6. Analyses indicate that if one warhead detonates, the remaining warheads and all the solid propellant will sympathetically detonate. OP-5¹ and Porzel² indicate that for the PENGUIN propellant, a TNT equivalency of 25% is appropriate for determining the MCE. Based on a single missile (warhead plus propellant contribution) the ESQD arc is 300 feet. For a four missile (MK 3) configuration the ESQD arc is 485 feet. Again in this instance, blast determines the arc, not fragmentation.

Because of the questions raised by this and other studies, the NESIP has undertaken a program to determine the TNT equivalency of several standard Navy gun and rocket propellants. The tests will be conducted on several types of propellants (single and double base solid propellants as well as two types of gun propellants). Care is being taken to maintain that all charges are above their critical diameter for detonation, and that the initiation stimulus is more than sufficient to achieve detonation (explosive boosters whose weights are approximately 10% of the propellant weight being tested).

Another recently completed study is that of the Mine Neutralization System Bomblet (DESTRUCTOR MK 14 MOD 0) (Figure 7). This is an underwater bomb designed to be dropped from a submersible. The case is non-metallic, with a nine-pound lead ballast in the nose. Calculations indicate that the weapon in its shipping container will mass detonate when stacked in a side-by-side configuration. The ESQD hazard range is determined solely by airblast; the case and container fragments do not contribute to the range. Up to nine weapons can mass detonate and still meet the desired hazard criteria at 500 feet. The palletized configuration of this weapon has not, as yet, been determined. These results will be used in defining a "pallet load." The lead ballast in the nose of each bomblet constitutes a special fragment hazard, in that it is massive

and may be expelled nearly intact. If the ballast is expelled near an optimum launch angle, it could go up to four miles. Moreover, the ballast would constitute a single fragment or a relatively small number of fragments so that the areal density at 500 feet should not exceed the acceptable hazard criterion.

The NESIP (Milestone II-1) program effort has been an on-going program for about eight years. During this time, it has answered safety/hazard questions for many Navy weapon systems. Moreover, it has produced a broad data base which can be applied not only to safety problems but to vulnerability problems as well. One example of this data base is the answer to the question "What are the initial fragment velocities produced by Navy weapons?" The answer is usually known for fragmenting weapons; however, fragmentation data is usually not of concern to the torpedo designer. Table 3 presents a compendium of NESIP fragment velocity data extracted from the data base.

The results of the entire Milestone II-1 effort can be summarized as follows:

All current Navy weapons and scenarios which have been tested or analyzed thus far are either acceptable hazards near 500 feet or could be made so.

The program is continuing. As indicated above, the emphasis this year has been on problems associated with submarine tenders (ESQD arcs for workshop accidents and sympathetic detonation inhibitors for MK 48 torpedoes) and the TNT equivalency of propellants. Future efforts will continue the propellant equivalency work and begin studies of preformed fragment warheads and LFORM ammunition and ships.

TABLE 1 NESIP PROGRAM

MILESTONE NO.	TASK
	I. OVERSIGHT AND REVIEW OF PROGRAM
I-1	PROVIDE NESIP SUPPORT SERVICES TO OPNAV
I-2	CONDUCT PERIODIC REVIEWS OF NESIP
I-3	CONDUCT AMHAZ REVIEWS
I-4	MAINTAIN WAIVER DATA BANK
I-5	MAINTAIN CAPABILITY FOR EXPLOSIVES SAFETY INSPECTIONS/SURVEYS, ON AN 18-MONTH BASIS, AFLOAT AND ASHORE
I-6	REVIEW ACTIVITY MASTER PLANS FOR EXPLOSIVES SAFETY IMPLICATIONS
I-7	COMBINED WITH ACTION ITEM I-5
I-8	MAINTAIN CURRENT THE STANDARD EXPLOSIVES SAFETY INSPECTION CHECKLIST FOR SHIPBOARD INSPECTIONS
	II. ISSUES WITH DDESB
II-1	PROSECUTE NAVAL EXPLOSIVES SAFETY TEST PROGRAM
II-2	INCORPORATE MAGAZINE IMPROVEMENTS IN LFORM AMMUNITION SPACES IN AMPHIBIOUS WARFARE SHIPS
II-3	CHANGE HOMEPORT OF NORFOLK-BASED AOE's
II-4	PREPARE AND PRESENT ACTIVITY OR REGIONAL MASTER PLANS TO DDESB
II-5	CORRECTION OF DDESB-REPORTED EXPLOSIVES SAFETY DEFICIENCIES
II-6	FORMALIZE NAVY INTERIM EXPLOSIVES SAFETY STANDARDS (OPNAVINST 8023.21A)
II-7	ESTABLISH STANDARD PROGRAM FOR COMPUTING NET EXPLOSIVE WEIGHT (NEW)
	III. OTHER SIGNIFICANT PROBLEM AREAS
III-1	IDENTIFY MILCON PROJECTS FOR INCLUSION IN INVESTMENT PROGRAM 55 (DIRECTED EXPLOSIVES SAFETY INVESTMENT PROGRAM)
III-2	PROCESS WAIVER REQUESTS/UPDATES/VALIDATIONS
III-3	ANALYZE ABSLA'S TO MINIMIZE WAIVER NEEDS
III-4	NO ITEM ASSIGNED
III-5	CANCELLED
III-6	CLOSURE OF PORT CHICAGO HIGHWAY
III-7	SMALL ARMS TARGET RANGES: DESIGN, CERTIFICATION, WAIVERS
III-8	PROSECUTE THE NAVY EXPLOSIVES SAFETY FACILITIES PROJECT
	IV. POLICY GUIDANCE MATTERS
IV-1	MAINTAIN CURRENT THE NAVY EXPLOSIVES SAFETY POLICY GUIDANCE DOCUMENTS (e.g., OPNAVINSTS 8023.2/13/20/21, 8020.8, 5101.1, ETC.)
IV-2	INSURE CURRENCY OF EXPLOSIVES ACCIDENT AND INCIDENT (EXPLOSIVES MISHAP) REPORTING DIRECTIVE AND RESPONSIVENESS THERETO AT COMMAND LEVELS

TABLE 2 WEAPONS AND SCENARIOS TESTED/ANALYZED

<u>TORPEDOES</u>	<u>PROJECTILES</u>	<u>MISSILES</u>	<u>BOMBS</u>
MK 16	5"/54 (A-3)	TOMAHAWK	MK 82
MK 46	5"/54 (EXP. D)	HARPOON	MK 83
MK 48	5"/54 HIFRAG	PENGUIN	
	76 mm	2.75" FFAR	
	5" GUIDED	TOW	
		SPARROW	

ESQD FOR SHIPS

SSN 688 CLASS*
SSN & SSRN (ALL CLASSES)*
MK 3 PATROL ROAT*
FFG-7**

MCE/NEW: MAGAZINES

FFG-7
AS-18*
MACHRIHANISH

SHIP VULNERABILITY TO PIER-SIDE ACCIDENTS

DDG-2

SYMPATHETIC DETONATION INHIBITOR DESIGN

MK 16 TORPEDO
MK 46 TORPEDO
5"/54 (A-3) PROJECTILE
MK 48 TORPEDO

- * INCLUDES NESTED SHIPS
- ** WORK IN PROGRESS

TABLE 3 NESIP FRAGMENT VELOCITIES

MUNITION	EXPLOSIVE	CASE MATERIAL	CASE THICKNESS (IN.)	AVERAGE VELOCITY (FT/S)**	INITIAL VELOCITY (FT/S)***
MK 16 TORPEDO	HBX-1	BRONZE	0.125	9100	—*
MK 46 TORPEDO	PBXN-103	ALUMINUM	0.250	8200	—*
MK 48 TORPEDO	PBXN-103	ALUMINUM	0.250	9300	—
5"/54	A-3	STEEL	0.66	4360	4630
76 mm (BARE)	A-3	STEEL	0.66	3530	3680
76 mm (CANNISTERED)	A-3	STEEL	0.66	3070	3160
TOMAHAWK (BULLPUP WARHEAD)- IN SHIPPING CONTAINER	H6/ PICRATOL	STEEL	0.78	6000	7300
MK 82 (SINGLE BOMB)	H-6	STEEL	0.50	6300	8000
MK 82 (PALLET)	H-6	STEEL	0.50	9300	11,500
MK 83 (SINGLE BOMB)	H-6	STEEL	0.50	7300	8500
MK 83 (PALLET)	H-6	STEEL	0.50	10,200	12,700

* EXTRAPOLATIONS ARE NOT INCLUDED FOR THINLY-CASED MUNITIONS

** AVERAGE VELOCITIES ARE BASED ON DIFFERENT MEASURED DISTANCES FOR EACH MUNITION

*** BASED ON EXPONENTIAL VELOCITY DECAY MODEL

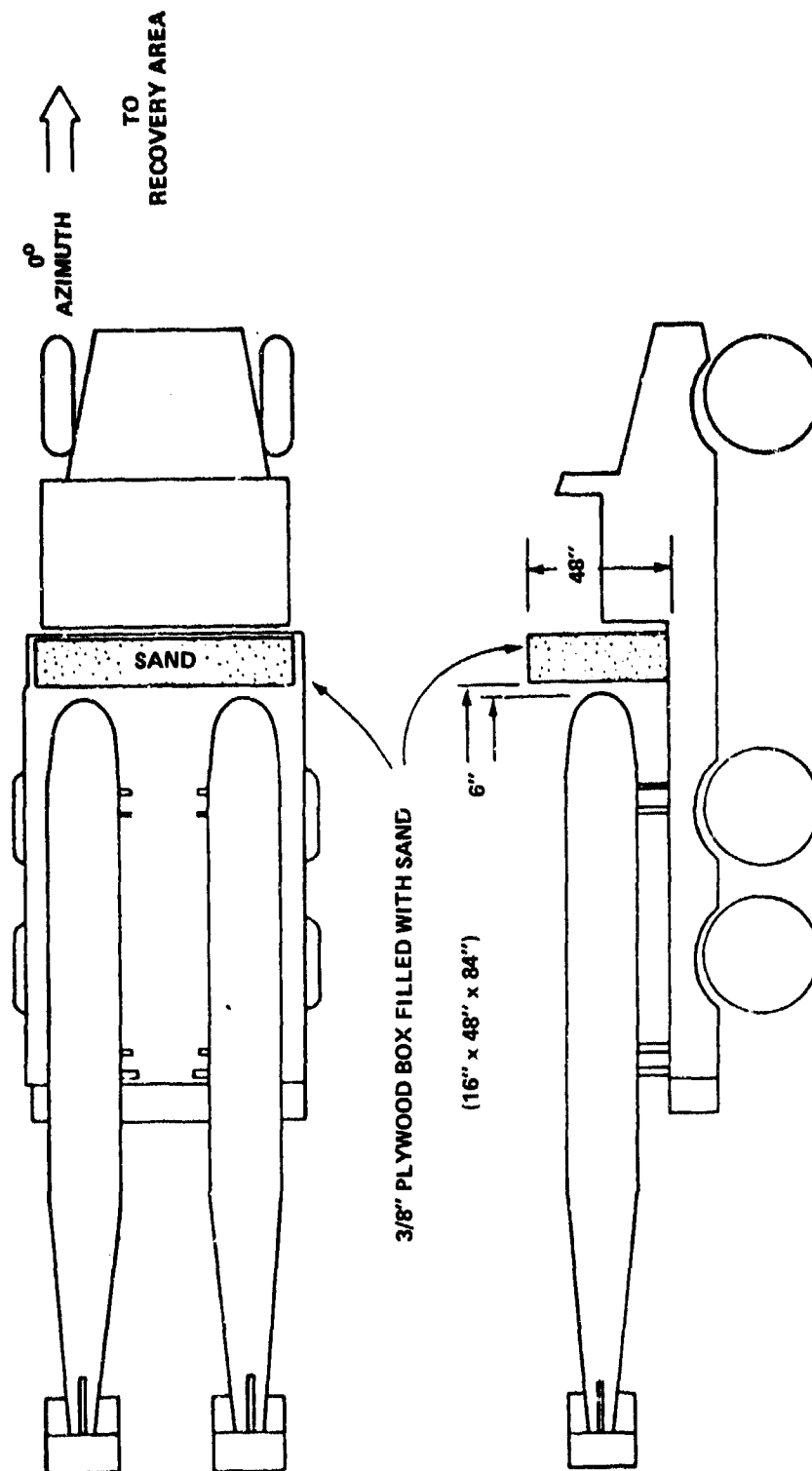


FIGURE 1 MINIMAL BLAST AND FRAGMENT SHIELD

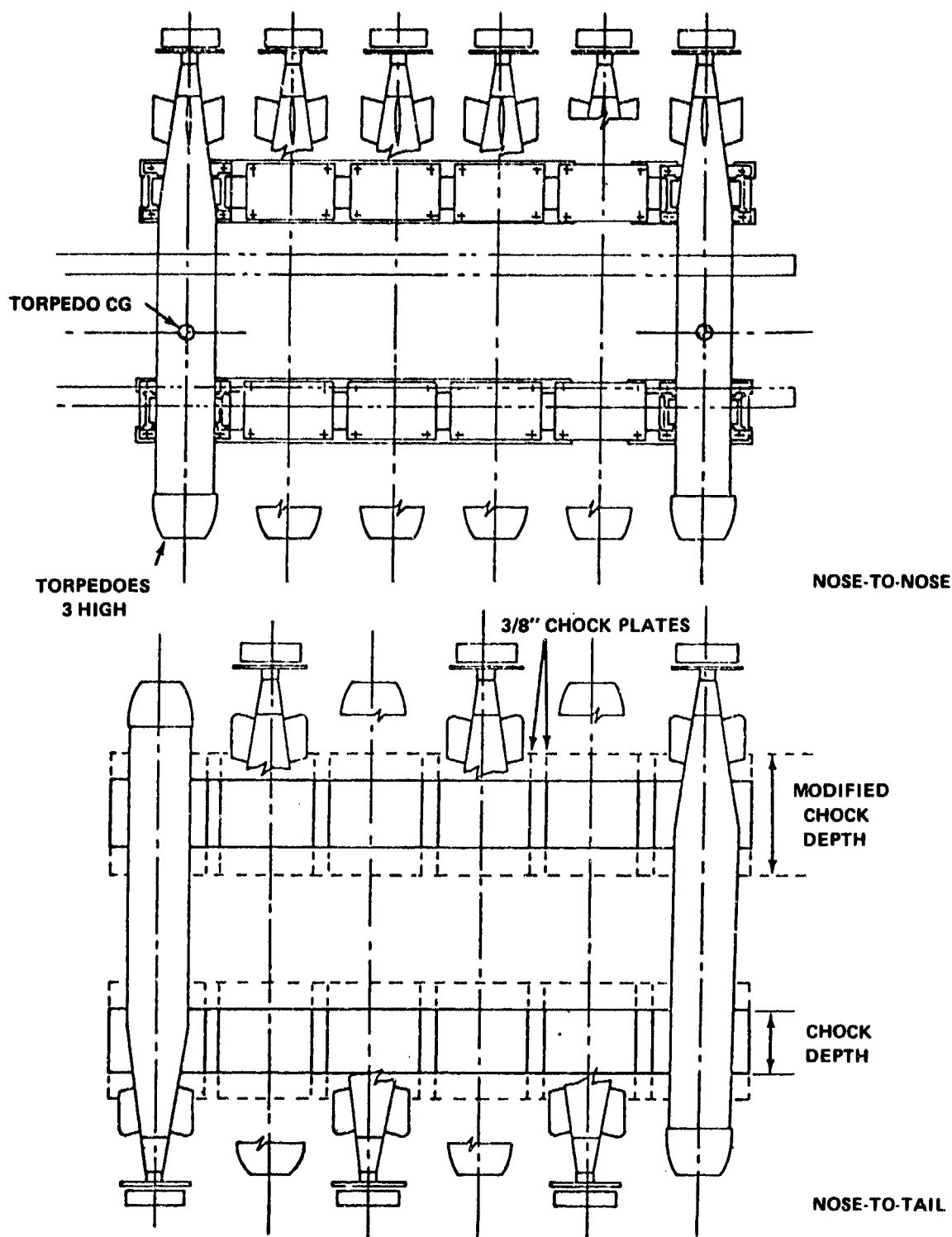


FIGURE 2 NOSE-TO-NOSE VS NOSE-TO-TAIL TORPEDO ARRANGEMENT

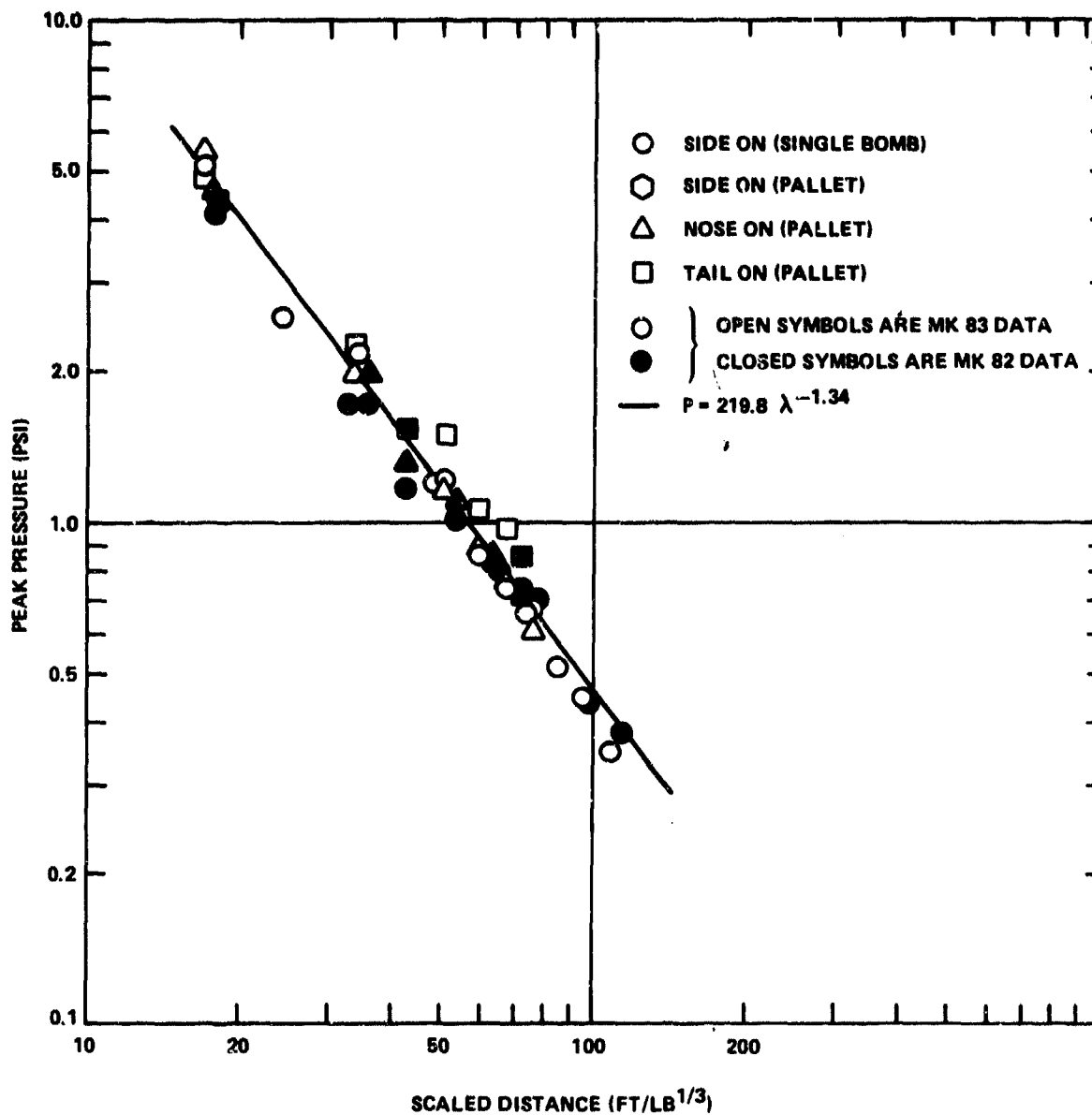


FIGURE 3 NESIP GENERATED MK 90 DATA

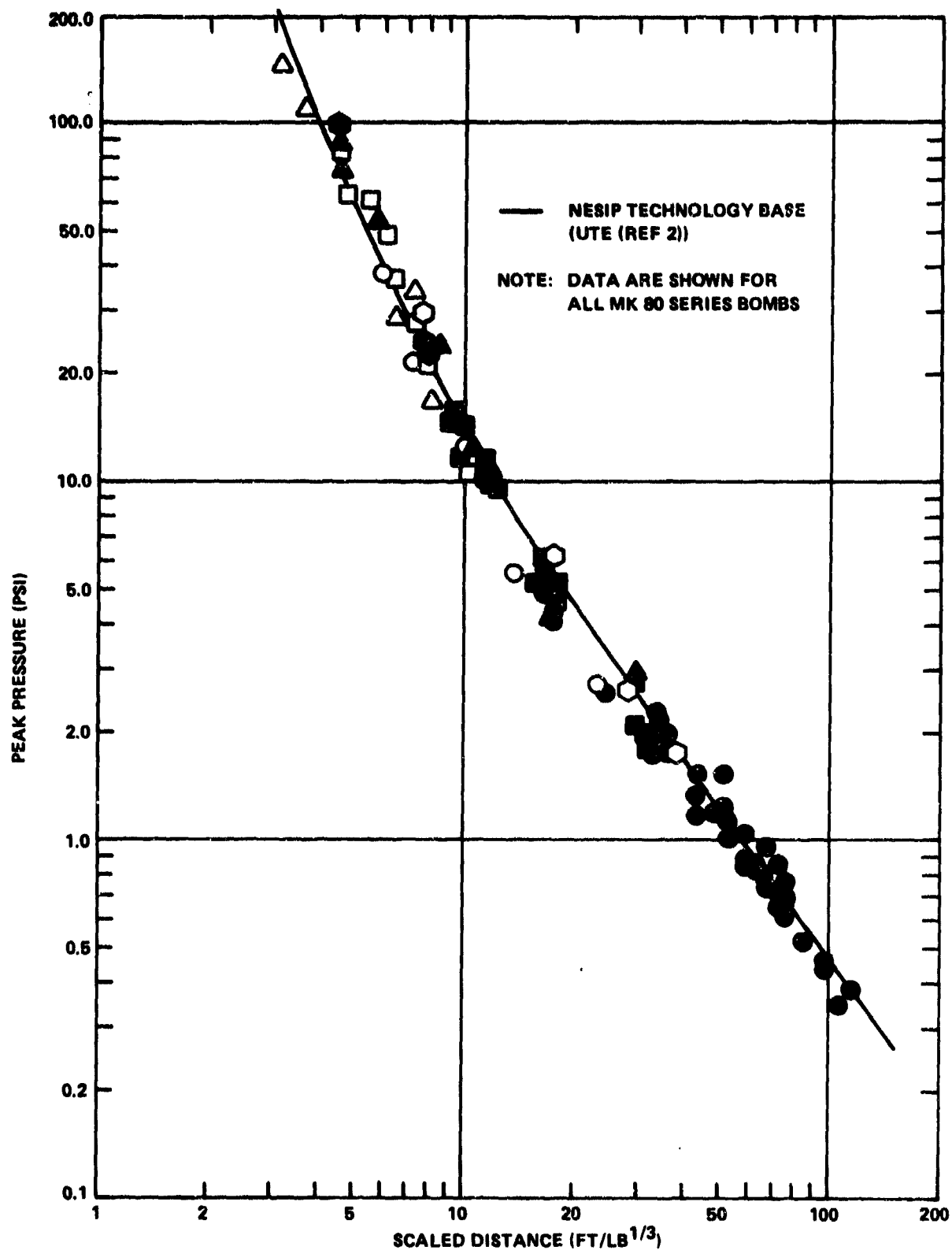


FIGURE 4 COMPILED MK 80 SERIES AIRBLAST DATA

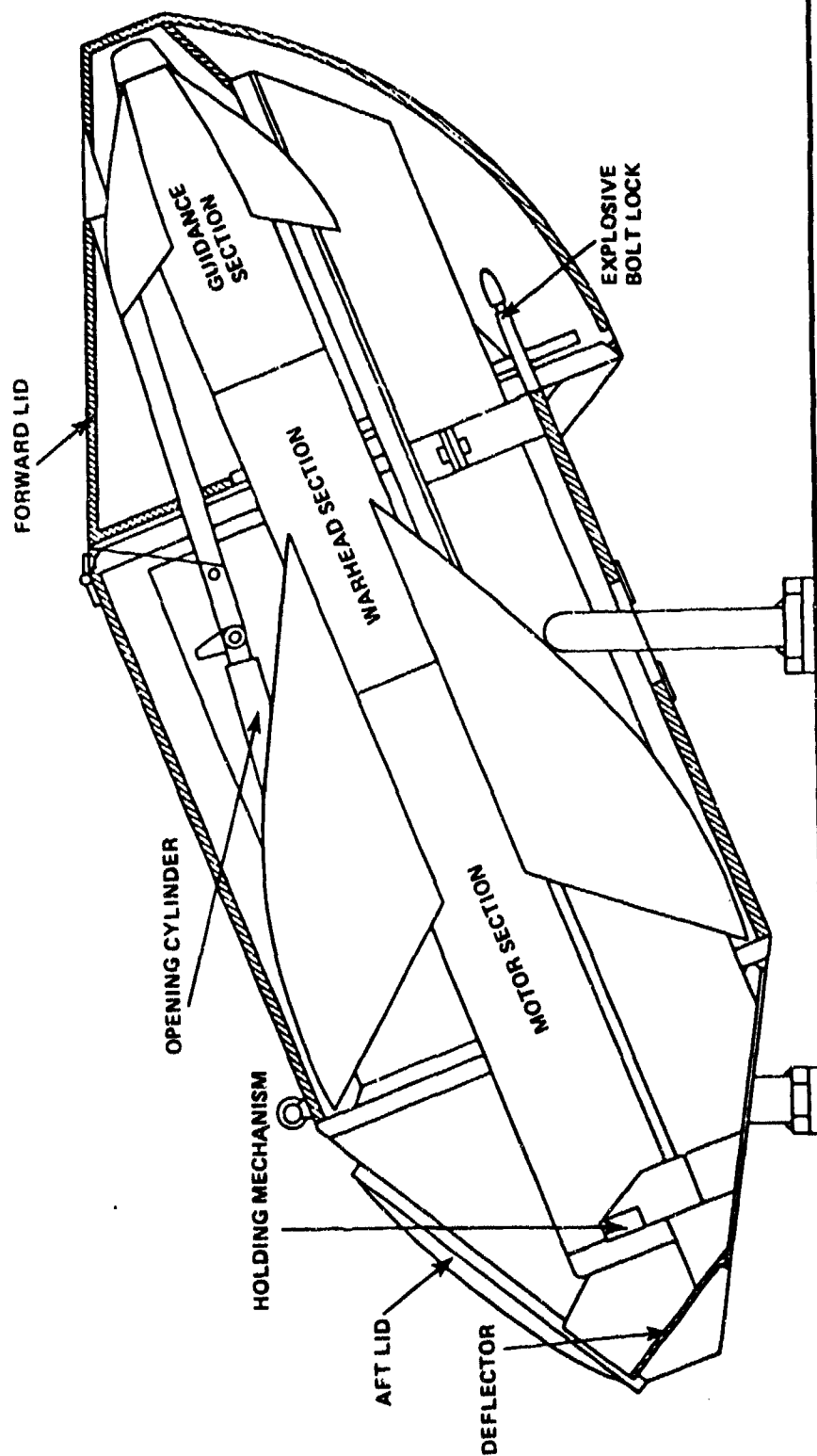


FIGURE 5 PENGUIN IN BOX LAUNCHER

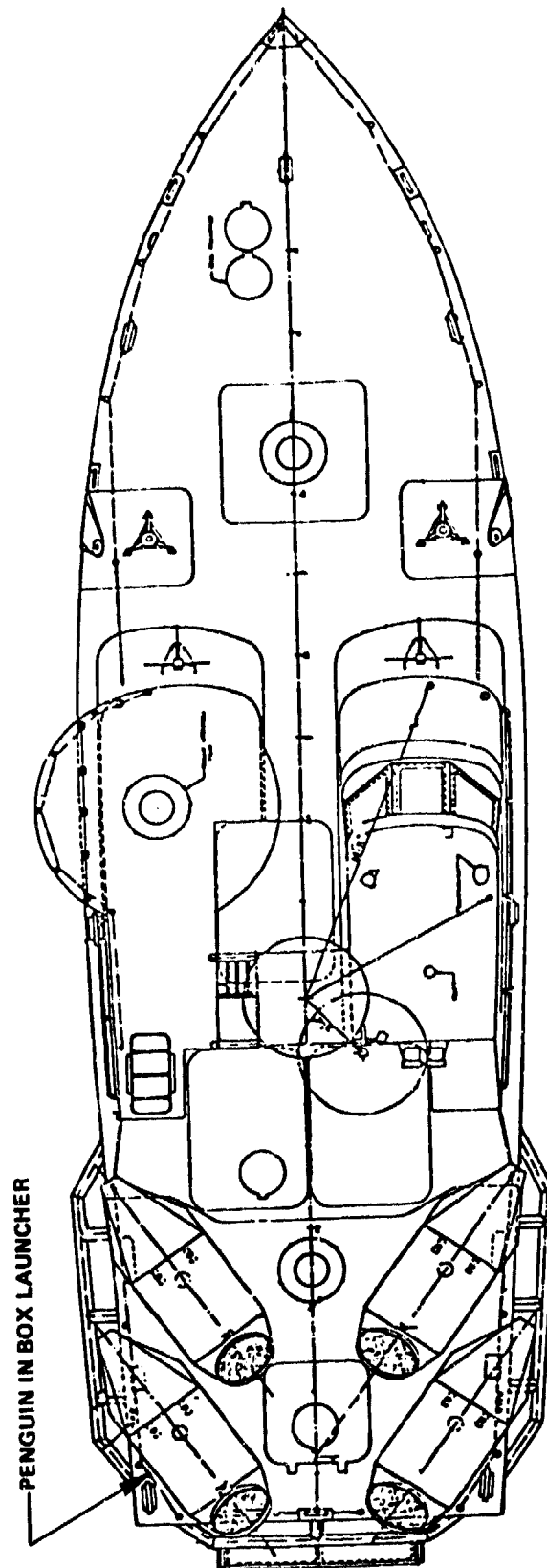


FIGURE 6 PATROL BOAT MK 3 CONFIGURATION FOR PENGUIN/BOX LAUNCHERS

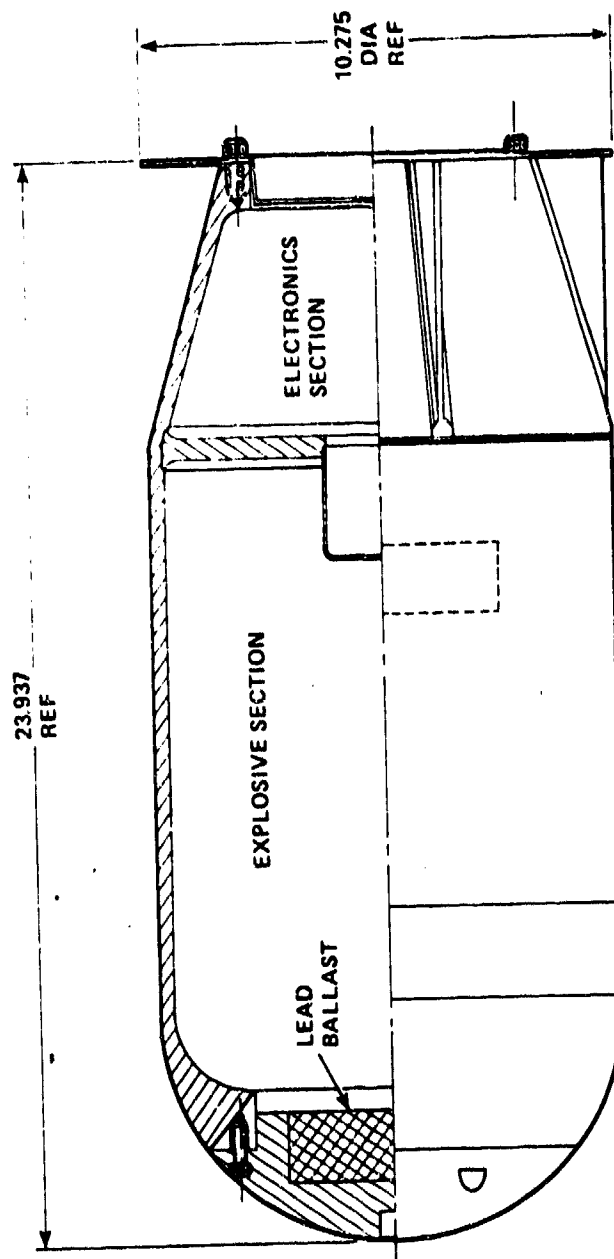
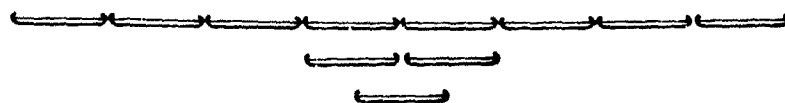


FIGURE 7 MINE NEUTRALIZATION SYSTEM BOMBLET (DESTRUCTOR MK 14 MOD 0)

AD P000437

**YIELD AND BLAST ANALYSES
WITH A
UNIFIED THEORY OF EXPLOSIONS**



**FRANCIS B. PORZEL
NAVAL SURFACE WEAPONS CENTER**

YIELD AND BLAST ANALYSES WITH A UNIFIED THEORY OF EXPLOSIONS (UTE)

Summary

Yield is the most significant single number measured on any explosion because all effects --sympathetic reactions, fragments, blast damage-- derive from it. UTE offers the only adequate way to relate all explosions: non-ideal, any media, over all ranges in air, underwater, underground, confined spaces, heavy cases etc. The Form Factor and Lead Time are new extensions intended for safety analyses. A key idea in the form factor is to define average energy density in the blast wave relative to the peak value at the shock; it is the tacit assumption in scaling now. Lead Time means the difference in TOA between a sound signal and a shock wave; it scales, is a sensitive measure of yield and is nearly constant at long range. Applications include: absolute measure of prompt and delayed yields for blast, sympathetic reactions, fragments, propellant yield, surface effects, analysis with sparse data and simplified instrumentation.

YIELD AND BLAST ANALYSES WITH A UNIFIED THEORY OF EXPLOSIONS

Francis B. Porzel
Naval Surface Weapons Center

1. UTE Methods for New NESIP Problems

Yield means the blast or hydrodynamic energy released by any explosive and is the single most significant number to be measured in tests of any explosion.

All effects derive from yield and in principle can be predicted using it:

- * Primary fragments: their sizes, shape, number, initial velocity of trajectory,
- * Close-in blast, regarding both initial containment and secondary fragments,
- * Low pressure damage, especially to specify the range where 1 psi occurs,
- * All sympathetic reactions -detonation, deflagration, burning, their degree- be it directly from blast or via fragment and thermal loads it produces.

In fact, the Maximum Credible Event (MCE) really means the overall yield.

The Unified Theory of Explosions (UTE)¹ was developed for just such needs. UTE offers the only general way to describe any explosion: nuclear, non-ideal HE, over all ranges in air, underwater, underground, confined spaces, heavy cases etc. UTE offers two dozen concepts as tools to treat dozens of real non-ideal effects, nearly all being unknown or ignored in idealized classic theory and hydrocodes. A key idea in UTE is "prompt vs delayed" energy; it asserts that natural processes release some energy instantly, some more slowly, reinforcing blast farther out; much is trapped behind the negative phase too late ever to support the shock front. This separation is manifest by phenomena like afterburning, secondary shocks, and the most dramatic feature of any explosion: The fireball is delayed energy.

The NESIP Technology Base² itself rests on the Unified Theory of Explosions and much success in NESIP tests is due to versatile and accurate analyses with UTE.

Current NESIP problems now raise new and more specific questions about yield. For sympathetic reactions and in the design of inhibitors to prevent them:

- * How much energy is released in a partial or in a low-order detonation?
- * What are the actual prompt and delayed fractions in afterburning explosives?
- * How to live with the large scatter of pressures measured in the real world?
- * How to live with the narrow range of feasible, affordable measurements?
- * What are the absolute energies involved in various modes of energy release?

For hazards involving propellants:

- * What are the yields of a propellant on an absolute basis, detonated alone?
- * If set off by an explosive warhead, how much does the propellant add to the prompt or delayed yield of the main explosion? Any new hazards?

To meet these new needs for NESIP, two major advances have been developed for UTE:

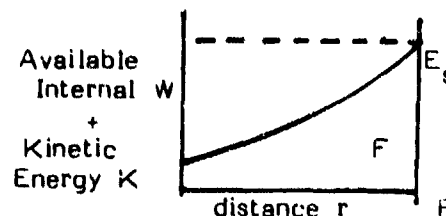
- * A "form factor" method for bookkeeping the energy within a blast wave, to describe variable rates of afterburning, notably in heavily aluminized HE.
- * A "lead-time" method, a simple reliable way to get yield from time-of-arrival.

They have widespread application to many explosion problems for NESIP and others. The purpose of this paper is to describe these new methods briefly, show the code and to test them by comparisons with a broad spectrum of field measurements.

1. All references are listed at the end of the text, before Appendix A.

2. Form Factor Concept and Method

The form factor F is defined to mean the average hydrodynamic energy $W+K$ in the wave relative to their peak sum E_s at the shock front. It is the ratio of the area shown here as F to the "square wave" as if E were constant at E_s .



If we define the yield $Y(R)$ at any shock radius R as the integrated sum

$$Y(R) = 4\pi \int_0^R (W + K) r^2 dr$$

normalize the integral, multiplying/dividing by the peak overpressure $P_s - P_0$, and by the mean value of any factor (like the available fraction A of energy at P)

$$Y(R) = \frac{4\pi}{3} R^3 (P_s - P_0) A \int_0^1 \left[\frac{W + K}{P_s - P_0} \right] \frac{1}{A} \left[\frac{r}{R} \right]^2 \frac{dr}{R}$$

Thus F becomes the dimensionless fraction specified by the definite integral.

Rigorously, we can just simply define a form factor F such that

$$Y(R) = \left(\frac{4\pi}{3} \right) R^3 \frac{P_s - P_0}{P} A F$$

This definition for F is deceptively simple but is a powerful hydrodynamic tool. Many man-years and \$millions were spent since World War II on elaborate hydrocodes, mostly to calculate pressure-distance curves with highly over-simplified models. Yet, both A and F are readily prescribed by the overpressure ratio $(P/P_0 - 1)$; so we can always obtain the shock radius R at any pressure P simply from

$$R^3 = \frac{Y(R)}{(4\pi/3) P A F} \quad P = \text{overpressure, units consistent with } Y \text{ and } R$$

To calculate R , the code decreases $Y(R)$ from its initial value Y_0 by decrements

$$dY = -4\pi \underbrace{Q R^2}_{\text{losses}} dR + \underbrace{\text{Afterburning}}_{\text{gains}}$$

This can be done in bold steps, decreasing the pressure about 25% at each step. The same steps are used also for integrating the time of arrival of the shock wave.

A and F always appear together and here is an exact way to calculate AF . For exposition, let Q here mean the net loss (waste heat) and gain (afterburning). Then the ratio of the dissipation equation ($dY=$) to the definition for F ($Y=$):

$$\frac{dY}{Y} = \frac{-4\pi Q R^2 dR}{(4\pi/3) R^3 P A F} = -\frac{3(Q/P) dR}{A F R}$$

gives

$$\frac{dY/Y}{dR/R} = \frac{3Q/P}{AF} \quad \text{and} \quad AF = \frac{3Q/P}{d \ln Y / d \ln R}$$

The machine code uses the local value of $d \ln Y / d \ln R$ from each previous step, because $d \ln Y / d \ln R$ varies slowly, from about -0.5 at high pressure to -1 at low. Thus AF is bounded between $6Q/P$ at high pressures and $3Q/P$ at low pressure. Figure 1 shows these bounds and the transition region for the function AF vs P .

Analysis shows that AF goes like $A(\text{shock})/3$ at high pressure, like $AP^2/3$ at low, and a suitable approximation, to a few percent in Y , without use of $d \ln Y / d \ln R$, and with a single parameter $1/3$ for both high pressures and low, is:

$$AF \approx \frac{A(\text{shock})}{3(1 + P_0/P)^2}$$

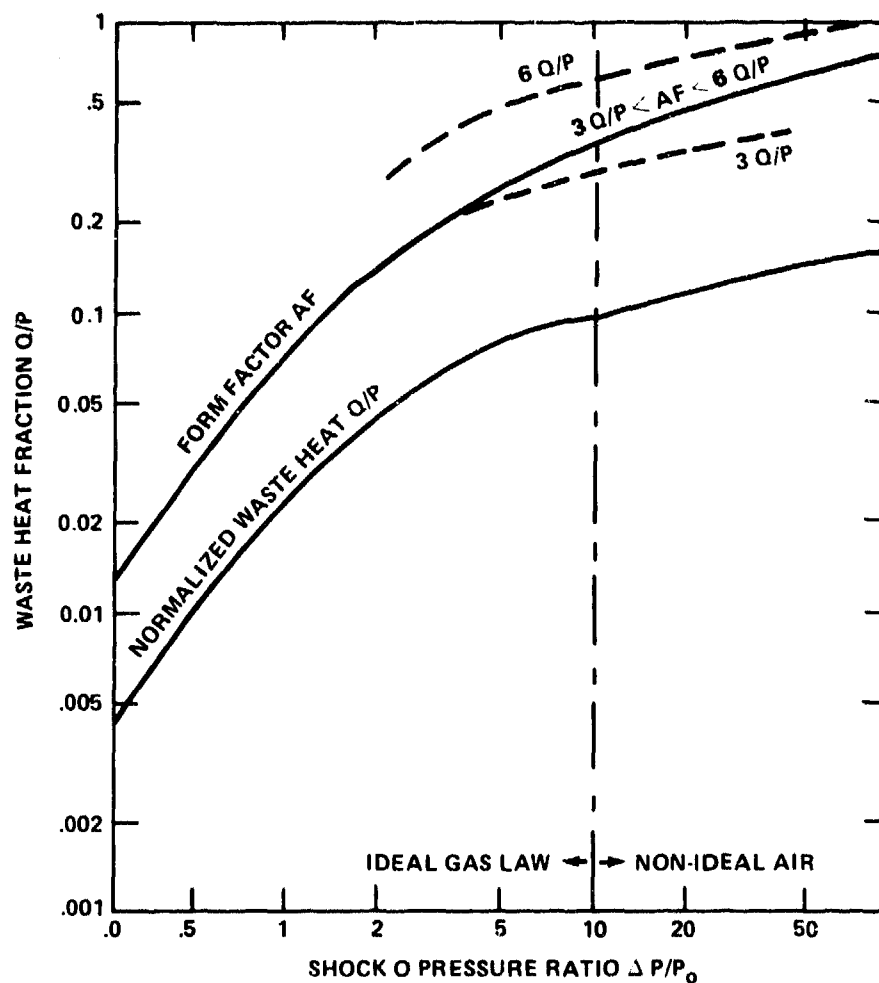


FIGURE 1. WASTE HEAT FRACTION AND FORM FACTOR VS. OVERPRESSURE

3. Lead-Time Concept and Method

Lead-time is a time-of-arrival method for measuring yield. With it we seek:

- * An over-all measure of the shock history, sensitive to its early behavior.
- * A way to circumvent uncertainty in yield from scatter in pressure measurements.
- * Simpler instrumentation than the sophistication needed for good pressure data.

Time-of-arrival is an excellent measure for high pressure supersonic blast^{3, 4, 5}; but at low pressure, TOA becomes sonic and an insensitive measure of shock strength. On the other hand, time-of-arrival can be measured with exceedingly high accuracy. Let us then measure the difference in time between the shock and a sound signal and define, at any range R:

$$\text{Lead-time} = \text{sound arrival} - \text{shock arrival time}$$
$$LT \quad R/C \quad - \quad T$$

This quantity ought to and does ⁹scale, is a sensitive measure at low pressures. Best of all, it becomes insensitive to the range at acoustic strength, so that one does not need an accurate gauge location --if the sound arrival is also measured.

As shown in Figure 2a, the early shock is highly supersonic: $U \gg C$. There

$$R = \int U dt \quad \text{or} \quad T = \int dR/U \quad \text{are both sensitive measures of } q_{\text{yield}}.$$

If we plot $\ln R$ vs. $\ln T$ as in Figure 2b, sound speed is a straight line, slope 1. But the shock time-of-arrival approaches it, partly because of the logarithmic plot. Also, the lead-time ceases to grow as the "overvelocity" vanishes at low pressure. As shown in Figure 2c, the lead-time approaches a scalable constant at long range.

In machine calculations, time-of-arrival adds up, using the same steps as for $Y(R)$:

$$TOA = \int dR/U \quad U = \text{local shock velocity}$$

Because of the finite step size, an average value for $1/U$ is used; thus

$$dT = T_{i+1} - T_i = [1/U_{i+1} + 1/U_i] * [R_{i+1} - R_i] / 2$$

The time-of-arrival and the lead-time are scaled just as for distance scaling.

When the shock is strong, it is convenient, and a more independent measure to scale

$$\text{Relative yield} = (\text{Measured TOA} / \text{reference TOA})^3.$$

When the shock is weak (below the transition pressure) we scale lead-times as

$$\text{Relative yield} = (\text{measured LT} / \text{reference LT})^3.$$

Figures 3 and 4 illustrate practical reasons for developing the lead-time method.

Large scatter in field pressure measurements is no doubt real, probably intrinsic, because a pressure gauge "feels" only the pressure at its surface, regardless of how rapidly pressure may vary in a boundary layer next to that surface^{6, 7}.

Figure 3 shows how pressure suffers from real variations both in space and in time

Spacewise, the dust-laden boundary layer, brush, rough terrain all deplete yield.

Timewise, the shock jets, and "rings" as it goes, in patterns that shift with time.

The time-of-arrival will more nearly follow the grand-scale average growth

of the hemisphere in free air above the ground surface, as idealized in Figure 4.

While some lag may occur due to drag in the boundary layer, the corresponding error in lead-time is not nearly as severe as the pressure reduction from the same layer.

Field measurements will test whether this expectation of less scatter is realized.

We also expect the lead-time will better "remember" the early history of the wave.

If the explosion starts at low speed, is then sustained by afterburning,

the TOA could be longer, the lead-time less, than by an instantaneous explosion.

On the other hand, compensation occurs: the energetic shock wastes more energy early and after running a long time more slowly, may arrive later than the afterburner.

UTE form factor calculations will show which is the stronger effect and how much.

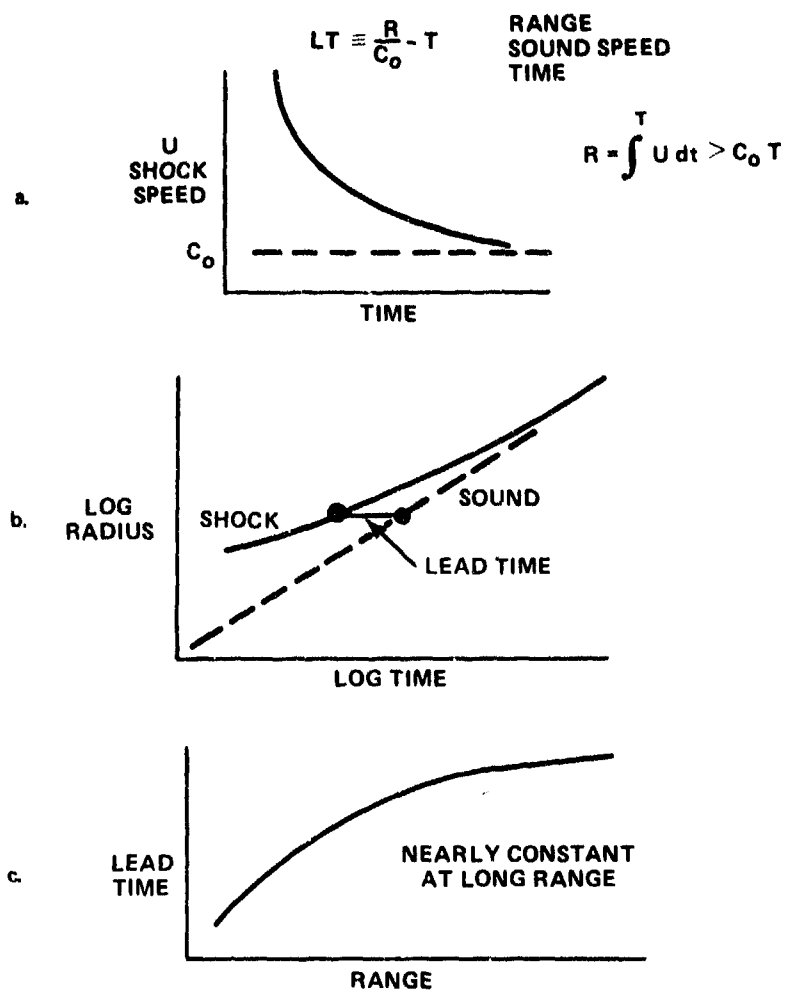


FIGURE 2. LEAD TIME METHOD

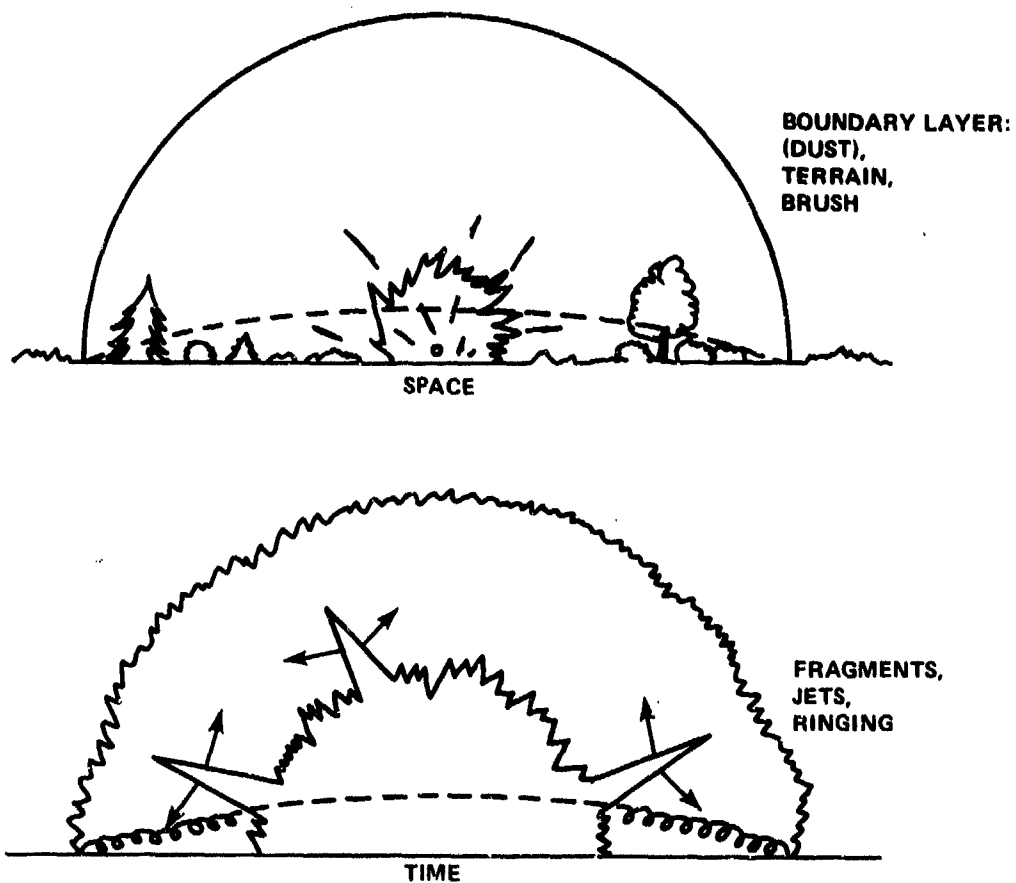


FIGURE 3. LOCAL PRESSURE VARIATIONS IN SPACE AND TIME

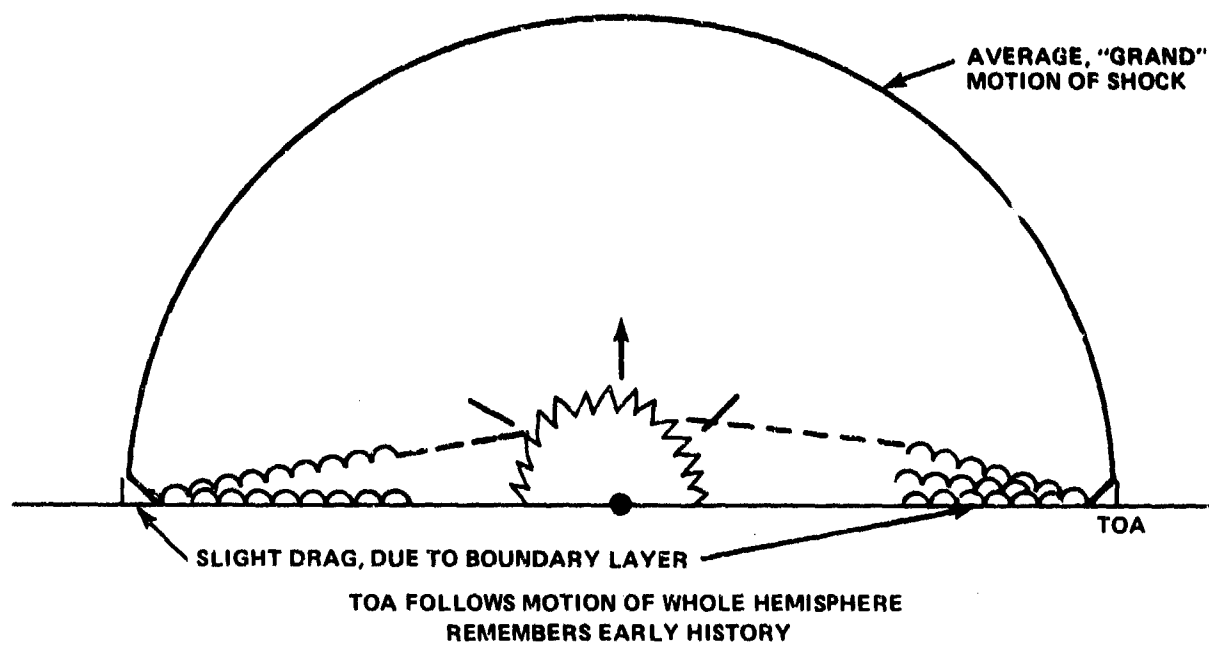


FIGURE 4. PERTURBATIONS ON TIME OF ARRIVAL

4. Machine Code and Printout

Appendix A lists the complete code, is well-annotated and may be self-explanatory. Written in advanced BASIC for a personal computer, it uses two-digit variables, compound statements in lines etc., but in principle could be copied and run as is.

Input parameters appear at the top of the printout (Tables 1, 2). They include:

Trial yield Y_0 , here in joules; 4.188×10^{12} joules = 1 KT, 4.188×10^6 = 1 KG,
Mass M of explosive and immediate case, their specific energy H relative to air,
Initial radius R_0 : HE charge, isothermal sphere (nuclear), isobaric sphere (gas),
Ambient conditions: pressure P_0 , sound speed C_0 , and/or density D_0 ,
Afterburning fraction AB of Y_0 ; Transition pressure P_t , strong to weak shock.
If any above are missing, the code usually supplies a default value or computes one.
Input measurements for evaluation of yield include pressure P , range X , and/or TOA.

Major Options are included regarding input parameters, input data, and print-out.

Input any 3 of 4: yield Y_0 , initial pressure P_i , mass M or specific energy H .

If any are omitted (usually P_i is unknown), the code will calculate it.

If all are given, the code will recompute H to make it consistent with the rest.

If P , X or T data are omitted; the code prints predictions anyway.

Time may be input either as discrete data or by a fitted curve. (So could distance).

Print-outs can be predictions only, + diagnostics, or yield analyses with graphs.

Major Computation Blocks (15 in all) are set off by remarks in the LIST.

Of interest as a guide to the code, they are listed on the first page of Appendix A.

Computation Procedure. After the predictions for conditions at the charge radius:

1. Select a new pressure; next data or reducing the previous P by $10^{-1} = 1/1.26$.
2. Compute waste heat Q , afterburning increment YA , available energy fraction A , form factor w/A as AF , shock velocity U ; all are functions of the pressure.
3. Compute yield decrement Y_1 , afterburning YA , new yield $Y = Y_i - Y_1 + YA$, then iterate for "mass-corrected" radius $Z = (R^3 + H \cdot M)^{1/3}$, then get R from Z .
4. Calculate TOA from $dT = dR/U$, and new TOA = old TOA + dT .
5. Calculate relative yield from range, essentially as (measured/calculated)^{cubed}
6. Calculate relative yield from TOA or lead-time, as (measured/calculated)^{cubed}.
7. Summarize with an average yield relative to input yield, for range and/or TOA including the standard deviation of the measured yields about their mean.

Table 1 illustrates a printout of close-in predictions of a massless explosion: $M=0$. The initial pressure P_i and radius R_0 mark the end of a nuclear radiative phase. The isothermal sphere implies a "square wave", i.e. larger form factor than normal, nor can the interior gas be accelerated instantly to reproduce a normal blast wave. The code allows it to do so gradually by computing an "inertial mass" as shown. The point is: In a gaseous explosion, spark gap, or any other non-ideal blast wave, a like initial dissimilarity occurs and will be so accommodated with all UTE codes. We note that the inertial mass found, 544 kg \approx mass of air engulfed at that radius.

Table 2 illustrates another printout option that graphs the relative yield from TOA. It compares predicted lead-times for a Mk 48 torpedo with the field test data. Initial yield included a ground reflection factor 1.5 and afterburning of PBXN 103. The ambient conditions are for the test site at Socorro, NM, altitude \approx 3200 feet. The input mass was 1038 pounds, essentially the warhead, most of which is PBXN-103. This was the very first test of the code. The relative yield is plotted as T (time). The TOA yield, .90 predicted, means lead-time itself is within $.9^{1/3} = .965$, 3.5%. Also shown, not plotted, are the pressure results: relative yield 1.099, 3.2% in R .

TABLE 1

RUN

UNIFIED THEORY OF EXPLOSIONS (UTE), FORM FACTOR METHOD AND TIMES
NUCLEAR COMPOSITE DATA, NOLTR 72-209

Total Yield = 4.18879E+12		Input mass = 0		Input H = .25
Ambient pressure = 100000		Ambient density = 1.16271		
Ambient sound speed = 347		Inertial mass = 544.037		
Afterburning fraction = 0		Complete at Pt/Po = 1.99526		
O'PRESSURE	RADIUS	YIELD	ARRIVAL TIME	LEAD TIME
79432.9	4.21063	.839084	9.50147E-06	.0121249
63095.8	4.51563	.818802	1.31606E-05	.0130002
50118.7	4.83647	.798519	1.74959E-05	.0139205
39810.7	5.17656	.778182	2.26698E-05	.0148954
31622.7	5.60958	.75347	3.00725E-05	.0161359
25118.8	6.06141	.728707	3.8739E-05	.0174293
19952.5	6.53499	.703973	4.89312E-05	.0187839
15848.9	7.03314	.679343	6.09603E-05	.0202075
13600	7.37917	.663073	7.01477E-05	.0211955
12589.3	7.55862	.654897	7.51919E-05	.0217076
10000	8.11427	.630716	9.20832E-05	.023292
7943.29	8.70291	.60686	1.12161E-04	.0249683
6309.56	9.32753	.583393	1.36065E-04	.0267445
5011.86	9.99126	.560374	1.64565E-04	.0286287
3981.06	10.6957	.537912	1.98504E-04	.0306249
3750	10.8641	.532836	2.07216E-04	.0311015
3162.28	11.3621	.518595	2.34559E-04	.0325092
2511.89	12.079	.499882	2.78187E-04	.0345317
1995.26	12.8509	.481772	3.30994E-04	.0367034
1584.89	13.6825	.464255	3.9494E-04	.0390359

TABLE 2

RUN

UNIFIED THEORY OF EXPLOSIONS (UTE), FORM FACTOR METHOD AND TIMES

INHIBITOR TESTS ON MK48 TORPEDOES, JUNE 1982, PRELIMINARY DATA SHOT #1

Total Yield = 3.85452E+09 Input mass = 471.252 Input H = .5
 Ambient pressure = 83000 Ambient density = .991783
 Ambient sound speed = 342.29 Calculated Initial Pressure = 1.08279E+07
 Afterburning fraction = .3 Complete at Pt/Po = 1.99526

P/PO	TOA Yield	Meas. T	.6	Relative TOA Yield	1.4
.456874	.884941	.0679804	.	T	.
.376298	.762048	.0809575	.	T	.
.223453	.938644	.128332	.	T	.
.201855	.88243	.140158	.	T	.
.154507	.983428	.176062	.	T	.
.0930362	.933178	.268408	.	T	.
.0880522	.915598	.280596	.	T	.

Yield, relative to input = 1.09959

Standard deviation, % = 21.1099 based on 7 samples, P=> 1 psi

TOA Yield, relative to input = .900038

Standard deviation, TOA yield, % = 7.77284 based on 7 samples

5. Test of Methods with Nuclear and HE Data

The form factor and lead-time methods were tested against a broad spectrum of data. Nuclear data check on absolute yields by their radiochemical and hydrodynamic yields and check the equation of state more severely at higher pressures than HE reaches. HE data check non-ideal effects like large mass, afterburning, and secondary shocks. The broad range of data checks for self-consistency and exposes systematic errors. Figures 6 to 10 graph the detailed results and Table 3 summarizes them.

Blast theory is usually checked against data by pressure-distance plots like Fig. 5. But as seen there, UTE matches composite data so closely that graphs are inadequate. Instead, UTE computes the relative yield at each pressure level and we plot that. On Figure 5, the line widths approach 3% in radius, 10% in yield, too small to see. On Figures 6 to 10, the three central lines are relative yields of $1.0 \pm 10\%$, as if the graph of Fig 5 were blown up to broaden the lines to the band width shown.

1 KT Nuclear Composite^{1, 7} (Fig 6) covers from 13600 to .07 bars, 10^5 times. ⁷ The average yield 1.024 KT $\pm 5.3\%$ matches the line width of the source curve ⁷ and is significant because the high pressures are superbly accurate fireball data. The TOA yields also are excellent at high pressures; overall is 1.08 KT $\pm 14\%$. The excursion at low pressures is probably due to a fitted time-of-arrival curve. The consistency in yield is assurance that the high pressure UTE equation of state is realistic relative to the ideal gas law, used for air at pressures below 10 bars.

KING Fireball³ (Fig 7) is probably the best pressure-distance data in existence: high yield, air drop, negligible mass effect, all-fission, a perfect circle fireball. Radiochemistry gave 545 KT, hydrodynamic yield 555 KT, fireball scaling 595 KT. Here, pressure and TOA both give 586 KT; scatter of 3-7% is round-off error in data. This one test is definitive: all the measured data are digital --no graphing errors.

Nuclear Blast Standard⁸ (Fig 8) is not data but an artificial viscosity hydrocode. The absolute value of yield .997 KT checks superbly, but the scatter is over 14%. Its initial pressures are known to be 50% low from actual fireball theory and data. At low pressure its P-R curve decays like $R^{-1.1}$, flatter than UTE, $P \sim R^{-1.33}$. Classic theory predicts R^{-1} , but field measurements always decay much faster.

1 KG TNT Composite⁹ (Fig 9): splendid agreement/consistency, up to the charge ^{1.4} and for $.07 < P/P_0 < 2$, the UTE calculation agrees well with often-measured $P \sim R^{-1.4}$. The excursion below .07 bars is probably not real, but old data piously fit to R^{-1} . The absolute yield is .714 KG, 714 cal/gm; earlier UTE methods gave 720 cal/gm.

1KG H6 Composite⁹ (Fig 10) is a check with a heavily aluminized explosive, where the afterburning fraction is estimated as .30. The consistency 5% is superb. The absolute yield is 1.014 KG HE, or 1014 cal/g, equivalent to 1.4 times TNT.

Previous UTE, DSC¹ (not shown) has been used successfully on so many NESIP and other tests that it is of interest to use a DSC calculation ($M=0$) as input data here. The result: Relative yield 1.00000, $\pm 3.5\%$, no sensible difference between them.

TABLE 3
TESTS OF $\left\{ \begin{array}{l} \text{FORM FACTOR} \\ \text{LEAD-TIME} \end{array} \right\}$ **- METHODS**

VERSUS	NOMINAL	SPAN,	BARS	YIELD	%	CONSISTENCY
NUCLEAR COMPOSITE (FITTED TOA)	1 KT	13,600	→	.07	RANGE 1.029 KT TOA (1.087)	± 5.3 (14.8)
KING FIREBALL	555- 595 KT	1,900	→	46	RANGE 586 KT TOA 586 KT	± 3.6 ± 6.8
AIR FORCE 1 KT STANDARD	1 KT	10,000	→	.07	RANGE .997 KT	± 14.6
TNT COMPOSITE	1 KG	47	→	.07	RANGE .714 KG	± 8.6
H-6 COMPOSITE	1 KG	8.3	→	.16	RANGE 1.02 KG	± 5.1
UTE DSC CONSTANT "q"	1	13,600	→	.07	1.00005	± 3.6

INDIVIDUAL POINTS

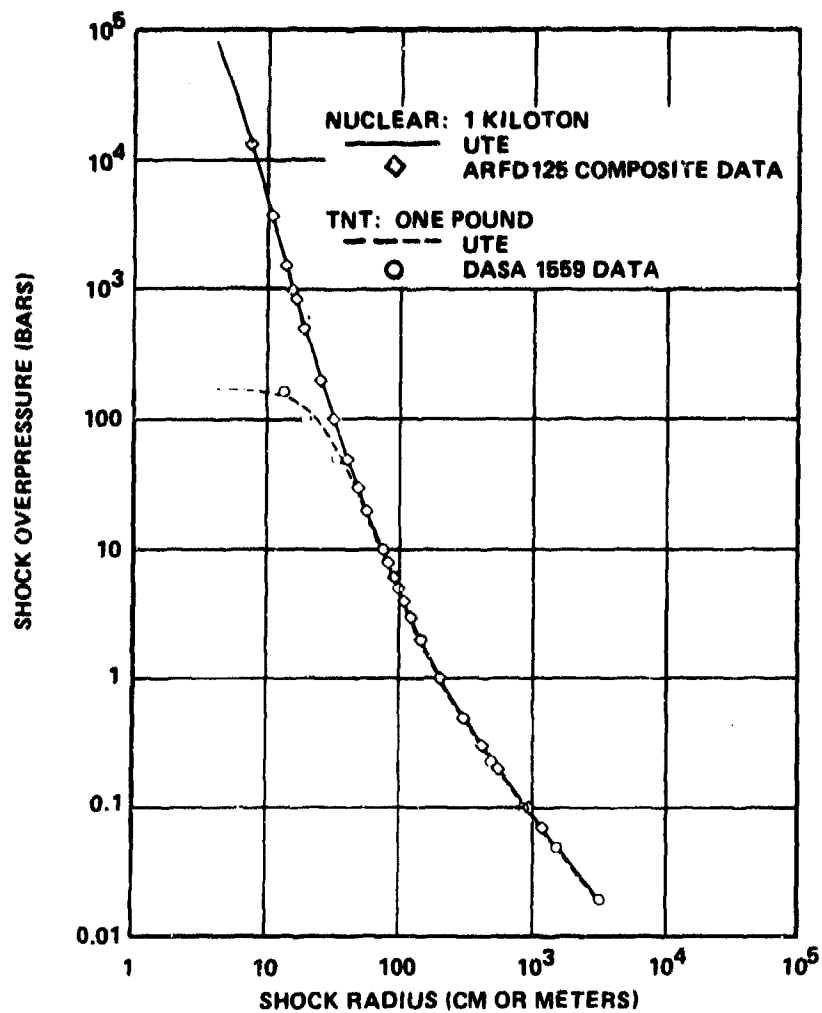
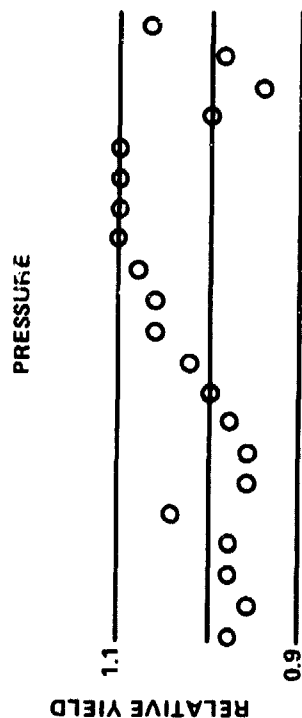
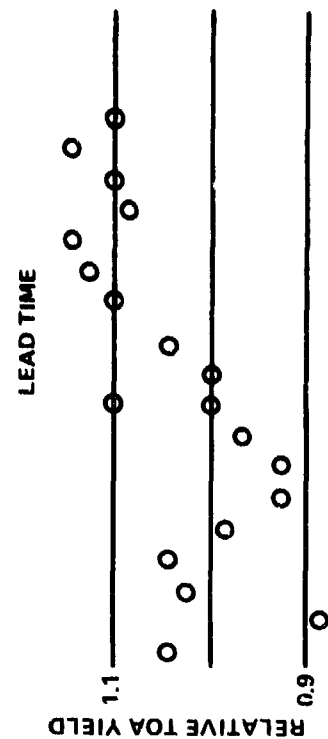


FIGURE 5. COMPARISON OF UTE PREDICTIONS WITH NUCLEAR AND TNT DATA

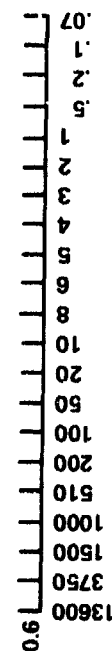
1KT NUCLEAR COMPOSITE



RESULT: 1.024 KT \pm 5.3%



RESULT: 1.08 KT \pm 14.8%



OVERPRESSURE RATIO P/P₀

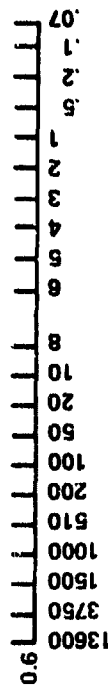


FIGURE 6. RELATIVE YIELD VS OVERPRESSURE, 1 KT NUCLEAR COMPOSITE

KING FIREBALL 555-595 KT

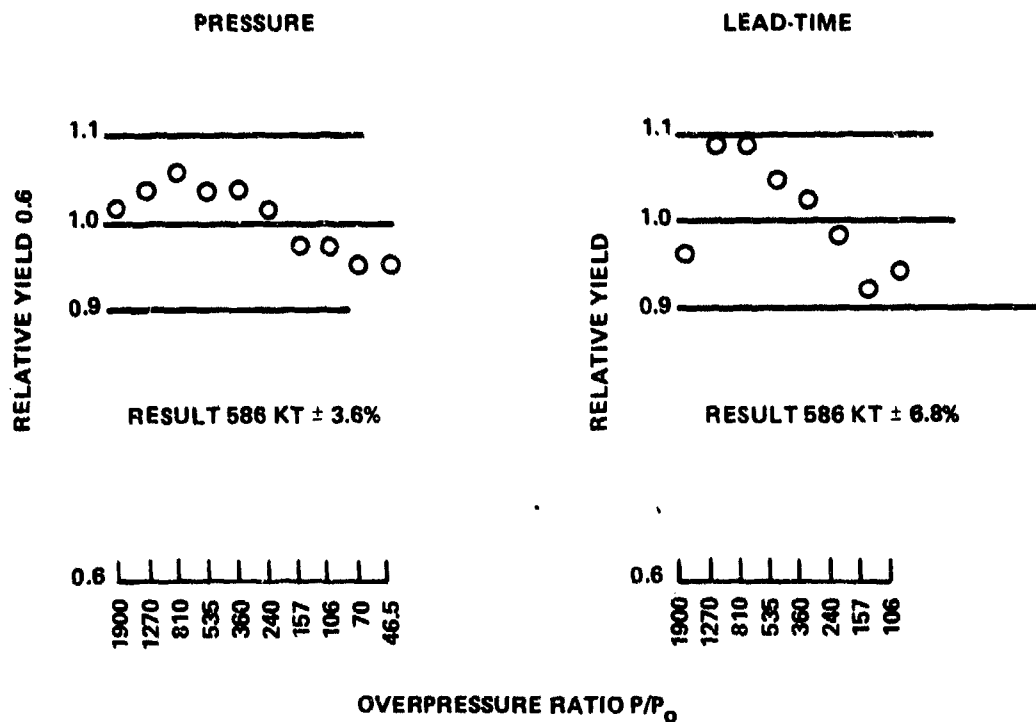


FIGURE 7. RELATIVE YIELD VS OVERPRESSURE, KING

AIR FORCE 1 KT STANDARD PRESSURE PREDICTIONS

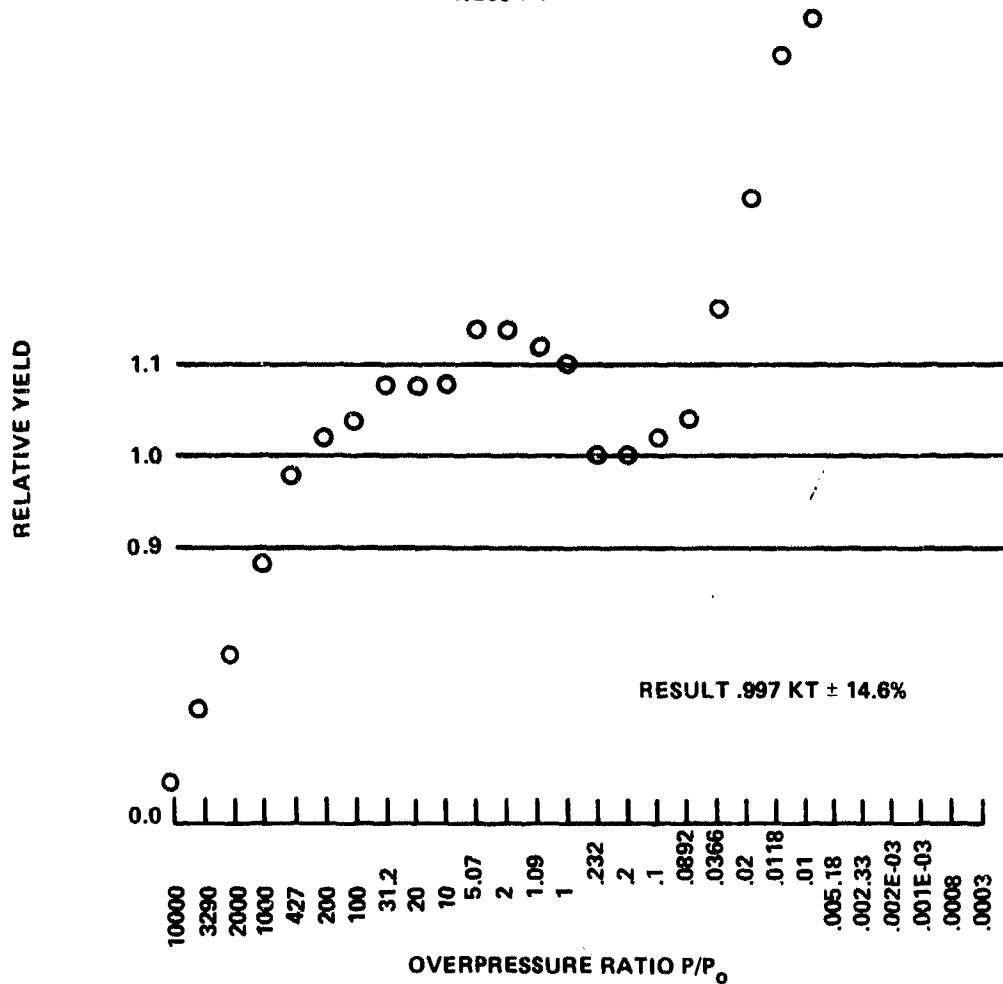


FIGURE 8. RELATIVE YIELD VS OVERPRESSURE, AF 1KT

PRESSURE

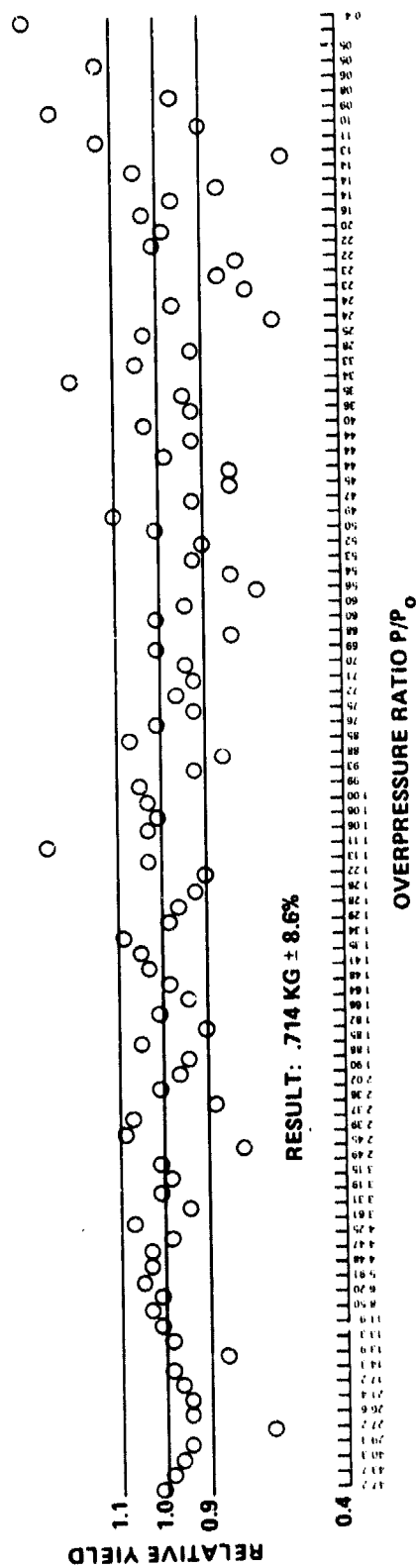


FIGURE 9. RELATIVE YIELD VS OVERPRESSURE, TNT COMPOSITE

H-6 COMPOSITE, 1 KILOGRAM
PRESSURE MEASUREMENTS

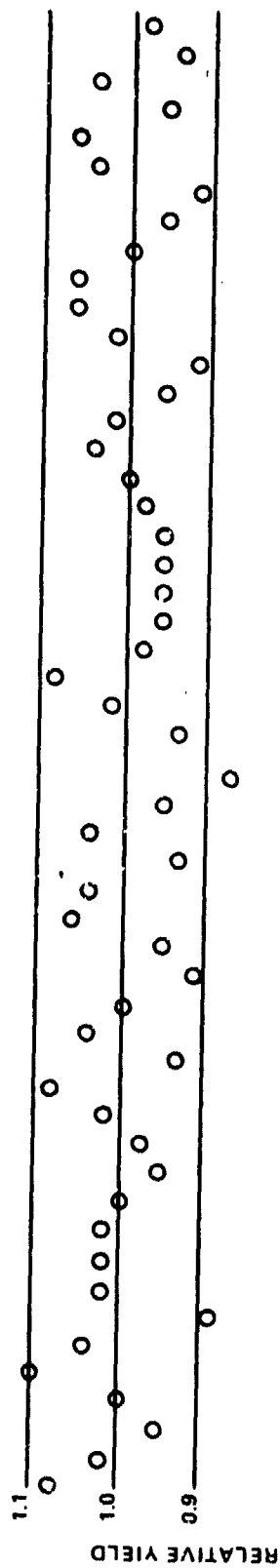
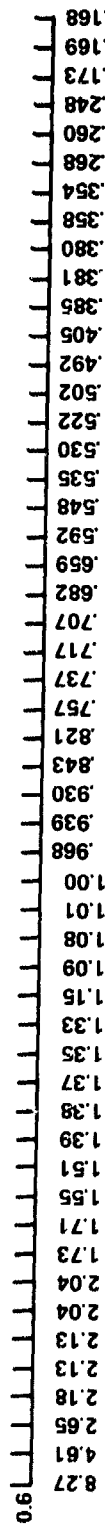


FIGURE 10. RELATIVE YIELD VS OVERPRESSURE, H-6



6. MK. 48 Torpedo Inhibitor Tests

Recent field experiments on the design of inhibitors^{2, 10} for the Mk 48 torpedo provide an opportunity to test/apply these new methods to a typical NESIP problem. The test set-up is shown at the top of Table 4; essentially, it was a donor warhead flanked by two acceptor warheads, with inhibitor plates between them, on each side. On one side the plates were steel, on the other side aluminum, thicknesses as shown. Detonation was suitably instrumented with witness plates, cameras and flash panels and in a blast line by pairs of pressure-time gages near 140, 240, 300, 400 feet. Even so, critical questions arise in all such tests:

If the witness plate did hole, did full detonation of the entire warhead occur?

If it did not hole, could the charge have moved and a delayed detonation occur?

To understand either case, we need to measure the yield output for each event.

The test results were unequivocal and corroborative among all the test evidence.

Shots 1 and 2: no acceptor detonated. Shot 3: the aluminum side holed in situ.

The 140 and 240 foot gages on Shot #3 had double pulses that coalesced by 300 feet. Still the critical questions remain: How much energy did each shot yield?

Peak pressure results are compared on Figure 11 with the pre-shot calculations.

The data on #1 seem somewhat low, on #2 somewhat high. But scatter makes it doubtful:

Excepting two "low" points on #1, one "high" on #2, 13 remaining points replicate.

Shot #3 leaves no doubt the curve beyond 300 feet represents twice the yield.

The corresponding pre-shot estimates and lead-time data are shown on figure 12.

Now there is no doubt that Shot #2 was larger than #1, nor that Shot #3 was double.

Considering this was the first test of a lead-time prediction on HE, it checks well.

Relative yields on shots 1 and 2 are plotted on Figures 13-14, summarized on Table 4.

Compare the pressure results: 1012 KG \pm 21.1% vs. 1386 KG \pm 17.9%.

The ratio 1386/1012 = 1.37 is impressive, except that 37% is not far different from the arithmetic or the Pythagorean sum of deviations, 21.1+17.9. One is just not sure.

Now compare lead-time yields: 828 KG \pm 7.8% vs. 1108 KG \pm 6.8%.

Again: 1108/828 = 1.34 is impressive and 34 is more than twice any sum of 7.6 and 6.8

These confidence levels make a strong, objective case for the merits of lead-time.

As Table 4 indicates, the yields on shot 3 were definitely doubled, by either method, but no predictions had been made with history effects for catch-up of second pulses.

We have yet to resolve why the lead-time gives lower yields on both shots 1 and 2.

Compare range/lead-time: 1012/828 = 1.23 (shot 1) and 1306/1108 = 1.25 (shot 2).

It is precarious to prognosticate with preliminary data until they really do firm up, but two main ideas are noteworthy here: 1. measuring sound velocity, 2. reflection.

Among many ways to measure sound velocity --absolute temperature + wind velocity, a microcharge fired just before the main shock, or compute C_g from the P-t data-- all three differed at the field tests, and we have not yet resolved why.

On the other hand, the lead-time could well be telling us a real fact:

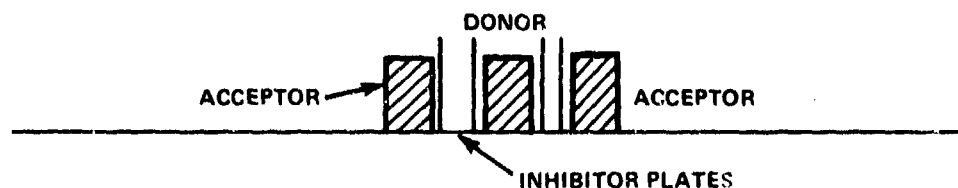
The calculations assumed the torpedo explosion reflected instantly off the ground.

Whereas we know it must have run for some time as a free air explosion, and was slowed by the inhibitor plates and by the acceptor in that direction.

We also know that the shock is slowed by the dust-load in the boundary layer

The present results are based on sound velocity as calculated from pressure gages.

TABLE 4.
MK 48 TORPEDO INHIBITOR TESTS



			YIELD (REFLE 1.)	CONSISTENCY
SHOT #1 1 1/2" ALUMINUM	NOMINAL 1000 KG	SPAN, PSI 10 → 1	RANGE: 1012 KG TOA: 328 KG	± 21.1% ± 7.8%
#2 3/4" ALUMINUM	1000 KG	10 → 1	RANGE: 1386 KG TOA: 1108 KG	± 17.9% ± 6.8%
#3 3/8" ALUMINUM	1000 KG	10 → 1	DOUBLED. DOUBLED:	

PRELIMINARY DATA AND ANALYSES

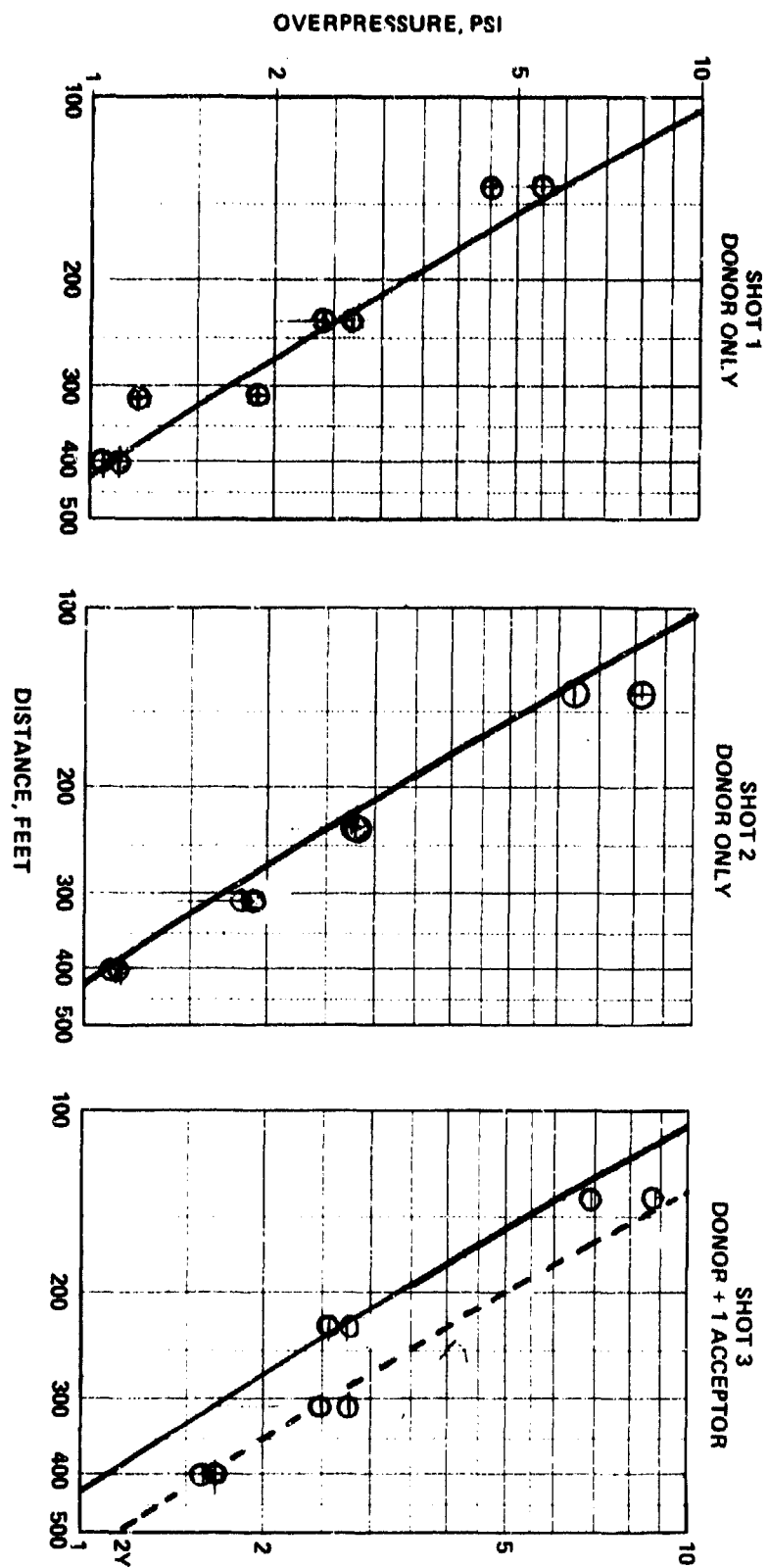


FIGURE 11. MK 48 TORPEDO INHIBITOR TESTS
(Preliminary Data)

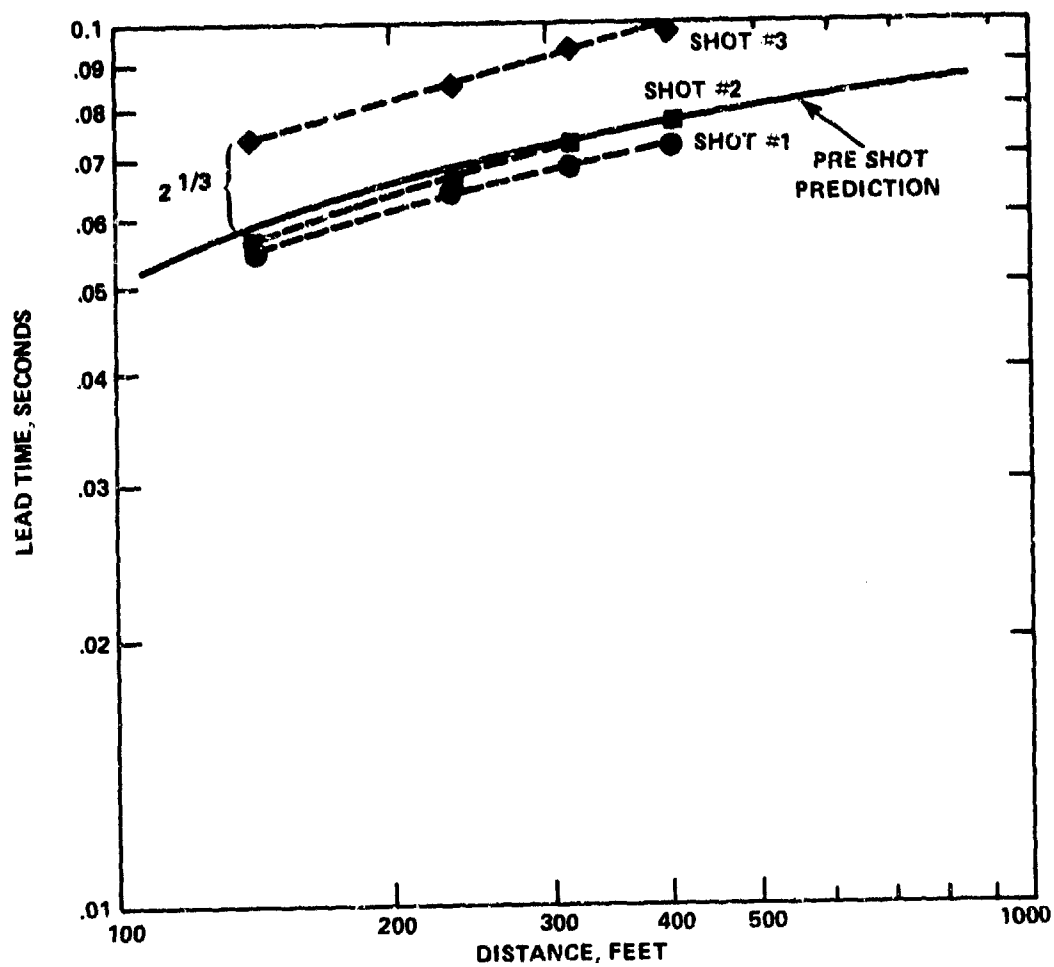


FIGURE 12. TEST OF LEAD TIME OF MK 48 TESTS

MK 48 TORPEDO INHIBITOR TESTS
SHOT #1

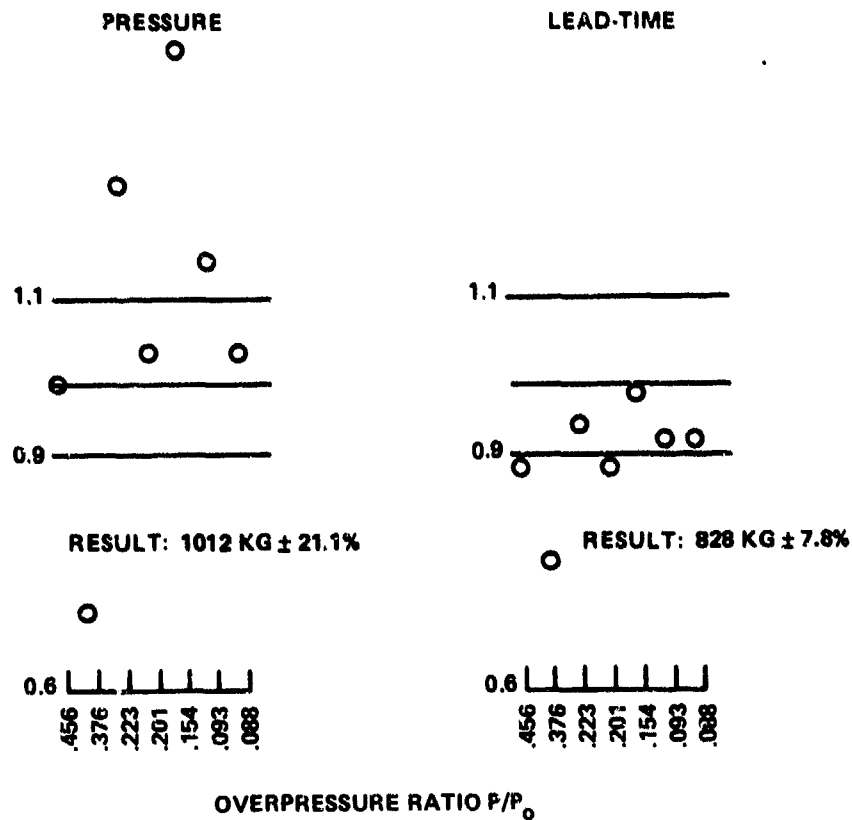


FIGURE 13. RELATIVE YIELD VS OVERPRESSURE, SHOT 1

**MK 48 TORPEDO INHIBITOR TESTS
SHOT #2**

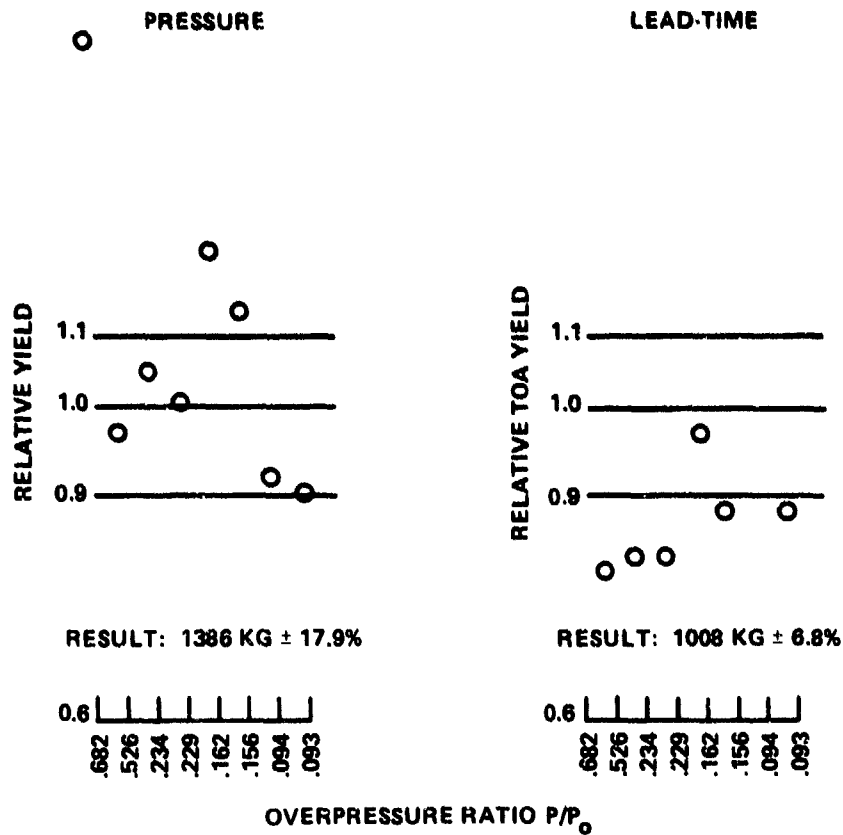


FIGURE 14. RELATIVE YIELD VS OVERPRESSURE, SHOT 2

7. Conclusions

1. Form Factor. The form factor method with the unified theory of explosions (UTE) agrees well with nuclear and high explosive data, with earlier methods of UTE and offers a facile way to describe non-ideal and non-spherical explosions.
2. Lead-Time. The lead-time method is a simply instrumented way to measure yield at high and low shock strengths, with much less scatter than pressure measurements.
3. UTEFORM. Form factor and lead-time together offer a new powerful diagnostic tool to solve the unpredictably broad problems which explosion safety requires such as sympathetic reactions, early blast history, unusual afterburning or energy release.
4. Absolute Yield. The definition $10^{12} \text{ cal/KT} = 10^6 \text{ cal/KG} = 10^3 \text{ cal/gm}$ is a modern rational way to correlate any explosion: nuclear, chemical, other source. It is necessary because:
Different HE's do not necessarily scale with each other nor with other sources.
That is, equivalent weight is certainly not constant at high shock strengths and is not necessarily constant even at acoustic shock strengths.

REFERENCES

1. "Introduction to A Unified Theory of Explosions (UTE)", F. B. Porzel, TR 72-209, U.S. Naval Ordnance Laboratory, September 1972, AD 658000.
2. "Technology Base of the Navy Explosives Safety Improvement Program", F. Porzel, 19th Explosives Safety Seminar, DOD Explosive Safety Board, September, 1980.
3. "Preliminary Hydrodynamic Yields of Atomic Weapons"(U), F. B. Porzel, WT 9001, Los Alamos Scientific Laboratory, Dec 1953 (then SECRET RD, KING is Unc).
4. "Close-In Time-of-Arrival of Underwater Shock Wave" F. B. Porzel, WT 1034, Final Report, Project 4.4, Operation WIGWAM, 1956.
5. "Close-In Time-of-Arrival Measurements for Yield of Underground RAINIER Shot", WT 1495, F. Porzel, W.C. Anderson, Project 23.1 Operation PLUMBOB, Jul 1959.
6. "Height of Burst for Atomic Bombs, Part II, Theory of Surface Effects" F. Porzel LA 1665, Los Alamos Scientific Laboratory, March, 1954.
7. "Surface Effects on Blast Loading" F.B. Porzel and L. Schmidt, 1959 ARF D126, Armour Research Foundation for Special Weapons Cmd. SWC-OS-20579-V-II.
8. "Nuclear Blast Standard (1KT)" Needham, C. Havens, M., Knauth, C. AFWL 73-55 (Rev), Air Force Weapons Laboratory, April, 1975.
9. Michael Swisdak, NSWC, private communication.
10. "Module to prevent sympathetic detonation in munitions" F.B. Porzel, U.S. Patent 4,286,708.

Appendix A

LIST for UTEFORM Form Factor and Lead-Time Methods With the Unified Theory of Explosions

Major Computation Blocks by Line Numbers:

0-199 Input parameters
200-299 Compute P_1 , given Y_0 and H
299-300 Compute M or H , given Y_0 , P_1 and either M or H
400-450 Compute trial Y , if unspecified
450-500 Print column headings
500-570 Data processing and pressure selection
570-699 Energy gains, losses, new yield and range
700-800 Equation of state sub-routine
800-850 Energy gain and loss sub-routines
850-899 Form factor sub-routines
900-999 Time-of-Arrival sub-routine
1000-1400 Input data: pressure, distance, time
1400-1500 Example: Fitted time-of-arrival sub-routine for a nuclear composite.
1500-1599 Relative yields from range and time-of-arrival
1600-2000 Yield, standard deviations and termination.

Hints:

1. Any consistent set of units may be used.
If energy is in joules, R in meters, M in kg, then P is in pascals $= 10^{-5}$ bars.
Line 50, as written, converts from KT ($4 \pi/3 * 10^{12}$) to joules;
use line 51 to enter the KT , KG or cal/gm .
2. Change data with a line editor, it will save retyping the remarks in that line.
3. In general, the variables are defined by remarks the first time used in the LIST.
4. For help, call Fran Porzel, 202 394 1166 (office) or 703 533 7973 (home).

```

0 J =2                '0 = Predictions, 1= analysis, 2,3 = range or TOA yield
1 REM..Any self consistent units may be used; P is in pascals for Y kg, R meters
5 PRINT "NUCOMP/UT8", DATE$, TIME$; IF J=0 THEN 15
15 PRINT "UNIFIED THEORY OF EXPLOSIONS (UTE), FORM FACTOR METHOD AND TIMES"
23 PRINT "NUCLEAR COMPOSITE DATA, NOLTR 72-209"
25 B = 4*3.141592/3    'Form factor for sphere; mech. eq of heat, 13.6 deg cal.
30 P0 = 1E5            'Ambient pressure; 1 bar = 1E5 pascals = 1E5 kg/m/sec^2
31 P0 = 1*P0           'Erases possible previous entry
35 E0 = 2.5 : K0 = 1/E0 +1 'energy and adiabatic coefficients, ambient
40 D0 = 1.1613 : C0 = 1138.45*.3048 'input ambient density D0 or sound speed C0 or both
41 D0 = 1.1613         'Erases possible previous entry for D0
43 IF C0 > 0 THEN D0 = K0*P0/C0^2 : GOTO 50 'Override D0 by equation of state
46 IF C0 = 0 THEN C0 = SQR(K0*P0/D0)
50 Y0 = B*10^12        'Yield; 1 KT = 10^12 cal = 4pi/3*1e12 kg m^2/m^3/sec^2
51 Y0 = Y0*1.0         'Relative yields from earlier runs or fits
52                     '1 KG = 10^6 cal = 4pi/3*1e6 kg m^2/m^3/sec^2
53 AB=.00              'Afterburning fraction
56 Y0 = Y0*(1-AB)      'Yield before afterburning
60 R0 = 4.2            'Radius of isothermal sphere or charge radius, 1 KT
61 R0 = 1*R0           'Erases possible previous entry
70 H = .25             'specific energy of debris to air; use .5 for massive
80 M = 0
83 M = H*MD/B/D0       'converts mass to equivalent volume of air
85 IF R0 = 0 THEN R0 = (MD/B/1500)^(1/3) ELSE 86 'Replace 1500 w/ D of charge
86 Z0 = (R0^3 + M)^(1/3) 'Z = Sahock radius corrected for UTE mass effect
90 PI = 8E9
93 PT = P0*10^-.3      'Transition pressure, book-keep end of afterburning
95 QZ = 3.5: YZ = .5   'Default initial values for dlnQ/dlnZ, dlnY/dlnZ (ideal)
100 PRINT "Total Yield ="Y0/(1-AB), "Input mass ="MD, "Input H ="H
120 PRINT "Ambient pressure ="P0, "Ambient density ="D0
140 PRINT "Ambient sound speed ="C0,
199 REM.....OPTION TO CALCULATE PI, GIVEN Y0 AND H.....
200 P = PI : IF PI > 0 THEN 300
210 PI = Y0/B/Z0^3     'Trial value; A*F approx 1 for strong shocks
220 P = PI
230 GOSUB 700
240 AF = A/3
250 Y = Y0*(1-Q/P)     'Estimate for waste heat of charge or isothermal sphere
260 P = Y/B/AF/Z0^3
270 IF ABS(P/PI -1) <.001 THEN 285
280 PI = P: GOTO 230   'Iterate for PI
285 PC = PI            'Save revised pressure PC at charge surface
290 PRINT "Calculated Initial Pressure ="P
296 GOTO 445
299 REM.....OPTION TO CALCULATE H, GIVEN PI AND Y.....
300 GOSUB 700
315 IF Y0 =0 THEN 400
320 Y = Y0*(1-Q/P)     'Waste heat in radiative phase or chargew/af = 1
330 IF MD>0 AND H>0 THEN 390
340 Z0=(Y/B/PI/AF)^(1/3)
350 MH = B*D0*(Z0^3 -R0^3)
360 IF MD = 0 THEN MD = MH/H ELSE 380
370 PRINT "Inertial mass ="MD : IF J = 0 THEN 380
380 IF H = 0 THEN H = MH/MD ELSE 390
385 PRINT "Calculated specific energy H ="H
390 M = H*MD/B/D0      'Computes "inertial volume" from apparent mass

```

```

399 REM.....OPTION TO CALCULATE Y (Needs debugging)
400 IF Y = 0 THEN Y = B*PI*A*F*Z0^3 ELSE 430
405 GOTO 930
410 Y0 = Y/(1- PI/P0)^(1/K -1))
420 PRINT "Calculated initial yield Y0 ="Y0
430 P = PI
445 PRINT"Afterburning fraction ="AB, "Complete at Pt/Po ="PT/P0
450 IF JK2 THEN PRINT"O'PRESSURE", "RADIUS", "YIELD","ARRIVAL TIME","LEAD TIME"
470 IF JK2 THEN PRINT " ", "Measured","Range Yield","Measured", "TOA Yield"
475 IF J = 1 THEN PRINT " Q/P"," Z", " YZ", " QZ". " AF"
480 IF J = 2 THEN PRINT "O'Press."TAB(10)"Rel. Yld" TAB(20)"dlnY/dlnZ" TAB(30)".6",
490 IF J = 3 THEN PRINT "P/P0" TAB(10)"TOA Yield" TAB(20)"Meas. T" TAB(30)".6",
491 IF J = 2 OR 3 THEN PRINT "Relative Yield" TAB(69)"1.4"
499 REM.....PRESSURE SELECTION.....
500 READ PX,X : IF PX = 0 THEN 1600
510 PX= PX*1E5
513 REM Use GOTO 525 with no measured times or if TX is in seconds
515 GOSUB 1400 'Sub-routine for fitted TOA curve
520 TX = TX/1000 'Fitted curve was in milliseconds
525 IF P>PX THEN N = .1*INT(10*LOG(PI)/LOG(10) ) : GOTO 540
526 PI = PX : H=0 : X0 =X : GOTO 300
530 N = N - 0.1
540 P = 10^N
545 IF ABS(PI/P -1)<.001 THEN 530
550 IF P <PX THEN P = PX
560 GOSUB 700
570 REM,.....GAINS, LOSSES, NEW YIELD AND ARNGE.....
580 IF QI = 0 THEN 630 'By-pass gain or loss at R0; avoid /0 error @600
590 YH = Y +YA 'Add afterburning; hold Y as Z is iterated
595 IF QZ = 0 THEN 605 'IF Q = QI THEN Z =ZI and Y1 = 0
600 Y1 = 3*B*QI*(ZI^3)/(QZ -3)*(1 - (Q/QI)^(1-3/QZ))
605 IF P<PT THEN YA = 0 'No afterburning beyond transition pressure
610 Y = YH -Y1
630 Z =(Y/B/P/AF)^(1/3)
631 IF QI = 0 THEN 637
632 IF Q = QI OR Z = ZI THEN 635 'Circumvents repeated pressure problem
633 QZ = LOG(QI/Q)/LOG(Z/ZI)
635 IF ABS(Z2/Z - 1)>.00001 THEN Z2 = Z : GOTO 595
637 IF M>Z^3 THEN Z = (M +R0^3)^(1/3)
640 R = (Z^3 - M)^(1/3)
645 ON ERROR GOTO 650 'Avoids d/0 on initial pass
646 YZ = LOG(YI/Y)/LOG(Z/ZI) 'Calculate dlnY/dlnZ for later use in 870
650 GOSUB 900. 'Get time increment
660 T = T +T1
675 IF J >1 THEN 687
680 PRINT P/P0, R, Y/Y0, T, R/C0 -T
687 IF ABS(P/PX-1)<.001 THEN GOSUB 1500
690 IF J = 1 THEN PRINT" "Q/P, Z, " "YZ, " "QZ, " "AF
696 PI=P : QI = Q : ZI =Z : RI =R :UI =US :YI = Y:AI=AF
698 IF ABS(P/PX -1)<.001 THEN 500 ELSE 530
Ready
>

```



```

699 REM.....EQUATION OF STATE SUB-ROUTINE.....
700 P = P/PO      'Equation of state is described best by pressure ratio
710 IF P<10      THEN E=2.5 :GOTO 760      'E is ratio =energy/PV, i.e.epsilonh
720 IF P<100     THEN E= 2.5 + 1.5*LOG(P/10)/LOG(10) :GOTO 760
730 IF P<700     THEN E= 4.0 + 1.55*LOG(P/100)/LOG(7) :GOTO 760
740 IF P<1000    THEN E =5.55 -.55*LOG(P/700)/LOG(10/7) :GOTO 760
745 IF P<4000    THEN E =5.0 - LOG(P/1000)/LOG(4) :GOTO 760
750 IF P<40000   THEN E = 4.0 :GOTO 760
755 IF P>40000   THEN E = 4.0 - .67*LOG(P/40000)/LOG(2) :GOTO 760
760 D = ((2*E +1)*(1 +P) +1)/(P + 2*E0 +2)      ' density ratio, real gas
770 A = E*(1 +P)/P*(1- (1+P)^(-1/(E +1))) 'Prompt energy factor A =Work/(P-PO)V
780 K = 1/E +1      'Same as epsilon = 1/(k-1)
790 P = P*PO      'get back to absolute overpressures
799 REM.....ENERGY LOSS AND GAIN SUBROUTINE.....
800 IF P/PO < .06 THEN 840      'Q will soon truncate to 0 if you don't do this
805 IF P/PO <11.3 THEN 830      'Exact match w/ ideal gas @ P=11.3, 3.4
810 L = .4342948*LOG(P/PO)      'convert pressure ratio to log base 10
820 Q = PO*10^((21.75-L)*(L-1)/16) :GOTO 845      'Semi-empirical fit for real air
830 Q = PO*((1 +P/PO)^(1/K)/D -1)/(K-1) :GOTO 842      'classical adiabat
840 Q = PO*(K+1)*((P/PO/K)^3)*(1 - 1.5*P/PO)/12      'acoustic dissipation
842 IF P>PT THEN 845      'Argument: wave form and losses are manifest at shock
843 Q = Q*(1 +AB)      'Argument: secondary shock, other losses
845 ZP= 1/4      'dlnZ/dlnP; assumes YA goes as volume and time
846 YA = AB*YO*((PC/P)^ZP -(PC/PI)^ZP)/((PC/PT)^ZP - 1) 'AB is prop. to Z-zl
847 IF P<PT THEN YA = 0
850 REM.....AF = A*F SUBROUTINE.....
860 IF P>PT THEN AF =A/3/(1 +PO/P)^2/(1 + AB) :GOTO 890
861 REM: Strong shock, F= .42, mean A=.8*A(shock), /(1 +AB) is peaked wave form
865 IF YZ = 0 THEN YZ = 1
870 IF P<PT THEN AF =3*Q/P/YZ      'Weak and second shock, YZ stable
880 IF AF>AI OR AF<=0 THEN AF= AI      'By passes troubles at transition pressure
890 RETURN
900 REM .....TIME-OF ARRIVAL SUB-ROUTINE.....
910 IF P/PO >450 THEN K =1.2 +.2*LOG(P/PO/450)/LOG(2) : GOTO 940      'real gas K
920 IF P/PO >15 THEN K = 1.4 - .2*LOG(P/PO/15)/LOG(30): GOTO 940      'real gas K
930 K = K0
940 US = SQR(P/DO/(1 -1/D))      'used previous K to calculate U
945 IF ZI = 0 THEN UI = US      ' UI not yet initialized as in 696
950 UB = (1/US + 1/UI)/2      'Mean for integrating dt as dx/U
960 T1 = UB*(R -RI)      'Time increment
970 IF ZI = 0 AND P/PO >10000 THEN T1 = .2*T1 : GOTO 990      'Radiative phase
980 IF ZI = 0 THEN T1 = .5*T1      'ball park estimate for detonations
990 RETURN
999 REM.....INPUT MEASURED DATA. AND/OR LOWEST PRESSURE FOR CALCULATION.
1000 DATA 13600, 7.32, 3750, 10.7, 1550, 13.7
1010 DATA 1000, 15.5, 510, 19.2, 200, 25.6
1020 DATA 100, 32.2, 50, 41, 20, 57.3
1030 DATA 10., 75.1, 8, 82.4, 6, 91.5
1040 DATA 5, 98.8, 4, 108.5, 3, 122.5
1050 DATA 2, 147.4, 1.0, 208, .5, 302
1060 DATA .2, 544, .10, 905, .07, 1200

```

```

1400 REM..... SUB-ROUTINE FOR FITTED TIME OF ARRIVAL.....
1410 IF (PX/P0) < 500 THEN 1430
1420 TX = (PX/P0/500)^(-4/5) : GOTO 1490
1430 TX = (PX/P0/500)^(-6/7)
1435 TX = TX*TX^(LOG(TX)/175)
1440 IF ABS(T2/TX -1) < .00001 THEN 1490
1450 T2 = TX :GOTO 1430
1490 RETURN
1499 REM.....RANGE AND TIME OF ARRIVAL YIELD.....
1500 IF ABS(P/PX -1)>.001 THEN 1595 'Passes only measured points
1510 YX= (X^3 +M)/Z^3
1533 TB = INT(50*YX + .25)
1534 IF TB>77 THEN TB = 77
1535 IF J = 2 THEN PRINT P/P0 TAB(10)YX TAB(20)YZ TAB(30)". "TAB(TB)"Y" TAB(70)". "
1545 IF US/CO >2 THEN YT = (TX/T)^3 : GOTO 1555
1550 YT = ((X/CO -TX)/(R/CO -T))^3
1555 TT = INT(50*YT + .25)
1560 IF TB>77 THEN TB= 77
1570 IF J = 3 THEN PRINT P/P0 TAB(10)YT TAB(20)T TAB(30)". " TAB(TT)"T" TAB(70)". "
1575 IF P<.068*P0 THEN 1590
1576 I = I +1
1580 SX = SX +YX
1585 VX = VX + YX^2
1586 IT = IT +1
1587 ST = ST + YT
1588 VT = VT + YT^2
1590 IF J = 1 THEN PRINT" Meas:", X, "*"YX, TX, "*"YT
1595 RETURN
1599 REM.....YIELDS AND STANDARD DEVIATIONS.....
1600 IF I <2 THEN 2000
1602 S = VX/(I-1) - (SX^2)/I/(I-1)
1604 IF IT < 2 THEN 1610
1606 S2 = VT/(IT-1) - (ST^2)/IT/(IT-1)
1608 PRINT
1610 PRINT "Yield, relative to input =" SX/I
1630 PRINT "Standard deviation, % =" 100*SQR(S)*(I/SX) "based on" I "samples, P=> 1 psi"
1640 IF ST = 0 THEN 1680
1650 PRINT "TOA Yield, relative to input =" ST/IT
1670 PRINT "Standard deviation, TOA yield, % ="100*SQR(S2)*(IT/ST)"based on "IT"samples"
1990 DATA 0, 0, 0
2000 END

```



AD P000438

DESIGN CRITERIA FOR FRANGIBLE COVERS IN ORDNANCE FACILITIES

Prepared for the
Twentieth DOD Explosives Safety Seminar
Norfolk, Virginia

24 - 26 August 1982

by

William A. Keenan

and

James E. Tancreto

Naval Civil Engineering Laboratory
Port Hueneme, California 93043

1.0 PURPOSE

This paper presents preliminary design criteria for frangible surfaces intended to "break-up" and "blow-away" quickly enough to limit the internal blast environment, structural damage and exterior debris hazard from explosions inside structures. The design criteria relate the critical design parameters of the structure, frangible surface and explosive to the internal loading -- in a format that facilitates the design of frangible covers and the prediction of internal blast loads.

2.0 BACKGROUND

2.1 Internal Explosions

Shock Pressures. Consider an explosion inside a hardened building with a frangible cover as illustrated in Figures 1 and 2. The detonation generates shock waves. The initial wave strikes the frangible cover, and all other interior surfaces, and is reflected. The energy in the reflected wave depends, in part, on the physical characteristics of the reflecting surface. When the incident wave first strikes the frangible cover, the pressure in the incident wave is shocked up to a reflected pressure. If this pressure accelerates the cover fast enough then the relative velocity between the incident shock wave and cover decreases. This reduces the total energy (total impulse) in the reflected wave to a value less than if instead the cover was non-frangible. In any case, the reflected waves, bouncing back and forth between the walls, floor and roof, produce a shock pressure loading on interior surfaces of the structure. The contribution from the cover to the total shock impulse on other interior surfaces depends, to a large degree, on the number of covers, cover size (surface area and aspect ratio), location of cover

relative to the explosive, physical properties of the cover (mass, strain energy capacity and failure mode) and boundary conditions of the cover (resistance of supports to moment, shear and tension).

The Naval Surface Weapons Center is currently developing criteria to predict the reflected-shock impulse on covers and the effects of cover characteristics on the reflected-shock impulse applied to other interior surfaces of a structure. At this point in the study it appears that for the practical range of design parameters, covers experience the full-reflected-shock impulse. Further, covers should be considered non-frangible surfaces when computing the reflected shock impulse on other interior surfaces of the structure.

Gas Pressures. If the explosion is confined inside an enclosed space, such as a building, the heat released by the detonation and the subsequent after-burning raises temperatures of the air and gaseous by-products of the explosion. This phenomenon generates gas pressures, in addition to shock pressures, in the same time period. The gas pressure inside the structure rises to some peak value, the value depending on the ratio of the net explosive weight to volume of the structure. The gas pressure then gradually decays as gas temperatures drop and gases vent from the structure. The gases vent through openings created by breakage of building components, such as windows, doors and frangible covers.

The peak gas pressure is characteristically small compared to the peak reflected-shock pressure. However, the duration of the gas pressures can be many times greater than the duration of the reflected-shock pressures, especially when the vent area is small compared to the volume of the structure. Progressive breakup of the building increases the total vent area. This increases the rate of escaping gases which, in turn, increases the rate of decay in gas pressures, and thus, decreases the duration of the gas pressure.

Blast hardened or massive structures often have little or no inherent escape paths for gases. In such cases, vent areas must be built into the structure. In practice, these vent areas are openings with frangible covers. The frangible covers are intended to breakup and blow away

quickly enough to reduce the gas pressure environment inside the structure. This strategy reduces the extent of structural damage and secondary debris.

2.2 Frangible Covers

Frangible covers are especially important in hardened structures that contain explosives. For example, safety standards may require a hardened structure to protect its inhabitants and contents from effects of possible explosions located outside the structure. Typically, such structures are massive and capable of absorbing large amounts of internal strain energy. Consequently, the benefits of protection provided against effects from an external explosion may be more than offset by the increased risk to inhabitants and contents from an internal explosion. Further, explosions in hardened structures increase the risk to nearby facilities since the greater blast loads inside a hardened structure produce greater launch velocities of flying debris threatening nearby facilities. A compromise solution to this dilemma is to install one or more frangible covers in exterior surfaces of the structure. The covers are placed at strategic locations that do not compromise protection from effects of an external explosion. The frangible covers reduce the internal blast environment and thus the external debris hazard.

Ordnance test structures, such as missile test cells, are also frequently blast hardened, especially if the test cell is immediately adjacent to the Weapons Maintenance Building that supports test operations. For this case, the test cell is blast hardened to reduce blast and debris on the adjoining building. Typically, one wall of the test cell is made frangible to relieve internal blast loads and focus explosion effects in prescribed directions outside the structure.

3.0 PROBLEM

The NAVFAC P-397 (Ref 1) states that "although frangibility is imperfectly understood and difficult to measure, it has been assumed that a material whose weight is 10 psf of surface area or less may be

considered frangible for both the shock-front pressures and gas pressures resulting from detonation of explosives greater than 100 lbs." NAVFAC P-397 further states "if a large portion (one or more surfaces) of a structure whose weight is greater than 10 psf fails, then this surface of the structure is considered frangible for the gas pressures. However, because the heavier surface will take longer to fail than the lighter surfaces, full reflection of the shock pressures will occur." In design practice, this criteria is interpreted to mean that any surface less than 10 psf is fully frangible, i.e., the surface does not contribute shock impulse to other interior surfaces of the structure and the degree of venting for gases is the same as if no surface covered the opening. This interpretation may contribute large errors in the design process and result in unsafe designs.

Trends in safety regulations require less risk to exposed individuals in ordnance facilities. This trend demands a better understanding of frangibility. For example, recent changes in NAVSEA OP-5 (Ref 2) require personnel working in a missile test cell to be exposed to no more than 2.3 psi from effects of possible explosions in other test cells. This requirement is difficult to satisfy in a multiple test cell complex. The facility designer desires one wall to be frangible in order to reduce the internal blast environment from an internal explosion, thereby, lowering the MCON cost of the facility and external debris hazard. However, to protect personnel in that cell from explosions in other cells, the designer must strengthen the frangible wall to safely resist external blast pressures. But strengthening the wall invariably results in a massive wall which violates current frangibility criteria. The solution to this dilemma usually requires severe restrictions of test operating procedures and lower production levels. Strengthening the "frangible" wall is the practical and cost effective solution, provided the designer has design criteria which account for effects of wall mass on internal blast environment.

The same problem is faced in trying to satisfy physical security regulations. A massive wall is desired to increase the denial time to forced intrusion into a missile test cell, but a light wall is required

to control construction costs. Again, physical security requirements must be compromised because of a lack of criteria on effects of wall mass on internal blast environment.

In view of the problems cited above, the Naval Civil Engineering Laboratory has undertaken a study to refine design criteria for frangible surfaces. The work is being sponsored by the Department of Defense Explosives Safety Board. The criteria presented herein is preliminary and requires further test validation.

4.0 SOLUTION FORMULATION

Consider an explosion inside either the missile test cell or the building shown in Figure 2. An opening of area A is located in one surface of either structure. The opening is covered with a frangible panel. The panel has a mass γ , area A and dimensions ℓ by h . The normal distance from explosive W to the panel is R .

The blast loading (combined shock plus gas pressure-time history) acting on an interior surface of the box is shown in Figure 3. This is also the blast loading on a cover placed over the opening provided the cover is non-frangible for shock pressures (i.e., the cover provides full-reflection of all shock waves striking its surface), but fully frangible for gas pressures (i.e., the cover does not decrease the vent area, A , for escaping gases; the vent area is A from the instant of detonation).

4.1 Shock Pressure Loading

If the reflected-shock pressure on the cover at any time t is $P_r(t)$ then the total reflected-shock impulse, i_r , is

$$\frac{i_r}{W^{1/3}} = \int_0^T \frac{P_r(t)}{W^{1/3}} dt \quad , \text{solution obtained from NAVFAC P-397} \quad (1)$$

The solution of Equation 1 is obtained from charts presented in NAVFAC P-397 (Ref 1). The charts predict the average reflected-shock impulse applied to a prescribed surface of a box-shaped structure. The charts are based on analytical procedures and empirical data derived from explosives tests. The P-397 procedure involves entering appropriate charts with a series of dimensionless parameters related to the geometry and size of the structure and the location of the explosive. The parameters are the length, L , and height, H , of the box-surface of interest; net weight of explosive, W ; number of adjacent reflecting surfaces, N ; normal distance from charge to box-surface of interest, R ; distance from charge to nearest adjacent reflecting surface, ℓ_1 ; and the height of the explosive, h_1 .

The accuracy of the P-397 value for i_r depends on the size of the cover relative to the size of the face of the box. The predicted value of i_r is the average value for the entire face of the box, including the area of the cover. Consequently, the procedure may underestimate i_r applied to the frangible cover if the area of the cover is small compared to the total area of the face of the box. In this case, computer programs, such as BARCS (Ref 3), should be used to estimate i_r . BARCS outputs i_r at each node point of a mesh simulating the surface area of the box. The proper value of i_r for the cover is the value of i_r averaged over nodal points within the area of the cover.

4.2 Gas Pressure Loading

4.2.1. Fixed Vent Area. Given a constant vent area, A , and the time constant, α , describing the rate of exponential decay in pressure, the gas pressure, P_g , inside the box at any time, t , is:

$$P_g(t) = B_g \left(1 - \frac{t}{T_g} e^{-\alpha(t/T_g)} \right) \quad (2)$$

According to analytical work by Proctor and Filler (Ref 4) and explosives tests by NCEL (Ref 5), the peak gas pressure, B_g , inside the box is

a function of the ratio W/V , the explosive weight, W , relative to the volume of the box, V . The relationship between B_g and W/V is plotted in Figure 4.

$$B_g = f(W/V), \quad \text{from Figure 4.} \quad (3)$$

Based on explosives tests by Keenan and Tancreto (Ref 5), the scaled duration of the gas pressure, $T_g/W^{1/3}$, inside the box for a constant vent area, A , and box volume, V , is:

$$\frac{T_g}{W^{1/3}} = 2.26 \left(\frac{A}{V^{2/3}} \right)^{-0.86} \left(\frac{W}{V} \right)^{-0.86}, \quad \text{provided } A \text{ \& } V = \text{constant} \quad (4)$$

and the corresponding scaled total impulse of the gas pressure, $i_g/W^{1/3}$, is:

$$\frac{i_g}{W^{1/3}} = 569 \left(\frac{A}{V^{2/3}} \right)^{-0.78} \left(\frac{W}{V} \right)^{-0.38}, \quad \text{provided } A \text{ \& } V = \text{constant} \quad (5)$$

$A/V^{2/3} \leq 0.21$

Equations 4 and 5 are empirical relationships derived from the gas pressure-time history measured inside a box with A , V and W held constant in each test but varied between tests. In these tests, pressure measurements indicated no gas pressure developed inside the box for $A/V^{2/3} \geq 0.60$.

$$\frac{i_g}{W^{1/3}} = 0, \quad \text{provided } A = \text{constant} \quad (6)$$

$A/V^{2/3} \geq 0.60$

No test data is available to derive the expression for $i_g/W^{1/3}$ where $0.21 < A/V^{2/3} < 0.60$. However, for the purpose of this paper it is arbitrarily assumed that the log of $i_g/W^{1/3}$ varies linearly with the log of $A/V^{2/3}$ for $0.21 \leq A/V^{2/3} \leq 0.60$.

Given A , V and W it is possible to derive an explicit expression for the time constant, α , based on the following requirement.

$$i_g = \int_0^{T_g} P_g(t) dt \quad (7a)$$

Combining Equations 2 and 7a

$$i_g = B_g \int_0^{T_g} \left(1 - \frac{t}{T_g}\right) e^{-\alpha(t/T_g)} dt, \text{ provided } A\&V = \text{constant} \quad (7)$$

where B_g , T_g and i_g are fixed values obtained from Equations 3, 4, and 5 (or 5a), respectively, based on given values of A , V and W .

4.2.2 Variable Vent Area. Consider a frangible cover over an opening in a structure containing an explosion as shown in Figure 3. The combined shock and gas pressures force the cover to move away from the opening. This motion results in a variable vent area that increases with time. Calculation of the gas pressure history inside the structure requires an iterative process because of the variable vent area. The iterative process proceeds as follows.

Referring to Figures 5 and 6, at time t_i the known gas pressure is P_i and the known acceleration, velocity and displacement of the cover, acting as a rigid plate, are \ddot{x}_i , \dot{x}_i and x_i , respectively. If P_{i+1} is the assumed gas pressure at time t_{i+1} , then

$$\begin{aligned} t_{i+1} &= t_i + \Delta t \\ \ddot{x}_{i+1} &= P_{i+1}/m \\ \dot{x}_{i+1} &= \dot{x}_i + (\ddot{x}_i + \ddot{x}_{i+1})(\Delta t)/2 \\ x_{i+1} &= x_i + \dot{x}_i \Delta t + (\ddot{x}_i + \ddot{x}_{i+1})(\Delta t)^2/4 \end{aligned} \quad (8)$$

During the time interval Δt , the average displacement of the cover is $(x_i + x_{i+1})/2$. If the perimeter of the opening is s , then the average vent area, \bar{A}_{i+1} , available for gases to escape from the structure is

$$\bar{A}_{i+1} = (x_i + x_{i+1})s/2 \quad (9)$$

Considering \bar{A}_{i+1} to be a fixed vent area during the time interval, Δt , the gas pressure impulse, i_g , is calculated from Equation 5, the gas pressure duration, T_g , is calculated from Equation 4, and the time constant, α , is calculated from Equation 7. Knowing α_{i+1} , the gas pressure, P_{i+1} at time t_{i+1} is calculated from Equation 2. The calculated value of P_{i+1} becomes the new assumed value of P_{i+1} and the above process is repeated until the difference between the assumed and computed values of P_{i+1} is within a prescribed error limit. Given agreement, time is incremented by Δt and the entire process is repeated for the next time step. If during this process, \bar{A} becomes equal to the area of the opening, then the effective vent area is fixed and $\bar{A} = A$ for all succeeding time intervals.

Eventually, the gas pressure decays to zero. The time corresponding to this point is the gas duration, T_g , inside the structure, and the total gas impulse, i_g , is equal to the total area under the gas pressure-time curve. The above computational process was the basis for NCEL computer program REDI which was used to develop design criteria for frangible covers.

5.0 DESIGN CRITERIA

Computer program REDI was used to generate design criteria for frangible covers. The following criteria are considered preliminary and require further test validation.

5.1 Gas Impulse

Criteria for the gas pressure impulse inside a structure with a frangible cover are presented in Figures 7-10. In each figure, the scaled gas pressure impulse, $i_g/W^{1/3}$, is plotted as a function of the scaled vent area, $A/V^{2/3}$, for several values of the frangible cover mass, $\gamma/W^{1/3}$. Each family of curves in Figures 7-10 are for fixed values of the scaled reflected shock impulse, $i_r/W^{1/3}$, acting on the frangible cover and the ratio of the net explosive weight to structure volume, W/V . The

curves assume the total reflected shock impulse, i_r , is applied to the cover at time $t = 0$, i.e. the reflected shock impulse imparts an initial velocity to cover equal to i_r/m where m is the mass per unit surface area of the cover. This assumption reduced significantly the number of parameters required to display the design criteria.

Use of the criteria require interpolation between values corresponding to the curves in Figures 7-10. Linear interpolation on a log-log scale is recommended for obtaining an intermediate value of any parameter, using either mathematical relationships or log-log graph paper. Further, it is recommended that i_r in Figures 7-10 be interpreted as the value predicted by procedures outlined in NAVFAC P-397 or computer program BARCS (Ref 3).

5.2 Peak Gas Pressure

As stated earlier, the peak gas pressure, B_g , depends on the ratio of the net explosive weight to structure volume, W/V , and is obtained from Figure 4.

$$B_g = f(W/V), \quad \text{from Figure 4} \quad (3)$$

5.3 Effective Gas Duration

The effective duration of the gas pressure based on a linear time decay in the pressure is

$$T'_g = \frac{2 i_g}{B_g} \quad (10)$$

where i_g is the total gas pressure impulse obtained from Figures 7-10 and B_g is the peak gas pressure obtained from Equation 3.

6.0 TEST VALIDATION

6.1 Method of Validation

Experimental data obtained from explosive tests designed to evaluate the performance of earth covered structures was used to validate the design criteria for frangible covers shown in Figures 7-10. The experiment involved detonating explosives inside a series of small earth-covered missile test cells having one frangible wall and a soil-covered roof slab. The frangible wall and roof slabs were not fastened to their supports. Test variables were the mass of the frangible wall, γ , mass of the soil covered roof, $\gamma_s + \gamma_r$, and weight of explosive, W . The motion of the roof and wall slabs was measured in each test with a high speed camera.

The total reflected-shock plus gas impulse, i_T , imparted to the roof was derived from the measured maximum vertical displacement of the roof slab, x_m , by applying the principle of conservation of energy. Since the roof is unrestrained, the total work done by the gravity forces of the roof must equal the total change in its kinetic energy.

$$\text{Work} = -(\gamma_s + \gamma_r) x_m \quad (11a)$$

Since $\dot{x} = 0$ at $x = x_m$, the total change in kinetic energy, ΔKE , is

$$\Delta KE = \frac{1}{2} \left(\frac{\gamma_s + \gamma_r}{g} \right) \left(0^2 - \dot{x}_T^2 \right) \quad (11b)$$

Equating Equations 11a and 11b,

$$y_m = \frac{\dot{x}_T^2}{2g} \quad (11c)$$

From the principle that the total impulse applied to the roof must equal the change in its momentum,

$$\int_0^T P(t) dt = \left(\frac{\gamma_s + \gamma_r}{144 g} \right) (\dot{x}_T - 0)$$

$$i_T = \left(\frac{\gamma_s + \gamma_r}{144 g} \right) \dot{x}_T \quad (11d)$$

Combining Equations 11c and 11d and dividing the result by $W^{1/3}$, the scaled total impulse of the reflected-shock plus gas impulse on the roof is:

$$\frac{i_T}{W^{1/3}} \text{ (measured)} = 1.731 \left(\frac{\gamma_s + \gamma_r}{W^{1/3}} \right) 2\sqrt{x_m} \quad (11)$$

Since γ_s , γ_r , W , and x_m are known values for each test, the scaled total impulse applied to the roof was calculated from Equation 11. This value was considered to be the "measured" value of $i_T/W^{1/3}$ acting on the roof of the missile test cell.

The predicted value of $i_T/W^{1/3}$ was taken to be the sum of the scaled reflected-shock impulse, $i_r/W^{1/3}$, predicted from criteria presented in NAVFAC P-397 (which is based on the parameters shown in Figure 3), plus the scaled gas impulse, $i_g/W^{1/3}$, predicted from the criteria presented in Figures 7-10. In other terms, the predicted scaled total impulse acting on the roof of the missile test cell was taken as:

$$\frac{i_T}{W^{1/3}} \text{ (predicted)} = \frac{i_r}{W^{1/3}} \text{ (NAVFAC P-397)} + \frac{i_g}{W^{1/3}} \text{ (Fig. 7-10)} \quad (12)$$

The predicted value of $i_r/W^{1/3}$ in Equation 12 assumed four reflecting surfaces ($N=4$), i.e., the frangible wall, in addition to the other three walls, was considered to be a non-frangible surface for shock waves striking its surface. The difference between $i_T/W^{1/3}$ obtained from Equations 11 and 12 was the basis for validating the reliability of the design criteria for frangible covers presented in Figures 7-10.

6.2 Test Description

Design details of the test structure are shown in Figure 11. The structure was a one-sixth geometric-scale model of a HARPOON missile test cell. The floor, sidewalls, backwall and floor were constructed from 3-inch-thick steel plate, joined together with full-penetration welds. The backwall had no door opening. The bottom face of the floor was flush with the ground surface.

The roof slab was 1-1/8-inch-thick plywood (3.3 psf) with No. 10 gauge sheet metal (5.63 psf) nailed to the inside face. The roof slab was covered with sand to depth, d_s , in a berm-like fashion. The berm was configured so that the soil depth, d_s , extended a distance d_s beyond the vertical extension of the walls, except at the headwall. The surface of the berm was spray painted white to improve photographic contrast in recording the failure mechanism of the earth-bermed roof. The total roof mass was varied between tests by changing the depth of sand, d_s .

The test charge was Composition C-4 explosive shaped into a right cylinder with a length-diameter ratio equal to 1.0. The charge was positioned midway between the walls and 7 inches above the floor, the typical scaled location of a HARPOON missile during a testing operation. The test charge ranged from $W = 1.0$ to 3.0 lbs which corresponds to approximately $W = 216$ and 640 lbs full-scale, respectively.

The frangible wall was absent in two tests. In all other tests, the frangible wall was either 1-1/8-inch plate glass (one test) at $\gamma = 1.64 \text{ lb/ft}^2$, or 3/8-inch plywood with 28 gauge sheet metal on the inside face (6 tests) at $\gamma = 1.73 \text{ lb/ft}^2$ or 1.0-inch plywood with 13 gauge sheet metal on both faces (two tests) at $\gamma = 10.50 \text{ lb/ft}^2$. Based on scaling laws, $\gamma = 1.73$ and 10.50 lb/ft^2 are equivalent to $\gamma = 10.38$ and 63.0 lb/ft^2 full-scale, respectively.

A view of a typical test setup prior to detonation is shown in Figure 12. Note the adhesive tape used to secure the frangible wall to its supports. Also note the soil berm spray painted white.

The values of critical parameters for each test are presented in Table 1. Note: The listed values of γ_s and γ_r have been increased by

9% to account for a 2-inch overlap of the roof slab onto each wall. Further, γ for the frangible wall has been increased by 5% to account for a 1/2-inch overlap of the wall onto its supports.

6.3 Predicted Versus Measured Results

The measured and predicted results for each test are compared in Table 2. The small difference between the measured and predicted $i_T/W^{1/3}$ for tests 23 and 24 (no frangible wall, i.e. $N=3$) indicate the NAVFAC P-397 procedure for the predicting the reflected-shock impulse on interior surfaces of a structure are quite accurate, at least for the range of parameters tested.

The value of test parameters in tests 25 and 27 are nearly identical, except for the properties of the frangible wall. The frangible wall was plate glass in test 25 and plywood/metal in test 27. The small difference between measured and predicted $i_T/W^{1/3}$ for these tests suggests that the brittleness of a frangible wall does not significantly effect the gas pressure environment inside a structure.

Test 29 provides the best measure of the reliability of the design criteria since the gas impulse was a large percentage of the total impulse. Note that the difference between the measured and predicted i_T is largest for this test.

The ratio of measured to predicted i_T averaged over all tests is 0.99. This suggests that the design criteria for frangible covers is adequate, at least for the range of parameters tested.

7.0 APPLICATION OF CRITERIA

The following problems and their solutions illustrate the application of the design criteria for frangible covers.

7.1 Missile Test Cell

The missile test cell shown in Figures 1 and 2 supports testing and checkout of the LUNI missile. The net weight of explosive for the LUNI is 343 pounds TNT equivalent. The center of gravity of the explosive is positioned such that the scaled reflected-shock impulse on the frangible wall is $i_r/W^{1/3} = 100$ psi-msec/lb^{1/3}, according to NAVFAC P-397 (or computer program BARCS). The frangible wall is a 3-inch-thick reinforced concrete slab with a total surface area equal to 150 ft². The volume of the missile test cell is 8575 ft³.

(a) Problem: Find the peak gas pressure, B_g , gas impulse, i_g , and effective gas duration, T'_g , inside the missile test cell.

Solution: The scaled area and mass of the frangible wall and the density of explosive in the missile test cell are

$$A/V^{2/3} = 150/(5277)^{2/3} = 0.49$$

$$\gamma/W^{1/3} = (3 \times 145)/12/(343)^{1/3} = 5.2 \text{ psf/lb}^{1/3}$$

$$W/V = 343/5277 = 0.040 \text{ lb/ft}^3$$

Entering Figure 4 with $W/V = 0.040$, find

$$B_g = 240 \text{ psi}$$

Entering Figure 9 with $W/V = 0.040$, $\gamma/W^{1/3} = 5.2$, $A/V^{2/3} = 0.49$ and $i_r/W^{1/3} = 100$, find

$$i_g/W^{1/3} = 325 \text{ psi-msec/lb}^{1/3}$$

$$i_g = 325(343)^{1/3} = 2275 \text{ psi-msec}$$

From Equation 10, the effective gas duration for design purposes is

$$T'_g = \frac{2 i_g}{B_g} = \frac{2(2275)}{240} = 19.0 \text{ msec}$$

(b) Problem: Find the percent reduction in the gas impulse if the LUNI missile is moved closer to the frangible wall such that $i_r/W^{1/3} = 1000$ psi-msec/lb^{1/3}.

Solution: Entering Figure 9 with $W/V = 0.040$, $\gamma/W^{1/3} = 5.2$, $A/V^{2/3} = 0.49$ and $i_r/W^{1/3} = 1000$, find

$$i_g/W^{1/3} = 92 \text{ psi-msec/lb}^{1/3}$$

$$i_g = 92 (342)^{1/3} = 644 \text{ psi-msec}$$

Therefore, the reduction in gas impulse applied to all surfaces of the missile test cell is

$$\text{Reduction in } i_g = \left(\frac{2275 - 644}{2275} \right) 100 = 72\%$$

This reduction in i_g will reduce significantly the construction cost of the missile test cell but increase significantly the possible strike range of debris from the frangible wall which is roughly proportional to the square of the total impulse. For example,

$$i_T = i_r + i_g = 100(343)^{1/3} + 2275 = 2975 \text{ psi-msec (problem a)}$$

$$i_T = i_r + i_g = 1000(343)^{1/3} + 644 = 7644 \text{ psi-msec (problem b)}$$

Therefore, without an exterior barricade in front of the frangible wall, the possible increase in the strike range of debris, R_s , is

$$\frac{R_s \text{ (problem a)}}{R_s \text{ (problem b)}} = \left(\frac{7644}{2975} \right)^2 = 6.6$$

7.2 Weapons Maintenance Building

The weapons maintenance building shown in Figures 1 and 2 is for maintenance of the HARPOON missile. The workbay, shown in Figure 2, is 100 feet long, 40 feet wide, and 20 feet high and contains no more than 2400 pounds TNT equivalent at any one time. The roof and walls are

massive reinforced concrete slabs designed to protect operating personnel from an inadvertent explosion in an unrelated ordnance facility located nearby. A large equipment door at both ends of the workbay is 25 feet long and 15 feet high. The doors are not blast-hardened and weigh 13.3 psf.

(a) Problem: Find the peak gas pressure, B_g , gas impulse, i_g , and effective gas duration, T'_g , if the scaled reflected-shock impulse, $i_r/W^{1/3}$, on the doors is 100 psi-msec/lb^{1/3}.

Solution: The door area is $A = (25 \times 15)2 = 750 \text{ ft}^2$. The volume of the workbay is $V = 40 \times 20 \times 100 = 80,000 \text{ ft}^3$. The weight of explosive is $W = 2400 \text{ lb}$. The door mass is $\gamma = 13 \text{ psf}$. Therefore, the critical scaled parameters are

$$A/V^{2/3} = 750/(80,000)^{2/3} = 0.40$$

$$W/V = 2400/80,000 = 0.040 \text{ lb/ft}^3$$

$$\gamma/W^{1/3} = 13.3/(2400)^{1/3} = 1.00 \text{ psf/lb}^{1/3}$$

Entering Figure 9 with these values, find

$$i_g/W^{1/3} = 120; \quad i_g = 120(2400)^{1/3} = 1606 \text{ psi-msec}$$

Entering Figure 4 with $W/V = 0.040$, find

$$B_g = 240 \text{ psi}$$

From Equation 10, the effective duration of gas pressure in the workbay is

$$T'_g = 2(1606)/240 = 13.4 \text{ msec}$$

(b) Problem: Find the gas impulse in the workbay if the mass of the equipment doors is increased to 67 psf to improve physical security of the building.

Solution: The scaled door mass is $\gamma/W^{1/3} = 67(2400)^{1/3} = 5.0 \text{ psf/lb}^{1/3}$. Entering Figure 9, find

$$i_g/w^{1/3} = 350; \quad i_g = 350(2400)^{1/3} = 4686 \text{ psi-msec}$$

Thus, increasing the door mass from 13.0 to 67 psf increases the gas impulse applied to interior surfaces of the building by

$$\text{increase in } i_g = \left(\frac{4686 - 1606}{1606} \right) 100 = 192\%$$

8.0 FUTURE WORK

Explosive tests are planned for 1983. The tests will extend the range of test parameters and include large scale tests. The large scale tests are considered important since the theory used to develop the design criteria is based on empirical relationships derived from small scale tests.

9.0 REFERENCES

1. Naval Facilities Engineering Command. NAVFAC P-397, Army TM 5-1300 and Air Force AFM 88-22: Structures to resist the effects of accidental explosions. Washington, D.C., Jun 1969.
2. Naval Sea Systems Command. NAVSEA OP-5: Ammunition and explosives ashore, vol 1, rev. 5. Washington, D.C., Oct 1976.
3. Civil Engineering Laboratory. Technical Note N-1494: Optimum dynamic design of nonlinear reinforced concrete slabs under blast loading, by J. M. Ferritto. Port Hueneme, Calif., Jul 1977.
4. J. F. Proctor and W. S. Filler. "A computerized technique for blast loads from confined explosions," from Minutes of the 14th Annual Explosives Safety Seminary, New Orleans, La., Nov 1972, p 99.
5. Civil Engineering Laboratory. Technical Report R-828: Blast environment from fully and partially vented explosions in cubicles, by W. A. Keenan and J. E. Taureto. Port Hueneme, Calif., Nov 1975.

10.0 LIST OF SYMBOLS

A	Area of the opening without the frangible cover, ft^2
\bar{A}	x_p , effective vent area, ft^2
B_g	Peak gas pressure extrapolated to time $t = 0$, psi
B_r	Peak reflected-shock pressure, psi
d_s	Depth of soil cover, ft
$E(x)$	Total strain energy absorbed by structural element at displacement x relative to its support, ft-lb/ft^2
g	Gravity = 32.2×10^{-6} , ft/msec^2
h	Height of frangible wall, ft
h_1	Height of explosive (c.g.) above floor, ft
i_B	Total reflected shock impulse, psi-msec
i_g	Total gas impulse, psi-msec
i_r	Total reflected-shock impulse, psi-msec
i_T	Total impulse; sum of reflected-shock plus gas impulses, psi-msec
l	Length of frangible wall, ft
l_1	Distance from explosive (c.g.) to sidewall, ft
m	Mass per unit area of surface, $\text{psf-msec}^2/\text{ft}$
N	Number of adjacent reflecting surfaces.
$P(t)$	Pressure at time t , psi
$P_g(t)$	Gas pressure at any time t , psi
$P_r(t)$	Reflected-shock pressure at any time t , psi
R	Normal distance from c.g. of explosive to a surface of structure, ft
s	Perimeter of the opening providing escape path for gases, ft
T_g	Duration of gas pressure, msec
T'_g	$2i_g/B_g$ = Effective duration of the gas pressure based on a linear time decay, msec

t	Elapsed time after detonation, msec
t_1	Time when reflected pressure equals the gas pressure, msec
T_r	$2i_r/B_r$ = Effective duration of the reflected shock pressure based on a linear time decay, msec
V	Volume of structure containing the explosion, ft^3
W	Net weight of explosive, lb (TNT equivalent)
x	Displacement at any time t , ft
\dot{x}	Velocity at any time t , ft/msec
x_m	Maximum displacement, ft
\dot{x}_T	Velocity at time T_r , ft/msec
α	Exponential decay constant for $P_g(t)$, msec^{-1}
γ	Mass of frangible cover per unit area of surface, lb/ft^2
γ_r	Mass of roof slab per unit area of surface, lb/ft^2
γ_s	Mass of soil cover per unit area of surface, lb/ft^2
ρ_s	Density of soil, lb/ft^3

Table 1. Test Parameters for Missile Test Cell

Test No.	Test Charge				Test Cell ^a				Frangible Wall				
	W (lb)	R (ft)	h _I (ft)	λ_I (ft)	d _S (ft)	ρ_S (lb/ft ³)	γ_S^b (lb/ft ³)	γ_r^b (lb/ft ³)	h (ft)	l (ft)	P (ft)	A (ft ²)	γ^c (lb/ft ²)
23	1.00	3.00	0.583	1.833	0.667	85.0	61.8	9.73	2.58	3.75	12.3	9.17	0.00
24	3.00	3.00	0.583	1.833	0.833	84.9	77.1	9.86	2.58	3.75	12.3	9.17	0.00
25	1.00	3.00	0.583	1.833	0.667	87.5	63.6	9.73	2.58	3.75	12.3	9.17	1.72
26	1.00	3.00	0.583	1.833	0.833	89.0	80.8	9.73	2.58	3.75	12.3	9.17	1.82
27	1.00	3.00	0.583	1.833	0.667	85.8	62.4	9.04	2.58	3.75	12.3	9.17	1.82
28	3.00	3.00	0.583	1.833	1.000	83.0	90.5	9.04	2.58	3.75	12.3	9.17	1.82
29	1.00	3.00	0.583	1.833	0.833	84.2	76.5	9.86	2.58	3.75	12.3	9.17	11.03
30	3.00	3.00	0.583	1.833	1.000	84.0	91.6	9.86	2.58	3.75	12.3	9.17	11.03
31	3.00	3.00	0.583	1.833	0.833	84.6	76.8	9.86	2.58	3.75	12.3	9.17	1.82
32	1.00	3.00	0.583	1.833	0.333	84.6	30.7	10.0	2.58	3.75	12.3	9.17	1.82
33	3.00	3.00	0.583	1.833	0.333	85.0	30.9	10.0	2.58	3.75	12.3	9.17	1.82

^aV = 55.1 ft³; L = 6.0 ft; H = 2.50 ft; w = 3.67 ft.^b γ_S and γ_r increased by 9% to account for overlap of roof slab onto its supports.^c γ increased by 5% to account for overlap of frangible wall onto its supports.

Table 2. Comparison of Measured and Predicted Total Impulse on Roof

Test No.	Scaled Parameters				Measured		Predicted			i_T (meas.) i_T (pred.)
	$A/V^{2/3}$ (-)	$R/W^{1/3}$ (ft/lb ^{1/3})	W/V (lb/ft ³)	$\gamma/W^{1/3}$ (lb/ft ² -lb ^{1/3})	y_m (ft)	$i_T/W^{1/3}$ ^a (psi-msec/lb ^{1/3})	$i_r/W^{1/3}$ ^b (psi-msec/lb ^{1/3})	$i_g/W^{1/3}$ ^c (psi-msec/lb ^{1/3})	$i_T/W^{1/3}$ ^d (psi-msec/lb ^{1/3})	
23	0.633	3.17	0.018	0.0	2.4	192	161	0	161	1.19
24	0.633	2.20	0.054	0.0	6.4	264	253	0	253	1.04
25	0.633	3.17	0.018	1.72	4.4	266	198	100	293	0.89
26	0.633	3.17	0.018	1.82	4.2	321	198	105	297	1.06
27	0.633	3.17	0.018	1.82	5.4	287	198	105	297	0.95
28	0.633	2.20	0.054	1.26	~9.8	374	311	61	410	1.01
29	0.633	3.17	0.018	11.03	9.5	461	198	368	540	0.81
30	0.633	2.20	0.054	7.64	--	--	311	237	548	--
31	0.633	2.20	0.054	1.26	--	--	311	59	370	--
32	0.633	3.17	0.018	1.82	--	--	198	99	297	--
33	0.633	2.20	0.054	1.26	55	364	311	61	370	0.98

Avg. = 0.99

^aFrom Equation 11.^bFrom Equation 1 based on N = 3 for tests 23 & 24 and N = 4 for tests 25-33.^cFrom Figures 7-10.^dFrom Equation 12.

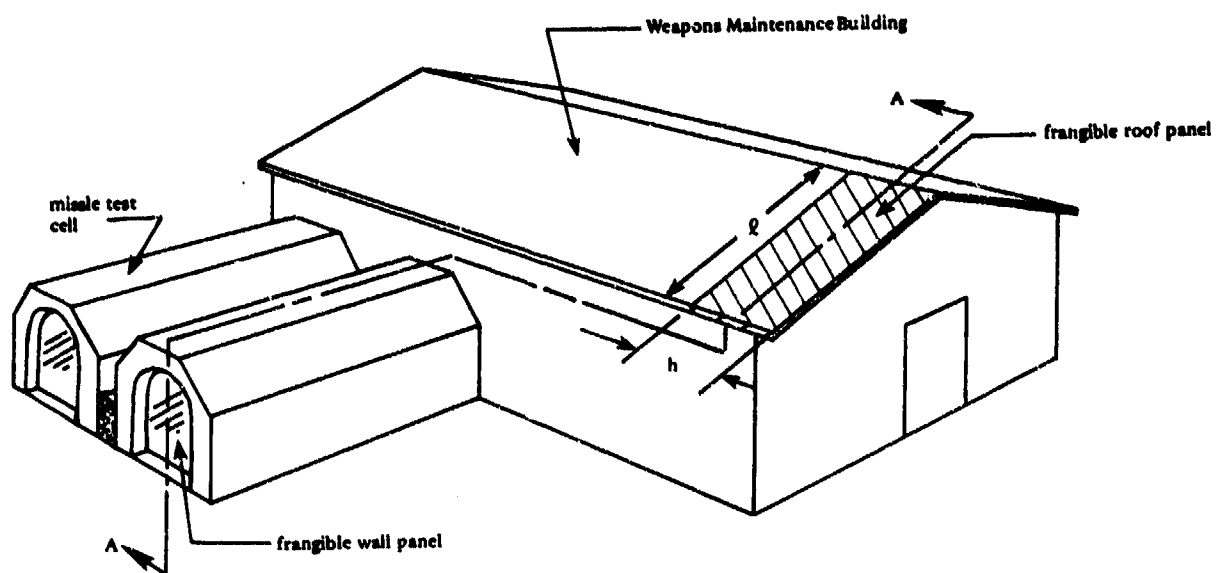


Figure 1. Frangible panels in Weapons Maintenance Facility.

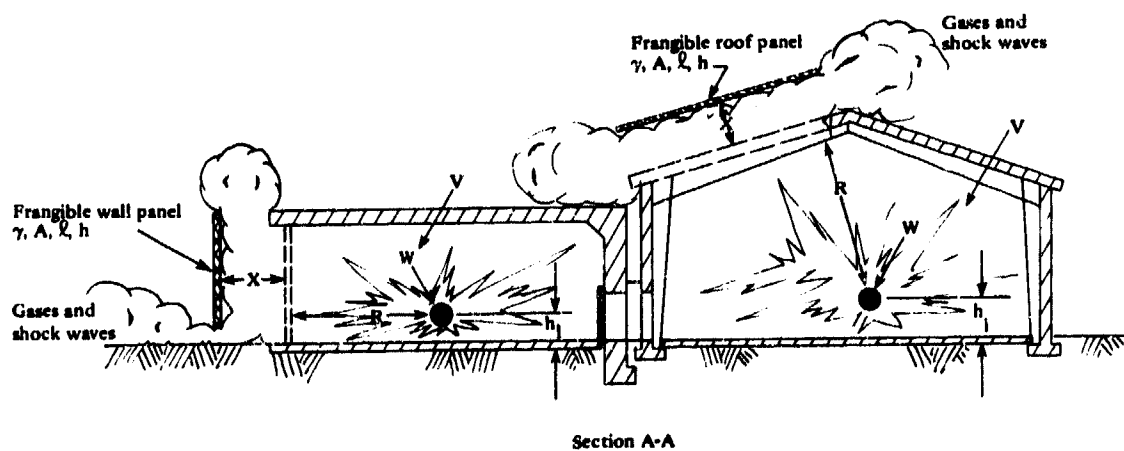


Figure 2. Design parameters for frangible panels.

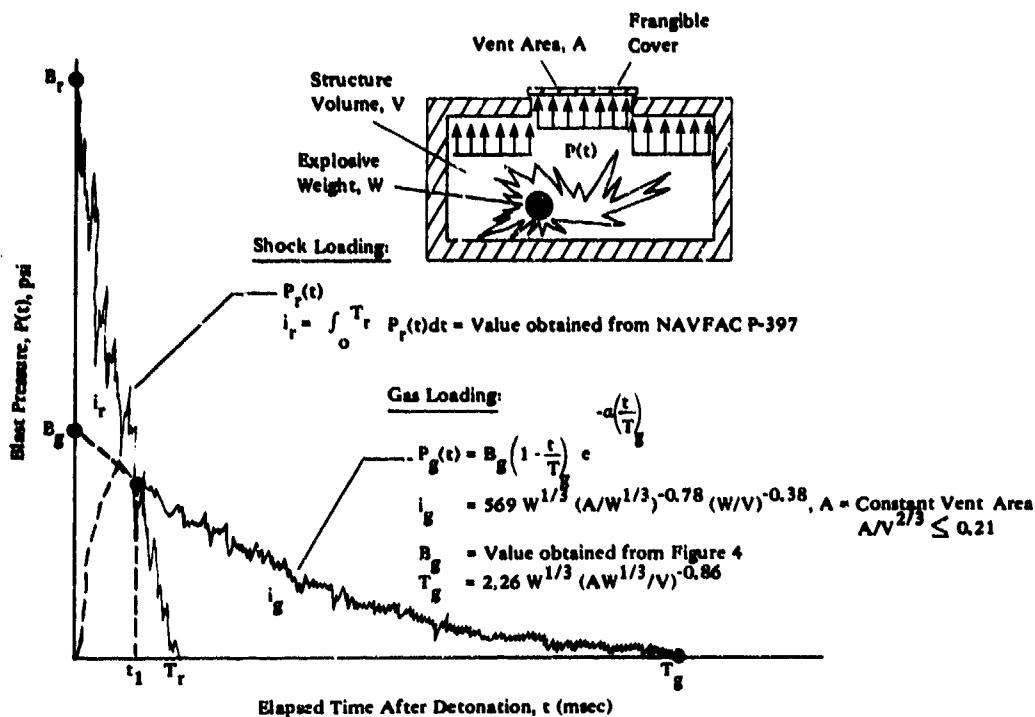


Figure 3. Internal blast loading for constant vent area; loading on a cover that is non-frangible for reflected-shock pressures but fully frangible for gas pressures.

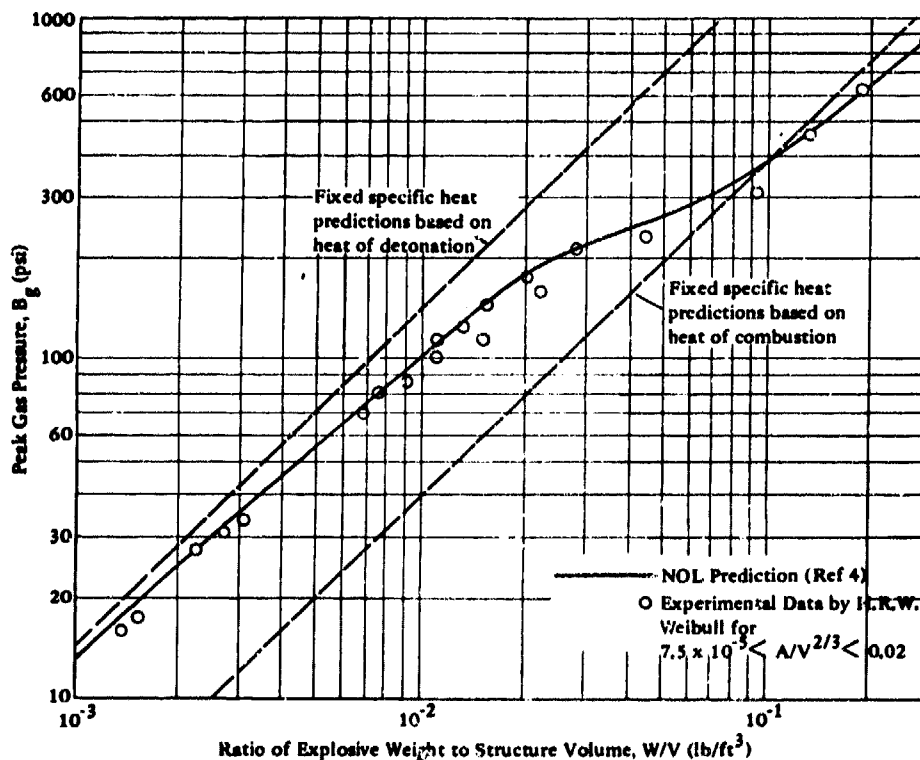


Figure 4. Peak gas pressure inside a structure.

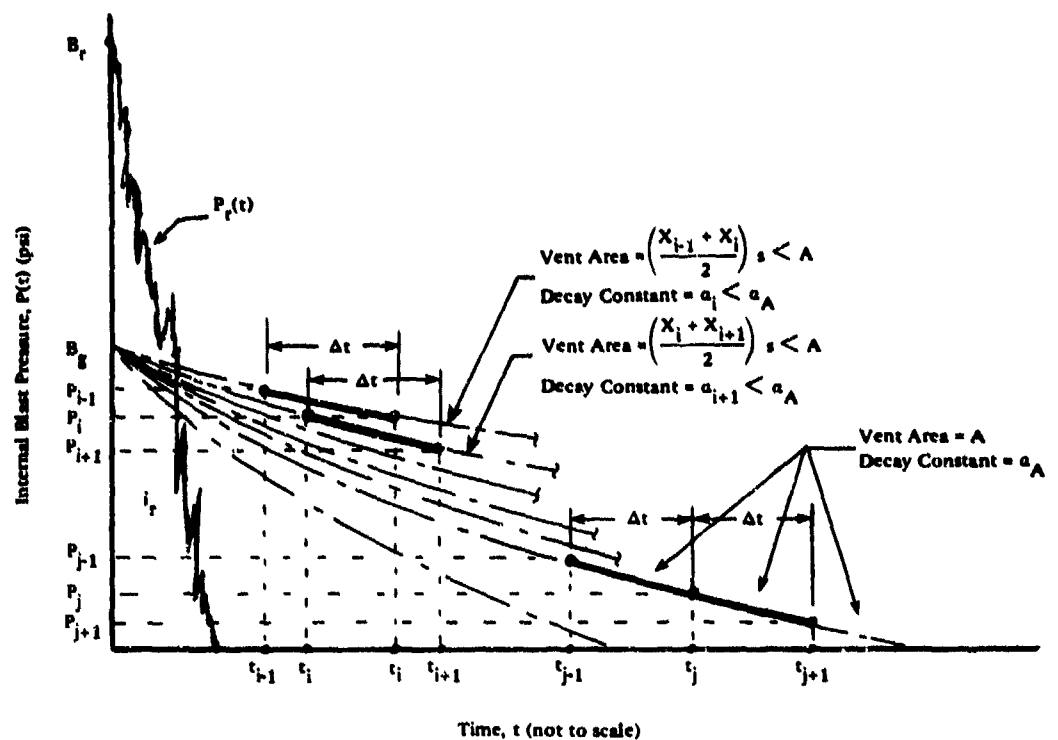


Figure 5. Graphical display of solution method for gas pressure history when response of cover controls venting and later when area of opening controls venting.

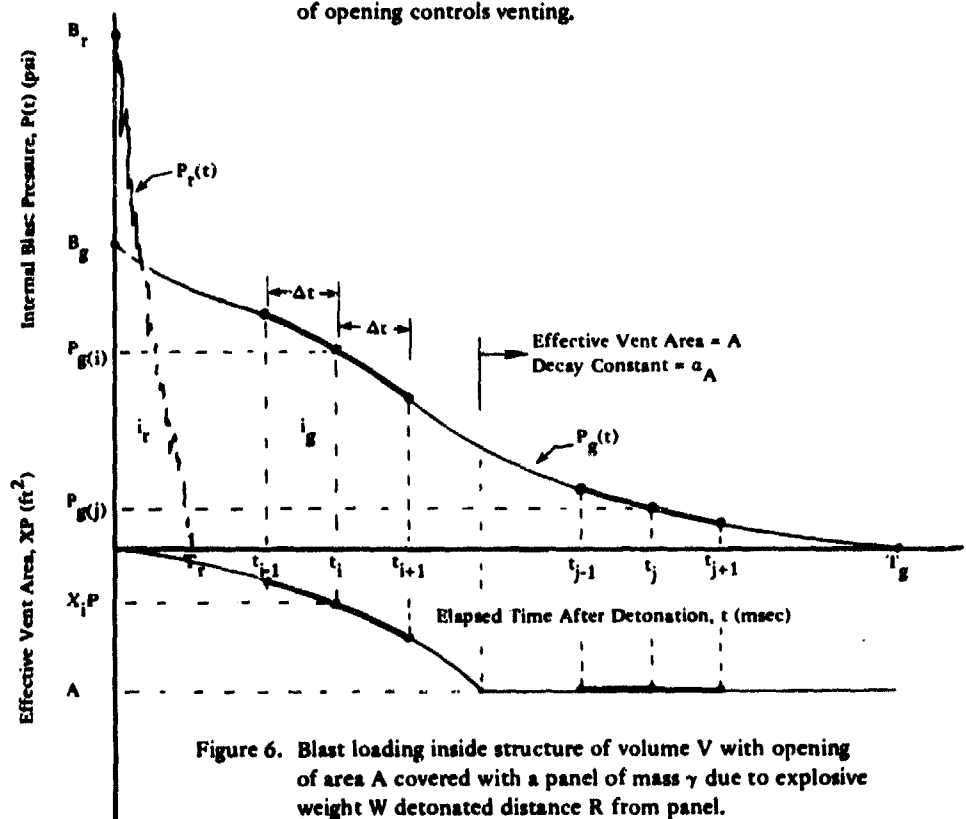


Figure 6. Blast loading inside structure of volume V with opening of area A covered with a panel of mass γ due to explosive weight W detonated distance R from panel.

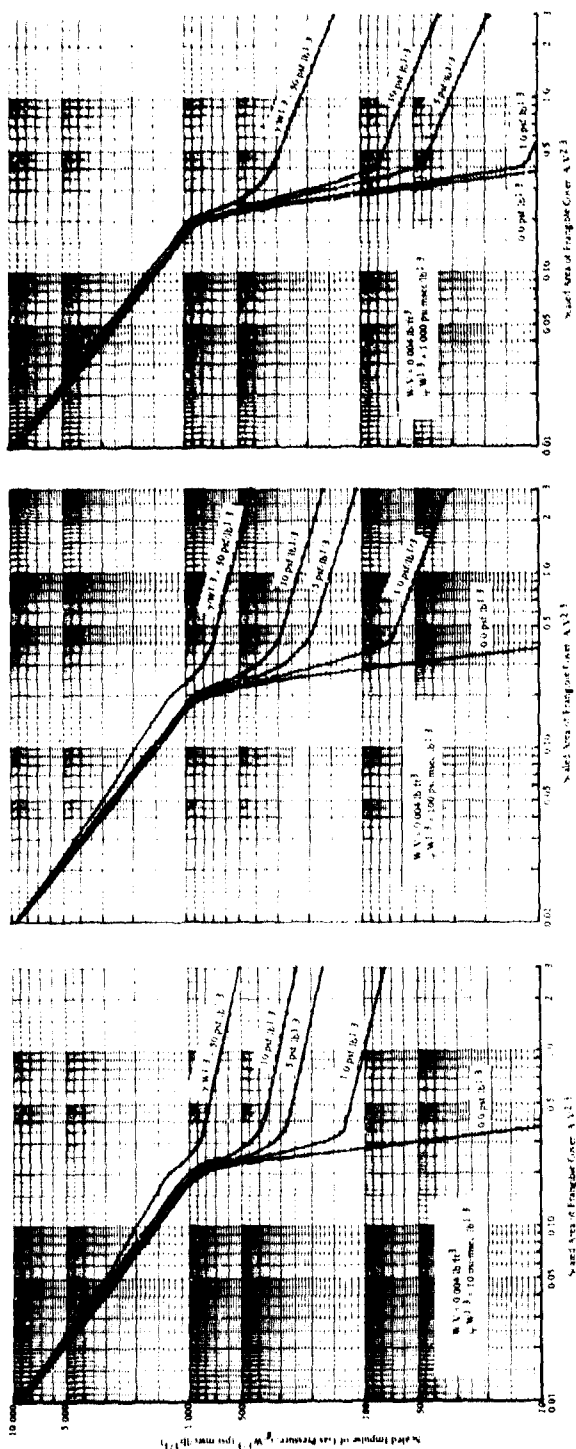


Figure 7. Design criteria for frangible covers for $W/V = 0.004 \text{ lb/ft}^3$.

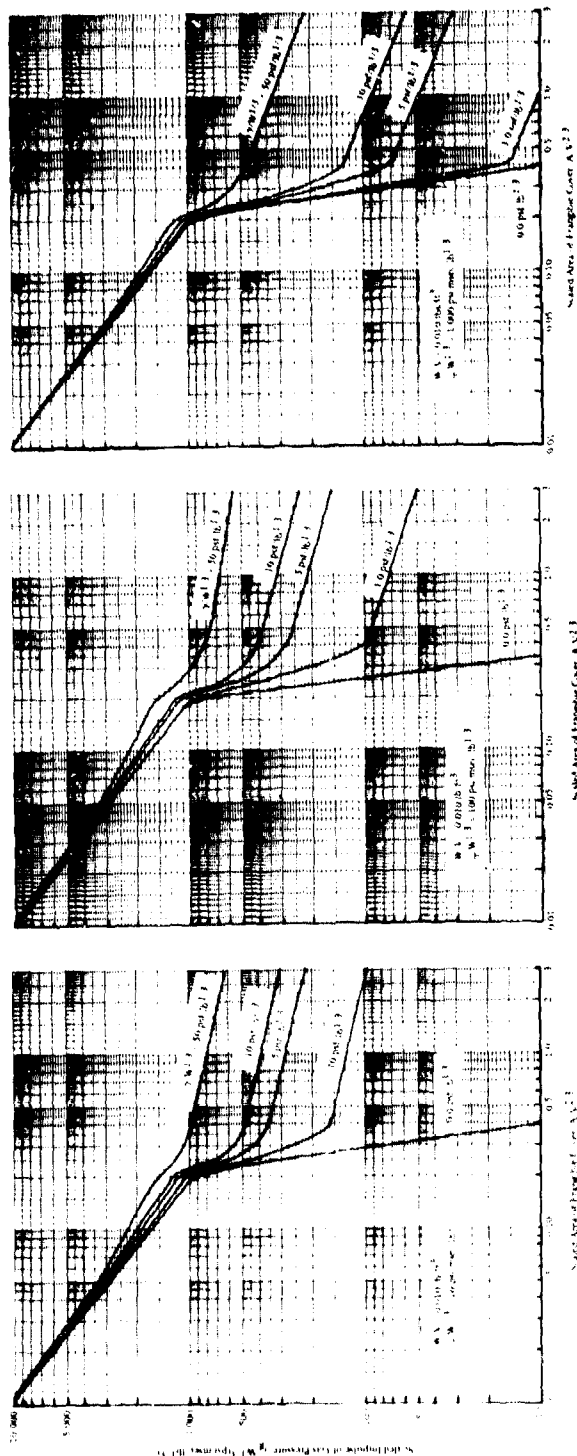


Figure 8. Design criteria for frangible covers for $W/V = 0.010 \text{ lb/ft}^3$.

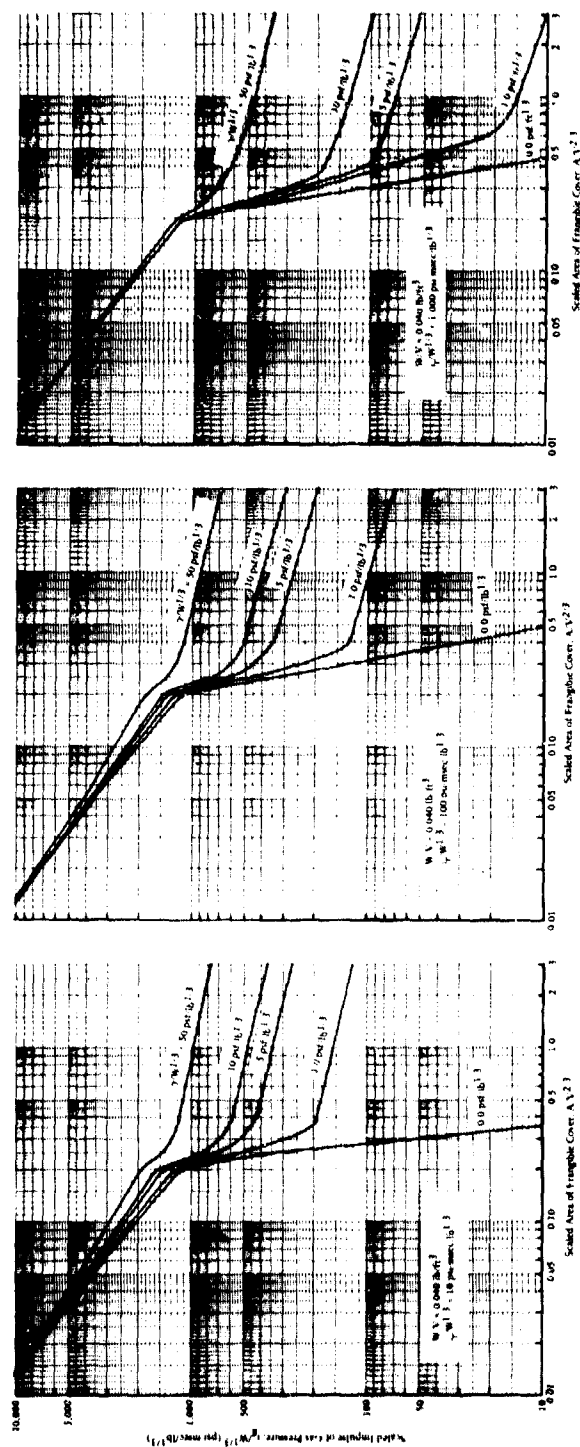


Figure 9. Design criteria for frangible covers for $W/V = 0.040 \text{ lb/ft}^3$.

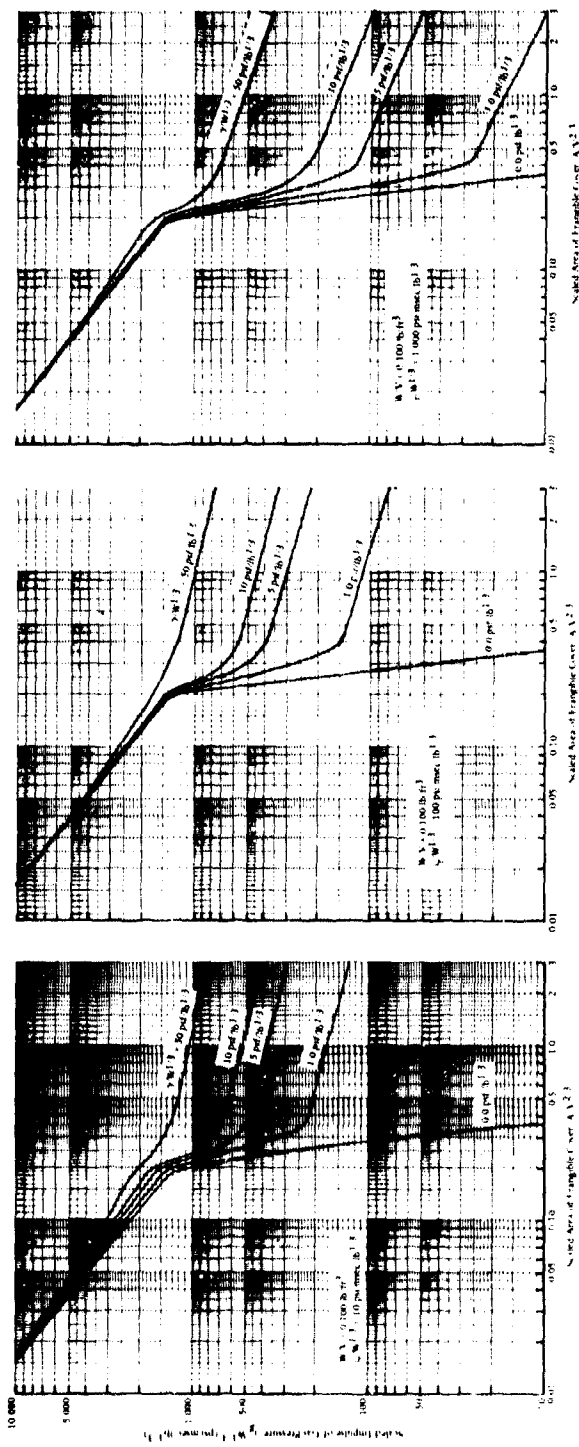


Figure 10. Design criteria for frangible covers for $W/V = 0.100 \text{ lb/ft}^3$.

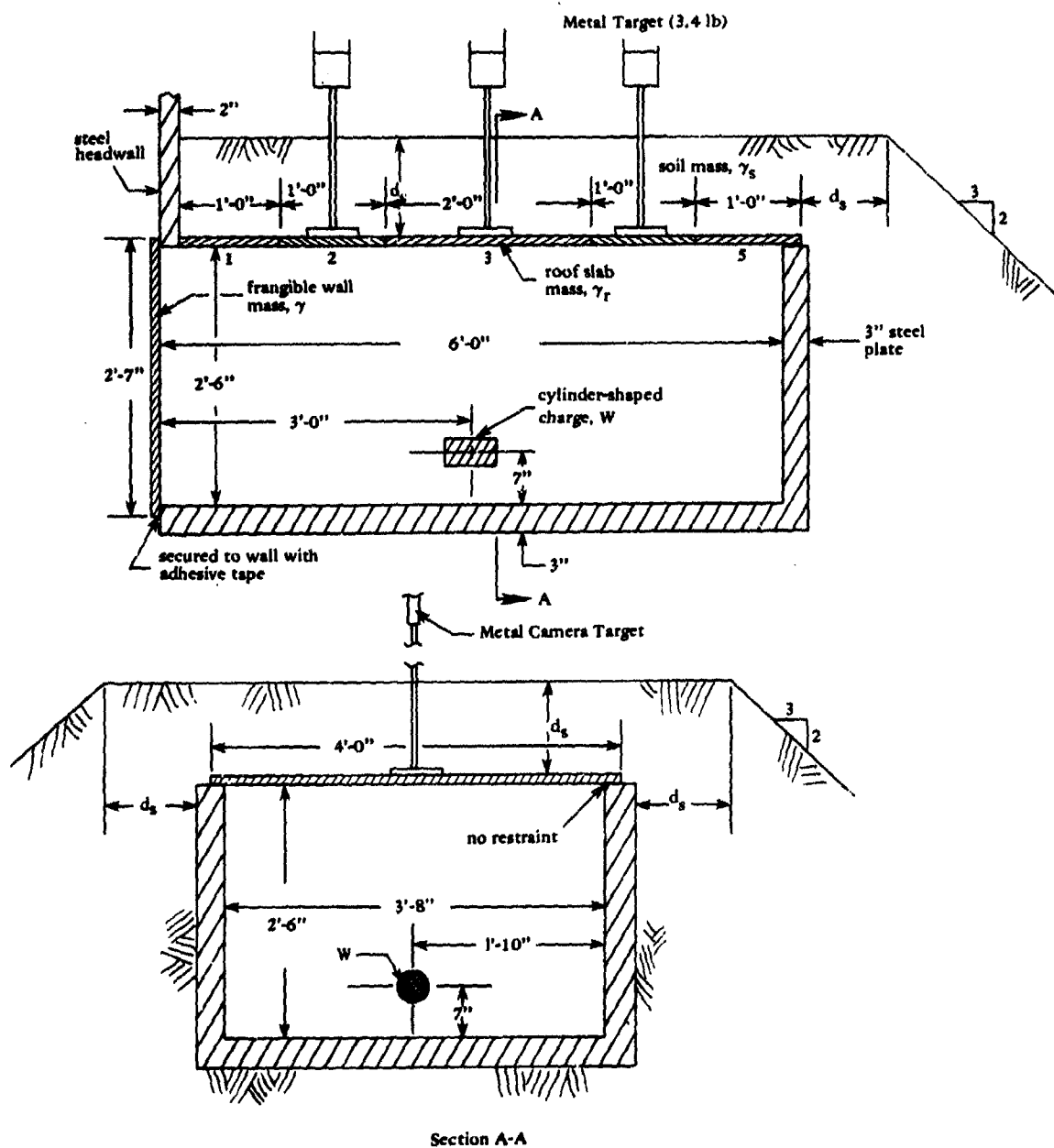


Figure 11. Design details of missile test cell.

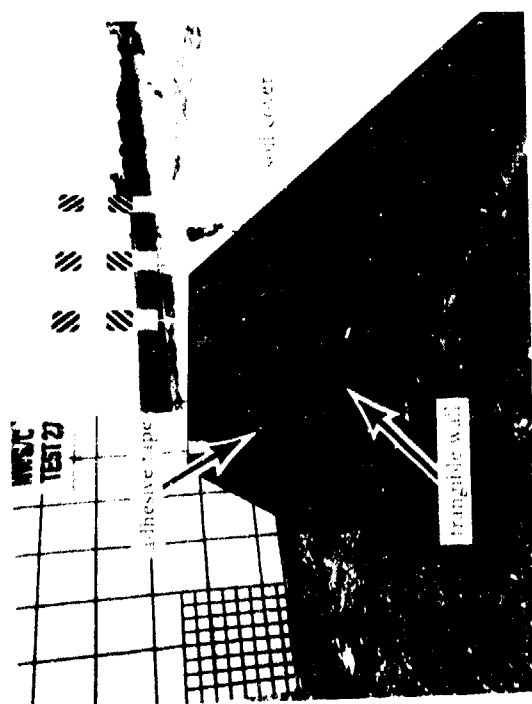


Figure 12. View of missile test cell.

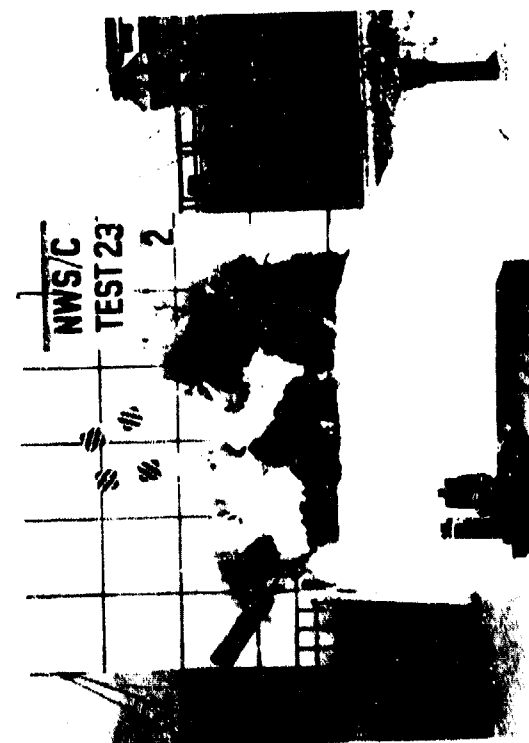


Figure 13. View of missile test cell near time of maximum response of roof slab - Test 23, no frangible wall ($\gamma=0$ psf), $W = 1.0$ lb.



Figure 14. View of missile test cell near time of maximum response of roof slab - Test 25, plate glass wall ($\gamma=1.73$ psf), $W = 1.0$ lb.

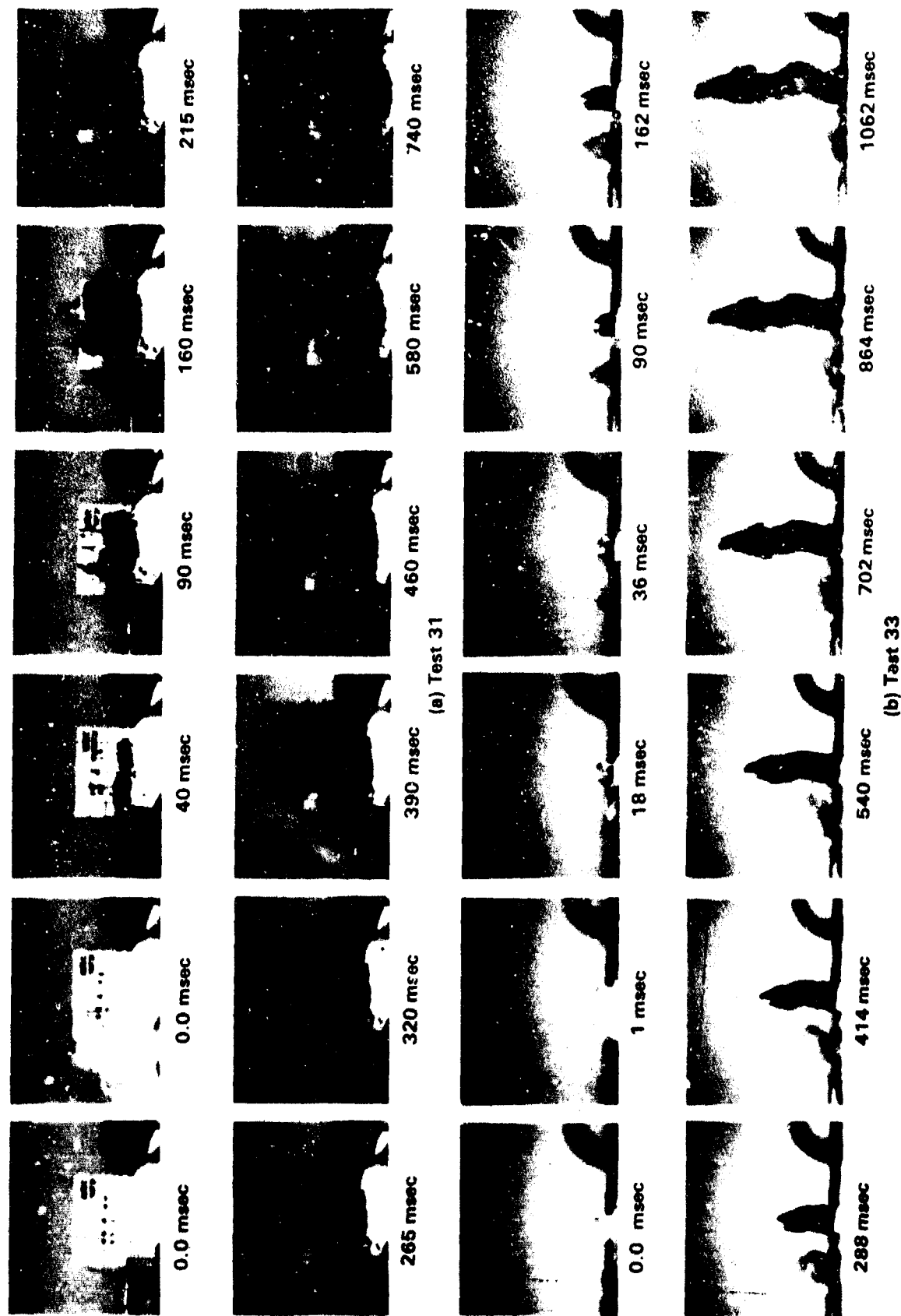


Figure 15. Dissipation and directional effects of kinetic energy of roof mass.

Internal Blast Measurements in a Model of the Pantex Damaged Weapons Facility

By

J. C. Hokanson, E. D. Esparza, W. E. Baker and N. R. Sandoval,
Southwest Research Institute

AD P000439

ABSTRACT

The Damaged Weapons Facility (DWF), planned for construction at the Pantex Plant, will consist of several rooms and interconnecting corridors. It is being designed to essentially completely contain explosive effects in the event of an accidental explosion during weapon disassembly. Because of the complex geometry of the facility, the rational prediction of initial and later reflected shock wave loading, and the longer-term gas pressure loading, is very difficult. Accordingly, a one-eighth scale, overstrength, steel "loads" model of the facility has been built and tested. Tests include detonations within the model of various weights and types of spherical and cylindrical explosives, at several charge locations within the high bay area of the facility. This paper summarizes shock and gas pressure measurements taken within the model, and compares test results to current methods for estimating these transient pressures and to data from other investigators.

INTRODUCTION

General

This paper summarizes results of a two-phase test program conducted by the staff of Southwest Research Institute under Purchase Order No. F0913400, for Mason and Hanger-Silas Mason Company, Inc., Pantex Plant, Amarillo, Texas.

The work involved the design, preparation of construction drawings, fabrication, instrumentation, and internal blast testing of a one-eighth geometric scale model of the Damaged Weapons Facility (DWF) planned for construction at the Pantex Plant. The full-scale facility, which is to be used as a disassembly facility for damaged weapons, is being designed for Department of Energy, Amarillo Area Office, by the firms of Gibbs and Hill, and Ammann and Whitney. Since these weapons contain high explosives as well as toxic material, their disassembly must be performed within a structure which in the event of the occurrence of an accidental detonation, will contain, within acceptable limits, the explosive and toxic materials output.

The Damaged Weapons Facility will consist of several rooms and interconnecting corridors. The disassembly of a weapon will take place in the main room or bay. This room is fully enclosed except for an access opening to surrounding staging areas, corridors, and equipment and personnel blast locks. Methods for determining the blast loads produced by spherical charges which are detonated within fully enclosed cubicle type bays are well known (Refs. 1 and 2). However, only a minimal amount of data are available pertaining to the evaluation of the blast loads and overpressures which leak out of a bay into the adjoining confined areas.

To determine these latter blast loads, a series of tests has been conducted. These tests included the initiation of various explosive charges within a one-eighth scale model of the Damaged Weapons Facility and recording the magnitude of the resulting blast overpressures, impulse and thermal variations. The data obtained from these tests will enable the verification (or nonverification) of the estimated blast loads used for the building design (Phase I). Also, the test results provide an insight into internal blast loads produced by (1) multiple charges, (2) charge geometry, (3) charge confinement and (4) TNT equivalency (Phase II).

Purpose and Objectives

The primary purposes of the tests in Phase I were to obtain measurements of the blast and gas pressure loads, both within the high bay where explosions may occur, and within corridors and staging bays adjacent to the high bay. All but one of the explosive charges detonated in this phase were single PBX 9404 spheres weighing about 0.990 lb (this represents 507 lb in full scale). The charge location was varied, as well as the pressure measuring stations. Tests were replicated three times to determine reproducibility of measured dynamic loads.

The objectives for Phase II were the determination of internal blast loads associated with:

1. "TNT equivalency" of PBX 9404, PBX 9502, and Pentolite;
2. Multiple charges;
3. Short cylindrical charges;
4. Lightly used charges.

In support of the first of these objectives, there was also a requirement for measuring heats of combustion for explosives to be tested in this program, as well as explosives for which there was an extensive data base of internal explosion measurements.

An additional objective during this phase was to obtain better transient thermal measurements by use of fast-response calorimeters, and to use these measurements to predict temperature-time histories for critical components in the prototype structure.

Paper Content

In following sections, we describe the design and construction of the model, give our plan for instrumentation, describe the plan for reduction of the many channels of data recorded during each test, and give the test plan for both phases of the tests. Then, test results are summarized. The paper concludes with a discussion of the test results. A reference list is appended. Much more complete descriptions of this internal blast project appear in Ref. 3 and 4 for Phase I and Ref. 5-7 for Phase II.

SCALING

The Hopkinson-Cranz scaling law for air blast waves from explosive sources (Ref. 8) predicts that the entire history of shock loading of a complex structure should scale properly in subscale experiments, provided that:

1. Exact geometric similarity is maintained,
2. All times scale in exactly the same proportion as the geometric (length) scale factor λ ,
3. Types of explosive sources are identical and total source energy E scales as λ^3 , and
4. Initial atmospheric ambient conditions are unchanged.

Furthermore, References 9 and 10 show that explosions within vented or unvented containment structures will generate long-term (quasi-static) pressures whose amplitudes and durations (when vented) also scale according to the Hopkinson-Cranz law.

The implications of the blast scaling law are as follows:

1. At similar locations and similar scaled times, pressure amplitude and velocities are identical in model and full-scale tests.
2. Because times are compressed by the scale factor λ , shock arrival times, pressure rise times, overpressure durations, and all characteristic times in complex pressure-time histories scale by λ .
3. Specific impulses also scale as λ , because the amplitudes (pressures) are unchanged and the durations scale as λ .

Inherent in the Hopkinson-Cranz law is the assumption (and proof by many, many tests) that, for the very rapid shock loading and still rapid gas pressure rise processes in contained high explosive loading, heat transfer processes lag so greatly that they have insignificant effect on the transient loads.* The scaling of the complex process of heat transfer by radiation, convection and conduction is very difficult (see Chapter 12 of Ref. 8), and obeys quite different scaling laws than for the pressure loads from contained explosions.

Basically, the model of the DWF which we built and are testing maintains close to the exact geometric internal shape of the full-scale DWF design. However, outer wall, roof and floor thicknesses are not exactly geometrically scaled, but are instead designed for strength to withstand many scaled internal explosions with no damage. No attempt whatever was made to scale or model heat transfer processes in model design and construction.

*Eventually, even the quasi-static pressure within a gas-tight container will very nearly equilibrate, as the hot explosion gases and compressed air mix and cool by heat transfer through the container walls.

Basically, the model of the DWF which we built and are testing maintains close to the exact geometric internal shape of the full-scale DWF design. However, outer wall, roof and floor thicknesses are not exactly geometrically scaled, but are instead designed for strength to withstand many scaled internal explosions with no damage. No attempt whatever was made to scale or model heat transfer processes in model design and construction.

There is ample evidence that the Hopkinson-Cranz blast scaling law applies for very small geometric scale factors λ (see Ref. 8). So, the choice of λ is dictated by other factors. As the scale factor becomes smaller, the required frequency response for blast transducers and recording systems must be increased proportionally, because all times are also shortened by λ . Also, as model size decreases, access to the model becomes more difficult. These negative factors must be weighed against reduced construction cost with smaller size. The choice of $\lambda = 1/8$ for this model was dictated primarily by the need for internal access to change model configuration and to inspect, replace or rearrange instrumentation between tests. Someone had to be able to crawl inside the model, and that would have been impossible at a smaller scale.

MODEL DESIGN AND CONSTRUCTION

Model Design

All-welded construction was chosen for this model, because of strength, economy in construction and ease of making the model pressure-tight. The basic construction material was chosen to be a pressure vessel steel, ASTM A 537 Class 1. This material has high yield strength and ductility, even at low temperatures. It also can be welded in thick sections with little loss in material strength and ductility.

We conducted some limited analyses to predict blast loads and response of elements in the structures, to allow us to size the steel plate thicknesses for various parts of the structure.

Most of the blast loading predictions were made for the surfaces of the high bay area, using worst-case (nearest charge locations) for each surface. The methods for predicting local and average peak overpressure and specific impulse loading are described in detail in Reference 2. Details appear in Ref. 1. Quasi-static pressures were also predicted from a curve in Reference 2, using the maximum charge weight and the volumes of the high bay area for one pressure, and the entire internal volume of the model for another pressure.

Using the maximum calculated blast and quasi-static loads within the high bay area, plate thicknesses were sized assuming elastic beam strip theory, clamped-clamped boundary conditions, and a factor of safety (FS) of 1.5, based on static yield strength for the A 537 Class 1 steel. Scaled pressure-impulse (P-i) diagrams from Reference 11 were used for these calculations. The results showed that $h = 3$ inches was adequate for all surfaces in this part of the structure. Details appear in Ref. 1.

Calculations of blast loads within other parts of the structure are very questionable (which is, indeed, the reason for this program). So, to achieve a conservative design and to allow choice of a suitable hydrotest pressure,

we established Dynamic Load Factors for the heavily-loaded high bay structural elements, based on the vibration frequencies of appropriate beam strips, and then computed equivalent static pressures to give the same maximum stresses, using again the safety factor of 1.5. The recommended hydrotest pressure was $P_T = 210$ psi. Based on this pressure, plate sizes were chosen for the remainder of the model. These were 1.5 inches for walls outside of the high bay, and 2.0 inches for roof outside the high bay. Although there are no good methods for predicting blast loads outside the high bay area, we felt that we could obtain at least order of magnitude estimates by exercising a two-dimensional blast wave code and representing the three-dimensional model structure by a two-dimensional analog. The results of these calculations could give a rough idea of blast pressures and rise times, and thus help in selection of appropriate transducers, as well as indicate possible areas of blast focusing causing local high pressures. The results of these calculations appear in Appendix C of Ref. 1. Although the absolute numbers were not expected to correlate well with test data, relative amplitudes between the high bay area and other areas were helpful in planning our instrumentation. They were also comforting to the designers, because no high local overpressures were predicted outside the high bay area.

The final design of the model evolved on the basis of the above design calculations; the need for access to all outer surfaces of the model for installing and for changing instrumentation; and the practical requirements for welding, assembling, inspection, and stress relief. A support structure allowing access from below was designed as a welded grillage of deep section I-beams, with seven large access holes cut through the webs. In the model itself, the design allowed subassembly of units, which were then welded together for final assembly. The method and sequence of construction was planned to minimize welding distortions, and to allow complete nondestructive inspection of critical welds.

In the final design, there are two hinged manhole covers for access, many transducer holes, sliding doors for the equipment and personnel locks which can be bolted in place in the closed position or held open, and a small vent pipe which is normally closed, but can be opened through a pneumatically actuated valve.

Model Construction

The model was fabricated at Southwest Research Institute. Steel plate was cut to size, beveled as needed, and welded into subassemblies using machine and hand welding equipment and methods. All "outer envelope" welds which must withstand significant blast and quasi-static pressure loads were fully inspected using approved methods of nondestructive inspection. Any critical flaws were ground out and rewelded.

The model was assembled in several subassemblies, which were separately stress relieved. These two major subassemblies were then welded together, and other small parts welded in place. While still in the welding shop, the model was hydrostatically tested to 210 psig. It was then painted and installed at our test range. The completed model is shown in Fig. 1 and 2.

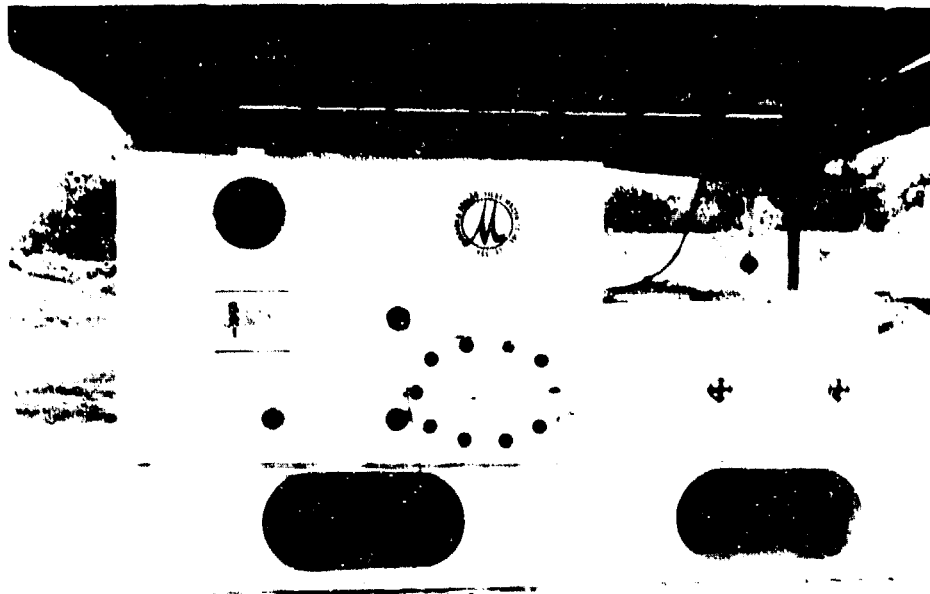


Figure 1. Completed Model Installed at Test Range

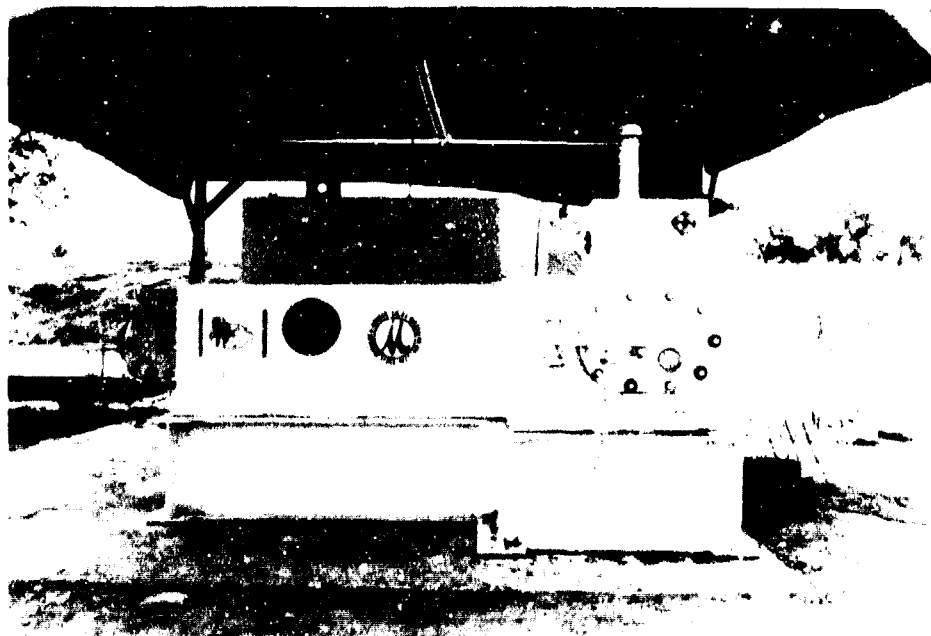


Figure 2. Completed Model Installed at Test Range

INSTRUMENTATION

In these tests, three types of transient measurements were made during Phase I:

1. Blast pressure
2. Gas pressure
3. Temperature.

In addition, heat fluxes were measured during Phase II. There were 53 measurement locations during Phase I, increased to 63 during Phase II. These locations are shown schematically in Fig. 3 and 4. On any one test, only certain locations were instrumented. The rest of the sensing locations were sealed with blind covers to maintain model pressure tightness.

Blast Pressure

The majority of the measurements made were blast pressures. The transducers selected for these measurements are made by PCB Piezotronics, Inc., and are miniature dynamic sensors specifically designed for blast wave measurements which require very high frequency response. Two basic models were used, Model 102 and Model 109A. All Model 102 transducers have the same mechanical configuration but have four different ranges (250; 1,000; 5,000; and 10,000 psi). For those gage locations very close to the charge, Model 109A (80,000 psi) transducers were used because of the higher blast pressures expected. This higher range transducer does differ in mechanical configuration from the lower range transducers.

Each PCB transducer utilizes an acceleration compensated, quartz, piezoelectric, pressure sensing element coupled to a miniature source follower within the body of the transducer. This micro-electronic amplifier converts the high impedance output of the quartz element into a low impedance, high level output signal. Regardless of range or configuration, all of these transducers have a rise-time capability of one microsecond.

Recording of all blast pressure data was done on two, 14-track, Wideband II FM tape recorders at a speed of 60 ips. The data bandwidth (-3db) at this recording speed is 0-250 kHz.

Gas Pressure

For gas pressure measurements made at locations where the blast pressure amplitude was expected to be only slightly higher than the quasistatic gas pressure, Endevco Model 8510M transducers, with a range of 500 psi, were used. At gas pressure locations where high amplitude blast pressures were expected (primarily in the high bay) Endevco Model 8511A with a range of 2,000 psi, and Kulite Model HKS-375 with a range of 5,000 psi were used to sense the higher gas pressure.

All of these transducers use a four-arm Wheatstone bridge diffused into a silicon diaphragm. These piezoresistive transducers feature greater than 100 mV full-scale output voltage, high resonant frequency, good linearity, and static pressure response. These transducers are capable of recording blast pressures.

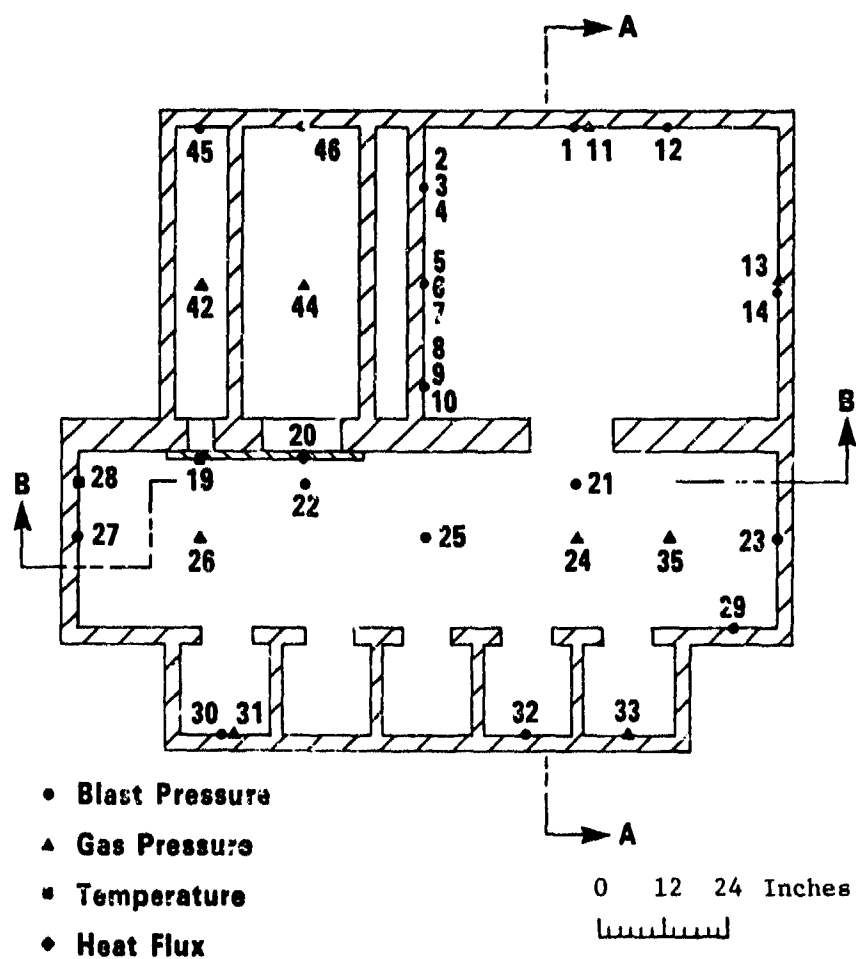


Figure 3. Transducer Locations, Plan View

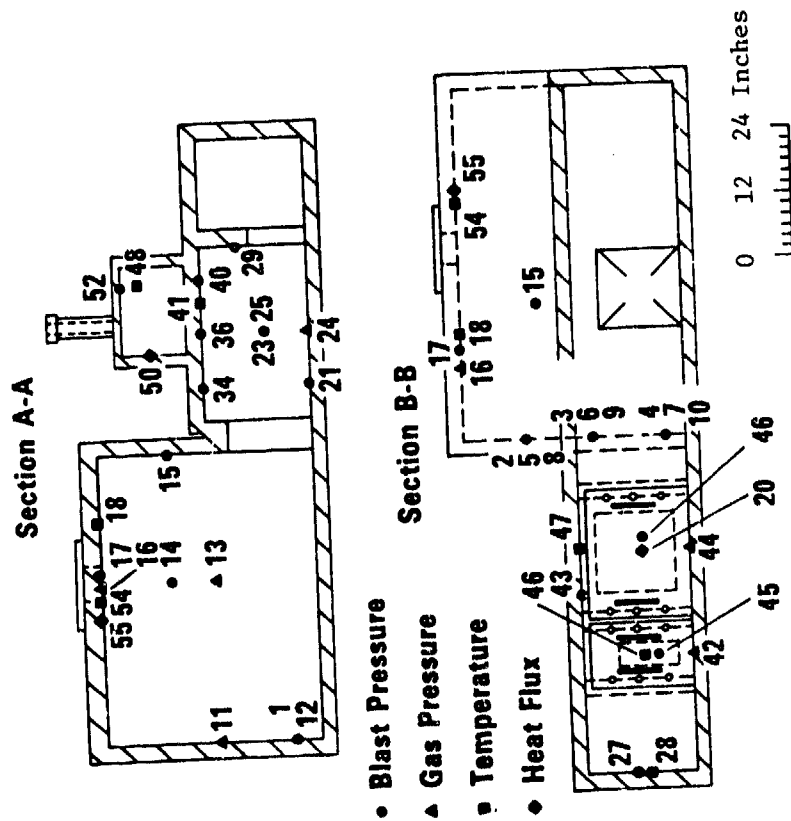


Figure 4. Transducer Locations, Vertical Sections

However, because of their static pressure response capability, they were set up to sense the gas pressure rise within the model structure, while at the same time providing a reasonable survival rate to the higher blast pressures.

Bridge power and output signal amplification was provided with Vishay Model 2310 signal conditioning amplifiers. These units accept low-level signals from strain gages, piezoresistive transducers, thermocouples, etc., and condition and amplify them into high-level outputs suitable for multi-channel magnetic tape recordings.

Recording of all gas pressure data was made on a 14-track, Intermediate band, FM tape recorder at a speed of 30 ips. The data bandwidth (± 1 db) at this recording speed is 0-10,000 Hz. This bandwidth was more than sufficient to record the gas pressure data.

Temperature and Thermal Flux

Although some inner surface temperature measurements were made during Phase I testing, and more temperature and thermal flux measurements during Phase II, the primary thrust of the testing was to obtain pressure measurements. So, we do not detail the instrumentation for recording transient temperatures and thermal fluxes. See Ref. 3-7 for details.

Playback Electronics

The test data recorded in both phases were played back and digitized using the system shown in Figure 5, to produce the data plots. Up to four channels of data were played back at one time through the analog filters into a Biomation Model 1015 four-channel transient recorder. This recorder digitizes the incoming analog signals at sample intervals of 0.01 milliseconds or greater. Since this unit has four separate analog-to-digital (A/D) converters, the samples for each of the four data channels are time correlated. The maximum number of samples which can be taken is 1024 per channel. The A/D units are 10 bit units, which means that the analog signals are digitized with a resolution of one part in 1024 of the full-scale voltage setting. The minimum full-scale voltage setting is 0.1 volts.

Once the test data (or calibration pulses) are properly formatted in digital form, the DEC 11/23 computer extracts the data from the transient recorder memory through the CAMAC* data buss and stores them on an eight-inch flexible diskette. A graphics terminal is used to display each data trace for verification.

The stored data on the diskettes were read into a DEC 11/70 minicomputer; then, the appropriate data processing plots were prepared using a Printronix 300 printer/plotter.

DATA REDUCTION

General

The test data were digitized using the equipment described in the previous section with the following procedure. The calibration signals, 1 kHz, 1 volt

*Computer Automated Measurement and Control ANSI/IEEE-583 Buss

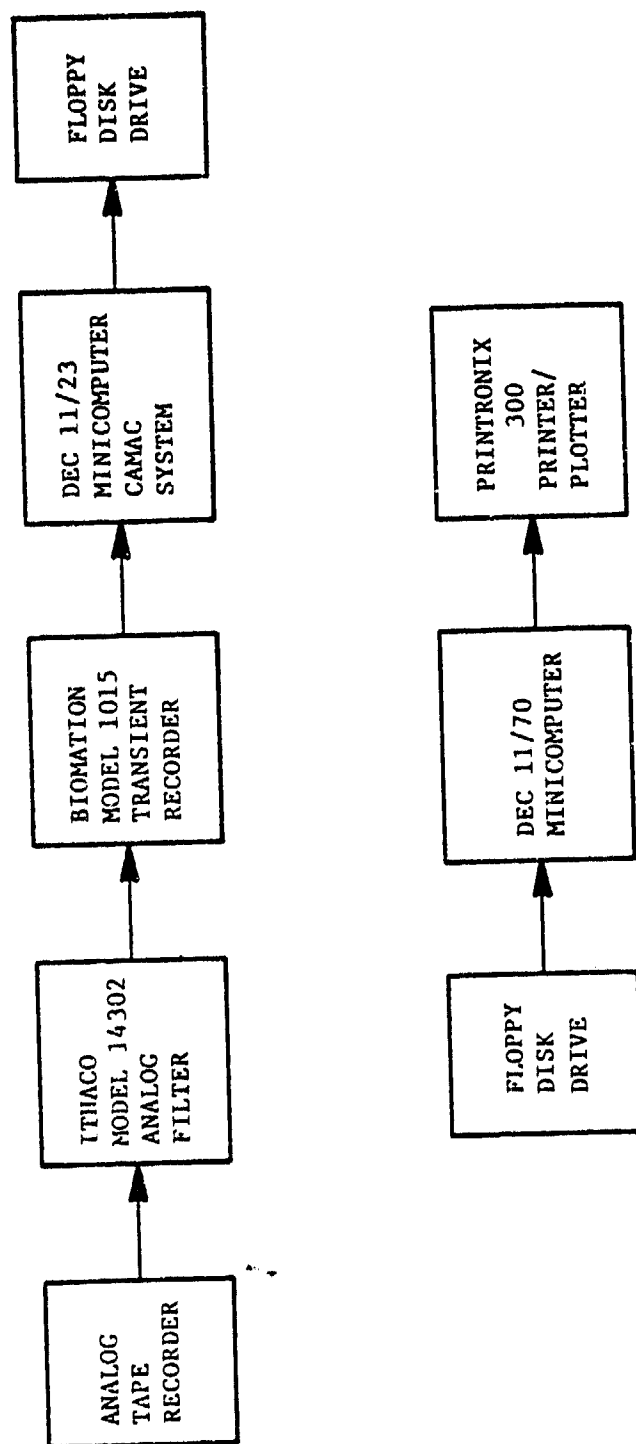


Figure 5. Test Data Playback System

p-p, recorded on each tape recorder channel prior to each test, were digitized by the Biomation unit and transferred to the 11/23 computer. The analog filters were set to a low pass cutoff frequency of 200,000 Hz for the calibration signal playback. The digitized calibration signal was analyzed to establish the factor required to convert the test data to engineering units.

The calibration factor was calculated individually for each gage on each test. Then the analog data were played into the Biomation recorder. The filters were generally set at a low pass cutoff frequency of 2000 Hz for the gas pressure gages and 2000 Hz for the blast pressure gages in the low bay. The filters were generally set at a low pass cutoff frequency of 200,000 Hz for the blast pressure gages in the high bay. To ensure that all data channels were time correlated, the signal which caused the charge to explode was recorded on channels 1 and 2 of each tape recorder. This signal, which we call time zero, was also digitized unfiltered in channel 1 of the Biomation recorder each time data were played back. The data digitized by the Biomation have units of counts. The data amplitude in engineering units of psi is then determined using calibration data for each transducer and the calibration factor also.

Extraction of Engineering Design Parameters from the Pressure Traces

The pressure records digitized as described above were examined to obtain certain parameters useful in the design of a structure loaded by an internal explosion. The parameters desired are:

- o quasi-static pressure, P_{QS}
- o shock pressure, P_S
- o shock impulse, I_S
- o duration of shock loading, D_S .

The definitions of these parameters are given in Figure 6. The maximum quasi-static pressure is quite difficult to define because it is obscured by the initial shock and the first few reflected shocks. Obviously, several reflections must take place before an irreversible process attenuates the shocks and converts the energy into the quasi-static pressure. We have decided to set the P_{QS} by examining the record and locating the time at which the shocks appear to be well attenuated. The amplitude at this time is then defined as the quasi-static pressure. This point also defines the duration of the shock loading. If we assume that the quasi-static pressure builds linearly from zero to P_{QS} , then the shock impulse is defined as the integral of the net pressure amplitude above the ramp increase. This is shown in Figure 6 as the shaded region of the curve. The shock pressures are then the amplitudes of the initial shock and the first few peaks, again above the ramp increase in the quasi-static pressure.

The quasi-static pressures are estimated using the same techniques as the blast pressure records. The shock pressure, impulse, and duration were not extracted from these records.

LOC=27 TEST=09

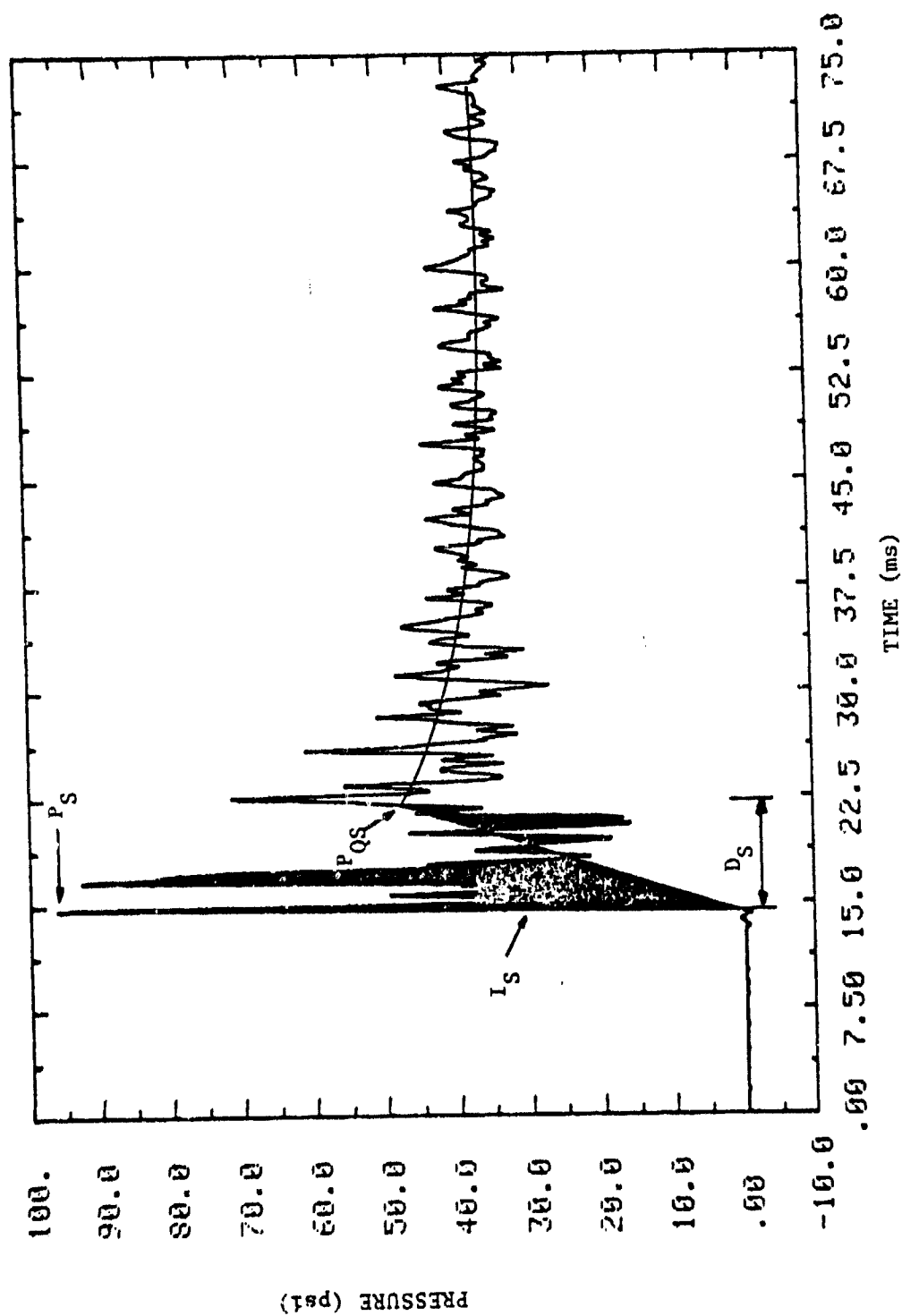


Figure 6. Definition of Parameters Extracted from the Blast Pressure Traces

TEST PLAN

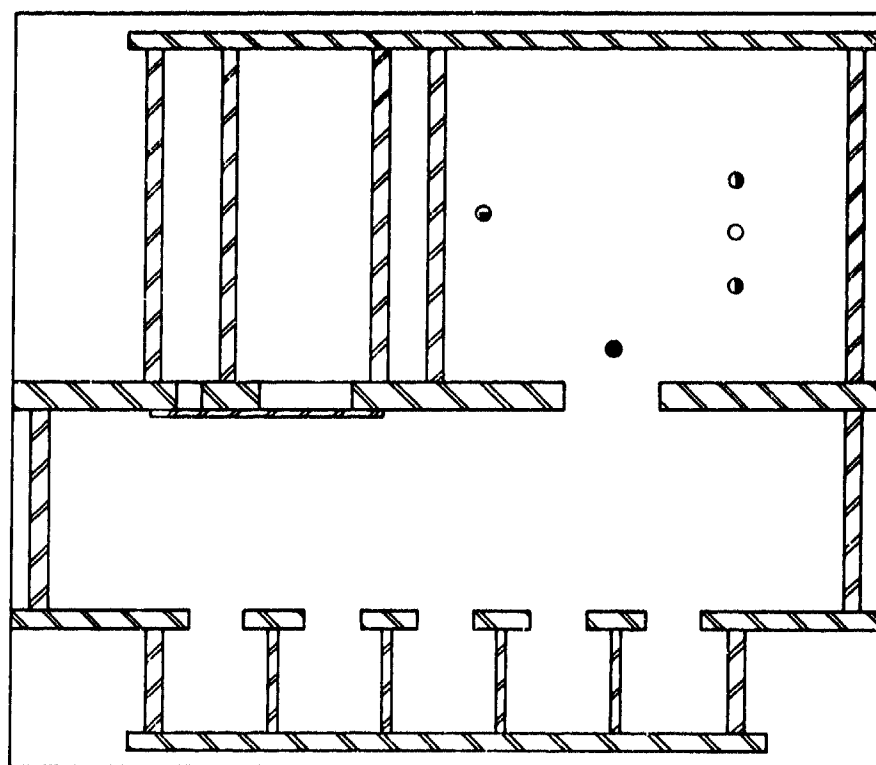
Test Procedures

All of the explosive charges used in this program were provided by Mason and Hanger. Mason and Hanger also conducted a number of tests to determine a reliable method of initiation so that output (breakout) from the spherical charges was as simultaneous as possible. (See Ref. 12.) Prior to conducting the Phase I experiments, 12 PBX-9404 charges, two pentolite charges and two TNT charges were selected at random and were assembled under the direction of personnel from Pantex. The assembly consisted of gluing the Reynolds Industries RP-2 exploding bridgewire detonator into the specially machined cavity in each charge. Extra care was taken when assembling the TNT charges, since these charges had a small PBX-9404 pellet at the bottom of the cavity (to provide reliable and consistent high order ignition) which has to be properly seated. These assembly procedures were followed throughout the test program.

Each test began with the preparation of a data sheet which defined the gage location, gage serial numbers, amplifier gain, charge location, and other test information for the range personnel. The technicians would then install the gages in the model and connect them to the instrumentation system. If a gage had already been installed, then all exposed wiring was inspected and corrected if necessary. The gages were checked for continuity at the amplifier to ensure that each channel was properly connected and that the transducer was electrically sound. The test prolog and the 1.0 volt, 1 kHz calibration were then recorded on each of the three analog tape recorders.

A technician then examined each transducer from the inside of the model. Any debris on the transducer diaphragm was carefully cleaned off. The Endevco gas gages have a recessed diaphragm. The cavity on the exposed face of the transducer must be filled with an opaque grease to protect the transducer and to prevent a photoelectric response from the light emitted from the fireball. This cavity was filled with a syringe prior to each test (after Test 4) with the grease provided by Endevco. A thin coat of Dow Corning DC-4 was applied over the diaphragm for thermal shielding. The last step in preparing for the test was to suspend the charge at the location specified for the test. This was accomplished by placing the charge in a portion of a fish net, and hanging the net from one of several nuts which had been welded to the roof of the high bay. Charge locations are shown in Fig. 7. Nuts welded to strategic points on the floor provided additional tie-down points to ensure that the charge was suspended as close as reasonably possible to the desired charge location. Still photographs of the suspended charge were taken before the two manhole doors were closed. The pneumatic valve used to relieve the pressure in the model after a test was checked to ensure that the valve was closed. The range was then cleared of all personnel.

At this point, the tape recorders were placed in the record mode, and the charge was fired. The tape recorders were left on for a minimum of 10 seconds before being turned off. Once all recorders had been shut down, the pneumatic valve was opened remotely, and the pressure in the model was allowed to vent. The lead technician then checked the current weather conditions and made the appropriate entries on the data sheet. The manhole covers were opened, and fans were placed in front of the openings to clear the detonation products from the model. The fans were run for one hour before any personnel had access to the



- Location A
- Location B
- ⊙ Location C
- ⊗ Location D (Multiple)

Figure 7. Charge Locations

inside of the model. Then the exterior and interior of the model were examined for any signs of damage and/or gas pressure leakage.

Phase I Test Matrix

The 12 tests planned for Phase I are summarized in Table 1. Test 0 was planned for a leakage check of the model, but also yielded some useful transient pressure data, so it is included in the matrix. As noted earlier, the primary purpose of this phase was to define transient and long-term pressure loads in areas out of the high bay, so instrumentation was concentrated there for most tests in this phase.

Phase II Test Matrix

This phase included 37 tests, arranged according to the matrix in Table 2. Here, the high bay area was instrumented more completely. Note that, in both phases, tests in any specific configuration were replicated at least once, and usually twice, to determine repeatability of measurements. For Tests 40-45, the model was modified by welding a closure over the high bay door, to lower the internal volume and increase quasi-static pressure.

TEST RESULTS AND DISCUSSION

We recorded useable data on most recording channels on all tests, except during Tests 12, 13 and 22 when a tape recorder malfunctioned, or during most of the tests when transducers were damaged by severe thermal, shock, or fragment impact loads.

The reduced data, in a format of one time history per page, are truly voluminous, and appear in Ref. 4, 6, and 7. They are much too extensive to reproduce here. Typical blast pressure records are shown in Fig. 8, and gas pressure records in Fig. 9. The multiple shocks were quite pronounced in the high bay area, but were markedly attenuated at almost all locations out of the high bay. Quasi-static pressures in this gastight model quickly equilibrated throughout the model (within 15-35 ms). The test data replicated very well, with all features of the complex time histories of pressure being essentially repeated during repeat tests, and small scatter in quasi-static pressure measurements.

During the Phase I testing, it quickly became apparent that quasi-static pressures for PBX 9404 explosive were considerably lower than predicted from methods in Ref. 2 which are based on TNT data and comparative heats of detonation of the two explosives. A summary of these measurements from the Phase I tests appear in Table 3.

In the Phase II testing, much more data were accumulated on quasi-static pressures, because explosive charge weight, test chamber volume and type of explosive were all varied. The average values for P_{QS} for all tests are plotted in Fig. 10 versus the "loading density" W/V . The line for TNT is reproduced from Ref. 2. Note that all data for PBX 9404 lie below the prediction line, while data for cylindrical and cased cylindrical charges lie above the line.

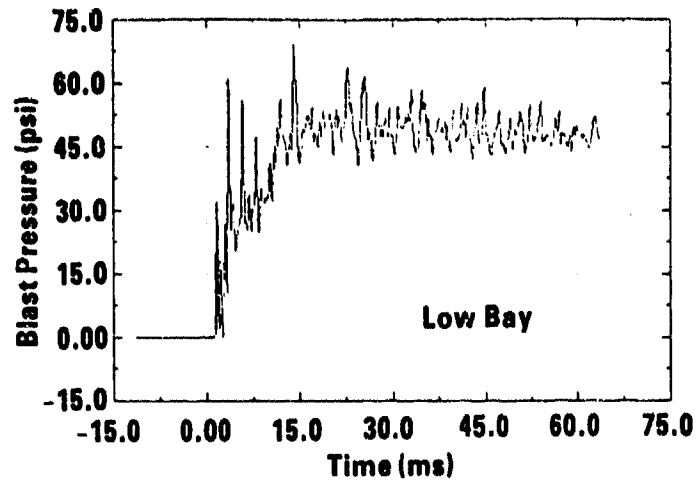
Table 1. Phase I Test Matrix

Test No.	Purpose	Charge	Blast Door Position	Charge Location
1 2 3	Instrumentation Testing	PBX 9404	Closed	Location A
0	Leakage Check	TNT	Closed	Location B
4 5 6	Equivalent Charge Location	PBX 9404	Closed	Location B
7 8 9	Load Verification	PBX 9404	Opened	Location B
10 11 12	Donor Bay Doors	PBX 9404	Closed	Location C

Table 2. Phase II Test Matrix

Test No.	Purpose	Charge	High Bay Door Position	Charge Location
14	Donor Bay Load	PBX-9404	Open	Location C
15-17	TNT Equivalence	TNT	Open	Location A
13, 18-22	TNT Equivalence	PBX-9404	Open	Location A
23-25	TNT Equivalence	PBX-9404	Open	Location A
27-29	Multiple Charges	PBX-9404	Open	Location D
30-31	Charge Geometry	PBX-9404	Open	Location A
32-39	TNT Equivalence	PBX-9582	Open	Location A
40-41	TNT Equivalence	PBX-9582	Closed	Location A
42-43	TNT Equivalence	PBX-9404	Closed	Location A
44-45	TNT Equivalence	Pentolite	Closed	Location A
46-47	TNT Equivalence	Pentolite	Open	Location A
48-50	Charge Confinement	PBX-9404	Open	Location A

**Blast Loads in the Pantex Damaged Weapons Facility
Test No. 39 Location 40**



**Blast Loads in the Pantex Damaged Weapons Facility
Test No. 20 Location 6**

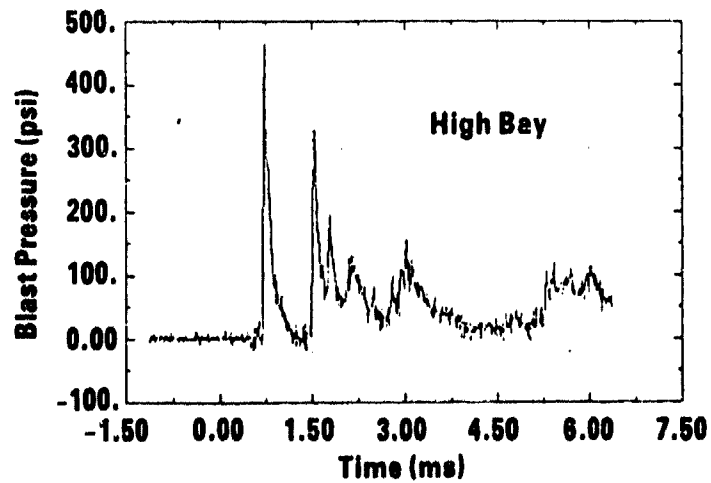
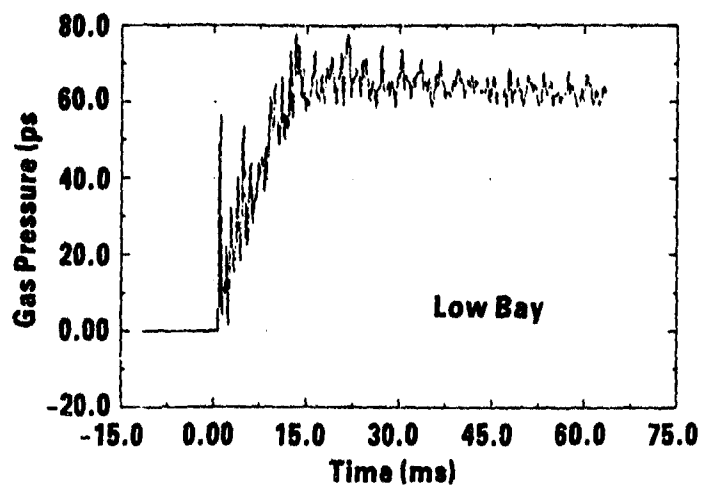


Figure 8. Blast Pressure Records

**Gas Loads in the Pantex Damaged Weapons Facility
Test No. 46 Location 24**



**Gas Loads in the Pantex Damaged Weapons Facility
Test No. 28 Location 11**

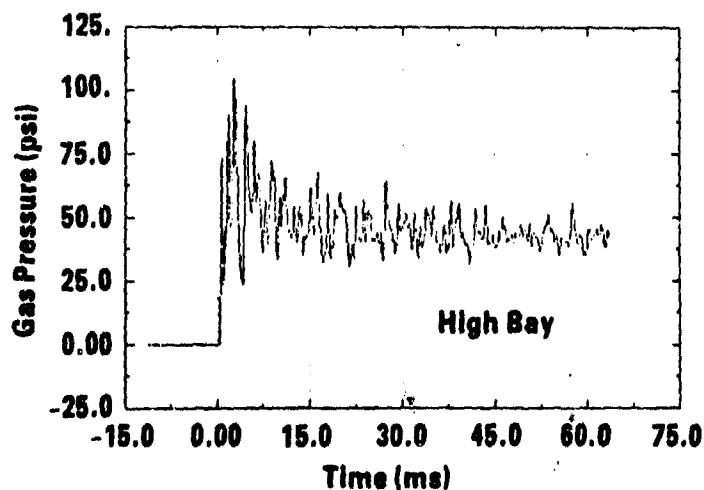


Figure 9. Gas Pressure Records

Table 3. Summary of Quasi-Static Pressure Measurements
from Phase I Tests

Test No.	Blast Door Position	PQS (PSI) Estimated From			
		Gas Gages		Blast Gages	
		PQS	S.D.	PQS	S.D.
1	Closed	43.3	1.1	41.2	6.3
2	Closed	49.1	2.0	51.7	6.0
3	Closed	45.9	0.7	48.6	8.1
4	Closed	46.9	4.2	44.4	4.6
5	Closed	41.0	0.9	46.2	6.4
6	Closed	43.7	2.7	46.0	7.1
10	Closed	51.5	5.5	50.6	6.1
11	Closed	47.3	1.5	44.7	5.1
12	Closed	49.7	3.5	—	—
		46.5 ± 3.4		46.7 ± 3.5	
7	Open	40.5	2.5	38.0	7.8
8	Open	40.1	1.6	39.5	4.3
9	Open	40.2	1.6	39.0	6.2
		40.3 ± 0.2		38.8 ± 0.8	
0	Closed (TNT)	77.0	6.3	85.4	10.5

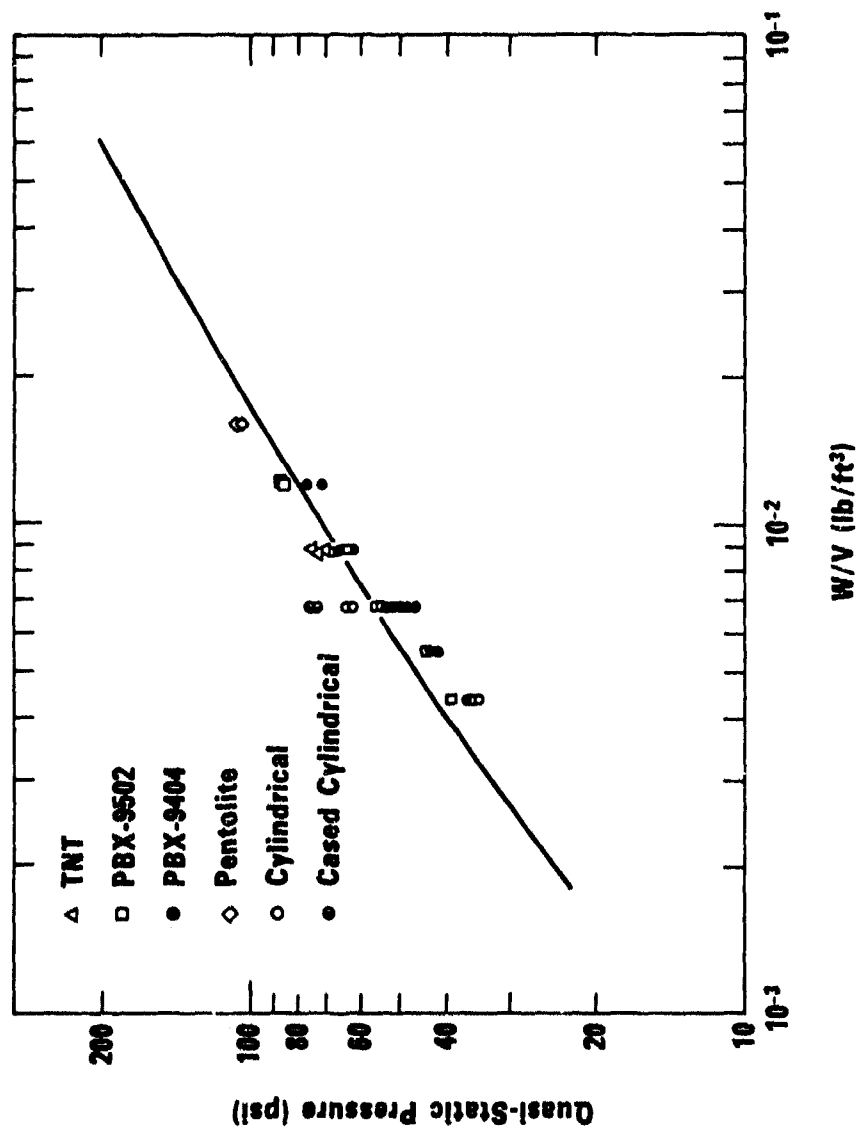


Figure 10. Summary of Quasi-Static Pressure Data

We realized that the quasi-static pressures in this range of loading density must depend on the heat of combustion of the explosive, as much as the heat of detonation, because there is enough oxygen in the air in the chamber to allow considerable afterburning and consequent heat addition to raise the pressure. Measurements of heats of combustion during Phase II allowed us to adjust the effective charge weights for the explosives, in a manner described in Ref. 5. The high quasi-static pressures for the cylindrical charges were at first puzzling, until we realized that both types of cylindrical charges had combustible plastic discs in intimate contact, and that the aluminum casing for the cased charges could also be partially combustible. Accounting for the effect of these energies on the quasi-static pressure allowed us to adjust the correlation with W/V , as shown in Fig. 11.

Unlike the quasi-static pressure data, there were no particular surprises in the shock pressure data. We did note, however, that the effects of changing charge geometry from spherical to cylindrical with L/D ratio of 1:1 were minimal. Also, the change from single spherical charges to pairs of spherical charges with the same total weight produced only minimal changes in shock pressure signals, for the particular charge location and gage measuring stations chosen in this program.

CONCLUSIONS

We can summarize by giving the major conclusions of the Phase I and Phase II testing as follows:

- o Replication of tests yielded consistent results
- o Shock loading is strongly attenuated by propagation through the highbay door into the lowbay
- o The quasi-static pressure is independent of charge location
- o The quasi-static pressure is dependent on the explosive type, explosive weight and the enclosed volume
- o Cylindrical charges with L/D ratios of 1:1 produce shock loading similar to equal weight spherical charges
- o For the configuration tested, multiple charges yield the same results as an equivalent single charge
- o Material near the charge can substantially increase the quasi-static pressure.

The reduced data for shock loading on the walls of the high bay area are voluminous and could be used as a data base for verifying analytical or empirical shock loading prediction methods in design manuals. That task was not, however, part of the scope for this work.

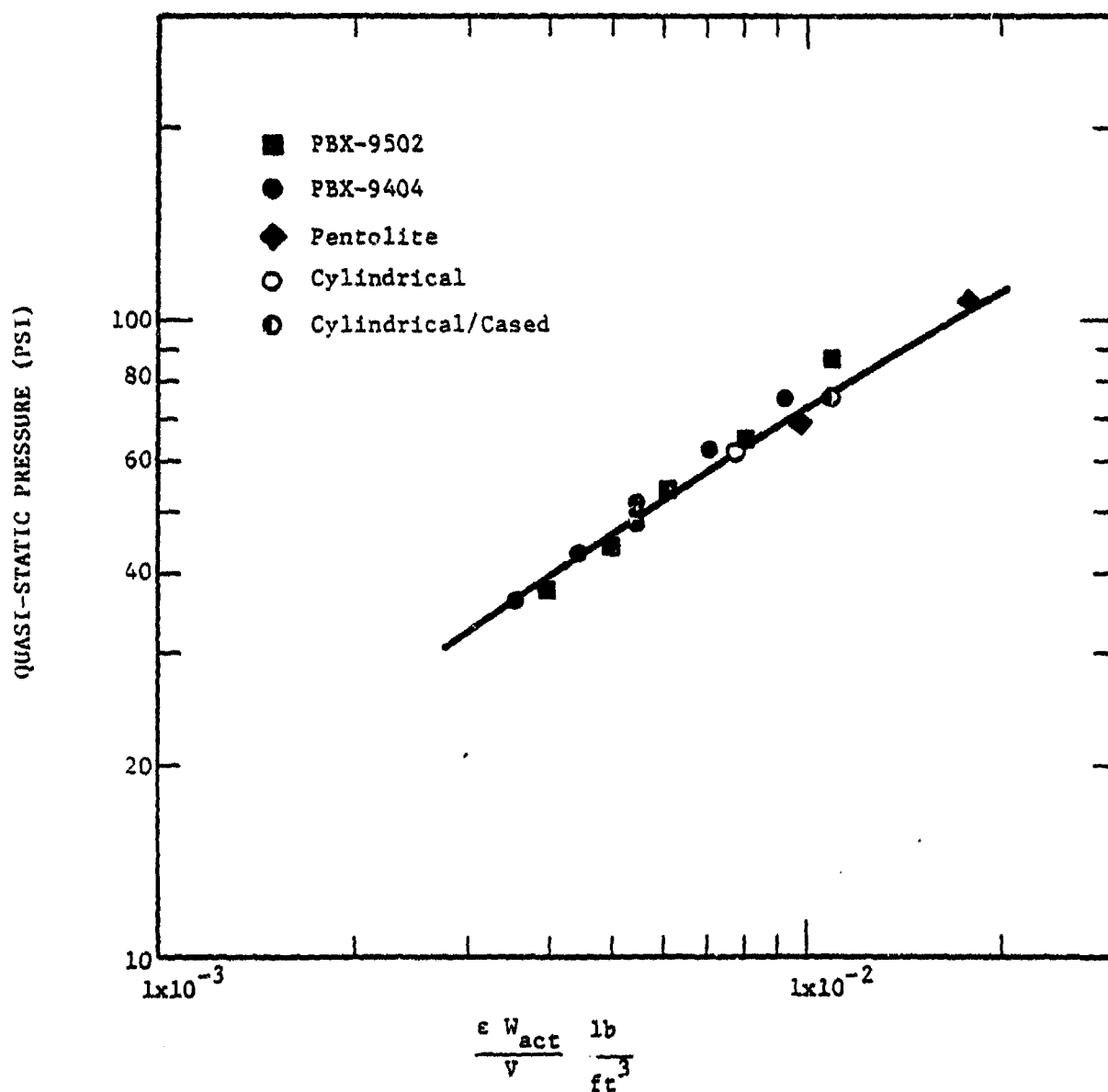
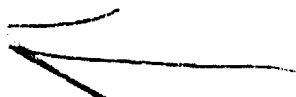


Figure 11. Quasi-Static Pressure versus Effective Charge to Volume Ratio

REFERENCES

1. Structures to Resist the Effects of Accidental Explosions (1969), Dept. of the Army Technical Manual TM5-1300, Department of the Navy Publication NAVFAC P-397, Department of the Air Force Manual AFM 88-22, Department of the Army, the Navy, and the Air Force, June 1969.
2. Baker, W. E., Westine, P. S., Kulesz, J. J., Wilbeck, J. S., and Cox, P. A., (1980) A Manual for the Prediction of Blast and Fragment Loadings on Structures, DOE/TIC-11268, U.S. Dept. of Energy, Albuquerque Operations Office, Amarillo Area Office, Amarillo, TX, Nov. 1980.
3. Hokanson, J.C., Esparza, E.D., Baker, W.E., and Sandoval, N.R., "Determination of Blast Loads in the Damaged Weapons Facility, Vol. 1, Final Report for Phase I," prepared for Mason and Hanger-Silas Mason Co., Inc., January 1982.
4. Hokanson, J.C., Esparza, E.D., Baker, W.E., and Sandoval, N.R., "Determination of Blast Loads in the Damaged Weapons Facility, Vol. 2, Final Report for Phase I," prepared for Mason and Hanger-Silas Mason Co., Inc., January 1982.
5. Hokanson, J.C., Esparza, E.D., Sandoval, N.R., Baker, W.E., and Anderson, C.E., "Determination of Blast Loads in the Damaged Weapons Facility, Vol. 1, Final Report for Phase II," prepared for Mason and Hanger-Silas Mason Co., Inc., May 1982.
6. Hokanson, J.C., Esparza, E.D., Sandoval, N.R., Baker, W.E., and Anderson, C.E., "Determination of Blast Loads in the Damaged Weapons Facility, Vol. 2, Final Report for Phase II," prepared for Mason and Hanger-Silas Mason Co., Inc., May 1982.
7. Hokanson, J.C., Esparza, E.D., Sandoval, N.R., Baker, W.E., and Anderson, C.E., "Determination of Blast Loads in the Damaged Weapons Facility, Vol. 3, Final Report for Phase II," prepared for Mason and Hanger-Silas Mason Co., Inc., May 1982.
8. Baker, W.E., Westine, P.S., and Dodge, F.T., (1973) Similarity Methods in Engineering Dynamics: Theory and Practice of Scale Modeling, Spartan Books, Rochelle Park, N.J.
9. Suppressive Shields Structural Design and Analysis Handbook, (1977) HNDEM-1110-1-2, U.S. Army Corps of Engineers, Huntsville, Division, November 1977.
10. Keenan, W.A., and Tancreto, J.E., (1974) Tech. Rept. 51-027, "Blast Environment from Fully and Partially Vented Explosions in Cubicles," Civil Engineering Laboratory, Naval Construction Battalion Center, Port Hueneme, California, February 1974.
11. Baker, W.E., Cox, P.A., Westine, P.S., Kulesz, J.J., and Strehlow, R.A., (1978) "A Short Course on Explosion Hazards Evaluation," Southwest Research Institute, San Antonio, Texas.

12. West, G.T., "Initiation of PBX 9404, Pentolite and TNT Spheres," Mason and Hanger Technical Report No. MH-SMP-82-01, December 1981.



AD P000440

QUASI-STATIC PRESSURE, DURATION, AND IMPULSE FOR EXPLOSIONS IN STRUCTURES

W. E. Baker
Charles E. Anderson, Jr.
Bruce L. Morris
Donna K. Wauters

Southwest Research Institute
6220 Culebra Road
San Antonio, Texas

ABSTRACT

Similitude analysis has been used to obtain dimensionless parameters for peak quasi-static pressures, blowdown duration, and specific impulse for blast loading within enclosures. Data from the United States and Europe have been collected and analyzed, and then displayed graphically according to relationships derived from the similitude analysis. Three graphs are presented, along with appropriate curve fits, of the peak quasi-static pressure versus the ratio of charge weight to enclosure volume, the reduced duration versus the reduced pressure, and the reduced specific impulse versus the reduced pressure.

NOMENCLATURE

A = surface area of enclosure
F = unit of force
L = unit of length
T = unit of time
V = enclosure volume
W = unit of energy
= charge weight
 a_0 = sound speed of air
c = exponential decay constant
f = functional relationship
g = functional relationship
h = functional relationship
 i_g = specific (gas) impulse
p = pressure
 p_0 = ambient pressure
PQS = peak gage quasi-static pressure
 p_1 = peak absolute quasi-static pressure
t = time

t_{max} = duration
 a_{eff} = ratio of effective vent area to total enclosure surface area
 γ = ratio of specific heats
 π = nondimensional term
 τ = nondimensional duration
 σ = standard deviation

Superscripts:

- (bar) = nondimensional term
 ^ (carrot) = calculated quantity from curve fit

INTRODUCTION

The loading from an explosive charge detonated within a vented or unvented structure consists of two almost distinct phases. The first phase is that of reflected blast loading. It consists of the initial high pressure, short duration reflected wave, plus perhaps several later reflected pulses arriving at times closely approximated by twice the average time of arrival at the chamber walls. These later pulses are usually attenuated in amplitude because of irreversible thermodynamic process, and they may be very complex in waveform because of the complexity of the reflection process within the structure, whether vented or unvented. Maxima for the initial internal blast loads on a structure can be estimated from scaled blast data or theoretical analyses of normal blast wave reflection from a rigid wall. Following the initial and secondary shock wave reflections from the internal walls, the pressure settles to a slowly decaying level — the shock wave phase of the loading is over. The second phase of a slowly decaying pressure is a function of the volume and vent area of the structure, and the nature and energy release of the explosion.

The process of reflection and pressure buildup in either unvented or poorly vented structures has been recognized for some time, dating from World War II research on effects of bombs and explosives detonated within enclosures. However, very little data were available from WWII and no attempt was made to understand or relate the physical processes until 1968 when Weibull [1] correlated peak quasi-static pressure versus the charge weight for a series of experiments with TNT detonated within a vented enclosure. More recently, study of these pressures has revived because of interest in design of vented and unvented explosion containment chambers.

A typical time history of pressure at the wall of a vented structure is shown in Figure 1. One can see that the maximum quasi-static pressure is quite difficult to define because it is obscured by the initial shock and first few reflected shocks. Obviously, several reflections must occur before irreversible processes attenuate the shocks and convert their energy to quasi-static pressure. Therefore, it seems inappropriate to call point A in Figure 1 the peak quasi-static pressure, although this is the point used by Kingery, et al. [2] to compare with code predictions from Proctor and Filler [3] and

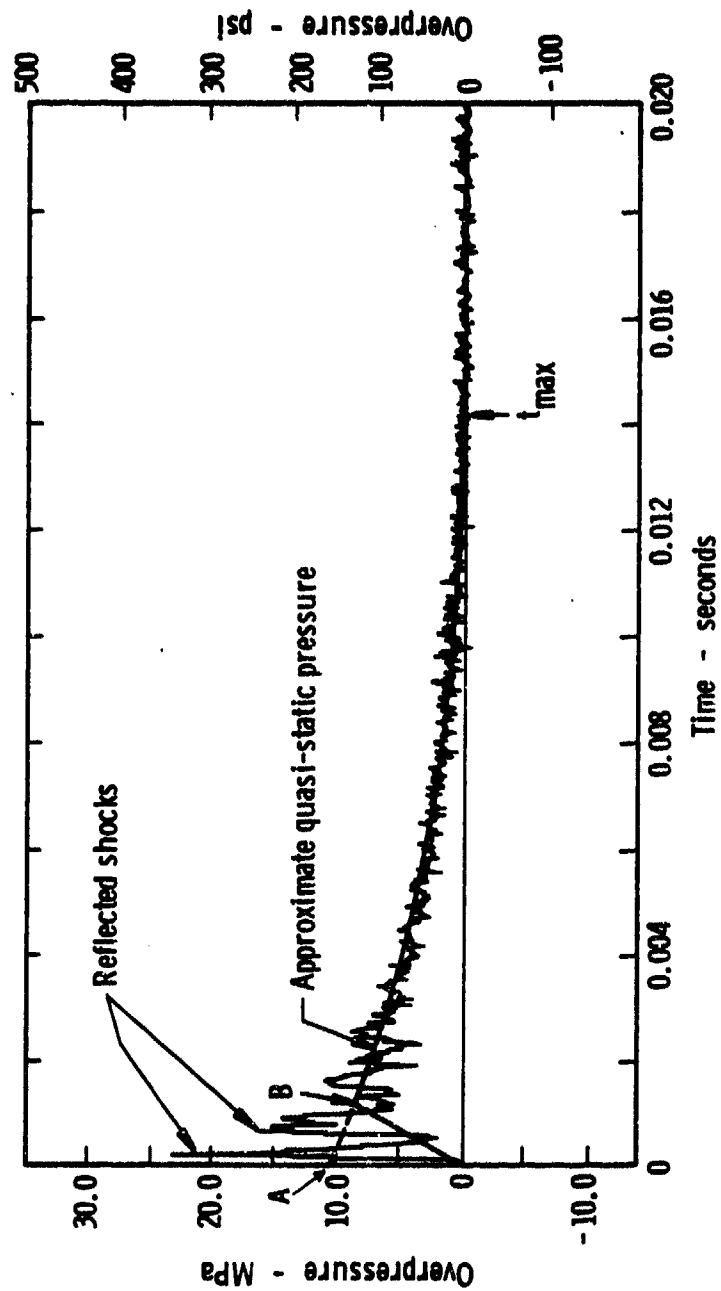


Figure 1. Typical Pressure-Time History of an Explosion in a Vented Structure

the Kinney and Sewell equation [4]. A better approach is to allow some time for establishing the maximum pressure, such as point B in Figure 1. The smaller the vent area to the total wall area, the closer the pressure at point B will be to that at point A, and in the limit of the vent area being zero (that is, an unvented enclosure), the pressures at points A and B will coincide.

Figure 1 also illustrates another problem inherent in reduction of vented pressure data: accurate determination of duration of this pressure. When the pressure approaches ambient, the shock reflections have largely decayed. But, the pressure approaches the baseline nearly asymptotically so that the duration is quite difficult to determine accurately. A possible duration t_{max} is shown in the figure.

In spite of complexities in the venting process, gas pressures and their durations can be predicted with reasonable accuracy, particularly if one differentiates between these relatively long term and low amplitude pressures from the internal blast pressures resulting from blast wave impingement and reflection. Generally of great interest in the blast loading of structures resulting from interior explosions are the peak quasi-static pressure, the duration, and the total impulse. The following paragraphs will develop and describe relationships among various physical parameters. Functional relationships will be derived from similitude analysis, but the exact functional form cannot be ascertained from this analysis without invoking restrictive, simplifying assumptions. However, a large quantity of experimental data, from a variety of sources [1-22], allow empirical relationships to be obtained.

SIMILITUDE ANALYSIS

A model analysis was performed to determine the functional form of the quasi-static pressure versus physical parameters pertinent to a vented structure. The problem is envisioned as an instantaneous energy release of magnitude W inside a confined volume V . A vent area ($\alpha_{eff} A$) exists through which internal gases can escape, where α_{eff} is the effective ratio of vent area to total cross-sectional area of the walls. Ambient atmospheric pressure p_0 exists initially inside and outside the confined volume. To define an equation-of-state for the gases in this problem requires two additional parameters which are the ratio of specific heats γ and speed of sound a_0 . Table 1 summarizes the parameters in this problem and lists their fundamental dimensions in a system of units of force F , length L , and time T .

Nondimensional numbers, or π terms, can be developed from the list of variables in Table 1. The assumptions in this analysis are all in the definition of the problem. Phenomena are not considered which do not have parameters listed in the table. Probably the major assumption invoked is that thermal effects are ignored — in other words, the pressures dissipate through venting and not through the conduction of heat into the walls of the structure. An acceptable set of π terms which result are:

Table 1. Parameters Determining Quasi-Static Pressure Inside Vented Containment Vessel

<u>Parameter</u>	<u>Symbol</u>	<u>Fundamental Dimensions</u>	<u>Reason for Including</u>
Volume	V	L^3	Describe Geometry of Boundaries
Vented Area	$(a_{eff} \Delta)$	L^2	
Energy Release	W	FL	Input Energy
Atmospheric Pressure	P_o	F/L^2	Define the State of Air
Sound Speed in Air	a_o	L/T	
Specific Heat Ratio Air	γ	—	
Pressure Increase	p	F/L^2	Loading Functions
Time	t	T	
Impulse	i_g	FT/L^2	

$$\pi_1 = p/p_0 \quad (1)$$

$$\pi_2 = \frac{(a_{eff} A)}{v^{2/3}} \quad (2)$$

$$\pi_3 = \gamma \quad (3)$$

$$\pi_4 = \frac{W}{p_0 V} \quad (4)$$

$$\pi_5 = \frac{a_0 t}{v^{1/3}} \quad (5)$$

$$\pi_6 = \frac{1}{p_0 t} \quad (6)$$

Note, however, that π_6 adds no new information since the impulse can be explicitly obtained by integrating the pressure with respect to time.

In general terms, dimensional analysis states that the functional format for the reduced pressure, π_1 , is given by:

$$\frac{p}{p_0} = f \left[\frac{W}{p_0 V}, \frac{(a_{eff} A)}{v^{2/3}}, \gamma, \frac{a_0 t}{v^{1/3}} \right] \quad (7)$$

If we are only interested in predicting the peak quasi-static pressure, the result will not depend upon time, hence the functional form must be invariant with respect to the last pi term. Likewise, for γ a constant (as it would be for air), the functional form will not depend upon γ , hence:

$$\bar{p} = f \left[\frac{W}{p_0 V}, \frac{(a_{eff} A)}{v^{2/3}} \right] \quad (8)$$

where \bar{p} is the ratio of the maximum absolute quasi-static pressure to ambient pressure, i.e.:

$$\bar{p} = \frac{p_{QS} + p_0}{p_0} \quad (9)$$

and p_{QS} is the conventional gage quasi-static pressure. Provided the flow through the vent is small relative to the rate of energy release, the maximum pressure will occur before significant venting has transpired. And since the ambient pressure is essentially an invariant, Equation (8) can then be written for the maximum quasi-static pressure:

$$p_{QS} = f \left[\frac{W}{V} \right] \quad (10)$$

The blow-down time, or duration, can also be expressed as a functional relationship with respect to the other pi terms:

$$\frac{t a_o}{V^{1/3}} = g \left[\frac{p}{p_o}, \frac{(a_{eff} A)}{V^{2/3}}, \gamma, \frac{W}{p_o V} \right] \quad (11)$$

But it just has been shown, if the maximum quasi-static pressure is reached before significant venting occurs, that the last term $W/(p_o V)$ is a function of the first term, p/p_o . And, since γ is an invariant, Equation (11) becomes:

$$\frac{t a_o}{V^{1/3}} = g \left[\frac{p}{p_o}, \frac{(a_{eff} A)}{V^{2/3}} \right] \quad (12)$$

Based on a theoretical analysis of chamber venting by Owczarek [22], Baker and Oldham [24] showed that

$$\frac{t a_o}{V^{1/3}} = \frac{V^{2/3}}{(a_{eff} A)} \quad (13)$$

or

$$t = \frac{V}{a_o (a_{eff} A)} \quad (14)$$

In physical terms, Expression (14) states that the blowdown time is directly proportional to the chamber volume divided by the effective venting area, not an unexpected result. Expression (13) thus allows us to simplify Equation (12) by defining a new scaled time \bar{t} :

$$\bar{\tau} = \left(\frac{t_{a_0}}{V^{1/3}} \right) \left(\frac{a_{eff} \Lambda}{V^{2/3}} \right) = s \left[\frac{p_1}{p_0}, 1 \right] \quad (15)$$

$$\bar{\tau} = s \left[\frac{p_1}{p_0} \right] \quad (16)$$

Thus, the scaled duration is also only a function of the reduced pressure.

The last relationship to obtain is a nondimensional, or reduced, impulse \bar{i}_g . Figure 2 shows a simplified form for gas venting pressures. In this simplified form, the gas venting pressure is assumed to follow the solid curve which rises linearly from time zero until it reaches, at time t_1 , a curve which is decaying exponentially from an initial maximum value of p_1 , where p_1 is the absolute quasi-static pressure at time $t = 0$. The decay then follows the time history

$$p(t) = p_1 e^{-ct} \quad (17)$$

until it reaches ambient pressure p_0 at time $t = t_{max}$. The exponential decay is shown to agree well with experiment (Kingery, et al. [2], and Schumacher, et al. [5]). The cross-hatched area under the overpressure curve is defined as the gas impulse i_g , and is found by integrating Equation (17) with respect to time:

$$\begin{aligned} i_g &= \int_0^{t_{max}} [p(t) - p_0] dt = \int_0^{t_{max}} (p_1 e^{-ct} - p_0) dt \\ &= \frac{p_1}{c} (1 - e^{-ct_{max}}) - p_0 t_{max} \end{aligned} \quad (18)$$

The duration, t_{max} , will be obtained from Equations (15) and (16). Likewise, as will be shown later, the exponential decay factor, c , can be written in terms of t_{max} and $\bar{\tau}$. As stated earlier, the impulse can thus be found explicitly from the other nondimensional relationships, but it is still useful to display the impulse graphically. Since the impulse depends upon the duration and the pressure, and the scaling factor for time is given by Expression (14), then a suitable choice of parameters to scale the impulse is:

$$\bar{i}_g = \frac{i_g a_0 a_{eff} \Lambda}{p_0 V} \quad (19)$$

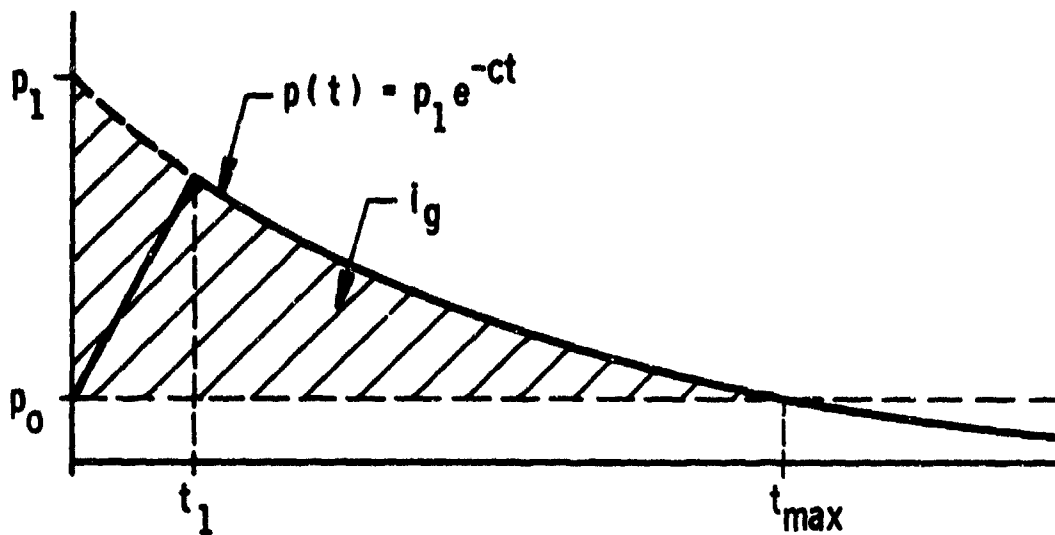


Figure 2. Simplified Pressure-Time History for Venting

But the maximum pressure and the scaled duration are functions only of the reduced pressure, hence

$$\bar{i}_s = h \left[\frac{p}{p_0} \right] \quad (20)$$

Equations (10), (16), and (20) express the functional relationships between the various physical parameters. The next section will empirically determine the functional forms via curve-fitting of experimental data. However, a brief discussion of the effective vent area ratio, a_{eff} , is in order.

Venting can be geometrically quite complicated for some structures, particularly those structures referred to as suppressive structures which often have three to six wall layers with various staggered venting patterns so fragments will not escape the confinement. For multi-walled confinement, an effective vent area ratio must be computed. To compute a_{eff} for a multi-walled structure, we have used

$$\frac{1}{a_{eff}} = \sum_{i=1}^N \frac{1}{a_i} \quad (21)$$

where N is the number of elements in a suppressive structure panel. Although no proof of this relationship is presently possible, it does reach the appropriate limits for small and large numbers of plates. For example, if only one plate is present, $a_{eff} = a_1$ as it should. If an infinite number of plates is present, $a_{eff} = 0$, with the flow completely choked. If one of the plates is solid, and thus has a zero a , $a_{eff} = 0$ as it should. If all plates have the same value for a , $a_{eff} = a/N$, which is a number smaller than a for a single plate as would be expected. In each member, a is defined according to:

$$a = \frac{A_{vent}}{A_{wall}} \quad (22)$$

For plates, the meaning of this definition is obvious. However, in angles and louvres, the definition is less obvious since angles and louvres are more efficient in constricting flow than are plates with holes. Details for computing the a 's for more complicated geometries can be found in Baker and Oldham [24] and Baker, et al. [25].

GRAPHICAL DISPLAY OF DATA

The preceding discussion determined which physical parameters are interrelated. This analysis permits the judicious choice of parameters to

display experimental data graphically. Equation (10) states that the peak quasi-static pressure is only a function of the charge energy-to-volume ratio. Thus, a plot of experimental data of p_{qs} versus W/V will determine this functional relationship. Figures 3 and 4 display the data from 177 tests, and as can be seen, the experimental data range over several orders of magnitude. Figure 3 is a graph of the data in metric units, while Figure 4 is the identical graph except it is displayed in English units. The data include tests conducted with the following high explosives (HE): TNT, PETN, PBX-9502, 50/50 Pentolite, dynamite, C-4, Comp B, and RDX.

One approximation has been made in plotting these data. For any given high explosive, the charge energy is directly proportional to the explosive mass. Also, the energy-to-mass ratio for most high explosives is approximately the same. Figures 3 and 4, for convenience, use the mass of the explosive for the symbol W . No attempt has been made to normalize all the high explosives to TNT since the scatter in data from experiments with the same high explosive often masks the effects of slight variations of the energy-to-mass ratio differences between explosives. (For carefully controlled experiments, the differences in effects of energy variation between explosives can be measured. Indeed, for a series of experiments conducted by Hokanson, et al. [21], where quasi-static pressures were measured for bare explosive and the same explosive mass encased in plastic and aluminum, the contribution of the oxidized casing to the peak quasi-static pressure was theoretically computed and measured experimentally.) It should be noted, however, that if explosion scenarios other than HE detonations are of interest, e.g., various fuel/air mixtures, then the TNT equivalent weight should first be determined and then used for W if these graphs are to be used to determine the peak quasi-static pressure.

It is reasonable to expect the peak quasi-static pressure to be directly proportional to the charge weight, and examination of the data in Figure 3 confirms this supposition for small and large W/V . For intermediate values of W/V , a transition region is evident. For $W/V < 0.4 \text{ kg/m}^3$, complete oxidation of the explosive occurs. But if W/V is too large, insufficient oxygen is available to convert all the potential energy available in the explosive charge, and the energy release is reduced by the ratio of the heat of detonation to the heat of combustion. Thus, for $W/V > 11.0 \text{ kg/m}^3$, the primary oxidizer available is that in the explosive itself. A transition region, $0.4 < W/V < 11.0$, connects the two regions. Linear least-squares curve fits have been performed on the data in the two end regions, and are shown in Figure 3.* A seventh-order polynomial of the form:

* All curve fittings in this article have been performed in log-log coordinates. Linear thus refers to the form of the curve in a log-log plot.

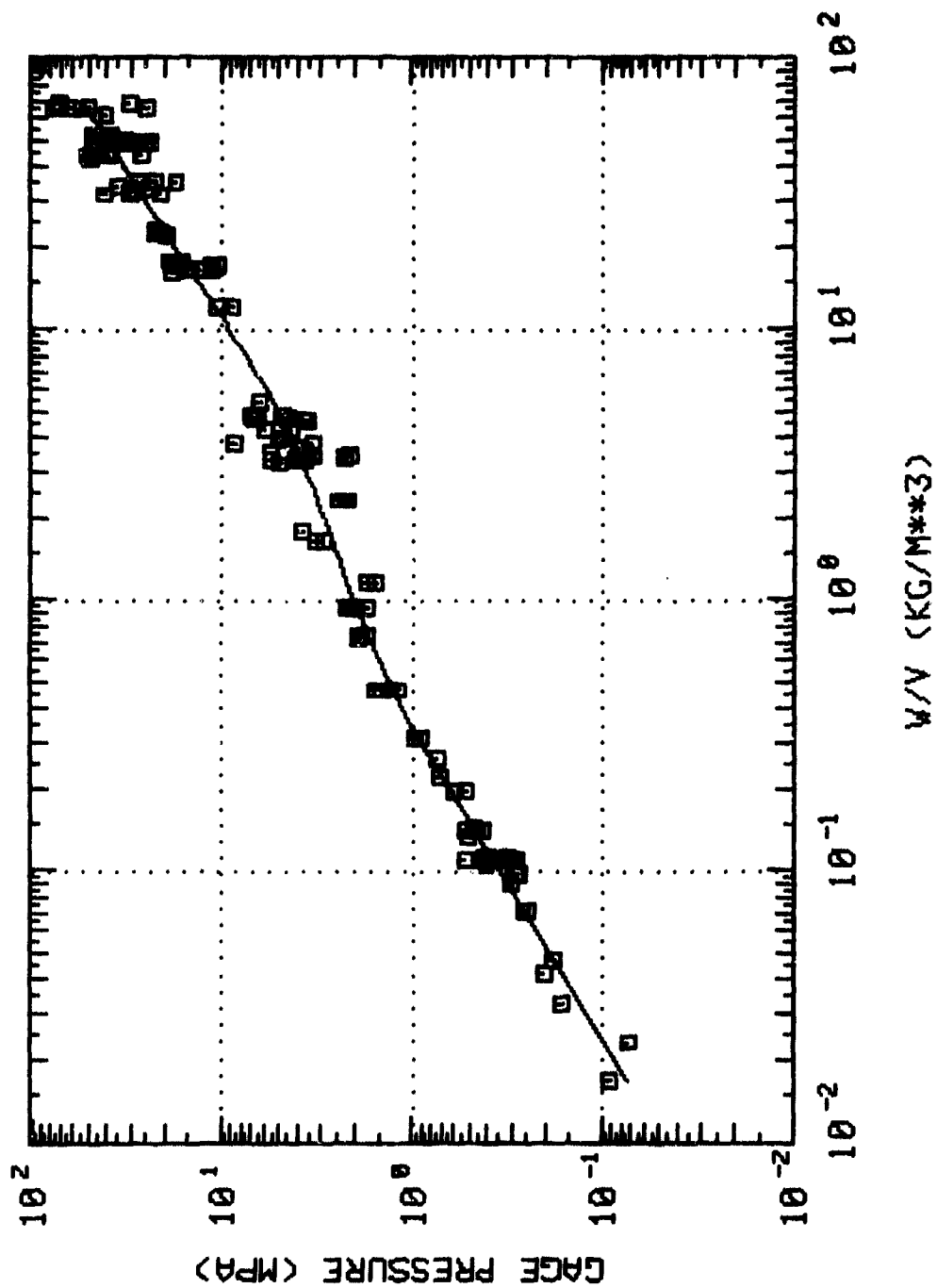


Figure 3. Peak Quasi-Static Pressure Versus the Ratio of Charge Weight to Enclosure Volume (Metric Units)

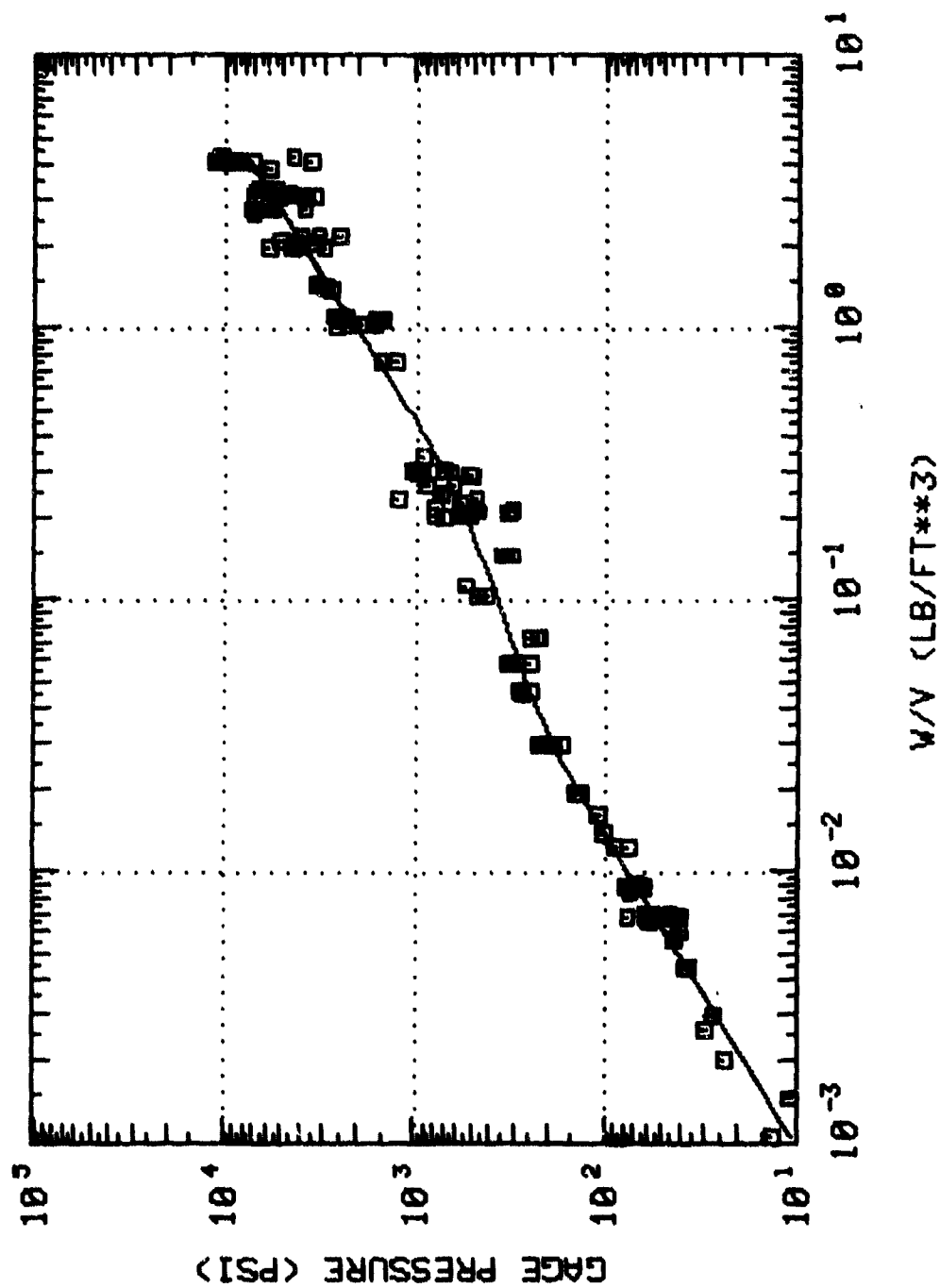


Figure 4. Peak Quasi-Static Pressure Versus the Ratio of Charge Weight to Enclosure Volume (Engineering Units)

$$\begin{aligned} \log p_{QS} = & a_0 + a_1 \log (W/V) + a_2 [\log (W/V)]^2 + a_3 [\log (W/V)]^3 + \\ & a_4 [\log (W/V)]^4 + a_5 [\log (W/V)]^5 + a_6 [\log (W/V)]^6 + \\ & a_7 [\log (W/V)]^7 \end{aligned} \quad (23)$$

was then used to curve fit the entire range of data, where \log represents the logarithm to the base 10. Such a high order polynomial is required because of the number of constraints: the slopes and intercepts at each end, the points where the polynomial connects with the straight lines, and the constraint that the curve be a least-squares fit. This is a total of seven constraints which stipulates at least a sixth-order polynomial for the curve fit. But the appearance of the data in Figure 3 implies that an odd function (as opposed to an even function) should be used. Hence, a seventh-order polynomial becomes the minimum order polynomial stipulated. Table 2 lists the coefficients of Equation (23) as well as the linear expressions for the two asymptotes. Table 3 lists the comparable coefficients and asymptotes for pressure in psi and W/V in lb/ft^3 (Figure 4).

The standard deviation for Equation (23) has also been computed but needs to be interpreted properly. The standard deviation, σ , is usually used as an estimate of the scatter in data, or error in predictions. One standard deviation encompasses approximately 68 percent of all data values. The uncertainty in estimating an observable is often written as the calculated quantity plus or minus one standard deviation:

$$\log p_{QS} = \log \hat{p}_{QS} \pm \sigma_0 \quad (24)$$

where p_{QS} is the estimated quasi-static pressure, \hat{p}_{QS} is the computed quasi-static pressure from the curve fit, and σ_0 is the computed standard deviation. Define σ_0 such that

$$\log \sigma_0 = \sigma_0 \quad (25)$$

The right-hand side of Equation (24) can then be written as

$$\log \hat{p}_{QS} \pm \log \sigma_0 \quad (26)$$

so that Equation (24) can be rewritten as:

Table 2. Summary of Peak p_{QS} Versus W/V
[MPa Versus kg/m^3]

$$\begin{aligned} \log \hat{p}_{QS} = & 0.30759 + 0.51815 \log (W/V) - 0.150534 [\log (W/V)]^2 + \\ & 0.31892 [\log (W/V)]^3 + 0.10434 [\log (W/V)]^4 - 0.14138 [\log (W/V)]^5 + \\ & - 0.019206 [\log (W/V)]^6 + 0.021486 [\log (W/V)]^7 \end{aligned}$$

Correlation Coefficient, r : 0.993

One Standard Deviation: $\sigma_o = 1.247$

$$\frac{\hat{p}_{QS}}{1.247} \leq p_{QS} \leq 1.247 \hat{p}_{QS}$$

Asymptotes:

$W/V \leq 0.4 \text{ kg/m}^3$	$\hat{p}_{QS} = 2.347 (W/V)^{0.8395}$	$\sigma_o = 1.143$
$W/V \geq 11.0 \text{ kg/m}^3$	$\hat{p}_{QS} = 1.1004 (W/V)^{0.9202}$	$\sigma_o = 1.300$

Table 3. Summary of Peak p_{QS} Versus W/V
[psi Versus lb/ft^3]

$$\begin{aligned} \log \hat{p}_{QS} = & 3.3138 + 0.952133 \log (W/V) + -0.023074 [\log (W/V)]^2 + \\ & - 0.317807 [\log (W/V)]^3 + 0.149364 [\log (W/V)]^4 + 0.374595 [\ln (W/V)]^5 + \\ & 0.161978 [\log (W/V)]^6 + 0.021486 [\log (W/V)]^7 \end{aligned}$$

Correlation Coefficient, r : 0.993

One Standard Deviation: $\sigma_o = 1.247$

$$\frac{\hat{p}_{QS}}{1.247} \leq p_{QS} \leq 1.247 \hat{p}_{QS}$$

Asymptotes:

$W/V \leq 0.025 \text{ lb/ft}^3$	$\hat{p}_{QS} = 3495. (W/V)^{0.8435}$	$\sigma_o = 1.143$
$W/V \geq 0.70 \text{ lb/ft}^3$	$\hat{p}_{QS} = 2049. (W/V)^{0.9393}$	$\sigma_o = 1.300$

$$\log (\hat{p}_{QS}/\sigma_o) \leq \log p_{QS} \leq \log (\sigma_o \hat{p}_{QS}) \quad (27)$$

$$\frac{\hat{p}_{QS}}{\sigma_o} \leq p_{QS} \leq \sigma_o \hat{p}_{QS} \quad (28)$$

Tables 2 and 3 give σ_o , as well as the correlation coefficient (which is a measure of the confidence of the curve fit).

Here we would like to mention our uncertainty of whether the slopes of the two asymptotes should have the same value. The slopes are not appreciably different, and particularly with the scatter prevalent for large W/V , it is not unreasonable to speculate that the slope should be identical. However, for the present, we have elected to report the linear least-squares, that is, the best fit to the data.

In deriving Equation (10), the assumption was made that the flow through the vent (for $a_{eff} \neq 0$) is small relative to the rate of energy release so that the maximum quasi-static pressure occurs before significant venting has transpired. Keenan and Tanoreto [22] obtained no measurable quasi-static pressure for values of $(a_{eff} A/V^{2/3}) \geq 0.772$. Of the data plotted in Figures 3 and 4, the maximum reduced vent area ratio was 0.3246. Thus, Figures 3 or 4, and Tables 2 or 3, are valid for

$$0 \leq \frac{a_{eff} A}{V^{2/3}} \leq 0.3246 \quad (29)$$

For a vented enclosure ($a_{eff} \neq 0$), Equation (16) suggests that the duration, $\bar{\tau}$, be plotted versus the reduced pressure, \bar{p} , given by Equation (9). Seventy of the data points from Figure 3 or 4 represent vented enclosures, and these are plotted in Figure 5. It can be seen that the duration has considerable scatter because of the difficulty in determining when the overpressure has returned to ambient. Note, however, that the uncertainty in duration has negligible impact on the impulse since the total area under the pressure time curve is not sensitive to the exact location of t_{max} . A linear least-squares curve fit has been performed on the data and is shown in Figure 5, and the results are summarized in Table 4.

From the linear curve fit, it is straightforward to compute t_{max} from Equation (15) as a function of \bar{p} :

$$t_{max} = \frac{V}{a_o a_{eff} A} (0.4284) \left(\frac{p_{QS} + p_o}{p_o} \right)^{0.3638} \quad (30)$$

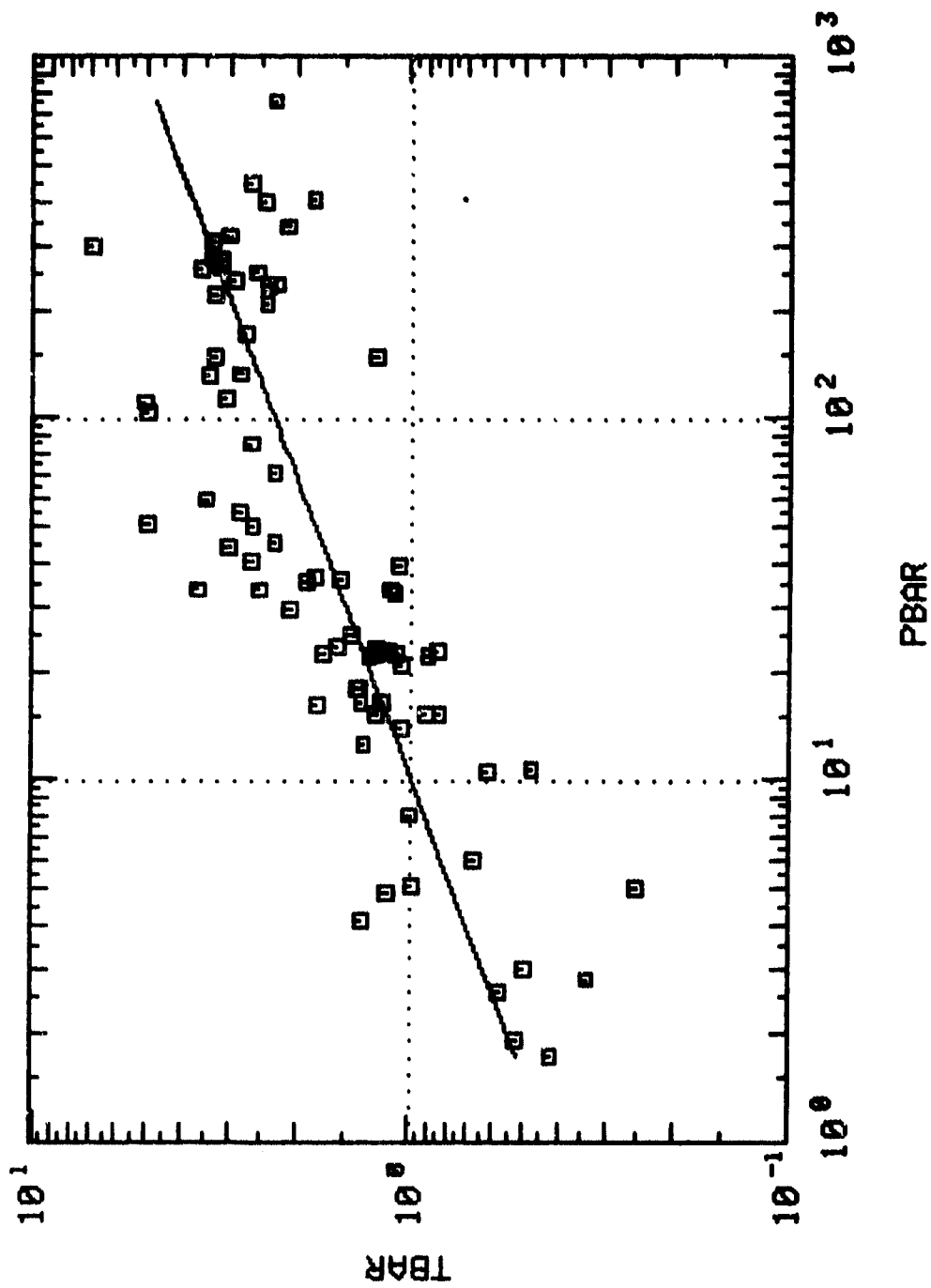


Figure 5. Reduced Duration Versus Reduced Pressure

Table 4. Summary of $\bar{\tau}$ Versus \bar{p}

$$\bar{\tau} = \frac{t_{a_0}}{v^{1/3}} \frac{a_{eff} \Lambda}{v^{2/3}}$$

$$\bar{p} = \frac{p_{QS} + p_0}{p_0}$$

Linear Curve Fit:

$$\frac{\Lambda}{\tau} = 0.4284 (\bar{p})^{0.3638}$$

Correlation Coefficient, r : 0.799

One Standard Deviation: $\sigma_0 = 1.50$

$$\frac{\frac{\Lambda}{\tau}}{1.50} \leq \bar{\tau} \leq 1.50 \frac{\Lambda}{\tau}$$

The constant c in Equation (17) can now be evaluated:

$$p_o = (p_{QS} + p_o) e^{-c t_{\max}} \quad (31)$$

$$c = \frac{1}{t_{\max}} \ln \left(\frac{p_{QS} + p_o}{p_o} \right) \quad (32)$$

The specific impulse is then obtained from Equation (18), which after some rearrangement of terms, reduces to:

$$i_s = \left(\frac{p_{QS}}{\ln \bar{p}} - p_o \right) t_{\max} \quad (33)$$

where \bar{p} is given by Equation (9) and t_{\max} is given by Equation (30).

As we have already stated, and just shown with Equation (33), the specific impulse can be obtained directly from the peak quasi-static pressure and the duration. However, because of the interest in specific impulse for computing the loading of structures, it is often convenient to have a graphical representation of specific impulse. Equation (20) indicates that an appropriate parameter for the abscissa is the reduced pressure. Sufficient information was reported to compute specific impulses for 75 of the tests. Figure 6 displays these reduced impulses, \bar{i}_g , versus the reduced pressure. A linear least-squares curve fit was also performed on these data, and is displayed in Figure 6. Table 5 summarizes the curve fitting information.

Quadratic least-squares curve fits were also performed on the data in Figures 5 and 6. However, the standard deviations differed by less than seven percent between the linear and quadratic curve fits for duration, and differed by only two percent for the reduced impulse. A two-sample comparison of variance was performed using the F ratio test at a 99 percent confidence level. For the linear and quadratic curve fits to be different statistically, the ratio of their respective σ 's must exceed approximately 1.7. Since the ratio of their σ 's is much less than 1.7, there is no significant difference in the linear versus quadratic curve fits -- hence, only the expressions for the linear curve fits have been reported.

SUMMARY

A sizeable quantity of data have been compiled and analyzed to obtain peak quasi-static pressure, and the duration and impulse for explosions within structures. Similitude analysis indicated an appropriate choice of parameters for graphically displaying the data. Peak quasi-static pressure was found to

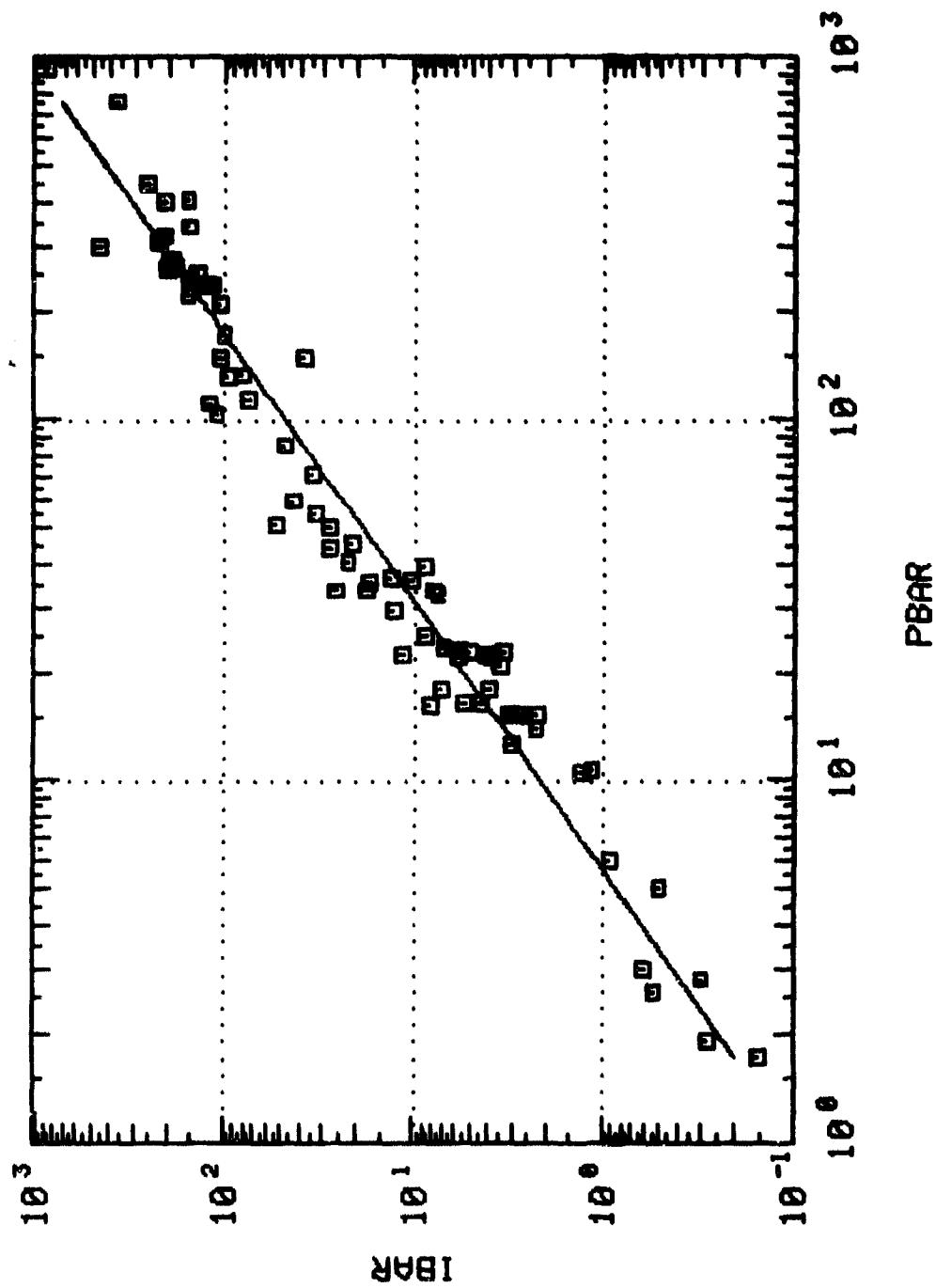


Figure 6. Reduced Specific Impulse Versus Reduced Pressure

Table 3. Summary of \bar{i}_g Versus \bar{p}

$$\bar{i}_g = \frac{i_{g, eff} A}{p_o V}$$

$$\bar{p} = \frac{p_{gs} + p_o}{p_o}$$

Linear Curve Fit:

$$\bar{i}_g = 0.0953 (\bar{p})^{1.351}$$

Correlation Coefficient, r : 0.977

One Standard Deviation: $\sigma_o = 1.53$

$$\frac{\bar{i}_g}{1.53} \leq \bar{i}_g \leq 1.53 \bar{i}_g$$

be a function of charge weight to chamber volume. Also, a nondimensional duration and a nondimensional specific impulse were found to be functions only of the reduced, i.e., nondimensional, pressure. The data range over several orders of magnitude and have thus been presented on log-log plots. Least-squares curve fits have been performed and reported, with their standard deviations, to provide appropriate analytic functions to relate the physical parameters. Thus, for high-order detonations within enclosures, the peak quasi-static pressure, and if the enclosure is vented, the duration and specific impulse, can be ascertained from the graphs on the respective analytic expressions.

ACKNOWLEDGEMENTS

The authors gratefully acknowledge the management of the Engineering Sciences Division of Southwest Research Institute who provided time and support for this research endeavor. Additionally, we would give special thanks to A. Jenssen of the Norwegian Defence Construction Service who graciously supplied a tremendous amount of the experimental data which have been analyzed and reported.

REFERENCES

1. Hans R. W. Weibull, "Pressures Recorded in Partially Closed Chambers at Explosion of TNT Charges," Annals of the New York Academy of Sciences, Volume 152, Article 1, October 1968, pp. 357-361.
2. C. N. Kingery, R. N. Schumacher, and W. O. Ewing, "Internal Pressures from Explosions in Suppressive Structures," BRL Memorandum Report ARBRL-MR-02848, USA Ballistic Research Laboratory, Aberdeen Proving Ground, Maryland, 1978.
3. J. F. Proctor and W. S. Filler, "A Computerized Technique for Blast Loads from Confined Explosions," Minutes of the 14th Annual Explosives Safety Seminar, New Orleans, Louisiana, 8-10 November 1972, pp. 99-124.
4. G. F. Kinney and R. G. S. Sewell, "Venting of Explosions," NWC Technical Memorandum 2448, Naval Weapons Center, China Lake, California, 1974.
5. R. N. Schumacher, C. N. Kingery, and W. O. Ewing, "Airblast and Structural Response Testing of a 1/4 Scale Category 1 Suppressive Shield," BRL Memorandum Report No. 2623, USA Ballistic Research Laboratory, Aberdeen Proving Ground, Maryland, 1976.
6. D. M. Koger and G. L. McKown, "Category 5 Suppressive Shield (TDP)," Report EM-TR-76001, Headquarters, Edgewood Arsenal, Aberdeen Proving Ground, Maryland, 1975.

7. E. D. Eparza and A. B. Wenzel, "Development of a Blast Simulator for Testing Simulated Aircraft Fuel Tanks," ITCG/AS-76-T-004, Naval Air Systems Command, Washington, D.C., 1978.
8. E. D. Eparza, W. E. Baker, and G. A. Oldham, "Blast Pressures Inside and Outside Suppressive Structures," Report EM-CR-76042, Headquarters, Edgewood Arsenal, Aberdeen Proving Ground, Maryland, 1975.
9. S. Zilliacus, W. E. Phyllaier, and P. K. Shorrock, "The Response of Clamped Circular Plates to Confined Explosive Loadings," Report No. 3987, Naval Ship Research and Development Center, Bethesda, Maryland, 1974.
10. J. F. Proctor, "Internal Blast Damage Mechanisms Computer Program," JTCG/ME-73-3, Air Force Systems Command, Wright-Patterson AFB, Ohio, 1973.
11. A. Skjeltop, T. Hegdahl, and A. Jenssen, "Underground Ammunition Storage, Report I: Test Programme, Instrumentation, and Data Reduction," Norwegian Defence Construction Service, Oslo, Norway, 1975.
12. A. Skjeltop, T. Hegdahl, and A. Jenssen, "Underground Ammunition Storage: Model Tests to Determine Air Blast Propagation from Accidental Explosions," Nr 59/70, Norwegian Defence Construction Service, Oslo, Norway, 1970.
13. A. Skjeltop, T. Hegdahl, and A. Jenssen, "Underground Ammunition Storage: Blast Propagation in the Tunnel System. Report IIA: Chamber Pressure," Nr 79/72, Norwegian Defence Construction Service, Oslo, Norway, 1975.
14. A. Skjeltop, T. Hegdahl, and A. Jenssen, "Underground Ammunition Storage: Blast Propagation in the Tunnel System. Report IIIA: Single Chamber Storage, Variable Tunnel Diameter and Variable Chamber Volume," Nr 81/72, Norwegian Defence Construction Service, Oslo, Norway, 1975.
15. A. Skjeltop, T. Hegdahl, and A. Jenssen, "Underground Ammunition Storage: Blast Pressure in the Tunnel System. Report III: Single Chamber Storage, Variable Tunnel Diameter and Variable Chamber Volume," Nr 81/72, Norwegian Defence Construction Service, Oslo, Norway, 1972.
16. A. Skjeltop, T. Hegdahl, and A. Jenssen, "Underground Ammunition Storage. Model Test to Investigate the Strength and Effectiveness of a Self-Closing Concrete Block, Test IV," Nr 85/72, Norwegian Defence Construction Service, Oslo, Norway, 1972.
17. A. Skjeltop, T. Hegdahl, and A. Jenssen, "Underground Ammunition Storage. Model Test to Investigate the Strength and Effectiveness of a Self-Closing Concrete Block, Test V," Nr 98/74, Norwegian Defence Construction Service, Oslo, Norway, 1973.

18. A. Skjeltnorp, T. Hegdahl, and A. Jenssen, "Underground Ammunition Storage: Blast Propagation in the Tunnel System. Report IVA: Connected Chamber Storage, Variable Chamber Volume and Variable Angle Between Branch and Main Passageway," Nr 82/72, Norwegian Defence Construction Service, Oslo, Norway, 1975.
19. A. Skjeltnorp, T. Hegdahl, and A. Jenssen, "Underground Ammunition Storage: Blast Propagation in the Tunnel System. Report IV: Connected Chamber Storage, Variable Chamber Volume and Variable Angle Between Branch and Main Passageway," Nr 82/72, Norwegian Defence Construction Service, Oslo, Norway, 1972.
20. J. C. Hokanson, E. D. Esparza, W. E. Baker, and N. R. Sandoval, "Determination of Blast Loads in the Damage Weapons Facility, Volume 1, Phase 1," SwRI Report 6578-101, Mason and Hanger-Silas Mason Company, Inc., Amarillo, Texas, 1982.
21. J. C. Hokanson, E. D. Esparza, W. E. Baker, N. R. Sandoval, and C. E. Anderson, "Determination of Blast Loads in the Damage Weapons Facility, Volume 1, Phase 2," SwRI Report 6578-102, Mason and Hanger-Silas Mason Company, Inc., Amarillo, Texas, 1982.
22. W. A. Keenan and J. E. Tancreto, "Blast Environment from Fully and Partially Vented Explosions in Cubicles," Technical Report 51-027, Civil Engineering Laboratory, Naval Construction Battalion Center, Port Huene-me, California, 1974.
23. J. A. Owczarek, Fundamentals of Gas Dynamics, International Textbook Company, Scranton, Pennsylvania, 1964.
24. W. E. Baker and G. A. Oldham, "Estimates of Blow-Down of Quasi-Static Pressures in Vented Chambers," Edgewood Arsenal Contractor Report EM-CR-76029, Report No. 2, Edgewood Arsenal, Aberdeen Proving Ground, Maryland, 1975.
25. W. E. Baker, P. A. Cox, P. S. Westine, J. J. Kulesz, and R. A. Streh-low, Explosion Hazards and Evaluation, Elsevier Scientific Publishing Company, Amsterdam, 1982.

Paper Distributed at the:

Twentieth DoD Explosives Safety Seminar
Norfolk, Virginia

AD P000441

VIPER ROUND CONTAINMENT VESSEL DEVELOPMENT

by

C. James Dahn
Safety Consulting Engineers, Inc.
Rosemont, Illinois

August 26, 1982

ABSTRACT

The purpose of this paper is to present the development of a new steel containment vessel to contain the explosion effects of two Viper rounds. The containment vessel was utilized in a production facility for the load/assemble and packout of Viper rocket systems. At one stage of the production process, continuity checks must be made on the live rounds. During this operation, there is a remote potential of accidental initiation, thus, a need arose to protect personnel from the explosion effects of the Viper rounds.

A vented containment vessel was developed to permit the explosion products to be vented out through the roof of the production facility. The containment vessel was designed to contain metal fragments, blast and shape charge effects. At the same time, the Viper rounds could be easily moved into and out of the containment vessel without hazard. During this development, additional fragmentation and blast output tests were conducted to determine precise output of the Viper rounds. This data yielded lower blast output than did previously recorded information. Thus, in the original design of the containment vessel, higher blast output and fragment effects were considered. The containment vessel of 6 ft. diameter by 30 ft. high can withstand 125 percent TNT equivalence of the two Viper rounds without deformation or adverse effects on personnel.

INTRODUCTION

In 1980, General Dynamics Incorporated rebuilt an abandoned loading facility at Camden, Arkansas for the purpose of load/assemble and packout (LAP) of Viper weapon systems. In the Viper Production Building, a critical electrical continuity check is required on the Viper round assembly. As a safeguard to personnel and facilities, a containment vessel was necessary to contain an accidental initiation at this point.

This vessel must contain blast output, fragments and shape charge effects to prevent hazard to personnel in the areas.

RISI Industries located in Chula Vista, California was contracted by General Dynamics to supply various shields, tables and tooling for the LAP operations. RISI Industries had contracted Safety Consulting Engineers, Inc. to develop a safe structural design against blast, fragments and shape charge for the containment vessel. The SCE analyses supplied RISI Industries with the parameters sufficient to provide detailed design of the containment vessel. In addition, Safety Consulting Engineers, Inc. was contracted to conduct qualification tests on the production containment vessel to be supplied to General Dynamics.

VIPER ROUND CHARACTERISTICS

A. Configuration

The Viper round consists of a rocket motor attached to a warhead assembly as shown in Figure 1. This entire round is placed into a launch tube and sealed accordingly for shipment to the field. The launch tube assembly contains the electrical power pack to charge a capacitor to fire the warhead and also to initiate the rocket motor. Normally, the sequence of events of firing the round is that of charging the warhead initiator power capacitor and then initiating the rocket motor. The rocket motor fires for approximately one second. The shape charge warhead is armed at a specific distance from the initiating point and is initiated upon impact with the hard target.

B. Blast Output

For the initial design input of the containment vessel, blast output data obtained at ARRADCOM on LX-14 billets (see Reference 1) was utilized. The peak side-on pressure and impulse for LX-14 as compared to TNT is shown in Figure 2. Since the TNT equivalency values of LX-14 appeared to be extremely high, additional TNT equivalency and blast pressure measurement testing was conducted of the Viper rounds. As a calibration, one pound of Pentolite charges were detonated. The results of the SCE blast tests are also shown in Figure 2. The peak reflected pressure/impulse of airburst TNT charges and LX-14 equivalent charges are shown in Figure 3.

This data is utilized for the design and structural considerations of the containment vessel from a blast standpoint. The TNT scaled distance-blast pressure and impulse data was obtained from Reference 2.

Previous TNT equivalency tests conducted on LX-14 per Reference 1 utilized cylindrical LX-14 Viper billets. To correlate this data to cylindrical TNT charges, correlation factors as given in Reference 3 are needed. The ratio of the cylindrical cylinder to sphere pressures as a function of scale distance is shown in Figure 4. Thus, for a scale distance of 5, the peak pressure of the cylinder is between 1.6 and 1.85 times that of the pressure of a sphere. Thus, when TNT equivalencies are being calculated, significant error can be realized in reporting blast output of cylindrical charges.

C. Fireball Size

Fireball radius of an explosive charge can be determined from equations in Reference 2 as a function of charge weight. The diameter of the fireball and the fireball duration can be calculated by utilizing the following equations taken from Reference 4:

$$D_f = 9.56 W^{0.325}$$

$$t_f = 0.196 W^{0.349}$$

where

D_f = fireball diameter, ft.

t_f = fireball time of duration, seconds

W = charge weight in pounds

Calculations were made from 0.5 to 4 pounds charge weight to determine the fireball radius and duration of time. The results of these calculations are shown in Figure 5. Actual LX-14 test data as recorded from Reference 1 indicates that the fireball radius is 4.5 ft. This radius is less than the radius of an equivalent TNT charge at one pound.

D. Fragments and Missiles

The case fragments, weight and velocity and distributions for the Viper round as obtained from Tecom testing per procedure TOP/MTP4-2-813 as reported in Report No. FRNOP-82754 is shown in Figure 6. Here, we see that the average aluminum case fragments are propelled at approximately 6,000 ft. per second and weigh between 5 to 10 grains. This data was utilized for the design of the fragment shield portion of the containment vessel.

E. Rocket Firing

The rocket, if accidentally initiated, has a total burn time of less than one second imparting a peak velocity to the round of about 900 ft. per second. Thus, the round must be adequately contained in the containment vessel so that if an accidental rocket firing should occur, the round will not move.

DESIGN PHILOSOPHY

The containment vessel was to be designed to occupy minimum space in the production facility and yet aid the production flow in the electrical checkout of the round. A vented containment vessel would provide the smallest occupied volume in a production facility, and thus was selected for this application. A cylindrical-shaped containment vessel was chosen to provide easy access and maximum strength for configuration and volume. An inner fragment shield was incorporated to assure integrity of the blast shield structure. Fragment impacts generate stress concentrations in the primary blast containment vessel which could lead to failure over a time period. The containment vessel was designed so that two Viper rocket assemblies could be moved into the chamber at one time and be electrically checked in a remote condition. Thus, two round feed doors are needed which would operate simultaneously to open both the fragment-shield portion and the outer containment vessel. The shield opening elevation should be convenient for the operators so they can move rounds in and out of the shield without difficulty. A summary of the design criteria is shown in Table 1.

CONTAINMENT VESSEL DESIGN

A. Fragmentation Shield

Calculations were made to determine the fragment velocities necessary for penetrating various mild steel plates using techniques from Reference 2. Aluminum fragment weights versus fragment velocities required to penetrate three steel plate thicknesses are shown in Figure 7. Here, we see that an aluminum fragment going at 10,000 ft. per second would penetrate a steel plate of a half-inch thickness if its weight was greater than 40 grains. A creditable fragment velocity and weight as seen from Figure 6 is approximately 9,000 ft. per second and 30 grains respectively. Thus, we see from Figure 4, that a half-inch steel plate would be adequate to prevent penetration of aluminum fragments from the warhead. Based on the round height in the containment vessel of approximately three feet, the maximum height of the fragment shield should be seven feet to prevent angle-spray impact onto the exterior containment vessel walls.

B. Containment Vessel Configuration

The containment vessel will be vented through the roof of the existing production building. The vent should be designed so that the maximum blast side-on pressure emanating from the end of the vent is less than 2.3 psi. The stack vent peak side-on pressure was calculated using techniques in Reference 2. The incident pressure outside of the stack was calculated using the following approximate equation:

$$P_s = 290 \left[\frac{A_{ex}}{v^{2/3}} \right]^{0.401} \left[\frac{W^{1/3}}{R} \right]^{1.496}$$

where

R = A distance from the stack exit to the point of interest in feet

W = Charge weight in pounds

Thus, for a 3.76 pound TNT equivalent charge initiated in the center of the containment vessel, the peak side-on pressure at the stack outlet as a function of height from the floor is illustrated in Figure 8.

C. Vessel Blast Constraint Configuration

Blast analysis in accordance with Reference 2 was conducted on the cylindrical containment vessel design to establish the optimum wall thickness of the outer blast containment vessel, the height of this vessel, and its structural integrity elements. Response equations were utilized to evaluate the effect of the shock pulse and gas pulse on the cylindrical structure. Optimization studies were conducted to determine the maximum height of a six-foot diameter cylinder to reduce the blast loads and gas pressure loads on the structure. Studies were conducted on vent diameters of 40 inches. A summary of the structural calculations for the inner fragment shields, the outer blast shield, transition and the stack are found in Table 1. Maximum deflections of each of the components were also calculated and listed in the same table.

A 12-foot high by six-foot diameter blast containment vessel of 0.75 inches thick was obtained to assure structural integrity of the containment vessel under a 3.76 pound TNT equivalent explosion charge (maximum output of two viper rounds.) A final structural configuration is illustrated in Figure 9. Inner fragment shield thickness was calculated to be one inch to insure its blast load structural integrity. The outer shield can safely withstand the blast loads with a wall thickness of 0.75 inches. The stack wall thickness of 0.5 inches is adequate to maintain stack structural integrity.

SPECIAL DESIGN CONSIDERATIONS

A. Access Door Analysis

The maintenance access door was necessary to clean out the interior of the containment vessel from time to time. It is desired that the maintenance door be as far away from the rounds in the design configuration to minimize the load on the door. The door design selected was an interior door placed on the interior of the blast containment vessel area so that loads imparted into it would be distributed onto the outer shield lip area. By utilizing techniques in Reference 2, the door thickness and position from the Viper rounds was optimized to maintain maximum door integrity. The overhang of the door was selected based on the blast stresses imparted from the door into the containment vessel. Peak reflected pressures and durations were calculated for the expected locations of the door. Explosion blow-down times were calculated and the access door natural period was determined. With this information, the structural resistance of the door could be calculated. In addition, the reaction loads on the door were also calculated. The door with the wall thickness of 0.75 inches meets structural integrity satisfactorily as a result of the explosion environment. The door was positioned approximately 5.5 feet away from the center of the potential burst to minimize the structural loading on the door. The final configuration of the access door is shown in Figure 10. Here, we see that there are six tabs that secure the door snugly up to the shield opening with a two-inch lip area around the opening.

B. Round Feed Doors

The rocket assembly feed door had to be at least 36 inches high and as wide as structurally permissible. Door locations were directly in line with the round in a horizontal direction. Structural analysis was conducted to determine the minimum thickness of door required and the maximum width of door permitted to maintain structural integrity. Also, the degree of overlap on the door was also determined. Both the fragment shield door and the containment vessel doors would operate simultaneously in opening and closing and would be placed on the interior of the respective walls. Natural frequencies were calculated for each door based on various door thicknesses and door widths. Calculations then were made of the pressures and response times of the blast wave and gas pressure pulse. The structural response and structural resistance to blast of a 3.75 pounds of TNT equivalent explosive were analyzed. The reaction forces on the door were also calculated by using methods in Reference 2. Dynamic stress loading on the door was calculated looking at the height and width effect of the door. These results are calculated as shown in Figure 11. According to this data, the maximum width permissible when stress reaches a minimum condition was approximately 9 inches.

By using energy methods, the calculated structural resistances and ductility ratios were calculated. From these calculations, the door width of 9 inches was most desirable because stresses were minimized at this width. As width increased from this level, the stresses reached failure levels.

By utilizing two-inch wide flanges around the opening in the fragment shield and the containment vessel exterior wall, the loads imparted to the wall by the door will be within safe limits. For a nine-inch wide door by 36 inches high, the reaction load imparts a stress on the long side of 19,471 psi and on the short side of 3,519 psi, both well within structural limits. Final configuration of the round feed door is shown in Figure 12. The two-inch wide flange welded to the exterior wall of the containment vessel is noted.

C. Door Cutout Stress Concentrations

Stress concentration analysis was performed on the two (2) round feed doors and the maintenance access door. The objective of the stress analysis is that of determining the minimum radius at the corners of the door cutouts to assure that the integrity of the structure will be maintained. Stress concentration factors for elastic stress and equations were used from Reference 5, "Formulas for Stress and Strain" by Roark and Young. These calculations yielded a minimum radius at the corners, of one inch for both the round feed doors and the access doors. In addition, a flange approximately two inches wide should be placed around the door cutout at the round feed station. The radius of curvature is shown in both Figures 9 and 11, as incorporated in the final design.

D. Shape Charge Effects

To mitigate the shape charge effect in case of an accidental initiation of the Viper round, five one-inch thick armored plates at various angles and spacings were utilized below the charge. Thus, if a shape charge should initiate, the effect would be mitigated before the steel bottom plate would be hit.

CONTAINMENT VESSEL QUALIFICATION TEST RESULTS

Based on SCE TNT equivalency tests of full-up Viper rounds, the maximum explosive weight of TNT in the containment vessel is considerably less than previously designed. Actually, for a 125 percent overtest in the containment vessel, a total weight of Pentolite explosive charge of 2.8 pounds is required. This would simulate 125 percent blast output of two Viper rounds going off at the same time. The containment vessel detail design by RISI Industries was fabricated by FEECO Corporation of Green Bay, Wisconsin and shipped to Safety Consulting Engineers', Inc. test site in Freeport, Illinois. The containment vessel as shown

in Figure 12, was erected for testing. Appropriate high-speed movie cameras and blast pressure gauges were utilized to monitor the qualification tests. The first qualification test was conducted by detonating one Viper round inside of the containment vessel. The second test was run by detonating 2.8 pounds of Pentolite charge in the containment vessel center to simulate 125 percent blast output of two Viper rounds. In both qualification tests, no fragments or blast overpressures were sensed in the vicinity up to thirty feet from the containment vessel. A small puff of escaping gas was noted at the initial detonation but stopped instantaneously according to high-speed camera coverage. Thus, the containment vessel met the requirements of the production facility and safety requirements by being able to withstand the fragmentation, blast, fireball output, and shape charge output of two Viper rounds. Actually, the shield easily withstood 125 percent blast overpressure in accordance with the military requirements.

REFERENCES

1. "TNT Equivalency of LX-14 High Explosives" ARRADCOM Contractor Report No. AR-TSD-CR.
2. "Suppressive Shields" U.S. Army Corporation of Engineers Publication HNDEM-1110-1-2, 18 November 1977.
3. Hazards of Chemical Rockets & Propellants Handbook - Vol. 1, General Safety Engineering Design Criteria, May 1972, AD 889763.
4. Rakaczky, J.A., "The Suppression of Thermal Hazards From Explosions of Munitions - A Literature Survey" BRL Interim Memorandum Report No. 377, Aberdeen Proving Ground, Maryland, May 1975.
5. Roark, R.J. & Young, W.G., Formulas For Stress & Strain, Fifth Edition, McGraw-Hill.

TABLE 1
CONTAINMENT VESSEL DESIGN CRITERIA

<u>PARAMETER</u>	<u>SUGGESTED LIMITS</u>
1. Minimum Floor Space	6 ft. Diameter
2. Separate Fragment Shield Configuration	Vertical cylinder
3. Fragment Shield Height	To stop fragment spray at ends
4. Fragment Shield Thickness	To stop fragment penetration and withstand blast effect
5. Vent Configuration & Diameter	Cylinder & diameter based on minimizing gas pulse load onto structure
6. Vent Height	To reduce blast over-pressure below 2 - 3 psi at top of vent
7. Outer Blast Containment Vessel Configuration	Vertical cylinder
8. Outer Blast Containment Vessel Configuration Thickness	Based on blast & gas pressure loads onto structure
9. Method to Hold Rounds	Dolly with propagation shield on it to move in & out of vessel
10. Round Entry	2 doors that open simultaneously
11. Electrical & Mechanical Entry	Fitting & maintenance door
12. Heat Effect	Angled plates
13. Bottom	Scaled

TABLE 2

VIPER CONTAINMENT VESSEL DESIGN
VESSEL STRUCTURAL ANALYSIS RESULTS

Condition: 2 Rounds Vent Diameter: 40" $W_{He} = 3.76 \text{ lb.}$

CONDITION	INNER SHIELD		OUTER SHIELD		*TRANSITION ($t=3/4"$)	STACK $r_{max} = 900 \text{ psi}$
	$r_{max} = 857 \text{ psi}$ ($t=1"$)		$r_{max} = 750 \text{ psi}$ ($t=3/4"$)			
1. Radius of Structure (ft.)	2.5		3.0		2.33	1.67
2. P_r (psi)	6000		4150		180	130
3. T_i ($\times 10^{-5} \text{ sec.}$)	6.22		7.34		60.4	74.2
4. P_{sq} (psi)	22		22		22	22
5. T_{BD} (sec.)	0.090		0.090		0.090	0.090
6. T_n Structure ($\times 10^{-4} \text{ sec.}$)	9.43		11.3		23.4	14.1
7. r_m (psi) (for $\mu = 1$)	1261		864		1295	1808
8. r_m (psi) (for $\mu = 6$)	385		266		396	551
9. Wall Thickness (inch) for $\mu = 1$	0.95		0.79		0.91	0.91
10. Wall Thickness (inch) for $\mu = 6$	0.29		0.24		0.28	0.28

*Utilized Bi-Axial Stress Analysis

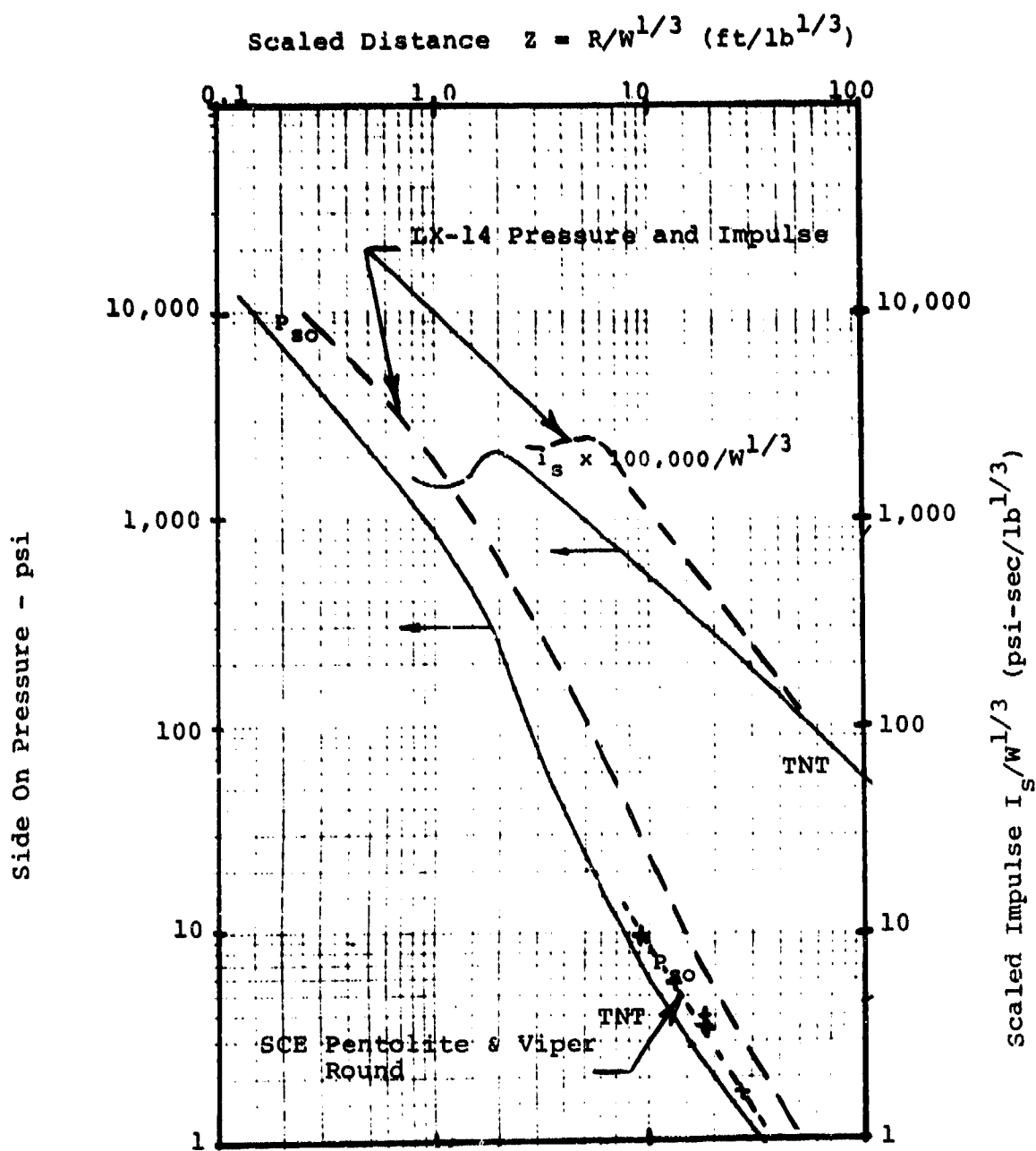


Figure 2. Peak Side On Pressure and Impulse For TNT Air Burst Charges LX-14 Billets (Reference 1) and SCE Results of Viper Rounds

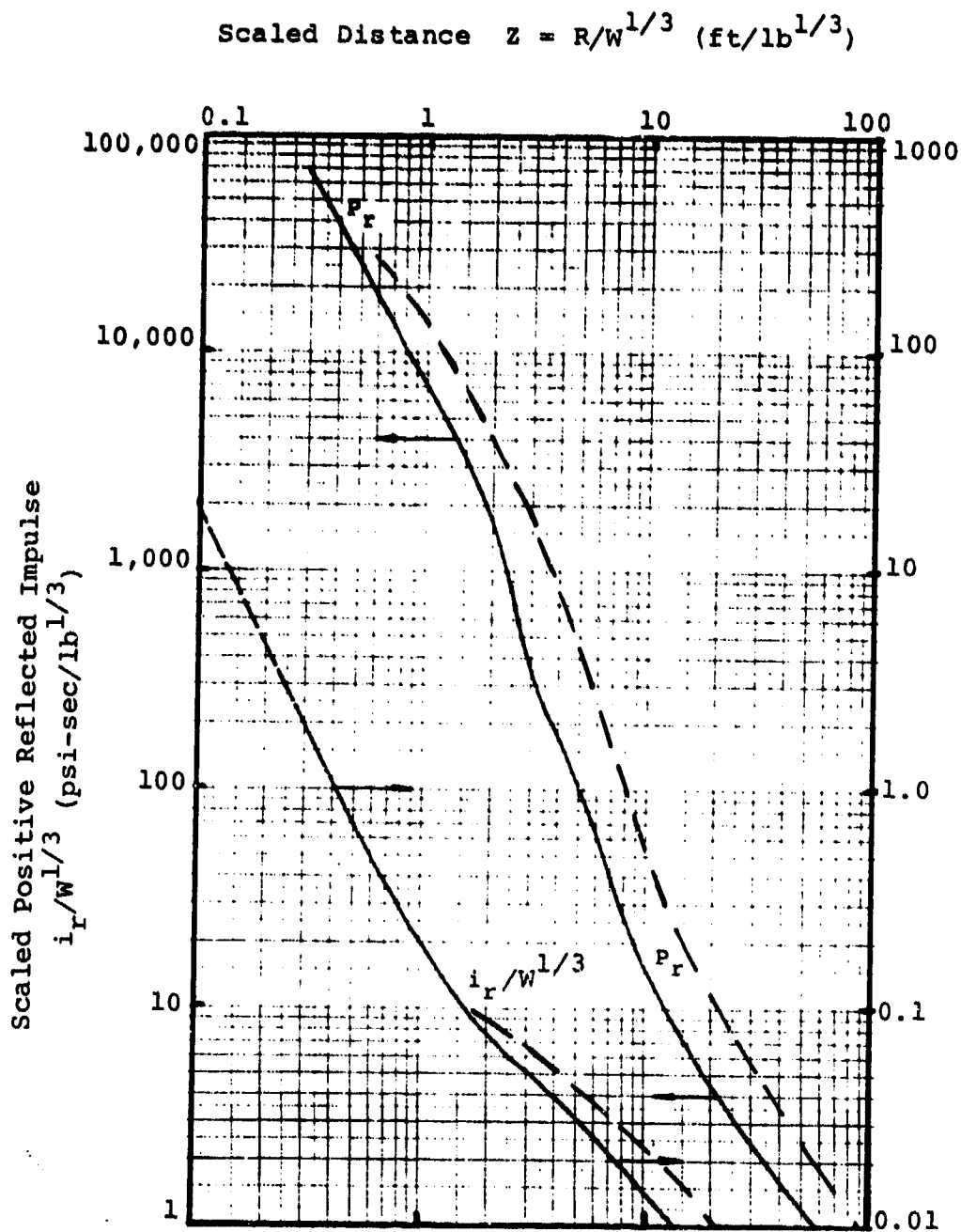


Figure 3. Peak Reflected Pressure and Impulse - Air Blast Charges of TNT Charges and LX-14 Equivalents (Estimated From Reference 1)

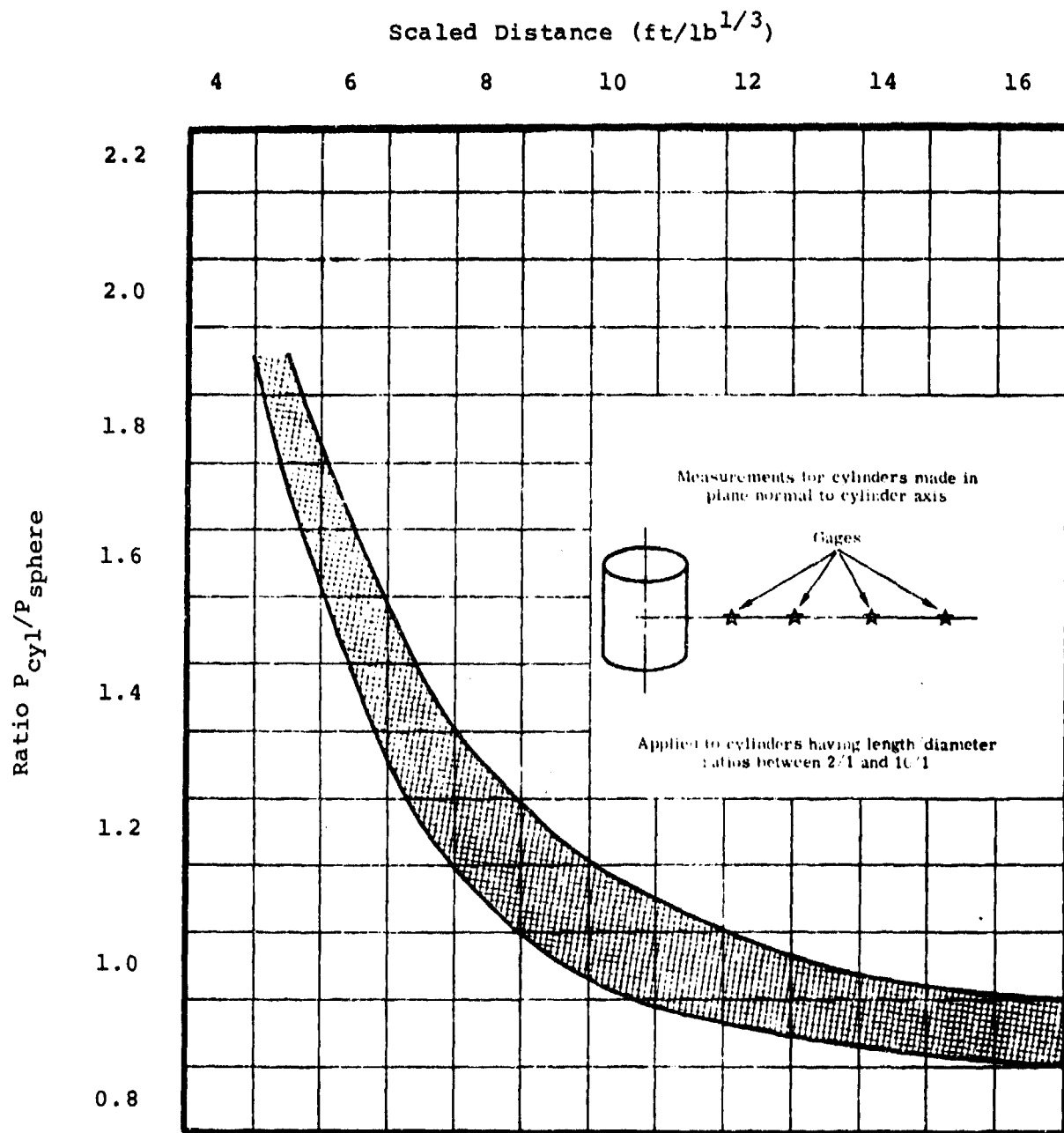


Figure 4. *Peak Overpressures From Cylindrical Charges Compared to Peak Overpressure From a Spherical Charge of the Same Equivalent Weight

*See Reference 2

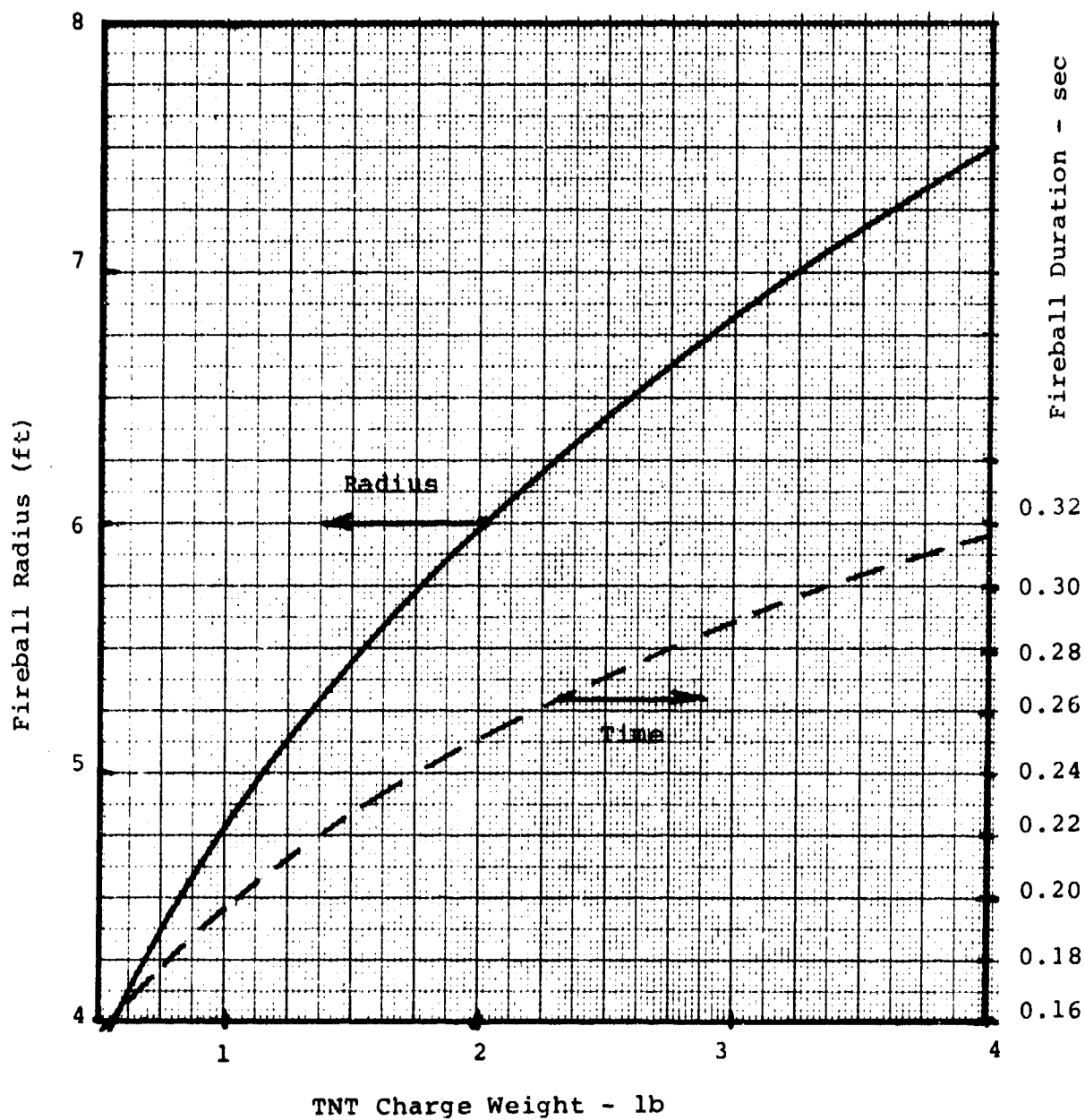


Figure 5. Calculated Fireball Radius and Duration for Various Charge Sizes

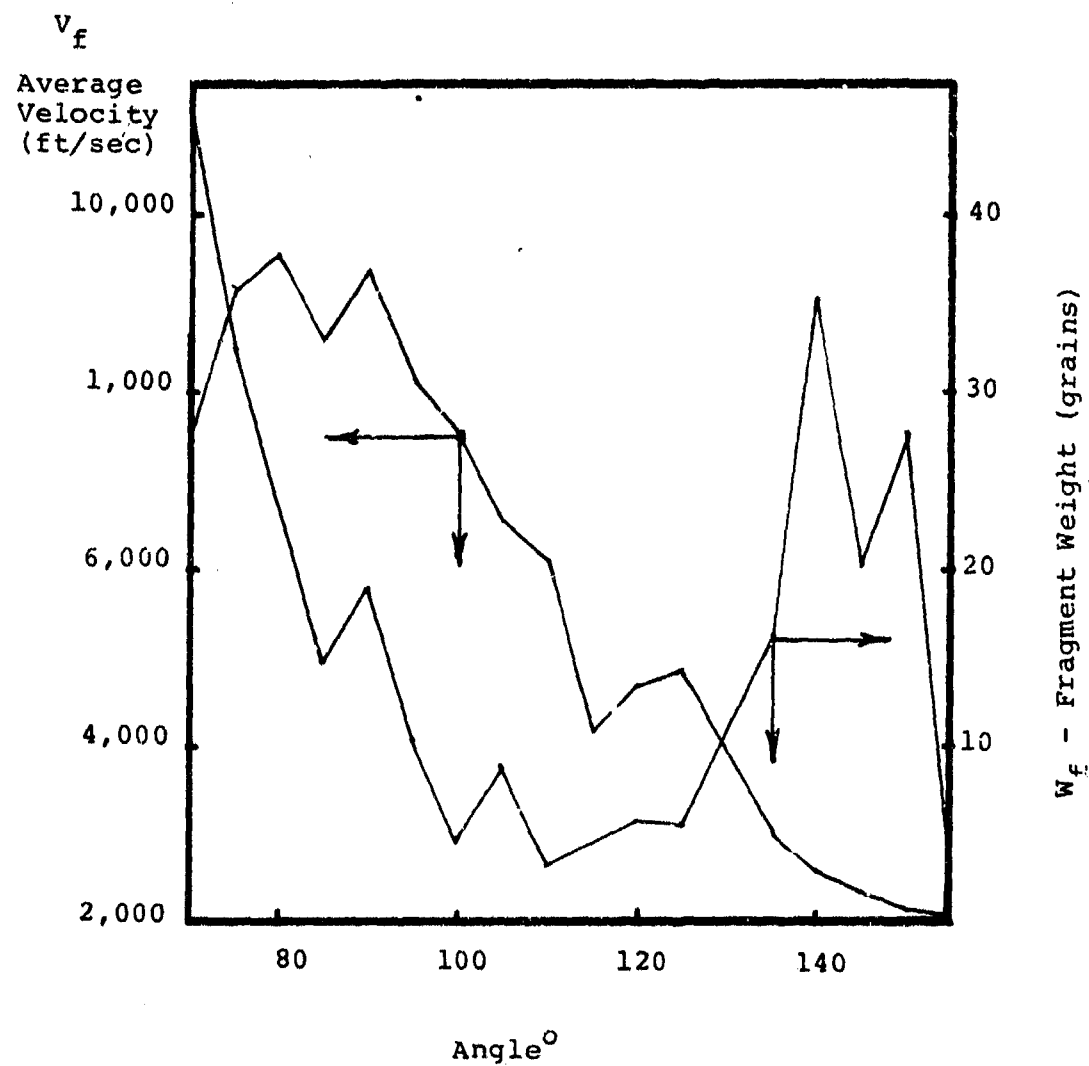


Figure 6. Case Fragment Velocity and Weight Distribution From Viper Round

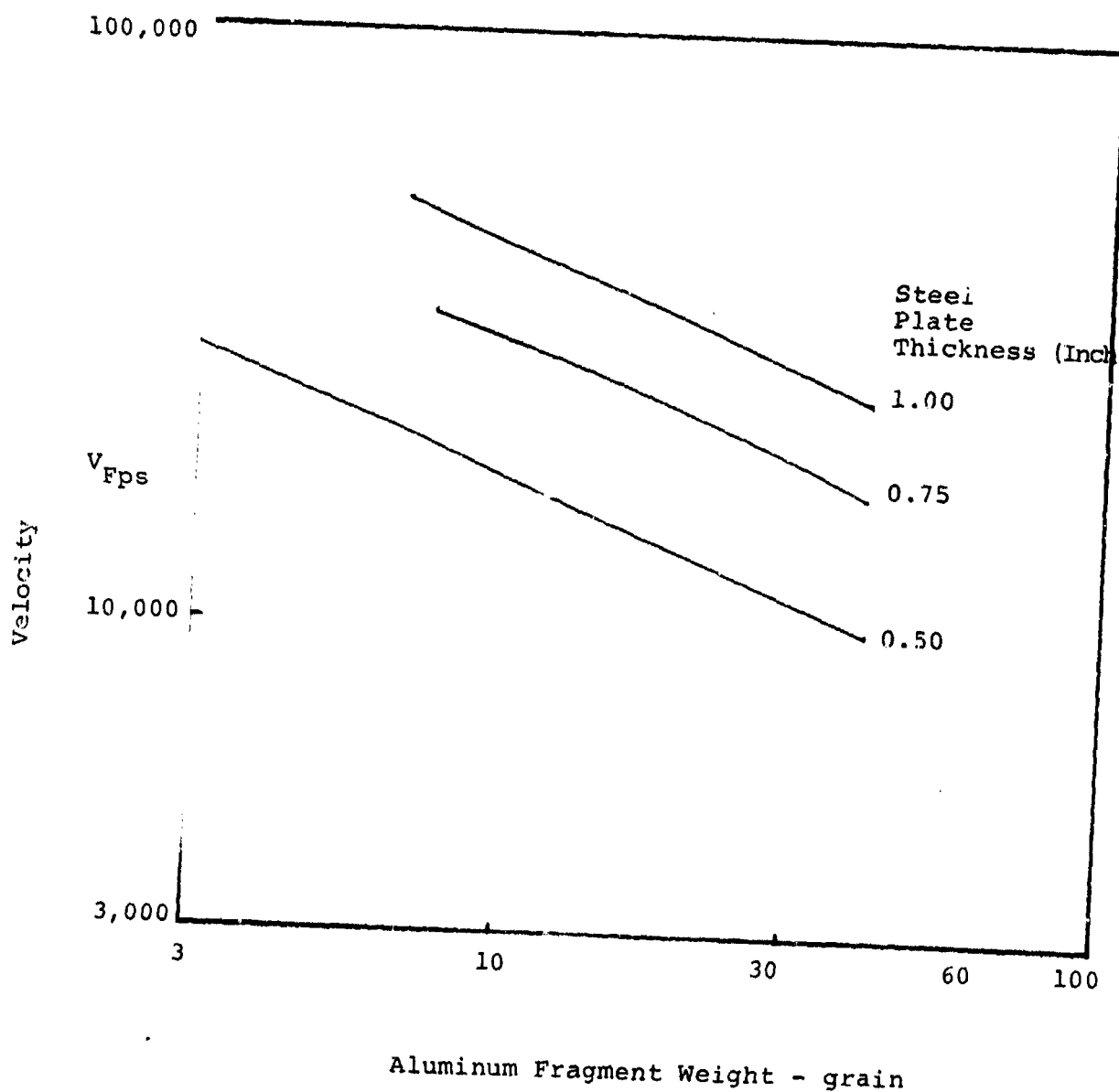
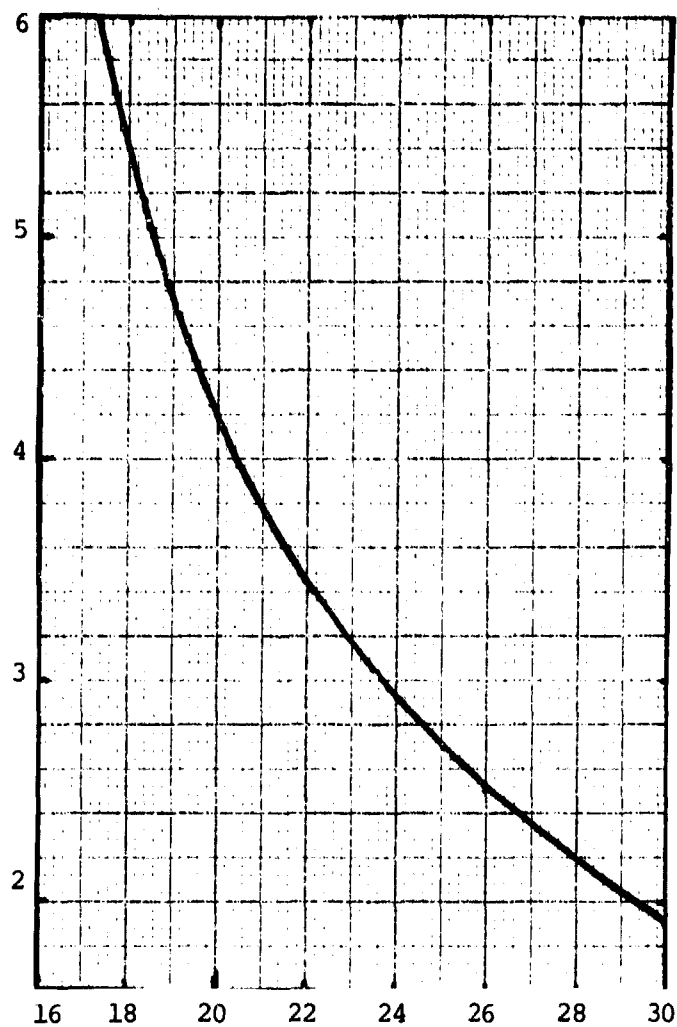


Figure 7. Fragment Velocity Required to Penetrate Mild Steel Plates at Various Aluminum Fragment Weights

Peak
Side-On
Pressure
at
Stack
Outlet
(psi)



Stack Height From Floor

Figure 8. Vent Stack Outlet Peak Side-On Pressure Versus Stack Height (2 Rounds)

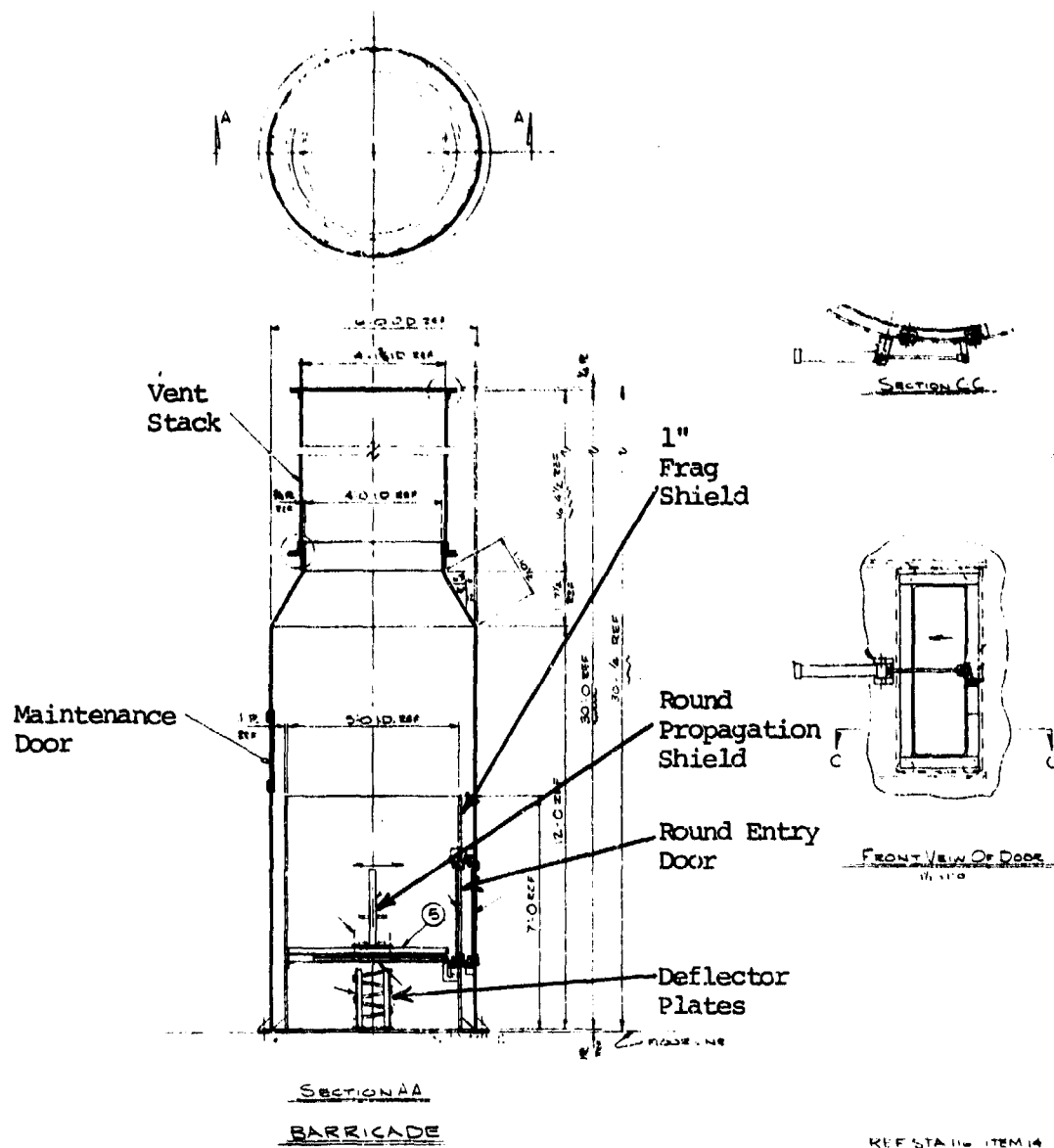


Figure 9. Viper Containment Vessel Design



Figure 10. Maintenance Access Door

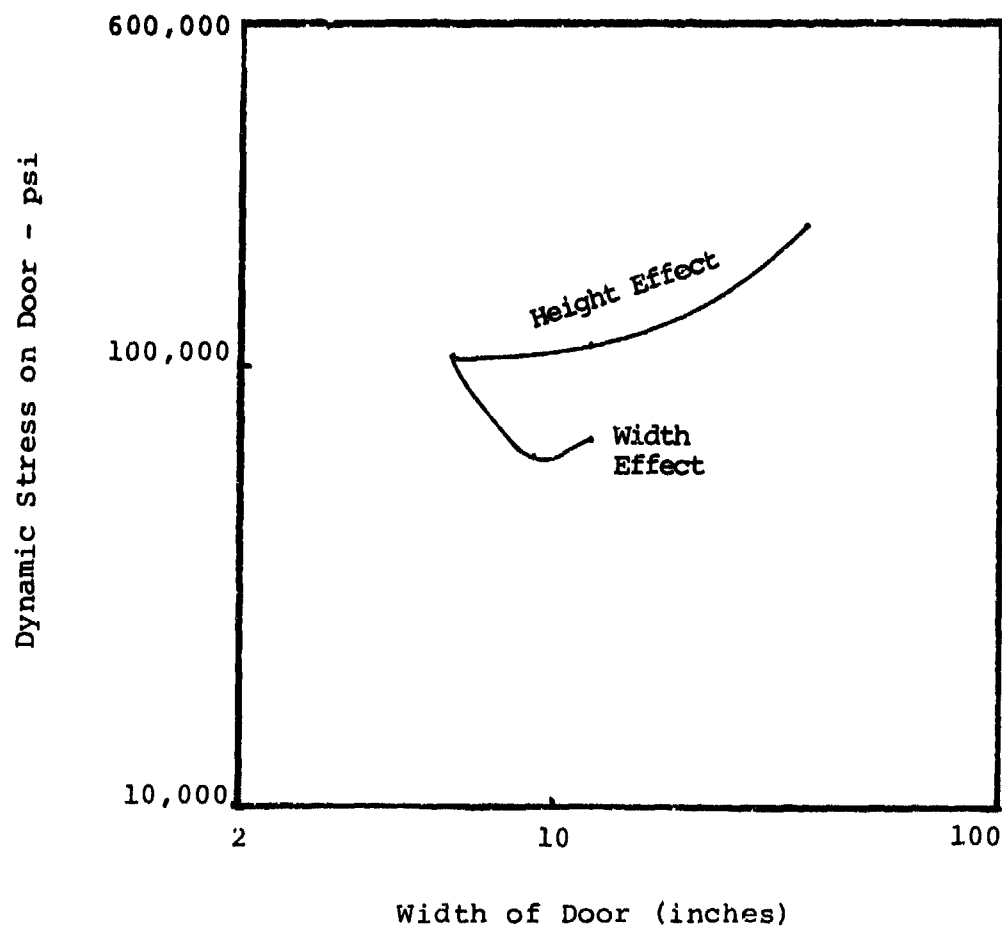


Figure 11. Dynamic Stress on a 1 Inch Thick Steel Door 36 Inches High

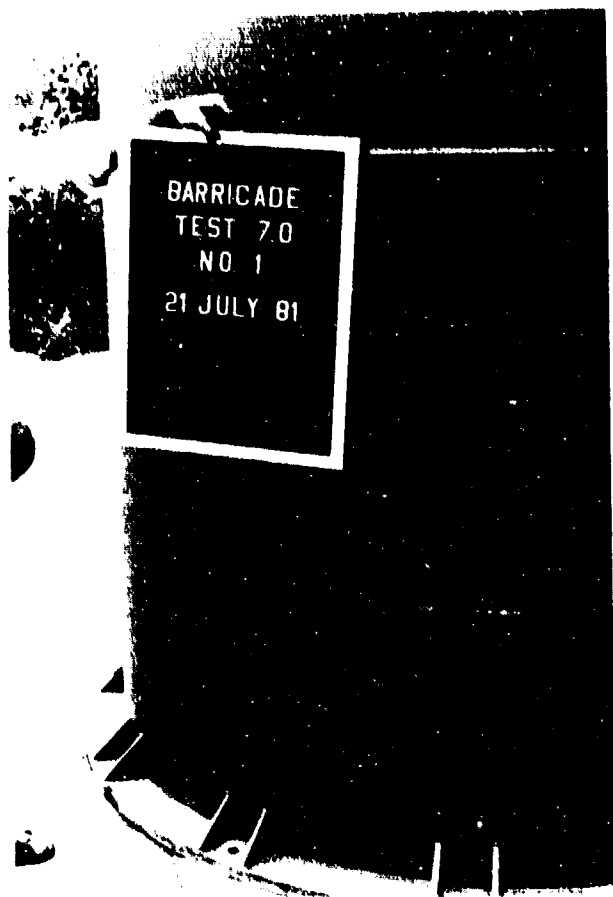


Figure 12. Round Feed Door

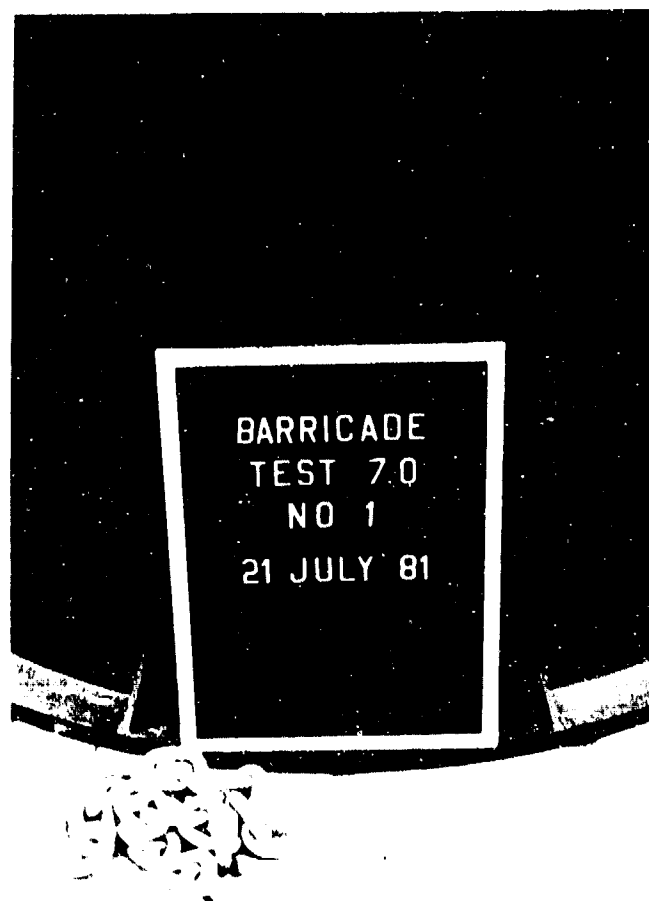


Figure 13. Electric Feedthrough of Vessel

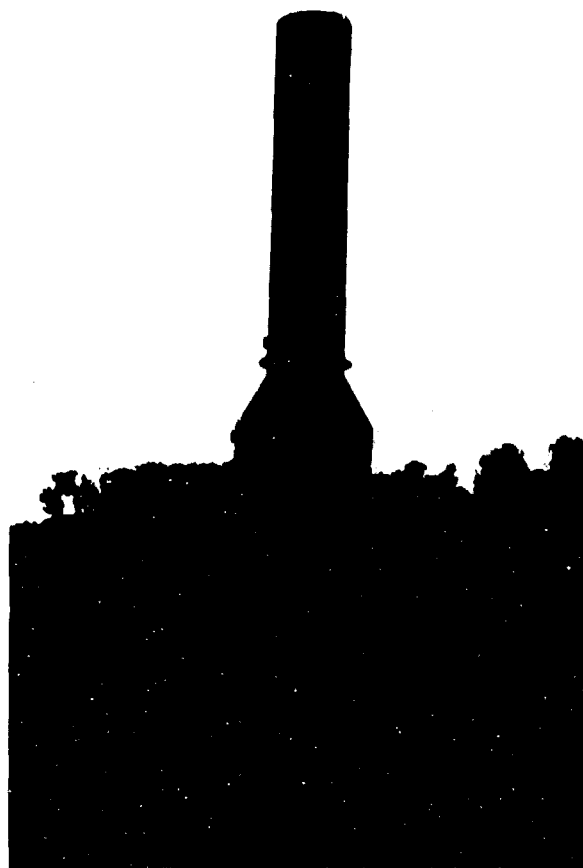


Figure 14. Photo of Viper Containment Vessel
Design

→ Behaviour of Gun Propellant to
Ignitions of Different Intensities

Roland Wild

Bundesinstitut für chemisch-technische Untersuchungen (BICT),
Großes Cent, 5357 Swisttal-Heimerzheim, FRG

1. Introduction

↓
In the case of large calibre ammunition, for example 105 mm and 120 mm, a uniform and accurate ignition of the propelling charge is of great importance.

A poor ignition may not only lead to a spread of the ballistic data (e.g. initial velocity of the projectile); the gas pressure inside the barrel may become so high, that the strenght of the barrel-material may be exceeded and hence the gun can be totally destroyed, even fatal casualties may happen.

It is known by experience, that different gun propellants react in different manner to poor ignition. Therefore it is desirable to have a small scale test at one's disposal (which can be performed in the laboratory) by means of which it can be checked which gun propellant responds in a dangerous manner to a poor ignition.

↑
Such a test should be not too expensive and nevertheless should yield reliable data.

In the following a test method is described which meets the above mentioned requirements.

2. Description of the test method

A sketch of the experimental set up is shown in figure 1. The propellant, with a mass of about 500 g is filled, with its bulk density, into a seamless steel tube, which is open at one side. The tube has a length of 350 mm, a wall thickness of approx. 5 mm and an inner diameter of 50,8 mm (2 inches). An igniter (fig. 2), also made of steel is fixed at the closed end of the tube. The tube then, with its open end is put onto a steel block. A quartz gage for measuring the pressure (up to 0.7 GPa) is built into this steel block. When performing the test, a steel block with a mass of 18 kg is put onto the whole assembly.

For igniting the propellant we use quite normal black powder. The amount of black powder, which is filled into the igniter can be varied.

Up to 22 g black powder can be packed into the igniter.

The test output is the pressure in the steel tube (measured by the quartz) produced by the different igniter strengths.

The tubes rupture at pressures of approximately 0.08 GPa, therefore the burning of the propellant can be monitored, under normal circumstances, up to a pressure of 0.08 GPa.

3. Results

In figure 3 typical pressure time histories, which were recorded when performing the tests, are shown.

It can be seen, that in the case of a weak ignition (5 g black powder) a regular burning of the propellant occurs, when using stronger ignition conditions, the burning characteristics significantly change, in other words

the pressure rise time drastically decreases, and in some cases even pressures up to 0.7 GPa are produced. Though the steel tubes normally rupture at pressures of 0.08 GPa, the pressure rise time in this case, is so fast, that due to the inertia of the confinement, such high pressures can be attained.

4. Applicability of the method and discussion

In order to check the applicability of the test method we performed the test with several seven perforated gun propellants (see table 1).

Propellant 1, 2 and 3 were triple base propellants which chemical compositions were nearly the same, only the web sizes were slightly different. The main difference between these propellants was the way how they were produced. Propellant 4 was a double base propellant and propellant 5 a single base propellant. All the propellants exhibited nearly the same interior ballistic data, which were determined in a closed vessel (see also table 1).

For ignition we used black powder charges of 5 g, 10 g, 15 g and 20 g. The relevant data for judging the response of the propellants to different ignition strengths are tabulated in table 2. As relevant data we took the maximum pressure, the pressure rise time and the maximum rate of the pressure rise ($\frac{dp}{dt}$).

When comparing the data it can be seen, that propellant 1 reacts most sensitively to the variation of the ignition strength, i.e. the rate of the pressure rise becomes greater when using a moderate ignition strength, whereas when looking at propellant 3 one can constate that very high pressure rise rates only occur, when using a very high ignition strength.

We think, that the very fast pressure rises, and hence the very high pressures, in the case of intense ignition, can be explained by assuming a fracture of the propellant grains. For theoretical calculations, using a gas dynamic model, yield similar pressure rises, when assuming that a part of the propelling charge (10 %-15 %) is fractured near the projectile base.

The fracturing of propellant grains, can be explained by a pressure gradient, produced by the ignition, which accelerates the charge downwards. At the steel block the motion is stopped and the grains can be fractured. The more intense the ignition, the greater will be the pressure gradient and the acceleration of grains and therefore the possibility of fracturing will rise.

The results, now, do not mean, in any way, that for example propellant 1 should not be used for constructing ammunition, but nevertheless the results show that, when using propellant 1 the ignition condition should be thoroughly investigated, in order to avoid a dangerous behaviour of the ammunition.

Furthermore it should be remarked, that at the present state of our investigations there exist no absolute, unambiguous criteria for judging the behaviour of the propellants, nevertheless the method can be used to compare different propellants, concerning the behaviour to changes in the ignition conditions.

5. Summary

A small scale laboratory test is described by means of which it becomes possible to judge the behaviour of gun propellant to different ignition strength in the ammunition. The applicability of the test method could be shown.

Table 1

Interior ballistic data determined in a closed vessel. Loading Density 0.1 g/cm^3
 $(p_{\text{max}}$ in all cases approx. 0.1 MPa)

Propellant	1 triple base	2 triple base	3 triple base	4 double base	5 single base
$L_D \text{ } [(\text{Pa s})^{-1}]$	$0.11 \cdot 10^{-5}$	$0.14 \cdot 10^{-5}$	$0.11 \cdot 10^{-5}$	$0.11 \cdot 10^{-5}$	$0.19 \cdot 10^{-5}$
$r_p \text{ } [\text{Pa}/\mu\text{s}]$	$0.52 \cdot 10^4$	$0.62 \cdot 10^4$	$0.55 \cdot 10^4$	$0.58 \cdot 10^4$	$0.61 \cdot 10^4$
$\left(\frac{dp}{dt}\right)_{p=0.08 \text{ GPa}} [\text{Pa}/\mu\text{s}]$	$0.08 \cdot 10^5$	$0.11 \cdot 10^5$	$0.09 \cdot 10^5$	$0.1 \cdot 10^5$	$0.11 \cdot 10^5$

L_D = dynamic vivacity =

$$= \left(\frac{dp}{dt}\right)_{0.5 p_{\text{max}}} \cdot \frac{1}{0.5 p_{\text{max}}^2}$$

r_p = pressure rise rate between $0.1 p_{\text{max}}$ and $0.9 p_{\text{max}}$

Propellant Ignition	No 1	No 2	No 3	No 4	No 5
	triple base	triple base	triple base	double base	single base
5g black powder	P_{max} [GPa]	0.08	0.10	0.08	0.08
	$\left(\frac{dp}{dt}\right)_{max}$ $\left[\frac{MPa}{\mu s}\right]$	0.15	0.12	0.10	0.46
	t_r [μs]	1050	1250	1300	420
10g black powder	P_{max} [GPa]	0.075	0.08	0.08	0.08
	$\left(\frac{dp}{dt}\right)_{max}$ $\left[\frac{MPa}{\mu s}\right]$	0.22	0.13	0.10	0.57
	t_r [μs]	500	1000	1000	275
15g black powder	P_{max} [GPa]	0.11	0.08	0.08	0.28
	$\left(\frac{dp}{dt}\right)_{max}$ $\left[\frac{MPa}{\mu s}\right]$	0.80	0.50	0.26	10.0
	t_r [μs]	150	300	400	20
20g black powder	P_{max} [GPa]	0.70	0.11	0.42	0.70
	$\left(\frac{dp}{dt}\right)_{max}$ $\left[\frac{MPa}{\mu s}\right]$	140	1.2	13	140
	t_r [μs]	5	100	32	5

Table 2

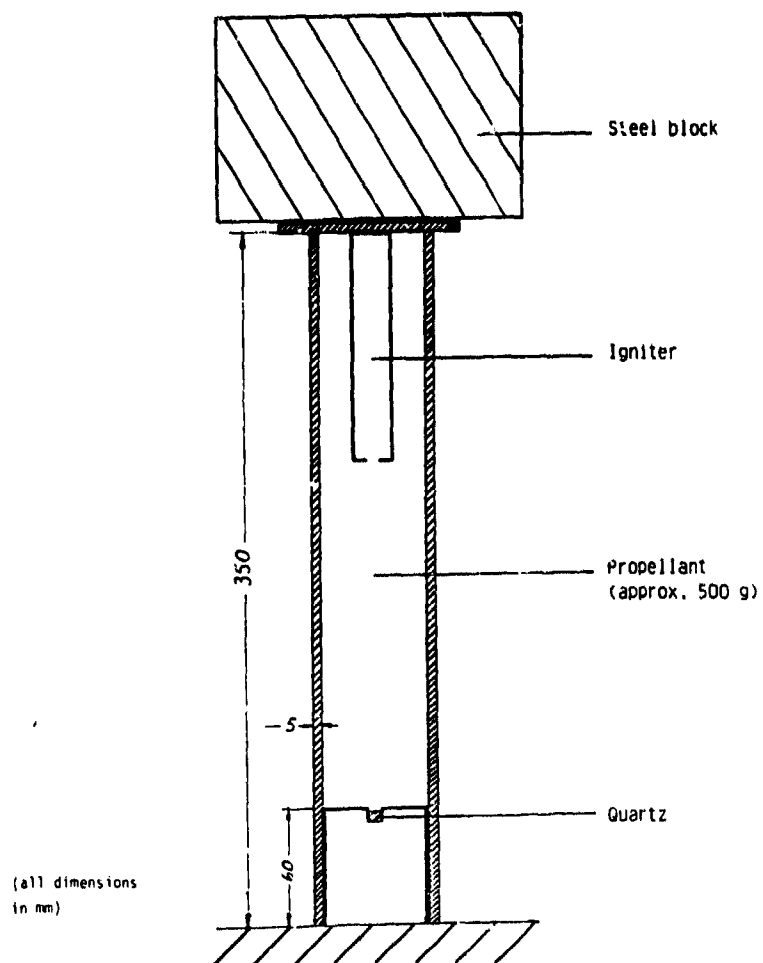


figure 1. Experimental Set up

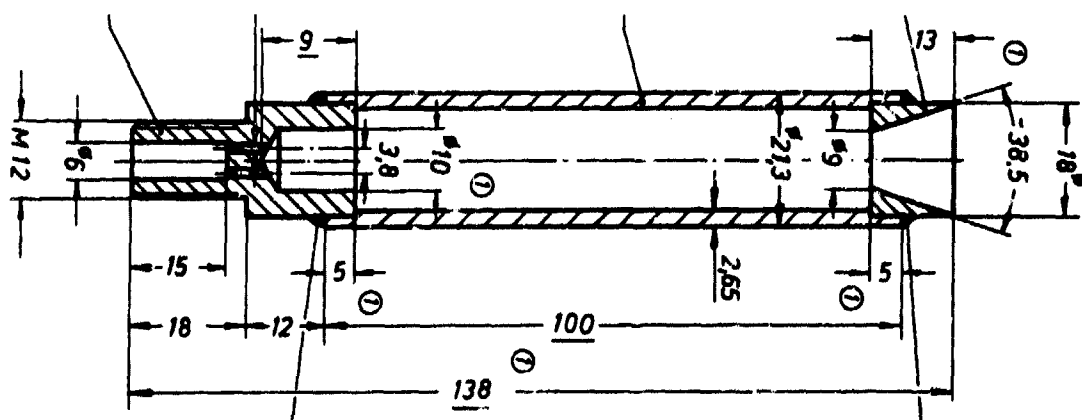


figure 2. Igniter 447

PRESSURE TIME HISTORY

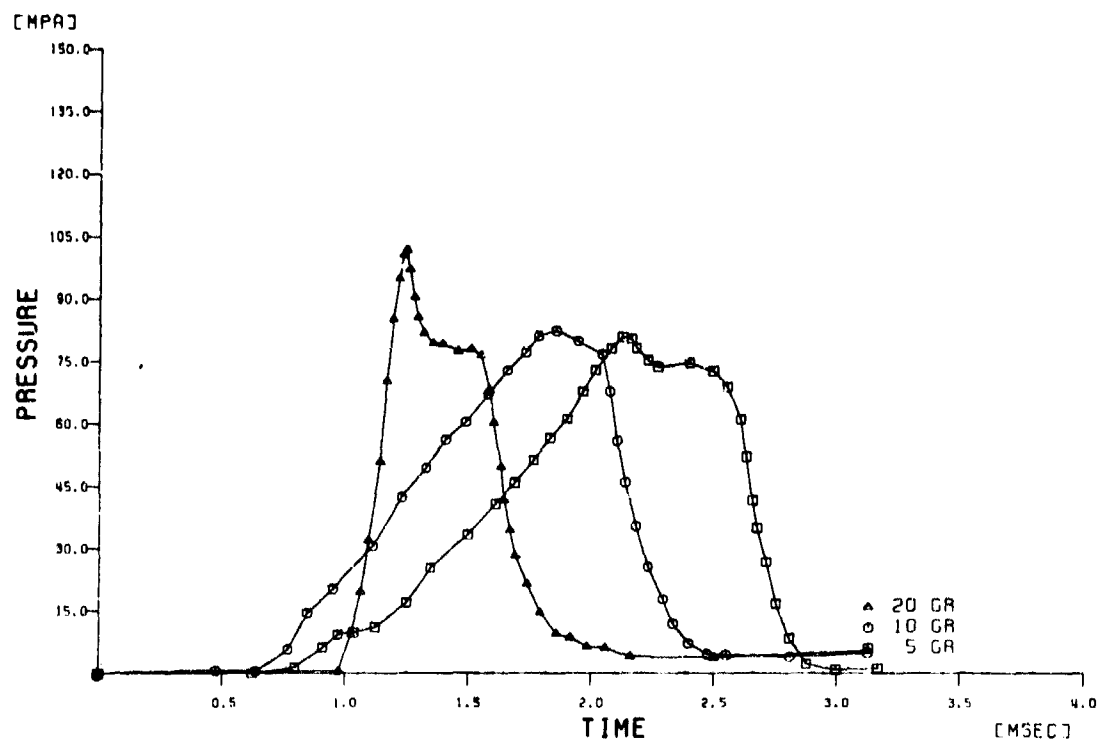
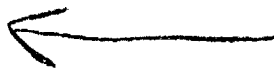


figure 3. Pressure Time History



MINISTRY OF DEFENCE

ROYAL ARMAMENT RESEARCH AND DEVELOPMENT ESTABLISHMENT

AD P000443

The Response of RDX/TNT Filled Shell to Thermal Stimuli

A S Dyer, C D Hutchinson, P J Hubbard and J Connor, Jr.

Paper for presentation at the
DOD 20th Explosives Safety Seminar, Norfolk, Virginia. August 1982

Summary

Trials have been conducted in which 155mm shell filled with RDX/TNT (60/40) have been subjected to internal ignition and to external flame. The effects on adjacent shell of internal ignition have also been assessed. Generally results are consistent with assessments of explosiveness based on RARDE Burning Tube Tests but in one trial base ignition appeared to induce detonation in adjacent shell. The significance of these results is discussed.

1 INTRODUCTION

The hazard which an explosive or an explosive filled store presents is determined by two factors:

a) the ease with which the store may be accidentally initiated which we designate as the sensitiveness

and

b) the consequences of that initiation, the explosiveness.

Each of these factors is, or may be, a function of the physical form of the explosive (eg whether it be in powder or charge form) of the type and level of the stimulus and of the environment - particularly the confinement. A complete hazard assessment of an explosive store should involve testing the store over a range of stimuli and levels of stimuli in environments which may be encountered in practice. The explosive should be tested as used, that is in charge form, but also in the form in which it is processed and in the form it might degenerate to after, for example, prolonged storage or vibration, that is in powder form.

A full evaluation of this type is expensive, time-consuming and rarely, if ever, attempted. Instead small scale tests are used to predict what might happen in practice. One such test has been employed by RARDE for the past several years to estimate the explosiveness of secondary explosives in charge form and under confinement. Known as the Burning Tube Test, the procedure involves ignition of the explosive charge contained in a mild steel tube sealed by end caps.

The Small Burning Tube Test normally carried out employs a charge of 350g of explosive in a tube with wall thickness of 6mm. Explosiveness is assessed by the degree of damage to the tube and by the extent to which the explosive is consumed.

The ranking order of explosiveness is unchanged when determined in the Large Burning Tube which employs a similar ignition system in an approximately 9kg charge in 12.7mm thick wall tubes. This size of charge and wall thickness is quite similar to the FH70 155mm shell.

Attempts have been made to increase the discrimination of the burning tube test by varying the confinement on RDX/TNT 60/40 and on TNT by using tubes with tapered or stepped walls but these have not been successful. On the other hand, increased confinement in weapons subject to rifle bullet attack has been shown to lead to enhanced explosiveness. Burning Tube Tests with heavier confinement are planned but in the interim the chance has arisen to carry out trials on 155mm FH70 shell filled with either RDX/TNT 60/40 or CW3. CW3 is a RDX/HMX/TNT 56/4/40 composition with other minor additives to improve its mechanical properties. These trials had their original impetus in reports from the USA on trials to assess the minimum non-propagation distance between detonating 155mm M107 shell filled Comp B. During these trials it was found that wooden pallets on which shell were standing caught fire when struck by hot fragments from shell detonating at 16 and 25m. The burning pallets were

said to have caused detonation in shell standing on them after intervals of 17 and 30 minutes. Both the US and subsequent UK tests were on unfuzed shell.

While external fire trials do form a major part of the study, it was decided to extend the trials to investigate the effects of varying confinement at internal ignition sites on explosiveness and also to investigate possible differences between RDX/TNT and CW3 filled shell. These studies are not yet complete but some interesting observations have been made and at least provisional conclusions can be drawn from them. The aim in this report is to describe the work which has been done and to discuss its interpretation.

2 INTERNAL IGNITION STIMULUS TRIALS AT AMBIENT TEMPERATURES

Previous work has shown that the most violent deflagrative events that could be produced in shell at ambient temperatures resulted from ignitions at the base of the shell. The fuzehead/propellant ignition system used in burning tube tests was adapted to produce an ignition at the base of 155mm shell. Empty shell were bored at the base and fitted with a threaded plug. Removal of this plug after filling the shell with either RDX/TNT (60/40) Type A or CW3 left a cavity 25mm in diameter by 20mm deep. The fuzehead and a 1.5g ballistite charge were placed in this cavity and retained by a plug of equal thickness to the shell base (35mm). Modified shell filled with CW3 incorporated vinyl alkyd paint bonding of explosive to the shell wall.

The following trials were conducted:

- a) Base ignition of RDX/TNT filled shell with 1 or 2 adjacent CW3 filled shell as acceptors to assess the possibility of propagation.
- b) Base ignition of a CW3 filled shell with 2 adjacent CW3 filled shell as acceptors as in Test 1.
- c) Base ignition of a single CW3 filled shell.
- d) Top ignition of CW3 filled shell.
- e) Base detonation of CW3 filled shell.

2.1 Results

Results of internal ignition trials are detailed in Table 1. Important features are summarised here.

Base ignited RDX/TNT filled shell behaved in a similar manner to that expected from Large Burning Tube Tests. The filling deflagrated violently, shattering the shell body into many pieces, but recovered fragments showed no signs of detonation and many small pieces of unconsumed explosive were found scattered around the test site. CW3 filled shell at 85 and 105mm from the donor were broken open but the major proportion of the shell bodies and the explosive were intact.

A test involving base ignited CW3 filled shell as donor gave rather different results. On ignition of the donor shell a very violent reaction ensued involving the donor and acceptor shells at both 95 and 135mm separation. Large fragments from the base of the donor were driven into the ground but there was no sign of other large fragments or of unconsumed explosive. Deep holes had been blown in the site by the violence of the reaction. Peripheral damage to stands and blast gauge equipment showed they had been struck by extremely fast moving fragments. The blast gauges indicated that overpressures had been generated somewhat greater than would have been expected from the detonation of a single shell.

Base ignitions of a single CW3 filled shell without acceptors also gave a very violent event but foil gauges were only dented, not punctured, and indicated an overpressure of less than 35kPa at 5m. In one test a 170mm long fragment from the nose section of the shell was recovered.

Using a transit plug modified to take the fuzehead/propellant system so as to give nose ignition, a single CW3 filled shell was tested. The shell was inverted with 100mm of the nose buried in the ground to increase the confinement. A mild reaction occurred which split open the tapered section leaving the lower section intact and filled. The majority of the CW3 from the top section was also recovered.

This test was repeated with a nose ignited CW3 filled shell upright between 2 CW3 filled acceptor shell both at 95mm separation. There was a little more damage to the donor but a large part of the filling was recovered unconsumed and the 2 acceptor shell were recovered intact.

A modified shell fitted with a base plug and filled CW3 was detonated from the base using a tetryl booster and an L2A1 detonator. Foil blast gauges recorded detonation overpressures with a spread of up to 50% around the predicted value at a range of radial distances. Base fragments recovered from the region of the plug were smaller than those obtained from base ignited shell but not so small as those from a nose detonated shell.

3 RESPONSE OF 155mm SHELL TO EXTERNAL FLAMES

This part of the trials derived from the US report of detonations of Comp B filled shell in pallet fires, but the opportunity was also taken to examine the effect of torching from an ignited shell on adjacent shell. All of these trials involved CW3 filled shell.

3.1 Results from Pallet Fires

In an attempt to repeat the US observation a test was arranged with a 155mm CW3 filled shell standing upright in an angle-iron stand on a wooden pallet. The standard pallet 4ft x 4ft was ignited remotely by a fuzehead with a 200g thermite mixture (SR877). An explosive event occurred after 17½ minutes. Large pieces of CW3 were found up to 150m from the test site, some of which showed evidence of having melted. Large fragments of the shell were recovered. There was no suggestion of detonation from this single shell.

The test was repeated with similar arrangements except that the shell was laid horizontally on the pallet. In this test an explosive event occurred after 4mins 17secs. Large pieces of CW3 were recovered again showing signs of having melted. Large sections of the shell body were also recovered.

3.2 Results from Torching Shell

Results are summarised in Table 2. Donor shell filled CW3 were ignited with a thermite igniter in the nose and the flames played on the centre, the driving band, the base and along the length of acceptor shell. Events occurred at times varying from about 40 seconds to several minutes after ignition with acceptor shell being split open and a large portion of their filling being recovered unconsumed.

4 DISCUSSION

4.1 Internal Ignition Trials at Ambient Temperature

The response of the base ignited RDX/TNT 60/40 Type A filled shell was much as anticipated from Large and Small Scale Burning Tube Tests. The filling was not completely consumed but showed fairly high explosiveness. Adjacent CW3 filled shell at 85 and 105mm were split open by fragment strikes and the filling was scorched without the event growing after the case was split.

The CW3 filled shell gave more violent events in single shell tests in that less explosive was recovered. However one large shell fragment and some unconsumed HE were recovered while no foil blast gauges were punctured. This indicated that the events were not detonations. A comparison of the high speed framing camera records from base detonated and base ignited shell shows a slower expansion of the fireball for the base ignited shell. It was surprising however, that such base ignited CW3 filled shell as donors could cause events in adjacent shell which gave every indication of being detonations. Whereas large fragments were recovered from the base of the donor shell no fragments were recovered from the acceptor shell. The foil blast gauge records indicate detonation of more than one shell when acceptors were present but gave no response to a single donor.

Although it is easy to mistake violent deflagrations for detonations, it is our impression that in these trials detonation in CW3 filled acceptor shell was induced by knock-on effect following deflagration in CW3 filled, base ignited donor shell.

A large difference was evident between the response and effect of CW3 filled donors as compared with RDX/TNT filled donors and there are several possible causes for this difference:

- a) The 4% HMX or the increased mechanical strength due to the minor additives in CW3 may have increased its explosiveness relative to RDX/TNT even though RDX/TNT and CW3 behaved similarly in Large and Small Burning Tube Tests.

b) The filling in CW3 filled shell is known to sediment such that the nitramine content at the base could be up to 7% greater, ie 57% nitramine.

It is known that 70/30 cyclotol and 75/25 RDX/TNT compositions show greater explosiveness than 60/40 RDX/TNT or EDCI in charge hazard tests (Spigot and Oblique Impact). CW3 was similar to RDX/TNT in the oblique impact test.

c) The CW3 filled shell were treated with a vinyl alkyd/TNT bonding paint while the RDX/TNT filled shell were not. This bonding agent may have increased the confinement marginally at the ignition site in the base of the shell.

d) The explosiveness of the CW3 may have been enhanced in the shell as compared with that in a Burning Tube because of the strong walls at the base of the shell. The tensile strength of STA 64 shell body material is twice that of the mild steel used in RARDE Large Scale Burning Tubes.

The tests on CW3 filled shell with nose ignition showed lower explosiveness which is probably due to the thinner walls reducing the confinement but may also be helped by there being no vinyl alkyd bonding or sedimentation at the top of the shell.

Further tests have been carried out in burning tubes with 25mm thick walls filled with RDX/TNT or CW3 both with and without vinyl alkyd bonding. Sedimentation in the CW3 filled tubes was enhanced by slow cooling. No significant differences in behaviour were observed. It appears that even these thick wall mild steel tubes provide less confinement than the shell.

Further evidence of the importance of confinement in determining the results of ignition of CW3 filled shell comes from an event which occurred recently when a shell was being sectioned longitudinally from the base. The filling ignited when it came into contact with the saw but the venting path provided by the saw-cut prevented the occurrence of anything more than a relatively mild deflagration.

4.2 External Flame Trials

The single shell pallet fire gave an event in a time similar to the US trials. Further examination of the US report suggests there were 3 shell on the burning pallet so in view of the knock-on effect postulated above it is conceivable that a detonation may have indeed occurred especially if adjacent shell were sensitised by heating.

The torching experiments gave deflagrative events with the violence increasing as the thickness of the heated region of the shell body and the time to the event increased. When replicate tests were carried out the times to the events were closely similar.

CONCLUSIONS

The effect of confinement on the consequences of deflagration initiated in 11kg charges of CW3 and RDX/TNT (60/40) Type A in a large test vehicle (UK 155mm shell) has been studied. Ignition in the very heavily confined base region of the shell gives rise to more violent events in CW3 fillings than in RDX/TNT fillings. It is believed that this is due to the increased confinement provided by the vinyl alkyd bonding of the CW3 filling to the inside of the shell case, a feature absent from the RDX/TNT filled shell. This bonding prevents venting of product gases along the path between the filling and the shell walls in the very early stages of reaction. CW3 and RDX/TNT filled shell behave identically when nose initiated; the area of ignition in these cases is in the fuze well and, by the time a process has burned to the outer surface of the charge, effects due to bonded or unbonded fillings are secondary to those from the failure of the relatively thin metal confinement. The vinyl alkyd bonding of CW3 to the 155mm shell is provided to ensure that no base air gaps are present which could lead to ignition by adiabatic compression during gun launch and to prevent rotation of the shell filling during flight. Given the very low probability of confined base ignition except as a consequence of set-back forces during gun launch, no safety advantage would accrue from removal of the bonding or from changing the filling to RDX/TNT (60/40).

This manifestation of high explosiveness in CW3 filled shell is not predicted by our Burning Tube Tests. We are forced to conclude from this that the confinement in the Burning Tube is substantially less than that at the base of the 155mm shell. This conclusion is important in reminding us of the variation in explosiveness with environment, of the need to carry out hazard assessments over a range of environments and of the dangers of extrapolating explosiveness data outside the range of confinement in which it was determined.

We intend to continue these studies using Burning Tubes of heavier confinement and also to carry out further trials with both internal and external ignition on CW3 filled shell to confirm that the events witnessed were indeed detonations and to determine the fragment velocities and overpressures which can lead to detonations in acceptor shell.

TABLE 1 Internal Ignition Trials

BASE IGNITION		
Donor	Acceptor	Observations
RDX/TNT	1 x CW3 at 85mm	Donor deflagrated violently. Acceptor broken open, filling mostly intact.
RDX/TNT	1 x CW3 at 105mm 1 x CW3 at 350mm	Donor and acceptor at 105mm - as above. Acceptor at 350mm displaced but intact.
CW3	2 x CW3 at 95mm	Very violent reaction involving donor and acceptors. No large fragments or unconsumed explosives. Overpressure greater than from a single detonated shell.
CW3	2 x CW3 at 135mm	As previous trial.
CW3	None	Violent reaction. Overpressure less than 5psi at 15 feet.
TOP IGNITION		
CW3 Shell inverted and 100mm of nose buried	None	Mild reaction splitting open tapered section of shell. Most of CW3 recovered.
CW3 Shell upright	2 x CW3 at 95mm	Donor slightly more damaged than in previous trial but large part of CW3 unconsumed. Acceptor shell intact.

TABLE 2 Torching Trials, CW3 Filled Shell

Layout	Time to Event	Observation
Donor 100mm from and at right angles to acceptor. Flames centred on a point 280mm from nose of acceptor.	48s	Donor and acceptor split open. Large fragments of CW3 recovered.
As previous trial.	38s	As previous trial except event extinguished donor.
Donor 100mm from and at right angles to acceptor. Flames playing on driving band.	330s	More violent than previous trials. Donor shell continued to burn for 70 minutes. Acceptor split into large fragments, unconsumed CW3 recovered.
Donor between two acceptor shell. Nose of donor set back 350mm behind noses of acceptors. Shell parallel and in contact. One acceptor fitted with transit plug. Other unplugged.	495s	CW3 in unplugged shell melted before event. Event in plugged shell opened up nose end. Donor and unplugged shell continued to burn. Unconsumed CW3 recovered from plugged shell.
Donor in line 100mm behind acceptor.	630s	Acceptor split lengthways, filling ejected forwards. Base of acceptor blown 100m backwards. Some unconsumed CW3 recovered. Donor knocked backwards but continued to burn.
As previous trial.	595s	As previous trial.



AD P000444

→ SPARROW (AIM/RIM-7M) WITH EX-114 MOD 1 WARHEAD

QUANTITY-DISTANCE STUDY FOR HANDLING OPERATIONS

DR. JERRY M. WARD AND RICHARD A. LORENZ

NAVAL SURFACE WEAPONS CENTER

EXPLOSION DYNAMICS BRANCH

WHITE OAK, SILVER SPRING, MARYLAND 20910

SPARROW (AIM/RIM-7M) WITH EX-114 MOD 1 WARHEAD
QUANTITY-DISTANCE STUDY FOR HANDLING OPERATIONS

SUMMARY

A quantity-distance study was performed for the SPARROW guided missile AIM/RIM-7M with the EX-114 MOD 1 warhead in pierside and shipboard transport/handling configurations.

The results of this study indicate that warhead-to-warhead propagation of detonation is expected in all the transport/handling configurations considered. As long as the SPARROW missiles are within 4.3 m (14 ft) of each other as determined from geometric considerations the warheads must be assumed to mass detonate.

The rocket motor propellant should not detonate, but could violently react if impacted by a high speed preformed fragment from an adjacent donor warhead. Under some accident scenarios, a violently reacting rocket motor may cause the forward warhead explosive to sympathetically detonate from rocket motor debris impact.

The maximum credible events and associated airblast hazard ranges for the transport/handling configurations considered are listed below.

Maximum Credible Events and Airblast Hazard Ranges

<u>Configuration</u>	<u>Contribution</u>	<u>Airblast Hazard Range, m (ft)</u>
Missile	1 Warhead	55 (180)
MK 470 MOD 0 Shipping Container	1 Warhead	55 (180)
MK 470 MOD 0 Stack of Three	3 Warheads	79 (260)
CNU-166/E Shipping Container	3 Warheads	79 (260)
CNU-166/E Stack of Three	9 Warheads	114 (375)
MK 29 MOD 0 Launcher	8 Warheads	105 (345)

Only detonations contribute to the airblast hazard range determinations. The fragment hazard ranges are governed solely by the preformed steel fragments from the warheads that detonate. The ranges for aluminum and polyvinyl chloride (PVC) fragments from shipping container and launcher surrounds are substantially less than those for the denser steel fragments, so that the aluminum and PVC fragments do not affect the fragment hazard range determinations.

The preformed fragments do not present an unacceptable hazard beyond 152 m (500 ft) for an eleven warhead mass detonation. However, for twelve or more warheads the hazard range extends well beyond the 152 m range out to the vicinity of the maximum fragment range because a large percentage (20%) of the fragments impact in this region.

The acceptable hazard handling arc that can be applied to all transport/handling configurations considered is 114 m (375 ft) as determined by the airblast hazard for nine warheads.

A total of twelve or more missiles within 4.3 m (14 ft) of each other are required to exceed the maximum acceptable hazard range of 152 m (500 ft).

Appendix A presents results of trajectory calculations performed for a generic preformed fragment warhead. These results illustrate the qualitative trends obtained for the classified SPARROW results.

INTRODUCTION

This task was part of the EX-114 warhead development program for the AIM/RIM-7M SPARROW to gain the Navy's Weapon Systems Explosives Safety Review Board (WSESRB) approval for service use of this version of the guided missile aboard Naval vessels.

The work request was in response to requirements that all programs for the development and introduction of new weaponry into the Fleet include analyses developed by the Naval Explosives Safety Improvement Program (NESIP) and/or verifying tests (as recommended by NESIP) to insure the timely availability of hazard information for review by the WSESRB. In particular, the Naval Surface Weapons Center was tasked (funded) by the SPARROW program to assess the sympathetic detonation characteristics and explosion hazard effects of the SPARROW weapon.

Methods developed for the NESIP Technology Base¹ were used to obtain the analytical results presented in this report.

The hazard definition of interest here is the acceptable hazard handling arc. The acceptable arc for an explosion event is determined by the minimum range at which both blast overpressure and fragment hazard criteria are satisfied. These criteria are:

(1) The blast overpressure must be less than 6.9 kPa (1 psi).

(2) The hazardous fragment flux evaluated for the ground surface area must be less than 1 hazardous fragment per 56 m² (600 ft²). A fragment is considered hazardous when it has an impact energy of 80 Joules (58 ft-lb) or greater. Note that the fragment hazard criterion specifies an acceptable areal density for hazardous fragments, not a maximum range for hazardous fragments. There can be hazardous fragments beyond the acceptable hazard handling arc; however, their areal density should be less than the level specified above.

OBJECTIVES

1. Determine the likelihood of sympathetic detonation and hence the maximum credible event (MCE) for the SPARROW weapon system for the pier and ship configurations.

2. Determine the acceptable hazard range (blast and fragment effects) for the MCE's.

3. If necessary, recommend possible handling procedure changes and/or inhibitor/shield designs (feasible solutions) for reducing the MCE's so that the acceptable hazard handling arc falls below the desired value of 152 m (500 ft).

¹Porzel, Francis B., "Technology Base of the Navy Explosives Safety Improvement Program," Minutes of the Nineteenth Explosives Safety Seminar, Department of Defense Explosives Safety Board, Los Angeles, CA, Sep 1980.

APPROACH

Figure 1 provides a general procedural flow chart for the weapon system investigation. The major program elements are described below.

- I. Review and evaluate the weapon input data.
- II. Determine the blast/fragment contributions of the propellant sections to the explosive effects generated by the donor warhead detonation.
- III. Determine the acceptable hazard range (blast/fragment effects) for a donor warhead detonation (which may or may not include a contribution from the propellant) for the numbers of configurations (assuming mass detonation of ordnance.) This represents the worst possible accident scenario.
- IV. Review the handling procedures for the weapon for all required transport/handling configurations.
- V. Determine the relative positioning of the weapon units for all required transport/handling configurations. Evaluate the potential for sympathetic detonation and determine the MCE's for these configurations.
- VI. Determine the acceptable hazard range (blast/fragment effects) for the MCE's for the various transport/handling configurations.
- VII. Contingent - Conduct sympathetic detonation tests according to the answer (and associated confidence) obtained from elements V and VI above. Tests may be needed to verify/clarify the analytical results obtained. Whether or not the propellant sections would be needed for these tests would be determined by the evaluation represented by element II above.
- VIII. Contingent - Investigate and recommend handling procedure changes and/or inhibitor/shield designs (feasible solutions not final engineered designs) to reduce the MCE and associated blast/fragment effects. This investigation is necessary only if the acceptable hazard range is greater than 152 m (500 ft).
- IX. Contingent - Conduct inhibitor/shield tests. These tests may be required to verify the design concept from element VIII.
- X. Perform a final analysis and provide a letter report documenting results, conclusions, and recommendations.

For the SPARROW quantity-distance study (referring to Figure 1):

- (a) The propellant was evaluated to not sympathetically detonate. Therefore, propellant effects were not required for element III.
- (b) There was sufficient confidence in the analytical evaluations of sympathetic detonation for the normal handling configurations that testing was not conducted (element VII) at this time.
- (c) The hazard ranges do not exceed 152 m (500 ft) for the missile configurations analyzed. Therefore, contingent shield/inhibitor designs and tests were not required (elements VII and IX).

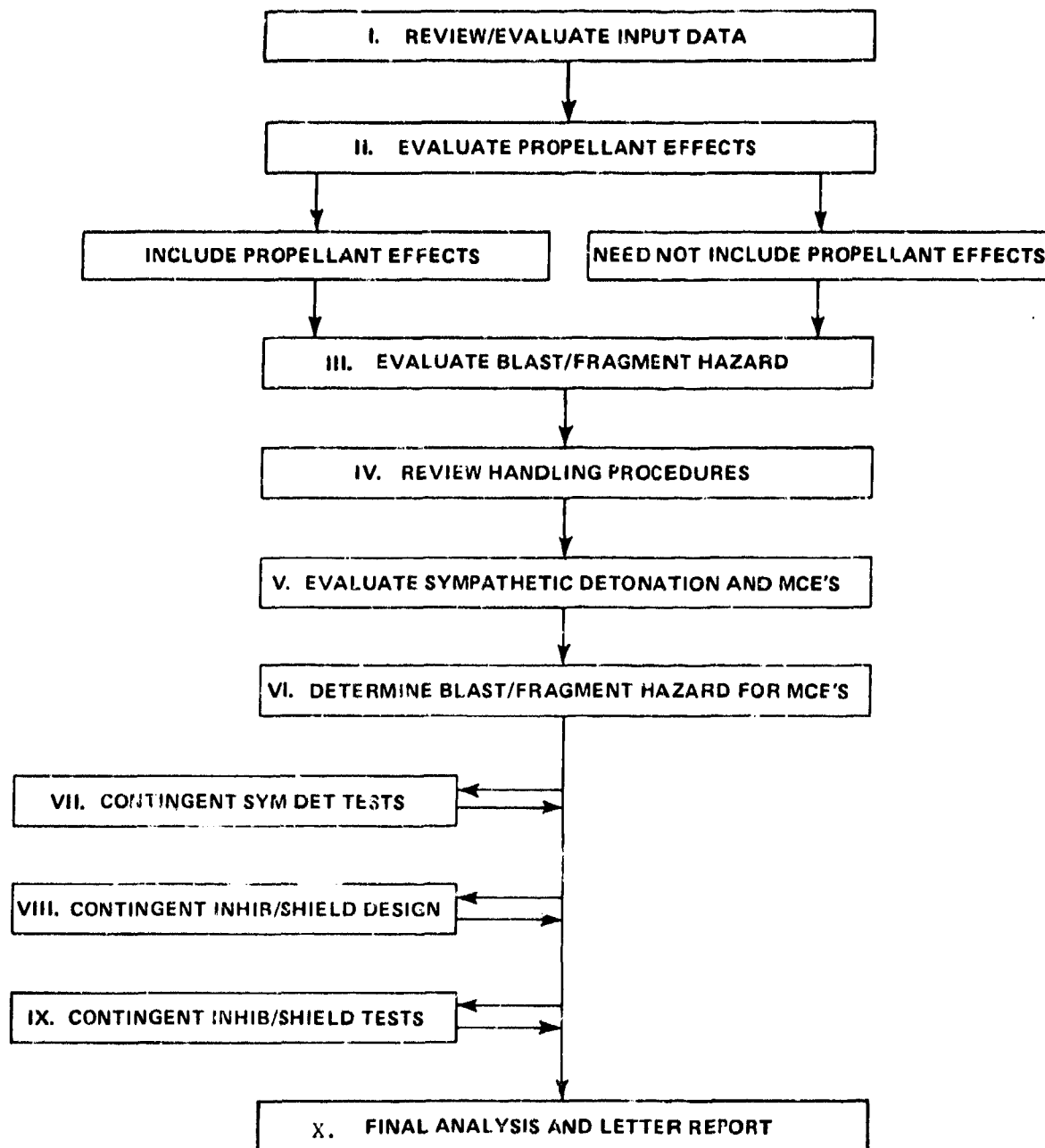


FIGURE 1. FLOW CHART FOR A GENERAL WEAPON SYSTEM QUANTITY-DISTANCE STUDY

MISSILE SYSTEM DESCRIPTION

The specific SPARROW weapon evaluated in this study is the AIM/RIM-7M (air-to-air/surface-to-air) with the EX-114 MOD 1 focused fragmentation controlled pattern (FFCP) warhead.* The missile is shown schematically in Figure 2.

The AIM-7M SPARROW will be transported in a CNU-166/E missile container (see Figure 3) that stores three missiles.

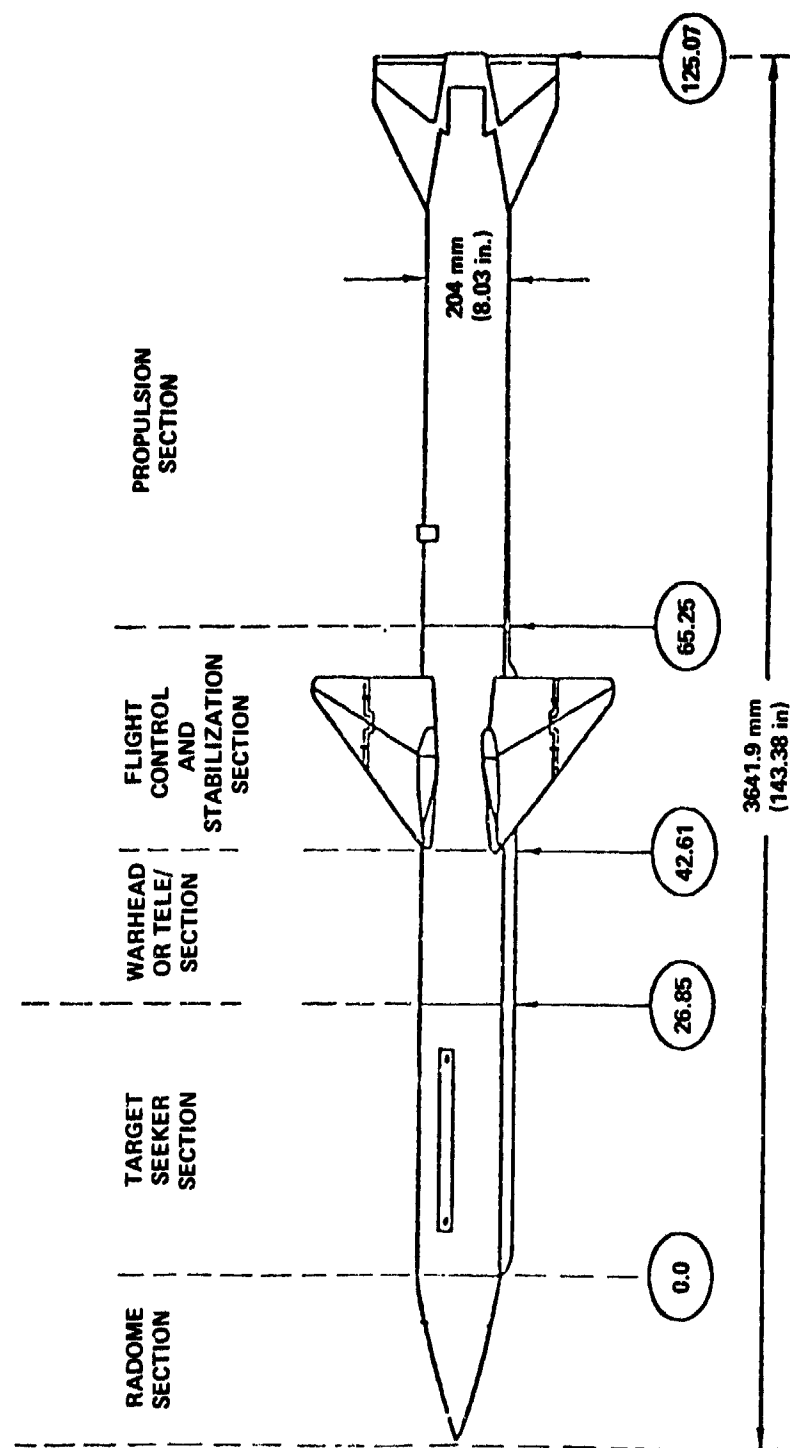
The RIM-7M SEASPARROW will be transported in a MK 470 MOD 0 missile container that houses one missile (see Figure 4). The RIM-7M SEASPARROW will be all-up loaded in the MK 29 Mod 0 box launcher for the Improved Point Defense System aboard ship. The launcher, shown in Figure 5, contains eight missiles. Three of these box launchers are to be mounted on aircraft carriers (CV and CVN) providing a total topside load of 24 all-up missiles. Between 24 and 48 missiles will be stored below deck in magazines. Other launch platforms under consideration include destroyers (DD) and support ships (AOE and AOR.)

Configurations of candidate Vertical Launch Systems (VLS) for the RIM-7M SEASPARROW are not addressed here. An analysis of all of the various candidate launcher designs is beyond the scope of this study.

Aircraft armament arrangements for the SPARROW were not addressed because these configurations would not be encountered in a tidewater port environment (the handling area of concern for this study.)

Specific unclassified missile data required for the quantity-distance study are listed in Table 1. The sound speed values for the explosive/propellants given in Table 1 represent estimates based on similar explosives/propellants at the same density.

*The term "preformed" is used in this paper to refer to the EX-114 MOD 1 warhead case fragments. The term is used in a general sense to describe fragments formed from scored warhead cases (producing explosively-formed fragments) and to describe the truly preformed fragments that are first (pre) formed and then embedded in the warhead case material.



NOTE: STATION LOCATIONS IN INCHES

FIGURE 2. SPARROW (AIM/RIM-7M) WITH EX-114 MOD 1 WARHEAD

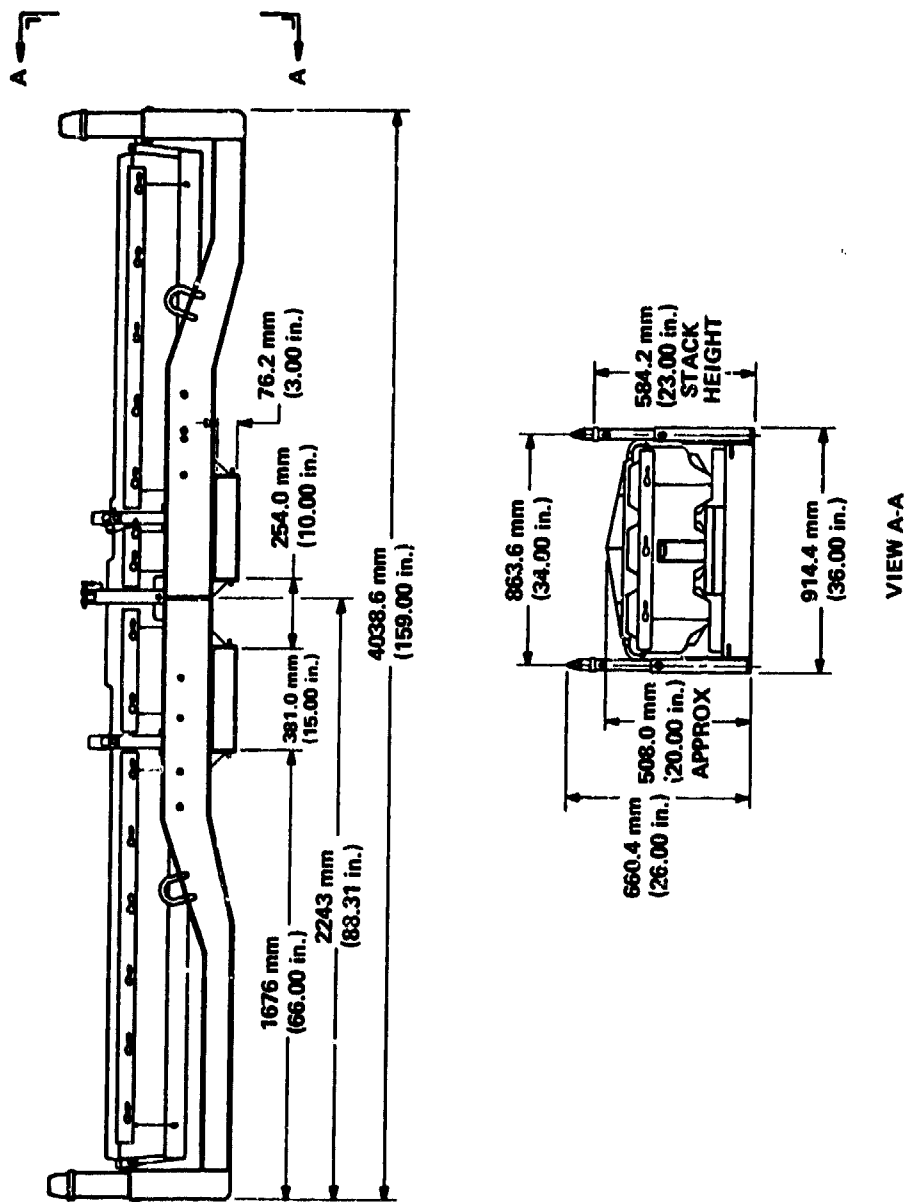


FIGURE 3. CNU-166/E MISSILE CONTAINER

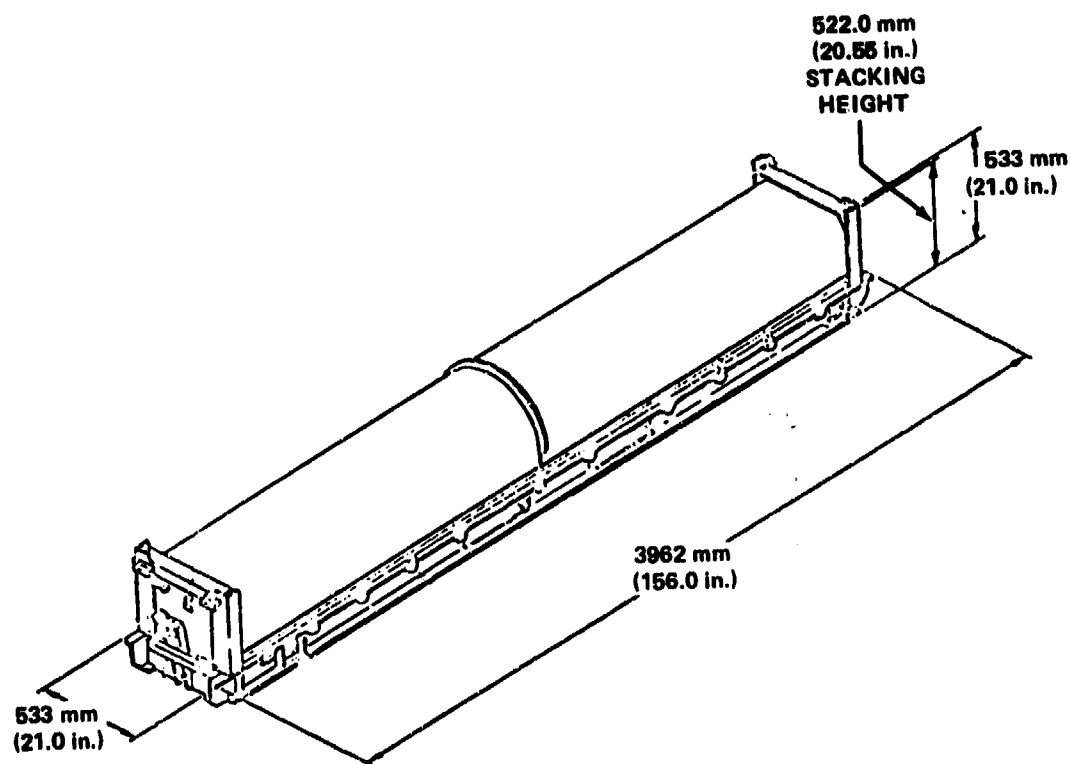


FIGURE 4. MK 470 MOD 0 CONTAINER, SHIPPING AND STORAGE

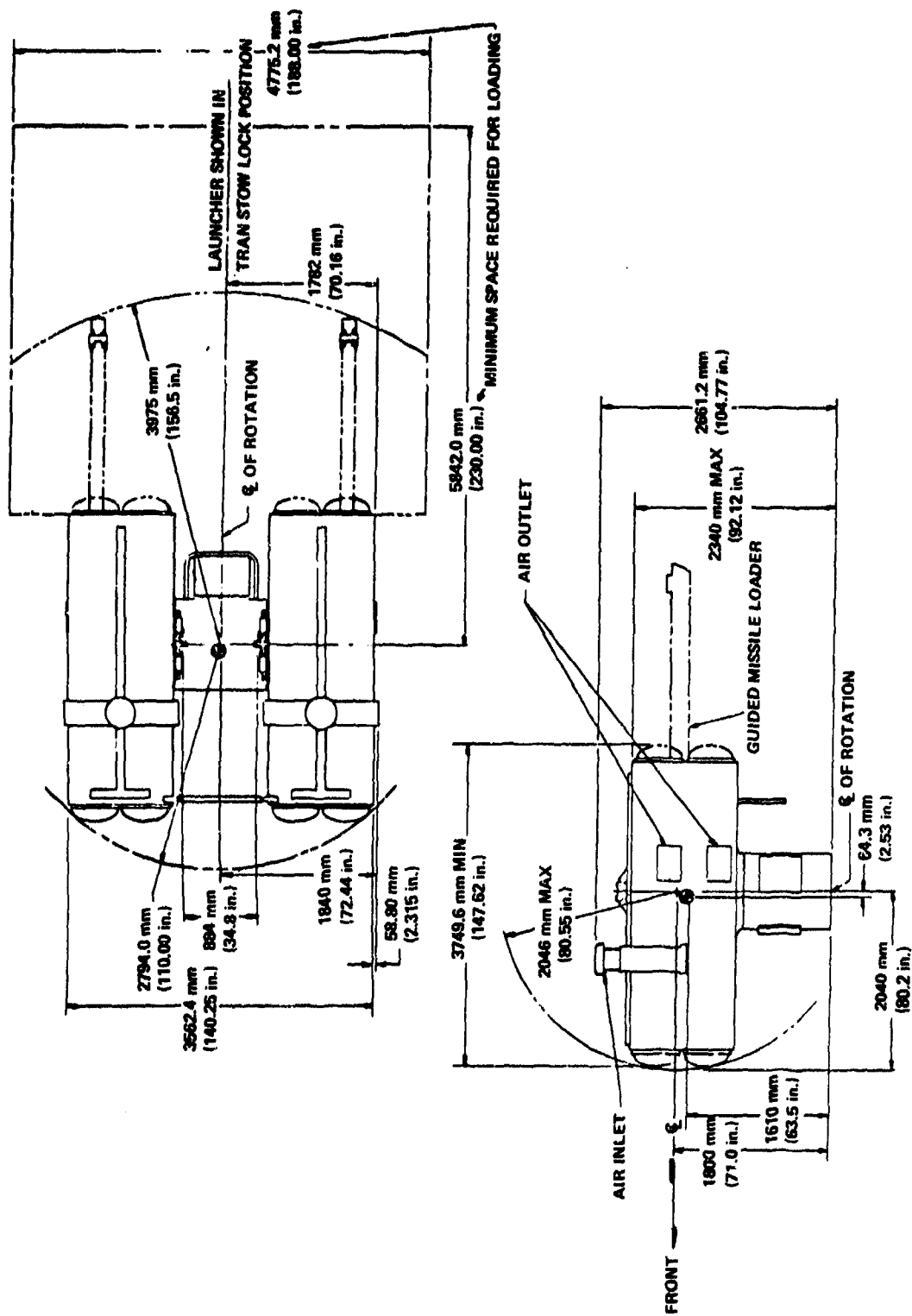


FIGURE 5. MK 29 MOD 0 MISSILE LAUNCHER

TABLE 1 AIM/RIM-7M SPARROW WITH THE EX-114 MOD 1 WARHEAD DATA

Warhead Section

Explosive Sound Speed (estimate), m/s (ft/s)	3000 (9800)
Total Warhead Mass, kg (lb)	38.6 (85.2)
Length, mm (in)	400.3 (15.76)
Diameter, mm (in)	204 (8.03)

Flight Control and Stabilization Section

Mass, kg (lb)	32.4 (71.4)
Length, mm (in)	575.3 (22.65)

Propulsion Section

Booster/Sustainer Propellants Sound Speed (estimate), m/s (ft/s)	3000 (9800)
Total Propulsion Section Mass, kg (lb)	95.7 (211)

CNU-166/E Shipping Container

Cover Material	Acrylic-Polyvinyl Chloride
Density, kg/m ³ (lb/in ³)	1260 (0.0455)
Thickness, mm (in)	6.35 (0.250)
Steel Rail Thickness, mm (in)	4.75 (0.187)
Alum. Clamp Double Thickness, mm (in)	6.35 (0.250)

MK 470 MOD 0 Shipping Container

Aluminum Thickness, mm (in)	2.5 (0.10)
-----------------------------	------------

MK 29 MOD 0 Launcher

Material	Aluminum laminate
inner wall thickness, mm (in)	1.0 (0.040)
outer wall thickness, mm (in)	1.0 (0.040)
inside corrugation thickness, mm (in)	0.81 (0.032)
Averaged areal density, gm/mm ² (lb/in ²)	8.16×10^{-3} (0.0116).

SYMPATHETIC DETONATION EVALUATION

The general missile configurations considered in the sympathetic detonation evaluation are: (1) the three-missile CNU-166/E missile container, see Fig. 3; (2) the single-missile MK 470 MOD 0 missile container, see Fig. 4; and (3) the eight-missile MK 29 MOD 0 Launcher, see Fig. 5. Most of the pertinent material dimensions and specifications required for the sympathetic detonation evaluations are noted in the figures. Additional information is provided in Table 1.

The maximum propellant web dimension for the SPARROW rocket motor, MK 58, MOD 3/4 is much smaller than the critical diameter for sustained detonation.² For this reason the propellant is assessed to have a zero card gap value² for the NOL Large Scale Gap Test (see Ref. 3) which means that pressures on the order of 20 GPa (200 kbars) or greater are required to initiate detonation.³ A representative calculation for the configurations studied is presented in this chapter; however, the conclusion is that the rocket motor propellant should not sympathetically detonate in the handling/transport configuration as a result of a donor warhead explosive detonation. Tests were not deemed necessary to verify this condition.

Table 2 lists the donor/acceptor combinations considered and the pressure thresholds necessary to sympathetically detonate. Note the representative calculation for the warhead-to-rocket-motor propagation (entry one in Table 2).

Additional configurations could have been included in Table 2 to account for donor-warhead-to-acceptor-rocket-motor geometries that arise if the missiles were housed in the CNU-166/E shipping containers in alternating nose-to-tail orientations (which would not be done because of center-of-gravity considerations) or if the missiles in the MK 470 MOD 0 shipping containers were arranged in a similar nose-to-tail fashion. However, calculations indicate that the rocket motor propellants would not sympathetically detonate in these configurations from either blast induced or fragment induced loadings. The sustainer section of the rocket motor does line up with the warhead section for a nose-to-tail stacking arrangement. In this arrangement the rocket motor propellants would most likely react violently (but not detonate) as a result of the detonation of an adjacent warhead. With no experimental data in hand, it must be assumed (for safety analysis purposes) that a violently reacting sustainer rocket motor could sympathetically detonate (from impact loads from rocket motor debris) the corresponding warhead section (forward of the missile control section) and any adjacent warhead (aligned by nose-to-tail stacking).

The detonation threshold pressure listed in Table 2 for the acceptor warhead explosive is a conservative estimate because no measured values were available. An actual value for the detonation threshold can be obtained by running the NOL Card Gap Test on the material.

²Camp, Albert T., Brentland Corporation, Personal Communication, 3 July 1981.

³Price, Donna, Clairmont, Jr., A. R., and Erkman, J. O., "The NOL Large Scale Gap Test. III. Compilation of Unclassified Data and Supplementary Information for Interpretation of Results," NOLTR 74-80, 8 Mar 1974.

TABLE 2 Sympathetic Detonation Predictions for SPARROW (AIM/RIM-7M) with EX-114 MOD 1 Warhead

Configuration*	Acceptor	Separation Distance ** mm (in)	Detonation Threshold GPa (Kbars)	Overpressure in Acceptor		Sympathetic Detonation
				Shock Induced GPa (Kbars)	Fragment Induced GPa (Kbars)	
1. Single Weapon	R/M (Same weapon)	635 (25.0)	20 (200)	0.11 (1.1)	2 (20)	No
2. CNU-166/E	W/H Adjacent	48 (1.9)	1.7 (17)	5.38 (53.8)	5.1 (51)	Yes
3. CNU-166/E	W/H Above S/C***	381 (15.0)	1.7 (17)	0.28 (2.8)	4.6 (46)	Yes
4. CNU-166/E	W/H Adjacent S/C	210 (8.1)	1.7 (17)	0.88 (8.8)	2.8 (28)	Yes
5. MK 470 MOD 0	W/H Above S/C	330 (13.0)	1.7 (17)	0.37 (3.7)	4.6 (46)	Yes
6. MK 470 MOD 0	W/H Adjacent S/C	330 (13.0)	1.7 (17)	0.37 (3.7)	4.6 (46)	Yes
7. MK 29 MOD 0	W/H Adjacent in same $\frac{1}{2}$ launcher	381 (15.0)	1.7 (17)	0.28 (2.8)	4.6 (46)	Yes
8. MK 29 MOD 0	W/H Adjacent in other $\frac{1}{2}$ launcher	1550 (61.0)	1.7 (17)	0.016 (0.16)	4.6 (46)	Yes

* Donor is the Warhead (W/H).

** Separation distance is measured from donor charge surface to acceptor charge surface.

*** S/C refers to Shipping Container.

A calculation of the total prompt energy released from the W/H explosive detonation is necessary for establishing a pressure distance curve. Reference 4 provides free-air airblast data for several explosives including the explosive used in the EX-114 MOD 1 warhead.

Shock induced pressures in the acceptor explosive/propellant were calculated in the following manner. The donor was assumed to be a spherical charge. UTE⁵ calculations provided normally reflected pressure estimates at the acceptor position.* Shielding effects of the intervening material were ignored, which results in the highest loads being calculated. Actually including the intervening materials as added mass surrounds in the UTE computations does not appreciably change the reflected pressures calculated. The reflected pressures computed at the charge-surface-to-charge-surface separation distance were assumed equal to the induced pressures in the acceptors and are listed in Table 2 under the heading of "Shock Induced."

Fragment induced pressures in the acceptor materials were computed in the following way. The maximum donor fragment velocity was used as the initial fragment velocity in the directions normal to the charge cylindrical surface. For the fragment velocity off the aft end of the warhead the following expression was used:

$$V_a = (E_a / M_a)^{1/2}$$

where V_a = initial fragment velocity in aft direction

E_a = energy flux in aft direction, about 10% warhead energy release

M_a = mass flux in aft direction, about 10% of the warhead mass plus the mass of the flight control section and the mass of the nose cap of the rocket motor.

The above expression is based on the assumption that energy is initially equi-partitioned between internal and kinetic energy. The energy flux was estimated by assuming that the relative energy directed through any part of the charge surface is proportional to that area.

The velocities determined above were then used in the following formula to estimate the pressure induced by the fragment impact in the acceptor material.

$$p = \rho c v / K_1$$

⁴Costain, Thomas S. and Motto, Rocco V., "The Sensitivity, Performance and Material Properties of Some High Explosive Formulations," Technical Report 4587, Picatinny Arsenal, Dover, New Jersey, Sep 1973.

⁵Porzel, Francis B., "Introduction to a Unified Theory on Explosions (UTE)," NOLTR 72-209, 14 Sep 1972.

*Program UTE was coded for the HP 41C programmable calculator.

where

p = pressure induced in acceptor, listed in Table 2 under the heading "Fragment Induced"

ρ = initial density of acceptor material

c = sound speed in acceptor material (see Table 1)

v = initial fragment velocity as determined above

k_1 = factor representing reduction in fragment velocity for configuration 1 in Table 2 due to conservation of momentum between donor fragments and material shielding acceptor explosive/propellant

The results in Table 2 indicate that an acceptor rocket motor propellant will not sympathetically detonate from either the shock or fragment loads produced by a donor warhead explosive detonation. However, if the missiles were stacked in a manner such that the warhead section of one missile were aligned with the rocket motor section of an adjacent missile, then higher fragment impact induced pressures (though less than the 20 GPa detonation threshold) could be generated in the rocket motor propellant than indicated for configuration 1 in Table 2. The assumption (for safety) is that the rocket motor propellant could violently react (though not sympathetically detonate) in response to these fragment impact induced loads. A second assumption (for safety) is that a violently reacting rocket motor could cause an adjacent (or the forward) warhead to sympathetically detonate from rocket motor debris impact loads. It should be pointed out that there are no data to support these (conservative) assumptions.

Acceptor warhead explosive should sympathetically detonate from fragment impact for all configurations investigated. For adjacent weapons inside the CNU-166/E shipping container (separation distance of 48 m (1.9 in)) the shock induced pressure is also sufficient to sympathetically detonate the acceptor warhead explosive.

Out to about 140 mm (5.5 in) separation distances shock pressures exceed the detonation threshold pressure of 1.7 GPa (17 kbars). The preformed SPARROW fragments can induce pressure in acceptor SPARROW explosives above the detonation threshold pressure out to ranges on the order of 440 m (1440 ft). However, at a range beyond 4.3 m (14 ft) the acceptor warhead section has only a 50 percent chance of being struck by a donor warhead preformed fragment when it is aligned in the beam spray.

MAXIMUM CREDIBLE EVENT

Single Missile - Configuration one in Table 2

The maximum credible event for the single missile is the donor warhead explosive detonation. The rocket motor propellant should not sympathetically detonate for any missile arrangement.

CNU-166/E Shipping Container - Configurations two, three, and four in Table 2

The maximum credible event for the loaded CNU-166/E shipping container that contains three missiles is the detonation of all three warhead explosives. The maximum credible event for a stack of CNU-166/E shipping containers, three containers per stack, is the detonation of all nine warhead explosives. Detonation should propagate between warheads in adjacent stacks of CNU-166/E containers if the warheads are aligned side-by-side.

MK 470 MOD 0 Shipping Container - Configurations five and six in Table 2

The maximum credible event for the loaded MK 470 MOD 0 shipping container that contains one missile is the detonation of the donor warhead explosive. The maximum credible event for a stack of MK 470 shipping containers, three containers per stack, is the detonation of all three warhead explosives. Detonations should propagate between warheads in adjacent stacks of MK 470 MOD 0 containers if the warheads are aligned side by side.

MK 29 MOD 0 Launcher - Configurations seven and eight in Table 2

The maximum credible event for the all-up MK 29 MOD 0 launcher that contains eight missiles is the detonation of all eight warhead explosives.

Nose-to-Tail Arrangement of Missiles in Shipping Containers

For both the CNU-166/E and the MK 470 MOD 0 shipping containers, a nose-to-tail arrangement of adjacent missiles lines up the warhead section with the sustainer rocket motor of the adjacent weapon. Even though the sustainer propellant should not sympathetically detonate (as indicated in Table 2), the propellant could violently react (see the discussion at the end of the previous section). The assumption (for safety) is that the violently reacting rocket motor propellant could sympathetically detonate forward and adjacent warhead explosives.

Optimum Stack Configuration for Shipping Containers

Detonation/violent-reaction propagation between warhead/rocket motor missile sections housed in adjacent stacks of CNU-166/E and MK 470 MOD 0 shipping containers can be eliminated, for the most part, by arranging the adjacent stacks such that the acceptor warhead/rocket motors do not lie within the beam spray of possible high speed preformed donor fragments from neighboring warheads.

AIRBLAST HAZARD PREDICTIONS

Airblast predictions for sea level conditions were calculated using the UTE model (References 1 and 5). The specific SPARROW configurations considered are defined in Table 3 along with the computed results.

Referring to Table 3, the airblast hazard range refers to the distance from the explosion source (ground zero) at which the blast overpressure has fallen to the 6.9 kPa (1.0 psi) level. The airblast calculations require specification of the explosive mass, TNT equivalent (airblast), and case mass. The case mass includes all mass in the immediate surround such as shipping container materials, and/or launcher structure. The configurations in Table 3 are discussed below.

1. One Missile - An all-up missile with no immediate surrounds such as shipping containers or launcher structure.
2. 22 Missiles - The maximum number of missiles in configuration one for which the airblast hazard criterion is satisfied at 152 m (500 ft).
3. CNU-166/E - Three missiles in the air launch missile shipping container.
4. CNU-166/E Stack - A stack of three air launch missile shipping containers that holds nine missiles total.
5. 7 CNU-166/E Containers - The maximum number of loaded CNU-166/E containers (configuration 3) for which the airblast criterion is satisfied at 152 m (500 ft).
6. MK 470 MOD 0 - One missile in the surface launch missile shipping container.
7. MK 470 MOD 0 Stack - A stack of three surface launch missile shipping containers that holds three missiles total.
8. 22 MK 470 MOD 0 Containers - The maximum number of missiles in configuration six for which the airblast hazard criterion is satisfied at 152 m (500 ft).
9. MK 29 MOD 0 Launcher - Eight missiles in the box launcher used on surface ships.

None of the configurations considered in Table 3 represent an airblast hazard at 152 m (500 ft). The detonation of 22 warhead explosives just satisfies the airblast criterion at 152 m (500 ft). The values for the airblast hazard range are reported in three significant figures only for the purposes of ranking. The computed values represent conservative (over) estimates of the actual hazard ranges.

TABLE 3 Airblast Hazard Predictions for Maximum Credible Explosions

<u>Configuration</u>	<u>Airblast Hazard Range</u>	
	<u>m (ft)</u>	
1. One Missile	53.9	(177)
2. 22 Missiles	151	(496)
3. CNU-166/E (3 missiles)	78.9	(259)
4. CNU-166/E Stack (9 missiles)	114	(374)
5. 7 CNU-166/E Containers (21 missiles)	151	(496)
6. MK 470 MOD 0 (1 missile)	54.3	(178)
7. MK 470 MOD 0 Stack (3 missiles)	78.3	(257)
8. 22 MK 470 MOD 0 Containers (22 missiles)	152	(499)
9. MK 29 MOD 0 Launcher (8 missiles)	104	(342)

FRAGMENT HAZARD PREDICTIONS

The preformed fragment (EX-114 MOD 1 warhead) trajectory predictions were computed using the computer program TRAJ.^{1*} The fragments formed from shipping container walls, launcher panels, or the rocket motor cases (contributed by violent reactions) are not significant hazards in comparison with the hazard associated with the preformed fragments. For this reason only the hazard results for the preformed fragments are presented here.

Preformed fragment initial conditions and computed trajectory results for a generic preformed fragment warhead are presented in Appendix A to illustrate the methods used and qualitative trends obtained for the classified SPARROW results.

The SPARROW preformed fragments do not present an unacceptable hazard beyond 152 m (500 ft) for a mass detonation of eleven warheads. However, for twelve weapons the hazardous fragment criterion is exceeded in the vicinity of the preformed fragment maximum range -- well beyond 152 m (500 ft) -- because a large percentage of the fragments impact in this region.

The computed trajectory results, therefore, indicate that the maximum number of SPARROW weapons (with the EX-114 MOD 1 warhead) handled shipboard or pierside at the tidewater ports should be restricted to eleven. For more than eleven warheads the fragment hazard criterion is exceeded beyond 152 m (500 ft) for a mass detonation of the warheads.

The above fragment hazard results do not include the following effects for the reasons stated:

1. Higher velocity fragments formed in the interaction zone between sympathetically detonating weapons -- this effect should only apply to adjacent weapons inside a CNU-166/E shipping container. The warheads should have too large a separation distance to form an interaction jet for the other configurations. However, an enhancement of the preformed fragment velocity by a factor of 1.5 (a typical value for sympathetic detonations) only increases the maximum trajectory range by about 10%, a negligible amount considering the uncertainties in input conditions.

2. Lower preformed fragment velocities produced by the added mass in the immediate surround of the warhead case; such as shipping container cases and launcher panels -- this effect reduces the initial fragment velocity (from momentum conservation considerations) by about 5% in general. The initial fragment velocity is not defined that precisely, so this effect is not considered. There is one exception to the 5% velocity reduction: preformed fragments that are adjacent to the aluminum clamps on the CNU-166/E shipping container have their velocity reduced by about 32%. This produces a 9% reduction in the maximum trajectory range and affects only about 4% of the fragments for the CNU-166/E shipping container configuration (three warheads). This effect on the fragment hazard range is negligible. Results presented in Appendix A indicate that variations of fragment drag coefficients and drag area have a much more pronounced effect on fragment impact range than does a similar variation of the initial fragment velocity.

* Program TRAJ was coded for the HP 41C programmable calculator. A FORTRAN version is coded for the CDC 6500.

3. Concentration of preformed fragments in a narrow beam spray directed towards vertical targets, not ground surface targets (on which the fragment hazard criterion is based) -- for the narrow beam spray region, the hazard range for vertical targets (greater than one hazardous fragment per 56 m^2) extends out to 323 m (1060 ft) for eleven warheads. Because the fragment hazard criterion applies only to prone personnel (horizontal target areas not vertical) the vertical target hazard is not addressed in this investigation. The effect of the concentration of fragments in the narrow beam spray is considered in the evaluation of the areal density of hazardous fragments impacting the ground surface.

It should be pointed out that the computed fragment areal density variation with range near the maximum fragment impact range is a function of the range increment size selected. This is because of the singularity in the trajectory solution at the maximum impact range. The results quoted for the SPARROW warhead are based on 30 m (100 ft) range increments that is well within uncertainty limits of the impact range for the preformed fragments. Twenty percent of the SPARROW preformed fragments fall within this range increment near the maximum range. Also, it should be mentioned that the computed fragment areal density results are based on cylindrical divergence (with a beam spray angle) and not spherical divergence because of the cylindrical design for the SPARROW warhead.

FINAL COMMENTS

The results and conclusions presented in the SUMMARY section will not be repeated here. However, a number of observations were made during the analysis that should be summarized. These are presented in the following paragraphs.

Three classes of configurations for the SPARROW were not addressed here: 1) vertical launch systems, 2) aircraft armaments, and 3) ship magazines. Including these configurations was beyond the scope of this study.

The fragment hazard criterion is exceeded (for a twelve warhead mass detonation) in the vicinity of the maximum range for the preformed fragments. This distance is many times greater than the 152 m (500 ft) range. The fragment areal density on the ground surface is greater in the region of the maximum fragment range bounded by the geometry of the beam spray than in any other ground location surrounding the warhead beyond the immediate ground zero location.

Substantially different (increased) fragment hazard ranges would be established if the hazard criterion were based on standing (vertical) personnel rather than prone (horizontal) personnel. The main problem with applying the criterion to prone personnel is that the prone position presupposes a warning when in fact the first signals to reach the personnel are high-speed lethal fragments.

The detonation threshold values for the EX-114 MOD 1 warhead explosive were obtained from card gap data for similar explosives by analogy. An actual card gap value should be determined for this explosive.

One mechanism for propagation of detonation between warheads is worth investigating further: Will a violent reaction response of the solid rocket propellant sympathetically detonate the forward warhead explosive? For the purposes of this study, the assumption was made that a violently reacting rocket motor could sympathetically detonate a forward or adjacent warhead. If this assumption were proven to be false, then nose-to-tail stacking of missiles could eliminate detonation propagation between adjacent warheads.

The enhancement of preformed fragment impacts in the vicinity of the maximum fragment impact range should be investigated experimentally. The computed results for SPARROW and for the generic warhead discussed in the appendix are based on the assumption that all the preformed fragments have the same mass, shape, and aerodynamic properties. These calculations tend to overestimate the fragment hazard produced by warheads of the preformed warhead design.

APPENDIX A

GENERIC PREFORMED FRAGMENT TRAJECTORY CALCULATIONS

Computer program TRAJ was used to compute the trajectories of fragments for a generic preformed fragment warhead. This generic warhead design was defined to illustrate the methods used and the qualitative trends obtained for the classified SPARROW results. Except for the fact that both the SPARROW and the generic warheads are of the "preformed fragment" design, there are no other similarities between them.

The trajectory calculations are used to establish the areal distribution of the preformed fragments as a function of range. The assumed fragment parameters for these calculations are given in Table A-1.

For the trajectory calculations, the fragments were uniformly distributed circumferentially around the warhead with the longitudinal axis of the missile oriented parallel to the ground surface. The angles of elevation for the fragments were varied between 0° and 90° (only one quadrant and hence only 60 fragments needed to be considered because of symmetry) to obtain the spread of impact ranges out to the maximum fragment impact range of 1280 m (4200 ft). These results are given in Figure A-1. All fragments impacted at hazardous energies (greater than 80 J (58 ft-lb)).

The fragment areal densities were determined from the data presented in Figure A-1 by proportioning the fragments in 30.5 m (100 ft) range increments out to the maximum range for the 15° side spray sector. Because of cylindrical symmetry, the proportion of fragments impacting at a particular range increment is equal to

$$F_i = \frac{\Delta\theta_{L_i} + \Delta\theta_{H_i}}{90^\circ}$$

where F_i = Proportion of fragments in 90° quadrant impacting in range increment i ; for example 4% of the fragments have impact ranges between 850 m and 900 m (see Figure A-1).

$\Delta\theta_{L_i}$ = Spread of initial elevation angles for fragments impacting range increment i from low angle trajectories*

$\Delta\theta_{H_i}$ = Spread of initial elevation angles for fragments impacting range increment i from high angle trajectories*

*For impact ranges less than the maximum range, there are two trajectory solutions. The low and high designations are referenced relative to the initial elevation angle θ_{MAX} corresponding to the maximum range.

TABLE A-1 GENERIC PREFORMED FRAGMENT WARHEAD DATA

Nominal Preformed Fragment Dimensions:

Length,	mm (in)	51	(2.0)
Width,	mm (in)	25	(1.0)
Thickness,	mm (in)	13	(0.50)
Average $C_D \bar{A}/m$, mm^2/gm (in^2/lb)			5.0 (3.5)
Drag Coefficient, C_D			1.0
Average Area, \bar{A} mm^2 (in^2)			645 (1.0)
Mass, gm (lb)			130 (0.29)
Maximum Initial Fragment Velocity, m/s (ft/s)			1500 (5000)
Number of Preformed Fragments			240
Fragment Beam Spray Width, degrees			15

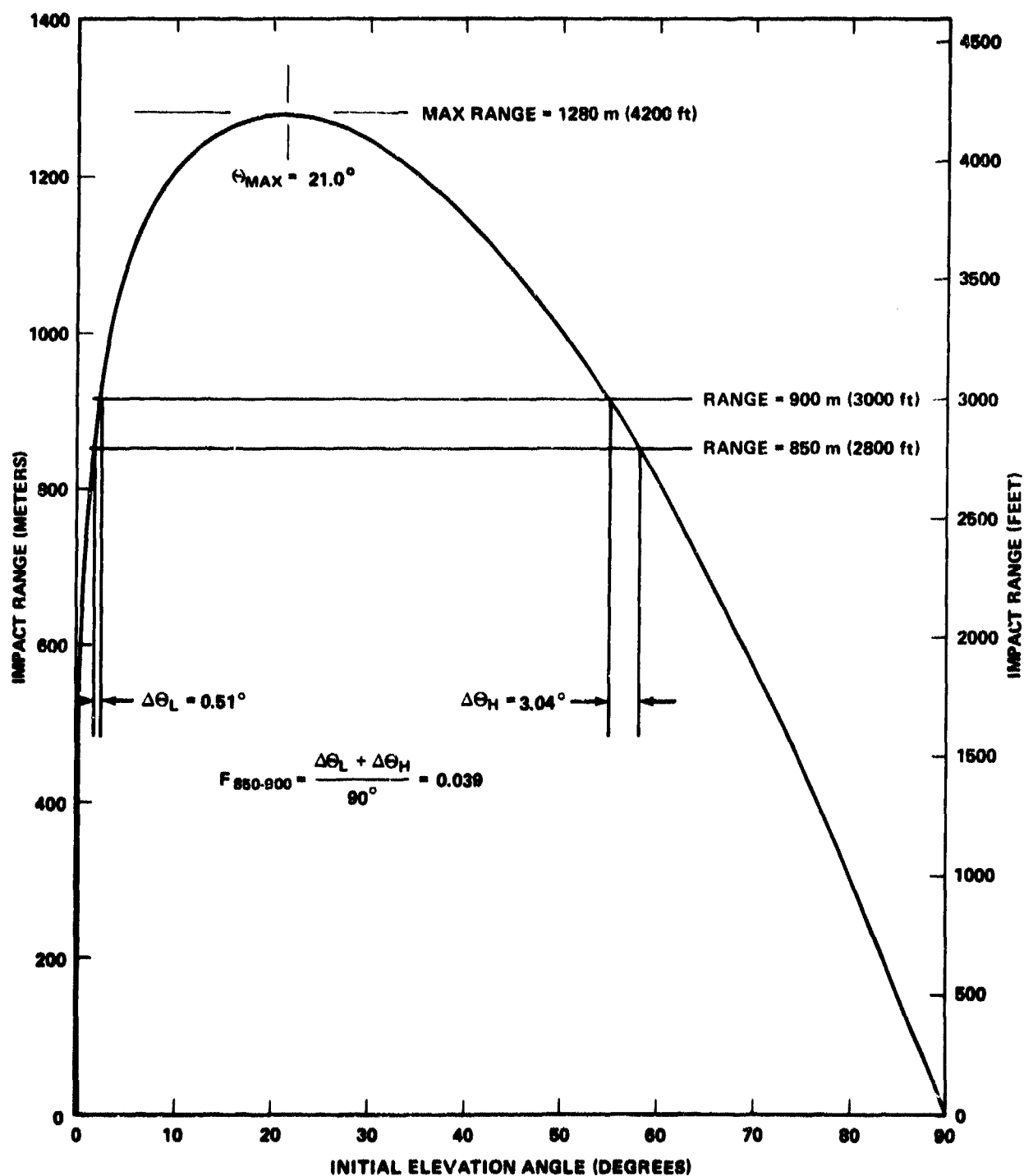


FIGURE A-1. GENERIC PREFORMED FRAGMENT IMPACT RANGE VERSUS INITIAL ELEVATION ANGLE

Table A-2 gives the range increments considered, the percentage of fragments impacting in each range increment, and the maximum numbers of mass detonating warheads allowed at ground zero such that the fragment hazard criterion is not exceeded; that is, such that there is less than one hazardous fragment which possesses 80 J (58 ft-lb) kinetic energy or greater impacting per 56 m² (600 ft²) ground surface area. Note in Table A-2 that 18% of the fragments impact within ~30 m (100 ft) of the maximum fragment impact range (1280 m (4200 ft)). For this reason, the range increment from 1250 m - 1280 m (4100 ft - 4200 ft) is the critical location for hazardous fragments -- 17 or more warheads produce sufficient fragments impacting at this range to exceed the fragment hazard criterion within the 15° beam spray. The next region that is hazardous for a minimum of 17 warheads is located less than 90 m (300 ft) from ground zero.

The percentage of fragment impacts within the (30.5 m) 100 ft increments (column 2 in Table A-2) are plotted in Figure A-2 to better display the enhancement of the fragment impacts in the vicinity of the maximum range.

A limited sensitivity analysis was performed with the trajectory calculations that gave the following results. The base calculation assumed $C_D = 1.0$, $\bar{A} = 645 \text{ mm}^2$, and $v = 1500 \text{ m/s}$.

(1) a $\pm 10\%$ variation in drag coefficient, $C_D = 1.1, 0.9$ gives a (-7.9%, + 9.6%) variation in maximum impact range.

(2) a $\pm 10\%$ variation in drag area* $\bar{A} = 710, 581 \text{ mm}^2$ gives a (-6.1%, + 11.8%) variation in maximum impact range.

(3) a $\pm 10\%$ variation in initial fragment velocity, $v = 1650, 1350 \text{ m/s}$ gives a (+2.5%, -2.7%) variation in maximum impact range.

The above results indicate that variations in fragment drag coefficients and/or drag areas (characteristic fragment lengths) have a more significant effect on the fragment impact ranges than do comparable variations in initial fragment velocities.

Note that the 30.5 m (100 ft) impact range increment used to define the fragment impact range distribution (Table A-2) is on the order of variation of the impact range for a 10% variation in initial fragment velocity.

*For the same shape fragment this corresponds to a (-7.0% + 13.6%) variation in characteristic fragment length. Note that the variation in impact range correlates more closely with changes in fragment length than with area.

TABLE A-2 GENERIC PREFORMED FRAGMENT IMPACT

RANGE DISTRIBUTION

<u>Range Increment *</u> (ft)	<u>% of Fragments to Impact Within Range Increment **</u>	<u>Maximum Number of Mass Detonating Warheads to Satisfy Fragment Hazard Criterion for Range Increment **</u>
0-100	1.1	3
100-200	1.1	10
200-300	1.1	17
300-400	1.1	23
400-500	1.1	29
500-600	1.1	35
600-700	1.2	41
700-800	1.2	47
800-900	1.2	52
900-1000	1.2	58
1000-1100	1.2	64
1100-1200	1.2	69
1200-1300	1.2	74
1300-1400	1.2	79
1400-1500	1.3	84
1500-1600	1.3	88
1600-1700	1.3	92
1700-1800	1.3	96
1800-1900	1.4	99
1900-2000	1.4	101
2000-2100	1.4	103
2100-2200	1.5	105
2200-2300	1.5	107
2300-2400	1.6	108
2400-2500	1.6	109
2500-2600	1.7	109
2600-2700	1.8	109
2700-2800	1.8	109
2800-2900	1.9	107

TABLE A-2 (CONT.)

<u>Range Increment*</u> (ft)	<u>% of Fragments to Impact</u> <u>Within Range Increment**</u>	<u>Maximum Number of</u> <u>Mass Detonating</u> <u>Warheads to Satisfy</u> <u>Fragment Hazard</u> <u>Criterion for Range</u> <u>Increment**</u>
2900-3000	2.0	106
3000-3100	2.1	103
3100-3200	2.3	100
3200-3300	2.5	96
3300-3400	2.6	92
3400-3500	2.9	87
3500-3600	3.2	82
3600-3700	3.5	76
3700-3800	4.0	69
3800-3900	4.6	60
3900-4000	5.5	52
4000-4100	7.4	39
4100-4200	18.4	16

* Computations were performed in English units (100 ft = 30.5 m).

** These results for 43 entries in the present table are interpolated using a four-point scheme from the results of 44 trajectory calculations.

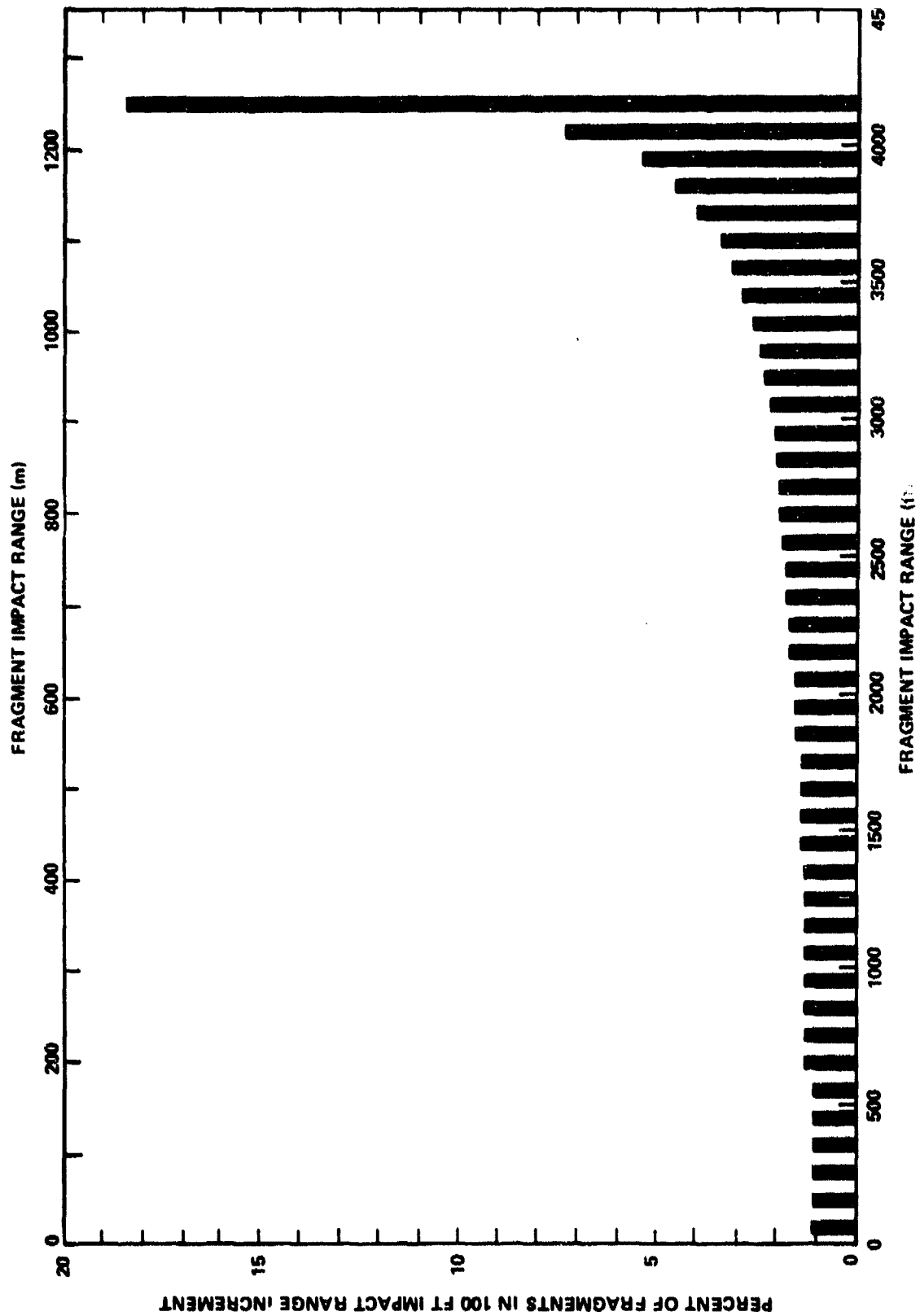


FIGURE A-2. PERCENT OF FRAGMENTS IMPACTING WITHIN 100 FT RANGE INCREMENT

AD P000445

BASIC TOW MISSILE (BGM-71A-1)
QUANTITY-DISTANCE HAZARD STUDY
FOR HANDLING OPERATIONS

RICHARD A. LORENZ AND DR. JERRY M. WARD

NAVAL SURFACE WEAPONS CENTER
EXPLOSION DYNAMICS BRANCH
WHITE OAK, SILVER SPRING, MARYLAND 20910

SUMMARY

A quantity-distance study was performed for the basic TOW guided missile BGM-72A-1 in pallet, weapon skid, and helicopter transport/handling configurations.

A sympathetic detonation test was conducted with the missiles in the pallet unit load (ADU-486/E pallet adapter) configuration to verify analytical predictions for detonation propagation. Flash x-ray tests were performed to verify estimates for the shaped charge slug mass, shape, and initial velocity. The tests supported the predictions. For differences that did occur between the test results and predictions, the predictions tended to be conservative -- that is, they over-estimated the hazard. Analyses of the test data indicate that propagation of detonation in the pallet configuration is highly unlikely. However, violent reactions did occur within the pallet but were limited to nearby missiles within a direct line of sight from the donor warhead.

Without shipping containers, all missiles are expected to detonate in the weapon skid configuration. Only a vertical pair of missiles in the four round modular launcher is expected to detonate in the helicopter configuration.

The maximum credible events and the associated hazard ranges for the transport/handling configurations considered are listed below.

Maximum Credible Event (MCE)

Configuration	Detonation Contribution	TNT Equivalent for Detonation, kg(lb)	Violent Reactions Contribution
Pallet	1 warhead plus flight motor	5.5 (12)	7 warheads plus 7 flight motors
Weapon Skid	16 warheads plus flight motor	55.2 (122)	15 flight motors
Helicopter	2 warheads plus flight motor	8.8 (19)	2 warheads plus 3 flight motors

Acceptable Hazard Range

Configuration	Airblast, m(ft)	Fragments, m(ft)
Pallet	37 (121)	71 (233)
Weapon Skid	77 (252)	87 (285)
Helicopter	42 (139)	58 (190)

Only detonations contribute to the airblast acceptable hazard range determination. The determination of the fragment acceptable hazard range also includes the effects of violent (non-detonating) reactions. As can be seen from the table above, the acceptable hazard handling arc that can be applied to all transport/handling configurations considered is 87 m (285 ft) as determined by the fragment hazard. Because no hazard ranges went beyond 152 m (500 ft), no inhibitor/shield design is needed.

There can be one unique hazardous fragment formed, the shaped charge slug, that can travel well beyond the fragment hazard ranges listed above. The slug, if it is formed, represents a significant hazard for the direction in which the missile is pointing. Controlling the orientation of the missile or using a massive shield appear to be the two basic methods available for reducing the slug hazard from a missile transported/handled in the all-up configuration. The jet associated with the shaped charge dissipates well within the acceptable hazard handling arc stated above. However, it should be pointed out that proper initiation of the shaped charge explosive is required for formation of the jet and slug. If the warhead explosive is not properly initiated near the detonator, it is highly unlikely that either the jet or the slug will be formed.

I. INTRODUCTION

This task was performed as part of TOW systems safety engineering support to satisfy the Weapon Systems Explosives Safety Review Board (WSESRB) approval for service use of TOW weapon equipped helicopters aboard Navy vessels.

Methods developed for the Naval Explosives Safety Improvement Program (NESIP) Technology Base were used to obtain the analytical results presented in this report. The methodology is described briefly in Reference 1.

Flash x-ray tests with a TOW missile warhead in shipping configuration (CNU-333/E) and with a bare warhead were conducted at the NSWC Montana Shelter Facility, Dahlgren Laboratory, to define the shaped charge slug parameters. A sympathetic detonation test for a unit load (ADU-486/E pallet adapter) of TOW missiles (quantity eight) with one donor and seven acceptors was conducted at the Naval Ordnance Missile Test Facility, DICE THROW Test Site, White Sands Missile Range, New Mexico to establish experimentally the airblast and fragment hazards associated with an accidental detonation in the pallet handling unit. These test results were required to verify and complement the analytical hazard predictions.

The hazard definition of interest here is the acceptable hazard handling arc. The acceptable arc for an explosion event is determined by the minimum range at which both blast overpressure and fragment hazard criteria are satisfied. These criteria are:

- (1) The blast overpressure must be less than 6.9 kPa (1 psi).
- (2) The hazardous fragment flux evaluated for the ground surface area must be less than 1 hazardous fragment per 56 m² (600 ft²). A fragment is considered hazardous when it has an impact energy of 80 Joules (58 ft-lb) or greater.

Note that the fragment hazard criterion specifies an acceptable areal density for hazardous fragments, not a maximum range for hazardous fragments. There can be hazardous fragments beyond the acceptable hazard handling arc; however, their areal density must be less than the level specified by (2) above.

An NSWC technical report that presents more detailed analytical and test results is to be published at a later date.

¹ Porzel, Francis B., "Technology Base of the Navy Explosives Safety Improvement Program," Minutes of the Nineteenth Explosives Safety Seminar, Department of Defense Explosives Safety Board, Los Angeles, CA, Sep 1980

II. BASIC TOW MISSILE DESCRIPTION

The basic TOW (Tube Launched Optical Tracked Wire Guided) Weapon (designated BGM-71A-1) is a guided missile propelled by solid propellant launch and flight motors that delivers a conical shaped charge warhead. The missile is shown deployed and in various transport configurations in Figures 1 through 6.

The mass breakdown for the missile and selected dimensions are given in Table 1. The explosive and propellant properties are given in Table 2.

III. SYMPATHETIC DETONATION

The configurations considered in this section are the palletized basic TOW missile in launch tube (Figures 1 and 2) and shipping container (Figure 3) as shown in Figure 4, the basic TOW missile in launch tube only as illustrated for the weapon skid in Figure 5, and the helicopter launcher in Figure 6. Tables 1 and 2 contain the pertinent values used in the calculations below. Only warhead (W/H) and flight motor (F/M) combinations were investigated because Reference 2 indicates that the W/H explosive and F/M propellant would sympathetically detonate each other,* and that the launch motor propellant would not sympathetically detonate for either a W/H explosive or a F/M propellant detonation. Table 3 lists the donor/acceptor combinations considered and the pressure thresholds necessary to detonate the acceptors. In the calculations below, the total prompt energy available from a W/H explosive detonation is taken to be 10.04 MJ and that from a F/M propellant detonation is 6.26 MJ.

Airblast Initiation Predictions

Blast induced pressures in the acceptor materials were calculated in the following manner. The donor was assumed to be a spherical charge. UTE (Ref. 3) calculations were made for the normally reflected pressures at the positions of the acceptors. Any shielding effects of the intervening materials were ignored, which results in the highest loads being calculated. It turns out for this particular TOW configuration that including the intervening materials as added mass surrounds about the donor does not appreciably change the reflected pressures calculated. The induced pressures were assumed to equal these reflected pressures in the acceptors and are listed in Table 3. All the blast induced pressures are significantly less than the detonation thresholds of the acceptors except for case 5 where the fragment induced pressure is even greater than the blast induced pressure. For these reasons no corrections were made to the UTE calculations to account for the cylindrical geometry of the charge or the effect of any shielding by intervening materials.

*The electronics section was not included in the Reference 2 tests. The present calculations do account for the electronics section.

²Lynch, C. L. and Tucker, W. L., "TOW Hazards Classification Tests," Report No. RT-TM-66-73, U.S. Army Missile Command, Redstone Arsenal, AL, 15 Sep 1966.

³Porzel, Francis B., "Introduction to a Unified Theory of Explosions (UTE)," NOLTR 72-209, 14 Sep 1972.

Fragment Initiation Predictions

Fragment induced pressures in the acceptor materials were calculated in the following manner. The donor was considered to be a cylindrical charge. Initially, the energy flux and mass motion of the donor are assumed to be directed normal to the charge surfaces. It was estimated for both W/H and F/M donors that approximately 60 percent of the mass and energy is directed radially outward from the sides and 20 percent is directed axially from each end face. Appropriate masses for materials located between donor/acceptor explosives and propellants were used in the velocity calculations. The more important mass values are given in Table 1.

The initial velocity of a fragment was calculated according to the formula:

$$v = \left[\left(\frac{1}{2} \right) \times \frac{2E}{M} \right]^{1/2}$$

where v = initial velocity of the fragment

E = donor energy propagating in the given direction

M = mass accelerated in the given direction

The additional factor of $1/2$ accounts for the initial partition of energy between kinetic and internal energy. The calculated velocity was used in the following equation to estimate the pressure induced by fragment impact in the acceptor material.

$$P = \rho cv/K$$

where P = pressure induced in acceptor

ρ = initial density of acceptor

c = sound speed in acceptor material

v = initial velocity of fragment as calculated above

K = factor representing reduction in fragment velocity due to conservation of momentum between fragment and shielding material

When the intervening mass increments (m_1) are accumulated and carried along with the original fragment mass (m_0), the K -factor is calculated as:

$$K = 1 + \sum m_1/m_0$$

where the summation includes all mass elements involved. When the intervening mass elements (m_1) are punched out and then separate from the original fragment mass (m_0) before striking the next plate, the K -factor is calculated as:

$$K = \prod (1 + m_1/m_0)$$

where the product function covers all appropriate mass elements. The first definition for the K-factor results in the highest calculated induced pressure in the acceptor material.

As summarized in Table 3, if the F/M propellant detonates, the associated W/H explosive should sympathetically detonate, but the adjacent F/M propellant should not. If the W/H explosive detonates, the associated F/M propellant should not sympathetically detonate but the adjacent W/H explosive may possibly sympathetically detonate. Since W/H to W/H sympathetic detonation is marginal, it can be expected in the pallet configuration that some adjacent warheads may sympathetically detonate, but that any propagation of detonations will rapidly die out. Note that even though the adjacent W/H may not detonate, the high induced pressures calculated indicate that the W/H explosive is very likely to experience an energetic reaction such as deflagration or rapid burning.

Sympathetic Detonation Test

A sympathetic detonation test was conducted by the Naval Ordnance Missile Test Facility personnel at the White Sands Missile Range, New Mexico. The objectives were to: (1) determine the maximum credible event (MCE) for the detonation of a single shaped charge W/H in a unit load pallet configuration (ADU-486/E) of eight all-up basic TOW missiles in CNU-333/E shipping and storage containers; (2) determine the airblast hazard range for the test configuration; and (3) determine the fragment hazard range for the test configuration.

Missile #2 in Figure 4 was the donor W/H. A high speed camera was set up to document the explosion event with a large field of view. A higher speed camera was aligned nose-on to record detonation propagation between missiles in the pallet. Two lines of pressure gages were set up to record the airblast generated by the event. Fragment recovery areas were set up out to 427 m (1400 ft) in 61 m (200 ft) radial by 20° angular sectors.

The test results pertaining to sympathetic detonation are discussed in the next paragraph. Results pertaining to the airblast and fragment hazards will be discussed in their respective sections.

Test Results

Post-test debris observations indicated that in addition to the donor W/H detonation, five acceptor warheads broke apart violently and five flight motors reacted violently. Six intact launch motors, one intact flight motor, and two intact TOW missiles (still in CNU-333/E containers) were located within the recovery area. The debris evidence, therefore, suggests that the maximum contribution to the MCE for this test would come from the explosive/propellant from six warheads and five flight motors (30 kg (67 lb) TNT)).

The donor missile is labeled #2 in Figure 4. Missiles #6 and #8 were recovered intact in their containers. This suggests the following propagation scheme. The donor missile #2 fragments cause missiles #1, #3, #4 and #5 to react. There is also a direct path for fragments between missiles #2 and #7. Missiles #6 and #8 were shielded from direct impact by fragments from missile #2. Therefore, missiles #6 and #8 did not react. If this propagation scheme is correct, then a corner donor such as missile #1 would cause acceptor missiles #2, #4, #5 and #6 to react. All seven acceptors, however, would react if either missile #4 or #5 were the donor.

The camera viewing the pallet nose-on, which could possibly have given photographic evidence of sympathetic detonation, did not operate during the test. However, the camera viewing the pallet side-on from a great distance with a large field of view did document that only one shaped charge jet/slug was formed, that of the donor warhead. This documentary film also showed that at least two rocket motors did go propulsive for a short period of time and that energetic reactions continued in the vicinity of ground zero for a considerably longer period of time.

The airblast data indicates that only the donor W/H explosive detonated. The violent reactions which were observed in the acceptor materials release a considerable amount of energy which can contribute to the fragment hazard, but which is too late to enhance the blast wave. Therefore, a warhead detonation is not expected to cause sympathetic detonation in the pallet configuration.

Conclusions

Pallet Configuration. The predictions summarized for cases 2 and 3 in Table 3 indicate that sympathetic detonation is marginal for the adjacent warheads. The pallet test which represented seven donor-acceptor detonation propagation tests showed that there was no sympathetic detonation, but that many violent reactions occurred. This agreement between predictions and test results allows us to rely on the predicted results, which are somewhat more severe, without having to test each of the other configurations.

The MCE for the pallet configuration shown in Figure 4 is the detonation of one flight motor and one warhead, with violent reactions occurring in the remaining warheads and flight motors.

Weapon Skid Configuration. Cases 5 and 6 in Table 3 indicate that the warheads will mass detonate if any one of them detonates. The detonation of a F/M will cause the detonation of a W/H (case 2), but will not cause the adjacent flight motors to detonate (case 6).

The MCE for the weapon skid configuration shown in Figure 5 is, therefore, the detonation of one flight motor and all warheads, with violent reactions occurring in the remaining flight motors.

Helicopter Configuration. Figure 6 shows that adjacent weapons in the vertical direction correspond to cases 5 and 6 in Table 3. There is sufficient launcher mass between horizontal neighbors that sympathetic detonation is not expected to occur.

The MCE for the four round helicopter configuration shown in Figure 6 is the detonation of one flight motor and two warheads, with violent reactions occurring for the remaining two warheads and three flight motors.

IV. AIRBLAST HAZARD

The airblast hazard range is defined as that distance from the point of detonation at which the side-on overpressure is equal to 6.9 kPa (1.0 psi).

Predictions

Airblast predictions for sea level conditions were calculated using the computer program UTEDMG (refs. 1 and 3). In the calculations, the total prompt energy available from a W/H explosive detonation is taken to be 10.04 MJ and that from a F/M propellant detonation is 6.26 MJ. The explosive/propellant masses and case/launcher/shipping-container masses surrounding the detonating materials were calculated using the data in Table 1. The predicted airblast hazard ranges for the MCE's defined in Section III are presented in the table in the Conclusions paragraph below.

Test Results

The airblast results from the sympathetic detonation test described in Section III indicate that the airblast hazard range is 25m (82 ft) for the pallet configuration. This is the result of a single W/H detonating. The predicted hazard range is larger because the MCE is the detonation of both a W/H and a F/M.

Conclusions

The airblast hazard ranges for the MCE's in the handling/transport configurations of interest are summarized below:

<u>TOW Configuration</u>	<u>Airblast Hazard Range</u>
Pallet	37 m (121 ft)
Weapon Skid (16 missiles)	77 m (252 ft)
Helicopter	42 m (139 ft)

The predicted maximum number of TOW weapons that can mass detonate and still not exceed the airblast hazard criterion at 152 m (500 ft) is 70 weapons.

V. FRAGMENT HAZARD

The fragment hazard range is defined as that distance from ground zero for which the hazardous fragment flux evaluated for the ground surface area falls below one hazardous fragment per 56 m² (600 ft²). A hazardous fragment has an impact energy greater than or equal to 80 Joules (58 ft-lb).

Predictions

In the present calculations, it was assumed that the energy from the violent reactions contributed to the fragment hazard as well as that from the detonations. The calculations indicate that the steel fragments from the F/M

case are more hazardous than the aluminum fragments from the W/H case. The predicted fragment hazard ranges for the MCE's defined in Section III are presented in the table in the Conclusions paragraph below.

The fragment predictions were calculated using the computer code FEN (ref. 1). The data in Table 1 were used to define the fragment characteristics for the calculations. The characteristic dimension of the aluminum fragments was taken to be equal to the thickness of the W/H case. That of the steel fragments was taken to be one half the thickness of the thicker F/M case. The larger the fragment dimension, the farther the fragments travel when all other trajectory parameters are equal. A drag coefficient of 1.28, corresponding to supersonic velocities, was used. A shape factor of 0.3, a typical value for irregularly shaped bomb fragments, was assumed. The shape factor (SF) is defined by the relationship: $\text{volume} = \text{SF} \times \text{frontal area} \times \text{length}$. The initial fragment velocity was taken to be equal to the velocity of the side spray fragments from the flash x-ray tests described in Section VI. The predicted fragment side spray velocity was quite close to the measured value.

Test Results

Thirty one large pieces of debris (fragments) were recovered from the pallet test described in Section III. only a cursory fragment recovery effort was performed in order to identify the major debris items. No comprehensive recovery of hazardous fragments was undertaken. However, based only on the recovered debris, the fragment hazard range for the test was evaluated to be 38 m (125 ft). Twelve of the recovered fragments landed farther than 38 m from ground zero, but their areal density did not exceed the hazard criterion.

Conclusions

The fragment hazard ranges for the MCE's in the handling/transport configuration of interest are summarized below:

<u>TOW Configuration</u>	<u>Number of Weapons</u>	<u>Fragment Hazard Range</u>
Pallet	8	71 m (233 ft)
Weapon Skid	16	87 m (285 ft)
Helicopter	4	58 m (190 ft)

The predictions indicate that the mass detonation of basic TOW weapons should not violate the defined fragment hazard criterion at 152 m (500 ft) until the number of weapons approaches the level of 185 weapons.

VI. JET/SLUG HAZARD

The basic TOW shaped charge W/H, if initiated properly, will produce a very high speed jet and a somewhat slower but more massive slug. Both the jet and the slug travel in the nose forward direction.

Proper initiation of the shaped charge explosive is required for formation of the jet and slug. If the W/H explosive is not initiated near the detonator, it is highly unlikely that either the jet or the slug will be formed. Detonation of the F/M propellant could possibly properly initiate its associated W/H. It is extremely unlikely that more than one jet/slug set would be formed in any given accident scenario.

Because of the sensitive nature of a number of the basic TOW warhead parameters, the results in this section are given in general, qualitative terms for this paper.

Predictions

An estimate was made of the propagation (penetration) in air of the TOW shaped charge jet using the expression below taken from Reference 4.

$$x_r = x_s - t \sqrt{\rho/\rho_s}$$

where x_r = Residual penetration in steel after penetrating a thickness t through a protective material of density ρ

x_s = Penetration in steel with no protective materials

t = Thickness of protective material

ρ = Density of protective material

ρ_s = Density of steel

By setting $x_r = 0$ the "thickness" t of air traversed by the jet can be solved for. This value of t will overestimate the distance travelled in air since the above equation does not take into account the breakup of the jet due to transverse instabilities over large distances of travel. Even so, the jet is predicted to dissipate well within the acceptable hazard range of 152 m (500 ft).

An estimate was made for the slug size and shape. Then a range of values was considered for the other trajectory parameters (initial velocity, angle, drag coefficient). The trajectory calculations were made using the computer program TRAJ (ref. 4). In the pallet configuration, where the slug started out horizontally three feet above the ground, it was predicted for all combinations of assumptions that the slug would travel well beyond the acceptable hazard range of 152 m (500 ft). If the missile were pointed upward at the optimum elevation angle between 20 and 25 degrees, then the slug could easily travel several miles before impacting the ground.

Flash X-ray Tests

Flash x-ray tests were performed by NSWC at the NSWC Montana Shelter Facility at Dahlgren, Virginia. The objectives were to: (1) determine the initial velocity, shape, and mass of the slug formed by the basic TOW shaped

⁴Pugh, Emerson M., "A Theory of Target Penetration of Jets," NDRC Report A-274 (OSRD-3752) May 1944.

charge; and (2) determine the initial velocity of the fragments ejected in the side spray of the W/H section.

Two TOW W/H configurations were tested. For Test 1 the W/H was housed inside the glass reinforced plastic launch tube and the aluminum shipping container. For Test 2 only the bare W/H section was set up.

The slug shape and velocity were determined from two x-ray pictures taken a known time interval apart. The slug mass was obtained from the shape on the x-ray film, assuming that the slug was a solid of revolution about its longitudinal axis. The initial velocities of the side spray fragments were determined using a high speed camera to obtain fragment times of arrival at a 22 gauge mild steel flash panel.

Test Results

A typical flash x-ray picture of the slug is shown in Figure 7. The slug shape and mass were quite close to the predicted values. The velocities of the slug and the side spray fragments were in the range considered for the predictions. The test results indirectly indicate that the shaped charge jet will travel substantially less than the predicted distance.

Conclusions

Because proper initiation of the shaped charge explosive is required for the formation of the jet and slug, it is unlikely that a fully formed jet and slug will be generated in an accidental detonation. It is extremely unlikely that more than one jet/slug set would be formed.

The jet is expected to dissipate well within the acceptable hazard range of 152 m (500 ft).

A slug, even partially formed, represents a significant hazard in the direction that the missile is aligned at the time of the accident. The slug could travel several miles before impacting the ground. Controlling the orientation of the missile or using a massive shield appear to be the two basic methods available for reducing the slug hazard from a missile transported/handled in the all-up configuration.

TABLE 1 MASS AND DIMENSIONS FOR BASIC TOW

TOW Missile

Warhead Section

Explosive Mass, kg (lb)	2.4 (5.3)
Total Mass, kg (lb)	3.9 (8.6)
Aluminum Case Thickness, mm (in).	1.3 (0.050)

Electronics Section

Total Mass, kg (lb)	1.61 (3.54)
-------------------------------	-------------

Flight Motor Section

Propellant Mass, kg (lb).	2.59 (5.72)
Total Mass, kg (lb)	5.65 (12.45)
Steel Case Thickness, mm (in)	3.2 (0.13)

Center (Guidance) Section

Total Mass, kg (lb)	2.44 (5.37)
-------------------------------	-------------

Launch Motor Section

Total Mass, kg (lb)	5.48 (12.08)
-------------------------------	--------------

TOW Total Mass, kg (lb).	19 (42)
----------------------------------	---------

Launch Tube

Glass Reinforced Plastic Mass, kg (lb)	2.0 (4.5)
Total Mass, kg (lb).	6.8 (15)
Thickness, mm (in)	1.9 (0.075)
Density, g/cm ³ (lb/in ³).	1.87 (0.0676)

Shipping Container

Aluminum Tube Mass, kg (lb).	4.63 (10.2)
End Cap Mass, kg (lb).	4.94 (10.9)
Total Mass, kg (lb).	14.5 (32)
Tube Case Thickness, mm (in)	1.6 (0.064)

Polyethylene Foam Cushion

Total Mass, kg (lb).	1.4 (3.0)
Radial Thickness, mm (in).	27.2 (1.07)
Density, g/cm ³ , (lb/ft ³)	0.032 (2.0)

TABLE 2 EXPLOSIVE AND PROPELLANT PROPERTIES

Warhead Explosive: OCTOL Type I - 75/25 (HMX/TNT)

Density, g/cm ³ (lb/in ³)	1.81 (0.0655)
TNT Equivalent.	1.38
Large Scale Card Gap Test	220 Cards
	1.64 GPa (16.4 kbars)
Sound Speed, m/s (ft/s)	2400 (7890)

Flight Motor Propellant: PNJ Double Base Propellant

Density, g/cm ³ (lb/in ³)	1.58 (0.057)
TNT Equivalent (Estimated).	0.8
Card Gap Test	55 Cards
	7.7 GPa (77 kbars)
Sound Speed, m/s (ft/s)	1580 (5180)

Launch Motor Propellant: M7 Double Base Propellant

Density, g/cm ³ (lb/in ³)	1.63 (0.059)
Card Gap Test	65 Cards
	3.5 GPa (35 kbars)
Sound Speed, m/s (ft/s)	1630 (5348)

TABLE 3

SYMPATHETIC DETONATION PREDICTIONS FOR PALLETIZED BASIC TOW

Case	Donor	Acceptor	Detonation Threshold GPa (kbar)	Overpressure in Acceptor		Sympathetic Detonation
				Blast Induced GPa(kbar)	Fragment Induced GPa(kbar)	
<u>Same Weapon</u>						
1	W/H	F/M	7.7 (77)	0.53 (5.3)	2.0 (20)	No
2	F/M	W/H	1.6 (16)	0.36 (3.6)	2.8 (28)	YES
<u>Neighboring Weapons, With Shipping Containers</u>						
3	W/H	W/H	1.6 (16)	0.37 (3.7)	1.6 (16)	Marginal
4	F/M	F/M	7.7 (77)	0.25 (2.5)	1.2 (12)	No
<u>Neighboring Weapons, Without Shipping Containers</u>						
5	W/H	W/H	1.6 (16)	1.5 (15)	2.5 (25)	YES
6	F/M	F/M	7.7 (77)	1.5 (15)	1.3 (13)	No

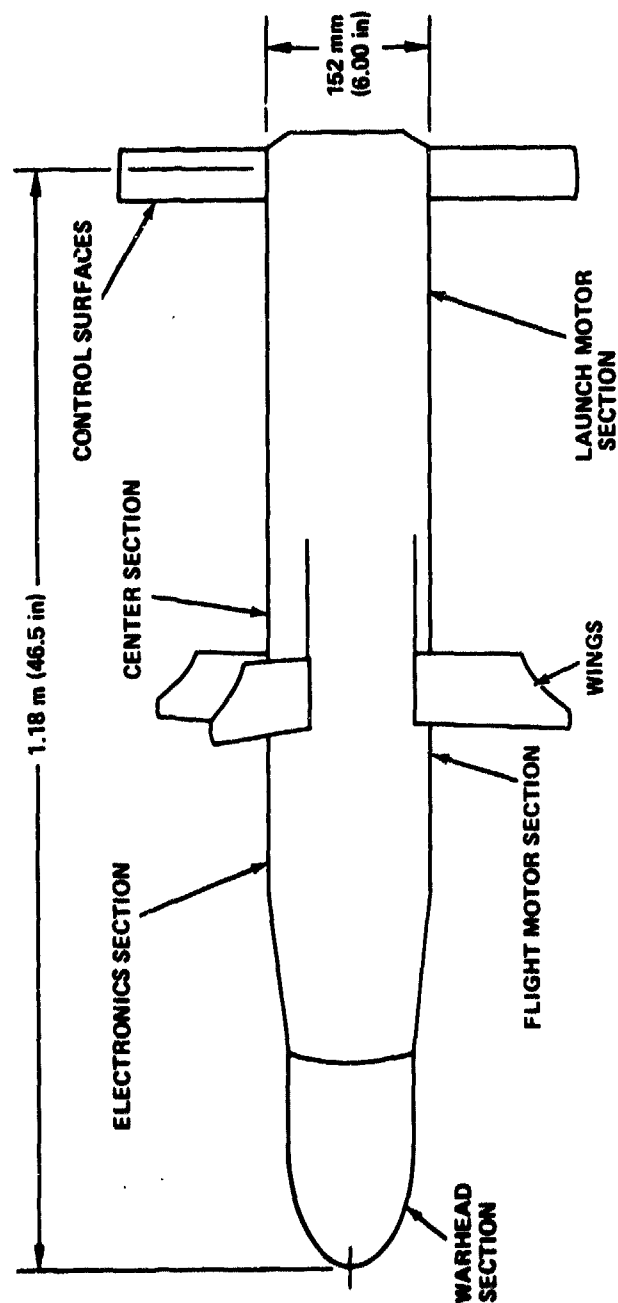


FIGURE 1. BGM-71A-1 TOW GUIDED MISSILE SURFACE ATTACK WEAPON COMPONENTS

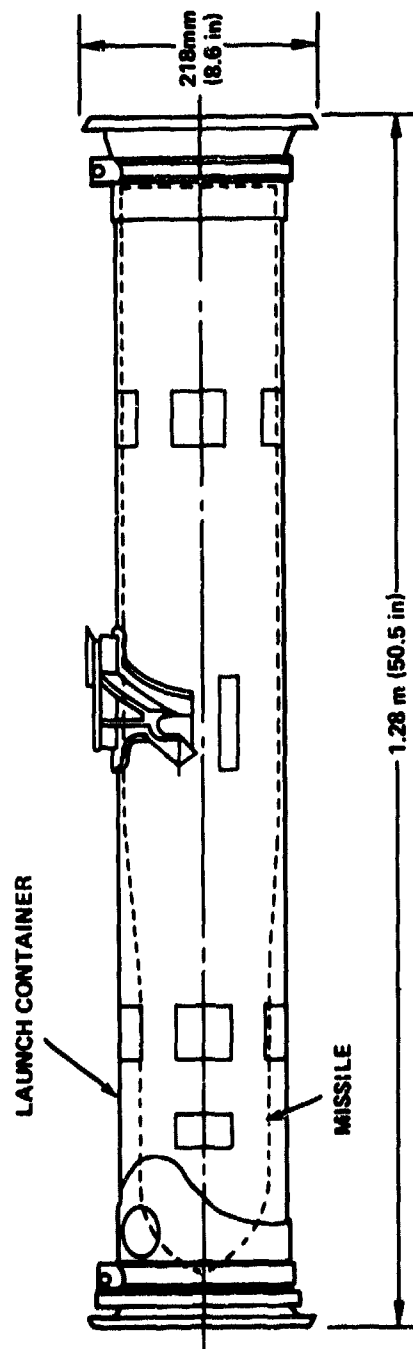


FIGURE 2. BGM-71A-1 TOW GUIDED MISSILE LAUNCH CONTAINER

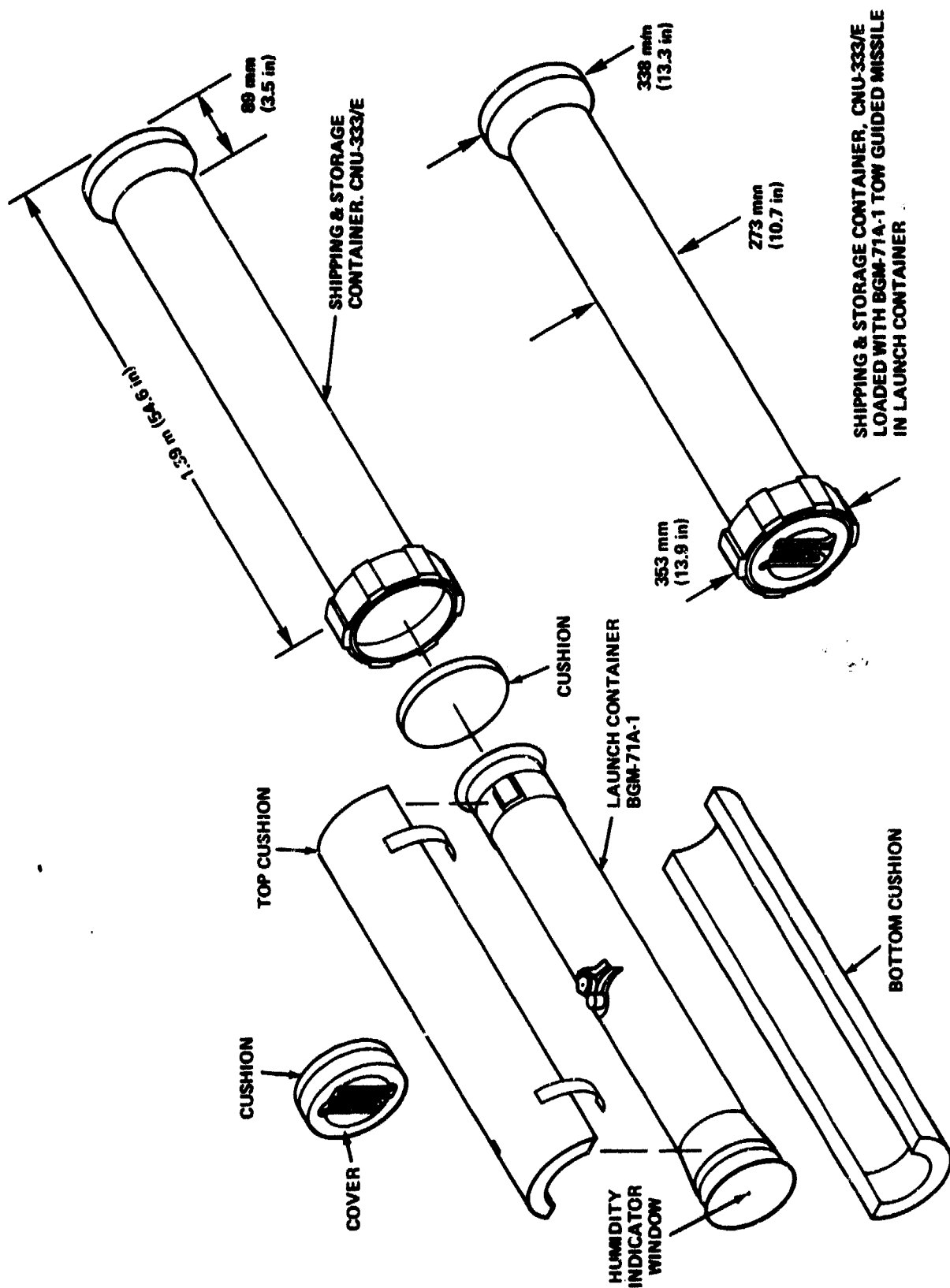


FIGURE 3. CONTAINER (CNU-333/E), SHIPPING & STORAGE, FOR BGM-71A-1 TOW GUIDED MISSILE

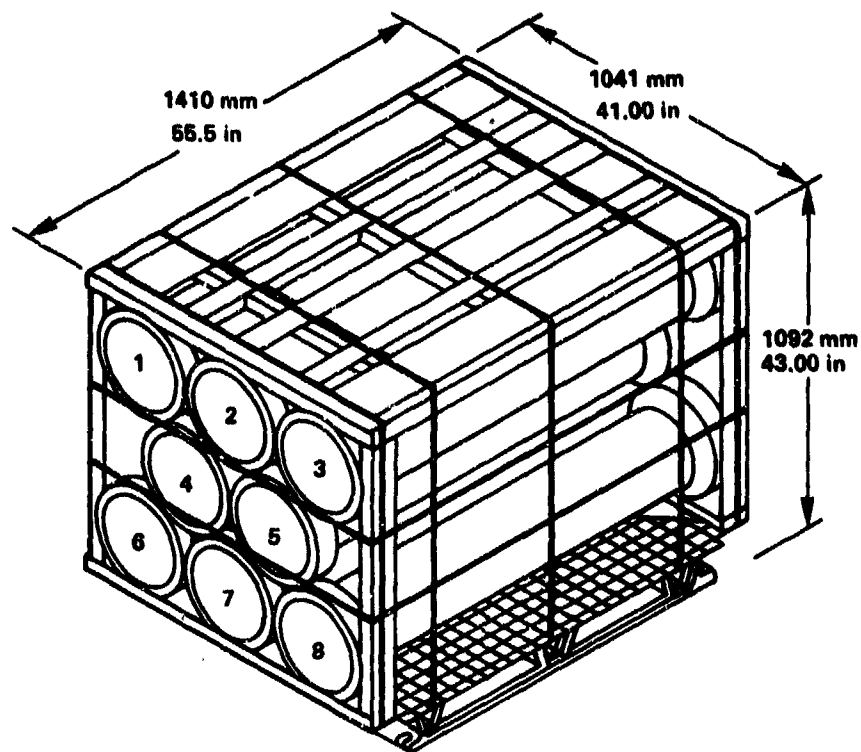
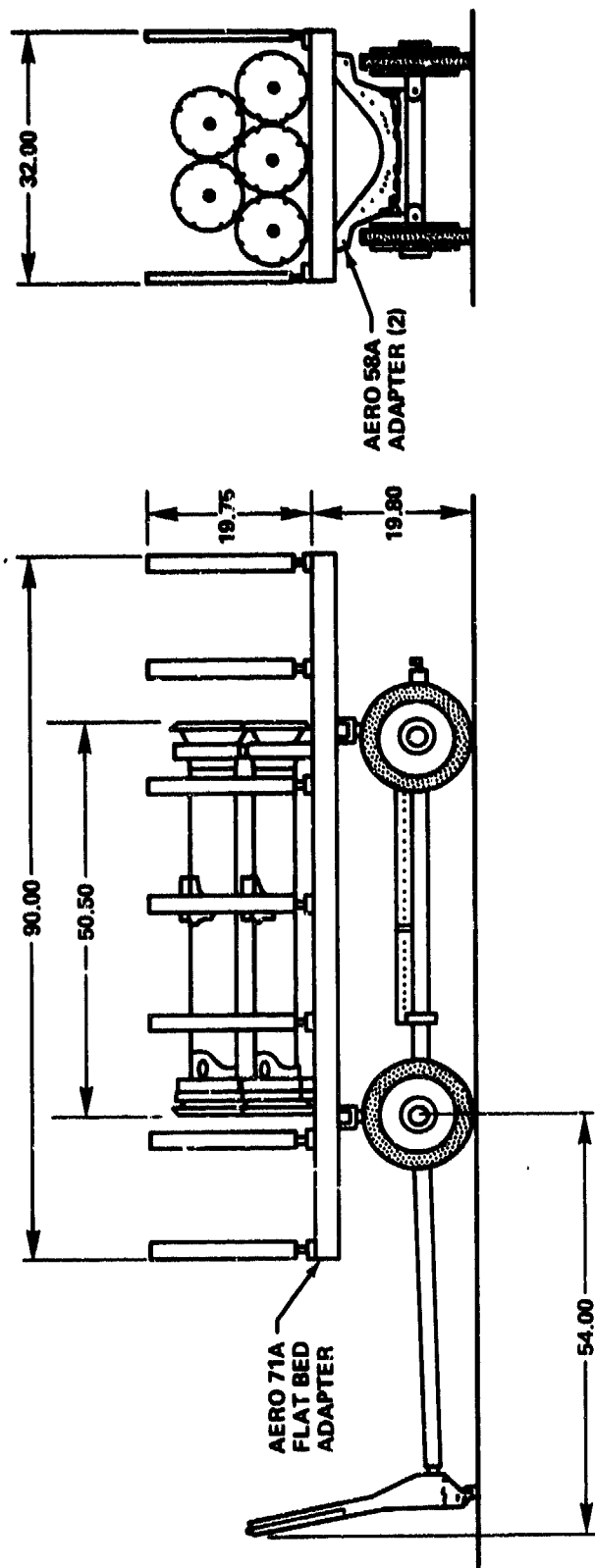


FIGURE 4. FLEET ISSUE UNIT LOAD, GUIDED MISSILE BGM-71A-1, BGM-71C (TOW) OR BTM-71C (INERT) IN ADAPTER ADU-486/E



NOTE: DIMENSIONS ARE IN INCHES.

FIGURE 5. TOW MISSILE IN LAUNCH CONTAINER ON AERO 21C WEAPON SKID
EQUIPPED WITH AERO 58A AND 71A ADAPTERS

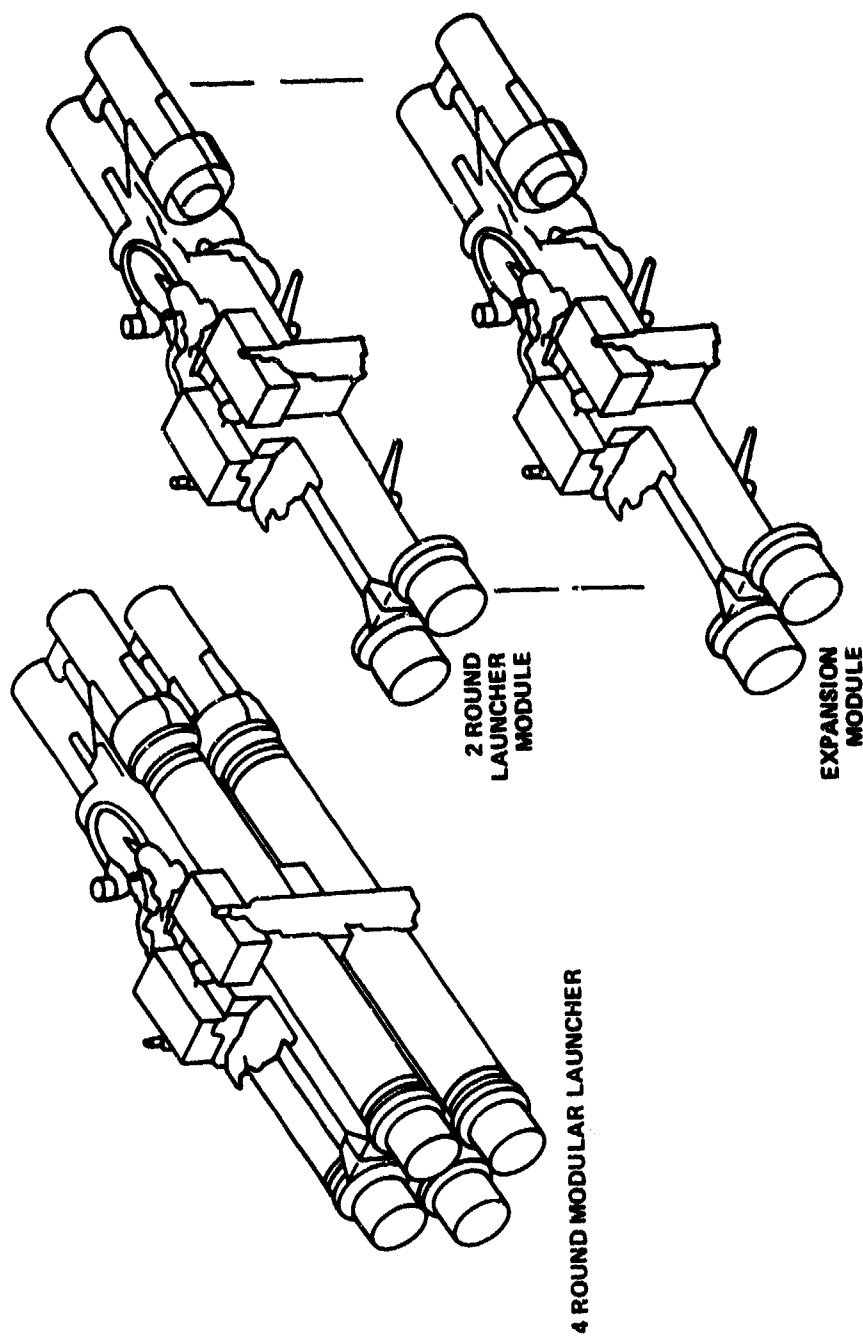


FIGURE 6. TWO (2) OR FOUR (4) ROUND MODULAR LAUNCHER



↑
DIRECTION OF MOTION

FIGURE 7. FLASH X-RAY PICTURE OF BASIC TOW SLUG

→ HALF-SCALE SUBMARINE TENDER WORKSHOP EXPLOSION HAZARDS

Joseph G. Connor, Jr.
Naval Surface Weapons Center
White Oak, Silver Spring, Maryland 20910

ABSTRACT

↙
As part of the Naval Explosive Safety Improvement Program (NESIP), a torpedo warhead was detonated inside a 1/2 scale model of a submarine tender workshop. The model was tightly confined on the bottom and three sides, lightly confined on the top and the remaining side - off which fragments were collected and shock overpressure measured. This test constitutes a worst case, since the bulkheads in the ship will provide much less confinement than was built into the model. Fragment hazards extend less than 300 feet from the model and 1 psi overpressure was observed 400 feet from the model (300 and 800 feet for a full scale tender). A second test was performed in which the sides of the model were less tightly confined than on the first. No fragments were recovered and 1 psi overpressure was observed 200 feet from the model (400 feet from a full scale tender).
↗

AD P000446

INTRODUCTION

The primary objective of the Naval Explosives Safety Improvement Program (NESIP) is to establish the Maximum Credible Event (MCE) and the acceptable hazard ranges pertinent to a variety of munitions handling situations. Acceptable hazards are defined as follows:

- less than one psi blast overpressure
- less than one fragment per 600 ft² of collection area with kinetic energy less than 58 ft-lb.

A specific NESIP goal is to determine acceptable hazard ranges for accidental explosions of torpedo warheads aboard a submarine tender. If these ranges are less than the hazard arcs specified by regulation, the proscribed arcs may be reduced by the DDESB.

BACKGROUND

Accidental torpedo warhead explosions aboard a submarine tender that may pose serious external threats will occur either in the workshop or in the magazine below the workshop: This portion of the ship is illustrated in Figure 1. Tests conducted under the aegis of NESIP (References 1 and 2) indicate that the MCE for an explosive accident in either compartment can be limited to a single warhead by shielding and judicious weapon placement.

These previous tests have led to the following conclusions:

For a single unconfined warhead outside the ship:

- torpedo propellant may burn vigorously, but will not detonate in the tender accident scenario
- one psi side-on overpressure will be observed at or inside the 500 ft range
- one hazardous fragment per 600 ft² will be found well within the 500 ft range.

For sympathetic detonation of warheads in the same compartment:

- detonation of a single warhead in the workshop will not induce subsequent detonations of another, properly oriented, warhead in the workshop, or of warheads in the magazine
- mass detonation in the magazine will not occur if the weapons are spaced, oriented and shielded properly.

¹ Connor, J. G., Jr., "Accidental Torpedo Detonation in Submarine Tender Workshops," 19th Explosive Safety Seminar, Los Angeles, CA, 9-11 Sep 1980.

² Connor, J. G., Jr., "Shipboard Effects of Accidental Torpedo Warhead Detonations," NSWC TR 81-289, June 1981.

The next step is to assess the hazards associated with detonation of a single warhead inside the workshop compartment. One model test has been completed and another is in the process of being analyzed. Both tests involved lighting off a half scale torpedo warhead inside a half scale model of the workshop area of the ship. Structural debris collection and side-on pressure observations confirm the 500 ft hazard range implied by the earlier unconfined warhead tests.

AS-18 MODEL: DISCUSSION

In the workshop a single torpedo warhead is normally located near a longitudinal bulkhead at one side of the workshop. Explosion of the warhead will cause the longitudinal bulkhead and the decks above and below to open. Hot explosion product gases then will vent to the neighboring ship compartments. The longitudinal bulkhead on the opposite side of the workshop is not likely to be ruptured by the shock front.

The hull plate aboard ship is not expected to be perforated, but pieces may separate from the (horizontal and vertical) stiffeners at the weld lines. The intact hull plate will confine the explosion gases and debris to the ship; it will also muffle the amplitude of the airblast observed outside the ship.

The initial outward velocity imparted to the hull plate by the explosion shock has been calculated (Reference 2). The result of the calculation is an upper limit on the initial velocity of the plate since it was based on the assumption of an unimpeded shock striking a uniform unreinforced steel plate. Reflected shocks from the nearby decks and bulkheads were not included in the assumed load on the hull plate. With these restrictions, the initial velocity of the plate was estimated to be just under 300 ft/sec. This velocity does not give the plate sufficient kinetic energy per unit area to exceed the strain energy required for rupture. Thus, no perforation is expected when the warhead is detonated behind an intervening bulkhead and various items of furnishings. The net permanent deformation is difficult to predict because of the many weld joints at the decks and plate stiffener junctions.

The structure is modeled carefully after the ship on the side closest to the expected location of the warhead - the area of the ship that can supply material for fragments, and the area through which the shock front must pass. The remainder of the model simply represents the structural mass and enclosed volume of the ship compartments that will be opened up by the blast front, and into which explosion gases can expand. Structural details are considered to be unimportant in areas of the model other than those in the exit paths for fragments and blast. Early time confinement approximating that supplied by the stiffened decks and bulkheads in the ship is provided by earthen restraints along the sides, back and over the roof of the model.

AS-18 MODEL: CONSTRUCTION DETAILS

Plan and elevation views of the models used for both tests are shown in Figures 2 and 3. In both cases, the portion of the model facing the fragment recovery pad and pressure gage line is modeled as closely as possible from the ship drawings.

For the first test, the two sides and back (the side away from the recovery pad) were formed by an excavation in a previously undisturbed hillside abutting the pad area. The roof was galvanized steel sheets not fastened to the supports, but covered with about 10 inches of earth so that it would remain in place for a short time but blow away after the initial confinement. Each end of the hull plate was anchored at two points by extending horizontal stiffeners into pockets cut into the hillside. The top of the hull plate was not restrained while the bottom was held back by several stakes driven into the ground.

The model for the second test was a replica of that used on the first test as far as internal volume and structural details of the hull plate are concerned. However, the two sides and back were much less tightly confined than they were on the first test. The back consisted of steel plating resembling in mass but not structural detail the side facing the pad. The sides were restrained by 4 ft of earth sandwiched between the steel model walls and 1 ft thick concrete pads. The roof was identical to that on the first model.

The construction changes on the second test resulted from a conscious effort to avoid the excessive confinement provided on the first test by the excavation walls in the virgin hillside.

On another series of NESIP tests (Reference 3) it was found that furniture inside the compartments close to the exploding warhead had a significant effect on fragment dispersion and hull breakout. Thus, each of the present models contained objects to simulate the items normally found in the torpedo workshop. The first test model was less heavily loaded than was the second.

TEST RESULTS

Photographs of the models before and after each test are shown in Figures 4 and 5.

First Test. The simulated hull plate was pulled loose from its moorings and thrown 300 ft. It was recovered with no penetrations and no evidence of fragment strikes on its inner surface. At a point opposite the warhead, it was bowed outward about 3 ft indicating that the fingers at each end of its length had provided insufficient restraint. The explosion pushed the center portion out until the fingers were no longer seated in their pockets in the hillside. The plate was then driven away from the model; the simulated furniture followed. Most of the structure and furniture fragments recovered from the pad were found in a circular segment 150° on either side of the center line of radius 400 ft from the warhead. The density of fragments recovered was less than 1 in 1200 ft² at the 400 ft radius.

The hard, lava-like material of the hill in which the model was constructed provided unyielding reflecting surfaces which enhanced the shock loading of the hull plate and furniture. Thus the fragments were subjected to a sustained driving pulse which pushed them out onto the recovery pad after the hull plate had departed.

³Swisdak, M. M., Jr., "Determination of Safe Handling Arcs Around Nuclear Attack Submarines," 19th Explosives Safety Seminar, Los Angeles, CA, 9-11 Sep 1980.

This megaphone effect also enhanced the amplitudes of the shock sensed by the pressure gages on the center line from 46 to 320 ft from the warhead. The pressure distance curve is plotted in Figure 6 together with that from the second test. On the first test, one psi is observed at 400 ft from the 1/2 scale warhead, corrected to sea level. For a full scale warhead, one psi would be expected as far out as 800 ft in similar circumstances.

Second Test. The simulated hull plate was anchored to two earth-filled steel boxes which were restrained by large concrete slabs as shown in Figure 3. The back of the model was unrestrained - while the first was set into a hill.

As a result of these differences, when the warhead detonated in the second model the hull plate and its anchors moved forward a few feet and tipped over without parting any welds. No debris left the model.

One psi overpressure was observed at 200 ft from the warhead - corrected to sea level conditions. Thus, one psi from a full scale warhead in a full scale ship at sea level would be expected at 400 ft from the warhead.

The motion of the hull plate was monitored with Doppler radar and a high speed camera. Preliminary measurements indicate that the maximum plate velocity was 10 to 20 ft/sec about a third of a second after motion began. This is much less than the prediction for an unstiffened, unconfined and unrestrained plate.

DISCUSSION

It is apparent that little, if any, debris will leave the side of a submarine tender following detonation of a full scale warhead in its torpedo workshop.

Earlier tests have shown that sympathetic detonation among warheads in the workshop and magazine is unlikely or can be prevented easily. The present tests were intended to involve the worst case of a single warhead accident: a single warhead detonates accidentally in the torpedo workshop near the hull. Detonation of a single warhead in the magazine, since it is further removed from the hull plate, will induce lesser hazards outside the ship than one detonated in the workshop.

CONCLUSIONS

For a single warhead detonated in the workshop:

- Initial velocity of any debris will be less than 25 ft/sec
- Any debris will be confined to a segment of radius 400 ft, 15° on either side of the normal to the hull plate
- One psi from a full scale warhead at sea level will be observed at 400 ft from the warhead.

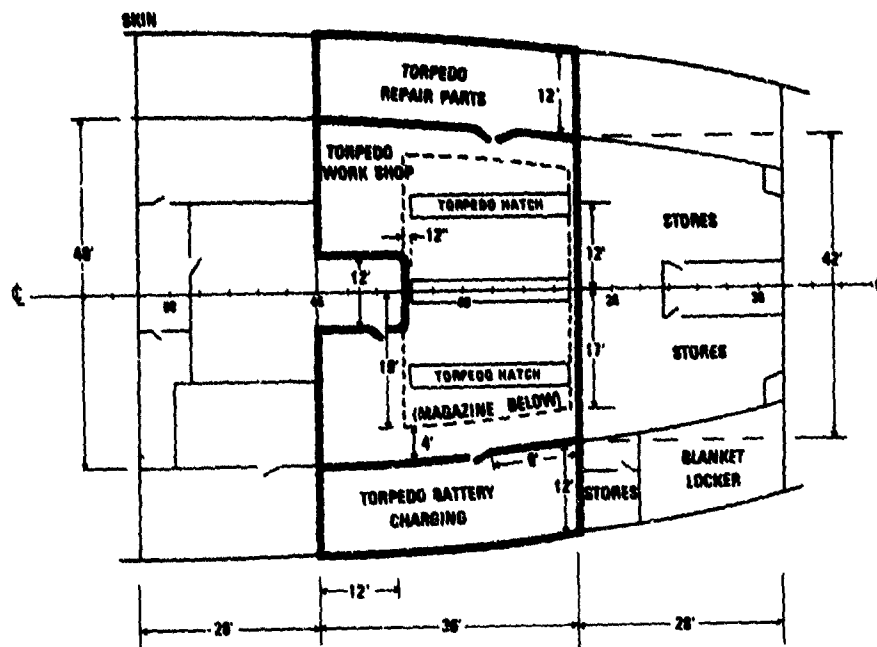


FIGURE 1a PLAN VIEW OF WORKSHOP DECK

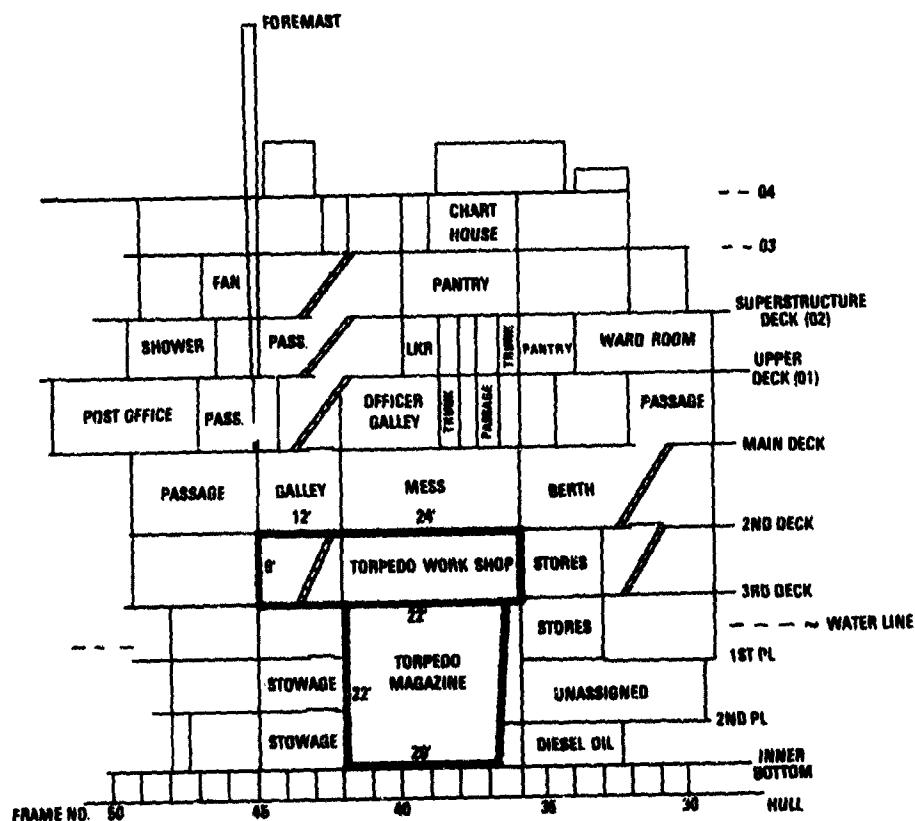


FIGURE 1b TENDER ELEVATION AT CENTER LINE

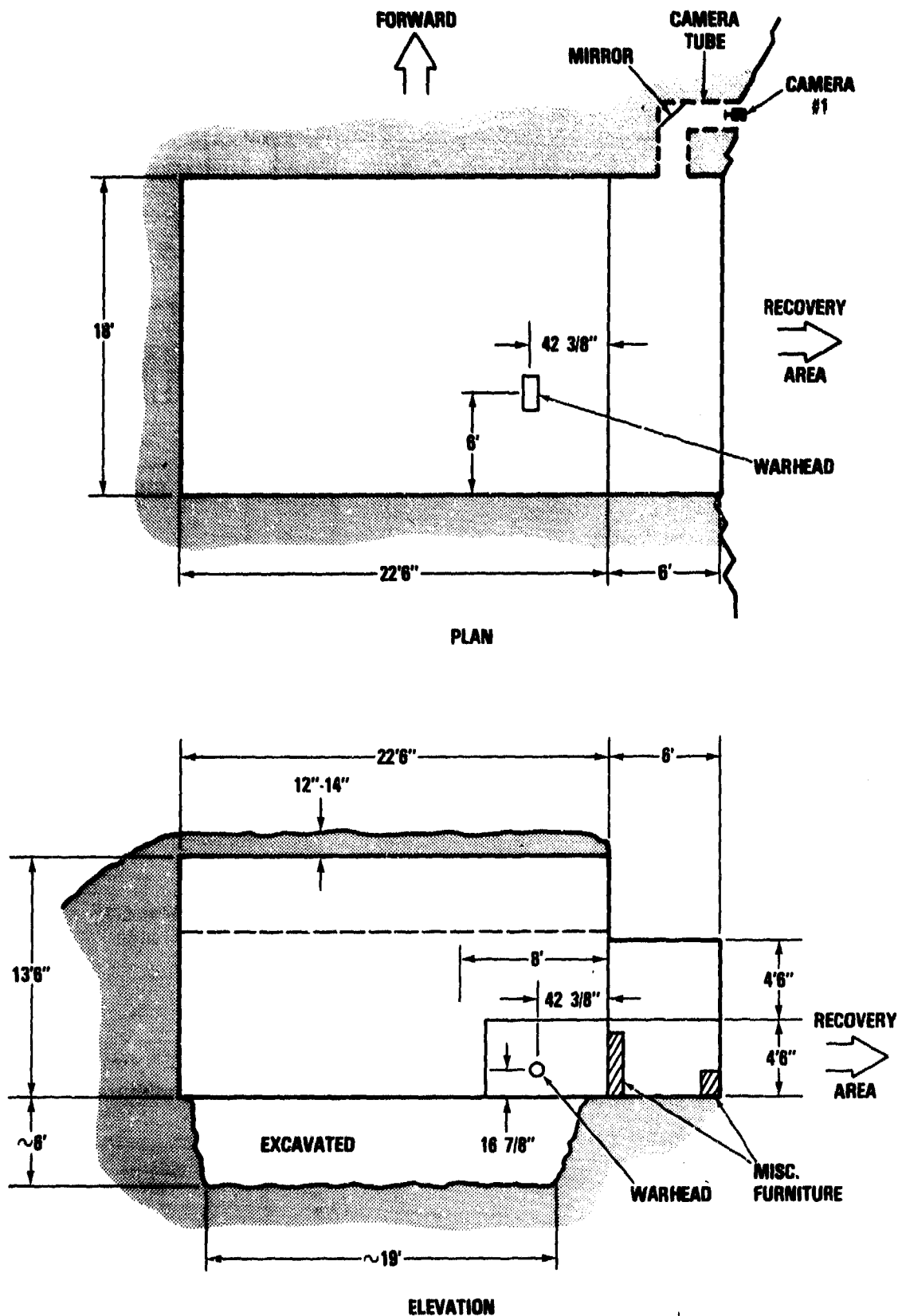


FIGURE 2 MODEL CONSTRUCTION FIRST TEST

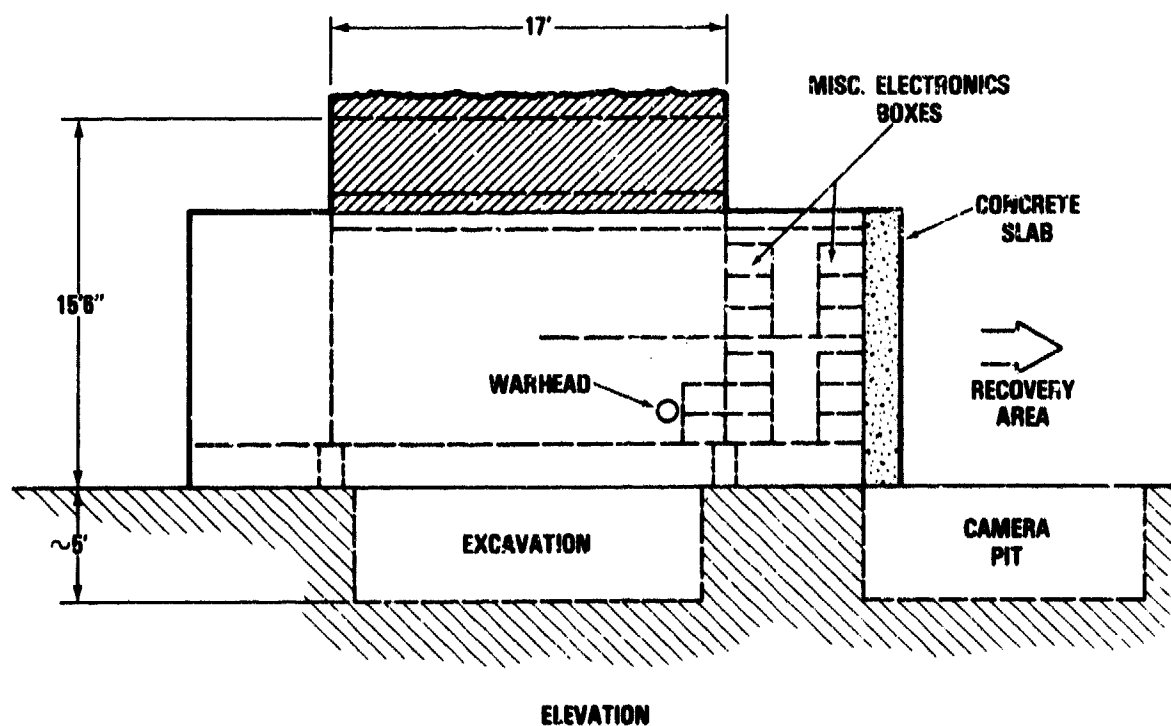
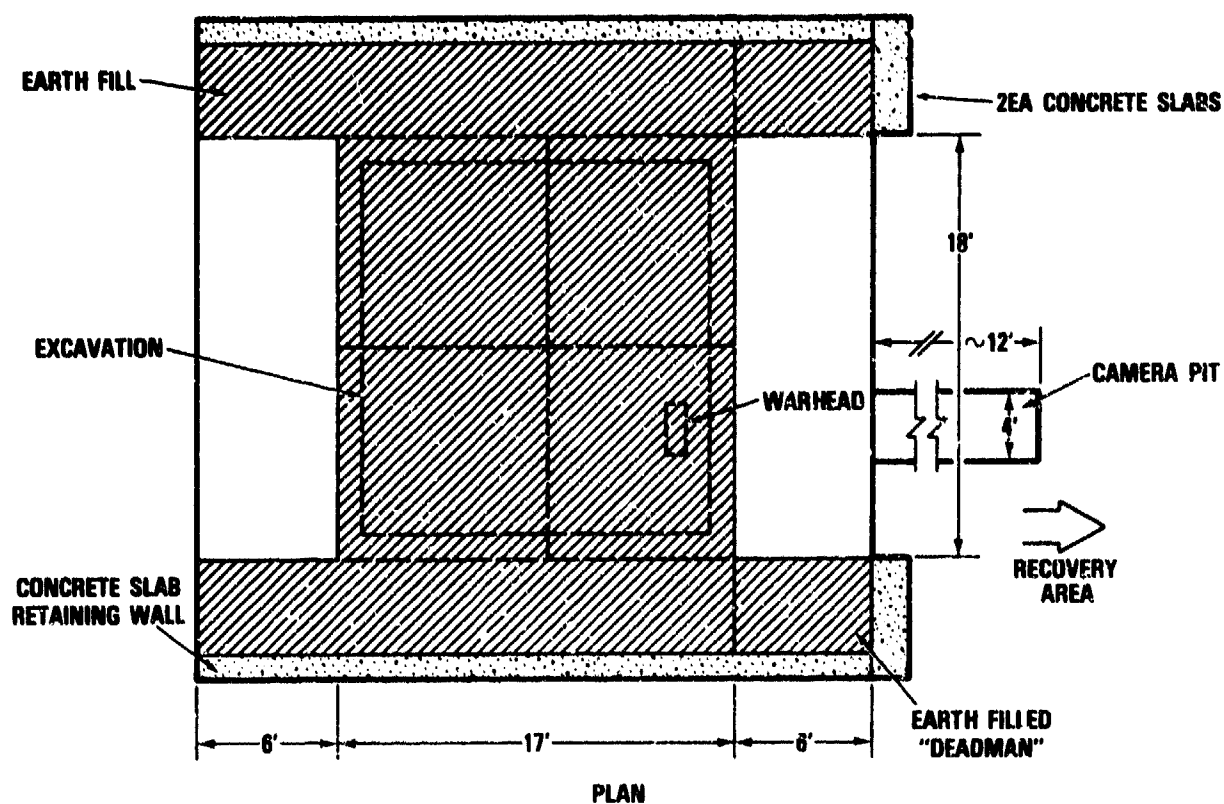


FIGURE 3 MODEL CONSTRUCTION SECOND TEST



A. BEFORE



B. AFTER

FIGURE 4. FIRST TEST MODEL

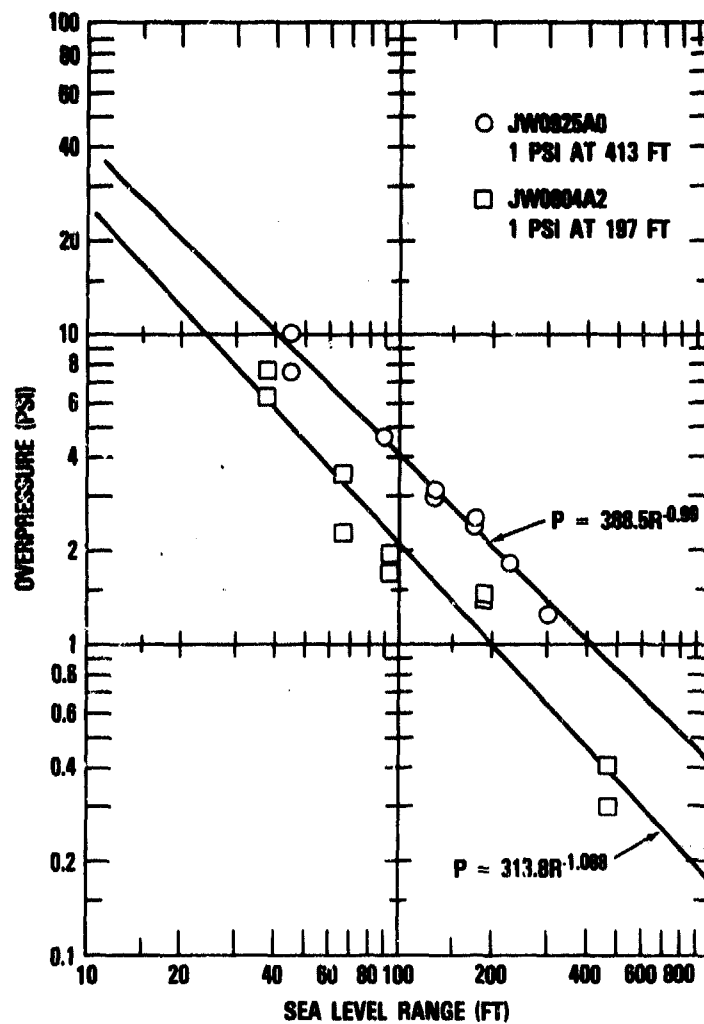


A. BEFORE



B. AFTER

FIGURE 5. SECOND TEST MODEL



**FIGURE 6 ½ SCALE SUBMARINE TENDER
SEA LEVEL AIRBLAST OVERPRESSURES**

AD P000447

→ EXPLOSION CONTAINMENT: PROGRESS,
SCALING LAWS, AND MATERIAL PROPERTIES*

by

John J. White, III and B. Dale Trott
Battelle, Columbus Laboratories
Columbus, Ohio

ABSTRACT

↓
The Battelle Ordnance Technology Section has been involved for several years with the development of Navy (Tri-Service) technology for the containment of explosions in portable spherical chambers. The central topic of this paper concerns the room temperature testing of a Frostline steel vessel with 22 repetitive explosions from 4.54 kg (10 lb) charges of Composition C-4 high explosive. The cumulative plastic deformation of the shell has been analyzed in the impulse approximation to give effective values for the Frostline mechanical equation of state. Evidence of work hardening is found. Scaling laws predicting the peak elastic response of explosively loaded spherical shells are compared. Recent literature on the topic of explosion containment, including Soviet interest, is briefly reviewed.
↑

* Sponsored, in part, by the U.S. Naval Explosive Ordnance Disposal Facility, Indian Head, Maryland, under Contract No. N00174-76-C-0103.

INTRODUCTION

Portable, reuseable, accessible explosion containment chambers offer a number of advantages to situations where unplanned or infrequent detonations should be confined.^(1,2) The unwanted effects of blast, fragments, noise, and toxic materials released by explosions can be contained by proper design. Fracture-safe design is a significant topic for all applications.⁽¹⁾ High containment efficiency (ratio of charge to vessel weight), which is essential to portable vessels, leads to the anticipation of elastic-plastic responses in the vessel design.^(3,4) The type-classified Mk 634 Mod 0 Explosive Devices Container⁽⁵⁾ represents the state-of-the-art in such portable chambers.

The principal application⁽²⁾ for portable explosion containment technology concerns the handling of terrorist bombs and related devices. Safe transport of the dangerous item to a preferred location for disposal is desired. The need in the civilian sector is for each major population center to have its own device. It is important for safety reasons to insure that the most reliable design information be disseminated. Similar thoughts apply to explosion containment design for manufacturing ammunition, demilitarization of ammunition, and advanced weapon development.

This paper documents a portion of an evolutionary development program,⁽⁶⁻⁸⁾ which led to the Mk 634 Mod 0 Device. A brief literature review is made to keep users of the technology abreast of related activities. Scaling laws for the prediction of elastic responses in spherical vessels are compared to show their usefulness and status. A room temperature explosion test series⁽⁹⁾ on a Frostline steel vessel is presented. Each 4.54 kg (10 lb) shot added to the cumulative residual strain in the vessel shell. The data is then analyzed in the impulse approximation to predict an effective mechanical equation of state for Frostline steel.

LITERATURE REVIEW

As steady contributors to the literature in the field of explosion containment, we make a practice of collecting and referencing relevant contributions of interest to our colleagues. To save space, we mention these contributions once, and refer our readers to previous papers⁽¹⁻⁹⁾ containing other significant references.

The student of technology development will find the Carlson report⁽¹⁰⁾ from 1945 very interesting. His objective was to analyze the design and test results for a prototype vessel called "Jumbo" and some tenth-scale versions called "Jumbinos". The vessel "Jumbo" was a cylinder capped by thinner gage hemispheres. It was expected to confine an explosion from a two-ton charge.

Developments on cylindrical vessels closely parallel efforts with spheres. M. C. de Malherbe, et al.⁽¹¹⁾ performed a successful analysis of a gas detonation wave propagating down the axis of a cylinder. A. G. Ivanov and coworkers⁽¹²⁾ extended a Soviet interest to optimize the weight efficiency of cylindrical containment chambers. They are using the approach of multilayer walls to stop crack propagation and avert catastrophic rupture of the whole structure. A. A. Buzukov⁽¹³⁾ has reported additional experimental data to confirm the loading history and vibrational response of cylinders to line charges.

Recent research on spherical containment includes contributions from LANL, BRL, and the Soviets. D. C. Moir⁽¹⁴⁾ of LANL performed a safety analysis to determine the capability of an outer safety sphere to contain all products of the catastrophic failure of an inner confinement vessel. This leads to the challenging problem of the penetration capability of a hemisphere striking a larger radius hemisphere internally. T. R. Neal⁽¹⁵⁾ of LANL has addressed the charge rating criteria for elastic responses of spherical shells, i.e., an equivalent of the scaling law published^(1,4,16) by the present authors. The practical interest in this case is to assure a reuseable confinement shell.

BRL⁽¹⁷⁾ has evaluated a novel approach to spherical containment that involves off-center detonation of bare charges. The shell is relatively thin, however the weld line is heavily reinforced with thick internal and external bands. The charge is rotated from the port to various positions off-center but within the weld plane. This device is one of the Army's more effective suppressive shield designs. The use of 1020 carbon steel is not attractive from a service temperature/fracture safety point of view.⁽¹⁾ The application is not stated, but a manufacturing process appears to be a good candidate. Battelle published pipe bomb containment results⁽⁸⁾ for a similar sized vessel in 1978.

T. A. Duffey and coworkers⁽¹⁸⁻²¹⁾ have been active in extending the theory of spherical explosion containment. They have considered the case of a thin shell surrounded by an infinite elastic medium, e.g., a vessel buried in concrete or sandstone.^(18,19) Some earlier calculations⁽²⁰⁾ on blast loading and free shell response were presented⁽²¹⁾ at the ASME Pressure Vessel and Piping Division Conference in Orlando, June 27-July 1, 1982.

The recent Soviet work on spherical vessels has concentrated on strength scale effects in water-filled shells and on the correct dynamic loading of an air-filled shell. Ivanov, et al.⁽²²⁾ conclude that the easier failure of scaled-up, water-filled vessels is not explainable in terms of strain rate effects. The calculations by Zhdan⁽²³⁾ and also the LANL group⁽²⁰⁾ raise the interesting question of resonant loading effects due to periodic pressure pulsations within the vessel. The impulse appears to be increased for distances less than 10 charge radii. The data of Buzukov⁽¹³⁾ on pulsations in cylinders is consistent with this line of investigation.

Some new information of equipment and facilities may be of interest. The FBI Total Containment Bomb Trailer⁽⁶⁾ is one of many interesting devices displayed in the recent book⁽²⁴⁾ by Michael Dewar.

The vessel and trailer were developed by Pictanny Arsenal with the technical support of the Battelle Ordnance Group. Individuals interested in permanent test facilities may wish to consult NSWC TR 3891 to learn about the Dahlgren blast confinement chamber. ⁽²⁵⁾ Similarly, Battelle is expanding its capabilities by building a new terminal ballistics facility. Laboratories wishing to study small-scale explosions may want to consider a Fike 20 Liter Test Sphere. ⁽²⁶⁾ The cost per pound of explosive contained may be rather high. A rather exceptional contribution on the topic of dust explosions and their control is the new English-language version of the book by W. Bartknecht. ⁽²⁷⁾

SCALING LAW FOR ELASTIC RESPONSE

We recently published a useful scaling law ^(1,16) for quickly predicting the peak first-cycle response of an elastic spherical shell loaded by the explosion of a centered, bare, spherical charge. The results for a given vessel material may be expressed in the form

$$\epsilon_{\max} = K_1 R^{-1.293} h^{-1.026} M^{0.772} \quad (1)$$

where ϵ_{\max} is the peak strain, K is a constant, h is the shell thickness, R is the shell radius, and M is the explosive mass. In the impulse approximation, Eq. (1) becomes

$$\epsilon_{\max} = K_2 R^{-1.39} h^{-1.00} M^{0.80} \quad (2)$$

The calculation of these equations involved computer runs of SPLAS ^(3,4) for a wide range of shell designs, shell materials, explosive charge weights, and peak stresses. The vessel was filled with air at STP.

Eqs. (1) and (2) can be compared with the experimental findings of Neal, (14,20,28) whose results may be written

$$\epsilon_{\max} = K_3 R^{-1.883} h^{-1.000} M^{0.961} \quad (3)$$

Eq. (3) is specific to 9 shots on steel vessels with 4 values of the air density in the vessel. The discrepancies among the exponents of R and M need to be resolved through further research. (20,23)

These equations also offer the opportunity to ask what effect the shell radius to thickness ratio, R/h , has on vessel performance. The answer is most easily answered in terms of the specific containment ratio, M/M_v , where M_v is the thin shell mass. Eqs. (1-3) can be rewritten and closely approximated by

$$\epsilon_{\max} = C_1 \left(\frac{R}{h} \right)^{0.252} \left(\frac{M}{M_v} \right)^{0.772}, \quad (4)$$

$$\epsilon_{\max} = C_2 \left(\frac{R}{h} \right)^{0.20} \left(\frac{M}{M_v} \right)^{0.80}, \quad (5)$$

and

$$\epsilon_{\max} = C_3 \left(\frac{R}{h} \right)^{0.039} \left(\frac{M}{M_v} \right)^{0.961}, \quad (6)$$

respectively, where C is a constant. Alternatively, these equations can be written as

$$\frac{M_v}{M} = \left(\frac{C_1}{\epsilon_{\max}} \right)^{0.772} \left(\frac{R}{h} \right)^{0.326}, \quad (7)$$

$$\frac{M_v}{M} = \left(\frac{C_2}{\epsilon_{\max}} \right)^{0.80} \left(\frac{R}{h} \right)^{0.25}, \quad (8)$$

and

$$\frac{M_v}{M} = \left(\frac{C_3}{\epsilon_{\max}} \right)^{1.0406} \left(\frac{R}{h} \right)^{0.0406}. \quad (9)$$

If M and ϵ_{\max} are specified, the BCL results expressed by Eq. (7) states that 25.4% more metal is needed if R/h is doubled. Thus thicker shells offer some advantage over thinner shells of the same mass. The LANL result expressed by Eq. (9) states that only 2.9% more metal is required if R/h is doubled. This comparison clarifies the incentive for obtaining better knowledge of the scaling law exponents.

EXPERIMENTAL MULTIPURPOSE BLAST CONTAINMENT CHAMBER

Our recent publications^(1,2,16) on explosion containment have emphasized materials performance at low service temperatures and also scaling laws for vessels having an elastic response. This section returns to a previous topic,^(3,4,7,8) namely the elastic-plastic response of a spherical vessel to repetitive explosion tests.

The multipurpose blast containment chambers⁽⁹⁾ discussed below were intended to meet the following objectives:

- Completely contain the blast from 4.54 kg (10 lb) of TNT detonated centrally within the chamber. Repeat at least 7 times.
- Reduce blast overpressures outside of the vessel at a 1.52 m (5 ft) radius to not over 27.6 kPa (4 psi).
- The chamber should be on a support cradle to facilitate transport in trucks or on trailers.
- The access port should be large enough to accommodate the passage of an attache case whose dimensions are 0.305 x 0.432 x 0.089 m (12 x 17 x 3-1/2 in.) in a random orientation.
- The total weight of the chamber and cradle should not exceed approximately 953 kg (2100 lb).
- Perform the blast containment role down to a temperature of -34.4 C (-30 F).

Difficulties meeting the last objective using Frostline* steel were vividly illustrated in our paper at the Nineteenth Explosives Safety Seminar.⁽¹⁾ The first five objectives were successfully met, and it is the data⁽⁹⁾ obtained to satisfy the first objective that is reported and analyzed below. The explosive charge and vessel weight constraints implied an elastic-plastic response by the vessel material.

Chamber Design

The diameter of the chamber was selected on the basis of the minimum diameter chamber which could incorporate a port of at least 0.536 m (21.1 in.) in diameter to pass the attache case as required by the objectives. Our experience^(4,8) had shown that port diameters equal to the radius of a spherical chamber performed satisfactorily, hence a sphere diameter near 1.07 m (42 in.) was selected.

The wall thickness of the chamber was selected on the basis of iterative design calculations⁽⁴⁾ of the weight of the reinforcing ring, door, cradle, and chamber itself to obtain a gross weight of chamber and cradle as near 953 kg (2100 lb) as possible. These calculations indicated a desired average wall thickness near 0.0229 m (0.900 in.). This led to ordering the rolled gage of plate to be hot-pressed in hemispherical shells at 0.0245 m (0.970 in.) with instructions to hold overweight down.

It was found by ultrasonic measurements that the average thickness of seven hemispherical heads at the pole was 0.8576 inches, indicating an average thickening of 0.044 inches from the minimum to the pole.

The average wall thickness of the vessel was calculated under the assumption that the heads have circular symmetry about their pole points, and each set of measurements at a given polar angle was weighted accordingly. The selected wall thickness led to an actual total vessel weight including cradle of the first vessel of 976 ± 11 kg (2150 ± 25 lb), within 2.4 percent of design objective.

*Trade-name of Lukens Steel Company

The Battelle method for designing the door reinforcing ring was employed. This approach has an excellent service record. Further details are given elsewhere.^(4,9)

The previously used door design criteria⁽⁴⁾ employed a flat disc door whose thickness was established on the basis of static, elastic stress formulas, such that the maximum stress in the door would equal that in the spherical vessel. Examination of the door performance realized^(4,8) using this criteria showed that no measurable distortion of the doors occurred, even for vessels which suffered catastrophic failure. An opportunity to reduce the vessel weight with no sacrifice of performance was recognized.

It is known from various stress analyses^(6,7) that the door stresses will be largest in the center, and gradually decrease toward the edges of the circular door. Hence, material was removed from the outer edges of the door. The central 1/3 of the door was left flat near the design⁽⁴⁾ thickness. The thickness of the outer edge was reduced by a factor of two. Thus, the back half-thickness of the door was converted from a right-circular disc to a frustum of a cone. This weight reduction amounted to 47 kg (103.5 lb) and resulted in satisfactory performance of the door.

The door operating mechanism selected for use in these chambers was suggested by B. S. W. Poe of the Naval Explosive Ordnance Disposal Facility (NEODF), Indian Head, Maryland and tested for operational feasibility in an approximately full-scale mock-up at NEODF. It consists of a 12 VDC-powered electric winch mounted on a plate attached to the outside top of the reinforcing ring. The winch lifts the door from a rest position near the bottom of the chamber up to the fully closed position by a steel cable attached to the outer face of the door. The door is not otherwise attached to the chamber. This door operating design is shown schematically in Figure 1 with the door shown both open (dotted), closed, and secured by the auxiliary support spider.

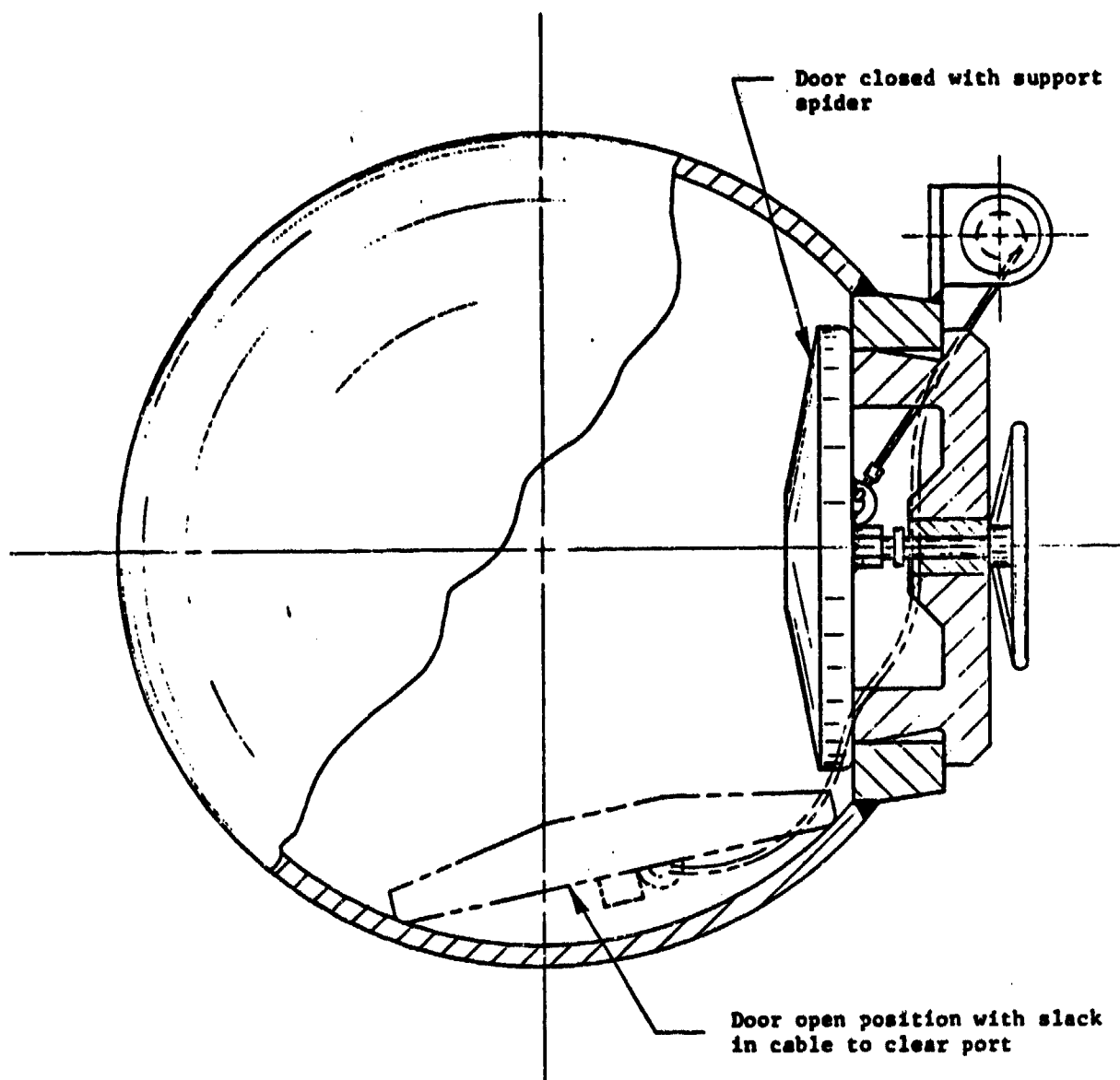


FIGURE 1. SCHEMATIC VIEW OF CHAMBER
SHOWING DOOR OPERATING
MECHANISM

Observation of the operation cycle of the door on the scale mock-up showed that only small, strong guides located at either side of the door along its horizontal centerline are needed to guide the door into its final centered position and keep it there. The guides chosen were 3/4 in. wide, 1 in. high, and 2 in. long. Analysis of the geometry of door lift in the vessel showed that efficient lifting action is obtained where the five-inch thickness of the reinforcing ring is considered, if the cable is attached 2 in. above the door centerline.

To provide positive support for the chamber door in the fully closed position during road travel, an auxiliary support mechanism was constructed. The mechanism consisted of a five-legged spider fabricated from 6061 T-6 aluminum alloy with a captive central 0.0254 m (1 in.) diameter bolt. The spider legs were machined to fit inside the reinforcing ring to provide positive centering and overlap the outside to provide positive closure. The central bolt attached to the door via a nut welded to the center outside face of the door. The bolt was tightened via a handwheel attached to the outer end of the bolt.

Materials Selection and Properties

The introduction of the blast containment service temperature requirement of -34.4 C (-30 F) led to a program to evaluate the effectiveness of available materials.^(1,29) This resulted in a search for a vessel steel that could be hot pressed into a hemisphere, has a modest cost, and has adequate low temperature fracture properties. A special heat of modified Frostline material was selected for the present application.

Frostline steel is quite similar to the A-537 material used successfully in previous vessel programs.^(4,7,8) Frostline has a small columbium (niobium) addition, which resulted together with special rolling practice in fine grain in the range of ASM grain sizes 12-14. The modified Frostline contains a calcium addition to control sulphide shapes to a nodular form, thus giving increased toughness. The cost of this material is comparable to that of A-537 material.

The Charpy V-notch energies of separately heat-treated Frostline at -59 C (-75 F) ranged from 79 to 262 J (58 to 193 ft-lb), suggesting good fracture resistance at the specified service temperature of -34 C (-30 F). Fracture-safe design practice suggests that the nil ductility transition temperature (NDT) for steels should be 120 F (67 C) below the operating temperature, however since successes with only 60 F (33 C) are reported. Unfortunately, the Charpy test data is not always sufficient to evaluate the NDT, and drop weight or dynamic tear test data must be used.

Difficulties with the fracture toughness of Frostline at -34.4 C (-30 F) developed when dynamic tear tests were made as part of the base metal and welding qualification procedures. Reheat treating of test pieces gave successful fracture properties, but the full thickness material did not respond adequately.

As reported previously,^(1,28) explosion bulge and full scale vessel tests confirmed that the modified Frostline material was not adequate to meet the low service temperature blast containment requirement. A vessel was successfully tested at -6.5 C (20 F). HY-80 material has subsequently been shown to completely satisfy the material requirements for this application.^(1,2,5,29,30)

The rings and doors of the present vessels would also have been fabricated from Frostline material. However, none of this material was available in the required thicknesses. The more costly, alternate alloy, HY-80 was selected based on its confirmed superior low temperature properties, and availability in the required thickness.

Explosion Testing At Room Temperature

Figures 2 and 3 give front and side views of a vessel fabricated from Frostline steel. It is 107 cm (3.5 ft) in diameter, has a 2.29 cm (0.90 in.) wall-thickness, weighs 998 kg (2,200 lbs) with aluminum cradle, and has a 55.3-cm (21.75-in.)-diameter access port with a circular door. Figures 4 and 5 show the explosive charge positioning system in the extended and retracted positions. Figure 6 gives a good



FIGURE 2. FRONT VIEW OF THE FIRST FROSTLINE
EXPLOSION CONTAINMENT VESSEL AFTER
SHOT NO. 23.

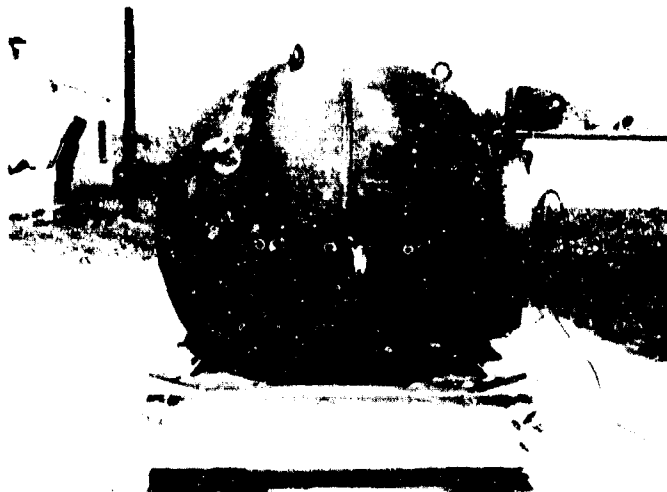


FIGURE 3. SIDE VIEW OF THE FIRST FROSTLINE VESSEL
CONTAINMENT VESSEL AFTER SHOT NO. 23.



FIGURE 4. VIEW OF THE FIRST FROSTLINE
EXPLOSION CONTAINMENT VESSEL
WITH THE CHARGE POSITIONING
SYSTEM EXTENDED.



FIGURE 5. VIEW OF A FROSTLINE VESSEL AND
CHARGE WITH THE CHARGE POSITION-
ING SYSTEM RETRACTED.

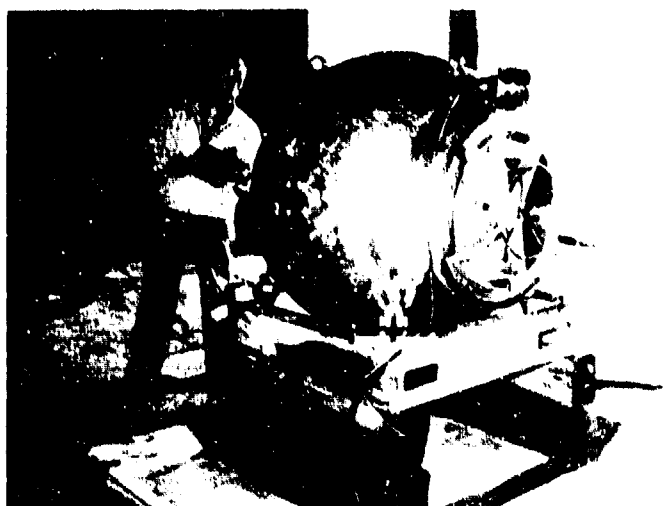


FIGURE 6. FRONT VIEW OF THE FIRST FROSTLINE
EXPLOSION CONTAINMENT VESSEL DURING
THE TEST SERIES. THE WINCH, CABLE,
AND ALUMINUM SPIDER SHOULD BE NOTED.



FIGURE 7. REAR VIEW OF THE FIRST FROSTLINE
EXPLOSION CONTAINMENT VESSEL AFTER
SHOT NO. 23. SLIGHT DIMPLES MAY BE
OBSERVED SLIGHTLY BELOW THE LIFTING
EYEBOLTS.

view of the aluminum spider, while Figure 7 indicates a slight dimpling effect after many tests that is characteristic of mass asymmetries.

An explosion testing series of 23 shots was carried out on the first of these vessels fabricated. The tests were conducted in the summertime inside a reinforced concrete test building. Thus the vessel temperature just prior to the explosion was at least 15.6 C (60 F) in every test completed.

The accumulated residual strain in the vessel material was determined by means of measurements between fiducial marks making up 18 gage lengths. The marks were placed on three orthogonal great circles so that the average response would closely approximate that of a simple spherical shell loaded by the explosion of centrally-positioned, spherical explosive charges.

Table 1 gives the average residual strain⁽⁹⁾ determined for 23 shots employing a centrally-positioned, spherical charge of Composition C-4 high explosive. The first 22 shots used 4.54 kg (10 lbs) charges, and the 23rd shot used 9.09 kg (20 lbs) of explosive.

Figure 8 gives a plot⁽⁹⁾ of the accumulated average residual strain for the first 22 shots versus shot number. The downward curvature indicates a work hardening effect. The average incremental increase was 0.045 percent per shot, indicating that the vessel would likely contain 100 or more shots with 4.54 kg (10 lbs) of C-4 explosive. It is known that large amplitude flexural vibrations occur near the pole,⁽⁴⁾ which could lead to fatigue problems with high usage. Further work is required to fully evaluate large numbers of usages. Service use based on metropolitan police experience suggests that high numbers of usages will not be required in the EOD role. In any event, the principal blast containment objective was easily met at room temperature.

It is truly shocking to compare these results with the first test at -34.4 C (-30 F) on the second Frostline vessel using 4.54 kg (10 lbs) of explosive.^(1,2,9) In this case, the vessel failed by brittle fracture.

TABLE 1. ACCUMULATED AND INCREMENTAL AVERAGE RESIDUAL STRAIN
FROM EXPLOSION TESTING OF THE FIRST FROSTLINE VESSEL
AT ROOM TEMPERATURE.

<u>Shot No.</u>	<u>Explosive Charge, lbs</u>	<u>Accumulated Strain, Percent</u>	<u>Incremental Strain, Percent</u>
1	10	0.086	0.086
2	10	0.166	0.080
3	10	0.242	0.076
4	10	0.307	0.065
5	10	0.360	0.053
6	10	0.392	0.032
7	10	0.471	0.079
8	10	0.499	0.028
9	10	0.548	0.049
10	10	0.572	0.024
11	10	0.620	0.048
12	10	0.631	0.011
13	10	0.684	0.053
14	10	0.716	0.032
15	10	0.752	0.036
16	10	0.808	0.056
17	10	0.832	0.024
18	10	0.854	0.022
19	10	0.899	0.045
20	10	0.909	0.010
21	10	0.944	0.035
22	10	0.994	0.050
23	20	1.674	0.680

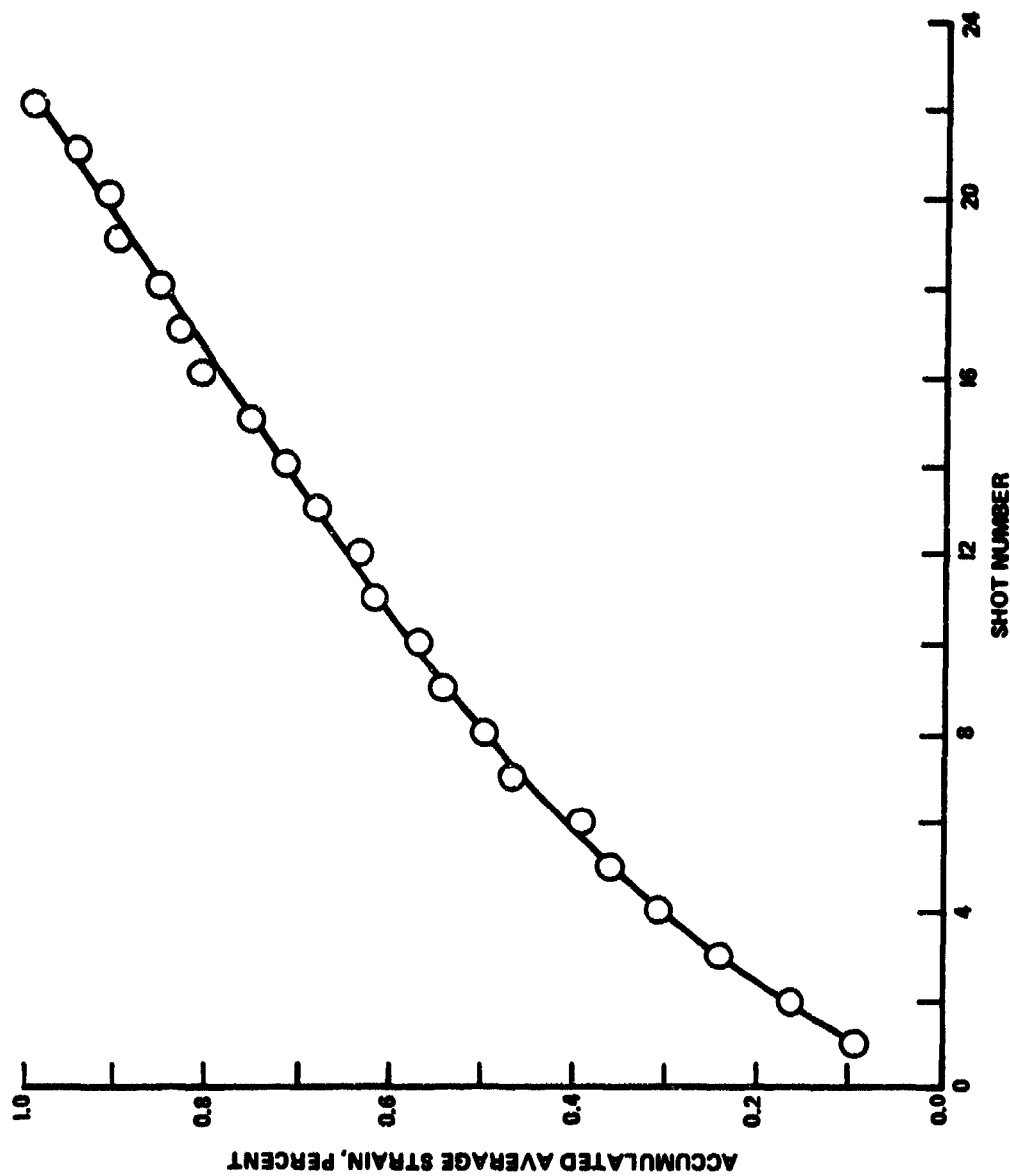


FIGURE 8. ACCUMULATED AVERAGE STRAIN FOR A SERIES OF EXPLOSIVE EXPERIMENTS WITH THE FIRST FROSTLINE EXPLOSION CONTAINMENT VESSEL. TEN POUNDS OF COMPOSITION C-4 WERE USED FOR EACH EXPERIMENT.

as expected, scattering pieces about the test site. Potential users of blast containment vessels who have no experience with nil-ductility transition temperatures are urged to read Reference 28.

The large deformation of 0.68% strain caused by the 9.08 kg (20 lb) shot should be noted. The shot deposited more than 3 times the amount of energy from a 4.54 kg (10 lb) shot. A large fraction of the energy is absorbed elastically with the 4.54 kg (10 lb) shots. Thus the incremental deformation is small. The elastic energy absorption is unchanged with the 9.08 kg (20 lb) shot, thus requiring a relatively larger amount of plastic flow to achieve containment.⁽³⁾

MECHANICAL EQUATION OF STATE ANALYSIS

A preliminary analysis has been made of the data in Table 1 and Figure 8 to determine an effective mechanical equation of state (EMES) for Frostline steel. The immediate application of the EMES would be the prediction of the elastic-plastic responses of Frostline vessels with differing radii R , thicknesses h , and/or explosive charges M .

Model Description

The major assumptions of this analysis were:

- The impulse approximation can be meaningfully applied.
- Strain rate effects can be estimated using an effective yield and flow stress.
- Loading can be estimated using the reflected impulse data of Goodman.⁽³¹⁾

The impulse approximation overestimates the peak vessel response by 15-30%. Thus the yield strength estimated will be too high by a significant amount. This means that the EMES should only be used in vessel response predictions using the impulse approximation. The strain rate assumption has been used by Baker⁽³²⁾ and many others to obtain useful solutions with minimum effort. The method implies

errors of 10-20 ksi in yield stresses if the loading strain rates of two vessels differ by an order of magnitude. Also, as noted previously, it would appear that corrections to the reflected impulse of Goodman⁽³⁰⁾ should be made at distances less than 10 charge radii.^(20,23)

The stress-strain model assumed here (see Figure 9) includes a linear elastic segment up to a yield stress σ_y . The plastic flow stress is represented by a linear segment with a small positive slope S to account for work hardening. The material unloads elastically and returns after damping to the residual strain state ϵ_r . If the work hardening coefficient S changes as ϵ_r increases, then a cusp is created by continuing the loading curve at some point with another linear segment. This type of loading curve is called a linear spline in mathematics, and the cusp points are called knots.

Mathematical Method

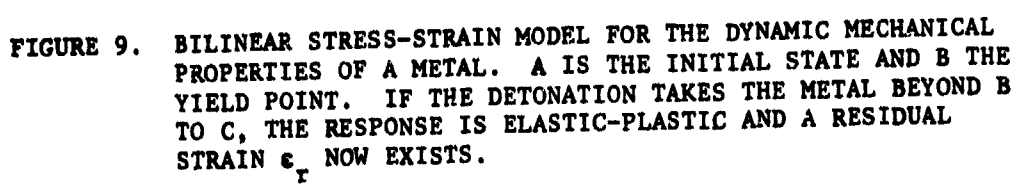
In the impulse approximation⁽³⁾, the shell acquires a jump in radial velocity in a time short compared with the natural response time. Momentum is conserved by writing

$$I_r = \rho h V_o, \quad (10)$$

where I_r is the reflected shock wave pressure impulse, ρ is the shell density, h is the shell thickness, and V_o is the initial radial velocity. The kinetic energy imparted by the explosive per unit volume of the shell is

$$U = \frac{\rho V_o^2}{2} = \frac{I_r^2}{2\rho h^2}. \quad (11)$$

For each explosive shot the area under the stress-strain curve out to the unloading point must equal $U/2$, allowing for the biaxial strain. The impulse I_r depends on both the charge size and the vessel radius.⁽³¹⁾



When the nth shot is fired, the vessel has the accumulated residual strain $\epsilon_{r,n-1}$ and a stress of zero. The mechanical state of the material proceeds to the yield point $(\epsilon_{y,n}; \sigma_{y,n})$, then across the flow curve to the unloading point $(\epsilon_{y,n+1}; \sigma_{y,n+1})$, and finally down to the new accumulated strain $\epsilon_{r,n}$. Energy is conserved using the relation

$$U_n = \sigma_{y,n} (\epsilon_{y,n} - \epsilon_{r,n-1}) + (2 \sigma_{y,n} + S [\epsilon_{y,n+1} - \epsilon_{y,n}]) (\epsilon_{y,n+1} - \epsilon_{y,n}). \quad (12)$$

Eq. (12) is a quadratic equation for the new unloading strain $\epsilon_{y,n+1}$. It is then possible to calculate

$$\sigma_{y,n+1} = \sigma_{y,n} + S (\epsilon_{y,n+1} - \epsilon_{y,n}) \quad (13)$$

and finally

$$\epsilon_{r,n} = \epsilon_{y,n+1} - \sigma_{y,n+1}/E', \quad (14)$$

where $E' = E/(1 - \nu)$ is the effective elastic modulus of the shell.

Computer Analysis

A computer program BILIN was written to perform a brute-force least squares fit of the predicted values of ϵ_r from Eq. (14) to the data given in Table 1 and Figure 8. The unknowns were the initial dynamic yield stress σ_y and the slopes S_1 , S_2 , etc. of the flow curve. The cusp points (knots) were only locally fixed by specifying their occurrence at a selected unloading point.

Table 2 describes the qualitative aspects of six model fit procedures used to investigate the EMES of Frostline steel that can explain the residual strain data. A global fit means that all unknown parameters were determined simultaneously. A sequential fit means that an additional spline segment was added on after a calculation for so many shots was

TABLE 2. SUMMARY OF ANALYSIS OF THE CUMULATIVE RESIDUAL STRAIN
IN A REPETITIVELY TESTED EXPLOSION CONTAINMENT VESSEL

CASE	MODEL	FIT [†]	COMMENT(S)
A-G	Elastic-Perfectly Plastic	Global	Poor fit, predicted curve has no curvature
B-G	Elastic-Plastic, One Segment	Global	Good fit, predicted curve does not change in curvature
C-S	Elastic-Plastic, Two Segments	Sequential Segments	Excellent fit with a model having a cusp
C-G	Elastic-Plastic, Two Segments	Global	Excellent fit with a model having a cusp
D-S	Elastic-Plastic, Three Segments	Sequential Segments	Good fit, error propagation leads to a non-physical model result
D-G	Elastic-Plastic, Three Segments	Global	Excellent fit, not optimized for knot positions

[†]The yield point was variable, but the plastic-plastic knots were locally fixed by specifying the number of explosion tests applicable.

completed. The sequential method was abandoned when the fifth procedure D-S gave a non-physical (negative) value of a slope.

Table 3 gives the quantitative results from the six procedures. Case A-G is an elastic-perfectly plastic model that yields a straight line on Figure 8 due to the fact that all 22 shots used 4.54 kg (10 lb) of explosive. Case B-G is the usual elastic-plastic model with a single plastic segment. This model introduced curvature (due to work hardening) and the fit greatly improved.

Cases C-S and C-G had two plastic segments with a knot after the ninth shot. The fits are excellent because the first slope accounts for the initial curvature and the smaller second slope accounts for the later linear portion of the data.

Cases D-S and D-G had three plastic segments with knots after the fifth and twelfth shots. Case D-S turned out badly, because the error distribution in Shots 7-12 caused S_2 to be larger than S_1 . This anomaly led to a negative value of S_3 , which is not physically acceptable for 1% total residual strain. Case D-G demonstrates the advantage of global fitting. The fit is not superior to Case C-G, presumably because the knot positions were not optimized.

Cases C-G and D-G are considered the results best describing the EMES for Frostline steel. The finding that the initial dynamic yield stress σ_y is 111 ksi is consistent with past experience^(4,7,8,30) using Case B-G in program SPLAS for such steels as A-537 and HY-80. The static tensile yield strength of this Frostline steel was 60 ksi with an ultimate tensile strength of 80 ksi. Due to the nature of the impulse approximation, the correct dynamic initial yield strength for this data is probably 90 ksi. Thus the material appears to have a 50% increase in yield strength due to the strain rate.

Referring to the analysis by Duffey,⁽³³⁾ we estimate that mild steel doubles in yield strength for a strain rate of 40.4 sec^{-1} . For the impulse approximation used here, the initial strain rate for the 4.54 kg (10 lb) shots was 56.5 sec^{-1} . The 50% increase in dynamic

TABLE 3. ELASTIC-PLASTIC MODEL ANALYSIS OF THE CUMULATIVE RESIDUAL STRAIN IN A REPETITIVELY TESTED EXPLOSION CONTAINMENT VESSEL

CASE	σ_{y1}, psi (ϵ_{y1}, Z)	$S_1, 10^6 \text{ psi}$	σ_{y2}, psi (ϵ_{y2}, Z)	$S_2, 10^6 \text{ psi}$	σ_{y3}, psi (ϵ_{y3}, Z)	$S_3, 10^6 \text{ psi}$	σ_{y4}, psi (ϵ_{y4}, Z)	$E_{\text{res}}, 10^{-3}$
A-G	127,300 (0.310)	0.00	127,300 (1.401)					0.800
B-G	116,700 (0.284)	2.05	137,400 (1.293)					0.195
C-S	112,050 (0.273)	3.19	130,900 (0.862)	0.93	135,000 (1.307)			0.110
C-G	111,500 (0.271)	3.39	131,400 (0.858)	0.56	133,900 (1.312)			0.099
D-S	111,600 (0.272)	3.25	124,400 (0.665)	3.34	135,600 (1.001)	-2.41	128,000 (1.318)	0.183
D-G	109,400 (0.266)	4.25	126,200 (0.662)	1.92	132,900 (1.011)	0.20	133,500 (1.312)	0.106

yield strength over static yield strength is thus quite reasonable if the analogy with mild steel is accepted.

SUMMARY

A progress report has been given on portable, spherical explosion containment vessels. Experimental data on the elastic-plastic response of a Frostline steel vessel has been given. It has been shown that a two plastic segment mechanical equation of state for the Frostline material can accurately account for the observations. The initial dynamic yield strength deduced is physically reasonable. Recent efforts by other research groups have been reviewed. The problem with scaling laws for elastic response and the possible problem of predicting the correct explosive loading on vessels have been introduced.

ACKNOWLEDGMENTS

The guidance of L. J. Wolfson and B. S. W. Poe of the Naval Explosive Ordnance Disposal Facility was useful and significant. The experimental assistance of W. F. Schola was particularly helpful. M. A. Lavender assisted with the manuscript. The encouragement of G. C. Throner is particularly appreciated.

REFERENCES

- (1) Trott, B. D., White, J. J. and Poe, B. S. W., "Explosion Containment Vessels and Materials Evaluation for Low Service Temperature Applications", Minutes of the Nineteenth Explosives Safety Seminar, Volume I, 351-386 (1980), AD A093 521.
- (2) White, J. J., "Containment and Control of Explosions", Proc. of the 11th Symp. on Explosives and Pyrotechnics, Franklin Research Center, paper 4, 1-14 (1981).
- (3) White, J. J., Trott, B. D., and Backofen, J. E., "The Physics of Explosion Containment", Physics in Technology, 8, 94-100 (1977).
- (4) Trott, B. D., Backofen, J. E., White, J. J., and Petty, J., "Design of Explosive Blast Containment Vessels for Explosive Ordnance Disposal Units", AMMRC MS 78-3, Proc. of the Army Symposium on Solid Mechanics, 1978 - Case Studies on Structural Integrity and Reliability, 215-288 (1978), AD A059 834.
- (5) Florschutz, G. B., "Development and Testing of the Mk 634 Mod 0 Explosive Devices Container", NAVEODFAC TR-229, Naval Explosive Ordnance Disposal Facility (March 1980), AD B047 693L.
- (6) "Explosive Confinement Vessel", General Information Bulletin 76-9, FBI Bomb Data Program (1976).
- (7) Trott, B. D., Backofen, J. E., White, J. J., and Wolfson, L. J., "Trailer-Mounted Chamber for Containment of 40 Pounds of TNT" Minutes of the Seventeenth Explosives Safety Seminar, Volume I, 687-708 (1976), AD A036 015.
- (8) Trott, B. D., Backofen, J. E., White, J. J., and Wolfson, L. J., "Blast and Fragment Containment Capability of Portable Chambers", Minutes of the Eighteenth Explosives Safety Seminar, Volume I, 687-708 (1978), AD A066 568.
- (9) Trott, B. D., and White, J. J., "Design and Evaluation of an Experimental Multipurpose Blast Containment Chamber", NAVEODFAC TR-196, Final Report to Naval Explosive Ordnance Disposal Facility, Contract No. N00176-76-C-0103, Battelle, Columbus Laboratories (October 1978), AD B033 126L.
- (10) Carlson, R. W., "Confinement of an Explosion by a Steel Vessel", LA-390, Los Alamos Scientific Laboratory, Los Alamos, New Mexico (September 1945).

- (11) de Melherbe, M. C., Wing, R. D., Laderman, A. J., and Oppenheim, A. K., "Response of a Cylindrical Shell to Internal Blast Loading," J. Mech. Eng. Sci., 8(1), 91-98 (1966).
- (12) Batalov, V. A., Ivanov, A. G., Ivanova, G. G., Sofronov, V. N., and Tsytkin, V. I., "Strength of Single Layer and Multilayer Cylindrical Vessels Loaded Internally by Pulses of Various Lengths", J. Appl. Mech. and Tech. Phys. (USSR), 19, 695-700 (1978).
- (13) Buzukov, A. A., "Forces Produced by an Explosion in an Air-Filled Explosion Chamber", Combustion, Explosions, and Shock Waves (USSR), 16 (5), 555-559 (1980).
- (14) Moir, D. C., "Safety Analysis of the M-2 Confinement Systems", LASL Report, M-2 TM-264, Los Alamos Scientific Laboratory, Los Alamos, New Mexico (circa December, 1979).
- (15) Neal, T. R., "Charge Rating System for a Confinement Vessel", LASL Report, M-2 TM-260, Los Alamos Scientific Laboratory, Los Alamos, New Mexico (January 1979).
- (16) White, J. J., and Trott, B. D., "Scaling Law for the Elastic Response of Spherical Explosion-Containment Vessels", Experimental Mechanics, 20, 174-177 (1980).
- (17) Jackson, W. F., "The Containment of Blast Effects from the Detonation of Small High Explosive Charges", ARBRL-MR-03124, Ballistic Research Laboratory, Aberdeen Proving Ground, Maryland (August 1981), AD A105 164.
- (18) Duffey, T. A. and Johnson, J. N., "Transient Response of a Pulsed Spherical Shell Surrounded by an Elastic Medium", Proc. of the Seventh Canadian Congr. of Appl. Mech., Sherbrooke, P.Q., May 27-June 1, 1979, pp 447-8.
- (19) Duffey, T. A. and Johnson, J. N., "Transient Response of a Pulsed Spherical Shell Surrounded by an Infinite Elastic Medium", Int. J. Mech. Sci., 23, 589-593 (1981).
- (20) Karpp, R. R., Duffey, T. A., and Neal, T. R., "Response of Containment Vessels to Explosive Blast Loading", LA-8082, Los Alamos Scientific Laboratory, Los Alamos, New Mexico (June 1980).
- (21) Duffey, T. A., Karpp, R. R., and Neal, T. R., "Response of Containment Vessels to Explosive Blast Loading", ASME Pressure Vessel and Piping Conf., Orlando, Florida, June 27-July 1, 1982.

- (22) Ivanov, A. G., Ryzhanskii, V. A., Tsypkin, V. I., and Shitov, A. T., "Scale Effect in the Strength of a Pressure Vessel Under Internal Explosive Loading", Combustion, Explosion, and Shock Waves (USSR), 17(13), 327-331 (1981).
- (23) Zhdan, S. A., "Dynamic Load Acting on the Wall of an Explosion Chamber", Combustion, Explosion, and Shock Waves (USSR), 17(2), 241-244 (1981).
- (24) Dewar, M., "Internal Security Weapons and Equipment of the World", Charles Scribner's Sons, New York, 1979, p 77.
- (25) Holt, W. H., Berger, T. L., Mock, W., "Explosive Shock Depoling of Ferroelectric Ceramics for the Pulse Charging of Capacitors to High Voltages", NSWC TR 3891, Naval Surface Weapons Center, Dahlgren, Virginia (June 1980), AD A107 700.
- (26) "Fike 20 Liter Test Sphere", descriptive flyer, Fike Metal Products Corp., Blue Springs, Missouri (1981).
- (27) Bartknecht, W., "Explosions: Course, Prevention, Protection", Springer-Verlag, New York, 1981.
- (28) Neal, T., "Blast Confinement and Scaling Laws", Bull. Am. Phys. Soc., 25, 516 (1980).
- (29) White, J. J., Trott, B. D., and Schola, W. F., "Development of Comparative Data on the Blast Containment Capability of Several Materials", NAVEODFAC TR-189, Final Report to Naval Explosive Ordnance Disposal Facility, Contract No. N00174-76-C-0187, Battelle, Columbus Laboratories (May 1978), AD B028 042L.
- (30) Trott, B. D., "The Construction and Evaluation of Prototype Blast-Containment Chambers", NAVEODFAC TR-210, Final Report to Naval Explosive Ordnance Disposal Facility, Contract No. N00174-77-C-0372, Battelle, Columbus Laboratories (May 1979), AD B040 696L.
- (31) Goodman, H. J., "Compiled Free-Air Blast Data on Bare Spherical Pentolite", Report 1092, Ballistic Research Laboratories, Aberdeen Proving Ground, Maryland (February 1960), AD 235 278.
- (32) Baker, W. E., "The Elastic-Plastic Response of Thin Spherical Shells to Internal Blast Loading", J. Appl. Mech., 27, 139-44 (1960).
- (33) Duffey, T., "An Elastic-Viscoplastic Solution for Impulsively Loaded Rings", Int. J. Solids Structures, 8, 913-921 (1972).

AD P000448

DESIGN OF A DETONATION CHAMBER
FOR DEMILITARIZING MUNITIONS

by

M. G. Whitney

W. E. Baker

J. R. Riegel III

L. R. Garza

ABSTRACT

In this paper, we present the ideas and methods used in the concept development of a detonation chamber for use in an ordnance disposal facility. Unstable, outdated munitions would be intentionally detonated in the chamber. The chamber had three important design criteria: 1) it should not allow missile or explosive products to escape to the environment, 2) it should operate on a 23-minute cycle (from disposal detonation to detonation), and 3) it should contain detonations involving up to 100 lb of TNT equivalent energy. To satisfy the environmental demands, simple disposal methods such as detonating the ordnance in the open are eliminated. An inventory of ordnance types intended for disposal was reviewed to define the "worst case" fragment hazard.

Various concepts were evaluated to resist blast loads, including both reinforced concrete and steel construction. Structural types included suppressive shield designs, cubicals, I-beam frames with curved membrane panels (steel only), spherical shells (steel only) cylindrical shells, and water tank designs. Of the various chamber concepts evaluated, four were selected for final evaluation. They were, 1) a cylindrical concrete water tank with steel dome above, 2) a cylindrical concrete water tank with concrete dome above, 3) a steel cylinder with ellipsoidal end caps and internal I-beam/angle fragment shield, and 4) a concrete cylinder with flat end caps and an internal I-beam/angle fragment shield.

Based on the evaluation of the four concepts, either of the first two (water tanks) was recommended as the preferred choice.

I. INTRODUCTION

In 1979 Southwest Research Institute (SwRI) performed analyses to design a detonation chamber for use in demilitarizing outdated munitions. This study by SwRI was but one part of a facility study prepared by Travis-Braun and Associates, Inc., in joint venture with Splawn-Munir and Associates, Inc. SwRI was subcontractor to the Architect-Engineer. The purpose of this facility being planned is to dispose of outmoded ammunition and contaminated waste products for Red River Army Depot, with the capability of disposing of some munitions from other military facilities. The disposal facility is intended for siting at the Red River Army Depot. The Ammunition facility study was prepared for the Fort Worth District, Corps of Engineers.

The entire facility concept includes the use of a fluidized-bed reactor complex, a decontamination oven, grinder areas, slurry house, shearing/sawing/shredding areas, and the detonation chambers. All disposal systems were required to meet the then existing Environmental Protection Agency criteria. A more in-depth discussion of the entire facility concept is provided in References 1 and 2.

As mentioned, the scope of the work described in this paper included only the concept development of the detonation chamber. Items intended for disposal in the chamber were deemed as unstable or unsafe for mechanical demil by the other processes. The demil process planned for the chamber was the intentional detonation of items with complete containment required. It is stressed that the scope of work under this study by SwRI was concept development only, and the resulting designs are not final designs.

II. DESIGN CONSTRAINTS

The detonation chamber concepts were determined with several restrictions. These included:

- 1) A design value of 100 lb of TNT equivalent explosive energy as a maximum for any one firing,
- 2) Total containment,
- 3) Explosive products scrubbed or filtered before release,
- 4) Reusable for numerous firings over a 10-year period,
- 5) A 23-minute cycle time between firings,
- 6) Use with a wide variety of munitions including fragmenting rounds, and
- 7) A safety factor of four applied to the yield stress of structural steel or rebar.

III. ANALYSIS

The analysis by SwRI included consideration of both blast and fragment loads and their effects on the containment structure. Several early, obvious concepts were investigated and reviewed for practicality. The initial design philosophy for the chamber was to contain the explosion with a blast-resistant structure which is designed to last more or less indefinitely under repeated blast loads and to contain fragments with replaceable liners or shields which will last for a number of shots, being replaced as needed. Structural analysis was performed for uniform loading and one-degree-of-freedom response. Asymmetries were left for a more detailed analysis. Efficient ordnance replacement, equipment needs, rapid cleanup, rapid scrubbing, and sufficient work area all must be considered in any concept. Fragment protection was determined to present a greater design problem than blast protection for the munitions considered and a water tank concept was included for consideration. Four concepts were selected for final evaluation and comparison.

Considerations for Blast Containment

The detonation chamber should measure about the same in all major dimensions so that all internal surfaces will feel approximately equal blast loads when ordnance is detonated near the center. Also, chamber shapes which leave small surface area for a given internal volume use material more efficiently in containing internal dynamic and static pressure loads than do chambers which are much larger in one dimension than in others. These considerations dictate such shapes as spheres, short-capped cylinders, or cubes as the basic containment chamber geometry. The following geometries, as illustrated in Figure 1, were considered.

- 1) Spheres (steel construction)
- 2) Cylinder with $L/D = 1$ and flat end caps (steel and concrete construction)

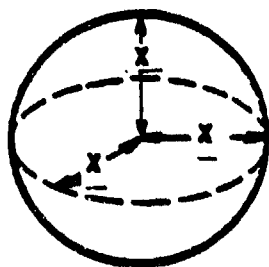
- 3) Cylinder with $L/D = 1$ and oblate spheroidal end caps
(steel construction)
- 4) Cube (steel and concrete construction).

For these four geometries, one can easily correlate the internal volume and various internal dimension with a single dimension, X , as shown in Figure 1. This dimension should be large enough to conduct normal operations conveniently; however, it is obvious that blast loads reduce as X increases. The minimum value of X was fixed as 10 feet for operational requirements and an upper limit of 50 feet was considered, for beyond this it is unlikely that the structure would be economical. The range of sizes considered was, therefore, $10 \text{ ft} \leq x \leq 50 \text{ ft}$.

Blast loads in air were determined using standard air blast curves for both the initial reflected shock and quasi-static loading. Blast pressure loading consists of several reflected short duration pulses and a relatively slow buildup to a much longer duration quasi-static pressure as illustrated in Figure 2. As suggested in Reference 3, the multiple reflected shocks are approximated for the dynamic analysis as a single triangular pulse with the same duration and 1.75 times the peak pressure as that predicted for the initial reflected pulse.

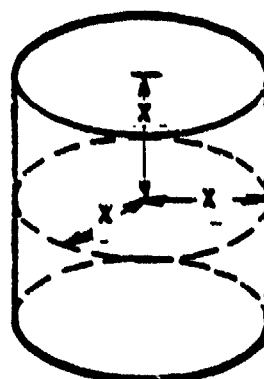
The above procedure was utilized for blast load prediction for loads in air-filled chambers. As mentioned, it proved difficult to provide fragment shielding for air-filled chambers, and water tank containment chambers were also investigated. Underwater blast curves are available in Reference 4. The minimum radii of the tanks were fixed by fragment stoppage distance but the magnitude of the underwater shocks increased the radius well beyond this. An additional step to reduce the magnitude of the underwater shocks was to provide an air cylinder about the charge to decouple the munition and the water. The prediction of underwater loads proceeded as follows:

- 1) Use air blast curves to determine shock loads at water/air cylinder interface



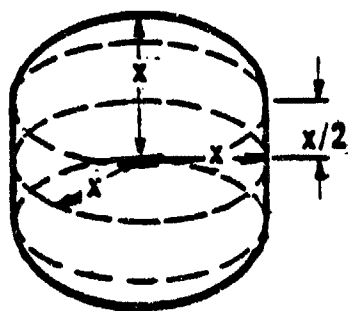
1. SPHERE

$$V = \frac{4}{3} \pi x^3$$



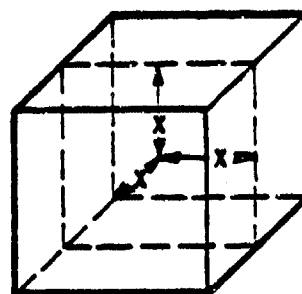
**2. CYLINDER WITH
FLAT END CAPS**

$$V = 2 \pi x^3$$



**3. CYLINDER WITH
SPHEROIDAL END CAPS**

$$V = \frac{4}{3} \pi x^3$$



4. CUBE

$$V = x^3$$

Figure 1. Geometric Shapes for Consideration

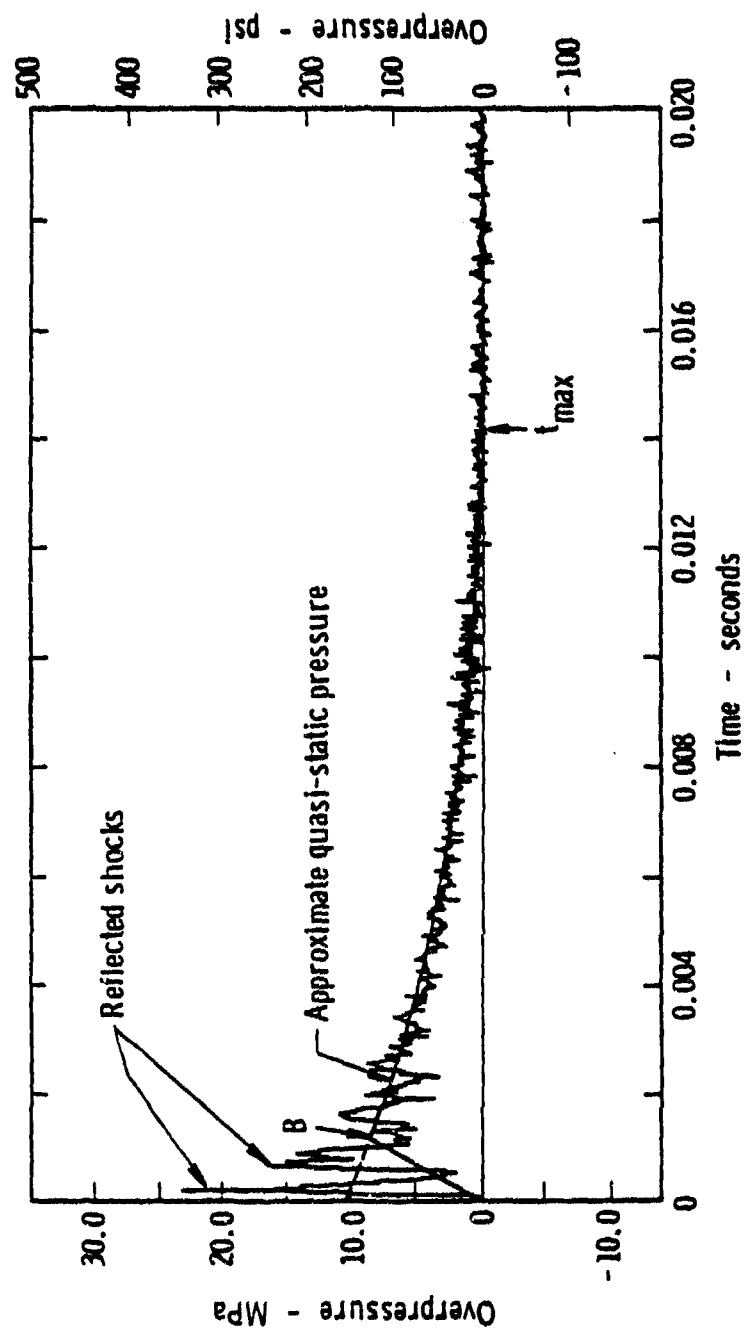


Figure 2. Typical Pressure History of an Explosion in a Vented Structure

- 2) Determine effective quantity of explosive energy which would produce the same loads at that distance in water
- 3) Use underwater shock curves to predict loading on the tank walls.

In addition to the tank loads, air shock loads and a water plume will develop above the tank, and these loads must be contained. These loads can be predicted using methods described in References 5 and 6.

Considerations for Fragment Containment

An important function of the detonation chamber is to arrest all fragments from internal munitions explosions. Because the chamber itself must be designed for quite a long life, only very low energy fragment impacts can be tolerated. Preferably, no fragment impacts should be allowed. So, this requirement dictates some type of inner structure or system which is capable of either completely arresting high speed fragments, or of slowing them and/or breaking them up so they cannot damage the blast-resistant structure. In the analysis, "worst case" fragments were identified from the inventory of munitions planned for disposal. As an example, one such fragment could be a piece of steel shell casing weighing about 3 lb, traveling at 1750 ft/sec. In assessing systems employing fragment retardation or arrest, one must consider a number of factors, which can be listed as questions:

- 1) Are proven design methods available?
- 2) Can an average recycle time of 23 minutes be attained?
- 3) Is periodic replacement needed? Is this easy or difficult?
- 4) What is the effect on gas scrubber system?
- 5) Does system complicate or ease design/construction for blast resistance?

There are a number of fragment arresting systems which could be used to protect the detonation chamber including the following:

- 1) Solid steel plate

- 2) Vented steel panels designed for suppressive shields
- 3) Spaced panels with sand fill between panels
- 4) Kevlar curtains or other exotic fragment-stopping material
- 5) Sand-filled expendable cylinders surrounding munitions
- 6) Large water tank.

Solid Steel Plate - A fragment shield can be made out of pieces of solid steel plate which will stop all fragments. These plates can be closer to the munitions than the blast-resistant structure itself, and would feel much stronger blast waves. They must be mounted on a very strong frame. Periodic replacement is mandatory, but can be minimized by using many panels and replacing only those which show severe fragment damage. Cleanup should be relatively simple, and there is no effect on a gas scrubber system. Blast loads on the blast-resistant chamber will be strongly attenuated, in fact, the blast-resistant design problem is transferred from the blast chamber to the frame for supporting the solid steel fragment arrest panels. The chamber itself could be thick enough to stop the fragments, but the structural integrity would be compromised and effect the blast-resistant capabilities.

Vented Steel Panels - A number of types of vented steel panels, employing assemblies of standard structural shapes, were designed and tested during the suppressive structures program. Two types which could easily be used to catch fragments are panels made up of nested angles and interleaved I-beams. Proven design methods for fragment arrest are readily available for these panels. (Reference 3) Because they are vented, they carry some blast loading but also pass some blast which will impinge on the chamber. So, an intermediate strength support frame will be needed. Because of blast attenuation by the vented panels, the loads on the blast chamber are reduced and a lighter design will suffice. Cleanup and periodic replacement problems should be similar to solid steel panel design, and there is no effect on the scrubber system.

Spaced Panels with Sand Fill - The main framework would consist of deep section I-beams. These are spanned by sections of commercial steel roof decking, with several feet of sand fill between inner and outer decking panels. The

decking panels are quite thin, so fragment arrest must be accomplished primarily by the sand fill. The I-beam frame must be of similar strength as for support of solid steel fragment panels, because the panels do not vent. Inner decking panels will probably require frequent replacement. Cleanup will be more difficult than for steel fragment panels, because sand will leak out of the panels when the inner decking is perforated. Dust may complicate scrubber functioning. Because this design carries the blast loads in the support framework for the sand-filled panels, the blast chamber design can be drastically lightened, as is true for any unvented fragment arresting design.

Kevlar Curtains or Other Exotic Fragment-Stopping Material - The relatively new DuPont fiber Kevlar has been found to be an excellent material for arresting high-speed fragments either as Kevlar cloth curtains or when formed into fiber-reinforced rigid panels using an epoxy resin matrix. The loose cloth could be used to catch fragments, suspended from a framework. Rigid Kevlar-epoxy panels or other exotic material could replace steel fragment arrestors. Although these concepts will work as well as any other unvented fragment stopping concept, the high cost would probably prohibit its use.

Sand-Filled Expendable Cylinders - Figure 3 illustrates this concept. The sand packed around the exploding munition arrests the fragments. The cylindrical sonotube container for the sand ruptures. Both sand and pieces of sonotube disperse and impinge on the detonation chamber inner surfaces. The air cavity shown in the figure may or may not be needed to decouple strong shock waves from the sand and prevent sand displacement before fragment arrest. The fragment arresting system is expended with each detonation in this concept. It is also a very "dirty" system, scattering debris all through the detonation chamber with every shot. Scrubbing and cleanup would both be difficult. Also, design concepts are not proven.

Even though this concept has certain advantages such as strong blast wave attenuation and very low initial cost, the other disadvantages probably outweigh these advantages.

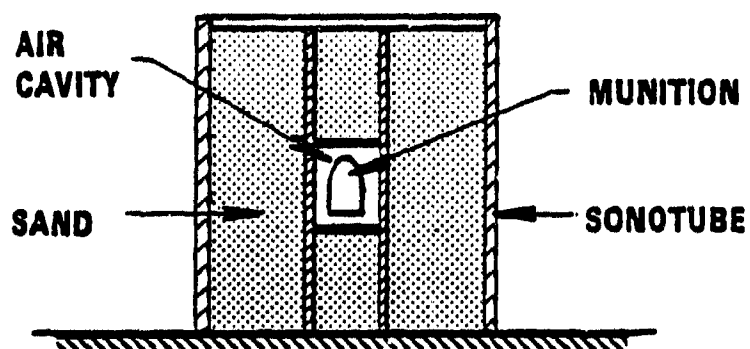


Figure 3. Concept for Expendable, Sand-Filled
Fragment Arrestor Placed Inside the Detonation Chamber

Large Water Tank - A system used in the Netherlands for complete recovery of fragments from detonating shells appears very attractive for this application. The Dutch system is described in Reference 7, and shown in Figure 4. This system has many advantages. The water slows the fragments so that they never impinge on the walls of the tank or emerge from the water surface with enough velocity to cause any structural damage. The water also drastically reduces air blast above the tank, so a very light chamber covering the tank will suffice. Rapid turnaround of munition detonation is possible, if a number of the expendable air cylinders are made up beforehand.

The air cylinder and bubble curtain shown in Figure 4 are needed to decouple direct underwater shock from the tank walls. The air cylinder can present an operational problem, because it is buoyant in water and must be drawn beneath the surface and held there by a pulley and cable system, as indicated in the figure.

Cleanup should be very simple with this system, because all fragments will remain in the tank and fall to the bottom. Periodically accumulated fragments can be cleaned out. Some filtering or cleanup system may be needed for the water, because explosion products will be intimately mixed with the water with each explosion.

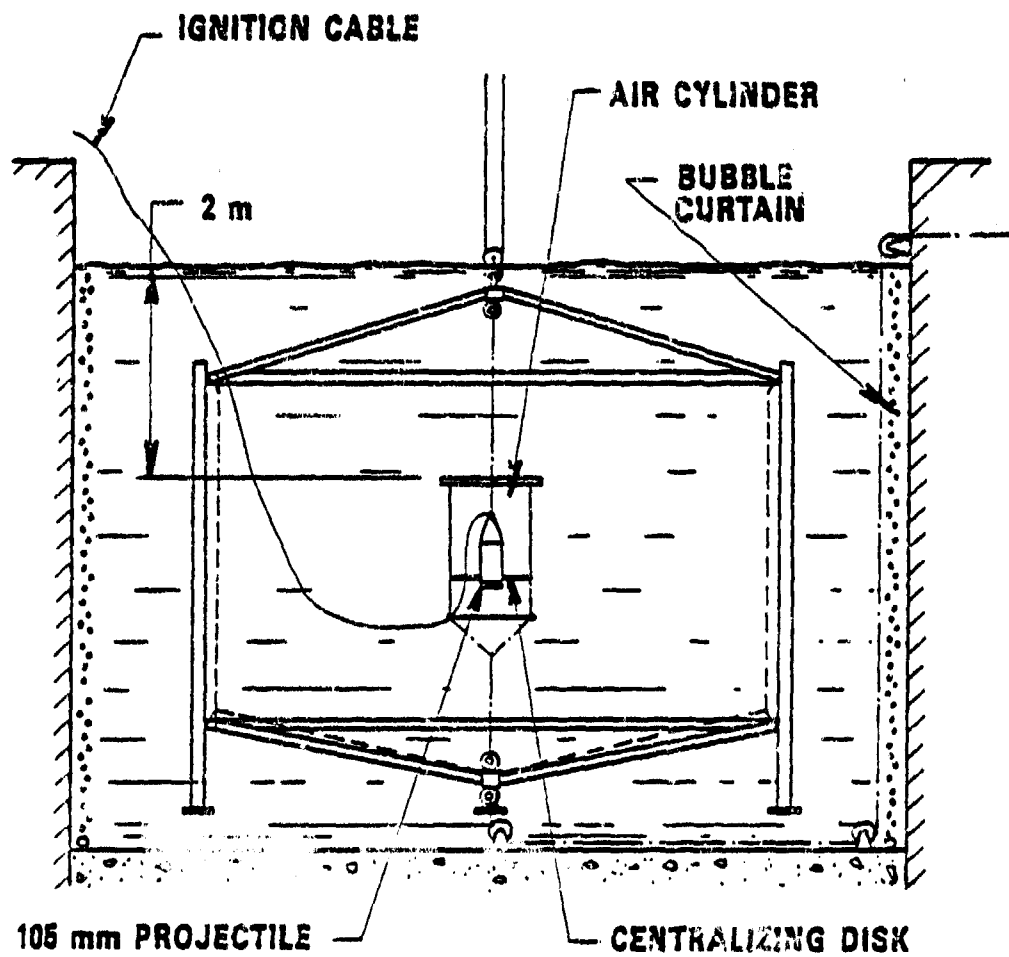


Figure 4. Test Basin Used in the Netherlands
For Complete Fragment Recovery

IV. CHOICE AND COMPARISON OF PREFERRED CONCEPTS

Weighing the various factors cited in previous sections of this paper it was felt that the last concept discussed, the water tank, has many advantages over all other systems. It was the recommended choice. As a backup in the event that the water tank is not operationally acceptable to the customer, the concept of vented steel panels similar to panels in suppressive shields was recommended as the second choice. The fragment arrestor would be placed inside cylindrical containment structures. The cylindrical shape was determined in structural calculations to be more material efficient than the box shape and more space efficient than the spherical geometry. The final four concepts include:

- 1) a reinforced concrete (R/C) tank with steel dome above,
- 2) a R/C tank with a concrete dome above,
- 3) a steel cylinder with oblate spheroidal end caps and internal fragment shield, and
- 4) a R/C cylinder with flat end caps and an internal fragment shield.

Figures 5 - 9 illustrate these concepts. As noted earlier, the air blast analysis was performed for direct loading to the structure from shock pulses driven through air above. Also, as suggested earlier, the use of a suppressive-type shield would significantly reduce the shock loads transmitted to the blast-resistant shell. The designs shown here have not been refined to include these reduced loads. If further consideration of these concepts is desired, then analysis should include this refinement. But, the basic conclusions made from this study are not expected to change.

A comparison of the four concepts was made and is summarized in Table 1. A cost comparison for "empty shell" structures (i.e., only the basic superstructure of walls, roof, and foundation) indicated that either of the two water tank designs was much less expensive than the air chambers. The same conclusion was made for expendable material costs. Operational considerations were also compared, and again the water tank concepts were rated superior.

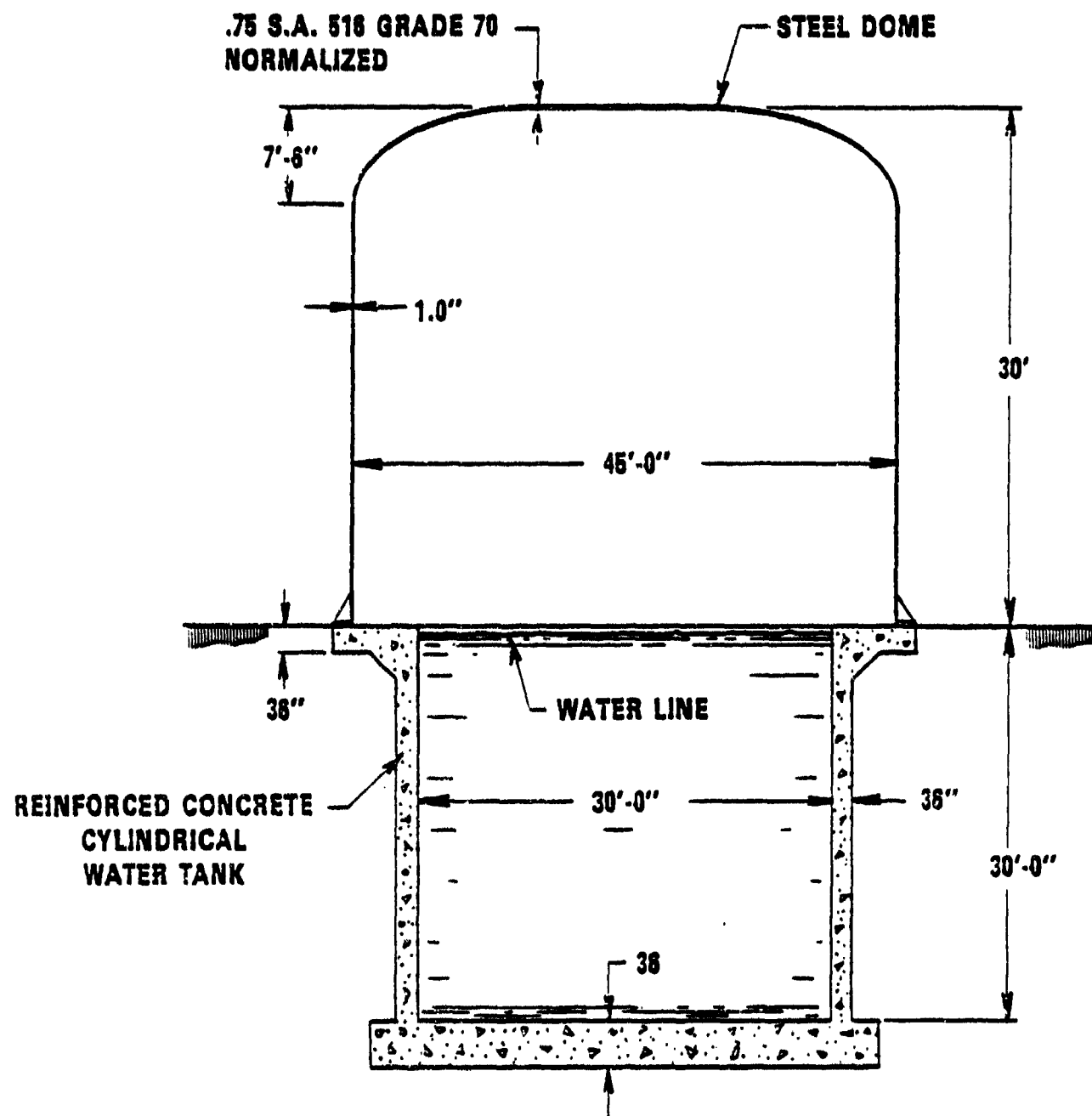


Figure 5. Concept No. 1 (Steel Dome)

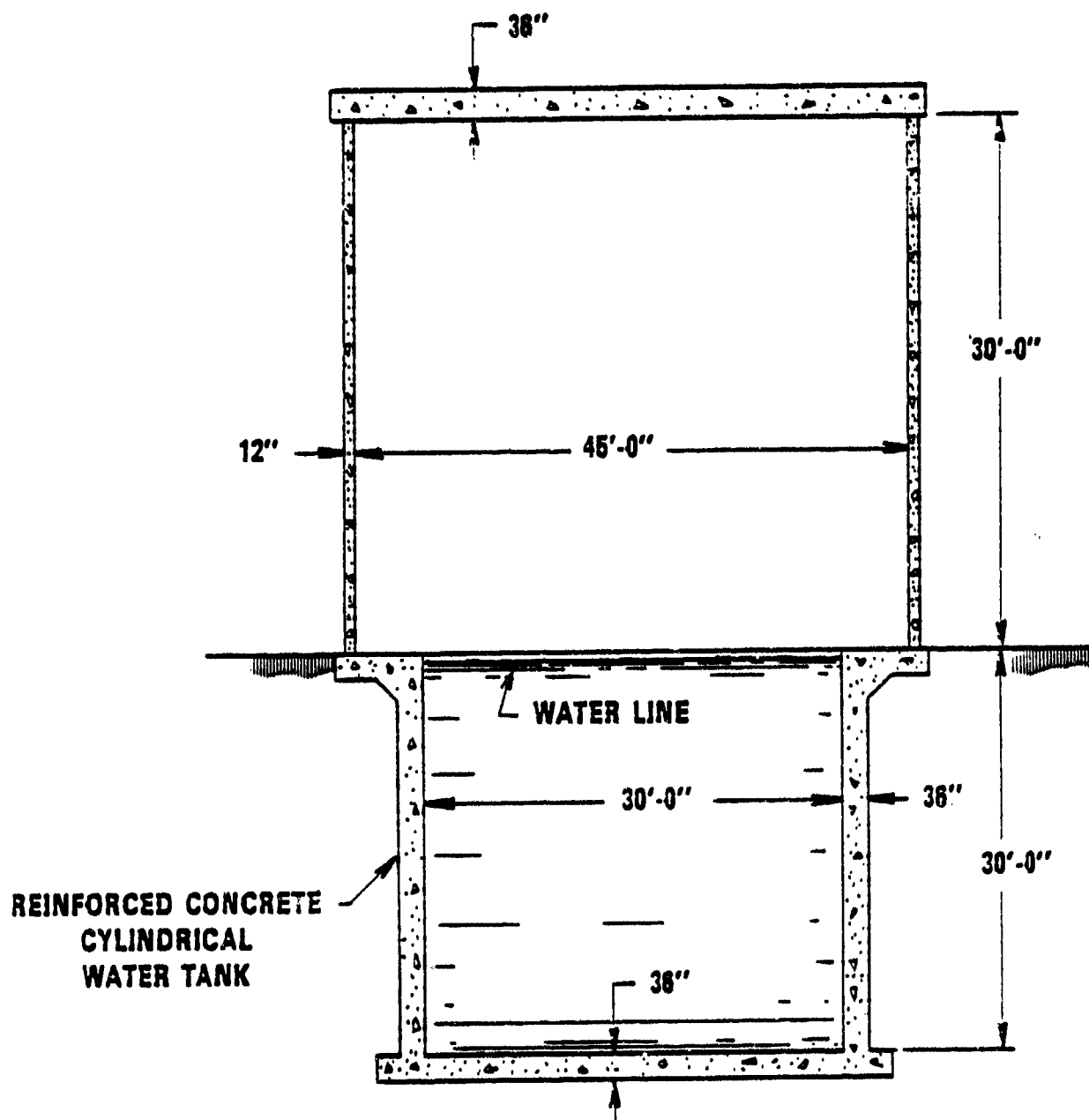


Figure 6. Concept No. 2 (Reinforced Concrete)

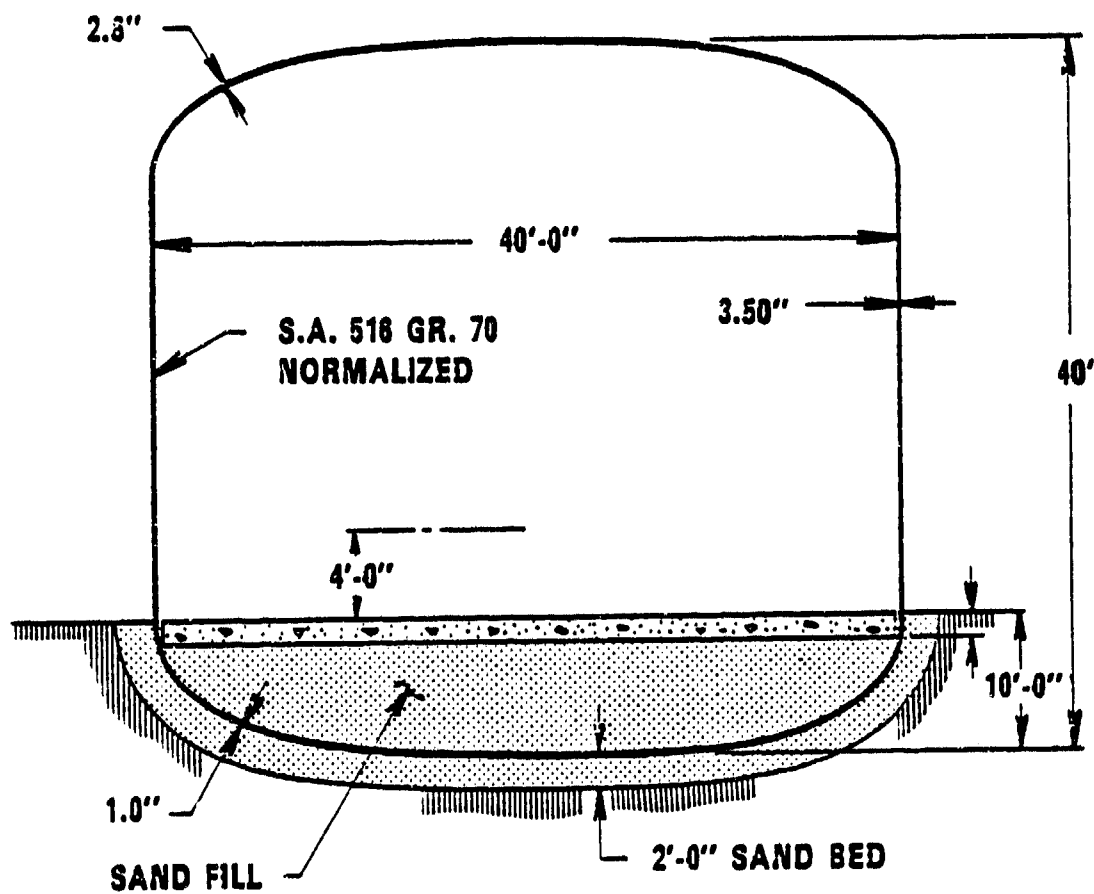


Figure 7. Concept No. 3 (Sheet 1. Outer Shield)
 565

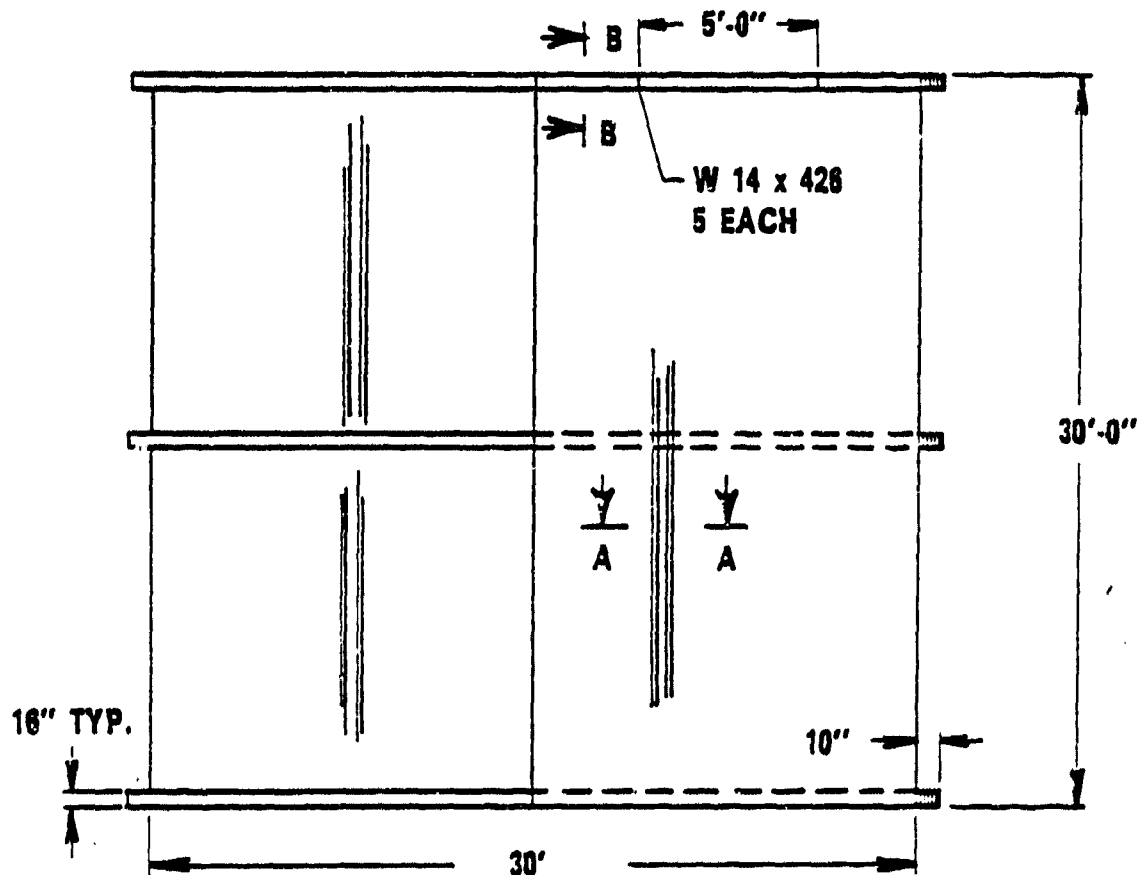
TEN LAYERS OF 1" THICK
STEEL HOOPS EACH.
EACH INSTALLED AND
WELDED INSIDE OUT
(TYP. 3 PLACES)

SECT. A-A

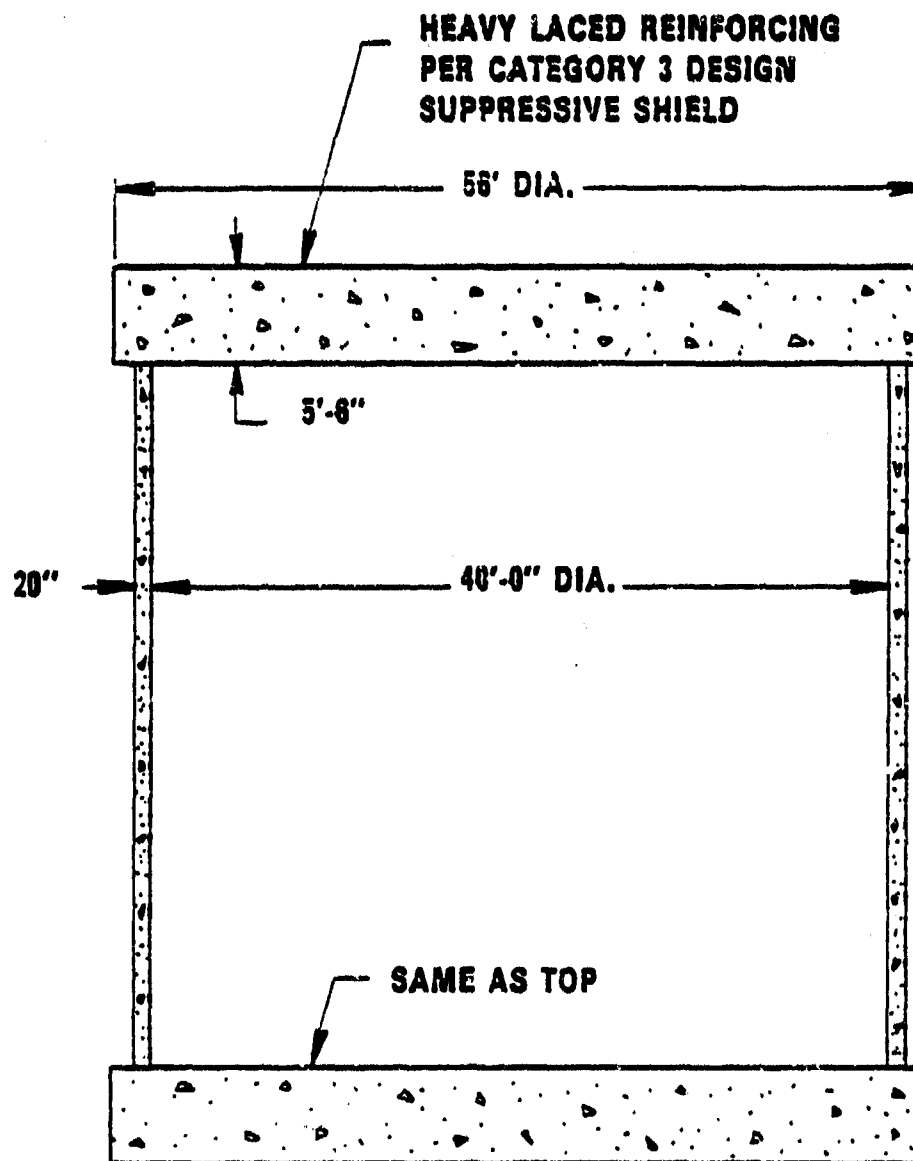
8 x 8 x 1-1/8 < 56.9 1/FT.
SPACED \pm 3" APART

SECT. B-B

ROOF NESTED < IRON
(TO BE SIZED)



Inner Frag Shield
Figure 8. Concept No. 3 (Sheet 2)



REINFORCED CONCRETE VERTICAL CYLINDER
(REQUIRES INNER FRAG SHIELD CONCEPT NO. 3)

Figure 9. Concept No. 4

V. RECOMMENDATIONS

We strongly recommended that the water tank concepts be evaluated further in detailed studies. Also, no mention has been made of the effect of a "bubble curtain" (see Figure 4) on the demil detonation chamber design, for the tank was designed without it. Further evaluation of this system should be incorporated in future studies. Additional consideration of the air-cylinder design and radii is necessary. Cycle times for the detonation chamber concepts need to be determined and modifications made accordingly.

REFERENCES

1. "Red River Army Depot Ammunition Depot Facility Study," Contract No. DACA63-78-C-0080, by Travis-Braun and Associates, Inc., and Splawn-Munir and Associates, Inc., prepared for the Department of the Army Fort Worth District Corps of Engineers, 15 September 1978.
2. "Concept Data Brochure - Ammunition Disposal Facility, Red River Army Depot, Texas," Contract DACA63-79-C-0164, Travis-Braun and Associates, Inc., and Splawn-Munir and Associates, Inc., prepared for the Department of the Army Fort Worth District Corps of Engineers, December 1979.
3. "Suppressive Shields Structural Design and Analysis Handbook," HNDM-1110-1-2, U. S. Army Corps of Engineers Huntsville Division, November 1979.
4. R. H. Cole, Underwater Explosions, Princeton Univ. Press, 1948 (Reprinted by Dover Publications, Inc., in 1965).
5. M. M. Swisdak, Jr., "Explosion Effects and Properties: Part I - Explosion Effects in Air," NSWC/WOL TR-75-116, Naval Surface Weapons Center, White Oak, Silver Spring, MD, October 1975.
6. M. M. Swisdak, Jr., "Explosion Effects and Properties: Part II - Explosion Effects in Water," NSWC/WOL TR-76-116, Naval Surface Weapons Center, Dahlgren, VA, February 1978,
7. B. Janzon and H. J. Pasman, "Fragmentation of H.E. Warheads. A Comparison Between Two Experimental Methods for Evaluating Fragment Mass Distribution," Proc. of First Int. Symp. on Ballistics, ADPA, Orlando, FL, November 1974, pp. IV - 131 through IV - 144.

DESIGN OF THE ADVANCED HIGH KINETIC ENERGY LAUNCH SYSTEM

W. V. Hill
Black & Veatch
Kansas City, Missouri

AD P000449

ABSTRACT

↓
This report describes the design of a facility to provide for destructive testing of U.S. and foreign munitions, up to and including 155 mm. The facility consists of a Range Tunnel designed to resist the muzzle blast of an artillery weapon and a large steel dome structure designed to contain the blast effects of 64 pounds of TNT.

INTRODUCTION

↑
The Advanced High Kinetic Energy Launch System is to provide the Ballistic Research Laboratory (BRL) a facility for the destructive testing of U.S. and foreign munitions, up to and including 155 mm. Munitions to be tested include kinetic energy projectiles (KE), advanced chemical energy (CE), self-forging fragment (SFF), and reactive armors (RA).

The facility consists of a Range Tunnel, 25 feet wide, 21 feet 3 inches high, and 280 feet long (See Figure 1). There is a suppressive door at the entrance to the tunnel to trap missiles and fragments should an accidental explosion occur in the tunnel. The Target Room is a steel dome-shaped structure 60 feet in diameter, designed to contain the blast effects of 64 pounds of TNT. The equipment door is 14 feet wide by 18 feet high. The Instrumentation Building is 16 feet by 33 feet and is constructed of concrete block. The well provides 30 gallons per minute of water for washdown of the Range Tunnel and Target Room. The Holding Tank contains the contaminated washwater and the exhaust filter system removes radioactive dust from the Target Room. Site work includes access roads, parking area, electrical power service, area lighting, underground telephone cable, and a cable trench from the Instrumentation Building to an existing Control and Firing Building. At the present time, the

facility is under construction at Aberdeen Proving Ground, Maryland and is scheduled to be completed early in 1983.

RANGE TUNNEL

The Range Tunnel is designed to resist the dynamic loads from the muzzle blast of an artillery weapon. The muzzle blast loads, at various angles of incident, were provided by Dr. Charles Kingery of BRL. From the blast data received, we developed the idealized pressure-time curves for an angle of incident of 0, 30, and 45 degrees. The idealized pressure-time curves were developed by the use of methods given in Reference No. 1. The maximum load occurs at an angle of incident of 45 degrees where the peak reflected pressure is 57 psi, duration of the positive phase is 4.5 milliseconds, and the positive reflective impulse is 128 psi-milliseconds (see Figures 2 and 3).

The original criteria and concepts called for the Range Tunnel to be constructed of existing armor plate. When the actual design of the Advanced High Kinetic Energy Launch System started, the armor plate had been used in another project. Both steel plate and reinforced concrete were investigated for use in the construction of the Range Tunnel. The reinforced concrete had the lower cost. An economic study on various thicknesses of concrete and the amount of reinforcing required was also made.

For the design of the Range Tunnel, we used a dynamic load factor calculated using Reference 2. The design of the roof slab was then checked by using the Acceleration-Pulse Extrapolation Method of Numerical Integration given in Reference 3.

As you can see from Figure 4, for the roof slab design the values for both the dynamic load factor method and numerical integration are identical, except for the time of maximum deflection. The 6.30 milliseconds was the increment of time nearest to the 6.21 milliseconds. The clear span of the walls are 16 feet and the roof slab spans 20 feet. The elastic unit resistance is 73.0 psi for the walls and 46.7 psi for the roof slab. The natural period of vibration for the walls is 11.9 milliseconds and 18.6 milliseconds for the roof slab. The dynamic load

factor for the walls is 1.03 and for the roof slab 0.71 milliseconds. The equivalent elastic deflection is 0.0503 inches and 0.0785 inches. The maximum deflection is 0.040 inches and 0.068 inches. The maximum deflection occurs at 4.32 milliseconds for the walls and 6.21 milliseconds for the roof slab. Dividing the elastic deflection into the maximum deflection gives a ductility ratio of 0.80 for the walls and 0.87 for the roof slab.

Using a thickness of 2 feet 6 inches, with No. 9's at 12 inches for the positive reinforcing steel and No. 11's at 12 inches for the negative reinforcing bars proved to be the most economical section (see Figure 5). Temperature reinforcing is No. 8 at 14 inches each face. The direct tension bars are No. 10's at 12 inches and No. 4 stirrups were used at 12 or 14 inches, as required. The reinforcement used was ASTM A615, Grade 60 except for the stirrups for which Grade 40 was used. Two 7/8-inch bolts were installed on the centerline of the roof for a future 5-ton monorail to be installed when funds become available.

TARGET ROOM

Figure 6 shows the floor plan of the Target Room. The structure is designed for repeated blast loads of 64 pounds of TNT equivalency. Some of the ammunition to be tested will contain heavy metal and it was necessary to design the Target Room to contain the explosion, except for leakage through the shot hole into the Range Tunnel and through the vents into the filter system. On each side of the doors you can see the structural tee stiffeners. The opening through the mat foundation in the center is for placement of the targets.

The upper part of the Target Room is designed as a dome with a radius of 29 feet 6 inches (see Figure 7). The dome is supported by a ring beam constructed of one-inch plates. The lower portion of the Target Room, below the ring beam, is a section of a cone. The diameter of the top of the cone, where it is attached to the ring beam, is 46 feet 9 inches and the diameter of the base of the cone is 59 feet. The height of the section of the cone, below the ring beam, is 18 feet one inch and the rise of the dome is 11 feet 6 inches.

The Target Room was designed by the trial-and-error method. We first assumed the structural members then we reviewed the structure to determine the stress in the members. The blast loadings on the interior of the Target Room from 64 pounds of TNT were also received from BRL. From these, we developed the idealized pressure-time curve (see Figure 8). The peak gas pressure is 15 psi. Even though there is some decaying of the gas pressure, we assumed a zero rate of decay and considered the 15 psi gas pressure to be constant. The peak positive reflected pressure was calculated to be 75 psi, giving a total peak positive pressure of 90 psi. The positive reflected impulse is 60 psi-milliseconds and the duration of the positive phase is 1.6 milliseconds.

To obtain the natural period of vibration of the various members of the Target Room, we used a computer program called the "Finite Element Method for the Dynamic Analysis of Structures Subject to any Dynamic Loading" (Reference No. 4).

The dynamic load factor was then calculated. For the gas pressure, a dynamic load factor of 1 was used and the gas pressure was considered constant. An equivalent static load was then calculated and STRUDL was used to find the stresses in the various members (Reference 5).

For our first trial, we used vertical stiffeners between the ring beam and foundation on 4-foot 2-inch centers completely around the structure. The analysis showed that the side wall plates were carrying the loads in ring tension and the stiffeners near the door were the only ones being stressed. The next step was to keep eliminating stiffeners. The final design has three stiffeners on each side of the equipment door and one on each side of the personnel door (see Figure 6). Additional steel plates were welded around the other openings. Everything was designed with a ductility factor less than 1 so all elements would remain in the elastic range.

Both the side walls and dome were constructed of one-inch plate. For the dome and ring beam, we used ASTM A516 steel, Grade 70, which has a minimum yield stress of 38,000 psi, and using a dynamic increase factor of 1.1 resulted in a dynamic yield stress of 41,800 psi. ASTM

A516 steel was used for the dome because it is easy to shape and is readily weldable. ASTM A572, Grade 60 is classified as a high strength, low alloy structural steel and was used for its availability, high strength, and weldability for the rest of the structure. The minimum yield stress is 60,000 psi and it has a dynamic yield stress of 66,000 psi.

The maximum circumferential stress in the dome is 7,560 psi and the maximum meridional stress is 9,050 psi (see Figure 9). The maximum stress in the ring beam, which occurs at the equipment door jambs, is 16,800 psi. Using ASTM A516 steel the dynamic yield stress was 41,800 psi. For the side walls the maximum circumferential stress is 14,780 psi and the maximum meridional stress is 7,410 psi. The maximum stress was in the door jambs which were subject to tension and bending in two directions. The stress was 45,700 psi. The stress in the door stiffeners along each side of the equipment door was 49,380 psi and the maximum stress in the equipment door itself was 51,300 psi. For the side walls, door jamb, door stiffeners, and door, the dynamic yield stress of the steel used is 66,000 psi.

Some of the armor piercing ammunition to be tested contains heavy metal which has a low grade of radioactivity. Upon striking the target, the projectile explodes and the dust formed cannot be discharged into the atmosphere. The air evacuation and filtration system consists of a fan which pulls 24,000 cubic feet per minute of air through the suppressive door (see Figure 10).

The door is constructed of interlocking wide flange beams. This allows air to pass through the door but will trap missiles and fragments should an accidental explosion occur in the tunnel. Air is pulled from the tunnel into the Target Room through the 36 inch diameter shot hole. The contaminated air leaves the Target Room through two 36 inch diameter ducts to the attenuators. The attenuators are used to protect the filters from excessive blast pressures. The attenuators were existing and furnished by BRL. They are 10 feet in diameter and 50 feet long, made up of one-inch plate. No attempt was made to determine how effective the

attenuators will be in reducing the blast pressure to the filters. Three sets of filters are used in series: prefilters, secondary filters, and high efficiency particulate air filters which have an efficiency of not less than 99.99 percent when tested with 0.3 micron smoke.

The personnel door and the equipment door are sealed by using compressed air seals. Provisions have been made to wash down the dust that gets into the Range Tunnel through the shot hole. Miscellaneous items in the Range Tunnel and Target Room include view ports for cameras and lighting, tie downs for the weapon, unistruts for attaching equipment to the walls, PA system, telephone, power receptacles, and lighting.

REFERENCES

1. TM 5-1300, Structures to Resist the Effects of Accidental Explosions, June 1969 and Change No. 1, dated March 1971.
2. TM 5-856-3, Principles of Dynamic Analysis and Design, March 1957 and Change No. 2, dated November 1973.
3. C. H. Morris, R. J. Hansen, M. J. Holley, J. M. Biggs, S. Manyet, and J. K. Minami, Structural Design for Dynamic Loads, 1959.
4. Computer Program S73, Dynamic Stress Analysis Axisymmetric Structures, Black & Veatch, February 1976, Revised January 1980.
5. Computer Program S50, Structural Design Language (Univac 1100 ICES/STRU DL), Black & Veatch, September 1975, Revised November 1980.

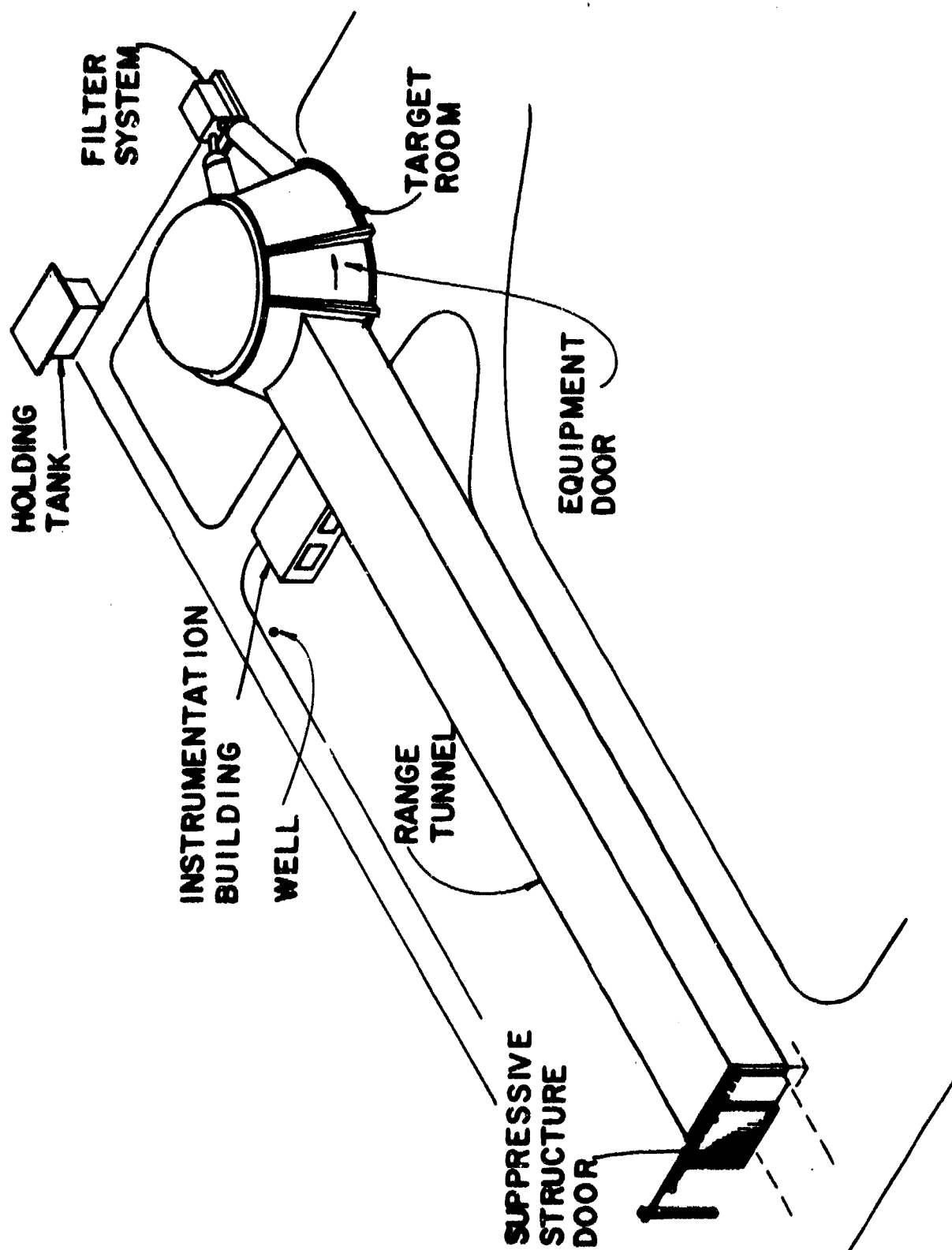
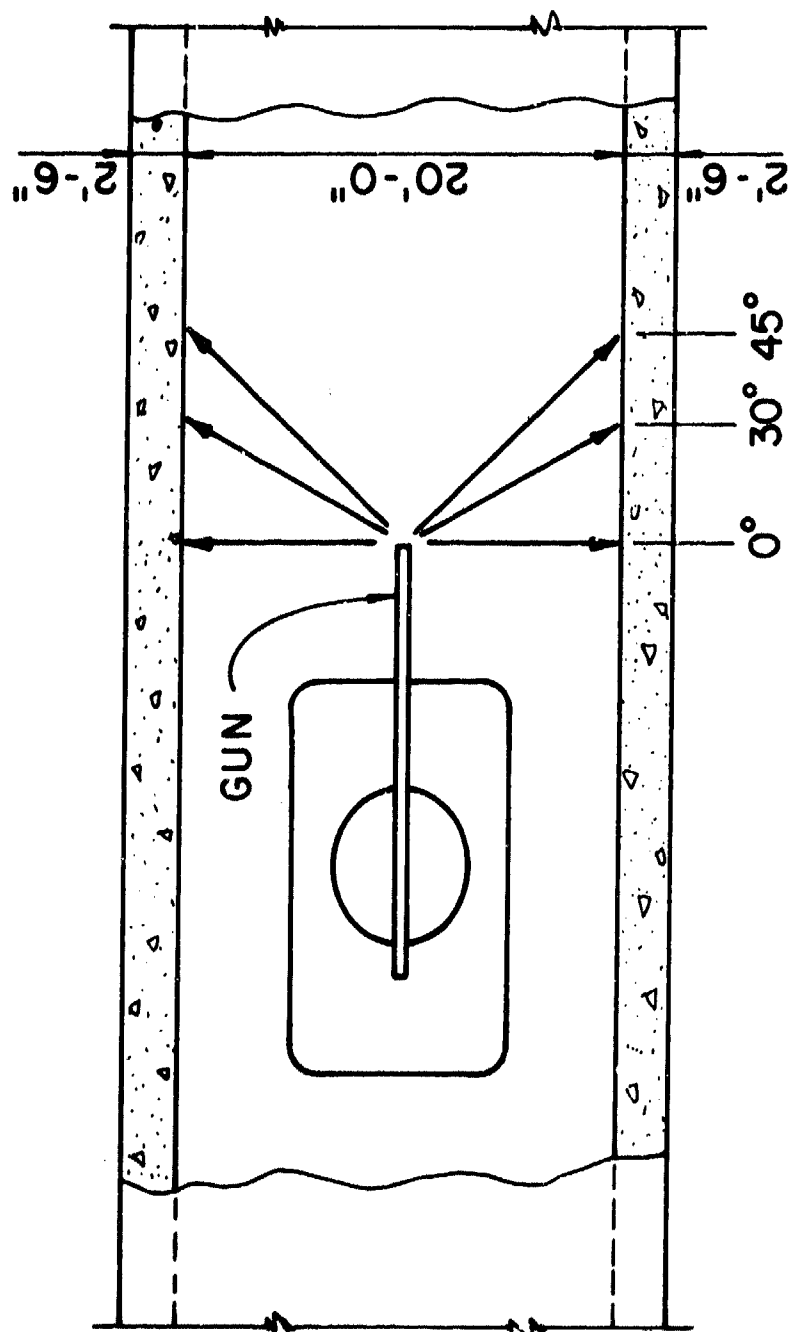
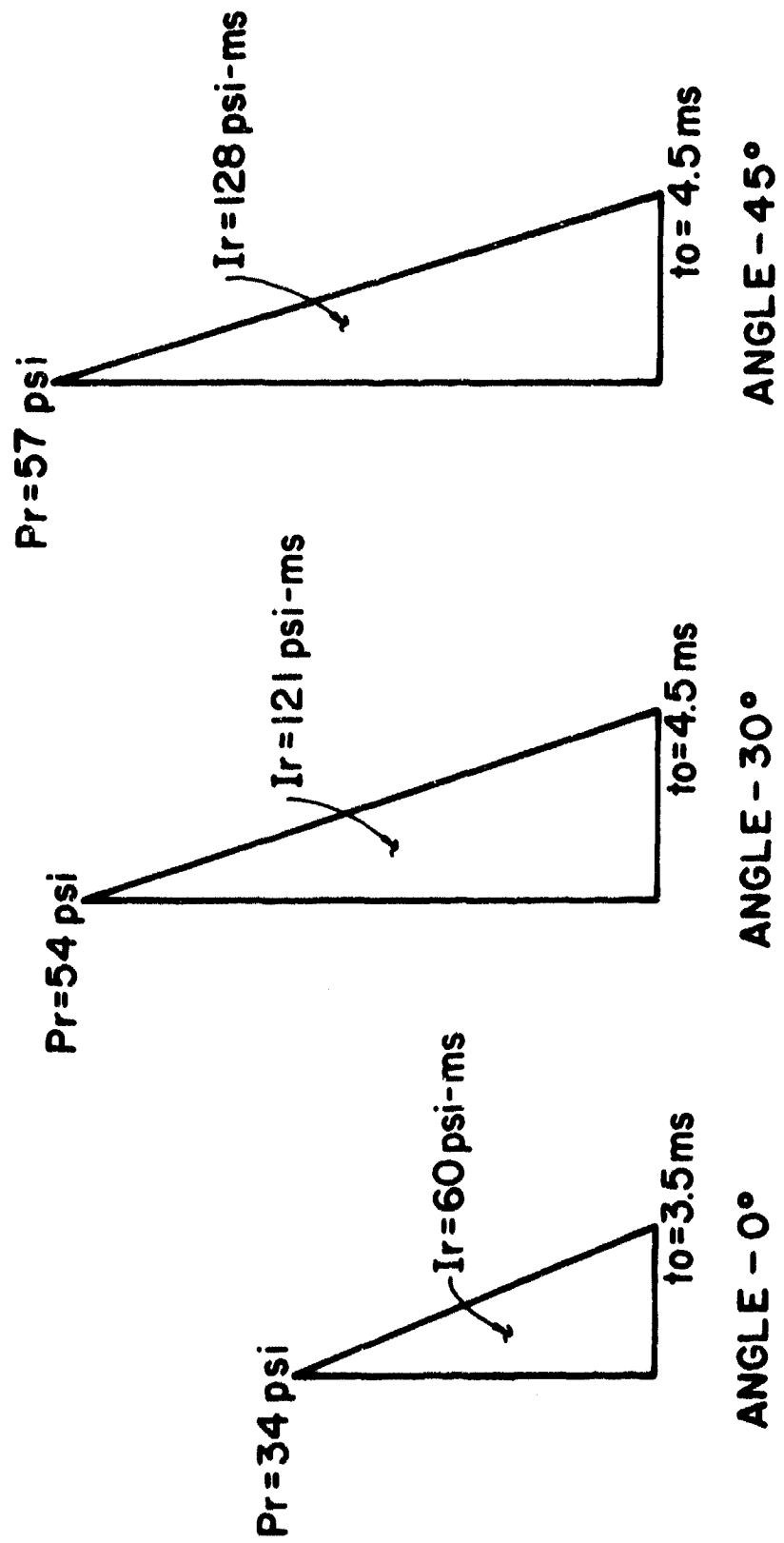


FIGURE 1



PLAN RANGE TUNNEL

FIGURE 2



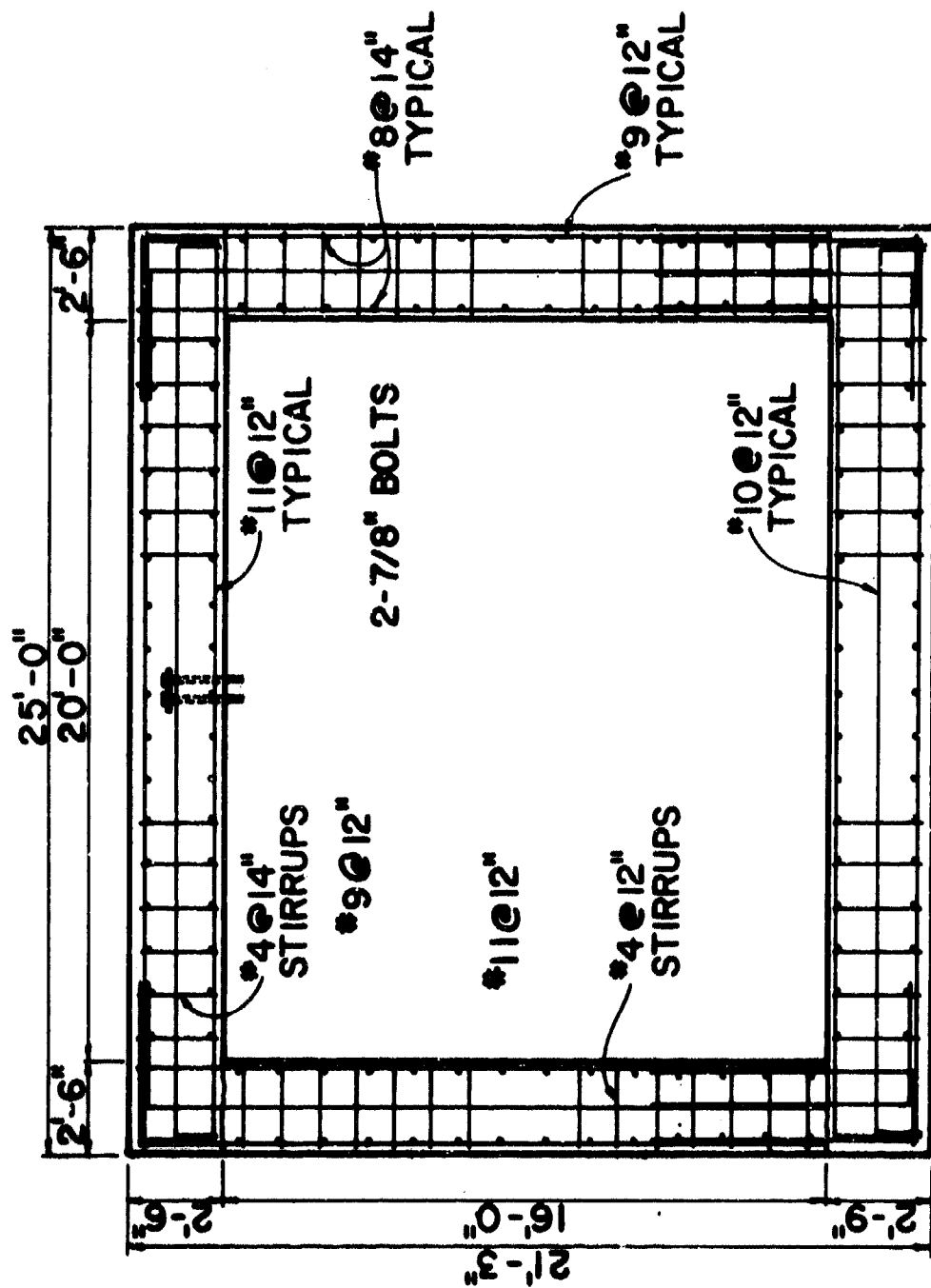
IDEALIZED PRESSURE-TIME CURVE

FIGURE 3

RANGE TUNNEL

	<u>ROOF SLAB</u>	
	<u>DYNAMIC</u> <u>LOAD FACTOR</u>	<u>NUMERICAL</u> <u>INTEGRATION</u>
SPAN	20.0'	20.0'
ELASTIC UNIT RESISTANCE	46.7 psi	46.7 psi
NATURAL PERIOD OF VIBRATION	18.6 ms	18.6 ms
DYNAMIC LOAD FACTOR	0.71	—
ELASTIC DEFLECTION	0.0785"	0.0785"
MAXIMUM DEFLECTION	0.068"	0.068"
TIME MAXIMUM DEFLECTION	6.21 ms	6.30 ms
DUCTILITY RATIO	0.87	0.87

FIGURE 4



RANGE TUNNEL SECTION

FIGURE 5

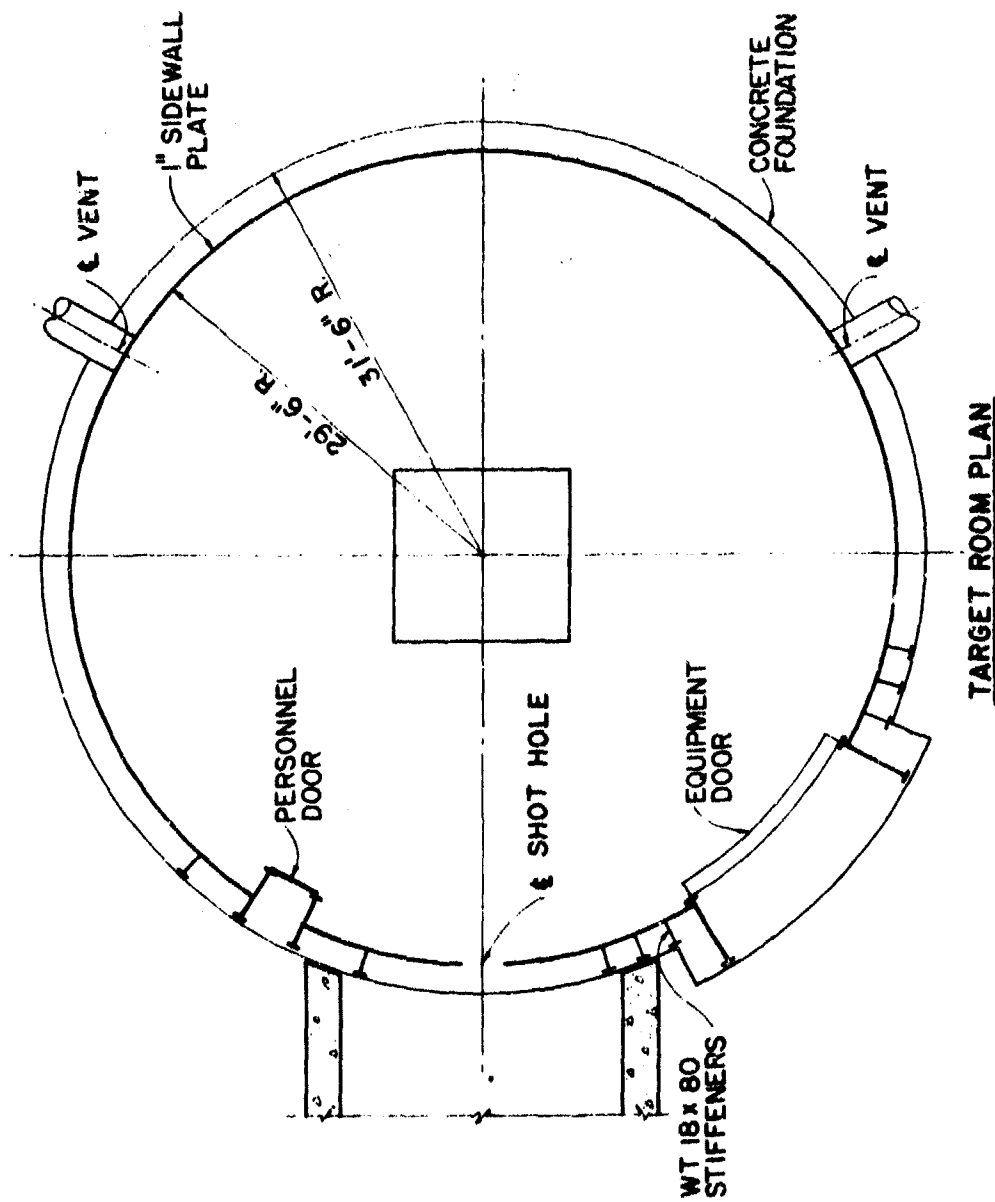


FIGURE 6

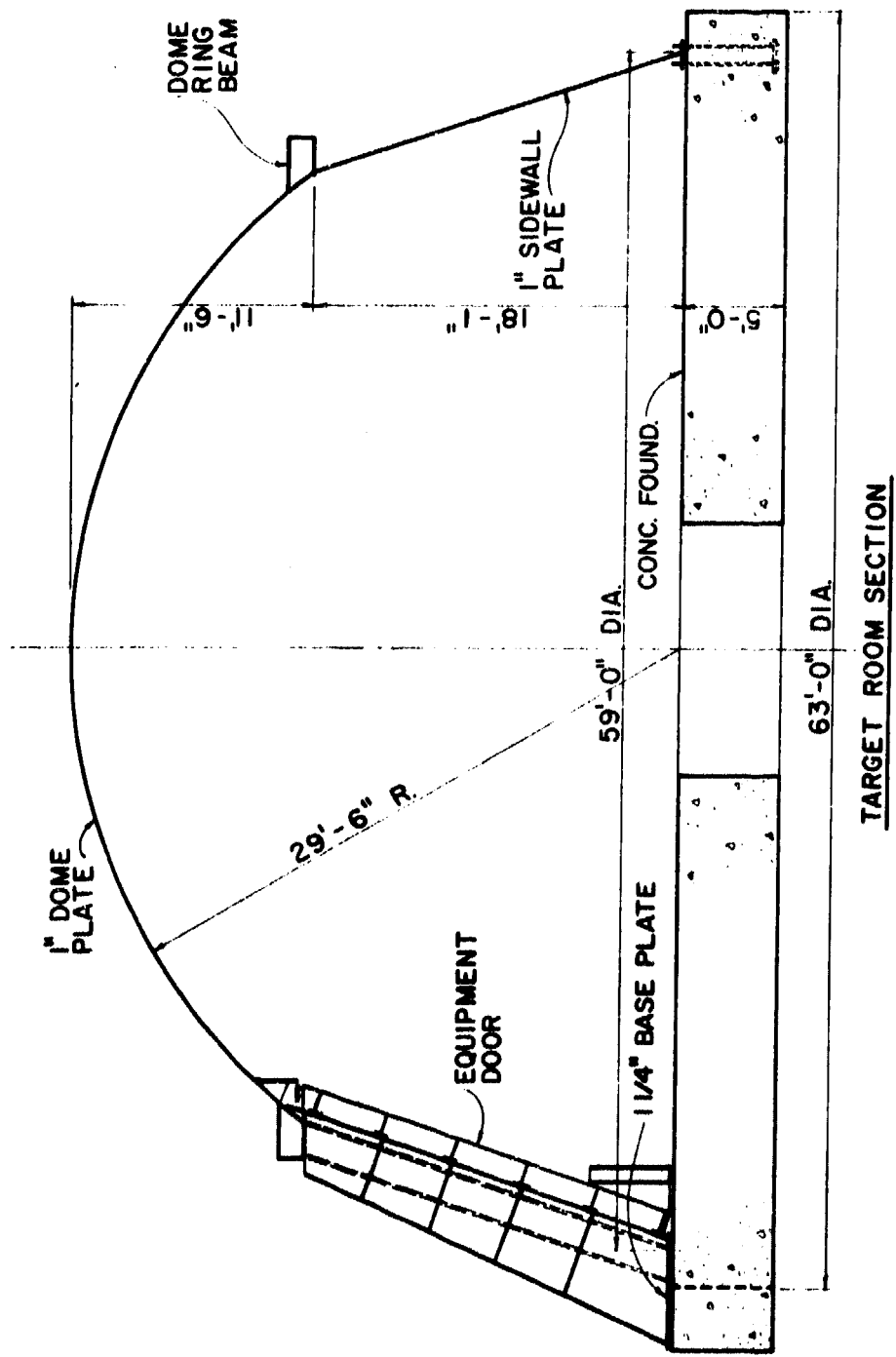
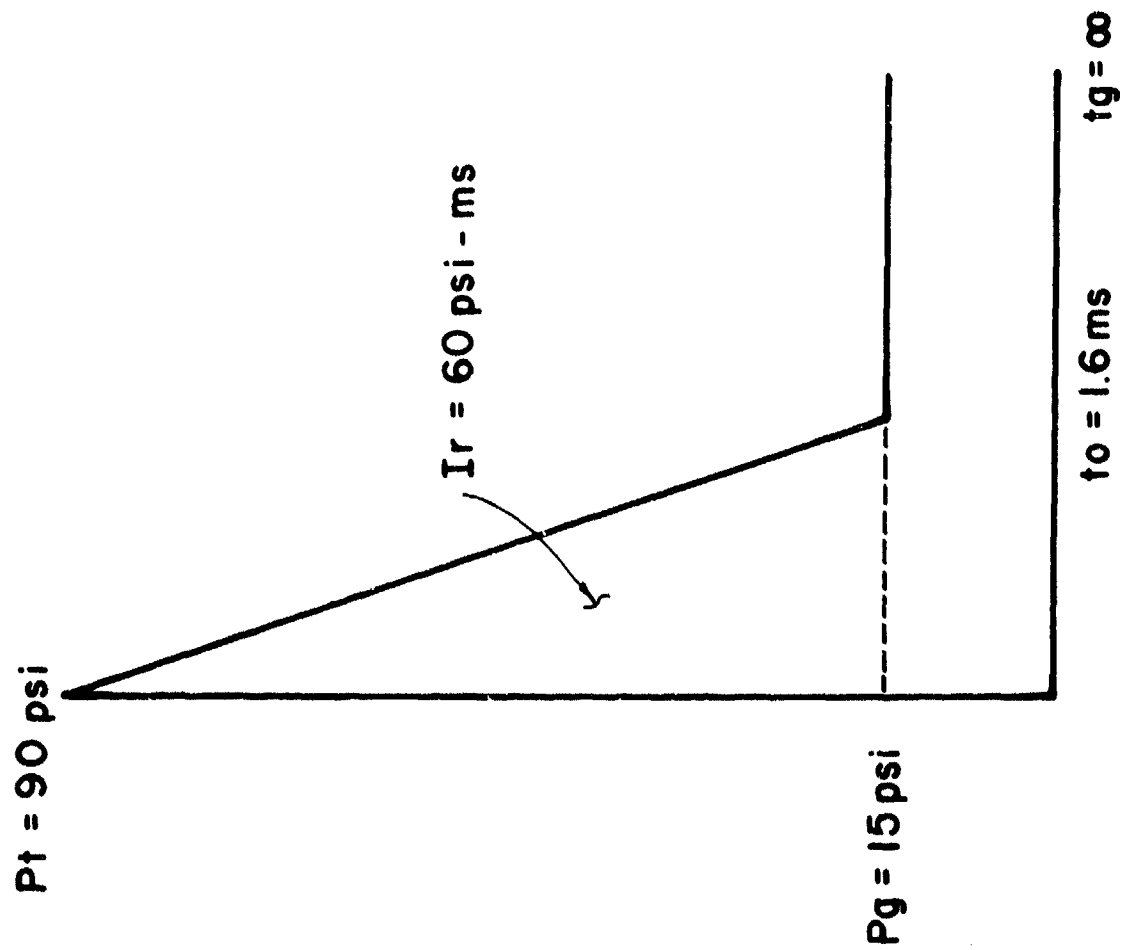


FIGURE 7

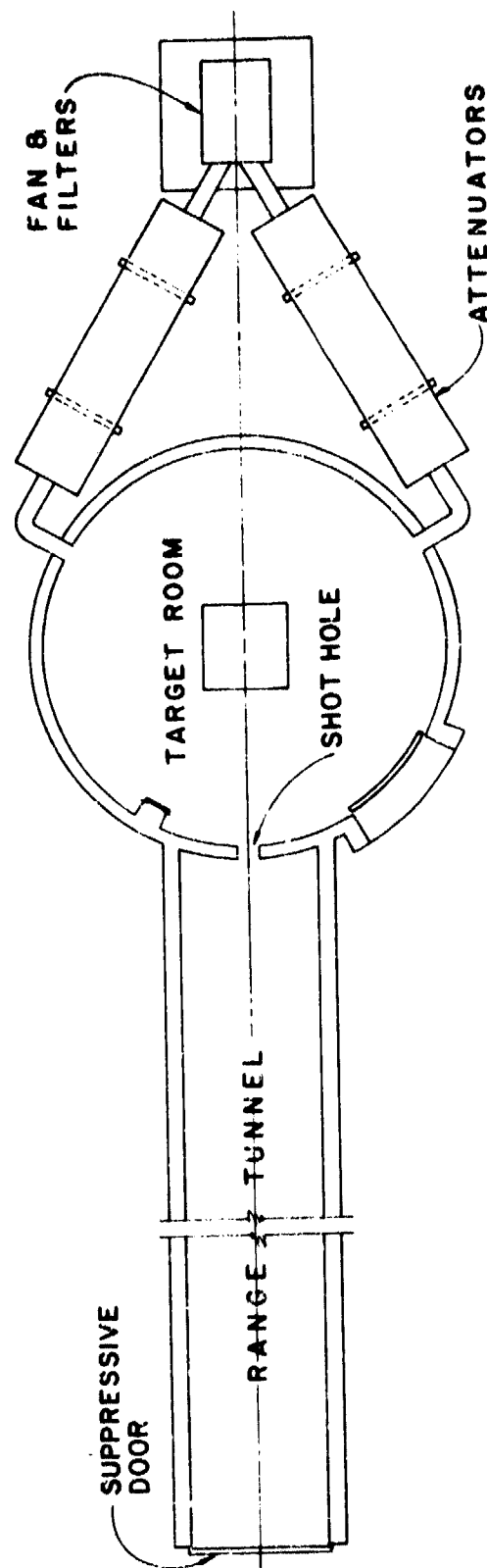


IDEALIZED PRESSURE - TIME CURVE

TARGET ROOM

<u>MEMBER</u>	<u>STRESS</u> (psi)
DOVE	
CIRCUMFERENTIAL	7,560
MERIDIONAL	9,050
RING BEAM	16,800
SIDE WALLS	
CIRCUMFERENTIAL	14,780
MERIDIONAL	7,410
DOOR JAMB	45,700
DOOR STIFFENER	49,380
DOOR	51,300

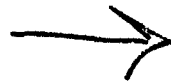
FIGURE 9



AIR EVACUATION & FILTRATION SYSTEM

FIGURE 10

AD P000450



DESIGN AND EVALUATION
OF
DAMAGED WEAPON FACILITY

By

Norval Dobbs
Samuel Weissman

AMMANN & WHITNEY, CONSULTING ENGINEERS

and

Larry Skeen

MASON & HANGER, SILAS MASON COMPANY

ABSTRACT

As part of the overall modernization of the Pantex Plant, Amarillo, Texas, the Department of Energy/Mason & Hanger, Silas Mason Co. has engaged the Joint Venture Firm of Gibbs & Hill/Ammann & Whitney to design the new "Production and Assembly Facilities". As part of this design, Ammann & Whitney was required to develop and design a "near full containment" structure titled "Damaged Weapon Facility". This facility will be used for the inspection and disassembly of components which have been damaged by accidental means.

11

DESIGN AND EVALUATION OF DAMAGED WEAPON FACILITY

Introduction

The criteria for the Damaged Weapon Facility (hereafter referred to as DWF) specified a Gravel Gertie type cell structure (Fig. 1) where venting of an interior explosion would occur through gravel fill which, in turn, would remove the radioactive material. However, due to operational requirements, it was determined that an oversize Gravel Gertie of at least 43 feet in diameter would be required as compared to the 34-foot standard Gravel Gertie cell which had previously been tested. Therefore, it would have been necessary to perform full-scale tests to verify the design for a large structure to meet the requirement for radioactive material capture. Thus, various other configurations were considered which ultimately resulted in the selection of a near full containment structural design as described below. Because of the presence of radioactive material, in combination with high explosives, containment type design is required to limit dispersion of the radioactive material in the event of an accidental HE detonation. In addition to describing methods of construction to attain this containment, a comparison of design blast loads with blast loads obtained from a set of 1/8-scale tests performed in conjunction with this project is presented.

Description of Structure

The DWF consists of a main high bay area and adjoining staging area; all within the containment area (Figs. 2, 3 and 4). The structure is a near full containment design consisting of laced reinforced concrete walls, roof and floor slab.

The adjoining area consists of two equipment rooms, six staging rooms, and staging corridor. The equipment room contains air-handling equipment, whereas the staging area contains various inert components. The staging corridor provides a means of access from the structure's entrance to the high bay.

The individual concrete elements have been designed to limit their support rotations to 2 degrees and thereby prevent through-cracking of the elements. The thickness of the laced concrete roof of the high bay is 6'-0" and of the walls, 4'-6"; the exterior and interior walls of the staging area are 1'-6" and 2'-0", respectively; whereas the staging area corridor roof is 3'-0" thick. All elements of the entrances are 1'-0" thick concrete.

An equipment air lock with two steel-plate, single-leaf interlocking blast doors is provided. These doors have been provided with compressed seals to prevent leakage of radioactive particles in the event of a detonation within the cell. To obtain an effective door seal, it was necessary that the door bear against the structure along all of its sides. To provide a bearing surface along the bottom edge of the equipment blast door, three alternative concepts were considered:

1. A fixed step with a removable ramp.
2. A retractable step and
3. A recess in the floor slab.

The first concept was not considered acceptable for the movement of items into the structure. The second concept was determined to be unreliable with regard to obtaining an effective continuous seal. The third concept, which was selected, is described below.

The equipment door closure is completely mechanized with electric motors which operate the pins that secure the door, operate the screw jack which raises the door out of the recess in the floor slab and operates the door to swing open and closed. A hydraulic unit is used to provide the necessary compression against the door seals.

Each personnel air lock blast door is a single leaf steel plate with radiation blast seals. Each door swings outward to provide emergency

egress in the event of an accident. In order to provide bearing for the seal along the bottom of each door, a 4-inch fixed step was provided at each door. This requires that personnel step down when leaving the structure. To provide this exterior swing of the personnel doors, each door had to be designed to "hang" from the locking pins and, therefore, the pins were designed to sustain the full impact of the interior blast. The personnel doors are provided with hydraulic systems which operate the pins, provide door seal compression and swing the doors. The operating mechanism of each personnel door is designed to open and close for two-speed conditions: normal speed of 30 seconds and emergency speed of 15 seconds. Redundant power is supplied to each door from three sources: normal commercial power, emergency generators and emergency batteries.

The high bay area is equipped with a 9-MEV Linac (X-ray machine) with crane and hoist, and with a trolley and hoist to provide movement of materials. Sufficient earth cover had to be placed over the structure to attenuate to a safe level any radiation leakage from the Linac.

Air intake and exhaust equipment rooms are located at each end of the staging corridor. The dehumidified air, which is supplied from the service area outside the DWF, is supplied to air-handling units within the intake equipment room. This air enters the DWF through a blast valve supply chamber (Fig. 5) which is located on top of the equipment room. The air-handling unit mixes the fresh dehumidified air with return air inside the structure. Air exhaust is accomplished through equipment hoods which are ducted to the exhaust equipment room. At this point, the exhaust air passes through a two-stage HFFA filter before being discharged to the atmosphere through a second blast valve housing above the exhaust equipment room.

Both blast valves are dual-actuated (remote pressure or blast). An initial pressure rise within the high bay, where all hazardous operations are performed, will be detected by pressure transducers which transmit an electrical signal to the blast valve operator to close the blast valves.

The valves will close in approximately 100 milliseconds after receiving the signal. In the event that the blast wave reached the valves prior to their closure, the blast pressures will assist in closing the valves. The valves are designed to resist this impact.

Located above the roof of the vestibules is a post-accident, single-stage HFOA filtration system to filter any contaminants which may escape past the blast doors. A fan connected to the emergency power source and located on the roof will exhaust the contaminants through the filters. This latter system is actually a redundant system to back up the blast door seals.

In the event of a detonation, the interior of the DWF will be pressurized. Relief of this pressure is accomplished through a pressure relief pipe which is connected to each blast valve chamber. The pipe is connected to a two-stage HFOA filtration system also located on the roof of the vestibule. Manual valves are provided to control the release of the internal pressure.

Design of Structure

The DWF was designed for an internal explosion of 423 pounds of spherical PBX 9404. The charge is located as shown in Figure 6 (1/8-scale model of DWF) and with the center of charge positioned 3 feet above the floor. The design criteria stated that a TNT equivalency equal to 1.3 be used for PBX 9404. With this equivalent weight of explosive and the use of a safety factor of 20 percent as defined in Reference 1, the total design charge weight was equal to 660 pounds of TNT.

Methods for determining the blast loads in the high bay were available (Ref. 1). However, there was no accurate means of predicting the blast loads at different locations outside the high bay; therefore, a design method was developed which involved the following steps:

1. The distance from the source of the explosion to the opening in the high bay was added to half the distance from the opening to the point in question outside the high bay. The one-half distance was used to account for the two-dimensional expansion of the blast

wave rather than the three-dimensional expansion for which the curves in Reference 1 were developed.

2. The total distance obtained by Step 1 was divided by the cube root of the equivalent charge weight.
3. The parameter calculated in Step 2 was used with Figure 4-12 of TM 5-1300 to determine the incident pressure, arrival time of the incident wave, and the duration of the incident pressure.
4. The angle of incidence of the wave at the point in question was determined geometrically and then used to determine the reflected coefficient from Figure 4-6 of Reference 1.
5. The product of the reflection factor and the incident pressure was used to obtain the reflected pressures, impulse and duration.
6. These reflected pressures were then averaged over a given area of the element (roof, wall, etc.) in question to obtain the average shock loads.
7. The gas pressures used were obtained from Figure 4-65 (Ref. 1) using a volume corresponding to a portion of the structure volume over which the shock loads were averaged.

A typical average pressure-time history of the calculated blast loads outside the high bay is shown in Figure 7. The initial peak pressure represents the shock load, whereas the flat portion of the loading illustrates the pressures produced by the build-up of the gaseous products and temperature rise produced by the confinement of the explosion.

Since the design blast loads outside the high bay were not well defined, a series of explosive tests were performed in a 1/8-scale model of the DWF (Ref. 2). These tests, which are described in more detail in another paper presented at this seminar (Ref. 3), covered a wide range of topics including:

1. Determination of blast loads

2. TNT equivalency
3. Effects of charge shape, and
4. Effects of charge casing.

The results of these tests indicate that the design loads, as used, were conservative and that the resistance of the building and, therefore, the amount of steel and/or concrete thickness outside the high bay could be reduced by 10 to 20 percent.

Figure 8 illustrates the comparison of the design blast loads to the test results.

Column 2 lists the blast loads used for the design of various areas of the structure outside the high bay, whereas Columns 3 through 6 list the corresponding test results. Column 1 lists the points within the structure at which the measurements were made. It may be noted that the charge weights listed in Columns 2 through 6 are 1/8-scale charge weights; e.g., 1.289 pounds is 1/8-scale weight of 660 pounds.

It may be noted, from Figure 8, that the design shock pressures in Area A (Fig. 6) are significantly higher than the shock pressures recorded in the tests. This is probably due to the choking effects produced as the blast wave passes through the relatively small opening between the high bay and the staging area. However, except for the roof slab, the impulse produced by these shock loads in the tests are closer in magnitude to those used in the design. The magnitudes of the shock pressures in Area B (Fig. 6) are also similar to those used in the design. The latter is attributed to the fact that the blast wave had more area to expand in Area B and that the magnitude of the shock loads were in the order of magnitude of those of the gas pressures.

The magnitude of the gas pressures recorded in the tests using 1.289 pounds of TNT are in the order of magnitude of the gas pressures used for the design of Area B. In the latter case, the entire volume of the structure was used to calculate the gas pressure for the design (81 psi). Therefore, it would appear that the volume of the entire structure should

be used to calculate the gas pressure at all points within the structure rather than the volume of individual sectors of the structure. Another important aspect of the gas pressure is its relatively long rise time. In all cases, except for the blast door and blast valve housing gas loads, the rise time was in the order of 15 milliseconds which is equal to 120 milliseconds in the full-scale structure. This very long rise time tends to produce a condition where the structure will not respond to the dynamic effects of the blast loads and thereby produce a structural response which is similar to that produced by a statically applied load.

The longer duration of the rise time of the gas pressures in the blast valve housing is attributed to the choking effects produced by the relatively small diameter (9- to 10-inch diameter) holes through which the air passes from the equipment room to the blast valve housing. The shorter rise time of the gas pressure acting on the blast door cannot be explained at this time.

An examination of the test results using 1.289 pounds of TNT indicates a higher gas pressure than that produced by an equal weight of PBX 9404. This would seem to indicate that the TNT equivalency of PBX 9404 is less than the 1.3 value used in the structure design. The results of other tests using pentolite also indicated a lower TNT equivalency for the gas pressures.

On the other hand, the cased PBX 9404 having a weight equal to 0.992-pound produced gas pressures in the same order of magnitude as 1.289 pounds of TNT, thereby indicating a TNT equivalency of 1.3 for the cased explosive. The values for 0.992 pound of uncased PBX 9404 are presented to show the effects on the gas pressure produced by the casing.

Conclusions

The following conclusions are offered:

1. The blast loads used for the design of the portion of the DWF outside the high bay area are conservative and therefore the concrete thickness and/or reinforcement can be reduced 10 to 20 percent.

2. The use of a TNT equivalency of 1.3 for uncased PBX 9404 is conservative. However, it is probably not conservative when casing effects are included.
3. Blast pressures produced by the blast waves passing through small openings will significantly affect the magnitude of the shock pressure as well as modify the pressure-time variation of both the shock and gas pressures.

REFERENCES

1. "Structures to Resist the Effects of Accidental Explosions", Departments of the Army, the Navy, and the Air Force, TM 5-1300/NAVFAC P-397/AFM 88-22, Washington, D.C., 17 March 1971.
2. HOKANSON, J.S., et al., "Determination of Blast Loads in the Damaged Weapons Facility", Volume 1, Final Report Phases I and II, SWRI-6578, Prepared for Mason & Hanger, Mason Company, Inc., Amarillo, Texas, by Southwest Research Institute, San Antonio, Texas, July 1982.
3. HOKANSON, J.S., et al., "Internal Blast Measurements in a Model of the Pantex Damaged Weapons Facility", a paper presented at the Twentieth DOD Explosive Safety Seminar, August 1982.

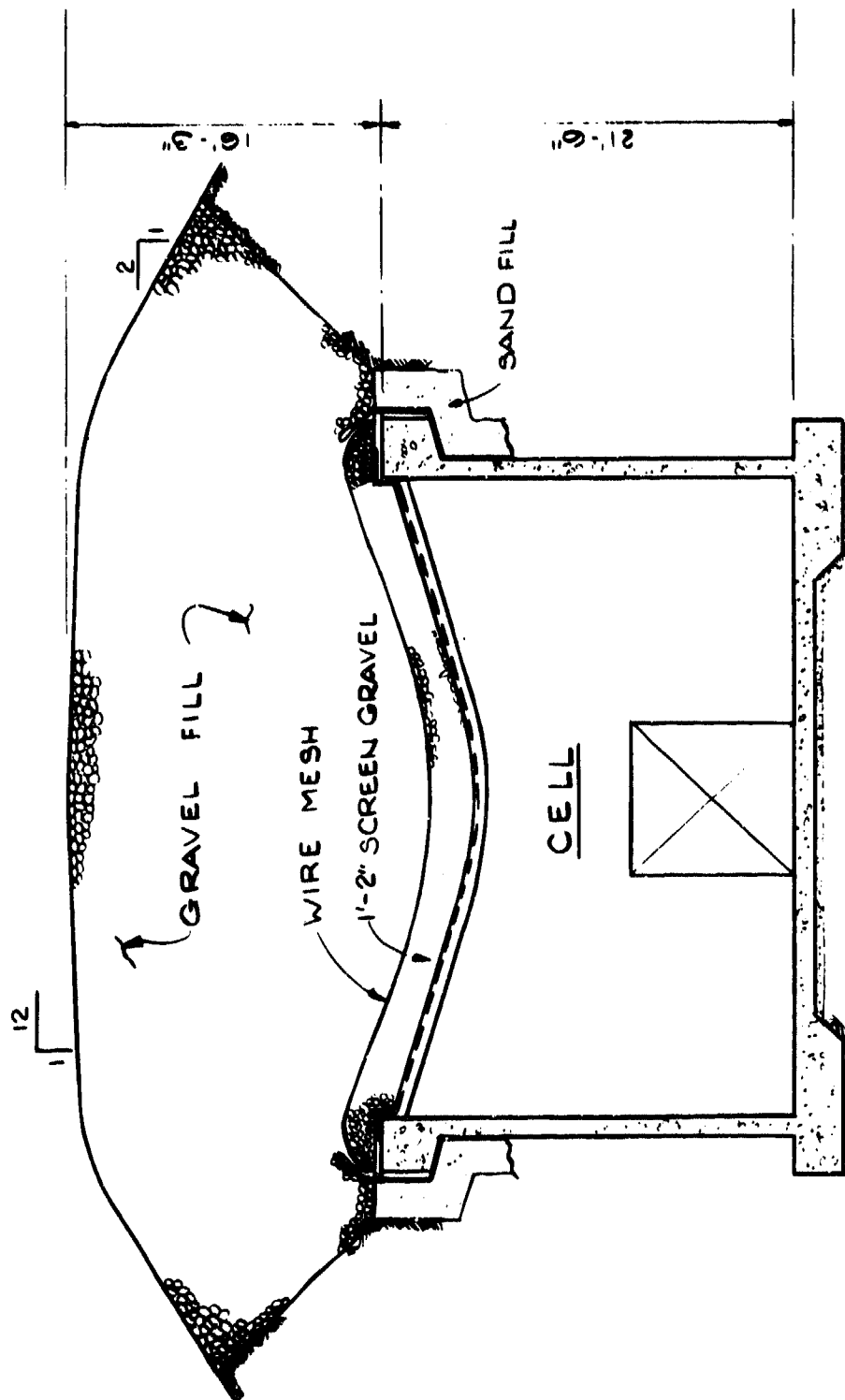


Figure 1 : GRAVEL GERTIE

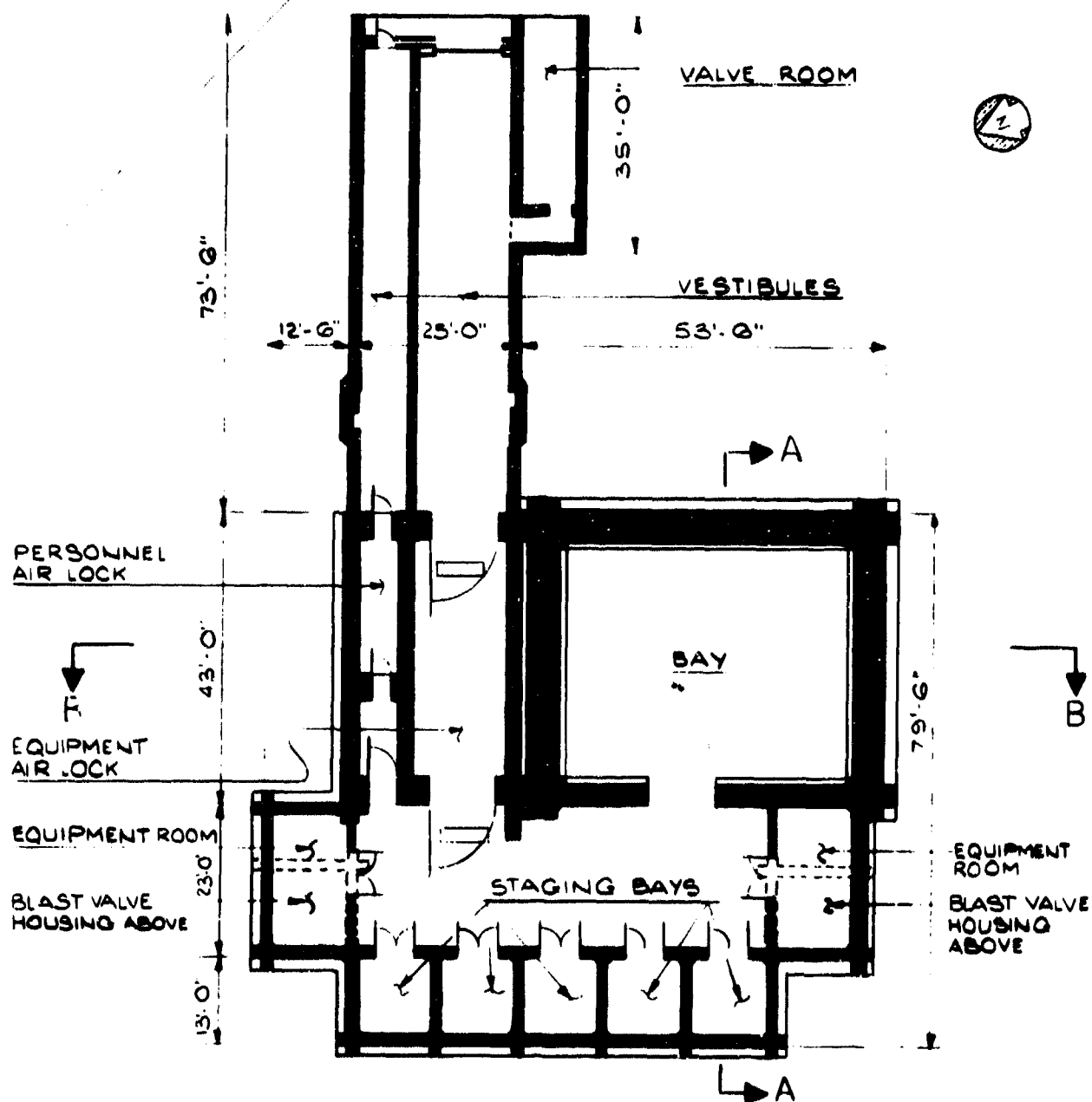


Figure 2 : DAMAGED WEAPONS FACILITY (FLOOR PLAN)

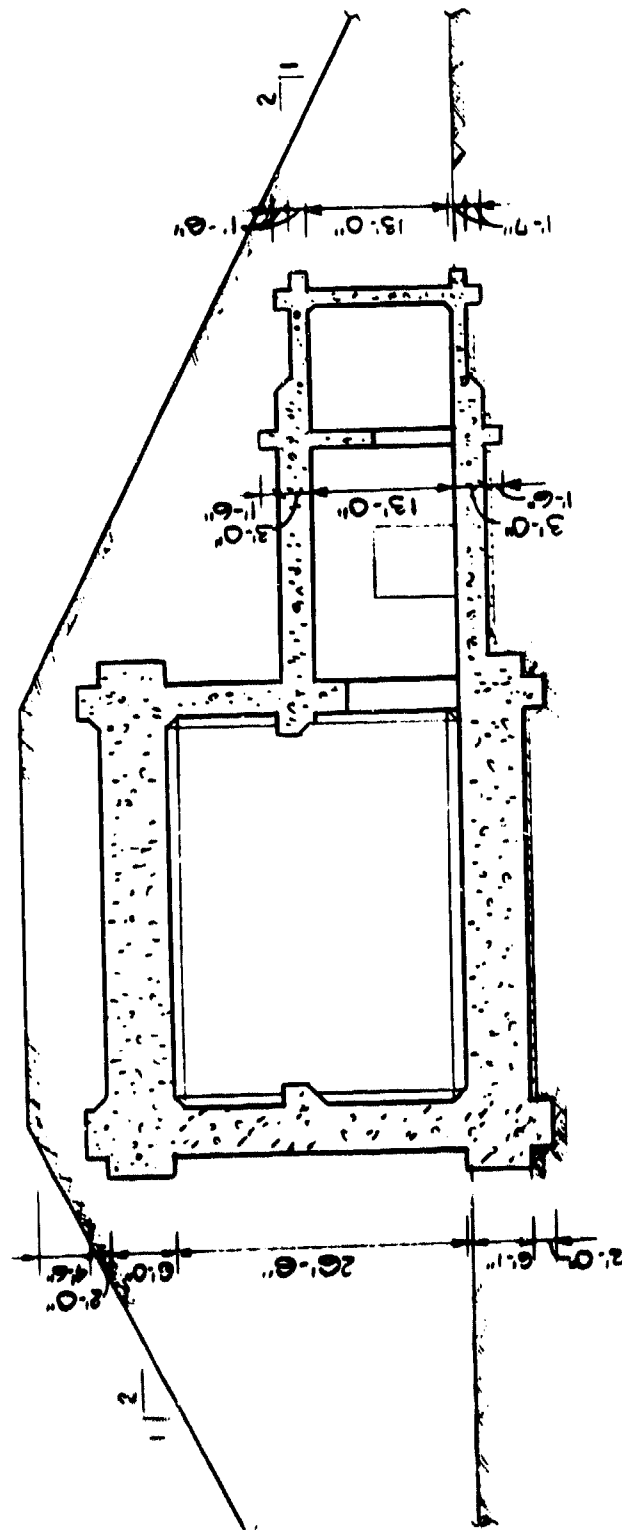
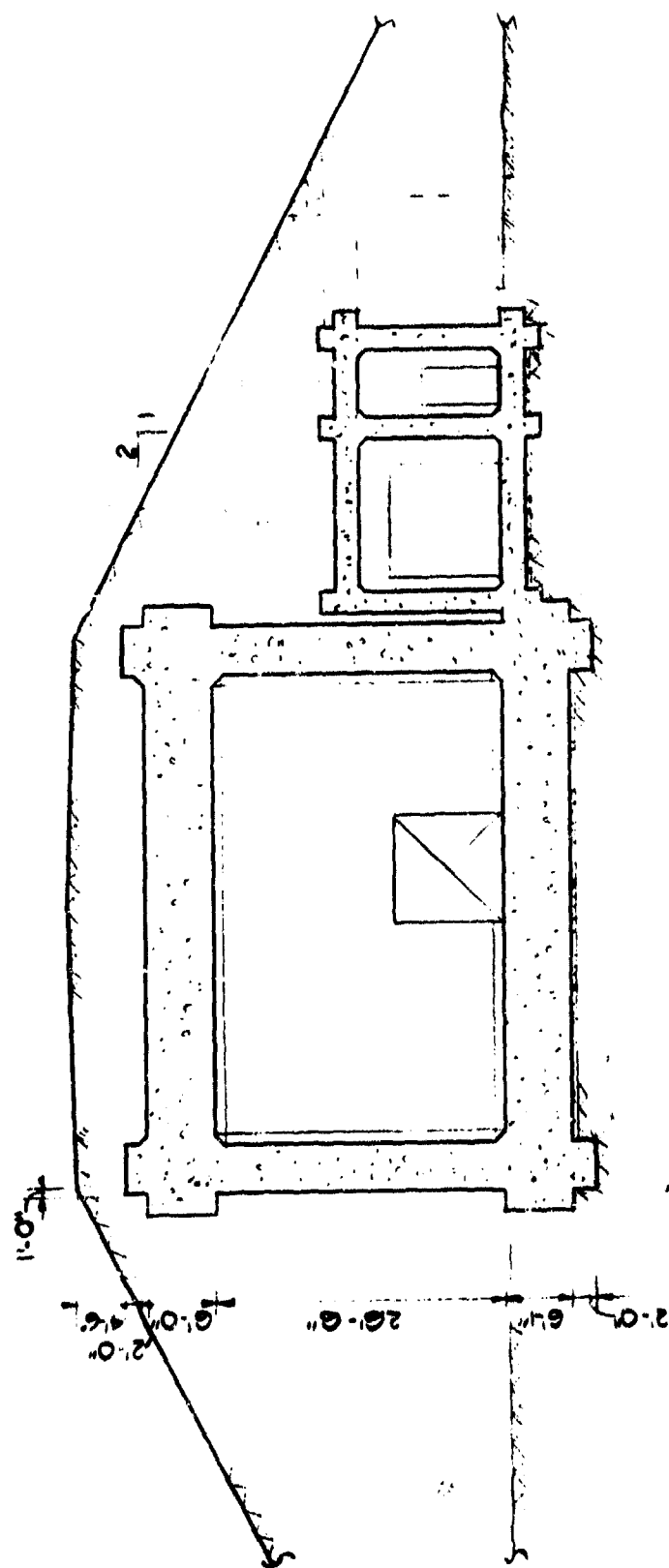
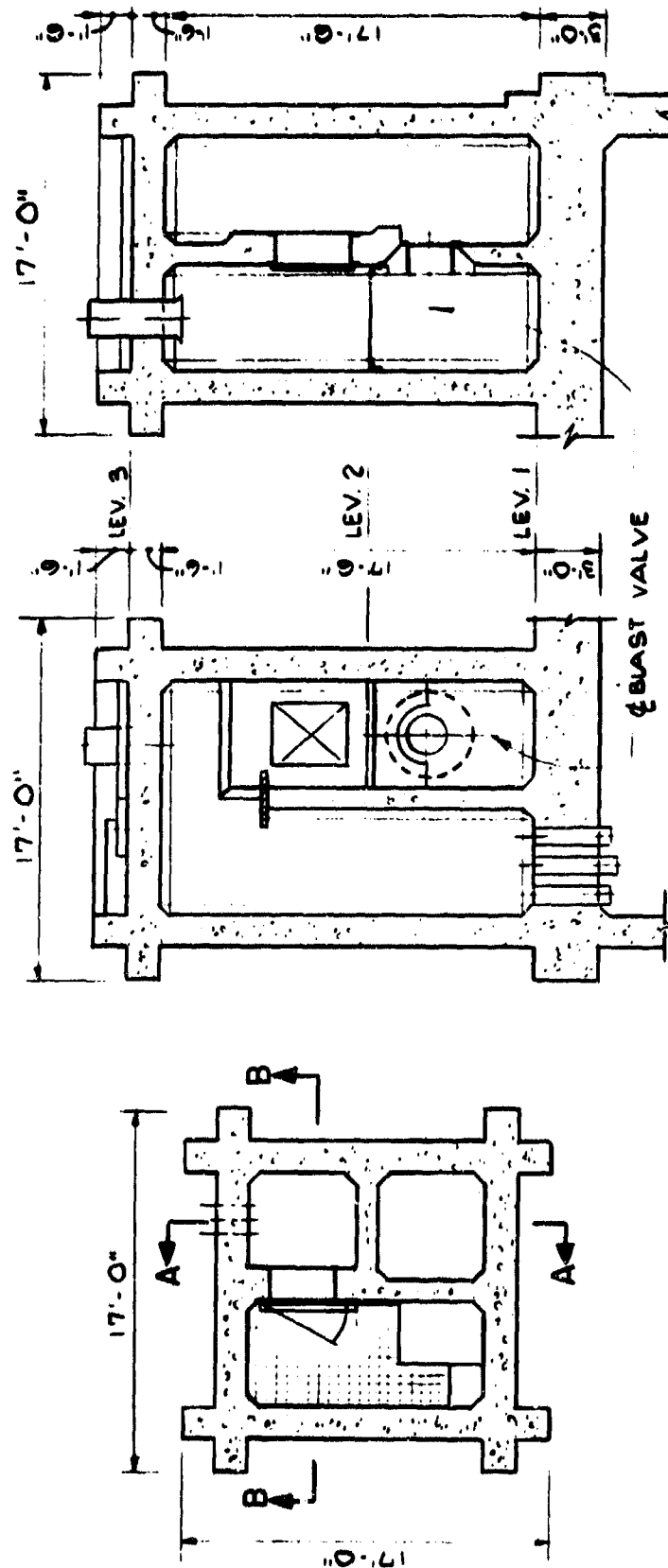


Figure 3: DAMAGED WEAPONS FACILITY (SECTION A)



602

Figure 4 : DAMAGED WEAPONS FACILITY (SECTION B)



FLOOR PLAN
(2ND FLOOR)

SECTION A

SECTION B

Figure 5: BLAST VALVE HOUSING

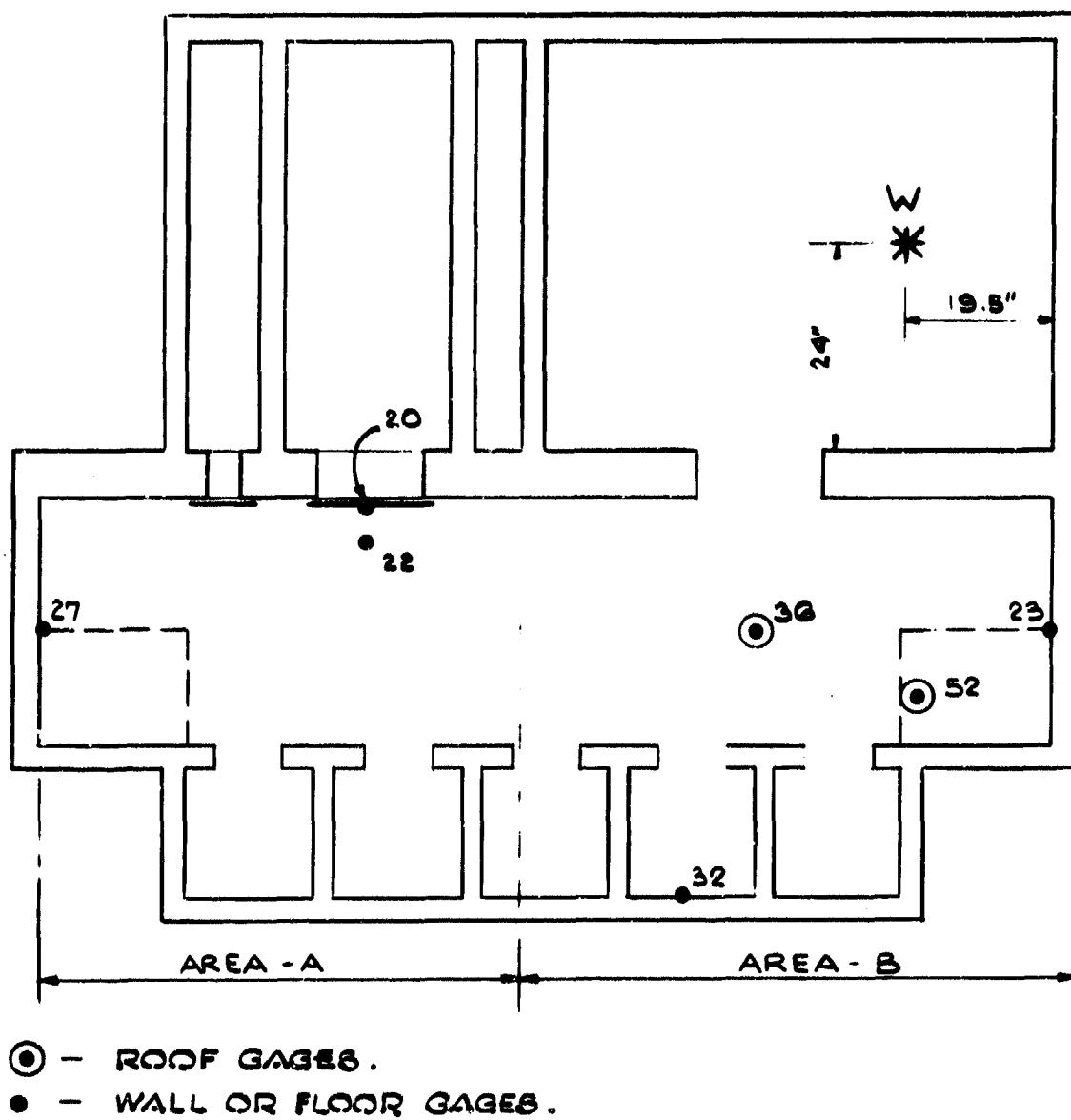


Figure 6: ONE-EIGHT SCALE MODEL

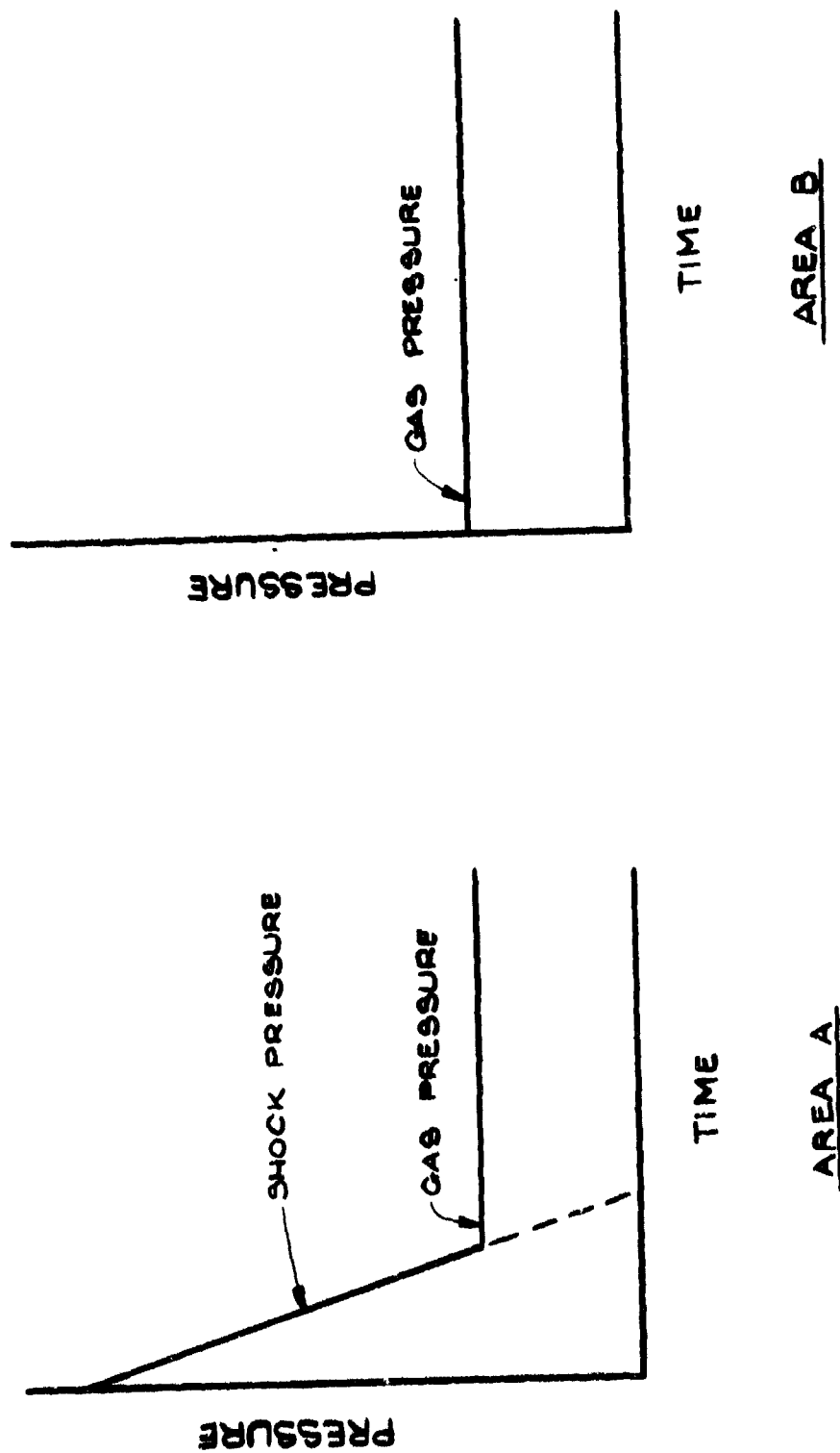
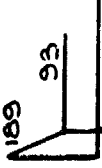
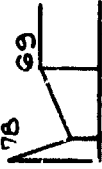
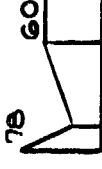
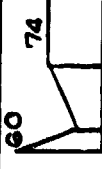

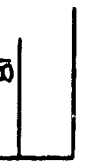








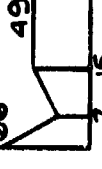
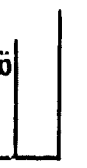
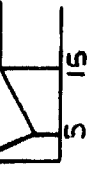


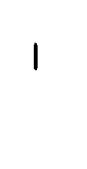
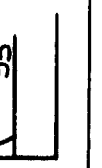
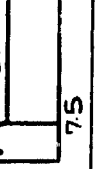
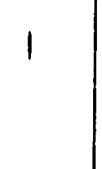

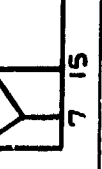
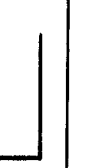





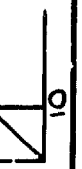





Figure 7: TYPICAL AVERAGE DESIGN BLAST LOADS

LOCATION (SEE FIGURE-6)	TEST RESULTS (1)						
	DESIGN	TNT W = 1.289*	TNT W = 1.289*	PBX 9404 W = 1.289*	PBX 9404 (2) W = 0.992*	PBX 9404 W = 0.992*	
ROOF SLAB (GAGE 36)							
FLOOR SLAB (GAGE 22)							
WALL (GAGE 23)							
WALL (GAGE 27)							
WALL (GAGE 32)							
BLAST VALVE HOUSING GAGE 52							
BLAST DOOR (GAGE 20)							

(1) PRESSURE - PSI TIME - MILLISECOND	(2) CAGED EXPLOSIVE
--	---------------------

(1) PRESSURE - PSI
TIME - MILLISECOND

(2) CAGED EXPLOSIVE

Figure 8: COMPARISON OF DESIGN AND TEST LOAD

AD P000451

DoD 5154.4S, "DoD Ammunition and Explosives Safety Standards,"
Chapter 13, Personnel Protection

R. A. Scott, PhD, FAIC
DDESB, Alexandria, VA 22331

The Department of Defense Explosives Safety Board by DoD Directive 5154.4 is charged with protecting personnel from the hazards associated with DoD ammunition and explosives. Chapter 13 of the subject standards establishes blast, fragments, and thermal hazards protection principles and applies to all operations/facilities where personnel are exposed to ammunition/explosives hazards during industrial, processing, manufacturing, and more routine operations.

Chapter 13 directs that an assessment of risk shall be performed on all new or modified industrial operations/facilities involving ammunition/explosives. Based upon this assessment, engineering design criteria for the facility-operation will be developed for use in the selection of appropriate equipment, shielding, engineering controls and protective clothing for workers. The assessment should include such factors as (1) initiation sensitivity; (2) quantity of materials; (3) heat output; (4) rate of burning; (5) potential ignition sources; (6) protection capabilities of shields, various types of clothing, and fire systems; and (7) personnel exposure with special consideration given to the respiratory and circulatory damage to be expected by inhalation of hot vapors and the toxicological effects due to inhalation of combustion products.

The exposures which are permissible are identified for each of the three hazards. For example, workers must be provided protection from potential blast overpressures, hazardous fragments, and thermal effects, with applicable respiratory and circulatory hazards, when assessments performed in compliance with the hazard assessment indicate the probability of accidental explosion producing overpressures, hazardous fragments, and accidental flash fires producing thermal hazards are above an acceptable risk level as determined on a case-by-case basis by the DoD Component. Thus protection afforded at the nearest work station must be capable of limiting incident blast overpressure to 2.3 psi, fragments to energies of less than 58 ft-lb, and thermal fluxes to 0.3 calories per square centimeter per second. Shields complying with MIL-STD-398 are acceptable protection.

Several protective measures may be used to assure that the permissible exposures of personnel are not exceeded in one or more of the following ways:

- a. Elimination or positive control of ignition/initiation stimuli.
- b. Sufficient distance or barricades to protect from blast and/or fragments.
- c. In those areas of facilities where exposed thermally energetic materials are handled which have a high probability of ignition and a large thermal output as indicated by hazard assessments performed, a fire detection and extinguishing system which is sufficiently quick-acting and of adequate capacity to extinguish potential flash fires in their incipient stage will protect both workers and property. Design and installation of the system must maximize speed of detection and application of the extinguishing agent.

d. In ammunition operational areas where it is essential for workers to be present, and the hazard assessment indicates an in-process thermal hazard exists, use of thermal shielding between the thermal source and the worker is an acceptable means of protection. If shields are used, they should comply with MIL-STD-398. If shielding is not possible, or if that provided is inadequate for protection of exposed personnel including their respiratory and circulatory systems, augmentation with improved facility engineering design, personnel protective clothing and equipment may be necessary.

e. Thermal protective clothing must be capable of limiting bodily injury to first degree burns (0.3 calories per square centimeter per second with personnel taking turning evasive action) when the maximum quantity of combustible material used in the operation is ignited.

f. Protective clothing selected must be capable of providing respiratory protection from the inhalation of hot vapors and toxicological effects when the hazard assessment indicates adverse effects would be encountered from the inhalation of combustion products.



AD P000452

FIRE HAZARDS OF COMBUSTIBLE
AMMUNITION IN STORAGE OR TRANSPORT

Prepared by

R. Pape
T. E. Waterman
H. Napadensky

IIT Research Institute
10 W. 35th Street
Chicago, Illinois 60616

IIT RESEARCH INSTITUTE

ABSTRACT

↓
The initial phase of work has been completed toward development of a standard test procedure to characterize the fire hazards of Class 1.3 and 1.4 munitions items, that is items that are primarily a fire hazard. Preliminary experiments considered fire damage or spread of fire to occur by radiant heat transfer from the flame or fireball, by direct flame impingement, or by firebrands (hot or burning objects). A "fast" burning propellant (a ball powder), a "slow" burning propellant (M1), an incendiary (ALA17 candles), and 2.75 inch rocket motors were used to identify the dominant phenomena and scaling relations, and to select the most promising instrumentation. Subsequent work will emphasize larger sample sizes to validate scaling relations and identify criteria for minimum realistic test size. ↗

1. BACKGROUND

Munitions items and materials in Hazards Classes 1.3 and 1.4 present mainly a fire hazard in storage and transport. Currently safety distance standards for these materials are based on $W^{1/3}$ (weight to the 1/3 power) scaling. $W^{1/3}$ scaling is appropriate for airblast phenomena, such as for Class 1.1 materials, and perhaps for a narrow set of fire hazards (i.e. those due to the explosive fireball). However, the overall fire hazard is complex, including "fireball" bursts as well as sustained flames, in both cases possibly propelling firebrands and debris to large distances. Munitions fires can occur in the open or inside storage structures. For most of these fire hazards, other scaling relations are more appropriate, and safe separation standards should be based on these more realistic scaling relations.

2. OVERALL DDESB PROGRAM FOR FIRE HAZARDS FROM COMBUSTIBLE AMMUNITION

In 1979, The DOD Explosives Safety Board initiated a five phase program to investigate fire hazards associated with combustible ammunition (materials in hazard divisions 1.3 and 1.4) and ultimately develop standard tests and rational safety distance standards to realistically characterize those hazards. The first phase of the program, Methodology Development, has been completed (Ref. 1). The objectives of that program were to develop an understanding of the phenomena that constitute the overall fire hazard, determine the appropriate scaling relations for these phenomena, and to evaluate experimental methods and instrumentation techniques required to characterize the hazards. During Phase 1, the most promising scaling and measuring techniques were identified and evaluated experimentally.

Emphasis in Phase 2 (to begin shortly) will be on size and configuration effects. During Phase 1 stacks of 8 or 12 boxes of munitions items were burned out in the open (essentially unconfined). During phase 2, larger stacks (perhaps up to 30 boxes -- "intermediate scale") will be burned in the open, as well as inside enclosures of several sizes. A plan for "large scale" testing is to be developed during Phase 2. Such "large scale" testing must be completed before the Safe Separation Standards and Classification Test methods can be finalized.

IIT RESEARCH INSTITUTE

Phase 3 is to consider the vulnerability of exposed targets to the different fire effects. Primarily, consideration will be given to radiant flux, total heat radiated, and firebrands of different types. Prolonged direct flame impingement may not exceed critical levels. Targets of concern may include exposed energetic materials (propellants, explosives, pyrotechnics, etc.), munitions items, materials of construction, nearby structures, persons, natural ground cover (eg. dry grass), vehicles, fuel tanks, etc. The vulnerability of targets of concern will define the criteria needed for developing safe separation standards.

Phase 4 is the development of safety distance standards. From Phases 1 and 2 the dominant phenomena, controlling parameters, and scaling relations will have been determined and verified. From Phase 3, the target vulnerability criteria will have been established. Under Phase 4, these basic building blocks will be combined to structure the safe separation distance standards.

The only missing element required to realistically characterize the fire hazards of combustible ammunition is a standard test for the Class 1.3 and 1.4 materials. The standard test must provide the parameter values that are needed to go into the safe separation distance tables or relations to establish the separation distance required. The tests must be realistic and practical to perform. This implies in part that the minimum quantity that realistically characterizes the hazard must be identified.

3. PHASE 1 RESULTS

The initial step of Phase 1 was to identify (from the literature) or develop scaling models for evaluating experimental results for free standing flames and fireballs, enclosure fires (i.e. storage facilities), and firebrand lofting. Flame characteristics of interest included the heat flux emitted from the flame and the flame geometry.

In addition to investigating the theoretical basis for scaling, the pertinent instrumentation techniques were surveyed and summarized. Instrumentation of interest included devices for measuring radiated heat flux, flame temperature, gas velocity, firebrand trajectories, and firebrand ignition potential. In each case, the most promising techniques were selected for experimental evaluation. In the case of ignition by firebrands, two experimental studies were completed. The first study was to determine the abilities of various types of firebrands to ignite host (target) materials characteristic of "real world" combustibles that could be exposed to such firebrands. A black powder layer was chosen as representative of a bare propellant in a storage or process facility. Wood and asphalt shingles were taken to represent roofing. Cardboard was tested because many materials are stored in cardboard containers. Canvas and plastic tarpaulins were evaluated. A typical vinyl covered seat cushion was tested, and dry timothy hay was taken as representative of a field of dry grass. The firebrands included the following:

- Smoldering cardboard
- NFPA "C" brand to represent smoldering wood
- An M30 pellet ignited while in contact with the host
- Solid copper cylinder heated to specified temperatures
- Hollow steel tube heated to specified temperatures

The results of this ignition study are summarized in Table 1. This study indicated the ignition potential for the range of firebrand types. To determine the ignition potential and lateral trajectory range of firebrands produced during field tests, several candidate catcher materials were evaluated. These are shown in Table 2. The most promising system was found to be a slab of polyurethane foam painted with an intumescent paint. For weak firebrands, the burn pattern on the painted surface was indicative of the brand type and intensity. For strong firebrands, the painted surface was penetrated. A hole was volatilized in the foam and the hole size was indicative of the brand's intensity.

For the remainder of the test program, four sample materials were selected. These were M1 propellant, Western Cartridge 844 (a ball powder), 2.75 inch rocket motors, and ALA 17 candles (an incendiary). These materials were tested both in their shipping containers and removed from the containers.

TABLE 1
EQUIVALENCY OF FIREBRAND IGNITION POTENTIAL

Host Material	Firebrand				
	Cardboard	C-Brand	M30 Pellets	Solid Copper	1/2 inch Pipe
Black Powder	Ignites	Ignites	Ignites	471°C (P=0.5)	579°C (P=0.5)
Wood Shingle	P=0.8	P>0.5	No Ignition	760°C- 954°C (flame P=0.5)	954°C (smolder P=0.5)
Cardboard	Ignites	P>0.8	P=0.8	Between 538°C and 649°C (P=0.5)	Between 538°C and 649°C (P=0.5)
Asphalt Shingle	---	No Ignition	No Ignition	Between 760°C and 982°C (P=0.5)	---
Canvas Tarpaulin	Ignites	P>0.7	P=0.4 (smolder)	649°C (P=0.83)	649°C (P=0.5 smolder) 760°C (P=1 flame)
Plastic Tarpaulin	No Ignition	P=0.8 (smolder) P=0.6 (flame)	No Ignition	at 871°C No Ignition	---
Dry Hay	Ignites	Ignites	Ignites	538°C (P=0.6 smolder) 649°C (P=0.2 flame)	954°C (P=1 smolder) and (P=0.8 flame)
Seat Cushion	No Ignition	Ignites	No Ignition	649°C and 760°C (P=0.4 smolder)	at 982°C No Ignition

TABLE 2
SUMMARY OF EXPERIMENTAL EVALUATION OF
CANDIDATE CATCHER MATERIALS (TESTS COMPLETED)

Catcher	Brand Type					Wind Velocity (mph)
	1/2 Inch Pipe	Solid Copper	Cardboard	M-30	C-3rand	
Polyethylene, painted	X	X	X	X	X	5-6
Polyethylene, unpainted	X	X	X	X	X	5-6
Polyurethane, painted	X	X	X	X	X	5-6
Polyurethane, unpainted	X	X	X	X	X	5-6
Kraft Paper, painted	X	X	X	X	X	5-6
Kraft Paper, unpainted	X	X	X	X	X	5-6
Smooth Asphalt Roofing	X	X	X	X	X	5-6
Polyethylene, painted				X	X	0
Polyethylene, unpainted				X	X	0
Kraft Paper, painted			X		X	0
Kraft Paper, unpainted				X	X	0
Milk Carton filled with water	X	X	X			0

Seven series of tests were conducted. The first test series was to screen the different instrumentation options so that the most promising could be selected for later tests. The second series was to determine how to safely test the 2.75 inch rocket motors. It was determined that the rocket motors would not self-propel themselves very far; and outdoor testing was found to be suitable. The third test series involved single packages (boxes) of each of the sample munitions items. The packages were exposed to a liquid hydrocarbon pool fire on one side. Typically, it would require a significant portion of an hour before the fire penetrated the packaging, and a fireball would result. Test series 4 involved stacks of several boxes to simulate realistic storage or transport configurations. With the M1, the Western Cartridge 844, and the rocket motors, the individual boxes usually reacted independently with long periods of time between events. The individual events were quite similar to the single box tests. With the incendiary, the stack of boxes burned significantly different from the single box. The single box produced individual flares "dancing around" on the ground or shooting like rockets into the air. The multiple boxes of flares produced individual flare burns as well as periods of a sustained churning white ball of fire spewing hot brands appearing like snow.

Test series 5 consisted of burning piles of bare propellant in the open, and test series 6 consisted of burning these materials inside of a small enclosure, simulating a storage structure. Both were idealized tests to evaluate scaling relations. Finally, test series 7 involved burning propellant inside of its storage container with the top removed. These seven types of tests provided a good overview of the different ways that the four sample materials can burn.

Figure 1 shows the range of heat fluxes (all scaled to 10 meters from the source) produced by each of the sample materials in the single and multiple box configurations. Figure 2 shows a similar comparison of firebrand travel distances observed in the tests.

Based on the Phase 1 program, much was learned that can be applied to the development of a standardized classification test for characterizing the fire hazards of combustible munitions. The burning behavior of the materials is better understood, therefore more realistic quantity-distance standards can be developed.

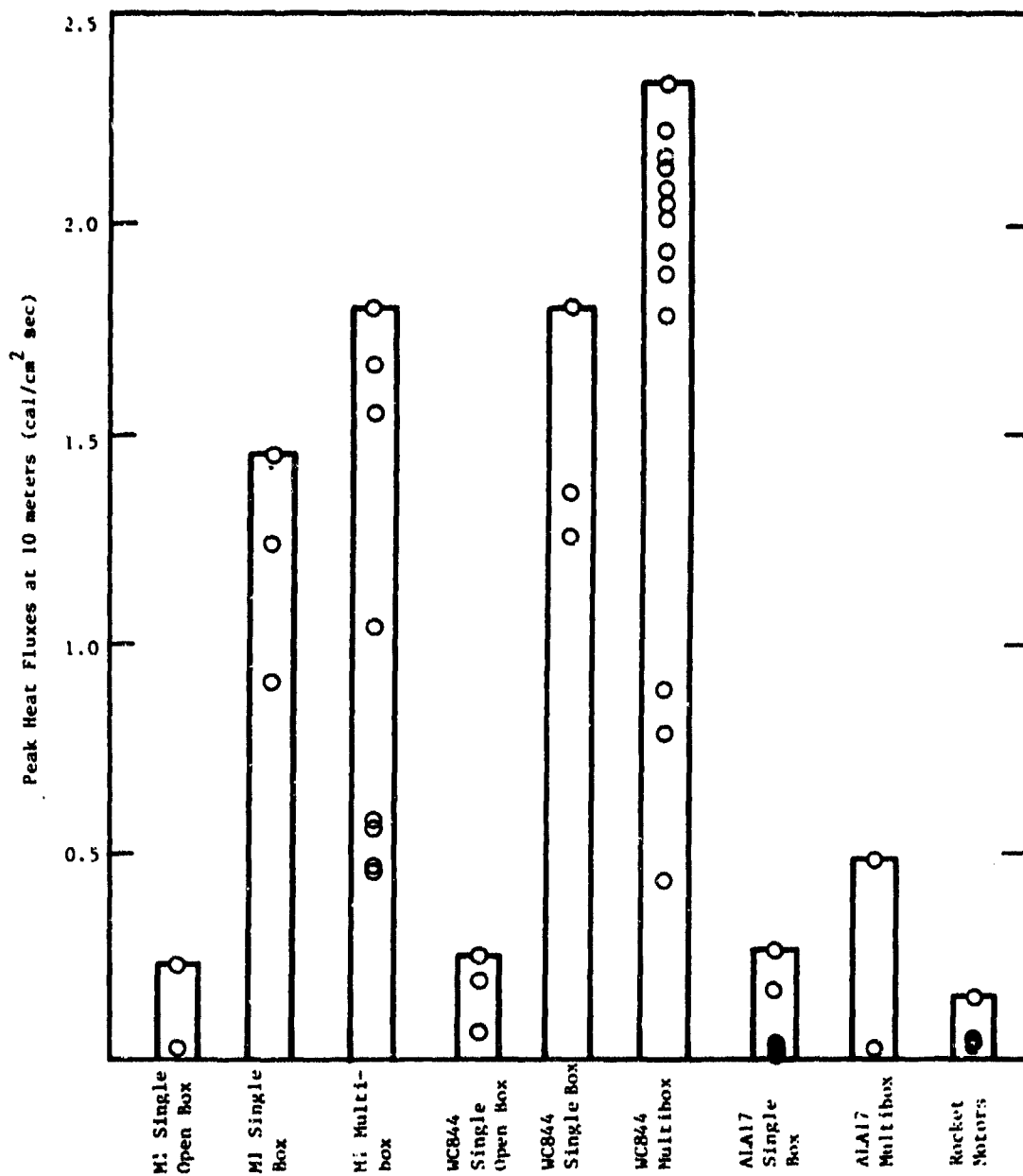


Figure 1 Comparison of Heat Fluxes

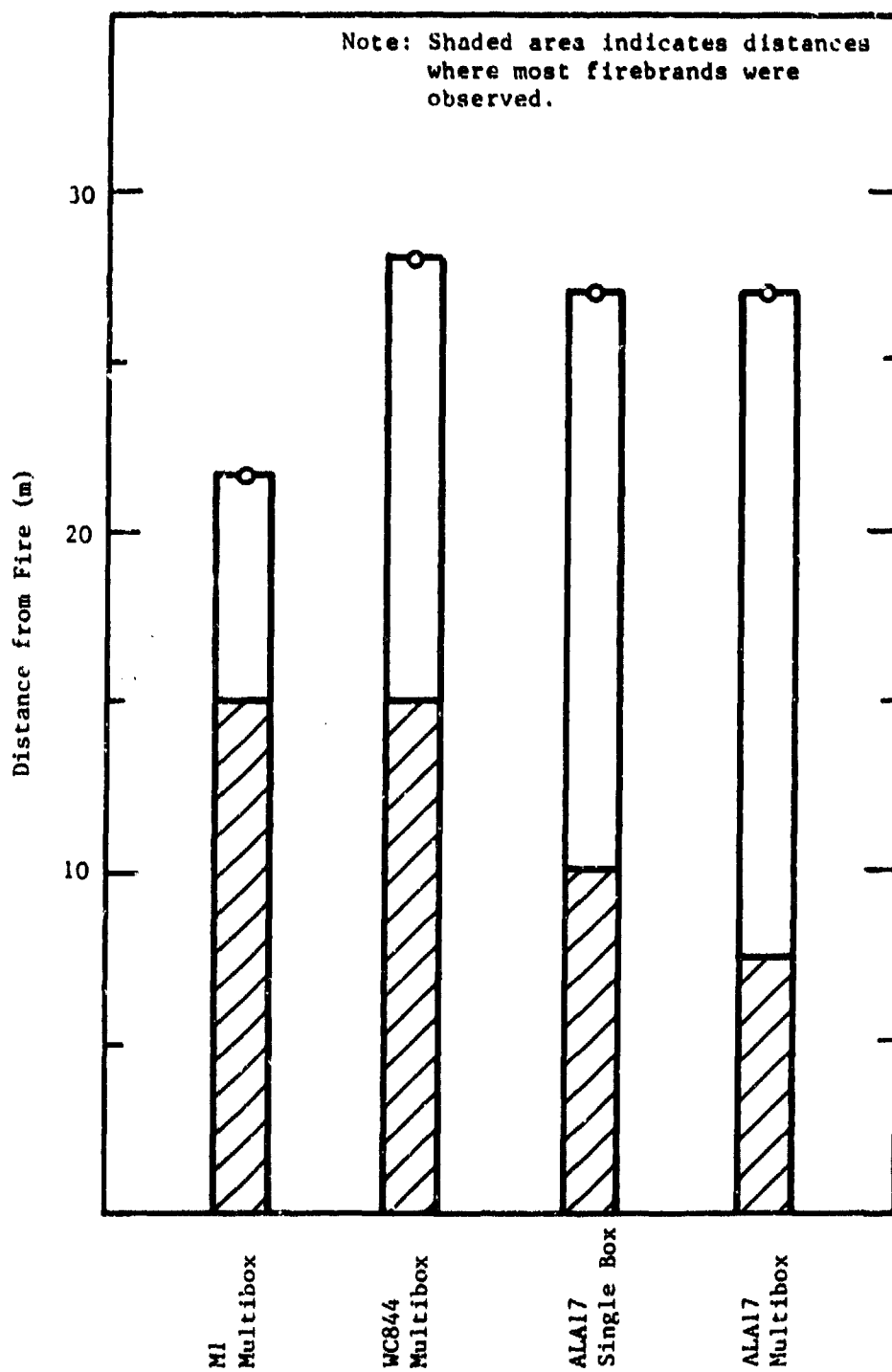


Figure 2 Comparison of Firebrand Distances

In addition, the results of Phase 1 clarified exactly what type of tests must be conducted during Phase 2 in order to verify scaling techniques for free air and enclosure fires.

IIT RESEARCH INSTITUTE

4. PHASE 2 REQUIREMENTS

The results of the Phase 1 investigations indicate that for some Hazard Division 1.3 and 1.4 materials, e.g. boxed bare propellants, the burning behavior of the individual box may be an adequate characterization of a large stack burning in the open. With other materials, e.g. ALA 17 candles, significant transition in burning behavior was observed as the stack size increased, even for the small scale tests conducted. Thus, one objective of Phase 2 will be to further verify that the individual box is indeed representative of large stacks burning in the open for the propellants. If this is the case, a small stack of boxes, or perhaps one box, will be an adequate quantity for the standard test for this subcategory of materials. For materials like the ALA 17 candle, at least a small stack is required (based on the Phase 1 results). In Phase 2, further transitions in behavior will be sought as the stack size is increased in an effort to identify a criteria for selecting the minimum allowable stack size for testing of materials in this subcategory.

During Phase 1, realistic size enclosure fires were not investigated. A 55 gallon drum was used as a model enclosure. Bare propellant was placed inside the enclosure and burned. A tongue of flame was observed to emerge out of an opening at one end of the drum and an attempt was made to identify the scaling relations and parameters that characterize this flame. For real items, such as the stacks of boxes, the question remains as to how the fire will progress inside the enclosure. In the open, the boxes generally burned independently --- individual fireball bursts dying as a sustained fire column in each case. In an enclosure significant interaction between boxes is anticipated. In recent British tests, boxes of propellant were burned inside such an enclosure and a long tongue of flame was seen to emerge from the enclosures open doorway. These test results were apparently quite similar to the 55 gallon drum results conducted by IITRI. Based on those results, the open air burns of stacked boxes will not characterize enclosure fires. Will 55 gallon drum scale tests adequately characterize these fires, or will a more realistic looking larger scale test involving actual packages be required? Answering these questions should be the essence of much of the Phase 2 work.

IIT RESEARCH INSTITUTE

Thus, for both the open air and enclosure cases an experimental parametric sensitivity study will be required. The major variables should include stack size, stack arrangement, ignition type, and ignition location. The major objectives should be to verify scaling relations and to determine the minimum stack size that will realistically characterize the fire behavior of the materials.

Two additional questions still remain to be answered under Phase 2. First, a great many materials and packaging arrangements are included in HD 1.3 and 1.4. The variety of items and packaging materials is summarized in Table 3. Under Phase 1 only four materials were evaluated:

M1 Propellant
Western Cartridge 844 (WC844-a, ball powder)
2.75 inch Rocket Motors
ALA 17 Candles (an incendiary)

These materials were selected to represent the range of items in HD 1.3 and 1.4. Unfortunately, only four materials could not possibly represent all the possible variations that exist in these categories. Therefore, one additional material (a smoke producing material such as white phosphorous) has been added to the list of sample materials during Phase 2. Small scale (Phase 1 type) to intermediate scale tests will be accomplished on this new material.

Second, the question remains as to the degree of confinement afforded by a typical unstrengthened above ground storage structure. Will such a structure act more like an igloo, containing the reaction and producing a tongue of flame that extends out of an open doorway or window, or will it provide negligible confinement resulting in essentially a free air burn of the munitions? An analysis is to be conducted to evaluate this problem and clarify which phenomena are more appropriate for characterizing the unstrengthened storage structure situation.

5. SUMMARY

A five phase program is being conducted by the Department of Defense Explosive Safety Board leading to revised safety distance standards and testing for Class 1.3 and 1.4 materials. The first phase of work has been

IIT RESEARCH INSTITUTE

TABLE 3
TYPICAL CLASS 1.3 AND 1.4
MUNITIONS ITEMS AND PACKAGING MATERIALS

Munitions Items*
Propellants (solid, powder, grains/pellets)
Incendiaries
Fireworks
Cartridges
Blasting Caps
Primers
Bombs
Cord/Cable
Fuses
Flares
Grenades
Rockets/Rocket Motors
Squibs
Tracers
Contrivances
Some Explosive Devices
Packaging Materials
Paper Bags
Kraft Paper
Plastic Bags
Fiberboard Boxes
Natural Wood
Rubberized Textile
Rubber
Sawdust
Wood Wool
Textile
Aluminum
Steel
Glass

* Some of the types of items listed may also be in other classes.

completed. During that program, scaling relations were evaluated. Primarily, instrumentation methods were scrutinized and the controlling phenomena were identified. It presently appears that a classification test procedure should evaluate stacks of boxes burning in the open, as well as enclosure fires (i.e. at least 2 tests are needed). Based on the results of the Phase 1 program, the essential features required in subsequent phases of work have been identified.

REFERENCE

1. Pape, R., T. E. Waterman and A. N. Takata, "Fire Hazards from Combustible Ammunition, Methodology Development. (Phase I)" Final Report--Project J6480, Contract MDA903-79-C-0327, June 1980.

IIT RESEARCH INSTITUTE

ACKNOWLEDGEMENT

The work presented in this paper was conducted under Contract MDA903-79-C-0327 for the Department of Defense Explosives Safety Board, Alexandria, Virginia (DDESB). Mr. W. G. Queen and Dr. T. Zaker were the DDESB technical representatives on the program.



IIT RESEARCH INSTITUTE

AD P000453

20 th DOD Explosives Safety Seminar
NORFOLK VIRGINIA



MEASUREMENT AND PREDICTION

OF HEAT FLUX IN

GUN PROPELLANT FIRES

J.P. LUCOTTE

Safety Technical Group (SNPE)

91710 VERT-LE-PETIT FRANCE

1. INTRODUCTION

Over a period of several years, SNPE has conducted tests using various, sometimes large quantities of hunting gunpowder and propellants.

These tests are designed to determine the effects on the environment of accidental ignition during the handling or storage of the materials concerned.

The hundred or so tests, performed on quantities ranging from a few kilograms to several dozen tons, served to determine empirical laws through systematic processing of the results, in order to predict the duration of combustion, the size of the fireball, and the heat flux emitted.

By means of a technical approach, these laws, associated with the data in the literature on human tolerance to heat flux, make it possible to define hazardous areas.

Before presenting these laws and offering an example of their application (related to French regulations), we shall first describe one of the many experiments involving large amounts of explosives.

2. EXAMPLE OF A TEST ON LARGE QUANTITIES OF MATERIAL

This test was designed to assess the behaviour of a storage building using a hunting gunpowder, and to determine the fireball produced.

This so-called "Captieux type magazine" was described in detail at the 17th seminar on safety of explosives by Messrs. Roure and Fontaine. The figure [1] recalls the main characteristics of this type of depot.

A standard storage configuration was reproduced for the test: the building was subdivided into 14 blocks each containing 72 drums. Since the capacity of each cardboard drum was 15 kg of powder, the building contained 15,120 kg of hunting powder.

Initiation was caused by the ignition - using hot wires - of 150 kg of powder spread on the ground around a central block. (Figure [IX]).

The film which we shall now see offers an idea of the progress of the fire and its consequences on the building (NOTE: the building had been used in a previous test, and the film shows the absence of a few roof tiles before the fire set in the experiment described here).

Heat flux measurements were taken close to the building to determine the flow around the fireball. Asymptotic Hy Cal Engineering calorimeters were employed.

The graph below (figure [III]) shows the heat flux recording at 20 m facing the building, as a function of time.

Immediately after ignition, the combustion of 150 kg of bulk powder used to set the fire can be observed. This combustion reaches a peak in 3 seconds, and the heat flux at 20 m is 8 W/cm². The flux then becomes practically null until the 85th second, when the whole building catches fire, the recorder is saturated but the maximum flux can be estimated at 50 W/cm² at 20 m (obtained 10 seconds after the start of the overall fire). Combustion lasts less than one minute, and is followed by a residual combustion (combustion of cardboard packings).

The depth of the flame front during total combustion is a maximum of 30 m at the facade. (This distance was minimized by a 5 m/s side wind, which caused the vegetation to burn

over a lateral distance of 200 metres). At the rear of the building, after projection of roof slabs, the flame front also reached 30 metres. (Figure [IV]).

3. EMPIRICAL FORECASTING EQUATIONS

These equations were obtained from the measurements and observations noted during about 100 tests.

They were established by a non-linear regression method.

3.1. Radius of the fireball

If the shape of the container does not cause any particular orientation of the flames, the fireball radius can be estimated by the equation:

$$R = 1.21 \cdot M^{0.366} \quad [1]$$

This equation is valid for $M < 10,000 \text{ kg}$.

3.2. Combustion time

The equation is not uniform over the entire weight range.

$$M < 800 \text{ kg} : t_1 = 3.225 \cdot M^{0.126} \quad [2]$$

$$800 \text{ kg} < M < 40,000 \text{ kg} : t_2 = 0.707 \cdot M^{0.405} \quad [3]$$

3.3. Radiant flux

$$\frac{\Phi}{S} = \frac{k}{4\pi} \cdot c \cdot t \cdot \frac{Q}{R^2} \cdot \frac{dM}{dt} \quad [4]$$

where:

- $\frac{Q}{A}$ flux density in W/cm²
- k unit conversion factor
- c energy conversion factor (reflecting the part of the energy available which is emitted in the form of radiant flux)
- t heat transfer coefficient (reflects the part of the radiant flux emitted which is effectively received at distance R)
- Q potential of the gunpowder (cal/g).
This is a simple way of expressing the energy available in the burning material.
- R distance (m)
- $\frac{dM}{dt}$ combustion flow rate per unit mass

The factors c and t are associated with the materials and the fire conditions.

As a first approximation, and based on the assumptions used, the following mean values can be taken for the product c.t. (values obtained empirically):

- c.t. = $\frac{1}{3}$ if the product is in bulk or in a container offering little fire resistance [4a]
- $\frac{1}{10} < ct < \frac{1}{3}$ if the product is in containers offering substantial fire resistance [4b]

These empirical equations provide a technical approach to the forecasting of danger zones in case of fire.

However, French regulations allow these zones to be calculated principally on the basis of material weight. Before using an example to compare the technical approach and the regulatory approach, it is essential to summarize the French regulations governing heat flux hazardous area calculation.

4. REVIEW OF FRENCH REGULATIONS

Materials or objects incurring a fire hazard are divided into two groups:

- . one includes materials and objects which burn with the generation of considerable heat radiation (1.3.a);
- . the second group includes materials and objects which burn fairly slowly, or in succession (1.3.b).

For each of these subdivisions, the boundaries of the danger zones are defined in principle on the basis of the weight involved, according to the following table:

DANGER ZONE	1.3.a.	1.3.b.
Z1 (mortal injury in more than 50% of cases)	$0 < R_1 \leq 2.5 M^{1/3}$	$0 < R_1 \leq 1.5 M^{1/3}$
Z2 (grave injury that may be mortal)	$< R_2 \leq 1.5 M^{1/3}$	$< R_2 \leq 2 M^{1/3}$
Z3 (injuries)	$< R_3 \leq 5 M^{1/3}$	$< R_3 \leq 2.5 M^{1/3}$
Z4 (possibility of injury)	$< R_4 \leq 6.5 M^{1/3}$	$< R_4 \leq 3.25 M^{1/3}$

M : Weight of explosible substance in kilograms.

R : distance of the boundaries of hazardous areas, in meters.

TABLE 1 : FRENCH REGULATION.

Moreover, the same regulations provide a definition of danger zones using the concept of heat flux.

- . zone Z1 corresponds to a flux above 1.5 W/cm^2
- . zone Z2 corresponds to a flux above 0.6 W/cm^2

This definition allows an initial technical approach if the flux measurements are known.

5. PRACTICAL PROCEDURE FOR THE APPROXIMATE PREDICTION OF DANGER ZONES CREATED BY HEAT FLUX.

Only the general case of non-directional combustion is dealt with here, for which the propagation of the radiant flux is not affected by any obstacle.

- a) Input data: . weight of material
. potential.
- b) Calculation of combustion time by equation 2 or 3.
- c) Finding on curve [v] the flux which, for exposure times calculated in b), cause first, second or third degree burns (NOTE: this curves are a compilation of the work of D.E. Jarret and K. Buettner, and of the recommendations of MIL STD 398 dated 5 November 1976, and does not account for burns by direct contact with the flames).
- d) Use of equation [4] to calculate the distances at which these critical flux are received.

6. SAMPLE FORECAST

To illustrate the procedure just described, the following table gives a comparaison between the danger zones calculated in accordance with French regulations and those which were estimated by our technical approach, in the case of the combustion of 15,120 kg of hunting powder (potential 1000 cal/g).

	Regulatory approach	Technical approach
21	61,8	/
22	86,5	90
23	123,6	110
24	160,7	180

TABLE 2 : RADIUS (m) OF HAZARDOUS AREAS.

This example reveals acceptable agreement between the two approaches.

7. CONCLUSION

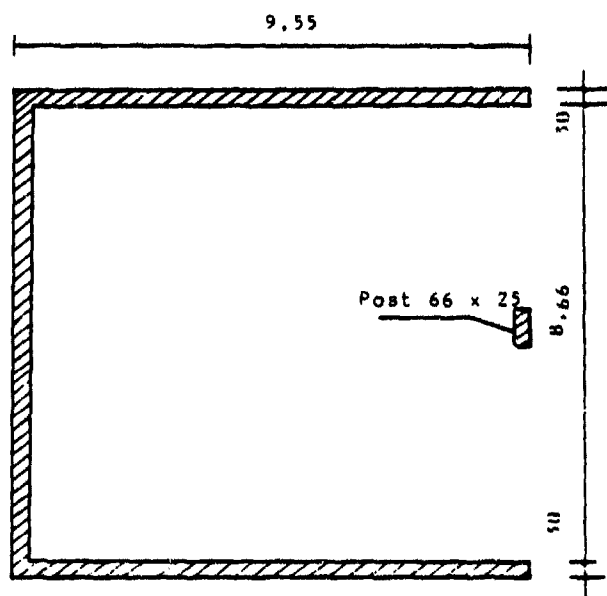
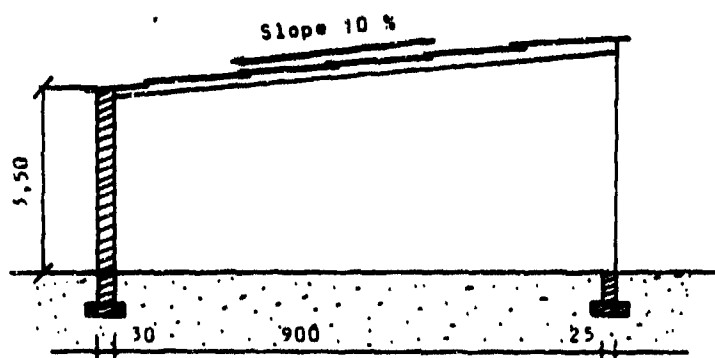
The many experiments conducted by SNPE helped to derive empirical equations to predict fireball sizes, combustion times and the radiant flux received.

In simple cases, these empirical equations allow a very rapid calculation of the danger zones. To deal with more complex cases, these empirical equations offer input data for computer programs, which must also account for the rate of expansion of the fireball, the role of shields and openings, and even the possibilities of operator flight.

TYPE
CRB
RIS

PROPELLANT STORAGE
MAGAZINE "CAPTIEUX" TYPE

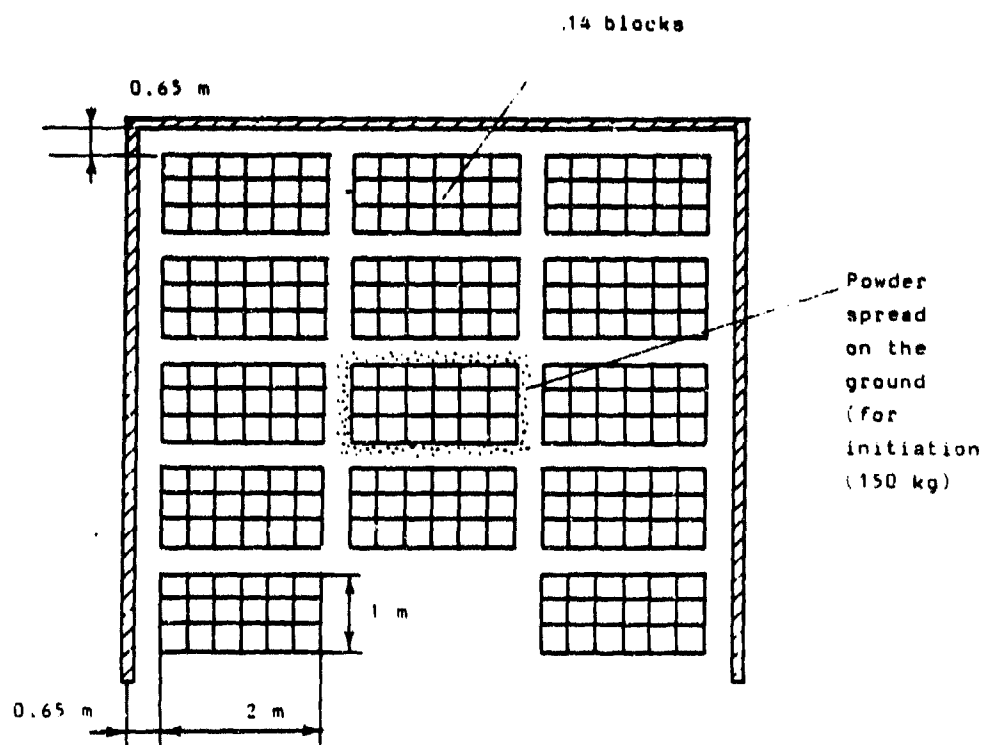
Fig. 1



SNPE
CRB
GTS

ARRANGEMENT OF POWDERS
FOR EXPERIMENTATION
IN THE MAGAZINE

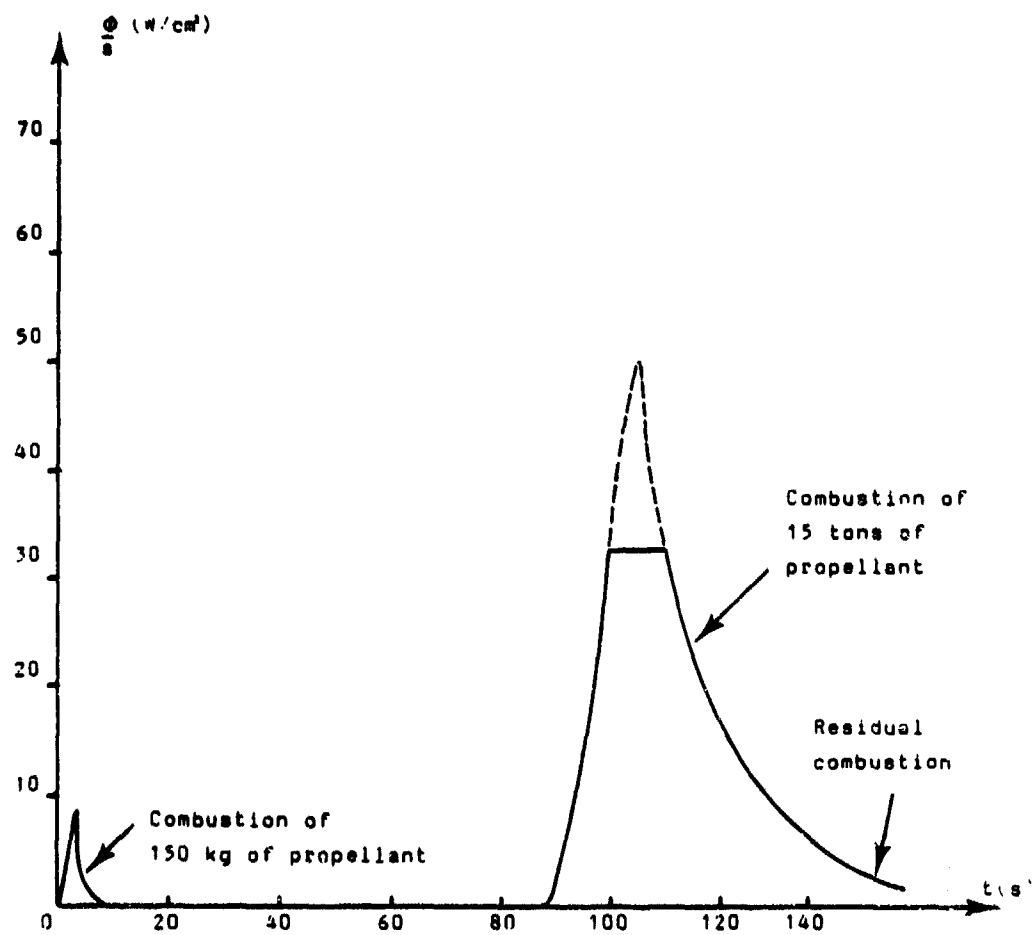
Fig. 11



SNPE
CRB
GTS

HEAT FLUX AT 20 METERS
IN FRONT OF THE MAGAZINE

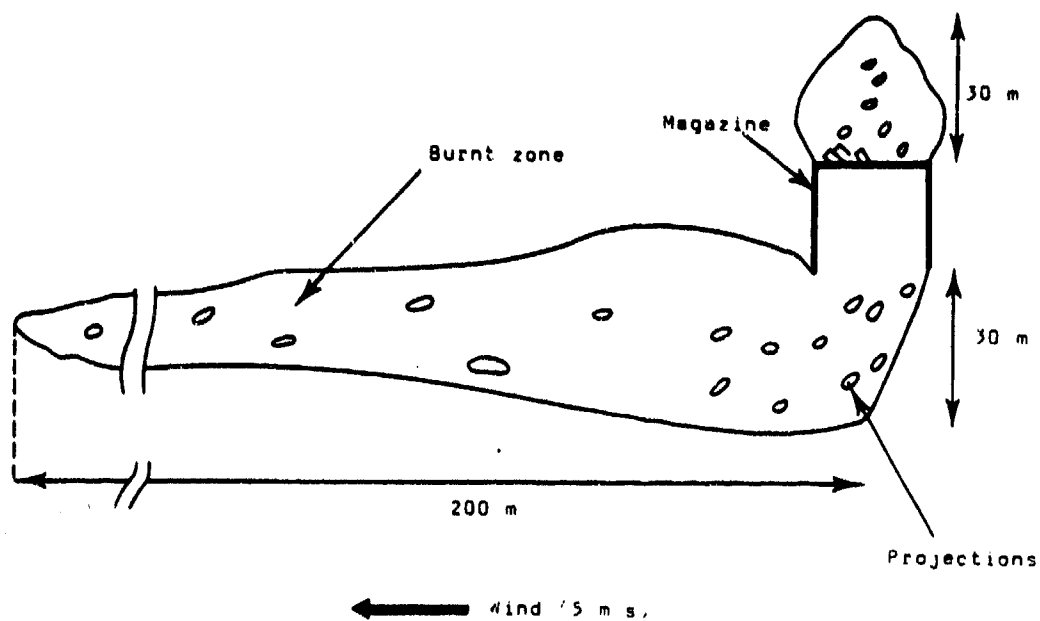
Fig. III



SVPE
CRB
GTS

BURNT ZONE AND PROJECTIONS
AFTER THE COMBUSTION

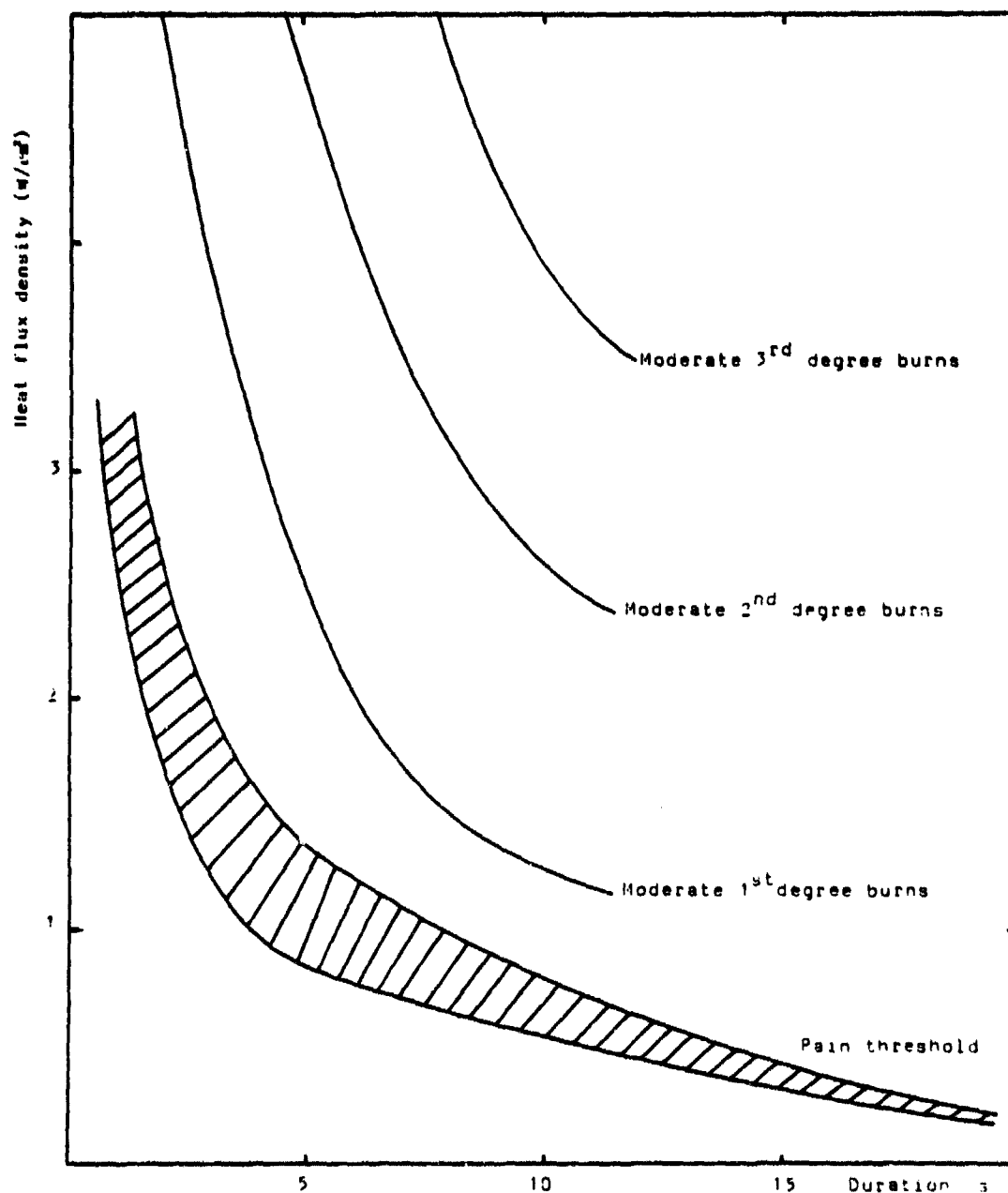
Fig. IV



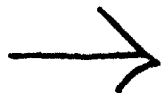
SVPE
CRB
GTS

HUMAN TOLERANCE
TO HEAT FLUX

Fig. V



AD P000454



QUANTITY-DISTANCES FOR HAZARD DIVISION 1.3
MASS FIRE RISK EXPLOSIVES

W. S. N. TINKLER
Safety Services Organisation (PE)
Ministry of Defence,
St Mary Cray, England

SUMMARY

Quantity-Distances for HD 1.3 explosives, particularly bulk gun propellants, are considered to be less soundly based than for HD 1.1 (mass exploding) and HD 1.2 explosives. Blast effects and projection hazards have been extensively studied and are comparatively well understood. The behaviour in a fire of bulk stocks, or loads, of HD 1.3 explosives depends primarily on the strength of the confining structure. Tests on tonnage quantities of boxed gun propellants in representative structures are reported. The unexpectedly energetic behaviour displayed indicates that existing Q-Ds for HD 1.3 explosives may give inadequate levels of protection. The orientation of entrances to propellant magazines may be a crucial element in the protection against communication between magazines and process buildings.

INTRODUCTION

The study of the effects of an incident involving explosives (used here in the widest sense to include ammunition, pyrotechnics and propellants), was naturally concentrated on those showing the most widespread damage and injury potential, i.e. those which mass explode. These explosives, classified using the international scheme as Hazard Division (HD) 1.1, produce a blast wave capable of damaging or destroying structures at a distance. The blast wave parameters are fairly consistent and mathematical relationships, which predict the range at which a particular degree of structural damage is to be expected from a known quantity of explosives, i.e. Q-Ds, are almost universally accepted. Licensing of explosives holdings simply requires a decision as to what is an acceptable degree of damage and hazard. In the writer's opinion this concept of relating the radius for a certain degree of (acceptable) hazard to the explosive quantity by a simple mathematical relationship is justified only when blast is the predominating effect producing the hazard. This implies that it is essentially wrong in principle for other than HD 1.1 mass exploding explosives.

Projections, both primary and secondary, from buildings etc surrounding the explosives, often accompany blast effects from a mass explosion. Although the range of lethal projections may extend as far as a damaging blast wave, the projection hazard is typically not the controlling factor at the IBD from larger quantities of explosives. For HD 1.2 explosives, which display negligible blast effects, the projection hazard is the predominant effect. The radius to a certain degree of acceptable hazard depends essentially on the particular design of explosive article concerned (in the military field typically HE gun ammunition not exceeding 100mm calibre). It must be borne in mind that the range of effects is not

significantly increased when the quantity is increased, since the articles react individually. A typical incident would begin as, or soon result in, a fire in a ammunition store or vehicle and continue possibly for hours in the absence of fire fighting action. This extended duration would allow spontaneous evacuation of personnel not seriously injured in the initial event. Both NATO and UK/MOD specify the distance function:-

$$D = 68 Q^{0.18} \text{ in metres and kg}$$

for the hazardous types of HD 1.2 explosives with a minimum of 270 m (900 ft). [In the writer's opinion this almost negligible factor of 0.18 is a sop to the gut feeling that if 2 tonnes of ammunition requires a "safe distance" of say 270 m then 20 tonnes must need more - why not 400m?] It is noted that UD DOD in Interim Change 1 to Table 5 of DOD 5154 simply specifies fixed distances for particular types of HD 1.2 explosives irrespective of quantity. Although historically less interest has been shown in the investigation of projection hazards than of blast, recently more attention has been given to the study and measurement of projections. A joint Australian/UK series of tests whose results are currently being analysed is merely the latest effort in this field.

Flame is produced when almost all explosives function. In a mass detonation the visible flame is very quickly extinguished and normally is not so effective as blast and projections in causing damage at a particular distance. Since HD 1.2 items react individually the flame produced is typically even less significant than for HD 1.1 explosives. By contrast HD 1.3 explosives display heat and flame as the predominant effect.

In contrast with the blast and projection effects typical of HD 1.1 and HD 1.2 explosives, the firey behaviour of HD 1.3 explosives has hardly been studied at all. This in spite of the large quantities of propellants which are used, particularly in military ammunition. It is by no means only for KE weapons that propellants are the predominant type of energetic material present. Again it is often overlooked that Nitrocellulose (NC) and Nitroglycerine (NG), traditionally used in propellant formulations, have a higher energy content per lb than almost all other High Explosives.

It is well known that the energy in the propellant can be harmlessly dissipated by burning when unconfined. It appears to have been tacitly assumed that the behaviour of bulk boxed propellant, if involved in a fire, will invariably approximate to that of an unconfined fire. Subsequent to the 1939-1945 War, ESTC revised the UK regulations, including Quantity-Distances, concerning the storage of propellants. During consideration of the matter it became apparent that then current Q-Ds were not based on reliable experimental evidence. The opportunity presented by the need to dispose of war surplus propellant in West Germany led to the controlled burning of up to 175,000 lb (800,00 kg) stacks at DUNE. It was then decided that more closely controlled tests should be carried out in UK and, after some simple preliminary trials a planned series of trials was



R 107.
General view of 40,000 lb. cordite stack before
firing, showing the instruments on line D.

initiated involving stacks of propellant up to 40,000 lb (18,000 kg) in mass in the open air.

TRIALS CARRIED OUT 1948-1949 (Ref.4)

A programme of trials was carried out involving wire cages to hold bare 'cordite' propellant in an approximate cubic heap. It was found that central ignition of the stack gave a faster development of maximum burn than peripheral ignition. The maximum flame radius at ground level with central ignition could be represented by the formula:-

$$\begin{aligned} R \text{ (ft)} &= 1.04 W^{0.44} & (W \text{ in lb}) \\ \text{or } R \text{ (m)} &= 0.45 Q^{0.44} & (Q \text{ in kg}) \end{aligned}$$

A simplified formula was proposed:-

$$\begin{aligned} F \text{ (ft)} &= 0.6 W^{\frac{1}{2}} & (W \text{ in lb}) \\ \text{or } R \text{ (m)} &= 0.27 Q^{\frac{1}{2}} & (Q \text{ in kg}). \end{aligned}$$

Both formulas giving the same distance of 25 m for 8500 kg (80 ft for 19,000 lb).

N.B. The influence of the wind has been ignored. It is known that wind velocities less than 10 ft/sec (3 m/sec) can significantly move the fire ball down wind from the propellant heap.

TRIALS CARRIED OUT 1958 (Ref.5)

A further series of trials were carried out using similar wire cages to restrain the bare cordite propellant. Essentially these were a repetition of the previous trials with, however, some sophisticated recording equipment including thermal dosage meters. It was determined that the maximum flame radius of the fire ball (irrespective of height) could be represented by the formula:-

$$\begin{aligned} R \text{ (ft)} &= 7.4 W^{0.28} & (W \text{ in lb}) \\ \text{or } R \text{ (m)} &= 2.8 Q^{0.28} & (Q \text{ in kg}) \end{aligned}$$

For 8500 kg this is 36 m (116 ft for 19,000 lb).

Again the influence of the wind is ignored.

PRACTICAL CONSIDERATIONS

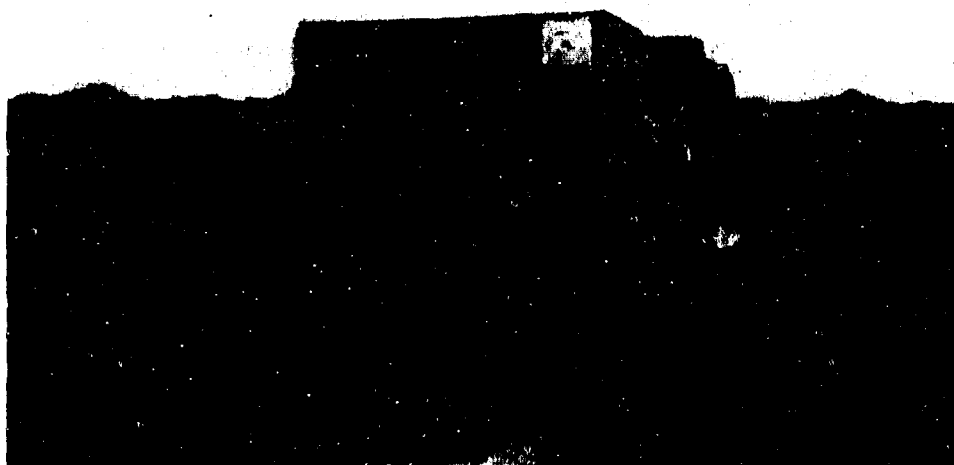
The implied assumption that propellant is stored and carried effectively in an unconfined state is crucial. Since it is known that the burning rate of propellant is markedly increased (by a factor exceeding 10^3) when greatly confined in a gun breech or a rocket motor it is surprising that no effort seems to have been made to allow for the effect on the burning rate of propellant by a structure which would provide limited confinement. Such a structure could be a brick or concrete walled storehouse with a concrete roof of say 6 inches (150 mm) thickness. In the UK such construction is widely used for stores and process buildings. A process building would be provided with windows but a typical storehouse would be without. The internal pressure required to lift such a roof, not tied down the walls, would be about 0.5 psi. It may be taken for granted that the weakest part of the structure would be the door(s) and that they would be forced open if propellant within took fire. This would allow some venting of combustion products from the propellant and it appears to have been assumed that such venting would effectively restrict the propellant burn rate to an acceptable degree, presumably dependant on the thermal protection afforded by the packages.

RECENT TRIALS OF BOXED GUN PROPELLANT (Refs. 7 & 8)

Between 1973-75 trials were carried out in the UK to compare the resistance to the spread of fire within a stack of boxed gun propellant. Boxes constructed of fibreboard were compared with re-useable C128 wooden boxes traditionally used to carry propellant in the UK by MOD. Rather surprisingly it was found that there was some difficulty in ensuring communication of fire from one box of propellant to adjacent boxes in a rough stack. The trials were carried out in the open and even slight winds seriously affected the impingement of the flames onto adjacent boxes. The details of the flame geometry from the ignited box was found to be significant. The propellant in the strong wooden boxes was found to communicate more quickly when the boxes were neatly stacked on pallets than the lighter fibreboard boxes which were effectively airtight. On a pallet the precision made wooden boxes were quite accurately aligned with other boxes in the same layer. These boxes were fitted with a simple clipped on lid overlapping the ends and sides. On igniting the propellant in one box the pressure within lifted the lid slightly without dislodging it and a laminar flame issued exactly aligned to play on the join between the next box and its lid. The result was a very fast communication of the fire to all boxes in a particular layer. Communication of fire between boxes on other layers took much longer and often the propellant was extinguished before layer to layer communication occurred. Communication between the fibreboard boxes proceeded by means of fire penetration of the box material itself. Although it took longer for the box to box



Fig. 1. General view of Pontine block stone.
(Log Ref 6301).



REMARKS: The block is a single unit of masonry, and is of a dark color. It is of a rectangular shape, and is of a size of approximately 1.5 meters by 1.0 meters. It is of a weight of approximately 1.5 tons. It is of a type of masonry known as Pontine block stone.

communication to occur it eventually encompassed all of the fibreboard boxes on a pallet, or pallets, provided these were touching or close together.

LARGE SCALE TRIALS OF BOXED GUN PROPELLANT (Ref. 9)

It was decided to investigate the rate of spread of fire along a row of pallets of boxed propellant within a representative building. A survey of magazines showed that a volumetric loading density of approx. 4 lb propellant per cubic foot was typical (64 kg m^{-3}). The typical pallet was approximately a 4 ft (1.2 m) cube and, when carrying propellant in fibreboard boxes, held approximately 1000 lb (450 kg) net. A long room was constructed of large concrete ('Pendine') blocks having a height and internal width both of 8 ft (2.4 m). The length was just in excess of 40 ft (12 m) with one end closed, and the other being completely free. The roof was formed of steel plates about $\frac{3}{4}$ inch (18 mm) thick and 12 feet (3.6 m) long butted together and set across the room width. It was realised the 'doorway' was an unrealistically large venting area for such a storehouse of volume of 2560 ft^3 (77 m^3). Ten pallets were placed along the axis of the room and touching as would be a typical stack in a magazine. The ten pallets held approximately 10,000 lb (4,500 kg) in total of propellant. The blocks forming the walls were carefully positioned to leave 'arrow slots' a few inches wide between. Cameras were placed to observe the spread of flame down the length of the building. One box of propellant on the pallet nearest the doorway was ignited. The test was repeated with a similar stack of pallets of wooden boxes of gun propellant. Because of the lost volume these ten pallets held approx. 7500 lb (3400 kg) in total of propellant. Each trial was repeated making four firings in all.

There was an initial delay whilst the first box fire communicated to the other boxes on the outermost pallet. The arrow slots then successively spurted flame and shortly after bright flames were seen at the last slot indicating, presumably that flame filled the whole volume of the room, the rate of combustion accelerated violently. The flame discharged from the open end of the room so increased that in the first (fibreboard box) trial a roaring flame jet swept for 200 ft (60 metres) horizontally along the ground. The roof plate at the closed end of the room lifted and was dislodged thereby somewhat reducing the confinement. This violent phase when presumably the greater part of the propellant reacted, lasted about 5 seconds. Unfortunately, the cameras were not aligned to monitor this flame projection. A similar result occurred with the other fibreboard box trial.

The trials involving the C123 wooden boxes proceeded very similarly although with a slightly less violent reaction. It is impossible to ascertain whether the reduced propellant loading density or the protective effect of the wood versus fibreboard caused the difference. Trial 2 of the wood box fire, is illustrated in the film clip. In trial 4 there was a delay, amounting to hours, before the fire was established. The established fire behaved identically to that in trial 2 but no film record was taken.



Fig 7. Firing 3. Fibreboard boxes. Fire has just reached end of store.
(Neg Ref 6398).



Fig 8. Firing 3. Flame beginning to vent fiercely from open end.
(Neg Ref 6399).



Fig 9. Firing 3. Burning fiercely, with flaming debris thrown from open end.
(Neg Ref 6400).



Fig 10. Firing 3. Pressure through open end reduced by venting through roof.
(Neg Ref 6401).

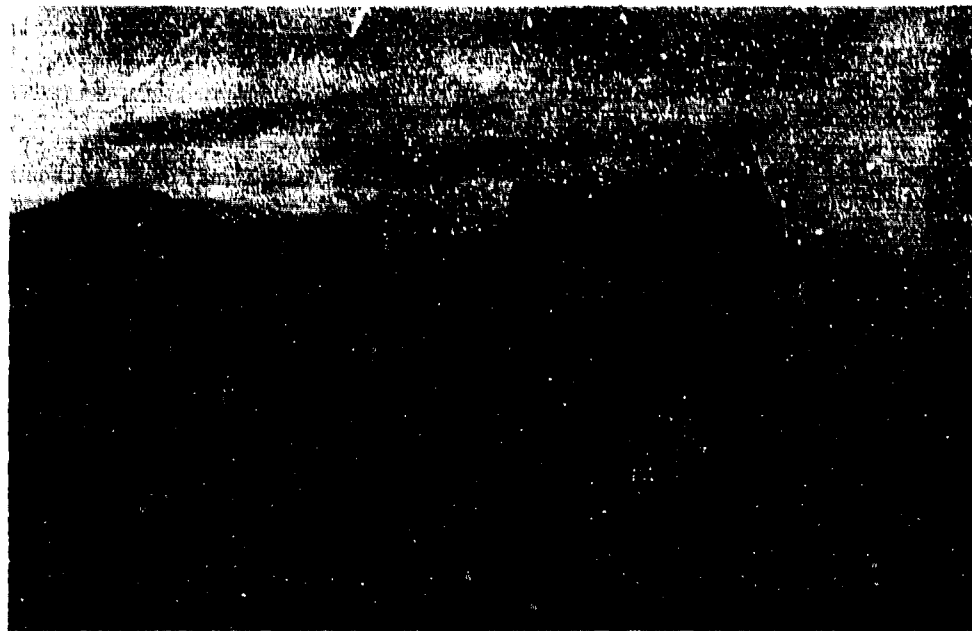


Fig. 13. Firing 3. Showing pallets thrown out.
(Neg Ref 6386).



Fig. 14a. Firing 3. Showing roof plate and half Pandine block thrown off.
(Neg Ref 6390).

OBSERVATIONS

The 18 mm steel roof of the model room constructed for the trials had a weight corresponding to 0.20 psi. It is reasonable to assume that leakage of the pressurised combustion products between the top of the concrete wall and the plate submits the whole area of the plate to much the same pressure and that this represents the maximum confinement of combustion products. It would be anticipated that the maximum internal pressure would occur remote from the vented end of the room. The structure, although it may appear to be of massive construction, is in fact much weaker against a sustained internal pressure than many common types of well built storehouses. This implies that the effects demonstrated are minimal and, apart from wooden sheds or thin pannelled buildings, might be exceeded should an incident occur in many existing propellant storehouses. It is relevant to note that French practice has been to store propellants in long buildings with one long side completely open, apart from a mesh screen, which arrangement produces negligible confinement of combustion products.

The strength of the anticipated flame jet from a doorway or other opening requires that a normally constructed propellant storehouse must never be orientated to allow the jet to play on the door or window of an adjacent building. If the building at the exposed site is constructed with concrete or brick walls without windows, integral concrete roof and is orientated with door(s) away from the potential explosion site it seems reasonable to assume that communication of fire would be effectively precluded. Earth covered buildings would, of course, be even more effective fire barriers. However, even a simple inperforate brick wall should be an effective fire barrier and not transmit the heat from a comparatively fast burning propellant fire at the PES. Communication should not occur provided the roof was also a fire barrier and there are no gaps between roof and walls. Distances based entirely on Quantity would seem to be more or less irrelevant in the close-in situation.

FACTORS INVOLVED IN A PRACTICAL PROPELLANT INCIDENT

The duration of a fire may be very variable, in particular the lead up time to the maximum rate of heat emission. Most of the combustion will take place during a very limited period, of the order of 5 seconds, if the high intensity fire surge does occur. Obviously, if the incident only involves intermittent burns of small quantities of propellant over an extended time the chances of communication or injury are negligible. It may be noted that both the bare propellant stack and the boxed propellant in a moderately strong storehouse show the same period (5 secs) of high intensity fire. The presence of boxes holding propellant is likely to delay the onset of the high intensity fire but not to greatly affect the high intensity burn rate in a moderately strong storehouse (e.g. brick walls with concrete roof).

Buildings of slightly greater strength e.g. of reinforced concrete with integral roof, or igloos, may by confinement provoke even faster high intensity burn rates.

The position of the 'fireball' from a storehouse door will not approximate to the building itself if radiation is being considered. Any calculation of radiative heat transfer is likely to be misleading on this account since the effective centre of the 'fire ball' may be 50 m in front of the doorway.

For concrete buildings the flame jet produced may approach 100 m in length. Direct flame impingement by the jet may give heat transfer rates up to 10 times that expected from radiation at distances of the order of tens of metres, typical of inter storehouse spacings. A wall traverse may be used to deflect an anticipated flame jet to protect against direct flame impingement. Radiation from the buoyant flame will still occur, however, over the top of the wall. Provided the roof of the acceptor building is fire resistant this may be tolerable. Windows are, of course, transparent to heat radiation.

Quantity Distances based on radiant heat doses to people may be inadequate if:-

- a. The radiant heat pulse is of much shorter duration than the 6 secs usually postulated, (Reference 11) as may be caused by strong building confinement.
- b. Building orientations are not taken into account unless well positioned door traverses are used to mitigate.
- c. A large quantity is stored in each chamber (or carried in a ship's hold). Considerations of radiation would indicate an inverse square law for Q-Ds. British experiments indicate that the flame radius scales as $Q^{0.44}$ but Q-Ds for HD 1.3 explosives are mostly scaled at $Q^{\frac{1}{3}}$ as for detonating explosives with, however, a much smaller k factor. It is well known that large quantities of propellants when stored underground can, when involved in a fire, lead to projection of the cover and blast effects approaching that to be anticipated from a similar quantity of detonating high explosive. It would appear logical, therefore, that Q-Ds for HD 1.3 explosives be markedly less than for HD 1.1 mass detonating explosives for quantities of the order of a ton or so (neglecting the flame jet effect). If the scaling increase were based on $Q^{0.5}$ or $Q^{0.44}$ the distance would eventually overtake the Q-Ds for HD 1.1 explosives based on $Q^{\frac{1}{3}}$. It would be particularly convenient if this occurred at a quantity 'Q' large enough for the transition from burning to high order deflagration to be plausible.

CONSIDERING INHABITED BUILDING DISTANCES

The inhabited building quantity distances for the storage of HD 1.3 explosives are (for larger quantities) currently calculated using the distance functions:-

$$D = 6.4 Q^{\frac{1}{3}} \text{ in metres and kg (16 } W^{\frac{1}{3}} \text{ feet and lb)}$$

in NATO and UK/MOD, Refs 1 & 2.

$$\text{and } D = 3.2 Q^{\frac{1}{3}} \text{ in metres and kg (8 } W^{\frac{1}{3}} \text{ in feet and lb)}$$

in USA, DOD, Ref.3.

It is reasonable to assume that most accidental fires have occurred with smaller quantities of explosives (i.e. 10 tonnes or less) since the majority of explosives storehouses fall into this group. It may also reasonably be assumed that most incidents were due to external effects and not to inherent chemical instability of propellant material, which can presumably be ruled out these days. The practicable experience of fires involving HD 1.3 explosives may have been given undue weight in setting out protection levels. The possibility that, for propellant storage buildings of quite common design when quantities exceed a few tons, the effects may be quite disproportionally more violent than normal experience has apparently been disregarded.

The IBDs prescribed in both NATO and UK for propellants are 29% of those specified for high explosives. In US military practice the ratios range from 20% for smaller quantities down to 16% for Q of 250,000 lb (110,000 kg). Again making the point rather differently:- The same spacings and presumably acceptance of injury levels to persons and damage, are used by NATO and UK for Process Building Distances and for Inhabited Building Distances in the USA.

CONSIDERING MAGAZINE DISTANCES

The quantity distances between magazines or explosives storehouses for HD 1.3 explosives are currently calculated using the distance functions:-

$$D = 0.22 Q^{\frac{1}{2}} \text{ in metres and kg (0.49 } W^{\frac{1}{2}} \text{ in feet and lb)}$$

in NATO & UK/MOD, Refs. 1 & 2.

$$\text{and } D = 2.0 Q^{\frac{1}{2}} \text{ in metres and kg (5 } W^{\frac{1}{2}} \text{ in feet and lb)}$$

in USA, DOD, Ref.3.

The NATO/UK value represents about 80% of the flame radius from an unconfined bare stack of propellant (Ref.4). Since the distance scales as the square root of the quantity it becomes progressively more conservative as Q increases. The US DOD value being scaled as the cube root of the quantity becomes progressively less conservative as Q increases. (Making the assumption that the effect is correctly represented by an index approximating to 0.45). However, the actual distances required by the US are longer for quantities up to 500 tonnes, which may possibly be the practicable limit.

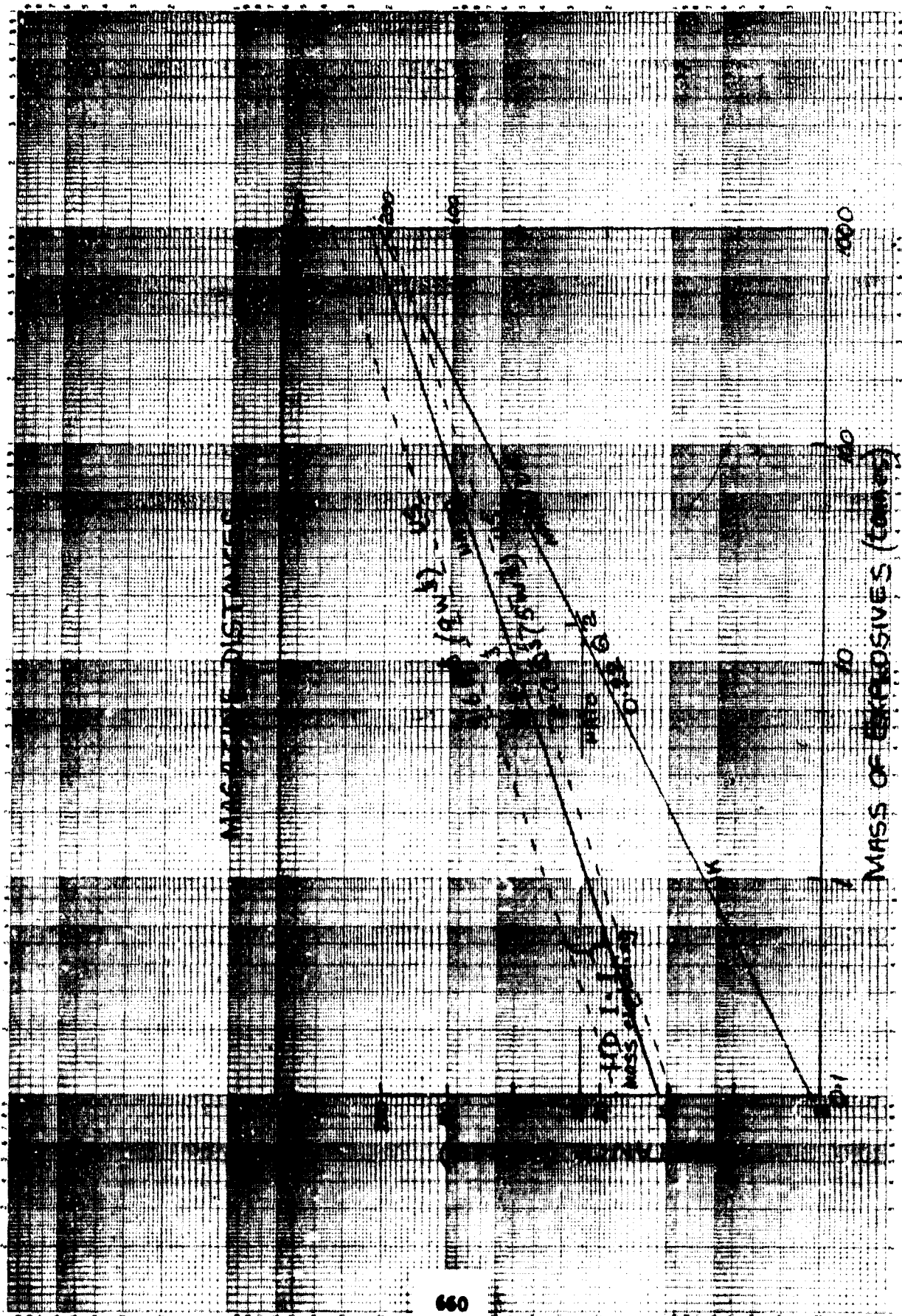
The inter-magazine distances with barricades prescribed in NATO/UK for propellants are 29% of those specified for high explosives for 1 tonne rising to 82% for 500 tonnes. In US military practice, the constant ratio is 55% of the US HD 1.1 Q-D of 9 W³ feet, and lb (3.6 Q³ in metres and kg). The NATO/UK distance for HD 1.1 is 2.4 Q³ in metres and kg (6 W³ in feet and lb), perhaps a traverse (UK) gives greater protection than a barricade (US)? If a Q of 8.5 tonnes (18,700 lb) is considered as a typical storehouse load then the US tabulated distance (Ref.3) is 125 ft (38 m) and the NATO/UK value (Ref 1 & 2) is 21 m (69 ft). One can only speculate as to the rationale behind the unusually conservative approach by US DOD compared with NATO. It may, presumably, be assumed that it was not based on flame jet considerations.

CONCLUSION

Consideration of some HD 1.3 quantity distances show many anomalies and imply that the level of protection they afford may be inadequate compared to HD 1.1 and 1.2 explosives whose effects are better understood. It is the strongly held view of the writer that the behaviour in a fire of boxed propellants, and the various types of rocket motor classified as HD 1.3, does not lend itself to theoretical study nor to modelling. Large scale test firings should therefore be carried out to confirm, or otherwise, the presently accepted quantity distances. More immediately, large quantity HD 1.3 storage facilities should be surveyed to ensure any probable jetting effects from buildings do not produce an unacceptable communication hazard.

REFERENCES

1. Manual of NATO Safety Principles for the Storage of Ammunition and Explosives, Part I, Table 3A, October 1976.
2. Quantity Distances for Military Explosives, ESTC/220/LEAFLET No.5 - Part 2, Table 3A, June 1979.
3. DOD Ammunition and Explosives Safety Standards DOD 5154.4S Table 5 - 6.1 Interim Charge 1, 29 August 1979.
4. Ministry of Supply, ARE Report No.5/52, D.E. JARRETT, January 1952.
5. Ministry of Supply, P&EE(S), Trial Report to SXR/108/01, June 1958.
6. ESTC Safety Distances Sub-Committee Working Paper 7A, October 1960.
7. P&EE Pendine, Trial Report 45/73 dated December 1973.
8. P&EE Pendine, Trial Report 91/74 dated March 1975.
9. P&EE Pendine, Trial Report 32/76 dated April 1977
10. The Radiant Heat from burning propellant in bulk. ESTC 100 C WP 7A. D.E. JARRETT. October 1966.
11. Derivation of the British Explosives Safety Distances. Ann. NY. Academy of Sciences Vol.152 D E JARRETT. October 1968



IMPROVED THERMAL PROTECTION FOR
PYROTECHNIC WORKERS

Jim I. Martin, Don W. Moore, Tracy K. Bramlett
Day & Zimmermann, Inc.
Lone Star Army Ammunition Plant

OBJECTIVE

The objective of this research was to determine the relative advantages and disadvantages of various types of fabrics and materials for providing protection for employees against flash fires. After determining the best materials for thermal protection, design requirements for a flashsuit, gloves, and visor assembly were to be established.

BACKGROUND

The selection of protective equipment and clothing to guard against thermal injury to ammunition and explosive workers must have a sound basis in fact. Until recently it did not. Assumptions had been made that protective equipment that has proven itself adequate for civilian firefighters, or for steel workers, or for airplane fuel firefighters, could be successfully used at ammunition plants. The unfortunate evidence provided by recent incidents and the results of a series of preliminary tests indicated that these assumptions were false.

As a result of these discoveries, a need for re-evaluating the protective qualities of the materials used became apparent. Alternative types of materials were considered. Product descriptions were obtained. The opinions of fabric manufacturers, of suit designers, and of protective suit users were solicited.

A bewildering variety of answers was obtained. Different fabric manufacturers used different types of tests which produced incompatible results. Suit designers and the users of protective suits had greatly varying requirements to meet their different sources of thermal stress. It became apparent that the only way to have a sound basis for selecting different fabrics was to conduct a methodical examination of the thermal protection properties of these fabrics and materials under a standardized testing procedure.

EXPERIMENTAL PROCEDURE

A series of tests was designed to evaluate the properties of protective fabrics and materials against various heat sources. Laboratory tests were conducted with a fixed heat source; field tests were conducted with one type of pyrotechnic materials; and burn envelope tests were conducted with quantities of different types of pyrotechnics.

Laboratory Tests

The laboratory tests gave the opportunity to obtain reliable and complete data on the benefits of different kinds of material. The tests were conducted under controlled conditions, with a defined heat source, with a fixed distance from the heat sources, and with a measured amount of time.

As a result of extensive trial and error, a reliable, practical, and relatively realistic experimental procedure was developed. It consisted of exposing samples of fabrics to an oxyacetylene torch for brief periods of time. A mechanical shutter allowed the fabric to be exposed to the flame for times

varying from 1/4 second to 1 1/4 seconds. The fabric was positioned so that it was in the most intensely hot part of the flame (2.5 inches from the orifice) where a thermocouple consistently indicated readings of over 2,600° F.

Samples of different fabrics were exposed to the flame while the temperatures on the unaluminized side were recorded using thermocouples and temperature indicator strips. Thermocouples were used for most of the testing because, in addition to indicating the maximum temperature reached, they could be used to determine the length of time it took to reach that maximum temperature and the total time that the temperature exceeded 140° F (blistering will occur if the base layer of skin reaches this temperature).

The same laboratory test series was conducted under conditions simulating the effects of deluge activation. Water was discharged onto the aluminized surface immediately after the flame was cut off. Under these conditions, the desirable characteristics (lower maximum temperature and shorter time above 140° F) of all fabrics showed improvement. Nevertheless, the same rank order of fabrics was found to hold in both the dry and wet conditions.

Additional tests were performed, using the same test apparatus and single or multiple layers of underlying fabric (unaluminized Nomex or cotton). With the addition of underlying fabrics, the desirable characteristics of fabric protection improved. In general, the same rank ordering of outer protective

fabrics was found to hold across all combinations of underlying fabrics. Greater variability in the results was found. Previous researchers have concluded this variability occurs because it is impossible to keep the multiple layers consistently separated from one test to another.

The tests in the laboratory setting using the oxyacetylene heat source permitted rigid control of the test circumstances. The heat source characteristics, the distance from the flame, and the time of exposure were all controlled with some precision. As a consequence, it was possible to make an accurate comparison between the protective properties of the different fabrics.

Field Tests

In the field tests, using pyrotechnic materials as the heat source, precise control of the factors cited above was impossible because of variations in the materials, the burn rate, and the evolution of the burn sequence. Nevertheless, it was necessary to determine to what extent the results of the laboratory tests applied to the actual field situation.

The field tests were performed with a movable arm which passed the sample of fabric or material through the flame of a burning pyrotechnic pellet at a fixed rate of speed. For most of the test series, the samples passed 1 inch over the burning pellet and were thoroughly immersed in the flame. Exposure times varied from approximately 0.5 seconds to 3.0 seconds. Temperatures were recorded with quick response thermocouples, and heat flux was measured with a calorimeter. Most of the tests were performed with single layer samples, but additional ones duplicated

the multi-layer and simulated deluge tests performed in the laboratory.

For the most part, the results of the field tests paralleled those of the laboratory. The one major difference was in the effectiveness of inerting a layer of reflective foil in the visor facepieces. The laboratory tests had shown little effect of the foil, but with some pyrotechnics, the foil greatly reduced the temperature increase, probably because of the higher radiant energy generated by the pyrotechnic material.

Burn Envelope Tests

The burn envelope tests were performed primarily with various quantities of a high-range pyrotechnic mix (one that had the greatest caloric output). Additional tests were conducted with mid-range and low-range mixes.

The burn envelope tests were the most difficult to control, to measure, and to replicate. Major differences in the growth, shape, and movement of the burn envelope from one test to the next made it impossible to ensure that samples mounted at the same position were actually exposed to the same thermal threat.

Analysis of the data showed, however, that the same general performance characteristics of the different test materials were maintained in the burn envelope tests. No major differences were determined, but valuable data about the shape and development of the thermal threat from pyrotechnic mixes were obtained.

RESULTS AND DISCUSSION

The test series generated volumes of data for a wide variety of samples under many different test conditions. The findings of the various test series are summarized in the following subsections by the major area of interest - fabric, glove, visor, and burn envelope results.

Fabric Results

Tests on various kinds of fabrics were performed with 25 types tested in the laboratory series and 40 in the field tests. Various weights and thicknesses of aluminized and unaluminized fabric were examined. Table 1 summarizes the types of fabrics examined.

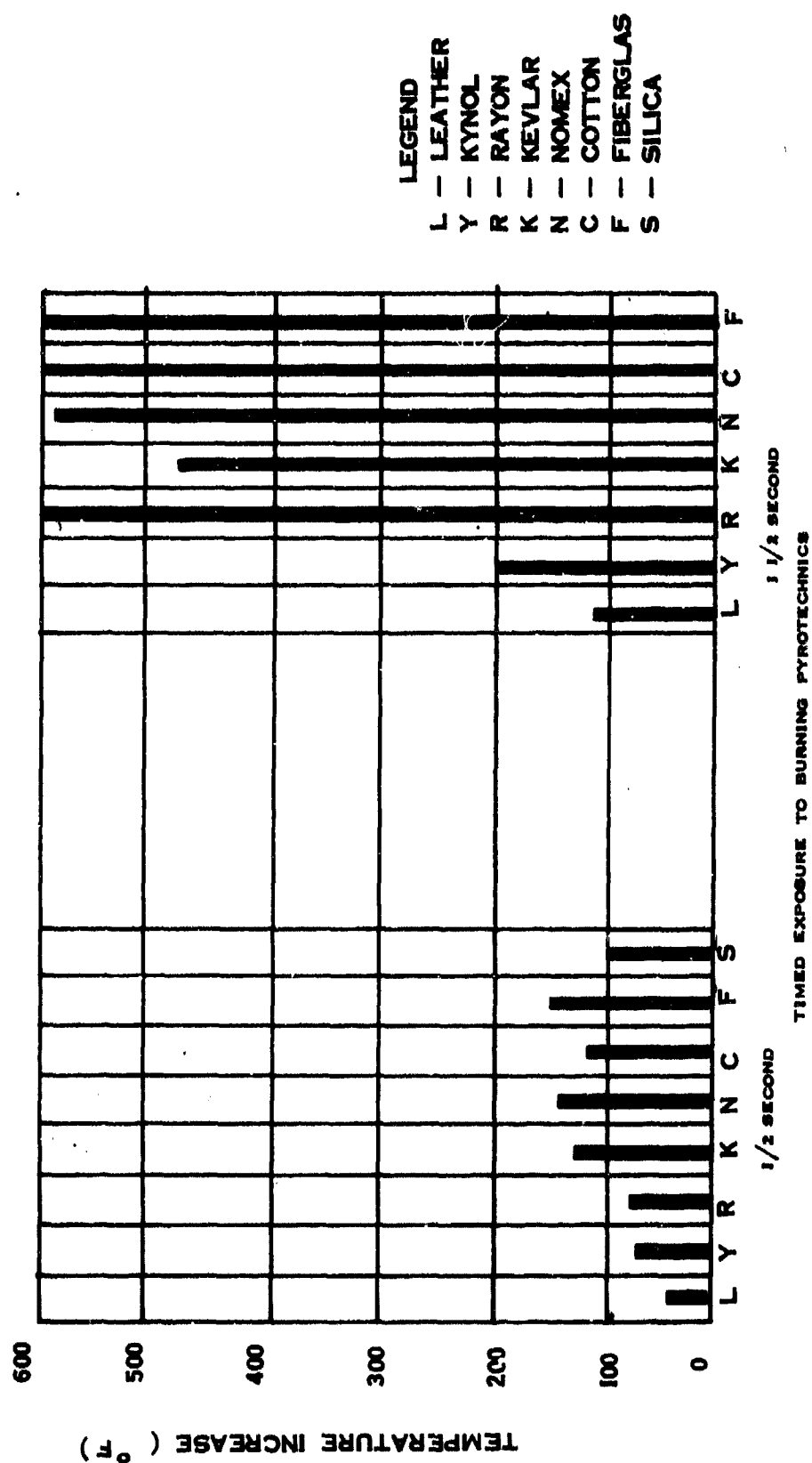
TABLE 1.

FABRICS TESTED

LAB	FIELD	TYPE
4	4	KYNOL
4	4	RAYON
5	5	KEVLAR
4	6	NOMEX
0	5	SILICA-BASED
3	4	OTHER SYNTHETICS
2	2	NATURAL FIBERS
3	10	LEATHER

The data from the laboratory tests and pyrotechnic field tests were in close agreement. Data from the field tests with single layers of protective fabric are summarized in Table 2 and illustrated in Figure 1. For short duration exposures,

Figure 1.
TYPICAL PYROTECHNIC TEST RESULTS



the differences between the various fabrics appear relatively inconsequential; for prolonged exposures, however, there are significant differences.

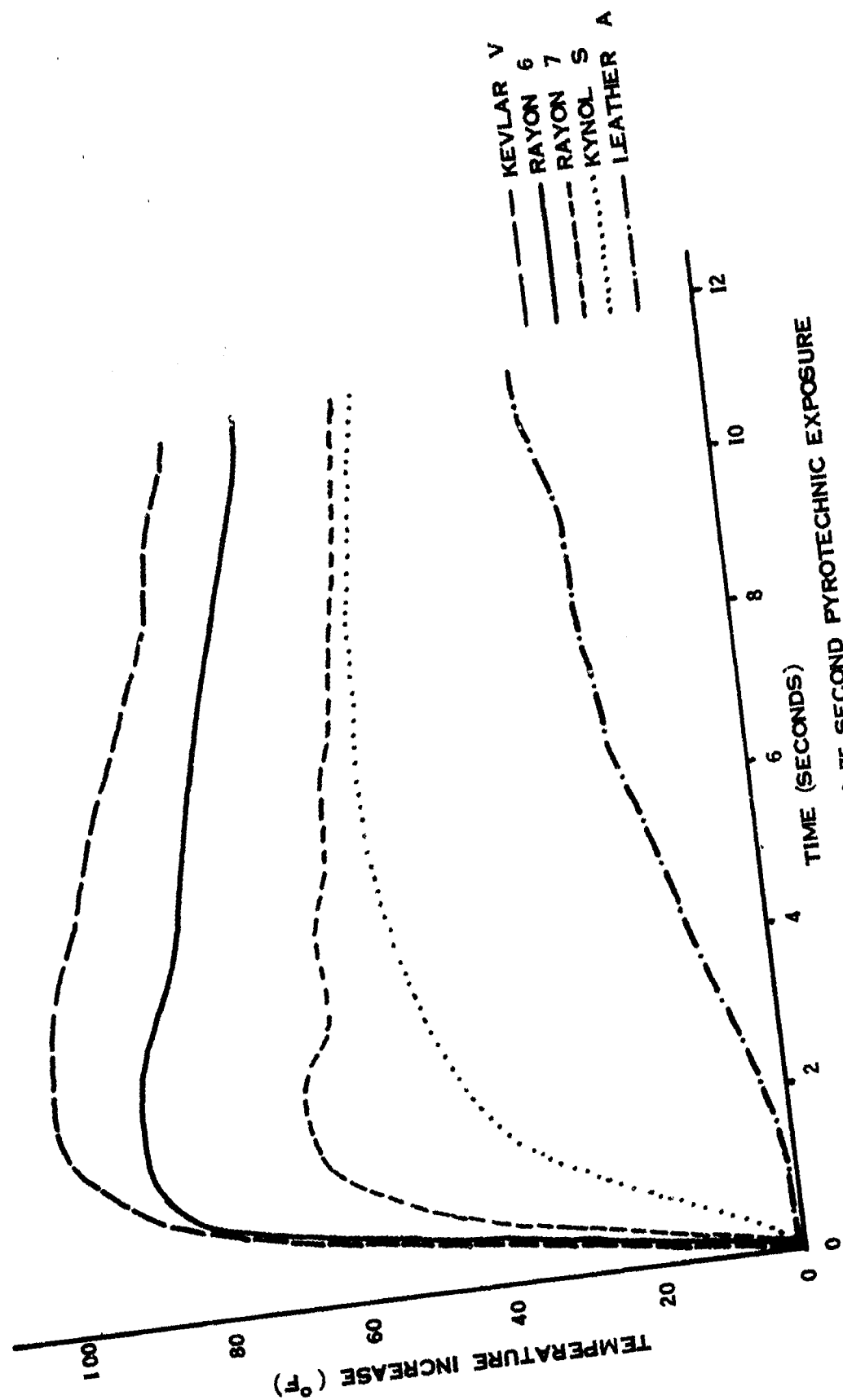
TABLE 2.

TYPICAL PYROTECHNIC TEST RESULTS

EXPOSURE TIME TO BURN	1/2 SEC	1 1/2 SEC
LEATHER	40	101
KYNOL	79	200
RAYON	81	CHARRED
KEVLAR	131	470
NOMEX	140	567
COTTON	134	BURNED
FIBERGLAS	150	670
SILICA-BASED	100	770

Leather consistently performed the best. Kynol-based fabrics also yielded good performance and were generally superior to other fabric blends; however, it is impossible to specify one fabric as the best under all test conditions, test measures, and operational requirements. Different materials proved superior under certain circumstances. In general, however, Kynol appeared the best of the synthetic fabrics.

The reason for some of the inconsistency in results is apparent in the following figures. For a short duration exposure to pyrotechnics, the results are relatively straightforward. (See Figure 2.) Leather appears the best with the lowest and slowest temperature rise. When the exposure time is lengthened

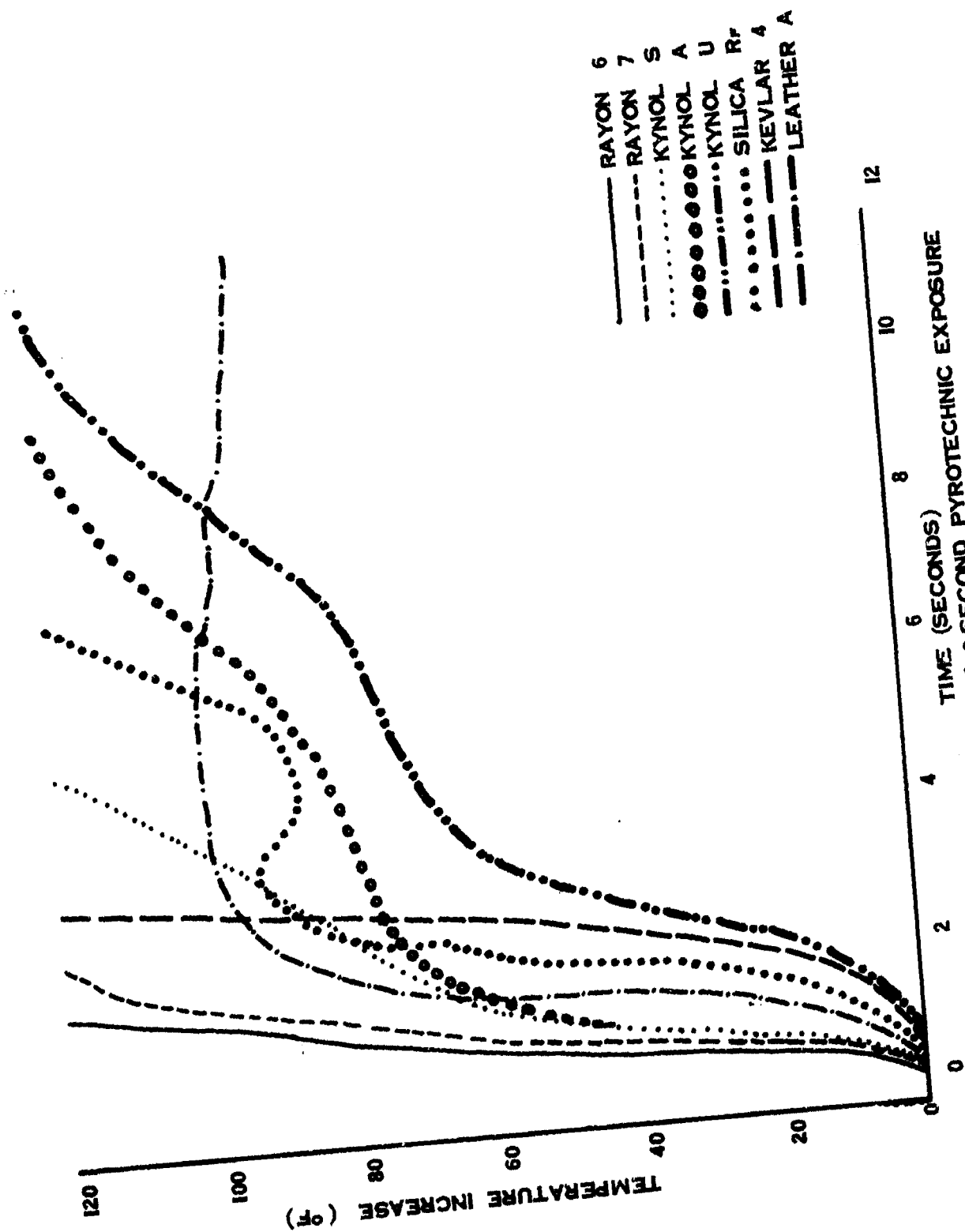


TEMPERATURE RISES FOR 0.75 SECOND PYROTECHNIC EXPOSURE
Figure 2.

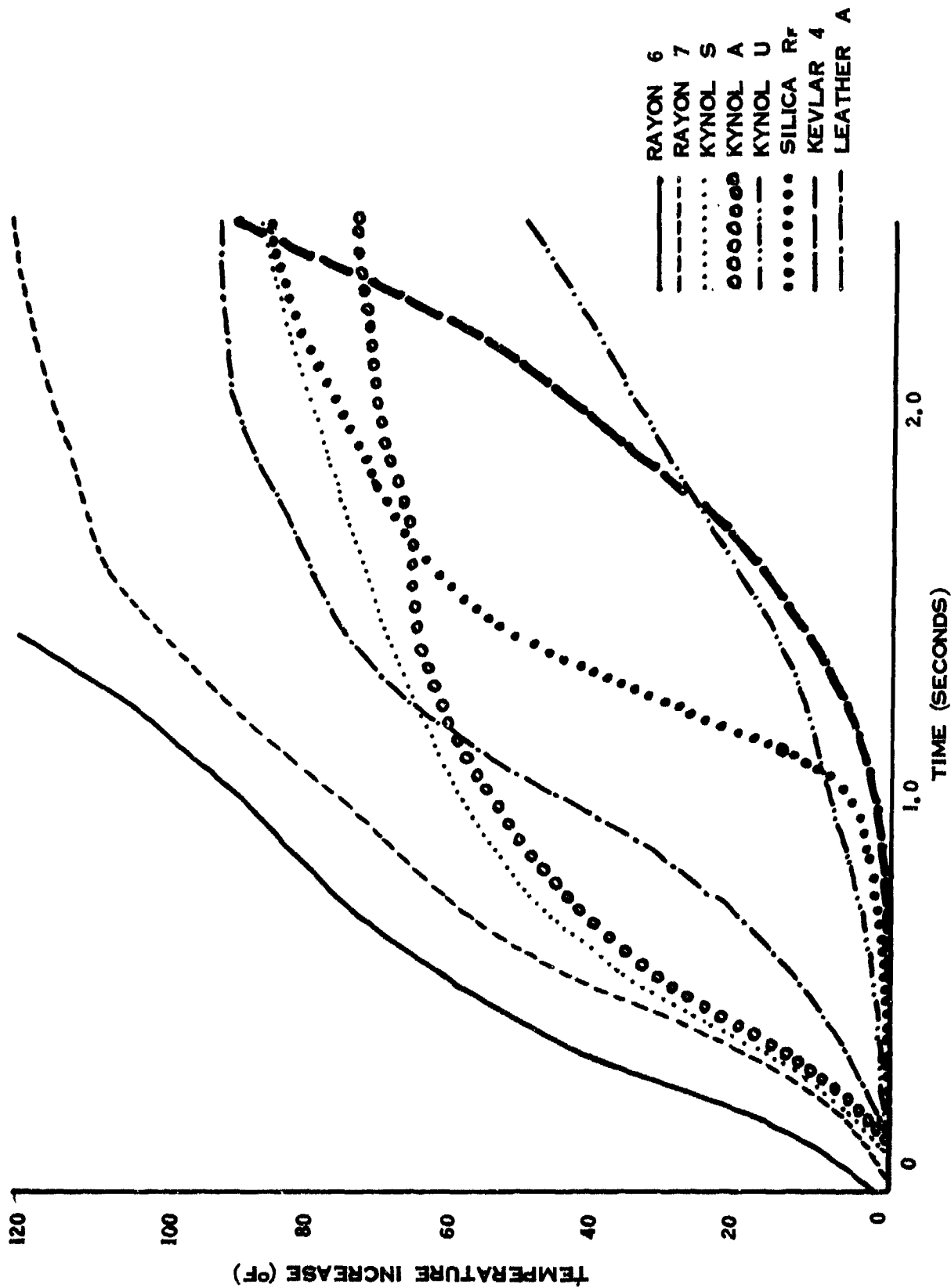
to 3.0 seconds (see Figure 3), the results become confusing. Is it more desirable to have a fabric with a slower temperature rise, even though the maximum temperature attained is significantly greater (e. g., the Kevlar as opposed to the Kynol S, or the Kynol A as opposed to the leather)?

The selection of fabrics becomes even more confusing when the early temperature rises occurring immediately after exposure to the flame are examined. In work operations where a deluge system is mounted, the rapid onset of water would dissipate the heat before it could penetrate the fabric, so it would appear that the fabric which would delay heat penetration the longest would be best. However, while failure of a deluge system is extremely rare, the consequences of such a failure would be more disastrous if a fabric with a slow, but ultimately higher, temperature rise were decided upon. Figures 4 and 5 show temperature and heat flux data for a few of the samples examined and illustrate the problem in making the selection. In general, however, by most measures, leather is the best material, and Kynol has qualities that make it the best of the synthetics.

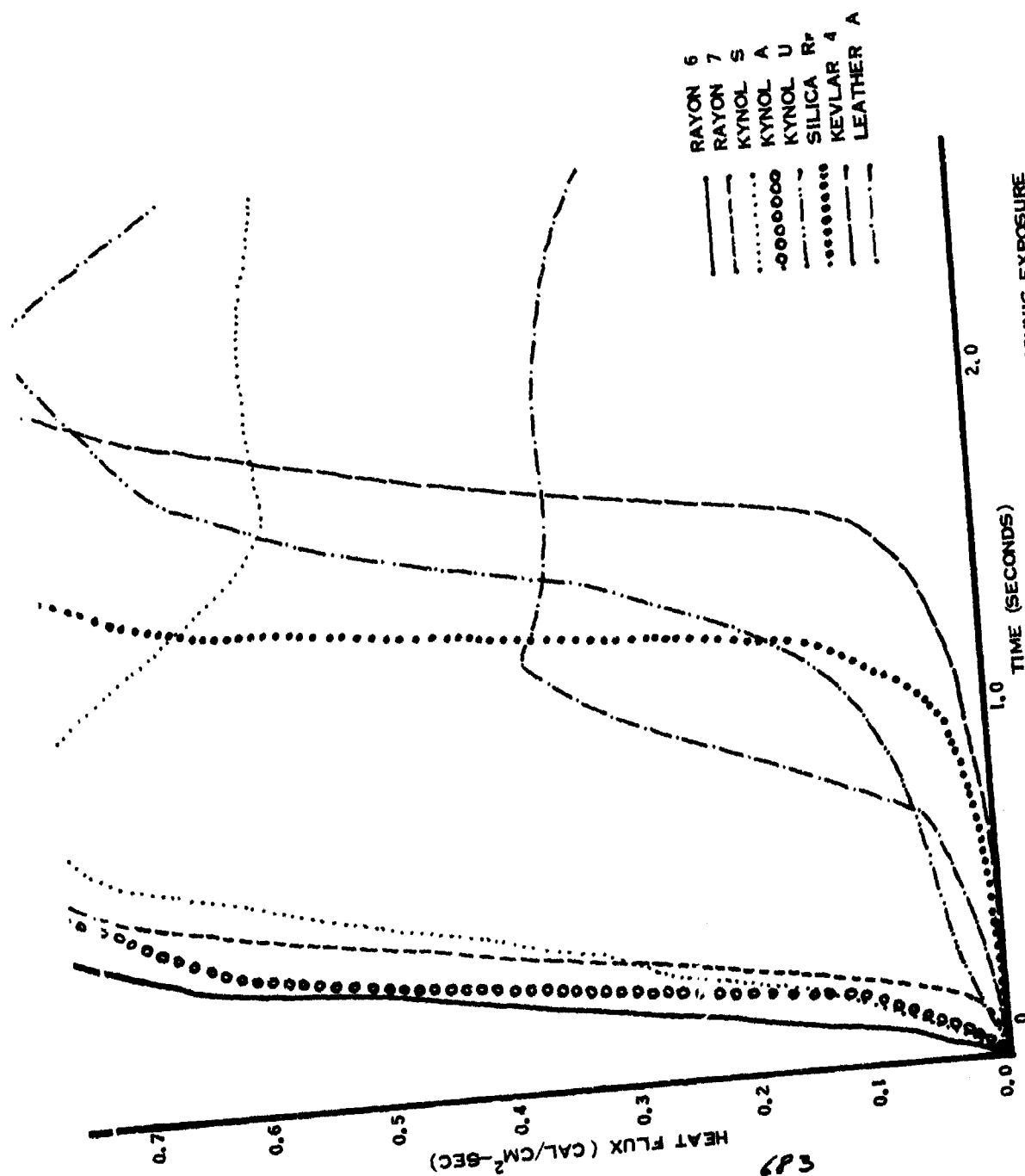
Multiple layers of Nomex underclothing reduce the temperature rise, and the rapid onset of water quickly cuts the peak temperature and promotes cooling. Tests with multi-layer and with simulated deluge conditions are illustrated in Figure 6. Despite the added protection provided by multiple layers of clothing and the deluge system, the major protection is afforded by the outer layer, and the selection of that material determines the additional effectiveness of other measures.



TEMPERATURE RISES FOR 3.0 SECOND PYROTECHNIC EXPOSURE
Figure 3.

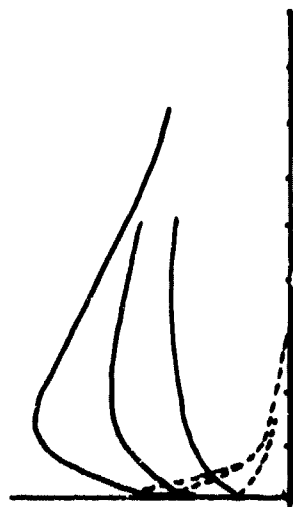


EARLY TEMPERATURE RISES FOR 3.0 SECOND PYROTECHNIC EXPOSURE
Figure 4.



EARLY CALORIMETRIC INCREASES FOR 3.0 SECOND PYROTECHNIC EXPOSURE
Figure 5.

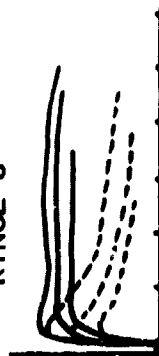
KEVLAR F



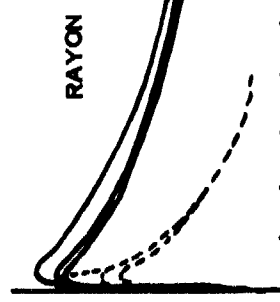
KYNOL A



KYNOL U



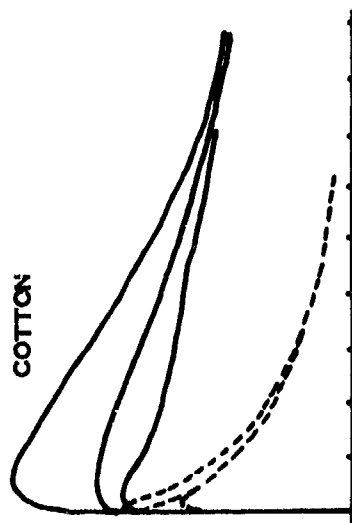
RAYON 6



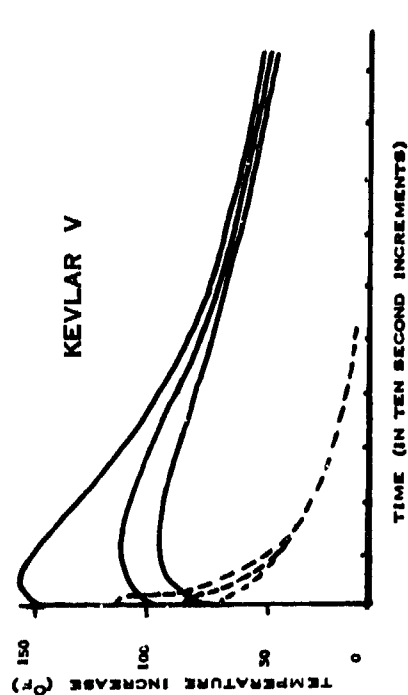
FIBERGLAS



COTTON



KEVLAR V



COMBINED MULTI-LAYER AND DELUGE TESTS

TEMPERATURE/TIME CURVES FOR FABRICS EXPOSED TO
1/2 SECOND FLAME AT 2000 °F

SOLID LINES ARE FOR DRY TESTS - DASHED ARE FOR DELUGE
CURVES DEPICT SINGLE LAYER, MULTI-LAYER 1, AND MULTI-
LAYER 2 IN DESCENDING ORDER

Figure 6.

Materials which were unaluminized showed substantially lower peak temperatures under the deluge conditions. Table 3 summarizes representative tests with some materials tested with pyrotechnic burns.

TABLE 3.

COMBINED MULTI-LAYER AND DELUGE TESTS WITH PYROTECHNICS				
TEMPERATURE INCREASES (°F)				
DRY CONDITION	KYNOL	RAYON	LEATHER	KYNOL
	ALUM.	ALUM.	UNALUM.	UNALUM.
SINGLE LAYER	81, 5	95	42	77
PLUS ONE LAYER NOMEX	32	68	48	50
PLUS TWO LAYERS NOMEX	43	61	46	45
DELUGE CONDITION				
SINGLE LAYER	81	89, 5	31	15
PLUS ONE LAYER NOMEX	44	78	10	28
PLUS TWO LAYERS NOMEX	38	47	19	4

The aluminization process makes materials relatively waterproof and retards the cooling effect afforded by the water. Although the aluminization does have this disadvantage, the advantages demonstrated in prolonged burns in the laboratory, field, and burn envelope tests provide compelling evidence that its use is warranted.

In working with pyrotechnics, it is possible that the suit or gloves may be wetted with acetone, alcohol, or water during some stage of the process. In order to determine if any of these wetting agents would have an adverse effect on the protection offered by a fabric, special laboratory and field tests were conducted. A summary of some of the data from the field tests is provided in Table 4.

TABLE 4.
EFFECTS OF WETTING AGENT ON PYROTECHNIC PROTECTION

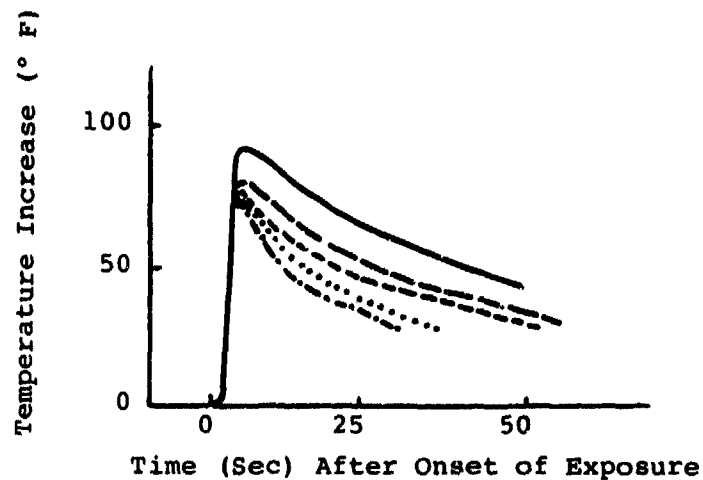
FABRIC	TEMPERATURE INCREASE - DEGREES F			
	DRY	ALCOHOL	ACETONE	WATER
KYNOL, UNALUMINIZED	107	80	49	32
KYNOL, ALUMINIZED	86	75	51	51
RAYON, ALUMINIZED	97	88	51	59

In neither series of tests was the protection impaired; all wetting agents resulted in a reduced temperature peak. There was some variation in the effectiveness of the enhanced protection. In the most prolonged burns of the pyrotechnic tests, the acetone apparently evaporated more rapidly than it did in the oxyacetylene tests, because no appreciable cooling effect could be noted.

During the course of use of a protective fabric suit, the aluminization may exhibit cracking or abrading. Tests were conducted to determine to what degree those conditions reduced protection. Surprisingly, in both the laboratory and field tests, the worn fabrics generally showed protection as good as, if not better than, new material. Figure 7 summarizes the typical results from the laboratory tests. The improved protection appeared to have resulted from the increased thickness of the fabric caused by the repeated flexing and bending which caused the cracking or abrasion. On prolonged exposure to a high thermal threat, the intact aluminization proved superior, but for a wide range of other exposure conditions, the used fabric samples were frequently superior.

The leather samples examined in the main body of tests proved to be consistently superior, but their weight was approximately twice as heavy as the heaviest synthetic fabric. It had

WORN FABRIC TEST RESULTS



Fabric Condition	Increase in Temp. (° F) Above Ambient	Time (Sec) to Peak Temperature	Time (Sec) Above 140° F
— Unused Rayon	92.0	2.0	52.0
Used Rayon:			
— Good Condition	85.5	3.6	31.4
- - - Slightly Abraded	84.5	3.5	23.0
- . - . Cracked Surface	78.0	3.0	19.2
..... Heavily Abraded	76.0	3.0	20.5

* Samples of fabric exposed to 2600° F for 1/2 second.

Figure 7.

been found throughout the tests that the degree of thermal protection generally showed some correlation to the weight and thickness of the samples examined. Additional tests with pyrotechnic sources were conducted with a wide range of weights and thicknesses of leather. The results are summarized in Table 5 and show that while there is some correlation of the weight of the leather, the aluminized leathers gave substantially better protection than did other leather samples of greater weight.

TABLE 5.

LEATHER SAMPLES IN PYROTECHNIC BURNS

LEATHER TYPE	WEIGHT	TEMPERATURE
UN-ALUMINIZED	(OZ/YD ²)	INCREASE (°F)
CREAM GRAIN	20	95
BUFFED GRAIN	21	105
CROME LEATHER	25	101
CROME LEATHER	40	105
THERMAL LEATHER	40	90
CROME LEATHER	50	91
ALUMINIZED		
SPLIT LEATHER	24	65
ALUMINIZED LEATHER	40	70

The general results of the fabric tests are summarized in Table 6.

TABLE 6.

FABRIC TEST RESULTS

NO ONE TYPE OF FABRIC IS BEST FOR ALL
TEST CONDITIONS
MEASUREMENT PROCEDURES
OPERATIONAL CRITERIA
KYNOL GENERALLY GAVE THE BEST RESULTS
FOR SYNTHETICS
LEATHER PERFORMED THE BEST OF ALL
BUT AT INCREASED WEIGHT
ALUMINIZATION IS BENEFICIAL FOR
HIGH THERMAL THREATS

Glove Results

Tests were performed on a variety of gloves and of glove materials in both the laboratory and field test series. Although tests were conducted with the gloves intact, data was also collected from tests in which the glove was taken apart and the sensor reassembled in such a way that the location of the sensor with respect to the liner and outer layer could be consistently positioned. Data collected with the glove materials reassembled in this manner tended to be more consistent.

The different gloves exhibited greatly varying degrees of protection. As with the fabric tests, leather gloves generally gave the best protection. Synthetics could match the protection afforded by the leathers only by greatly increasing their thickness. (See Figure 8 and Table 7.)

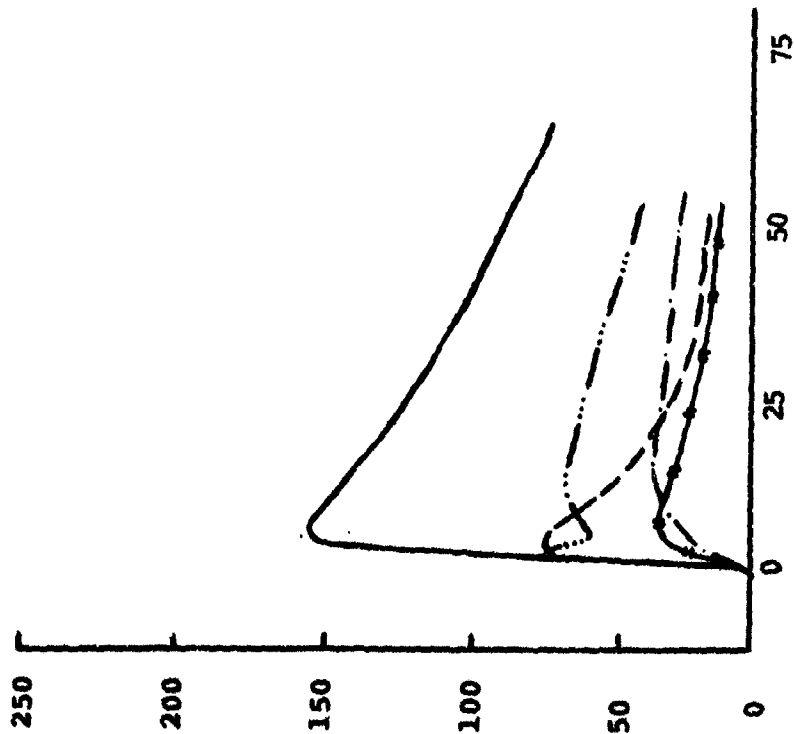
TABLE 7.

GLOVE MATERIAL PYROTECHNIC TESTS

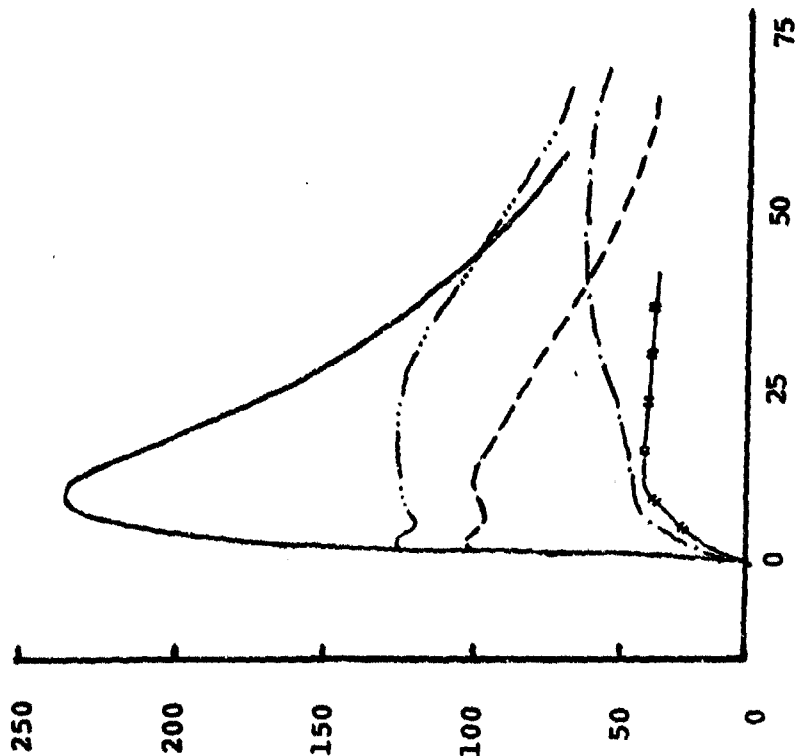
	TEMPERATURE INCREASES ($^{\circ}$ F)	
	WITHOUT LINER	WITH LINER
ALUMINIZED LEATHER	136	70
WORK LEATHER	96	68
PIGSKIN	128	94
KNIT KYNOL	188	89
KEVLAR 4	268	128
KEVLAR 7	308	136
FIBERGLAS	687	206

Liners enhanced the degree of protection afforded by any other material. A problem with many pyrotechnic operations,

1/2 Second



1 Second



Time (Sec) After Onset of Exposure

FIGURE 8. Temperature/Time Curves for Samples of Gloves

- Fiberglass
- Kynol
- - - Rayon
- · - Asbestos
- · - Leather, Work

Temperature Increase (°F)

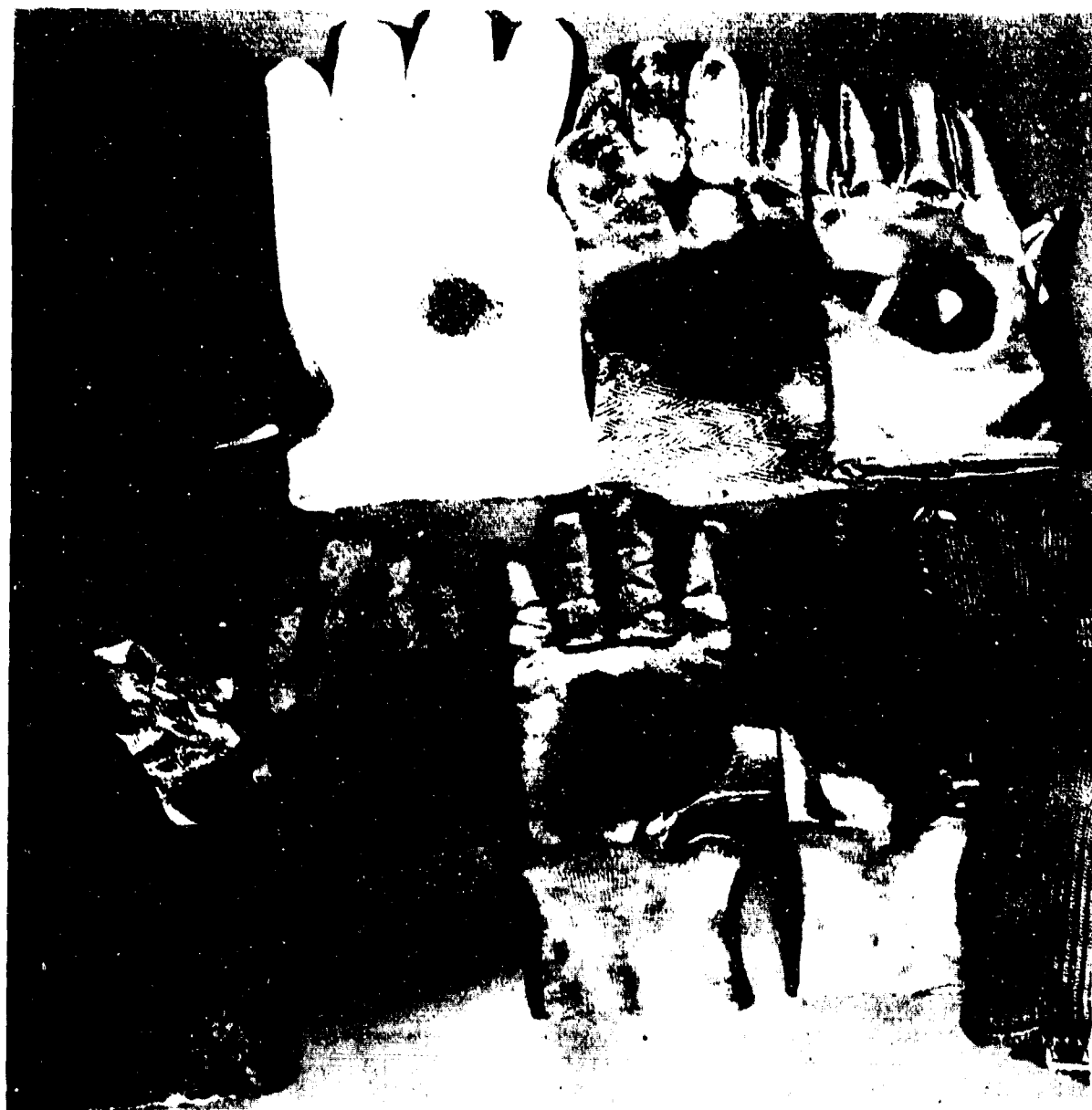


Figure 8(b). Effects on Gloves of 1 Second Laboratory Test Burns.

Top Row: Kelnit; Asbestos; Aluminized Rayon; Aluminized Fiberglas
Bottom Row: Leather; Work Leather; Aluminized Leather; Aluminized
Kevlar; Knit Kynol.

however, is that a substantial degree of flexibility and sensitivity is required for performing the work. Liners generally encumber the operation and could prove to be a greater safety hazard than a help.

Visor Results

Tests were performed with different visor faceshield materials in single and multiple layer tests. Table 8 summarizes the results for the laboratory tests performed with visor assemblies. Figure 9 shows the test apparatus for the laboratory test of the visors, and Figure 10 shows the results of burn tests of visor shields.

The results of the pyrotechnic tests varied from those of the laboratory in that the reflective foil proved to make a substantial contribution to reducing the thermal threat. (These results are discussed in a separate report.)

With all of the visor tests, the temperature rise in the multi-layer assemblies was substantially lower than than obtained under similar conditions with protective fabrics. For protection against damage to the inner shield and for enhanced thermal protection, a dual layer shield should be used. Reflective foil should be used against certain types of pyrotechnic threats with high radiant outputs. An inner shield of 1/8th inch Lexan, an air gap, and an outer shield of .040 acetate provides optimal protection.

TABLE 8. Thermal Protection With Outer Shield Variations

Temperature Rise ($^{\circ}$ F) and Time (Sec) to Maximum Temperature *

		Experimental Conditions									
Inner Shield	Outer Shield (Acetate)	Inner Shield Reflect. Foil		Inner Shield Air Gap		Inner Shield Reflect. Foil		Inner Shield Outer Shield		Inner Shield Outer Shield	
		Temp	Time	Temp	Time	Temp	Time	Temp	Time	Temp	Time
Lexan .125 inch	.044 in.	24 $^{\circ}$	164	20 $^{\circ}$	164	23 $^{\circ}$	174	28 $^{\circ}$	146		
	.040 in.	27 $^{\circ}$	171	26 $^{\circ}$	148	29 $^{\circ}$	146	35 $^{\circ}$	111		
	.020 in.	36 $^{\circ}$	81	26 $^{\circ}$	102	40 $^{\circ}$	77	32 $^{\circ}$	90		
	Average	29.0 $^{\circ}$	138.7	24.0 $^{\circ}$	138.0	30.7 $^{\circ}$	132.3	31.6 $^{\circ}$	115.7	74 $^{\circ}$	54
Plexiglas .118 inch	.044 in.	22 $^{\circ}$	213	24 $^{\circ}$	167	27 $^{\circ}$	122	29.5 $^{\circ}$	122		
	.040 in.	25 $^{\circ}$	143	31 $^{\circ}$	148	26 $^{\circ}$	149	37 $^{\circ}$	107		
	.020 in.	28 $^{\circ}$	105	38 $^{\circ}$	83	35 $^{\circ}$	103	38 $^{\circ}$	93		
	Average	25.0 $^{\circ}$	153.7	31.0 $^{\circ}$	132.7	29.3 $^{\circ}$	124.7	34.8 $^{\circ}$	107.5	61 $^{\circ}$	57
Cumulative Average		27.0 $^{\circ}$	146.2	27.5 $^{\circ}$	135.3	30.0 $^{\circ}$	128.5	33.2 $^{\circ}$	111.6	67.5 $^{\circ}$	55.5

* Visor combinations exposed to 2600 $^{\circ}$ F for one second.



Figure 10. Prolonged Burn Visor Test Results

Burn Envelope Results

The burn envelope tests were designed to determine the extent to which the flame generated by a burning pyrotechnic mix would expand. Samples of fabric were mounted on test stands to determine the temperature rises experienced within the burn envelope.

There were found to be massive differences between various pyrotechnic mixes in the heat output, the area and volume the burn envelope would occupy, and the duration of the burn. Examination of paper tape indicators and a review of single frames of motion pictures and videotapes showed that the border of the burn envelope was sharply defined but that the shape was continually changing.

As a result of these variations in the flame envelope, samples exposed to the burn received various amounts of thermal insult, and consistent results for samples located at the same place in the field could not be obtained. Nevertheless, by computing the averages of the rank order of effectiveness of the tested samples at each location, a generalized ordering of the effectiveness of the fabrics could be obtained. When this was done, as is shown in Table 9, leather proved to be the best, with the two varieties of aluminized Kynol in the following places.

TABLE 9.

BURN ENVELOPE FABRIC TEST RESULTS

LEATHER, ALUMINIZED	18.5	RAYON, ALUMINIZED 7	28
KYNOL, ALUMINIZED S	20.5	KEVLAR, ALUMINIZED V	26.5
KYNOL, ALUMINIZED A	22	FIBERGLAS, ALUMINIZED	23
KYNOL, UNALUMINIZED	26	NOMEX, ALUMINIZED	48
RAYON, ALUMINIZED U	24.5	KEVLAR, UNALUM, 4	45

RANK ORDER AVERAGES OF TEN TYPES OF FABRICS

Summaries of the findings for the temperatures recorded on fabrics exposed to a 16-ounce burn of a high-range pyrotechnic mix are indicated in Figure 11. The temperature readings are those obtained at positions approximately two feet apart above and away from the pyrotechnic source. Similar readings are shown for three quantities of pyrotechnic mix in Figure 12.

The rayon appeared to give substantial protection on some of these burns, but the protection was afforded by the char which developed over the sensor. When the fabric was touched, it crumbled. For a protective suit, this protection afforded by the char would be illusory. In conducting these tests, all fabrics were routinely examined to determine if spurious results such as this should have been discounted.

It should be noted that the temperatures recorded were obtained with temperature indicator strips. These strips are sensitive to both the total temperature and the duration of the rise, so it is unlikely that they represent the actual temperature attained behind the protective fabrics. Despite this drawback, they do permit comparison of the results of one fabric with those of another, and they allow the simultaneous sampling of many more fabrics than would have been possible by other means.

Despite the variations introduced by the experimental constraints of the burn envelope tests, when the results are examined in conjunction with the more rigidly controlled laboratory and field tests, they do appear to be consistent with the earlier, more accurate and replicable findings, and for that reason, appear to reflect a basic validity common to all three test processes.

TEMPERATURES RECORDED BEHIND PROTECTIVE FABRICS ABOVE 16 OUNCES
OF BURNING HIGH-YIELD PYROTECHNIC MIX

LEATHER ALUMINIZED	KYNOL S ALUMINIZED	KYNOL A ALUMINIZED	KYNOL U UNALUMINIZED
140	150 140	123	120 145 130
✓ 100	180 250	152	200 230 190
135	190 330	310	320 340 350 ⁺



RAYON U ALUMINIZED	RAYON 7 ALUMINIZED	KEVLAR V ALUMINIZED	FIBERGLAS ALUMINIZED
145	150 190	✓ 100	270 250 150
190	220 190	190	310 435 NR
150	270 240	✓ 220	465 500 NR



TEMPERATURES ARE IN ° F		NOMEX 0 ALUMINIZED		KEVLAR 4 UNALUMINIZED	
READINGS ARE AVERAGES FOR TWO FOOT INTERVALS WITHIN THE BURN ENVELOPE.		190	260 160 NR	330	370 350 ⁺ NR
		✓ 100	400 350 NR		



Figure 11.

READINGS ARE AVERAGES FOR TWO FOOT INTERVALS WITHIN THE BURN ENVELOPE OF THE MIX
TEMPERATURES ARE AVERAGES OF MAXIMUM RECORDED IN °F

Figure 12.

PROTECTIVE CLOTHING

A continuing effort is being made to apply the findings from this series of tests to the development of an improved pyrotechnic suit and to the selection of gloves and other protective gear for pyrotechnic operators.

Certain objectives were established as essential for the improved flashsuit. It must:

- Permit unassisted and quick removal.
- Allow routine body and arm movements.
- Cover the head and torso completely.
- Provide an uninterrupted front.
- Seal flaps and overlaps effectively.
- Allow a clear view of the operating area.
- Provide for air cooling with an automatic disconnect.

Other objectives were established as desirable. The suit should:

- Weigh less than 10 pounds.
- Permit unassisted entry.
- Require as few discrete actions as possible when putting the suit on.
- Allow operators direct access to fresh air via a detachable hoodpiece or hinged visor facepiece.

After attempting over ten prototype designs, the essential characteristics have been met, but the desirable characteristics could not be completely satisfied. Figure 13 depicts one of the latest models of a suit meeting the essential characteristics.



Figure 13. Side and Back Views of Aluminized Kynol Flashsuit.

Continued efforts are being made to increase the comfort and ease of entry into the protective suit, and to incorporate the latest findings into providing for increased protection. At the current time, the following recommendations (see Table 10) reflect the most recent developments.

TABLE 10.

SUIT DESIGN - RECOMMENDATIONS

KYNOL FABRIC FOR THE BODY
LEATHER FOR THE ARMS AND HOOD
ALUMINIZATION FOR HIGH THERMAL THREAT
AIR-COOLING WITH AUTOMATIC DISCONNECT
INTEGRAL SUIT AND AIR VEST PACKAGE
DUAL LAYER VISOR WITH FOIL AS REQUIRED

It must be emphasized that while the objective of this research has been to develop thermal protection, the most effective thermal protection is the removal of the operator from hazardous operations. Concurrent efforts are being undertaken at Lone Star Army Ammunition Plant to remote the most hazardous pyrotechnic operations.

Even when most of these operations have been successfully automated, there will always remain the necessity to provide personal protection for maintenance and other individuals who will, of necessity, come into proximity to pyrotechnic operations. The data obtained by these tests will therefore continue to prove of benefit in attempting to provide the most effective thermal protection to those engaged in pyrotechnic operations.

The views, opinions, and/or findings contained in this report are those of the authors and should not be construed as an official Department of the Army position, policy, or decision, unless designated by other documentation.

The data and conclusions contained herein are based on work believed to be reliable; however, we cannot and do not guarantee that similar results and/or conclusions will be obtained by others, and we do disclaim any liability resulting from the use of the contents of this report.

APPENDIX

TECHNICAL DATA

Table 11. Pyrotechnic Mixes Used in Burn Envelope Tests

<u>Type of Mix</u>	<u>Category</u>	<u>Heat Output</u>
M13 Tracer	High Yield	2774 cal/gm
M692 Delay	Medium Yield	1807 cal/gm
M549 Delay	Low Yield	583 cal/gm

Table 12. Fabrics Used in Pyrotechnic Tests.

Category Code	Description	Weight (oz/yd ²)	Thickness (inches)	Temperature Rise (°F) After Timed Exposure 0.5 sec	2 sec
KYNOL					
YA	alum. AKI	17.2	.053	74.5	302
YS	alum. Amatex	22.9	.063	85.5	199
YU	unal. Amatex	19.0	.064	78.5	326
YK	unal. Knit	27.4	.064	--	132
RAYON					
RU	alum. Gentex 1017 (used)	19.1	.053	81	222.6*
R6	alum. Gentex 1006	14.9	.031	78.5	351.6*
R7	alum. Gentex 1017	19.9	.041	89.5	158*
R9	alum. Gentex 1019	18.8	.044	70	194.6*
KEVLAR					
KW	alum. Gentex 1090	9.1	.030	138	Burn**
KV	alum. Fyrepel	11.3	.025	97	681.5
KH	unal. Amatex 11HT26	10.7	.040	149.5	476
K4	unal. Amatex 22PT7	21.9	.073	64	299.8
KF	unal. Flextra	15.3	.053	131	472
NOMEX/ARAMID					
NG	alum. Gentex 1055	13.3	.083	62	Burn**
NN	alum. Gentex 1056	10.0	.019	231	Burn**
NO	alum. Fyrepel 10oz	11.4	.025	112	Burn**
N3	alum. Gentex 1053	4.8	.012	140	Burn**
NC	alum. Fyrepel check	4.7	.018	222	Burn**
NB	alum. Fyrepel black	9.8	.018	150	587
SILICATES					
SR	unal. HAVEG 84CH red-back	22.9	.029	75	726
SH	unal. HAVEG 188CH	40.4	.053	92	256
SB	unal. HAVEG 84CH	18.9	.031	133	840
SC	unal. HAVEG UC-100-48	19.0	.031	118	771
SRF	unal. Refrasil	19.6	.034	91	895
OTHER SYNTHETICS					
FG	alum. Gentex Fiberglass	15.4	.020	150	624
PR	alum. Gentex Preox	16.7	.037	82.5	666.6
GT	unal. Amatex 24PT73WR	24.0	.073	74	237
GN	unal. Amatex 16HT65WR	16.0	.052	70	535.3
LEATHER					
CR3	unal. Cream grain	20.2	.053	--	97.9
BU3	unal. Buffed grain	20.8	.055	--	106.5
BL3	unal. Chrome split	26.2	.066	--	100.8
BL4	unal. Chrome split	39.5	.062	--	104.6
LA3	alum. split	33.8	.062	40.5	63.3
LA4	alum. split	44.7	.058	--	87.6
SC4	unal. split	44.8	.069	36	--
TH4	unal. Thermaleather	39.4	.072	--	79.7
LA5	alum. split	39.7	.069	45	70.0
BL5	unal. Chrome split	50.0	.087	--	80.6
OTHER ORGANICS					
CO	alum. Gentex 1003 Cotton	14.0	.025	124	Burn
WO	alum. Gentex 1009 Wool	20.5	.069	63	114.3

* Charred and disintegrated (insulated thermocouple gave false reading).

** Burned, melted, shriveled, or otherwise destroyed.

FIGURE 14.
Typical Test Results for
Samples of Fabrics Exposed to Temperatures in Excess of 2600 OF
for 0.5 Seconds.

Figure 14(a). Side Exposed to Flame.

Figure 14(b). Side Opposite Flame.

In both figures, the samples are displayed in the following order:

Top Row, Left to Right:

Rayon, Used
Rayon, 1006
Rayon, 1017
Rayon, 1019
Preox

Second Row, Left to Right:

Kynol, AKI
Kynol, Suit, Amatex
Kynol, Unaluminized, Amatex
Nomex, 1055
Nomex, 1056, Thin
Nomex, 10 oz., Thick

Third Row, Left to Right:

Nomex, 1053, Check
Kevlar, 1090
Kevlar, V
Kevlar, 11HT
Kevlar, 22PT
Kevlar, Flextra
Cotton, 1003

Bottom Row, Left to Right:

Wool, 1009
Refrasil
Fiberglass
Leather, 3
Leather, 5
Leather, Unaluminized

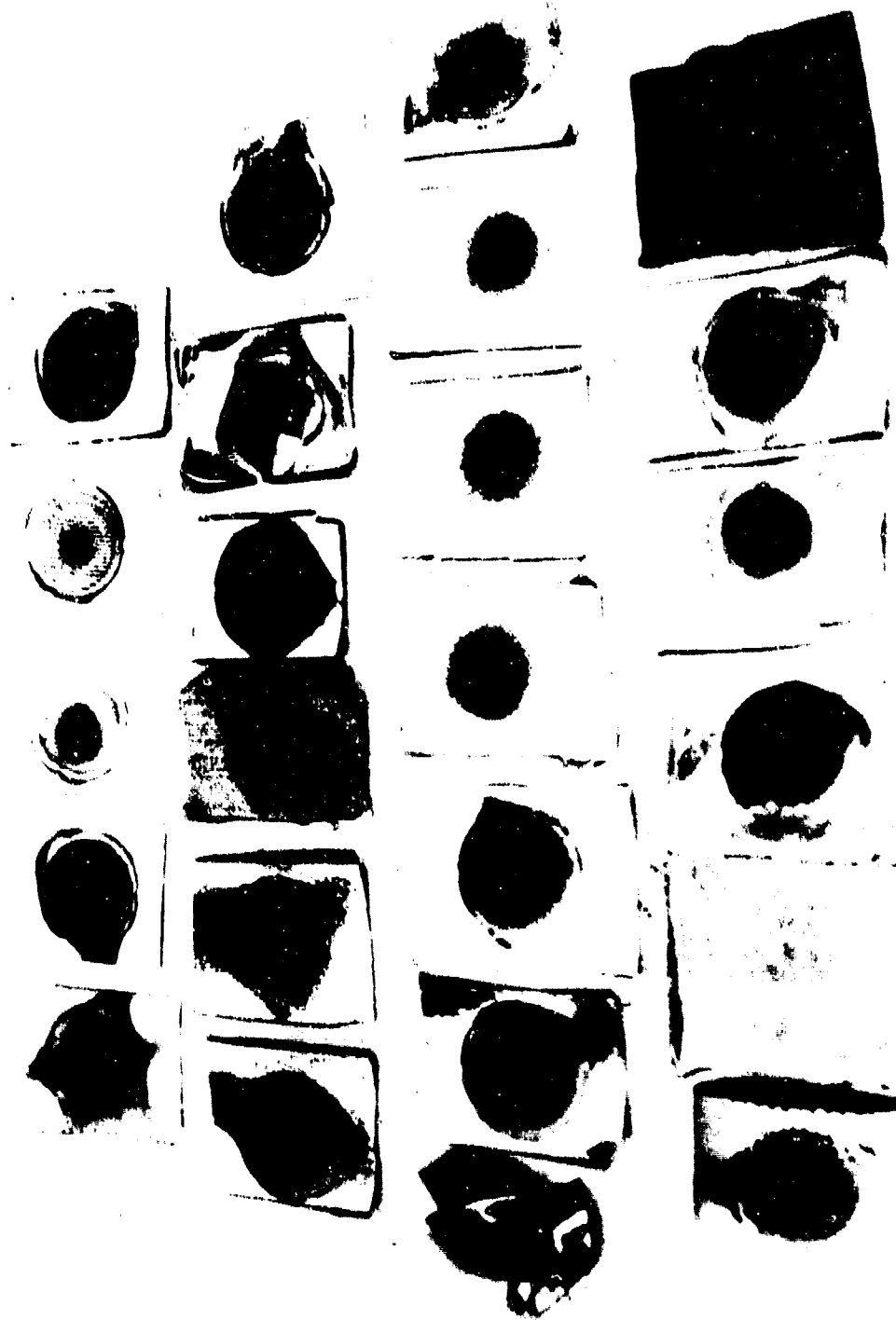


Figure 14(a). Laboratory Test Samples (Side Exposed to Flame).

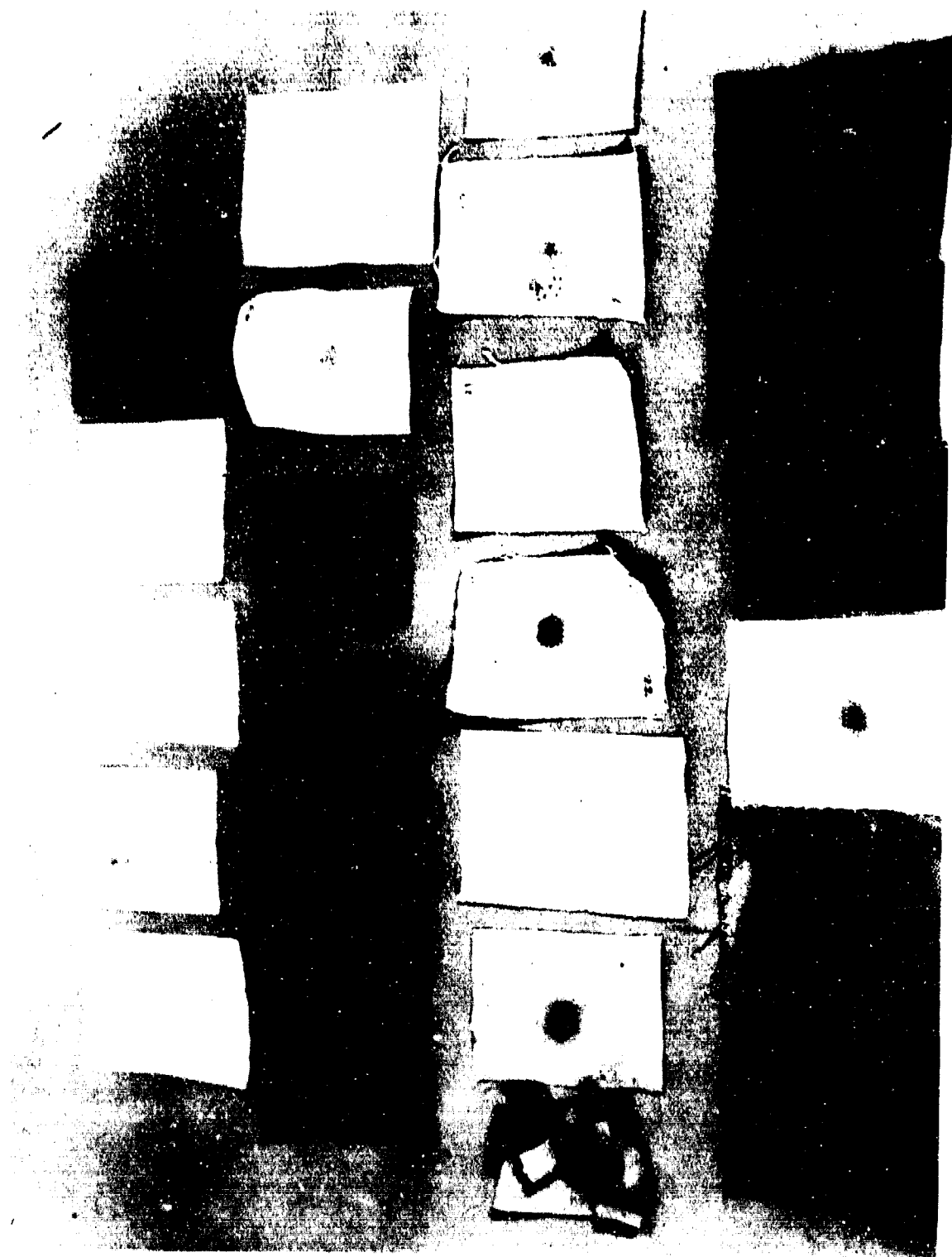


Figure 14(b). Laboratory Test Samples (Side Opposite Flame).

FIGURE 15.
Typical Test Results for
Samples of Fabrics Exposed to High Yield Pyrotechnic Burn
for 0.5 Seconds.

Figure 15(a). Pyrotechnic Test Samples (Side Exposed to Flame).

Figure 15(b). Pyrotechnic Test Samples (Side Opposite Flame).

In both figures, the samples are displayed in the following order:

Top Row, Left to Right:

YS Kynol, Suit, Amatex
 YA Kynol, AKI
 YU Kynol, Ualuminized, Amatex
 R6 Rayon, 1006
 R7 Rayon, 1007

Second Row, Left to Right:

KV Kevlar, V
 KF Kevlar, Flextra
 K4 Kevlar, 400
 KH Kevlar, KH
 N3 Nomex, 1053
 NB Nomex, Black
 NB Nomex, Black

Third Row, Left to Right:

SC Silicate, UC 100-48
 SB Silicate, 84CH
 SH Silicate, 188CH thick
 SR Silicate, red backing
 FG Fiberglass
 PR Preox
 GN NorFab, 16HT 65WR
 GT NorFab, 24PT '73WR

Bottom Row, Left to Right:

UA Leather unal (L5)
 L5 Leather L5
 L3 Leather L3
 WO Wool wool

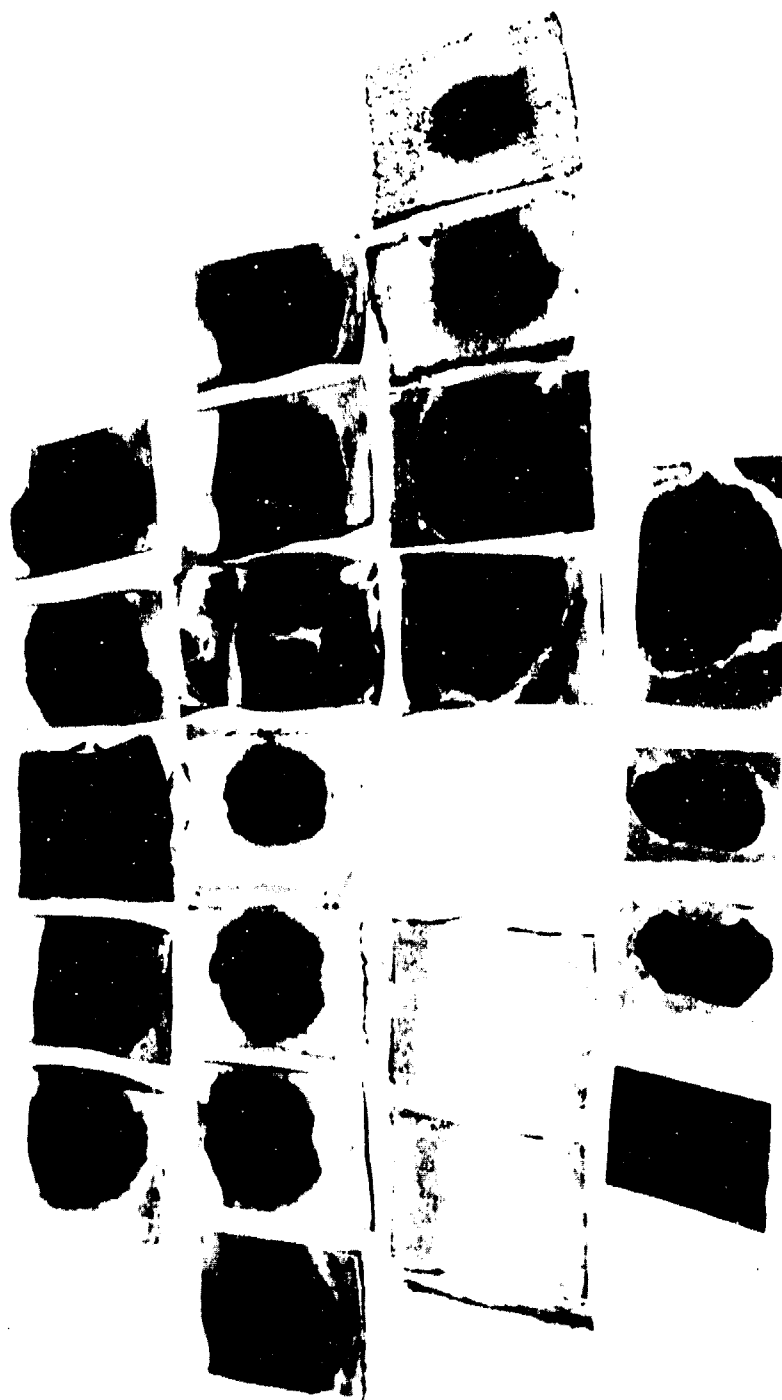


Figure 15(a). Pyrotechnic Test Samples (Side Exposed to Flame).

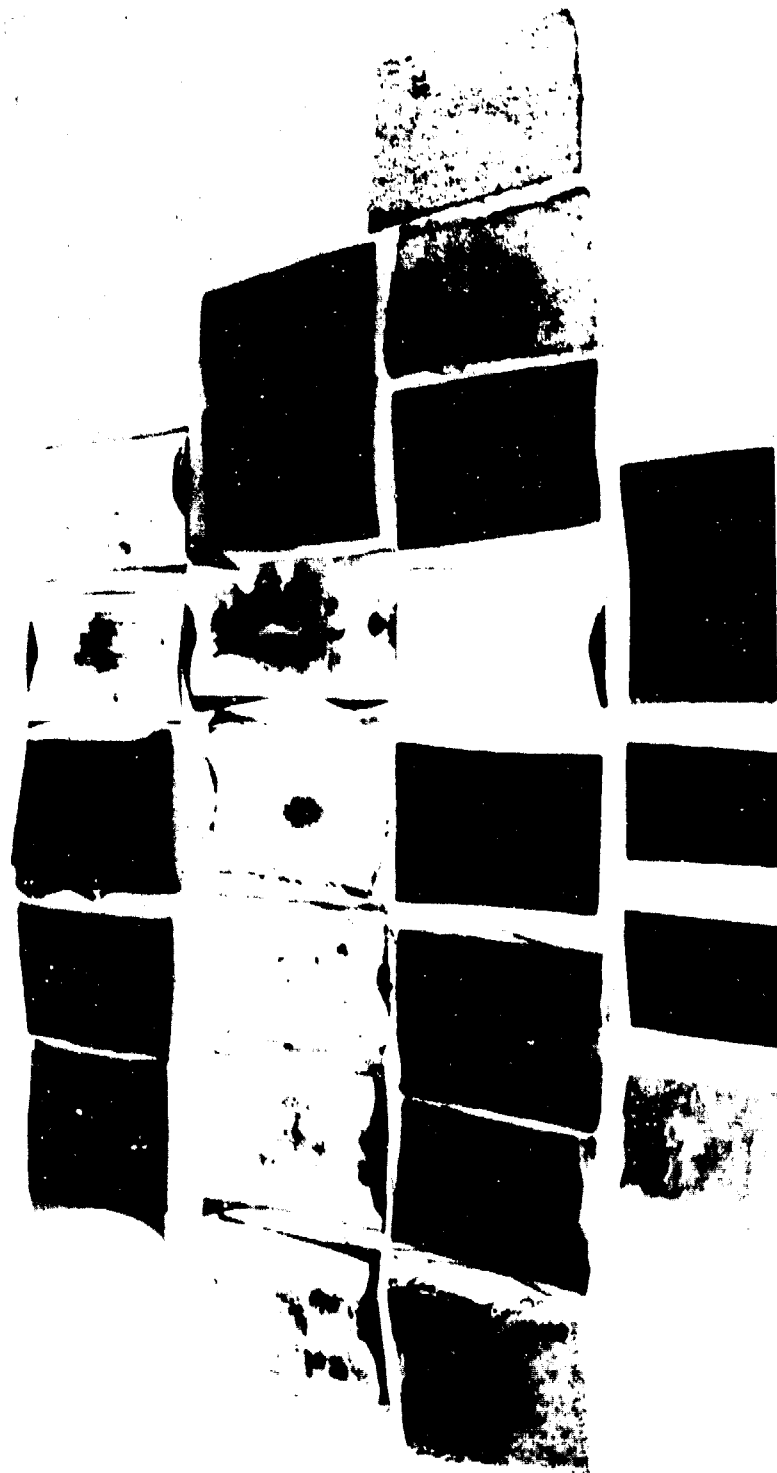


Figure 15(b). Pyrotechnic Test Samples (Side Opposite Flame).

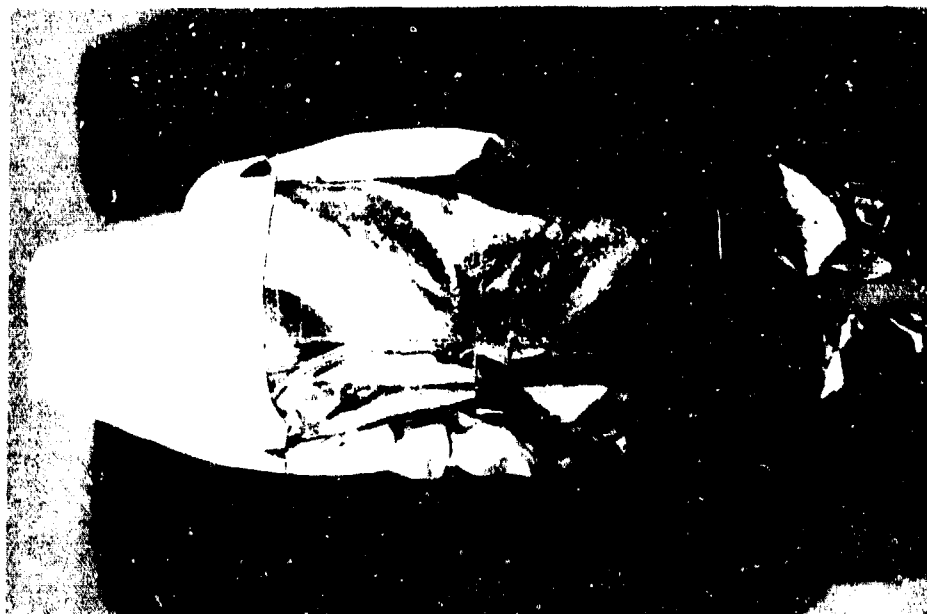


Figure 16 (a). Side and Back Views of Leather and Aluminized Kynol Flashsuit.

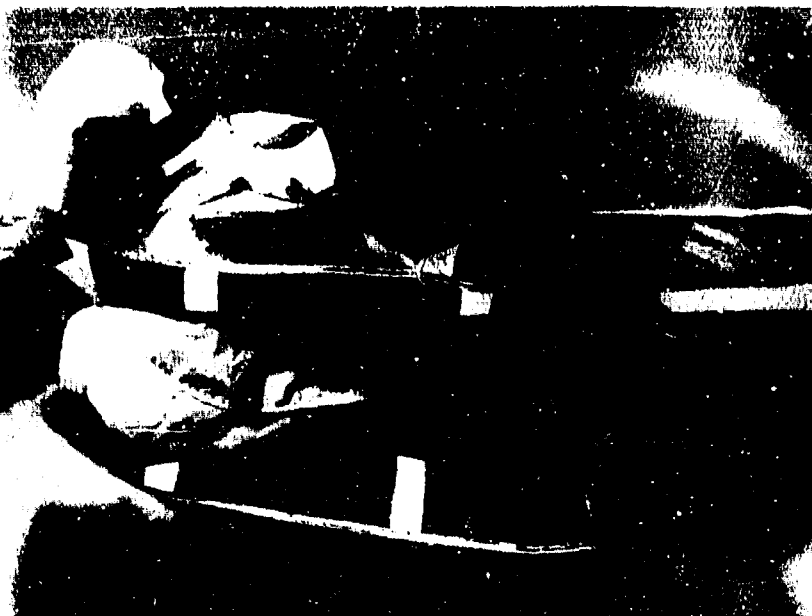
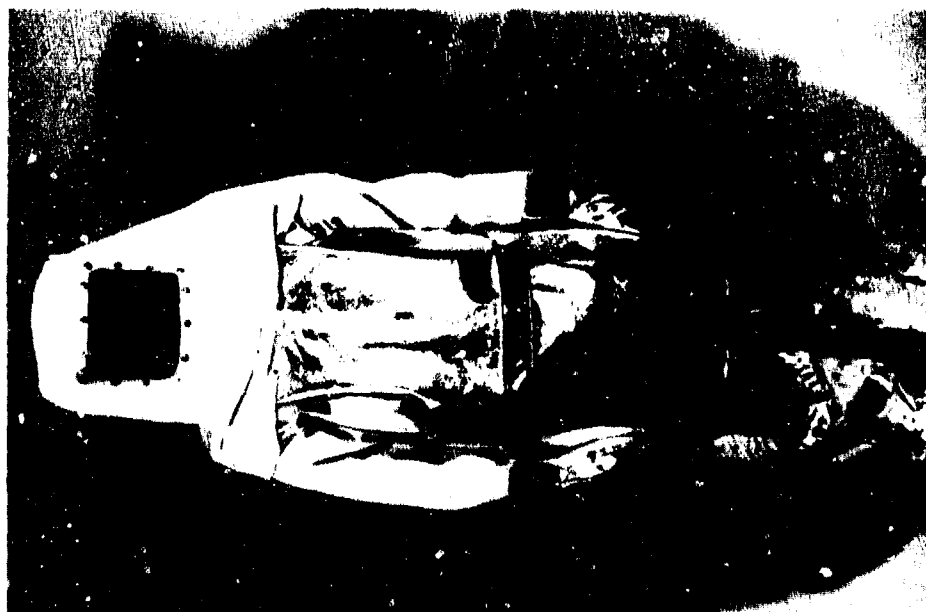


Figure 16 (b). Front View of Leather and Aluminized Kynol Flashsuit and
Three/Quarter View Showing Suit Being Placed over Air Cooling Vest.

→ GENERAL RISK ANALYSIS METHODOLOGICAL IMPLICATIONS TO
EXPLOSIVES RISK MANAGEMENT SYSTEMS

Prepared for the Twentieth DoD Explosives
Safety Seminar
Norfolk, Virginia
24-26 August 1982

By

Lloyd L. Philipson
J.H. Wiggins Company
1650 South Pacific Coast Highway
Redondo Beach, California 90277

ABSTRACT

AD P000456
↙ An investigation sponsored by the National Science Foundation has produced as one of its results a survey and evaluation of risk analysis methodologies. This paper presents some implications of the survey⁽¹⁾ to risk analysis and decision making for explosives hazards such as may ultimately be implemented in the Navy's proposed NOHARM System and other similar systems that may be contemplated by DoD organizations.

GLOSSARY

Risk

The probability distribution for the occurrences, due to faults or failures, or external events, of a set of possible losses, such as given numbers of casualties, deriving from a given activity, such as the operation of a specified facility under specified conditions for a particular period of time. Risk is often also used to mean the product of the probability and

⁽¹⁾ Supported under Grant No. PRA-8007228. Any opinions, findings, and conclusions or recommendations expressed here are those of the author and do not necessarily reflect the views of the National Science Foundation.

magnitude of a given loss, or the sum of such products over all the possible losses, i.e., the expected loss. Individual risk is the probability of a given loss (e.g., an injury) occurring to any member of the exposed population. Group or societal risk is the probability that a given number of individuals will suffer a given loss.

Risk Assessment

The integrated analysis of the risks of an activity, system or facility and their significance in an appropriate context. It incorporates risk estimation and risk evaluation.

Risk Estimation

The statistical, analytical and/or judgmental modeling process leading to a quantitative estimate of a given risk.

Risk Evaluation

The appraisal of the significance of a given measure of risk, as for example, the comparison of the expected number of casualties per year from a specified facility's operation, with that from a number of other, generally "accepted" sources of risk; or the appraisal of the risk of such casualties in relation to the socio-economic benefits of its acceptance.

Risk Management

The process whereby decisions are made to accept a known risk or hazard or to eliminate or mitigate it. Trade-offs are made among increased cost, schedule requirements and effectiveness of redesign or retraining, installation of warning and safety devices, procedural changes, and contingency plans for emergency actions.

INTRODUCTION

The application of probability-based decision criteria in explosives safety management appears to be gaining some ground at present in the military. Computer implementations of this application as management decision support systems are being considered. This has been due to the increasingly evident inadequacies and costliness of the traditionally employed, purely con-

sequence-orientated, Explosives-Safety-Quantity-Distance (ESQD) safety decision criteria. In particular, the Navy has carried to the preliminary requirements definition stage the NOHARM (Naval Ordnance Hazards Analysis and Risk Management) System concept for aiding decision making on the explosives hazards in the tidewater areas of Navy bases [1], [2], [3], [4], [5]. The Western Space and Missile Center at Vandenberg Air Force Base has initiated the conceptualization of an analogous system, PERMA (Probabilistic Explosives Risk Management Assistance), as a probability-based aid to safety decision making on rocket launch support facilities [6]. The general concept of an explosives risk management system is sketched in Figure 1.

While the belief in the value of such explosives (and other hazards, as well) risk management support systems has recently strengthened, it is nevertheless also generally recognized that the satisfactory implementation of the risk analysis functions of these systems is not easy, in large part due to the shortcomings of the data bases and fundamental physical information available for the carrying out of these functions. Furthermore, it is well understood that the philosophical foundations for the application of probability-based safety decision criteria where people are concerned are not yet firmly set, not only in the military but in society at large.

A recently completed review for the National Science Foundation of risk assessment methodologies and the uncertainties that arise in their various forms and applications has attempted to throw some light on these problems and on the various approaches to their possible resolution, or at least amelioration, that have been considered [7]. The intention of the present paper is to draw from this general review some pertinent implications to explosives risk management procedures. For the sake of brevity, only those especially critical procedures will be considered here that are involved in (1) the estimation of the occurrence probabilities of mishaps involving explosive materials, and (2) the use of risk estimates in the risk acceptability and risk mitigation cost-benefit evaluations that would be the basic outputs of explosives risk management assistance systems. The context of these specific considerations is first introduced in a discussion of a general risk estimation model and of the general objectives of risk evaluation.

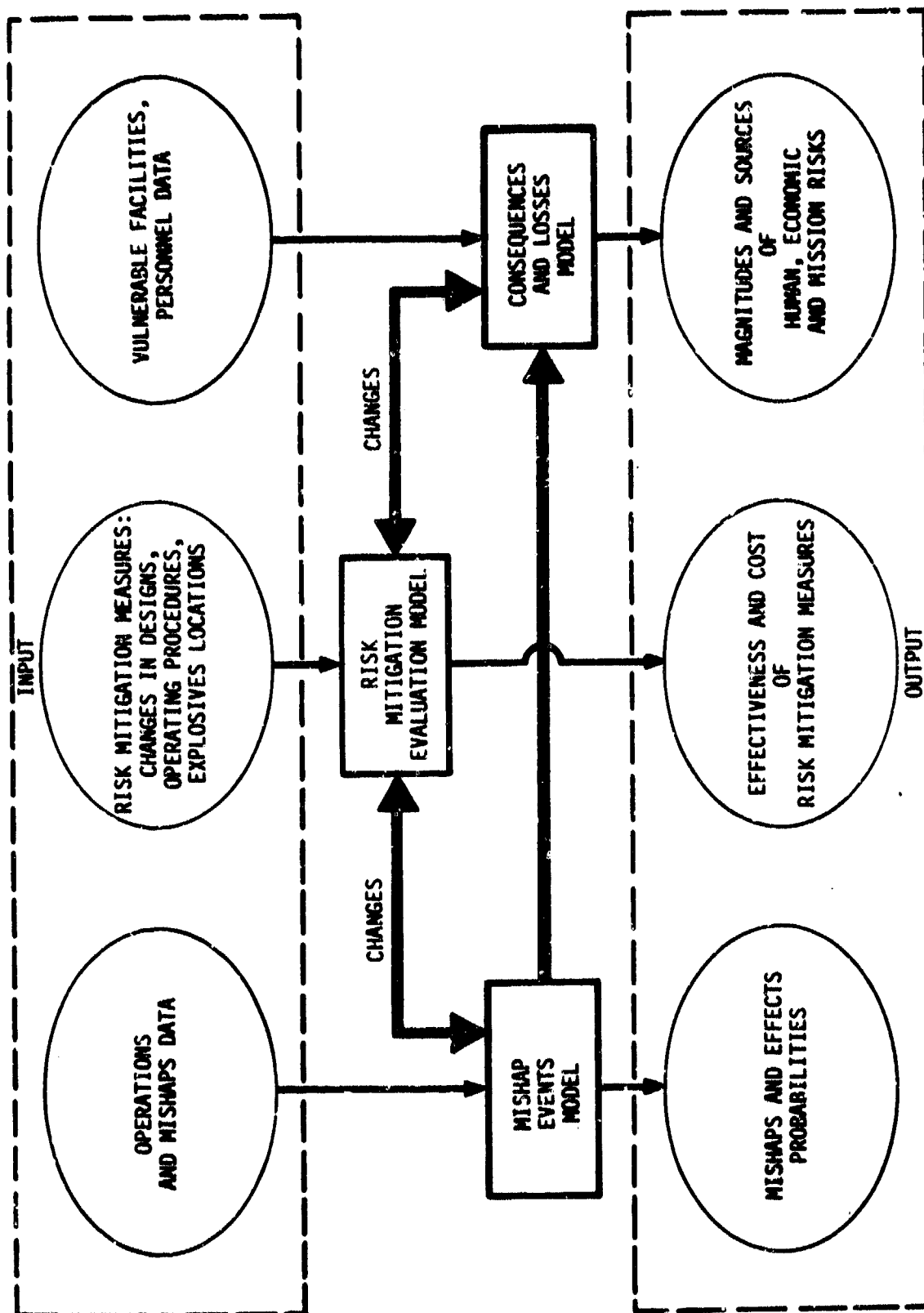


Figure 1. Explosives Risk Management System Concept

The General Risk Estimation Process

Possible losses (fatalities, injuries, property damage, mission delays) accrue from an explosives handling, transport or storage activity as the result of certain sequences of events. As illustrated in Figure 2, they may generally be considered to include the occurrence of a primary event, such as an equipment failure, e.g., of a crane, that leads to an initiated event (the occurrence of a particular mishap or accident), such as the dropping of an ordnance item. A reaction occurs and a container, such as the ordnance item's casing, ruptures and releases its material or energy content, and generates thereby one or more possible effects, e.g., a fire, an explosion of a given yield that produces blast, fragments, etc. When they impinge upon some target structure (adjacent people, buildings, etc.) these effects induce certain consequences and losses (number of casualties, etc.). The effects and losses may occur with a range of possible magnitudes. The losses may be treated as individual measures (numbers of fatalities, injuries of specified severities, property damage), or they may be integrated into a single measure, such as equivalent dollars.

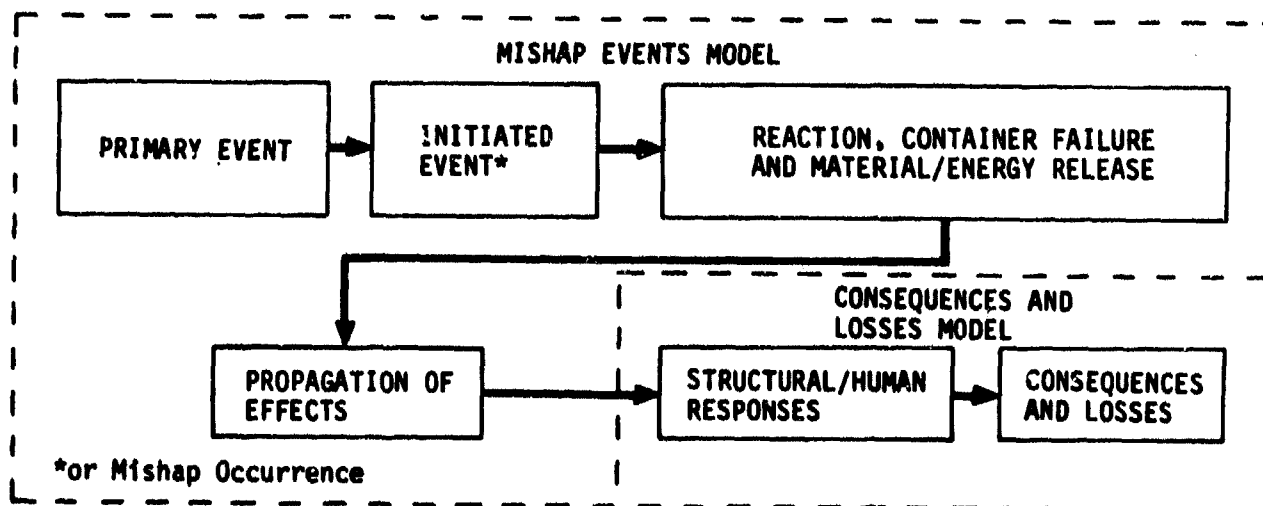


Figure 2. General Risk Estimation Process

The probability of occurrence of each event is then estimated, or, for effects and losses, perhaps only an average magnitude or a "credible worst-case magnitude" may be estimated. The results may then be combined into a

risk profile, such as is represented typically by Equation 1 (assuming only one kind of loss, say fatalities, is of interest). When it is adequate to do so,⁽²⁾ this is often compressed into a single expected loss measure, which is merely the mean of the probability distribution equivalent to the risk profile.

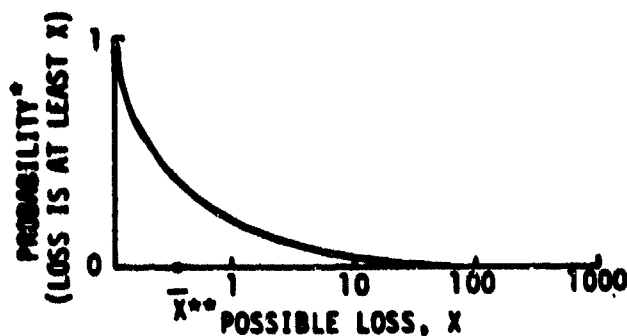
$$\begin{aligned} \text{Prob}^* (\text{Loss at least } x) = & \sum_i \sum_j \sum_k [\text{Prob} (\text{Loss at least } x \mid \text{Effect } k \text{ occurs}) \cdot \\ & \text{Prob} (\text{Effect } k \mid \text{Release of material or energy}) \cdot \\ & \text{Prob} (\text{Release} \mid \text{Mishap type } j \text{ occurs}) \cdot \\ & \text{Prob} (\text{Mishap type } j \mid \text{Primary event } i \text{ occurs}) \cdot \\ & \text{Prob}^* (\text{Primary event } i)] \quad (1) \end{aligned}$$

The asterisk in the equation signifies a given unit of exposure for the probability, as per year, per operation, etc. A vertical bar indicates that the probability involved is conditional on the occurrence of the event following the bar (and is read "given that"). As x is allowed to range over its possible values the risk profile is built up, as shown in Figure 3.

Risk Evaluation and the Character of Risk Assessment Applications

Risk evaluation is concerned with considerations of the significance of an estimated risk with respect to acceptability, and of ways to mitigate the risk where this is deemed desirable. These considerations relate to a set of possible kinds of applications of risk assessment, which perhaps may be usefully defined in terms of the questions below.

(2) An expected value results from the summation of the losses from all possible events weighted by their probabilities of occurrence. Thus, a low probability-high consequence event, which may be of the greatest importance to decision makers, may contribute only relatively little to the expected loss. A hazardous activity could then appear to be less risky than another because its expected loss is lower but could nevertheless entail a small chance of larger accidents and so in fact be of greater concern. This gives rise to the need to consider "the tail of the probability curve" as well as its expected value, or mean, in assessing risks, and so motivates the development of the risk profile.



*e.g., per operation, per year etc., for given hazardous activity

** \bar{X} is the expected loss (per operation, etc.), the mean of the distribution from which the risk profile derives

Figure 3. Illustrative Risk Profile

- How safe is a particular hazardous activity (i.e., what are its risks)?
- How does this safety compare with the safety of other activities?
- How much additional safety could be attained for a given cost, through some set of alternative modifications?
- How much would it cost to attain some required level of safety, through some set of alternative modifications?
- Which would be the safest means of accomplishing a given objective (e.g., transport of a given amount of an explosive material in a year over alternative routes or by alternative modes or by alternative shipment sizes)?
- Central philosophical issue: is the estimated (perceived?) risk "acceptable"? What are ways of appraising this?

THE APPLICABLE RISK ESTIMATION METHODOLOGIES

Four general risk estimation methodologies have so far evolved: statistical inference, fault tree modeling, analytical/simulation modeling, and subjective estimation of risk parameters. (Subjective estimation is also common in the development of inputs for the first three methodologies.)

For the sake of brevity, the discussion here of the four methodologies is orientated primarily around their utility in the first phase of an explosives risk analysis: estimation of the probability of occurrence of a mishap while handling an explosive material or item. The determination of the nature and probabilities of occurrence of an explosive reaction and its possible effects (blast, heat, fragments, fire, etc.) is the subject of other presentations of this seminar and, for brevity, will not be considered further. Neither will the determination of the possible losses that derive from these effects (e.g., number of fatalities, injuries, property damage) be treated here because this makes use of relatively familiar techniques.

Statistical Inference

The most regularly employed procedure for estimating mishap occurrence probabilities is that of statistical inference. However, it is directly usable only if an adequate data base exists, with significant sample sizes at the various levels of the specific hazardous conditions of concern. Also, it has to be able to be assumed that the past record satisfactorily represents (or can be modified so as to represent) what the future will hold.

In its basic form, the methodology of statistical inference assumes an activity's mishaps occur independently and with constant probabilities and develops estimates of these probabilities. The past record of such mishaps provides the frequency of their occurrence over the record period and thus, for instance, the frequency per year which is then extrapolated to future years. If the frequency per operation is desired, the "exposure" in terms of the number of operations that was accumulated during the record period must be known or estimated. The result is then an inference of the future probability of occurrence of a mishap as the ratio of the frequency of

mishaps to the frequency of operations. A confidence interval for the inferred probability can also be established.

A number of important problems arise in this superficially simple process, however. First, the estimation of the exposure requires that records on the operations conducted with the explosive material are kept and are accessible. Such records are not generally available. Thus, estimates may have to be made employing samples of operations data, often of uncertain accuracy or even validity, with liberal judgmental interpretation.

Second, adequate data for a meaningful statistical inference may also not exist on the mishap occurrences. This is always the case for the rare, potentially catastrophic events that are usually of greatest interest. If the record of exposure (e.g., number of operations) is great enough it may be possible nevertheless to estimate credible upper bounds on the probabilities of such events, but these are often too conservative (that is, too large) to support practical decision making on the control of future activities with just as large or larger rates of exposure.

A third problem area in statistical inference is that of the "stationarity" of the process giving rise to the mishaps. That is, it must be assumed that the past record also represents the future (or it is understood how to modify it so that it will). There are many reasons why this may not be the case; e.g., if a mishap occurs once, significant actions will be taken to decrease the chance of occurrence of such a mishap in the future. Or, "familiarity breeds contempt," or at least lack of concentration, among human operators so that the chance of a mishap where humans are involved may gradually increase over time. An increase in mishap frequency may also be due to wear of equipment under inadequate maintenance. The validity of statistical inferences that do not, or cannot, reflect such considerations is clearly questionable.

Overcoming fully in an explosives risk management system the problems that have been noted, and others that could also be brought forward [7], is not possible. But the situation can be improved by, first, making the uncertainties that the inference procedure gives rise to as explicit as

possible, so that the risk management system user can incorporate them in his decision process. Second, steps for improving mishap and exposure recordkeeping procedures can be defined comprehensively, and carried out. Finally, trend analysis methods can be applied to adapt the probability inferences to the effects of non-stationarity and other dependencies in the data.

Fault Tree Modeling

This approach synthesizes the possible sequences of events initiated by the activation of some hazard (a "Primary Event") and culminating in a particular mishap or failure "Top Event" with potentially deleterious consequences to people, property or the environment. Its application requires that all possible event sequences (system failure modes) will have been tracked back to their initiating primary events. To realize the full power of fault tree modeling the probabilities of occurrence of the primary events and all related action initiations (e.g., a successful or unsuccessful conduct of a corrective action) need to be estimated with adequate precision, and the magnitudes of the consequences accurately predicted. If these requirements are met a series of combinatorial probability calculations results in an assessment of the probability of occurrence of a Top Event and its consequences; i.e., the risk deriving from the hazards under analysis.

The principle difficulties with the fault tree procedure are the uncertainty that all significant event sequences have been considered, and the acquiring of sufficiently precise data for predicting, with reasonable accuracy, the initiating and related action event probabilities. If, nevertheless, fault tree methods can be applied, at least two important advantages not provided by statistical inference methods would accrue. First, the input data acquisition problem would be changed from that of obtaining meaningful samples of mishaps for all sets of conditions of interest at the activity level - to that of obtaining only primary event data, such as on specific failure modes of specific equipments, or procedures. It is, of course, recognised that primary event probability data generally still require statistical methods (and some subjectivity) to develop properly. What is emphasized here is that large enough sample sizes, even for different sets of

conditions, are clearly much more easily and correctly developed for primary events than for actual mishap occurrences. While certainly not trivial, this problem is at least possible to be solved from standard failure data sources and, for activity-specific events, with appropriate recordkeeping systems, experimentation, simulation and testing.

Second, fault trees lend themselves conveniently to the evaluation of the effectiveness of given mitigating measures. Any such measure should be able to be assessed through the changes that it would induce in the original fault tree describing the mishap occurrence that it is intended to prevent, or decrease the probability of. The evaluation of the effectiveness of mitigating measures using statistical models currently requires highly, if not entirely, subjective postulations of what the changes in the given mishap records would have been (and, it is presumed, would be in the inference for the future) if the mitigation had been in place during the period in which the records were acquired.

To gain these and other advantages [7], fault tree modeling techniques for explosives hazards analysis, especially, need to be deepened to better reflect mishap dynamics, including human operator actions. Improved means are also needed for acquiring activity-specific data on the probabilities of primary events, including human failures.

Analytical and Simulation Modeling

Analytical and simulation modeling approaches to risk analysis begin with functional descriptions of the activity or system under study. The operations of the system are then expressed in terms of appropriate performance parameters that express the functions, and the interaction of the functions, of system components (human, as well as equipment) and interfacing external factors. The conditions under which mishaps and their effects occur are associated with specific combinations of the values of these parameters. Their probabilities of occurrence and the consequences of their occurrence are then assessed by means of probability or effects formulas (in analytical models), through numerical accumulations from repeated runs of system oper-

ation "scenarios" (in simulation models), or by combinations of both procedures.

The main problems with analytical models are the need for acceptable simplifying assumptions that the derivation of their formulations usually require, and of the related departure of their modeled factors from direct physical significance. Simulations are better in these regards in that they usually tend to replicate real-world factors in a fairly recognizable way. However, to the extent that they avoid arbitrariness in their simplifications, their complexity and computational requirements increase. The need to repeat many runs of simulated operations in order to derive usable accident statistics (as in Monte Carlo simulations) exacerbates the computational requirements. Simulations are, therefore, expensive means for risk analysis (other than in specific, and limited, data development support roles).

Analytical and simulation models are not usually appropriate for mishap occurrence modeling, but are applicable primarily to assessments of mishap effects and consequences. However, this will not be discussed further here.

Subjective Estimation

The most generally applicable approach to developing risk estimates is that of subjective estimation by experts. These experts are assumed to be sufficiently familiar with the detailed circumstances of operations similar to those of interest that they can meaningfully extrapolate their experience to new conditions, employing only their individual judgments, in combination with those of the other experts as, for instance, in a Delphi procedure [8].

Subjective estimation is perceived as inherently a relatively low-confidence risk analysis methodology. However, this perception may be at least in part a result of the general lack of appreciation of the perhaps more subtle but sometimes just as significant subjective elements of the other possible methodologies. This has been evidenced to some extent in the preceding discussions of these methodologies. Moreover, "engineering judgment" is already the most employed method for at least categorizing hazards in terms of their qualitative risk levels (expressing relative frequencies of occur-

rence and relative severities or criticalities of possible consequences). To improve the quantitative subjective estimation process should therefore be a worthwhile endeavor, even if less formal procedures than, say, Delphi are considered. How this might be done is next briefly outlined.

Introduction to a Subjective Risk Estimation Process⁽³⁾

A Preliminary Hazard Analysis is first performed of the operations of a facility to identify a set of possible mishaps that have some potential for leading to explosions. Each mishap has some (unknown) probability of occurrence (ranging down, possibly, to very small values) each time the operation during which it can occur is executed. For simplicity here, it is assumed that for each mishap this probability is the same for any repetition of an operation and that the occurrence of a mishap during any one such repetition is independent of whether or not it occurs in any other.

Each of a group of experts familiar with the operations of interest and the bases for the identification of the subject set of mishaps is now asked to list the mishaps in descending order of their frequencies of occurrence per operation.⁽⁴⁾ He is then asked to judge how the frequency of the second mishap in his list compares to that of the first, and state this as a fraction, c_2 , less than or equal to one; how the third compares to the second, giving a fraction, c_3 ; the fourth to the third, c_4 ; etc. Finally, he is asked to give his best estimate of the frequency per operation, f_1 , of the first mishap on his list, the one that he believes would occur most often and thus the one whose frequency is easiest to estimate. Its occurrence may be a quite common event. (Recall that the mishaps of interest have only some potential for leading to explosions; by no means are explosions expected each time they occur. Such mishaps may occur ordinarily

(3) A basic process for mishap probability estimation is outlined here. Variations on it, and similar processes for other risk factors, can also be considered.

(4) This information is sometimes more easily elicited in terms of the number of times the expert expects an operation would be executed between mishap occurrences. The relative frequency estimates would of course be the reciprocals of these estimates.

but only rarely lead to explosions. The estimation of the probability of an explosion given the occurrence of a particular mishap is a distinct problem not considered in this paper; see however [3].)

In this way, each expert arrives at an estimate of the frequency of occurrence per operation for each mishap in the list: $f_1, f_2 = c_2 f_1, f_3 = c_3 f_2 = c_3 c_2 f_1$, etc. Note that this has been accomplished with judgments only of one relatively common mishap's occurrence frequency and of the comparative frequencies of successive pairs of mishaps with relatively similar occurrence probabilities. The probabilities of even rare mishap occurrences, all but impossible to estimate in isolation, are thus able to be estimated in a reasonable manner, a principal reason for the use of this procedure. A simple illustrative example of the technique that has been outlined is given in Figure 4.

For each mishap, the median (used as the output point estimate) and lower and upper extremes (used as subjective confidence bounds) of the estimates of its frequency of occurrence per operation by the several experts can be determined. If the spreads between the extremes of the estimates for some mishaps are deemed excessive, the process that has been described can be iterated by having the group reconsider together the reasons for the differences in the mishaps listing orders and comparative frequency estimates of the several individuals, and then, again as individuals, make such changes as then seem justified in the lists and estimates.

The result is the group's overall best point estimates (the median values) of the identified mishaps' probabilities of occurrence per operation, and also the ranges of uncertainty that should be considered in the use of these estimates as a complete risk analysis proceeds. (These ranges can be converted into uncertainty distributions, if desired, to support the derivation of uncertainty distributions for the ultimate overall risk estimates.)

APPROACHES TO RISK EVALUATION

Given a set of risk estimates, the problem remains of how judgments can be made on whether a calculated risk level for a given hazardous activity is

I. IDENTIFY MISHAPS OF CONCERN		II. ESTIMATE THEIR <u>RELATIVE</u> FREQUENCIES PER OPPORTUNITY	
1	(MOST COMMON)	-	
2		1/2	
3		3/4	
4		1/10	
5		1/10	
6		1/100	
III. ESTIMATE THE ABSOLUTE FREQUENCY OF MISHAP 1 = .2			
IV. DERIVE THE ESTIMATED FREQUENCIES OF ALL THE MISHAPS:			
1		.2	
2		.1	
3		.075	
4		.0075	
5		.00075	
6		.0000075	

Figure 4. Example of Subjective Estimation Process

sufficiently low for the activity to be instituted or continued, or whether mitigation measures may be needed. The proper selection of the most cost-effective such measures is then also of concern.

Risk Acceptability Evaluation

While no single approach has yet been established that enables a universally appreciated evaluation of the acceptability of the risk of a hazardous activity, a number of attempts have been made to develop such an approach. These are discussed here in three classes: comparisons to "ambient"/historical risks, comparisons to risks of equi-benefit alternatives, and balancing of risks and benefits.

Comparison to Ambient/Historical Risks - In 1969, Chauncey Starr [9] published the first of many articles on public risk acceptance in relation to benefits, as revealed by historical data. Expected fatalities per hour or per year, per individual in various groups exposed to potential accidents and other deleterious factors, and due to voluntary or involuntary hazardous activities, were estimated from past data and compared to assessments of the benefits accruing from these activities. Starr found historical levels of risk acceptance increased in proportion to the cube of the increase in benefits, and that voluntary acceptance levels were about three orders of magnitude greater than involuntary acceptance levels. (These particular conclusions have since been disputed. However, Starr's general demonstration of the dependencies of the level of risk accepted on benefits and on whether the acceptance is voluntary or involuntary is not questioned.)

Starr's concepts have been extended by many others in attempts to establish numerical acceptable risk levels for hazardous activities that provide specific benefits or meet specified societal needs. These numerical levels may also reflect the confidence in the risk estimates that are evaluated.

Risk Comparisons of Equi-Benefit Alternatives - A second risk acceptability evaluation approach is the standard operations research technique of assuming some activity must be put in place to satisfy a specific need, and

then establishing which alternative means of implementing it would give rise to the least risk. This minimum risk is then "acceptable," by definition.

Balancing of Risks and Benefits - Quantitative procedures exist for expressing the risks of a hazardous activity, as well as its benefits, in common economic terms, e.g., present value dollars. However, these procedures generally entail assuming a "value-of-a-life" (or of an injury or health insult), and this has been a difficult feature of the analysis to have agreement on. If it could be agreed to, it could then be argued that a hazardous activity was acceptable if the potential losses expressed by its risks are less than the dollar value (or a given fraction of this value) of its benefits.

Evaluation of Possible Mitigation Measures

Mitigation measures may reduce the risk by reducing the probability of occurrence of a mishap and/or by reducing its consequences should it occur. Mitigation measures may be procedural changes, equipment or facility design changes, or changes in the locations of the explosives whose presence and handling induce the risks.

Cost-Effectiveness of Alternatives - When evaluating alternatives for risk mitigation one first compares their effectiveness in terms of reduction in the estimated risk. Effectiveness can be measured in a variety of ways, such as the expected number of lives saved, the reduction in expected property damage, expected mission delay avoided, or, in more complex investigations, differences in selected characteristics of complete risk profiles. The cost of each alternative is next determined. Usually, the mitigation which provides the greatest effectiveness within an allowable cost budget, or the mitigation which provides a required level of effectiveness at the lowest cost, is then selected (see Figure 5a). In some cases, the mitigation that provides the most effectiveness per dollar (i.e., has the highest effectiveness-to-cost ratio) may be preferred.

Cost-Benefits of Alternatives - If the effectiveness of the alternative mitigations is first expressed as equivalent expected dollar losses avoided,

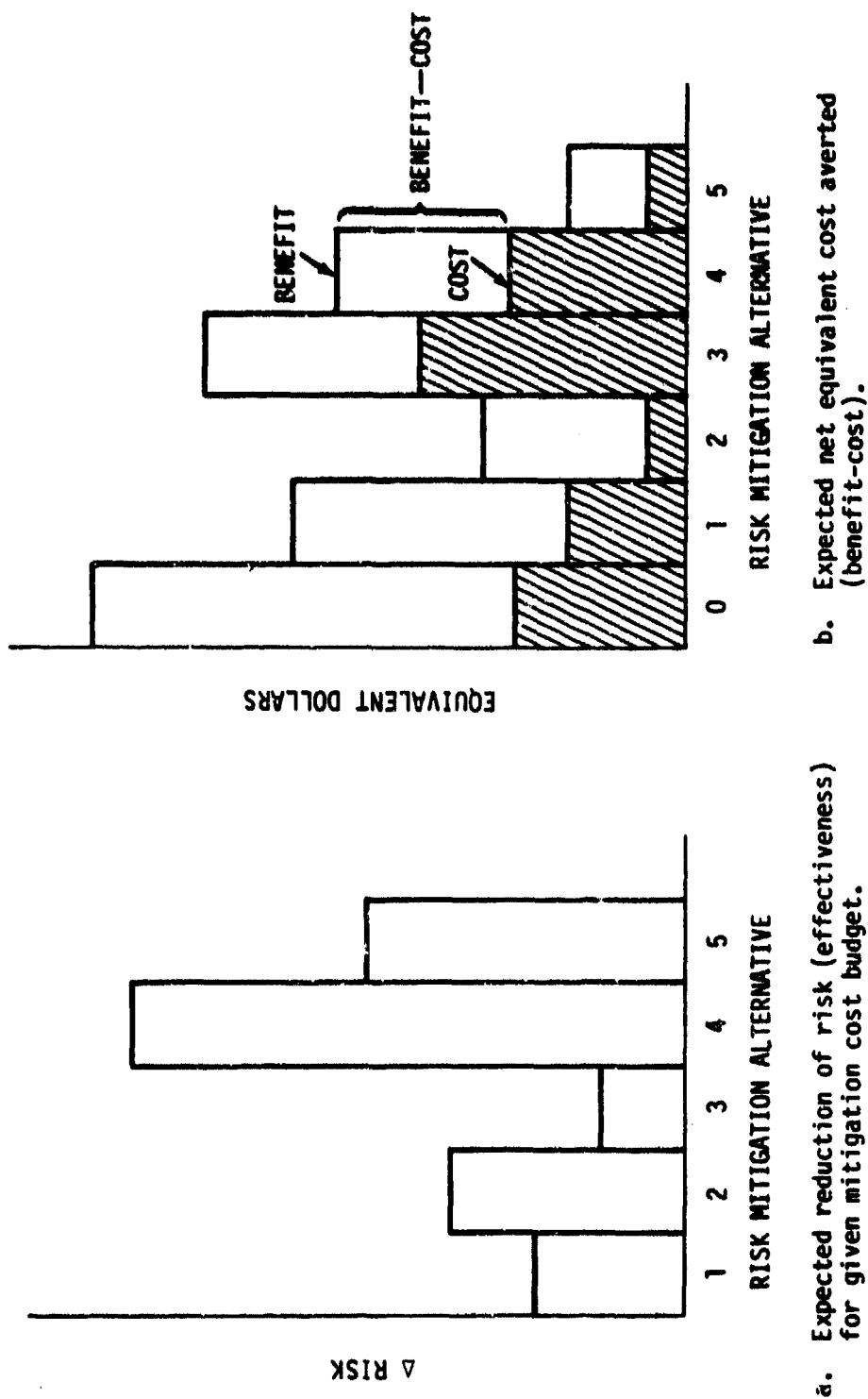


Figure 5. Typical Cost-Effectiveness and Cost-Benefit Evaluations of Alternative Risk Mitigation Strategies

which is generally termed "benefit," then the preferred alternative is that one whose benefit most exceeds its cost in common dollar terms (see Figure 5b).

THE TREATMENT OF UNCERTAINTIES

There are four general techniques available for the treatment of uncertainties. The four techniques are:

- The development of statistical bounds (when statistical estimates are involved).
- The establishment of subjectively-derived bounds; i.e., the employment of judgment to appraise the credible ranges of variation of the estimates.
- The conduct of parametric sensitivity analyses; i.e., the recalculation of the output estimates as the input factors are allowed to vary over their ranges of uncertainty. Monte Carlo techniques may be employed, or, when computing requirements would be excessive, only selected values (e.g., nominal and worst-case values) from the input uncertainty ranges might be considered.
- The carrying out of parallel analyses and peer reviews. Risk analyses should always be at least carefully reviewed by independent analysts, given the analyses' inherent uncertainties and subjectivities. When resources permit, two or more independent analyses should be executed in parallel, and their results compared. The results will help to define the ranges of uncertainty that can exist in the results. They will also help to decrease the uncertainties and raise the level of confidence that can be held in the results in areas where reasonable agreement obtains.

Primarily, these techniques can provide means for illuminating for a decision maker the possible ranges of variation in the risk estimates (and the cost and any other estimates, as well) he must deal with. They produce

confidence limits or other definers of the uncertainty ranges of the outputs of the estimation process. The decision maker can then consider whether and how the potential variability in the estimates might affect his preferences.

The application of these techniques, as appropriate, may also help to reduce uncertainties by identifying where they are most significant in a decision analysis, and motivating thereby additional investigations of the factors from which the significant uncertainties arise.

CONCLUSIONS

Risk analysis is a potentially important component of explosives risk management systems. Its main elements are:

1. The structuring of the problem, which includes selecting a method of analysis consistent with the characteristics of the hazardous activity or system of concern, the availability of data, and the needs and resources of the risk manager involved.
2. The estimation of the relevant risks (i.e., the probabilities of the consequences of all significant undesired events, with and without mitigating measures).
3. The evaluation and interpretation of the estimated risks, to result in the acceptance of a risk or the recognition of a need for risk reduction measures.

However, much must yet be done towards the reduction and/or better exposition of its uncertainties, so as to enable risk analysis to be as useful as possible in explosives risk management. A primary impediment to its successful implementation is the inadequacy of the data base for risk estimation--in both scope and detail. Mishap data are sparse. Also generally inadequate are operations records as sources of exposure data. Thus, pure statistical inference methods of risk estimation are not promising. (Some augmentations may be feasible, however [7].)

For fault tree methods, failure rate data on the equipments involved in the handling of explosive materials are also generally not available. Moreover, it is not yet possible to quantify very satisfactorily the extent to which errors or other variations in the performance of operating personnel affect the probabilities of mishap occurrence (although this is receiving considerable study by the nuclear power industry and the Nuclear Regulatory Commission).

Analytical and simulation models apply primarily to the effects and consequences factors in explosives risk estimates and have not been discussed in this paper. However, they are the subjects of other papers presented at this Seminar.

A structured subjective estimation process has been introduced that is a straightforward evolution from the judgment-based, qualitative hazards ranking procedures already employed in explosives safety management. It can enable the development of numerical risk values and some appraisals of their uncertainties for use in probability-based risk decision making.

A most controversial aspect of risk management is the evaluation and interpretation of the estimated risks. There is a lack of concurrence on the factors that should be included in the judgments that must be made. In addition to the relevant estimates of hazardous activity risks and mitigation effectiveness and cost estimates (incorporating assessments of their significant uncertainties), mission importance considerations, and socio-political risks can be of concern. The implementation in risk management systems of such evaluation approaches as have been noted in this paper can help to illuminate the judgments that must be made.

REFERENCES

1. Keenan, W.A., "Analysis of Risk and Risk Mitigative Policies." Presented to the 18th Explosives Safety Seminar, San Antonio, Texas, September 1978.

2. Philipson, L.L., "Initial Conceptualization of an Explosives Risk-Decision Model." Prepared for the Navy Civil Engineering Laboratory. J.H. Wiggins Company, Technical Report No. 79-1364-1, 30 September 1979.
3. Philipson, L.L. and E. Ostermann, "Further Development of Ordnance Hazards Modeling Logic for NOHARM System." Prepared for the Navy Civil Engineering Laboratory. J.H. Wiggins Company, Technical Report No. 79-1375/1376, March 1980.
4. Philipson, L.L. and W.A. Keenan, "The Navy's NOHARM System." Proceedings of the Fifth International System Safety Conference, Denver, Colorado, 27-31 July 1981.
5. Keenan, W.A. and L.L. Philipson, "System Performance Specification for the Naval Ordnance Hazards Analysis and Risk Management (NOHARM) System." Technical Memorandum No. 51-80-25, Naval Civil Engineering Laboratory, September 1980.
6. Task Assignment Definition, Probabilistic Explosive Risks Management Assistance (PERMA) System. Range Safety Support Contract F04703-79-C-0004, U.S. Air Force Western Space and Missile Center, 1 March 1982.
7. Philipson, L.L., "Risk Assessment Methodologies and Their Uncertainties: Volume I, A Review of Risk Estimation Approaches; Volume II, A Review of Risk Evaluation Approaches." Prepared for the National Science Foundation. J.H. Wiggins Company, Technical Report No. 82-1398, March 1982.
8. H.A. Linstone, and M. Turoff, eds. The Delphi Method. Addison-Wesley, 1975.
9. C. Starr, "Social Benefit Versus Technological Risk," Science, Vol. 165, September 1969.

→
↘

RISK ANALYSIS FOR EXPLOSIVES OPERATIONS
LT COL ALAN C. GRAHAM, JR.
HQ AIR FORCE INSPECTION AND SAFETY CENTER

In order to be of any military utility munitions must be placed at the intended point of use in the quantity necessary and within the time constraints of the situation. For most Air Force applications, that means on an aircraft ready for launch or, at the very least, on the base of intended use. However, many bases, particularly overseas locations, have limited capability because land and money are not available to construct enough munitions storage and operating facilities to meet all operational requirements. In addition, traditional philosophy emphasized "absolute" levels of safety. As a result, combat units must rely on centralized storage ammunition areas in overseas theaters of operation and CONUS storage for the bulk of their conventional wartime munitions requirements. In a short notice conventional conflict, these assets may have no utility because they will not be available during the first critical days when they will be needed most.

AD P000457

Eighteen months ago, the Air Force Safety Center decided that our conservative safety standards and our traditionally conservative interpretation of those standards prevented maximum or effective use of existing facilities, and were a strongly negative influence on readiness and combat capability. We initiated steps to test our existing criteria and to eliminate restrictions which did not provide a measurable increase in the level of safety. One of our more successful efforts was the distant runner test which is a discussion topic for another session during this seminar. In spite of these efforts to define appropriate levels of risk, there are still many cases where immediate operational needs cannot be met using established safety criteria, and waivers to that criteria are necessary to meet mission requirements. In the past, requests for waivers were accepted as a routine fact of life and no indepth analysis was conducted to quantify the additional risk the proposed procedure presented. As a result, some units accepted high levels of risk for marginal increases in capability. To correct this, we proposed a methodology for risk management to provide commanders with a more definitive assessment of the potential effects of a mishap on their operations.

If we are to become more accurate in assessing operational risk, we are forced to logically pursue the definition of the mission. Exactly what are the elements, that is, the people, equipment, facilities, and operations, that constitute the mission, and what are the specific conditions under which they will operate. Based on this definition of the mission, it is possible to identify hazards and factors or conditions which can generate hazards or result in a mishap. We are perhaps, most familiar with this process in its application to hardware systems safety. Preliminary hazard analyses, fault trees,

failure modes and effects analyses, and other similar systems analysis techniques are used to examine the systems, subsystems, components and their interrelationship as well as human factors which affect safety. These analytical tools were developed to assure that no stone remained unturned in the quest to assure adequate design and operational safety. No less rigorous approach is warranted for the risk analysis of explosives operations.

Risk is an expression of possible loss in terms of mishap probability, mishap severity and mission exposure. While there may be such a thing as a risk-free environment, for all practical purposes, a given level of risk exists in all situations. Whether that level of risk is "acceptable" is a purely managerial decision, and the Air Force explosives safety standards published in AFR 127-100 represent DDESB and USAF managerial decisions on acceptable levels of risk for normal munitions operations. However, commanders at all levels must make this managerial decision each time they face the safety-operational necessity confrontation.

Operational necessity cannot be separated from a discussion of risk because it is the factor which may cause a commander to "accept" a greater level of risk than is normally allowable. For example, the need for faster aircraft refueling and reloading during combat mandated these operations be conducted simultaneously which is normally prohibited. The Air Force conducted detailed systems safety engineering analyses (or SSEAs) of the simultaneous operations and developed procedures which represent an acceptable wartime risk. Because we had to be able to train in peacetime using these procedures, the analyses also addressed specific hazard abatement techniques and procedures necessary to limit risk during practice operations. As a result, we are able to simulate our wartime procedures more precisely and will be better prepared for combat.

Each one of us quantifies risk and makes many risk analysis decisions each day of our lives. Most of them are intuitive, almost reflex decisions, and the fact we are all still here is witness to the marvelous success rate we all enjoy. These individual risk decisions we all make impact few people other than ourselves. However, when we are dealing with explosives operations, the hazard, and the people exposed to that hazard may be multiplied manyfold. We can ill afford to rely solely on intuitive judgment in these risk decisions. We proposed this generalized risk management model to help commanders and safety staffs develop more methodical analysis techniques. The key to using this model is the accurate identification of the three elements of risk: mishap severity, mishap probability, and mission exposure. Let's take a brief look at these factors in relationship to explosives operations.

It would be convenient, even comforting if we were able to come up with a neat, mathematical relationship between these three elements of risk so we could plug in the numbers and crank out a solution that could be compared against a standard, acceptable risk. There have been several efforts to use this type of relationship. As an example, during the combat turnaround SSEAs we assigned hazard severity and hazard probability factors as shown on the chart and used simple multiplication to determine which hazards needed to be controlled. The standard, acceptable risk index was 8. Risks, even category I hazards, were acceptable if the probability was low enough. While this was a convenient decision tool, the probability index was often based on "soft" numbers, not hard, engineering data. In practice, we still must rely on subjective judgment to a great extent, but the proposed model allows greater objectivity and provides clues to areas where risk can be minimized.

Mishap severity can be thought of as the resultant damage that can be expected if the maximum credible event occurs and this damage is normally quantifiable, such as aircraft damaged or destroyed, people injured or killed, or facilities damaged or destroyed.

As an example, this is a map of a combat turnaround area. The area consists of nine aircraft parking spots with an explosive limit of 2344 lbs NEW each, and four service alleys which are used to preposition equipment and munitions with an explosive limit of 4688 lbs NEW each. Each spot is separated by an ARMCO revetment barricade to prevent simultaneous detonations of explosives from one potential explosion site or PES to another PES. Because the sites are so close together (K1.25 in this case), aircraft in adjacent cells will suffer various degrees of damage from slight to total destruction from the initial blast overpressure depending on the distance from the PES. Although simultaneous detonation would be prevented by the barricades, the resulting fuel fires may cause propagation of the explosion.

As you can see on the map, there are a large number of facilities located within the 1,250 foot minimum fragment hazard distance of the PES. These facilities house a wide variety of operations ranging from the squadron operations building to the flightline dining hall. For each facility we can compute the maximum expected blast overpressure and the resultant damage expected. For example, this is the dining hall. It is a wood frame structure located 450 feet from the PES. There is unbarricaded line of sight from the PES because of this entry road through the ARMCO revetment wall surrounding the parking ramp. At this distance (a K-factor of about 27) the expected overpressure would be 2 PSI. Personnel located in the building may be injured by direct fragments or secondary fragments such as broken glass or building debris. The building will receive minor blast damage, including broken window

glass, and direct fragment damage. For the limited quantity of explosives at the PES, the risk of personnel injury or facility damage due to low angle, high speed fragments can be reduced by construction of barricades at the dining hall. We would recommend the use of barricades in this case even though we obtain no reduction in the safety distance by their use. Note that many essential facilities are already barricaded to provide protection from enemy attack. It is convenient that these barricades can also protect us from inadvertent explosions of our own munitions.

Let's take a brief look at mishap probability. Although soft values were often used during SSEAs, we can arrive at some "hard" mathematical values here. Before a munitions item is accepted for use, the Air Force conducts an extensive safety analysis to identify failure modes and effects, single point failures, safe delivery parameters and so forth. In general, this review assures that the probability of inadvertent detonation of any munitions item is very remote; less than one in a million. However, we must insure that, in planning munitions activities, the operational procedures developed do not intentionally or unintentionally defeat design safety features.

Now, in general, the explosives safety standards do not recognize probability--or rather they are based on a probability of one that the maximum credible event, a high order detonation, for example, will occur. The notable exception to this is the use of public traffic route distances of 60 percent of the inhabited building distances based on the transient nature of the exposure. We were recently successful in our arguments before the DDESB that a similar case can be made for the transient exposure of aircraft on a taxiway or runway. Our goal in this case is to prevent damage to the runway or taxiway, and distant runner showed us K4.5 provided this level of protection. The previous criteria were K-30. If the commander is willing to accept the very low probability that aircraft will be on the taxiway at the exact moment of detonation, a large area is freed for storage of munitions. We believe wider acceptance of transient exposures and mishap probability is necessary in order to meet operational needs and maintain acceptable safety standards. Probability is widely used as a management decision tool in aircraft design, and its further extension to the explosives community is the next logical step in our evolution from black powder safety.

These three factors then combine to define the specific level of risk for a given situation, and the commander must answer the tough question "Is this level of risk acceptable?" If the risk analysis is thorough, this answer can be based on much more than mere intuition. That may not mean the decision will be any easier to make, but at least the commander will have a better understanding of the effects of the decision.

Once the decision is made, the model leads us to actions required. If the risk is acceptable but current standards are not met, a waiver or deviation request must be prepared for approval by higher headquarters. This merely formalizes and documents the decision process and using the model from the start simplifies this paperwork significantly. If the risk is unacceptable we must eliminate or reduce the risk, by modifying the system, using an alternate system, or canceling the operation.

In our combat turnaround example, the commander decided to evacuate nonessential personnel from the area of the operation and to prohibit passenger terminal operations while the combat turnarounds were in progress. Although a waiver was still required, the risk was significantly reduced. It is often hard to get the point across that waivers, deviations and risk assessments don't make things any safer, they just help us understand our weakness more completely. This greater level of understanding, however, allows us to focus our attention and to take action to prevent accidents caused by those weaknesses.

In the final analysis, the goal of risk analysis for explosives operations must be to provide the maximum operational capability within acceptable (not minimum) levels of risk. For too long, we in weapons safety have been a negative factor, only telling commanders why they could not conduct their operations. Risk analysis offers us the opportunity to be an active driving force by showing the commander how to do the job better.



RISK ANALYSIS FOR EXPLOSIVES OPERATIONS



LT COL ALAN C. GRAHAM, JR.

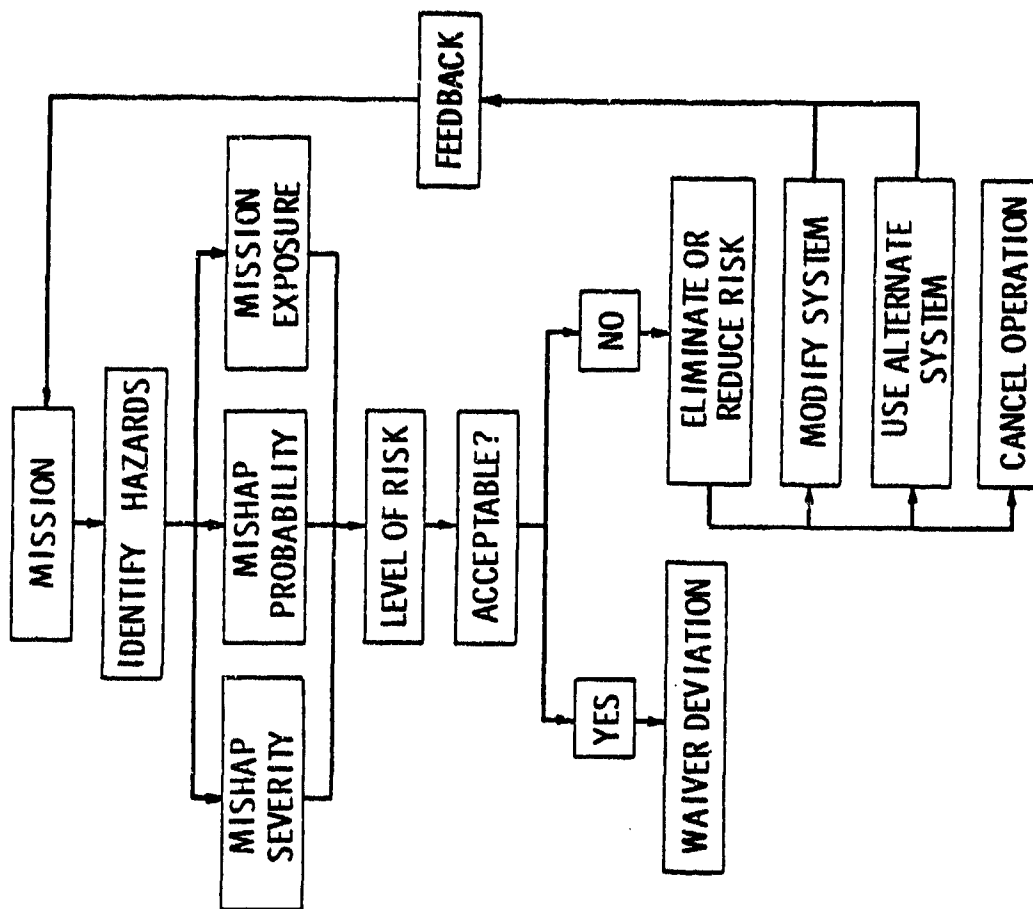
AIR FORCE INSPECTION AND SAFETY CENTER



- UTILITY OF MILITARY MUNITIONS
- VALIDATION/REVISION OF CRITERIA
- WAIVERS STILL NECESSARY
- METHODOLOGY FOR RISK MANAGEMENT
 - SPECIFY MISSION ELEMENTS
 - IDENTIFY HAZARDS
 - "QUANTIFY" RISK

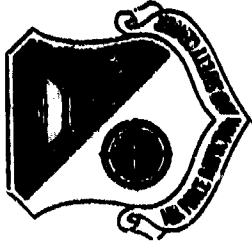


GENERALIZED RISK ASSESSMENT PROCEDURE





REAL HAZARD INDEX



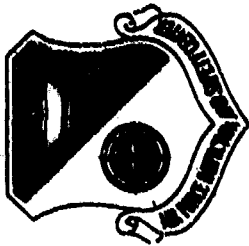
HAZARD SEVERITY

CAT I 4
CAT II 3
CAT III 2
CAT IV 1

HAZARD PROBABILITY

A 6
B 5
C 4
D 3
E 2
F 1

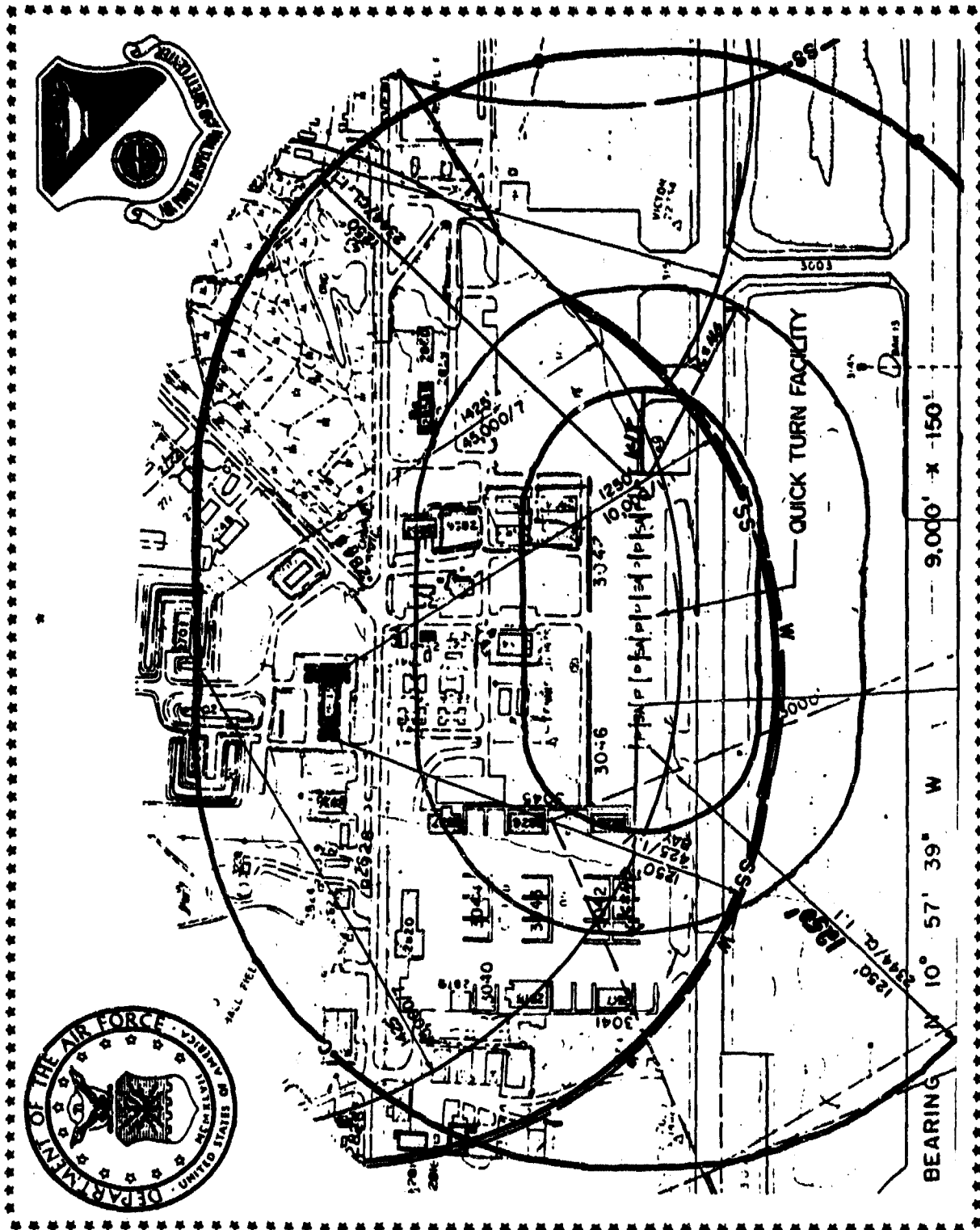
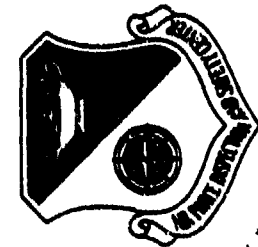
HIGHEST ←-----→ LOWEST



REAL HAZARD INDEX MATRIX

PROBABILITY

	<u>SEVERITY</u>			
	<u>I (4)</u>	<u>II (3)</u>	<u>III (2)</u>	<u>IV (1)</u>
A (6)	24	18	12	6
B (5)	20	15	10	5
C (4)	16	12	8	4
D (3)	12	9	6	3
E (2)	8	6	4	2
F (1)	4	3	2	1



BEARING N 10° 57' 39" W 9,000' x 150'



AD P000458

→ BUILDING DAMAGES DUE TO AIRBLAST FROM AN ACCIDENTAL EXPLOSION

by

Hansjörg Rytz
Defense Technology and Procurement Group
of the Swiss Federal Department of Defense
Technical Division 6
CH-3602 Thun / Switzerland

ABSTRACT

→ This paper describes the effects of airblast on buildings caused by an accidental explosion of about 1000 kg of a gelatine explosive in a Swiss explosives factory. The location of the detonated explosive charges and the course of the explosion are briefly summarized. The evaluated building damages are described and compared with damage criteria given in the literature. The location of persons at the time of the explosion is shown, and their injuries are described. The appendix contains photos of typical building damages and a checklist that was used to record building damages. ↗

Paper presented to

Twentieth Explosives Safety Seminar, 24 - 26 August 1982
The Omni Hotel, Norfolk, Virginia, USA

INTRODUCTION

On February 1st in 1982, an accidental explosion involving about 1000 kg of explosives occurred in the "Cheddite AG" explosives factory at Isleten, Switzerland. Two persons were killed and a number of employees suffered light injuries. The factory, founded in 1873 by the Alfred Nobel Society on the occasion of the construction of the Gotthard railway tunnel is located at a remote place on the shore of Lake Lucerne.

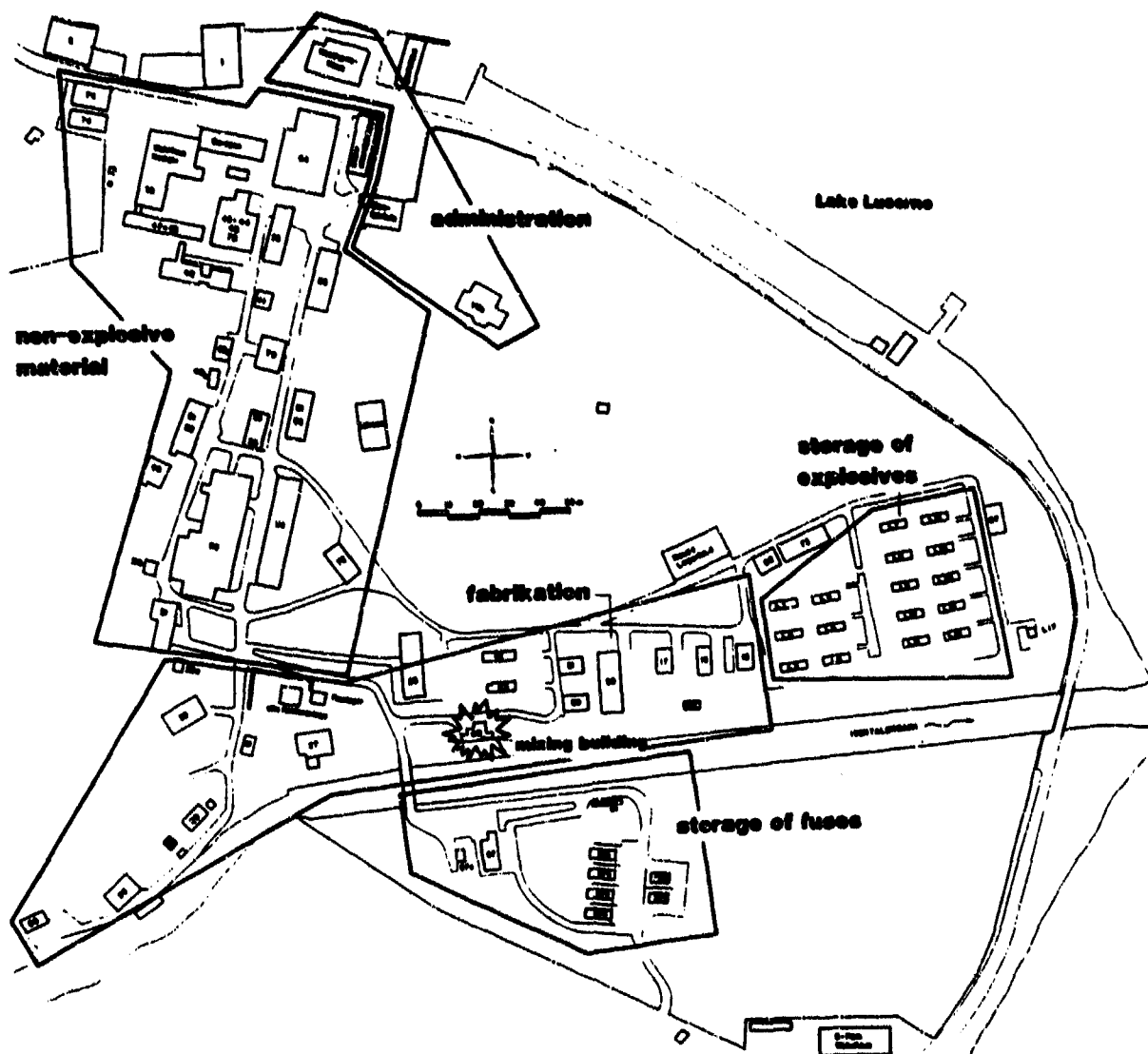


Figure 1: Layout of the Cheddite AG, Explosives Factory at Isleten, Switzerland

The factory encloses nearly 100 buildings which can roughly be divided into the divisions shown in figure 1.

The extensive damage to the buildings was registered and analyzed by the Swiss Defense Technology and Procurement Group. The primary goal of the investigation was to get first-hand and detailed information about the effects of airblast on buildings. This information is used to improve the basis for the quantitative damage prediction in risk analyses. In Switzerland, such risk analyses are performed for the purpose of safety assessment for all military ammunition storages and factories.

ORIGIN AND COURSE OF THE EXPLOSION

The explosion occurred in a mixing building, shown in Figure 2, in which the commercial gelatine explosive Titadyn 45 had been mixed.

As far as it is known from the official investigation, the explosion started when a person (A) was pumping a mixture of 49 % nitroglycerine, 47 % nitroglycol and 4 % Dinitrotoluol (DNT) from a vessel mounted on a small electrically operated car into a mixing and kneading vessel inside the building. The most likely initial event was the explosion of a few kilograms of this mixture which were left in the vessel of the car. In a second step, the explosion propagated to a container with 400 kg gelatine explosive Titadyn 45 standing outside the building. Then it propagated to the two vessels inside the building, one containing about 100 kg of the mixture of nitroglycerine, nitroglycol and DNT, the other one containing 400 kg gelatine explosive Titadyn 45.

For the purpose of the evaluation of building damages due to airblast, the TNT equivalent of the multiple explosions is estimated to be about 1000 kg.

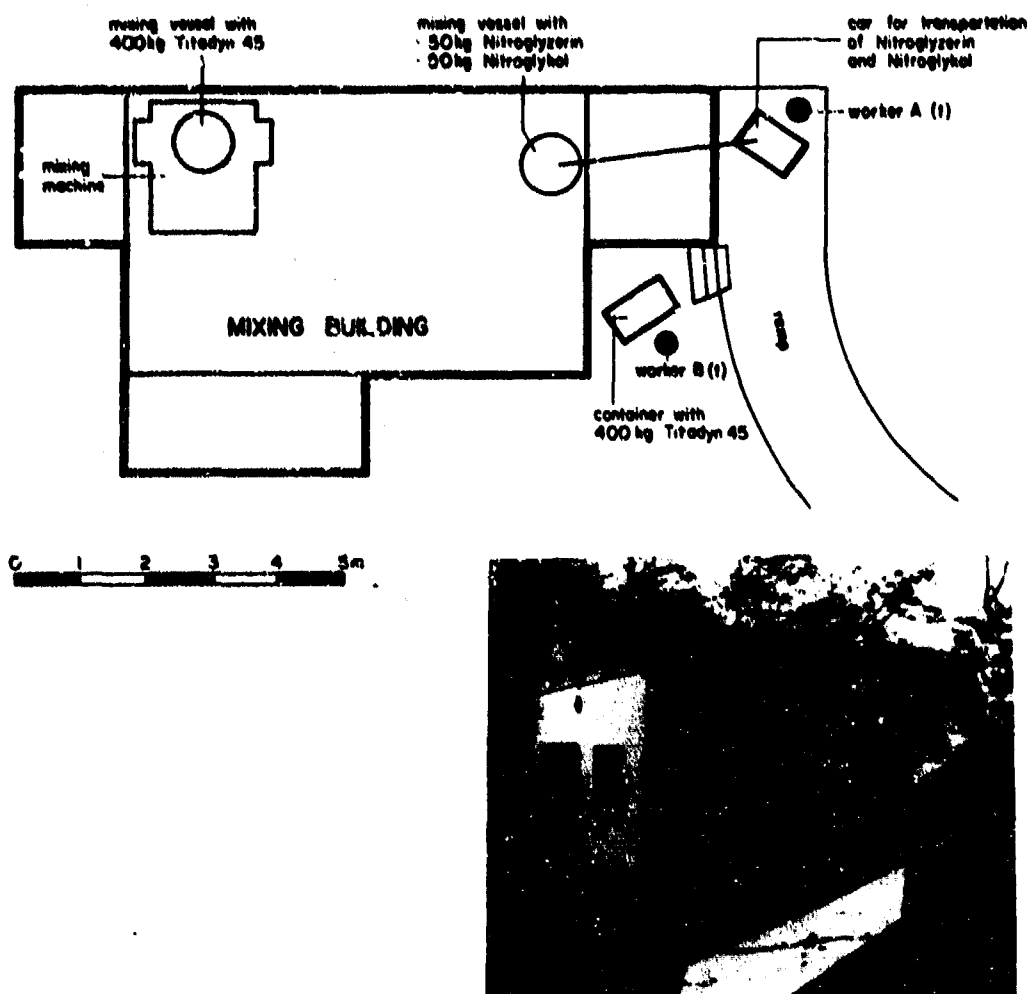


Figure 2: Horizontal section and photos of the mixing building in which the explosion occurred

OBSERVED BUILDING DAMAGES

The evaluation of the building damages was performed in order to get additional information for damage prediction models used in preliminary risk analyses. For this purpose simple and easily applicable models are required which enable a simple and reliable assessment of estimated building damages. Therefore, no distinction was made between buildings of different construction types, age, etc. In addition, the damage description was simplified by defining five representa-

tive damage categories (see Table 1). These definitions closely correspond to those in similar investigations found in the literature. In the appendix, illustrative examples are given for the damage level of each individual category.

Damage Category	Description
A	building totally demolished and collapsed
B	damage beyond repair and requiring demolition
C	seriously damaged; requires extensive repairs before reusable for any purpose
D	Slight damage to windows, glass panels, doors and roofs
E	Minor damage to glass or miscellaneous small items (similar to damage caused by strong wind)

Table 1: Definition of damage categories

The damages recorded for more than a hundred buildings were classified according to these five categories. Since the mixing building was almost completely surrounded by earth barricades, the debris throw from building and crater did not significantly contribute to the damages. Therefore, it can be assumed that practically all building damages were caused by the effects of the airblast only.

Figures 3 and 4 show the results of the classification of the building damages:

In Figure 4 the damage categories of the investigated buildings are plotted against their distance from the center of explosion.

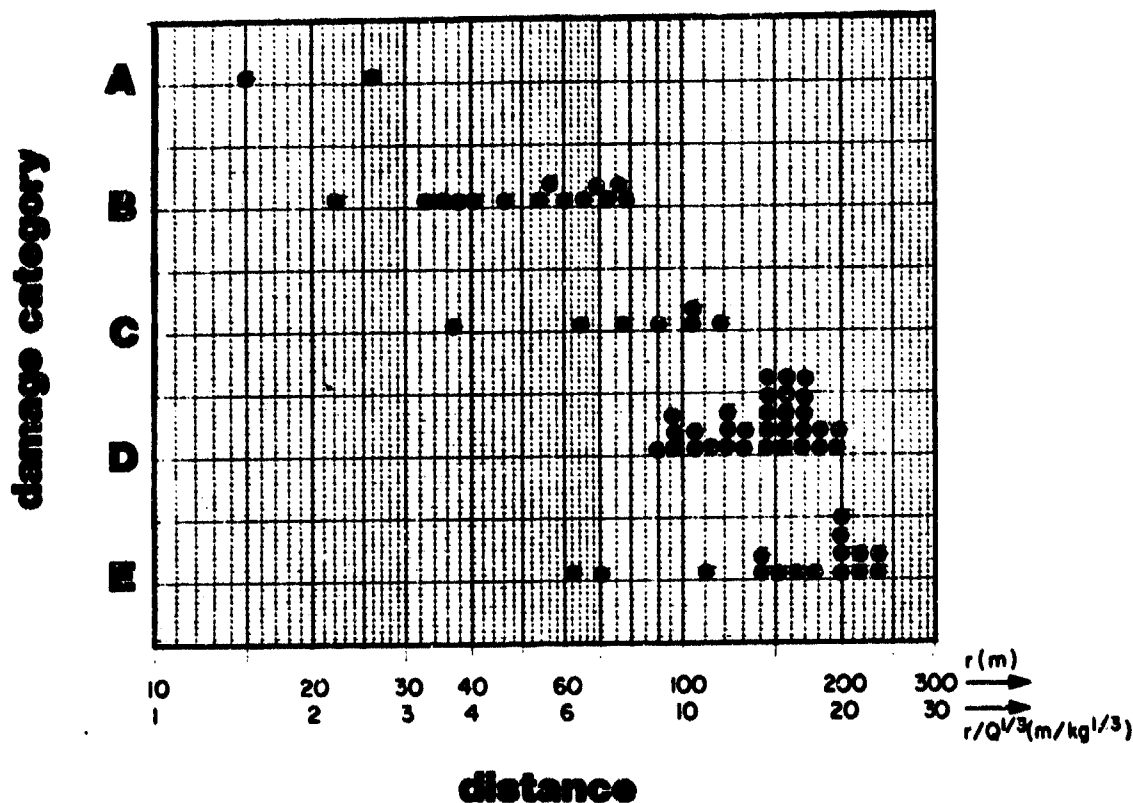


Figure 4: Building damages versus distance and scaled distance from the explosion source

As expected, a large scatter of the data points can be observed in each category. This scatter can be attributed to the differences in the buildings such as load bearing capacity and ductility of the structural elements, building height, form and material, existence of barricades, etc. All these factors may influence the actual damage level at a given airblast intensity.

Moreover, it can be observed that the data points of categories D and E sometimes heavily overlap. This is due to the fact that the classification of the building damage at low damage levels is not always clear-cut. Since these damage

levels are usually not relevant to injuries of persons, this inaccuracy is of no importance for risk analyses.

EFFECTS ON PERSONS

At the time of the explosion, 39 persons were present at a distance of about 200 meters around the explosion center. 34 of them were inside buildings and five in the open.

Figure 5 shows the positions of these 39 persons at the time of the explosion. Besides the two persons who were working in the exploded mixing building and who were killed instantaneously, only one employee walking at a distance of about 35 m ($p \approx 1$ bar!) was injured significantly. He was thrown away by the blast wave and suffered a shock and a few minor wounds. He was hospitalized for two weeks. About ten persons in the range of 40 to 200 m were slightly harmed by glass fragments. The rest of the staff was not injured.

COMPARISON WITH EXISTING DAMAGE CRITERIA

The most essential factor for the risk to which persons inside buildings are exposed usually is the behavior of the structure, i.e. whether it collapses or not (limit between damage criterion A and B). This statement can be illustrated by the heavily damaged, but not collapsed building number 20 (see Figure 5), where three persons were working. All of them were only slightly injured by glass fragments. The inspection of this building showed that a slightly stronger airblast would have caused the collapse of the ceiling which was already half a meter below its original position. A collapse would have killed the three persons instantaneously.

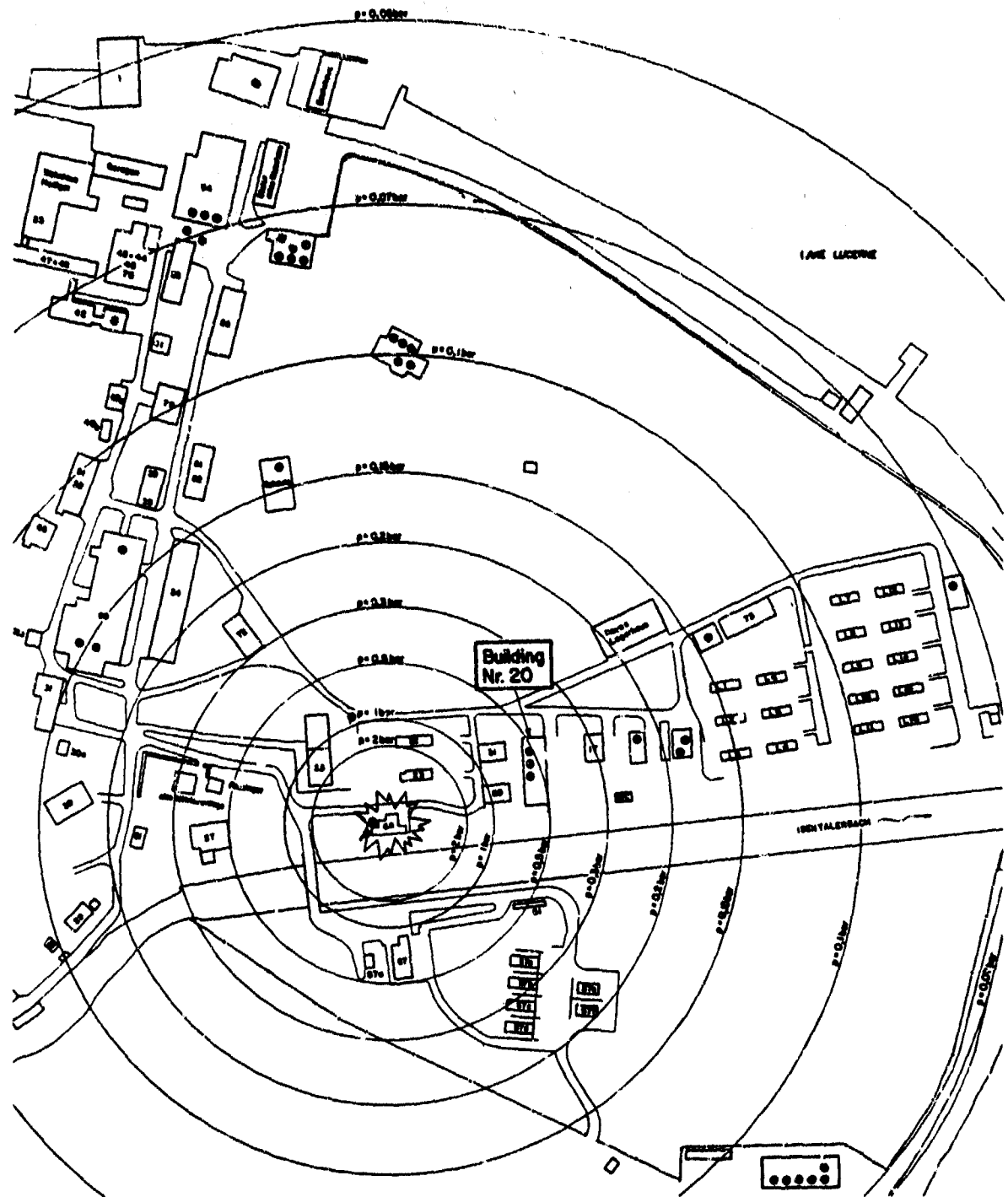


Figure 5: Position of the exposed persons at the time of explosion

Damage category A, being the most important one, has been chosen for comparison with damage criteria from the literature. The following damage criteria found in the literature were selected for comparison:

- a) Jarrett (Ref. 2, 1968) gives the following relationship for "almost complete demolition":

$$r = \frac{3.8 \cdot W^{1/3}}{(1 + (\frac{3180}{W})^2)^{1/6}}$$

r (distance in m)

W (charge in kg)

The investigation of Jarrett is based on the evaluation of several accidental explosions.

- b) Wilton (Ref. 3, 1966) (and various other authors) take the incident over-pressure as the characteristic value for building damages.
Total demolition of average inhabited buildings occurs at

$$p \approx 0.4 \text{ bar}$$

The investigation of Wilton is based on nuclear and large high explosive tests.

In Figure 6, the damage criteria of Jarrett and Wilton are presented in form of the well-known p - I -diagram (pressure-impulse diagram):

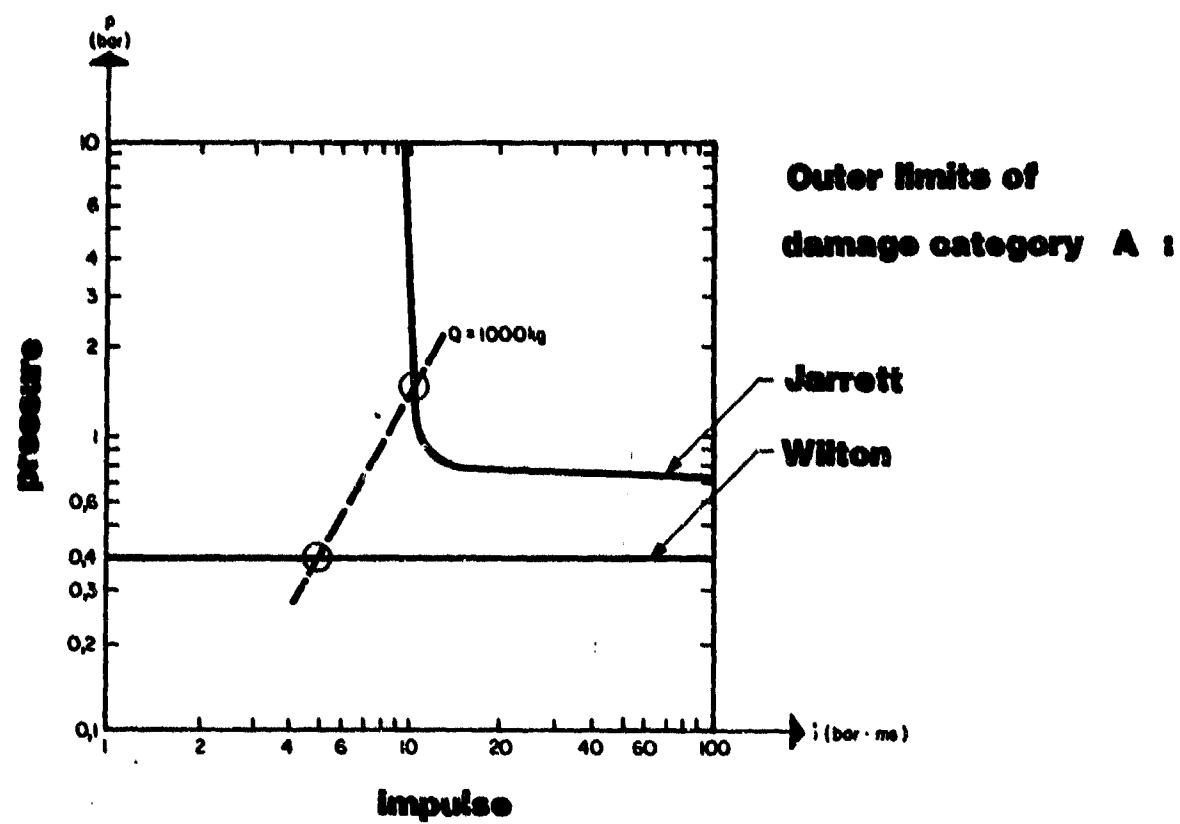


Figure 6: Damage criteria of Jarrett and Wilton for total demolition

For a charge weight of 1000 kg, the criterion of Jarrett leads to a radius of total demolition of 28 m. The criterion of Wilton, however, leads to a radius of 55 m. These values are shown in the map of Figure 7:

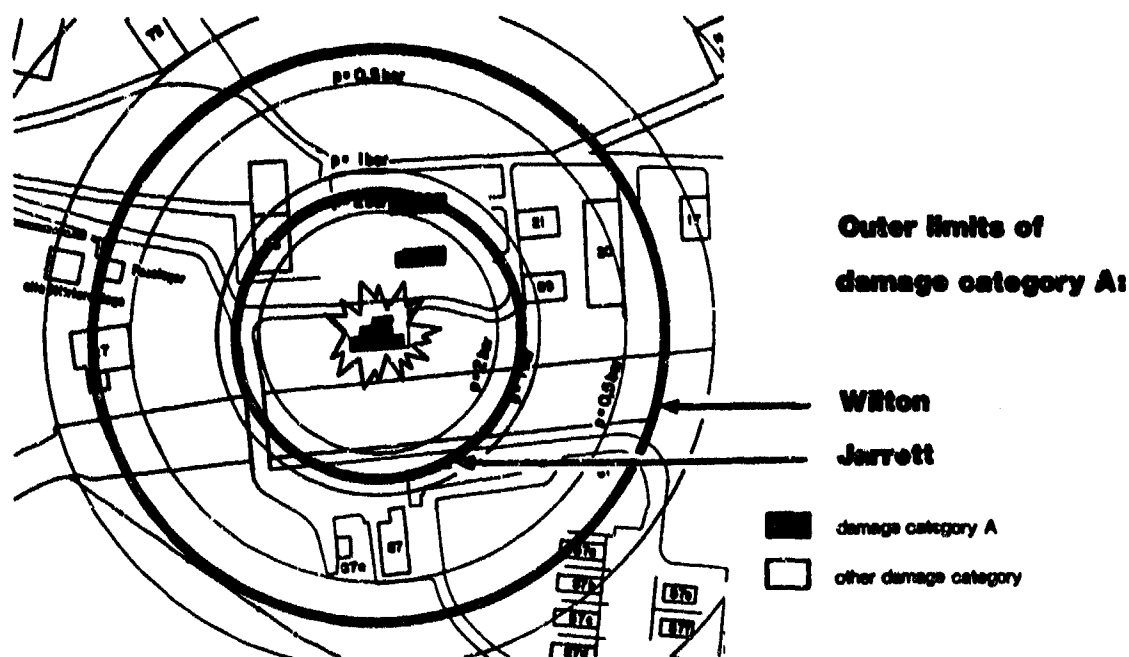


Figure 7: Outer limits of damage category A

As Figure 7 shows, the damage radius predicted by Jarrett closely corresponds to the actually observed damage, whereas the prediction of Wilton strongly overestimates the effects. The reason for these differences is that for small explosions the impulse is the important factor for the collapse of the building and not the pressure (see Figure 6).

SUMMARY AND CONCLUSIONS

On the occasion of an accidental explosion involving about 1000 kg of gelatine explosive in a Swiss explosives factory on February 1st, 1982, an extensive investigation of the damage on buildings by airblast was performed. The primary goal of this investigation was to improve damage prediction models for the pur-

pose of risk analyses of explosives and ammunition factories. In the course of this investigation the following conclusions were drawn:

- The risk to persons inside buildings due to an airblast is determined by the fact whether the building can withstand the blast load or whether it will collapse.
- In predicting the possibility of collapse, the peak overpressure or the impulse can be of importance. The impulse criterion is important for relatively small explosions, whereas the peak overpressure criterion is valid for large explosions only.
- The observed damages to buildings show a considerable scatter. This is due to differences in construction types, age, height, form, etc.
- The experience collected from this explosion is only a drop in the bucket. It does not allow to draw new conclusions with respect to damage prediction models for buildings. However, it has clearly shown that a systematic collection of data on building damages could lead to improved prediction models in the future. Besides an evaluation of explosion events in the past, it would be most beneficial to collect all information on building damages and the effects on persons as well as on explosives or other substances (propagation) from future accidents (see Appendix). The evaluation of actual accidents is still the best starting point to improve the safety in the explosives industry.

ACKNOWLEDGEMENT

The permission to report on this accident and the assistance in the preparation of the data by the management of the explosives factory "Cheddite AG" is gratefully acknowledged.

REFERENCES

- (1) Gruppe für Rüstungsdienste:
"Explosionsunglück vom 1. Februar 1982 in der Schweizerischen Sprengstoff AG Cheddite, Isleten; Schadenbilder"
P. Janser, Ernst Basler & Partner, TM 3113-10, Febr. 82
- (2) D.E. Jarrett:
"Derivations of the British Explosives Safety Distances"
Annals of the New York Academy of Sciences, Volume 152, Art. 1, Oct. 68
- (3) C. Wilton, B. Gabrielson:
"House Damage Assessment"
URS Research Company, San Mateo, Cal.
Defense Nuclear Agency Report DNA 2097 G, Jan. 73

APPENDIX

EXAMPLES FOR BUILDING DAMAGES

CHECKLIST TO RECORD BUILDING DAMAGES

DAMAGE CATEGORY A



Building Nr. 23

Distance from
source:

$r = 17 \text{ m}$

Incident over-
pressure:

$p = 2.5 \text{ bar}$

Incident impulse:

$i = 15 \text{ bar} \cdot \text{msec}$



Building Nr. 22

$r = 26 \text{ m}$

$p = 1.7 \text{ bar}$

$i = 10 \text{ bar} \cdot \text{msec}$

DAMAGE CATEGORY B



Building Nr. 20

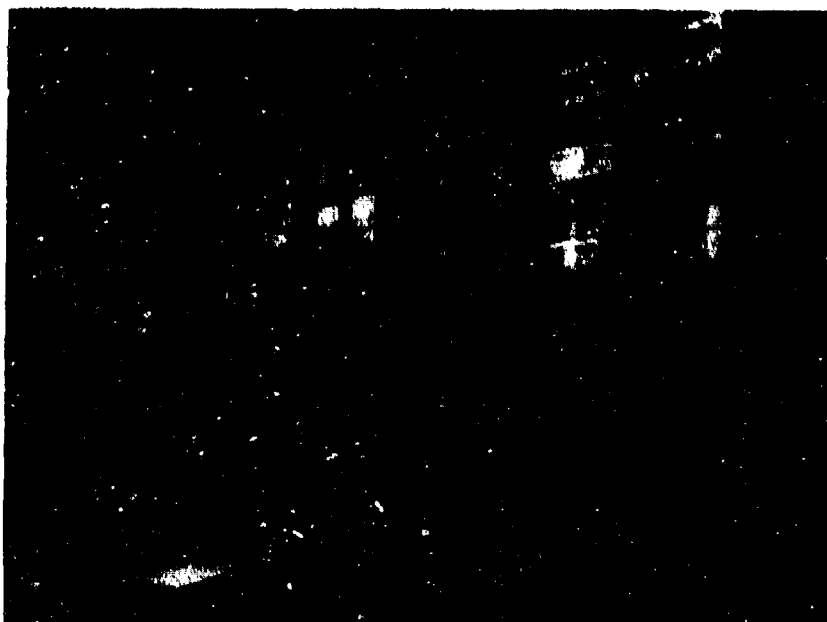
$r = 46 \text{ m}$
 $p = 0.55 \text{ bar}$
 $i = 6 \text{ bar} \cdot \text{msec}$



Building Nr. 72

$r = 72 \text{ m}$
 $p = 0.27 \text{ bar}$
 $i = 4 \text{ bar} \cdot \text{msec}$

DAMAGE CATEGORY C



Building Nr. 19

$r = 78 \text{ m}$

$p = 0.23 \text{ bar}$

$i = 3.7 \text{ bar} \cdot \text{msec}$



Building "Scheune"

$r = 105 \text{ m}$

$p = 0.15 \text{ bar}$

$i = 2.8 \text{ bar} \cdot \text{msec}$

DAMAGE CATEGORY D



Building Nr. 29

$r = 98 \quad m$

$p = 0.17 \text{ bar}$

$i = 3.0 \text{ bar} \cdot \text{msec}$



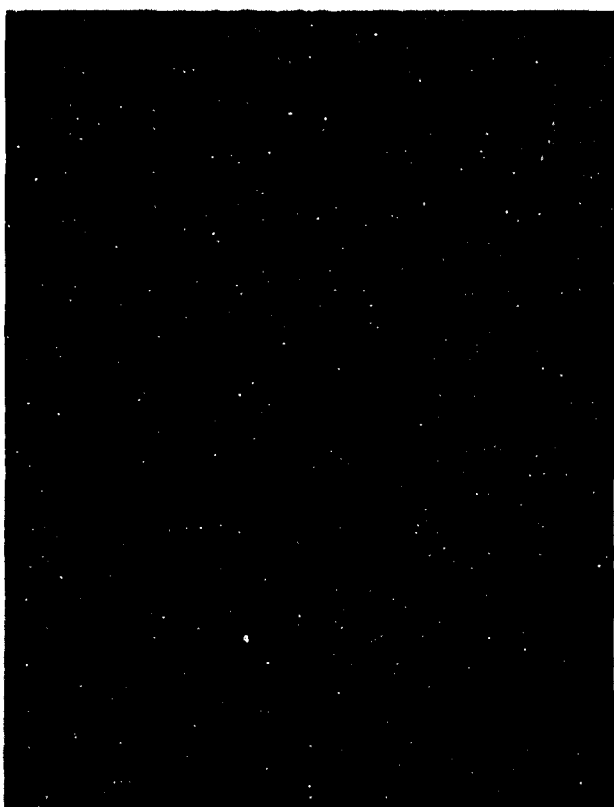
Building Nr. 67

$r = 183 \quad m$

$p = 0.075 \text{ bar}$

$i = 1.6 \text{ bar} \cdot \text{msec}$

DAMAGE CATEGORY E



Building WC

$r = 62 \text{ m}$

$p = 0.32 \text{ bar}$

$i = 4.7 \text{ bar} \cdot \text{msec}$



Building Nr. 53

$r = 215 \text{ m}$

$p = 0.06 \text{ bar}$

$i = 1.45 \text{ bar} \cdot \text{msec}$

CHECKLIST TO RECORD BUILDING DAMAGES

Place of Explosion:

Date of Explosion:

Estimated Charge Weight:

Building Nr.:

Photo of
Damaged Building

Location with
respect to Explosion

Description of Type and Construction of Building:

Description of Observed Damage:

Description of Injuries to Persons present during the Explosion inside and around the Building:

Description of Operation Performed during the Explosion:



AD P000459

MODELING DEBRIS EFFECTS PRODUCED BY A HIGH YIELD EXPLOSION

A. Longinow* T. E. Waterman** H. S. Napadensky**

INTRODUCTION

Among the objectives of the study (Ref. 1) on which this paper is based were determination of the combustible/noncombustible makeup and the distribution of debris piles that would be produced in an urban area subjected to a nuclear weapon attack. This paper describes the method used in meeting these objectives and illustrates its application by means of an example problem.

THE DEBRIS PROBLEM

Debris, as defined here, is material translated by the blast from a nuclear explosion. The sources of debris are varied and depend on the local area. Most debris comes from objects broken apart by the blast, such as buildings, garages, fences, utility poles, trees, shrubs, cars, etc.; also, whole objects such as gravel, picked up and transported by the blast wind. Such material can cause casualties and damage to facilities as a result of high energy impact and/or accumulation. Debris accumulations in streets can impede or prevent rescue operations and can also be a source of fuel for the spread of fires.

Knowledge of debris hazards is important to the civil defender who must identify areas where shelters can be sited and develop rescue plans, firefighting activities and debris clearance operations. This knowledge is important for the planner of critical facilities to design and site his structures sufficiently far away from potential debris sources.

Debris profiles in the direct vicinity of any given building will depend on certain characteristics of the neighborhood, i.e., types of neighboring buildings, their strengths, relative positions, separation distances, sizes, and contents. Direction, distance and intensity of blast also must be known.

* Department of Civil Engineering, Illinois Institute of Technology, Chicago, IL 60616 (Formerly Department of Civil Engineering, Valparaiso University, Valparaiso IN 46383)

** IIT Research Institute, Chicago IL 60616
IIT RESEARCH INSTITUTE

A building which does not fail while other buildings in its vicinity fail catastrophically may serve as an accumulator for some portion of upstream debris. The debris will pile up on its windward side and possibly inside the building itself. Should this building contain a basement shelter with an air intake located at ground level on the windward side, debris accumulation could block the vent. Also, depending on the composition and state (burning, smoldering) of this debris, the shelter may fill with toxic gases and smoke, and the shelter building may be ignited.

The local composition of a debris pile depends on a number of different parameters. Among these are the flight characteristics of individual items of debris and the extent to which they interact with each other while in transit. At a given accumulator, the debris from an upwind building may be segregated; with light, combustible debris at the bottom and heavy combustibles intermixed with noncombustible debris at the top of the pile. One can also postulate a situation in which the debris from the breakup and contents of a building are essentially segregated in terms of combustibles and noncombustibles.

Parameters that need to be considered in a local debris distribution analysis of a single building or group of buildings can be categorized as:

- 1) Building and neighborhood geometry (building heights, plan areas, separation distances, etc.)
- 2) Loading on building components and contents.
- 3) Failure characteristics of building and components (failure modes, failure loading, time to failure)
- 4) Physical characteristics of debris (size, shape, weight)
- 5) Aerodynamic characteristics of debris (drag and lift coefficients)

PREVIOUS WORK

"Debris production and distribution" has received a fair amount of attention among the agencies concerned with different aspects of this subject area. Experimental (field) studies conducted over the past two decades have dealt with the fracturing and destruction of individual buildings of brick, concrete masonry and wood framed construction, free standing masonry walls with and without mortared joints, trees, cars, special structures and equipment, etc. (Ref. 2 through 9). No field test work has been done on groups of buildings representing urban or suburban blocks or neighborhoods.

Concurrent with field studies, debris-related work was conducted in the laboratory using various shock tubes. The URS shock tunnel has been used extensively in the civil defense area to study the fracture strength of conventional masonry walls having various perimeter conditions.

Concurrent analytic studies in the civil defense sector have dealt with the gross distribution of debris, taking into account large urban areas and numerous building types (Ref. 10, 11), debris clearance studies (Ref. 12,13), debris formation and translation (Ref. 14, 15; 16). Comparatively little work has been directed at the combustible/noncombustible distribution within debris piles.

PREDICTING THE DISTRIBUTION OF BLAST-INITIATED DEBRIS

Loading and Response Analysis - The analytic process for determining the "incipient collapse" of a building and the corresponding debris characteristics is illustrated in Figure 1. It is described as follows:

Given a nuclear weapon attack condition, the first step is to determine the free field airblast environment at the location of the building. In this step the ideal airblast wave is modified by considering the influence of local terrain features such as neighboring buildings or other obstructions. Pressure-time histories acting on the external portions (walls, doors, roof, etc.) of the building are determined by further modifying the local blast environment as influenced by the building geometry.

Buildings contain numerous openings (doors, windows); therefore, the building will be subjected both to external pressures and internal fill pressures as the blast wave progresses through and engulfs the building. A method for determining average fill pressures and flow velocities in rooms having simple geometries is given in Ref. 14.

Having determined the time dependent net loading on the building and on its individual components, the next step involves a structural response analysis.

Buildings consist of closed networks of beam, column, and plate elements. Analysis of the structural, dynamic response of such a network as a continuous structure is currently a practical possibility only for sufficiently simple geometries and loading; then only if elastic response is sought. For this reason, and in order to produce usable results in the shortest time, the building analysis process is generally a step by step procedure which considers only

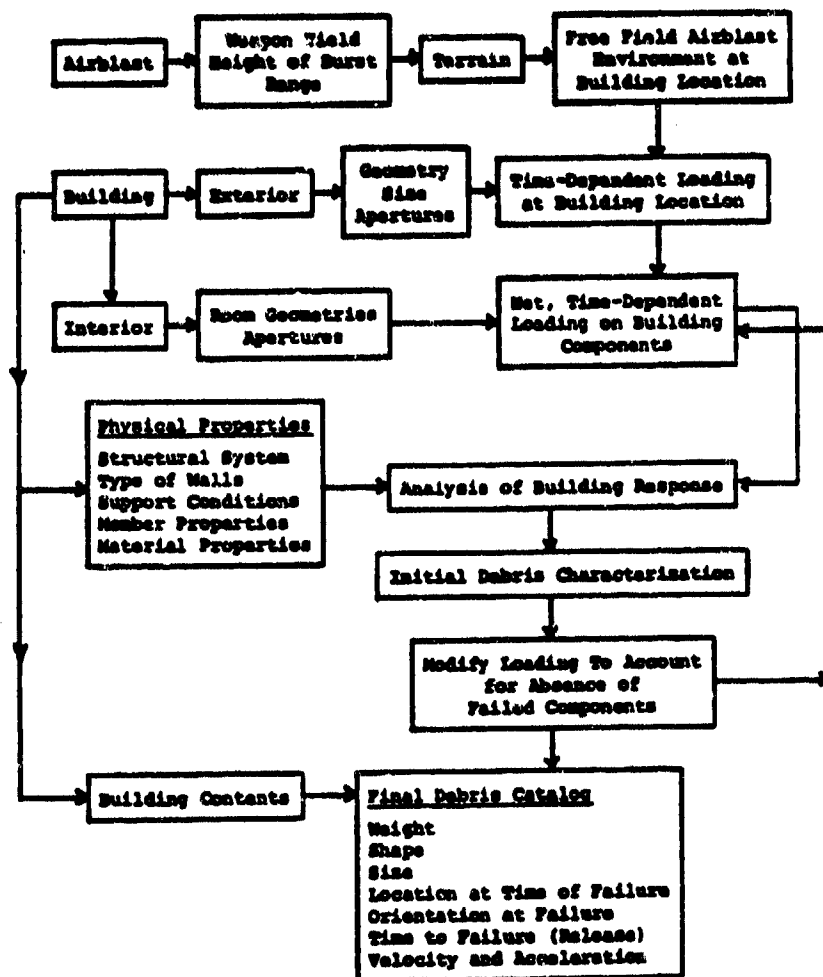
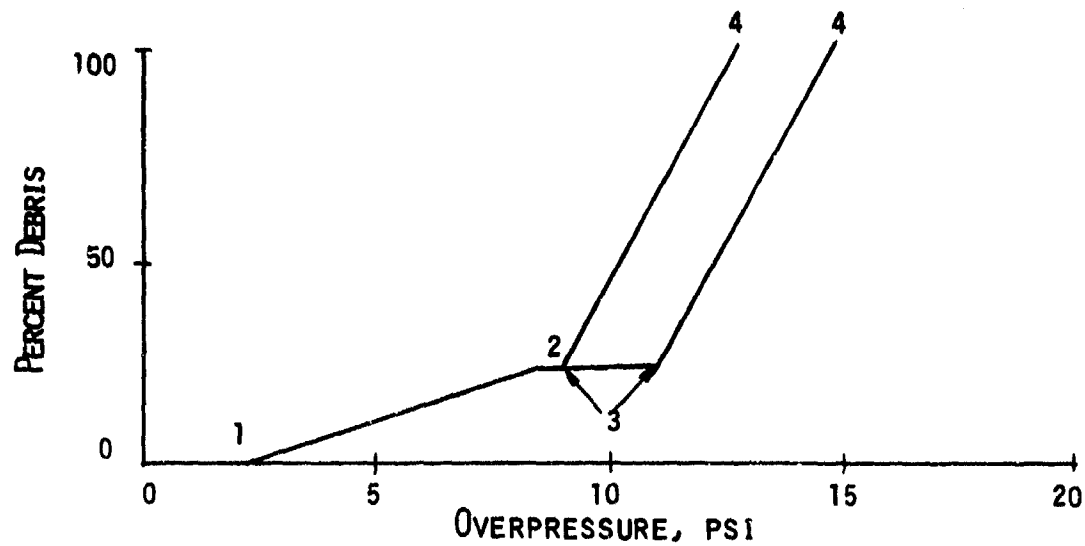


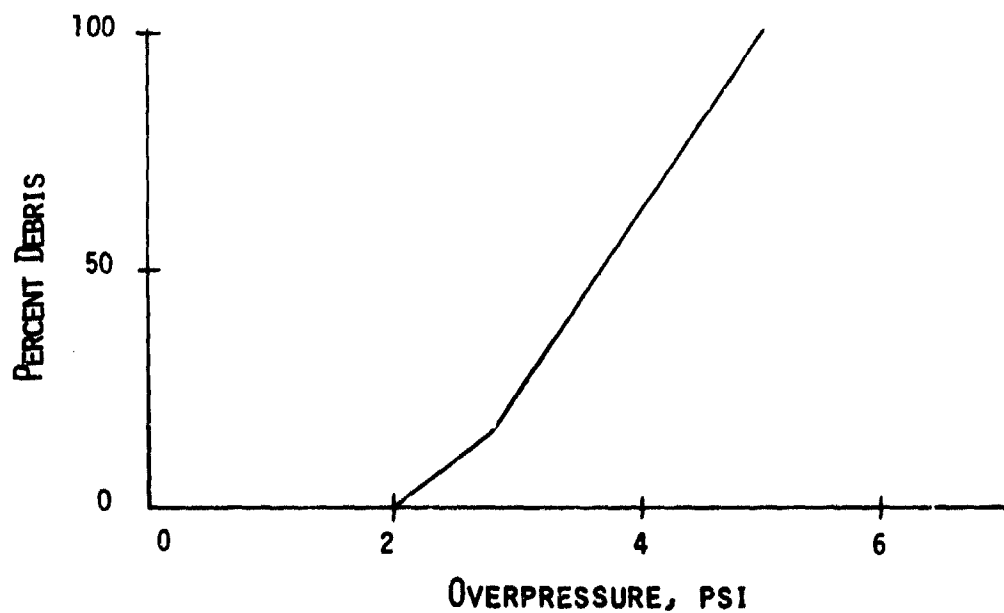
Figure 1 Loading and Response Analysis

the dominant modes of response and relies heavily on experimental data. In this approximate approach, the building is decomposed into its principal and subsidiary components. Subsidiary components are those which do not affect the response of the building as a whole to any significant degree, but which are still debris-producing. These are handled separately. The principal components are loaded using the net, time-dependent loading determined as described previously. Support conditions are approximated to correspond to those of the actual, combined structure. The response analysis proceeds on a component by component, time step by time step basis. Since the loading acting on each component in this chain depends on the net loading and response of adjoining components, the analysis is necessarily an iterative procedure as indicated in Figure 1. The end result consists of a debris catalog containing the size, weight, original location, etc. of each debris piece to be used in the transport-trajectory analysis.

Relationship of Debris to Building Damage - Unless a building is completely destroyed, only the parts of the structure that fail under blast loading (plus the contents of the failed part of the structure) become debris. Except for wood-frame and load-bearing masonry buildings, many buildings have relatively light walls and partitions that will fail at a much lower overpressure than the frame itself. Figure 2a is a typical "debris chart" (Ref. 11). Points 1 and 2 are the initiation and completion, respectively, of failure of frangible (diffraction phase sensitive) elements such as panels, doors, suspended ceilings, etc. The location of these points is relatively independent of weapon yield. The plateau from point 2 to point 3 is caused by the difference in overpressure between the final failure of the frangible parts of the building, and the start of failure of the drag-sensitive (ductile) portions of the building. The location of points 3 and 4 is determined by the failure characteristics of the main structural system, point 3 representing the overpressure at which elements of the main structural system would begin to fail, and point 4 representing the overpressure for complete destruction. The location of points 3 and 4 is weapon yield sensitive. Figure 2a shows the pattern for a multistory frame building for both 1-MT and 25-MT weapons. The height of the plateau is determined by the portion of the total building represented by the frangible parts and the contents of the above-ground floors.



a) MULTISTORY STEEL OR REINFORCED CONCRETE FRAMED BUILDING WITH LIGHT EXTERIOR WALLS



b) WOOD-FRAME BUILDING

Fig. 2 Debris Chart

Wood-frame and masonry buildings have very little ductility and points 2 and 3 practically coincide, eliminating the plateau effect. Figure 2b is a debris estimate for wood-framed residential buildings. Debris begins to form at about 2 psi and the building is completely collapsed at 5 psi. Load-bearing masonry structures may fail at somewhat higher overpressures but the debris chart looks very much like that shown in Figure 2b.

Debris Trajectory Analysis - Data Requirements

The input data and information required for the trajectory analysis are described in Figure 3. These include a physical description of the debris, such as its size, weight and geometry, and any other pertinent characteristics which can be determined such as moment of inertia. Secondly, the initial free-flight characteristics of the debris must be established. These include the time of release of the piece of debris into the blast environment, its location at the time of release, and initial motion data. These categories of input data are generated in part from the specific response analysis discussed in the preceding section, or estimated from experimental data.

The trajectory calculation also requires aerodynamic data on the class of debris shapes encountered. These data include drag and lift coefficients, each as a function of orientation angle (angle of attack). The data must include all orientations since most pieces of debris will be expected to tumble and rotate as they are transported through the air.

The blast wind is the primary driving force in the transport problem (which also includes gravitational effects) and a satisfactory treatment of this variable has already been developed (Ref. 17) and is used here.

Any piece of debris which impacts with the ground plane during the early portion of the blast environment may bounce, i.e., not be captured, and even if much momentum is lost as a result of the impact the aerodynamic forces will generally be sufficiently large to loft the piece of debris and cause it to be transported some additional distance. Once lofted, the piece of debris will acquire additional momentum and again represent a hazard.

Debris Trajectory Analysis - Transport Model - A simple rectangular block free to translate and rotate in two dimensions is used to represent a piece of debris. It is defined by four corner points. Symbols representing its dimensions are

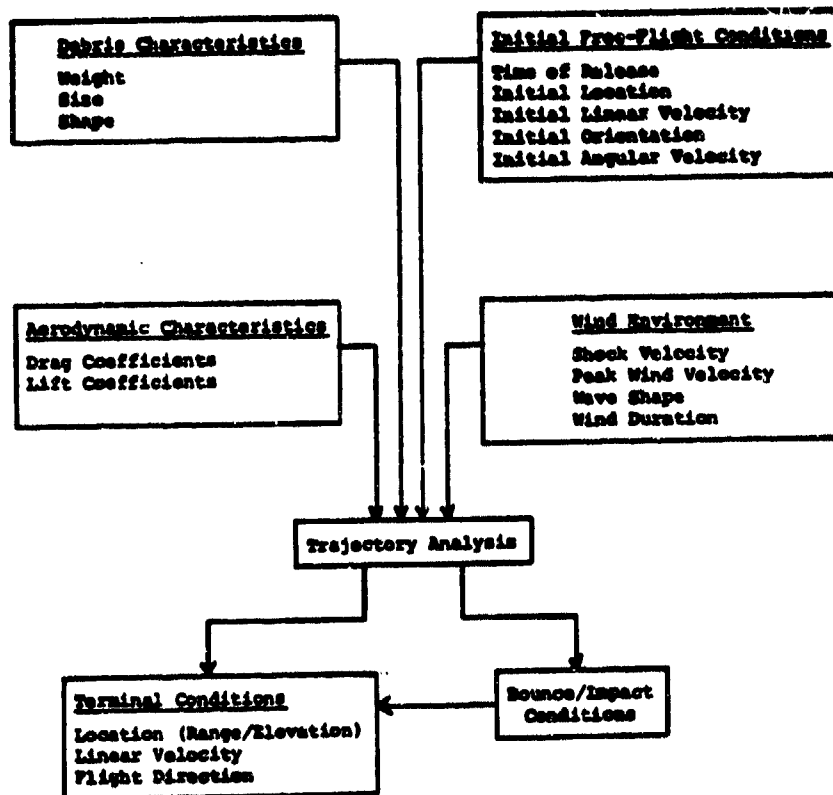


Figure 3 Debris Transport/Trajectory Analysis

shown in Figure 4a, and include D1, the vertical distance from corner point 1 to the center of gravity; D2, the vertical distance from corner point 2 to the center of gravity; H, the total height; S1, the horizontal distance from corner point 1 to the center of gravity; and S2, the horizontal distance from corner point 2 to the center of gravity. Additional parameters needed to describe a piece of debris include its width (normal to the plane of the paper), weight and mass moment of inertia. The model, therefore, requires that an irregular piece of debris must be idealized by means of a rectangular solid.

Blast loading consists of diffraction, drag and lift forces. Time dependent diffraction loading is applied as shown in Figure 4b and consists of forces acting at the center of each of the four planes. These forces are computed as follows:

$$\begin{aligned} P_{12} &= 1/2(P_1 + P_2) (S_1 + S_2) W \\ P_{23} &= 1/2(P_2 + P_3) H \cdot W \\ P_{34} &= 1/2(P_3 + P_4) (S_1 + S_2) W \\ P_{41} &= 1/2(P_4 + P_1) H \cdot W \end{aligned} \quad (1)$$

Where P_i ($i = 1, 4$) are pressures in the blast wave acting at the corner points and W is the width normal to the plane of the paper. The net effect of this loading vanishes once the shock clears around the block.

Drag and lift forces are applied as shown in Figure 4c and are defined as follows:

$$\text{Drag force: } D = q(t) A_d(\theta) \quad (2)$$

$$\text{Lift force: } L = q(t) A_l(\theta) \quad (3)$$

where $q(t)$ is the dynamic pressure of the flow and A_d and A_l are position depending drag and lift areas which are expressed as follows:

$$A_d = A_{dmin} + (A_{dmax} - A_{dmin}) \sin^2 \left(\theta - \frac{\pi}{2} \right) \quad (4)$$

$$A_l = A_{lmax} \sin(2\theta - \pi) \quad (5)$$

A_{dmin} , A_{dmax} and A_{lmax} are respectively the minimum drag area, the maximum drag area and the maximum lift area of the rigid block. They are obtained by multiplying the actual areas by appropriate drag and lift coefficients (Ref. 18).

As shown in Figure 4c, the drag force is assumed to act at the center of the projected horizontal area. Its eccentricity (Δ) is

IIT RESEARCH INSTITUTE

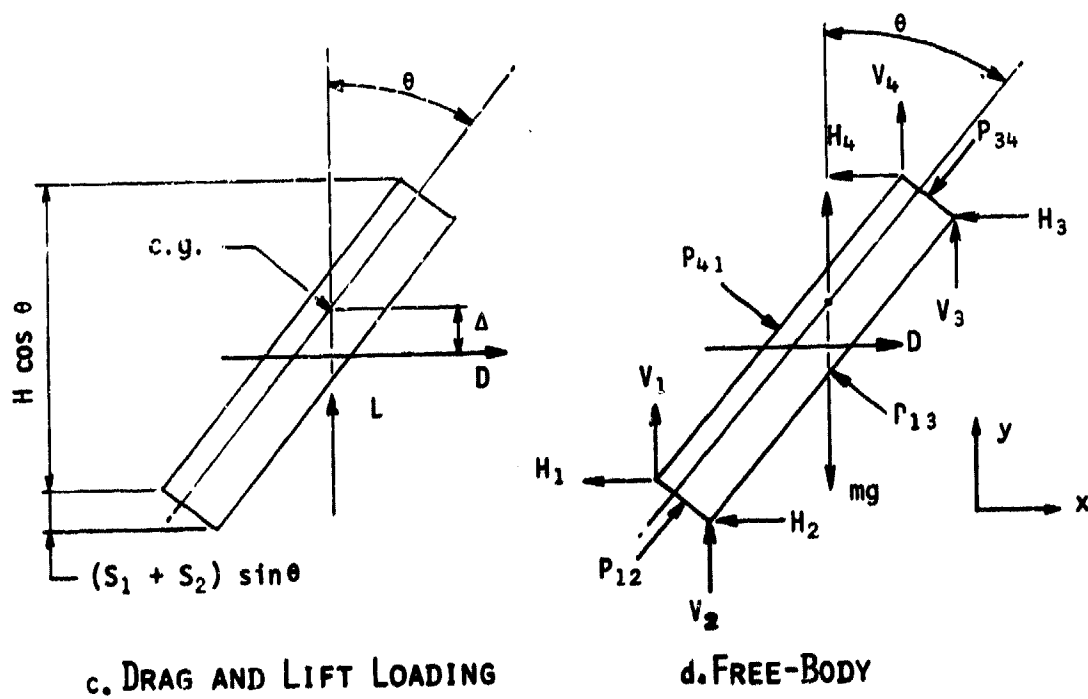
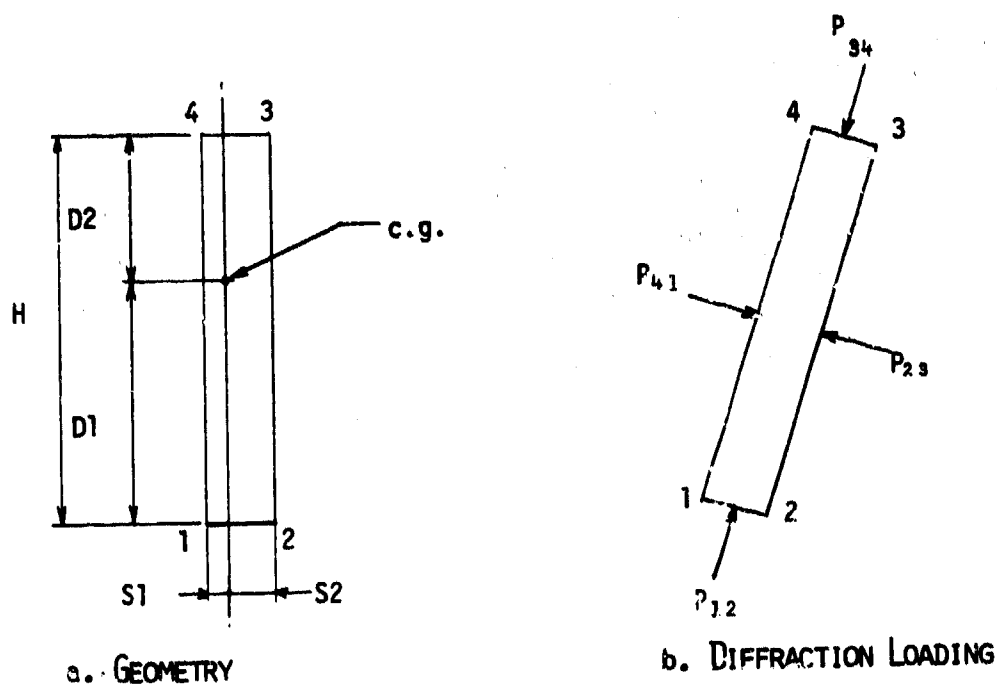


Fig. 4 Debris Translation Model

$$\Delta = \left(\frac{H}{2} - D_1\right)\cos\theta + \frac{1}{2}(S_1 + S_2)\sin\theta \quad (6)$$

The lift force is assumed to act at the center of gravity (c.g.) and, therefore, has no associated eccentricity.

The final set of forces which may act on the piece of debris are contact forces which occur on impact with either a horizontal or a vertical surface. These contact forces are broken down onto the horizontal (H), and vertical (V) components acting at the four corner points of the block (see Figure 4d).

The following forces apply (where the subscript i refers to the specific point in contact: i = 1,2,3 or 4).

For contact with floor:

$$\begin{aligned} V_i &= -KL y_i & y_i < 0 & \text{ and } \dot{y}_i < 0 \\ &= -Ku y_i & y_i < 0 & \text{ and } \dot{y}_i \geq 0 \\ &= 0 & y_i > 0 & \\ H_i &= \mu V_i (|\dot{x}_i| / \dot{x}_i) \end{aligned} \quad (7)$$

For contact with wall:

$$\begin{aligned} H_i &= KL(x_i - x_w) & x_i > x_w & \text{ and } \dot{x}_i > 0 \\ &= Ku(x_i - x_w) & x_i > x_w & \text{ and } \dot{x}_i \leq 0 \\ &= 0 & x_i < x_w & \\ V_i &= \mu H_i (|\dot{y}_i| / \dot{y}_i) \end{aligned} \quad (8)$$

where

- x_w - coordinate of the wall
- KL - spring constant for loading
- Ku - spring constant for unloading
- μ - coefficient of friction

The governing equations for computing the trajectory of the block are given as follows:

$$M\ddot{X} = D - H_1 - H_2 - H_3 - H_4 + P_{12}\sin\theta - P_{23}\cos\theta - P_{34}\sin\theta + P_{41}\cos\theta \quad (9)$$

$$M\ddot{Y} = L + V_1 + V_2 + V_3 + V_4 + P_{12}\cos\theta + P_{23}\sin\theta - P_{34}\cos\theta - P_{41}\sin\theta - Mg \quad (10)$$

$$\begin{aligned}
I\ddot{\theta} = & D\Delta + H_1(D_1\cos\theta - S_1\sin\theta) + H_2(D_1\cos\theta + S_2\sin\theta) \\
& - H_3(D_2\cos\theta - S_2\sin\theta) - H_4(D_2\cos\theta + S_1\sin\theta) \\
& + V_1(D_1\sin\theta + S_1\cos\theta) + V_2(D_1\sin\theta - S_2\cos\theta) \\
& - V_3(D_2\sin\theta + S_2\cos\theta) - V_4(D_2\sin\theta - S_1\cos\theta) \quad (11) \\
& - P_{12}((S_2 - S_1)/2) - P_{23}(H/2 - D_1) \\
& + P_{34}((S_2 - S_1)/2) + P_{41}(H/2 - D_1)
\end{aligned}$$

In equations (9), (10) and (11):

M = the mass of debris piece

I = the mass moment of inertia

The other parameters are as shown in Figure 4 and defined previously.

ILLUSTRATION OF DEBRIS DISTRIBUTION ANALYSIS

The building used in the analysis is shown in Figure 5 (Ref. 14, 21). This is a small, two-story office building whose basic building module has plan dimensions of 13-ft by 23-ft. The building consists of eight basic modules. The structural system is a reinforced concrete frame. Roof and intermediate floor consist of one-way reinforced concrete slabs. In the long direction the building is enclosed by unreinforced concrete masonry walls and window walls arranged in a staggered pattern. Exterior walls in the short direction consist of masonry without windows. Each module of the building is assumed to contain furnishings which include a sofa, a table, two arm chairs, four small chairs and a desk. The sizes and arrangement of these items in the room is described in Ref. 14 and 21.

The building is assumed to be located at the 5 psi range of a 1-MT near-surface burst. Its front wall (see Figure 5a) is oriented at right angles to the direction of the blast wave. At this range the longitudinal masonry walls, which have an incipient collapse overpressure of 0.5 psi, will fail catastrophically as will the transverse studwalls. The structural frame, including floor and roof slabs and the transverse masonry walls, are expected to remain in place. Debris will consist of broken, longitudinal masonry walls, transverse studwalls and furniture. Window glass will become debris; however, its transport is not considered in this analysis.

Before a debris transport analysis can be performed, it is first necessary to determine the number and size of primary pieces of debris that will be

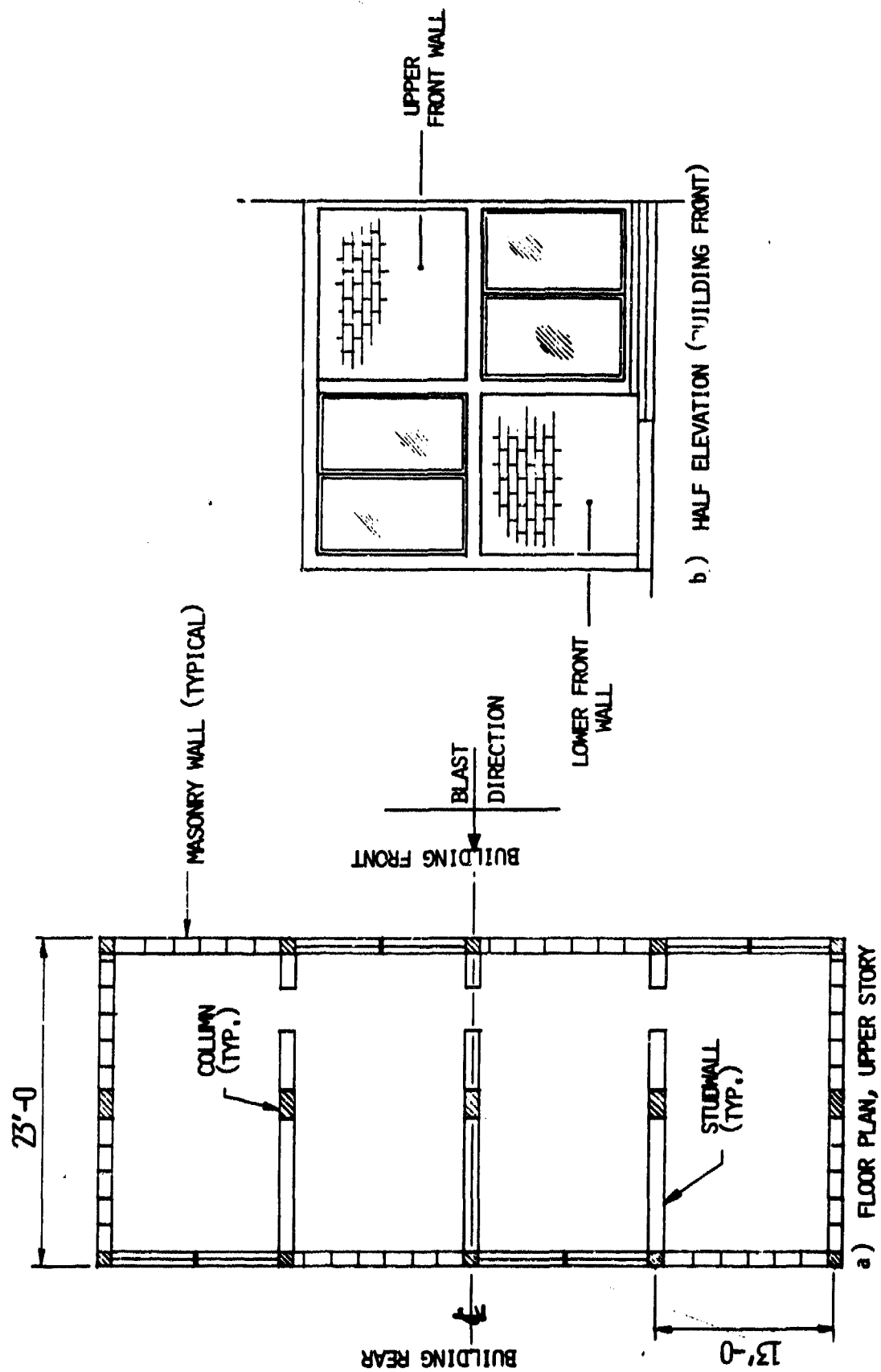


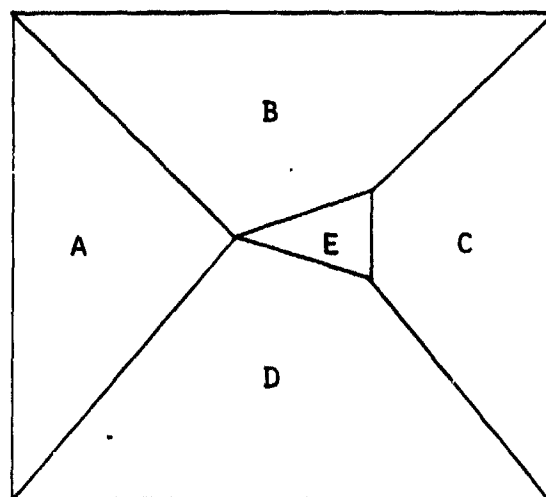
FIGURE 5 BUILDING USED IN ILLUSTRATION

produced when a given wall interacts with the blast wave, and the number and size of secondary pieces that will result when a primary piece impacts the floor. This was determined using experimental data.

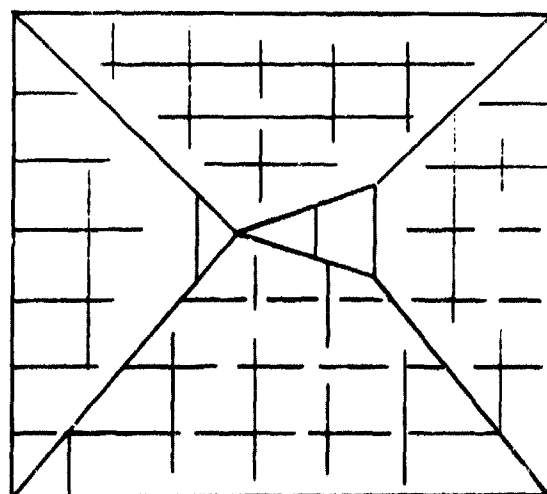
The initial crack pattern chosen for the longitudinal masonry walls is shown in Figure 6a and corresponds to experimental results (Ref. 19) for a simply-supported masonry wall having the same dimensions. This figure shows the primary pieces produced when the wall interacts with the blast wave. An assumed secondary debris pattern is shown in Figure 6b. Each primary piece is assumed to break up in pieces having four different sizes, i.e., one-, two-, three- and four-block sizes. These sizes correspond approximately to those obtained in the URS shock tunnel for similar walls.

A debris catalog was prepared in which each piece of debris was described, in terms of the data required by the transport model (See Figure 4), x, y, z coordinates of its center of gravity relative to one corner of the building, and time of separation. Initial velocity was set equal to zero. Time was taken to be zero when the blast wave was coincident with the plane of the front of the building, and, therefore, the time of separation for the front wall was also zero. The actual time to failure was estimated to be 0.04 sec. This was considered to be small in comparison to the positive phase duration of the blast and was, therefore, neglected. For the other items, furniture and the back wall, the time to separation was computed using the shock velocity and the distance from the front wall to the center of gravity of the given items.

The first part of the analysis dealt with the primary wall pieces (Figure 6a); their motion was traced until each piece touched the floor or the ground plane. At that point it was assumed to break up into the preassigned number of secondary pieces (Figure 6b). The initial conditions of forward distance, velocity, acceleration and time, were those for the center of gravity of the primary debris piece, the other two coordinates were pre-assigned. The transport of each secondary piece was continued until its velocity became smaller than a pre-assigned value. The final positions of wall debris produced by one half of the building (the four modules shown in Figure 5b) are shown in Figure 7. Only masonry wall debris is included. Furniture items and studwall debris traveled significantly greater distances. The debris from the four walls are identified in Figure 7. Two of the walls are similarly identified in Figure 5b.



a) PRIMARY FAILURE PATTERN



b) SECONDARY FAILURE PATTERN

FIGURE 6 MASONRY WALL FAILURE PATTERNS

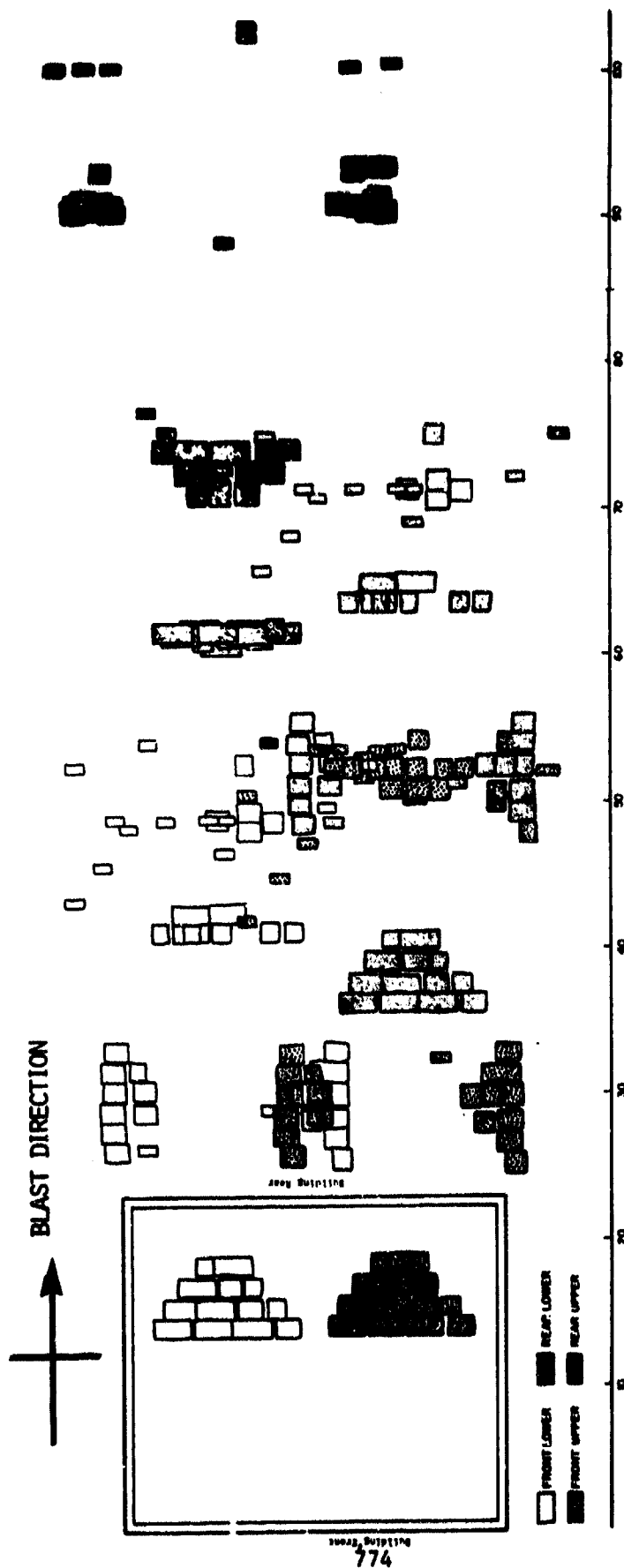


FIGURE 7 FINAL DISTRIBUTION OF MASONRY WALL DEBRIS

The debris from segments D (Figure 6a) of the two front walls travel an average of about 18 feet and remain within the building. The longest distance (about 100 feet) is traversed by the smaller pieces (one block in size) from the upper rear wall.

Calculations indicate that it takes approximately 0.04 sec for the wall to reach incipient failure, i.e., to form the crack pattern shown in Figure 6a. An average of 0.50 sec is then required for the individual (large) pieces to impact with the ground plane. Approximately 3 seconds would elapse from the time of wall failure to the time all of the pieces shown in Figure 7 come to rest.

Velocity histories of furniture items are shown in Figure 8. These curves contain numerous jumps indicating impacts with the ground plane. These items were assumed not to break up while in motion. Furniture debris were transported significantly faster and further than masonry wall debris. The longest transported distance was 330 feet for the table, and the shortest was 164.5 feet for the chair. The presence of an accumulator (stronger structure) in the path of the debris would create a pile with a high concentration of furniture near the ground against the accumulator, covered by a layer composed primarily of masonry. The order of arrival of debris pieces at any given accumulator location can be extracted from calculated position-time data for each debris piece.

CLOSURE

The method described provides a basis for determining 1) the makeup of debris piles from various debris sources, 2) the hazard to a facility due to debris impact and/or debris accumulation.

2. The task of accounting for each piece of debris as was done here is tractable when the source is relatively small and isolated. However, when dealing with a group of different buildings, the task of cataloging of debris piece by piece is impractical; and, unless gross simplifications are made, in all likelihood impossible. It is much more reasonable to consider groups of debris with average properties. Statistical distributions of debris within these groups can also be considered.

3. The building debris became segregated, e.i., the heavy noncombustibles remained relatively close to the building while the lighter, mostly combustible debris were transported significantly further.

Note: Numbers given below refer to horizontal distances traveled by the various items.

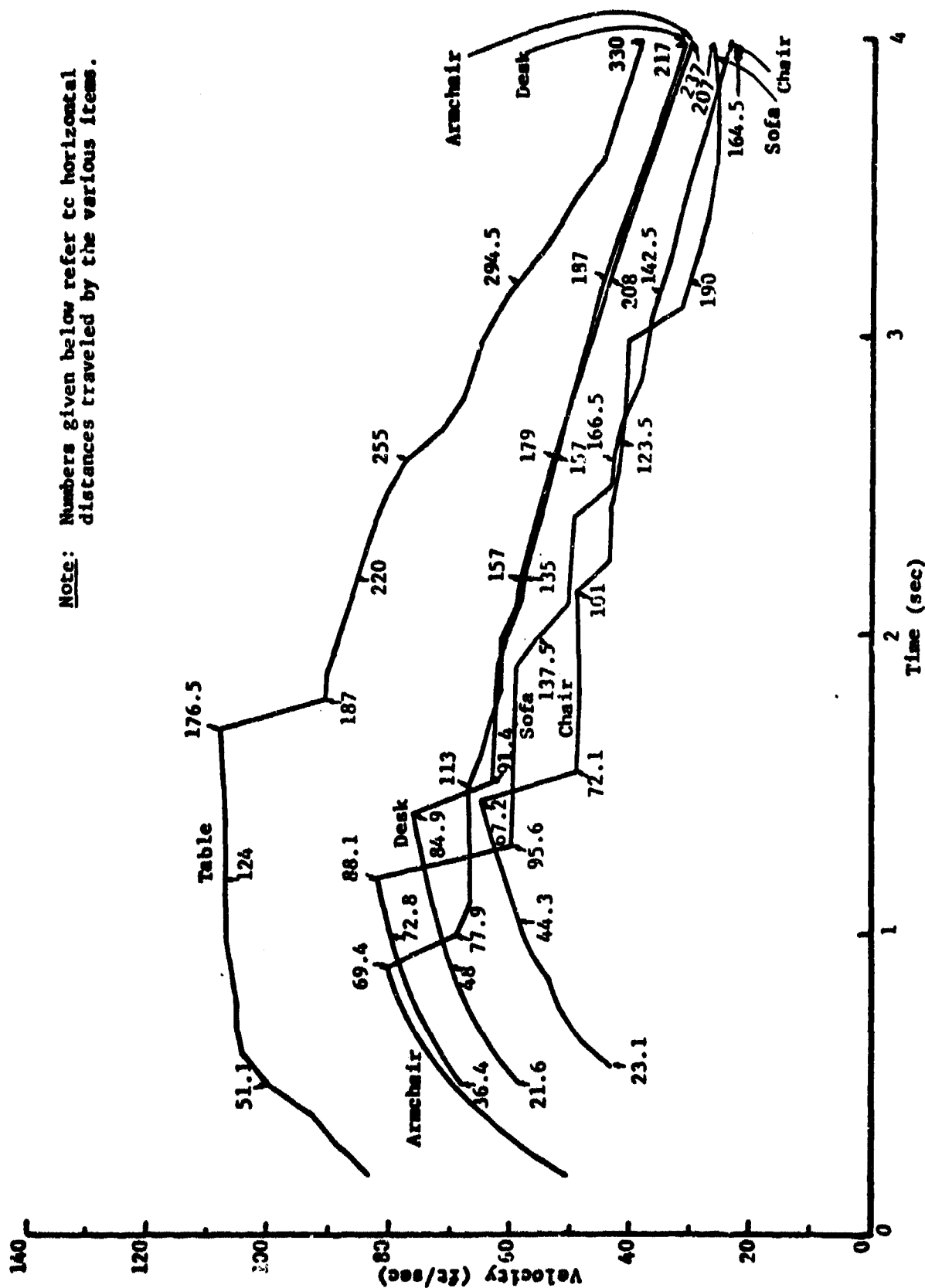


FIGURE 8 VELOCITY HISTORIES OF FURNITURE ITEMS (SECOND FLOOR)

4. Debris transport is sensitive to the peak overpressure of the blast wave at the affected location. Transport distances tend to increase at a rate greater than a linear function of peak overpressure.
5. Debris transport is sensitive to the weapon yield when the debris are sufficiently light and peak overpressures sufficiently high to keep the debris piece in the air long enough to be affected by the longer overpressure durations of the high yield weapons.
6. Most debris produced by a high yield weapon would spread apart as carried along by the blast wave. This would result in a deposition of debris in a fan shape originating at the source. The fan angle would be approximately 30 degrees (Ref. 20).

The two-dimensional (vertical plane) model used here does not allow for such dispersion. In this study an angle smaller than 30 degrees was chosen and the final debris positions were adjusted accordingly (see Figure 7).

7. Closely spaced debris sources may result in a lesser area covered by debris than that predicted assuming each source is isolated. This is due to shielding, accumulation, and interaction of debris with debris.
8. For larger weapon yields the distribution of debris at a given overpressure will increase because of longer pulse duration.

ACKNOWLEDGMENT

The authors wish to recognize the support of the Federal Emergency Management Agency, and in particular, the contributions of the Contract Officer's Technical Representatives, Messrs D. Benson, D. Bettge, and G. Sisson, to the programs which served as a basis for this paper.

REFERENCES

1. Longinow, A., Waterman, T. E., Takata, A. N., "Assessment of Combined Effects of Blast and Fire On Personnel Survivability", for Federal Emergency Management Agency, FEMA Contract DCPA01-79-C-0265, IIT Research Institute, Chicago, IL, June 1982
2. Witt, E. F., "Building Fragmentation Project 1.08," Operation DISTANT PLAIN Preliminary Report (U), Volume I, DASA1876-1, December 1966, pp 175-101.
3. DeCapua, N. J. and Witt, E. F., "Debris Studies Projects 1.05, 1.07, and 1.08", Operation DISTANT PLAIN Symposium (U), Volume I, DASA1947-1, September 1967, pp 264-283.
4. Witt, E. F., "Fragmentation of Buildings Project LN108", Operation PRAIRIE FLAT Preliminary Report, Volume I, DASA2228-1, January 1969, pp 147-176.
5. Warren, R. E., "Project LN108 Tree and Automobile Debris," Event DIAL PACK Preliminary Report, Volume I, Part I, DASA2606-1, May 1971, pp 153-184.
6. Morris, P.J. and Wilton, C., "Debris From Trees Subjected to Blast," URS Research Company, URS794-1, May 1970.
7. Sauer, F. M., Fons, W. L. and Storey, T. G., "Blast Damage to Coniferous Tree Stands by Atomic Explosions," Project 3.19 Operation UPSHOT-KNOTHOLE, WT-731, U. S. Forest Service, Division of Fire Research, January 1954.
8. Fons, W. L. and Storey, T. B., "Blast Effects on Tree Stand," Project 3.3 Operation CASTLE, WT-921, U. S. Department of Agriculture Forest Service, Division of Fire Research, March 1955.
9. Sauer, F. M., "Forest Blowdown - Comparison of the Results of High-Explosive Experiments and Predictions," DASA2300, SRI, July 1969.
10. Edmunds, J. E., Sears, P. M., "Debris Model Research and Five-City Study Application", for Office of Civil Defense, Contract 12471(6300A-310), OCD Work Unit 3312B, URS Research Company, Burlingame, California, June 1968.
11. Edmunds, J. E., "Debris Prediction Model" for Office of Civil Defense, Contract 12471(6300A-310), OCD Work Unit 3312B, URS Research Company, Burlingame, California, June 30, 1969.
12. Feinstein, D. I., "Debris Distribution", for Office of Civil Defense, Contract OCD-PS-64-50, Subtask 3322B, IIT Research Institute, Chicago, IL, August 1964.
13. Feinstein, D. I., "Debris Distribution", for Office of Civil Defense, Contract OCD-PS-64-50, Subtask 3322B, IIT Research Institute, Chicago, IL, March 1966.
14. Longinow, A., et al, "People Survivability In a Direct Effects Environment and Related Topics", for Defense Civil Preparedness Agency, Contract DAHC20-68-C-0126, Work Unit 1614D. IIT Research Institute, Chicago, IL, May, 1973.

15. Wiersma, S. J., Martin, S. B., "The Nuclear Fire Threat To Urban Areas", for Defense Civil Preparedness Agency, Contract DAHC20-70-C-0219, Stanford Research Institute, Menlo Park, California, April 1975.
16. Rempel, J. R., "Debris Distribution As A Parameter In Blast/Fire Interaction", for Federal Emergency Management Agency, Contract DCPA01-79-C-0269, Work Unit 2564C, SRI International, Menlo Park, CA, June 1980
17. Brode, H. L., "A Review of Nuclear Explosion Phenomena Pertinent To Protective Construction", The Rand Corporation, R-425-PR, May 1964
18. Hoerner, S. F., "Fluid Dynamic Drag", 1965 (published by the author).
19. Edmunds, J. E., "Experiments to Determine Debris Formation From Corrugated Steel And Brick Walls", for Office of Civil Defense, Contract DAHC20-69-C-0129, Work Unit 3313C, URS Research Company, URS 751-4, January 1970.
20. Warren, R. E., Witt, E. F., "SAFEGUARD Debris Studies, Information Presented at SAFSCOM meeting, Case 27950-2130
21. Waterman, T. E., "Fire Laboratory Tests - Phase III: Fires in Blast-Initiated Debris External To Shelters", for Defense Civil Preparedness Agency, Contract DAHC 20-70-C-0406, Work Unit 1135A, IIT Research Institute, Chicago, IL, February 1973.

AD P000460

Response of the Flash X-Ray
Building at Site 300 to
Explosions on its Firing Table

C. F. Baker, C. Y. King,
J. W. Lyle, R. K. Mullins,
D. S. Ravenscroft, and W. M. Shay

LAWRENCE LIVERMORE LABORATORY
University of California • Livermore, California • 94550

Response of the Flash X-Ray Building at Site 300 to Explosions on its Firing Table

ABSTRACT

The response of the new high-explosive Flash X-ray Radiography Facility at Bunker 801 at LLNL Site 300 to explosions on its firing table has been measured. Seven charges of the high explosive C-4, with increasing weights of from 18 to 585 lb, were detonated. Charges were placed on a pea-gravel firing table on the radiographic axis 10 ft from the face of the steel bullnose protection plate. No noteworthy damage to the new building or its installed equipment occurred during these tests.

Strains on 46 strain gauges were recorded during the explosive tests. During construction of the facility, these gauges had been welded to the steel reinforcing bars in various locations, or suspended between them, and were then embedded in the structural concrete. The gauges recorded strains as high as 220 $\mu\text{in./in.}$, which is equivalent to a stress of 5600 psi in steel. All elements of the structure remained well below their elastic limits, and should remain within these limits when subjected to detonations of up to 1000 lb of TNT on the firing table.

The measured strains were less than those given by simple engineering calculations by factors of from 1.7 to 3.9. Several safety factors and conservative simplifying assumptions were included in the strain calculations, and this may account for the large differences.

Work is underway with more elaborate structural-analysis models that use the laboratory's large digital computers. Future experiments and computer modeling should yield better agreement between theory and experiment.

INTRODUCTION

The design of LLNL buildings to withstand blast follows a fairly rigid procedure. Early in the process a firm of architects and engineers (A&E) is hired, meetings with laboratory staff are held to define requirements, and the A&E contractor designs the buildings according to our criteria. The contractor sometimes hires consultants to assist in the design of special facilities; this was done in the design of the recently completed high-explosive Flash X-ray Radiography Facility (FXR).

The design goal was to produce a structure capable of withstanding repeated detonations of 1000 lb of TNT on a gravel firing table 10 ft in front of the bullnose.

The Laboratory has conducted explosive tests near structures for about 30 years. It was realized early in the construction of FXR that our knowledge about structural response to blast could be improved if instrumentation were installed in the roofs and walls of FXR before the concrete was poured. The strength of FXR could be demonstrated and compared with design calculations, and explosive tests of different weights, geometries, and locations could provide useful data for the design of new structures.

Accordingly, 61 strain gauges were installed on and between the reinforcing bars and embedded in the concrete, and 8 accelerometers were mounted

at various locations in the completed building. (Of the 61 strain gauges installed, 49 survived the construction process; we had enough channels to record results from 46 strain gauges.) The locations of the strain gauges are shown in Fig. 1 and in Figs. A-1 through A-5 in Appendix A. The locations of the accelerometers are shown in Fig. B-1 in Appendix B.

Seven high-explosive charges, weighing up to 585 lb, were detonated at the shot point shown in Fig. 1, and the response of the structure was recorded. The measured strains were lower than those predicted by rapid-analysis calculations by factors of from 1.7 to 3.9. Some reasons for the differences between experiment and theory are suggested in the section "Discussion of Results."

The only damage caused by these tests was the shattering of a plastic cover on an outside lighting fixture. The building and its installed equipment were unaffected.

The following sections describe the tests and the data analysis, compare the observations with the results of simple calculations, and give our conclusions. The appendices give technical data on the strain gauges and accelerometers, summarize the strain-gauge data, and show calculations we did to supplement those done by the design consultants. Microfiche records of the actual data, after smoothing by computer, are included.

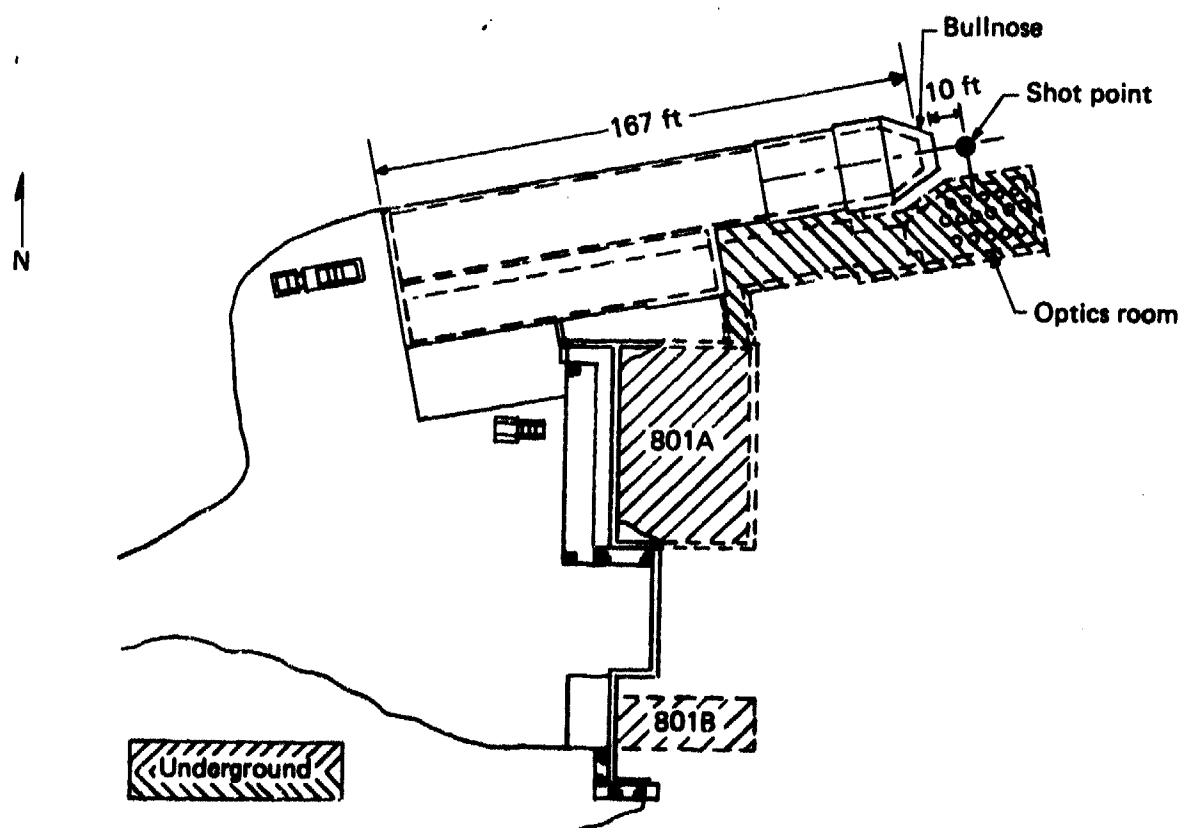


FIG. 1. The FXR addition to bunker 801A (plan view). Test explosives were placed on a gravel firing table at the shot point in front of the bullnose. The optics room is completely below the firing-table surface; it was covered with an 18-in. layer of gravel for all shots but one.

FLASH X-RAY FACILITY TESTING

HIGH-EXPLOSIVE CHARGES

C-4 explosive¹ was used for the testing because its heat of detonation is near that of the common PBX-9404 explosive and because its putty-like consistency makes assembly cheaper since machining is unnecessary. C-4 is 91% RDX mixed with 5.3% di (2-ethylhexyl)-sebacate, 2.1% polyisobutylene and 1.6% motor oil.

The heat of detonation of PBX-9404 is 1.38 kcal/g; the heat of detonation of TNT is 1.09 kcal/g. Reference 1 does not tabulate an experimental value of the heat of detonation for C-4; we assume its heat of detonation is equal to that of PBX-9404, because the *calculated* heats of detonation are nearly the same, 1.59 for C-4 and 1.56 for PBX-9404. The ratio of the experimental heats of detonation of PBX-9404 and TNT ranges from 1.25 to 1.27, depending on the observer (see Ref. 1). A rounded-up ratio of 1.3 was adopted for the purpose of calculating TNT equivalent weights, with C-4 assumed equivalent to PBX-9404.

Except for the 585-lb charge, the C-4 was packed into cardboard or sheet-metal cylinders with length-to-diameter ratios (L/D) of about 1. The 585-lb charge was built up on a wooden pallet, bag by bag, in an approximately right-circular cylinder of L/D = 1. To adjust the shot height, we placed the smaller charges by hand on plywood boxes; the larger charges, supplied on wooden pallets, were maneuvered into position with a fork-lift truck.

All charges were center-detonated. The charges were placed so their centers were on the axis of the linear-induction accelerator (LIA) and 10 ft from the exterior surface of the A-36 steel bullnose cover plate. The space in front of the bullnose adjacent to the optics room was filled with pea gravel about 15 ft deep, forming a firing-table surface about 2 ft below the LIA axis. The top few feet of pea gravel in the blast area was replaced after each shot. The firing table is shown in Fig. 2.

In shot 413, the pea-gravel surface was only about 6 in. below the LIA axis, so a hole about 18 in. deep and 6 ft in diameter was dug to bring the center of the explosive to the LIA centerline. This seemed merely an expedient at the time; we did not recognize that we had barricaded the shot.

In shot 414, which used the same weight of C-4 (182 lb), we levelled the entire firing table surface. (We also removed a 21-in. pea-gravel cover from the optics room roof to investigate static loading and the blast-attenuating properties of gravel.) The remarkable differences between the data from the two shots simply exhibit the effects of barricading.

We thought it prudent to fire shots of increasing explosive weight. We chose 585 lb as the maximum weight because it was the largest pressed-PBX-9404 spherical charge available and because it represents a practical maximum for the bunker during the next several years. The weights of the smaller charges were determined by the capacities of the containers available to hold them—55-gal oil drums, paper shipping drums, lard cans, and ice cream cartons.

The charges fired and the corresponding shot numbers are listed in Table 1.

TABLE 1. High-explosive charges fired, and equivalent TNT charges.

Shot No. RKM-	Date fired	Weight of C-4 (lb)	Equivalent weight of TNT (lb) ^a
408	12/22/80	18	23
409	12/22/80	18	23
410	01/07/81	69	90
413	01/12/81	182	237
414	02/17/81	182	237
415	01/13/81	325	423
416	02/11/81	585	761

^aWeight of C-4 \times 1.3; see text for the derivation of this factor.

PRECAUTIONS

Precautions taken to minimize damage included the following:

- The fire sprinkler system was turned off before each shot, although water pressure was maintained in the lines. This was to minimize the



FIG. 2. The FXR building during construction showing the bullnose, the gravel firing table in front, and the buried optics room on the left. The 4-ft-square opening in the bullnose had not been covered with its steel-and-plywood sandwich when this photograph was taken. Gravel has been removed from some of the optics ports, revealing circular temporary covers. The top edges of buried naval armor plate can be seen around the long side of the optics room and partially around the short side. This armor protects the turning-mirror equipment and the tops of the optics ports from shrapnel. The armor extends 15 to 20 ft below the gravel table and is separated from the optics room wall by 2 ft of gravel, which may substantially mitigate ground shock.

chance of water damage to the partially constructed linear induction accelerator, particularly to the many very clean electronic components that were still exposed. Fortunately, no water leaks occurred.

- The large doors at the west end of the new building are held closed by small bolts and striker plates of only a few in.² area. If the fasteners had failed during the negative phase of the blast wave, the swinging doors could have been damaged. Aluminum channels with styrofoam pads were therefore placed across the doors and bolted through the concrete walls. The styrofoam was

placed in the 2-in. space between the channels and the doors with negligible compression. This is shown in Fig. 3. The intention was not to prevent the doors from opening, but rather to test the fasteners and to prevent damage if the doors did swing open. The fasteners held, and the styrofoam was unmarked, but the lower striker plate on the larger door suffered some coining and plastic deformation.

- The bullnose opening was closed by a sandwich of plywood and steel plates held on by 48 breakaway bolts. The shots in which the HE was

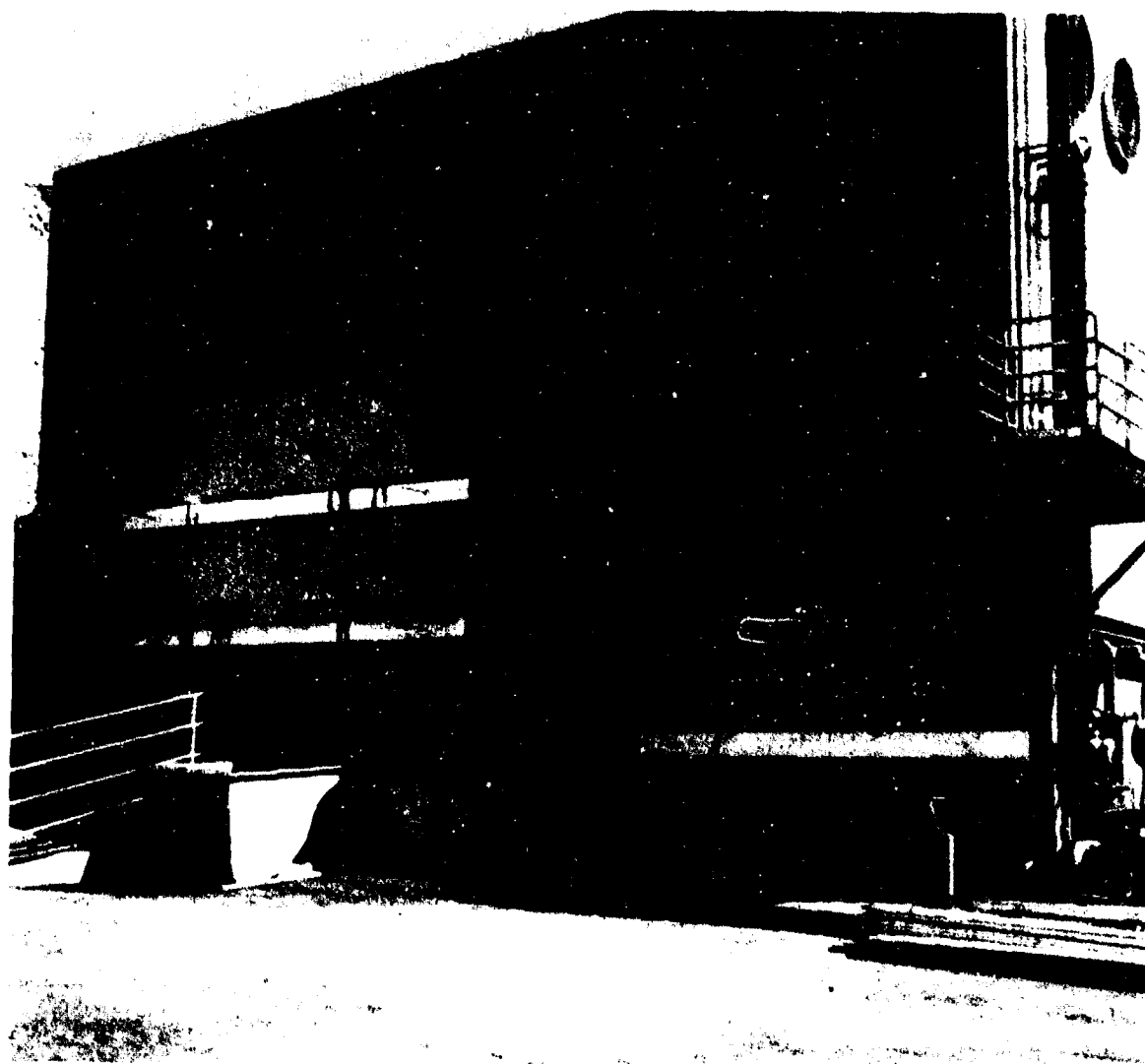


FIG. 3. As a precaution, fittings were installed at the rear doors of the accelerator building to prevent damage if the latches failed during the negative-pressure portion of the blast wave. The aluminum channel loosely held a strip of 2-in.-thick styrofoam against the doors. The latches did not fail, so these precautions probably will not be used again except for very large explosive charges.

cased in sheet metal caused some cosmetic pitting of the front 6-in.-thick steel cover, so sheets of scrap plywood were stacked in front for the heavier shots. For the 585-lb shot, two layers of pea-gravel bags were put in front of the bullnose to reduce the rebound forces on the breakaway bolts. Details of the bullnose sandwich, the method used to hold it together, and its performance are discussed in the next section.

BULLNOSE DESIGN

The bullnose design adopted for the FXR building was a result of experience with the structure of Bunker 851, including its early failure and successful rebuilding. In addition, facilities constructed for similar purposes were visited and compared: these included the Phermex installation at Los Alamos National Laboratory, the British

facilities at Aldermaston and Foulness, and the new x-ray facility at Moronvilliers, France.

At LLNL's linac Bunker 851, the bullnose is a monolithic, hollow, 300-ton steel-reinforced concrete structure. The bullnose is not fastened to the bunker, but is free to side on its own foundation. It is hollow to accommodate the linac beam-transport equipment and the x-ray producing target hardware. Rubber bumpers partially fill the 8-in. space between the bullnose and the bunker wall.

When the Bunker 851 bullnose was tested with explosives when it was completed in 1960, concrete was spalled from the inside front face. This occurred because the initial compressive shock reflected as a rarefaction from the interior concrete/air impedance mismatch, resulting in tensile stresses high enough to cause brittle failure of the concrete. The repair consisted of rebuilding the front 2.5 ft with much more reinforcing steel and facing both inside and outside surfaces with steel plates of enough tensile strength to prevent spall. Through-bolts in plastic pipe were embedded in the matrix, and their nuts were torqued to several hundred ft-lb after the concrete cured.

A sandwich of plywood and steel sheets with a 4-in.-thick front plate of case-hardened steel armor, attached to the bullnose with breakaway bolts, forms the primary shrapnel-protection and blast-mitigating structure for the Bunker 851 bullnose. This construction has performed quite well for 20 years. The armor plate is replaced every few years when shrapnel damage becomes excessive. The breakaway bolts have broken several times during rebound: the plate simply tilts over in the gravel and is set up again and rebolted.

In 1977, the French constructed a steel-reinforced concrete building at Moronvilliers to protect a new flash x-ray machine from blast and shrapnel damage. Their building is about 24 ft high and 31 ft wide. The bullnose is an integral part of the construction; its front face consists of two vertical planes that meet at right angles, so it looks like the bow of a ship. The concrete there is 4 ft thick and is pierced with a steel-cased hole for the emergence of the x-ray beam. Armor plate covers the concrete where it is likely to be damaged. The building has withstood many nearby explosions.

The FXR bullnose design combined the economical integral French style of construction with the through-bolted steel-plate anti-spall features of the Building 851 bullnose. For some ap-

plications it is important to have the x-ray target as close to the shot as possible while still providing shrapnel and blast protection for the accelerator. In FXR this requirement was met by providing a 4-ft-square opening in the bullnose to accommodate electron-beam-transport equipment and the x-ray producing target hardware. For the tests reported here, the opening was closed by a sandwich of plywood and steel plates held on by 48 breakaway bolts. This is shown in Fig. 4. In actual use the sandwich will be pierced to allow emergence of the x-ray beam, and the opening will be covered by light-weight x-ray transparent materials.

When the bullnose is dynamically loaded, the pressure forces on the front face compress the various construction materials and store elastic energy. As the blast wave dissipates and the pressure decreases, the compressed materials expand and accelerate the front steel plate back towards the firing table. The momentum thus imparted to the plate results in tensile stresses in the bolts holding it on; when the forces are high enough, the bolts are elongated. The bolts are designed to fail in tension and/or bending to avoid damage to the cast-in-place permanent bolts. A bolt is shown in Fig. 5, and the result of a laboratory tensile test to failure is shown in Fig. 6. The yield point in the tension test was 50 ksi; the elongation was about 35%, corresponding to about 1.5 in. total extension to failure in the reduced-section region of the bolt.

After each shot, the bolts above the level of the firing-table gravel were removed and measured to see if their yield point had been exceeded. No elongation occurred until the 325-lb shot. Some elongation occurred in the 585-lb shot, even though gravel bags were used in front of the bullnose in that shot. The data are shown in Table 2. The important result is that the total

TABLE 2. Bullnose bolt elongation in 325-lb and 585-lb shots.

Shot No.	C-4 weight (lb)	Minimum elongation (μ in./in.)	Maximum elongation (μ in./in.)	Average elongation (μ in./in.)
415	325	0.003	0.027	0.015
416	585	0.026	0.131	0.093

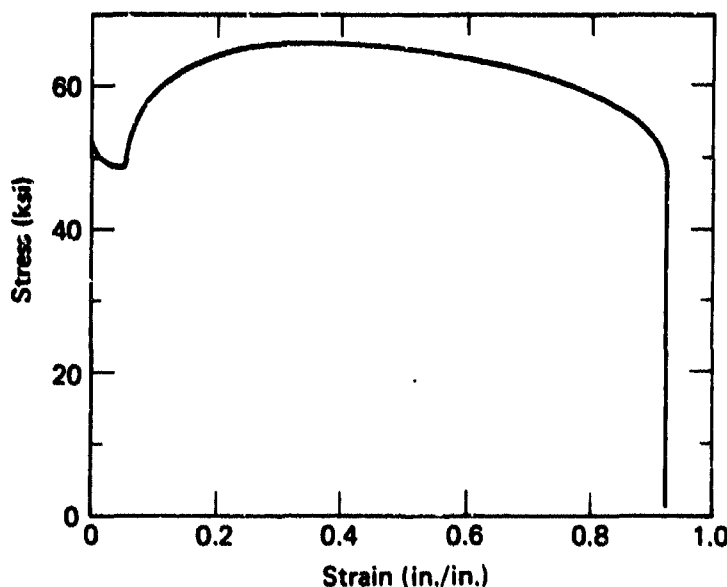


FIG. 6. Stress vs strain in a laboratory test of a breakaway bolt.

average overall bolt elongation in these tests, 0.147 in., is far less than the 1.5-in. total elongation to failure in the laboratory tension test.

After the tests were complete, the steel-and-plywood sandwich was removed and the permanent parts of the bullnose were inspected for damage; none was found. Sections were cut out of the plywood layers and compared with fresh material of the same lot; again, no permanent deformation or compression of the plywood was found. Thus, it appears that the breakaway bolts performed as intended. They will be scribed and occasionally removed for inspection.

STRAIN GAUGES

Strain gauges were installed during the construction of the building. Some gauges were welded to the steel reinforcing bars, and others were suspended in the spaces between them; the gauges were then embedded in the concrete as it was poured. Very rugged gauges were needed to survive the construction activities and the pouring of the concrete. For installation on the reinforcing bars we used a weldable gauge, the Ailtech Model SC129-6S; for suspension between the bars we used a so-called "embedment gauge," the Ailtech CG129-6-6S. Specifications for these gauges are given in Appendix A.

The weldable strain gauge consists of a nickel-chrome alloy sensing filament welded, with its leadout wire, into a small unit about 0.75 in. long. The strain filament itself is enclosed in a stainless steel tube welded to a stainless steel flange. The filament is mechanically coupled to the inside of the strain tube, but electrically isolated from it by magnesium oxide powder. The assembly is hermetically sealed and should function for many years.

For gauge installation, a small area on the reinforcing bar was ground smooth and the gauge flanges were spot-welded to the bar with a small capacitive-discharge welder. The strain in a reinforcing bar is transmitted through the spot welds on the mounting flange to the strain tube, and through the magnesium oxide powder to the alloy strain filament. The powder is so highly compacted that the strain is transmitted to the sensing element throughout its length. Dow Corning room-temperature vulcanizing silicone rubber (RTV) number 732 was applied all over the welded assembly and the newly cleaned steel surface to reduce rusting. Figure 7 shows a typical weldable gauge installed on a reinforcing bar.

Embedment strain gauges are available in various lengths appropriate to different average aggregate sizes. We used the 6-in. gauge recommended for our aggregate, whose average size

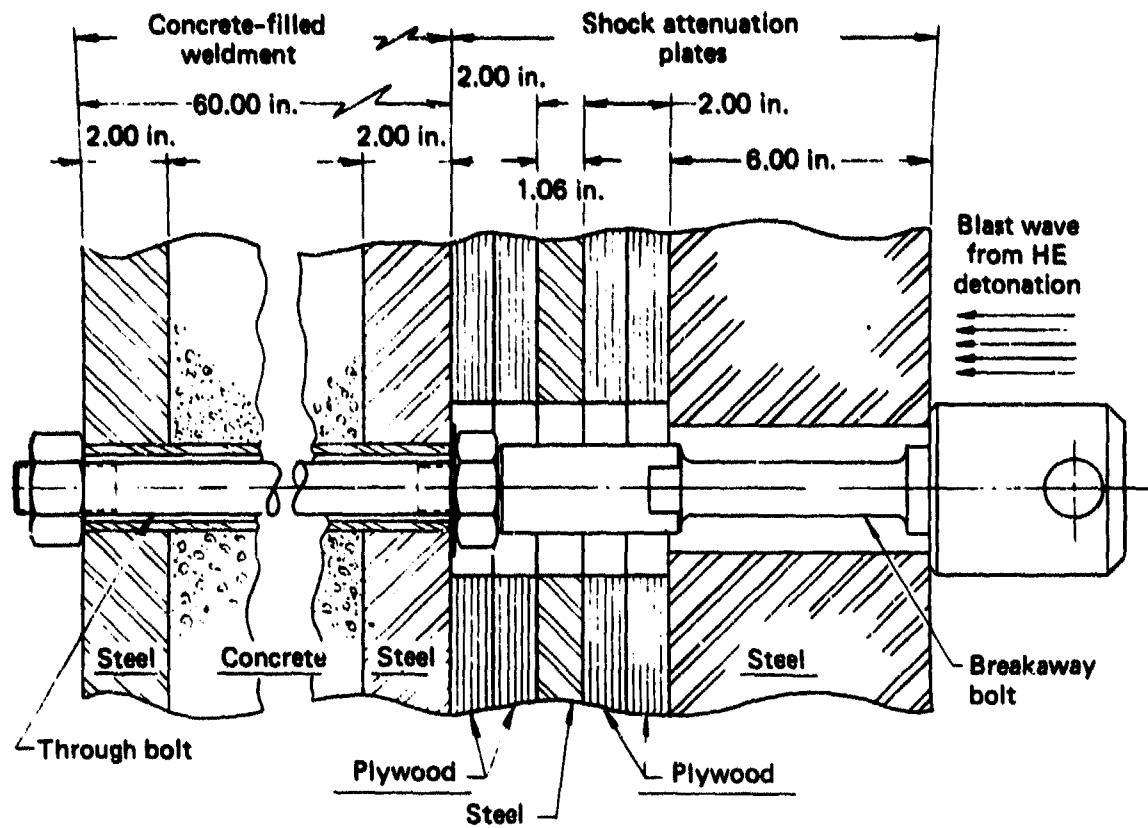


FIG. 4. Construction details of the bullnose front, showing the method used to close the opening for the x-ray beam and the method used to attenuate shocks transmitted to the building. Steel plates form the inside and outside surfaces of a weldment later filled with concrete and made an integral part of the building. Special breakaway bolts hold the armor-plate-and-plywood "sandwich" that attenuates the transmitted shocks. The bolts are designed to fail in tension to prevent plastic deformation of permanent parts of the building. At the end of these tests, the average bolt extension was 0.147 in., well below the 1.5-in. extension obtained when a bolt was pulled to failure in a tensile-test machine.

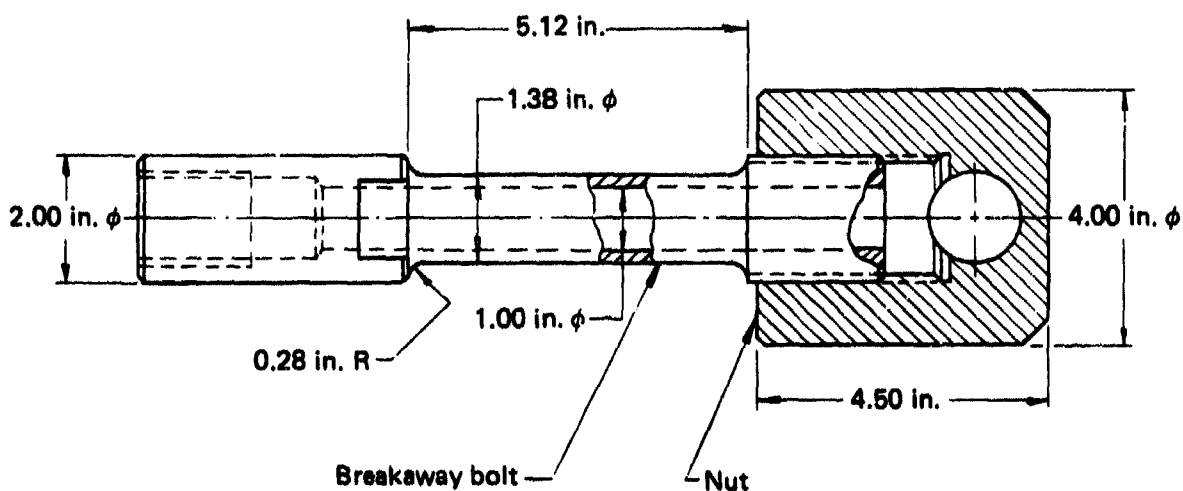


FIG. 5. Breakaway bolt used to hold the front plates onto the bullnose.

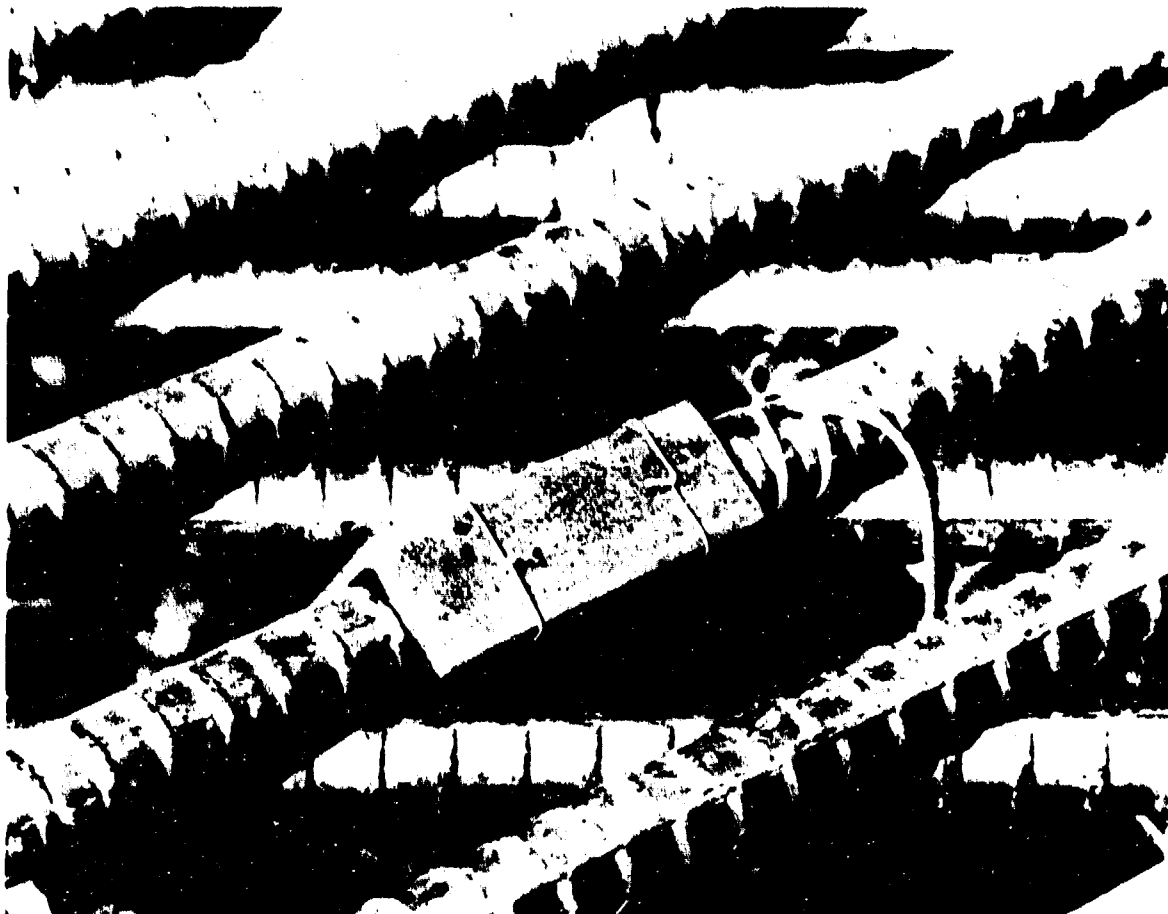


FIG. 7. A strain gauge spot-welded to a reinforcing bar and covered with Dow Corning RTV silicone rubber. A piece of steel angle has been wired to the bar to prevent damage from construction activities. The signal cable leads away to the right and down.

was 1.5 in. The sensing filament is contained in a stainless steel tube, at the ends of which are triangular plates mounted normal to the gauge axis. This assembly is shown in Fig. 8. The gauges were suspended from the reinforcing bars in the desired locations and orientations on wires threaded through the holes in the triangular plates.

Cable connections to the strain gauges were routed over the reinforcing mat to minimize damage during the pouring of the concrete. The cables were brought out to connection boxes on the interior walls of the bunker, where they are now available for use at any time.

Of the 61 gauges installed, 49 survived the construction activities and the pouring of the concrete. Most loss occurred with the embedment gauges, probably because of severe loads imposed

on the connecting cables by rapidly inflowing concrete. Appendix A gives the locations of the strain gauges and other information on their installation and use.

ACCELEROMETERS

Eight Endevco piezoresistive accelerometers were used to measure the structural response of the optics room floor, the bullnose floor, and two linear induction accelerator mounts. Appendix B gives the accelerometer specifications; Fig. B-1 shows their locations.

Accelerometers were fastened in pairs to aluminum blocks, which were epoxied to the structure in the locations shown in Fig. B-1 so that biaxial measurements could be made. By recording both



FIG. 8. Embedment strain gauge (6 in. long) suspended between supports in the middle of the optics room roof. The inner and outer double-layered reinforcement mat is clearly visible; two camera-port sleeves are on the left.

the horizontal and vertical components of acceleration at several locations, we hoped to distinguish between forces acting on the front face of the structure and those transmitted from underneath by ground shock. The two components were not significantly different at any location except at the bullnose floor for shot weights of 182 lb and more. At that location, the vertical component of acceleration was about 40 to 90% greater than the horizontal component.

DATA RECORDING

The signals were recorded with three magnetic tape recorders: a 32-channel recorder with 80-kHz frequency response, and two 14-channel recorders with 20-kHz frequency response. A real-time os-

cillograph was used to get a quick look at data from gauges in the most important locations. We recorded 54 channels: 46 strain gauges and 8 accelerometers. The remaining channels recorded a fiducial marker coincident with the detonation of the high explosive and a time-code generator for use in data reduction.

A bridge circuit was used to energize and monitor the change in resistance of the strain gauges and accelerometers. Precision resistors were used in the inactive bridge arms, and standard signal-conditioning equipment was used to supply power. The wire length from the strain gauges and accelerometers was about 130 ft, so the bridge excitation voltage was measured as close to each sensor or transducer as possible. (Safety considerations prevented us from making measurements close to the connection boxes.)

The voltage output from the strain gauges and accelerometers was preamplified by differential amplifiers whose frequency response was at least 100 kHz. Before each test, a calibration signal was recorded for each transducer, either by shunt calibration or by voltage substitution. These calibrations were used during data reduction to relate the recorded analog voltage to a strain or acceleration.

The recorded data was digitized and reduced by computer with the code ATD.² Because high-frequency signals propagated in a structure of this size are of little interest, noise above 2 kHz was removed from the strain gauge data with a 6-pole (36 dB/octave) Bessel-filter algorithm. The accelerometer data was unfiltered.

The highest recorded strains on the reinforcing bars were those in the middle of the optics room wall for the 585-lb shot; these are shown in Fig. 9. Figure 10 shows the strain recorded on that shot in the middle of the optics room roof. Zero time in Figs. 9 and 10 corresponds to the detonation of the high explosive.

STATIC TESTS

To check gauge response, we observed the response of ten strain gauges in the optics room roof to two static loadings with up to 20 steel blocks whose weight totalled about 186 tons. The first loading consisted of a layer five blocks long

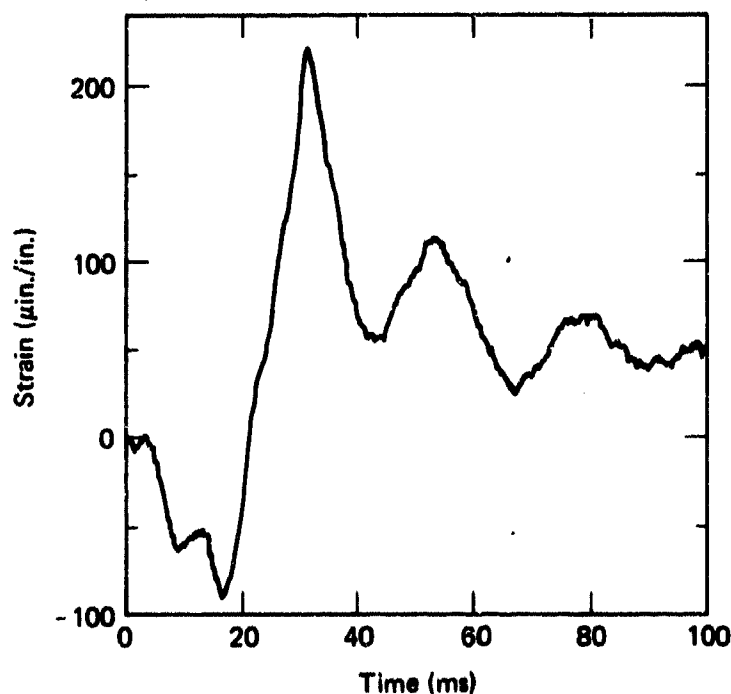


FIG. 9. The highest strains recorded in the building (except for those in the front steel plate) were those in the interior reinforcement mat, mid-span in the optics room wall by gauge 4. In this signal, from the 585-lb test, a peak compressive strain of nearly 90 $\mu\text{in./in.}$ occurred about 16 ms after detonation; a peak tensile strain of about 220 $\mu\text{in./in.}$ occurred about 32 ms after detonation. The signal has a fundamental frequency of about 40 Hz, which corresponds closely with the natural frequency of a wall of this shape and size, which we calculated to be 48.5 Hz.

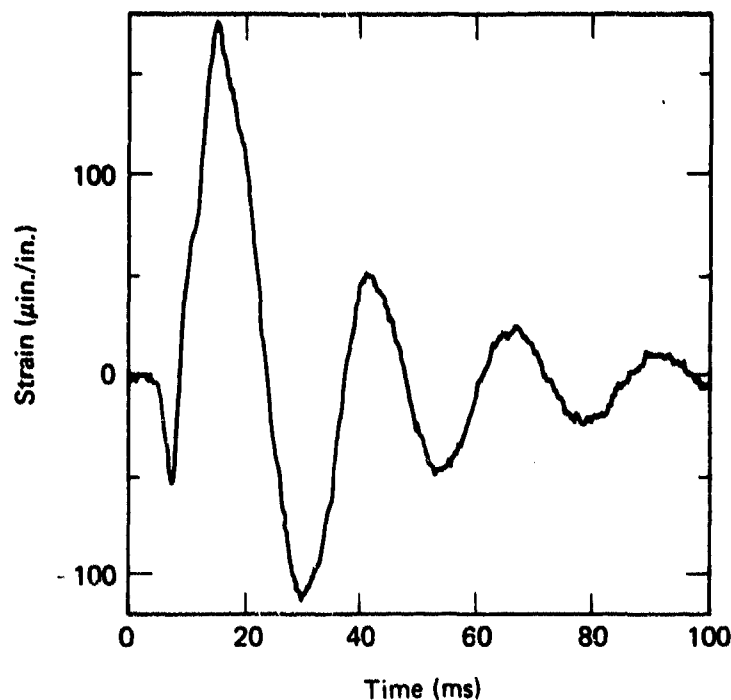


FIG. 10. One of the strongest and least noisy signals recorded in these tests was from gauge 28, mid-span in the optics room roof on the interior reinforcement mat. The signal shown here, from the 585-lb shot, indicates an initial compressive strain of $55 \mu\text{in./in.}$ about 8 ms after detonation, and a tensile strain of nearly $175 \mu\text{in./in.}$ 15 ms after detonation. This tensile strain corresponds to a stress in the reinforcement bar of 5250 psi, well below failure stress in both the steel and the concrete. The fundamental frequency was 40 Hz.

and three blocks wide across the centerline of the short span with three more blocks across the middle row. This loading put three blocks directly over each wall, and gave strains too small to measure. In the second loading, the blocks were arranged directly over the central gauges in two 3×3 layers, with the last two blocks on top. The strains achieved in this loading are reported in Table 3. Appendix D gives calculations of the strains expected in the static tests, shows the locations of the gauges used, and shows the arrangement of steel blocks in the second static test.

The strain readings were obtained using a strain indicator that reads directly in strain units. The gauge resistances were measured independently with an H-P 3456 digital volt-ohmmeter.

The bridge circuit for each strain gauge was completed near the active strain gauge, as in the dynamic tests. The wire length from each strain gauge to the measuring station was 50 ft.

Ordinarily this type of static strain measurement is routine. One measures the strain in the unloaded structure, then loads, measures, unloads, and remeasures. The interesting data are the strain changes caused by loading and unloading. Initial and final unloaded strain readings may differ by a few $\mu\text{in./in.}$, but for most structures this difference isn't critical. For the optics room roof, however, drift of up to $20 \mu\text{in./in.}$ occurred with no change in the applied load. The load-induced strains were not much bigger than this. The drift was probably caused by sunshine-induced thermal stresses on the

TABLE 3. Strain changes in loading and unloading in the static loading tests. Increase in gauge resistance, corresponding to tension, is indicated by a (+) sign; decreasing resistance, corresponding to compression, is indicated by a (-) sign. Uncertainties in strains are about 10 to 20 $\mu\text{in./in.}$ The calculations described in Appendix D gave 183 $\mu\text{in./in.}$ for the magnitude of the strain at the centerline.

Strain gauge No.	Location		Location on span	Loading strain ($\mu\text{in./in.}$)	Unloading strain ($\mu\text{in./in.}$)
	Exterior	Interior			
33	X		Centerline	-36	+50
31		X	Centerline	+40	-24
30	X		Centerline	-34	+50
28		X	Centerline	+40	-32
25		X	1/3-span	+38	-8
24	X		1/3-span	-30	+40
22		X	1/3-span	+44	-64
21	X		1/6-span	-3	+8
16		X	1/6-span	+4	+8
15	X		Wall-roof corner	+18	-8

exposed roof, so the strain change in unloading, which took 35 min, should be much more reliable than the strain change in loading, which took two days.

For each gauge, Table 3 lists the loading and unloading strain changes. The initial unloaded gauge resistances used in determining these changes were averages of three values obtained over two days; the loaded values were averages of two values obtained over eight hours; the final unloaded values were the results of single measurements.

Despite drift, the signs of the loading and unloading strain changes generally agree with what one would expect for gauges on a horizontal beam fixed at its ends. Gauge 15 does not show the expected sign of change in loading, but it is in a corner where the strain field is complicated. Gauge 16 does not show the expected sign of change in unloading, but both gauges 16 and 21 gave strain changes considerably smaller than the 20 $\mu\text{in./in.}$ thermal drift.

The magnitudes of these strains are very small—in fact, they are only two to three times greater than those due to thermal stress. The equivalent stress for the largest measured strain in the roof steel reinforcing bar is only 1920 psi, well below the yield point of the steel. Vehicular travel over the optics room roof should not be the problem it is in the older portions of the bunker.

The strains given in Table 3 have uncertainties of about 10 to 20 $\mu\text{in./in.}$

CANTILEVER-BEAM TESTS

A further verification of strain gauge factor and of the dynamic response of the recording systems was made at the Livermore site. A weldable gauge from the lot used for the bunker measurements was compared with a conventional metal-foil gauge when both were mounted side by side on a cantilever beam that was first statically loaded and then dynamically oscillated. These tests, described in Appendix A, confirm the gauge factors given by the manufacturer and provide a calibration of the gain of the recording system at the beam's natural oscillation frequency.

ERRORS

Errors in the strain measurements arise from uncertainties in the gauge factors, in the shunt-calibration resistances, and in the bridge excitation voltages. We estimate the uncertainty of the strain-gauge data to be less than 4% of the measured value, and that of the accelerometer data to be less than 2.5% of the measured value.

DATA ANALYSIS

All the reduced data from the strain gauges and accelerometers is reproduced on microfiche at the back of this report.

For each strain signal, we recorded the peak strain and the time from detonation to peak strain. A computer-generated Fourier analysis gave the major frequencies present in the signals from each gauge. These data are tabulated in Appendix C. The accelerometer data were particularly noisy. The peak accelerations recorded in each shot are given in Table 4.

The highest strains (see Fig. 11) were those on the interior face of the A-36 mild steel front cover plate for the 325-lb charge, and were about 700 $\mu\text{in./in.}$ This strain corresponds to a stress in the plate of 21 000 psi, about 60% of the minimum yield stress in simple tension. Clearly, the much lower strains in the 585-lb shot demonstrate the mitigating effect of the two layers of gravel bags placed in front of the plate. The fact that the strain was compressive in the 585-lb shot (rather than tensile, as in the other shots shown in Fig. 11), and the large difference between the vertical and horizontal strain signals, are probably accounted for by shocks transmitted through the gravel firing table. The barricading in shot 413 considerably lowered the strain, as Fig. 11 shows.

The highest strains in the structure itself occurred in the interior reinforcing bars of the optics room wall: in the 585-lb shot, the strain at this location was 220 $\mu\text{in./in.}$ See Fig. 12.

The strain in the center of the optics room roof is perhaps of greater interest than the strain in the optics room wall because it is most easily calculated. The average strain from two gauges on the interior reinforcing mat is shown in Fig. 13. The highest strain measured there was 180 $\mu\text{in./in.}$ in the 585-lb shot.

Strains in the sloping bullnose roof are also of interest and are shown in Fig. 14. Here again the effects of barricading in shot 413 are apparent, as are the effects of the gravel bags used for the 585-lb shot. The highest strain measured in the bullnose roof was about 210 $\mu\text{in./in.}$ in the 325-lb shot.

Peak strains measured elsewhere were all lower. The locations of the gauges were chosen to yield the highest strain readings. However, some forward regions in the bullnose and at other complex corners were inaccessible for gauging because of the density and routing of the reinforcing bars and plates. Strains in these locations could have been higher than any we recorded.

The signals from gauges at corners were rich in high frequencies.

TABLE 4. Peak accelerations in dynamic tests.

Accelerometer	Figure	Location	Orientation	Peak accelerations (in g's) for the following shot weights (in lb)						
				16	18	69	162	182	325	585 ^a
A-1	B-1	Optics room floor	Vertical	0.7	0.5	1.5	3.4	4	3.0	3.5
A-2	B-1	Optics room floor	Horizontal	0.7	0.5	1.1	3.4	5	3.4	3.0
A-3	B-1	North LIA support	Horizontal	1.4	1.4	5	9	12	15	20
A-4	B-1	North LIA support	Vertical	2.5	2.5	4	9	14	15	15
A-5	B-1	South LIA support	Horizontal	2.1	2.2	7	13	12	17	26
A-6	B-1	South LIA support	Vertical	1.4	1.9	5	14	10	13	19
A-7	B-1	Bullnose floor	Horizontal	5.0	4.5	17	40	35	44	21
A-8	B-1	Bullnose floor	Vertical	5.0	5.0	18	59	50	68	40

^aTwo layers of gravel bags.

FIG. 11. Peak strains on the inner surface of the 6-in.-thick A-36 steel bullnose front cover plate (gauges 62 and 63). The lower strain in the first 182-lb shot (RKM 413) results from barricading. The mitigating effect of the two layers of gravel bags in front of the cover plate in the 585-lb shot is clear. The peak strains were tensile strains for all but the 585-lb shot, in which they were compressive, suggesting that ground shock transmitted a strong force component to the front plate in that shot.

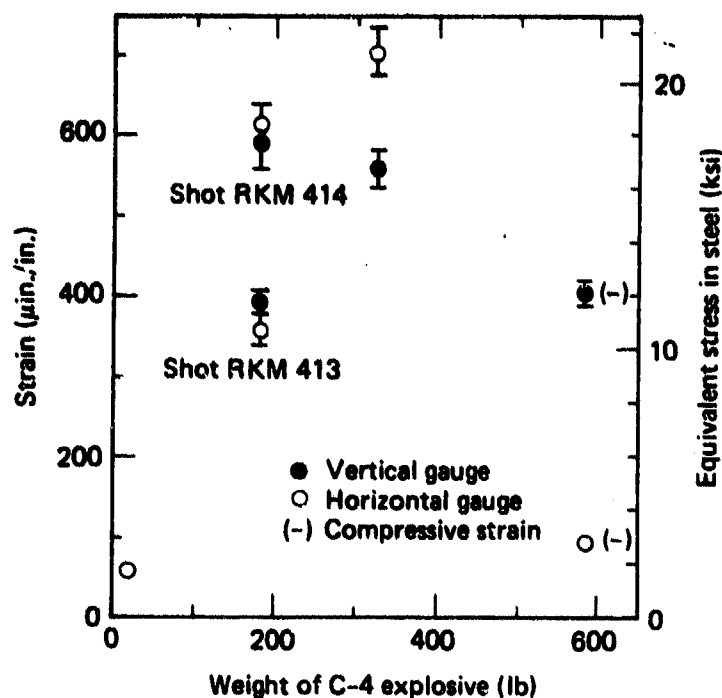
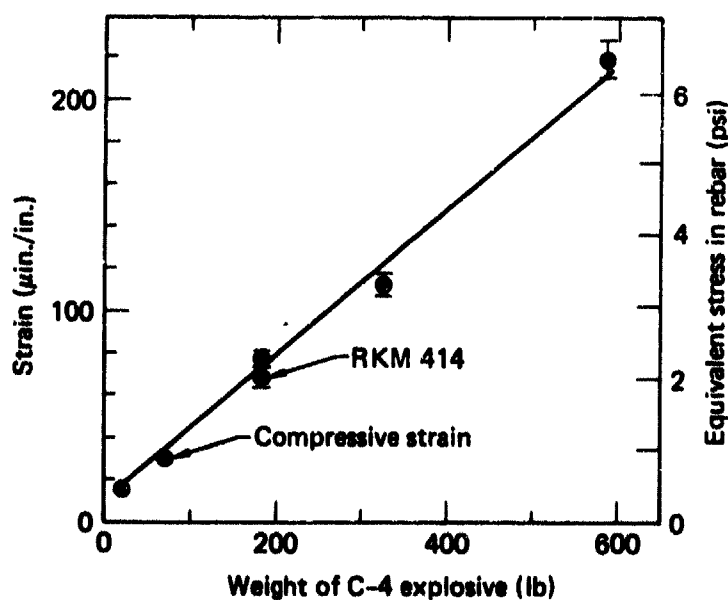


FIG. 12. Peak strains on the reinforcing mat on the interior mid-span of the optics room wall (gauge 4). All strains were tensile but one, which is indicated in the figure; the greatest was about 220 $\mu\text{in./in.}$



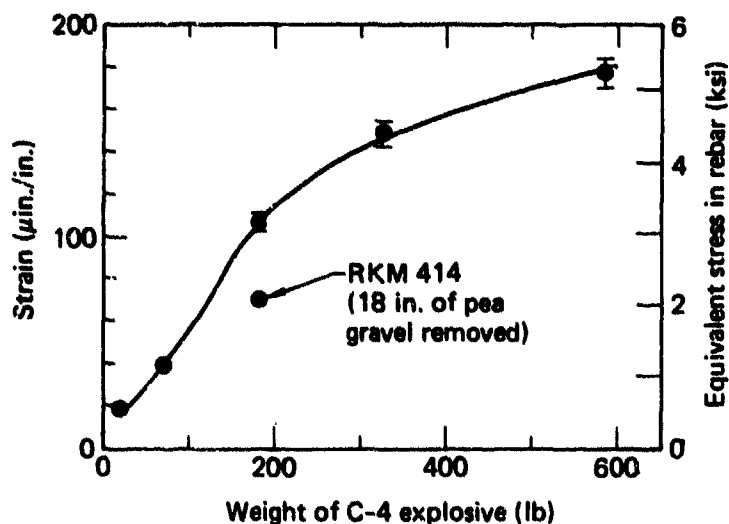


FIG. 13. Peak strains from gauge 28, mid-span in the optics room roof on the interior reinforcement mat. All strains were tensile. This gauge gave very clean signals, as Fig. 10 shows. In the 585-lb shot, the strain signals reached nearly 180 $\mu\text{in./in.}$

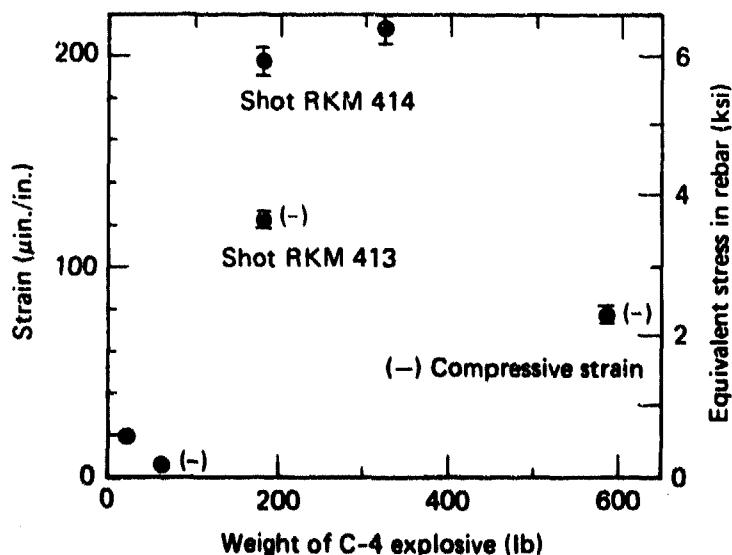


FIG. 14. Peak strains from strain gauge 57, on the interior reinforcement mat in the sloping bullnose roof. Barricading in shot 413 may account for the lower strain at that HE weight. The effect of the double layer of gravel bags in the 585-lb shot can be seen.

DISCUSSION OF RESULTS

Agbabian Associates, of El Segundo, California, was hired to perform the basic calculations for the design of the structures. These calculations are given in Ref. 3. Agbabian used rapid, simplified analysis methods based largely on experimental work reported in Refs. 4 and 5. The experimental data and conclusions reported in those references were adjusted and extrapolated by Agbabian to account, as closely as possible, for the differences between the experiments of Refs. 4 and 5 and the FXR design requirements. Their calculations are extensive and include many iterations; they represent the best analysis available in a field in which there is little experimental information or design verification.

Agbabian's calculations of building response to explosions made use of either of two models, as appropriate for the conditions of each shot. The first model is based on blast pressure and duration; the model assumes a triangular pressure pulse with zero rise time and assumes that the structural member in question has a single, undamped degree of freedom. The second model is based on blast impulse; the model equates the work done by the external force to the energy stored in the members. Strain energy due to both flexure and shear deformation was considered. Various safety factors were applied in both of these calculations. When a simplifying assumption was needed, the most conservative choice was usually made.

The ratio of the duration of the applied pressure to the period of oscillation of the member,

t_d/T , determines which model is used. Agbabian used the impulse model for $t_d/T < 0.08$.

One of us (C. Y. King) has extended the Agbabian calculations to predict the strains in the dynamic tests at a few locations, and for the static-loading tests of the optics room roof. Those calculations are reproduced in Appendix D. Because of its nearly rectangular form, the optics room roof was the easiest to treat mathematically; the signals from the gauges there also turned out to be the simplest, the least noisy, and the easiest to interpret. Table 5 gives the calculated stresses and strains at the centerline of the optics room for each of the dynamic tests.

The calculated strains shown in Table 5 are greater than the measured strains by factors of from 1.57 to 3.87. These large discrepancies are not the result of experimental error.

Table 6 gives the results of the static strain calculations for the optics room roof, and the corresponding experimental data. For the center of the roof, the ratio of predicted to measured strains is 4.8. Several conservative assumptions in the calculations of Appendix D probably account for this discrepancy. These include:

- The strength of the concrete in tension was neglected.
- The compression of steel was neglected in the tensile-stress calculation, even though steel reinforcement was provided equally in tensile and compressive sides of the members.

TABLE 5. Dynamic-test results: calculated and experimental data for the centerline of the optics room roof.

C-4 (lb)	TNT equivalent (lb) ^a	Calculated			
		Stress (psi)	Strain (μ in./in.)	Recorded strain (μ in./in.)	Ratio, calculated/recorded
18	23	2205	47	18	2.61
69	90	5222	151	39	3.87
182	237	6963	211	107	1.97
325	423	8358	259	148	1.75
585	761	8916	278	177	1.57

^aWeight of C-4 \times 1.3.

TABLE 6. Comparison of measured strain with design calculations for static loads. Static loads consisted of 20 blocks, each $38 \times 38 \times 47$ in., with a total weight of 370 930 lb. A 14-in.-diam hole 14 in. deep in the bottom of each block accommodates the lifting eye of a block on which it is stacked.

	Calculated				Measured strain ($\mu\text{in./in.}$)	
	Stress (psi)		Strain ($\mu\text{in./in.}$)		1/6 span ^a	Center ^b
	End	Center	End	Center		
Uniformly distributed over entire span	6713	3356	131	116	— ^c	— ^c
Partial uniform load at middle	8466	5306	292	183	6	38

^aAverage of gauges 16 and 21, loading and unloading.

^bAverage of gauges 28, 30, 31, and 33, loading and unloading.

^cToo small to measure.

- The roof of the optics room is a rectangle. The long span will take 8% of the load for negative moment and 9% for positive moment. In the one-way slab calculations, the short span dimension was assumed to take all of the load. Thus the calculated stress should be higher than the actual stress.

- The optics room roof is connected to its walls by a considerable amount of reinforcing steel.

During loading of the roof, the moment distribution will transfer some bending from roof to wall. In the calculations, we neglected this strengthening coupling.

- A single, conservative value of 3.32×10^6 psi was used for the modulus of elasticity of concrete; in fact, the modulus increases as the concrete cures, and may reach 4.62×10^6 psi for the type of concrete used in the bullnose.

CONCLUSIONS

The 4-ft-square bullnose aperture was successfully closed with the plywood-and-steel sandwich shown in Fig. 4. The steel plates did not suffer any plastic deformation, and the plywood sheets were not permanently compressed.

These experiments show that gravel bags effectively attenuate explosively driven strain in structures. In the 585-lb test, the accelerometers and strain gauges showed attenuation by a factor of two. While we commonly use gravel bags with explosive weights this high, all members of the building would probably have remained within their elastic limits even without the bags.

The many simplifying assumptions and safety factors used in the design calculations, and the lack of prior experimental verification, introduced a conservatism into the analysis that we believe accounts for the discrepancy between the calculated and observed strains. Work is underway with more elaborate structural-analysis models on the Laboratory's large digital computers. The gauges remain embedded in the structure, and we expect

that future experiments and computer modeling will yield better agreement between theory and experiment.

The stresses corresponding to the measured strains are very small fractions of the yield stresses of the members. For example, in the 585-lb shot, the peak strain of $185 \mu\text{in./in.}$ in the center of the optics room roof corresponds to a stress of 5265 psi (assuming a modulus of 29×10^6 psi for steel). This is only 8.9% of the nominal yield stress of the steel (60 000 psi). Thus, even for 585 lb of C-4, the optics room roof is well below the elastic limit and the yield strength of its reinforcing members. Careful examination of the data leads us to conclude that 1000 lb of TNT, detonated under the conditions of these tests, would produce a strain no higher than $500 \mu\text{in./in.}$ in any of the gauges. This corresponds to stress of 14 500 psi in the reinforcing steel, 24% of the yield stress. The building design goals have been achieved; in fact, the FXR facility is an extremely strong structure that should withstand detonations for many years.

ACKNOWLEDGMENTS

We acknowledge the superb gauge-installation work of J. Kuhlman and L. Meisner and the careful data recording and data reduction of J. Holm, B. Given, and G. Moxon. Herman Smith and his rigging crew adjusted their schedules

to accommodate our firing activity and carefully but quickly moved heavy plates and blocks on demand. Larry Simmons coordinated the activities of many disparate groups and ensured that the explosive tests were safely conducted.

REFERENCES

1. B. M. Dobratz, *Properties of Chemical Explosives and Explosive Simulants*, LLNL Explosives Handbook, Lawrence Livermore National Laboratory, Livermore, CA, UCRL-52997 (1981).
2. A. W. Shannon, *ATD User's Manual*, Lawrence Livermore National Laboratory, Livermore, CA, UCID-17394 (1977).
3. *Basis for Structural Design Flash Radiography Facility Addition to Building 801A, Site 300*, Agbabian Associates, El Segundo, CA, R-7825-4863 (1979).
4. *Structures to Resist the Effects of Accidental Explosions*, Armed Forces Explosives Safety Board, Washington, D.C., Department of the Army TM5-1300, NAVFAC P-397, AFM 88-22 (1969).
5. James K. Ingram, *CENSE Explosion Test Program, Report 1, CENSE 1, Explosions in Sandstone*, Waterways Experimental Station, Vicksburg, MS, TRN-77-6 (1977).

PWM/mc



AD P000461

STRUCTURAL DAMAGE TO BUILDING FRAMES FROM ACCIDENTAL OR TERRORIST EXPLOSIONS

Bruce L. Morris
Southwest Research Institute
San Antonio, Texas

INTRODUCTION

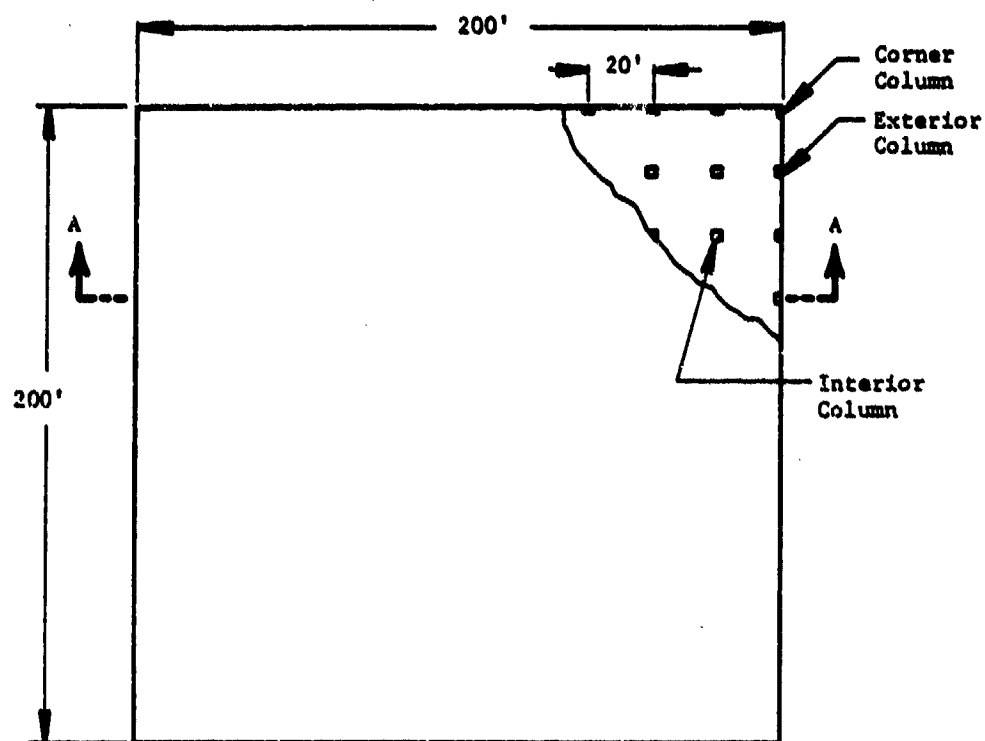
The response of structural building frames to blast loadings is of great interest to military attack planners, to safety-oriented personnel, and to persons required to prevent or lessen terrorist attack damage. This paper investigates the response of a number of structural steel or reinforced concrete columns to accidental or terrorist explosions by designing the columns for an assumed 'typical' office or hotel structure, determining the mid-height lateral deflection of the column which will lead to its subsequent collapse under the applied building loads, and then determining the blast pressures and impulses necessary to produce this critical mid-height deflection.

BUILDING DESIGN

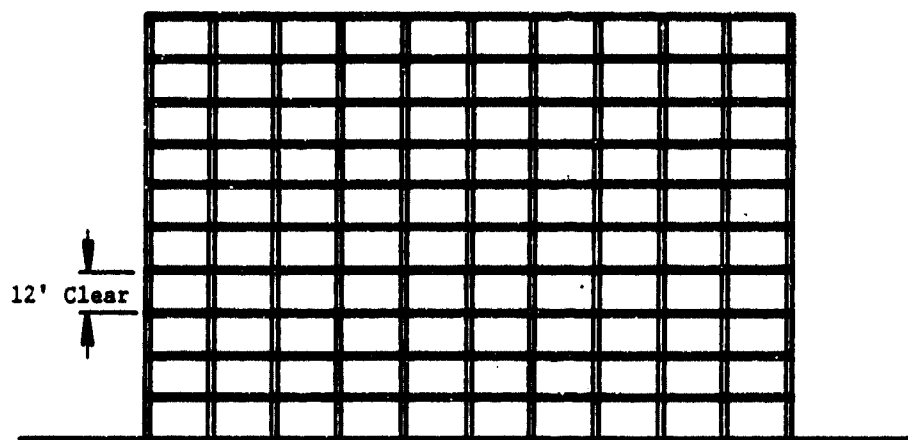
The typical building layout chosen is shown in Figure 1. Columns are placed at 20 foot centers in both orthogonal directions. A uniform live load of 90 pounds per square foot was applied to each floor in addition to a dead load equal to the weight of a 7-inch concrete floor slab. The total load on each column type (corner, exterior, or interior) was determined, and the column section selected using the 1963 American Concrete Institute (ACI) or 1967 American Institute of Steel Construction (AISC) specifications for the reinforced concrete or steel construction, respectively. Bending moments from connecting beams were ignored, and minimum code-applied eccentricities were used. Fixed support conditions at the top and bottom of the column were assumed, and a 12 foot clear-span height was used. The concrete design utilized ultimate strength design techniques with a concrete strength (f'_c) of 4,000 psi and a steel reinforcing bar yield strength (f_y) of 50,000 psi. The structural steel design utilized 36,000 psi yield strength sections. Table 1 summarizes the applied loads and section selections for the structural steel design, and Table 2 contains similar data for the reinforced concrete members.

CRITICAL DEFLECTIONS

The scenario for blast damage and subsequent collapse is presented in Figure 2. The blast is assumed to act from either direction (strong or weak axis) and deforms the column into the shape of Figure 2(c). The applied



PLAN



SECTION A-A

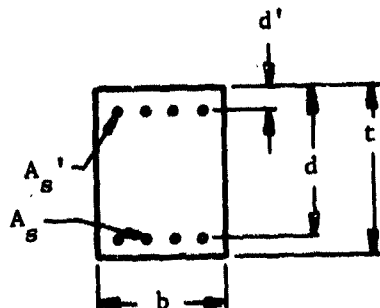
Figure 1. Typical Building Frame

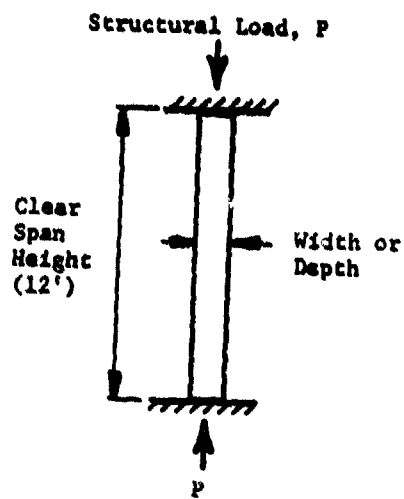
Table 1. Steel Column Design

<u>Column Location</u>	<u>Applied Load (Kips)</u>	<u>Section Selected</u>
Corner	189	W 8 x 67
Exterior	367	W 12 x 106
Interior	734	W 14 x 211

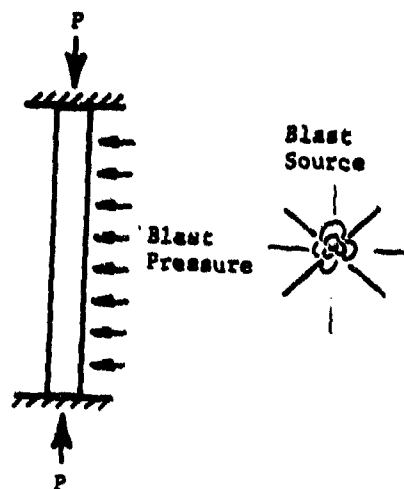
Table 2. Reinforced Concrete Column Design

<u>Column Location</u>	<u>Applied Load (Kips)</u>	<u>b = t* (inches)</u>	<u>d'* (inches)</u>	<u>A_s = A_s'* (sq. in.)</u>
Corner	226	12	2.5	2.54
Exterior	416	16	2.5	5.10
Interior	788	22	2.5	7.62

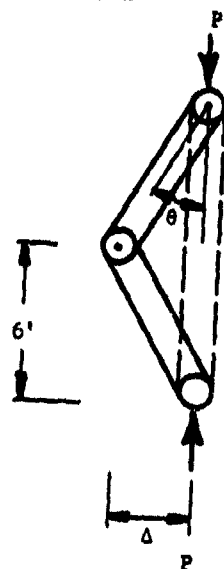




(a) Normal Column Action



(b) Blast Loading



(c) Deformed Shape

Figure 2. Blast Damage Scenario

structural load, acting through the deformed eccentricity, Δ , produces a moment which, if the deflection is sufficiently great, exceeds the combined axial load and moment capacity of the cross-section. The column will then fail.

The steel column sections were analyzed for bending in both the strong and weak axis directions. Figures 3 and 4 present the idealized cross sections and the completely plastic stress profiles for the two bending cases. The location of the neutral axis (N.A.) was determined. The distance from the tension flange to the neutral axis for the strong axis case was found to be

$$X_s = T_F + \frac{T_W H}{2W} - \frac{P}{2W F_Y} \quad (1)$$

where the variables are as defined in Figure 3. For the weak axis case, the corresponding distance from the tension edge to the neutral axis is given as

$$X_W = \frac{2T_F W F_Y + H T_W F_Y - P}{4T_F F_Y} \quad (2)$$

where the variables are as defined in Figure 4.

The eccentricity of the applied structural load, P , from the neutral axis necessary to produce a moment equal to the resisting moment was then determined. This leads to the following strong and weak axis eccentricities (about the neutral axis):

$$e_s = \frac{F_Y}{2P} \left[W X_s^2 + W (T_F - X_s)^2 + T_W H (H + 2T_F - 2X_s) + T_F W (2H + 3T_F - 2X_s) \right] \quad (3)$$

$$e_W = \frac{F_Y}{P} \left[T_F (W - X_W)^2 + T_F X_W^2 + T_W H \left(\frac{W}{2} - X_W \right) \right] \quad (4)$$

These eccentricities were then adjusted to measure from the original section centerline (where the structural load is assumed to be applied). This eccentricity about the centerline is then critical mid-height deflection, Δ . The results are summarized in Table 3.

The reinforced concrete columns of Table 2 were analyzed for bending about the strong axis only since, in reality, the steel placement would probably be uniform around the column and the sketch in the table represents an

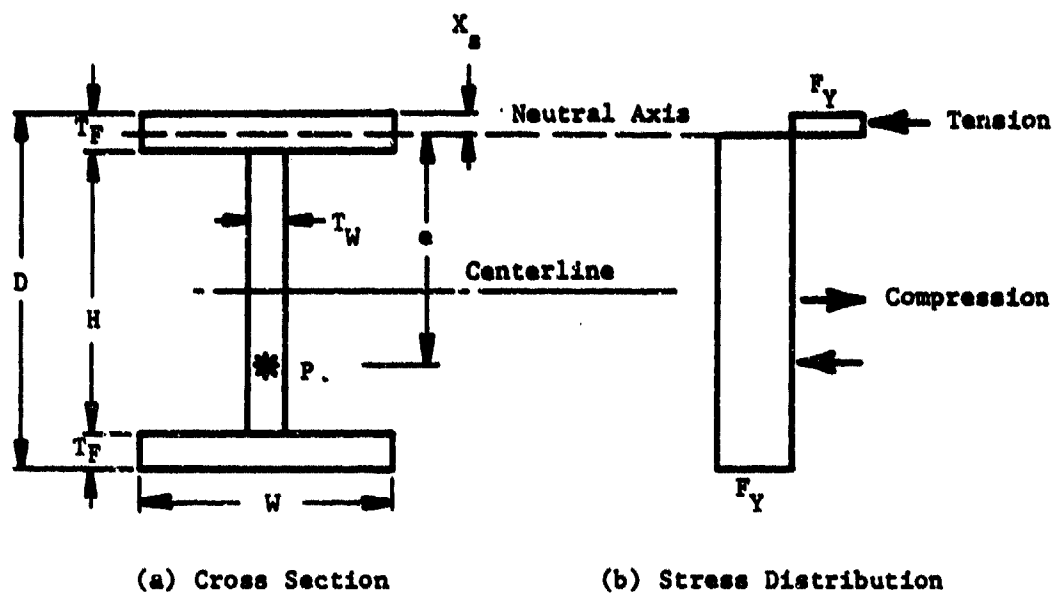


Figure 3. Strong Axis Bending of Steel Columns

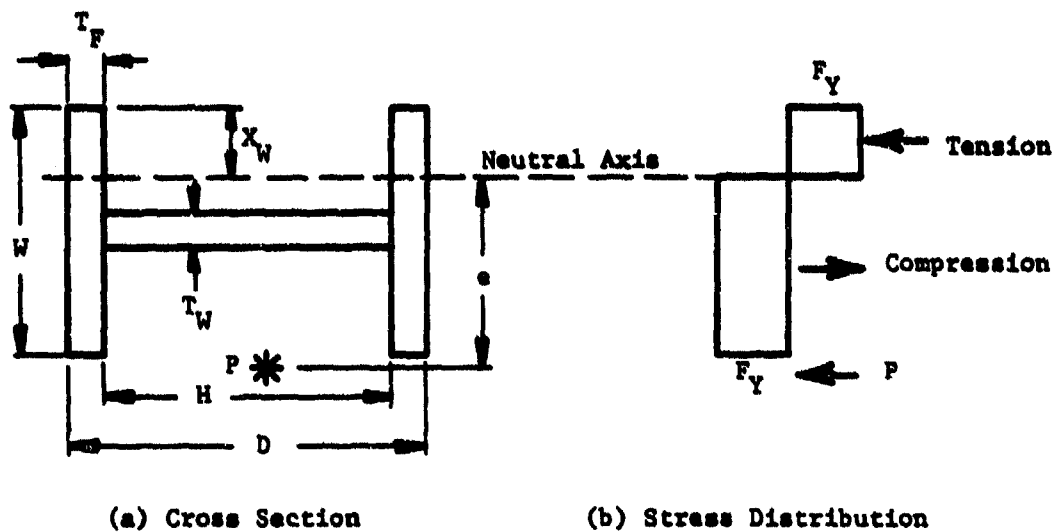


Figure 4. Weak Axis Bending of Steel Columns

Table 3. Bending of Steel Columns

<u>Property or Dimension</u>	<u>Column Section</u>		
	<u>W 8 x 67</u>	<u>W 12 x 106</u>	<u>W 14 x 211</u>
F_y (psi)	36,000	36,000	36,000
D (inches)	9.000	12.880	15.750
W (inches)	8.280	12.230	15.800
T_f (inches)	0.935	0.986	1.563
T_w (inches)	0.570	0.620	0.980
H (inches)	7.130	10.910	12.620
P (pounds)	189,000	367,000	734,000
I_x (inches)	0.860	0.840	1.310
Δ_s (inches)	11.070	12.200	8.460
I_w (inches)	3.830	5.250	6.620
Δ_w (inches)	6.050	7.080	9.310

idealization. The column response to combined axial load and bending was determined using interaction diagrams similar to that of Figure 3 which is for the case of the exterior column. Pertinent equations, based on Figure 3, are presented below.

$$P_o = 0.85 f'_c b t + f_y (A_s + A_s') \quad (5)$$

$$M_o = A_s f_y (d - d') \quad (6)$$

$$P_b = 0.72 f'_c b d \frac{0.003}{f_y/E_s + 0.003} \quad (7)$$

$$P_b e_b' = 0.85 f'_c a_b b \left(d - \frac{a_b}{2} \right) + A_s' f_y (d - d') \quad (8)$$

where

$$a_b = 0.85 d \frac{0.003}{f_y/E_s + 0.003}$$

and

e_b' = eccentricity from center of tension steel

$$M_b = P_b e_b \quad (9)$$

where

e_b = eccentricity from center of section

The moment capacity, M , corresponding to the applied structural load, P , is then interpolated as shown in Figure 3. The critical eccentricity, Δ , is then found from

$$\Delta = \frac{M}{P} \quad (10)$$

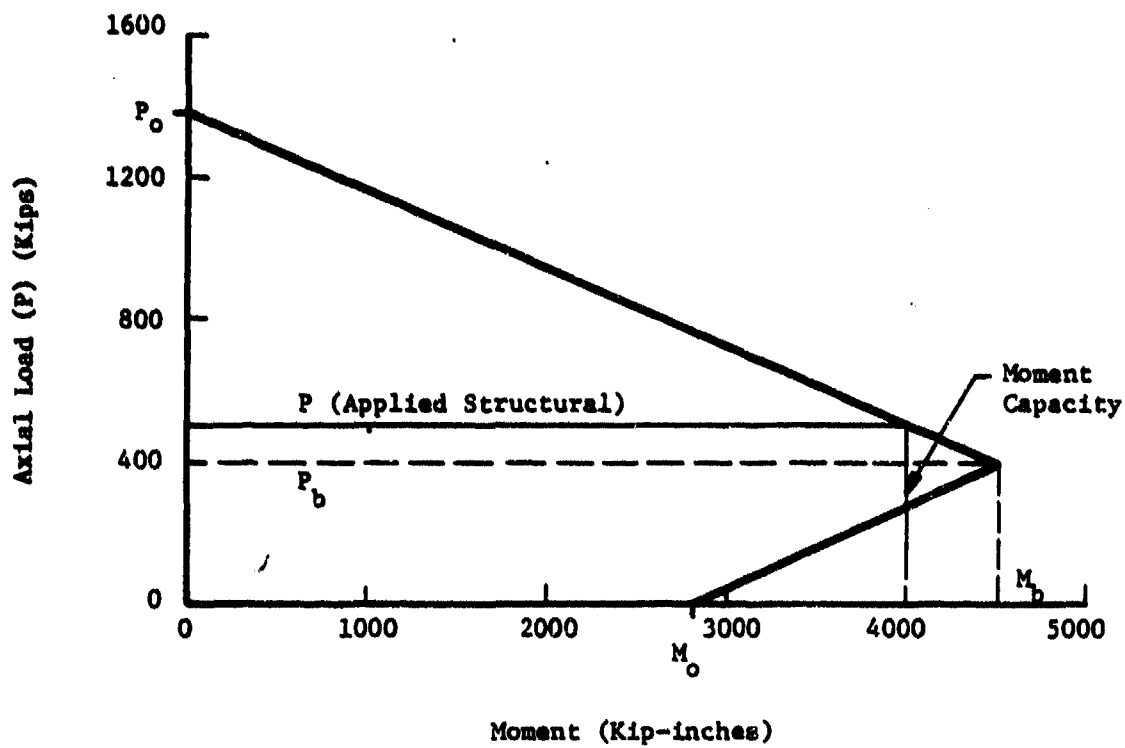


Figure 5. Interaction Diagram for Reinforced Concrete Columns

Results of these calculations are summarized in Table 4.

Table 4. Bending of Reinforced Concrete Columns

<u>Property or Dimension</u>	<u>Column Type</u>		
	<u>Corner</u>	<u>Exterior</u>	<u>Interior</u>
P_o (kips)	744.00	1,380.00	2,280.00
P_b (kips)	211.00	400.00	792.00
M_o (kip-inches)	889.00	2,805.00	5,400.00
M_b (kip-inches)	1,604.00	4,543.00	9,980.00
P (kips)	226.00	416.00	788.00
M (kip-inches)	1,559.00	4,463.00	9,980.00
Δ (inches)	6.90	10.73	12.60

BLAST RESPONSE

An explosion, either accidental or intentional, can load a structural column in a variety of ways. If the charge is close to the column, the blast can result in essentially a point load (the load being equal to the overpressure times the square of the exposed column width or depth as appropriate. If the charge is located some distance away from the column, the load is basically uniform over the column length. Both of these loads (the point and uniform) are produced by the initial blast. If the column is located along the wall of a room, the walls enclosing that room may produce reflections of this initial blast and may, depending upon the wall strength and charge placement, permit the rise of a quasi-static loading on the column. If the column is in the open area of a room, the quasi-static pressure buildup (if any) will act on all sides of the column and will not produce additional deformation over that caused by the initial blast.

The response of a structural member to a rapidly varying load is dependent upon both the peak value of that load and upon the loading duration. The precise shape of this load-time function is not important, and the triangular pulse of Figure 6 will be used in the remainder of this paper. The impulse, I , or area under the load-time curve, is then given as

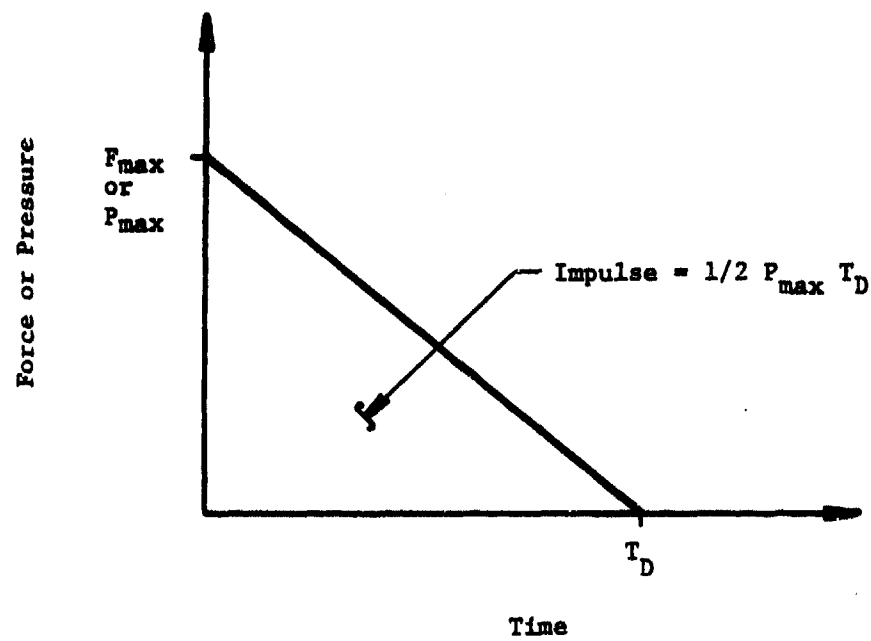


Figure 6. Idealized Load-Time History

$$I = 1/2 P_{\max} T_D \quad (11)$$

where P_{\max} is the peak overpressure (or force for a point load) and T_D is the load duration. Many combinations of peak overpressure and impulse will produce a specified displacement, and the compilation of these points produces a pressure-impulse (P-I) diagram for this deformation.

Determination of the pressure-impulse pairs was made using a single-degree-of-freedom (SDOF) numerical integration scheme based on the constant velocity or lumped impulse procedure found in Biggs [3]. This procedure begins with the dynamic equilibrium equation, for the undamped case,

$$F(t) - K_y - M\ddot{y} = 0 \quad (12)$$

where $F(t)$ is the time-varying loading function, K is the stiffness, M is the mass, y is the displacement, and \ddot{y} is the acceleration. A recurrence formula is developed to permit extrapolation of the displacement at time station $(i + 1)$ from data available for time step (i) or before. The formula for this procedure is given by

$$y^{(i+1)} = 2y^{(i)} - y^{(i-1)} + \ddot{y}^{(i)} (\Delta t)^2 \quad (13)$$

where Δt is the time step. The initial acceleration, $\ddot{y}^{(0)}$, is generally given as

$$\ddot{y}^{(0)} = \frac{F(0)}{M} \quad (14)$$

and the initial displacement, $y^{(0)}$, as

$$y^{(0)} = 0 \quad (15)$$

This initial acceleration, $\ddot{y}^{(0)}$, is assumed constant during the first time step, and the displacement at the end of this step, $y^{(1)}$, is found from

$$y^{(1)} = 1/2 \ddot{y}^{(0)} (\Delta t)^2 \quad (16)$$

The recurrence formula [Equation (13)] is then used to follow the system response.

Equation (12) implies that the structural resistance, R , to the applied loads, K_y , is linear with respect to system deflections. The resistance function (force-deflection relationship) used here instead is shown in Figure 7. Each of the three phases of the system response (i.e., elastic, elastic-plastic, and fully plastic) is represented by maximum resistances, R_M , stiffnesses, K , and load-mass factors, K_{LM} , all of which can be found in Reference 3 or 4 for varying support conditions and load types. The load-mass factor permits revision of Equation (12) to relate the equivalent SDOF mass, force, and stiffness to the original system. The dynamic equilibrium equation then becomes

$$F(t) - R(y) - K_{LM} M \ddot{y} = 0 \quad (17)$$

where $F(t)$, M , y , and \ddot{y} are the values from the original system.

The single-degree-of-freedom approach was used to determine the pressure-impulse pairs necessary to produce lateral column deflections as shown in Figure 2 and summarized in Tables 3 and 4 for the different column materials and bending directions. Results are shown in Figures 8, 9, and 10. The pressures for the uniformly loaded cases act over the entire length and width of the exposed face while those for the point loads are assumed to act over an area, at the center of the column, equal to the exposed width squared.

Now that these pressure-impulse pairs are known, all that remains is the determination of the high explosive quantity and distance from the member that will produce these critical deflections. Consider first the case of uniform loading. A standoff distance of 10 feet from the mid-height of the column will provide a relatively uniform load along the length of the 12 foot column. Consider also the case where the column is along the wall of a building room which will produce reflections of the blast wave. Baker, et al. [5] have shown that for a centrally located detonation, there will be three significant blast pressure pulses: the original incident pulse of magnitude P_{max} and duration T_R , a reflected pulse of magnitude $P_{max}/2$ and duration T_R , and another reflected pulse of magnitude $P_{max}/4$ and the same duration. Since the initial duration, T_R , and the times between arrivals of these pulses are generally short relative to the structural natural period, the pulses can be combined into a single one with an amplitude of $1.75 P_{max}$, producing an impulse 1.75 times that of the initial wave. With these reflections then, the pressures and impulses of Figures 8, 9, and 10 can be divided by this 1.75 amplification factor.

The short duration of blast loads, for relatively small charges, suggests that the impulse portion of the P-I diagram will be the hardest to satisfy. For that reason, the procedure to determine the quantity versus distance points is as follows:

1. For a given column and loading direction, determine the minimum impulse and the pressure at which it first occurs.

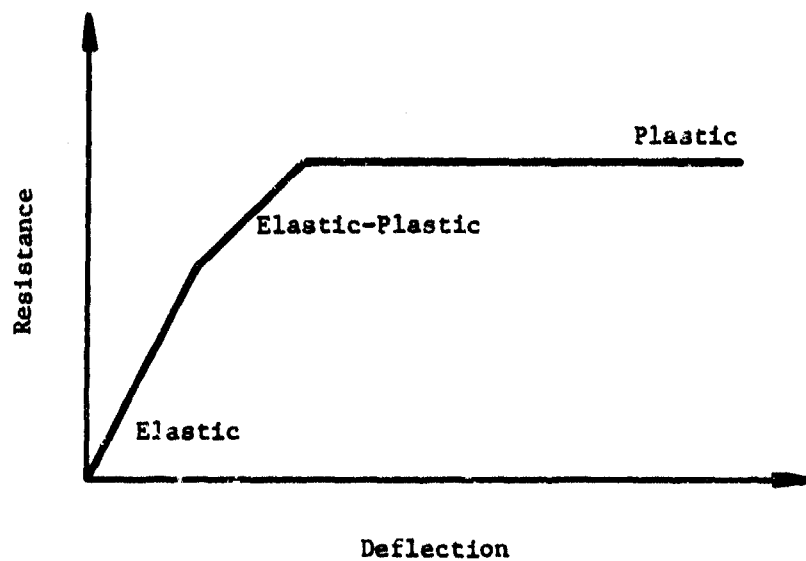


Figure 7. Force-Deflection Relationship

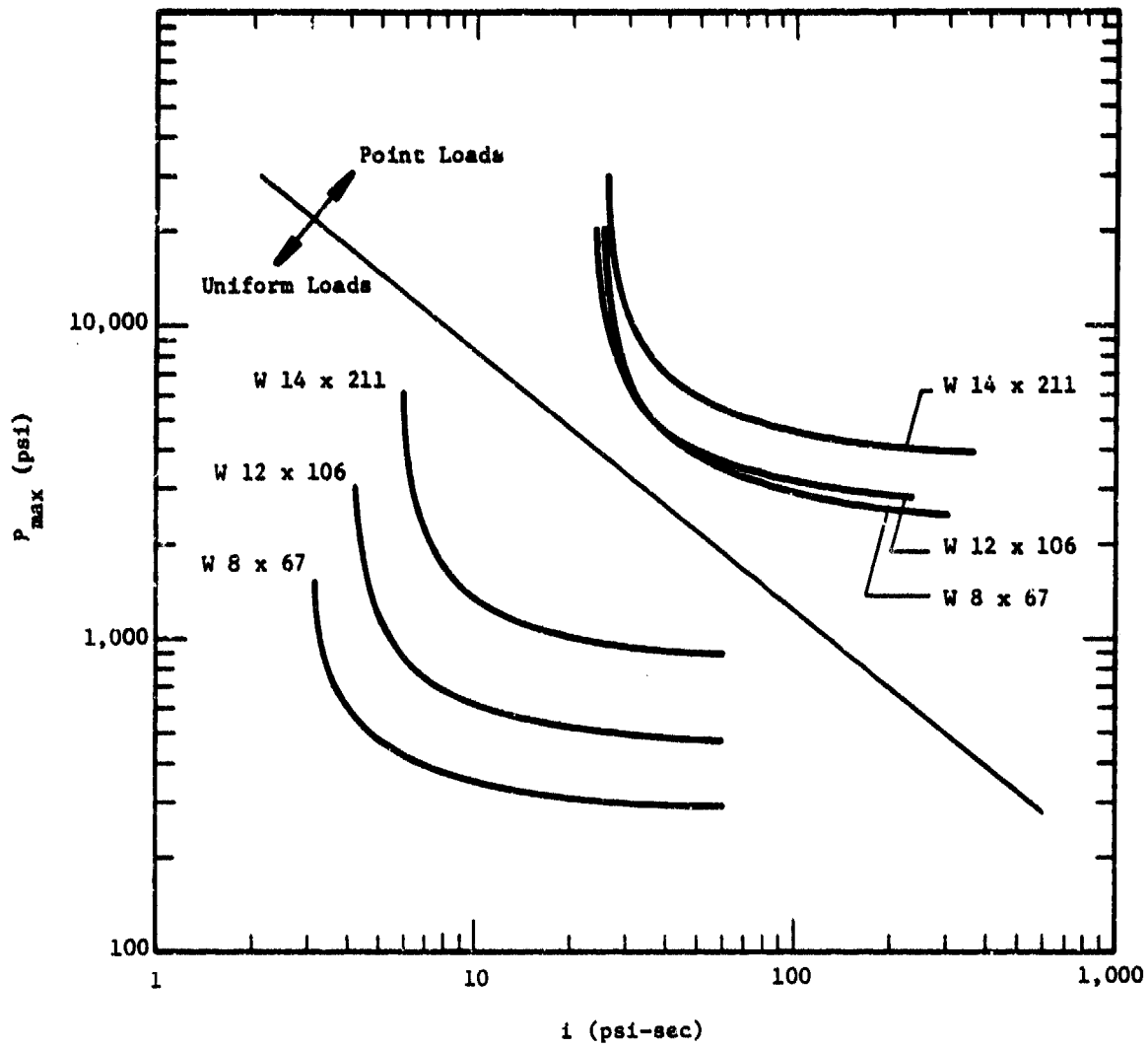


Figure 8. P-I Diagrams for Strong Axis Bending of Steel Columns

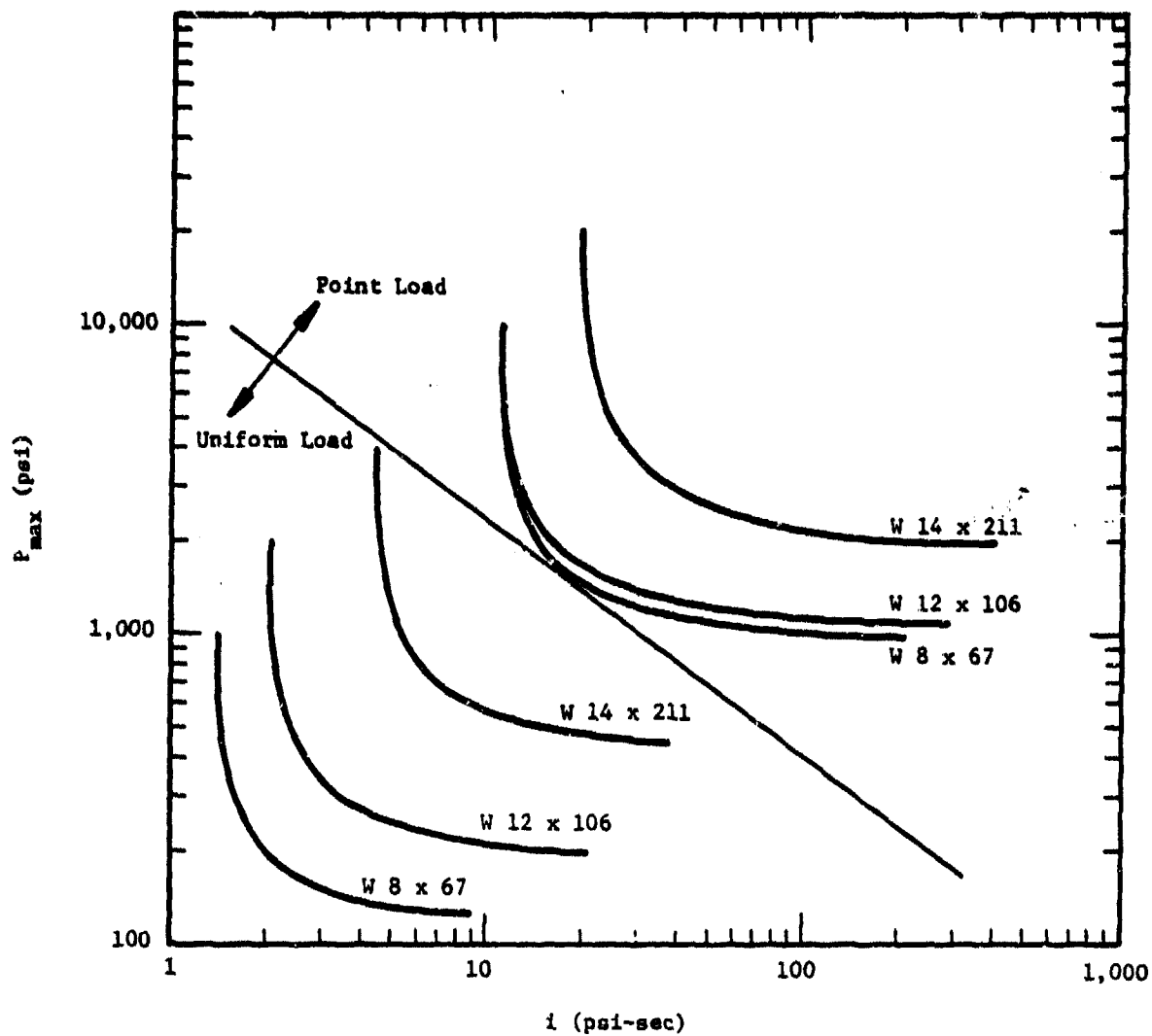


Figure 9. P-I Diagrams for Weak Axis Bending of Steel Columns

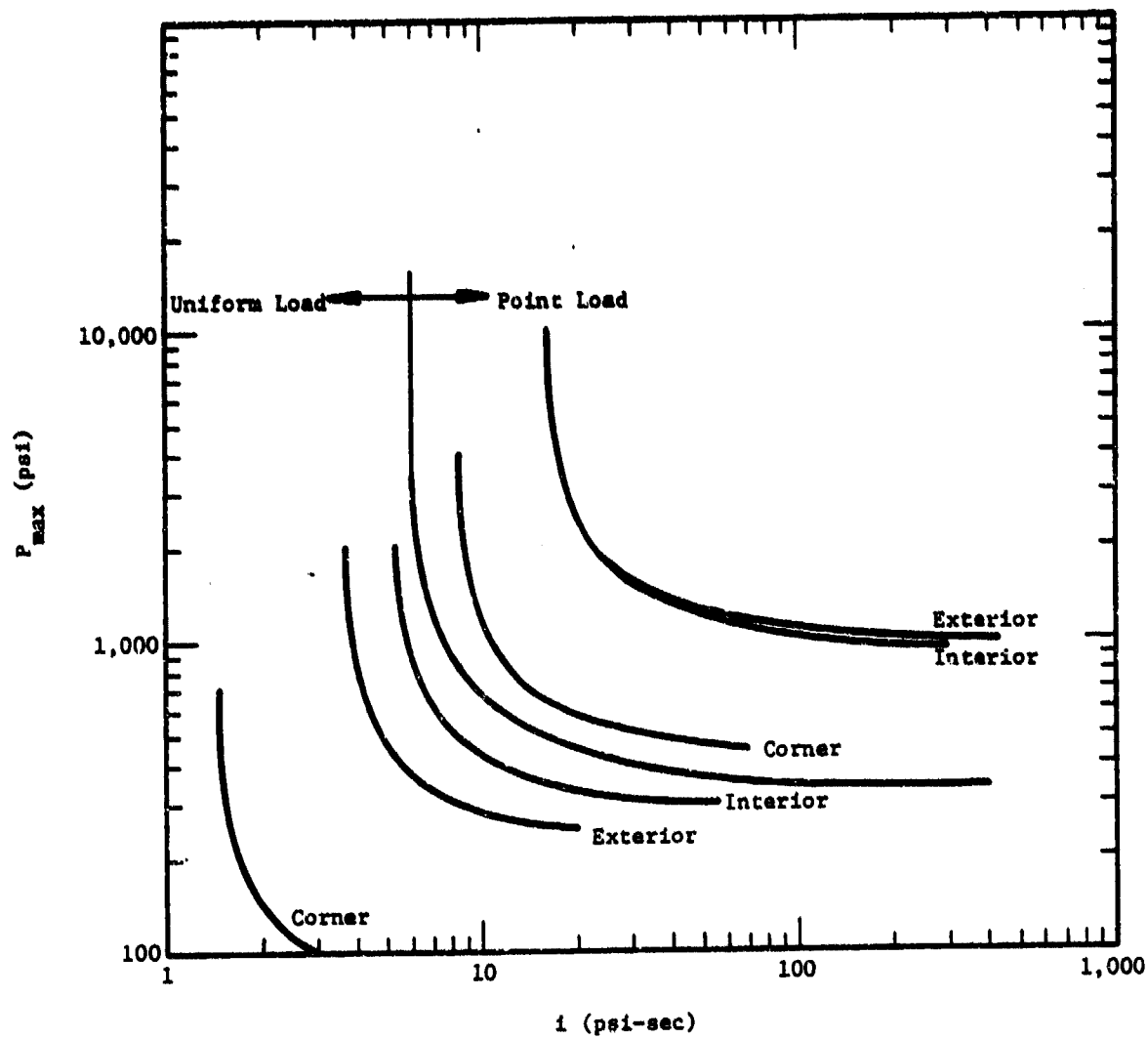


Figure 10. P-I Diagrams for Bending of Reinforced Concrete Columns

2. Determine required impulse, \bar{i} , and pressure, \bar{P} , by dividing by 1.75.
3. Select a charge weight, W , and determine $W^{1/3}$. Calculate the scaled impulse $\bar{i}/W^{1/3}$. Using blast overpressure/impulse versus scaled distance curves (such as those in Reference 5), determine the scaled distance, Z , ($\text{ft}/\text{lb}^{1/3}$) which produces the above scaled impulse.
4. Calculate the range for the charge, W , as $R = Z W^{1/3}$. If R is greater than 10 feet, the quantity-distance point is established. Repeat steps 3 and 4 for a number of points.
5. For \bar{P} , determine Z which produces this pressure. For this Z , determine ($i/W^{1/3}$) and set i equal to \bar{i} . This will permit calculation of $W^{1/3}$ and, hence, W . Determine R from $R = Z W^{1/3}$.
6. Use the Z above (where minimum impulse and minimum pressure are achieved) and increase W , determining the range from $R = Z W^{1/3}$. This portion of the curve provides minimum pressure and extra impulse.

These calculations are summarized in Figures 11 through 13.

Consider now the case of an explosive charge detonating close to the column at its mid-height. An approach similar to that above was used wherein, for smaller charges, the charge size and distance necessary to provide the minimum impulse from the P-I diagrams was determined, and the pressure checked to see that it exceeds the corresponding minimum pressure. The charge weight/distance pair providing the precise impulse and pressure was determined, and then charge weight and distance were determined for cases providing that minimum pressure and a greater impulse. It must be observed, however, that the nearness of the charge to the column and the very high intensity of the blast pulse are such that any reflections from room walls are insignificant and that there is no 1.75 factor which can reduce the required blast pressures. Results are displayed in Figures 14, 15, and 16.

A few comments on the results displayed in Figures 11 through 16 are in order at this time. The cusp in the curves for charge weight versus distance for the uniform loading case represents the transition from minimum impulse and a higher pressure, to the left of the point, to a higher impulse for the corresponding constant pressure to the right of the point. An arbitrary 10 foot minimum distance has been applied to approximately a uniform load over the 12 foot column. All of the curves for uniform loading represent the use of a 1.75 pressure-impulse factor caused by multiple reflections within a room. This factor is based on a roughly cubical room. While many of the distances would present great deviations from this idealized room shape, the reflections off the roof and floor would produce an amplification factor of some unknown magnitude. The use of the presented curves would be conservative from a designer's viewpoint since an amplification factor of less than 1.75 is practically assured.

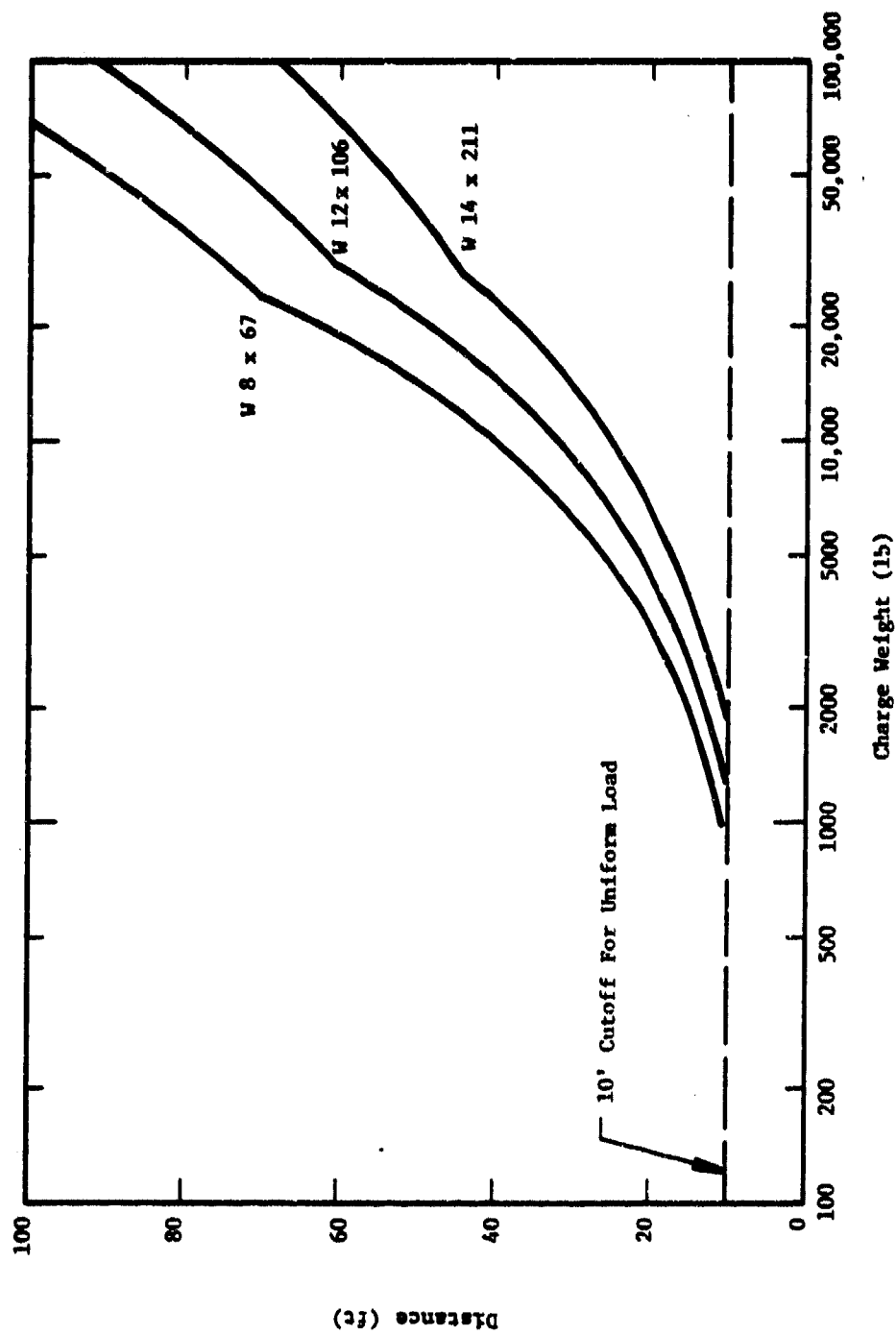


Figure 11. Charge Weight/Distance for Failure of Steel Columns Under Uniform Load - Strong Axis Bending

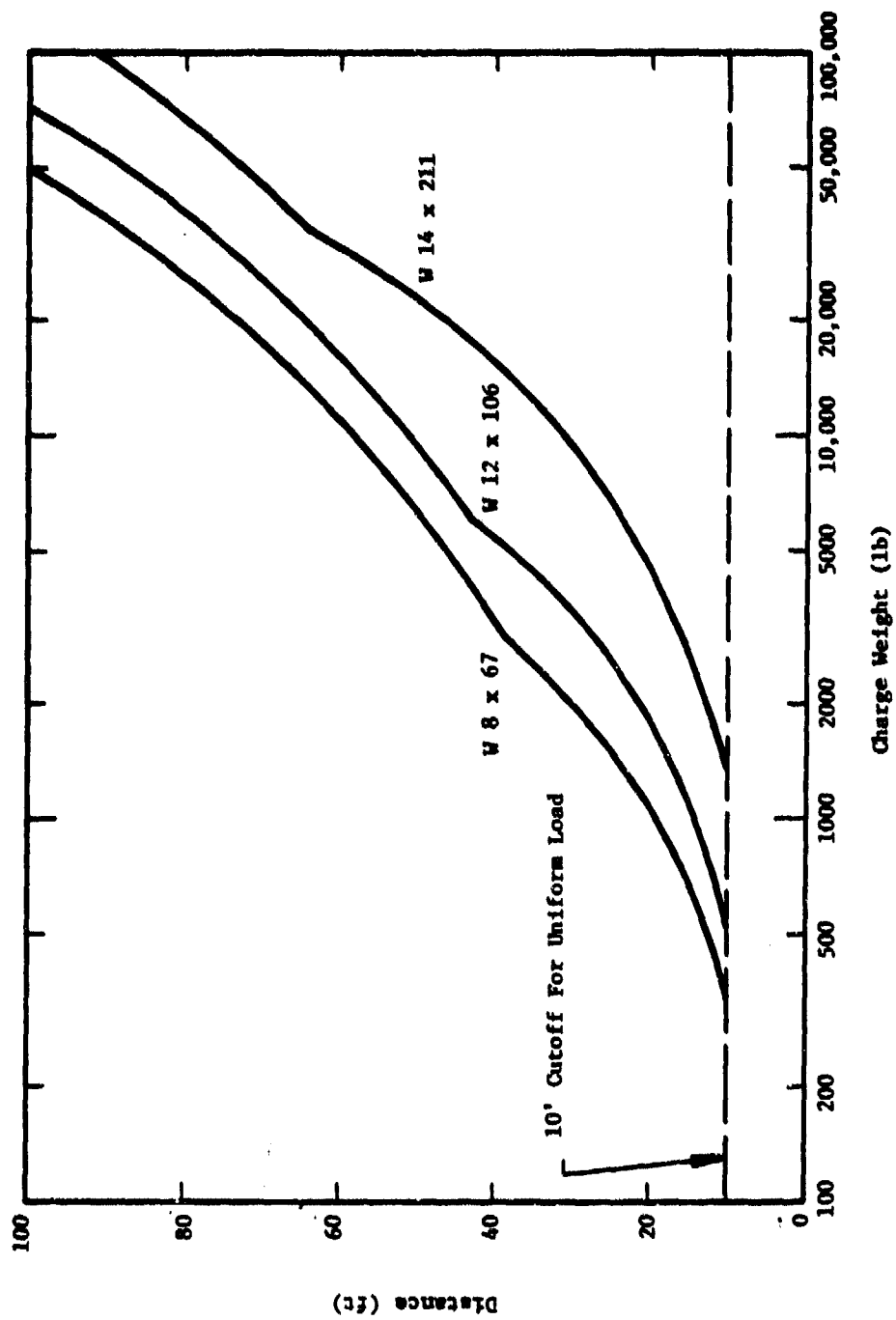


Figure 12. Charge Weight/Distance for Failure of Steel Columns Under Uniform Load - Weak Axis Bending

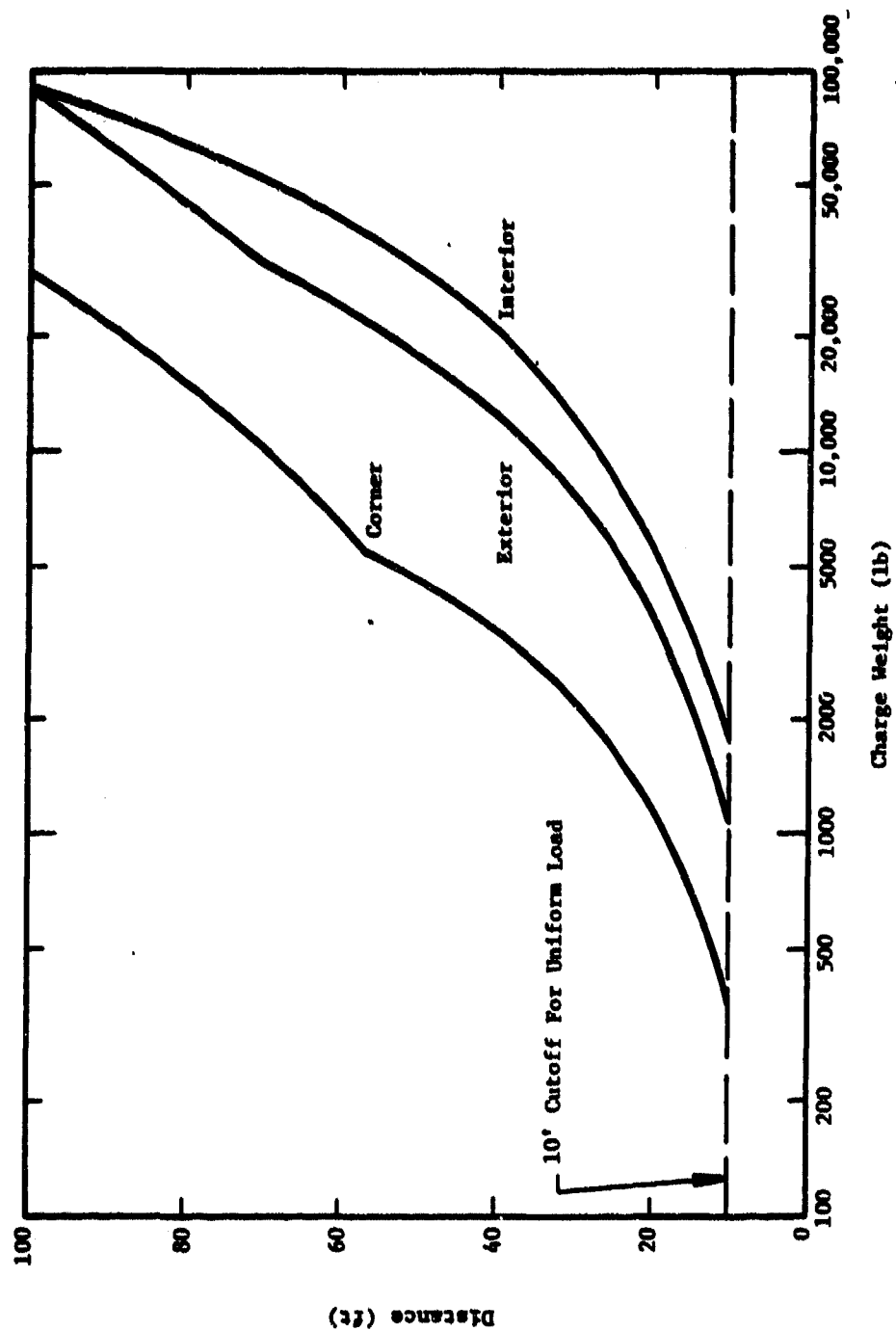
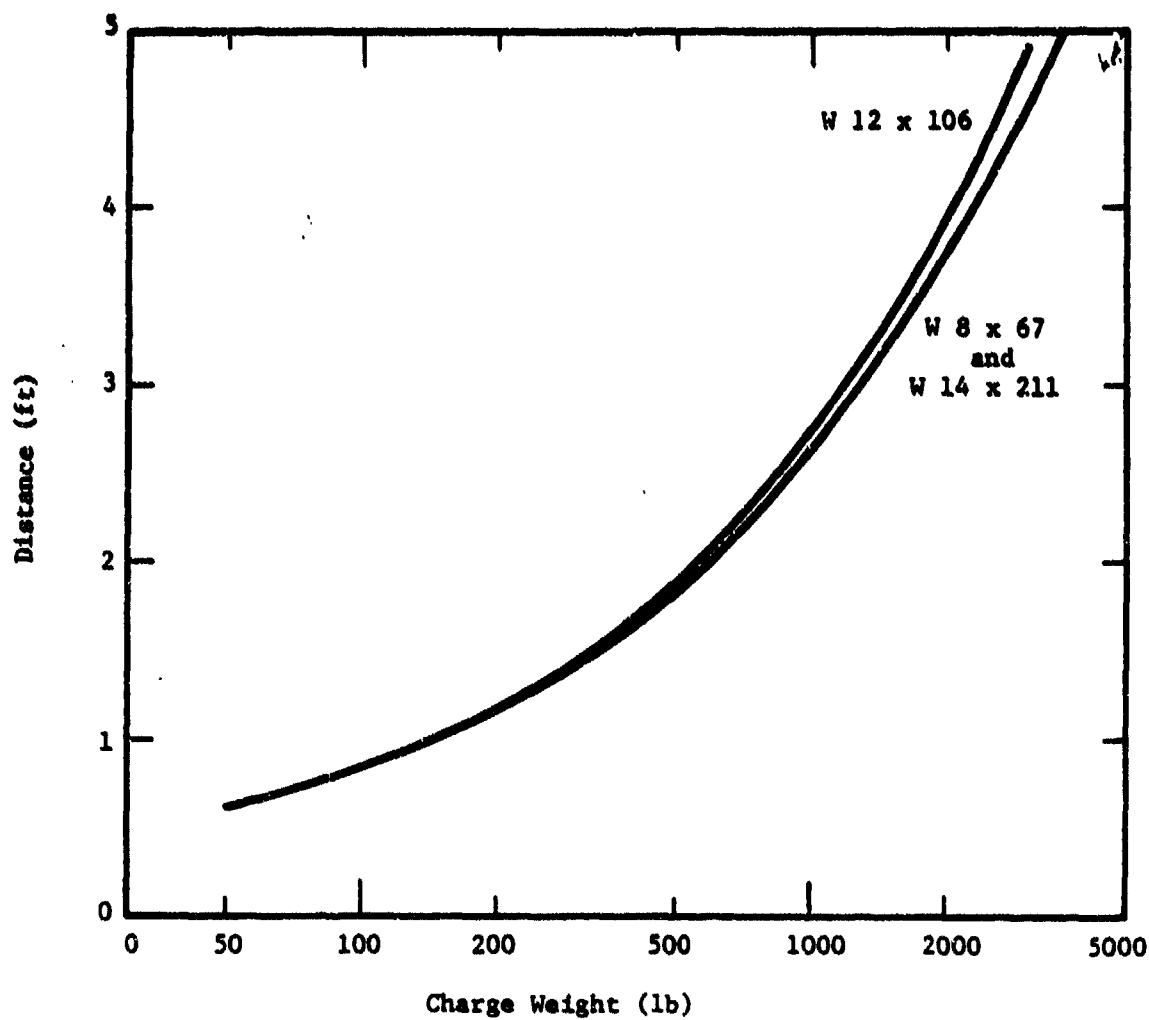


Figure 13. Charge Weight/Distance for Failure of Reinforced Concrete Columns Under Uniform Load



**Figure 14. Charge Weight/Distance for Failure of Steel Columns
Under Point Load at Mid-Height - Strong Axis Bending**

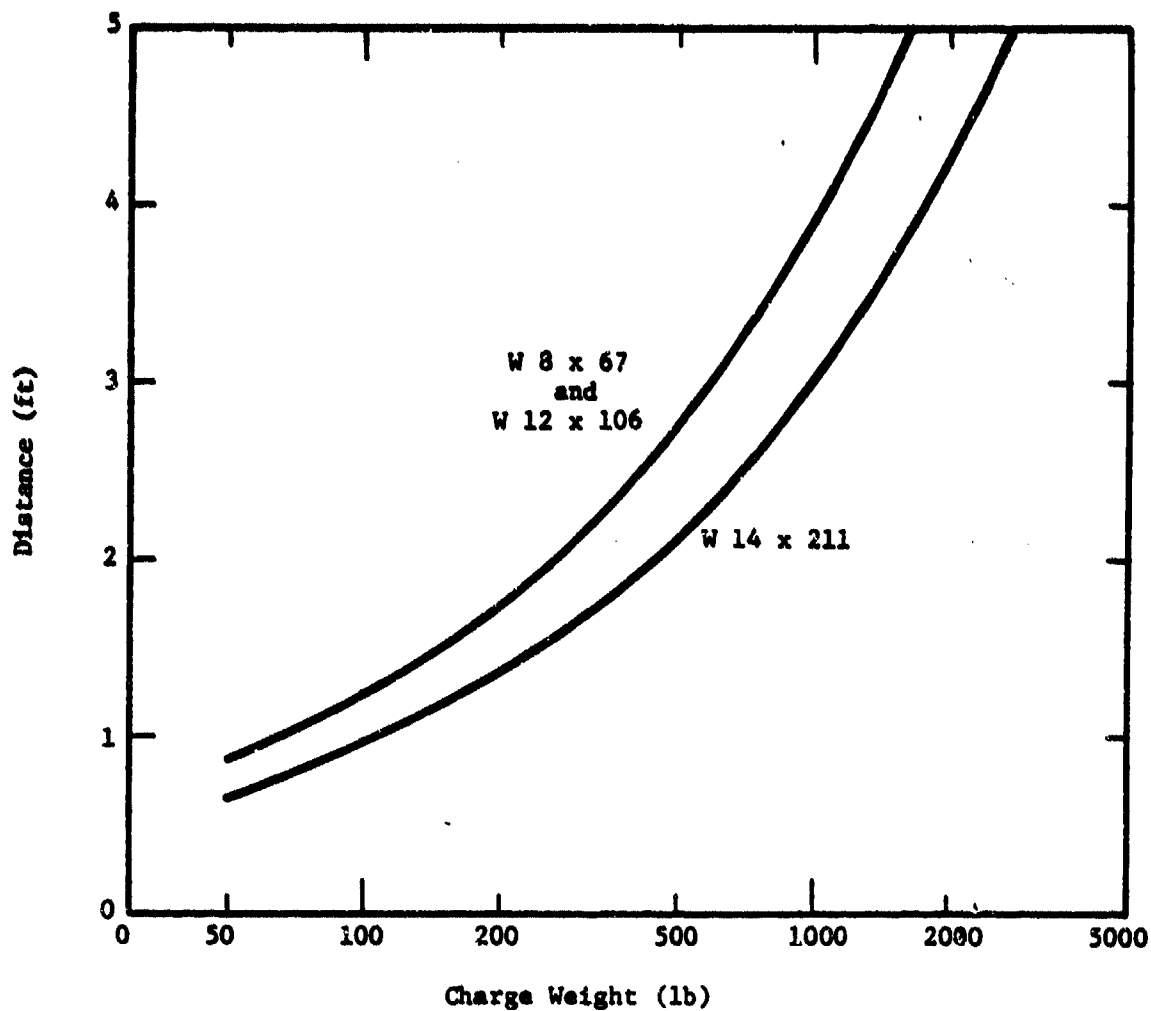


Figure 15. Charge Weight/Distance for Failure of Steel Columns Under Point Load at Mid-Height - Weak Axis Bending

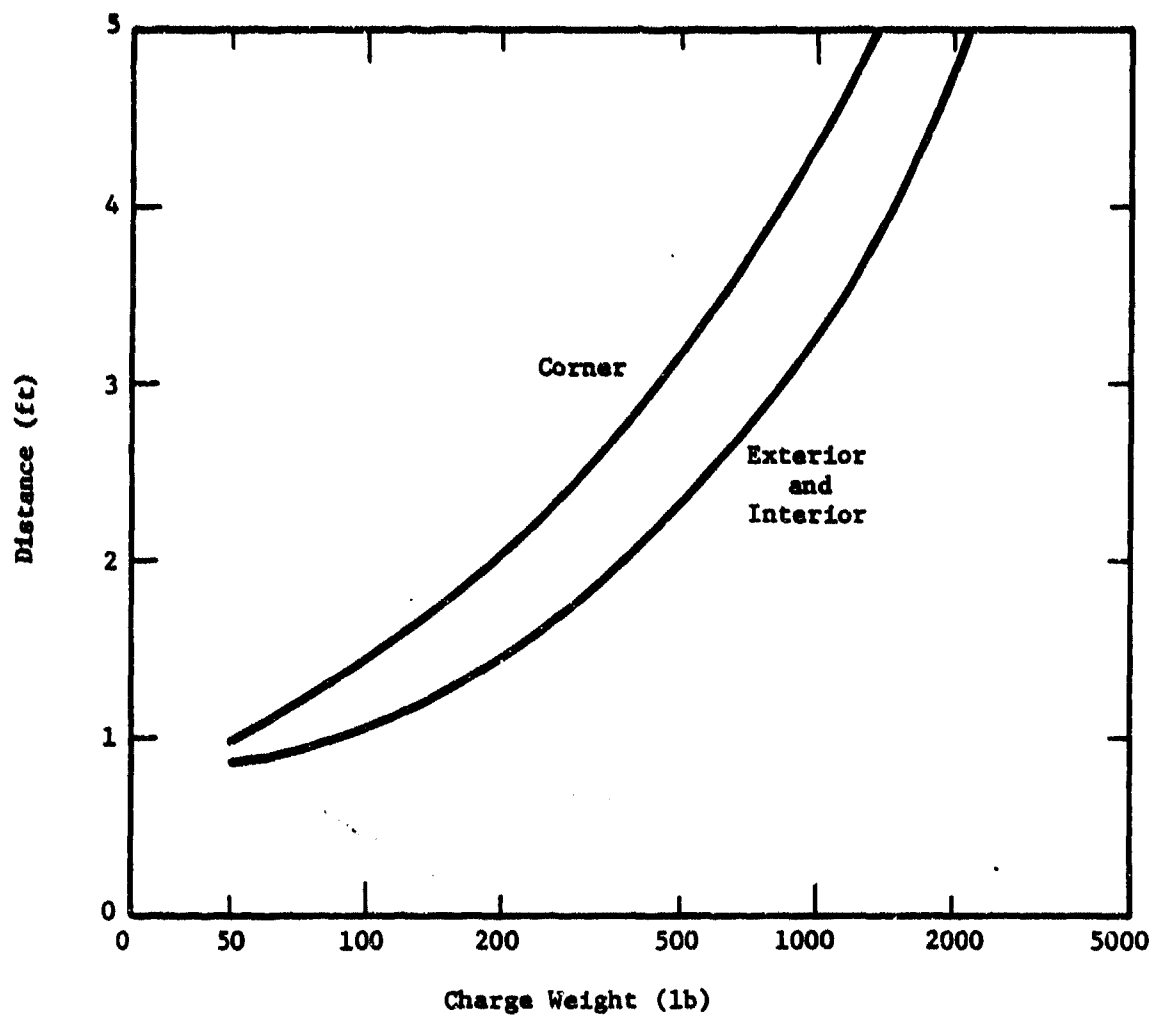


Figure 16. Charge Weight/Distance for Failure of Reinforced Concrete Columns Under Point Loading at Mid-Height

The charge weight/distance curves for the point load case (Figures 14, 15, and 16) have an arbitrary upper standoff distance of five feet to represent the end of point loading and a transition to uniform loading. If the actual loading on the entire column were considered, the curves in these figures would shift downward for distances greater than one or two feet.

APPLICATION OF THE RESULTS

While the numerical results presented above are strictly applicable to only six certain cross-sections and loading cases, the procedures used can be applied to any similar situation. The magnitudes of the charge weights and distances can also serve as indicators of similar values for other columns. These applications are explained below.

Consider first the design of a multi-story structure whose first floor is to be used as an explosives handling area. The charge weight versus distance curves of Figures 14 through 16 could be used to prescribe how close explosive charges can be placed or carried near the columns. For example, a 200-lb charge should not be placed any closer than 1.5 feet to a corner reinforced concrete column (see Figure 16). This same 200-lb charge presents no collapse-causing danger in a uniform load case.

The critical deformations calculated earlier can also be thought of as rotations rather than deflections (see Figure 2). Table 5 summarizes these rotations. Current design practice for accidental explosions, as contained in TM 5-1300 [6] indicates that partial failure will occur at a support rotation of 12° . This criterion of 12° does not consider any axial loads while Table 5 indicates collapse of the columns at rotations of from 4.8° to 9.9° . Clearly, structural loads should be considered in blast-resistant design.

Consider now some military implications of the calculational results. An 8-inch artillery shell (M106) contains less than 40 pounds of high explosive. As a point-load source, assuming that the casing does not reduce the blast effectiveness, the shell must be less than 12 inches from the columns at their mid-heights. Since there is no reliable way to detonate a shell at this location, the round would have to hit the column. Since the widest member considered here is only 22 inches wide, the likelihood of a hit, and consequently the likelihood of severe structural damage to a framed structure, is very small.

A 2000-lb bomb, such as the Mk 84 with 945 pounds of explosive, is capable of penetrating concrete roofs and, once inside a building, poses a very severe threat to the structural frame. In a uniform-loading mode, this explosive size has a damaging distance of from around 10 to almost 20 feet for the different columns and orientations studied. A 500-lb bomb, such as the Mk 82 with 192 pounds of explosive, would have limited capability in a uniform-loading mode and would have damaging distances of from 1.1 to 2.0 feet as a point-load source.

Table 5. Critical Deformations Expressed as Rotations

<u>Column Designation</u>	<u>Bending Direction</u>	<u>Critical Deformation (inches)</u>	<u>Rotation (degrees)</u>
W 8 x 67	Strong	11.07	8.7
W 8 x 67	Weak	6.05	4.8
W 12 x 106	Strong	12.20	9.6
W 12 x 106	Weak	7.08	5.6
W 10 x 211	Strong	8.46	6.7
W 14 x 211	Weak	9.31	7.4
R. C. Corner	—	6.90	5.5
R. C. Exterior	—	10.73	8.5
R. C. Interior	—	12.60	9.9

An explosive charge placed in our typical structure by a terrorist could have its damaging effects assessed using either the point or uniform loading curves as appropriate to the charge location. If the charge is in the center of a room, for example, and the figures predict structural collapse, one approach to limiting this damage could be removal of the nonload-bearing room walls to eliminate the 1.75 pressure-impulse amplification factor included in the uniform load curves. If an explosive charge, which is to be disarmed by EOD personnel, poses a collapse threat to a column, temporary shoring could be installed to support the structural loads in the event of a detonation.

The results of the calculations presented here can also be used in accident or post-attack investigations. An example of this application can be found in the attack on the embassy in Beirut in April 1982. An explosive-laden truck was driven into the embassy compound and detonated, removing many of the structural supports and toppling the multi-story structure. Assume

that the structural design was equivalent to the corner reinforced concrete column used here. Since the detonation was allegedly outside of the structure, the 1.75 pressure-impulse amplification factor cannot be used. The minimum impulse from this member's P-I diagram (Figure 10) is 1.48 psi-seconds with a minimum pressure of 500 psi. Table 6 contains a listing of explosive weights and distance combinations which will satisfy these requirements. Suppose now that the truck was loaded with 5000 pounds of explosive. Table 6 indicates that this charge weight would have to be within 30.8 feet of each exterior column to cause their collapse. Photographs of the toppled structure indicated that many of the interior columns were also destroyed, indicating that other factors, such as pre-emplaced cutting charges on the columns, may have been involved.

Table 6. Explosive Weight/Distance for Corner Reinforced Concrete Column

<u>Explosive Weight</u> <u>(lb)</u>	<u>Distance</u> <u>(feet)</u>
500	8.3
1,000	12.3
2,000	18.3
4,000	27.0
5,000	30.8
7,000	37.3
10,000	47.4

SUMMARY

This paper has presented a methodology for investigating blast effects on structural columns. This procedure has been followed on a typical urban structure and the effects quantified. Applications of this methodology to both design and post-event investigation have been outlined and qualitatively demonstrated.

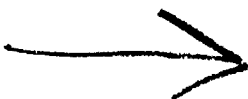
ACKNOWLEDGEMENTS

This paper is based upon work performed under Contract Number DAAK11-81-C-0042, "Evaluation of Indirect Fire Munitions for Use in Built-Up Areas," with the U. S. Army Human Engineering Laboratory, Aberdeen Proving Ground, Maryland. Technical Monitor for USAHEL was Ms. Brenda Thein and I wish to acknowledge her support, and that of Mr. Elsworth Shanks, in the publication of this paper.

REFERENCES

1. "Building Code Requirements for Reinforced Concrete (ACI 318-63)," American Concrete Institute, June 1963.
2. "Manual of Steel Construction," Sixth Edition, American Institute of Steel Construction, 1967.
3. Biggs, John M., Introduction to Structural Dynamics, McGraw-Hill, 1964.
4. "Design of Structures to Resist the Effects of Nuclear Weapons," U. S. Army Corps of Engineers Manual EM 1110-345-415, 1957.
5. Baker, W. E., Westine, P. S., Kulesz, J. J., Wilbeck, J. S., and Cox, P. A., "A Manual for the Prediction of Blast and Fragment Loadings on Structures," DOE/TIC-11268, November 1980.
6. "Structures to Resist the Effects of Accidental Explosions," Department of the Army Technical Manual TM 5-1300, June 1969.

AD P000462



LIGHTNING WARNING SYSTEMS

FOR

EXPLOSIVE OPERATIONS/FACILITIES

by

Mitchell A. Guthrie
Naval Surface Weapons Center
Code N42
Dahlgren, Virginia

✓

ABSTRACT

This report presents a review of lightning warning techniques with emphasis on explosive facilities and operations. An explanation of how each technique is used to detect the presence of conditions that can lead to these discharges, with the advantages and limitations of these techniques is given. In addition, an attempt is made to show how the lightning detection hardware can be incorporated into a facility's Hazardous Weather Plan.

↖

I. INTRODUCTION

Lightning can pose a severe safety hazard during explosive manufacturing and handling operations due to very strong electric and magnetic fields that are produced. Each of the services of the Department of Defense recognize this threat and require that explosive operations be curtailed at the approach of a thunderstorm. However, little guidance is given to the responsible party in determining when a thunderstorm is about to appear over his facility. In response to this problem, the Naval Sea Systems Command (NAVSEA 04H) has tasked the Naval Surface Weapons Center to investigate the current state-of-the-art in lightning detection technology and determine the effectiveness of each technique in applications involving explosive operations. This paper is a preliminary report of the information gained from the first phase of the program. It will review current lightning detection techniques available to explosive facilities and describe how each technique can be used to provide an advance warning of thunderstorm activity.

LIGHTNING DAMAGE MECHANISMS

The protection of a structure from the effects of lightning is based on statistical considerations of key lightning parameters. Even though facilities that house explosive materials are well protected, it is often not economically feasible to provide complete (100%) protection even to a "one-of-a-kind" facility. For this reason, it is essential to have an advance warning of lightning activity to terminate all explosive operations, or to evacuate all non-essential personnel from the area when termination of operations is not practical.

Lightning damage mechanisms are both mechanical and electrical in nature. The heat produced in the lightning channel by return stroke currents, which can reach 200 kA (200,000 amps), is adequate to burn holes in metal plates at the attachment point, fuze wires, burn through insulators such as glass, and cause explosions in masonry and trees due to the rapid expansion of trapped moisture. The 30,000°K temperatures generated in the channel produces pressures of over 400 psi. The expansion of the channel produces a strong cylindrical shock wave whose pressure decreases with the square of the distance from the channel, until it becomes thunder. In addition, the return stroke currents produce mechanical forces which can crush metallic conduits, pull wires from walls, and arc through insulating materials. These mechanical effects are generally associated with a direct lightning strike and typically result in much physical damage at the point of attachment.

In contrast to the mechanical damage mechanisms, the electrical damage mechanisms can also be caused by distant lightning. Each lightning stroke produces an electromagnetic wave due to the rapidly changing return stroke current. This electromagnetic pulse induces currents in closed loops of wire and exposed conductors such as overhead power lines, telephone lines, instrumentation lines, and detonator leads. The resulting surges can cause severe damage due to arcing if not properly protected.

With the advent of plant modernization came the increased use of solid-state electronics in explosive operations. These electronic devices are much more susceptible to transient over-voltages and surges, requiring much less energy to cause catastrophic failure. The use of devices of this type in

manufacturing facilities where an immediate shutdown is not practical, requires that a programmed shutdown be initiated well before a thunderstorm reaches the facility. However, equally important are the economic considerations due to a shutdown when no lightning hazard exists.

The primary task of the Thunderstorm Hazards to Ordnance Research (THOR) program is to determine when explosive operations should be curtailed due to lightning hazards and define the warning levels adequate for each type of warning technique. This is a very complex problem and will take the reduction of years of lightning detection data from differing geographical locations.

WARNING REQUIREMENTS

The first step in selecting a warning device is to determine how much advance warning is required. As stated earlier, lightning can create a hazardous condition well before it reaches the location of the explosive operation. In addition, the spatial separation of successive strikes is about 3km (2mi.) with separations of up to 10km (6mi.) recorded.

The amount of warning time required from a lightning detection system will vary considerably from facility to facility. The following factors influence the amount of warning time necessary:

1. Type of operations being conducted and the sensitivity of the ordnance being handled in that configuration -

For example, a missile in its "all-up" configuration with electrical out-of-line devices is much less sensitive than a detonator with its firing leads attached. In addition, the sensitivity of electronic control systems must also be considered in modern manufacturing plants where an immediate shutdown introduces an unacceptable hazard.

2. Length of time required to terminate operations -

Explosive operations that require only minutes to terminate need less sophisticated warning systems than will a manufacturing plant that may require an extended period to complete a programmed shutdown.

3. Schedule criticality -

Sites with little incidence of lightning activity can afford to be much more cautious in terminating operations than a site that will experience greater than 60 thunderstorm days per year. For operations whose scheduling is critical, the early warning of lightning activity is a critical problem.

4. Location of operations -

The orographic effect due to the location of the facility is often critical in determining the type of storm warning necessary. Mountains and large bodies of water often provide some of the conditions necessary for the development of

thunderstorms. Facilities near orographic features such as these may find a larger number of storms building directly over their facility than would a plant in a flat, open area. Storms also tend to follow these features in terrain during their normal movement. In addition, the geology of the area can be important. Lightning has been observed striking in a valley just below cliffs that are composed of high resistivity earth.

5. Typical storm characteristics -

An experienced observer at an ordnance facility can often forecast the onset of a thunderstorm because of the years of observation of the characteristics of these storms. Some of these characteristics are the type of storm normally experienced, typical direction of speed of storm movement, typical times of day of storm occurrence, and normal ambient conditions leading to storm. The experienced observer can use the observed deviation in these characteristics to see how useful each can be when trying to decide whether to terminate operations or not.

The relative importance of each of these factors will vary with each individual operation. In addition, some operations may have some factor that influences the type of warning system necessary that is peculiar to that particular operation only. Therefore, before selecting a warning system each operation performed at the facility should be considered.

II. LIGHTNING WARNING TECHNIQUES

It is not yet possible to make accurate lightning forecasts for any given location, but it is possible to detect the occurrence of distant lightning and detect the conditions that can lead to lightning, and thus a nearby discharge. Some detection techniques are still primarily research tools and are not yet advanced enough to be used reliably as a warning device. An example of these are the detection of the optical and audible spectrum of lightning. Research in these areas have not been directed toward lightning location except in crude form. For example, the difference in propagation time between the light and sound waves produced by lightning is used today at many facilities for locating the distance from a storm. AFR 127-100 states that a storm is "in the vicinity" when the difference in time between seeing the lightning flash and hearing the thunder (referred to as flash-to-bang time) is 15 seconds or less, which places the flash about 3 miles away. However, as reported earlier, the spatial difference in successive flashes can be as much as 6 miles. Moore, et. al. (1982), suggests that if the flash-to-bang technique is used for lightning location, at ordnance facilities, the storm should be considered in the vicinity when this time reaches 30 seconds or less.

The flash-to-bang technique has some serious limitations. Uman (1969) reports a case where thunder was not audible from a storm only 5 miles away. If the flash-to-bang technique is used, it is imperative that the responsible authority also know the speed of the movement of the storm at the time it approaches the vicinity of the facility. This speed can vary greatly from storm to storm, averaging 10 to 45 miles per hour, and even during the same storm. Although thunder can be heard from as much as 15 miles away, the operations carried out at ordnance testing facilities can mask this thunder until the storm is already "in the vicinity".

The flash-to-bang technique is prone to false alarms, also. Due to irregularities in the velocity and direction of storm movement, it is impossible to determine whether or not the storm will pass over the facility. This technique therefore is limited to applications at facilities which have few thunderstorm days per year and the scheduling of operations is not critical.

WEATHER FORECASTS

Local radio and television weather forecasts are generated with information from the National Weather Service, based on the statistical analysis of many meteorological inputs. These forecasts only predict the probability of a thunderstorm occurring during the day in the given forecast area. This does not mean that the storm will pass over the facility. This method is unreliable when used alone due to the expansiveness of the forecast area and the lack of a defined time when the storm will occur.

NATIONAL WEATHER SERVICE

In addition to the climatological data supplied by the weather service, weather radar is often used to determine the location of thunderstorm activity. Kasemir (1976) reported that it is probably the temperature rather than altitude that determines the onset of electrification. However, the higher the altitude a cloud reaches, the lower the temperature becomes.

CHARGE DISTRIBUTION OF TYPICAL CLOUD CELL

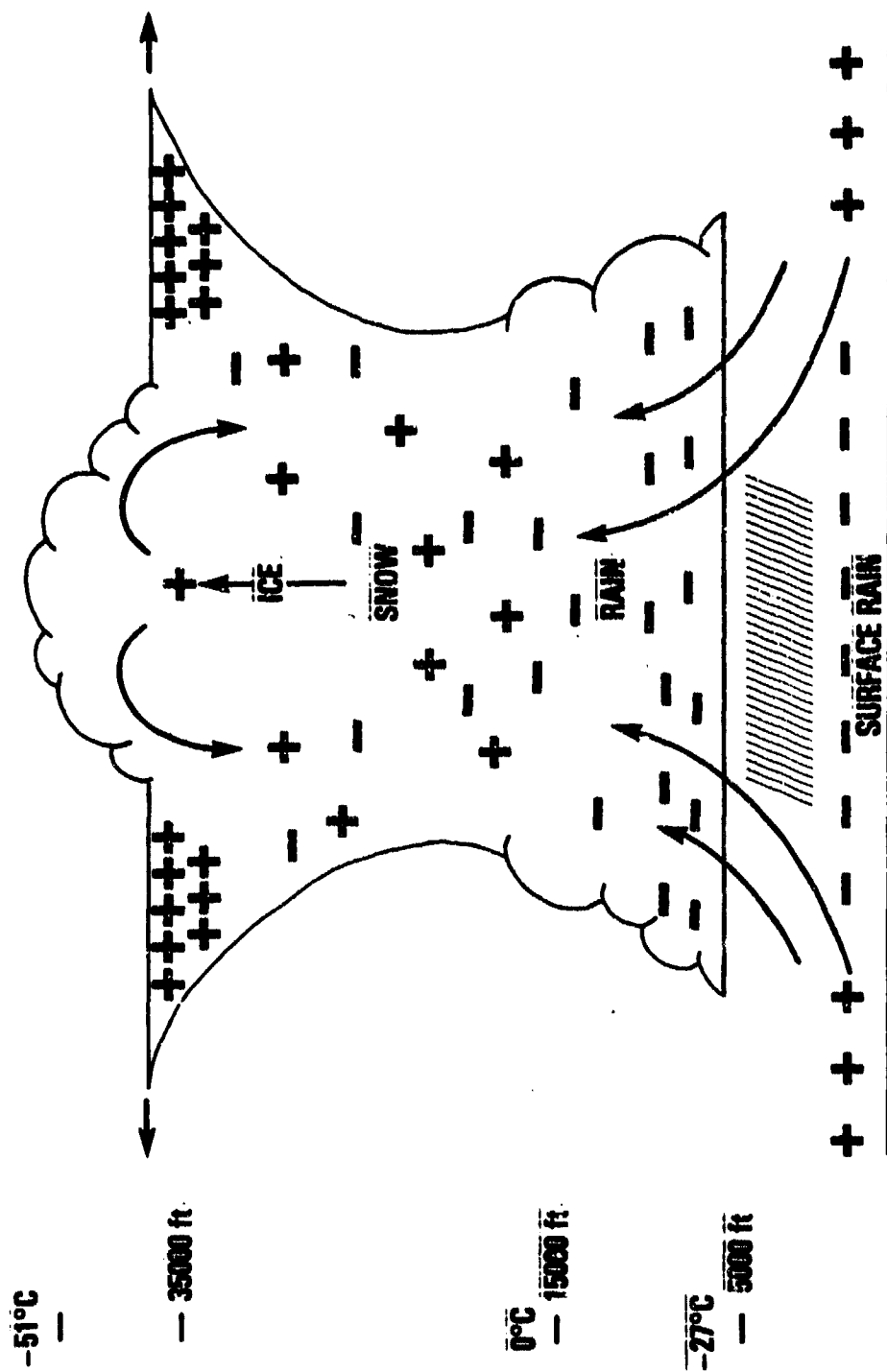


Figure 1

EXAMPLE OF RECORDING OF ΔE FIELD DETECTION INSTRUMENT

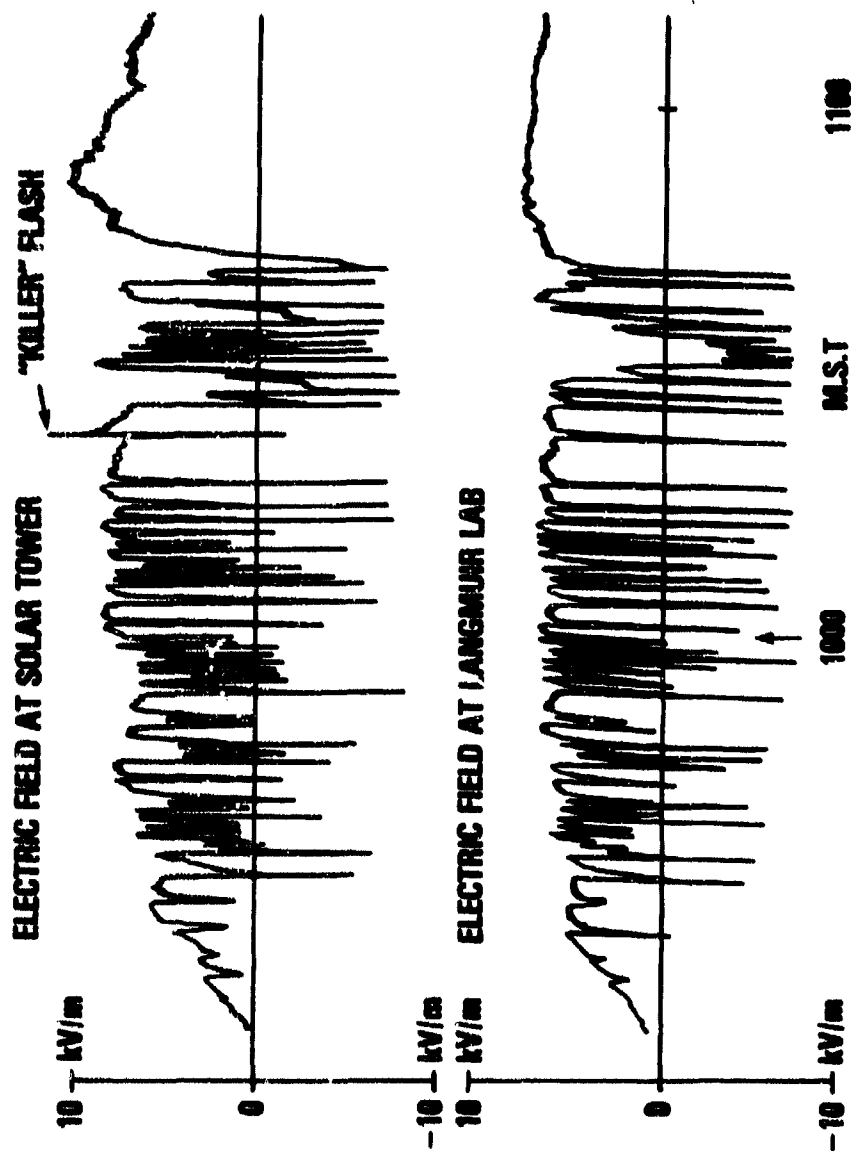


Figure 2 (courtesy of C. B. Moore
New Mexico Institute of Mining and Technology)

Cumulus clouds with tops below 16,000 feet do not contain electric fields adequate to generate cloud-to-ground lightning. When these cloud altitudes reach 25,000 feet or more, the fields in the cloud reach adequate levels to generate breakdown.

The National Weather Service radar displays can accurately identify the precipitation center of a cloud and determine from the density and altitude of the radar reflection whether this cloud is likely to contain lightning activity. However, Burger (1967) cites events showing that detonation of explosive devices can occur as much as 5 miles from the precipitation center of a storm. In addition, the radar data available is approximately 30 minutes old before it is released and the position of the storm could be as much as 15 to 20 miles off from the actual location by the time the information is used.

ELECTRIC FIELD MEASUREMENT

Under fair weather conditions, the electric field at the surface of the earth is generally +100 V/m. As a thunderstorm begins to build, the electric field gradient starts to increase. This change in the static electric field can be detected and then used to determine when local conditions are adequate for lightning to occur.

Changes in the static electric field can signal the approach of a storm. Figure (1) illustrates the charge distribution of a typical thunder cloud cell. As a charged cell approaches, the fair weather field becomes masked by the positive charge in the top of the cell, increasing the amplitude of the electric field gradient. As the cell gets closer, the negative charge at the base of the cell becomes more prominent and the electric field begins to change polarity. As the cell moves directly overhead, the electric field reaches its maximum negative value. Once the cell passes the measuring point the field again reverses polarity and finally relaxes to its fair-weather value.

FIELD MILL

The "field mill" is the most accurate and widely used device to measure the static atmospheric electric field. It measures the strength and polarity of the local electric field by having it alternately charge and discharge an electrode, which produces an alternating current whose amplitude is proportional to the magnitude of the external electric field. The information produced by the field mill is normally output on a strip-chart recorder to observe the onset of cloud electrification and track the passage of a storm.

In addition, the fast response time of the field mill allows it to detect the electric field changes produced by lightning. Figure (2) shows the output of a field mill for a storm recorded by C. B. Moore on 7 August 1979. The sharp discontinuities in the trace are due to lightning. The magnitude of the field change due to this lightning is somewhat proportional to the distance from the discharge. Most field mills marketed today use a combination of the static and dynamic electric field measurements to determine whether a lightning hazard exists.

The field mill can clearly indicate the presence of electrically disturbed weather patterns, but it has limitations. The device can only measure the atmospheric disturbances for the area immediately overhead, which can limit its warning time. In addition, it is easily influenced by the presence of space charge due to corona from nearby objects which can mask a much larger field strength aloft. To illustrate, Kasemir (1976) has detected lightning discharges when the surface field was only 500 V/m even though point discharge does not normally occur at field strengths below approximately 3000 V/m. Finally, the field mill is a sensitive research tool that is difficult to interpret when more than one storm cell is present, requires maintenance at periodic intervals, is sensitive to site location, and a go/no go criteria for alarm is difficult to establish. However, used in an array with the go/no go criteria specified in NAVSEA OP-5 (2000 V/m), the field mill can be a valuable tool for a safety director in evaluating the development of hazardous conditions due to lightning.

CORONA CURRENT

The corona current detector is the simplest measuring technique that can be used to determine the onset of a thunderstorm. As discussed earlier, strong electric fields are generated in thunderstorms, however, these fields are rarely observed to reach values over 15 kV/m over land surfaces. This phenomenon is due to corona discharges that occur at the tips of trees, bushes, towers, and other sharp objects attached to the earth. The space charge generated by the corona creates a screening layer that reduces the magnitude of the electric field at the ground. Although this space charge can limit the effectiveness of a field mill due to this screening, its generation can be used to detect potentially hazardous conditions.

A sharp point raised some height above a ground plane (earth) causes an enhancement of the atmospheric electric field around the point. This discharge process is initiated in a small volume of air close to the tip. As electrons are accelerated in the field, collisions with gas molecules ionize these gas molecules which release more electrons. This process, called electron avalanche, continues until a corona discharge is produced to decrease the concentration of the local electric field.

The value of the corona current produced by the point depends on the strength of the electric field, the presence of other points in the area, height of the point, curvature of the tip, and local wind speed. Therefore, for a given wind speed, the corona current is directly proportional to the electric field strength.

Although simple to build and instrument, the corona current detector has limitations. The wind speed is very important when determining warning levels of corona current. In addition, the system is not responsive to field strengths of less than approximately 1000 V/m, resulting in little advance warning.

RADIOACTIVE PROBE

Radioactive probes can also be used to measure the atmospheric electric field. These probes can be designed to measure either corona currents or voltage potentials; although all devices available commercially measure only

the voltage potentials. In either case, the radioactive material (polonium or tritium) is used as a source of ionization. Though their response time is slow, the probes are reliable and accurate.

In contrast to the corona current detector, the radioactive probe is less reliable in calm winds than in strong winds. In addition, the radioactive source must be changed about once a year to maintain adequate sensitivity.

SPHERICS

A sudden change in current flow will produce an electromagnetic wave that can be detected from a considerable distance. The waves produced by lightning currents are capable of propagating thousands of miles even though the strength of the signal decreases with distance. It is estimated that over the surface of the earth there are approximately 100 flashes every second. These waves are trapped by the earth's atmosphere and form a continuous background of crackling noise (static) on all but the highest frequency bands. These radiated waves, called atmospherics or spherics, can be detected and used to determine the actual location of the lightning discharge.

FLASH COUNTER

The flash counter is a narrow-band receiver designed to detect the electromagnetic wave produced by lightning or the electric field change which results. The counter detects the flash, computes its range, and displays the number of discharges occurring in preselected ranges. The most popular ranges used are 100, 50, 25, and 10 miles. By observing the number of discharges per range, one can determine the distance of the storm from the site.

Counters that detect the radiated wave follow the relationship that the amplitude decreases linearly with distance. These counters have a greater range than those that sense electric field changes. However, the electrostatic field change decreases with the cube of the distance, resulting in greater accuracy in the decreased range.

The flash counter also has limitations. The range information is based on the theory that each discharge is of average intensity, although Berger (1975) and others indicate these values can vary greatly (7 to 10 dB standard deviation). In addition, nearby intra-cloud lightning may be detected as a distant earth flash. Although the counters do not indicate direction of storm movement, the device can be used effectively at facilities where storms do not generally build overhead and the mature storms moving into the area always come from the same direction.

AZIMUTH/RANGE LOCATOR

The location of distant lightning by using two crossed loops arranged at right angles is an old, well established technique. The system responds to a narrow band in the VLF frequency range. The range of lightning location is determined the same way as does the spherics flash counter. To determine bearing, the ratio of signal amplitudes are compared. A monopole electric field antenna furnishes polarity information to eliminate the 180° ambiguity in bearing. The resulting location is generally displayed as a point on a CRT. The technique is relatively simple and has been used in land-based

systems and in aircraft. Some variations of this technique use a wide-band amplifier tuned to somewhat higher frequencies to eliminate some problems caused by the reradiation of the magnetic field.

Although the conventional crossed-loop locator has an effective range of up to 200 kilometers (km), it is inaccurate at close ranges. Bearing errors have been known to exceed 20° at ranges of less than 150 km due primarily to the horizontal components of the electromagnetic wave and reradiation of the wave by metallic bodies, buried conductors, or the ionosphere. Krider, et. al. (1976) devised a wideband system that samples the magnetic field at its peak, where the lightning channel is most vertical. However, this system is still subject to bearing errors due to the reradiation of the wave which can be a problem at military facilities where security fences are used extensively.

CROSSED-LOOP TRIANGULATION

The accuracy of a crossed-loop location system can be enhanced greatly by using three or more antennas to locate the same flash. Figure (3) is a block diagram of a typical triangulation network. The range and bearing information from each of the antennas is fed to a central computer where the data is analyzed statistically and the ground strike location is determined and plotted on a CRT.

Lightning Location and Protection Inc., the manufacturer of the crossed-loop triangulation system, has developed software to try to reduce the effect of the reradiated waves. The system is used operationally by the Bureau of Land Management and several utility companies, and is also used as a research tool by many studying key lightning parameters.

The major disadvantages to this type of system is the cost and the criticality of antenna site selection. The optimum site for an antenna would be in a large field with no buried conductors or metallic objects nearby. Sites such as this are not common at most military facilities. However, triangulation networks now cover a large portion of the United States and in these areas use of the system could be economical.

TIME-OF-ARRIVAL TRIANGULATION

The time-of-arrival (TOA) triangulation network is identical to the crossed-loop network with the exception of the detection method used. In a TOA network, each antenna detects the spherical wave and labels the time the wave was received. The information from each antenna is transferred to the central computer where it is analyzed and plotted. The system operates in the VHF frequency band and is not affected by reradiated waves. Pierce (1977) states that this is a very powerful technique, but it has not been practical to implement in the past. Today's technology in electronics now allows the precise timing of the received signal and therefore very accurate lightning location over a large area. The major limitation of this system to date is that it is not a proven system as is the crossed-loop system, but preliminary evaluations show it to be promising. In addition, antennas for the TOA network are not site sensitive, which may be important at military facilities.

BLOCK DIAGRAM OF TRIANGULATION LIGHTNING DETECTION NETWORK

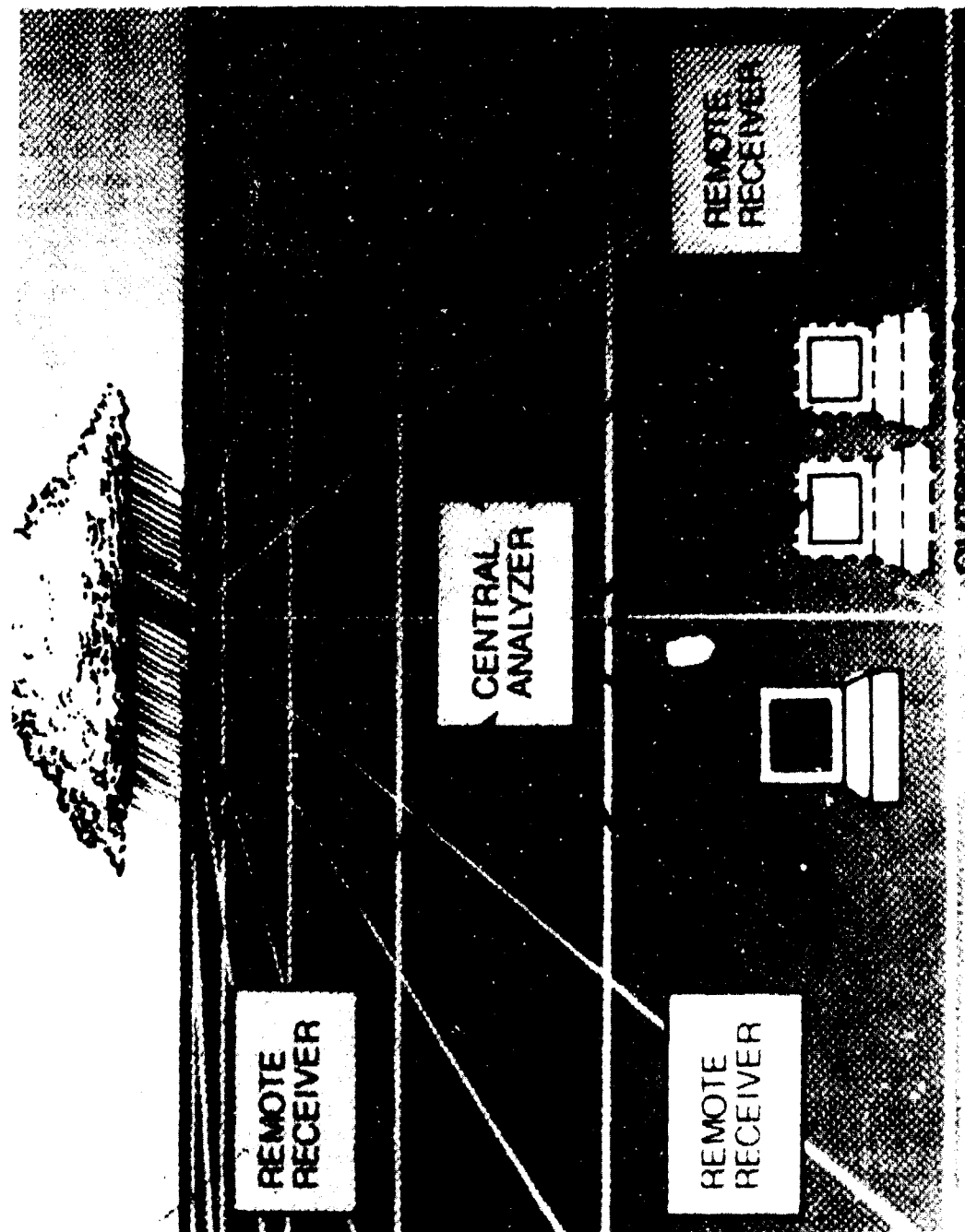


Figure 3 (Courtesy of Atlantic Scientific Corporation)

III. EVALUATION OF TECHNIQUES

The Bureau of Mines sponsored an evaluation of six lightning warning devices during the summer of 1979 because of their concern in using detonators in blasting operations. The results of the study were reported by Johnson, et. al., in the May 1982 Journal of Applied Meteorology. These results are summarized in tables 1 and 2.

Data were gathered from three locations which have different types of characteristic storms. As shown in these tables, the triangulation locator exhibited the best overall performance, although it is the most expensive to operate. In addition, the radioactive probe and field mill consistently gave 20 minutes or greater warnings, but both had high failure-to-alarm rates. In summary, no system was found to be ideal in all categories. A decision on the type of system required by a facility should be based on a tradeoff of the characteristics which are most important to the operations being conducted at the facility and the systems ability to meet these criteria.

TABLE 1

FRONTAL TYPE STORM SUMMARY

DEVICE	AVERAGE WARNING (min)	FALSE ALARM RATE (%)	FAILURE TO ALARM RATE (%)	ALARM RELIABILITY (%)	TIME TO CLEAR (min)
RADIOACTIVE	33	9	9	91	15
FIELD MILL	40	18	9	82	22
CORONA POINT	-20	27	55	73	-19
FLASH COUNTER	35	0	9	100	44
TRIANGULATION LOCATOR	21	0	9	100	5
AZIMUTH/RANGE LOCATOR	121	73	0	27	100

FROM BUREAU OF MINES EVALUATION

TABLE 2

CONVECTION TYPE STORM SUMMARY

DEVICE	AVERAGE WARNING (min)	FALSE ALARM RATE (%)	FAILURE TO ALARM RATE (%)	ALARM RELIABILITY (%)	TIME TO CLEAR (min)
RADIOACTIVE	28	0	10	100	9
FIELD MILL	27	0	15	100	9
CORONA POINT	-15	0	80	100	22
FLASH COUNTER	32	0	55	100	-10
TRIANGULATION LOCATOR	21	0	0	100	-4
AZIMUTH/RANGE LOCATOR	30	0	5	100	17

FROM BUREAU OF MINES EVALUATION, 1979

MOUNTAINOUS TYPE STORM SUMMARY

DEVICE	AVERAGE WARNING (min)	FALSE ALARM RATE (%)	FAILURE TO ALARM RATE (%)	ALARM RELIABILITY (%)	TIME TO CLEAR (min)
RADIOACTIVE	21	0	27	100	23
FIELD MILL	50	6	20	100	67
CORONA POINT	-20	0	83	100	40
FLASH COUNTER	-4	0	64	100	23
TRIANGULATION LOCATOR	20	0	0	100	0
AZIMUTH/RANGE LOCATOR	101	82	0	10	117

FROM BUREAU OF MINES EVALUATION, 1979

IV. SUMMARY/CONCLUSIONS

In summary, the major lightning detection techniques have been reviewed and their respective limitations discussed. No single system or single technique has been found that can reliably detect a mature storm moving into the area and a storm that may be building directly overhead. The field mill and radioactive probe were found to have promise, but were not 100% reliable. Although expensive to purchase and operate, the triangulation locator is the most sophisticated technique available, but cannot detect storms building directly overhead.

The optimum solution to the advance warning of potential lightning hazards seems to be a combination of techniques based on spherics detection and the electric field measurement. The selection of equipment should be based on actual detection requirements, frequency of lightning activity, scheduling criticality, and cost. At this time, it appears that the most reliable combination available would be a triangulation network for long range detection and tracking of mature storms, with a field mill array to detect the development of dangerous fields building directly overhead.

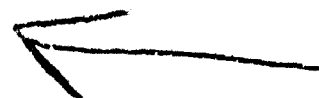
BIBLIOGRAPHY

- Anderson, R. B., "Measuring Techniques," Lightning, Volume 1-Physics of Lightning (edited by R. H. Golde), Academic Press, London, 1977.
- Barlow, J. S., Frey, Jr, G. W., and Newman, J. B., "Very Low Frequency Noise Power From the Lightning Discharge," Office of Naval Research, Contract No. N6-ONR-24311, September 1954, pg. 187-203.
- Berger, K., "The Earth Flash," Lightning, Volume 1-Physics of Lightning, (edited by R. H. Golde), Academic Press, London, 1977.
- Boggs, S. A., and Stone, G. C., "Fundamental Limitations in the Measurement of Corona and Partial Discharge," IEEE Transactions on Electrical Insulation, Volume EI-17, No. 2, April 1982, pg. 143-150.
- Brooks, M., and Ogawa, T., "The Cloud Discharge," Lightning, Volume 1-Physics of Lightning (edited by R. H. Golde), Academic Press, London, 1977.
- Burger, J. P., and Rost, D. L., "Preliminary Report of the Initiation of Various Types of Electroexplosive Devices by Induced Lightning," NTIS Report AD 827746, 1967.
- Chalmers, J. A., Atmospheric Electricity, Pergamon Press LTD, Oxford, 1967.
- Chauzy, S., and Raizonville, P., "Space Charge Layers Created by Coronae at Ground Level Below Thunderclouds: Measurements and Modeling," Journal of Geophysical Research, Volume 87, No. C4, April 20, 1982, pg. 3143-3148.
- Cianos, N., and Pierce, E. T., "Methods for Lightning Warning and Avoidance," SRI Technical Report, May 1974.
- Cianos, N., and Pierce, E. T., "A Ground-Lightning Environment for Engineering Usage," Stanford Research Institute, Technical Report TR-No.1.
- Dennis, A. S., and Pierce, E. T., "The Return Stroke of the Lightning Flash to Earth As a Source of VLF Atmospherics," Journal of Research NBS/USNC-URSI, Volume 68D, No. 7, July 1964, pg. 777-794.
- Department of The AirForce, AFR 127-100, "Safety Manual,".
- Department of Defense, MIL-HNDK-419, "Grounding, Bonding, and Shielding for Electronic Equipments and Facilities," Volume 1, 21 January 1982.
- Department of Defense, MIL-HNDK-419, "Grounding, Bonding, and Shielding for Electronic Equipments and Facilities," Volume 2, 21 January 1982.
- Durfee, G. H., "Effects of Lightning on Electrostatic Fuzing Systems," General Electric Technical Report TR-R59SD390, July 1959.

- Gething, P. J. D., Radio Direction-Finding, Peter Peregrinus LTD, London, 1978.
- Golde, R. H., Lightning Protection, Edward Arnold LTD, London, 1973.
- Greene, D. R., and Clark, R. A., "An Indicator of Explosive Development in Severe Storms," 1971.
- Gumley, J. R., "Lightning Prediction Techniques," Electrical Engineering Transactions, Institute of Engineers, Australia, 1973, pg. 13-18.
- Horner, F., and Bradley, P. A., "The Spectra of Atmospherics From Near Lightning Discharges," Journal of Atmospheric and Terrestrial Physics, Volume 26, 1964, pg. 1155-1166.
- Johnson, R. L., Janota, D. E., and Hay, J. E., "An Operational Comparison of Lightning Warning Systems," Journal of Applied Meteorology, May 1982, pg. 703-707.
- Kasemir, H. W., "Final Report to KSC Contract Number CC-59753," NOAA-APCL Technical Report June 1976.
- Krider, E. P., Noggle, R. C., and Uman, M. A., "A Gated Wideband Magnetic Direction-Finder for Lightning Return Strokes," Journal of Applied Meteorology, Volume 15, 1976, pg. 302-306.
- Latham, J., and Stromberg, I. M., "Point-Discharge," Lightning, Volume 1-Physics of Lightning (edited by R. H. Golde), Academic Press, London, 1977.
- Lee, W. R., "Lightning Injuries and Death," Lightning, Volume 2-Lightning Protection (edited by R. H. Golde), Academic Press, London, 1977.
- Malan, D. J., Physics of Lightning, English Universities Press LTD, London, 1963.
- Moore, C. B., Brook, M., and Krider, E. P., "A Study of Lightning Protection Systems," The Office of Naval Research Contract No. N00014-78M-0090 Final Report, October 1982.
- Naval Sea Systems Command, NAVSEA OP-5, "Ammunition and Explosives Ashore," Volume 1, Fourth Revision, 15 October 1974.
- Naval Surface Weapons Center, "Ammunition Evolution Curtailment at Sea Due to Thunderstorms; Criteria for," NSWC ltr DT-52:RAV:ac 8000, SAFEORD, DU 1L - 2C, 17 September 1975.
- Naval Surface Weapons Center, "Thunderstorm Hazards to Ordnance," NSWC ltr N42:MAG:rsm 8020 of 28 August 1980.
- Nordgard, J. D., and Chen, C. L., "Lightning-Induced Transients on Buried Shielded Transmission Lines," 1975 IEEE Symposium on EMC, September 1975, pg. 3A1C1-3A1C3.

- Orville, R. E., and Salanave, L. E., "Lightning Spectroscopy - Photographic Techniques," Applied Optics, Volume 9, August 1970, pg. 1775-1781.
- Parekh, H., and Srivastava, K. D., "Effect of Avalanche Space Charge Field on the Calculation of Corona Onset Voltage," IEEE Transactions on Electrical Insulation, EI-14 No. 4, August 1979, pg. 181-192.
- Parker, L. W., and Kasemir, H. W., "Airborne Lightning Warning Systems: A Survey," AFGL-TR-80-0226, July 1980.
- Pierce, E. T., "Atmospherics and Radio Noise," Lightning, Volume 1-Physics of Lightning (edited by R. H. Golde), Academic Press, London, 1977.
- Pierce, E. T., "Latitudinal Variation of Lightning Parameters," Journal of Applied Meteorology, Volume 9, February 1970, pg. 194-195.
- Pierce, E. T., "Lightning Location and Warning Systems," Lightning, Volume 2-Lightning Protection (edited by R. H. Golde), Academic Press, London, 1977.
- Prentice, S. A., "Frequency of Lightning Discharges," Lightning, Volume 1-Physics of Lightning (edited by R. H. Golde), Academic Press, London, 1977.
- Salanave, L. E., "The Infrared Spectrum of Lightning," IEEE Region Six Conference Record, 1966.
- Salanave, L. E., "The Optical Spectrum of Lightning," Science, Volume 134, No. 3488, 3 November 1961, pg. 1395-1399.
- Schonland, Sir Basil, The Flight of Thunderbolts, 2nd edition, Clarendon Press, Oxford, 1964.
- Standler, R. B., and Winn, W. P., "Effects of Coronae on Electric Fields Beneath Thunderstorms," Quarterly Journal of the Royal Meteorological Society, Volume 105, No. 443, January 1979, pg. 285-302.
- Stansfield, R. G., "Statistical Theory of D. F. Fixing," Ministry of Works Technical Report, 1947.
- Uman, M. A., Lightning, McGraw-Hill, New York, 1969.
- Uman, M. A., Lin, Y. T., and Krider, E. P., "Errors in Magnetic Direction Finding Due to Nonvertical Lightning Channels," Radio Science, Volume 15, No. 1, January - February 1980, pg. 35-39.
- U. S. Army Materiel Development and Readiness Command, DARCOM-R 385-100, "Safety Manual", 17 August 1981.
- Weidman, C. D., and Krider, E. P., "The Fine Structure of Lightning Return Stroke Waveforms," Journal of Geophysical Research, Volume 83, No. C12, December 20, 1978, pg. 6239-6247.

Winn, W. P., and Byerley, III, L. G., "Electric Field Growth in Thunderclouds," Quarterly Journal of the Royal Meteorological Society, Volume 101, 1975, pg. 979-994.



AD P000463

DIELECTRIC RADIO FREQUENCY HEATING
OF PROPELLANTS
INCIDENT INVESTIGATION AND APPLICATIONS

by

Melvin C. Hudson

Naval Ordnance Station
Indian Head, Maryland

ABSTRACT

Double-base propellant is heated to ease extrusion by utilizing the propellant dielectric properties in a radio-frequency oscillatory circuit. This paper presents information developed during investigation of a series of fires which were found to be related to the heating methodology and dielectric properties of the propellant. The content of this paper was extracted from reports and memorandum prepared by the incident investigation team of Chester E. Davis, E. Gordon Powell and the author. That the first two members were the major contributors to the investigation team is acknowledged.

This paper prepared for presentation at the 20th Department of Defense Explosives Safety Seminar, 24-26 August 1982, the Omni International Hotel, Norfolk, Virginia, USA.

DIELECTRIC RADIO-FREQUENCY HEATING OF PROPELLANTS

by Melvin C. Hudson

Double-base propellants are extruded to form rocket motor grains. Hydraulic presses and dies are utilized and the process is well documented. To ease extrusion, the propellant is softened by heating, normally to 130-140°F. Heating is accomplished basically in two ways; oven heating or radio-frequency heating utilizing the dielectric properties of the propellant. Problems encountered and information developed while utilizing dielectric heating at the Naval Ordnance Station are summarized in this discussion.

To assure understanding, a brief familiarization with the double base propellant process is in order. In this process, the ingredients, nitrocellulose, nitroglycerin, plasticizers and burning rate modifiers are mixed together in a water damp paste. This paste is put through heated rollers to drive off the water and give desired physical properties. The product of these rolling mills is a sheet, nominally 0.080 inch thick. These sheets are cut into strips 4 inches wide which are rolled into right circular cylinders called carpet rolls (nominally 15 inch diameter). The carpet rolls are heated and placed in the extrusion press for forming the propellant into rocket motor grains. The two principal means of heating the propellant carpet rolls are thermal ovens and dielectric heaters.

The thermal method of heating requires the carpet rolls be placed in an oven and allowed to come to a uniform temperature throughout. Because the carpet roll is fairly thick, a considerable period of time is required to attain desired temperature in the center. Also the thermal oven must be set near the final temperature desired for the propellant and this reduces thermal force and results in long heating periods. For these reasons, the thermal ovens are known as "soaking" ovens. Problems associated with soaking ovens are the investment in ovens required to support even a modest production capability and the effects of extended thermal soaking on the propellant. Of the latter, the major effects are volatilization of plasticizer and hardening of the propellant. Consequences are process and quality problems in the extrusion of carpet rolls to form propellant grains.

The second method of heating, that is dielectric heating, applies a high or radio-frequency electric field to carpet rolls situated as the dielectric in a parallel plate capacitor as shown in Figure 1. This is basically a resonant capacitive-inductive circuit. The electric field takes effect throughout the propellant thus eliminating thermal diffusivity as a factor. Heating time is reduced from ~24 hours for soaking ovens to ~20 minutes.

The phenomena involved in dielectric heating can be simplified to the following concepts: (1)

- a. The electric field potential gradient causes distortion and orientation of atoms and molecules by displacement of electrons with respect to the nucleus;
- b. Both polar and non-polar molecules are affected;

c. The effect of the displacement is to reduce the field gradient within the dielectric material.

These concepts are illustrated in Figures 2 and 3.

To digress a bit, note that both metallic conductors and dielectric or non-conductors can be heated by radio-frequency fields. The phenomena involved are different but pertinent to some of the events to be discussed. In heating conductive (metallic) materials, the imposed electric field induces motion of free electrons. Resistance to their motion by the atomic matrix results in heat generation. This is known as inductive heating and has extensive application. (2) Suffice for this discussion to visualize conditions occurring within a conductor located in an electric field; the free electrons concentrate at extremities and negate the field within the conductor thus creating concentrated charges and high electrical potentials. (1)

Returning to dielectric materials which have few free electrons, the distortion and displacement of atomic and molecular charges and resistance of the material matrix to orientation generates heat. As these phenomena occur throughout the material, heating does also.

An aid to visualizing the properties of the material in an electric field is to determine an equivalent circuit for the material. The basic circuit illustrated by Figure 4 shows that if a field is applied across a cube of material, the admittance (reciprocal of impedance) has both a capacitive or susceptive component and a conductive component. The conductive/resistance component is representative of metallic response; susceptive/capacitive component is representative of dielectric response to imposed fields. Note that when high frequency changes are made in the field, the molecules and electrons do not have time to achieve equilibrium with the field. This creates conditions such as anomalous dielectric dispersion. (3)

The admittance of RF electrical energy into a material equivalent circuit can only be described in mathematical terms by complex number notation. (2)(3)(4) This notation utilizes real and imaginary components. Application includes real and imaginary terms in the power factor, a concept involved in supplying energy to a dielectric in a resonant capacitive-inductive circuit and in other alternating current electrical circuits. In vector notation, the angle between vectors representing capacitor charging current and total current is the loss angle. The loss tangent or dissipation factor is the ratio of loss current to charging current.

The preceding remarks were intended to give a brief familiarization with the nomenclature of extruded double-base propellant processing, RF heating, and dielectric material phenomena. More detailed discussion can be found in references 1 thru 4 and any good text on high frequency electrical circuits.

There are various conditions inherent in dielectric heating which should be mentioned. Some that are important but not well characterized are changes which occur in the materials conductivity, dielectric constant and power factor or loss tangent as the frequency and material temperature vary. For example, as the material heats up, its electrical parameters change which cause change in the resonant frequency of the circuit. The dielectric constant, power factor and conductivity all vary with frequency. Also, it is important to note that a general property of dielectrics is for the imaginary part of the dielectric constant to increase with temperature. These interactions can lead to properties changes causing frequency shift toward better coupling and greater energy absorption by the dielectric. Sometimes these can cause problems in controlling heating of propellant.

Another condition which occurs is creation of standing waves, i.e., non-uniform voltage distribution. This is a function of electrode dimensions and wave length. Standing waves can be tuned out, however, they and the material characteristics previously mentioned can generate significant potential gradients within the material.

At Naval Ordnance Station, Indian Head, RF dielectric heaters have been utilized for heating propellant carpet rolls. The propellant enters the circuit as the dielectric in a parallel plate capacitor arrangement as illustrated in Figure 1B. Note that Figure 1A shows insulating rubber pads which separate the propellant from all metal surfaces. This eliminates direct application of high electrical potential from a conductor to the propellant. The pads are of low-loss dielectric material.

During the period 1950 to 1973, ten fires had occurred in the high frequency heaters. In most of these, foreign material or defects in the insulating cover of the electrode plates were considered as the most likely cause. For example, a metal stem thermometer for determining propellant temperature, if left in the carpet rolls during heating, can cause localized heating. The metal conducts in the applied electric field and concentrates the field at edges and points. This concentrated field causes localized heating in the propellant and could result in an arc. As these would occur within the carpet roll where the thermometer is utilized, ignition is a possibility. Other possible causes are water which is a highly polar molecule that may lead to localized concentrated fields and corona and arc discharge from various parts of the heater. Minor amounts of water are considered likely to evaporate before ignition temperature is attained. Corona discharge and arcs have been observed however they consistently are located on parts of the heater remote from the propellant.

In 1973, and early 1974, a series of five fires occurred with one particular propellant. As the investigations progressed from one fire to another, the obvious foreign item causes were ruled out. This led to the conclusion that the ignition cause was involved in heater operation and propellant proper-

ties. Following paragraphs discuss items considered and action taken without regard to chronology except that intensive effort was initiated after the fourth fire and the fifth fire occurred during this time.

Note that this was the first aluminized propellant subjected to dielectric heating. Limited tests had indicated that aluminized propellant could be heated safely. Over 1 1/4 million pounds had been heated prior to the first fire so aluminum can not be considered the sole cause of ignitions. X-ray examination of carpet rolls from the lot involved in the last fire showed areas ~1/16 inch diameter with increased attenuation. Visual examination did not reveal any cause for the attenuation and the propellant was subsequently dielectrically heated and extruded without incident.

The possibility that corona discharge or arc discharge was the ignition source was considered. Operating personnel had occasionally observed corona discharge during normal operation of the heaters. However, the corona was always observed on parts of the heater some distance from the propellant. One function of the insulating pads is to smooth the interface between propellant and electrodes and eliminate sharp points which are likely sources of discharge. Also, tests indicated the propellant in question would withstand current densities substantially in excess of typical corona discharge for a time longer than the cycle time of the heater. Hence corona discharge was considered an unlikely cause but the sharp edges of conductors were blunted to eliminate high field potential points that cause discharge.

Arc discharges were considered a less probable cause than corona as none had been seen or heard and plate current meters had not indicated erratic fluctuations typical of arc discharges. Tests indicated arc discharge current density was capable of igniting the propellant. Regardless, the absence of evidence of arc discharge under any condition of heater operation led to the conclusion that they were not the cause of the fires.

Foreign material in the propellant or facility was considered. Metallic foreign material discussed previously in regard to fires prior to 1973, was ruled out for lack of evidence. Also, experienced operators were in charge and thoroughly inspecting for foreign material. Dielectric foreign material was determined unlikely after determining the dielectric constant of the propellant as few materials have a constant with an imaginary part which exceeds that of the propellant. Ordinary water is one but was ruled out as known not to be present in most of the fires. In any case, minor amounts of water would tend to vaporize before ignition temperature is reached.

Possible erratic problems with the heater operations were considered. Manufacturer service personnel inspected the equipment following one of the fires. In this effort, the RF voltage sensor was relocated from the power supply to the heater plates in order to measure the voltage impressed across the propellant.

Parallel measurements across the propellant and the generator output were taken during the change. As expected, the voltage across the capacitor (heater plates) in the resonant inductive-capacitive series circuit was higher than the voltage across the total circuit measured at the generator output. Based on these limited results, the voltage across the propellant was reduced by retuning the RF generator. Output voltage was reduced from 4-5 kilovolt to 1.5-2 kilovolts.

During the investigation following the fifth fire, operators mentioned that the plate current meter readings were always higher with the aluminized propellant. Also, there had been a gradual increase in heating rates in the interval between fires. Periodically control adjustments had been made to keep within the $3\frac{1}{2}^{\circ}\text{F}/\text{minute}$ heat rate. A specific cause of the increase in heating rates was not determined. Two possibilities are a gradual change in propellant properties or drifting of the heater electronics. The first might explain the onset of fires after more than a million pounds of incident free operations. The second, drifting of heater electronics, had not been a detectable phenomena in prior operations with any propellant. Drifting may have occurred by some subtle feedback mechanism. This conjecture is based on the subsequent finding that the heaters having fires were tuned such that as the propellant heated, the change in dielectric properties caused the RF generator frequency to shift toward better resonant coupling. This produces higher voltage across the propellant which in turn causes higher heating rates, a feedback situation. If there was initially any localized inhomogeneity in the propellant in either temperature or dielectric properties, the feedback could result in a localized thermal runaway situation. The higher the temperature in the inhomogeneous element, the faster it heats. If the localized heating rate exceeds the thermal diffusivity then ignition temperature can be reached. Unfortunately, no localized inhomogeneities could be found though this was not considered as confirming their absence.

Eventually, the dielectric properties of the aluminized propellant NOSIH-AA-6, were hypothesized to be directly involved in causing fires. An investigation of these properties was made in comparison to N-5 propellant which had extensive history without fires. Tests were also made on a "non-hazardous" dummy propellant of nitrocellulose, dibutyl phthalate and aluminum that is sometimes used to check extrusion processing. Results were that the real part of the dielectric constants of AA-6 and N-5 were about the same (approximately 10). As hypothesized, AA-6 showed an imaginary part of the dielectric constant about twice that of N-5. The dummy propellant had a real dielectric constant lower than N-5 or AA-6 but the imaginary part greater than that of AA-6. (This dummy propellant should not be used to check out dielectric heaters as it will burn.) As the power factor or energy absorption is directly proportional to the imaginary part of the dielectric constant, it follows that AA-6 heats faster than N-5 for the same heater conditions.

To confirm the laboratory findings, full-scale tests were made. These measured the dielectric properties of N-5 and AA-6 as normally loaded into the heaters. Low power lab equipment was connected in place of the RF power gene-

rator to preclude actual heating of the propellant. The measurements were not entirely reliable because of poorly known transmission line effects, however, it was apparent that AA-6 had a significantly higher imaginary dielectric constant. These tests gave a rough indication of change in dielectric properties as a function of frequency. Also, by using propellant conditioned to different temperatures, frequency variation with temperature was briefly studied.

Measurements were made of the tuning of each of the three operational heaters. The oven which had not experienced any fire with the AA-6 propellant was found to be tuned somewhat differently from the others but no firm conclusion could be established as that oven was seldom utilized for AA-6 propellant processing.

All of the evidence indicated that the problem had been outlined sufficiently to attempt a solution. The obvious approach was to change the RF generator tuning so that the heating rate was less. Initially, it was planned to achieve this by tuning such that the changing properties of the propellant would pull the load circuit away from resonance with the generator as the propellant temperature increased. After other adjustments, this detuning was achieved.

Lowering of the heating rate was attained in trials but not as much as desired for safe operation. Adjustment of the normal controls made little progress toward lowering the heating rate. A study of the generator circuit determined that changing the tap on the output RF transformer was a modification that would allow improved control range. The tap was changed to a lower position with respect to ground which had the effect of lowering power input to the load. Controls then functioned normally to adjust the heating rate to 3.50F/minute with AA-6 propellant. Rate with other propellants was lower.

As the fires had occurred early in the heating cycle, it was considered that initial propellant temperature condition was a factor. To even out any inhomogeneities, a split heating cycle was utilized. This cycle applied heat, then a rest period of a few minutes before heating again. This inefficient technique was no longer required after the heaters were improved by the addition of automatic load controls.

With the heating rate dependent on propellant properties, control settings had to be changed with each propellant. This was achieved by manually relocating (by cranking mechanism) the output tap on the plate current load coil. Note must be made that for all propellants, the plate current and consequently the heating rate changed as the powder temperature changed. With the ovens tuned to decrease coupling as the propellant temperature increased, the plate current and heating rate decrease with time in the heating cycle.

This discontinuous and decreasing rate heating cycle and need for changing

control settings for different propellants adversely affected operations. Therefore, efforts were made to determine modifications to equipment that would return to continuous heating cycles without causing fires. This was accomplished by noting that the plate current load coil, normally set at a point by manually cranking, was amenable to controlled positioning. Coupling this positioning with the tuning to pull the generator away from resonance as the propellant heats up appeared to provide a means for safe and efficient operation. To understand this, it had to be noted that for fixed control settings the initial heating rate would be near the maximum of 3.5°F/min and would decrease with cycle time and increase in propellant temperature to 42°F/min at cycle end.

Automatic load controls were installed which controlled heating rate by changing the position of the plate current load coil output tap. The controls were programmed to automatically position the tap at the low current control set point at the end of each cycle. This was intended to assure that initial heating of each propellant charge was at low power thus reducing the effects of any inhomogenities and reducing chances for ignition which normally occurs early in the heating cycle. As the propellant heats up and internal conditions become uniform, the controls change tap position to increase plate current to a set level and thus apply more power to the propellant. Since the heaters are tuned to pull away from resonance as the propellant increases in temperature, balancing plate current increase/maintenance to set point against resonance detuning allows achieving a uniform heating rate through the cycle. It was found that with these controls, maximum heating rate could be reduced within the time allotted for heating. This was considered an improvement in safety.

Because there are individual system differences, each of the three heaters was characterized for plate current versus heating rate. The automatic load controllers were adjusted to start at a minimum setting below the operating level. As the cycle progresses, plate current output coil tap is automatically repositioned to increase current to attain and maintain the operating level. The improved heaters have been operated without a fire since 1974.

There still remains one unanswered question, what change occurred to trigger a series of fires after initially processing 1 1/4 million pounds without incident. Admittedly, data generated in the investigations revealed that operation with AA-6 must have been closer to ignition conditions than is the case with prior propellants processed.

Furthermore, the fact that two heaters were involved in fires would indicate that drifting of the RF generator and circuits was not the sole cause. Duplicate failure modes in two separate systems at nearly the same time is a low probability occurrence. This heater drift rationale has one weakness, and that is maintenance and adjustment, which, consistently performed in one direction on both heaters, may have eventually shifted them from no-fire to fire condition. This could not be determined and is thought unlikely based on operating and maintenance records and personnel memories.

Subsequent to the last fire, another aluminized propellant (2 1/2 Al) has been processed successfully although it is probably more sensitive than AA-6 to the power loading rate. This conjuncture is based on limited observation of the plate current when heating cycles begin for the two different propellants.

Only one item is left, the propellant. Some subtle change in propellant ingredient or processing changed the dielectric properties. Conjecture would be that the change was in the plasticizers as they generally have greater dielectric properties change with frequency and temperature than the other materials. This is supported by the observation that the second aluminized propellant with half the aluminum content of AA-6 appears more sensitive and has a higher plasticizer content. (Note that Nitroglycerin, a major ingredient has a real dielectric constant of 19.)⁽⁵⁾ The same difference would tend to rule against aluminum as the culprit. Although processing resulting in concentrations of aluminum could result in a tendency toward fires, it is more likely that aluminum (less than 5%) is an accomplice rather than the culprit. Further studies of the dielectric nature of propellants would be interesting but not necessary items and are not planned as current operations are satisfactory.

Reference:

1. UNIVERSITY PHYSICS, F. W. Sears and M. W. Zemansky, Addison-Wesley Publishing Co.
2. RADIO FREQUENCY HEATING, G. H. Brown, C. N. Hoyler, R. A. Bierwirth, D. Van Nostrand Co.
3. SCIENTIFIC ENCYCLOPEDIA, Van Nostrand, 5th Edition
4. COMPLEX VARIABLES AND APPLICATIONS, R. V. Churchill, McGraw-Hill
5. CHEMISTRY AND TECHNOLOGY OF EXPLOSIVES, Vol. 2, T. Urbanski. Pergamon Press

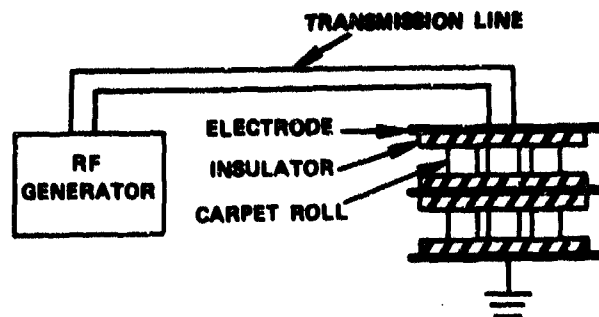


FIGURE 1A. DIELECTRIC OVEN

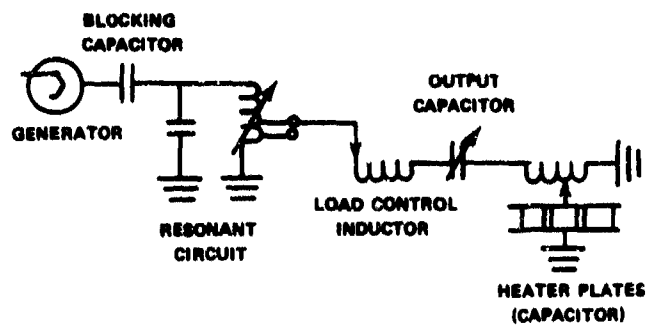


FIGURE 1B. EQUIVALENT CIRCUIT OF RF DIELECTRIC HEATER.

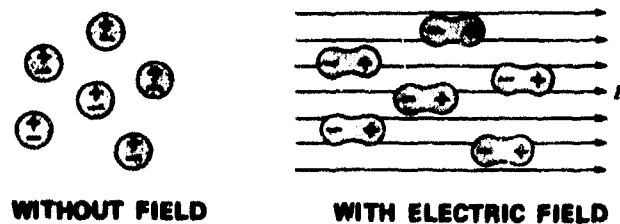


FIGURE 2A. BEHAVIOR OF NONPOLAR MOLECULES IN THE ABSENCE AND IN THE PRESENCE OF AN ELECTRIC FIELD
(From Sears - University Physics)

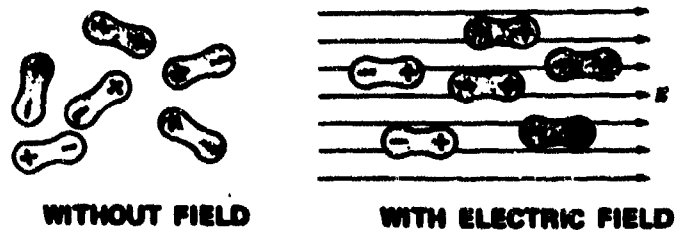


FIGURE 2B. BEHAVIOR OF POLAR MOLECULES IN THE ABSENCE AND IN THE PRESENCE OF AN ELECTRIC FIELD
(From Sears - University Physics)

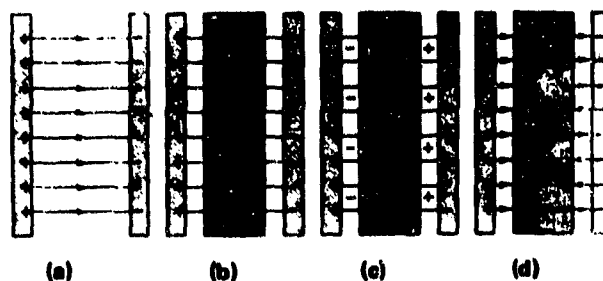


FIGURE 3. (a) ELECTRIC FIELD BETWEEN TWO CHARGED PLATES. (b) INTRODUCTION OF A DIELECTRIC. (c) INDUCED SURFACE CHARGES AND THEIR FIELD. (d) RESULTANT FIELD WHEN A DIELECTRIC IS BETWEEN CHARGED PLATES.
(From Sears - University Physics)

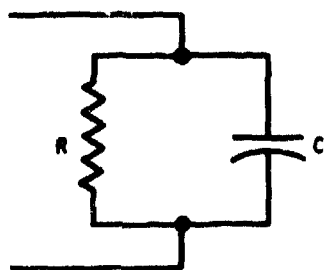
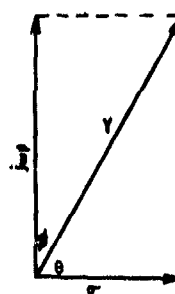


FIGURE 4A. EQUIVALENT CIRCUIT FOR A CUBE OF MATERIAL
(From Brown, - Radiofrequency Heating)



$$Y = \frac{1}{R} + j\omega C$$

or alternately

$$Y = G + j\omega p$$

$$\text{Power Factor or loss angle.} = \frac{G}{\omega p} = \tan \phi$$

FIGURE 4B. ADMITTANCE DIAGRAM OF A COMPLEX CAPACITOR
(From Brown - Radiofrequency Heating)

AD P 000 464

→ SAFETY OF HIGH EXPLOSIVES COMMINUTION PROCESSES

R Applin

AWRE ALDERMASTON

1. INTRODUCTION

Many properties of explosives are influenced by the particle size of the explosive, eg.

- (a) Consolidation characteristics of pressable, castable and extrudable HE systems.
- (b) Rheological and mechanical properties.
- (c) Hazard potential of both powders and consolidated compacts.
- (d) Initiation and propagation properties.

UK military explosives are supplied from the Royal Ordnance Factories in a restricted number of grades, therefore, AWRE is involved in comminution of secondary high explosives in order to

- (a) to do necessary research on the effects of particle size on various properties, and
- (b) based on that research, to tailor explosives to meet particular requirements.

↓
The explosives which are of interest include HMX, RDX, TATB, NQ, TNT, PETN and HNS and mixtures of these materials. These explosives are subjected to a variety of milling processes on the experimental and pilot plant scale. The quantities involved range from 1 or 2 kg to several hundred Kg.

↙ Various methods of comminution are in use;

- (a) end-runner milling (a mechanical pestle and mortar)
 - (b) ball-milling
 - (c) colloid or paste milling
 - (d) slurry or attrition milling
-

↓
(e) fluid-energy milling, *only*

↓
(f) precipitation from solvent combined with fluid-energy milling.

↖ This paper will outline the methods of comminution used at AWRE and then deal in more detail with how a number of safety problems have been dealt with.

2. COMMINUTION METHODS

2.1 All comminution operations on explosives at AWRE are carried out under remote control. Precipitation methods where no milling is involved are carried out under close control.

2.2 End-Runner Milling

This is essentially a mechanical pestle and mortar, (See Figure 1). The mortar is turned by an air-driven motor; the pestle revolves by the effects of friction and the material to be milled is crushed between the bottom of the mortar and the surfaces of the pestle.

Compositions such as TNT flake or Comp B are milled dry; other materials are milled under water. PETN is not milled by this method.

Many of the compositions prepared at AWRE contain rubbery binders and are in the form of coarse agglomerates which are not suitable for testing by our standard powder safety tests. Crushing at room temperature often is not effective in reducing the size of the agglomerates. However, milling in liquid nitrogen in the end-runner mill, where the temperature has been reduced to well below the glass transition temperature of the binder, is effective. The liquid nitrogen also acts as a diluent and ignition quencher in the same manner as water.

One disadvantage of the method is that atmospheric moisture is condensed onto the milled sample which necessitates a further drying stage and also means that it cannot be used for moisture sensitive compositions.

2.3 Ball Milling

This method is now only used on a small scale for experimental purposes. There are two reasons for this:

- (a) the relatively large quantities of explosive being processed at one time if the process is being used to produce worthwhile quantities of powder;
- (b) contamination of the product by material from the balls.

2.4 Colloid (paste) Milling

This is a method developed at AWRE in the late 1950's and it is used to produce our standard fine HMX (HMX Type B). Figure 2 shows the particle size distributions of three grades of HMX in use at AWRE.

The mill consists of a conical rotor, driven at high speed, turning inside a matching stator with a gap of a few thousandths of an inch; both the rotor and stator are made in carborundum. Figure 3 is a drawing of the stones. Stainless steel rotors and stators have been tried but the stability of rotation is not good enough to prevent the milling surfaces touching and binding.

The mill is fed with slurry from a circulation circuit which is designed to keep the slurry in suspension by the velocity of the circulating flow. The circuit is shown diagrammatically in Figure 4 and in place of Figure 5.

The product of this type of milling is a bimodal powder with good packing properties. However, a minute number of carborundum particles contaminate the product and, although they do not present a safety hazard and there is no problem in meeting the stringent grit clause of the specification, the grit particles occasionally manifest themselves in embarrassing situations. Because of this AWRE is moving away from colloid milled material to that produced by fluid-energy milling where there are no moving parts or carborundum stones.

2.5 Slurry Milling (Attrition Milling)

The kinetic energy of the circulating slurry in the circulation system for the colloid mill has been put to use in a form of milling known as slurry milling. The flow from two centrifugal pumps is directed to the opposing arms of a Tee piece of reduced diameter. The impact of the colliding explosive crystals is of sufficient violence to cause their attrition. This method, run on a continuous recirculation system, produces a powder with a particle size distribution, for HMX, intermediate between Type A and Type B. An important attribute of the material produced in this way is the rounded nature of the crystals.

2.6 Fluid-Energy Milling (Micronizing)

The second major method of milling, and the currently preferred method, in use at AWRE is fluid-energy milling. The milling takes place by collision of particles of material, one with another, in the very vigorous turbulence created inside the mill by colliding high pressure air jets. The centrifugal motion of the air flow partially classifies the powder so that the coarser material is retained in the milling area, thus allowing further comminution to take place. Figure 6 is a sketch of the mill; Figure 7 shows the two 300 mm mills installed at AWRE.

The milling is carried out with an aqueous slurry of the explosive and a considerable proportion of the energy input is used in moving water around. For use with TATB, a small fluid-energy mill has been installed which is being fitted up for use with dry powder. This is shown in Figure 8.

The product of this type of milling is unimodal.

2.7 Precipitation

Precipitation of explosives from solution in a variety of solvents by feeding the solution into stirred water is a recognised procedure for producing materials with closely tailored characteristics.

At AWRE this form of precipitation has been combined with fluid-energy milling to produce very fine and very pure powders.

PETN with a surface area of about $3 \text{ m}^2/\text{g}$ has been produced by this method.

3. SAFETY CONSIDERATIONS

3.1 Sources of Hazard in Comminution

There are several sources of hazard in our methods of comminution ie.

- (a) impact
- (b) friction
- (c) viscous heating
- (d) electrostatic discharge (dry powders and fuel/air mixture ignition).

The response to these stimuli are influenced by -

- (a) the particle size of the explosive
- (b) the concentration of the slurry, dust cloud, or solvent
- (c) the nature of the explosive.

The over-riding objective when any explosive process is introduced is to eliminate, if possible, the sources of hazard, but, if this cannot be achieved to reduce the hazard to the minimum. This has been done with the comminution processes used at AWRE and the following paragraphs discuss individual areas of operation.

3.2 Slurry Pumping

There are two slurry pumping circuits installed in our milling building:

- (a) A 25 mm diameter circuit pumped by an orbital lobe pump for use when preparing 1 - 10 kg quantities of product using the fluid-energy mill. The circuit is shown diagrammatically in Figure 9.
- (b) A 50 mm diameter circuit pumped by one or two (depending on the process) centrifugal pumps delivering 35 - 40 imperial gallons per minute against zero head. This circuit is used when preparing large quantities of product using the fluid-energy mill, colloid mill or by slurry milling. The circuit is shown diagrammatically in Figure 10.

The orbital lobe pump was chosen for the 25 mm circuit because of its inherently safe design. The body of the pump is rubber and the lobe is rubber coated. This design avoids any metal to H₂O friction in the pump.

The centrifugal pumps on the larger circuit have been modified with an AWRE designed gland lubrication system that prevents ingress of slurry into the gland from the pump. Figure 11 is a diagram of the system.

The gland was modified by having a PTFE bush with a helical groove fitted and the pump body was tapped in two places to communicate with this bush. An additional tapping into the pump body communicates directly with the pumping chamber. A filtered water flow is supplied through a flow controller to the bush. The downstream side of the water flow is connected to a pressure relief valve; the pump chamber is connected to the same valve. The water flowing around the gland is drained through the pressure relief valve whilst the pressure of the water flow is greater than the pressure being generated in the pump chamber. If the pressure in the pump chamber exceeds that in the bush the pressure release valve closes and the water flow in the gland flushes into the pump body, so preventing ingress of solids into the gland.

Although the centrifugal pumps have a good safety record at AWRE, it is recognised that there is a slight risk involved in their use. It has therefore been decided to replace them with an inherently safer design of pump, probably of the diaphragm type.

3.3 Slurry Circuits

When the major pieces of milling equipment were installed in the late 1950's experiments were carried out to find the concentration threshold of the propagation of detonation for slurries of HMX in water confined in 50 mm diameter stainless steel tube. It was found that, for

both suspended slurries and settled slurries in horizontal tube, detonation would not propagate at 30 per cent solids concentration when boosted by a 25 mm diameter, x 25 mm long cylinder of Comp B.

Guided by these results, the upper concentration limit for slurries of HMX and RDX permitted in the AWRE plant is 25 per cent. PETN has only been milled at low concentration (< 10 per cent).

More recent studies by Petrino et al (1) using gelled slurries have shown that detonations can be obtained in 30 per cent HMX slurries, but have confirmed that detonation will not propagate in 25 per cent HMX slurry. However, they obtained detonations in settled 5 per cent HMX slurry. They recommend that HMX slurries should not be allowed to sediment.

The approval that was given to work at 25 per cent HMX slurry concentration at AWRE, was conditional on

- (a) the pipe work being clear plastic to enable points of sedimentation to be identified and cleared;
- (b) each pipe run having a vertical section in the plant room to provide a break in any sedimented train of explosive and so prevent propagation of any ignition to the slurry preparation room.

Before and after each run using the fluid-energy mill or the colloid mill the slurry systems are flushed well with water to minimise sedimentation.

3.4 Colloid Mill

The major source of hazard with this type of mill is feeding dry material to the mill on start up, eg. between periods of use, slurry sedimenting and drying out; or failure during a milling run of the slurry pump leading to the loss of liquid feed to the mill.

These situations are guarded against by having the mill fitted with an independent, gravity fed, supply of water that is used to flush the mill before and after use; it is also capable of being switched in and out during a milling run.

3.5 Electrostatic Hazards

All fixed equipment and all other equipment above approximately 1 cubic foot volume is bonded to the earth bond of the building. This will prevent the build up of electrostatic charge of sufficient energy to ignite dusts of the explosives in use at AWRE.

When flammable solvents are in use a high level of ventilation is maintained to prevent the build up of solvent/air mixtures of ignitable proportions.

3.6 Viscous Heating

This is more of a nuisance than a hazard. When slurry milling or producing fine powders by the continuous recirculation of product to either the colloid mill or the fluid energy mill, the energy deposited in the slurry from the pumps appears as heat and consequently the slurry warms up. To remove this heat, which would soften the plastic pipes of the circulation system, the slurry is passed through a water cooled heat exchanger.

4. CONCLUSIONS

The explosives comminution operations at AWRE are run in as safe a manner as can be devised. The equipment and methods of operation are regularly reviewed to determine whether improvements can be made. However, the probability of an explosive event, although low, is greater than would allow the equipment to be run under close control.

This paper has presented the reasons for that conclusion and the steps that have been taken to minimise the likelihood of an explosive event.

REFERENCE

1. Petino G, Westover D, Scola R :
Detonation Propagation Tests on Aqueous Slurries of RDX
and HMX
Hazards Research Corp. Denville N.J.
ARLDC-CR-77002 April 1977.

COPYRIGHT © CONTROLLER HMSO 1982

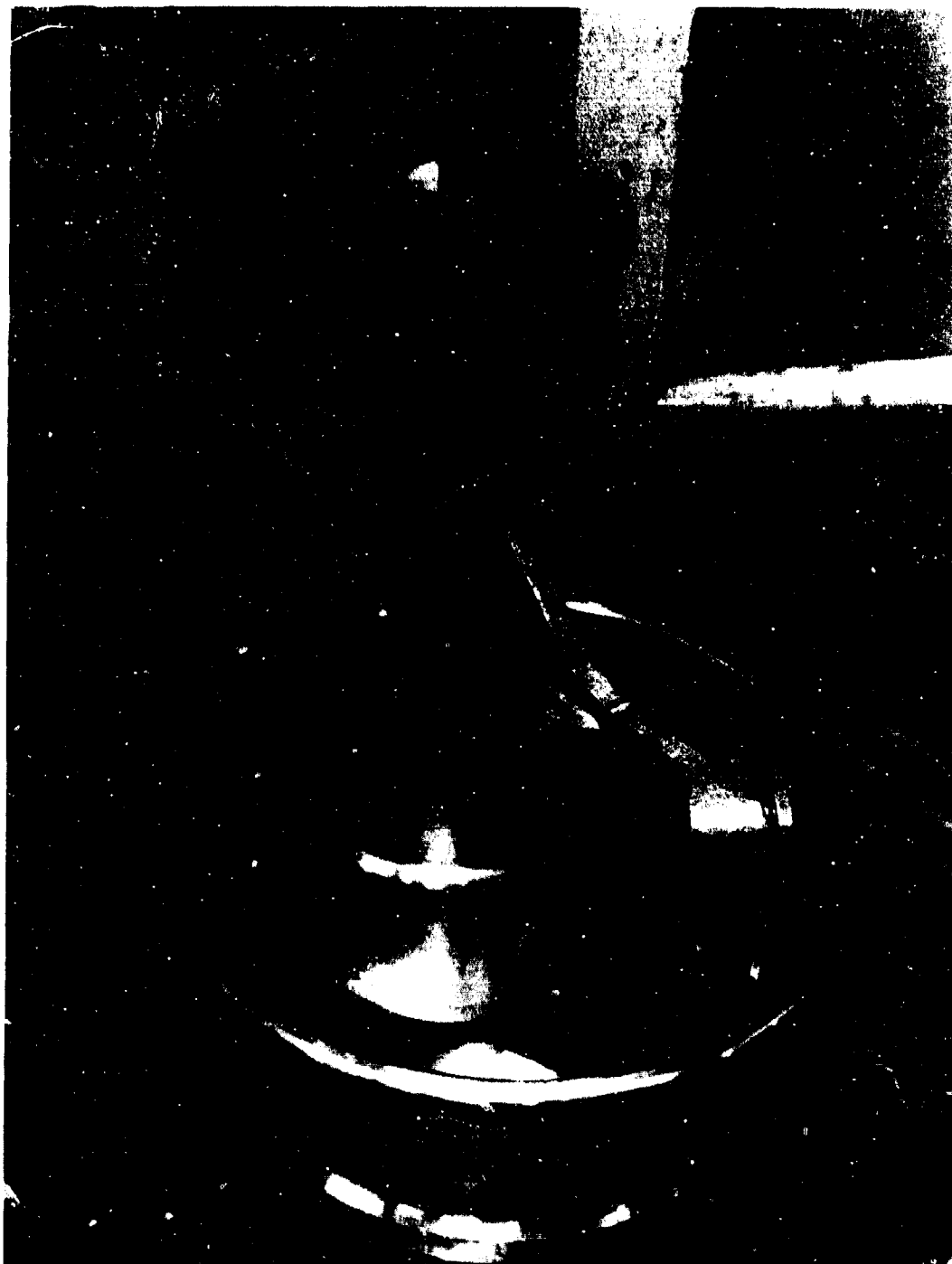


Figure 1 End-runner mill

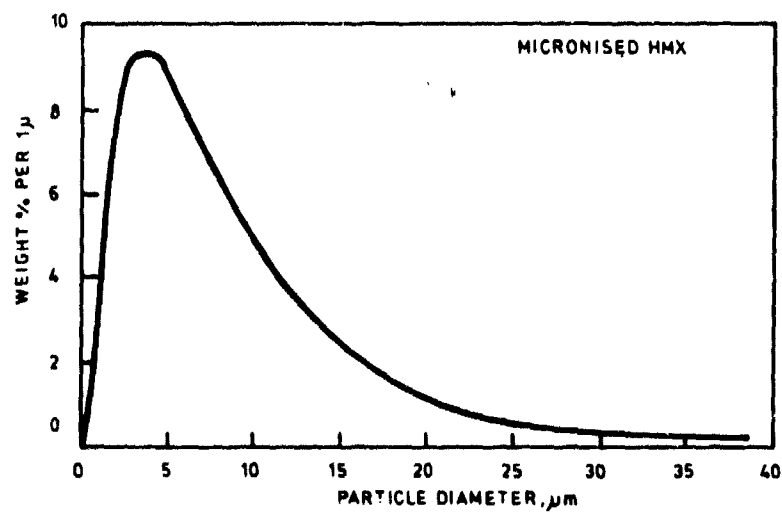
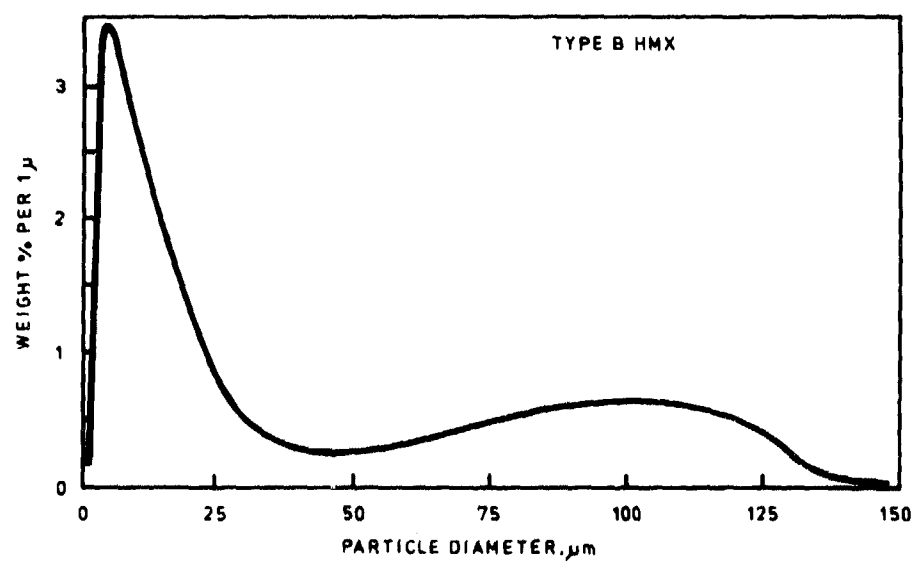
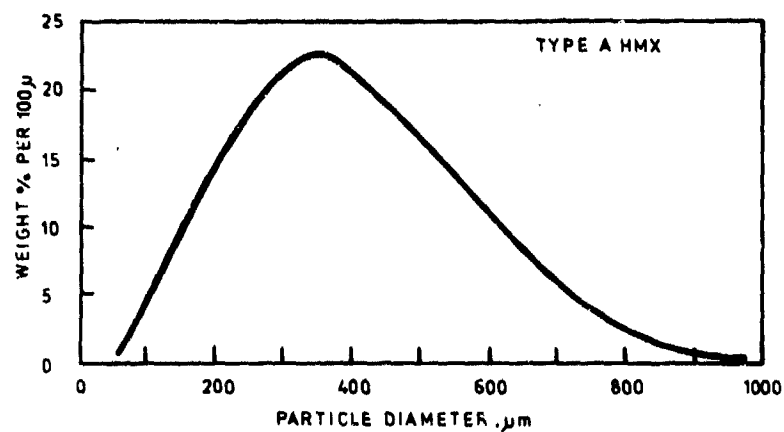


FIGURE 2 Particle Size Distribution of HMX Types Used at AWRE

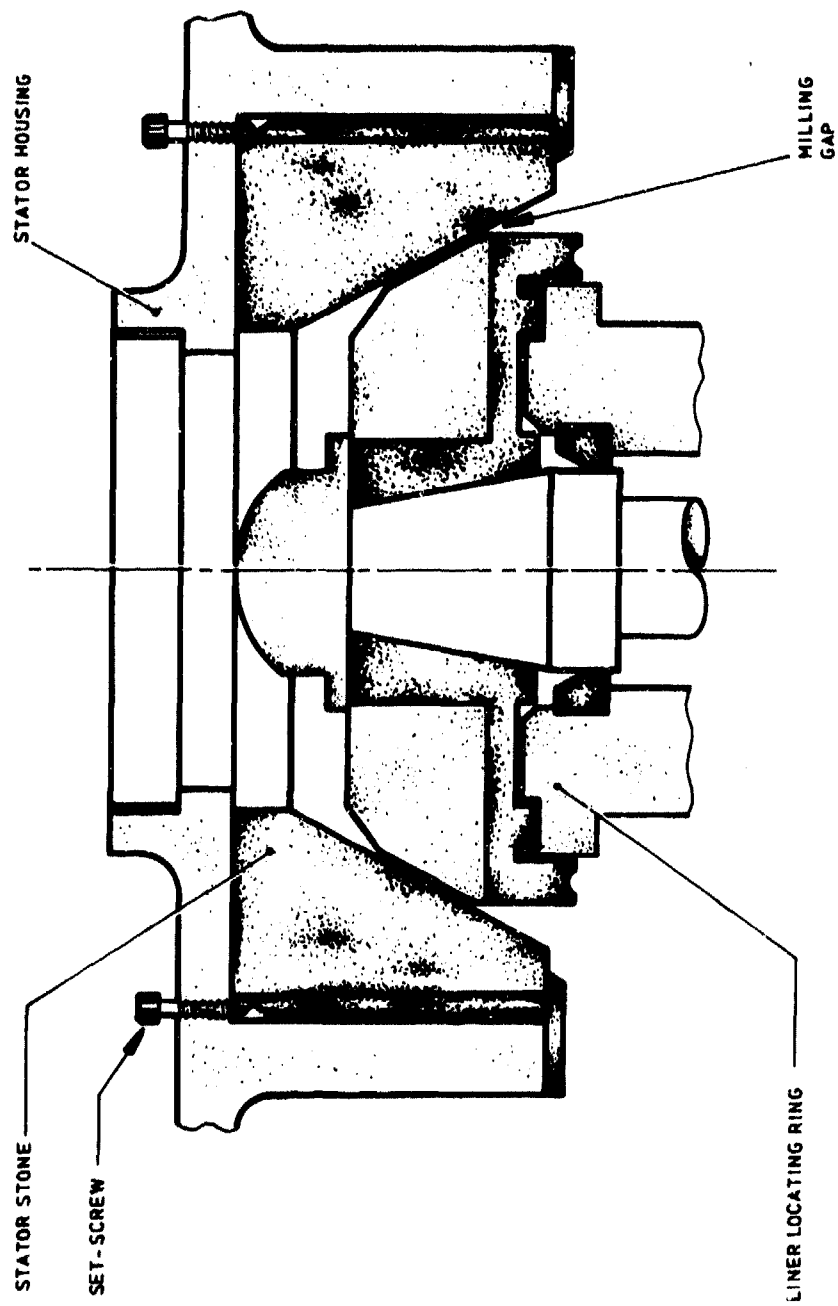


FIGURE 3 Carborundum Milling Units

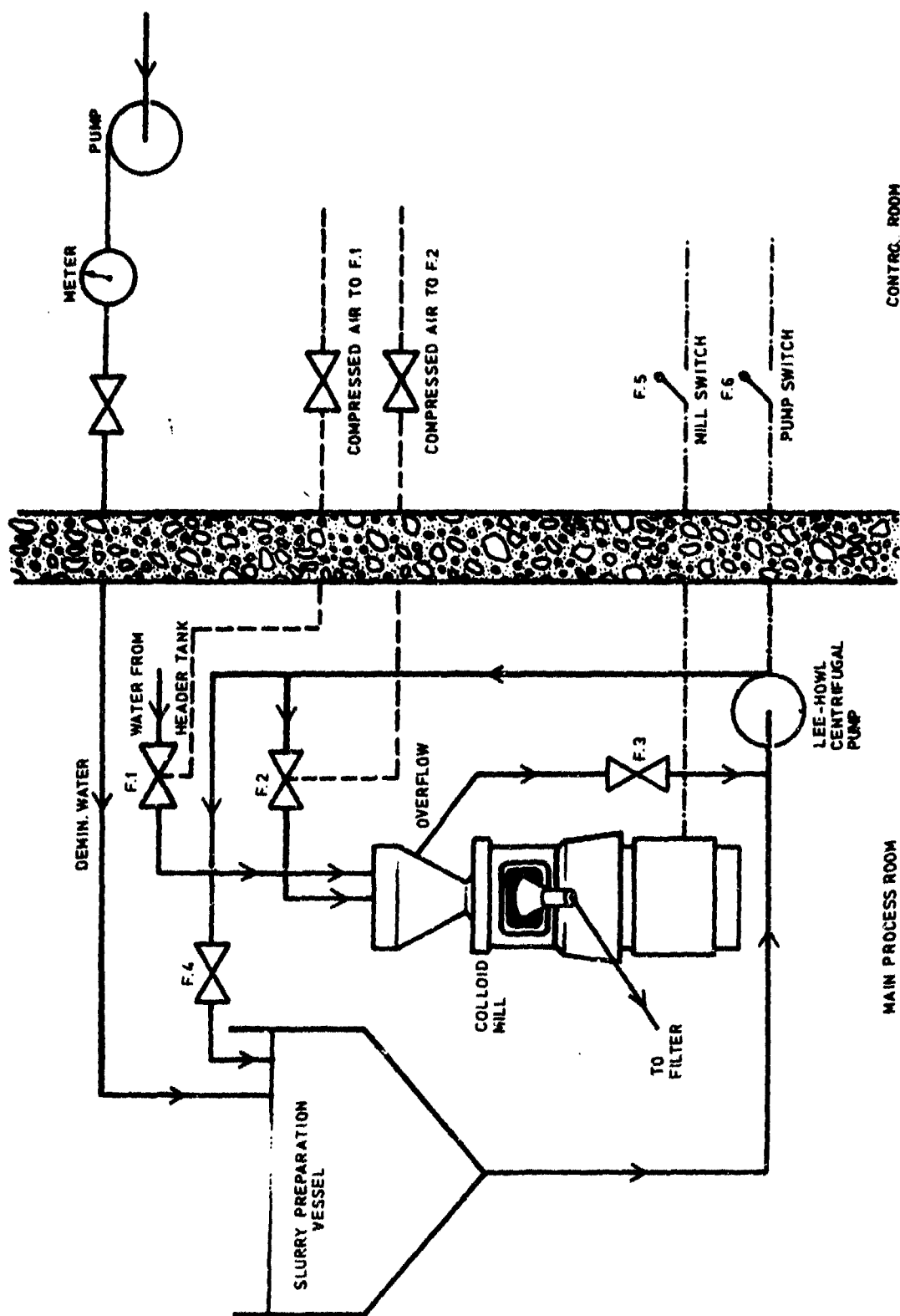


FIGURE 4 Colloid - Milling Circuit



Figure 5 Colloid mill

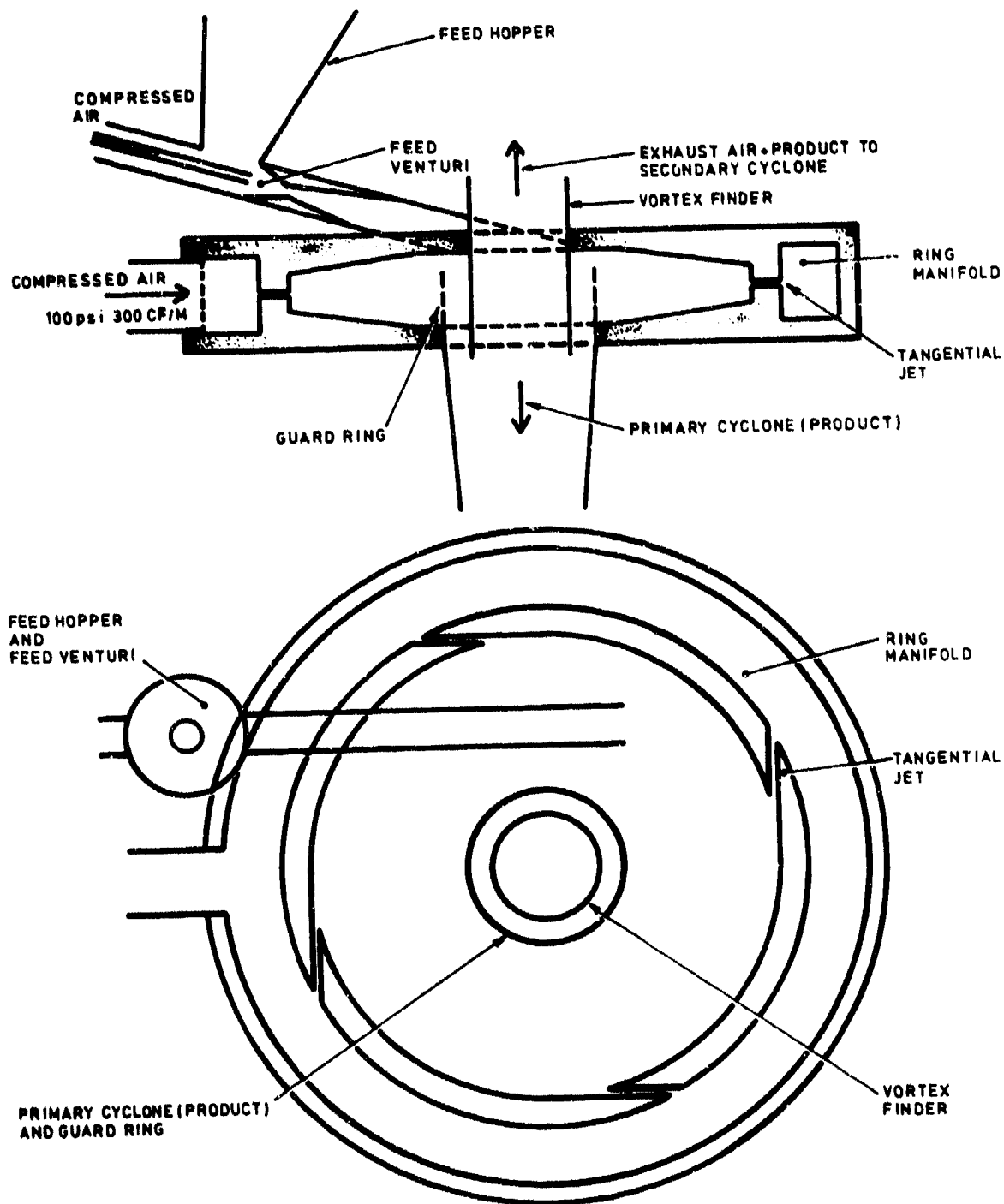


FIGURE 6 Fluid-Energy Mill (Micronizer)

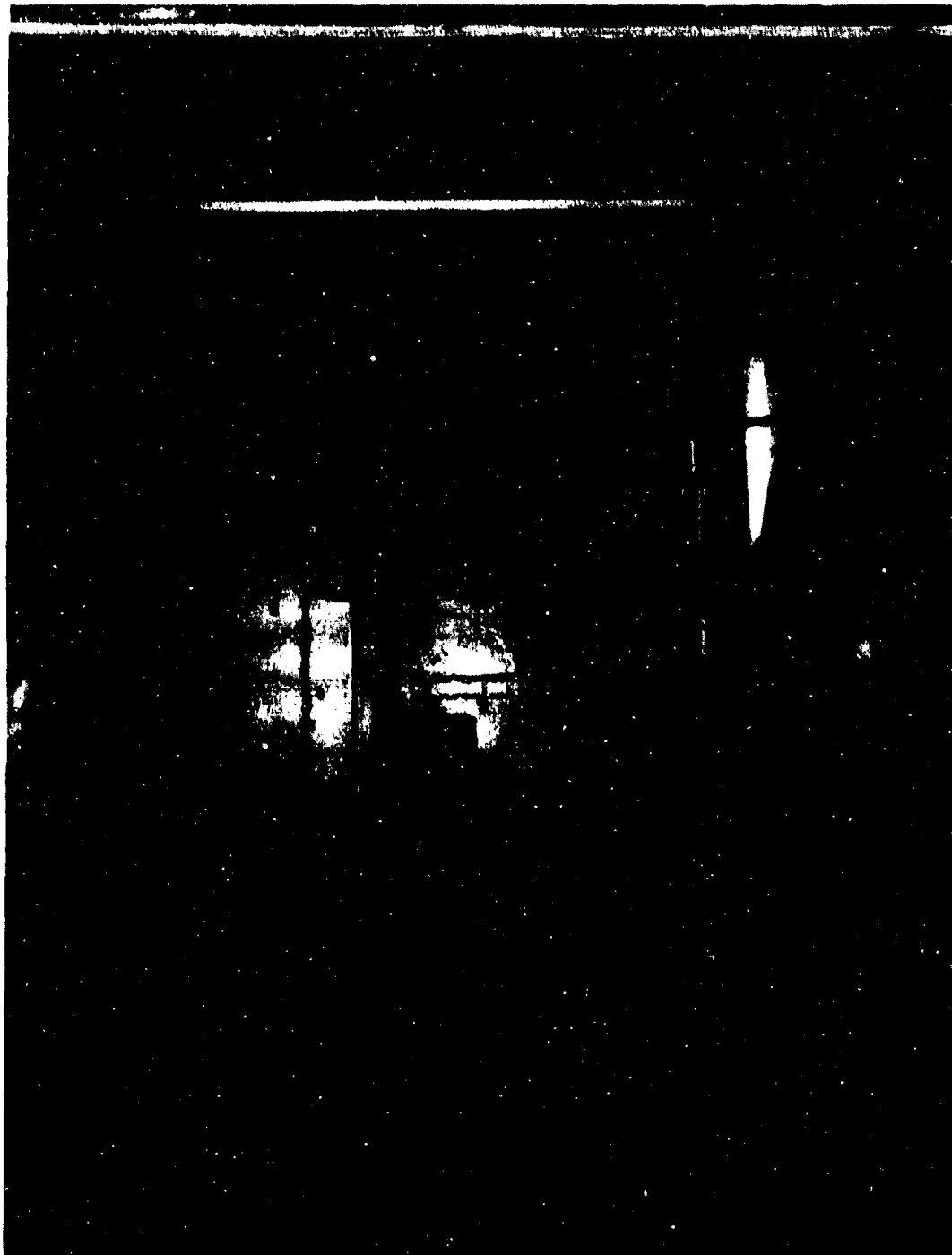


Figure 7 Fluid-energy mills



Figure 8 Small fluid-energy mill

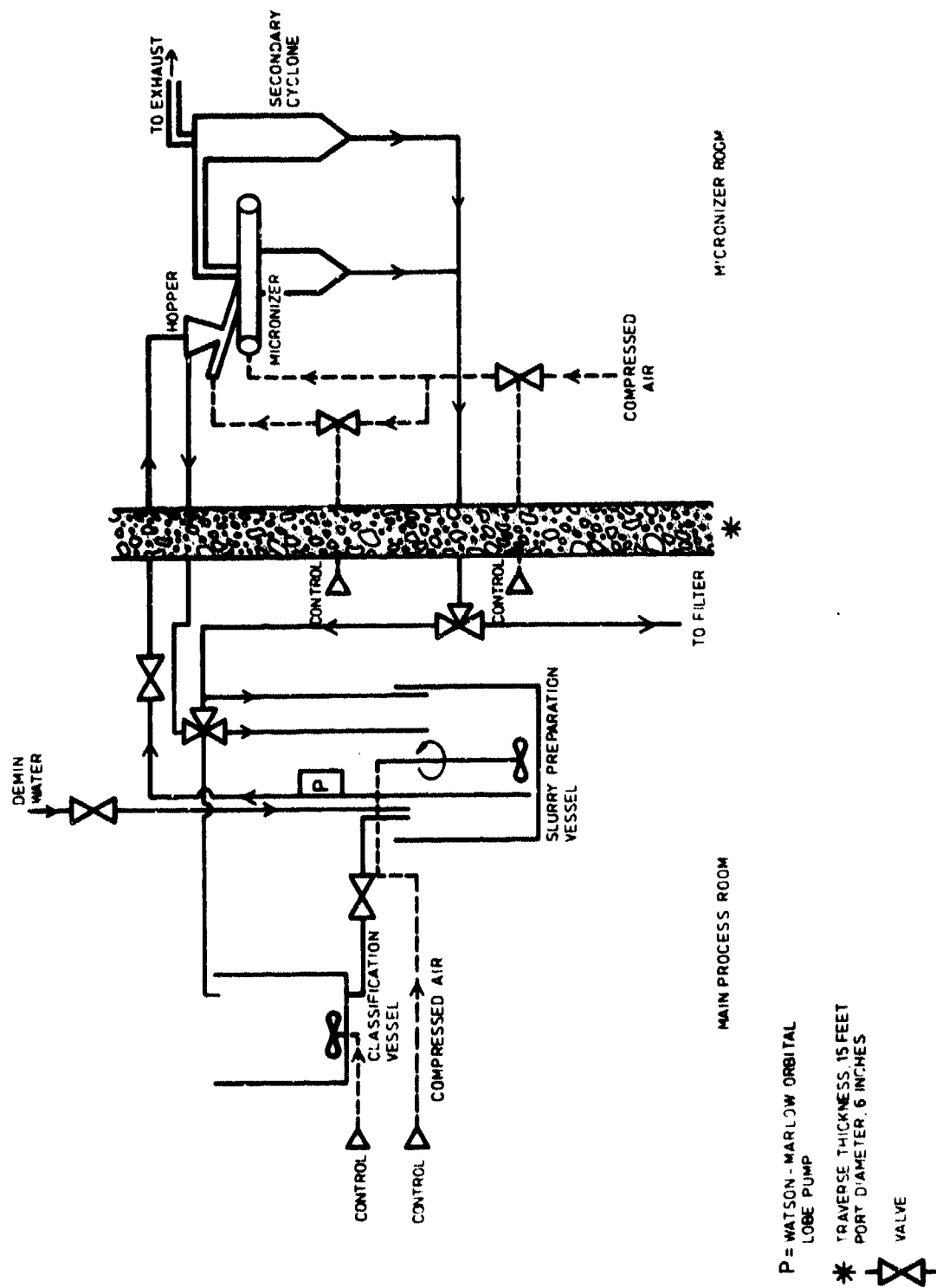


FIGURE 9 25mm Milling Circuit

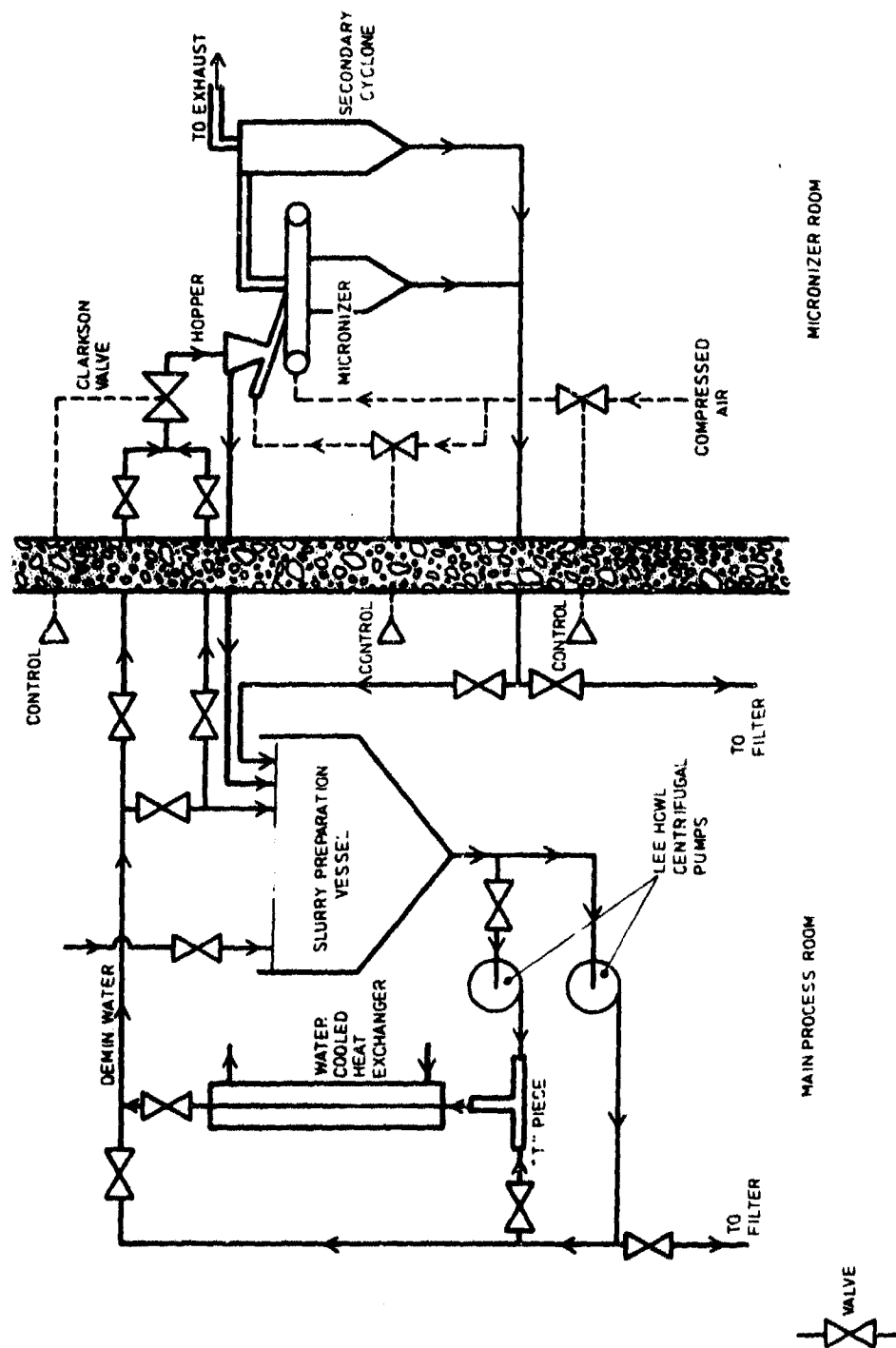


FIGURE 10 50mm Slurry-Milling / Micronizing Circuit

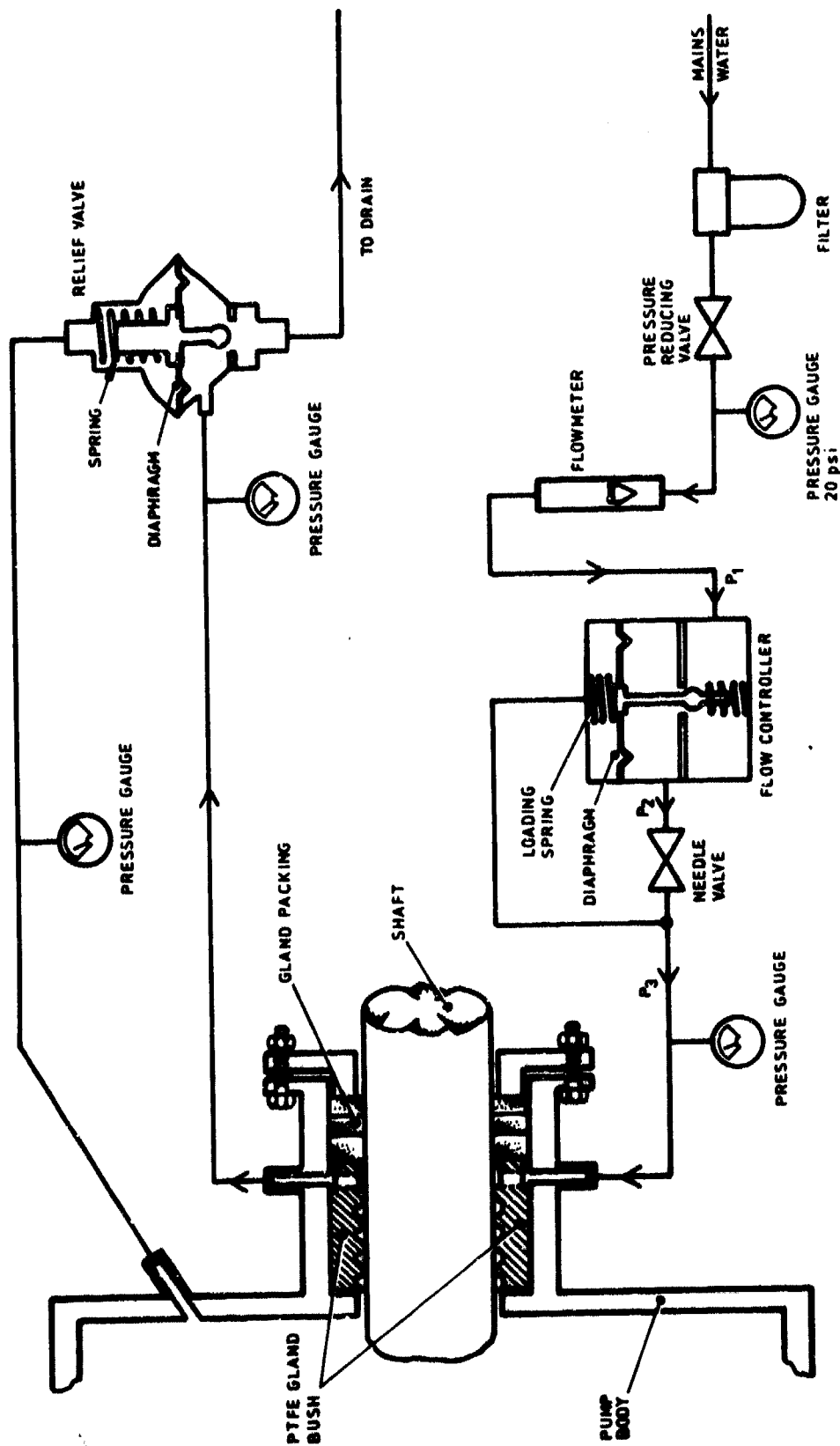


FIGURE 11 Pump Gland Lubrication System

AD P000465

→
STATIC ELECTRICITY PHENOMENA

IN THE MANUFACTURE AND HANDLING OF SOLID PROPELLANTS

by Ralph KENT

Safety Technical Group (SNPE) (1)

and Roger RAT

Saint Medard en Jalles Factory (SNPE)

Société Nationale des Poudres et Explosifs

↙
The studies described herein show that capacitive discharges and constant potentials may ignite the combustion of composite propellants.

The results analysis allowed SNPE to point out criteria based upon percolation phenomena and specific laws of volumic resistivity as a function of temperature. The above criteria should be able to predict, - with a rather good approximation, - the behavior of some propellants in regard to static electricity.

↑
1. INTRODUCTION.

Within the safety conditions improvement framework, SNPE has tried to evaluate the margins of safety in presence of static electricity. Various measurements, performed in the workshops, have highlighted the presence of static electricity during some operations.

(1) 91710 - VERT-LE-PETIT - FRANCE

Significant electric charges were observed on inhibitors and packings material, it has been possible to record the electric potential accumulated on a core during the core pull out operation. The above potential may go up to several thousands of volts at the end of the pull out operation. Thus, SNPE has implemented a large set of preventive operations which seem to be efficient such as, for instance, the use of graphit and systematic grounding of inhibitors. In the field of safety, preventive operations cannot provide an absolute warranty for any hazard.

Therefore, in the event of electric charges generation, SNPE has tried to understand the behavior of propellants, and more particularly of composite propellants, with regard to electric discharges.

2. CAPACITIVE DISCHARGE TESTS.

2.1. Presentation. :

At the beginning of the study worked out by SNPE we had at our disposal an electric spark priming test which had been used for a long time by most of the pyrotechnical plants which have to characterize primer explosives in regard to static electricity. The principle of the testing, (sketch depicted in figure 1) consist to determine the minimum energy for which twenty no reaction successive tests were performed. It is understood that the application of an immediate upper energy, would generate a reaction.

This test, involving a maximum energy of 726 mJ (i.e. a 3000 - pF capacity charged under a 22-KV voltage) does not result in the ignition of solid propellants whatever may be their configurations : either on a chipped form or on a pellet form similar to the dimensions of the negative electrode recess.

It should be noted, however, that propellant pellets are sometimes perforated in their center, after a capacitive discharge.

The analysis of the first results lets us assume that the ignition of some propellants would be possible, should the values of the following parameters be increased :

- size of samples (masse effet)
- duration of discharge in the RC circuit (R is used as the propellant resistance, and C as the capacity applied to the propellant extremities (time required for ignition),
- energy delivered.

In view of the above parameters, an equipment was created, it is depicted in figure 2.

The propellant sample to be tested is a cylindrical 90 mm diameter grain and 100 or 200 mm long (investigation of the constant of time impact $RC = f(L, C)$). The grain was located between two electrodes. The electrode system is a "point-plane type" ⁽¹⁾ to a sharp area is more intense. In order to get an adequate contact and distribution of the electric current, the rounded surface of the propellant grain facing the negative circular electrode is coated with a silver lacquer.

In order to investigate the influence of ambient hygrometry, the propellant grain was placed inside a $4 \cdot 10^{13} \Omega \text{m}$ volumic resistivity plexiglass chamber.

In order to measure the current accross the propellant grain an adequate resistor following the negative electrode was inserted into the discharge circuit. The electric equipment could deliver a 5.6 Joules energy (i.e. a 34.7-nF capacity charged under a 30-KV voltage).

2.2. Results.

A lot of tests were conducted and the main results are described here under :

2.2.1. - some propellants react and the reaction can take two forms :

. Ignition : films taken at 2000 frames per second show that, during ignition, cracks appear in the propellant. Through the above cracks, thick bursts of flames are generated. Then the combustion spread out.

(1) which is very penalizing because the electric field close.

According to the sharp noises heard, reactions are very severe most of the time.

. Cracking : the no-ignition tests after discharge show large cracks. These cracks, according to X-ray pictures, were made of a large quantity of small ducts (approximately 5/10 th mm diameter).

Outside, the cracks appear mostly on the lateral surface and on the silver-coated rounded surface. The sketch of figure 3 shows a cracked propellant grain.

On the other hand, it should be pointed out that the cracking phenomenon took place always before the ignition phenomenon.

2.2.2. - the reaction is very casual and may happen after successive capacitive discharges. (number of discharges is called n). For example, a propellant grain may crack at the 2nd and at the 10th discharge and may ignite only at the 20th one.

However, it was observed that usually n is less than 30.

2.2.3. - in case of no reaction the discharge current complies with the Ohm's law i.e. the measured time constant almost equals the time constant calculated in accordance with the relation : $\tau = RC$, C is the capacity applied to extremities of the propellant grain and R the propellant grain resistance.

Calculation of resistance R is based on the geometric dimensions of the grain and on the volumic resistivity measured by a KEITLEY-type cell (this measurement is taken on a 90 mm diameter and 5 mm thick propellant slice).

2.2.4. - In case of reaction, the measurements of discharge currents show that cracking or ignition phenomena appear as soon as the outside capacity is connected to the propellant grain extremities .

During the ignition phenomenon, the current shifts from 0 to several amperes within a few microseconds.

After cracking the current generally becomes 1000 times higher than measurements conducted prior to cracking. Therefore, cracks degrade the propellant and lower down the volumic resistivity. Typical examples of discharge currents are shown in figure 4.

2.2.5. - Parameters such as :

- . block length (100 to 200 mm),
- . presence of inhibitor,
- . outside hygrometry,

do not seem to have an important impact in the above tests.

2.2.6. - The casual nature of the results cannot allow to estimate a minimum energy of non-reaction, for a given propellant.

For this type of test, it should be noted that some propellants ignite at an 100 mJ energy level, approximately. This energy was calculated in accordance to the equation $Q = \frac{1}{2} CU^2$.

2.2.7. - Composite propellants (tested so far), with a volumic resistivity from 10^5 to $10^6 \Omega m$, do not react to a maximum energy of 15.6 joules.

2.2.8. - Composite propellants, with a volumic resistivity ranging from 10^8 to $10^{11} \Omega m$, are likely to react to capacitive discharges. In that case, the resistivity is not a discriminative criterion in regard to sensitivity to discharges.

2.3. Analysis.

In compliance with above results, a discriminating procedure was worked out : 3 identical grains from the same composition are submitted to 30 (above 30 it was noticed that the probability of ignition is virtually non-existent) 15.6 Joules (i.e. a 34.7 nF capacity under 30 KV).

A composition is called sensitive to capacitive discharges when, out of the 90 discharges, at least one cracking phenomenon is observed.

3. CONSTANT POTENTIAL TESTS.

3.1. Presentation.

Based on the observation that the reaction starts as soon as the capacity is connected to the propellant grain extremities, it is assumed that application of one voltage step (without capacity) would be sufficient to generate similar effects. For that reason, a second coupling shown in figure 5 was developed.

The cylindrical, 90 mm diameter and 100 or 200 mm long, propellant grain, the round surfaces of which were coated with a silver lacquer, is placed, along the symmetric axis, between two plane circular electrodes.

The constant potential was applied by 2-KV increments every five minutes in order to verify the influence of the joule effect.

3.2. Results.

3.2.1. - Propellants reacting to the capacitive discharge test, also react as soon as a potential, is applied. The above potential is called critical potential. The reactions are similar to the above ones.

3.2.2. - Conduction current, described in figure 6, complies with the Ohm's law below the critical potential. Occasionally, before the applied potential reaches the critical potential level, the current is submitted to "variations".

For most of the tests, the reaction is obtained as soon as the modification of the voltage level is applied.

A test, for which the last voltage level applied was very close to the critical potential, shows a very specific conduction current (see figure 7).

Starting from the 12-KV level and after a one minute period of time, pulses period of which are approximately constant, are noticed. The period value is close to the measured time constant of the propellant considered ($\approx 1,2$ s) amplitude of which exponentially increases. Each of these pulses was accompanied by a sharp snapping noise.

After a 2-minute period of time, a large crack is observed and the current stabilized at a 3,5 mA value, i.e. 1000 times the value of the initial current.

Then again, reactions are casual and it is very difficult to evaluate a propellant dielectric strength K such that :

$$K = U_c/L$$

where U_c is the critical potential and L the length of the propellant grain.

3.2.3. - Some propellants ignite at very low voltage, around 1 KV.

3.2.4. Even during long periods of time (30 minutes) the joule effect which may be characterized by the equation : $E = RI^2t$, does not cause any reaction.

4. ASSUMPTIONS ABOUT THE REACTION MECHANISM.

For propellants classified as "sensitive to capacitive discharges", the analysis of the facts such as, for example, initiation of the cracking phenomenon prior to the ignition phenomenon, let assume that the reaction mechanism is divided into two main phases :

- 1st phase : initiation of the cracking phenomenon in connection with a critical potential U_c .

- 2nd phase : initiation of an ignition phenomenon in connection with a critical energy E_c .

The above is explained in figure 8.

All the facts combine to prove out that the reaction starts inside the propellant material. The reaction start is located in microscopic areas. As a matter of fact, if the propellant, in its general form, may be considered as an isotropic environment, this is no longer true at the level of various particles such as aluminum, ammonium perchlorate, etc.

The existence of a critical potential shows that cracking is caused by one or several electric phenomena.

Among the well-known electric phenomena such as semi-conduction (case of the ZENER diode which becomes conductive at a given potential by avalanche effect), piezo-electricity, micro-breakdown (between two conductive particles separated by a dielectric) it is assumed that micro-breakdown can be considered as the most probable because the two following observations are support any this hypothesis.

- The measurements of volumic resistivity of aluminum powder (used for propulsion) packaged in a plexiglass tube show that, for a critical potential, the value of resistivity shifts from 10^7 to $10^3 \Omega m$. This corresponds to a breakdown, for a number of particles, of the alumina layer that covers pure aluminum particles on approximately 40 Å thickness.

- Assuming that the electric diagram for a propellant grain is a dielectric with a parallel RC circuit, it can be imagine that this grain is a complex assembly of RC circuits and that the junction points are conductive particles (e.g. aluminum grains).

Admitting that the breakdown between two conductive points, results in the destruction of the dielectric connection between these two points, and setting up arbitrary initial conditions, it can be proved, by simulation with electronic components or by calculation, that a U potential applied to the extremities (see sketch shown in figure 9) can produce a current (layout is depicted in figure 10). It must be noted that the above layout looks like figure 7 layout.

5. DETERMINATION OF A CRITERION BASED ON RESISTIVITY
AS A FUNCTION OF TEMPERATURE.

Over all the compositions tested, the volumic resistivity measurements, from -40 to + 80°C (-40 to + 176°F) show that 3 different laws of resistivity may be encountered versus temperature. The laws, shown in figure 11 are represented by one or two straight lines (1 and 2) with different slopes and equations as follows :

$$\ln (\rho v) = \frac{E}{KT} + \text{constant}$$

where : T = absolute temperature in K degree

K = BOLTZMANN's constant

E = energy in eV.

This law is similar to semiconductors. The existence of 2 straight lines points out a change in the type of conduction starting from a given transitional temperature. The values of the energies calculated from the slopes of the straight lines range from 0 to 2 eV.

The most remarkable observation is that the compositions which react to capacitive discharges follows a type-I law (i.e; the proportion E_1/E_2 is above 1) where as the compositions which do not react have a type II or III-law (i.e. the proportion E_1/E_2 is lower or equal to 1).

6. DETERMINATION OF A CRITERION BASED UPON PERCOLATION.

A factorial investigation of the propellants active constituents was carried out. A compromise between a strict investigation of parameters and the feasibility of specific formulations was worked out.

The results of this investigation mainly emphasize :

- the aluminum particle size.
- the electric characteristics of the binders
(binder = prepolymer + miscellaneous additives).

Since the aluminum granulometry is concerned, and for a constant aluminum content the decrease in diameter of aluminum particle size, (i.e. their increase in number), results in sensitive to capacitive discharges compositions.

The impact of the number of conductive particles was quite naturally the next step to investigate percolation phenomena.

Percolation, as theoretically defined, is independent of the voltage applied and allows - (for a given conducting and insulating particle system) - to determine the critical level of N_c/N_i ratio (N_c = number of conducting particles and N_i = number of insulating particles) above which the entire system is fully conducting.

In the case of a composite propellant, it does not seem possible to obtain such a level, because aluminum particles are working as insulations, although conductive inside.

In fact, the phenomenon that we have to work with comes from theoretical percolation phenomenon and, therefore, a "P breakdown percolation" coefficient was defined as follows :

$$P = \frac{N_c/N_i}{\sigma_L V_L}$$

where : σ_L = binder conductivity
 V_L = binder unit volume

The above coefficient covers 9 parameters.

Currently, the validation phase was conducted over about fifty different formulations. It is now possible to know a range for the critical P value : above this value, formulations are sensitive to capacitive discharges, under they are not.

However the above critical P value is not clean and there remains an area where this criterion is uncertain.

CONCLUSION.

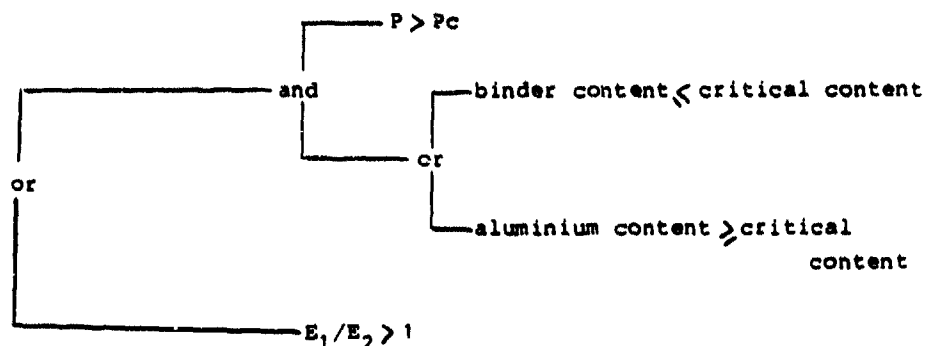
As we tried to demonstrate, it looks probable that the reaction mechanism is, first, conducted by a micro-breakdown phenomenon.

In order to understand this mechanism, a theoretical and fundamental study will be worked out.

Critical electrical fields between particles will be more specially studied.

To currently carry out our safety problems, two empirical criteria may be used, one is based on percolation phenomenon, the other is based on specific resistivity laws versus temperature.

So, a propellant will be classified as sensitive to static electricity if the following conditions are carried out.



Above criteria are systematically applied during new formulations developments. Propellant behaviour may be anticipated and may be modified if necessary so that safety cautions are taken to prevent any risk either during conception or carrying out of the materials.

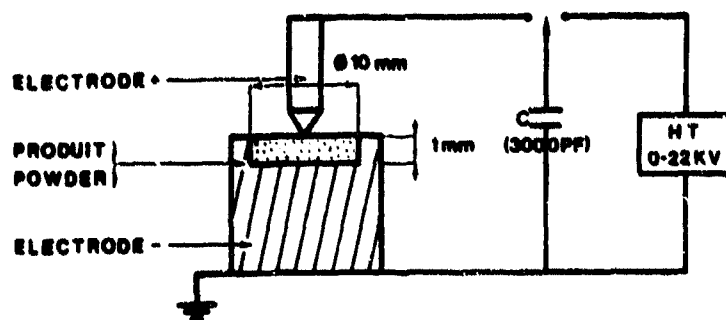


fig 1

Schematic arrangement of ignition test by electrostatic spark

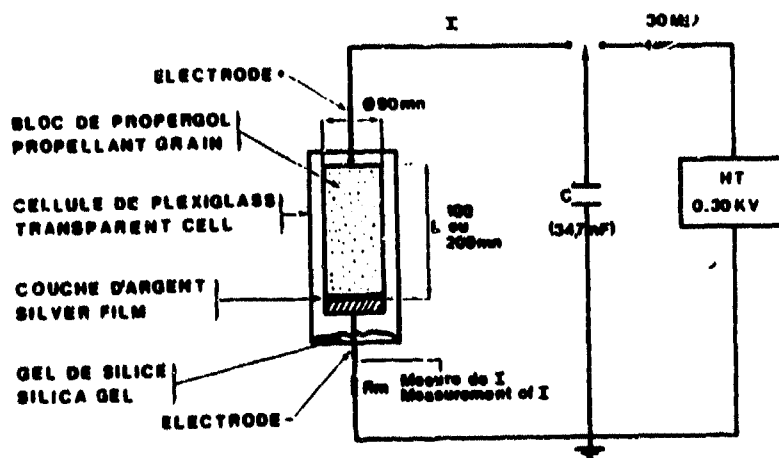


fig 2

Schematic arrangement for capacitive discharges test on the propellant grains

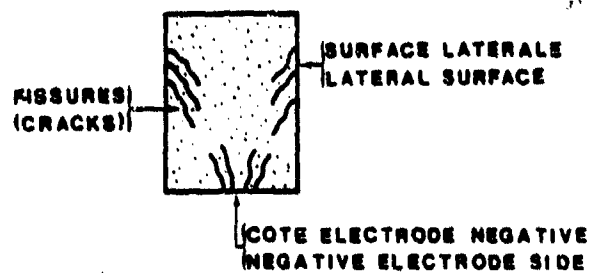


fig 3

Schematic diagram of a cracked propellant grain

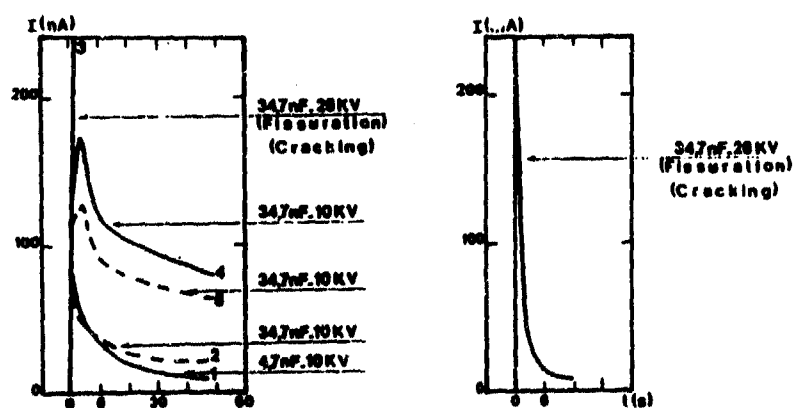


fig 4

Curves of discharges current(I) versus time (t) for different discharges in a "sensitive" propellant

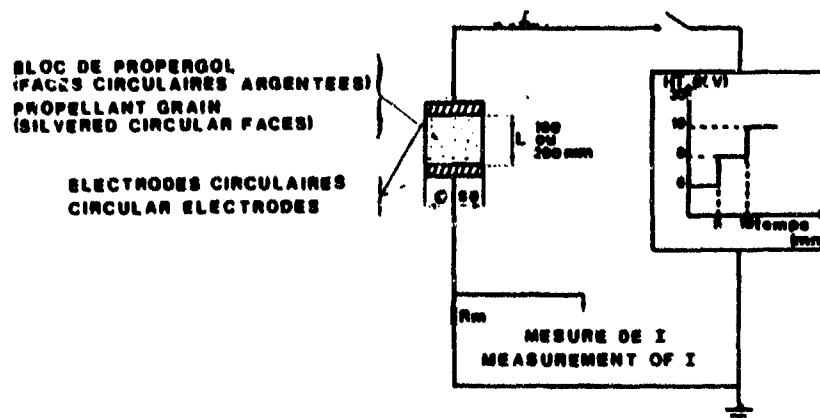


fig 5
SCHEMATIC ARRANGEMENT FOR POTENTIAL TEST

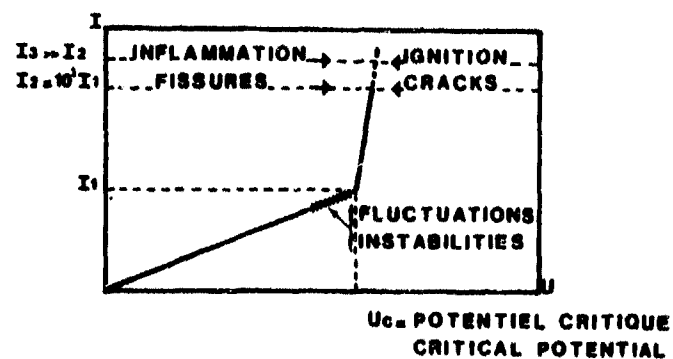
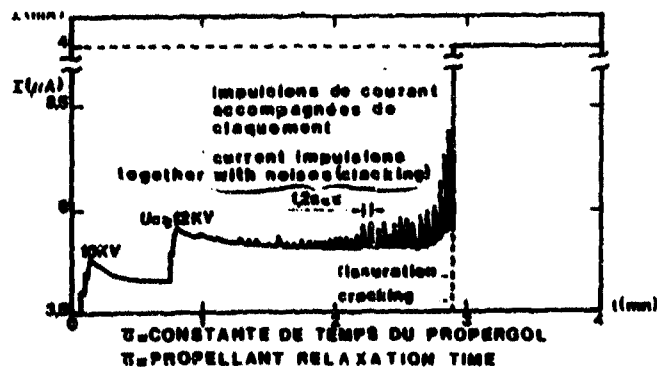


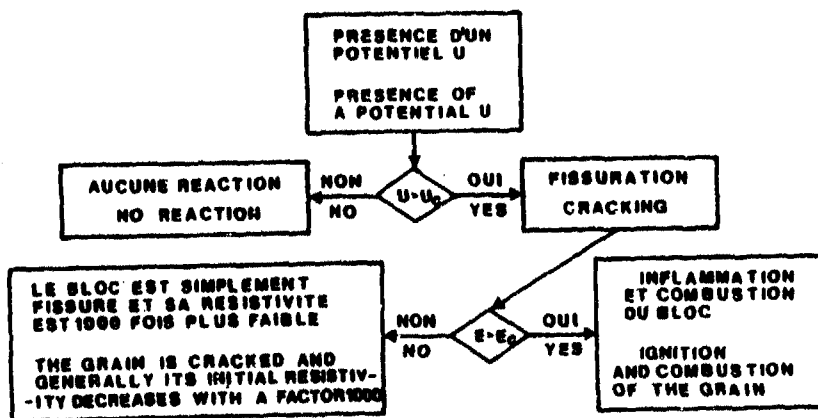
fig 6

General evolution of conduction current (I)
versus potential (U)



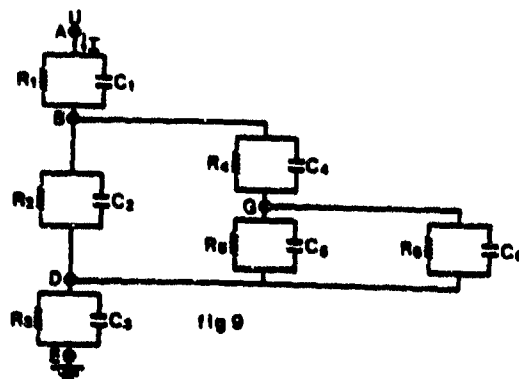
1197

Typical curve of conduction current (I) versus time (t) in a "sensitive" propellant (initial $\psi_v = 10^{-4}$ (2m))

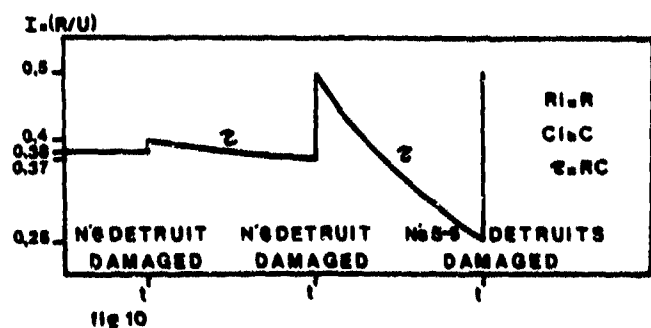


1198

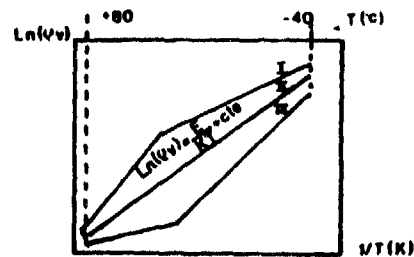
Schematic diagram of the reaction mechanism



Schematic diagram of a complex system of RC circuits



Evolution of current (I) versus time (t) circulating from point A to E



LOI I. PROPERGOL "SENSIBLE"
LAW I. "SENSITIVE" PROPELLANT $E_1/E_2 > 1$

LOIS II ET III. PROPERGOL "NON SENSIBLE"
LAWS II AND III. "NO SENSITIVE" PROPELLANT $E_1/E_2 < 1$

fig 11

Volumic resistivity (Vv) as function of $1/T(K)$

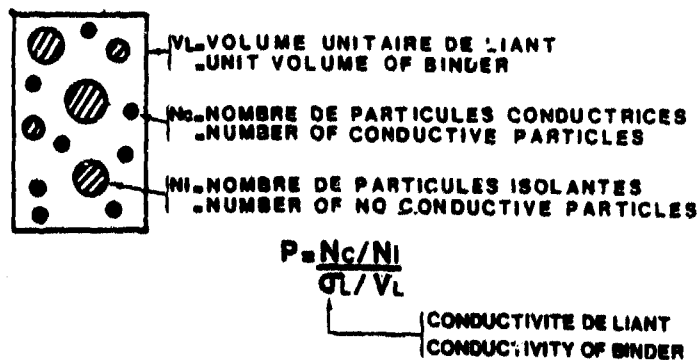


fig 12

Definition of the "breakdown percolation" coefficient (P)

RISK ANALYSIS - GRASPING THE NETTLE

R R Watson

Health & Safety Executive

United Kingdom

SUMMARY

1. This paper describes a recent problem where risk analysis enabled the British Government to formulate a compromise solution which avoided costly extreme courses of action. A major leisure centre had been built inside the Inhabited Building Distance of a busy explosives wharf. The paper indicates the techniques of the analysis and discusses ways to present data on casualties and damage in order to provide policy makers with a realistic basis for decisions.

INTRODUCTION

2. Some of the audience today will recognise in Figure 1 the former town of Port Chicago, California which was a constraint on the explosives limit for the loading piers of Naval Weapons Station Concord, a primary facility for the Armed Forces and the Military Assistance Programme. Others may view the picture differently and recognise what for many years constituted an ever-present threat to the lives and property of the residents of the town. It was not a hypothetical threat. Figure 2 shows the damage to the theatre in 1944 when a cargo ship being loaded with ammunition exploded killing 320 people in the area and causing \$ 12 million damage to property. A solution was found when Congress, after a careful study of the options in 1967, authorised \$ 20 million to eliminate the hazards to the locality by compulsory purchase of the town to provide a buffer zone of 2 miles radius from the piers.

3. This solution might not have been adopted if the town had been as large as that shown in Figure 3. In 1978 the Health and Safety Executive (UK) became aware of the existence of a new leisure centre (Figure 4) within the Inhabited Building Distance of a busy explosives wharf. There were proposals to develop the area into a major recreational complex (Figure 5). The centre had received planning approval when there were no requirements for consultation with the HSE or its predecessors. Explosives ships were about 700 metres from the leisure centre as shown in Figure 6 which is the view of the wharf from the cafeteria in the leisure centre.

SIMPLE BUT DRASTIC SOLUTIONS

4. Traditional concepts of explosives safety embodied in Quantity-Distance tables indicated two obvious solutions. Either the leisure centre should be closed down or the explosives operations at the wharf should cease. Neither of these courses of action was acceptable. The community would not accept closure of its multi-million dollar showpiece which attracted up to 45,000 people per week. Some of them worked in

Paper written for the Department of Defense Explosives Safety Seminar, Norfolk, Virginia 25 August 1982 and also presented to Ministry of Defence (ESTC) Seminar on Risk and Hazard Analysis in the Explosives Field, Fort Halstead, Kent 30 September 1982.

the explosives factory whose operations would be drastically curtailed by closure of the wharf; and with unemployment running at nearly 20%, the resultant loss of jobs was unacceptable. It was necessary to set aside quantity-distance concepts and adopt a fresh approach to the problem.

NEW WAYS OF APPRAISING EXPLOSIVES SAFETY

5. In 1969 the Explosives Storage and Transport Committee of the Ministry of Defence and the Inspectorate of Explosives in the Home Office reviewed the methods of determining explosives limits in British harbours. The joint committee decided to introduce weighting factors into the calculation to take cognizance of the different degree of risk (probability of explosion) presented by (for example) fused, unshuttered ammunition compared with unfused ammunition and packages of stable high explosive. This was the first departure from the traditional doctrine that explosives limits must be based on the assumption that the maximum credible accident will occur sooner or later so that consequences alone should be considered, not the likelihood of the postulated event in conjunction with the consequences (overall risk).

6. There have been several papers at recent Explosives Safety Board Seminars which have shown how risk analysis or risk appraisal may be used to supplement traditional tables of quantity-distances. Schneider of Switzerland and Jenssen of Norway have argued for a greater willingness to use these techniques when the orthodox approach is too inflexible. (Risk analysis appears to have become a respectable topic for these seminars; the topic session includes 5 papers this week). The Health and Safety Executive decided in 1978 to apply risk analysis to the intractable problem of the explosives wharf and the leisure centre.

7. Several speakers have uttered warnings at these seminars that although it is relatively simple to calculate the individual risk and the societal risk corresponding to various courses of action, a more difficult task lies at the interface between the safety engineers who present these options and the administrators or politicians who are asked to decide which option to adopt. There is understandable reluctance to endorse a proposal which, after all reasonably practicable precautions have been taken, acknowledges a residual but acceptably remote risk of serious casualties. It is this "nettle" that has to be grasped if the techniques of risk appraisal are to be exploited fully.

ASSESSMENT OF THE POSSIBLE CONSEQUENCES OF AN EXPLOSION

8. The first part of the analysis of the wharf problem was to predict the cost of damage to property in the vicinity and the number of casualties. Experience from past accidental explosions gives an indication of what to expect. The locale is at least important as the quantity of explosives involved. An explosion near Portsmouth, England in 1950 (Figure 7) was at an isolated jetty with no dwellings within the

Inhabited Building Distance so the majority of claims were for broken windows in the city. At Gibraltar (Figure 8) the sloping terrain and dense development close to the dockyard would be expected to maximise the consequences of an explosion but owing to the relatively small quantity of explosives involved in an explosion there in 1950, most serious damage was confined to the installation. The variability of fatalities for a given quantity of explosives is illustrated in Figure 9; there is some correlation between the quantity and the fatalities but clearly it is important to take account of the disposition of people at the time of an explosion.

9. In order to make a realistic prediction, a large scale map of the town was obtained and circles were drawn around the assumed centre of the explosives wharf at intervals of 50 metres out to 2500 m. This represented the expanding blast wave, the intensity of which could be determined by well known techniques assuming a maximum credible explosion of 50, 100, 200 tonnes etc of explosives of Division 1.1 (mass risk). Although casualties are more important than property damage, it was convenient to start by assessing damage. The value of property in each 50 m ring was calculated by laboriously counting the buildings of each type on the map. For each ring, the average cost of repairs was calculated using the combined data from World War II bombing of British brick dwellings and the report of the Port Chicago explosion involving different types of construction. The costs were then integrated over all the rings to give the total cost of damage for each assumed size of explosion at the wharf. The total cost was not unduly large and was less than the cost of damage to the leisure centre. In any case concern over the likely casualties among patrons and in the town as a whole eclipsed these materialistic considerations.

10. Next, an estimate was made of the likely number of casualties in consequence of the calculated levels of damage to dwellings, on the assumption of one occupant during working hours but four occupants at night and weekends. This type of prediction was somewhat crude, being based on statistical data from a variety of accidents, but was nevertheless useful for making comparisons. The most difficult prediction was the number of casualties in the leisure centre. Neither data from brick built houses nor that from US timber frame buildings is really relevant for a large span building of steel frame construction with modern cladding materials and extensive areas of glazing. The number of occupants at risk varies from a skeleton staff in silent hours to around 4,500 at peak hours. The number of patrons was introduced as a parameter in the presentation of results of the analysis.

11. The assessment had reached the stage at which the ramifications of the various options could be communicated from the safety engineers to the administrators. Figure 10 shows how the expected number of fatalities increases with the explosives limit and with the number of patrons who happened to be present at the moment of the postulated explosion. Consideration of this data led to the conclusion that some administrative arrangement should be sought to ensure that large quantities of explosives

would never be handled on the wharf or ships while the leisure centre was operating near its peak, and vice versa. Despite the practical difficulties of operating such an arrangement, it has been put into effect by the mutual collaboration of the authorities backed up by the powers of the Health and Safety at Work etc Act 1974. The relationships in Figure 10 were used to determine practical guidelines for the numbers of occupants to be permitted at different times of day, night and weekends. This should ensure that the chances of the worst credible accident occurring were sufficiently remote to be acceptable.

ASSESSMENT OF THE LIKELIHOOD OF AN EXPLOSION

12. The statement that a certain number of casualties would be tolerable raises many questions which are familiar to those involved in risk analysis. "Tolerable to whom?" asks the local resident. Curiously in this case there was no local pressure group demanding a reduction in hazards. Explosives had been made and shipped through the area for over a century; many residents were economically involved in the trade or had relatives who had benefited from it. In this situation it is a function of government to judge whether risks, which people are prepared to accept based on their own perception of the risks, should be permitted to continue or whether, in the light of specialist knowledge not available to those at risk, there should be change. A recurring problem in a democracy with high technology is how and to what extent government should make available to the public the plethora of information necessary to make well informed judgements. Paternalistic government may be resented; on the other hand it is very difficult for scientists and engineers to communicate highly technical information about risks and casualties in a form which is both neutral and unlikely to be misinterpreted. Should the people at risk have the same opportunities as the administrators and politicians to say whether the risks are acceptable? If so, would they grasp the nettle?

13. In the present case the government and its officials tried to steer a middle course. In order that the government could judge what numbers of patrons could be permitted in the leisure centre and what explosives limit should be assigned to the wharf, it was necessary to estimate the likelihood of an explosion involving simultaneously 50 or 100 or 200 tonnes etc of high explosives. This phase of the analysis involved the development of the usual fault tree, to ascertain what events could lead to the explosion and to assign probabilities to each factor. It also necessitated assessment of loading operations at the wharf to determine the likelihood that an explosion would involve only a small quantity of explosives (say one package or pallet) or an intermediate quantity (a rail vehicle full) or the whole of the explosives on the wharf and in the ship(s) just at the time that this quantity was at its peak.

14. Figure 11 is a much simplified indication of the factors which were taken into account. More or less subjective values of probability were assigned to the factors, using historical data or experimental results to check them wherever possible. Items like the risk of a spectacular suicide were very difficult to assess. The analysis was comprehensive and therefore much too expensive to adopt as a technique for tackling routine

problems with explosive quantity-distances. It was a collaborative effort, with the company concerned conducting the detailed analysis while government officials prescribed the guidelines for the study and monitored progress.

15. Many useful lessons were learnt from this study. A number of improvements were identified which would reduce the risks considerably. The explosives industry has always tried to design fail-safe features into its operations, as shown in Figure 12. This is not, as you might think at first sight, a Scotsman tending his moonshine on a grand scale. It is an early fail-safe monitoring device for nitroglycerine production. The worker is carefully watching the temperature to make sure it does not rise excessively; if he should fall asleep during this monotonous task, his one-legged stool would make sure he woke up again.

16. The analysis identified those factors which contributed most to the possibility of explosion of a ship. These included impact of packages of explosives during manhandling operations at the wharf; friction-initiated explosion of split powder explosives during loading/unloading; and fires started aboard the ship which spread to the explosives. The introduction of palletised loading, or better still freight containers with appropriate lifting equipment, would reduce the first two risks considerably but such changes could not be brought about quickly. On the other hand fire prevention measures, already at a high standard, could be further improved quickly. This involved some inconvenience, such as the banning of fires in the ship's galley, and additional effort such as the institution of a fire risk survey before loading operations commenced to remove potential fire risks like paints, solvents, rags which usually abound on board ships. It may be remarked that the intuition of any good safety officer might have led to similar observations but the risk analysis quantified the risks attaching to these factors and so highlighted those deserving most attention. The analysis also showed up a number of factors which were less obvious.

PRESENTATION OF THE RESULTS

17. After all the recommendations for improvements had been made, and the administrative arrangements had been worked out to restrict activities at both the leisure centre and the wharf so that they might co-exist, the crucial question remained: "Was the residual risk tolerable?" It should be emphasised that we were dealing with a fait accompli. Unquestionably the risk would not have been tolerated in the case of a proposal for a new project to build such a leisure centre so close an explosives wharf. Risk analysis begins only when quantity-distances fail to deal with a situation.

18. An earlier study on a much larger scale had been completed by the Health and Safety Executive and had been openly published in the report "Canvey: an investigation of potential hazards from operations in the Canvey Island/Thurrock area" (June 1978). Figure 13 shows the societal risk at the explosives wharf and that of a particular installation in the Canvey complex, before and after certain improvements. One could devote a seminar to the caption for the shaded zone at the bottom of the graph. Is any particular value of risk generally deemed to be "negligible" or should the value vary with the magnitude of the consequences?

19. Comparisons can be misleading. The word "fatalities" is sometimes used to include seriously injured people rather than deaths. The hazard from high explosives at a fixed site is different in character from explosive or toxic gas clouds which drift downwind and can therefore affect much greater numbers of people. The capital investments in facilities may be quite different and so may the shift of resources required to effect a significant reduction of risk. Despite all these reservations, this comparison was instrumental in resolving the problem without recourse to either of the costly extreme courses of action mentioned earlier.

20. The press devised some emotive headlines (Figure 14) but the general reaction of the public and local organisations seemed to be that the government had got it about right. The compromise solution was not strongly opposed by anyone.

LOOKING TO THE FUTURE - AND THE PAST

21. In conclusion, risk analysis served well in this instance. It will not usurp the role of traditional explosives quantity-distances criteria because it is much too time consuming, if done properly. Its function will be to provide the means to explore and evaluate other courses of action, and particularly to rank them to help decide the most cost effective option, when the traditional rules cannot be observed for some compelling reason.

22. In the case of this wharf, the analysis highlighted the potential advantages of unitised loading of explosives (Figure 15). Incidentally, this could be a tricky operation at an anchorage which is sometimes required in other harbours because of strict observance of quantity-distance concepts at berths. It could be even more tricky in the case of a freight container at an anchorage (Figure 16) unless loading is restricted to reasonably calm seas and winds. The ideal would be the use of freight containers at dedicated container berths but Harbour Masters are reluctant to risk their valuable installations for goods of Division 1.1.

23. Life was much simpler 100 years ago. Figure 17 shows how explosives used to be loaded near this troublesome wharf. One simply carried a package down the beach, paddled to a rowing boat, and rowed out to the ship. Not only was the operation safe, it was secure thanks to the ubiquitous British policeman.

*

*

*

ACKNOWLEDGEMENTS

British Crown copyright (1982) is reserved for this paper which is published by permission of the Controller of Her Britannic Majesty's Stationery Office. Illustrations are reproduced by kind permission of:

Daily Express	(Figure 7)
Irvine Development Corporation	(Figures 3 and 5)
Nobel's Explosives Co Ltd	(Figures 12 and 17).



FIG 1 FORMER TOWN OF PORT CHICAGO

Damage sustained by Port Chicago theater
in 1944 explosion, 5940 feet from blast.



FIG 2

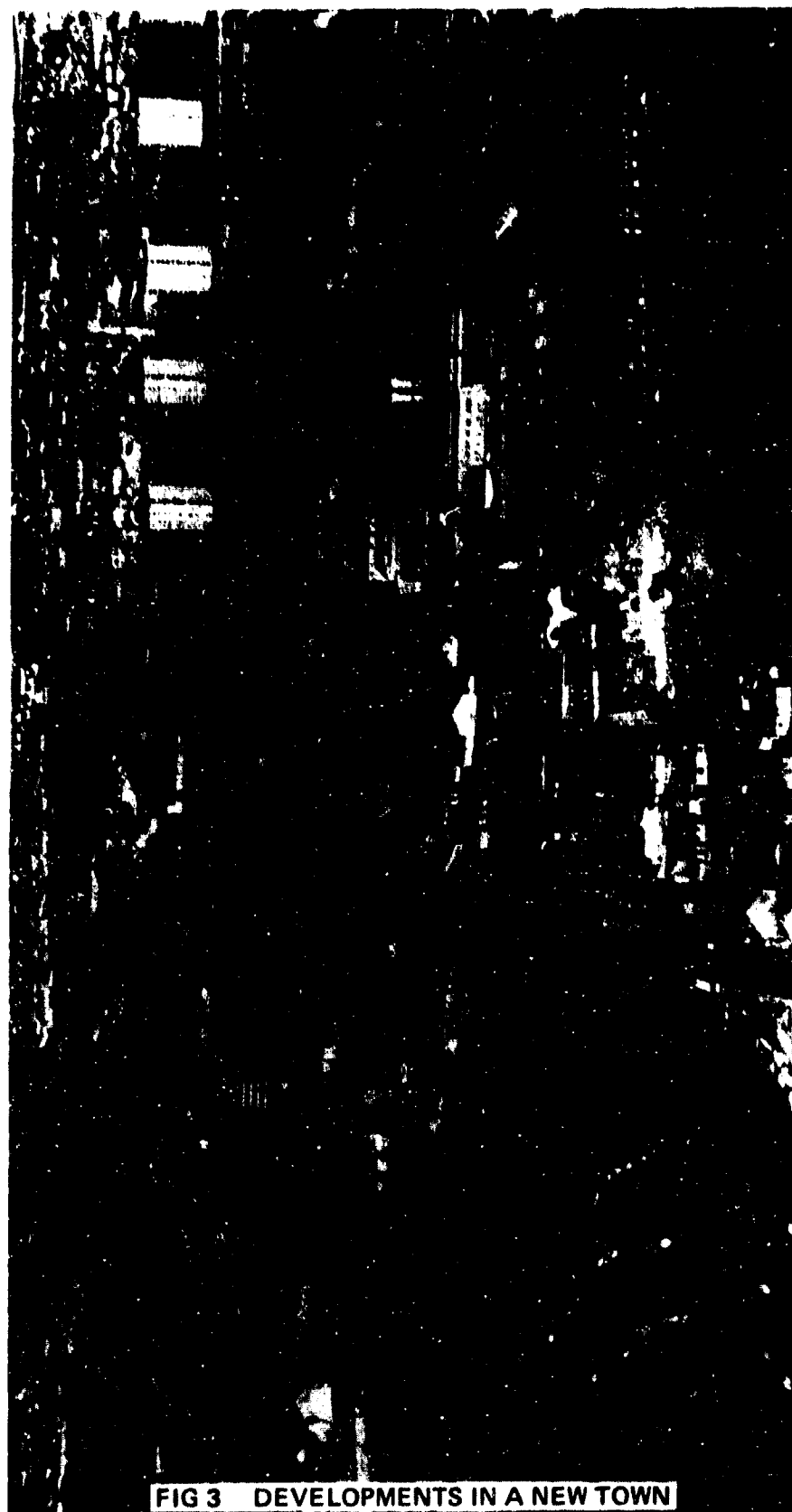


FIG 3 DEVELOPMENTS IN A NEW TOWN



FIG 4 LEISURE CENTRE



FIG 5 PROPOSED RECREATION CENTRE



FIG 6 EXPLOSIVES SHIPS VIEWED FROM LEISURE CENTRE

No. 15,624

SATURDAY JULY 15 1950

CONTROLLING SHAREHOLDER
LORD BEAVERBROOK

Weather: Rain; wind



DAILY EXPRESSES

EXPLOSION *TWO ELASTIC FIRE*
Naval Ammunition

WOMEN crouch in ditches
waiting for all clear

BATTLE

Beds cross river—
all round G.L.s
more troops

BOMB BARGES BLOW UP

Train flung in sea

FIG 7

NAVY DEPOT BLAST

Explosion built up: Portsmouth, Friday

AN explosion in a naval ammunition barge—one of a string of eight—being loaded with 500lb. bombs in Portsmouth Harbour tonight touched off a second barge laden with cordite and depth charges.

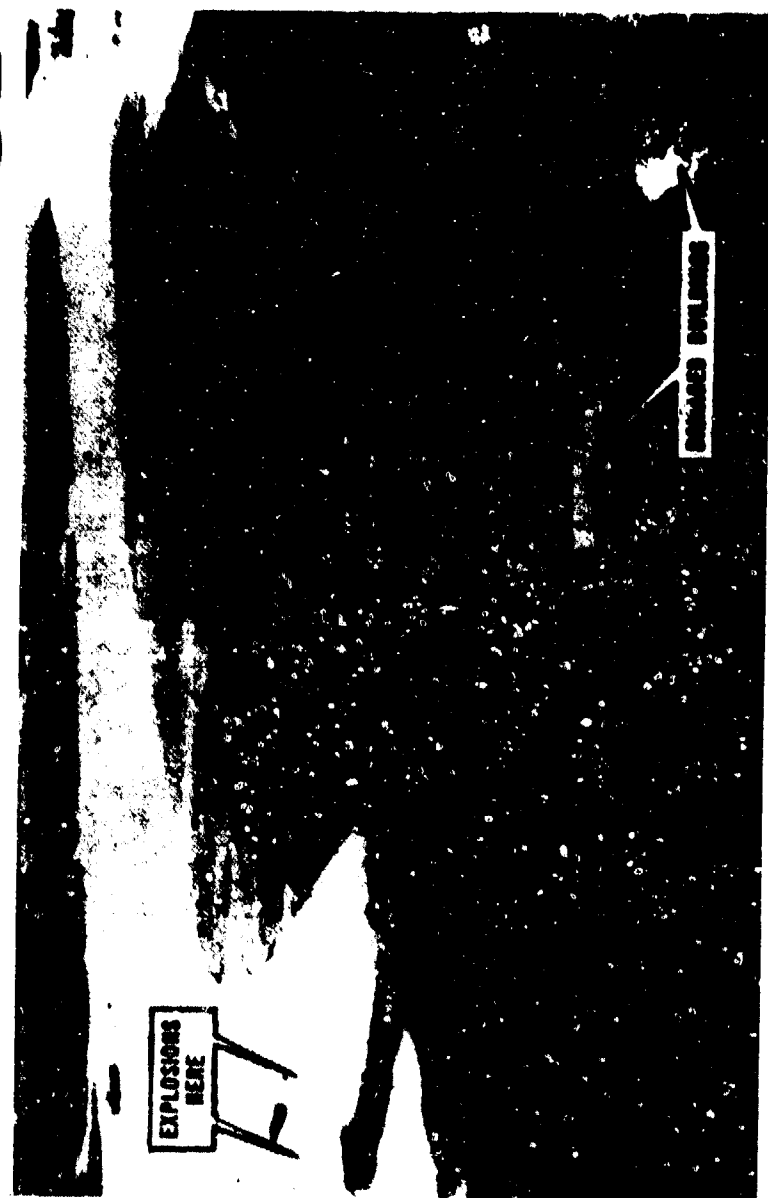
This second explosion wrecked the end of the jetty of the Royal Naval Ammunition Depot at Bechtam, Gosport, causing an ammunition train to plunge into the water.

SLASHED THE ROPES

Moorings ropes were slashed in an attempt to drift the other six barges further out into the harbour, but they did not go far before they too blew up. Their ammunition was to have been taken to a warship in the harbour.

The blast rocked the coast-side 20 miles round the harbour, damaged property over a two-mile radius, and sent thousands of people to cellars in fear of further blasts.

Hundreds of other people, many of them women, sheltered in roadside ditches, waiting for the "All clear". Only six people were detained in hospital—they were



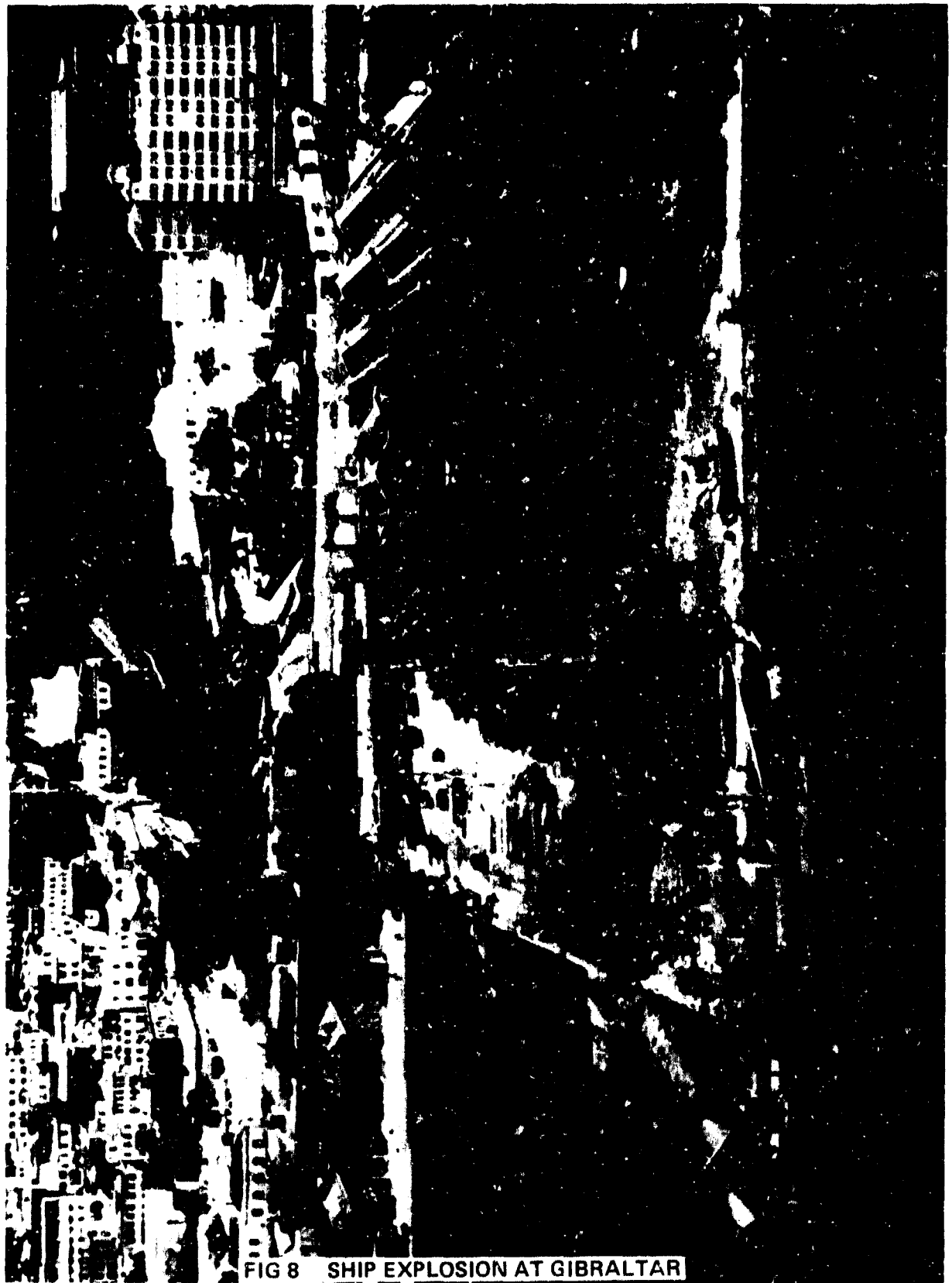
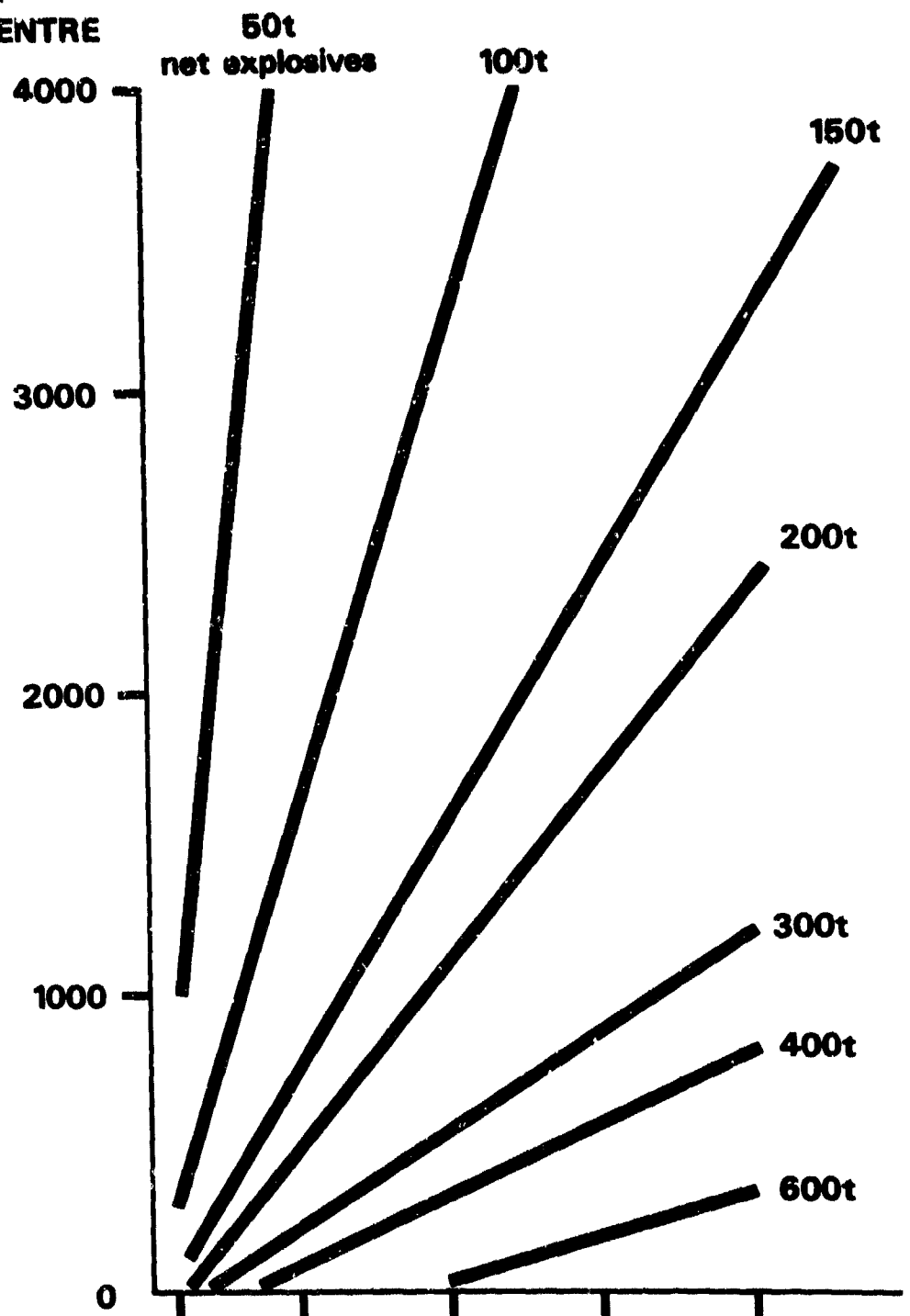


FIG 8 SHIP EXPLOSION AT GIBRALTAR

**No. of PERSONS
AT RISK IN
LEISURE CENTRE**



No. of FATALITIES IN THE LEISURE CENTRE & TOWN

FIG 10 ESTIMATED FATALITIES

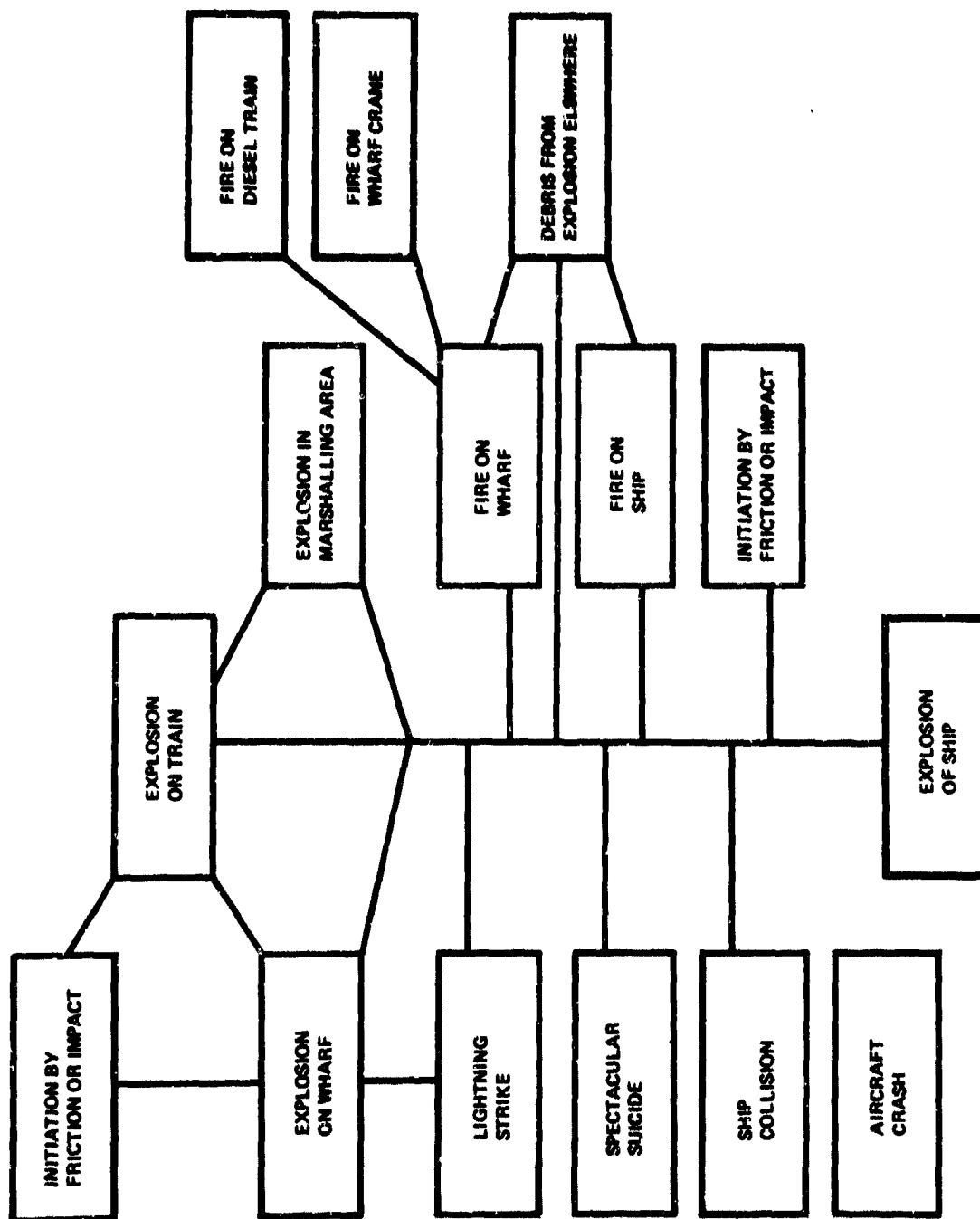


FIG 11 SIMPLIFIED LOGIC DIAGRAM



FIG 12 SCOTCH PRODUCTION METHODS HAVE BEEN
CONSTANTLY IMPROVED FOR GENERATIONS

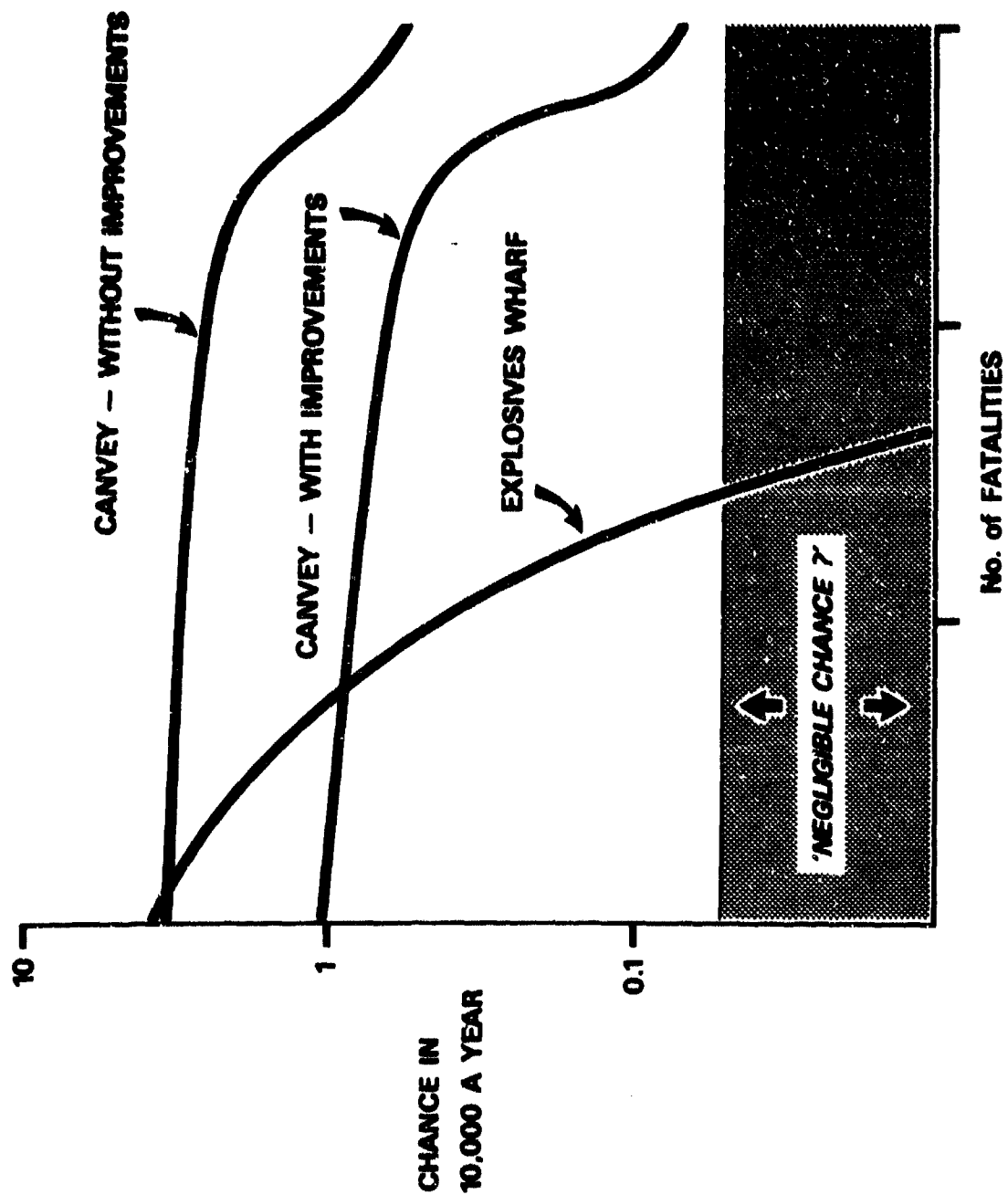


FIG 13 COMPARISON OF SOCIETAL RISKS AT CANVEY AND EXPLOSIVES WHARF

Explosives report
rock a new town

BOOMWATCH

DECISION FOR

CIL FURY

THE PRICE
OF SAFETY

Watch

file is ready

ST

leisure centre

safety do

WOMAN

Appeal to

'danger' n

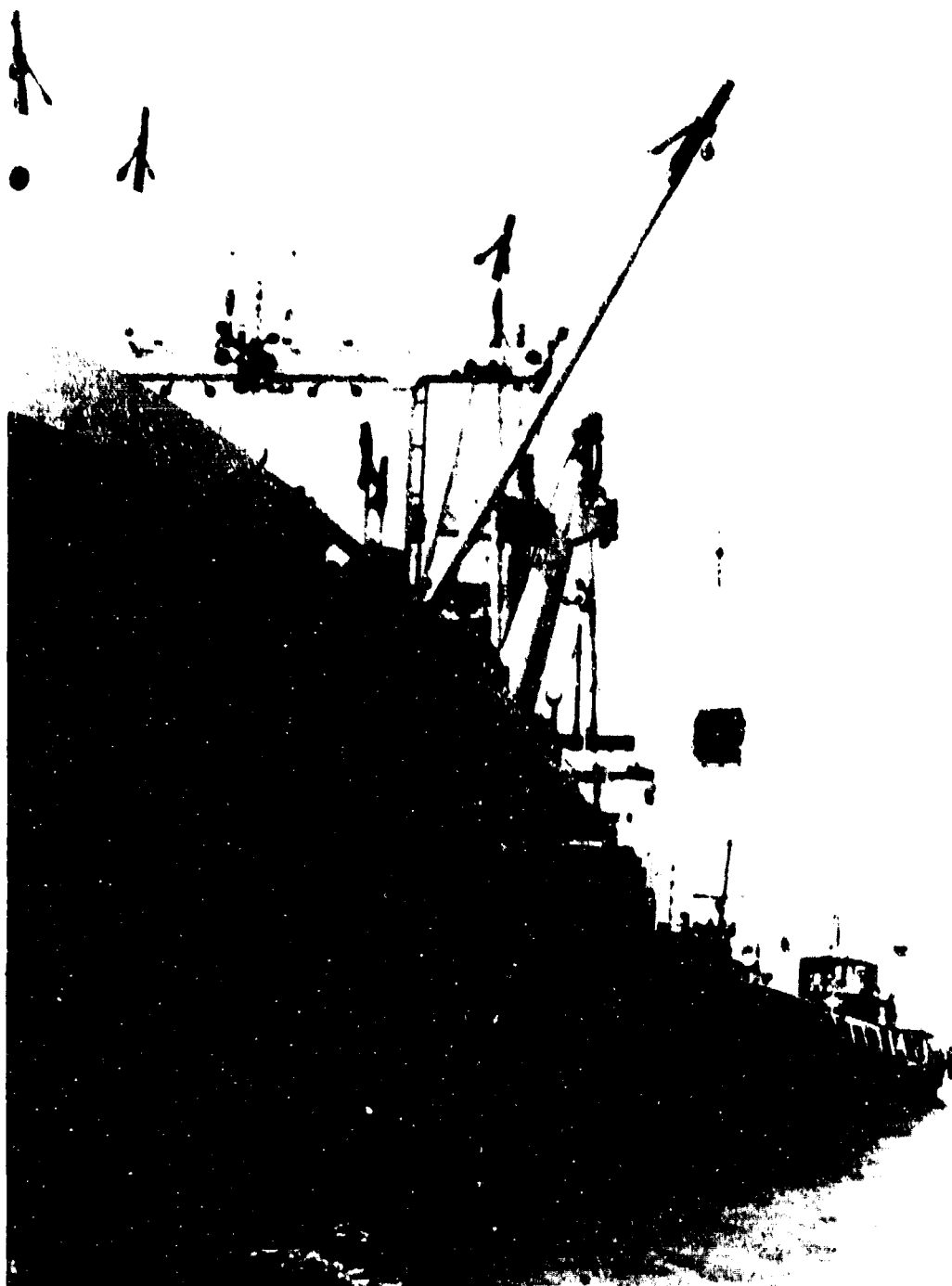
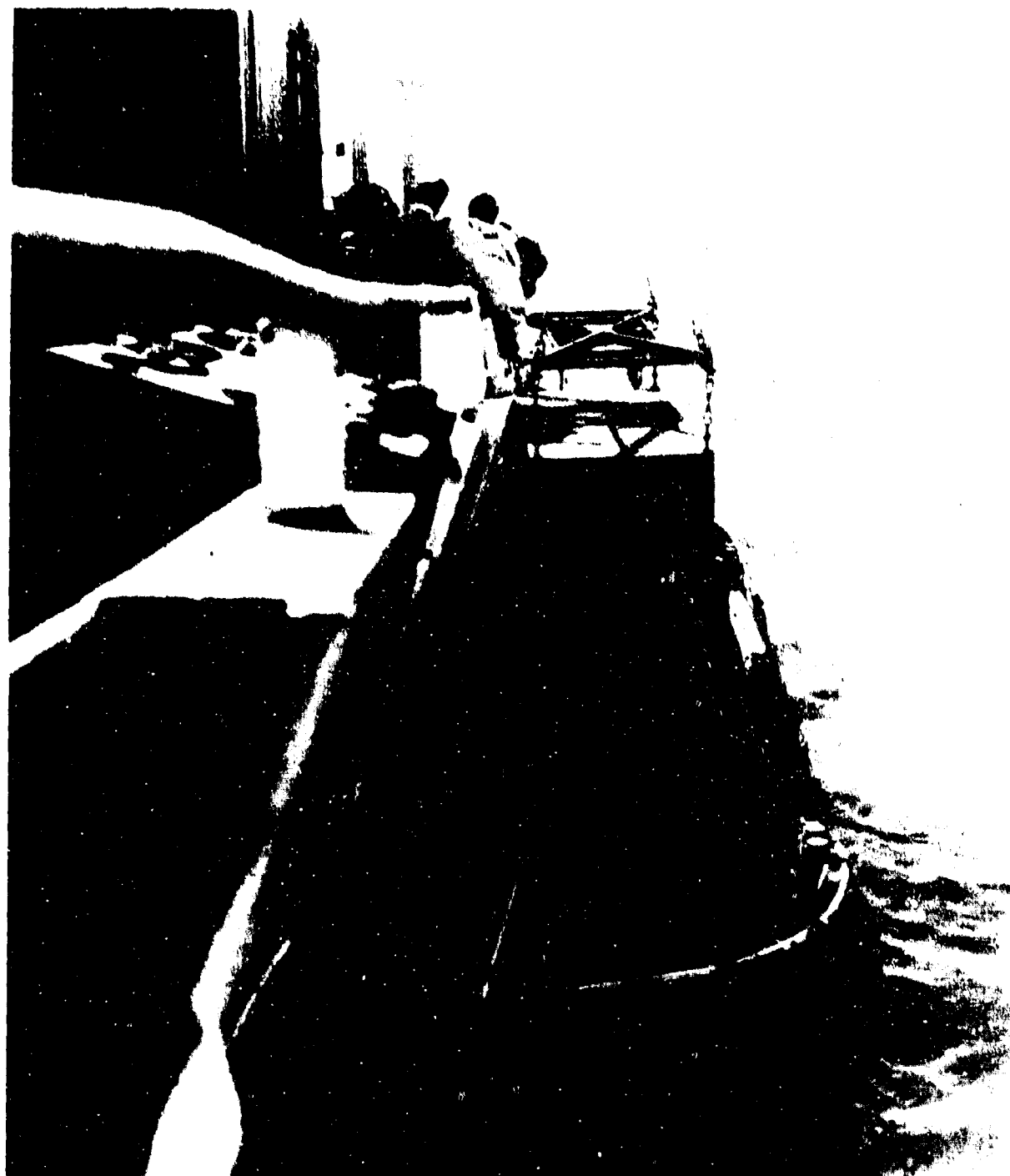


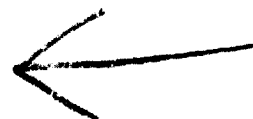
FIG 15 TRANSHIPMENT OF EXPLOSIVES IN A PALLET



**FIG 16 TRANSHIPMENT OF EXPLOSIVES IN A FREIGHT
CONTAINER**



FIG 17 TRANSHIPMENT OF EXPOLOSIVES - "EARLY DAYS"



AD P000467

→ THE LOW PROBABILITY OF ACCIDENTAL EXPLOSIONS:
ISN'T IT WORTH A CENT IN EXPLOSIVES SAFETY?

by

Hans A. Merz, M.ASCE/SIA
Ernst Basler & Partners
Consulting Engineers and Planners
Zurich, Switzerland

ABSTRACT

↓
In recent years, the problems in complying with well-known safety-distance regulations for ammunition and explosives storages steadily increased in Switzerland. As a reaction, the concept of quantitative risk assessment was developed to guarantee the safety of such storages. This concept allows to take into account both the probability of an explosion and its consequences.

It is shown that the safety-distance concept was originally developed as a reaction to the numerous large explosions which occurred around the turn of the century. Since that time the conditions have changed. Today, such explosions are rare events. Therefore, it is proposed to modify the safety-distance concept by introducing the low probability as main guarantor of safety. Necessary steps to promote this change include: demonstration that the probability is actually low, investigation into the reasons why it is low, and development of a model to take into account both probabilities and consequences of accidental explosions. The Swiss experiences with such a concept have shown that problems with storage facilities not complying with safety-distance regulations can often be solved efficiently and economically.

↑

Paper presented to

Twentieth Explosives Safety Seminar, 24 - 26 August 1982
The Omni Hotel, Norfolk, Virginia, USA

ORIGIN OF THE QUANTITY-DISTANCE TABLES

Around the turn of the century, a large number of storage magazines, primarily of the commercial explosives industry, exploded. The famous "History of Explosions" compiled by Ralph Assheton ¹⁾ tells us that during the period between 1875 and 1925 large and disastrous explosions involving up to 100 tons of explosives and causing up to 10 fatalities occurred at an average rate of one per year. At the same time, an even larger number of small and less damaging explosions took place (Figure 1).

The reaction of the public to these accidents was, at that time, clear and straightforward: storage of explosives is an extremely dangerous activity. Therefore, we demand that the consequences in case of an explosion be kept as low as possible.

Based on this attitude and on damage records collected during those years, the famous "American Table of Distances" was elaborated by a group of experts of the explosives industry in 1909. This was the first recognized regulation in the United States which specified safe distances for explosives magazines. It was based on the assumption that beyond the specified safe distances damage to persons and structures should be minimal (Figure 2).

Though use of the American Table of Distances was primarily intended for the commercial explosives industry, it was adapted by the US Government for the ammunition storage following a series of spectacular explosions in such magazines. Since then, minor changes and refinements of the quantity-distance relationship were made on various occasions, but the basic philosophy of the original American Table of Distances remained unchanged up to this day: the consequences in case of an explosion must be kept low.

Whereas the philosophy remained the same, a distinct change of entirely different nature can be observed: the frequency of large explosions in storage magazines

¹⁾ Ralph Assheton: "History of Explosions on which the American Table of Distances was Based". Published under the direction of the Institute of Makers of Explosives, Charles Story Press Co., Wilmington, Delaware, 1930

with potentially serious consequences continuously dropped to a level where large explosions in storages can be considered rare events. This decrease can be attributed to a number of factors, first of all to more rigorous safety rules for the handling and storage, and to better quality and control of explosives and ammunition. A look at probable causes of some of the explosions which happened at the beginning of this century clearly demonstrates how drastically things have changed in the meantime (see Figure 3).

There is no doubt that today's storage and handling conditions and the improved quality of explosives and ammunition are not comparable to those prevailing at the time when the American Table of Distances was created. *Today, we find ourselves in the situation that we apply rules to modern explosives and ammunition which were developed at a time, when the explosives industry was in its infancy. Isn't this reason enough for reconsidering the philosophy of strictly limited consequences and for taking into account the numerous efforts in reducing the frequency of explosions?*

In the present concept of quantity-distance relationships, efforts to reduce the probability do not pay off. They are, so to speak, treated as additional hidden reserves. Nobody has to fear the blame of having done too little for safety with this concept. But the day might come when we will be blamed for having done too much and for having wasted money which could have saved more lives in other potentially hazardous activities of our society.

The problem finally boils down to the simple question whether we can afford to limit both, probabilities and consequences, to a low level at the same time. This is not to say that the present concept should be abandoned immediately and everywhere. But when actual difficulties arise in complying with safety distances during the operation of existing magazines or in connection with the location of new magazines, the present concept has to be questioned.

It is this situation which has come up in Switzerland in the last ten to twenty years because of its densely populated areas. Practical problems have forced us to explore new ways of guaranteeing the safety of ammunition magazines. In a first step, the concept of safety distances was replaced by the concept of quantitative risk assessment, on which we reported in former papers to this semi-

nar ¹⁾. Such risk assessments basically allow to take into account both, the probability of explosions and their consequences. Since the limitation of the consequences, which was of primary concern at the beginning of the era of risk assessment, became increasingly difficult in practice, a comprehensive investigation into the probability part has been initiated. This paper summarizes some of the experiences and results obtained so far.

THE CONCEPT OF THE PARTNERSHIP OF PROBABILITY AND CONSEQUENCES

When exploring ways to guarantee the safety of different potentially hazardous activities in our society, we can notice marked divergencies:

- . As an example, the safety of large dams or of airplanes is mainly based on the low probability of accidents. Nobody would dare to require safety distances for dams or beneath air-routes. Airplane passengers can only rely on a low probability. And there are many other activities in our society where the low probability is an accepted guarantor of safety.
- . Even in the explosives industry, we can observe different ways of warranting safety:
 - In the production of ignitors, for instance, events might be very frequent, but their consequences are kept negligible. The machine might not even stop the production.
 - In the short-time intermediate storage of large production batches, on the other hand, we might completely rely on the small probability of an accident, though we know that the consequences could be disastrous. The same is true for the transportation of explosives on the road.

¹⁾ See Papers by Th. Schneider in the Proceedings of the 17th, 18th and 19th DDESB Seminars

These examples lead us to two conclusions:

1. There are marked differences in the way safety is guaranteed for various hazardous activities in our society. Whether we rely on low probabilities or low consequences is a matter of technical possibilities, practicability and, last but not least, tradition. However, it is hardly ever explicitly stated why the one or the other concept is used.
2. Relying on a small probability is neither an immoral nor an evil thing. Instead, in our society, it is considered an equal partner to the low consequence concept. Though we can observe a strong tendency to reduce safety problems to either a probability case or a consequence case in practice, *the equal partnership of probability and consequence is generally accepted.*

In conclusion, it can be stated at this point that recognizing this partnership of probability and consequences can be a way of getting away from the pure consequence thinking in explosives safety and throwing off the burden of unfavorable historical accident records.

APPLYING THE PARTNERSHIP IN AMMUNITION STORAGE

The reason for the application of the consequence concept in the safety of ammunition storages is merely traditional. There is many an argument for reconsidering this traditional concept:

- . The probability of a large explosion in ammunition storages lies in the same order of magnitude as the break of a major dam, for instance (Figure 4).
- . There are large differences in the probabilities of explosions between individual magazines. A storage full of shells filled with TNT and removed fuses is less probable in going off than a magazine with the same amount of highly sensitive explosives (Figure 5).

- . A difference of a probability factor of 10 or more between two magazines could result in a reduction of safety distances of 1/3 or more, if the same safety level for individual, exposed persons were maintained.

However convincing these arguments may be, the most effective promoters of the concept of equal partnership of probability and consequence are acute problems and the necessity of solving them.

The increasing urbanization in Switzerland made it more and more difficult and impossible to meet quantity-distance requirements and to reduce the consequences calculated in quantitative risk assessments to tolerable levels. As a reaction to this situation, a comprehensive investigation is presently performed to guarantee the safety of particularly critical magazines, primarily on the basis of small probabilities. The goal of this investigation is to develop a rational and transparent model for the partnership of probabilities and consequences.

In order to proceed in this new direction, three major areas of investigation were identified:

- *We need to show how large or small the probability of explosions is in reality. We need a statistical analysis, based on accident records and corresponding reference data such as number of operated magazines, total amount of stored ammunition, etc.*
- *We need to show why the probability is low, how it was decreased and how we can decrease it further. We need a model for assessing the effectiveness of safety measures acting on the probability side.*
- *We need to show on which rationale a reduction of the probability is set off against a reduction of the consequences. We need a model which links probability and consequence to something like a tolerable safety level.*

Though much work still has to be done in this investigation, some of the preliminary results can be mentioned:

- Based on the fact that not a single explosion occurred in our country since 1950, the average probability of an explosion in a storage magazine is esti-

mated to lie somewhere around 10^{-5} per year and magazine.

- The difference between the "best" and the "worst" magazine can be as large as a factor of 100 or more.

These differences are primarily due to type and sensitivity of the ammunition stored in a particular magazine, and type and equipment of the magazine.

- Based on an investigation into the causes and the development of possible explosions, the following safety measures contribute most significantly to low probabilities:

- . Generally safe ammunition produced today
- . Continuous quality control during manufacturing and storage of explosives and ammunition
- . Rigorous safety rules for the personnel involved in the storage
- . Early warning devices and fire protection
- . Rigorous security protection

The rationale on which we set off probabilities against consequences is the model of quantitative risk assessment. This model allows an easy numerical consideration of both quantities.

As a result of the work performed so far, buildings erected in the immediate vicinity of storage magazines could be tolerated in individual cases, because special and individually determined safety measures were taken to keep the probability at extremely low levels.

SUMMARY AND CONCLUSION

It is known experience that traditions are not easily given up. The application of quantity-distance relationships in the safety of ammunition magazines has its roots in a tradition going back to the turn of the century. It's an equally known experience that traditions are only given up when actual problems force to do so. In Switzerland, this situation has come up, and new ways have been sought to gua-

rantee safety. The features of this new method are as follows:

- The quantity-distance concept or the concept of limited consequences of accidental explosions was developed under the impression of the unfavorable accident records at the beginning of this century. Today's situation in ammunition storage is so markedly different and better that the low probability of large explosions must be taken into account.
- As safety concepts in other hazardous activities of our society show, probability and consequences are considered and generally accepted as equal partners in the safety business.
- The Swiss safety concept for ammunition storages is based on the partnership of probability and consequences. it concludes the demonstration that probabilities are indeed low, why they are low and the rationale of the model of quantitative risk assessment for setting off probabilities against consequences.

This new way has offered solutions for the economic operation of existing storage facilities, which otherwise would have needed safety waivers, or which were about to be given up.

NUMBER OF LARGE EXPLOSIONS OF STORAGE MAGAZINES AROUND THE TURN OF THE CENTURY

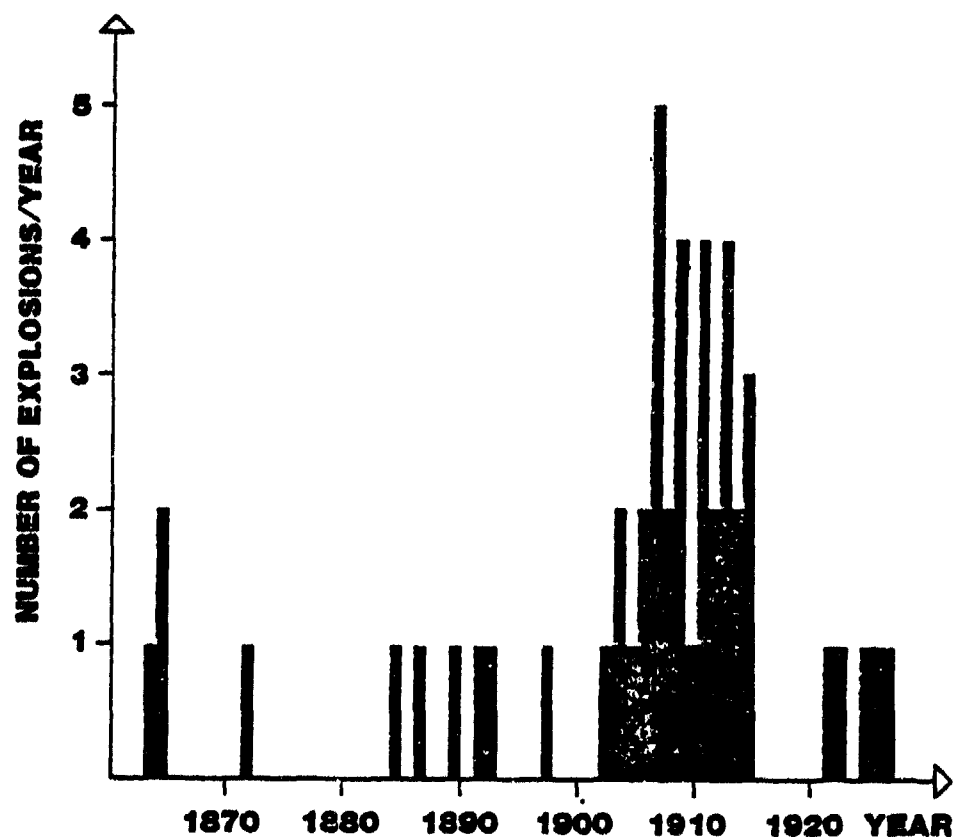


Figure 1

THE SAFETY DISTANCE CONCEPT

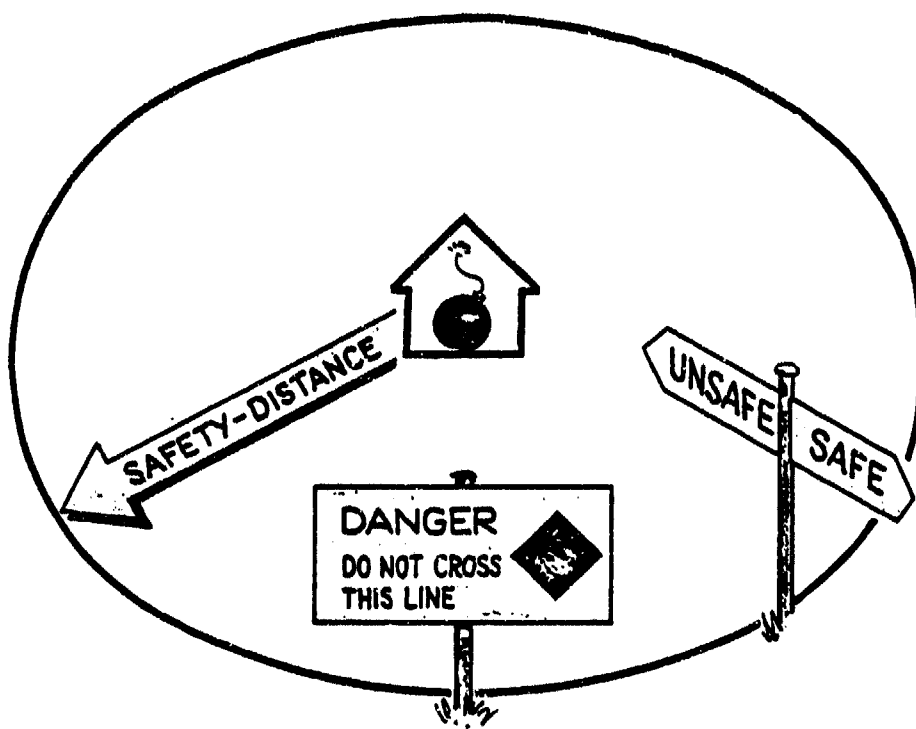


Figure 2

THE CAUSE OF EXPLOSIONS AROUND THE TURN OF THE CENTURY

(Taken from the "History of Explosions" by R. Assheton)

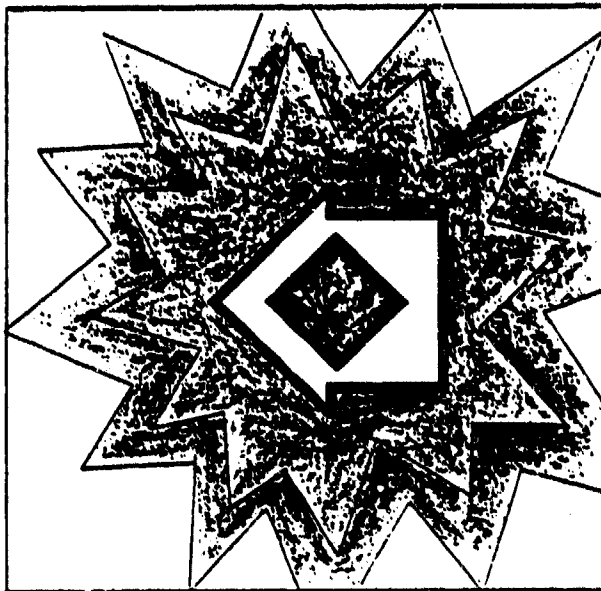
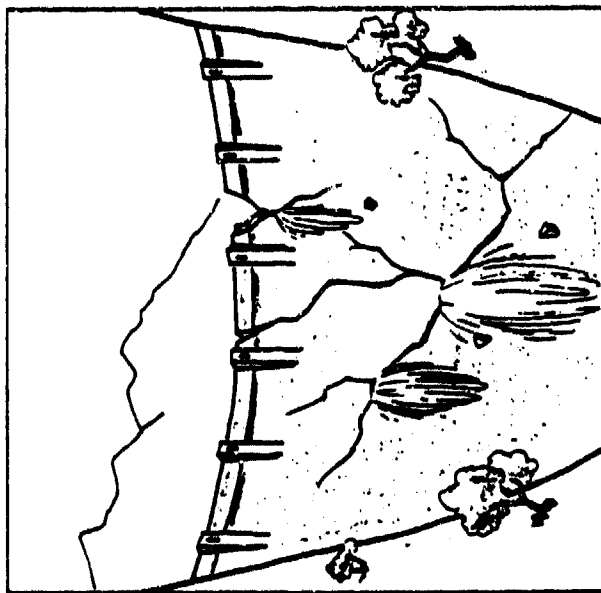
"____the accident may have happened through the carelessness of the soldiers as the most elementary rules of safety were violated."

"____an agent sent some years before (the explosion) to destroy some old dynamite in the magazine ,so old that it was in a dangerous condition, said that he found difficulty in persuading the officer in charge to throw away his cigarette at the door of the powder room. He also said that the floor was a quarter of an inch thick in loose black powder and only by refusing to enter could he induce the officer to remove his nailed soled shoes."

"____the storekeeper ____ said that a carpenter was repairing (leaking) powder boxes at the time (of the explosion) and he thought that driving nails in the lids set the powder off."

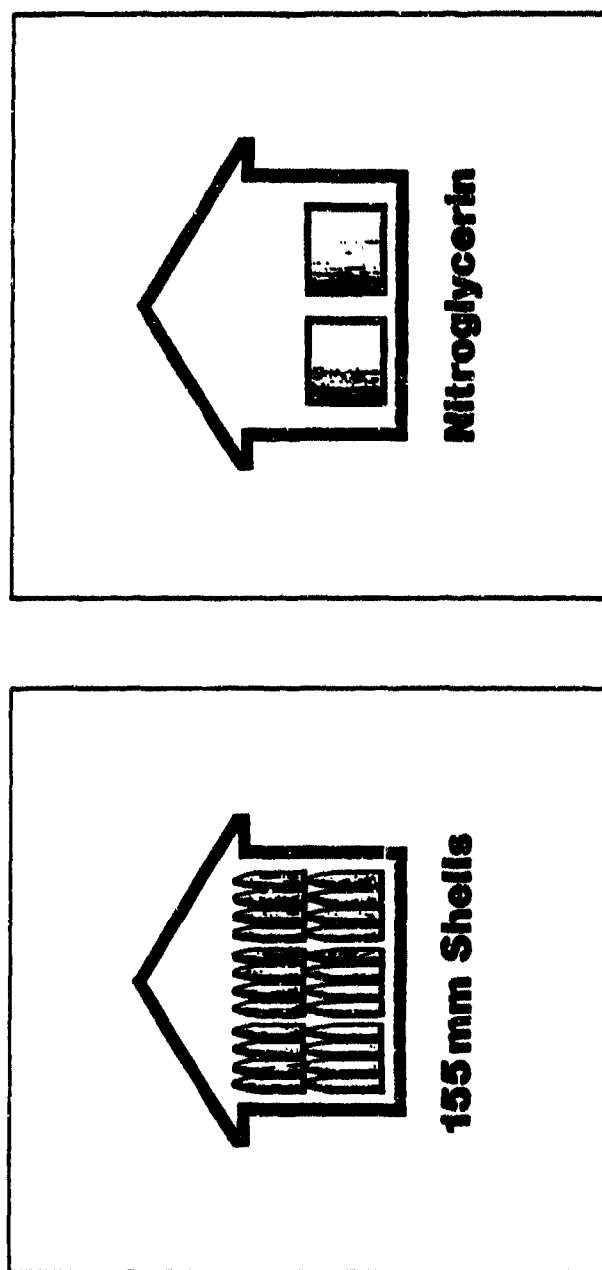
"____spontaneous decomposition ____ is thought to have been the cause of the explosion."

Figure 3



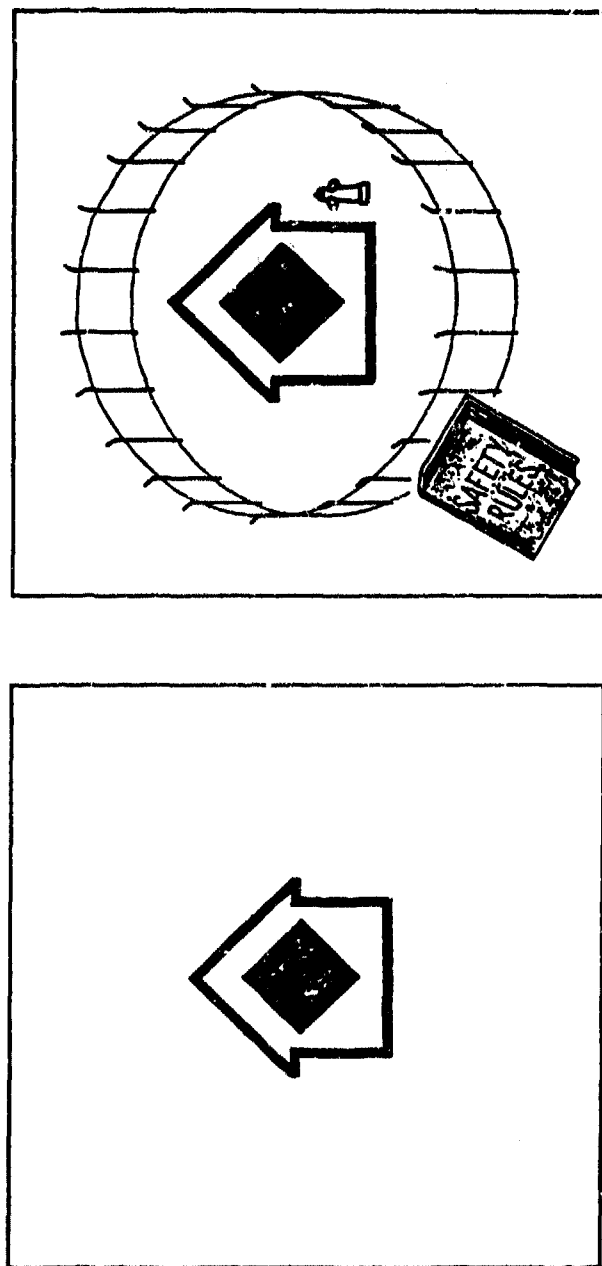
**The probability of the break of a major dam
is in the same order of magnitude as the probability
of a large explosion in an ammunition storage.**

Figure 4



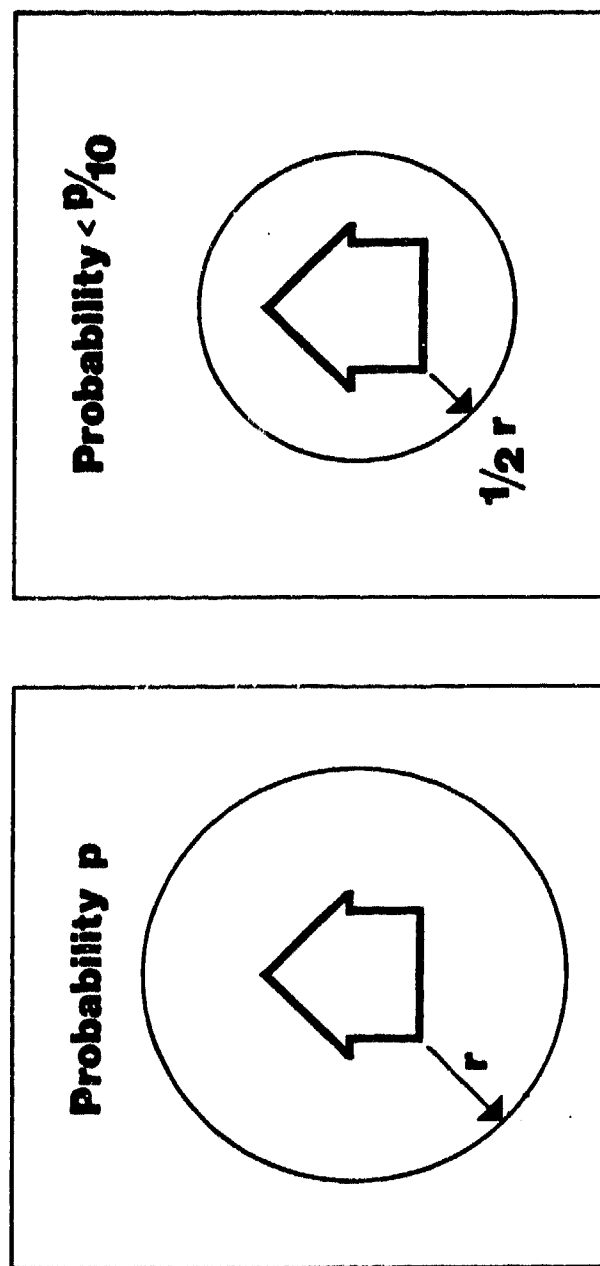
The probability of accidental explosions differs between magazines.

Figure 5



**Special safety measures reduce the probability
of accidental explosions.**

Figure 6



A lower probability justifies a reduction of the safety distances.

Figure 7